Newcastle University, UK

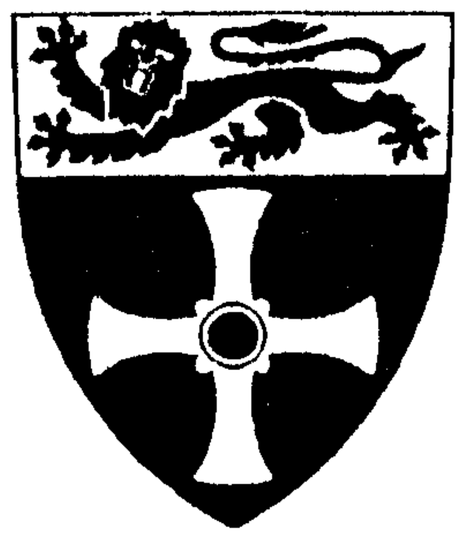

THE BEHAVIOUR OF FLEXIBLY BEDDED CONCRETE PAVER PAVEMENTS

This Ph.D. Thesis Presented to the Civil Engineering Department, the Division of Structural Engineering

By
Halil Murat Algın

September, 1996

ACKNOWLEDGMENTS

This Ph.D. Research was supervised by Professor John Knapton and financially supported by the Turkish Republic the Institution of Higher Education.

First of all, I would like to express my gratitude to my supervisor for his excellent supervision, criticism, continuous enthusiasm and encouragement throughout the three year program. I am grateful for the financial support given by the Turkish Republic the Institution of Higher Education. The UK and Newcastle University would have just been a figment of my imagination without their support. I am also deeply indebted to my parents and my dear friend Marie for their patience which immensely aided the accomplishment of this Thesis.

TABLE OF CONTENTS

ABSTRACT

The growth in the international usage of flexibly bedded pavers since World War II has brought about the need fully to understand how pavers bedded in sand function. The design methods are based upon the concept of making pavers and their bedding sand equivalent to conventional pavement construction materials. Experience has shown that pavers do not behave as a collection of individual units but rather interlock so that they behave in a manner close to that of flexible materials. The nature of a pavement surfaced with pavers is therefore depending on the pavers, the joints, and the way in which the two relate as well as the foundation on which the pavers rest.

In this Thesis, a way in which pavers distribute stresses resulting from rolling loads has been investigated and an understanding of the interlocking process thereby developed. This Thesis explains the theoretical analysis and demonstrates how it can be used to establish the nature and value of interlock. Chapter 1 concentrates on this process by starting to introduce concrete paver pavements and goes on outlining the principles upon which the remainder of this Thesis is based. The achievement of full interlock in the surface level of a paver pavement is an essential part of any successful paver pavement. It is important to understand the principles and specifications for the materials and construction process in order to satisfy the requirements of paver pavement components. Because of this reason, Chapter 2 outlines the major contents of UK specifications for the materials and construction methods likely to be used for the construction of paver pavements. Chapter 3 is concerned with the existing structural design of concrete paver pavements carrying vehicular traffic ranging from trucks to heavy industrial vehicles and aircrafts. Design criteria for such pavements are established and a range of methods for their analysis and design are reviewed. Chapters 4 and 5 show how the variations of patch loading on the surface of pavers can be calculated. Chapter 6 presents the bedding sand stress calculation method which can be used to determine the patterns of stress within the bedding material and it shows how these patterns develop as a patch loading rolls across pavers. All possible

eccentric load patches on the surface and their all vertical compressive stress distributions in bedding sand were calculated for chamfered rectangular pavers (with and without interlock), non-chamfered rectangular and nine proprietory shaped pavers. The nine proprietory shaped pavers analysed in this Thesis are commercially important on a worldwide basis. Chapters 7, 8 and 9 explains how the bedding sand stress calculation method can be applied to proprietory shaped pavers. A common proprietory shaped paver has been selected as an example in Chapter 7 to show how all possible vertical compressive stress regimes of proprietory shaped pavers can be calculated for all realistically possible load patches. The remaining proprietory shaped pavers are analysed in Chapter 8. The results of the analyses presented in Chapters 5, 7 and 8 are shown in Chapter 9. The results are being used in the development of paver jointing systems and it is now possible to assess more effectively the tolerances required in paver installation.

Although paver pavements appear to be very simple structures they are in reality very complicated, possibly one of the most complicated of all civil engineering structures. In order to predict the future performance of paver pavements, a vast number off simplifications must therefore be made. One of the most promising approaches to this is to apply accurate modelled Finite Element Analysis obtaining the data related with systematic behaviour of paver pavements on the surface level from the results of this Thesis.

GLOSSARY OF NOTATION

$0.\bar{3}$ the decimal 0.3 repeats indefinitely (see Sections 5.2 to 5.10 and 7.2)

σ_A the vertical compressive stress value beneath the circumscribing rectangular border of a paver's corner A (see Sections 6.2, 6.3, 7.2, 8.2 to 8.9, 9.2 and A.2)

N total applied load (see Sections 4.2, 4.3, 5.2 to 5.10, 6.2, 6.3, 7.2, 8.2 to 8.9, 9.2 and A.2)

F surface area of patch loading (see Sections 4.2, 4.3 and 5.2 to 5.10)

V volume of a vertical compressive stress block (see Sections 6.2, 6.3, 7.2, 8.2 to 8.9, 9.2 and A.2)

$\overline{X}$ applied load patch or the vertical compressive stress block's centroid distance in the x axis (see Sections 4.2, 4.3, 5.2 to 5.10, 6.2, 6.3, 7.2, 8.2 to 8.9, 9.2 and A.2)

$\overline{Y}$ applied load patch or the vertical compressive stress block's centroid distance in the y axis (see Sections 4.2, 4.3, 5.2 to 5.10, 6.2, 6.3, 7.2, 8.2 to 8.9, 9.2 and A.2)

$f(x)$ line function according to the x axis (see Sections 4.2, 4.3, 5.2 to 5.10, 6.2, 6.3, 7.2, 8.2 to 8.9, 9.2 and A.2)

$f(y)$ line function according to the y axis (see Sections 4.2, 4.3, 5.2 to 5.10, 6.2, 6.3, 7.2, 8.2 to 8.9, 9.2 and A.2)

$f(x,y)$ surface function of vertical compressive stress block beneath a paver (see Sections 6.2, 6.3, 7.2, 8.2 to 8.9, 9.2 and A.2)

abx the boundary line function of a paver which through corners a and b in the x axis (see Sections 5.2 to 5.10, 6.2, 6.3, 7.2, 8.2 to 8.9, 9.2 and A.2)

aby the boundary line function of a paver which through corners a and b in the y axis (see Sections 5.2 to 5.10, 6.2, 6.3, 7.2, 8.2 to 8.9, 9.2 and A.2)

T_{1x} the distance of intersection point 1 in the x axis for the proprietory shaped paver's tetrahedral stress block (see Section 7.2.1)

T_{1y} the distance of intersection point 1 in the y axis for the proprietory shaped paver's tetrahedral stress block (see Section 7.2.1)

S_{1x} the distance of intersection point 1 in the x axis for the proprietory shaped paver's short-pentahedral stress block (see Section 7.2.2)

S_{1y} the distance of intersection point 1 in the y axis for the proprietory shaped paver's short-pentahedral stress block (see Section 7.2.2)

L_{1x} the distance of intersection point 1 in the x axis for the proprietory shaped paver's long-pentahedral stress block (see Section 7.2.3)

L_{1y} the distance of intersection point 1 in the y axis for the proprietory shaped paver's long-pentahedral stress block (see Section 7.2.3)

P_{1x} the distance of intersection point 1 in the x axis for the proprietory shaped paver's partial-hexahedral stress block (see Section 7.2.4)

P_{1y} the distance of intersection point 1 in the y axis for the proprietory shaped paver's partial-hexahedral stress block (see Section 7.2.4)

M_{1x} the distance of intersection point 1 in the x axis for the proprietory shaped paver's absolute-hexahedral stress block (see Section 7.2.5)

M_{1y} the distance of intersection point 1 in the y axis for the proprietory shaped paver's absolute-hexahedral stress block (see Section 7.2.5)

a.....z corner names or distances (see Sections 4.2, 4.3, 5.2 to 5.10, 6.2, 6.3, 7.2, 8.2 to 8.9, 9.2 and A.2)

$\doteq$ is a approximation symbol in numeric analysis which implies equal when rounded to places shown (see Section A.2.1)

A, B, C and D the corner names of a paver's circumscribing rectangular border (see Sections 4.2, 4.3, 5.2 to 5.10, 6.2, 6.3, 7.2, 8.2 to 8.9, 9.2 and A.2)

CHAPTER ONE

BASIC INTRODUCTION TO THE BEHAVIOUR OF FLEXIBLY BEDDED INTERLOCKING PAVER PAVEMENTS

Synopsis

The paver pavement and its surfacing are a structurally major element in modern highway, industrial and airport projects. The full understanding of their behaviour, function and performance under different load regimes and environmental conditions is fundamental to providing adequate paver pavements. This Chapter concentrates on this process by starting to introduce concrete paver pavements and goes on outlining the principals upon which the remainder of this Thesis is based.

1.1. Introduction

Since the first UK application of concrete paving blocks as a highway pavement material in 1973[1], the development of flexible concrete paver pavements has brought about the need for fully understanding the mechanical behaviour of segmental paving systems. This is structurally imperative if a satisfactory level of performance in segmental pavements is to be achieved. Block paving consists of a large number of small, rigid slab with flexible joints between them. The nature of a block paved surface may therefore depend on the blocks, the joints, and the way in which the two relate - as well as the foundation on which the blocks rest. Block paving is particularly useful paving material in that it provides a very strong and flexible surface which can support concentrated loads indefinitely without suffering deformation.

The research reported in this Thesis describes the mathematical solution to the behaviour of the surface components of flexibly bedded concrete paver pavements. In order to understand the mechanical problem associated with the behaviour of paver pavements it is necessary to have a basic understanding of their principals and functions. This Chapter briefly outlines the general overview, and the nature of concrete paver pavements in engineering applications.

1.2. A brief historical note on segmental paving and general outlook

Segmental paving has been used for many years in road construction as a surface material. Initially, it was used by the Minoans, on the island of Crete some 5000 years ago[2]. Stone paved roads were used in Egypt around the time of Christ's birth[2]. These roads were used to transport the large stone blocks in the construction of the Great Pyramid[2]. It is probable that the joints between the paving stones were grouted with bitumen. The jointing serve the following functions.

- tabulate to make a smoother surface which is more comfortable to walk on
- easier for wheels to roll over
- it was used to prevent rain water from entering the embankments upon which many historic roads were constructed.

During the Roman Empire these kind of roads rapidly spreaded from Rome, to Italy, Northern Europe and parts of Asia and Africa[2]. Sand, a mixture of sand and bitumen, granulated slag, dry cement mortar or damp cement mortar were used. The original Greek paving systems based on the use of flat, irregularly shaped stones is still used today for surfacing village roads[2]. When they were designed, the weight and volume of traffic, and the strength of the underlying soil was taken into consideration[2]. Roman roadbuilders realised that the strength of many soils was influenced by its water content. Centuries after the demise of the Roman Empire, many European countries attempted to rebuild national road systems[2]. In order to satisfy the needs of people for an economic transportation system.

Until the invention of concrete flags, segmental paving was limited to stone and later clay products, the choice depending on their relative costs. In the nineteenth century, factories started to experiment with the production of wet-cast concrete flags, essentially copies of stone products. Large hydraulic presses were invented and used by the manufacturers. This technique allowed high-speed production of good quality and very uniform, durable products, at much lower cost than stone flags. The process is used for the manufacture of concrete kerbs and products of different cross-sections. Concrete blocks were first used as a substitute for the traditional clay products[2]. Originally all the operations in building segmental pavements were carried out manually and these traditional methods were also adopted in block laying. Fortunately, block paving and plate vibrators were being developed at the same time and the compaction of the laying course and levelling of the pavement surfaces with these plates was a natural outcome.

Engineering progress has led to the need for paving system that is adaptable, economic, long lasting and easy to maintain. In more recent years, the qualities of segmental paving have been revived. The merits of segmental paving are such that they provide uniform and close dimensional tolerances in order to be competitive in many situations with most other paving methods. Segmental paving construction costs had to be reduced.

Segmental paving intended to inspire architects, planners and engineers to look forward and develop further ideas and applications. The advantages of segmental paving include its good resistance to softening by oil or petroleum spillage, and its resistance to staining. Another advantage is its hard surface that resists indentation from high local stress, such as storage racks, or loaded trailer-legs, but it can also accommodate major ground movements, such as those that often occur over reclaimed land. Surfacing with flexible segmental units allows easier and lower cost opening and closing of a paved surface over trenches dug as compared with other paving forms[3]. Concrete blocks, flags, and clay pavers can be made to retain adequate skid and slip resistance, thereby satisfying the highway requirements. Architects have welcomed segmental paving systems that have given them opportunities to improve the appearance of the floorscapes of residential areas, pedestrian precincts, town centers, gardens and parks and ample scope to expertise their aesthetic design skills. Small units allow the paving of the most complex plan and vertical shapes which can be considered with variations in surface texture and color within a pavement.

Some examples of segmental paving include[4] : Accident prevention zone, airfield paving, bulk storage areas, bus terminals and stops, car parks, crawler lanes, residential roads, cycle tracks, deterrent paving, dockside paving, emergency roads, farm roads and yards, floors, footways, forecourts, industrial estates, junctions, landscape paving, light-reflecting surfaces, lorry parks, markets, roundabouts, overlays, petrol stations, playgrounds, quadrangles, railway stations platforms, roll on/roll off terminals, speed deterrents and traffic barriers. Concrete blocks are being used for the paving of airfields although their use on airport runways seems unlikely, at least in the near future[5]. The very flat surfaces

required from modern runways, with maximum longitudinal falls of 1%, means that the surface regularities achieved with normal block pavement construction techniques precludes their use in such situations[6]. Concrete paving blocks have been used for paving aircraft hard-standings and turning areas for both civil and military airfields[6]. Ben-Gurion International Airport, Israel and Luton International Airport in England are prime examples of military and civil applications respectively[3].

1.3. The role of paver pavements in highway engineering applications

The pavement design can be divided into two parts, firstly the plan and elevation, and secondly the structural design which involves the selection of the thickness and types of materials used in the various layers. Both parts of the design process depend upon the type and volume of traffic. The aim is to achieve the best possible combination of performance, durability, safety, maintenance, appearance, low-cost and general surface water free, resulting in an economical pavement. Initially four factors are important for structural pavements, which are subgrade strength, traffic loading, traffic volume and intended design life, measured in either number of traffic movements or time.

The manufacture of segmental pavement elements ranges from the digging out of suitable stones with simple hand tools, through to the use of modern, computer controlled machinery for making both concrete and clay products[7].

In an ever expanding industry, trying to prophesy the future is difficult. In 1989, Knapton[8] estimated the worldwide annual sales of blocks and pavers as 240 million square metres and growing rapidly. There is also other evidence that the various forms of segmental paving meet the present and future needs of very many different industrial, commercial and residential pavements where aesthetics are important. Segmental paving is considered by some to be somewhat better than either bituminous or in-situ concrete paving[4]. Co-ordination of different segmental materials, which will develop, will allow designers to

create even more interesting patterned paved area, introducing symbols and information as paver inlays. It is very likely that blocks will also be more widely used for heavy duty pavements and urban roads as a simple means of improving road safety[4].

New methods of pavement design as opposed to overlays are being developed for use in block pavements on new construction sites[9]. The normal pavement design problems are achieved by equivalence approach which provides high strength and dimensional consistency of pavements connected with their low-cost. In a wide range of paving applications, concrete blocks can offer advantages in such different areas as costs, construction, aesthetics and characteristics. The experience at Luton Airport has shown that block paving can resist aircraft loads (including turning movements) and jet engine blast[4]. It has also offered resistance to aviation fuel, hydraulic oil, anti-icing and de-icing fluids[4]. Concrete blocks can successfully resist erosion caused by the efflux of a jet engine[4]. However, special heat and erosion resistant joint-sealers must be used instead of the traditional jointing sand. It was concluded that block pavements were suitable for all airfield pavement which are subjected to slow-moving aircraft[4].

1.4. The nature of flexibly bedded concrete paver pavements

Figure 1.1 illustrates the principal elements of concrete block pavement consisting of a number of layers which have various functions ensuring the pavement remains stable, durable and safe for a period of time, under the action of weather and large numbers of load applications.

It can be seen in Figure 1.1, apart from pavers (wearing course) and bedding sand (laying course) the details of the modern concrete paver pavement varies little from a conventional flexible pavement.

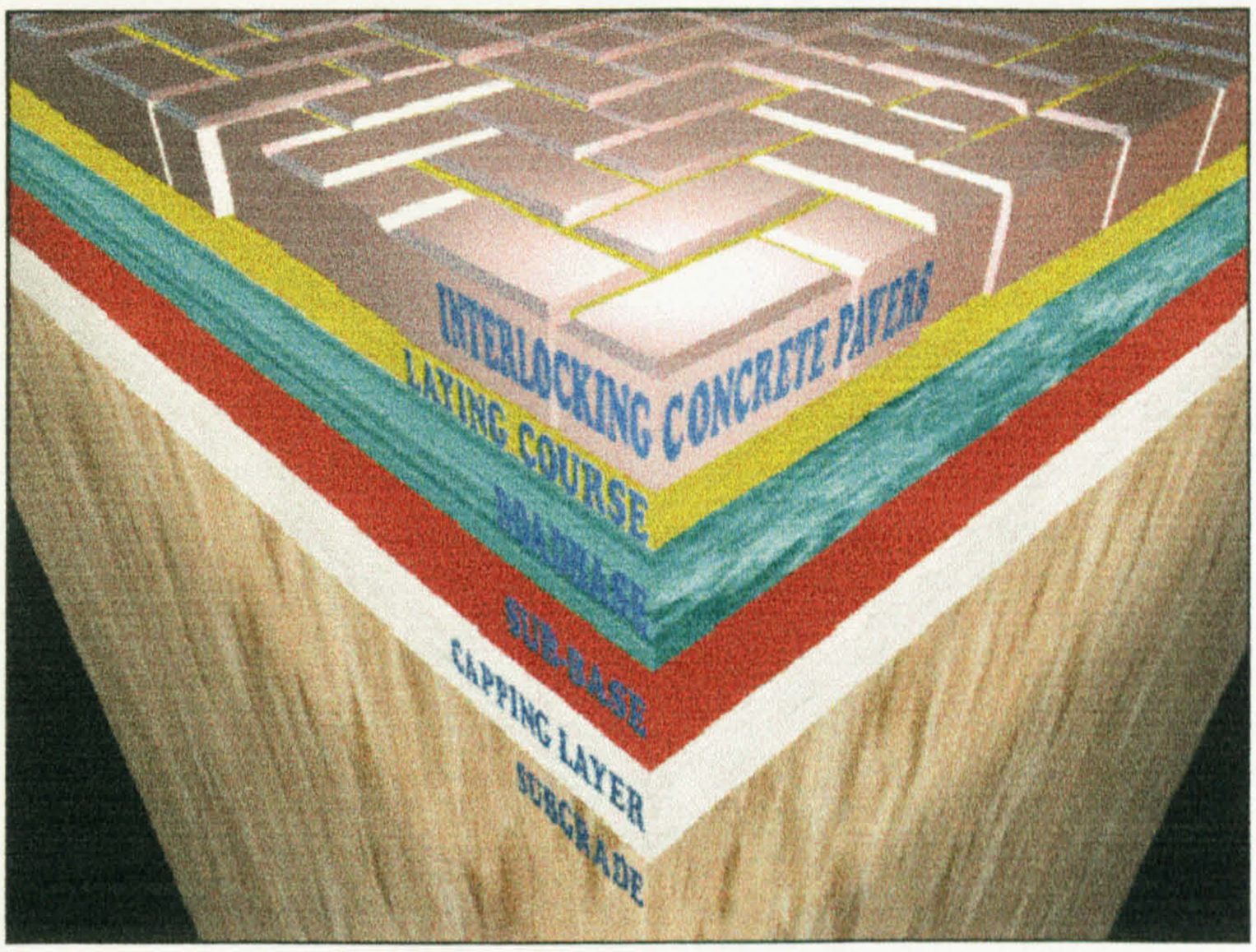

Figure 1.1: Principal elements of a concrete paver pavement.

The general experiences of concrete paver pavements indicates that the principal elements of a block pavement can be grouped in three components the surface, the structure and the foundation. Figure 1.2 shows a typical cross section of a pavement surfaced with pavers. The roadbase comprises the pavement structural course and the sub-base and capping represent the foundation.

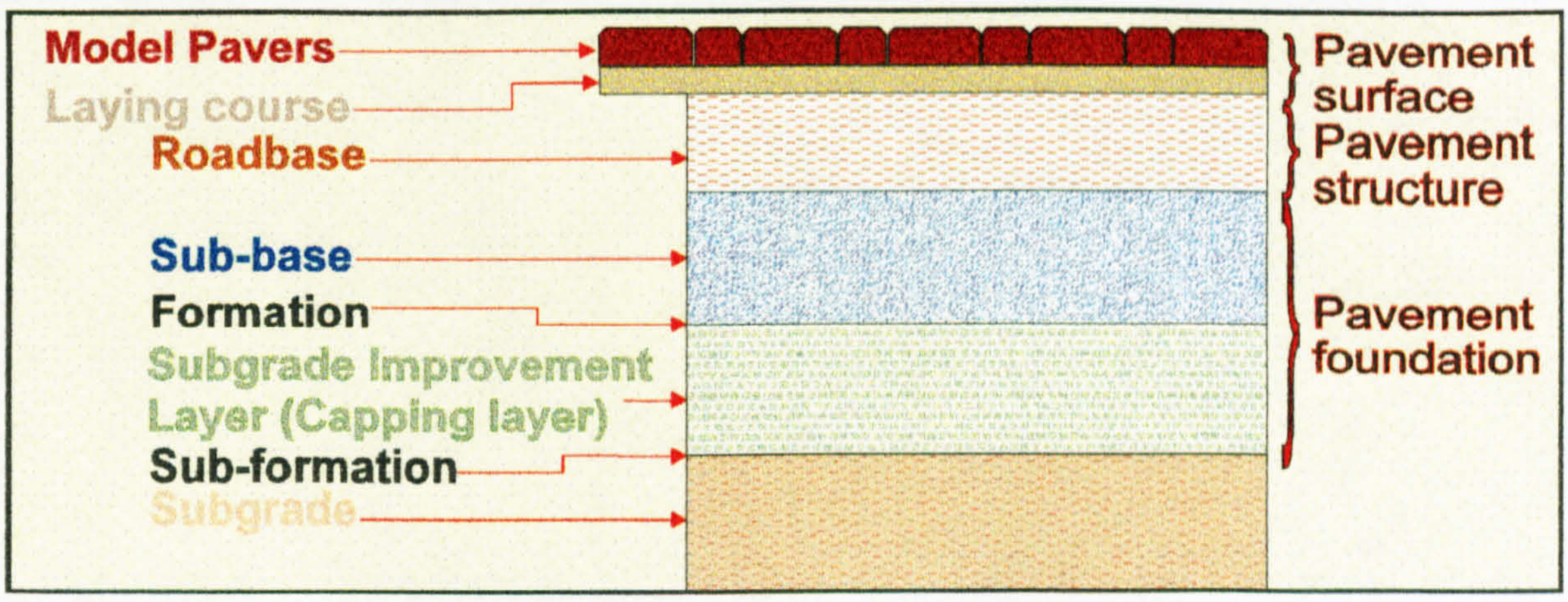

Figure 1.2: Typical cross section of a pavement surfaced with pavers.

1.4.1. The Surface

The surface of a concrete paver pavement is that component which most immediately affects traffic. The needs of traffic are that the surface should be sufficiently uniform to allow traffic to pass in comfort and safety at reasonable speeds, that it should not be so slippery as to allow vehicles to skid in wet whether, and that it should be sufficiently free-draining to avoid intrusive spray or pools of standing water in wet weather.

The surface of a concrete paver pavement structurally carries the applied loads by traffic and distributes the resulting loading over the layers beneath so that the stress transmitted to the soil does not exceed a safe value for the subgrade. Therefore, It should provide a running surface that will be safe and sufficiently strong to resist the effects of traffic and weather, with a minimum of maintenance over a long period. The surface also protects the underlying soil from the ingress of water and consequent variations in moisture content and thus assists in the maintenance during the design life of a uniform state of stability in the soil. Hence, it should provide a durable, non skid, non-slip, rideable and attractive upper surface to the pavement. In addition, the bedding sand layer in the surface reduces the friction between the pavers and the sub-base, and prevents the movement of paving blocks into a porous sub-base.

Flexible paver pavements are structurally complex systems consisting of individual pavers at surface level. Paver paving forms the top surface of the pavement and must therefore meet the significant requirements for a wearing course. It should support traffic loads without undue deformation, present a surface with suitable characteristics for the safe and comfortable passage of traffic, and provide protection to the underlying layers of the pavement and its foundation from the harmful effects of weather and traffic. An understanding of the way in which these objectives are achieved is important to the successful use of the joint materials (could be sand). Joints 0-6 mm wide are formed around each paver.

1.4.1.1. Interlock

From the earliest use of pavers, it was observed that the combination of rigid paving units and flexible joints formed a stable surfacing material with inherent strength and stability grater than might have been anticipated.

The matrix of joint material should effectively prevent any block from moving downwards or rotating, and thus ensure that the surface remains stable. The stress transferring between adjacent pavers at the surface level of paver pavements produce a flexible surface in which pavers act together as a system. The frictional forces provide stress transferring between joint material/paver interface are set up by compacted sand in the surface level. This systematic mechanism of flexible paver pavement is the crucial part of the behaviour of paver pavements.

The structural benefit provided by concrete block pavers has been defined in terms of interlock and Knapton[8] originally defined interlock as the inability of an individual paver to move independently of its neighbours. He categorised interlock into its three components viz.: rotational, vertical and horizontal.

Horizontal interlock is achieved by herringbone laying pattern or possibly by the use of a proprietory shaped paver. A pavement incorporating full interlock can sustain high levels of applied load. An interlocking paver pavement can be observed to behave in a manner whereby the pavers act together as a system such that the pavement has more of the character of a flexible homogeneous material rather than that of a collection of individual units behaving independently. Because of this, virtually all of the research into the behaviour of concrete block paving has focused upon establishing relative performance factors between pavers and conventional flexible pavement construction materials.

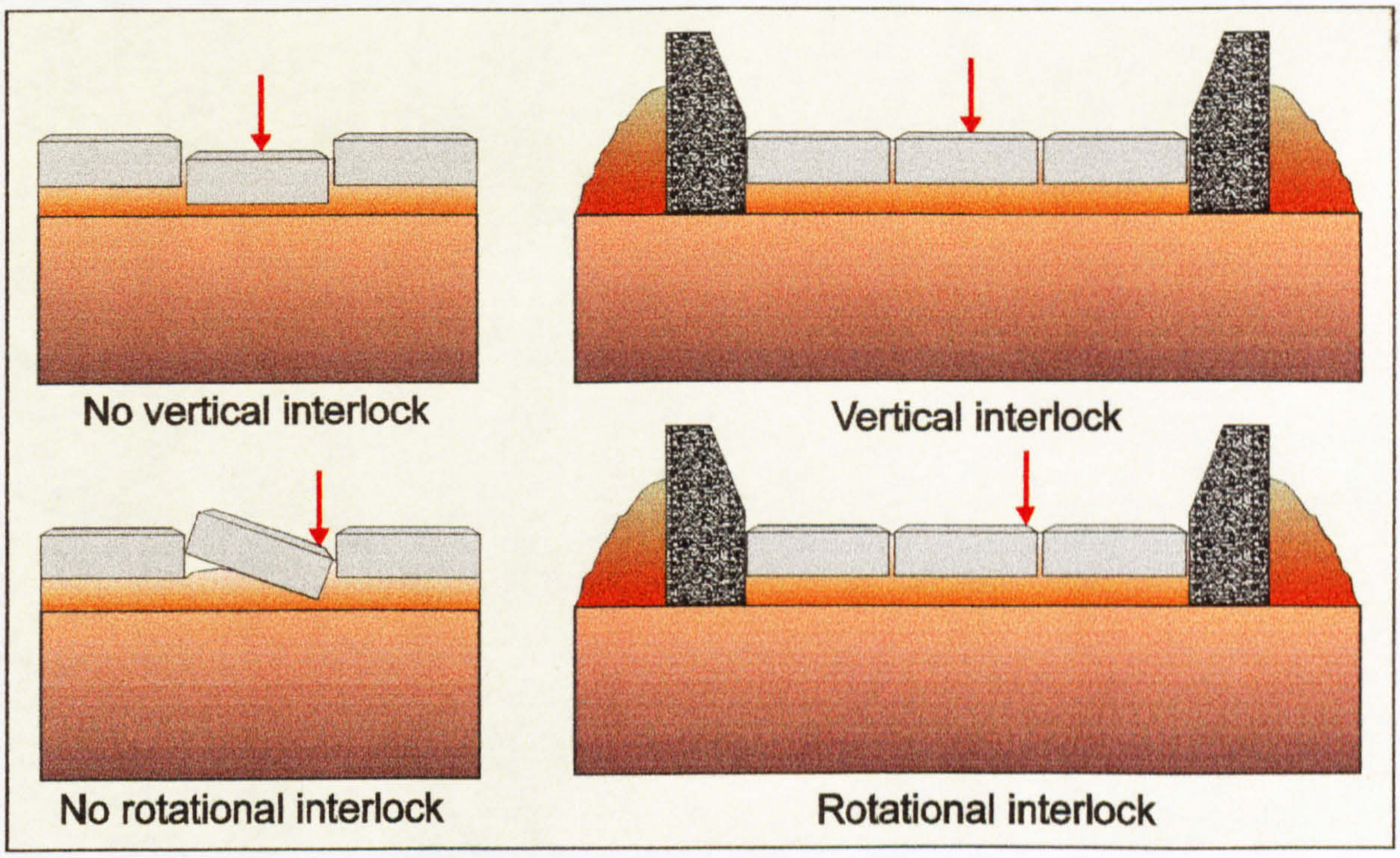

Figure 1.3. Interlock in pavers.

Figure 1.3 illustrates how rotational interlock is achieved by providing edge restraint and how vertical interlock is provided by the joint filling material. These concepts and definitions were first postulated by Knapton[8].

Interlock is developed during the installation of the pavers. The paving is commonly agitated by a vibrating plate compactor, the effect being to cause the laying course material to flow into the open joints and to be compacted, thus providing conditions in which full interlock can develop. The functions of the laying course are twofold: to fill any irregularities in the surface upon which the material is to be laid, and to bed the paving blocks and filling of the joints so that interlock may develop.

The effect of the applied loading is to tend to cause the block to move laterally, in the direction of the applied load and to rotate, owing to the eccentricity of the load. Rotation is resisted by the interlock. Rotational interlock is sufficient to prevent block rotation in all but the most severe circumstances. It has been found that in certain applications - for

example where lateral forces are large, frequently repeated and always in the same sense and at the same positions- even the deepest block with the best resistance to rotation is to a limited degree liable to be moved but the general experience in all but the most difficult applications is that the surface of the pavement will remain stable.

Lateral movement of blocks is resisted partly by the frictional forces which develop between block and laying course. However these alone are often incapable of preventing total movement and so the designer seeks to prevent the movement of individual blocks by laying them to a pattern or bond so that no block may move in isolation and so that no lines of weakness exist in the surface.

If a single isolated paving block subjected to a vertical patch load is considered with uniform support conditions in its bedding sand, the applied force is distributed over the lower face of the block, causing the sand below the block to become compacted and particularly if the load is repeated a number of times in same place and the sand initially is uncompacted, this tends to cause the underlying sand to flow from beneath the block to less highly stressed adjoining areas. If there is a lack of symmetry in the loading or support conditions there will be a corresponding lack of symmetry in the resulting movement of the block. Its downward movement will be associated with rotation and with the compaction of the laying course beneath and on one or more sides of the block. Frictional forces on the sides of the block are created which tend to resist vertical movement. In order to resist the deformation one ensures that the sand in the laying course is well compacted before traffic is admitted to the surface of the pavement.

Each of these three types of interlock is now considered in detail.

1.4.1.1.1 Vertical interlock[1] (see Figure 1.3.)

Once a vertical load is applied to an individual paver without vertical interlock, that paver can slide down vertically between its neighbours. Vertical interlock is achieved by vibrating the pavers into a well graded sharp sand during construction. This induces the sand particles to rise 25 mm into the pavers' gaps which are from zero to 6 mm. These well graded sands in pavers' gaps include particle of size from almost zero to 6 mm. Therefore, this circumstance allows a vertically loaded paver to transfer its load to its neighbours through shear.

1.4.1.1.2 Rotational interlock[1] (see Figure 1.3.)

If a vertical load were applied to a paver asymmetrically, that paver would rotate laterally toward the direction of applied load . Therefore, if the neighbouring pavers are prevented from moving laterally by edge restraint, an individual paver is prevented from rotating and rotational interlock is achieved. If sand is brushed into the surface, this can help to cause rotational interlock. Knapton and Barber[1] suggested that maximum particle size of 3 mm sand should be used for this purpose.

1.4.1.1.3 Horizontal interlock[1]

According to Knapton and Barber[1], particularly when rectangular blocks were laid in stretcher bond pattern with their longer axis transverse to the principal direction of traffic, horizontal braking and accelerating forces move pavers along the line of the road and eventually the pavers break as the corners of one row of blocks transmit high local tensile stress into the next row. This circumstance may be removed by using a shaped block or by using a rectangular block laid in a herringbone pattern. It has been said by Knapton and Barber[1] that although creep cannot be totally eliminated at severe braking locations, its

effect can be reduced to a level whereby breakage is eliminated and there is no visual consequence.

1.4.1.1.4 The effect of interlock in stress dissipation[1]

In 1976, a test area comprising a 2 m x 2 m concrete paver pavement was constructed over a group of 24 pressure measuring cells in order to quantify the effect of interlock in dissipating applied load. A static vertical load of 50 kN was applied to the surface of a series of 8 pavements which had six different paver shapes (see Figure 1.4.) and the stress at the bottom of a 50 mm layer of sand was measured by means of recording the pressure cells' data. Figure 1.5. shows the recorded vertical stress expressed as a percentage of the applied surface pressure. As can be seen in Figure 1.5, as load increased, the measured percentage of the applied load decreased, reducing to 60%. This implies that the greater the applied stress the greater the load spreading ability of the pavers. It was found that the load spreading ability of a paver pavement was substantially independent of paver shape, block thickness and bond pattern.

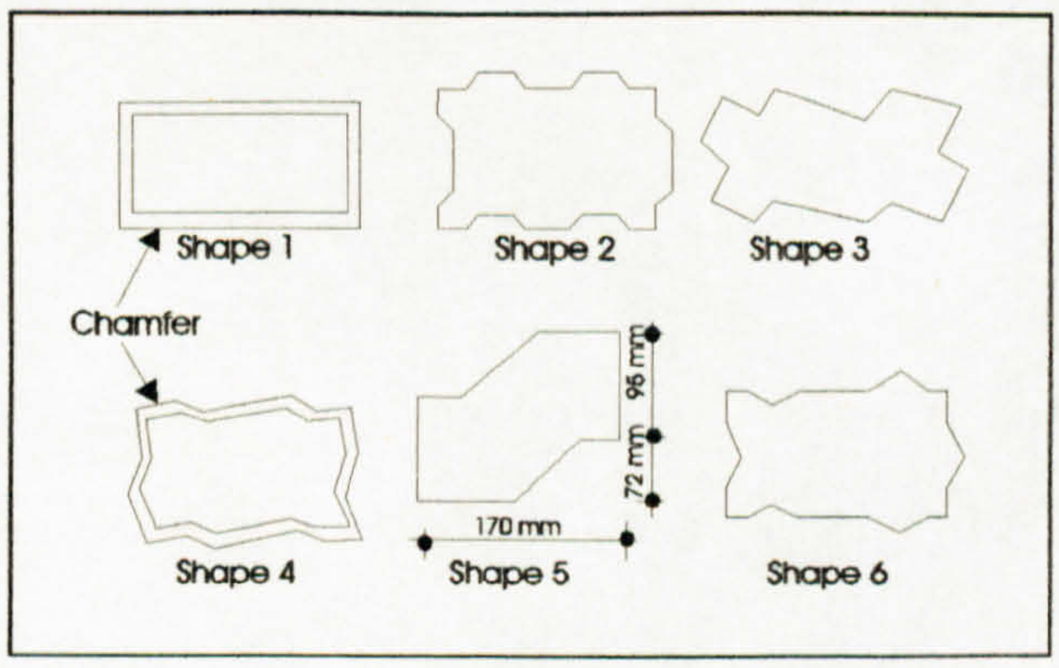

Figure 1.4: The six different paver shapes tested.

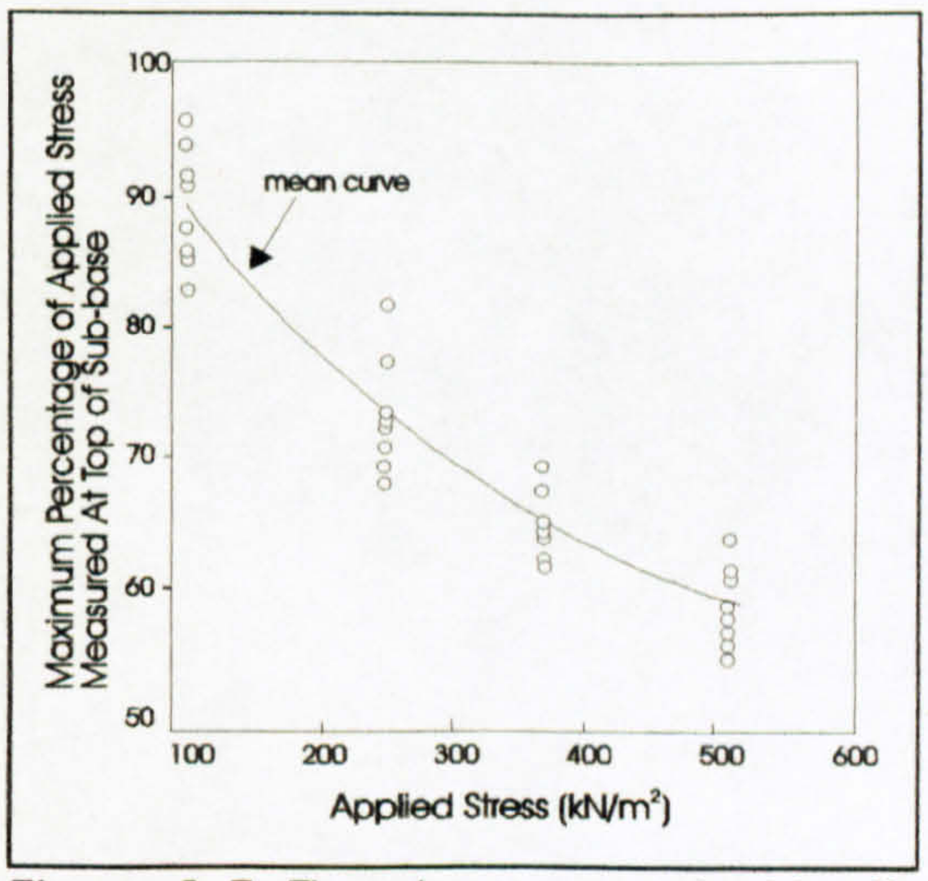

Figure 1.5: The stress recorded by the pressure cells.

It was inferred by means of comparing the load dissipating ability of concrete pavers with that of a conventional flexible pavement, that 80 mm pavers over 50 mm sand is equivalent to 160 mm of bituminous material. Interlock allows a concrete paver pavement to be considered as a flexible pavement.

The principal UK paver pavement design guide, BS7533:1992[9] uses conventional flexible pavement design technology with a one to one equivalence factor between pavers and asphalt, i.e. 100mm thickness of bedding sand and pavers is equivalent structurally with 100 mm asphalt. This assumption is supported by observations of the performance of pavers on trafficked areas[10].

1.4.2. The Structure

The purpose of the pavement structure component is to distribute traffic loads so that the stresses and strains developed by them in the subgrade and the sub-base are within the capacity of the materials in these layers.

The roadbase material comprises lean concrete, dense tarmacadam, dense bitumen macadam, rolled asphalt, wet-mix macadam, dry-bound macadam, soil-cement or cement-bound granular material. The sub-base is also a load-distributing layer but is of weaker material than the roadbase. The sub-base, in addition to reducing the stresses and strains developed in the subgrade, may help to protect it from frost action. It also provides a suitable working platform on which to construction the upper layers of the pavement. The load-distributing capacity of individual layers is a function of both their thickness and the mechanical stiffness of the materials in them.

For a conventional heavily trafficked pavement, the thickness of roadbase subjected to a high number of standard axles was determined by Knapton and Barber[1] using the conclusions from the initial research by the Cement and Concrete Association[11]. It was assumed that 80 mm pavers plus 50 mm sand was equivalent to 160 mm rolled asphalt, 225

mm lean concrete or 170 mm dense macadam. It was possible to deduct these thicknesses from the total thickness of surfacing plus roadbase specified in Road Note 29[12] to obtain the residual thickness of roadbase required underneath the sand. The resulting roadbase thickness is shown in Figure 1.6. As for residential roads, the sub-base was obtained from Figure 6 of Road Note 29[12]. Cross-falls to drainage channels of 1:40 and longitudinal falls to drainage channels of 1:180 were suggested. 80 mm paver thickness was recommended[1].

A significant experiment concerned with the use of heavy vehicles on a concrete paver pavement was reported in the Proceedings of the Institution of Civil Engineers[13]. A pavement consisting of a poorly graded sand sub-base, a 50 mm sand laying course and 80 mm pavers was constructed over a subgrade with a CBR of 3%-5%. The pavement was trafficked by heavy commercial vehicles in an industrial yard and despite the poor quality of the underlying layers, the pavement performed well. Where the pavement was constructed over a soft spot, a deformation of 100 mm took place rapidly. It was assumed that no structural failure was obtained although this pavement was underdesigned and although a localised serviceability failure took place.

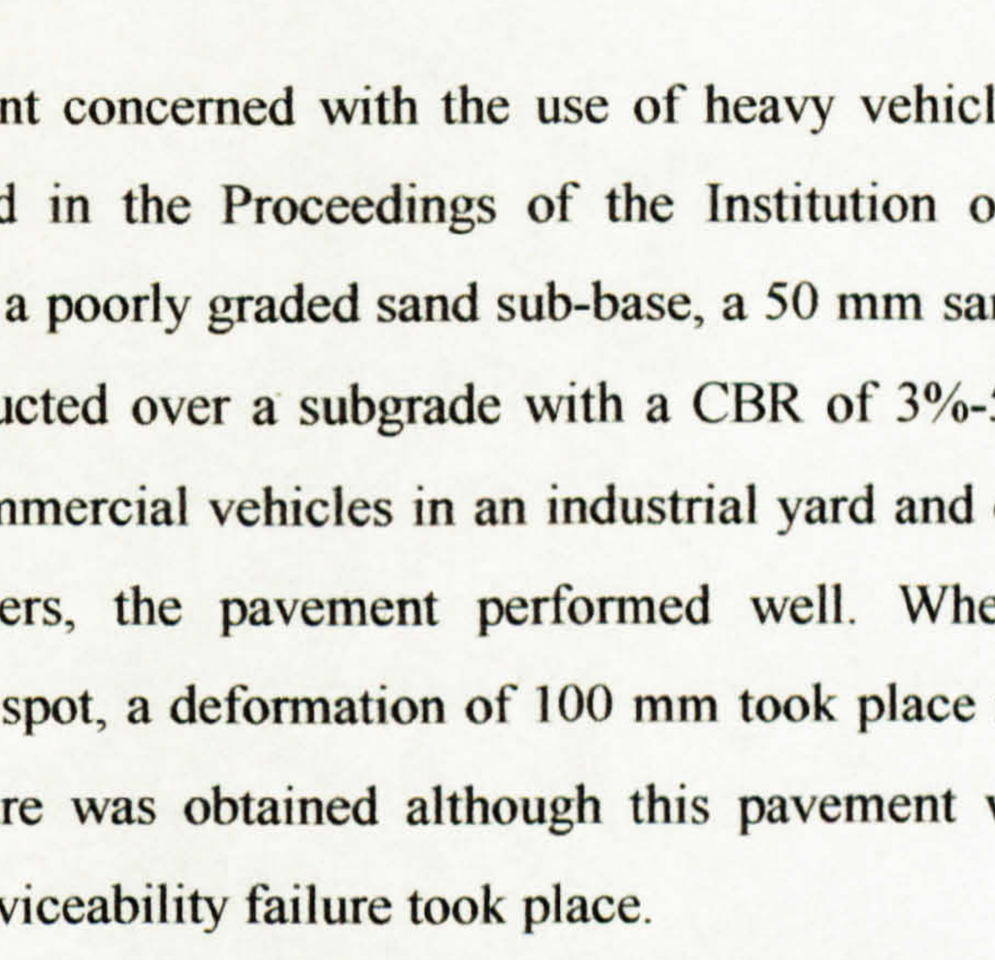

Figure 1.6: Roadbase thicknesses required beneath pavers for pavements carrying up to 80 million standard axle loads[1].

1.4.3. The Foundation

The purpose of the sub-base beneath a flexibly bedded concrete paver pavement is to form a surface which will enable the pavement to be constructed without damage to the subgrade or its protective seal and it provides a smooth and even interface between the pavement and its substrate at low cost. In addition, it improves the uniformity of the support given to the pavement and it contributes to the structural strength of the pavement.

Sub-base materials must be hard, durable, chemically inert and frost resistant. They must be suitably graded so that they are capable of being compacted to a high density and, when in this condition, they must not be susceptible to shrinkage, swelling or loss of stability resulting from changes in moisture content. The sub-base materials may consist of granular materials, stabilised soils or lean concrete. The range of materials includes naturally occurring gravel, crushed stone or concrete, industrial waste materials such as hard clinker, burnt colliery shale, spent oil shale and crushed slag.

The surface of sub-bases should be as regular as possible, in order to produce the interlock and friction between the underside of the pavement and the top of the sub-base and so to promote easier temperature movement and stress relief in the pavement.

The required thickness of sub-base is determined from the cumulative number of standard axles to be carried and the California Bearing Ratio (CBR) of subgrade (see 1.4.4).The thickness of subgrade improvement layer (Capping layer) can be determined in terms of the subgrade CBR values. If the value of CBR is 2% to 5%, the designer can choose the thickness of subgrade improvement layer, this allowance depends on the discretion of the engineer. It is dependent on how, when and where the CBR was measured, the knowledge of behavior of subgrade soil, and the extent of subgrade improvement layer and sub-base, how often it will be trafficked, closeness of subgrade drainage, and the likely construction time. According to BS 7533:1992[9], if the CBR of the subgrade is more than 5%, subgrade improvement layer (Capping layer) materials are not required.

During construction of industrial, commercial and housing projects, the sub-base layer in carriageway construction is often used as a site access road. It is therefore essential to provide an adequate thickness of sub-base with a suitable specification. LR 1132[14]-The Structural Design of Bituminous Roads-shows that soils can have lower Californian Bearing Ratio (CBR) values during construction than when measured in-situ. This is because drainage may be poor and the soil is disturbed by trafficking. Many clay soils in the UK exhibit CBR values of 1 to 2% during construction. In such circumstances LR 1132[14] recommends the use of a 600mm capping layer with a minimum 150mm thickness of DTp Type 1 granular sub-base material. If less is provided, contamination, initially of the capping layer, and loosening of the sub-base material can occur during site operations. The use of geotextile materials at the subgrade/capping layer interface can cure the problem of contamination from below but, even with a geotextile, the LR 1132[14] thicknesses of material are still required. If the subgrade and/or sub-base become overstressed during construction, a permanent loss of strength can occur leading to poor performance of the finished pavement. Cement or lime stabilisation is often used for the capping layer material to provide a firm foundation for the 150mm thickness of sub-base material. Geotextiles should not be considered to provide any enhancement of strength to the pavement construction.

1.4.4. The Subgrade

Pavement thickness is a function of the cumulative number of standard axles to be carried during the design life and the strength of the subgrade is also a principal factor in determining the thickness of the pavement. The strength of subgrade is assessed on the California Bearing Ratio (CBR) scale. In the UK the CBR test is used almost exclusively by engineers for soil strength classification, although the Plate Load Test is used in some countries. Details of the CBR test are now documented as follow[15]:

This test has been carried out by California State Highway Department since 1929. This method is carried out to determine the relationship between force and penetration when

the force is applied to a cylindrical plunger of cross-sectional area 1935 mm^2. The value of penetration and the ratio of force which is defined as a standard force are expressed as a percentage of the California Bearing Ratio (CBR). The test is more applicable in tropical and subtropical areas where there are drier conditions under roads and airfields.

In order to apply this test the following apparatus as described in BS 1377 : Part 4 : Page 21:1990[15] is required: 5 mm and 20 mm BS test sieves, a cylindrical metal mould, three metal plugs described in the same reference, a cylindrical metal plunger having a cross-sectional area of 1935 mm^2, a machine for applying the test force through the plunger, apparatus for measuring the penetration, three annular surcharge discs, two different metal rammers, a compression machine for static compaction, an electric vibrating hammer, a steel rod, a steel straightedge, a spatula, a means of measuring the movement of the top of the specimen during soaking, a balance capable of weighing up to 25 kg readable and accurate to 5 g, an apparatus for moisture content determination, filter papers.

The test is applied on material which passes the 20 mm BS test sieve. If the soil contains particles larger than this the fraction retained on the 20 mm test sieve is removed and weighed before preparing the test sample. If this fraction is greater than 25%, the test cannot be applied. The maximum particle specimen size does not exceed 20 mm. The test conditions are described in BS 1377:Part 4: Page 20[15]. Thorough mixed soil is kept for 24 h before compaction. One of the alternative compaction methods can be used. There are two main compaction methods: Static and Dynamic compaction. These methods comprise different alternative application methods.

Static compaction : *For compaction of the mass of wet soil to appropriate dry density, the requiring mass of wet soil is calculated from the equation:*

$$m_1 = \frac{V_m}{100}(100 + w)P_d$$

Where :

m_1 is *the mass of soil (in g)*

V_m is *the volume of the CBR mould (in* cm^3)

w is the moisture content of soil (in %)

P_d *is the specified dry density (in* Mg / m^3)

For air voids specification the following equation is used:

$$P_d = \frac{1 - \frac{V_a}{100}}{\frac{1}{P_s} + \frac{w}{100\,P_w}}$$

Where:

P_d *(in* $Mg \cdot m^3$*) is the dry density*

V_a *(in %) is the air voids expressed as a percentage of the total volume of soil*

P_s *is the particle density (in* $Mg \cdot m^3$)

w is the soil moisture content (in %)

P_w *is the density of water (in* Mg / m^3)

Method 1 : *The mould is taken with its collar and baseplate, and is covered by a filter paper. The weighed soil is poured slowly into the mould, while being tapped constantly by the steel rod. The tapping is continued until the level of soil reaches the level (about 5 mm to 10 mm) above the top of the mould. After tapping , a filter paper is placed on the top of the soil followed by a 50 mm thick plug and the specimen is compressed in the compression testing machine until the top of the plug is even with the top of the collar. The load is applied constant for at least 30 s and then released. After compaction the plug and filter paper is removed with the collar. If the specimen is not tested immediately the top plate of the mould is screwed to prevent evaporation. Where the air content is less than 5% in the compacted soil, the sample is allowed to stand for 24 h before testing.*

Method 2 : *The mould is taken as in Method 1. The wet soil is split into three equal parts, and each sealed in a container to prevent loss of moisture. One third of the soil is poured into the mould. The three plugs is then fitted , with handles removed, and the soil is compressed using the compression machine until the thickness of the soil, after removal of the load, is one third of the depth of the mould. The second and third layers is added in a similar manner to the first. In this last stage one plug only is used and it is pushed in*

until the top surface is even with the top of the collar. Storage and curing of the spacimen is as in method 1.

Dynamic compaction : *Three methods can be used for dynamic compaction. The first two are used where the required density can be obtained by a process of dynamic or vibrational compaction. The third is used where a given amount of compactive effort is to be applied to the soil as in the standard compaction test.*

Method 1 : *The mould is taken with its baseplate and is weighed to the nearest 5 g (m2). The collar is then fitted and a filter paper placed in the bottom. The dry density of the mass of wet soil is prepared as for the static compaction. This quantity is divided into five equal parts and sealed in a container to prevent loss of moisture by evaporation. The soil is then compacted into the mould with the collar which is attached in five equal layers using either the BS 2.5 kg rammer or 4.5 kg rammer. Each layer is given evenly distributed blows over the surface to ensure that the layer after compaction occupies one fifth of the height of the mould. The final level of the soil is just above the top of the mould. The collar is then removed and the soil trimmed evenly with the top of the mould using a steel straightedge. The mass of the mould with baseplate attached and containing the sample is then measured to the nearest 5 g (m3).*

Method 2 : *The mould and the wet soil is prepared exactly as in Method 2 for static compaction. One third of the wet soil is poured into the mould and compacted by a vibrating hammer. Vibrational compaction is applied until the thickness of the layer is equal to one third of the depth of the mould. The second and third layers are added and compacted in the same manner so that the final surface of the soil is level with the top of the mould. The mould with baseplate is then weighed (m3).*

Method 3: *The mould with its baseplate is prepared and weighed as in Method 1. The collar is then fitted and a filter paper placed in the bottom. About 6 kg of the soil at the required moisture content is prepared. Two levels of compaction can be used ; the first is*

the BS 2.5 kg rammer and the second the BS 4.5 kg rammer. Enough soil is placed in the mould using the light rammer with the collar attached. Two further layers are added and compacted in the same manner so that the final level is less than 6 mm above the top of the mould. The collar is then removed and any excess soil trimmed evenly with the top of the mould using a steel straightedge. The mould with baseplate is then weighed (m3).

Soaking procedure: *Soaking of CBR test samples is not normally used in the UK, but in certain cases it may be used. It can be carried out as given below. After compaction the baseplate is replaced. The collar is fitted to the other end of the mould and the thread packed with petroleum jelly. The specimen is then placed in a bath of water and the water level kept just below the top of the collar. Surcharge masses as required are then placed on the specimen. The time taken for the water to reach the top of the specimen is observed. Unless this happens within 3 days, the top of the specimen is flooded and the specimen left to complete its normal soaking period. The normal soaking period is 4 days. When soaking is complete, the sample is removed from the bath and allowed to drain for 15 min. The baseplate is replaced, the collar and perforated plates are removed and the specimen is then weighed to the nearest 5 g (m4).*

Test procedure : *The mould , containing the sample, with the baseplate in position, but the top face uncovered, should be placed on the lower platen of the testing machine. Surcharge masses as required are placed on the specimen. The plunger is seated under a force of 50 N for a bearing ratio of up to 30 % or 250 N for bearing ratio above 30 %, and is made to penetrate the specimen at a uniform rate of value mm/min. The baseplate is removed from the lower end of the mould, and fixed on the upper end, and the mould and contents are then inverted. The testing procedure described above is repeated on the other end of the specimen. After the penetration tests have been completed, samples of the soil each of about 350 g are taken from immediately below the penetrated surface of the two ends of the specimen and the moisture contents determined. Filling material used in the end first tested is not included in the moisture content sample.*

Calculations : *A graph indicating force on the plunger against penetration is drawn on the graph. The points are drawn through and a smooth curve is found. The curve is normally convex upwards. If the initial portion is concave upwards, correction is necessary. In this case a tangent is drawn at the point of greatest slope and is extended to cut the penetration axis. The curve is then shifted to the left so that the point of intersection of the tangent with the penetration axis coincides with the origin. This gives the corrected curve for CBR values.*

The standard force penetration curve corresponding to 100 % CBR. value for given penetration is defined as the force (read from the smoothed curve) required to cause a given penetration expressed as a percentage of the force required to cause the same penetration on the standard curve. The CBR value is calculated at penetrations of 2.5 mm and 5 mm, and the higher value taken.

For calculations of dry density of unsoaked specimens, the bulk density (ρ in Mg/m^3) of the specimen is calculated. For statically-compacted or vibatory specimens this is done from the equation.

$$P = \frac{m_1}{2305}$$

For dynamically-compacted specimens this is done from the equation.

$$P = \frac{(m_3 - m_2)}{2305}$$

The dry density, p_d in Mg/m^3, of the specimen is calculated from the equation.

$$P_d = \frac{100P}{100 + w}$$

w is the moisture content of the soil (%).

During the service life of the pavement, saturated subgrade may occur and should be taken into account in design and the CBR method should include the soaking procedure. Alternatively equilibrium suction index CBR values may be used when it is clear that saturated condition will never occur. For fine grained soils, the equilibrium suction index CBR can be determined from the plasticity index (PI) as shown in Table 1.1.

Effective subgrade drainage is need to maintain long-term CBR values at the equilibrium suction index value. The CBR values measured in the test must be truly representative of those obtaining throughout the site. In this case the lowest recorded values should be used, or for the places on which lower values are recorded, appropriate designs should be provided for different parts of the site. In addition soft spots which have given lower CBR values may be removed so that those unrepresentative CBR result would be ignored. The strength of soil is a function of its moisture content. The in-service strength may be much lower than the recorded CBR values. In the interpretation of investigation data, this situation must be taken into account since CBR values may have been obtained as a high figure e.g. in summer because of dryness of soil. More detail is provided in BS 6717:part 3[16] or BS 6677: part 3[17].

It can be concluded that although the procedure of the CBR test is very complex to prepare for most design situations, the test has a worldwide applicability to assess the strength of the subgrade which is principal factor in determining the thickness of the pavement. In UK practice, usually the Atterberg limits are measured instead of CBR for clay and other fine grained soils, because determining the Atterberg is much more convenient than determining CBR directly and more importantly, the Plasticity Index (PI) values allows the engineer to determine not just the CBR of the soil as tested but a design CBR which takes into account how the soil will be treated, or mistreated during construction (see Table 1.1). The two Atterberg Limits are Liquid Limit (LL) and the Plastic Limit (PL). Each of these limits is a moisture content: LL is the moisture content at which a soil passes from the plastic to the liquid state and PL is the moisture content at which a soil becomes too dry to be in a plastic condition. Each of these moisture contents is determined by a simple test set

in BS 1377:1990[18] "Methods of Test for Soils for Civil Engineering Purposes". Once these values are found for a soil, the value of the PI is subtracted from the value of the LL to obtain the Plasticity Index (PI). Then PI can be used to assess the CBR of the soil as shown in Table 1.1.

Table 1. Equilibrium suction index CBR values

Type of soil	Plasticity Index	High water table			Low water table		
		Construction conditions			Construction conditions		
		Poor	Average	Good	Poor	Average	Good
Heavy clay	70	1.5 to 2	2	2	1.5 to 2	2	2 to 2.5
	60	1.5 to 2	2	2 to 2.5	1.5 to 2	2	2 to 2.5
	50	1.5 to 2	2 to 2.5	2 to 2.5	2	2 to 2.5	2 to 2.5
	40	2 to 2.5	2.5 to 3	2.5 to 3	2.5	3	3 to 3.5
Silty clay Sandy clay	30	2.5 to 3.5	3 to 4	3.5 to 5	3 to 3.5	4	4 to 6
	20	2.5 to 4	4 to 5	4.5 to 7	3 to 4	5 to 6	6 to 8
	10	1.5 to 3.5	3 to 6	3.5 to 7	2.5 to 4	4.5 to 7	7 to > 8
Silt	-	1 1	1 2	2 1	1 2	2 2	2 2
Sand(poorly graded)	-	← 20 →					
Sand(well graded)	-	← 40 →					
Sandy gravel (well graded)	-	← 60 →					

Note 1: This table indicates reasonable estimates of equilibrium values of CBR for combinations of poor, average and good construction conditions with high and low water tables. Good conditions pertain where the subgrade is protected promptly with a subgrade improvement layer or sub-base and the site is well drained with adequate falls. This results in subgrades never getting wetter than their equilibrium moisture contents beneath the finished road. Poor conditions pertain where there is little or no subgrade protection and rainfall occurs on a poorly drained site so that the soil is fully wetted.
Note 2: A high water table is one 300 mm or less below formation level and is consistent with ineffective sub-soil drainage. A low water table is 1 m or more below formation level.

Table 1.1: Equilibrium section index CBR values.

Experience has shown that on wet cohesive soils commonly found in Britain, CBR values are very low and values usually range between 2% and 7%. Here lies one of the problems inherent in using CBR values for most UK design situations. For most design situations it can have one of only five values viz: 2%, 3%, 4%, 5%, or 7% or more, beyond which the ground is so strong that a nominal sub-base or foundation layer is required and the road section design is based entirely upon the amount of traffic. If the CBR of the subgrade is less than 2%, then the ground needs to be improved in some way before the road is built.

The three construction conditions shown in Table 1.1 refer to the effectiveness of site surface drainage during construction. For example, poor construction conditions apply

when no subgrade drainage is introduced so that the soil can become fully wetted during rain. Good construction conditions apply when the subgrade is protected by the construction of the pavement as soon as the subgrade is exposed so that it is never wetted. PI actually helps the paver pavement designer who may not be able to predict site conditions during the design process. In such a case, the design could be based upon average construction conditions. This will often result in the provision of a 300mm thick capping layer beneath a 150mm thick sub-base. Should the site conditions differ from the average assumption, then either the 300mm capping material can be eliminated, or an additional 300mm capping is added. In this way, the decision on how much subgrade protection to introduce is left to the contractor who can make a judgment based upon all technical and commercial issues applying at the time. Since the overall serviceability of the paver pavement is strongly dependent upon the characteristics of the subgrade soil, an error of assessment of CBR at subgrade can result in significant problems and an inappropriate design can be expensive to rectify. It is recommended that the most appropriate approach to provide a measure of the subgrade is to determine the Plasticity Index and then adopt the design philosophy of LR1132 Appendix C[14].

1.5. The modes of failure in paver pavements

Replacing a failed concrete paver pavement can be a very costly operation, especially when the pavement fails for no apparent reason although it has been properly designed and constructed. Some appreciable vertical movement or partial individual paver disorientation or deterioration does take place owing to external or internal force applied to the block paving itself (such as partial failure of the subgrade or disregarded maximum stress functions cause bedding sand failures can occur beneath the wearing course) cannot be tolerated in some cases by the paver paving which will disengage its integrity and will not keep the mechanism in physical balance. It may be that such a deformation will render the pavement unable to satisfy the requirements of traffic for the reasonably stable surface. This structural deterioration can be prevented considering the maximum stress values

which is described in Chapters 6 and 9. For full interlock, the jointing materials must successfully transfer maximum shear stress without any failure.

The types of paver pavement failure can be defined by taking a very broad view:

- The failure below the surface
- The failure of the surface

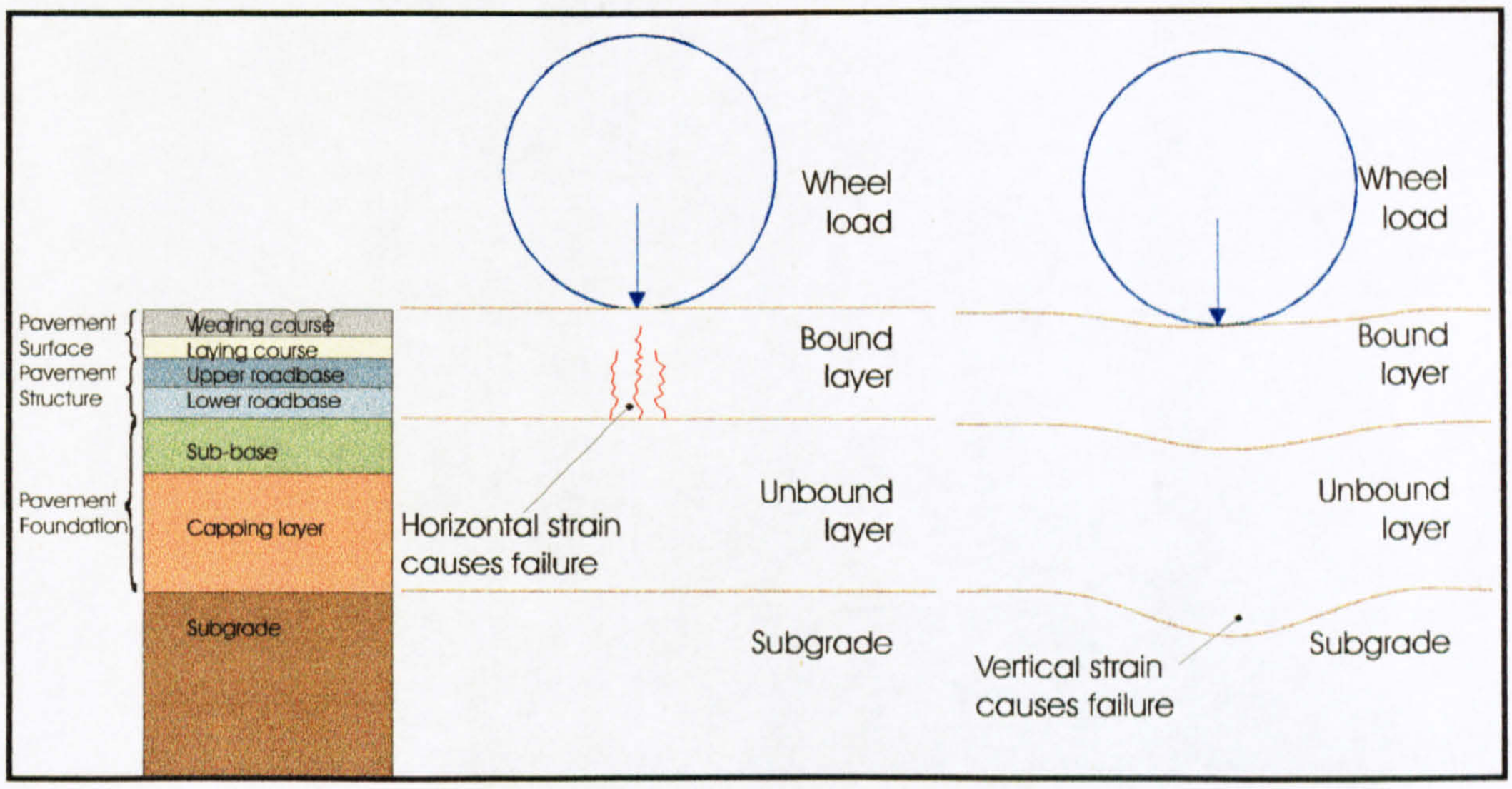

Figure 1.7: Examples of failure modes.

Figure 1.7 shows a flexible paver pavement whose structure is simplified to one bound and one unbound layer and which is subjected to a vertical wheel load. The modes of failure illustrated are horizontal strain at the bottom of the bound layer, causing the upward propagation of vertical cracks through the layer; and vertical strain at the top of the subgrade, causing consequent deformation in the bound and unbound layers and possibly leading to deformation at the surface. Tensile failure at the bottom of the bound layer may be avoided either by the provision of sufficient thickness of bound material to contain horizontal stresses within acceptable limits for a given material, or by providing a material

of sufficient strength to resist the stresses which will arise in a bound layer of sufficient thickness.

The thickness, the grading and the angularity of the bedding sand have been shown to be crucial to the behaviour of block pavements under traffic. Several[19, 20, 21] investigations on the influence of bedding sand on paver pavement failure concluded that particularly fine crushed rock sand grains in the bedding sand were breaking down under a large number of repeated loads with the result that a high percentage of the sand grains became as fine as silt which was then squeezed upwards as a paste through paver joints and fine crushed rock material appears to perform less well than naturally occurring silica sands. Knapton[20] reported that fine crushed rock often suffers from two inherent weaknesses. Firstly, grains of size 1mm or less are usually very angular such that very small pieces (less than 50 microns) easily become detached. These small pieces are easily transported by moisture and can form a lubricating slurry. Secondly, fine crushed rock usually contains a proportion of very fine material from the start and this also can form a lubricating slurry. In extreme cases there can be such a high proportion of this very fine material that the sand becomes effectively solid and prevents the free flow of water. The performance characteristics of different sands were assessed using micrographs to distinguish between suitable and unsuitable sands.

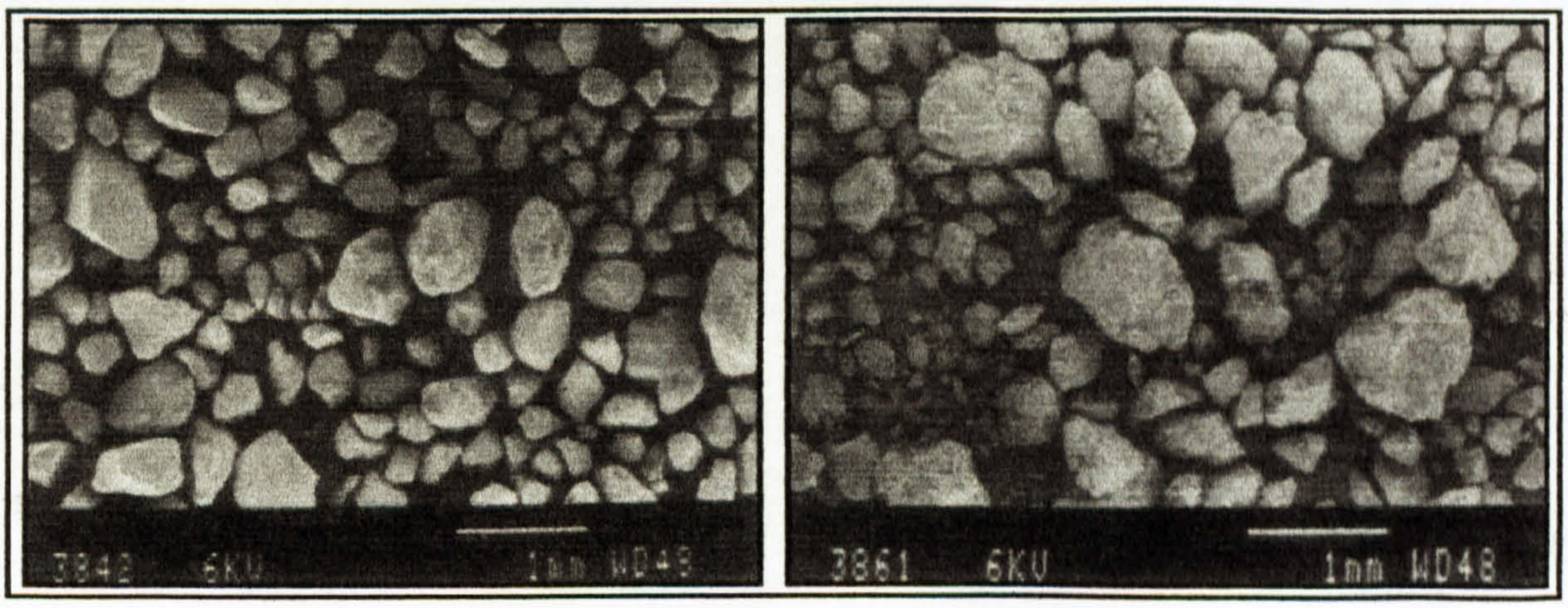

Figure 1.8: Micrographes of the naturally occurring sand and fine crushed rock sand.

Micrographes of two sands are shown in Figure 1.8. It was reported that the first sand (3842) in Figure 1.8 the naturally occurring sand was suitable for heavily trafficked paver pavements and the second sand (3861) in Figure 1.8 fine crushed rock was found to perform poorly in practice. Because this material has not been subjected to natural weathering small protrusions on each particle may become dislodged under channelised traffic.

The photograph shows many such loose grains of diameter less than 100 microns. It is these grains which form a lubricating paste and lead to loss of bedding sand strength. The principal sources of naturally occurring sands are the quaternary alluvium deposits, which were deposited in relatively recent times and have not been compacted to form solid rock. For this reason the individual grains of sand have retained their structure and are rounded with a smooth and natural glassy surface. Their intact structure and their smoothed spherical surface means that the grains do not abrade each other and break down into smaller particles, but remain intact, thereby maintaining a stable sand bedding course. Knapton and Cook[21] also categorised the sands in UK. This categorisation can be seen in Figure 1.9. The Geological Survey Ten Mile Map of the UK illustrates the nature of river alluvial deposits. Typically they exist in narrow bands, usually less than 1km wide, in either present or former river valleys (see Figure 1.9). Alluvial deposits were formed in recent geological time and individual particles of sand have not been cemented together to form solid rock. For this reason the grains of sand have a smooth and natural glassy surface. Categorisation is based on how much of a particular sand passed the 600 micron and 75 micron aperture sieves. These sizes were selected to eliminate single size materials and to place controls on the percentage of 'fines'. Essentially the less the percent passing the two designated sieve sizes, the better is the sand suited to heavy duty applications (see Figure 1.9).

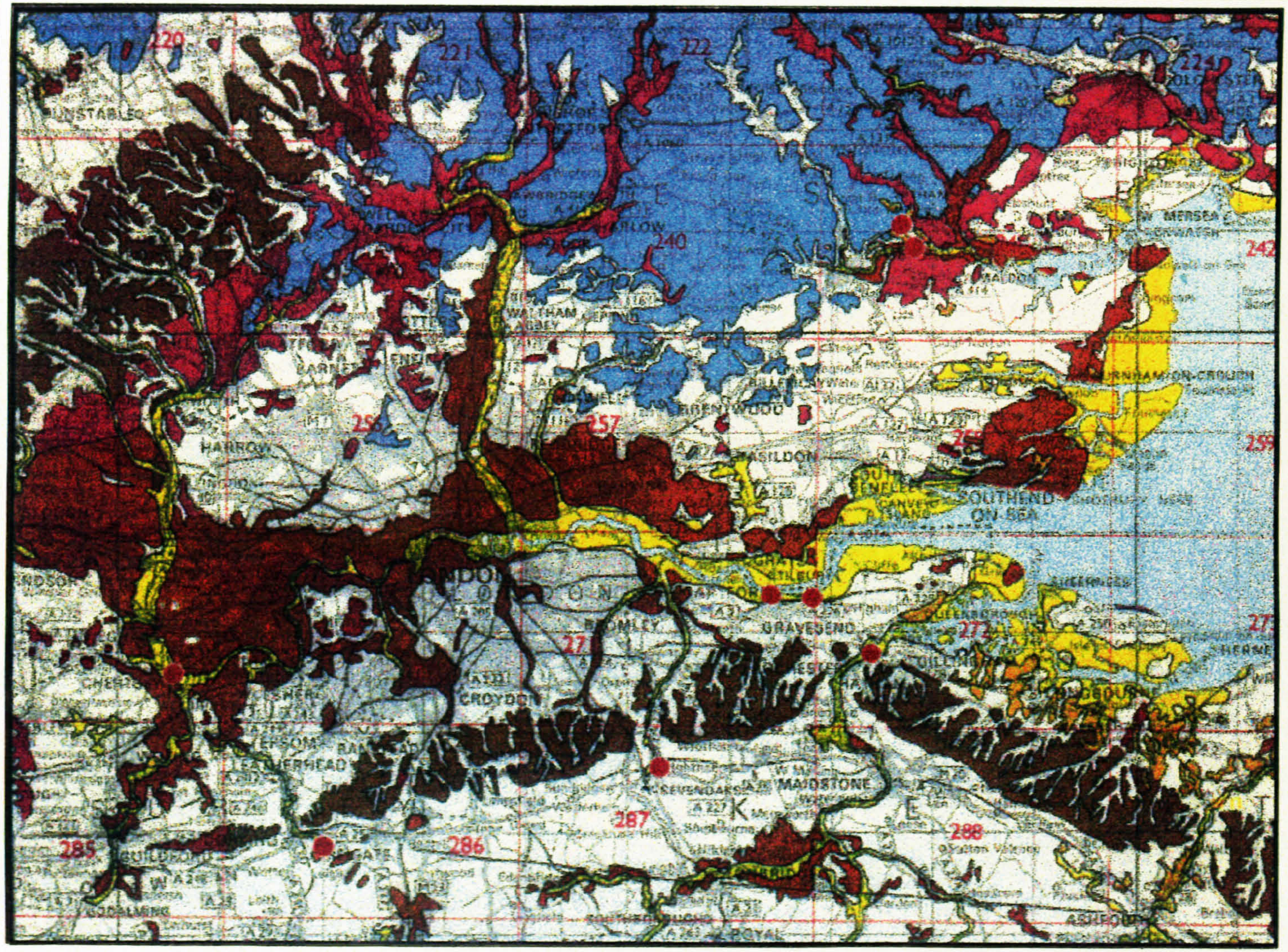

SAND CATEGORIES

Catgory	Application
1	Pavements receiving severely channelised traffic Industrial pavements Bus stations Loading bays
2	Adopted highways Petrol stations forecourts Pedestrianisation projects receiving regular heavy trafficking Car parks receiving occasional heavy vehicles Aircraft pavements
3	Pedestrianisation projects receiving occasional heavy trafficking Car parks receiving no heavy vehicles Private driveways Public areas receiving pedestrian traffic only Footpaths likely to be overridden by vehicular traffic
4	Footpaths not likely to be overridden by vehicular traffic Private areas receiving pedestrian traffic only

- Alluvium
- River Terrace Deposits (mainly sand and gravel)
- Raised Beach and Marine Deposits
- Glacial Sand and Gravel
- Boulder Clay and Morainic Drift
- Sand and Gravel of uncertain age or origin
- Clay-with-flints
- Brickearth, mainly loess
- Crag
- Sand Source

Category	% of sand passing 75 micron sieve	% of sand passing 600 micron sieve
1	Less than 0.1%	Less than 60%
2	0.1% to 1.0%	Less than 60%
3	1.0% to 3.0%	Less than 70%
4	3.0% and above	Less than 70%

Figure 1.9.

1.6. Conclusion

This Chapter outlined the principals upon which the remainder of this Thesis is based. The observed interlocking behaviour and typical bedding sand failures of paver pavements were propounded. One of the major conclusions of this Thesis is that the pattern of stress development in paver bedding sand is complex and depends upon the size, shape, orientation and speed of the load as well as paver geometry and laying pattern. Many of the hitherto unexplained bedding sand failures can be understood by examining the way in which local vertical stress transients develop and travel through bedding sand. The bedding sand failures can be prevented considering the maximum stress values which are developed in Chapters 4, 5, 6, 7, 8 and 9. For the full interlock, the joint materials must successfully transfer maximum shear stresses without any failure. The performance to date of paver paving in providing a durable low maintenance surface for traffic has resulted in wide acceptance. Paver paving provides the designer and specifier with more options for constructing safe and environmentally acceptable pavements than most alternative forms of construction. Accordingly, the use of segmental paving to satisfy the requirements of safety and the environment is likely to increase as the designer becomes more familiar with these advantages. The inherent structural benefit associated with well fitting small element pavement surfacing systems has been recognized and is now used commonly in pavement constructions. This development of flexible small element paving constructions has brought about the need for fully understanding the complex mechanical behaviour of segmental paving system. This Thesis seeks to define the state of the art and to explore more fully the true behaviour of paver systems in order to explain the observed behaviour.

References

1 Knapton J. and Barber S.D., (1980), *UK Research into Concrete Block Pavement Design*. Proc. 1st Int. Conf. on Concrete Block Paving, Pp 33-37, University of Newcastle upon Tyne, UK.

2 Lilley A. A.,(1991), *A Handbook of Segmental Paving*, Chapman & Hall, London.

3 Shackel B.,(1990), *Design and Construction of Interlocking Concrete Block Pavements*, Chapman & Hall, London.

4 Barber S.D., (1980), *Pavement Design For Port Areas*, Ph.D. Thesis, University of Newcastle upon Tyne, UK.

5 Knapton j., (1996), *The Use of Pavers in Aircraft Pavements*, CAA Report No. 960XX, Civil Aviation Authority, London.

6 Lilley, A.A., (1993), *Concrete Block Paving in the United Kingdom*, Paving Stone 83, Toronto.

7 Smith, R., (1989), *The development of clay pavers in the United Kingdom and their technical specification.* Proceedings vol. 44, Clay Paving Bricks, The Institution of Ceramics, Pp 1-7.

8 Knapton J., (1984), *Concrete Block Pavement Design in the UK*. Proc. 2nd Int. Conf. on Concrete Block Paving, Pp 129-138.

9 British Standards Institution, (1992), *The Structural Design of Pavements Surfaced with Clay Pavers or Concrete Block Paving*, BS7533:1992, BSI, London.

10 Knapton J.,(1985), *The Structural Design and Performance of Concrete Block Roads.* Proc. 3rd Int. Conf. on Concrete Pavement Design & Rehabilitation, Purdue University, Pp127-135.

11 Lilley, A. A. and Knapton, J., (1976), *Concrete block paving for roads. Cement & Concrete Association*, Wexham Springs, Publication 46.021, 19 pp.

12 Transport and Road Research Laboratory, (1970), *A Guide to the Structural Design of Pavements for New Roads* ,Road Note 29, Third Edition, HMSO.

13 Barber S.D. and Knapton J., (Jan.1980), *Terminal surfacing- higher loads to support*, Cargo Systems Int. (Jrnl. of ICHCA), Pp 67-73.

14 Powell W. D., Potter J.F., Mayhew H. C. and Nunne M.E., *The Structural Design of Bituminous Roads*, TRRL Laboratory Report LR 1132, Transport and Road Research Laboratory, Crowthorne, UK.

15 British Standards Institution, (1990), *Methods of test for soils for civil engineering purposes*, BS 1377:Part 4:1990, BSI, London.

16 British Standards Institution, (1988), *Precast Concrete Paving Blocks*, Part1: *Specification for Paving Blocks*, Part 3: *Code of Practice for Laying*, BS 6717:1988, BSI, London.

17 British Standards Institution, (1986), *British Standard for Clay and Calcium Silicate Pavers for Flexible Pavements*, Part 1: *Specification for Pavers*, Part 2: *Code of Practice for Design of Lightly Trafficked Pavements*, BS6677:1986, BSI, London.

18 British Standards Institution, (1990), *British Standard Methods of test for soils for civil engineering purposes*, BS 1377:Part 9:1990.

19 Lilley A. A., Dowson A. J., (1988), *Laying Course Sand for Concrete Block Paving*, 3rd Int. Conf. on Concrete Block Paving, Rome, Pp 457.

20 Knapton J., (1994), *Paver Laying Course Materials: State of the Art*, Proc. of 2.Int. Workshop on Concrete Block Paving, Oslo.

21 Cook, I. & Knapton, J., *Bedding Sand Guide*, Blockleys Brick Limited, Sommerfeld Road, Trench Lock, Telford, Shropshire, TF1 4RY, UK.

CHAPTER TWO

UK SPECIFICATIONS FOR ROAD MATERIALS AND CONSTRUCTION METHODS

Synopsis

This Chapter outlines the major contents of UK specifications for the materials and construction methods likely to be used for the construction of paver pavements. The achievement of full interlock in the surface level of a paver pavement is an essential part of any successful paver pavement. It is important to understand the principals and specifications for the materials and construction process in order to satisfy the requirements of paver pavement components. Specifications for paver pavements worldwide show considerable commonality in the requirements of all the paving materials. Where major differences are found these usually arise from differences in the indigenous materials and, more frequently, from differences in climate or ground conditions. Variations also result from differences in sampling and testing procedures. The Chapter concentrates on explaining the actual material properties and construction methods used in paver pavements which are directly related with the advanced material modelling under most loading conditions.

2.1. Introduction

Fundamental in the analysis of material strength properties are the underlying assumptions of how these properties should be characterised. Actual material properties are complex in several ways. A non-linear stress-strain relationship is the rule rather than the exception under most loading conditions. This can be accounted for but it normally requires advanced material models as well as appropriate information from tests. If this is not completed in a satisfactory manner there will be a model uncertainty which might be significant. Material properties are complex in many respects. At least to the extent where these characteristics can be revealed from experimental information. Based on such information it is possible to identify several aspects which could be of importance in a failure state design.

In the UK, the Department of Transport (DTp) "Specification for Highway Works"[1] is used commonly for many categories of pavements even those where DTp is not involved. It is used for all categories of pavement particularly those surfaced with pavers. Due to this fact the DTp specification is explained in this Chapter, particularly in relation to block paving can be seen in Figure 1.2 which shows pavement cross section illustration, the courses in a typical pavement material suitable for each of those courses are described in this Chapter.

Figure 1.2 shows that a pavement comprises three elements, the surface (pavers in this case), the structure and the foundation (generally granular materials are used in the foundation and sometimes these may be stabilized) and bound material are used in the structure. The construction of granular materials is undertaken according to a method specification whereby the contractor selects a combination of material and compaction equipment which will ensure a stable pavement course. On many contracts the engineer will need to be satisfied that the proposed method is satisfactory and may require that a trial area be constructed. He will then undertake density tests prior to approving the proposed method. The trial area is usually part of the finished work. In this respect, it could be argued that the DTp is a performance

specification and the method adopted is a means of ensuring that the performance achieved during the trial remains consistent throughout the contract.

2.2. Unbound materials for sub-base and roadbase

Slag materials are described in BS 1047[2] in order to be used in sub-base and roadbase whether or not it is air cooled blast furnace slag. BS 1377[3] accepts that a 2:1 water to material ratio can be used for the materials other than slag when placed within cement-bound materials, concrete pavements, concrete structures or concrete products. BS 1377[3] states that up to 225mm compacted specified unbound material thickness can be spread in one layer. (thickness after compaction is specified by the designer). Greater than 225mm compacted thickness unbound material should be laid in two or more layers, the minimum compacted thickness should be 110 mm. The lowest layer in several layers of unbound material should be the thickest layer.

DTp specification[1] states that after the material has been laid, compaction should be performed as soon as possible and full compaction should be applied to the area of longitudinal and transverse joints. Table 2.1 shows alternative method for the compaction of unbound materials. Unless the contractor proves an alternative method, equivalent or better than the specified method at site trials, Table 2.1 can be used. Before overlaying, in the process of compaction, the surface should be free of any layer ridges, cracks, loose materials, pot holes, ruts or other defects. It is concluded that defective areas should be removed and new material should be laid and compacted.

It is stated in DTp specification[1] that Table 2.1 can be applied for following purposes.

The number of passes is the number applying to each point on the surface of the layer in the process of compaction. Each point on the surface of layer should be traversed by the compaction plant in its operation mode. In Table 2.1, the compaction plant is classed in terms of static mass. When the total mass on the roll is divided the total roll width, the mass per

metre width of roll can be found. If a roller has more than one axle, the class of the machine can be categorised in terms of the axle giving the highest value of mass per metre width. For pneumatic-tyred rollers the mass per wheel can be found if the total mass is divided by the number of wheels. Vibratory rollers can either be self-propelled or towed, whereas smooth-wheeled rollers require mechanical vibration, applicable to one or more rolls. On a self-propelled machine with mechanical transmission the vibratory rollers have to use the lowest gear and the speed should be 1.5-2.5 km/h for a towed machine or a self-propelled machine. When higher gear or speeds are used the increases of passes should be arranged. In addition, the mechanical vibration is applied to two rolls which are working together.

TABLE 2.1:Compaction Requirements for Granular Materials Types 1 (Clause 803) and 2 (Clause 804) and Wet-Mix Macadam (Clause 805)

Type of compaction plant	Category	Number of passes for layers not exceeding the following compacted thicknesses: 110 mm	150 mm	225 mm
Smooth-wheeled roller(or Vibratory roller operating without vibration)	Mass per metre width of roll:			
	over 2700 kg up to 5400 kg	16	unsuitable	unsuitable
	over 5400 kg	8	16	unsuitable
Pneumatic-tyred rolled	Mass per wheel:	12	unsuitable	unsuitable
	over 4000 kg up to 6000 kg	12	unsuitable	unsuitable
	over 6000 kg up to 8000 kg	10	16	unsuitable
	over 8000 kg up to 12000 kg			
	over 12000 kg	8	12	unsuitable
Vibratory roller	Mass per metre width of vibrating roll:			
	over 700 kg up to 1300 kg	16	unsuitable	unsuitable
	over 1300 kg up to 1800 kg	6	16	unsuitable
	over 1800 kg up to 2300 kg	4	6	10
	over 2300 kg up to 2900 kg	3	5	9
	over 2900 kg up to 3600 kg	3	5	8
	over 3600 kg up to 4300 kg	2	4	7
	over 4300 kg up to 5000 kg	2	4	6
	over 5000 kg	2	3	6
Vibrating plate compactor	Mass per square metre of base plate:			
	over 1400 kg/m2 up to 1800 kg/m2	8	unsuitable	unsuitable
	over 1800 kg/m2 up to 2100 kg/m2	5	8	unsuitable
	over 2100 kg/m2	3	6	10
Vibro-tamper	Mass:			
	over 50 kg up to 65 kg	4	8	unsuitable
	over 65 kg up to 75 kg	3	6	10
	over 75 kg	2	4	8
Power rammer	Mass:			
	100 kg-500 kg	5	8	unsuitable
	over 500 kg	5	8	12

Table 2.1: Compaction requirements for granular materials Type 1, Type 2 and wet-mix macadam.

Half the number which is given in Table 2.1 for the applicable mass per metre width of one vibrating roll can be taken as the minimum number of passes. However if the mass per metre

width of the rolls compare to each other and if the result of this comparison show differences, the number of passes can be determined as for the roll with the smallest value. Furthermore, the minimum number of passes may be calculated in terms of treating the machine, the roll with the higher value of mass per metre which can be equaled to a single vibrating roll with a mass per metre width. If Vibratory rollers work without vibration, this roller can be categorised as smooth-wheeled rollers. It is added that the recommendations of the manufacturers should be taken into consideration in the operation of the vibratory rollers. All such rollers should be equipped with apparatus which show the frequency of the mechanism of operating and speed of travel. Vibrating-plate compactors are machines with a base-plate by which a source of vibration consisting of one or two eccentrically weighted shafts are attached. If the vibrating-plate compactor's area in relation with the surfaces of material being compacted is divided by the total mass of the machine in its working condition, the mass per square metre of base-plate of a vibrating-plate compactor can be determined. The recommendation of the manufacturer about the frequency of vibration should be used in the process of operation of vibrating-plate compactors. Less than 1 km/h traveling speed is generally used for operation but in some cases higher speeds can be imperative, in these cases the number of passes can be raised in terms of the increasing proportion of travel speed. Vibro-tampers are engine driven machines with reciprocating mechanism on a spring system by which oscillations occur in the base-plate. Power rammers are manually operated machines which are induced by explosions within an internal combustion cylinder. When the compacting shoe makes one strike, one pass of a power rammer has been made. Either type of compaction plant or different categories of the same plate may be allowed such that the number of passes for each is proportional to the appropriate number in Table 2.1 or the combination can produce the same compactive effort as singular operated ones (see Table 2.1).

The DTp specification[1] defines two categories of pavement sub-base materials Type 1 and Type 2. The requirements are as follows.

2.2.1. Granular sub-base material Type 1

This is high quality material whose strength is largely independent of moisture content. Type 1 Granular materials consists of the following: Crushed rock, crushed slag, crushed concrete or well burnt non-plastic shale. This material must be well-graded and in accordance with Table 2.2. Materials passing the 425μm BS sieve are deemed as non plastic by BS1377[3], which have been tested as such. This material may be transported laid and compacted without the possibility of it drying out or segregating. This material also consists of 10% fine values of 50 kN or more when it is tested in compliance with BS 812[4]. However, these samples must be tested in a saturated and surface dried condition. Prior to carrying out the tests the selected test portions must be soaked in water at room temperature for 24 hours without having previously been oven dried.

Table 2.2: Sub-base Type 1 Range of Grading	
BS sieve size	Percentage by mass passing
75 mm	100
37.5 mm	85-100
10 mm	40-70
5 mm	25-45
600 μm	8-22
75 μm	0-10
The particle size shall be determined by the washing and sieving method of BS 812[4] Part 103	

Table2.2: Sub-base Type 1 range of grading.

2.2.2. Granular sub base material Type 2

This is not high quality material whose strength is dependent on moisture content. Type 2 granular material usually consist of these : Natural sands, gravels crushed rock, crushed slag, crushed concrete or well burnt non-plastic shale. According to DTp specification[1] these materials should be well graded and should lie within the grading envelope of Table 2.3. In addition, Type 2 materials can usually lose strength in wet conditions and contain some clay and it may be necessary to protect it from weather more effectively.

Table 2.3: Sub-base Type 2 Range of Grading	
BS sieve size	Percentage by mass passing
75 mm	100
37.5 mm	85-100
10 mm	45-100
5 mm	25-85
600 µm	8-45
75 µm	0-10
The particle size shall be determined by the washing and sieving method of BS 812[4] Part 103	

Table 2.3: Sub-base Type 2 range of grading.

Materials passing the 425µm BS sieve, tested in compliance with BS 1377[3], should have a Plasticity Index (PI) of less than six. This material should also comply with the minimum CBR requirement and BS 1377[3] Test 16, with surcharge discs. It should be tested at the density and moisture content likely to develop in equilibrium pavement conditions. Additionally, the density should correlate to a uniform air voids of 5% content and an optimum moisture content as specified by BS 5835[5]. According to DTp specification[1], the material can be transported, laid and compacted at a moisture range of 1% above to 2% below the optimum as determined by BS 5835[5] and also without drying out or segregating. When tested in accordance with BS 812[4], the material must have a 10% fine value of 50 kN or more, except that these samples shall be tested in saturated and surface dried conditions. The selected test portions should be soaked under water at room temperature for 24 hours without having been oven dried.

2.2.3. Wet-mix macadam

Wet-mix macadam is a mixture of granular material and water which binds it together. Wet-mix macadam can be made and consist as follows:

The coarse and fine aggregate consist of crushed rock or crushed slag. This aggregate is shown in Table 2.4. According to DTp specification[1], the materials should be tested in a saturated and surface dried condition with 10% fine value of 50 kN and in accordance to BS 812[4]. Prior to testing the selected test portion is soaked under water at room temperature for 24 hours without having been oven dried. When determined against BS 812[4]: Section 105.1, the flakiness should

be less than 35. This material is mixed in a mixer as specified by BS 1305[6] or approved by the Engineer. The wet-mix macadam can be laid and compacted at the optimum moisture content of - 0.5% as specified by BS 5835[5]. Additionally, the compacted thickness of each layer should not be more than 200 mm. Any area with loose surface in fines should be removed and replaced with properly graded material.

Table 2.4: Wet-mix Macadam Range of Grading	
Bs sieve size	Percentage by mass passing
50 mm	100
37.5 mm	95-100
20 mm	60-80
10 mm	40-60
5 mm	25-40
2.36 mm	15-30
600 µm	8-22
75 µm	0-8
The particle size shall be determined by the washing and sieving method of BS 812 Part 103	

Table 2.4: Wet-mix macadam range of grading.

2.3. Bituminous roadbase and surfacing materials

Two types of bituminous material can be used, DBM (Dense Bituminous Macadam) and asphalt. The most important difference between these materials is that DBM is stiffer than asphalt material but can crack whereas asphalt material is more flexible than DBM material.

According to DTp specification[1], aggregates should be clean, hard and durable. Clean vehicles should be used in order to transport bituminous materials under the discretion of the consulting engineer. It should be covered over in the process of transit or awaiting tipping. It can use dust, coated dust or water inside of the vehicles in order to help tipping of the mixed materials. However the amount should be minimum. An approved self-propelled paving machine can be used for spreading, leveling and tamping practically. The mixed material should be supplied to the paver continuously without delay after arrival at the site. The rate of delivery of material should be taken into account. The type of paver and its rate of travel should be determined and also its uniform flow of laying width should be provided. The material

should be laid in accordance with the recommendations of British Standard BS 594[7]. If bituminous material is hotter than 145°C , laying of material can be dangerous because of heat damage. Refer to the British Standard Guide Page 19, section 901 Bituminous Roadbase and Surfacing Materials sub-section Laying. DTp specification[1] states that the following stages can be allowed in the situation of hand laying of any bituminous material;

- For laying regulating courses of irregular shape and varying thickness;
- In confined spaces where it is impracticable for a paver to operate;
- For footways;
- At the approaches to expansion joints at bridges or viaducts;
- For laying mastic asphalt in compliance with BS 1447[8].

According to DTp specification[1], in order for regularity requirements to be satisfied for compaction, bituminous material should be laid and compacted in layer thicknesses otherwise full strength is not attained. The minimum thickness in one pass of the paver must be 90 mm . If the full course thickness then it is less than 90 mm. The material mentioned should be uniformly compacted without causing any undue displacement of the mixed material. This process should be completed whilst the temperature of the mixed material is greater than the minimum rolling temperature as stated by British Standard. The rolling should continue until all roller marks are removed. The compaction is carried out using 8-10 tonnes of dead-weight smooth wheeled rollers with a width of not less than 450 mm or multi wheeled pneumatic tyred rollers of equivalent mass or by vibratory rollers or a combination of these. Wearing course and base course material should always be surface finished with a smooth wheeled roller (either a dead-weight or vibratory roller in non vibrating mode). However note that vibratory rollers should not be used on bridge decks. A vibratory roller can be used if it is capable of the standard compaction of an 8-tonne dead-weight roller. The performance of these rollers can be measured by the following:

- TRRL Report 1102[9]

- Producing the necessary evidence under comparable conditions by the Engineer.

The material is rolled in a longitudinal direction with the driven rolls nearest the paver. The roller first compacts the material closest to the joint and then move from the lower to the upper side of the layer, overlapping on successive passes with half the width of the rear roll or in the case of a pneumatic- tyred roller, at least the nominal width of the tyre. Rollers should be prevented from standing on newly laid material ,as there is a risk of deformity. The adequacy of these compaction is determined by the Engineer using the Percentage Refusal Density of the laid material in the following manner:

2.4. Trial areas

The construction of granular materials is undertaken according to a method specification whereby the contractor selects a combination of material and compaction equipment which can ensure a stable pavement course. On many contracts the engineer can need to be satisfied that the proposed method is satisfactory and may require that a trial area is constructed. The engineer can then undertake density tests prior to approving the proposed method. The trial area is usually part of the finished work. In this respect, it could be argued that the DTp is a performance specification and the method adapted is a means of ensuring that the performance achieved during the trial remains consistent throughout the contract.

According to DTp specification[1], prior (at least 3 days) to laying the dense macadam, the Contractor should lay a trial area to demonstrate the compaction plant and rolling procedure selected to achieve the specified Percentage Refusal Density. Trial tests should be carried out so that the engineer can approve the construction materials and methods. On the main project, the tests are done as a check. The trial should not be less than 30m nor more than 60m in length. If this trial complies with the contract, then it can form part of the works. Materials used in the trial are similar to that of the main works. Three pairs of cores

(each 150 mm nominal diameter) is taken from trial areas, each cut in compliance with BS 598[10] by a coring machine approved under BS 4019[11]. Two core pairs, at least, can be from the wheel track zones of a completed carriageway. Wheel track zones referred to here range from: (0.1m and 1.1m), (2.55m and 3.15m) from the center of the "nearside" lane markings for each running lane. In order for material to be considered "acceptable", the British Standards Manual states that the "Percentage Refusal Density" should not be less than 93 %. The "Percentage Refusal Density" is calculated according to the procedures (refer to the BSM). Furthermore, where the required level is not achieved the trial area shall be removed and the trial repeated.

2.5. Main works

According to DTp specification[1], no material can be laid until the engineer has accepted the material laid in the trial area. The contract is judged by determining the Percentage Refusal Density for areas of 1000 m^3 or from the material laid in any one day which is less than areas of 1000 m^3. The core pairs mentioned above is then taken from each area for determination as directed by the Engineer. Longitudinal joints in materials should not be situated in wheeled track zones whenever they are to undergo the percentage Refusal Density Test. The bituminous material laid should be in a continuous length with 300 tonnes from one source before material from another source is used. However this requirement may be waived by the Contractor with the approval of the Engineer (i.e. the constituents of materials from different sources are identical in quantity and quality and laying and compaction characteristics are similar). In accordance with BS 4987[12], the walls and base of all holes from which core samples are cut should be dried, painted with hot bituminous binder and filled to the underside of the wearing course level with dense laid macadam, well rammed in the layers not exceeding 50 mm. In order to prevent entrance of loose material into the joint when the joint of a structure is expanded or approached, a paver laying basecourse or wearing course should be taken out of use. All chippings should be applied uniformly to the surface and be rolled into the wearing course in such a manner that they are effectively held and provide any specified texture depth. Hand-raking of wearing course material which has been laid by a paver and the additions of

such material by hand-spreading to the paved area for adjustment of level can be permitted only in the following circumstances:

- At the edges of the layers of material and at gullies and manholes;
- At the approaches to expansion joints at bridges and viaducts;
- Where otherwise directed by the engineer.

According to DTp specification[1], joints between laying widths or transverse joints should be made in wearing courses, the material has to be fully compacted. All joints should be made up at least 300 mm from parallel joints in the layer beneath and in a layout agreed by the engineer. Bituminous material should be kept clean and uncontaminated. Upper roadbase material, in pavements without basecourse, and basecourse material should not be left uncovered for more than three consecutive days after being laid. The engineer may extend this period in terms of requirements.

2.6. Dense tarmacadam roadbase

Dense tarmacadam roadbase is described in BS 4987[12]. DTp specified that the aggregate should be in dry surface condition in the process of mixing. If the coarse aggregate is gravel, admixtures can be added as much as 2% of Portland cement. The mass of the total mix and the percentage of fine aggregate can thus be decreased accordingly. If the gravel is limestone, cement is not required. The tar should comply with BS 76[13].

2.7. Dense bitumen macadam roadbase

Dense bitumen macadam roadbase is described in BS 4987[12]. According to DTp specification[1], the aggregate should be in dry surface condition in process of mixing. If the coarse aggregate is gravel, admixtures can be added as much as 2% of Portland cement or hydrated lime. The mass of the total mix and the percentage of fine aggregate can thus be

decreased accordingly. If the gravel is limestone ,cement is not required. Binder should be petroleum bitumen complying with BS 3690[14]. Part 1 or tar bitumen complying with BS 3690[14] Part 3. The penetration of the bitumen or tar bitumen mixture should be either 100 pen or 200 pen grade.

2.8. Rolled asphalt roadbase

Rolled asphalt roadbase is described in BS 594[7]: Part 1 for roadbase mixtures. If the coarse aggregate is gravel, admixtures can be added as much as 2% of Portland cement .The mass of the total mix and the percentage of fine aggregate can thus be decreased accordingly. If the gravel is limestone, cement is not required. The binder should comply with BS 3690[14].

2.9. Rolled asphalt basecourse

Rolled asphalt base course is described in BS 594[7]: Part 1 for base course mixtures. If the coarse aggregate is gravel, admixtures can be added as much as 2% of Portland cement .The mass of the total mix and the percentage of fine aggregate can thus be decreased accordingly. If the gravel is limestone, cement is not required.

2.10. Dense bitumen macadam basecourse

Dense bitumen macadam course is described in BS 4987[12] for dense graded basecourse macadam. According to DTp specification[1], the aggregate should be in dry surface condition in process of mixing. If the coarse aggregate is gravel, admixtures can be added as much as 2% of Portland cement or hydrated lime. The mass of the total mix and the percentage of fine aggregate can thus be decreased accordingly. If the gravel is limestone, cement is not required. The binder should be petroleum bitumen complying with BS 3690[14]: Part:1 or tar bitumen is described in BS 3690[14] :Part 3.

2.11. Dense tarmacadam basecourse

Dense tar macadam base course is described in BS 4987[12] for dense graded basecourse macadam. According to DTp specification[1], the aggregate should be in dry surface condition in process of mixing. If the coarse aggregate is gravel, admixtures can be added as much as 2% of Portland cement. The mass of the total mix and the percentage of fine aggregate can thus be decreased accordingly. If the gravel is limestone, cement is not required.

2.12. Bitumen macadam basecourse

Bitumen macadam base course is described in BS 4987[12] for 40 mm nominal size single course material. According to DTp specification[1], the aggregate should be in dry surface condition in process of mixing. If the coarse aggregate is gravel, admixtures can be added as much as 2% of Portland cement or hydrated lime. The mass of the total mix and the percentage of fine aggregate can thus be decreased accordingly. If the gravel is limestone, cement is not required.

2.13. Tar macadam basecourse

Tar macadam base course is described in BS 4987[12] for 40 mm nominal size single course material. According to DTp specification[1], the aggregate should be in dry surface condition before mixing. If the coarse aggregate is gravel, admixtures can be added as much as 2% of Portland cement .The mass of the total mix and the percentage of fine aggregate can thus be decreased accordingly. If the gravel is limestone, cement is not required.

2.14. Rolled asphalt wearing course (recipe mix)

The material is described in BS 594[7]:Part 1 for wearing course recipe mixtures. According to DTp specification[1], composition of the material should be accounted for by the method which is described in BS 594[7]. 40 pen HD bitumen can be used under the discretion of the Engineer.

Rock or slag which is crushed with a polished stone value not less than 45 should be used. Nominal coarse aggregate content should be 30% by mass of the total mix for new works. The Marshall stability and flow for wearing course design mixtures is described in BS 594[7]:Part 1. BS 598[10]: Part 3 can be used for determination of the design method and the design binder content for compaction. BS 598[10]: Part 1 can be used for determination of the plant mixture and also the requirements for the wearing course design mixture should be suitable for the engineer.

2.15. Dense bitumen macadam wearing course

Dense bitumen macadam wearing course is described in BS 4987[12]. According to DTp specification[1], the aggregate should be in dry surface condition in process of mixing. The course aggregate should have the minimum polished stone value.

2.16. Dense tar surface wearing course

Dense tar surface wearing course is described in BS 5273[16]. According to DTp specification[1], the course aggregate content for road use should be 35% and for hand standing 5%.

2.17. Cold asphalt wearing course

Cold asphalt wearing course is described in BS 4987[12]. According to DTp specification[1], the course aggregate should have the minimum polished stone value. The aggregate should be in dry surface condition in process of mixing.

2.18. General requirements for cement-bound materials

These are usually concrete with low cement and water content so they can be constructed using paving machines rather than conventional structural concrete method. According to

DTp specification[1], the following clauses can be a guide for construction of cement-bound materials.

Cement-bound materials should comply with Table 2.5. Water should comply with BS 5328[17] Section 11.3 and slag should comply with BS 1047[2]. When the materials other than slag and the test is carried out in compliance with BS 812[4], 500mm of cement-bound materials, concrete pavement, concrete structure or concrete product which should have a soluble sulphate content not exceeding 1.9 g of sulphate (expressed as SO_3) per litre is added to this material. Table 2.5 can be used for convenient manner of the test of batching and mixing. The mix-in-plant method which is described in Table 2.5 is used and materials are batched by mass. The materials should be batched and mixed in accordance with BS 5328[17] Section 13.2. Continuous mixers are used and materials are batched by mass, the continuous mixers should comply with Table 2.5 of BS 1305[6] when tested in compliance with BS 3963[18].

Table 2.5: Cement-bound Materials

		Field Requirements						Specimen Requirements		
category	Clause	Mixing Plant	Method of Batching	Moisture Content	Minimum Compaction	Compaction	Curing	Compressive Strength Testing	Minimum 7 Day Cube Compressive Strength N/mm2	
									Average (Note 2)	Individual (Note 3)
CBM1	1036	Mix-in-Place or Mix-in-Plant	Volume or Mass	To suit requirements for strength, surface level, regularity and finish	95% Of Cube Density (Note 1)	Clause 1040	BS 1924 (Test 11)	BS 1924 (Test 11) or BS 1881 (Part 116)	4.5	2.5
CBM2	1037								7.0	4.5
CBM3	1038	Mix-in-Plant	Mass				BS 1881 (Part 111)	BS 1881 (Part 116)	10.0	6.5
CBM4	1039								15.0	10.0

Table 2.5: Cement-bound materials.

Plant-mix cement bound material should be removed immediately from the mixer and transported directly to the point at which the material is laid. During the transit from the mixer to the laying site and whilst awaiting tipping, the material should be protected from the weather. In order to prevent segregation and drying, the cement-bound material should be laid

and spread evenly. As soon as possible spreading should proceed without delay. In order for spreading of roadbase cement-bound material, paving machine or a spreader box can be used. Cement bound material should be spread in one layer evenly so that the total thickness is determined after compaction. Longitudinal or transverse construction joints, unless vertical forms are used, the edge of compacted cement-bound material should be reduced to a vertical face where the correct thickness of properly compacted cement-bound material has been obtained. In the case of cement-bound sub-bases under a concrete surface slab or continuously reinforced concrete roadbase, longitudinal construction joints in the sub-base should be staggered by at least 300mm from the position of the longitudinal joints in the concrete surface slab or continuously reinforced concrete roadbase, and by 1m for transverse joints. In order to prevent segregation, after the spreading of the cement-bound material, compaction should be performed at once. Around the longitudinal and transverse construction joints, special care should be applied to obtain full compaction. Table 2.5 can be used for testing of compaction. Compaction should be done within 2 hours of the addition of the cement. This period that is necessary or appropriate can be modified under the discretion of the Engineer. After completion of compaction, compacting equipment should not be carried on the cement-bound material for the duration of the curing period. On completion of compaction, the surface of any layer of cement-bound material should be well-closed, free from movement under compaction plant and from ridge, cracks, loose material, pot holes, ruts or other defects. The areas having the loose segregation or defect, should be removed to the full thickness of the layer, and new cement-bound material laid and compacted. According to DTp specification[1], one of following methods should be applied to cure on completion of compaction layers of cement-bound material during a minimum of 7 days.

- Covering with an impermeable sheeting with joints overlapping at least 300 mm and set to prohibit egress of moisture.
- Bituminous spraying
- Spraying with a curing compound

10 days prior to the start of the main cement-bound material works, a trial area (at least has the proportions 400m length and 222m width) should be laid to evaluate the suitability of the proposed materials, mix proportions, mixing, laying, compaction plant and construction procedures. The applicable area should include one longitudinal and one transverse construction joint. The test should be carried out with the specification. Unless the test is approved by the Engineer, the main works should be started. After confirmation, the materials, mix proportions, mixing, laying, compaction plant and construction procedures should not be modified without the permission of the engineer.

2.19. Use of nuclear density gauges with cement-bound material

According to DTp specification[1], the operation, warming up and the standardisation of the gauge should be done in accordance with the manufacturers recommendations. The gauge should be applied by the direct transmission mode of operation. Prior to the preliminary trial and in the process of changing the compound of the mix to the cement-bound material, the material should be checked in the following manner. With similar proportions of the cement-bound material which is suggested for use in the main works, two blocks should be made approximately 380 x 500 x 200 mm (deep). Blocks should be made by compacting the cement-bound material into a mould in four equal layers. During the four minutes, each layer should be compacted uniformly by using a vibrating hammer. The top layer should be even with the mould by traveling to obtain a smooth surface. A hole 18-25 mm in diameter should be formed through the full depth of the block (200 mm) and at a normal to the surface. The hole shall be 125 mm from one end of the block and in the center of the 380 mm dimension. The wet density of the blocks should be calculated from the dimensions and mass of each block. A nuclear density gauge can be used within one hour of weighing each block in order to take three density readings with source rod lowered to a depth of 150 mm and the gauge in the same position. The variation between the calculated density and the average of the three measured density values of each block should be determined as a percentage of the calculated density. If the difference between the variations for the two blocks is 1% or less, then readings taken by

nuclear density gauges used to measure the field density of the cement-bound material should be corrected by the average amount of the variation for the two blocks. The correction should be done either by using the gauge biasing device in compliance with the manufacturers instructions or by multiplying the derived in situ wet density by the appropriate factor. In all other cases the gauge manufacturer should be advised. The gauge should be at least 150 mm away from any vertical projection or edge. A smooth and level surface should be prepared on which to place the gauge in compliance with the manufacturers instructions. The manufacturers guide plate can be used to form an 18-25 mm diameter hole to the required depth, normal to the surface, by driving in a steel pin. The gauge should be positioned and the source rod lowered to the required depth. The gauge should be firmly seated by rotating it about the source rod with a slight back and forth motion. The gauge should be pulled so that the source rod is in contact with the wall of the hole and no air gap exists between the source and detection tube. One reading of one minute duration should be taken and recorded. The in situ wet density should be determined in compliance with the manufacturers instruction.

2.20. Manufacturing specifications for precast concrete paving

BS 6717[19]: Part 1 shows the manufacturing specifications for precast concrete paving blocks which are used for the construction of low speed roads and industrial and other paved surfaces in terms of all categories of static and vehicular loading and pedestrian traffic. Paving blocks are produced using one or more binders or binder constituents which are ordinary Portland cement (BS 12[20]), Portland-blastfurnace cement (BS 142[21]:Part 2), Portland pulverized-fuel ash cement (BS 6588[22]), pulverized-fuel ash (BS 3892[23]:Part 1), ground granulated blastfurnace slag (BS 6699[24]) in terms of requirements of the relevant British Standards. Paving blocks are produced using one or more aggregates which are natural crushed or uncrushed aggregates(BS 882[25]: 1993), air-cooled blastfurnace slag (BS 1047[2]:1983), pulverized-fuel ash (BS 3892[23]: Part 1,2), ground granulated blastfurnace slag(BS 6699[24]) in terms of the requirements of the relevant British Standards. The fine aggregate which passes a 5 mm sieve according to BS 410[26] should not include more than

25% by mass of acid-soluble material either in the fraction contained on, or the fraction passing, a 600 mm sieve.

According to DTp specification[1], the water should be very clear like drinking quality or the recommendations of BS 3148[27]:1980 should be taken into account. This can be used for different accelerating, delay and water-reducing agents which should comply with BS 5075[28]: Part 1. For pigments BS 1014[29] is used and calcium chloride should comply with BS 3587[30]. Concrete described as natural colour contains no pigment. The surface layer should be formed as an integral part of the block and should be not less than 5 mm thick in composite paving blocks. Additionally, the binder content of the compacted concrete should be not less than 380 kg/m^3. Paving blocks constructed of different binder constituents should have a higher binder content than paving blocks made in a similar way using only Portland cement for equivalent durability. According to DTp specification[1], the size thickness of paving blocks should not be less than 60 mm. Type R blocks should be rectangular and its work sizes are 200 mm length, 100 mm width. Type S blocks can be of any shape fitting within a 295 mm square coordinating space and the work size is not less than 80 mm. The preferred work size thicknesses are 60 mm, 80 mm and 100 mm. The measured maximum dimensional deviations from the stated work should be for length ± 2 mm, for width ± 2 mm, for thickness ± 3 mm and each side should be perpendicular to the wearing surface and the opposite face for paving blocks. The compressive strength of paving blocks should not be less than 49 N/mm^2 and the crushing strength of any individual block should not be less than 40 N/mm^2.

According to DTp specification[1], in order to carry out the compressive strength test the following sampling procedures should be taken into account.

- The paving blocks are divided each designated approximatcly equal section, including not more than 5000 blocks before laying. All samples are clearly marked at the time of sampling so that they are clearly defined. Two blocks are taken from each group.

- The samples are send to the test laboratory, and in order to prevent the blocks from the damage in transit, precautions are taken.
- The paving blocks are protected from damage and contamination factors until they have been tested. As soon as possible the tests are carried out after the samples have been taken.

DTp specification[1] states that in process of marking the following particular notes have to be written.

- the name, trade mark or other means of identification of the manufacturer
- the number and date of the British Standard
- the type of binder constituent(s) used
- the type of admixture(s) used

2.21. The installation of interlocking paving

BS 6717[19] is a British Standard used in the manufacturing of pavers (Part 1) in their installation (Part 3). The aspect of BS 6717[19] relevant to the reasons are as follows:

Installation of pavers has to be codified because the structural behavior of the surface depends upon joint spacing sand stability, sand thickness and joint material, all these factors are dependent upon quality of laying.

2.21.1. Construction of pavement

Construction should be in compliance with the Department of Transport Specification for Highway Works 1986[1]. The subgrade and sub-base (and roadbase where necessary) is prepared with consideration to the following specifications.

- The surface levels are within the tolerances given in Table 2.6.
- The longitudinal falls and crossfalls are such that no depressions hold water. (A minimum longitudinal fall of 1.25% and a minimum crossfall of 2.5% are recommended.)
- The surface should be tight and dense enough in order to prevent laying course material during the design life.
- Provision is made to:

  (1) Water should be drained from the laying course in service, e.g. by installation of drainage when the laying course is on impermeable foundations.

  (2) Migration and loss of laying course material should be prevented from draining, e.g. by using a geotextile.
- The extent of the site prepared for block laying includes enough room to provide adequate foundations and backing for any edge restraint.

Table 2.6: Tolerances on surface levels	
Layer of pavement	Maximum permissible deviation from design level
	mm
Sub-layer	
sub-base	±20
roadbase	±15
Surface course:	
overall	±6
flatness	10 under a 3m straightedge
adjacent to gullies, surface drainage channels and outlets (see note)	2 between adjacent blocks + 6, -0
Note. The permissible deviations for the upper level of drainage inlets and channels should be +0, -0 mm to ensure positive drainage.	

Table 2.6: Tolerances on surface levels.

According to DTp specification[1], edge restraints should be adequate to support traffic load and in order to prevent loss of laying course material from under the surface course. Figure 2.1 shows edge restraints. Additionally, the surface course should not be vibrated until the edge restraint, together with any concrete haunching which has given sufficient strength.

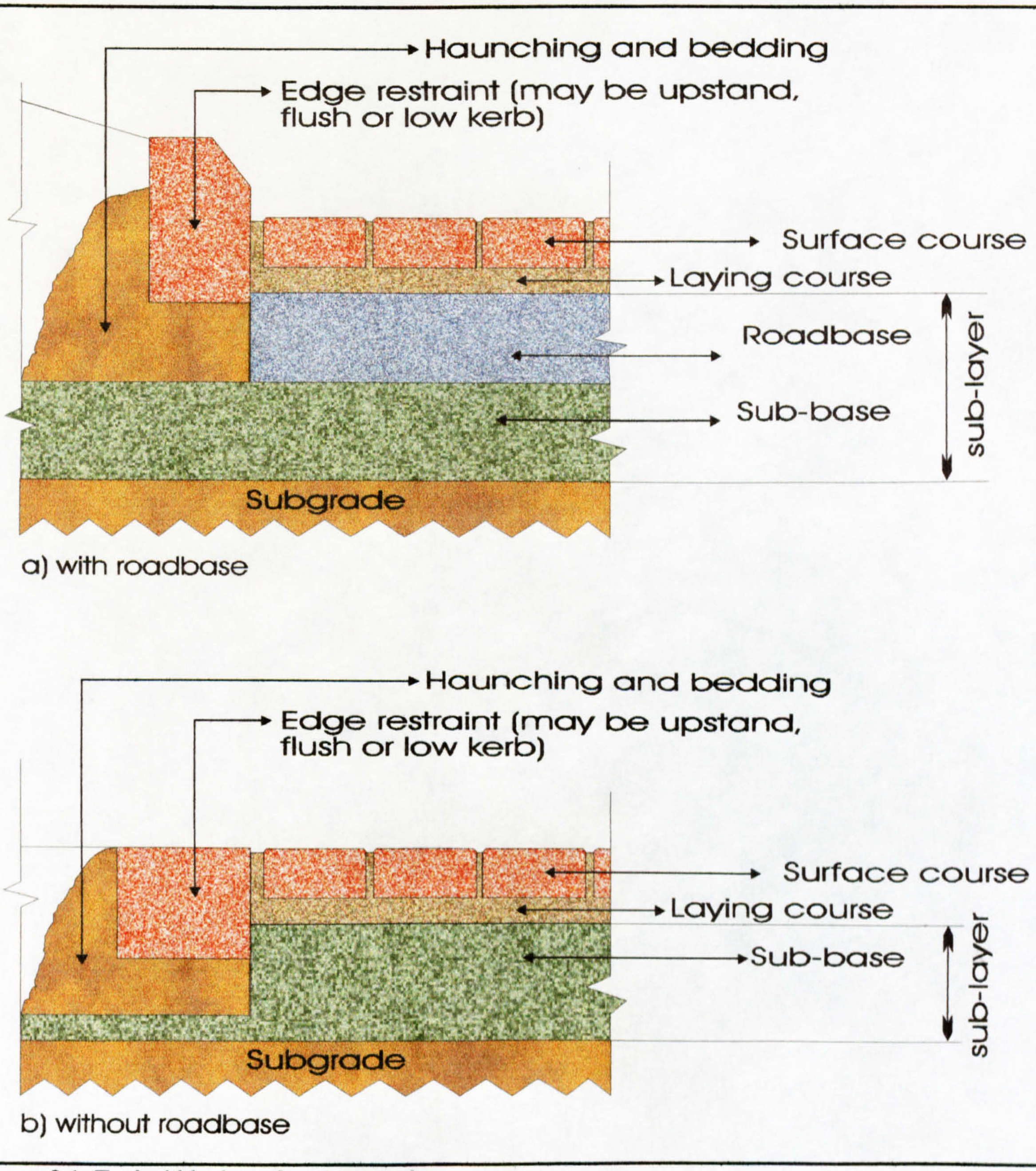

Figure 2.1: Typical block paving construction

Haunching is made to an edge restraint on the paving face vertical down to the level of the underside of the laying course.

Laying course:

According to DTp specification[1], naturally occurring sand can be used or crushed rock fines graded in compliance with Table 2.7. The moisture content of the laying course material should be as uniform as possible and the material should be moist without being saturated. The material should be covered with any material to be stockpiled. Furthermore, the laying course should be compacted so that after the compaction it forms a layer. It should be constructed approximately 50 mm thick below the paving blocks, (where closer tolerances are given in Table 2.6 for the level of the sub-base have been achieved, or where a roadbase has been used, a thinner laying course can be used, however, the materials should not be less than 25 mm thick at any point.). According to DTp specification[1], the laying course should be constructed using the method explained in the following items (a) and (b).

Table 2.7. Grading for laying course sand and jointingsand (using sieves comlying with BS410[26])		
Naminal aperture of sieve size	Percentage by mass passing through sieve	
	Laying course sand	Jointin sand
	%	%
10.00 mm	100	100
5.00 mm	90 - 100	100
2.36 mm	75 - 100	95 - 100
1.18 mm	55 - 90	90 - 100
600 µm	35 - 70	55 - 100
300 µm	8 - 35	15 - 50
150 µm	0 - 10	0 -15
75 µm	0 - 3	0 -3
NOTE. Sand should be graded by washing, decanting and dry sieving in accordance with BS 142[21], Part 103		

Table 2.7: Grading for laying course sand and jointing sand.

(a) Pre-compaction: The material which is in a loose uncompacted layer should be spread to about the required final depth below the surface profile. This layer should be compacted

using a vibrating plate compactor. Another layer of material is spread 15 mm thick and it is leveled to create a loose surface on which the paving blocks can be placed.

(b) Compaction after laying: The material should be spread loose in a uniform layer, and it should be leveled to a thickness required to the paving blocks have been laid and vibrated into place. The aim of spreading the laying course is to produce a uniform surface and for specifying design profiles and falls, at the uniform degree of compaction.

If any disturbance to the prepared laying course sand owing to pedestrian or wheel traffic occurs, before placing the paving blocks, the area of laying course material should be leveled again.

Surface course:

According to DTp specification[1], the paving blocks should be laid in terms of tolerances given in Table 2.6. The small changes can be done in order to keep up the bond pattern and the joints should remain enough for sand filling. Additionally, the blocks should be in the correct order and the first row of the blocks should be aligned against the edge restraint or by using a straightedge or string line. The uniformity of the blocks should be checked periodically e.g. by using string lines, and necessary changes can be done. All paving blocks are laid followed by closers. Infilling of the blocks is completed before compaction commences. Whenever possible, infilling to boundaries and obstructions should be completed as the laying of the surface course proceeds. The paving blocks can be trimmed to shape and size to form boundaries.

DTp specification[1] states that one-third of the full blocks should not be used. The edge of the paving blocks area should be restricted with blocks which have different placing shape against the edge of the area. Working around any obstruction or iron ware the paving blocks should be made with concrete with a maximum aggregate size of 10 mm and a 28-

day cube compressive strength of 40 N/mm^2 to form a more regular shape, and the paving blocks should be cut to be adjacent to this area. The iron ware is being provided in combination with the paving blocks. In addition, the surface course should be fully compacted using a plate compactor with a plate area which is not less than 0.25 m^2, transmitting an effective force on the plate not less than 75 kN/m^2 and frequency of vibration is in the range 75 Hz to 100 Hz. Otherwise, any compacting equipment which is given the same degree of compaction or better can be used. It is important to fill the lower portion of the block-to-block joint with the laying course material. After laying all areas of paving except edge strip should be compacted as soon as possible. The tolerances of finished surface level can be checked using Table 2.6. Over the surface course sand or crushed rock fines should be spread and brushed into the joint after compaction of the surface course. The sand which can stain the pavement colour should be taken into consideration. Filling between the joints is very important. The dry material can cause rapid joint penetration; that is why materials complying with the grading in Table 2.7 should be used. The block paving should be vibrated to ensure complete filling of the block-to-block joint by the surface-applied sand. Joint filling and final compaction should be completed as soon as practicable after laying. Further compaction may be necessary for block paving which is used for industrial vehicles or high point loads after joint filling. According to DTp specification[1], if weather conditions put the performance of the pavement into risk, all operation should be cancelled. After an early period of traffic use the surface of the pavement should be checked and additional sand filling must be brushed.

2.22. Conclusion, comments and discussion

It can be concluded that unbound materials are usually complying with one of several possible particle size grading envelopes. The most widely used specification for paving materials is the Department of Transport (DTp) "Specification for Highway Works"[1], which includes three forms of unbound material and two broad forms of cement-bound material, roller compacted and poured, that may be used as sub-bases. The unbound materials are known

as Type 1, Type 2 and wet-mix macadam. Type 1 materials have to be made of crushed rock, crushed slag, crushed concrete or well-burnt, non-plastic shale. Surface water can penetrate the joints of newly laid flexible paver pavements and therefore the requirement for a non-moisture-susceptible material immediately beneath the laying course is important. Type 2 materials can be made from the same aggregates as Type 1, but also from natural sands and gravels. The Department of Transport design requirements[31] permit the use of Type 2 materials beneath bituminous surfaced roads only for pavements designed to carry less than 400 commercial vehicles a day at opening and they should have a CBR of 30% or more when tested in accordance with the method described in BS 1377[3]. This type of material is not recommended directly beneath the laying course of a segmental pavement, as it may be weakened greatly when wet, owing to the presence of the plastic fractions. Wet-mix materials are made from a combination of sand and crushed rock or slag sand. The coarse fraction of the aggregate is required to have a 10% fines value of 50 kN or more when tested in accordance with BS 812[4], the tests being made with the aggregate in both a dry and saturated states, to ensure that the aggregate particles do not break down in service. There are some other requirements concerning the aggregate and its grading. These aggregates are mixed with water and laid and compacted within 0.5% of their optimum moisture content. These materials would be suitable for use beneath paver pavements although their use in practice is uncommon.

The Cement-Bound Material form 1 (CBM1) is a soil cement, either mixed in-situ, or pre-mixed, which has to contain sufficient cement to reach a minimum average seven-day cube compressive strength of 4.5 N/mm^2 and not lose more than 20% of its strength after seven days immersion in water, a simple way of detecting an excess of soluble sulphates. CBM 2 materials are made of selected aggregates within a broad grading envelope and with a 10% fines values of 50 kN or more[4], mixed with enough cement to give an average seven-day cube strength of not less than 7.0 N/mm^2. Mixing is allowed to be either in-situ or at a central plant. CBM 3 and CBM 4 materials are made of closely graded aggregates complying with the requirements of BS 882[25] and mixed with cement in a central mixing plant. The amount of cement added is that required to give seven-day cube strength of not

less than 10 N/mm2 and 15 N/mm2 for each material, respectively. In addition, for the heavily trafficked roads which require a roadbase, any of the following materials may be used: dense tar macadam, dense bitumen macadam, rolled asphalt, CBM 3 or 4, all of which are detailed in this Chapter. Bituminous-bound roadbases have not been used extensively beneath paver paving, probably because of the relative costs of bitumen and cement-bound materials, rather than for any technical reason. Only one case has been reported in the UK[32], apart from situations where pavers have been used as overlays to existing bituminous pavements. CBM 3 materials are the most popular bound roadbase beneath paver pavements. There is no reason why any material known to be suitable for a roadbase cannot be used for the construction of a sub-base, although this should usually be too expensive. In the UK the laying course materials for paver pavements are usually defined as a clean, sharp concreting sand[33],with less than 3% of silt and clay and not more than 10% retained on a 5mm BS sieve. A low silt/clay content is required to ensure that the sand can be easy to screen to a uniform level and cannot become unstable when wet.

The major contents of UK specification outlined in this Chapter facilitates the progress of the construction and the material types which can be used in the construction of paver pavements rather than to ensure the highest quality of engineering. An example of this is the trial area which allows plenty of initial testing so as to prove the method and materials, after which the trial method is adopted with very little testing. Efficient specifications for all the materials and construction processes used are an essential part of any successful pavement. Many manufactures deliberately increase their range of products to meet particular wishes of clients and to be able to offer a greater choice. To extend or restrict the range of products should be a commercial management decision. Complying with any specification requires the introduction of a quality control system and, increasingly, a quality assurance scheme, which in turn demand sampling and testing procedures to monitor the variation of the products, not just to be assured that they comply with a particular specification but also to be able to predict production trends that will, if left unchanged, cause the product to pass outside the specification limits. BS 6717[19] requires

that the minimum average compressive strength for pavers, based on a sample of 16 pavers, should be 49 N/mm^2, with no individual strength less than 40 N/mm^2. A specification should contain both upper and lower limits for properties of products, such as strength. The manufacturer does not wish to set the average too far above the minimum because increasing strength is usually synonymous with increasing costs. In addition, researche[34,35,36] has shown that in typical highway loading situations, the pattern of stress development in paver bedding sand (laying course) is complex and depend upon the size, shape, orientation and speed of the load as well as paver geometry and laying pattern. Many of the hitherto unexplained bedding sand failures can now be understood by examining the way in which local vertical stress transients develop and travel through bedding sand (see Chapters 6 and 9). For the full interlock, the jointing materials and/or laying course materials must transfer maximum shear and vertical stress transients without any failure[34, 35, 36]. In cases where water is present in sands including a significant fraction of fine material, the mechanism whereby sand instability can develop has been explained. Rapidly changing stress levels can result in pressure developing in water in bedding sand which can lead to instability. It is recommended[34, 35, 36] that sands should be specified which permit water to flow as freely as possible where traffic and water may occur concurrently. The data relating to pavers of different geometries indicates that there are differences in performance of different pavers although the effect is likely to be of minor structural consequence. The only exception to this is the difference between chamfered and non-chamfered pavers. By forcing the load patch inboard of the paver perimeter, chamfered pavers reduce bedding sand stress levels and are therefore to be preferred in trafficked pavements. Because of the described reasons, particularly, the specifications of the strength of laying course materials under different moisture contents are as important as their other defined properties.

References

1 Department of Transport, Scottish Development Department, Welsh Office, Department of Environment for Northern Ireland, (1986), *Specification for Highway Works*, Part:3, HMSO, London, 70pp.

2 British Standards Institution, (1983), *Air-cooled blast furnace slag aggregate for use in construction.* BSI, London, BS 1047.

3 British Standards Institution, (1990), *General requirements and sample preparation and classification tests.* BSI, London, BS 1377: Part 1&2

4 British Standards Institution, (1985), *Method for determination of particle size distribution.* BSI, London, BS 812: Part 103.

5 British Standards Institution, (1980), *Recommendations for testing of aggregates, Compactibility test for graded aggregates.* BSI, London, BS 5835: Part 1.

6 British Standards Institution, (1974), *Batch type concrete mixers.* BSI, London, BS 1305.

7 British Standards Institution, (1992), *Constituent materials and asphalt mixtures* BSI, London, BS 594: Part 1.

8 British Standards Institution, (1988), *Mastic asphalt (limestone fine aggregate) for roads, footways and pavings in building.* BSI, London, BS 1447.

9 Powell, W. D. & Leech, D., (1983), *Compaction of Bituminous Road Materials Using Vibratory Rollers*, Department of the Environment Department of Transport, TRRL Laboratory Report LR 1102, Crowthorne, pp 19, (Transport and Road Research Laboratory).

10 British Standards Institution, *Sampling and examination of bituminous mixtures for roads and other paved areas.* BSI, London, BS 598 Part 104:1989, Parts 105, 106, 107, 108 & 109:1990.

11 British Standards Institution, *Rotary core drilling equipment.* BSI, London, BS 4019 Part 1:1974, Part 2:1973, Part 3&4:1993.

12 British Standards Institution, (1993), *Constituent materials and for mixtures and transport, laying and compaction.* BSI, London, BS 4987:Parts 1&2.

13 British Standards Institution, (1974), *Tars for road purposes.* BSI, London, BS 76.

14 British Standards Institution, *Bitumens for building and civil engineering.* BSI, London, BS 3690 Part 1:1989, Part 3:1990.

15 British Standards Institution, (1992), *Hot rolled asphalt for roads and other paved areas.* BSI, London, BS 594 Parts 1&2.

16 British Standards Institution, (1975), *Dense tar surfacing for roads and other paved areas.* BSI, London, BS 5273.

17 British Standards Institution, *Concrete specifications.* BSI, London, BS 5328 Parts 1&2:1991, Part 3:1990, Part 4:1991.

18 British Standards Institution, (1974), *Method for testing the mixing performance of concrete mixers.* BSI, London, BS 3963.

19 British Standards Institution, *Precast concrete paving blocks.* BSI, London, BS 6717 Part 1:1993, Part 3:1989.

20 British Standards Institution, (1991), *Portland cement.* BSI, London, BS 12.

21 British Standards Institution, (1992), *Information and requirements for all protection relays.* BSI, London, BS 142, Part 1.

22 British Standards Institution, (1991), *Portland pulverized-fuel ash cements.* BSI, London, BS 6588.

23 British Standards Institution, *Pulverised-fuel ash.* BSI, London, BS 3892, Part 1:1993, Part 2:1984.

24 British Standards Institution, (1992), *Ground granulated blast furnace slag for use with Portland cement.* BSI, London, BS 6699.

25 British Standards Institution, (1992), *Aggregates from natural sources for concrete.* BSI, London, BS 882.

26 British Standards Institution, (1986), *Test sieves.* BSI, London, BS 410.

27 British Standards Institution, (1980), *Water for making concrete (including notes on the suitability of the water).* BSI, London, BS 3148.

28 British Standards Institution, *Concrete admixtures* BSI, London, BS 5075, Parts 1&2:1982, Part 3:1985.

29 British Standards Institution, (1975), *Pigments for Portland cement and Portland cement products.* BSI, London, BS 1014.

30 British Standards Institution, (1963), *Calcium chloride(technical).* BSI, London, BS 3587.

31 Department of Transport, (1987), *Structural design of new road pavements.* Department Standard HD 14/87, London, 87pp.

32 Parkinson j.,(1979), *Concrete block paving beats unstable ground*, in New Civil Engineer, London, 38-9.

33 Lilley, A. A., and Clark, A. J., (1978), *Concrete block paving for lightly trafficked roads and paved areas.* Cement and Concrete Association, Wexham Springs, 16pp, Publication 46.024.

34 Knapton, J., Algin, H.M., (1995), *The Mathematical Solution to Interlock in Flexibly Bedded Clay Paving.* Proc. of the 4th. Int. Masonry Conf. No. 7, Vol. 2, p 307-313. London.

35 Algin, H.M., Knapton, J., (1996), *Research into paver interlock*, Jrnl. of the Institution of Highway & Transportation & IHIE, Vol. 43, No. 03, p 20-24.

36 Knapton, J., Algin, H.M., (1996), *The Mathematical Solution to Interlock in Concrete Block Paving.* Proc. of the 5th. Int. Conf. on Concrete Block Paving, p 261-278, Tel-Aviv.

CHAPTER THREE

STRUCTURAL DESIGN OF PAVER PAVEMENTS

Synopsis

This Chapter is concerned with the existing structural design of concrete paver pavements carrying vehicular traffic ranging from trucks to heavy industrial vehicles and aircrafts. Design criteria for such pavements are established and a range of methods for their analysis and design are reviewed. The Chapter also focuses upon the principles of the structurally equivalence thickness technique based on the development of the bedding sand stress calculation method which is presented in Chapters 4, 5, 6, 7, 8 and 9.

3.1 Introduction

This Chapter outlines paver structural design procedures, methods and analytical techniques. Three main current approaches to the analysis of paver pavements can be described.

1) Layered elastic system analyses

2) Finite element analyses.

3) Mathematical analyses in the surface course.

1) Layered elastic system analyses: The layered elastic theory is a conventional and widely used approach to analyse the paver pavement. Such procedures are already well established for conventional flexible pavement design. Some local road authorities recommend a hierarchy of computer-based elastic analyses of the design of road pavements[1]. Here a pavement is modelled as a succession of layers each having linear elastic properties. The stresses and strains throughout the pavement may then be calculated as functions of the load magnitudes and placement and the layer thickness and properties.

2) Finite element analyses: The use of both slab and elastic layer theory presupposes that the paver course can be modeled in terms of an equivalent continuous elastic layer whose properties can be determined by plate load tests, accelerated trafficking studies or Falling Weight Deflectometer measurements. An alternative to this is to use finite element techniques to model the pavers as an articulated surfacing having defined load or displacement transference characteristics at the joints between neighboring paving units. Finite element studies of paver paving have been reported both in Japan and Netherlands. The Japanese study[2] was restricted to a consideration of the paver surfacing. The Dutch study[3, 4, 5, 6, 7, 8, 9, 10] was more comprehensive in that the analysis included an assessment of a complete paver/base/sub-base/subgrade system.

3) Mathematical analyses in the surface course: An alternative format mathematical analysis is developed in this Thesis (see Chapters 4 to 9) in which vertical stresses in the bedding sand are calculated by considering vertical and rotational equilibrium of the pressures applied to the upper and lower horizontal paver surfaces. It is assumed that the paver is structurally rigid in relation to the bedding sand so a planar stress regime can be assumed at the paver/sand interface. This assumption is justified by the values of Young's Modulus which would normally be applied to concrete (30,000N/mm^2) and to sand in compression (300N/mm^2). If tension were to be permitted to develop between the paver and the bedding sand the solution would be relatively straightforward. Tension cannot be developed in uncemented sand so it is assumed that compressive stress is developed in some parts of the interface and zero stress is developed elsewhere. By ensuring vertical and rotational equilibrium, three equations can be developed (one vertical equilibrium and two rotational equilibrium equations, one in each orthogonal direction) which can be solved to obtain the values of the vertical stress in the bedding sand at each corner of the lower horizontal surface of the paver. The stress at any point along the paver boundary can then be determined by linear interpolation. Loading is applied asymmetrically to each paver at all times and the resulting pattern of compressive stress in the underlying bedding sand cannot be calculated on a simple load spreading basis since the laying course material cannot accommodate tensile stress. Before the mathematical stress calculation in the bedding sand can be analysed, it is necessary to select a particular patch loading on a paver. The benefit of this type of analysis is that it provides a very clear understanding of the complex pattern of time dependent stresses in bedding sands when the pavement is subjected to rolling loads. This work is fully described in Chapters 4, 5, 6, 7, 8 and 9.

In this research, a choice had to be made between these three techniques. The finite element method although shown to be capable of closely modelling the observed load/deflection behaviour of paver pavements, is more suited as a research tool than for routine design. In particular the method is slow and requires expert adjustment of the model to account for any change in the properties or sequence of the pavement layers, also

it is difficult to model interfaces between pavers and jointing materials have different elastic properties. By contrast, a wide range of elastic layer analyses are already in common use for pavement design. These analyses may be quickly and easily varied to model a wide range of pavement types even by technically naive users. The mathematical analyses address accurately the nature of interlocking paver pavements at the surface level and provide more accurate inputs for analysing the behaviour of paver pavement's courses beneath the surface.

Accurate computation of stresses and strains in pavement structures consisting of different layers and materials whose behaviour is usually influenced greatly by time, temperature, moisture, etc., is an extremely complex task. Although the use of modern techniques such as the finite element method, in dealing with the non-linear response of pavement materials, is useful as a research tool, it still lacks practical applicability. The most promising design approach still appears to be that based on the use of linear elastic theory. In this approach, the non-linear characteristics of the material can be handled by an iterative process, whereby a different set of values for the elastic constants is used for each stress level. Other changes in material properties with time, temperature and moisture may be dealt with in a similar manner. In addition, the Finite Difference Method[14] may also be used in solving such types of problems. In this method the paver surface is divided into a grid, and a general fourth-order difference equation is developed for each nodal point in the grid. The deflection at any specific point is expressed in an individual difference equation for that particular point, and then is replaced by finite difference equations. Therefore the problem reduces to solving a large number of simultaneous algebraic equations instead of one complex differential equation. The solution produces the value of the deflection at each individual grid point. Once the deflections are obtained, they are substituted into the appropriate difference expressions to determine moments, shear and reactions at the nodal points in the paver. The difference equations for mesh points near or on the boundaries of the paver have to be modified from the general pattern of finite difference coefficients at interior points, in order to satisfy the boundary conditions. The modification of the

boundary conditions is one of the difficulties of the finite difference method, and sometimes limits its use.)

The finite element method has been used for analysing rigid pavements on elastic foundations, considering the subgrade either as an elastic continuum or as a Winkler-type foundation[15] and then this technique has been adapted to the flexible pavements[15] (see Figure 3.1). If a Winkler-type foundation is considered, the subgrade is represented by springs having a constant modulus of reaction Ks. This means that the subgrade reaction per unit area at any point is proportional to the vertical deflection at that point, but independent of the vertical deflection of any other point. If an elastic continuum foundation is considered in the finite element solution, the slab is treated as an assemblage of plate elements, while the foundation is treated as an idealised half-space. A Winkler-type foundation is much more representative than the elastic continuum foundation for paver pavements because of the individual paver behavior of pavements occurs non-interlocking case (see Figure 3.1). The flexibility matrix for the foundation is obtained by determining the deflections at all points for each location of a unit vertical point load. The stiffness matrix of the foundation is obtained by inverting the flexibility matrix. It is then combined with that of the paver to obtain the complete stiffness matrix of the structure.

The existing usage of the finite element method is as follows[8]. The pavement is first divided into individual rectangular elements joined at discrete finite numbers of nodal points. The foundation is considered as consisting of a series of rectangular pressure areas whose centers coincide with and remain in contact with the nodal points of the pavement. The pressure is assumed to be constant within each rectangle (see Figures 3.38 and 3.40). The stiffness coefficients at the nodal points of the foundation are determined by inverting the flexibility matrix of the foundation. The flexibility matrix can be obtained by using the Boussinesq equation, relating the vertical displacement, of the upper surface of an elastic half-space, to an applied vertical force. As a result the finite element method needs correct and appropriate inputs modelling the true behavior of interlocking paver pavements.

Therefore, the result of mathematical analysis can be used in finite element analysis in order to achieve more accurate design procedures for the whole pavement structure, but the accurate behaviour of the paver/bedding sand interface is difficult to model.

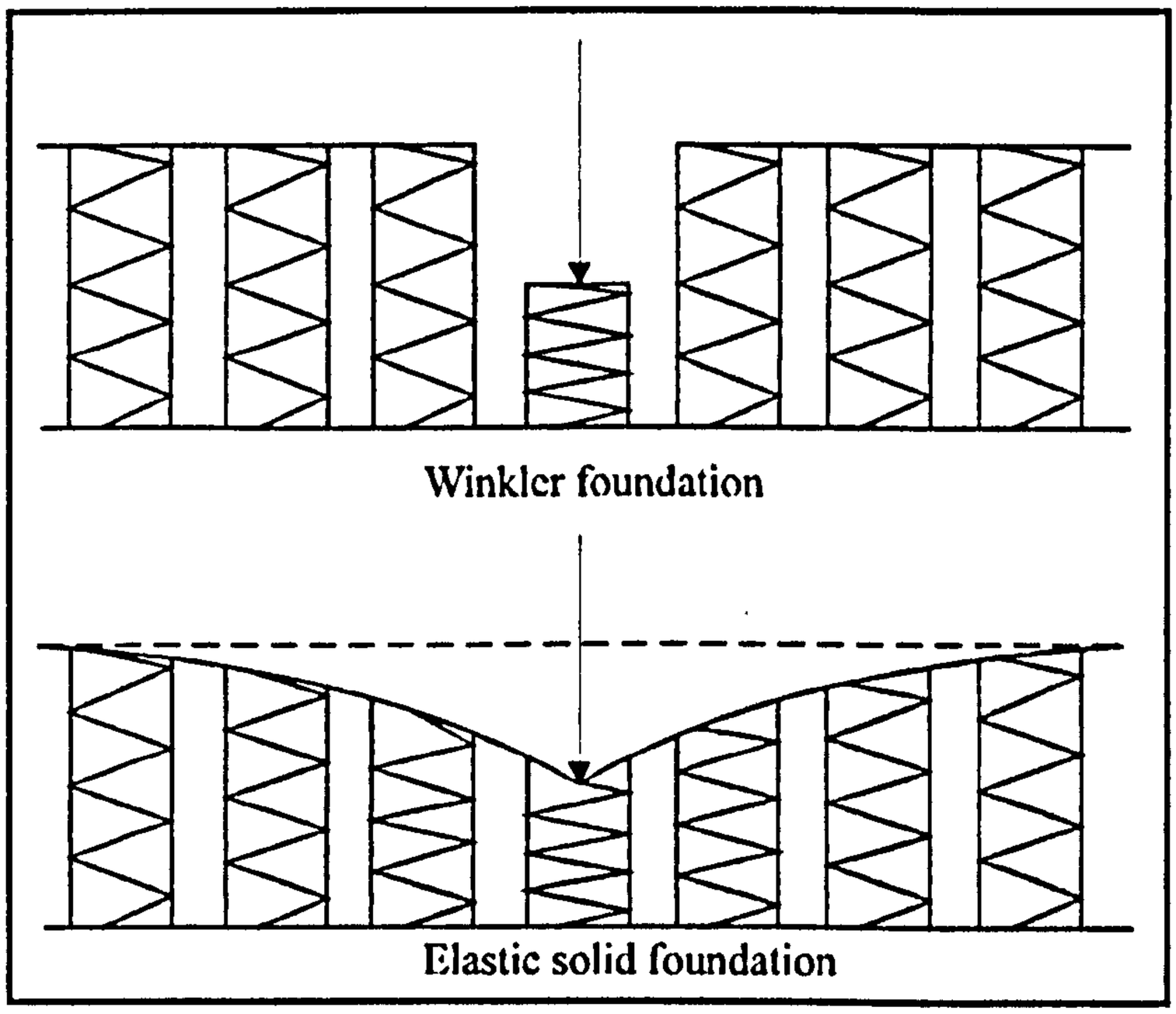

Figure 3.1: Difference between a Winkler subgrade and an elastic subgrade.

A paver pavement incorporating full interlock can sustain high levels of applied load. An interlocking paver pavement can be observed to behave in a manner whereby the pavers act together as a system such that the pavement has more of the character of a flexible homogeneous material rather than that of a collection of individual units behaving independently. Because of this, virtually all of the research into the behaviour of concrete block paving has focused upon establishing relative performance factors between pavers and conventional flexible pavement construction materials. This Chapter also explains design methods based on the flexible behavior of a paver pavement.

3.2. Paver pavement design methods

The identification of the design parameters is crucial to the formulation of a design methodology for paver pavements. It is therefore necessary to understand how pavements behave in service. This can only be possible by studying full-scale paver pavements under the action of actual or simulated traffic. Generally paver pavements tend to perform in a manner which is qualitatively similar. The thickness of pavers can be changed from 60 to 100 mm in practical pavements. Under traffic, paver pavements tend to develop interlock. Once the load-spreading ability of the pavers increases, the rate of accumulation of deformation reduces. When a paver pavement constructed on a granular base course becomes fully interlocked, it reaches a stable equilibrium condition which is unaffected by either the amount of traffic or by the magnitude of the wheel load (within the range from 24 to 70 kN). In the process of developing interlock the pavers behave as a structural layer rather than just as a wearing course. Paver pavements can typically reveal elastic deflections between 1 and 2 mm and yield only small rutting deformations. Consequently, the main design criterion for paver pavements including those with granular bases is that the deformation which accumulates during the development of interlock should be kept within suitable limits so that riding quality and drainage characteristics of the road surface are not substantially impaired. If a paver pavement has a stabilised base or sub-base, large deflections should not be tolerated in the pavement under traffic, although in the case of pavements that include a granular base large deflections may not be harmful to the pavers themselves. They may lead to the development of cracking within the base or sub-base. Once the cracks occur, they may tend to open the joints between the pavers and thereby, destroy or diminish the degree of interlock. In addition, the cracks may assist the progress of the movement of rain water down through the pavement with a consequent loss of strength in the subgrade. For these reasons deflection should be limited to values which will not cause cracking during the design life of the pavement. As a result, the design should include some measure of both load and traffic intensity. In this respect, the load influences the magnitude of the deflection while the traffic intensity can be related to the amount of deflection that can be tolerated if a fatigue failure is to be avoided.

The existing design procedures of paver pavement may be assigned to four basic categories:

1-) Design based on experience;

2-) Design based on field experience and laboratory tests (empirical design method);

3-) Design based on equivalence;

4-) Design based on mathematical models.

3.2.1. Design based on experience

Here, block and base thicknesses are chosen on the basis of experience. Not only must the existing pavement be materialistically the same, but also it should be old enough, and able to maintain satisfactory long term performance according to road construction specifications. The design procedures are often presented as a design catalogue which is a summary of local knowledge (see Figures 3.2, 3.3 and 3.4). The materials to be used in the catalogue are standard materials and it is not possible to adjust for better or poorer materials. The catalogues do not give any indications on what will be the performance of the different structures. It is therefore severely restricted since they cannot be extended beyond the bounds of the constraints used in the initial development.

3.2.2. Design based on field experience and laboratory tests (empirical design method)

Until the publication of the Department of Transport's present guide[19] for highway pavement design in 1984 all categories of highway pavement in the UK were designed according to Road Note 29[20]. This manual provides the design background for road construction. It is based on the performance of experimental roads interpreted in the light of structural theory. The advances which have been obtained from the research of the Transport Research Laboratory have been used to develop a new method for the structural design of road pavements. The structural design has been used for bituminous roads in order to build public road networks. Design curves were developed to measure

the thickness of each layer and all pavement thicknesses in terms of traffic volume and strengths of the subgrade. The empirical method of design was used in developing Road Note 29[20]. However, according to the TRRL Laboratory Report 1132[19], the empirical method of design does not provide a satisfactory basis for the design of roads for traffic levels such as those observed on experimental roads. Furthermore, this method does not accommodate for new or improved materials. After the publication of Road Note 29[20], experimental roads have carried more traffic, some over 20 msa, and for new design procedures, the effect of traffic volumes has been taken into consideration in order to design pavements. This was done by Monismith and Witczak[21] in 1983. The TRRL Laboratory Report 1132[19] is based upon stress analysis supported by the previous empirical experiments. For many conditions, the dynamic stress and strain that come from changing traffic loads can be calculated with reasonable accuracy using a multi-layer linear elastic model.

The stress of each layer can also be calculated, taking into account the variation in stiffness of bituminous materials with changing temperature. These calculations are necessary using cracking and deformation data (based on laboratory testing) for long-term performance. The results are suitable for characterising the stress and strain behaviour of pavements. Prediction of long-term performance from them is much less certain. Road pavements which demonstrate long-term performance are based on models in Laboratory tests which attempt to simulate conditions whereby road pavements are much simplified.

Although the results of these tests are generally suitable for the determination of the dynamic stress and strain behaviour of pavements, determination of long-term performance is much less limited. Some assumptions are made to simplify calculations such that the materials of pavements are treated as idealised material (It is assumed that idealised material treat as homogeneous or isotropic layers). As a result structural theory has been used quite often in many complex models developed with the principally objective of characterising particulate material used in road construction. Specifically inhomegenious particulate materials. Road Note 29[20] had been used for 20 years before 1970. Further significant increases have been observed of the damaging

power of commercial vehicles since 1970, when the last third edition of Road note was published.

3.2.2.1. Design criteria for designs based on field experience and laboratory tests (empirical design method)

The basis of mechanistic design method is that pavements must adhere to structural criteria to give satisfactory service. TR 1132[19] explains that the more important design criteria are (see Figure 3.5):

- When the subgrade sustains traffic loading, excessive deformations that are controlled by the vertical compressive stress or strain at formation level, are not desired.
- The cracking of bituminous and cement bound materials used in roadbase designs are not desired for long life performance under the influence of traffic. Horizontal tensile stress or strain, at the bottom of the roadbase must be considered to provide control.
- In order to create a satisfactory construction platform the load spreading ability of granular sub-base and capping layers must be sufficient.
- The internal deformations of considerable thickness of bituminous materials must be restricted. These deformations are a function of their creep characteristics.

In practice, other factors also have to be considered such as the effects of drainage.

The basic inputs that must first be acknowledged for road design include the determination of design life, the traffic loading and strength of the subgrade on which the road is to be built. According to TRRL 1132[19] these basic inputs must be taken account in the first stage of road design.

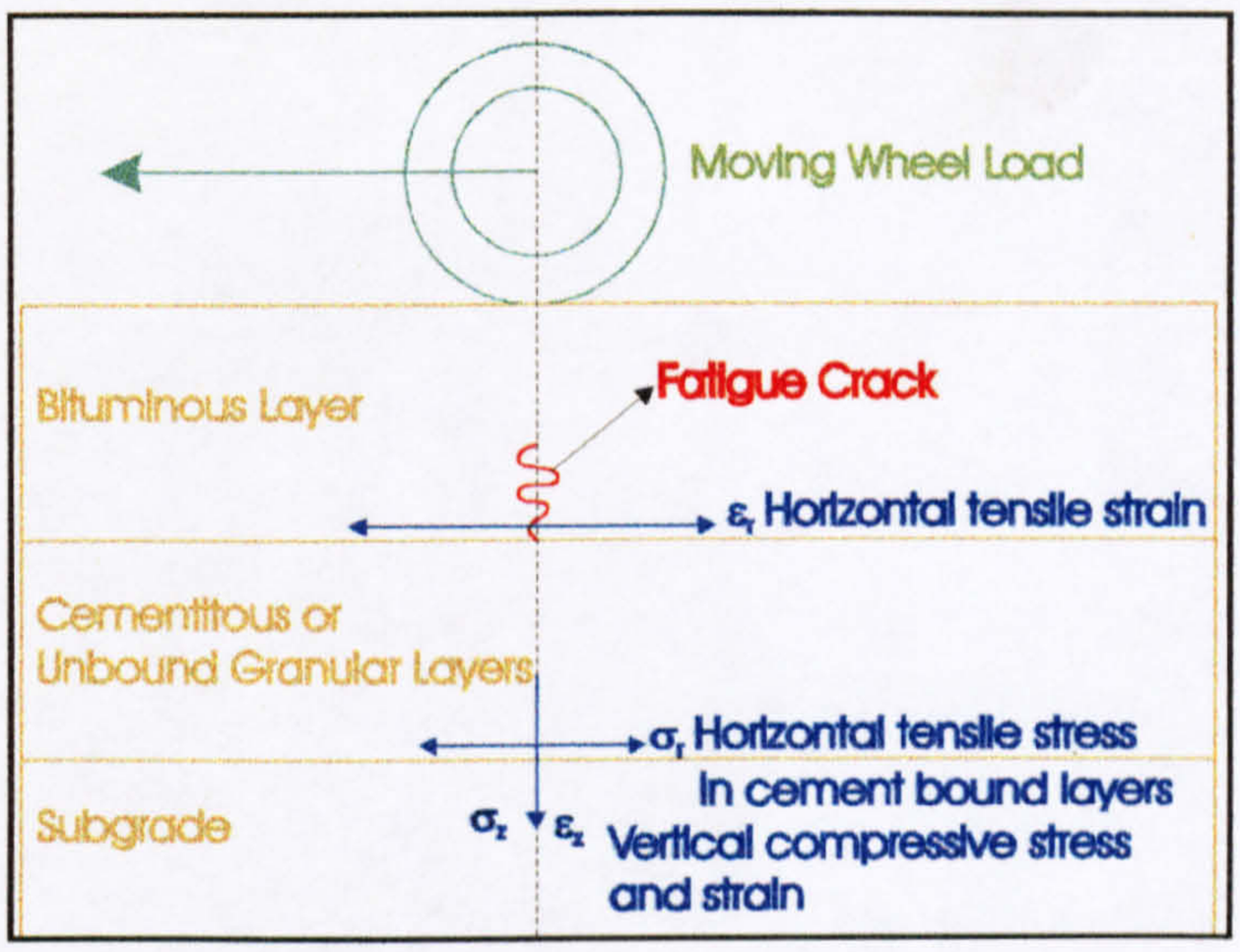

Figure 3.5: Critical stress and strains in a bituminous pavement.

3.2.2.2. Design life considerations for design based on field experience and laboratory tests (empirical design method)

The recommended design life according to Road Note 29[20] and LR 1132[19] is 20 years for bituminous roads and 40 years for concrete roads. In addition, the end of the design life was associated with surface ruts of 20 mm in the case of flexible pavement or cracking, and crazing in the case of rigid pavement. Roads in a failed state such as this are in need of a strengthening overlay or partial reconstruction. However, it is added that strengthening a pavement in such damaged conditions does not necessarily result in satisfactory subsequent performance.

TRRL 1132[19] showed how Lister[22] (1972) examined the surface state of the road and distinguished between both sound and critical conditions. The basis of this approach was the comparison between surface condition and structural integrity. Lister[22] (1972) defined the beginning of critical structural conditions such as rutting or the onset of cracking in the wheel paths. In the analysis of the performance of experimental roads, when the rutting in the wheel path is greater than 10 mm or when cracking is seen, the design life has been decided as a surface condition. When there is indication of damage to the road it is best to overlay at this point instead of allowing the road to achieve critical damage conditions. This is not only cheaper but also takes advantage of the

stability of the existing road structure. Failure to strengthen the road at the onset of surface failure may lead to structural failure and the resulting remedial work will then involve complete road reconstruction.

Abell[23] (1983) recommended that the initial design life might be longer than 20 years. Furthermore he states that when design life is calculated, variability of pavement performance, cost of traffic delay and other extra costs must be taken into account. Figure 3.6 summarised his work.

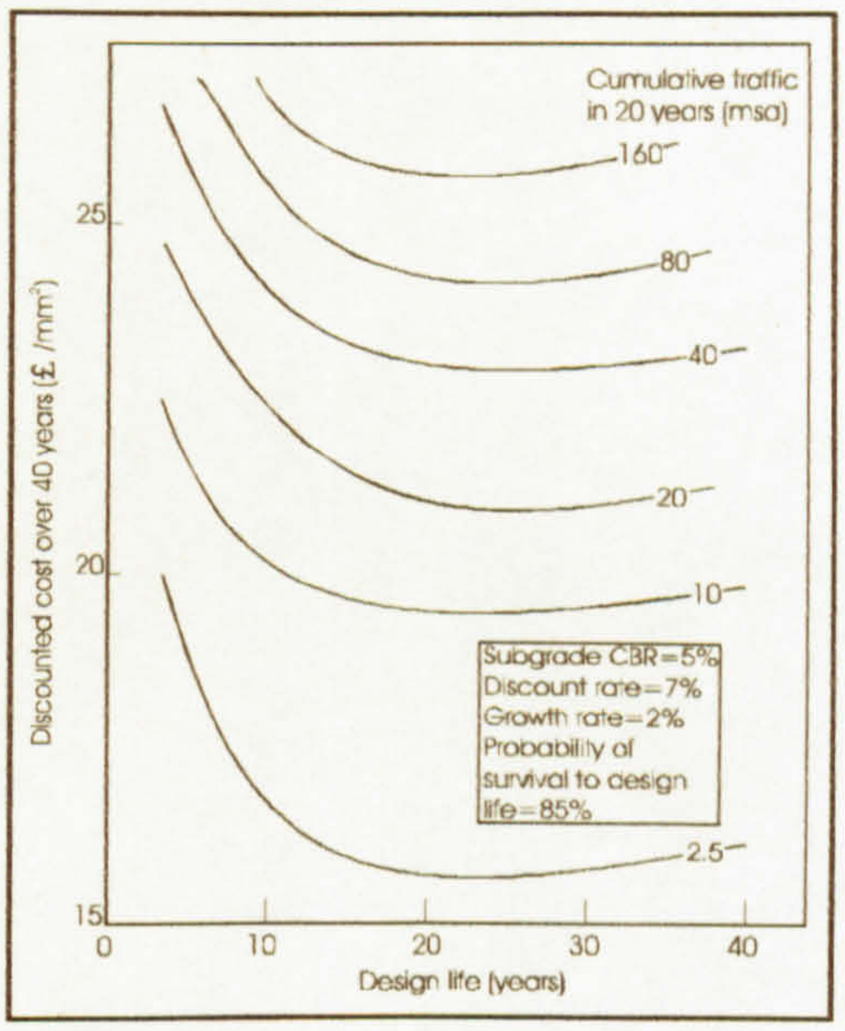

Figure 3.6: Discounted cost over 40 years for different design lives of roads with a bituminous roadbase.

Accordingly it can be noted that for bituminous pavements, the optimum design life costs shown for 40 years life does not differ markedly from 20 years costs. Abell[23] states that roads would survive with 85 per cent probability without requiring a strengthening overlay to extend their lives. This design that uses 10 mm rut criteria for structural deterioration will give a longer life than Road Note 29[20] which is based on 20 mm rut deterioration. Using deflection measurements, the life of the road can be extended by using strengthening overlay methods unless there are some factors that deter the overlay approach.

The method which Abell[23] (1983) uses is not very sensitive because it cannot predict the design life for 40 years. This method has risks and analysis is more complex. 20 years design life seems more appropriate. At the end of the 20 years, the life of the road can be extended, structural deterioration can be reconstructed, and may be adapted to the real design life. Roads can be re-aligned or widened to accommodate increased traffic density.

3.2.2.3. Traffic considerations for design based on field experience and laboratory tests (empirical design method)

Cumulative numbers of 80 kN standard axle loads are taken as a criteria in Road Note 29[20]. The designer has to estimate the number of standard axle load from the number of commercial vehicles. This is referred to as the vehicle damage factor on motorways and other heavily trafficked roads. Currer and O'Connor[24] (1979) suggested that vehicle damage factors should be calculated for the design of new roads. Later, Addis and Robinson[25] (1983) developed an equation for calculating the total number of commercial vehicles using the slow lane of a public road carriageway T_n, over a design life of n years, based on a knowledge of the initial traffic flow F_0 and for an annual growth rate of r. Their equation is:

$$T_n = 365\, F_0 \frac{\left[(1+r)^n - 1\right]}{r} \qquad (3.1)$$

If r=0, that is no traffic growth is anticipated, then the equation reduces to:

$$T_n = 365\, F_0\, n \qquad (3.2)$$

It has also been determined that the number of standard axles per commercial vehicle, i.e. the vehicle damage factor, can be calculated from:

$$D = \left(\frac{0.35}{0.93^{t} + 0.082}\right) - \left(\frac{0.26}{0.92^{t} + 0.082}\right)\left(\frac{1.0}{3.9^{\left(F/1550\right)}}\right) \quad (3.3)$$

Where:
D: The vehicle damage factors.
t: year of opening relative to 1945 (e.g. t for a road to be opened in 1996 = 1996 - 1945 = 51).
F: average annual daily flow (AADF).

From equations 3.1 and 3.2, Table 3.1 has been calculated and shows the total number of commercial vehicles after 20 years, for initial daily commercial vehicle flow (IDCVF) of 50 to 1000 and for annual traffic growth rates from 0 to 5%.

	Growth Rate %					
IDCVF	0	1	2	3	4	5
50	0.37	0.40	0.44	0.49	0.54	0.60
100	0.73	0.80	0.89	0.98	1.09	1.21
200	1.46	1.61	1.77	1.96	2.17	2.41
300	2.19	2.41	2.66	2.94	3.26	3.62
400	2.92	3.21	3.55	3.92	4.35	4.83
500	3.65	4.02	4.43	4.90	5.43	6.03
600	4.38	4.82	5.32	5.88	6.52	7.24
700	5.11	5.63	6.21	6.87	7.61	8.45
800	5.84	6.43	7.09	7.85	8.70	9.66
1000	7.30	8.04	8.87	9.81	10.87	12.07

Table 3.1: Cumulative number of commercial vehicles-millions; design life=20 years

Table 3.2 shows the calculated values for vehicle damage factors, from equation 3.3, for public roads opening in the UK any year from 1990 to 2020.

	Daily flow of commercial vehicles ADDF								
Year	50	100	200	300	400	500	600	800	1000
1990	0.55	0.65	0.84	1.02	1.18	1.32	1.46	1.69	1.89
1992	0.60	0.71	0.90	1.08	1.25	1.40	1.54	1.78	1.98
1994	0.65	0.76	0.96	1.14	1.31	1.47	1.61	1.86	2.07
1996	0.69	0.81	1.01	1.20	1.38	1.54	1.68	1.94	2.16
1998	0.74	0.85	1.07	1.26	1.44	1.60	1.75	2.02	2.24
2000	0.78	0.90	1.12	1.32	1.50	1.67	1.82	2.09	2.31
2002	0.83	0.94	1.17	1.37	1.55	1.72	1.88	2.15	2.38
2004	0.87	0.99	1.21	1.42	1.60	1.78	1.93	2.21	2.44
2006	0.90	1.02	1.25	1.46	1.65	1.82	1.98	2.26	2.50
2008	0.94	1.06	1.29	1.50	1.69	1.87	2.03	2.31	2.55
2010	0.97	1.09	1.32	1.54	1.73	1.91	2.07	2.36	2.60
2012	1.00	1.12	1.36	1.57	1.77	1.95	2.11	2.40	2.64
2014	1.02	1.15	1.39	1.60	1.80	1.98	2.14	2.43	2.68
2016	1.05	1.17	1.41	1.63	1.83	2.01	2.17	2.47	2.71
2018	1.07	1.20	1.43	1.65	1.85	2.03	2.20	2.49	2.74
2020	1.09	1.22	1.46	1.67	1.87	2.06	2.23	2.52	2.77

Table 3.2: Vehicle damage factors

3.2.2.4. Subgrade considerations for design based on field experience and laboratory tests (empirical design method)

In the design of road pavements, the strength and stiffness of the subgrade are required to fulfil two design functions:

- to characterise the subgrade as a foundation of the road to carry traffic.
- to find out the likely in-service long-term strength and stiffness of the subgrade after the construction stage.

The stresses of the subgrade resulting from traffic loads must be reduced until the deformation is at the prescribed level at the end of the design life. The strength and stiffness of the subgrade are directly related to the magnitude of stresses at the formation level. Thereby, the stresses and strains experienced by the overlayers are directly influenced by the stiffness of subgrade.

Moisture conditions directly affect the stiffness and strength of the subgrade. It is assumed that during the in-service life of the pavement, both pavement and foundation should be drained. The values of subgrade stiffness and strength related to moisture conditions of the subgrade in the design of a road is taken into account under wet conditions. These however might differ significantly from their values in dry weather.

The relationship between the various physical properties of a soil and its stiffness and strength are complex and vaguely understood. The California Bearing Ratio (CBR) test (see Section 1.4.4.) is used for the assessment of stiffness and strength in spite of its limited accuracy. However, the CBR test gives unrealistically low results on wet cohesive soils near saturation. For the design of new roads it can be applied to laboratory samples that have been compacted at the appropriate field moisture content. It can also be used to test material in-situ. This situation is very useful because subgrade strength needs to be measured when existing roads are being reconstructed. This can be done by in-situ CBR testing in pits or by making bore holes and using the cone penetrometer described by Black[26] (1979). According to the TRRL 1132[19], for the

cohesive soils CBR can be estimated with a soil suction method described by Black and Lister[27] (1979). Measurements of the stiffness modulus of subgrade soil is necessary to calculate stress and strain in the road pavement and in the subgrade soil. The value of CBR is a measure of stiffness, at large strain and low strain rate.

$$E = 17.6(CBR)^{0.64} \text{ MPa} \qquad (3.4)^{19}$$

Where CBR is in per cent; this can be used between 2 and 12 per cent

3.2.2.5. Capping layer considerations for design based on field experience and laboratory tests (empirical design method)

If the CBR of the subgrade is less than 5 per cent, the Department of Transport[28] (1978) suggested using a suitable capping layer constructed from low costs local available materials. In addition, the capping layer reduces the risk of damage during construction by providing a firm platform for compaction of the sub-base. Cement-bound materials above the capping layer can improve the structural contribution of these layers. Black and Lister[27] (1979) observed that extra capping layer eliminates any reduction in the strength of subgrade.

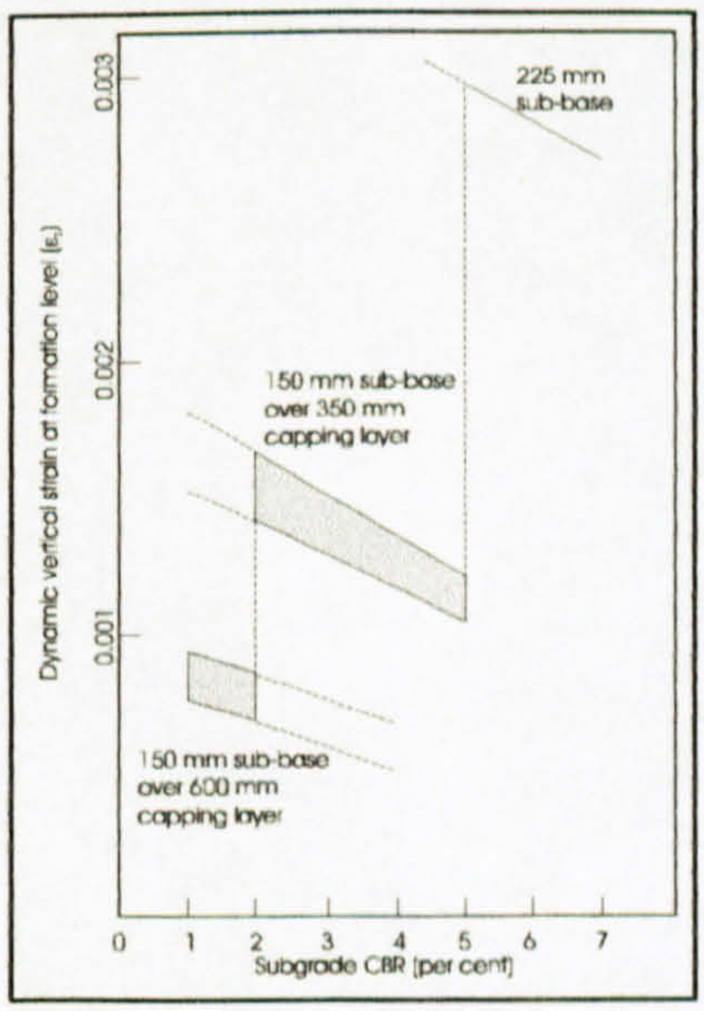

Figure3.7: Dynamic vertical strain at formation level beneath a 40 kN wheel load

For capping layers, analysis of dynamic vertical strain, for various combination of capping layer stiffness and thickness, has been performed for 150 mm sub-base. This is illustrated in Figure 3.7.

3.2.2.6. Sub-base considerations for design based on field experience and laboratory tests (empirical design method)

Sub-bases that use granular material are structurally meaningful and provide a working platform for transportation, laying and compaction. This layer must be frost-resistant and unyielding to the action of weather. In wet weather, cement-bound sub-bases may be preferred. For construction of granular sub-bases and cement bound sub-bases, linear elastic theory can be used. The stress generated by construction traffic and temperature in a cemented sub-base will generally cause it to crack. The magnitude of the crack will be influenced by the amount of traffic, strength and thickness of the sub-base and the stiffness of the subgrade and any capping layer.

$$\text{Log}N_{75} = \frac{h(CBR)^{0.63}}{190} \text{ -------} \quad (3.5)$$

where:
h: the thickness (mm) of granular material required to limit rut depth to 75 mm for a given traffic level and subgrade CBR.
N: the number of standard 80 kN axle.

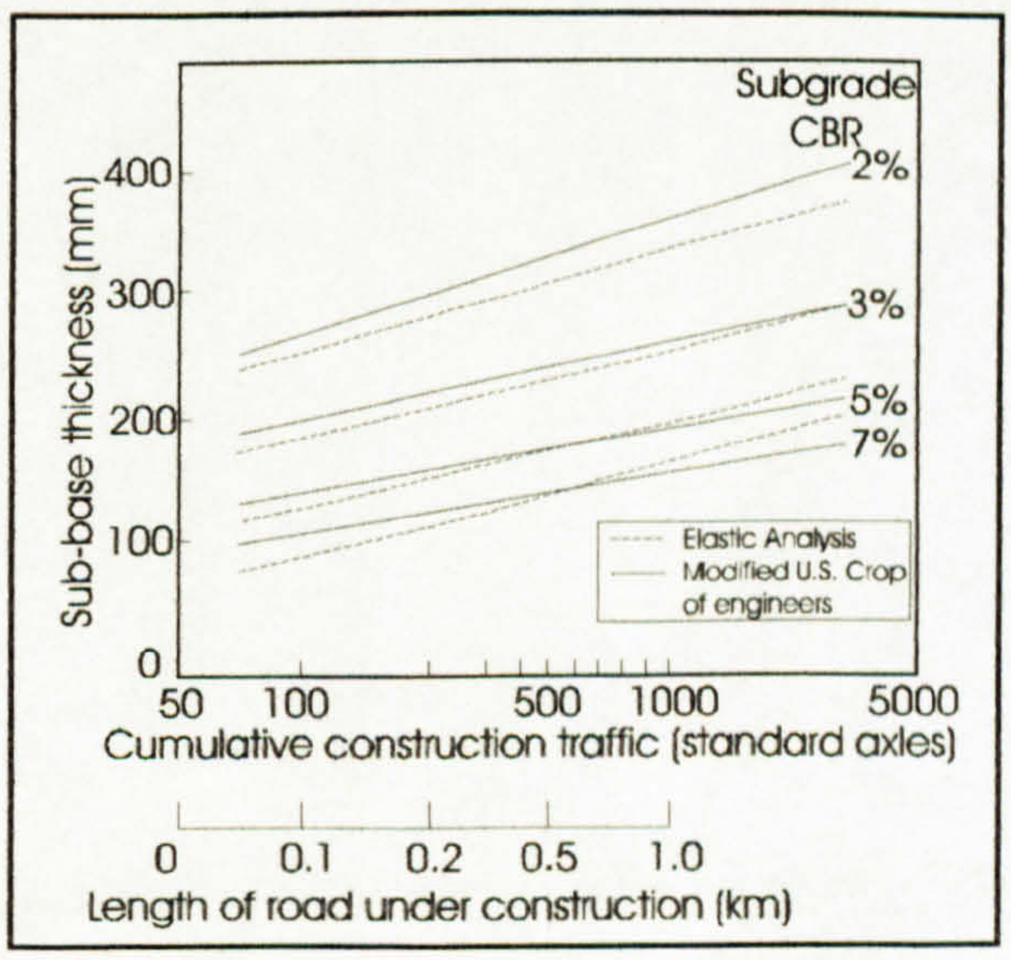

Figure 3.8: Thickness of sub-base required to carry construction traffic

Tests on unpaved roads were carried out by the US Corps of Engineers[29] to determine the thickness (h) mm of granular material required to limit rut depth to 75 mm. N is the number of standard 80 kN axles. The formulation was developed by Webster and Alford[30] (1978) and characterized by Giroud and Noiray[31] (1981). In addition, for limited deformation, about 40 mm, the following equation was demonstrated by Pike, Acott and Leech[32] (1977).

$$\text{Log}N_{40} = \frac{h\,(CBR)^{0.63}}{190} - 0.24 \qquad (3.6)$$

where:
h: the thickness (mm) of granular material required to limit rut depth to 75 mm for a given traffic level and subgrade CBR.
N: the number of standard 80 kN axle.

This equation has been used to determine the thickness of sub-base required for different levels of cumulative construction traffic as shown Figure 3.8.

3.2.2.7. Multi-layer linear elastic analysis to paver pavement design

A design method developed by Barber and Knapton[33] has been formulated in a way which preserves the engineers' freedom to specify sub-base and base material types and thickness in the pavement. This method was the paver pavement design method based upon multi-layer linear elastic analysis to be used widely. Therefore, it is described in detail. Barber and Knapton[33] define four primary requirements for a pavement:

1-) Low cost of construction.
2-) Low maintenance costs.
3-) High reliability.
4-) Known design life.

It is assumed that paver pavements with cement bound bases are the best solution available for these requirements. It is also stated that a successful design should take the following parameters into account:

- port layout and operation (Barber and Knapton[33]'s paper was written in the port pavement context)
- future uses and development
- type of trafficking (vehicle speeds; wheel loadings; number of loadings)
- static loading (point loads; impact loading)
- surface pollution (hydraulic oil; de-icing salts)
- strength of subgrade
- anticipated settlement (short term; long term)
- climate
- availability of local materials

The development and use of a series of design charts that have been derived from a basic design philosophy was described by Barber and Knapton[33]. The wide use of computers supported the development the semi-analytical approach in highway design and this made it possible to extend the empirical design rules beyond their original bounds to include motorways and industrial pavements. The most successful of these analysis techniques has been the multi-layer elastic model. It was stated that several computer programs of varying degrees of complexity had been developed, and their work used a simplified analytical technique developed by Ullidtz and Peattie[34]. This has been adopted because of its speed of execution, particularly when several hundred pavement structures are being analysed, as was the case for each design chart. The pavement model used in this work is illustrated in Figure 3.9. The assumption was that the contact area between the tyre and the pavement was circular with a contact stress equal to the tyre pressure. The analysis program gives the vertical stress and strain, and the radial strain at each interface. Two design criteria have been established and generally applied to pavements:

1-) Fatigue cracking of base material.

2-) Progressive vertical deformation of the subgrade.

In the structure of the paver pavement, the tensile radial strain at the bottom of the bound layer and the compressive vertical strain at the top of the subgrade were considered as the two design parameters. A relationship was developed between these two strains and the design life, i.e. numbers of load repetitions to failure of the pavement. These critical strains for a whole range of pavement structures were established and the results were plotted as a design chart. Figure 3.10 was given as an example of design charts. For each chart the following variables are held constant:

- Surfacing (material type - 80 mm thick concrete pavers)
- Base (material type - cement bound material)
- Sub-base (material type, granular; thickness; elastic modulus)
- Subgrade (CBR - California Bearing Ratio)

The variables for each chart are:

- Base (thickness; elastic modulus)
- Loading (magnitude of loading)

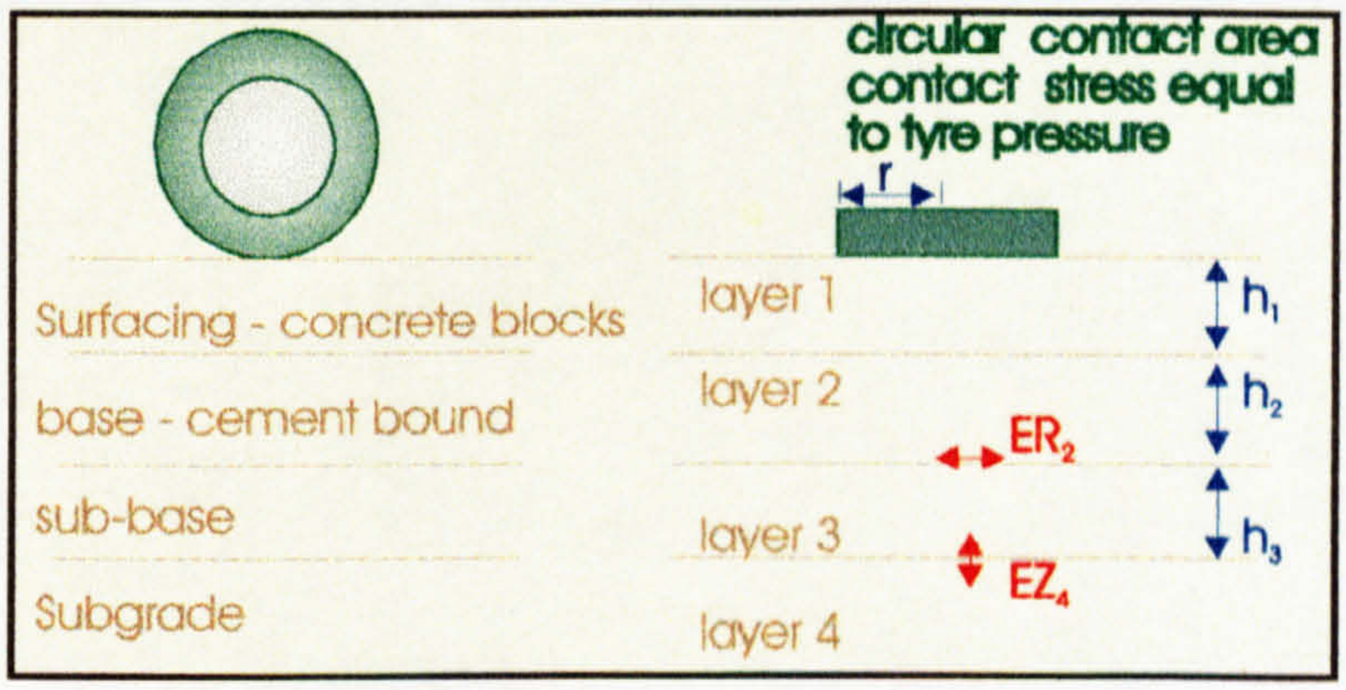

Figure 3.9: Pavement model developed by Barber and Knapton[33]. ER_2 is the critical strain in the base, EZ_4 is the critical compressive strain in the sub-base.

On each chart an example line has been drawn showing how the graphs are related:

i-) The strength of the basecourse, i.e. its elastic modulus, is the starting point on the ordinate of the bottom graph. Project horizontally to the intercept of the curve representing base thickness and then vertically to the centre graph.

ii-) This graph has two ordinate scales; the one on the left is the tensile radial strain at the bottom of the bound layer and the right hand scale is the compressive vertical strain at the surface of the subgrade (both are scaled in microstrain). Unlike highway design, where there is a statutory maximum axle load for pavements, in port areas the maximum load is variable. Consequently the central graph has a series of curves representing the magnitudes of loading, which are given in Port Area Wheel Loads' (PAWL's) increasing in multiples of two.

iii-) The two outer graphs represent the fatigue characteristics of the pavement base, on the left, and the subgrade, on the right. Thus projecting horizontally across both outer graphs and descending to the abscissae gives the anticipated design life for each constraint. The actual design life is the lower of the two values.

The wheel loading is characterised in terms of the Port Area Wheel Load, or PAWL, which is defined as a 12 tonne wheel load with a damaging factor of unity. Table 3.3 gives typical values for handling equipment in common use. The design charts given in Barber and Knapton[33]'s paper cover a range of subgrade strengths, Figure 3.10 gives a typical example of the design charts for CBR 5% with a surfacing of 80 mm concrete pavers. Table 3.4 gives typical values for the elastic moduli of various base materials necessary for the input in (i). Barber and Knapton[33] suggest that if possible the true values should be established from laboratory tests since they are dependent on the characteristics of locally available materials.

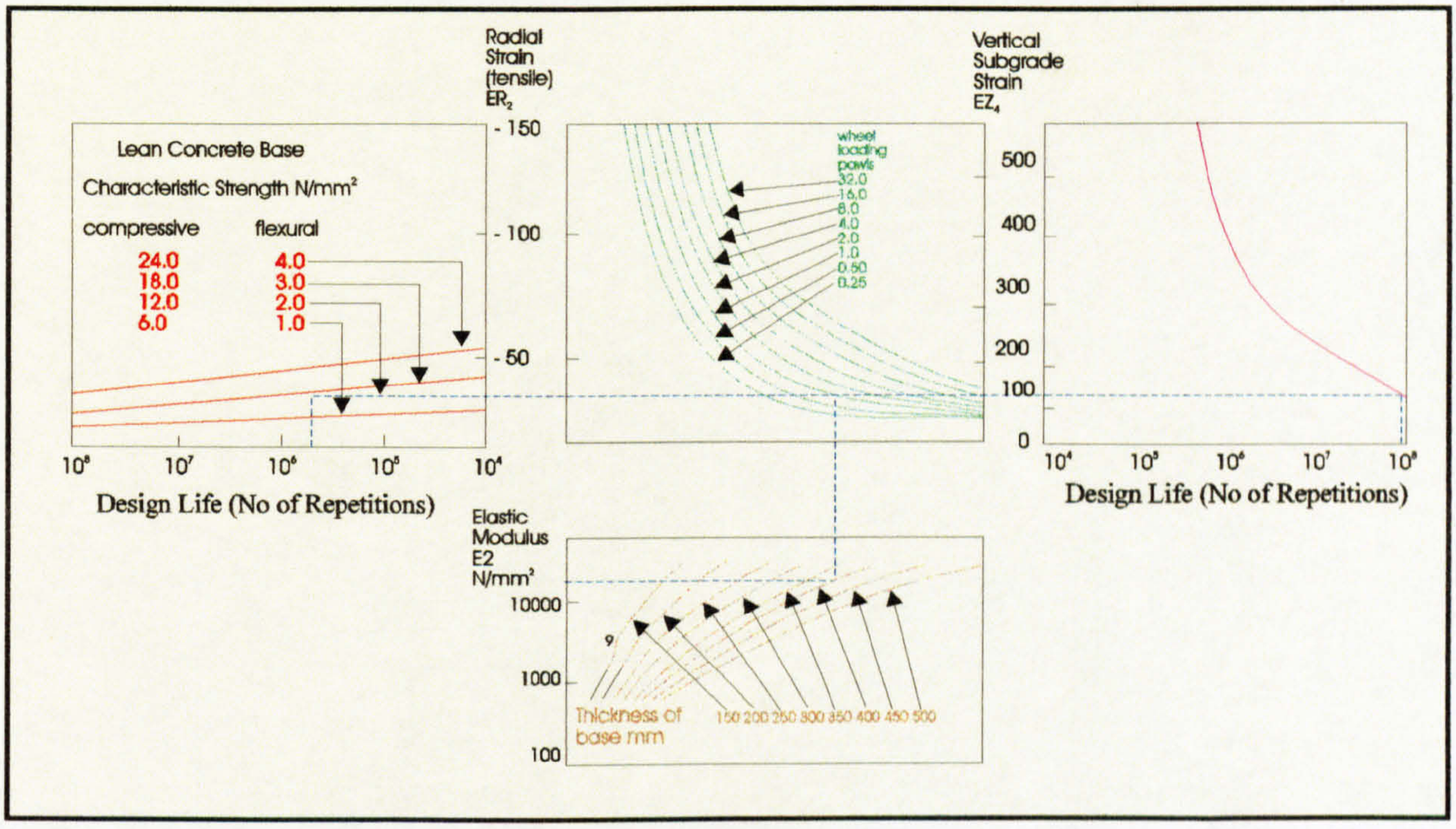

Figure 3.10: The design chart cover a range of subgrade strength, CBR 5%, with a surfacing of 80 mm concrete pavers.

Type of vehicle	PAWL ratings		
	unladen	average laden	most damaging wheel load
Road trailer	0.00	0.02	0.02
20 ft terminal trailer			
1x20 ft containers	0.01	0.10	0.14
2x20 ft containers	0.01	0.94	1.55
40 ft terminal trailer			
1x40 ft containers	0.01	0.05	0.02
2x24 ft containers	0.01	0.26	0.18
2x40 ft containers	0.01	0.39	0.25
4x20 ft containers	0.01	2.62	2.01
Front lift trucks			
23.5 t capacity	0.80	10.0	15.0
28.0 t capacity	1.05	11.0	17.5
37.0 t capacity	5.0	20.0	35.0
Straddle carrier			
4 wheels	0.80	3.00	2.06
8 wheels	0.80	1.40	0.60

Table 3.3: Typical Pawl values for handling equipment in common use.

It was stated by Barber and Knapton[33] that there are two principal elements in a pavement:

Surfacing. Should be of a high durability and strength to resist the severe surface loads and high contact stresses.

Base. The principal structural component of the pavement that spreads the load so the subgrade is not overstressed.

	Compressive Strength N/mm²	Flexible Strength N/mm²	Elastic Modulus N/mm²
Lean concrete	6 12 18 24	1 2 3 4	27,000 35,000 42,000 48,000
Cement Bound granular material	3 6 9 12	0.6 1.0 1.5 2.0	15,000 17,000 20,000 22,000
Soil Cement	2.5 5.0	0.5 1.0	3-7,000 5-11,000

Table 3.4: Typical values for the elastic moduli of the various base materials.

A secondary element is the sub-base that is provided where the pavement is constructed over a weak subgrade to give extra strength at low cost and to provide a good working surface for subsequent construction.

Despite the variety of pavements most structures can be divided into one of six broad categories, as indicated in Figure 3.11. It was assumed that asphaltic materials have been used extensively for both highway and aircraft pavements and their applications to industrial paving seemed logical. However, three characteristics of the asphaltic mix have resulted in an overall poor performance in port applications:

1-) The stiffness, or strength, of a bituminous material decreases as the temperature rises.

2-) The stiffness of a bituminous mix decreases as the loading time increases; i.e. the slower the vehicle the lower the strength.

3-) Surface oil pollution slowly dissolves the bituminous binder, leaving it more susceptible to scuff and frost attack.

Figure 3.11.

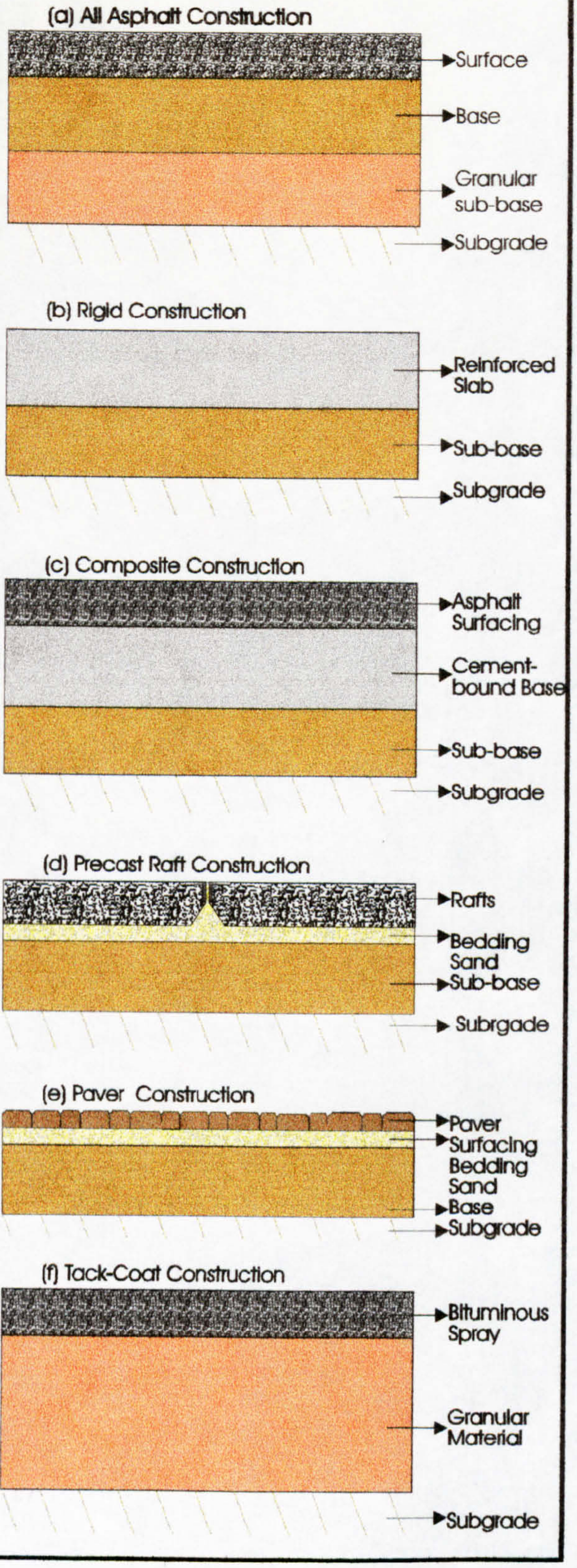

Figure 3.12.

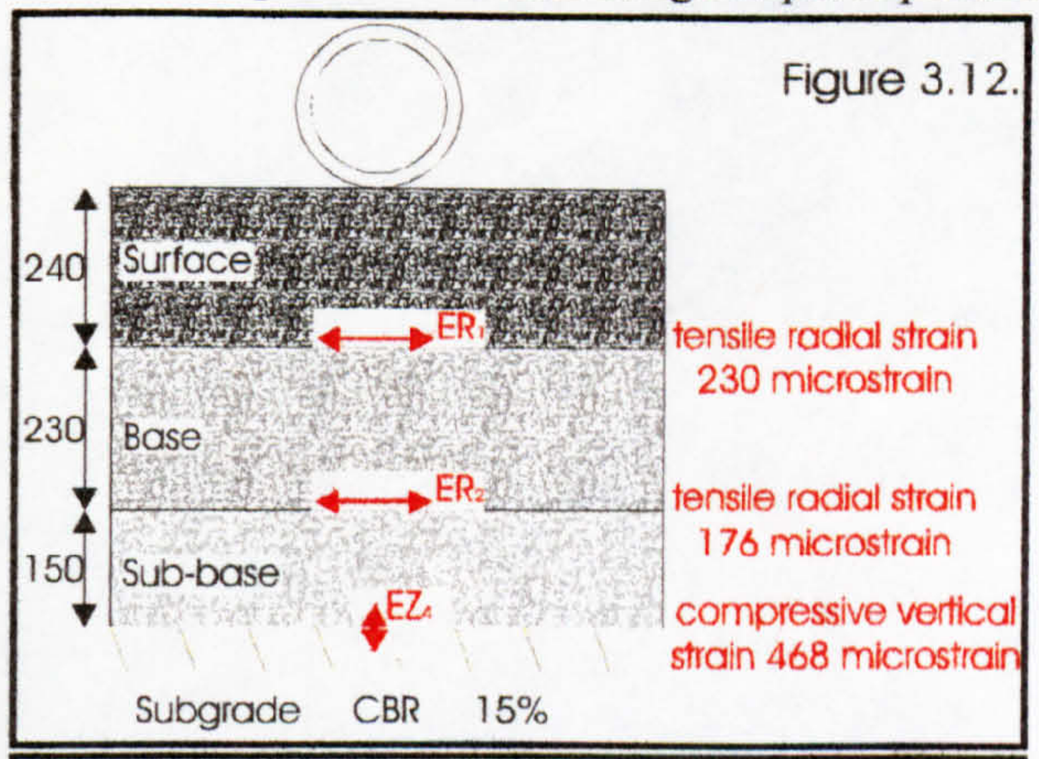

Figure 3.13.

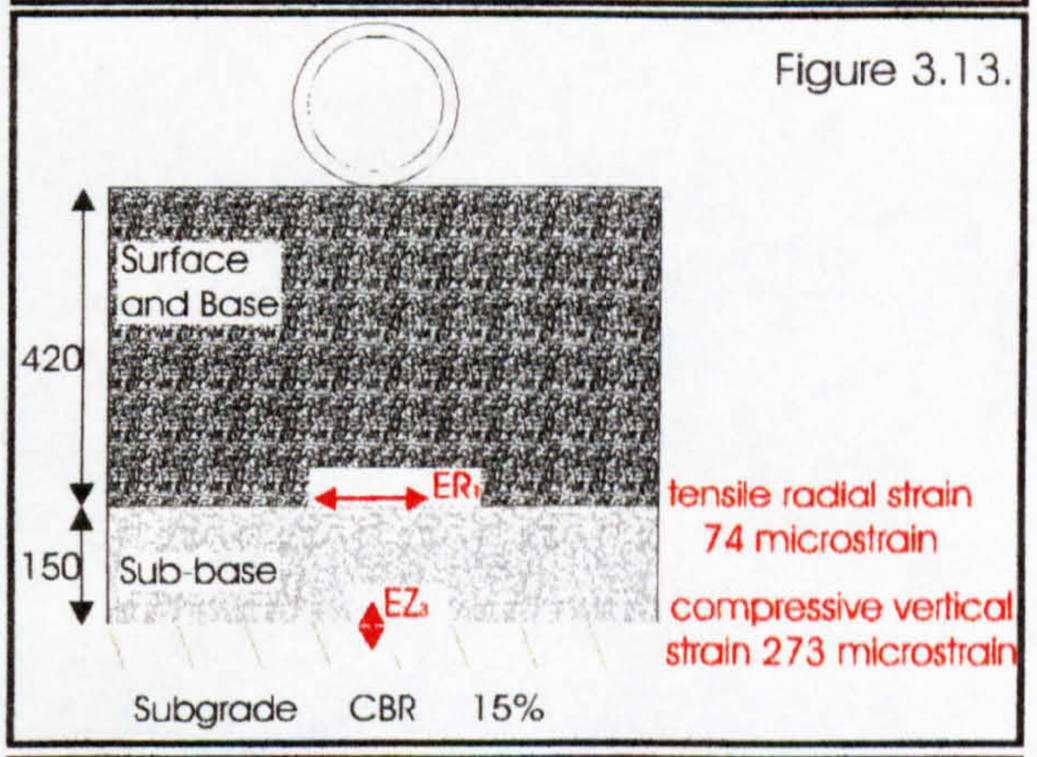

Figure 3.14.

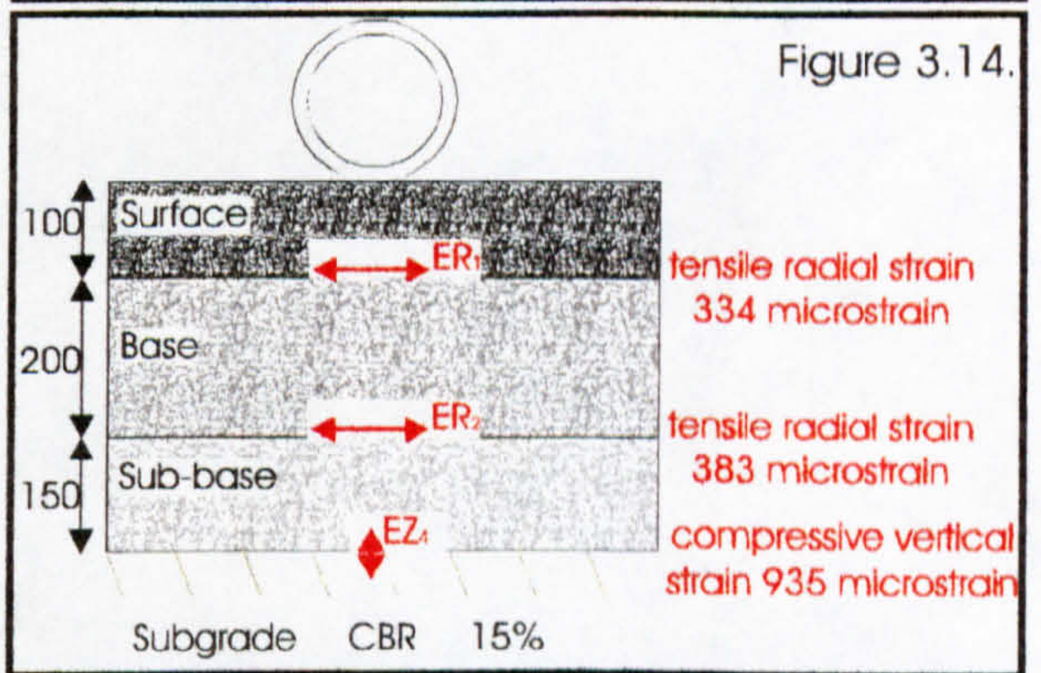

Figure 3.15.

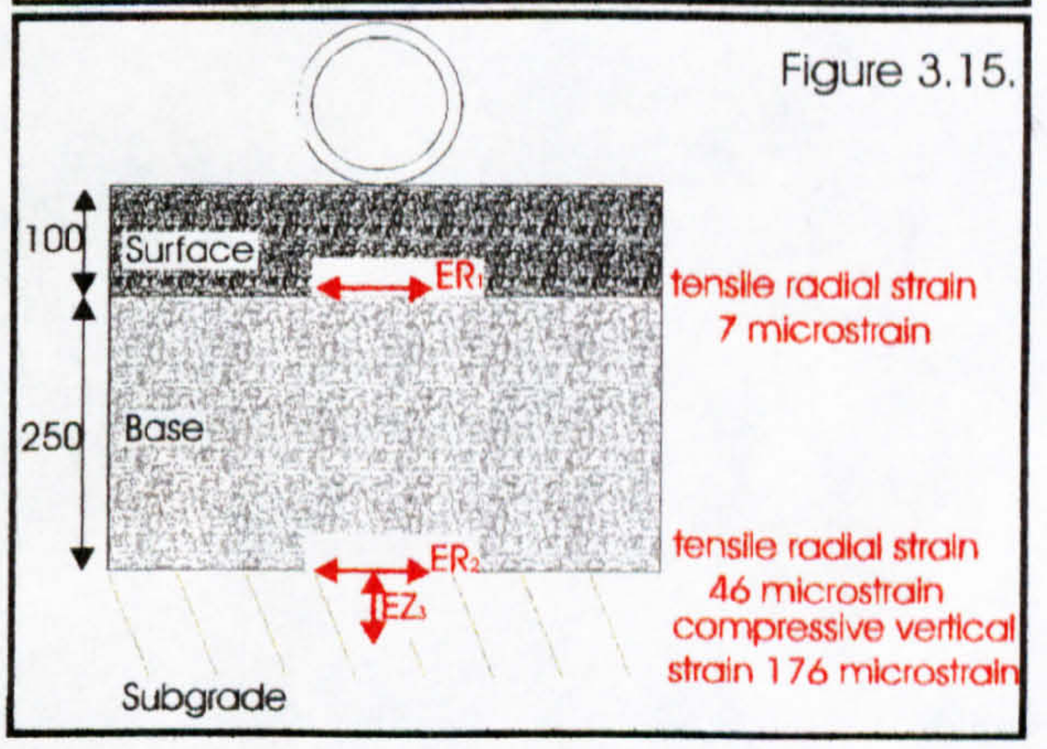

Figure 3.11: Pavement constructions generally fall into one of six broad categories.
Figure 3.12: Original pavement specification in Denmark. Wheel loading: 1 Pawl. Construction: 40 mm asphalt concrete wearing course (100 pen); 200 mm asphalt base course (100 pen); 230 mm Macadam base; 150 mm mechanically stabilised gravel.
Figure 3.13: Modified pavement specification in Denmark. Wheel loading, 1 Pawl. Construction: 40 mm asphalt wearing course (100 pen); 80 mm asphalt base course; 300 mm asphalt base; 150 mm mechanically stabilised gravel.
Figure 3.14: Typical all-asphalt paving. Wheel loading: 1 Pawl. Construction: 100 mm asphalt wearing course and dense bitumen macadam base course; 200 mm wet mix macadam base; 150 mm Type 2 granular sub-base.
Figure 3.15: Typical cement-bound base pavement. Wheel loading: 1 Pawl. Construction: 100 mm high stone content asphalt wearing and base course; 250 mm lean mix concrete.

It is reported by Barber and Knapton[33] that for low speeds, a typical mix stiffness for a 100 Penetration bitumen mix is approximately 2300 N/mm^2, compared to 7000 N/mm^2 used in highway design calculations where the speed is nearer 80 km/hr. This is reflected directly by rutting and indentation, particularly in the summer months. The durability of asphalt surfacing can be greatly improved if a high stone content and a low penetration bitumen is used. In this case the mix stiffness is more likely to be 4500 N/mm^2 (50 Penetration bitumen, 55-65% stone content), and this gives much greater durability against indentation, rutting and oil damage. However, the stiffer mixes generally exhibit poorer fatigue characteristics and are more prone to structural cracking. Also low binder contents are more susceptible to surface damage from severe tyre screwing. Fatigue cracking may be overcome by the use of a cement bound base. Although an asphaltic pavement is considered to be flexible, excessive differential settlement will lead to cracking and subsequent breakdown of the bound layer. The surface can be patched easily, but this is rarely satisfactory as pneumatic tyres rapidly pull the new material out. In large settlement areas, therefore, asphaltic surfacing is often rejected in favour of a more durable material.

Generally, bitumen bound bases have not been used widely except in Denmark because of their low stiffness and their poor fatigue characteristic. There is an established asphalt industry, and two construction techniques have been used in Denmark. The first illustrated in Figure 3.12 was based on highway design methods with modified thickness to accommodate increased loading. The structure's performance was not completely satisfactory and when a further area was laid the specification was changed to that indicated in Figure 3.13. This proved to be satisfactory. The diference in performance can be explained when the two structures are analysed. The two critical strains in the first structure are much greater than those in the second. It was also assumed that the latter was quicker, easier and less expensive to construct. In the UK, the port areas in which asphaltic construction has been used have experienced very severe problems with critical pavement damage. An analysis of the structure in Figure 3.14 indicates why; both of the critical

strains are very high and well above the material's ultimate strains. The performance of these three structures should be contrasted with that of composite structures, i.e. asphaltic surfacing over a lean mix concrete base as shown in Figure 3.15. Here, with a high strength base, the tensile strain in the asphalt is very low and may become compressive in some structures; the critical strain is then that at the base of the cement bound layer. The vertical subgrade strain is also very low. It is generally found that this form of construction gives a much more durable pavement. A wet mix macadam has been used as the base material in two of the structures given above. This has also been used under a concrete paver surfacing for an industrial pavement in the UK. It is a relatively weak material being almost analogous to soil cement but is claimed to be more tolerant to subgrade settlement. Traditionally, asphaltic materials have been economical for paving, but the recent increasing cost of oil, in the UK, has made it comparable to other more expensive surfacing materials such as concrete pavers.

It is also stated that it is possible to improve the surface durability of asphalt with a cement based grout. A surface layer of approximately 40 mm thickness of open texture, bitumen coated aggregate (no fines) is laid. Into this is rolled/vibrated a resin cement grout that is left to harden. It takes around 28 days to develop its full strength. The final stiffness of the surfacing is high, about 12,000 N/mm^2, and gives much greater resistance to surface loads. However, high strength, or semi-rigid, surfacings are very susceptible to cracking owing to the high tensile stresses developed under loading. The strength of the supporting base material is critical and the manufacturers have carried out design research based on the multi-layer elastic model. Since the material is not as flexible as a true asphalt, experience indicates that, under conditions of modest differential settlement, surface cracking will occur whereas a traditional asphalt mix would roll out. However, these cracks are fine and widely spaced and do not affect the overall integrity of the pavement. An alternative to cement resin is an epoxy asphalt mix which is highly resistance to oil attack. Construction is fast and efficient as the thermosetting mix hardens in about 90 minutes. Its use in port areas is not very widespread and where it is used is restricted to heavily polluted areas such

as loading bays. Although both these methods provide increased durability, they have higher construction cost. The use of these materials may not be adopted for large parking and operating areas owing to higher cost rate.

It is reported that in-situ concrete pavement gives very durable surface that can withstand high contact stresses, and provides good riding quality. However, it is noted that there are two difficulties which make the use of rigid pavement construction impracticable in many cases:

- Subgrade settlement cannot be accommodated without excessive cracking.
- Some provision for thermal expansion/construction must be made.

It was stated that in the older port developments that concrete paving was commonly used, either unreinforced or with a single layer of mesh reinforcement and regular expansion joints. Reinforced concrete is adequate for all but the heaviest of loading providing the site is not prone to settlement. Unfortunately this is rarely the case in a modern development and if a concrete structure is laid cracking must be expected. It is also noted that unreinforced concrete is completely unsuitable, and even at sites where extensive top and bottom steel reinforcement have been used problems with cracking have not been overcome. It is also added that regular expansion joints are necessary, but these are expensive to install and form inherent weaknesses within the structure. Cracking usually manifests itself across the corners and along the joints. Problem associated with expansion joints can be overcome with a continuously reinforced pavement. Here adequate reinforcement is included to distribute the stresses evenly through the concrete. Thus, instead of large cracks developing at intervals of 5 to 7 metres, transverse cracking is fine and closely spaced, 1 to 2 metres. A hard concrete surface is ideal and the necessary flexibility can be achieved by using a precast concrete surfacing material that can be relaid as settlement takes place.

It is noted that precast concrete surfacing gives several advantages:

- Good quality control in manufacture.
- Full strength achieved in off-site curing.
- Little plant needed for laying.
- Immediate trafficking.
- Easy relaying as settlement takes place.

Reinforced rafts or slabs are generally 2 metres square and usually have a protective steel angle surround or have a chamfer around the top edge instead. Various thicknesses are available but the heavy duty 150 mm thick slabs are recommended. The high cost of construction has, unfortunately, not been reflected by a good performance record in the port environment. The principal problem seems to be settlement of the subgrade. Uneven settlement leads to steps developing between adjacent units and pumping. This has to be rectified as quickly as possible as surface water and rocking washes out the supporting sand, making the problem worse. Some experiences indicated that the problems of hogging and high wheel loads made the precast rafts inappropriate for use in areas operated by rubber tyred terminal trailers. Overall costs are significantly greater than the alternative precast concrete surfacing, concrete pavers.

According to Barber and Knapton[33], concrete pavers give the same advantages as the raft system, a highly durable and hard surface, but they also have the flexibility associated with asphaltic construction. The dimensions of pavers are 100 mm x 200 mm and because they have adequate thickness, tensile cracking does not occur. Since the structure is already "cracked" the surfacing can accommodate extensive deformation without damage. The pavers are laid by hand on a layer of screeded but uncompacted sand.

The surface is vibrated to give the final profile and this forces the sand up into the joints, so converting the individual units into a homogeneous surfacing. If the pavers are made of high quality concrete the surface durability is excellent, it can withstand the very harsh

loading from trailer dolly wheels without any problems. Once interlock has developed, the strength of the surface layer is high and thus a large elastic modulus is used in the design chart. 80 mm pavers are common and performance has been perfectly satisfactory in port areas. The initial cost of construction may be slightly higher than that of an asphaltic construction, but existing paver pavements have required little maintenance. The overall costs, therefore, are lower. Surface water will drain through the backfill and if settlement around any soft spots becomes excessive, the pavers can be lifted and relaid in a few hours. This makes for one of the most cost effective forms of paving available for port areas.

It was stated that cement bound base materials are the most successful form of construction. Cement bound materials are divided into three broad groups by Barber and Knapton[33]:

- rolled dry lean concrete
- cement bound granular material
- stabilised soil cement

It is noted that which of these materials is the most suitable depends on materials and plant available; soil stabilisation of a sandy gravel subgrade can be significantly less expensive than lean concrete, despite the greater thickness and higher cement content required. All cement bound materials require a curing period to develop full strength, but this rarely causes a delay as the surfacing can be laid during this time.

It is generally recognised that the higher the strength the better, although this aggravates problems of shrinkage cracking. Lean concrete is generally regarded as a non-flexible material, but it has proved to be sufficiently flexible to follow site settlement to a remarkable degree. It is assumed that in areas of settlement, an angular aggregate will give better durability as frictional interlock across cracks is very high.

3.2.2.8. A Mechanistic design using the design parameters obtained from laboratory test

Shackel[35]'s design procedure described here involves two stages, comprising:

- The empirical characterisation of paver paving systems.
- The application of mechanistic analyses to paver pavements.

According to Shackel[35], the justification for an empirical approach to characterising paver pavements is that pavers can be manufactured and laid to much more consistent tolerances and specifications than most other types of flexible pavement materials. Therefore, the properties of pavers are less likely to vary from one project to another. Shackel[35] carried out a series of accelerated trafficking tests of paver pavements. It was shown that just two criteria are important in assessing the response of paver pavements to traffic.

In the case of paver pavements incorporating granular bases, the prime indicator of performance is the permanent or rutting deformation. By contrast, for pavements using stabilised bases the principal performance criterion is the elastic deflection. The results of the tests are shown in Figures 3.16 and 3.17 for rutting and deflection respectively. According to Shackel[35], mechanistic analysis can be important because of the complexity, cost and length of time involved in accelerated trafficking evaluations of pavements. The levels of performance achieved in a prototype pavement would be applied under conditions where the insitu subgrade has a strength at least equal to that studied in the accelerated trafficking tests. For each level of subgrade strength considered in paver pavement design it would be necessary to test a series of prototype pavements.

A study of relationships between pavement thickness and subgrade CBR indicates that for increases in CBR beyond 50% there is usually little significant reduction in pavement thickness. Accordingly, the relationship between CBR and thickness can effectively be

replotted as a series of factors, Fs (the thickness factor) by which the thickness at a CBR of 50% or greater must be multiplied to yield the necessary depths of cover. This is shown in Figure 3.18. Shackel[35] assumed that it is possible to calculate the thickness needed to achieve the some level of performance at some other CBR value.

There are two analysis techniques which are based upon elastic deflection and rutting deformation in mechanical design method. The CHEVRON[36] linear elastic computer analysis was used to examine the structure shown in Figure 3.19(a). The load used in the deflection analysis was a single 40kN wheel with a tyre pressure of 0.6N/mm^2. The purpose of the analysis was to examine the effects of varying the subgrade modulus (and hence CBR) and the base course thickness. The values of moduli assigned to each of the flexible material layers were selected from tables of typical values collated by Paterson and Maree[36] from both accelerated trafficking and laboratory tests of actual pavement materials.

The selection of suitable values to characterise the pavers was more difficult. Values of the apparent modulus of a paver layer vary from 0.415N/mm^2 reported by Seddon[37] to 8N/mm^2 quoted apparently without any experimental justification by Tait[38]. The results of the CHEVRON[36] analysis were rearranged using the techniques of multiple regression to determine how the base thickness should vary in order to maintain a constant level of elastic deflection at the surface of the pavement. This information was used to draw curve c in Figure 3.19. The relationship between CBR and modulus, was based on data given NAASRA[39], Paterson and Maree[36] and others, is taken into consideration in Shackel's work.

It should be noted that the relationship given as Figure 3.18(c) is relatively insensitive to changes in the material properties given in Figure 3.19(a) and can therefore be used with confidence to cover most practical situations. Inspection of Figure 3.18 indicates that the thickness factor, Fs, based on the criterion of maintaining a constant level of deflection in the pavement requires the pavement thickness at low CBR to be rather greater than that

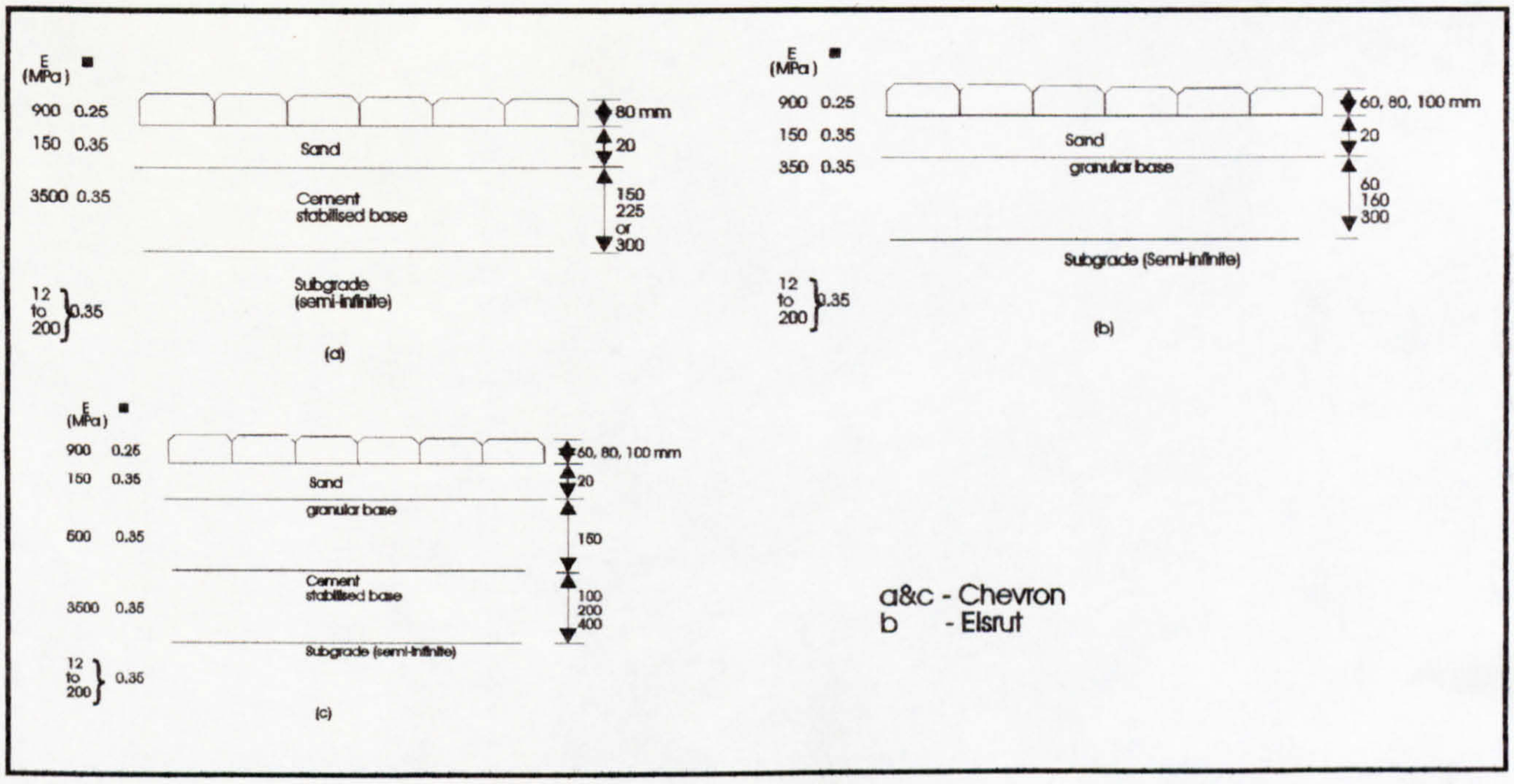

Figure 3.19: The idealised pavement structures used in the mechanistic CHEVRON and ELSRUT analyses.

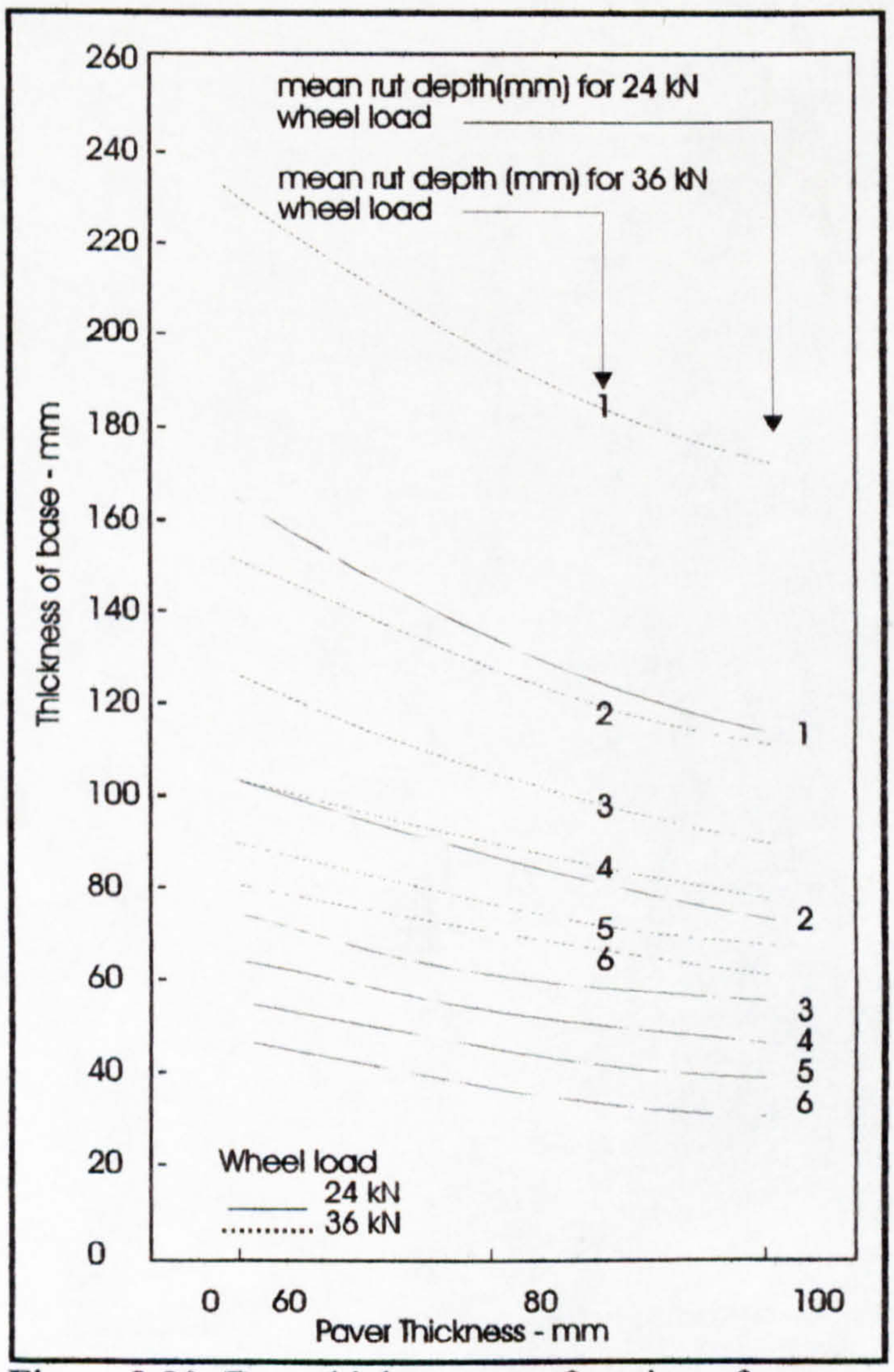

Figure 3.20: Base thickness as a function of paver thickness and rut depth.

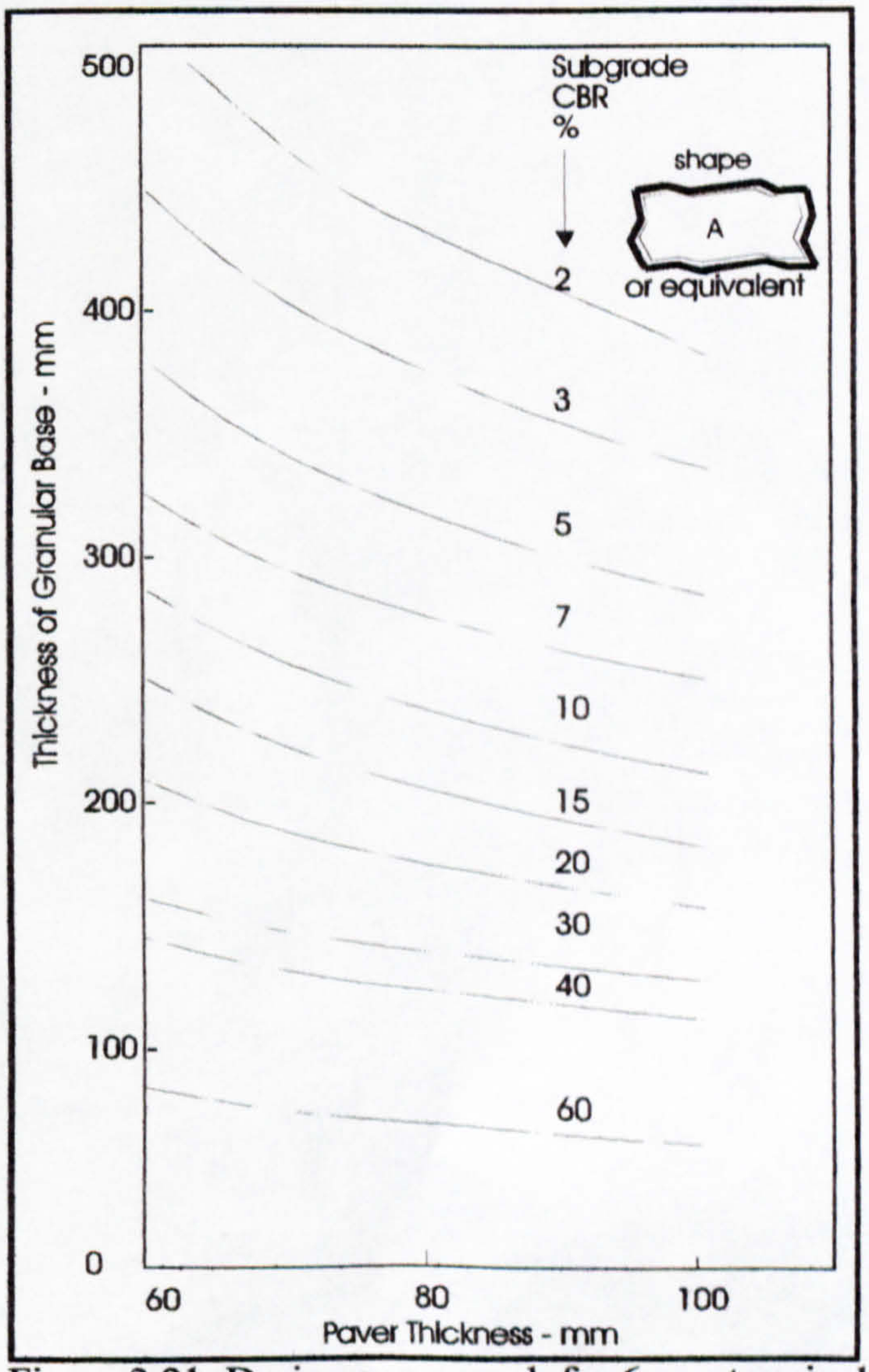

Figure 3.21: Design nomograph for 6 mm terminal rutting.

given by the conventional CBR, cover relationship (curve **b** and **d**). This shows that the criterion of constant deflection is suitably conservative for general use. According to Shackel[35], it is necessary to design such pavements in accordance with the criterion of maintaining the deflection within acceptable limits. In other words the design should be based on curve **c** in Figure 3.18.

According to Shackel[35], it is appropriate to base the design on considerations of deformation only for granular bases. The ELSRUT computer program developed at the University of California and described by Freeme and Monismith[40] was used in order to determine how the thickness of a granular base should be varied to maintain the deformation in the pavement constant. This program may be allowed to determine the deformation in a pavement resulting from a specified number of load repetitions. This program was used to calculate the rut depth after 10 000 repetitions of a 40kN single wheel load (tyre pressure 0.6N/mm^2) in the pavement structure shown in Figure 3.19(**b**). Then, using multiple regression techniques, the thickness factor/CBR relationship given as curve **a** in Figure 3.18 was obtained. Shackel[35] assumed that the criterion of maintaining a constant level of deformation (rutting) requires greater pavement thickness than that given by the CBR/cover relationships (curves **b** and **d**) except at low CBR as may be seen in Figure 3.18. CBR/cover relationships of ELSRUT[40] was used as a reference in Shackel's design procedures.

Shackel's original design curves were published for granular materials only. Suitable base materials for this form of construction are expensive. Using this form of construction is expensive where the subgrade CBR is low and therefore requires substantial pavement thickness. For this reason the design method has been revised to cover three types of pavement structure. The structures and the recommended range of subgrade CBR for which each is thought to be most economical are as follows:

- Granular base on subgrade (CBR>30%).

- Granular base on cement-stabilised sub-base (CBR<30%).
- Cement-stabilised base and sub-base (CBR<10%).

The data has been plotted in Figure 3.16 and has been obtained for prototype pavements in a fully interlocked condition. The data may be rearranged using the techniques of multiple regression to show the thickness of granular base needed beneath various thicknesses of paver to yield specified degrees of rutting. This is shown in Figure 3.20. From Figure 3.20, the combinations of base thickness and paver thickness needed to give a specified level of rutting at the development of full interlock may be selected for all pavements constructed on a subgrade similar to that used in the prototype pavements. In Figure 3.20 subgrade CBR was in excess of 60%. For pavements having CBR below 60% the thickness as given in Figure 3.20 should be multiplied by the suitable value of Fs given as curve a in Figures 3.18.

Figure 3.18 and 3.20 were combined in a single nomograph for the design of road pavements in order to provide suitable design parameters and performance criteria. Figure 3.21 has been plotted on the basis of a design single wheel load of 36kN and a specified rut depth of 6mm. This degree of rutting is considerably less than that which would be tolerated in actual roads. The designs shown in Figure 3.21 are believed to be conservative. The upper limit of thickness of a granular base is typically between 150 and 200 mm but economically this thickness varies from country to country. (When the pavement incorporates a stabilised layer it becomes necessary to consider both the magnitude of the applied load and the number of load repetitions in order to ensure that the sub-base will not crack.)

In order to determine the thickness of sub-base, the pavement structure shown in Figure 3.19(c) was analysed using the linearly elastic CHEVRON[36] computer program. The effects of varying the paver thickness, sub-base thickness and subgrade modulus on the surface

deflection are shown in Figure 3.22 for a 40kN single wheel load. The subgrade modulus may be assessed in terms of the CBR of the subgrade material.

Figure 3.22 may be interpreted as a relationship between traffic intensity, subgrade CBR and sub-base thickness and may be used for design purposes (as shown by line (a) on the figure for 0.6 million standard axle loads). A study of Figure 3.22 shows that it is not possible to reconcile the requirements of a high volume of traffic with a low subgrade CBR. In this kind of situation some alternative form of construction should be used. It should be noted that the relationship between deflection and pavement life assumed in Figure 3.22 was derived for pavements with bituminous surfacing whose tolerance to deflection is much less than that of paver pavements. The design in Figure 3.22 assumes that no cracking can be tolerated in the sub-base whereas in practice the granular base would act as a barrier against crack propagation. The resilient deflection of the pavement provides the principal criterion of performance. The elastic deflections of paver pavements with a granular base appear to be little affected by either the load magnitude or number of load repetitions. Typical data were given in Figure 3.17. These data may be rearranged by multiple regression techniques to show graphically the relationship between basecourse thickness and paver thickness (for specified levels of elastic or resilient deflection) This is shown in Figure 3.23.

From Figure 3.23 the basecourse thickness may be selected beneath any designated paver thickness to yield a specified surface deflection. This deflection may be related to the design life of the pavement expressed in numbers of standard axle loads by using the relationships published by Croney[41]. These values can be seen in Figure 3.23 which is plotted in terms of the thicknesses of granular base needed to control the deflection to designated levels.

It has been assumed that each centimetre of stabilised base is equivalent in performance to 1.5 centimetres of granular base. This assumption has been checked using elastic deflection

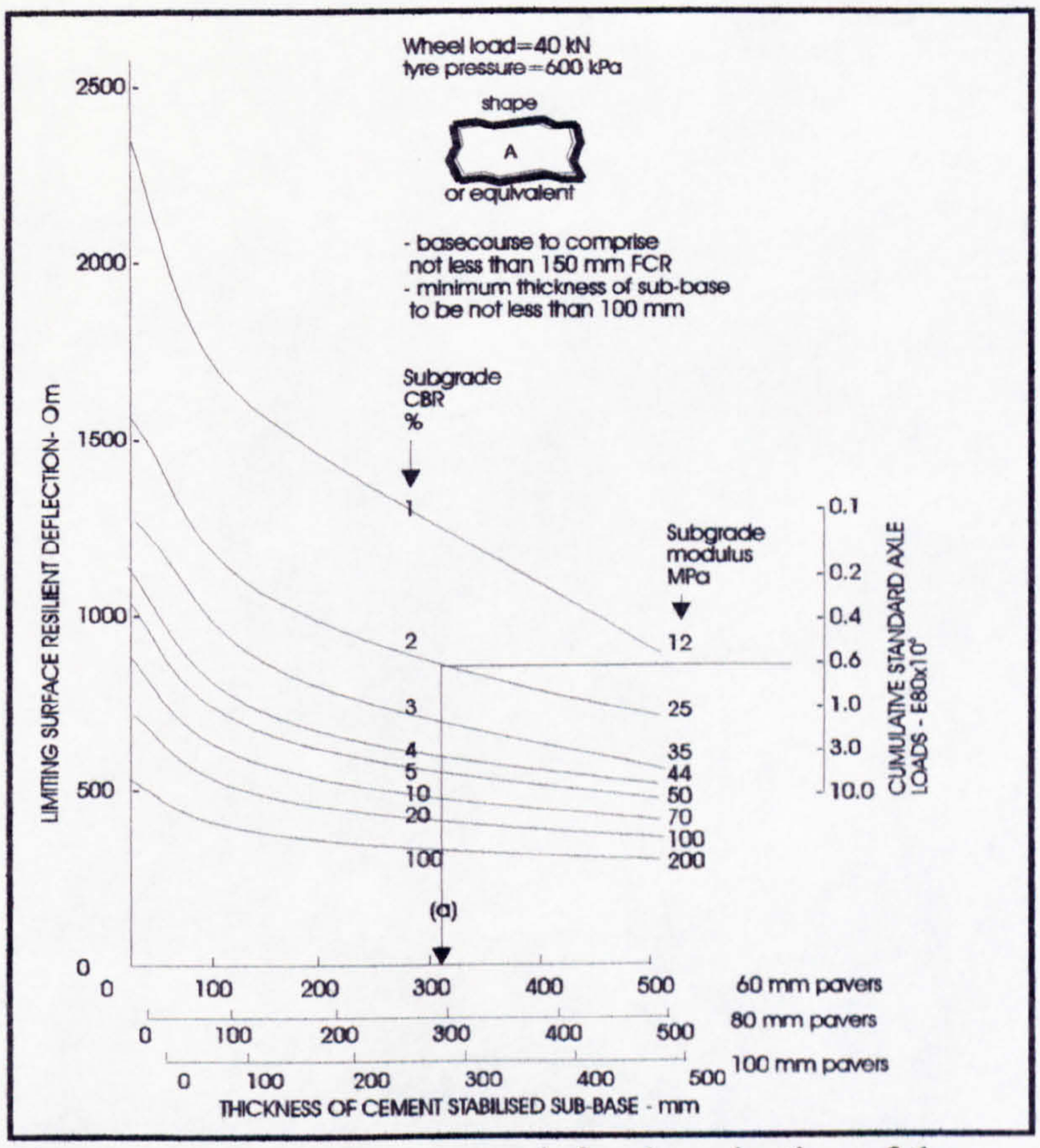

Figure 3.22: Design nomograph for the selection of the thickness of cement-treated sub-base needed beneath 150 mm of granular base.

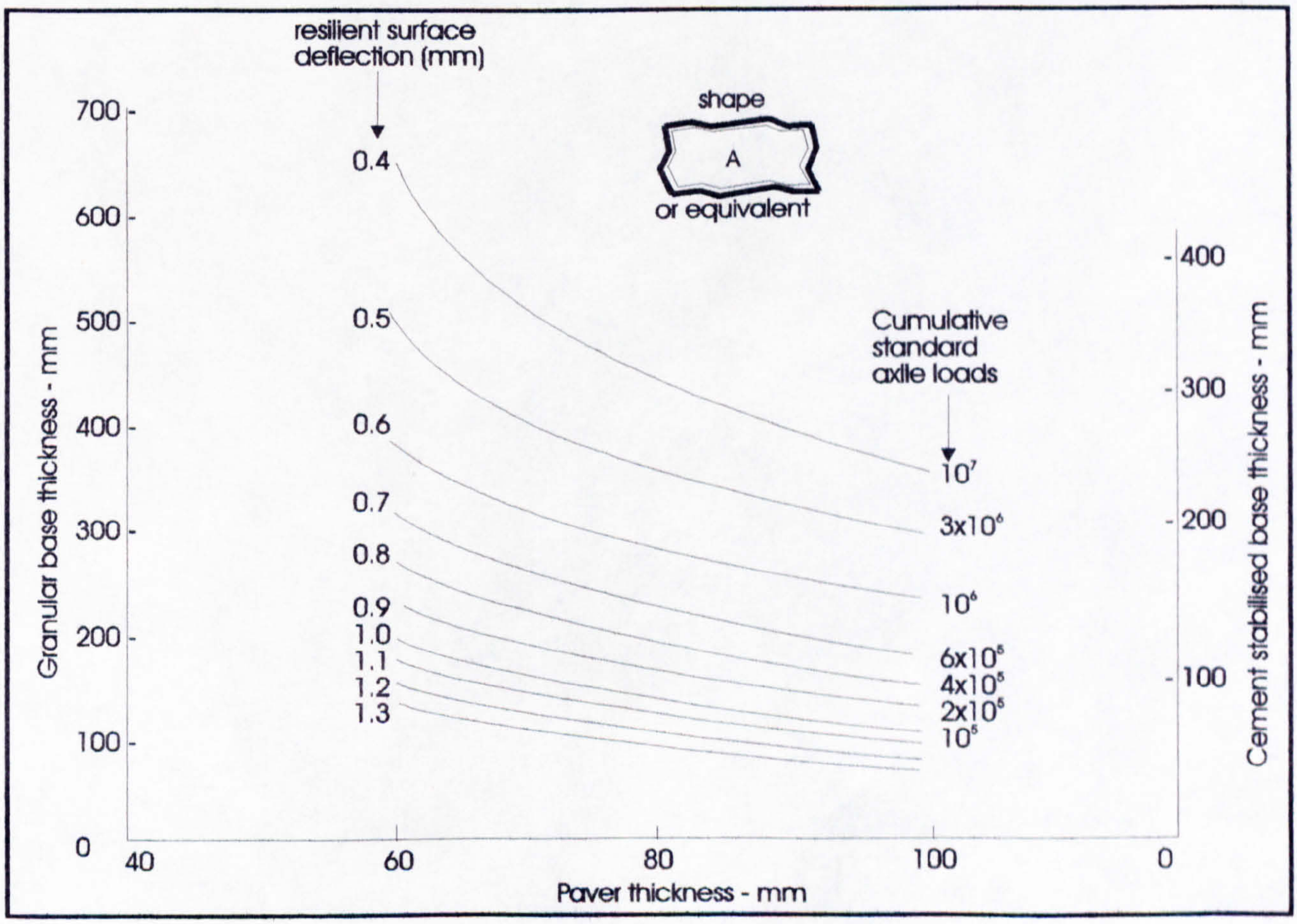

Figure 3.23: Base thickness as a function of paver thickness and resilient deflection.

as the equivalence criterion by means of a series of CHEVRON[36] computer analyses for a range of base thicknesses and moduli. Figure 3.23 may be used to design a pavement to yield a given design life provided that the subgrade CBR is equal to that used in the prototype pavement (>60%). For other values of subgrade CBR the thickness of stabilised base given in Figure 3.23 should be multiplied by the appropriate factor. Figure 3.18 in which Fs is taken from curve **c** and Figure 3.23 may be combined as a nomograph such as that given in Figure 3.24.

Property	Bedding sand	Granular base	Cement-treated base	Cement-treated sub-base	Untreated sub-base
(a) *Particle size distribution*					
percentage passing 53.0 mm	-	100	-		
37.5	-	85-100	100		
26.5	-	-	84-94		
19.0	-	60-90	71-84		
13.2	-	-	59-75		
9.52	0	-	-		
4.75	95-100	30-65	36-53	Max size	Max size
2.36	80-100	-	-	2/3 layer	2/3 layer
2.00	-	20-50	23-40		
1.18	50-95	16-43		thickness	thickness
600 µ	25-60	-	-		
425 µ	–	10-30	11-24	or 63 mm which-	
300 µ	10-30	9-27	-	ever is smaller	
150 µ	5-15	-	-		
75µ	0-10	5-15	4-12		
(b) *Plasticity*					
Liquid limit (max) %		25	-	-	-
Plasticity index (max) %	non-plastic	6	6	6	12
Linear shrinkage (max) %		3	-	-	-
(c) *Strength*					
Unconf. comp. strength (MPa)	n/a	-	1.5 (min) 3.0 (max)	0.75 (min)1.5 (max)	-
10 % FACT (min)	n/a	60 kN	110 kN	-	-
ACV (max)	n/a	-	20 %	-	-
Soaked CBR at 95% mod. MDD	n/a	80 %	-	-	45%
Max swell at 100% mod MDD	n/a	0.5 %	-	-	0.5%
(d) *Compaction*					
Min % mod. AASHTO MDD	n/a	98 %	97 %	95 %	95 %

Table 3.5: Recommended minimum standard for base and sub-base materials.

The relationship between the wheel loading first applied to the pavement and the in situ subgrade CBR was plotted in terms of the performance of the pavements under accelerated

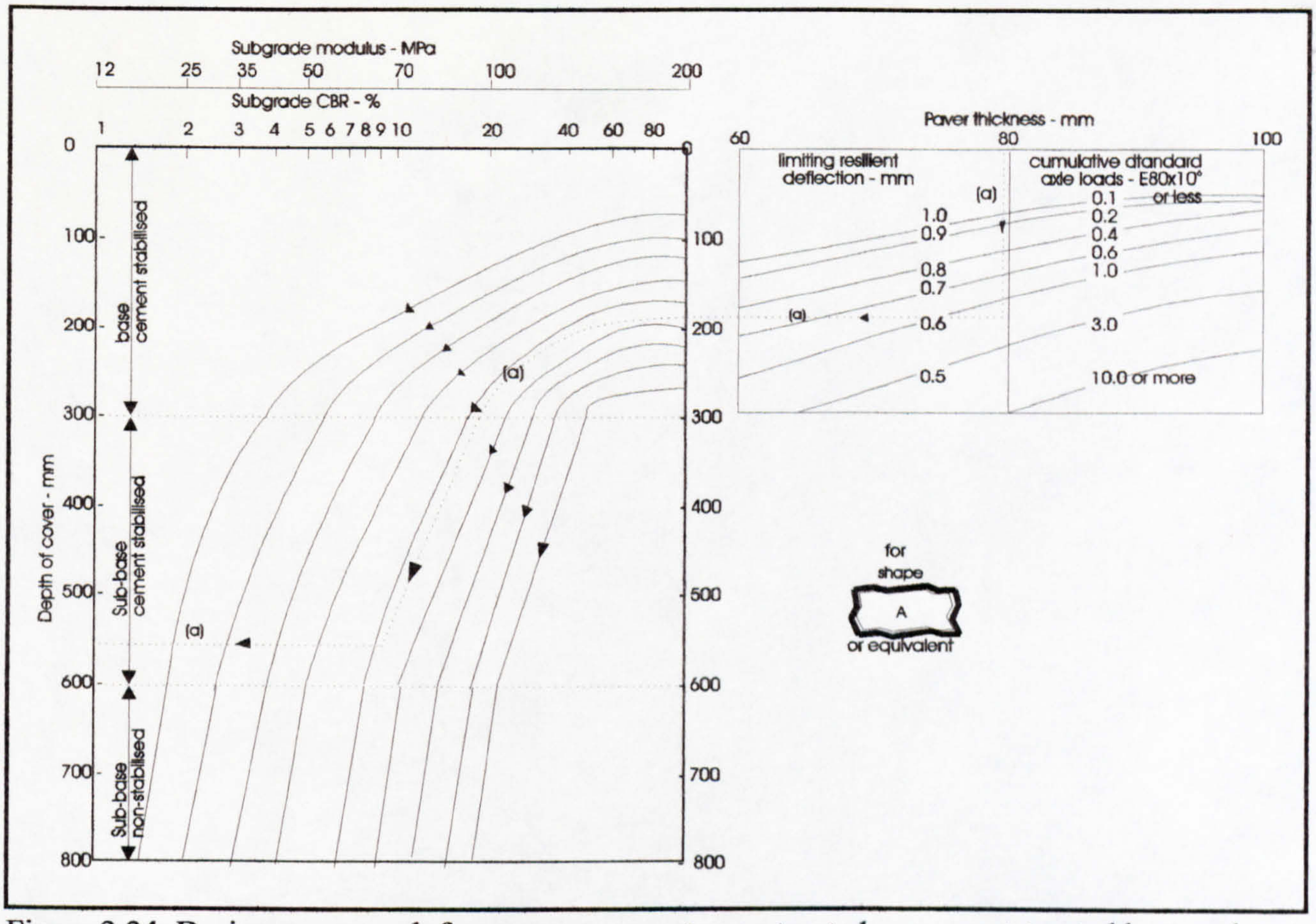

Figure 3.24: Design nomograph for paver pavements constructed on cement-treated base and sub-base.

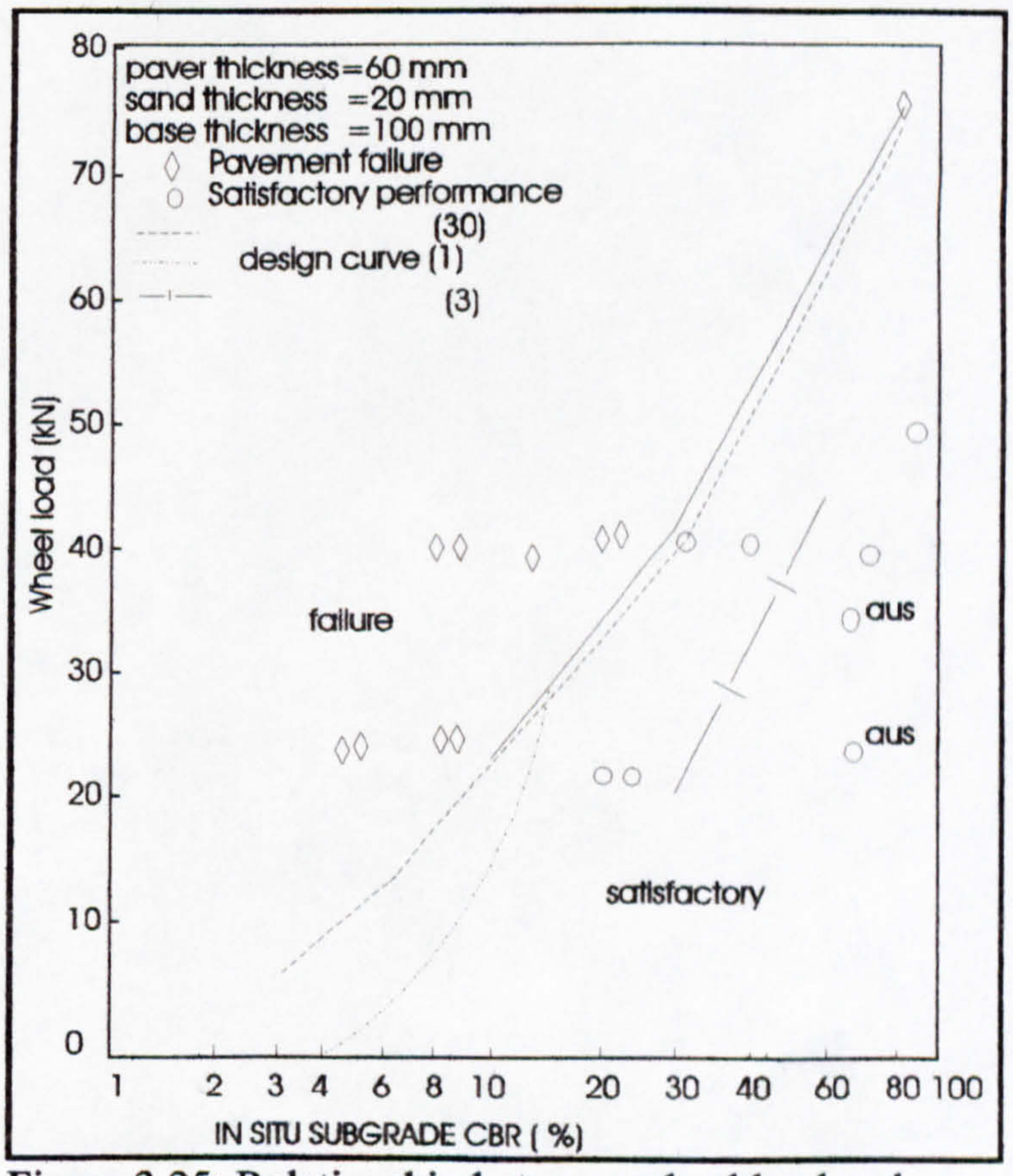

Figure 3.25: Relationship between wheel load and subgrade CBR necessary for support.

trafficking, as shown in Figure 3.25. Here all results have been included irrespective of paver shape or laying pattern. Figure 3.25 should be considered only as the first approximate check of the design methods and much more testing will be needed before the validity or safety of any design method can be determined with certainty. In using the design method, it is important to use materials whose quality is at least equal to that used in the various accelerated trafficking tests. A list of the minimum recommended standards to be achieved in each layer of the pavement is given in Table 3.5.

3.2.3 Design based on equivalence

This section deals with BS 7533[42]:1992 which is an adaptation of the methodology propounded in TRRL Laboratory Report LR 1132[19] (see Section 3.2.2). Pavers are substituted in place of asphaltic material by using BS 6677[43]:Parts 1,2,3 and BS 6717[44]:Parts 1&3 which define the characterisations of surfacing materials. BS 7533[42]:1992 is dealt with in this section because it describes the UK's principal design method for highways surfaced with pavers. BS 6677[43]:Parts 1,2,3 and BS 6717[44]:Parts 1&3 indicate how clay and concrete block pavers can be manufactured and laid. These guides give procedures for pavements constructed with clay or concrete block pavers.

The British Standards can be used for all pavements up to 18000 kg axle load and up to 12,000,000 cumulative standard axles including both highway pavements and industrial pavements where traffic shows similarity with highway vehicles: it excludes very heavy duty pavements. Pavers can be clay or concrete. Laying course (bedding course) is a layer on which pavers are bedded between the roadbase and pavers. Subgrade is natural or constructed soil layer below the pavement layers which transmit the load. Subgrade Improvement Layer (Capping Layer) is laid at the top of the subgrade in order to improve the strength of the foundation of the pavement. The sub-base comprises one or more layers below the roadbase. The roadbase comprises one or more layers above the sub-base. The component of the pavement are illustrated in Figure 1.2. The design of new pavements is

based on the method which is given in TRRL Report (Transport and Road Research Laboratory)1132[19] "The structural design of bituminous roads".

3.2.3.1. Subgrade assessment

The strength of the subgrade is a principal factor in determining the thickness of pavement. The strength of subgrade is assessed on the California Bearing Ratio(CBR) scale. This test is used for determination the strength of subgrades (see Section 1.4.4). During the service life of the pavement saturated subgrade may occur and should be taken into account in design and the CBR method can be used the soaking procedure. Alternatively equilibrium suction index CBR values may be used when it is clear that saturated condition will never occur. For fine grained soils, the equilibrium suction index CBR can be determined from the plasticity index (PI) as shown in Table 1.1 (see Sections 3.2.2.4 and 1.4.4 for details).

Volume of traffic	Cumulative traffic				[1] Volume of traffic which is in excess of this table. NOTE: This table is based upon the normal spectrum of light to heavy commercial vehicles in typical UK highways. Where the designer believes there is a greater proportion of light commercial vehicles than normal, these will be less damaging, hence more can be permitted. Conversely if a higher proportion are rear engined buses or heavy commercial vehicles fewer may be permitted and calculations based on axle damage factors are recommended, as described in TRRL Report 1132.
	20 years design life		40 years design life		
	Zero growth	2 % growth	Zero growth	2 % growth	
cv/d 30	msa 0.2	msa 0.3	msa 0.4	msa 0.6	
120	0.9	1	2	3	
250	2	3	7	9	
500	6	8	[1]	[1]	
1000	[1]	[1]	[1]	[1]	

Table 3.6: Relationship between commercial vehicles per day and the number of standard axle for design lives of 20 years and 40 years at growth rates of 0% and 2% per annum.

If the rut depth exceeds 10 mm, resetting the pavers may be necessary during the life of a pavement.

3.2.3.2. Design life

The number of standard axles (msa) or the number of commercial vehicles per day (cv/d) should be taken into consideration for design of the pavement. Table 3.6 was taken from

BS 7533[42]:1992 page 7. According to BS 7533[42]:1992, a 20 year design life is generally applicable unless access for possible maintenance of the roadbase is likely to be difficult and expensive. Zero growth is likely to be applicable for the pavement which serves a finite area. However, 2% growth is recommended in BS 7533[42].

3.2.3.3. Selection of pavement components

Figure 1.2 shows the general cross-section of the pavement not all components need to be present in every pavement. According to BS 7533[42], design can proceed with the determination of CBR values. Figure 3.26 illustrates a flow chart which can be used to determine pavement course thickness for various combinations of CBR and traffic loads. Firstly, the design CBR and the amount of traffic expected to use the pavement, expressed in million standard axles, are determined as described in Section 1.4.4. The thickness of subgrade improvement layer (capping layer) has been described in Section 1.4.3.

3.2.3.3.1. Sub-base

According to BS 7533[42]:1992, in road construction if the sub-base is not to be employed as a site access road and a subgrade improvement layer is present then the thickness of sub-base should be 150 mm, or if there is no subgrade improvement layer the thickness of sub-base should be 225 mm. If a subgrade improvement layer has been used and the road is to be employed as site access road, the sub-base thickness should be increased as indicated in Figure 3.26 in terms of the amount of traffic which will flow directly over the sub-base. The number of standard axles trafficking the sub-base or the number of dwellings being constructed or the equivalent size in square metres of the industrial or commercial property being constructed should be determined for the amount of traffic. If one of these three ways cannot be chosen then it can be assumed that the road will serve a large development trafficked by 5000 standard axles. If the projected traffic loading exceeds 2 msa the sub-

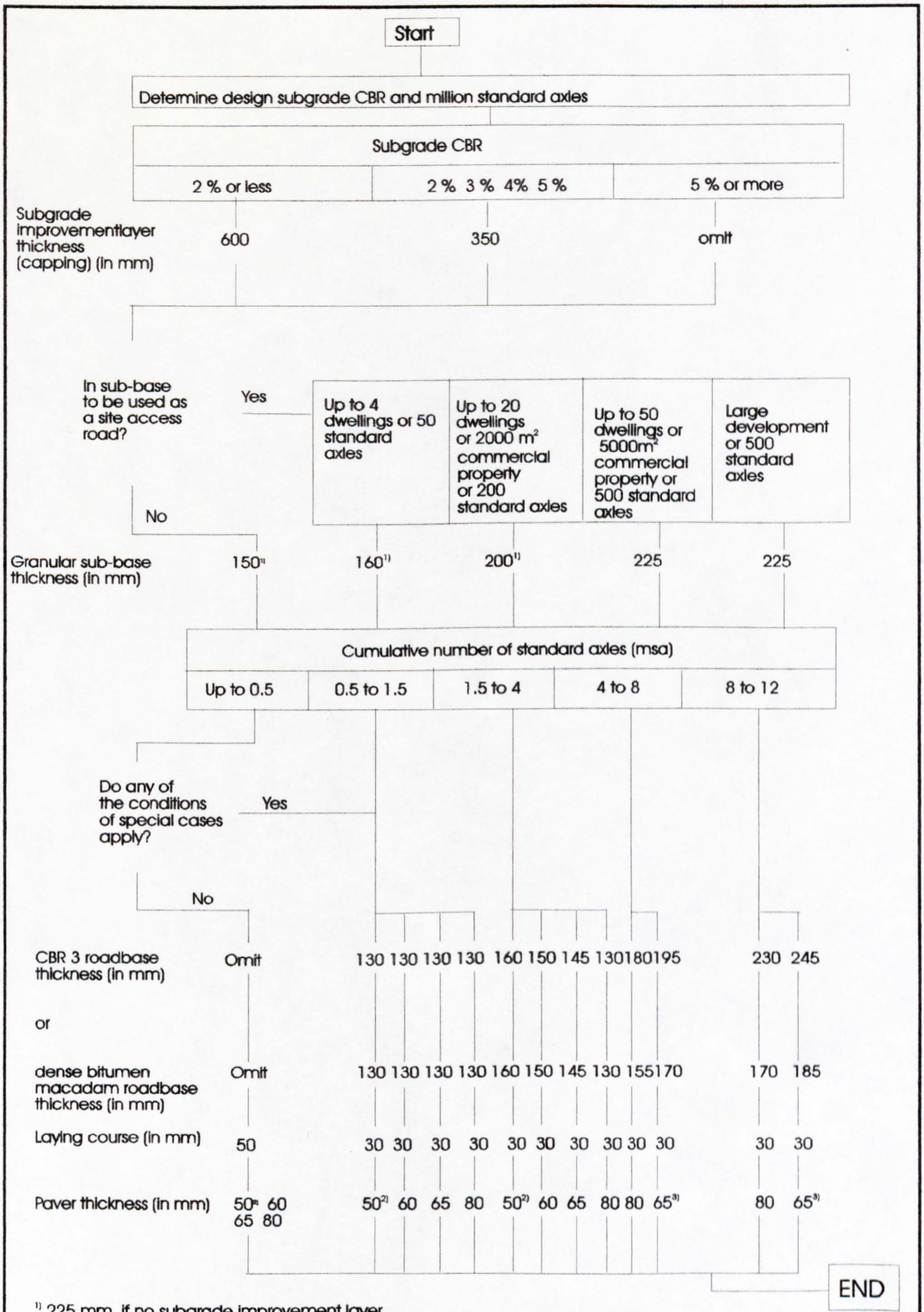

[1] 225 mm if no subgrade improvement layer.
[2] For clay pavers only.
[3] There is no long term evidence concerning the performance in service of 65 mm pavers beyond 4 msa so this design information has been extrapolated.

Figure 3.26: New pavement design procedure (from BS 7533[42]:1992 Page:7)

base strength should be at least equivalent to a CBR of 30%. The sub-base should be protected from the effects of weather when its surface is exposed.

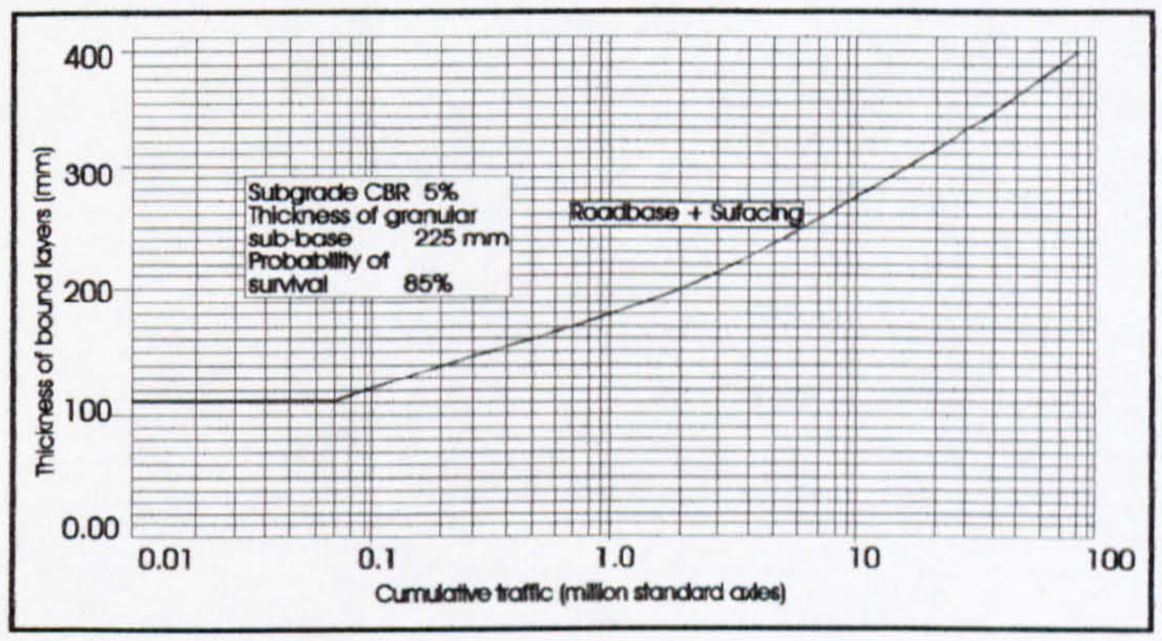

Figure 3.27: Design curve for roads with bituminous roadbase (from TRRL Laboratory Report 1132[19]: page 18).

3.2.3.3.2. Roadbase, Laying Course, Pavers

According to BS 7533[42], for the roadbase and laying course, BS 6717[44]:Part 3 or BS 6677[43]: Part 3 the following may be appropriate to use.

Roadbase: Roadbase specifications for Cement Bound Materials (CBM) and Dense Bitumen Macadam (DBM) are defined in Clauses 1038 and 908 of the Department of Transport Specification for Highway Works[45] and Figure 3.27 indicates these definitions. When the level of cumulative traffic is less than 500,000 standard axles and the pavement cannot be found in special categories, then it is not required to provide a roadbase. However, a minimum roadbase thickness of 130mm has been included in Figure 3.26 by taking into account practical construction issues.

Laying Course: BS 6717[44] or BS 6677[43] require the preparation of the Laying Course. The nominal thickness of Laying Course is assumed to be 50mm for unbound roadbases and 30mm for bound roadbases.

Pavers: Pavers are generally 50mm or 65mm for clay and 60mm to 65mm or 80mm for concrete. In this research, the experiments have been conducted on 80mm thick rectangular concrete pavers since they are the most widely used in the UK.

3.2.3.4. Pavement course specification

Pavement construction materials are specified in terms of the relevant clauses indicated by the Department of Transport Specification for Highway Works[45], Table 3.7. The recommendations of BS 6677[43]:Part 2 for clay pavers and BS 6717[44]:Part 3 for concrete block pavers can be used for the laying course and jointing.

Table 3.7: Specification for Highway Works clauses

Category of material	Clause number
Cement bound material 1	1036
Cement bound material 2	1037
Cement bound material 3	1038
Cement bound material 4	1039
Pavement quality concrete	1001 to 1034
Dense bitumen macadam	903
Hot rolled asphalt	904
Type 1 granular sub-base material	803
Type 2 granular sub-base material	804
Wet mix macadam	805
Subgrade improvement material	613

Table 3.7: Specification for Highway Works clauses*

3.2.3.5. Pavement overlay design

There are two design methods for pavement overlay design.

1) Deflection beam method

2) Component overlay design method.

---

* The following Clauses from the Department of Transport Specification for Highway Works, 1986 edition, are referred to in the text; Clause number: 613, 616, 803, 804, 805, 903, 904, 908, 1001 to 1034 inclusive, 1036 to 1039 inclusive.

In BS 7533[42], the deflection design method is preferred for existing flexible roads, the component overlay method is mentioned for other types of roads or industrial areas.

Deflection Beam Method: This method is described in TRRL Reports 833[46],834[47] and 835[48]. It is assumed that the overlay material will be a bituminous bound material. These Reports were adapted by BS 7533[42]:1992 to overlaying with clay or concrete block pavers and the material conversion factors shown in Table 3.8 are taken for these applications.

Table 3.8: Material conversion factors for evaluating highway pavement materials

Category of material	Material conversion factor	
	Suggested value	Range
Cement boundmaterial 1 (CBM1)	0.4	0.2 to 0.6
Cement bound material 2 (CBM2)	0.5	0.3 to 0.7
Cement bound material 3 (CBM3)	0.7	0.5 to 0.9
Cement bound material 4 (CBM4)	0.7	0.5 to 0.9
Pavement quality concrete	1.7	1.5 to 1.9
Dense bitumen macadam	1.0	0.9 to 1.1
Hot rolled asphalt	1.1	0.9 to 1.1
Open textured macadam	0.7	0.5 to 0.9
Wet-mix or dry	0.45	0.3 to 0.6
Type 1 granular sub-base material over material with a CBR of > 5 %	0.3	0.15 to 0.4
Type 1 granular sub-base material over material with a CBR of < 5 %	0.2	0.1to 0.25
Type 2 granular sub-base material over material with a CBR of > 5 %	0.2	0.1 to 0.25
Type 2 granular sub-base material over material with a CBR of < 5 %	0.1	0.05 to 0.15
Subgrade improvement material	0.1	0.05 to 0.15

Component Overlay Design Method: The condition of each course in an existing pavement is expressed as an equivalent thickness of a standard material. This allows the present conditions of material to be taken into account.

The thickness and condition of each course of the existing pavement is determined. It can be done by undertaking trial excavations or by taking cores. After identification of each type of material in the pavement, an MCF (Material Conversion Factor) is assigned to that material (Table 3.8). The thickness of each course is multiplied by the MCF to get the equivalent thickness of DBM. The equivalent thickness of pavers is given in Table 3.9.

Table 3.9: Equivalent thickness of pavers	
Paver thickness (mm)	DBM equivalence (mm)
80	120
65	105
60	100
50	90

Table 3.9: Equivalent thickness of pavers.

The degradation which can take place in each course of the pavement can eventually be resurfaced. The equivalent thickness of each course is multiplied by two factors which are CF1 and CF2. CF1 is applied by taking account of cracking and spalling. CF2 is used for rutting and settlement. (If the failure is in the sub-base, the subgrade improvement layer or the subgrade BS 7533[42] assumes that it may not be possible to overlay the existing pavement.) CF1 and CF2 are found for each course in terms of the condition of the material in the existing pavement as indicated in Tables 3.10 and 3.11.

Table 3.10: Condition factor CF1	
Condition of material	CF1
As new	1.0
Slight cracking	0.8
Substantial cracking	0.5
Fully cracked, or crazed and spalled	0.2

Table 3.11: Condition factor CF2	
Degree of localized rutting or localized settlement	CF2
mm 0 to 10	1.0
11 to 20	0.9
21 to 40	0.6
41 and above	0.3

Tables 3.10 and 3.11: Condition factors CF1 and CF2.

3.2.4. Design based on mathematical models

An alternative analysis to the design of concrete paver pavements is to use finite element techniques to model the pavers as an articulated surfacing having defined load or displacement transference characteristics at the joints between neighboring paving units. Finite element studies of paver paving have been reported both in Japan and Netherlands. The Japanese study[2] was restricted to a consideration of the paver surfacing. The Dutch

study[3, 4, 5, 6, 7, 8, 9, 10] is propounded in this section because it is more comprehensive in that the analysis included an assessment of a complete paver/base/sub-base/subgrade system. The benefit of this type of analysis is that it provides a very clear understanding of the complex pattern of time dependent stresses in foundation when the pavement is subjected to rolling loads.

A wheel track apparatus was used to determine the effect of an unbound base on the structural behaviour of concrete paver pavements so that six test sections (at the pavement test area of The Road Railroad Research Laboratory of Delf University of Technology[5]) can be tested and 275000 repetitions of 6kN wheel load were applied concurrently. The wheel track apparatus is a joint steel construction, consisting of eight beams. A little wagon with rubber tyre which could be turned centrally was fixed at each beam. The tyres were able to load up to P=6kN, the tyre pressure p=0.6N/mm^2 and the maximum running speed was 10 km/h. The difference between the six concrete paver test sections was in the thicknesses of the unbound base. The pavement structure of each section is as follows:

- The thickness of rectangular concrete pavers is h_1=80 mm in herringbone bond for each test section.
- The thickness of the bedding layers is h_2=50 mm of crushed sand for each test section.
- The thicknesses of the crushed concrete unbound bases (h_3) are given in Table 3.12.
- The thicknesses of the Eastern Scheldt sand unbound bases (h_4) are given in Table 3.12.
- The subgrade consists of about 1.5 m Eastern Scheldt sand on clay (see Figure 3.28).

The average in-situ dry density of the crushed concrete base material is 93.3 % of modified maximum Proctor density (mpd). The average in-situ water content is 6.9 percent. In test sections 2 through 5 the average in-situ dry density of Eastern Scheldt sand sub-base material is 100.1 % mpd, the average in-situ water content is 8.9 percent. However, the average in-situ dry density of the Eastern Scheldt sand in sections 1 and 6 is only 96,7 % mpd with a average water content of 8.2 percent.

Traffic Category	Category Symbol	Equivalent No. of Repetitions of 18-kips Standard Axle
Occasional	1	$0.7\ 10^5$
Very-Light	2	$2.0\ 10^5$
Light	3	$0.7\ 10^6$
Medium-Light	4	$2.0\ 10^6$
Medium-Heavy	5	$7.0\ 10^6$
Heavy	6	$2.0\ 10^7$
Very-Heavy	7	$7.0\ 10^7$
Heavy-Industrial	8	$4.4\ 10^8$
Very-Heavy-Industrial	9	$2.0\ 10^9$

Table 3.12: Thickness of unbound base and sand sub-base in the six concrete block test sections.

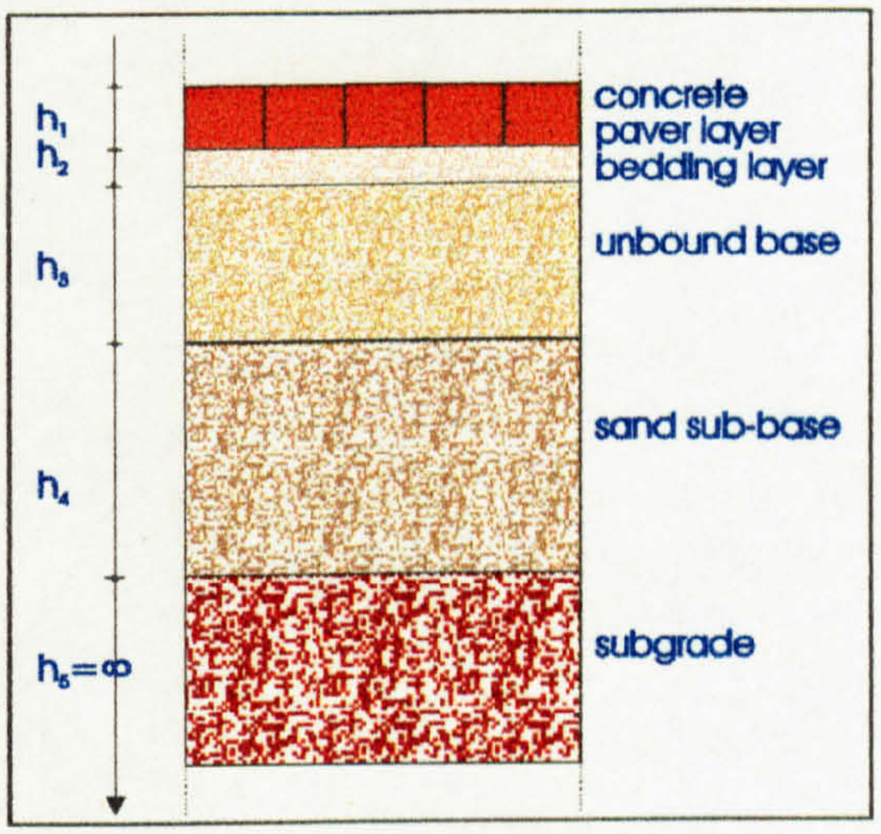

Figure 3.28: Concrete paver pavement structure used in the Dutch study[5].

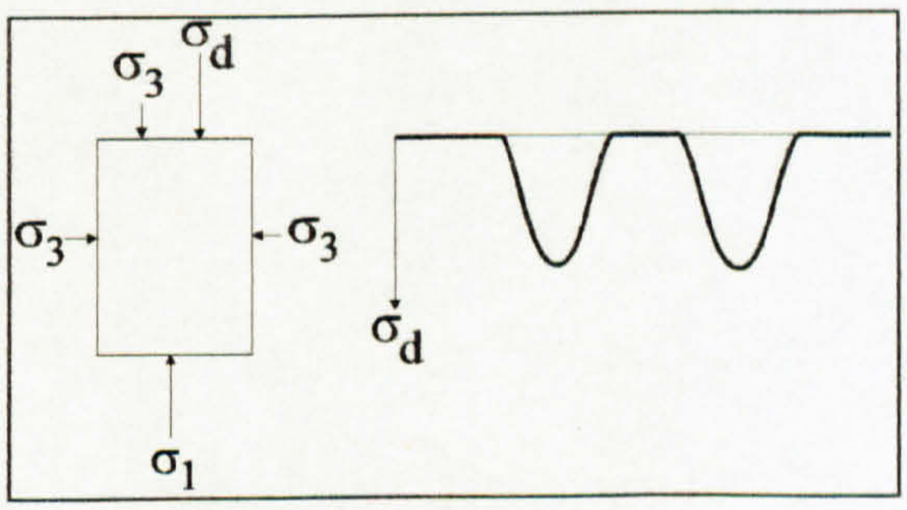

Figure 3.29: Stresses applied to specimen in the cyclic loading triaxial tests.

Cyclic loading triaxial tests are undertaken to determine fundamental stress/strain parameters for the unbound materials. A sample size of 400m x 800m is used for this test

(see Figure 3.30). The constant, all around confining stress (σ_3) simulates the constant overburden stress in the road construction (see Figure 3.29).

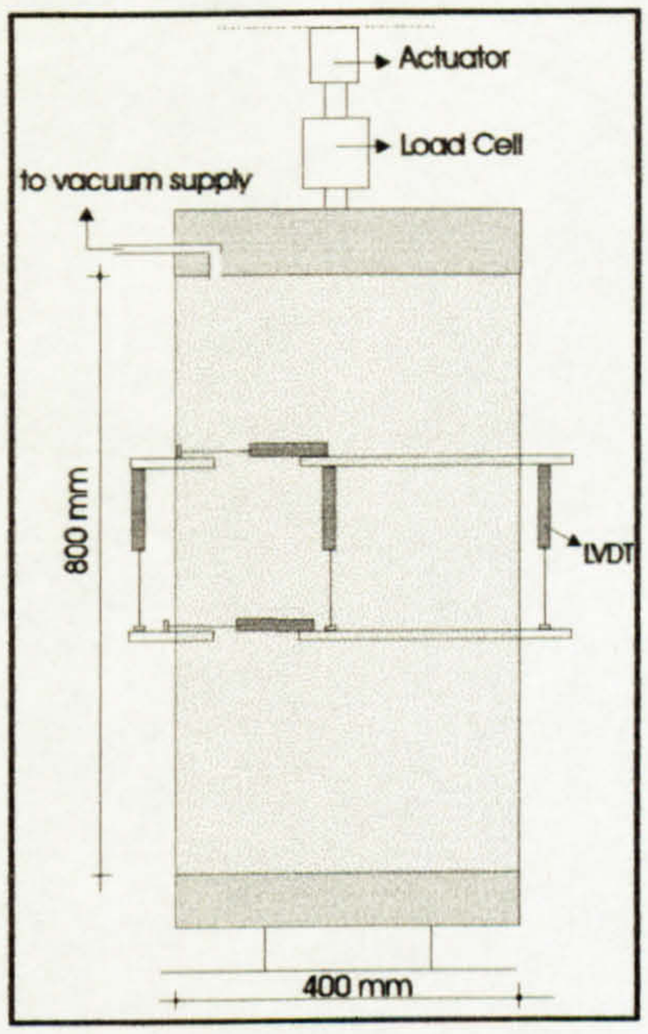

Figure 3.30: The outline of 400mm x 800mm cyclic loading triaxial apparatus used in Dutch study[5].

The cyclic deviator stress(σ_d) which simulates the in-situ stress resulting from traffic load varies between zero and a preset value at a frequency of 1 Hz. The major principal stress (σ_1) is then equal to $\sigma_1 = \sigma_d + \sigma_3$. The intermediate principal stress (σ_2) is equal to the minor principal stress (σ_3) and the total of principal stress θ is equal to:

$$\theta = \sigma_1 + \sigma_2 + \sigma_3 = \sigma_d + 3\sigma_3$$

In order to generate the confining stress (σ_3) the apparatus is adapted a partial vacuum inside the sample. A 100kN hydraulic actuator is used to apply cyclic deviator stress (σ_d) to the sample (see Figure 3.30). Two pexiglass rings mounted on the sample at 1/3 and 2/3 of sample height respectively support four vertical Linear Variable Displacement Transducers (LVDT) in order to determine the axial deformation Two horizontal LVDT are used to determine the radial deformation. The resilient and plastic behavior of the unbound

materials of the test sections were determined with the cyclic loading triaxial tests. The triaxial sample is tested at various levels of the confining stress (σ_3) and the deviator stress (σ_d) in order to determine the resilient strain parameters of the materials. The resilient modules Mr and Poisson's ratio (ν) can be calculated for characterizing the resilient behavior of unbound materials as follows.

$$Mr = \frac{\sigma_d}{\varepsilon_{a,r}} \qquad \nu = \frac{\varepsilon_{r,r}}{\varepsilon_{a,r}}$$

Where:

Mr = resilient modulus

ν = Poisson's ratio

$\varepsilon_{a,r}$ = axial resilient strain of the sample

$\varepsilon_{r,r}$ = radialresilient strain of the sample

The stress-depency of Mr is usually described with the following equation

$$Mr = k_1 \theta^{k_2}$$

where:

Mr = resilient modulus

k_1, k_2 = material parameters

θ = sum of principal stresses

Mr-θ relationships resulting from the Dutch study[5]'s cyclic loading triaxial tests are illustrated in Figure 3.31.

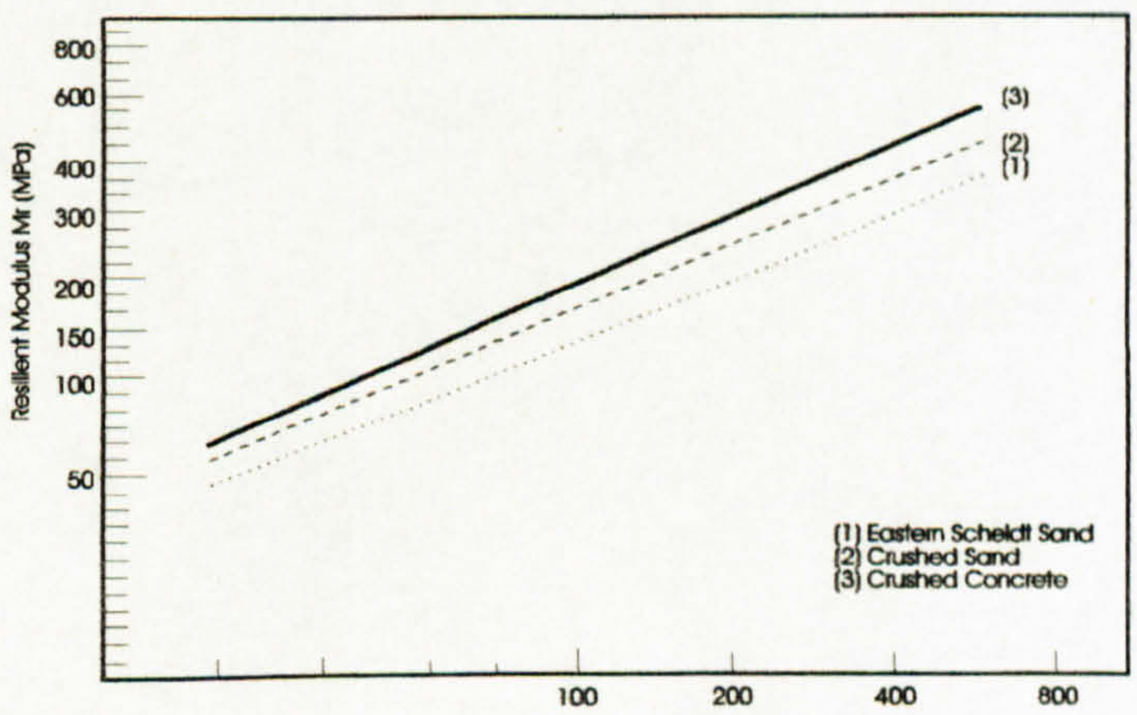

Figure 3.31: Mr-θ relationships is used in the Dutch study[5] for the unbound materials applied in the six concrete block test sections.

In order to determine plastic strain parameters three samples of each material which are the crushed sand, the crushed concrete and the Eastern Scheldt sand are tested at the same confining stress (σ_3) with a different level of the deviator stress (σ_d). Figure 3.32 illustrates three different stress ratio of $n = \sigma_d / \sigma_3$, the axial permanent strain ($\varepsilon_{a,p}$) against the number of load applications (N) for the crushed concrete and Eastern Scheldt sand. Falling weight deflection measurements were regularly undertaken on the test section in order to find resilient deformation behaviour. A dynamic load (loading time 0.02 s) is applied on the pavement structure by using a circular plate (diameter θ=300mm). Deflections (d) were determined for the distance of 0, 0.3, 0.5, 1.0, 1.5 and 2.0 m from the centre of the loading plate (see Figure 3.33).

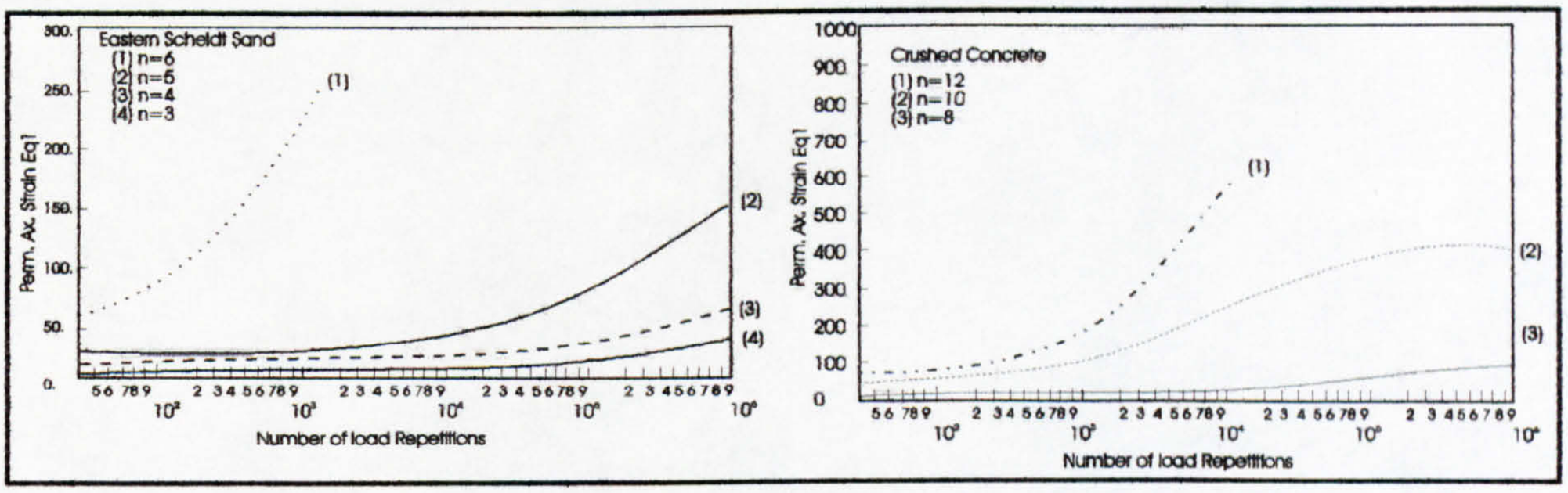

Figure 3.32: $\varepsilon_{a,p}$-N relationship of the unbound materials applied in the six concrete block test sections.

In order to measure the deflections, a 6kN load was applied by the wheel track in the concrete paver test sections . The some of the test results can be seen in Figure 3.34. As can be seen in Figure 3.34 and 3.35 when the base thicknesses increase, the deflections decrease. It is assumed that the load spreading capacity of concrete paver pavements increases with increasing base thickness. In addition, when the number of load repetitions increases, the deflections decrease and it is therefore assumed that the load spreading capacity increases with increasing number of repetition.

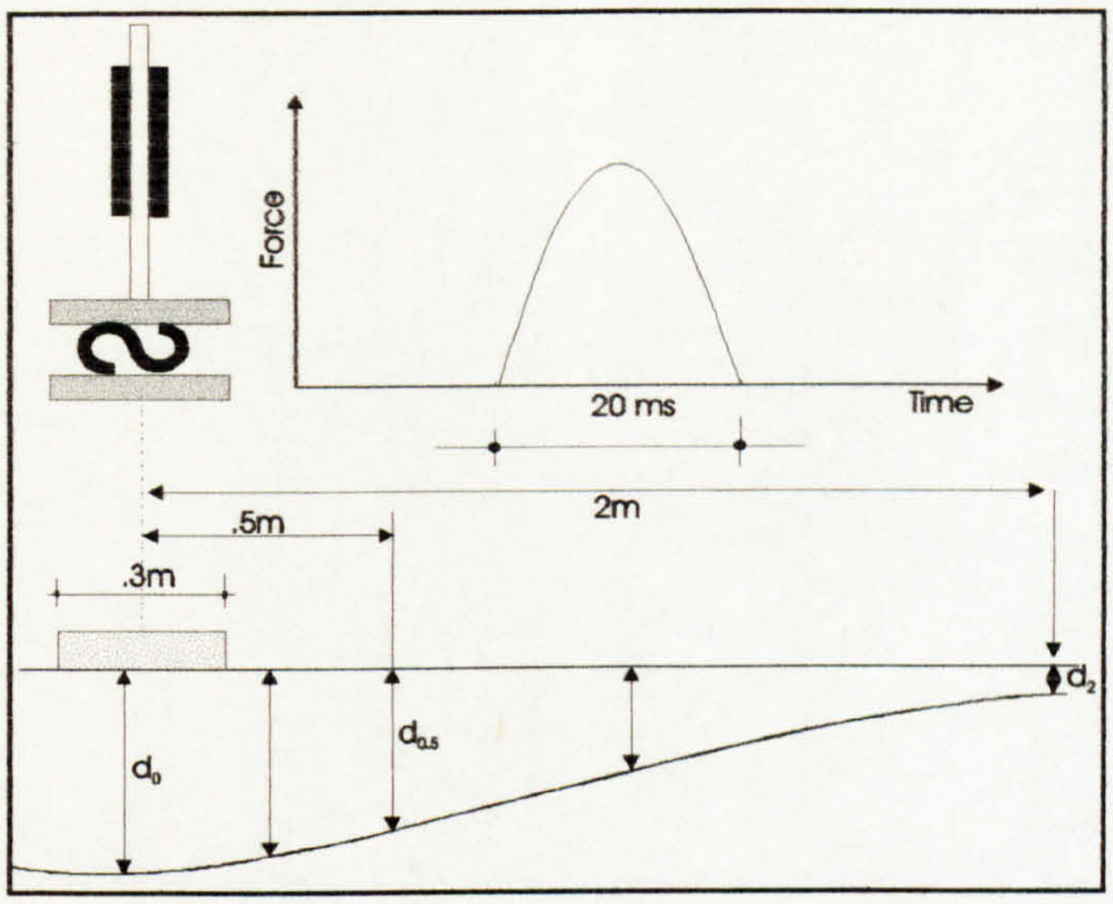

Figure 3.33: Outline of a falling weight deflection measurement.

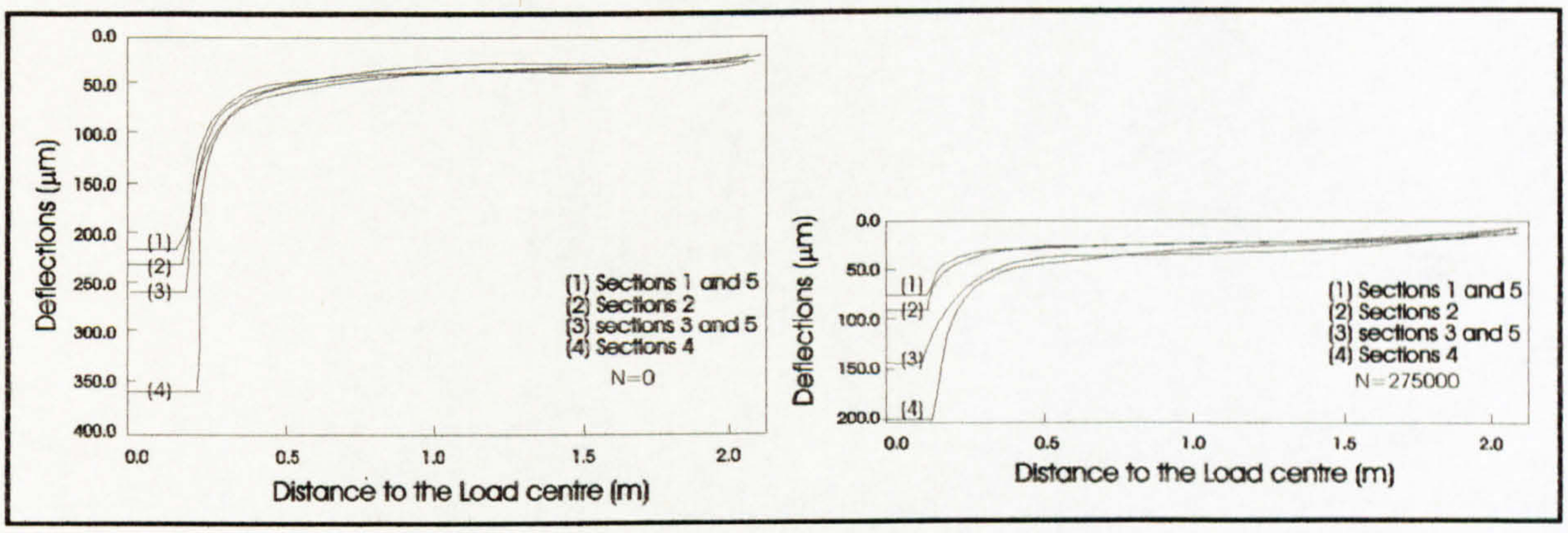

Figure 3.34: Average deflection curves of the concrete block test sections after N=0 and after N=275.000 wheel load repetitions.

Deflection measurements are applied to determine the permanent deformation behaviour (rutting) of the test sections. Figure 3.36 gives the average cross section profiles of the test sections at various numbers of applied wheel load repetitions. Figure 3.37 indicates the progress of the rutting with increasing number of load repetitions. The Figure 3.36 and 3.37 indicates that the rutting behavior of sections 1 and 6 are much worse than the behaviour of section 2 through 5, and the thickness of the unbound base has a slight effect on the rutting behaviour of the test sections.

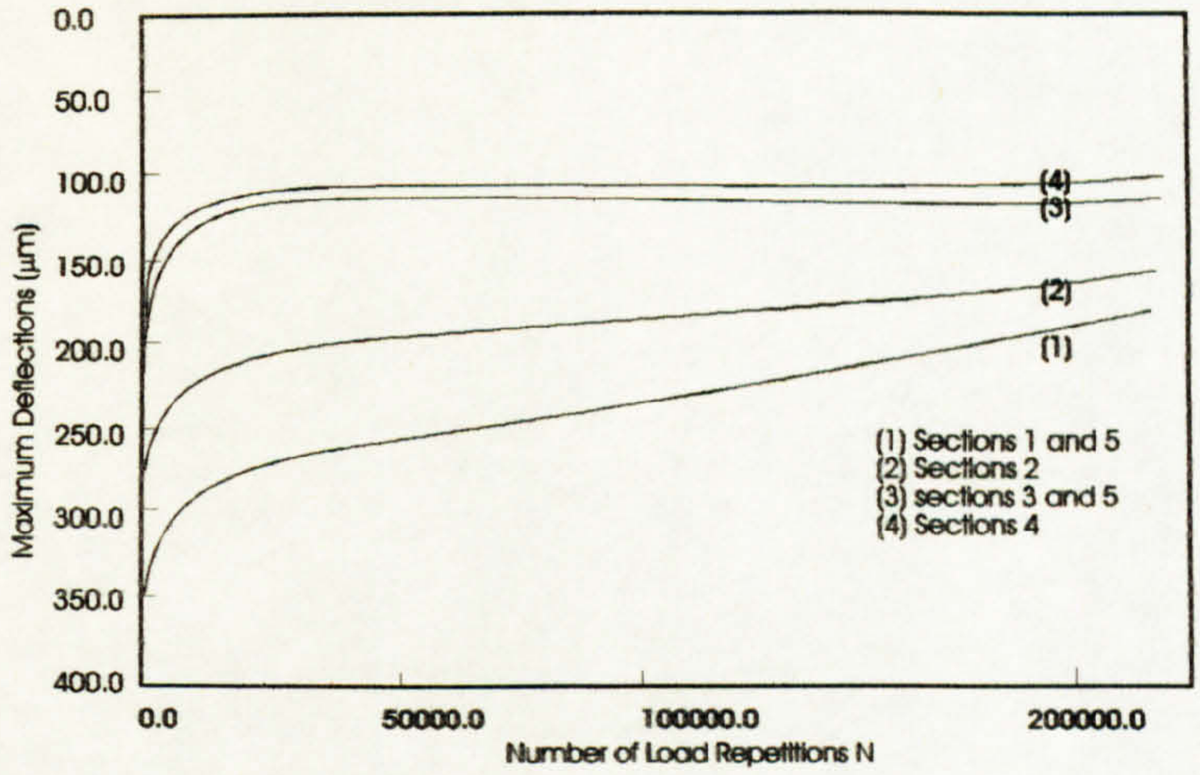

Figure 3.35: Average maximum deflection (d_0) of the concrete paver test sections as an function of the number of wheel load repetitions.

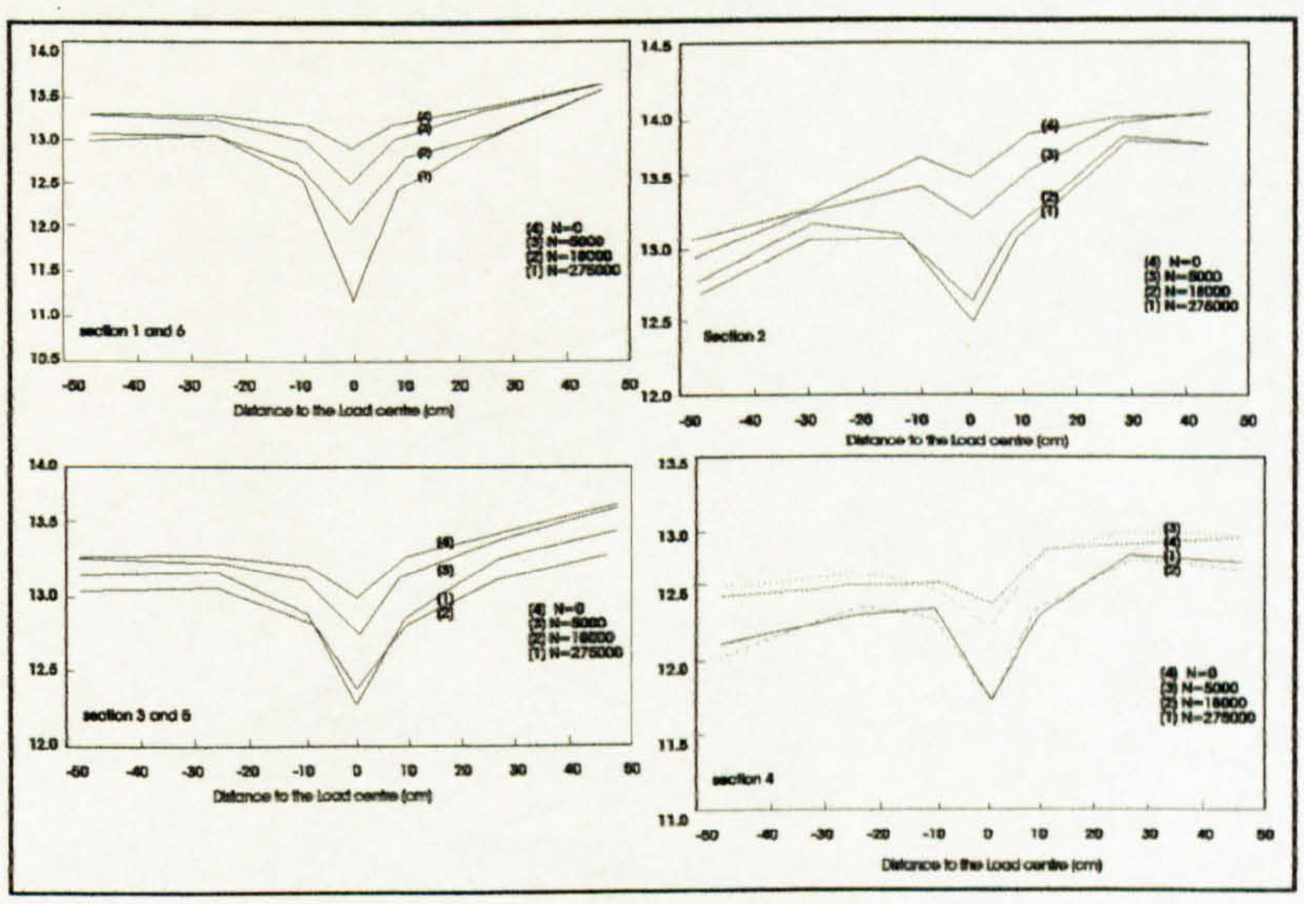

Figure 3.36: Average cross profiles of the concrete paver test sections after various numbers of wheel load repetitions.

The development of rutting in Dutch study[5] is defined by the following equation

$$RD = a_{p6/0.6} (N_{6/0.6})^{b_{p6/0.6}}$$

Where:

RD = mean rut depth (mm)

$N_{6/0.6}$ = cumulative number of (wheel track apparatus) wheel loads (P = 6 kN, p = 0.6 N / mm^2) repetitions

$a_{p6/0.6}$ and $b_{p6/0.6}$ = rutting coefficients for the total pavement structure, subjected to wheel loads.

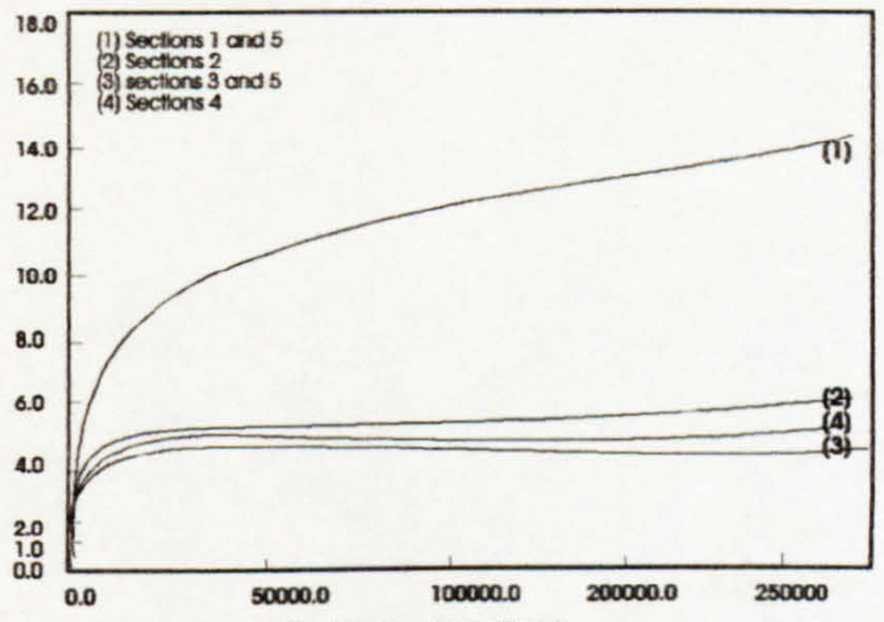

Figure 3.37: Average rut depth of the concrete paver test sections as a function of the number of wheel load repetitions.

The calculated rutting coefficients $a_{p6/0.6}$ and $b_{p6/0.6}$ and the regression coefficient r in Dutch study[5] are given in Table 3.13.

Sections	wheel track apparatus loads (P=6kN, p=0.6N/mm^2; $N_{6/0.6}$)			falling weight loads (P=6kN, ϕ=300mm; $N_{6/\phi300}$)		equivalent standard wheel loads (P=40kN, ϕ=300mm; $N_{40/\phi300}$)	
	$a_{p6/0.6}$	$b_{p6/0.6}=b_p$	r	$a_{p6/\phi300}$	$b_{p6/\phi300}=b_p$	$a_{p40/\phi300}$	b_p
1 and 6	0.853	0.225	0.988	0.315	0.225	2.146	0.225
2	0.795	0.177	0.941	0.299	0.177	2.006	0.177
3 and 5	0.753	0.156	0.893	0.283	0.156	1.889	0.156
4	0.818	0.162	0.942	0.306	0.162	2.059	0.162

Table 3.13: Rutting coefficients a_p and b_p (with respect to the mean rut depth) of the test sections for various types of wheel loads.

The maximum deflection d_0 (in the centre of the load) in Dutch study[5] is considered by Boussinesq's equation.

$$d_{0,6/0.6} = 2.63\, d_{0,6/\phi300}$$

where:

$d_{0,6/0.6}$ = maximum deflection due to a wheel track apparatus wheel load

$d_{0,6/\phi300}$ = maximum deflection due to the falling weight load (P = 6 kN, ϕ = 300 mm)

$$N_{6/\phi 300} = 2.65^{\frac{1}{b_{p6/0.6}}} . N_{6/0.6}$$

where:
$N_{6/\phi 300}$ = cumulative number of falling weight load repetitions
$b_{p6/0.6}$ = see the relevant equation
$N_{6/0.6}$ = see the relevant equations

The rutting of the concrete paver pavements in Dutch study[5] is defined by the following equation:

$$RD = a_{p6/\phi 300} \cdot (N_{6/\phi 300})^{b_{p6/\phi 300}}$$

Where,
RD = mean rut depth (mm)
$N_{6/\phi 300}$ = see the relevant equation
$a_{p6/\phi 300}$ and $b_{p6/\phi 300}$ = rutting coefficients for the total pavement structure, subjected to wheel loads

The rutting coefficients $a_{p6/\phi 300}$ and $b_{p6/\phi 300}$ ($=b_{p6/0.6} = b_p$) of the various test sections in Dutch study[5] are calculated as follows. The number of actual traffic wheel loads (for instance P=40kN, ϕ=300mm) is calculated from the number of falling weight loads using an AASHTO* -type load equivalency factor in terms of rutting.

$$N_{40/\phi 300} = (\frac{6}{40})^{\frac{1}{b_p}} . N_{6/\phi 300}$$

Where,
$N_{40/\phi 300}$ = cumulative number of equivalent standard single wheel loads
$N_{6/\phi 300}$ = see the relevant equation
b_p = rutting coefficient for the concrete paver pavement under construction

The rutting of concrete paver pavements in terms of repeated equivalent standard single wheel loads is defined in Dutch study[5] by the following equation.

---

* One of the major conclusions of the AASHO (American Association of State Highway Officials) Road Test was the development of equivalence damage factors for different axle loads. The tests showed that damage sustained by a pavement was dependent on the vehicle's axle load, but independent of pavement structure. The relationship has been verified by results from other test pavements and studied in more detailed by Heukelom and Klomp[51].

$$RD = a_{p40/\phi300} \cdot N_{40/\phi300}^{b_p}$$

where:
RD = mean rut depth (mm)
$N_{40/\phi300}$ = see the relevant equation
$a_{p40/\phi300}$ and b_p = rutting coefficients
for the total pavement structure,
subjected to equivalent standard single
wheel loads (P = 40 kN, ϕ = 300 mm)

The one of the analysis type conducted in Dutch study[5] was two-dimensional finite element modelling technique and this two-dimensional ICWS STRUDL[5] finite element model was used in the analysis of the concrete paver test sections. The details of the two-dimensional finite element modelling are as follows.

The model thickness is 1 mm. The concrete paver layer is modeled by a number of indeformable rigid body elements that represent the concrete pavers which are joined together using vertical linear springs symbolising the shear resistance of the joints (see Figure 3.38). The spring stiffness k (N/mm) of the joints is defined by the following equation.

$$k = \frac{G.h_1.1}{2w} = \frac{G.h_1}{2w}$$

Where:
G = shear modules of the joints (N / mm^2)
h_1 = concrete paver thickness (mm)
w = actual joint width (mm)

The concrete pavers are joined to the underlying bedding layer using vertical linear springs. The spring stiffness k'(N/mm) in Dutch study[5] is defined by the following equation.

$$k' = \frac{c.b.1}{2} = \frac{c.b}{2}$$

where:
c = bedding constant (N / mm^3)
b = concrete paver length or width (mm),
considering herringbone bond

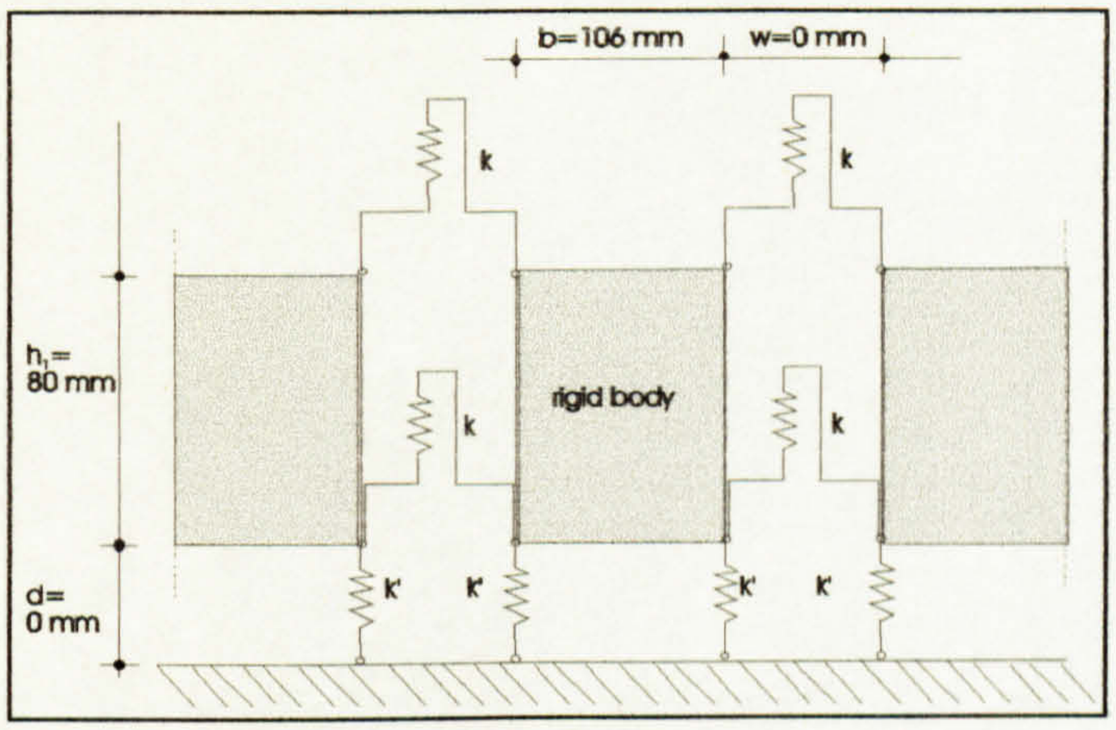

Figure 3.38: Two-dimensional finite element model is used Dutch study[5] for concrete paver pavements.

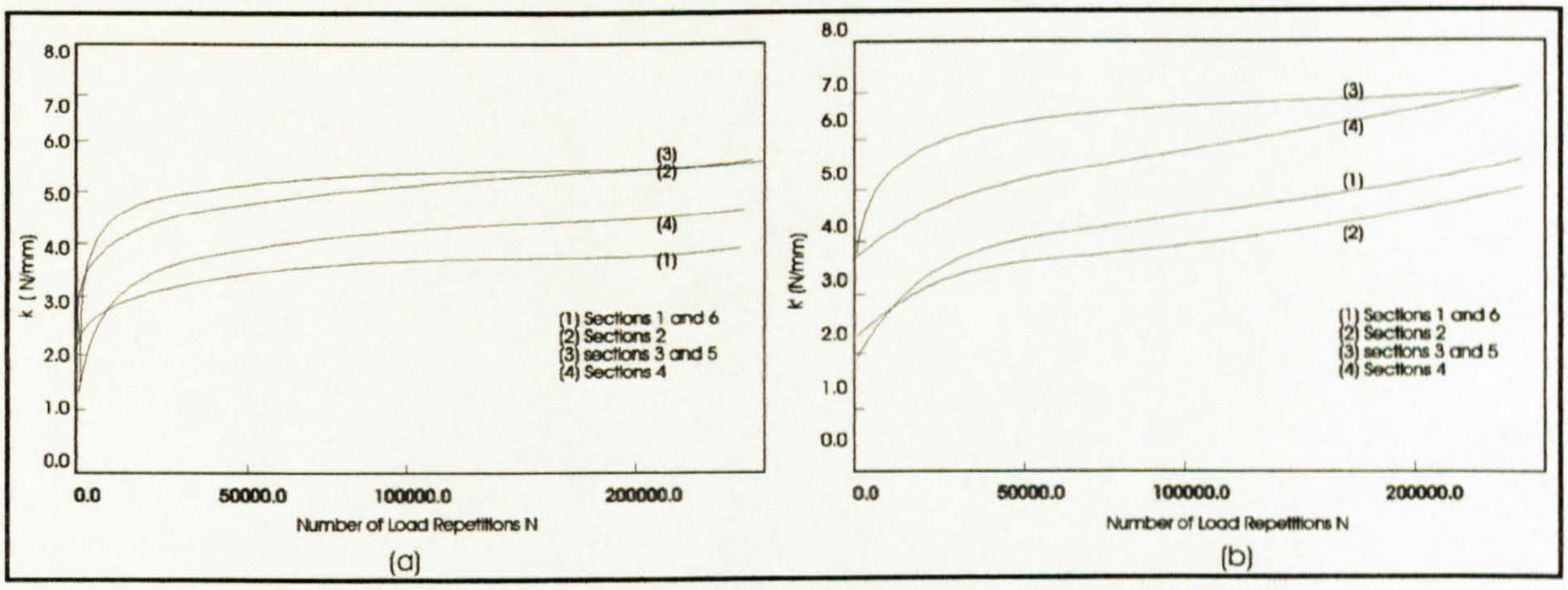

Figure 3.39-**a** and 3.39-**b**: **(a)** Joint stiffness (k) of the concrete paver test sections as a function of the number of wheel load repetitions, **(b)** Support stiffness (k') of the concrete paver test sections as a function of the number of wheel load repetitions used in Dutch study[5].

It is assumed in Dutch study[5] that no bending moments are transmitted in the paver layer and only vertical displacements of the pavers occur. The measured maximum deflection (d_0) is used as a displacement in two dimensional finite element model. The spring stiffnesses k and k' are calculated by means of trial and error. In Figures 3.39-a and 3.39-b, the progress of k and k' is illustrated with the number of wheel load repetitions. It is shown

in Figures 3.39-a and 3.39-b that the characteristic progressive stiffening behaviour and the supporting spring k' increases with increasing base thickness, but the joint stiffness k is hardly related to the base thickness.

A linear-elastic multilayer computer program BISAR[5] in Dutch study[5] is used to calculate the elastic compression of each layer for every deflection measurement because the calculated stresses, strains and displacements within the bedding layer, the base, the sub-base and the subgrade are not reliable owing to the supporting springs k' taking a significant part of the load in the two dimensional finite element analysis (see Figure 3.38).

Another analysis type was conducted in Dutch study[5] was the axial-symmetric finite element modelling technique in which the calculation of stresses, strains and displacements within the pavement structure below the rigid body top layer were determined in the axial-symmetric finite element model instead of the two-dimensional model. The details of the axial-symmetric finite element modelling are as follows.

The concrete paver layer is shown as a pure shear layer consisting of a number of indeformable rigid bodies which are joined together by vertical linear springs. The stiffness K of these springs is (see Figure 3.40):

$$\boxed{K = 2\pi rk}$$

Where:
k = spring stiffness according to the relevant equation(N / mm per mm)
r = distance to the loadcenter (mm)

The pavement (the bedding layer, the base, the sub-base and the subgrade) are modeled by the resilient modules Mr and Poisson's ratio (ν). The rigid body elements in the axial-symmetric finite element representation are fixed to the underlying bedding layer. All rigid bodies are only fixed at one point to prevent tensile stresses in the bedding layer except the loaded rigid body. The springs in the other points was introduced with very low stiffness k".

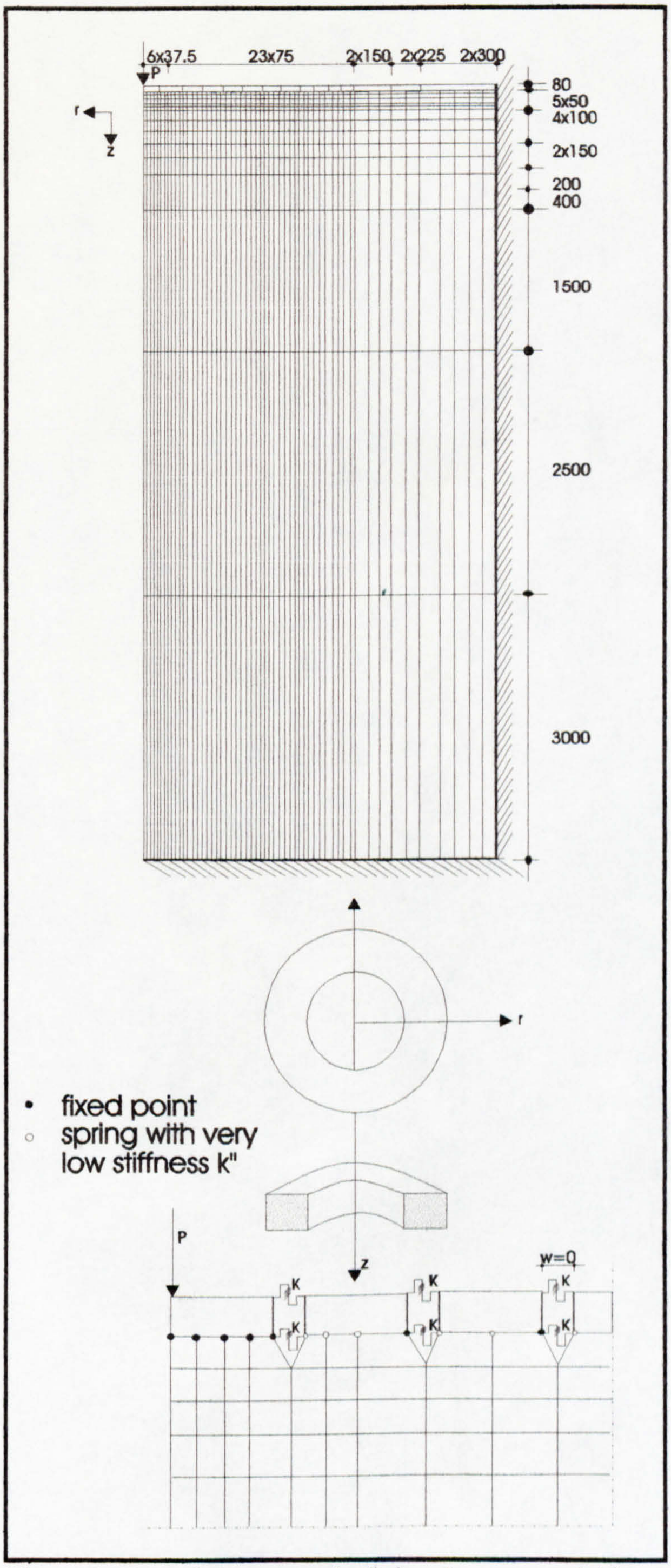

Figure 3.40: Axial-symmetric finite element model is used in the Dutch study[5] for concrete block pavements (dimentions in mm).

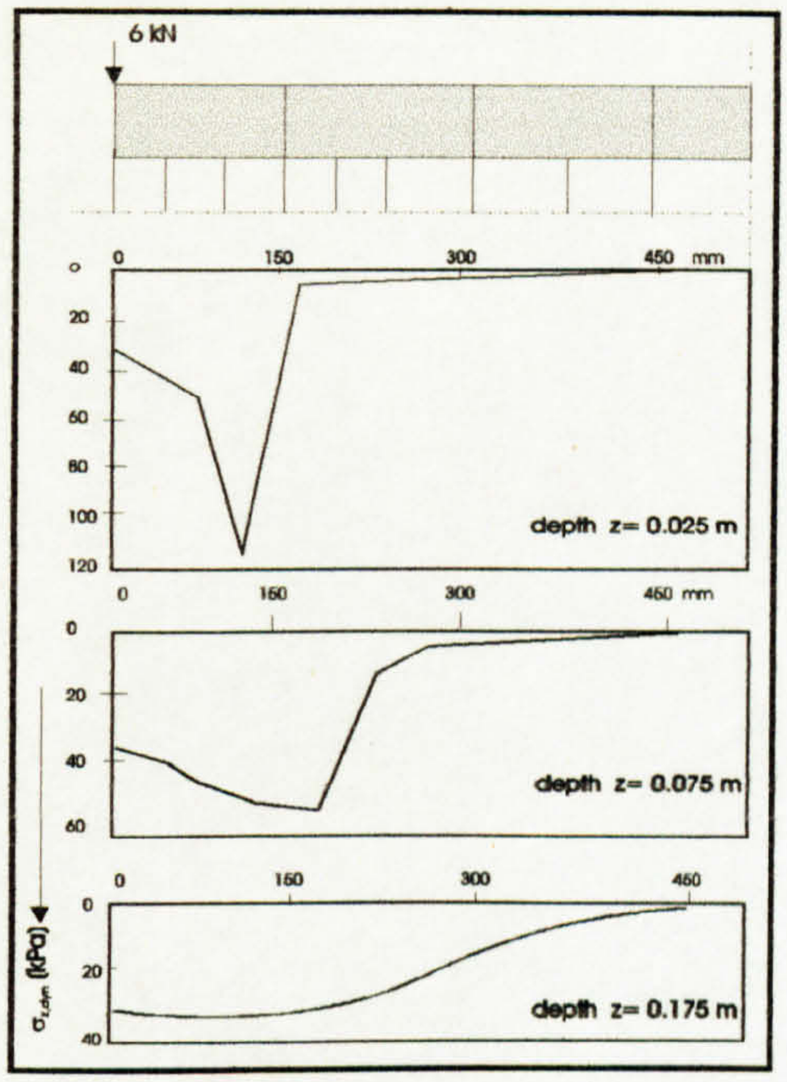

Figure 3.41: Vertical dynamic stresses within the test sections 1 and 6 at several depths below the concrete paver layer (load P=6kN and joint stiffness k=2.0N/mm).

The measured deflection curves of the test sections 1 and 6 in Dutch study[5] were calculated considering the axial-symmetric finite element model (see Figure 3.40) for 180,000 wheel load repetitions. In this calculation the Mr-θ relationships from Figure 3.41 and the minimum joint stiffness k=2.0N/mm (from two-dimensional finite element calculations, see Figure 3.39-a) were used. It is assumed that there is hardly load transfer from the loaded rigid body concrete paver to adjacent pavers and the vertical dynamic stress distribution below the loaded rigid paver is similar to the stress distribution below a very stiff foundation, with peak stresses below the edge of the loaded paver, as can be seen in Figure 3.41. It is noted in Dutch study[5] that the regular vertical dynamic stress distribution is reached at depth of about 0.2 m below the concrete paver layer. In addition, it is also assumed that especially in long term performance there is admirable correspondence between measured load and calculated rut depth (see Figure 3.42). In the Dutch study[4, 5, 6, 8] the resilient (deflections) and permanent(rutting) deformation behaviours of the test pavement were determined by falling weight deflection measurements and level measurements. Rigid body and permanent deformation behaviours were analysed using

progressive stiffening theory in Dutch study[6]. The analysis was conducted using elastic and permanent progressive stiffening coefficients for the various layers of the test pavement structure. The Dutch study[6] concluded that the load equivalency coefficient is dependent on the total pavement structure, especially on the subgrade modulus of elasticity.

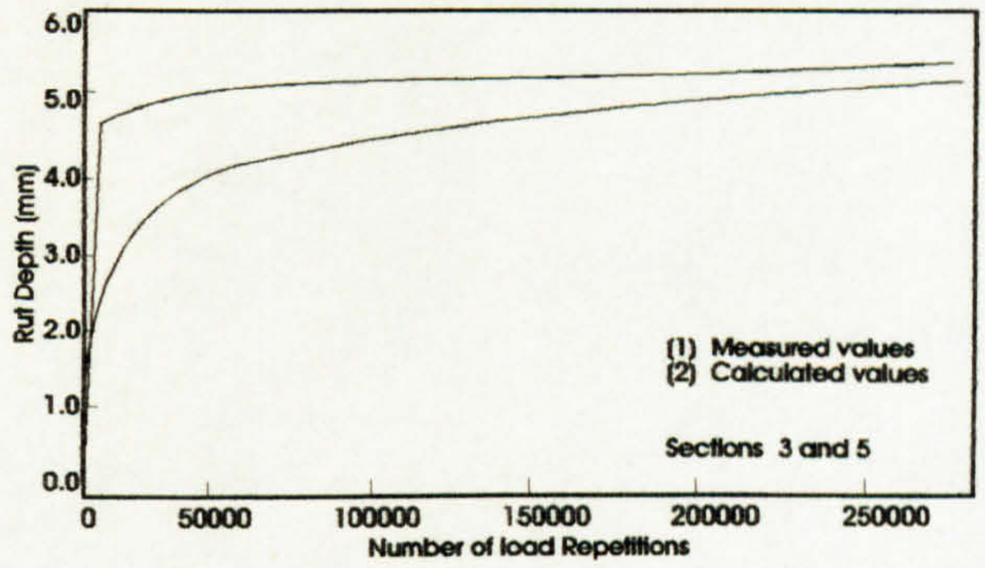

Figure 3.42: Comparison of the measured load and calculated rutting behaviour of the test sections 3 and 5 (load P=6kN, p=0.6N/mm^2).

The falling-weight deflection measurements were used to determine the resilient and the permanent deformation behaviours of the concrete paver test pavements. A 50kN dynamic load was applied through a circular plate of diameter 300mm. The contact pressure was 0.707N/mm^2 and the loading time was 0.02s. The deflections (d) were measured at distances of 0, 0.3, 0.5, 1.0, 1.5 and 2.0 m from the centre of the loading plate. The modulus of elasticity E_0 (N/mm^2) of the subgrade in Dutch study[6] was calculated by the following formula.

$$\log E_0 = 3.869 - 1.009 \log d_2$$

Where:

d_2 = deflection (μm) at a distance of 2m from the centre of the loading plate (50kN load)

E_0 = The modulus of elasticityof the subgrade (N / mm^2)

It was assumed in Dutch study[6] that maximum deflection decreased with increasing time (number of axle load repetitions) and all the test pavements indicated the characteristic progressive stiffening behaviour of stable concrete paver pavements. The level

measurements indicated that the rut depth increased with decreasing bearing capacity and with increasing traffic loading of the test pavement. The progress of rutting on the test pavements in Dutch study[6] is described by the following equation.

$$RD_c = a_p N^{b_p}$$

Where:
RD_c = charecteristic rut depth (mm), 30 per cent probability of exceeding
N = cumulative number of equivalent 80kN standard axle loads per lane
a_p, b_p = rutting coefficients with respect to the total pavement structure.

The cumulative number of equivalent 80kN standard axle loads N is obtained by addition of the relative damage. The most widely used model for this relative pavement damage uses the AASHTO-type load equivalency factor l_e according to:

$$l_e = \left(\frac{L}{L_{st}}\right)^m$$

where:
L = axle load (kN)
L_{st} = standard axle load (= 80 kN)
m = load equivalency coefficient

With respect to rutting, m for concrete paver pavements is given by:

$$m = \frac{1}{b_p}$$

where:
b_p = rutting coefficient

It was assumed that the rutting behaviour (such as rutting coefficients a_p and b_p) of concrete paver pavements is highly dependent on the total pavement structure, or the measured characteristic rut depth, the estimated number of load repetitions and the distribution of axle loads. In the two dimensional finite element representation the concrete paver layer is modeled as a pure shear layer. The concrete pavers are represented as indeformable rigid body elements which are interconnected by linear vertical springs with stiffness k, can move only in the vertical direction. The rigid body paver elements are supported by linear vertical springs with stiffness k', which represents the connection of the concrete paver to

the underlying bedding layer. The layers below the concrete pavers , the bedding layer, the unbound base, the sand sub-base and the subgrade are investigated with a system of continuous elements and characterised by the modulus of elasticity and Poisson's ratio. The following empirical equation is used for calculation of the modulus of elasticity E_i (N/mm^2) of the sand sub-base and unbound base.

$$E_i = l.E_{i+1} \quad \text{with } l = 0.206\, h_i^{0.45} \quad (2 \le l \le 4)$$

where:
h_i = thickness(mm) of the course considered
E_{i+1} = modulus of elasticity (N / mm^2)of the underlying course.

The two dimensional finite element model is loaded so as to induce a displacement equal to the measured maximum deflection d_0 at the centre of the load. The ICES STRUDL[6] finite element program is used to determine the parameters of each deflection curve. The spring stiffnesses k and k', were found for the test pavements wheel track by means of trial and error. It was assumed that the joint stiffness k substantially increases with time (number of load repetitions) and the support stiffness k' slightly increases with time on the test pavements. The progressive stiffening theory developed at Delft University of Technology[6] is used for the analysis of the permanent deformation behavior of the test pavement. The basic equation of the progressive stiffening theory is (see Figure 3.43):

$$\frac{d(\Delta h_p)}{dN} = f_1 \frac{df_2}{dN}$$

Where:
Δh_p = permanent deformation in a layer of unbound material
f_1 = elastic compression of the layer (= the deflection at the top of the layer minus the deflection at the bottom of the layer) due to an equivalent 40kN standard wheel load (80kN standard axle load)
f_2 = permanent deformation relationship of the unbound material.

for a granular material the compaction relation f_2 is given by:

$$f_2 = a_m N^{b_m}$$

where:
N = number of equivalent 80kN standard axle load repetitions per lane (in the wheel track)
a_m, b_m = permanent deformation coefficients of the granular material.

The elastic compression f_1 of a granular layer can be described as:

$$\text{if } N \le N_1: f_1 = d_{max} = \text{constant}$$
$$\text{if } N > N_1: f_1 = p + q.e^{-\log N}$$

where:
N_1 = initial number of equivalent 80kN standard axle load repetitions per lane (in the wheel track) until progressive stiffening occurs
d_{max}, p, q = elastic deformation coefficients of the granular layer

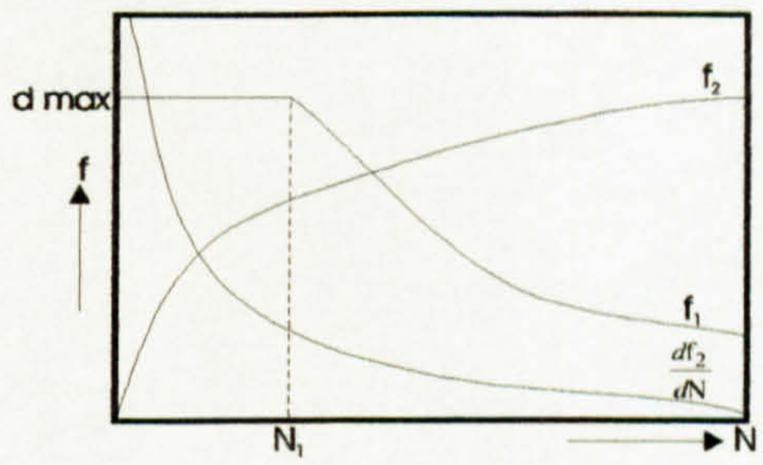

Figure 3.43: Schematical representation of permanent deformation functions.

The permanent deformation Δh_p in a layer of granular material in a concrete paver pavement was obtained from the equations described below:

$$\text{if } N \le N_1: \Delta h_p = d_{max}.a_m.N^{b_m}$$
$$\text{if } N > N_1: \Delta h_p = d_{max}.a_m.N_1^{b_m} + a_m.p.\left(N^{b_m} - N_1^{b_m}\right) + \frac{a_m.b_m.q}{b_m - 0.4343}\left(N^{b_m - 0.4343} - N_1^{b_m - 0.4343}\right)$$

Where:
N = number of equivalent 80kN standard axle load repetitions per lane (in the wheel track)
N_1 = initial number of equivalent 80kN standard axle load repetitions per lane (in the wheel track) until progressive stiffening occurs.
Δh_p = permanent deformation in a layer of unbound material
d_{max}, p, q = elastic deformation coefficients of the granular layer
a_m, b_m = permanent deformation coefficients of the granular material.

On the concrete paver pavement, the degree and extent of rutting were taken into account in the Dutch design method[6]. The permanent deformation (rutting) calculations were carried out according to the progressive stiffening theory. The initial number of equivalent 80kN standard load repetitions before progressive stiffening coefficients (d_{max}, p, q) was determined by means of calculations according to Ivanov[49]'s equivalency theory. $\overline{N}$-values of the concrete paver pavement is calculated with following formulation:

$$\overline{N} = \left(\frac{\overline{RD_c}}{a_p}\right)^{\frac{1}{b_p}}$$

Where:

$\overline{N}$ = acceptable number of equivalent 80 kN standard axleload repetitions per lane in the wheel track (making allowance for the lateral load distribution)

$\overline{RD_c}$ = charecteristic rut depth (30 per cent probability of exceeding); standard: $\overline{RD_c}$ = 15mm

a_p, b_p = rutting coefficients with respect to the total pavement structure.

The load equivalency coefficient m of concrete block pavements is calculated from the following equation:

$$m = 1.87 + 183\ E_0^{-1.5}$$

where:

E_0 = modules of clasticity (N / mm^2) of the subgrade, according to the relevant equation.

(It was assumed that the pavement life mainly depends on the subgrade modulus E_0 and, in case of a low E_0-value, also on the sand sub-base thickness.) In addition the value of the E_0 should fulfill the following equation.

$$E_0 \cdot (h_{sand})^{0.6} \geq 33$$

where:

E_0 = modulus of clasticity (N / mm^2) of the subgrade

h_{sand} = sand sub - base thickness (m).

Five design charts were developed for concrete paver pavements with an unbound base and a sand sub-base, for subgrade modulus values of 30, 40, 60, 100 and 140 N/mm^2. Each design chart applies to both a crushed concrete base material and a crushed concrete/crushed clay bricks base material. Two design charts are shown in Figure 3.44.

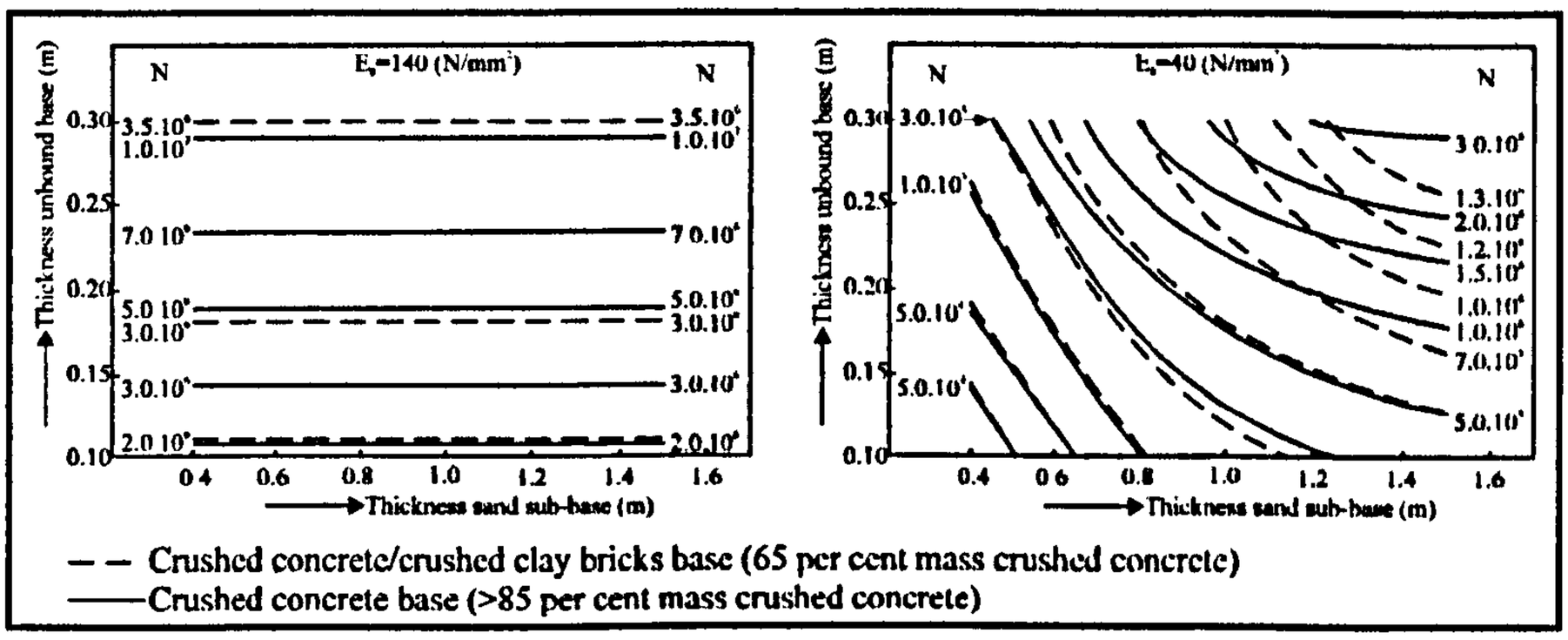

Figure 3.44: Design charts of the Dutch study[6] for concrete paver pavements installed with rectangular pavers (thickness≥0.08m) in herringbone bond, 0.05 m crushed sand bedding layer, an unbound base and a sand sub-base.

It was assumed that under normal road traffic shear failure of a concrete paver pavement with an unbound base is most unlikely. It was also assumed that the pavement life depends on the base material and the base thickness, and the load equivalency coefficient m also depends on the base material, base thickness, the sand sub-base thickness, and the subgrade modulus. For concrete paver pavements with a crushed concrete base the following values were calculated in the Dutch study[6]:

maximum m value:	$m = 3.81 + 242E_0^{-1.5}$
mean m value:	$m = 2.97 + 95E_0^{-1.5}$
minimum m value:	$m = 2.30 + 70E_0^{-1.5}$

Table 3.14 illustrates two design examples of the Dutch study[6]. It is assumed in the design examples of Table 3.14 that the total thickness of unbound base and sand sub-base should be minimum to reduce construction costs. Table 3.14 includes two traffic loadings:

- case 1 for residential street: total number of axle load repetitions per lane in the wheel track during design life: 2.10^6; axle load distribution: 5kN: 85%, 10kN: 5%, 40kN: 5%, 50kN: 5%.

-Case 2 for industrial road: total number of axle load repetitions per lane in the wheel track during design life: 15.10^6; axle load distribution: 5kN: 50%, 10kN: 10%, 30kN: 15%, 50kN: 15%, 70kN: 6%, 90kN: 2.5%, 110kN: 1.2%, 130kN: 0.3%.

Subgrade modulus of elasticity E_0 (N/mm^2)	40						140					
Traffic	case 1			case 2			case 1			case 2		
Pavement structure[1)]	S	CCS	CBS	S**	CCS	CBS**	S	CCS	CBS	S**	CCS	CBS
Load equivalency coefficient m (the equations* respectively)	2.6	3.3	3.1	2.6	3.3	3.1	2.0	3.0	2.8	2.0	3.0	2.8
Total number (N) of equivalent 80kN standard axle load repetitions per lane in the wheel track during design life (.10^6)	0.048	0.032	0.035	2.57	2.44	2.46	0.072	0.038	0.042	2.87	2.47	2.51
Concrete paver thickness (m): minimum	0.08	0.08	0.08	-	0.08	-	0.08	0.08	0.08	-	0.08	0.08
Crushed bedding sand layer (m)	0.05	0.05	0.05	-	0.05	-	0.05	0.05	0.05	-	0.05	0.05
Crushed concrete base (m)	-	0.10	-	-	0.30	-	-	0.10***	-	-	0.13	-
Crushed concrete/crushed clay bricks base (m)	-	-	0.10	-	-	-	-	-	0.10***	-	-	0.15
Sand sub-base (m)	0.90	0.40	0.40	-	1.10	-	0.00	0.00	0.00	-	0.00	0.00

[1)] S =sand sub-base only
CCS=crushed concrete base and sand sub-base
CBS=crushed concrete/crushed clay bricks base and sand sub-base

* equations: $m=1.87+183E_0^{-1.5}$, $m=2.97+95E_0^{-1.5}$, $m=2.72+95E_0^{-1.5}$

** pavement structure impossible for the present combination of traffic loading N and subgrade modulus E_0

*** overdesigned because a base and a sub-base are not necessary, as concerns the bearing capacity of the concrete paver pavement structure

Table 3.14: Some design examples of the Dutch study[6] for rectangular concrete paver pavements.

3.3. Discussion and comments

This Chapter has shown that a wide variety of methods are available for the design of concrete paver pavements. The methods vary widely in the degree to which they incorporate design and performance criteria which are appropriate to paver pavements. A variety of design methods based on the use of charts and nomographs have been presented. However, it is important to recognise that such methods are, in general, unlikely to yield as an optional design solution as the various analytical procedures. Once an analysis procedure has been selected the designer's task is to select that combination of paver, base, and (where appropriate) sub-base that will most economically satisfy the service

requirements of the pavement. Usually the designer has a choice of material. Moreover, he must decide whether a sub-base is needed or whether in-situ stabilisation of the subgrade should be considered. The number of feasible design solutions is normally large. Therefore, different design alternatives need to satisfy the speed, convenience and performance of the construction techniques in different climates and traffic conditions. The availability of the construction materials are also important to select a design type. This criteria needs to be established to help choose amongst the various alternatives. The criteria such as initial construction costs and discounted annual costs are largely subjective or judgmental and, therefore, rely on the skill and knowledge of the designer as well as they are quantifiable and are usually perceived by the pavement owner or user as paramount in the choice of a particular pavement design for their successful application. For this reason cost is being increasingly treated as a routine input to modern paver paving design procedures.

Consideration of the preceding sections show that designers have a wide and sometimes bewildering choice of design methods for paver pavements. Often the thicknesses indicated by one method will differ significantly from that required by some other procedure. The following example is applied to the design methods described in Section 3.2.3 and Section 3.2.2.8 respectively in order to reveal that how paver pavement designs vary from one design method to another.

If a road which has 20 years design life and is planned to be built in the UK on the heavy clay subgrade which has 4% CBR value and if its initial traffic flow is expected to be 500 commercial vehicles per day in each direction with an annual traffic growth of 5%, the solution could be as follows by using the design based on equivalence technique (see Section 3.2.3).

Commercial vehicles per day at opening (F_0) is 500. Annual growth rate (r) is 5%. Design life (n) is 20 years. The total number of commercial vehicles (T_n=6.0345 million cvs) can be calculated using Equation (3.1) can be seen in Section 3.2.2.3. Assuming road to be

opened in 1997, then t=52 and F=500 and, from Equation (3.3), D=1.5718 and therefore total traffic=6.0345 x 1.5718=9.4850 msa. Following the recommendations given in LR 1132[19], for the CBR 4% a capping layer of at least 350mm thickness and a sub-base of 150mm are required (see Figure 3.7). From Figure D2 of LR 1132[19], the roadbase thickness of dense bound macadam or hot-rolled asphalt required to satisfy the traffic conditions would be 300mm. Replacing part of this bituminous material with pavers (80mm) and sand (30-50mm) from Table 3.8, it can be seen that this allows the asphalt thickness to be reduced to 150mm. Alternatively, examining the use of a cement-bound base, complying with the requirements of CBM 3 (see Section 2.18), the required lean concrete roadbase thickness = 150/0.7≅214mm. This results in two alternative designs, as follows:

80mm pavers	80mm pavers
30 - 50mm laying course	30 - 50mm laying course
150mm hot - rolled asphalt roadbase	214mm CBM 3 roadbase
150mm sub - base	150mm sub - base
350mm capping layer	350mm capping layer

The UK approach to design has been criticized by many who regard the adoption of Road Note 29[20] sub-base design curves as conservative. Technically, this criticism has some justification but there is no doubt that the use of a familiar design technique has been of major benefit to the development of paver paving in the UK. Also, virtually all UK paver pavements are performing satisfactorily and first time users frequently respecify the material for subsequent work. It is also true that the formal approach to design adopted in the UK has prompted engineers in traditional paver paving countries to reassess their approach to design. The paver pavement design method is based on concept of making pavers and their bedding sand equivalent to conventional pavement construction materials. Experience has shown that pavers do not behave as a collection of individual units but rather interlock so that they behave in a manner close to that of flexible materials such as asphalt (see Figure 6.17). This observation is also used as an assumption to develop the bedding sand stress calculation method described in Chapters 4, 5, 6, 7, 8 and 9. The mathematical solutions of the vertical compressive stress distributions beneath the paver

types described in Chapters 6, 7, 8 and 9 concluded that there are minor differences in the performance of different pavers and the load spreading capability of both shaped and rectangular pavers is similar (see Figures 6.21, 9.1, 9.2, 9.3, 9.4, 9.5, 9.6, 9.7, 9.8 and 9.9). The equivalent design method does not restrict the use of the paver types which is commercially available at present. In conclusion, it can be emphasised that equivalent design technique addresses to the true behaviour of paver pavement.

If Shackel[35, 50]'s design curves, diagrams and recommendations (see Section 3.2.2.8) are used for the same inputs, the results could be:

80mm unipave / interpave blocks
20mm laying course
300mm gravel base
550mm cement - stabilized sub - base

The condition of the road network is of vital importance to the economy of any country. The task of the highway authorities is to maintain the system to those standards that will provide for the lowest overall costs of transportation, as related to paver pavements. The comparison of the last two design results reveal that Shackel[35, 50]'s design method is of limited value in this context. By implication Shackel[35, 50]'s design method described in Section 3.2.3.8 can also be considered to be conservative because it requires substantially higher cost base thicknesses. In addition Shackel[35, 50]'s design curves, diagrams and recommendations based upon the assumption that interpave pavers (see proprietory shaped paver 1 in Figure 5.1) perform better than rectangular pavers in service. However, as noted above, one of the major conclusion of this Thesis is that the data relating to pavers of different geometries indicates that there are differences in the performance of different pavers although the effect is likely to be of minor structural consequence (see 6.21, 9.1, 9.2, 9.3, 9.4, 9.5, 9.6, 9.7, 9.8 and 9.9). It can be seen from the figures that the only exception to this is the difference between chamfered and non-chamfered pavers. By

considering the load patch as a paver perimeter, chamfered pavers reduce bedding sand stress levels and are therefore to be preferred in trafficked pavements.

3.4. Conclusion

Each of the design methods described in this Chapter has benefits and disbenefits but none of them model paver pavements accurately subjected to rolling loads. It is important to consider paver pavement's bedding sand specification for accurately modelling. The applicability of some design methods presented in this Chapter can be disputed because of both lack of input-variables about behaviour of pavers at surface level and accuracy of modelled materials used in pavement construction are non-isotropic and exhibit varying degrees of elastic, plastic and viscous characteristics. Their input-variable deficiencies at surface level were formed the bedding sand stress calculation method described in Chapters 4, 5, 6, 7, 8 and 9. Two characteristics have to be established if paver pavement levels are to be modeled accurately; these are resilient (or elastic) behaviour and permanent (or plastic) behaviour. These are generally regarded as the relationship between applied stress and recoverable strain, and permanent strain and number of load applications, or design life. The result of the mathematical model analysis researches into the behaviour of pavement structures relates directly with the accurate determination of the component material ultimate strengths. All materials used in pavement construction are non-isotropic and exhibit varying degrees of elastic, plastic and viscous characteristics. A mathematical model can be no more accurate than the accuracy of the input variables, hence research into material characterisation has followed closely behind the development of the analysis methods. The only analytical technique available that encompassed this degree of complexity is the finite element method. Unfortunately this requires a vast amount of computer resources, and the information currently available on materials is too variable to justify the material characterisation has, therefore been directed toward quantifying the elastic, both linear and non-linear, and the visco-plastic behaviour. This Chapter also outlined the design method based upon finite element analysis research (see Section 3.2.4)

in which the parameters depend on simple empirical relationships. However, these techniques whose reliability directly related with the accuracy of the modeling are very useful in developing an understanding of the essential problems of paver pavement design.

The assumptions which are accepted in Dutch study[5, 6, 7, 8, 9, 10] (see Section 3.2.4) do not address the true dynamic behaviour of paver pavement because of the following reasons:

In principal, it can be assumed that spring constants (k) are not different from each other at the surface (see Figures 3.38 and 3.40). However, in the process of time assemblage of spring elements' constant can chance because of number of applied load, moisture, temperature, concentrated dynamic or static load application etc. The behavior of paver pavement at the surface shows unique characteristics (see Figure 6.17), the solution by directly applying the flexible pavements' mathematical modeling techniques cannot be compatible. The patch load applications on the surface varies in terms of contact load area's position (see Chapters 4 and 5). There are five main vertical compressive stress regimes which can occur beneath pavers according to magnitude and position of patch loads. These are conceptually (see Chapters 6, 7, 8 and 9):

- tetrahedral stress regimes
- long-pentahedral stress regimes
- short-pentahedral stress regimes
- partial-hexahedral stress regimes
- absolute-hexahedral stress regimes

The compression area beneath pavers bounded by force equilibrium line can only behave elastically and the other bottom surface area (apart from compression section) has zero stress value, (so elastic behaviour in this area cannot occur because tension cannot be developed in uncemented sand so that compressive stress is developed in some parts of interface and zero stress is developed elsewhere.) (Deflections and stress distributions are

function of applied tyre pressure and they change three dimensionally by exceeding tyre pressure in certain points beneath pavers.) In the Dutch study[5, 6, 7, 8, 9, 10] the force-deformation relationship at the surface of the paver pavement does not satisfy the equilibrium of applied load pressure because of the analysed model (exp. See Figures 3.38 and 3.40). The expression of the equilibrium at each nodes is not compatible in terms of the patch loadings and the vertical compressive stress regimes vary in bedding sand. Behaviour of paver pavement systems should not be attempted to solve by referring first to conceptually simple structural assemblies involving linearly elastic springs, because force-deformation relationships of construction materials are also function of time, moisture contents, temperature etc.) The problem relates with dynamic and non-linear mechanistic behaviour of paver pavements and equilibrium of force, force-deformation relationships should be satisfied. In addition, material categorisations are closely related with accuracy of mathematical modeling. Especially bedding sand has direct influence to stress distribution. It has to be categorised properly in terms of maximum stress values. Stress distribution can change for stabilised and non-stabilised joints. This should also be considered in mathematical modeling. Uncertainties in paver pavement design often may be overcome by changing to a computer-based analytical design methodology. Here the designer may freely specify the properties of the pavers, base, sub-base and subgrade. Accordingly each design may be tailored to suit such factors as the cost and availability of materials. Moreover, no simplifying assumptions concerning the loading conditions need to be made. Analytical paver pavement design involves the formulation and solution of a boundary value problem. This requires the determination of the stresses and strains at critical locations throughout the pavement. These are compared with the values that would, theoretically, be predicted to cause failure of the pavement. Failure may be the result of either excessive rutting or, in the case of bound materials, of extensive cracking leading to a loss in both strength and stiffness (see Figure 1.7). Typically, as shown in Figure 3.5, the critical stresses and strains occur either on or near the vertical load axis at the bottom of all bound layers and at the top of the subgrade. Provided the critical stresses and strains can be calculated it is possible to predict the service life of the pavement. Conversely, for a

designated service life, it is possible to calculate what values of stress and strain can be tolerated to determine what combination of layer thicknesses is required if these stresses and strains are not to be exceeded. The Dutch design method[6] described in this Chapter (see Section 3.2.4) is based on finite element analysis. Even though it is specific to particular types of base material and varies narrow ranges of subgrade conditions, its fundamental analysis technique can be very useful to understand the complex pattern of time dependent stresses by applying advanced accurate paver pavement modelling subjected to rolling loads. A particular advantage of such analysis technique is that they are capable of modelling non-linear visco-elastic shear sensitive anisotropic materials and complex dynamic and/or static loading conditions.

References

1 Lilley A. A.,(1991). *A Handbook of Segmental Paving*, Chapman & Hall, London.

2 Nishizaw, T., Matsuno, S. and Komura, M., (1984), *Analysis of Interlocking Block Pavements by Finite Element Method*, Proc. of 2nd. Int. Conf. on Concrete Block Paving, Delf, pp 80-85.

3 Molenaar, A. A. A., Moll, H. O. and Houben, L. J. M., (1984), *Structural Model for Concrete Block Pavements*, paper submitted to Annual Meeting of Transportation Research Board.

4 Houben, L. J. M., Molenaar, A. A. A., Fuchs, G. H. A. M. and Moll, H. O., (1984), *Analysis and Design of Concrete Block Pavements*, Proc. of 2nd. Int. Conf. on Concrete Block Paving, Delf, pp 86-99.

5 Houben, L. J. M. and Jacobs, M. M. J., (1988), *Wheel Tracktesting and Finite Element Analysis of Concrete Block Pavements*, Proc. of 3rd. Int. Conf. on Concrete Block Paving, Rome, pp 102-113.

6 Houben, L. J. M., et al., (1988), *The Dutch Design method for Concrete Block Road Pavements*, Proc. of 3rd. Int. Conf. on Concrete Block Paving, Rome, pp 156-169.

7 Huurman, M., (1994), *Development of the Non-linear Finite Element Program NOLIP for Concrete Block Road Pavements*, Proc. of 2nd. Int. Workshop on Concrete Block Paving, Oslo, pp 157-166.

8 Huurman, M., (1996), *Resilient Behaviour of Concrete Block Road Pavements and the Granular Materials Used in the Substructure*. Proc. of 5th. Int. Conf. on Concrete Block Paving, Tel-Aviv, pp 239-251.

9 Huurman, M., (1996), *Rut Development in Concrete Block Road Pavements Due to Permanent Strain in the Substructure*. Proc. of 5th. Int. Conf. on Concrete Block Paving, Tel-Aviv, pp 293-304.

10 Huurman, M., (1996), *Structural Design of Concrete Block Road Pavements Based on Transversal and Longitudinal Unevenness*, Proc. of 5th. Int. Conf. on Concrete Block Paving, Tel-Aviv, pp 349-364.

11 Algin, H.M., Knapton, J., (1996), *Research into paver interlock*, Jrnl. of the Institution of Highway & Transportation & IHIE, Vol. 43, No. 03, p 20-24.

12 Knapton, J., Algin, H.M., (1995), *The Mathematical Solution to Interlock in Flexibly Bedded Clay Paving*. Proc. of the 4th. Int. Masonry Conf. No. 7, Vol. 2, p 307-313. London.

13 Knapton, J., Algin, H.M., (1996), *The Mathematical Solution to Interlock in Concrete Block Paving*. Proc. of the 5th. Int. Conf. on Concrete Block Paving, p 261-278, Tel-Aviv.

14 Julian, L. D., (1986*), Finite Difference Methods in Dynamics of Continuous Media*, Macmillan Publishing Company, New York, 866 Third Avenue, NY 10022.

15 Ullidtz, P., (1987), *Pavement Analysis*, Published by Elsevier., pp 318.

16 Forchungsgesellschaft fur das Strassenwegen, (1980), *Merkblatt fur die Hesellung von Betonsteinpflaster*, Cologne.

17 Dansk Beton Industri, (1978), *Fliser Handbog*, DBI.

18 Clifford, J. M., (1981), *Structural Design of Segmented Block Pavements for Southern Africa*, National Institute for Transport and Road Research, CSIR, Pretoria, Technical Report, RP9.

19 Powell W. D., Potter J.F., Mayhew H. C. and Nunne M.E., (1984), *The Structural Design of Bituminous Roads*, TRRL Laboratory Report LR 1132, Transport and Road Research Laboratory, Crowthorne, UK, pp 62.

20 Transport and Road Research Laboratory, (1970*). A Guide to the Structural Design of Pavements for New Roads* ,Road Note 29, Third Edition, HMSO, pp 36.

21 Monismith, C. L. and Witczak, M. W., (1983), Moderators' Report. Papers in Session 1, Pavement Design, Proc. of 5th. Int. Conf. on Struct. Des. Asph. Pavements, Delf, 1982, (University of Michigan), vol. 2, p. 2.

22 Lister, N. W., (1972*), Deflection Criteria for Flexible Pavements*, Department of the Environment Department of Transport, TRRL Report LR 375, Crowthorne, (Transport and Road Research Laboratory).

23 Abell, R., (1983), *Economics of Staged Construction of Flexible Road Pavements*, Department of the Environment Department of Transport, TRRL Report LR 1069, Crowthorne, (Transport and Road Research Laboratory).

24 Currer, E. W. H. and O'Connor, M. G. D., (1979), *Commercial Traffic: Its Estimated Damaging Effect, 1945-2005*, Department of the Environment Department of Transport, TRRL Report LR 910, Crowthorne, (Transport and Road Research Laboratory).

25 Addis, R. R. and Robinson, R. G., (1983), *Estimation of Standard Axles for Highway Maintenance*, Proc. of the Symposium on Highway Maintenance and Data Collection, University of Nottingham, Nottingham, UK.

26 Black, W. P. M., (1979), *The Strength of Clay Subgrades: Its Measurement by a Penetrometer*, Department of the Environment Department of Transport, TRRL Report LR 901, Crowthorne, (Transport and Road Research Laboratory).

27 Black, W. P. M., and Lister, N. W., (1979), *The Strength of Clay Fill Subgrades: Its Prediction in Relation to Road Performance*, Department of the Environment Department of Transport, TRRL Report LR 889, Crowthorne, (Transport and Road Research Laboratory).

28 Department of Transport, (1978), *Road Pavement Design*, Technical Memorandum, No: H6/78, London, (Department of Transport).

29 US Department of the Army, (1980), *Engineering and Design, Flexible Pavements for Roads, Streets Walks and Open Storage Areas*, TM 5-822-5, Washington, DC.

30 Webster, S. L. And Alford, S. J., (1978), *Investigation of Construction Concepts for Pavements across Soft Ground*, US Army Waterways Exp. Station, Tech. Report S-78-6, Vicksburg.

31 Giroud, J. P. and Noiray, L., (1981), *Geotextile Reinforced Unpaved Road Design*, Proc. of the American Society of Civil Engineers Journal of the Geotechnical Engineering Division, Vol. 107, No. GT9.

32 Pike, D. C., Acott, S. M. and Leech, R. M., (1977), *Sub-base stability: A Shear-box Test Compared with other Prediction Methods*, Department of the Environment

Department of Transport, TRRL Report LR 785, Crowthorne, (Transport and Road Research Laboratory).

33 Barber, S. D. and Knapton, J., (1980), *Structural Design of Block Pavements for Ports*, Proc. of the 1st. Int. Conf. on Concrete Block Paving, University of Newcastle upon Tyne, UK, pp 141-149.

34 Ullidtz, P. and Peattie, K. R., (1980), *Pavement Analysis by Programmable Calculators*, Transportation Engineering Journal, American Society of Civil Engineers, September 1980.

35 Shackel, B., (1980), *The Design of Interlocking Concrete Block Pavements for Road Traffic*, Proc. of the 1st. Int. Conf. on Concrete Block Paving, University of Newcastle upon Tyne, UK, pp 23-32.

36 Paterson, W. D. O. and Maree, J. H., *An Interim Mechanistic Procedure for the Structural Design of Asphalt Pavements*, Tech. Rpt. RP/51.

37 Seddon, P. O., (1980), *The Behaviour of Interlocking Concrete Block Paving at the Canterbury Test Track*, Paper submitted to 10th. Aust. Rd. Res. Bd. Conference, Sydney.

38 Tait, J. B., (1978), *Heavy Duty Pavements in Interlocking Concrete*. New Zealand Conc. Const., November 1978.

39 National Association of Australian State Road Authorities, *Manual of Pavement Thickness Design*, 1978.

40 Freeme, C. R. and Monismith, C. L., (1974), *The Analysis of Permanent Deformation in Asphalt Concrete Pavement Structures*, Proc. of 2nd. Int. Conf. on Asphalt Pavements for Southern Africa, Durban, August 1974.

41 Croney, D., (1977), *The Design and Performance of Road Pavements*, HMSO, London.

42 British Standards Institution, (1992). *The Structural Design of Pavements Surfaced with Clay Pavers or Concrete Block Paving*, BS7533:1992, BSI, London.

43 British Standards Institution, (1986). *British Standard for Clay and Calcium Silicate Pavers for Flexible Pavements.* Part 1: *Specification for Pavers.* Part 2: *Code of Practice for Design of Lightly Trafficked Pavements.* BS 6677:1986, BSI, London.

44 British Standards Institution, (1988). *Precast Concrete Paving Blocks.* Part1: *Specification for Paving Blocks.* Part 3: *Code of Practice for Laying.* BS 6717:1988, BSI, London.

45 Department of Transport, Scottish Development Department, Welsh Office, Department of Environment for Northern Ireland, (1986), *Specification for Highway Works*, Part:3, HMSO, London, 70pp.

46 Kennedy, C. K., Lister, N. W., *Prediction of pavement performance and Design of Overlays*, Department of the Environment Department of Transport, TRRL Report LR 833, Crowthorne, (Transport and Road Research Laboratory).

47 Kennedy, C. K., Fevre, P. & Clarke, C., *Pavement Deflection: Equipment for measurement in United Kingdom*, Department of the Environment Department of Transport, TRRL Report LR 834, Crowthorne, (Transport and Road Research Laboratory).

48 Kennedy, C. K., *Pavement Deflection: Operating Procedure for Use in United Kingdom*, Department of the Environment Department of Transport, TRRL Report LR 835, Crowthorne, (Transport and Road Research Laboratory).

49 Ivanov, N. N., (1962), *Calculation of Flexible Pavements Subjected to Repeated Dynamic Loads* (in French), Revue Général des Routes et des Afrodromes, No. 294.

50 Shackel, B., (1988), *The Evolution and Application of Mechanistic Design Procedures for Concrete Block Pavements*, Proc. of the 3rd. Int. Conf. on Concrete Block Paving, Rome, pp 114-120.

51 Heukelom, W. and Klop, A. J. G., (1967), *Consideration of Calculated Strains at Various Depths in Connection with the Stability of Asphalt Pavements*, Proc. of the 2nd. Int. Conf. on Struct. Design of Asphalt Pavements, Ann Arbor, Univ. Michigan, pp 155-168.

CHAPTER FOUR

PATCH LOADING ON RECTANGULAR PAVERS

Synopsis

This Chapter presents a method to calculate the static vertical compressive pressures applied onto rectangular pavers (chamfered and non-chamfered) by rolling loads. It examines in detail the way in which patch loading applied to the wearing surface of rectangular pavers is transmitted as vertical stress into the underlying bedding material. The vertical compressive stresses in the bedding material are calculated for rectangular pavers (see Chapter 6) by considering vertical and rotational equilibrium of the pressures applied to the upper and lower horizontal paver surfaces. There is a direct relation between the pressure applied onto a paver surface and resulting vertical compressive stress distribution beneath the paver (see Chapters 6, 7, 8 and 9). It is therefore necessary to select a particular patch loading applied onto paver before the stresses in the bedding material can be analysed. This Chapter develops the general equations to the total applied pressures and the centroid distances of the variations of all realistically possible patch loadings for rectangular pavers.

4.1. Introduction

This Chapter defines the patch loads on chamfered rectangular pavers. These patch load calculations are the first step of the bedding sand stress calculation method[1, 2, 3] described in Chapter 6. Paver paving consists of a large number of small, rigid units with flexible joints. The nature of a paver paved surface may therefore depend on the pavers, the joints and the way in which the two relate - as well as the foundation on which the pavers rest. The effect of the applied loading is to cause loaded pavers to move vertically owing to the value of the applied load and to rotate owing to the eccentricity of the load. Rotation is resisted by the interlock[4]. Most pavers produced in the UK are chamfered[5]. The introduction of a chamfer may aid laying by indicating the top face of the block. The chamfer reduces sharp edges which, in turn, makes work more comfortable for the layer who may handle several thousand pavers in a day. Chamfers also lessen spalling and reduce the effect minor differences in level between adjoining pavers[5]. Normally a chamfer reduces the wearing surface area by 20%-30%. Because of this the stress distribution beneath rectangular pavers was analyzed for both chamfered and non-chamfered cases. Throughout the research, the total applied load (N) onto pavers was calculated using the following equation for $0.8 N/mm^2$ tyre pressure (Figures 4.1 and 4.2).

$$N = 0.8\,F$$

Where,
$N = \sum$ applied load onto paver (N)
$F = \sum$ load patch surface area (mm^2)
0.8 = tyre pressure of highway vehicle (N / mm^2)

4.2. Patch loadings on chamfered rectangular pavers

Figure 4.1 shows the relationship between contact zone of a commercial vehicle's dual rear wheels and pavers laid on 45 degree "elbow" pattern, that is, with the visually strong herringbone effect running orthogonally to the direction of the vehicle. This is a common laying arrangement on highways and industrial areas[1, 2, 3]. The green shaded areas represent

a part of full contact between tyre and pavers and have been produced by applying wet paint to a vehicle's tyres and lowering them onto the pavers. The tyres were inflated to a pressure of 0.8N/mm^2 and a load of 10,000kg was applied through the entire axle such that each individual wheel transmitted 2,500kg into the pavers. From this, it was found that the applied patch loads could be idealised by Line 1 and Line 2 shown in Figure 4.1 cutting through each other orthogonally. The chamfered rectangular model paver illustrated in Figure 4.1 is used in the stress analysis. This paver is 200x100x80mm (length, width, thickness) with a chamfer of width and depth 5mm around its upper perimeter. The paver's thickness is of no consequence in the determination of the vertical stress values.

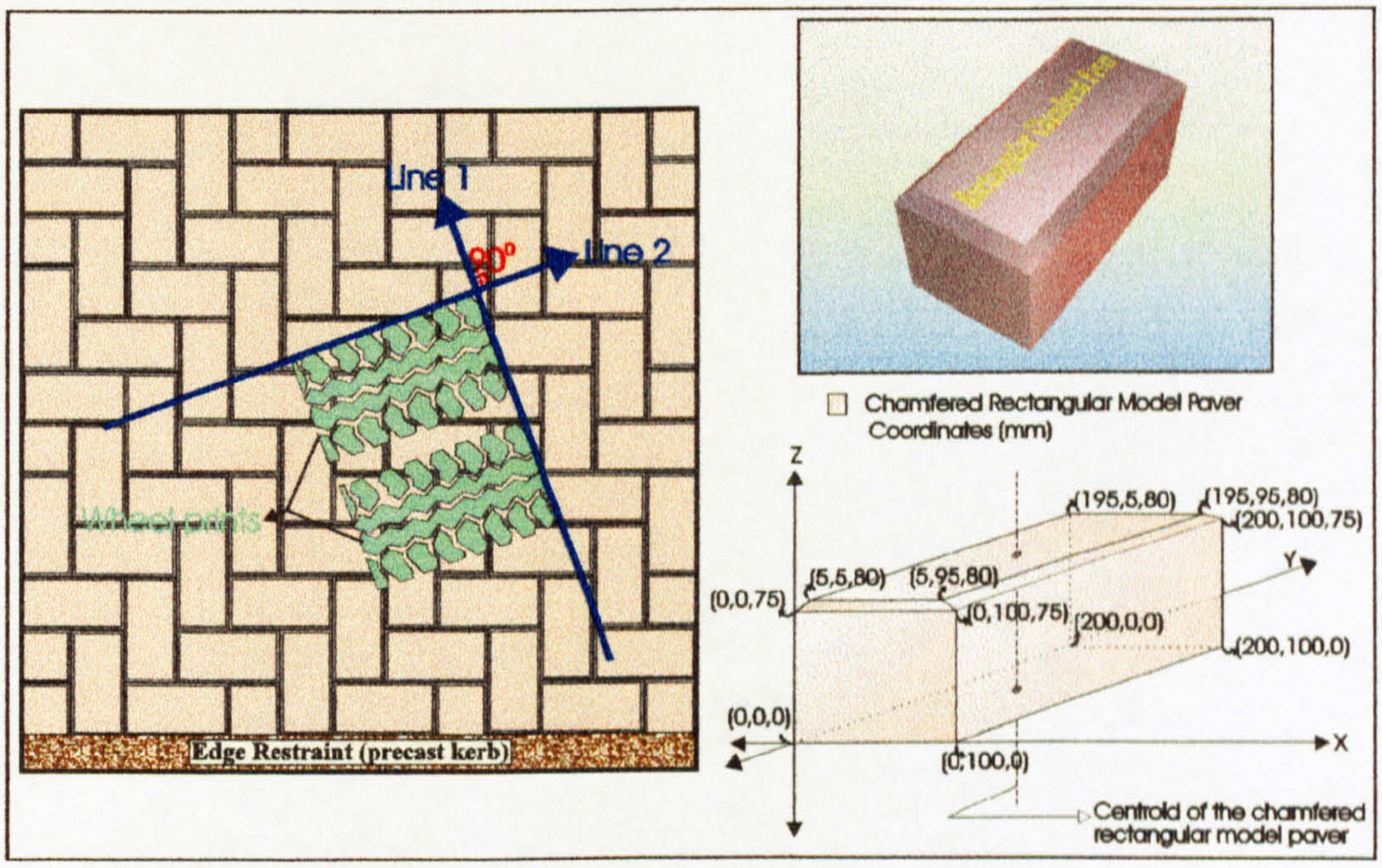

Figure 4.1: Contact load patch resulting from typical dual rear wheels of a commercial vehicle and the dimensions assumed for pavers in the stress analysis.

It is assumed that each tyre contact area has rectangular proportions (380 x 220mm) and the distance between the wheel prints is 50mm. Ten different plan relationship were calculated by turning the local wheel axes θ^{o} through relative to the global axes. As can be seen in Figure 4.2, the resulting pattern of compressive stress in the underlying bedding sand cannot be calculated on a simple load spreading basis, because loading is applied

asymmetrically to each paver most of time. The red shaded lines on the contact load areas illustrate some examples of the patch loadings on the chamfered rectangular pavers laid to 45 degree herringbone pattern.

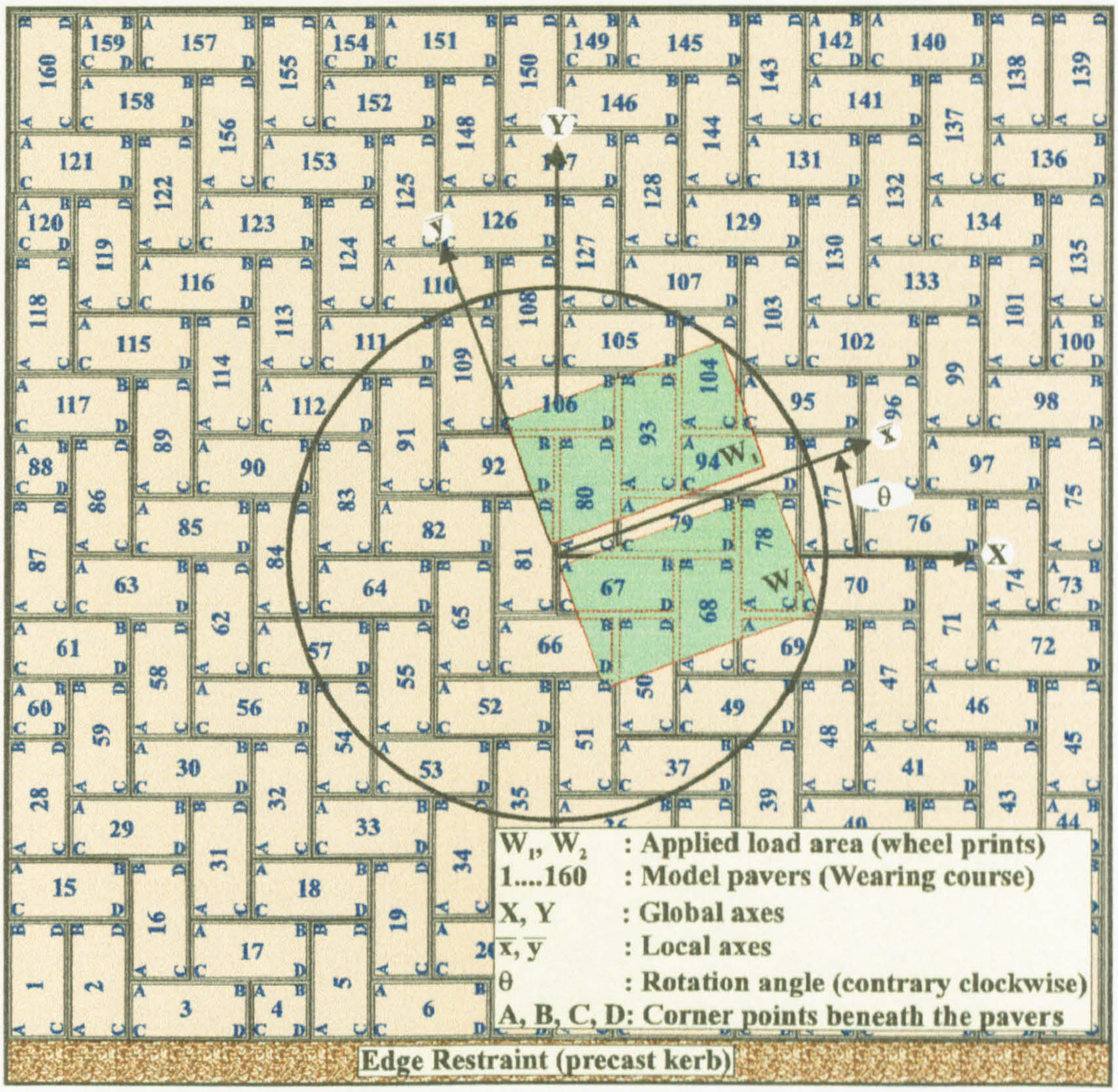

Figure 4.2: The plan relationship between contact zone of a commercial vehicle's dual rear wheels placed θ^{o} angle to the global axes.

Before analysing the vertical stresses in the bedding sand, it is necessary to select a particular patch loading on a paver. Figure 4.3 shows representative examples of patch loading arrangements on pavers from which it can be seen that in the general case the centre of gravity of the paver is displaced from the centre of applied pressure. The

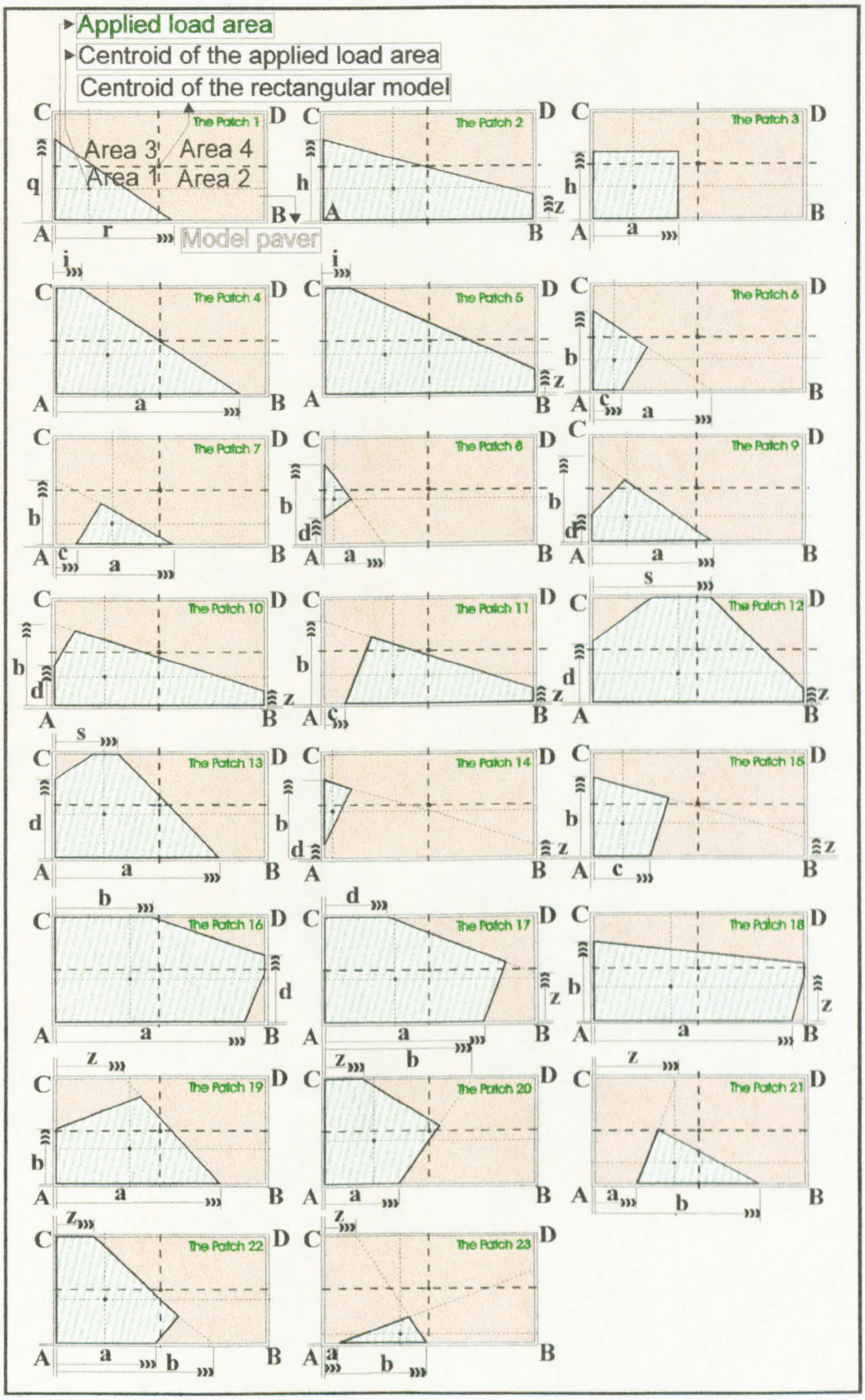

Figure 4.3: Typical load patches applied to individual rectangular pavers by highway vehicle tyres. In virtually all load situations, the centroid of the applied load do not coincide. This results in a complex pattern of stress in the underlying bedding material.

determined 23 different load patches which are commonly applied to the individual rectangular pavers illustrated in Figure 4.3. In the general case, the patch load centre is displaced in both the transverse and the longitudinal directions of the paver. The distances **a**, **b**, **c**, **d**, **h**, **i**, **q**, **r** and **z** characterise the patch loading and are used in the development of bedding sand contact pressure. In those calculations, a paver of thickness 80mm and plan dimensions 200mm x 100mm with a chamfer of width and depth 5mm around its upper perimeter is used. **A, B, C** and **D** are the corner points of the bottom surface of the rectangular model paver. In each of these load applications the centroid of the chamfered rectangular pavers divides the surface into four equal parts and the centroid of the possible applied load areas should be in **Area 1** in order to be able to force the stress at corner **A** positive and maximum all the time. Corner **A** was selected as a pivot point. If the centroid of the applied load is in **Areas 2, 3** or **4**, by changing the position of the model paver and by using one of the 23 possible applied load patches shown in Figure 4.3, the correct stress function can be found for the individual chamfered rectangular pavers. Therefore, wherever the centroid of the possible applied load patches is on the surface of the model paver, it can be found by using the same logic. Before analysing the stresses in the laying course, it is necessary to select a particular patch load on the chamfered rectangular paver shown in Figure 4.3. The general geometric solutions of the surface areas (F) and the centroids ($\overline{X}$ and $\overline{Y}$) of 23 possible patch loads on chamfered rectangular pavers can be calculated as follows.

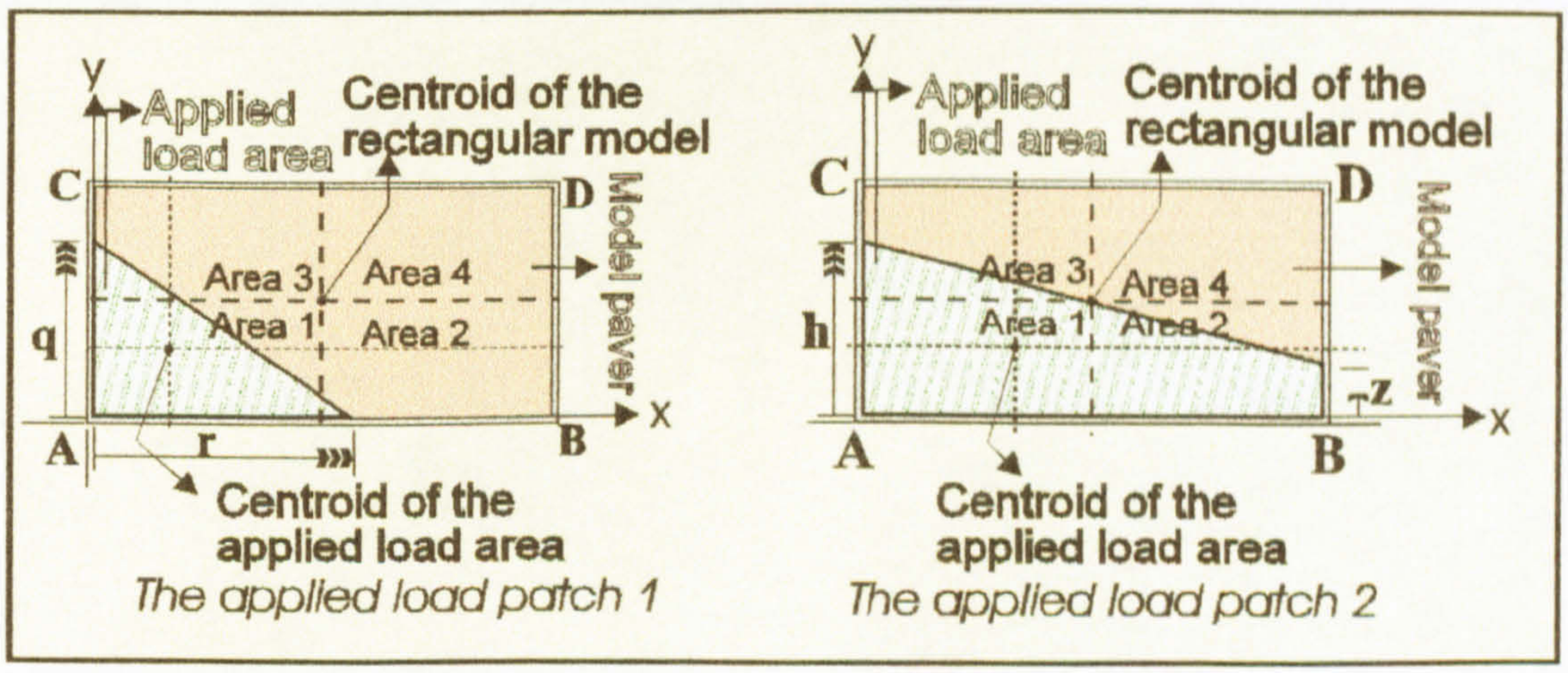

Figure 4.4: The applied load patches 1 and 2.

As can be seen in Figure 4.4, as the distance **q** in the load patch 1 changes from corner **A** to **C**, the distance **r** scans the model paver from corner **A** to **B**. Therefore, in this simple geometric patch load application which can search the half of the chamfered rectangular model paver, the variable surface areas of the triangle patch and their centroids in x and y direction are:

$$F = \frac{q\,r}{2},\ \overline{Y} = \frac{q}{3} \text{ and } \overline{X} = \frac{r}{3}$$

Similarly, in patch 2, when the distance **h** varies from corner **A** to **C**, the distance **z** scans the paver from corner **B** to **D**. In order to simplify the vertical stress calculations, the stress analysis was conducted in terms of the pivot point **A** which must have positive and maximum stress, it is therefore necessary to keep the centroid of the applied load in **Area 1**, so, in that case $\mathbf{z} \leq \mathbf{h}$. Hence, the general solution of these changeable patch load surface areas and their centroids can be calculated by the following simplified equations according to the distances **h** and **z**.

$$F = 95\,(h+z),\ \overline{Y} = \frac{h^2 + hz + z^2}{3\,(h+z)} \text{ and } \overline{X} = \frac{190\,(h+2z)}{3\,(h+z)}$$

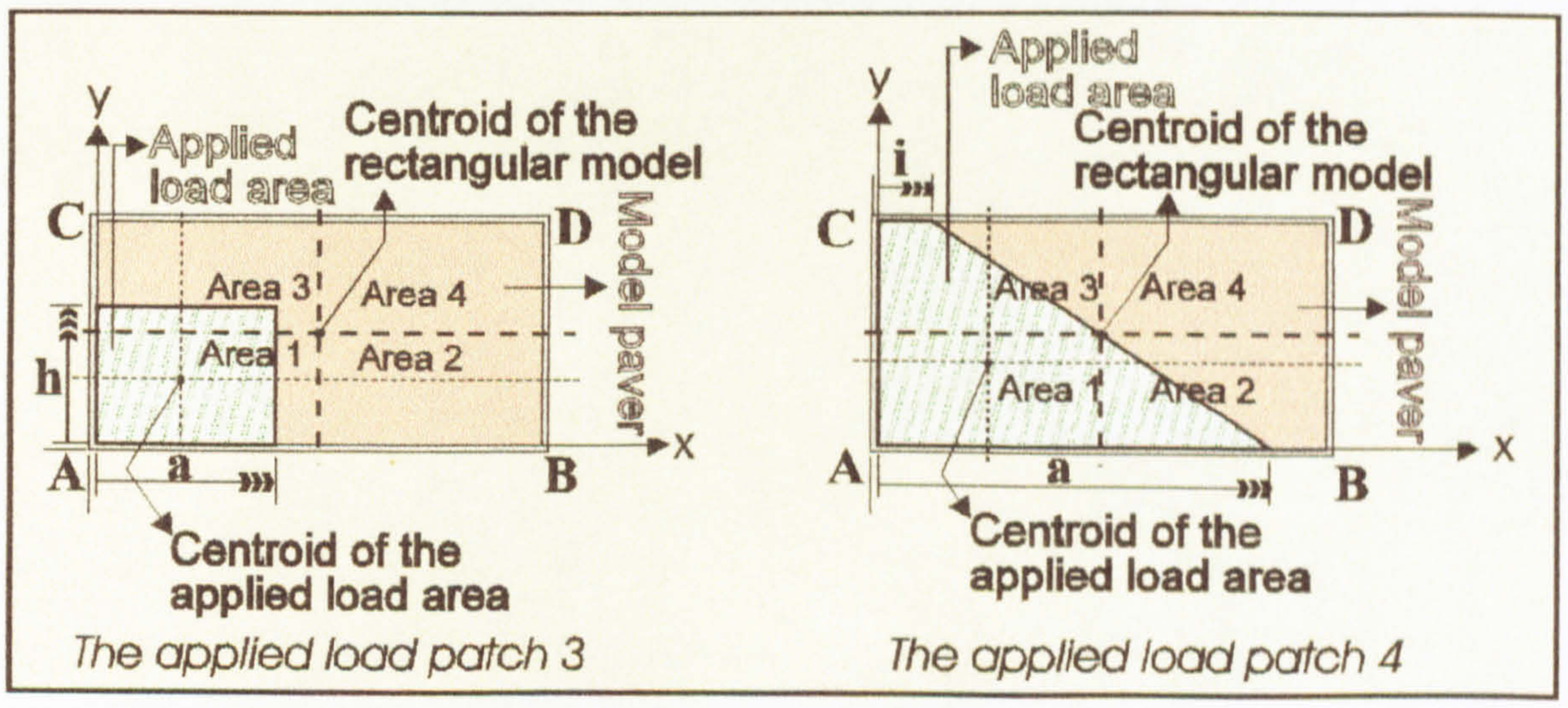

Figure 4.5: The applied load patches 3 and 4.

Figure 4.5 shows two possible load patches. The solution to patch 3 is straightforward according to the changeable distances **h** and **a** which scan the paver surface in the y and x direction respectively. $F = h\,a$, $\overline{Y} = \frac{h}{2}$ and $\overline{X} = \frac{a}{2}$. In patch 4 ($\mathbf{i \le a}$), the distance **i** changes from corner **C** to **D** while **a** varies from corner **A** to **B**. Therefore the solution to the surface load areas and their centroids are:

$$F = 45\,(a+i),\ \overline{Y} = \frac{30\,(a+2i)}{a+i} \text{ and } \overline{X} = \frac{a^2+ai+i^2}{3\,(a+i)}$$

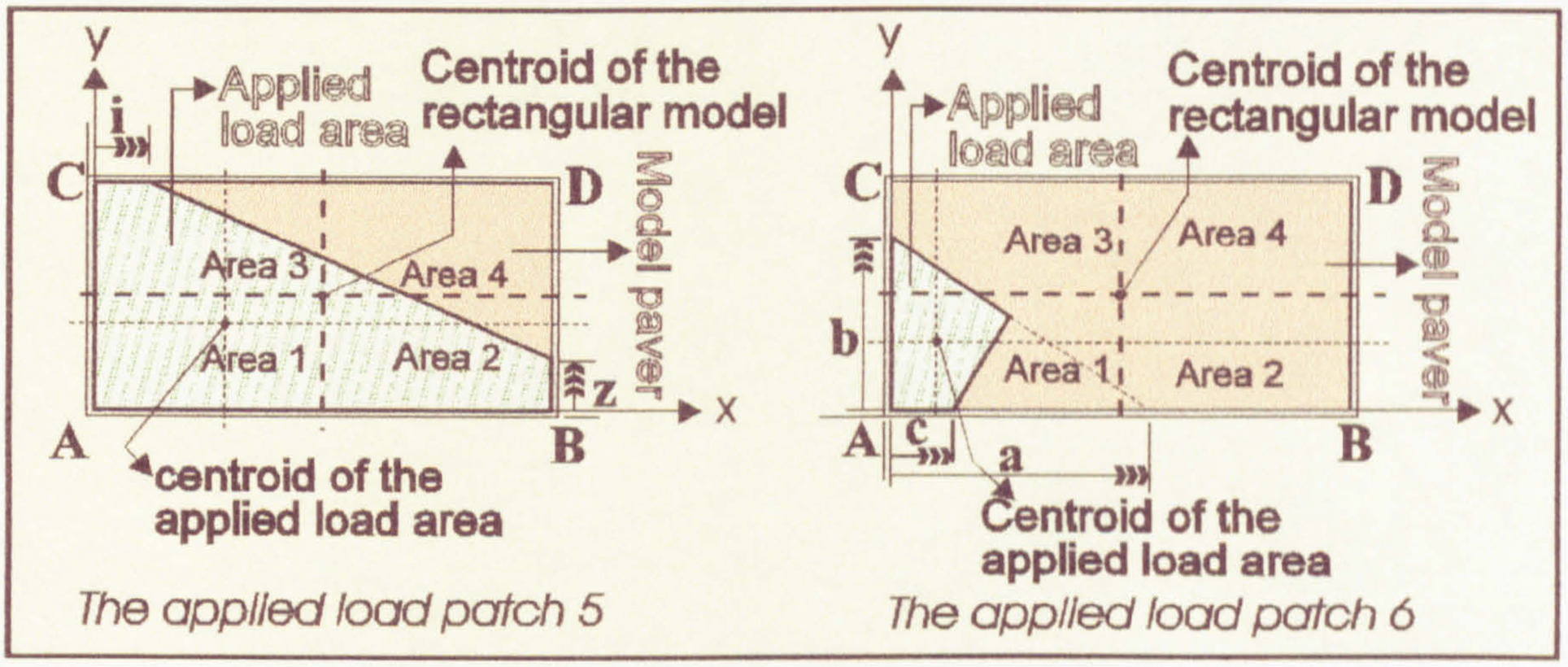

Figure 4.6: The applied load patches 5 and 6.

Figure 4.6 illustrates load patches 5 and 6. Patch 5 scans the chamfered model paver by the changeable distances **i** and **z**. The general solution to these variable surface areas and to centre of gravities is as follows:

$$F = 0.5\,(17100 + 90\,i + 190\,z - i\,z),$$

$$\overline{Y} = \frac{-1539000 - 16200\,i - 17100\,z + 90\,i\,z - 190\,z^2 + i\,z^2}{3\,(-17100 - 90\,i - 190\,z + i\,z)}$$

$$\overline{X} = \frac{-3249000 - 17100\,i - 90\,i^2 - 72200\,z + 190\,i\,z + i^2\,z}{3\,(-17100 - 90\,i - 190\,z + i\,z)}$$

Patch 6 illustrated in Figure 4.6 has three changeable distances which are **a**, **b**, **c**. While the distance **b** chances in the y direction, the distances **a** and **c** (**c**≤**a**) similarly scan the paver in the x direction. By calculus,

$$F = \frac{a\,b\left(b^2 + 2\,a\,c - c^2\right)}{2\left(a^2 + b^2\right)},$$

$$\overline{Y} = \frac{b\left(2\,a^2\,b^2 + b^4 + 3\,a^3\,c - 3\,a^2\,c^2 + a\,c^3\right)}{3\left(a^2 + b^2\right)\left(b^2 + 2\,a\,c - c^2\right)}$$

$$\overline{X} = \frac{a\,b^4 + 3\,a^2\,b^2\,c + 3\,a^3\,c^2 - 2\,a^2\,c^3 - b^2\,c^3}{3\left(a^2 + b^2\right)\left(b^2 + 2\,a\,c - c^2\right)}$$

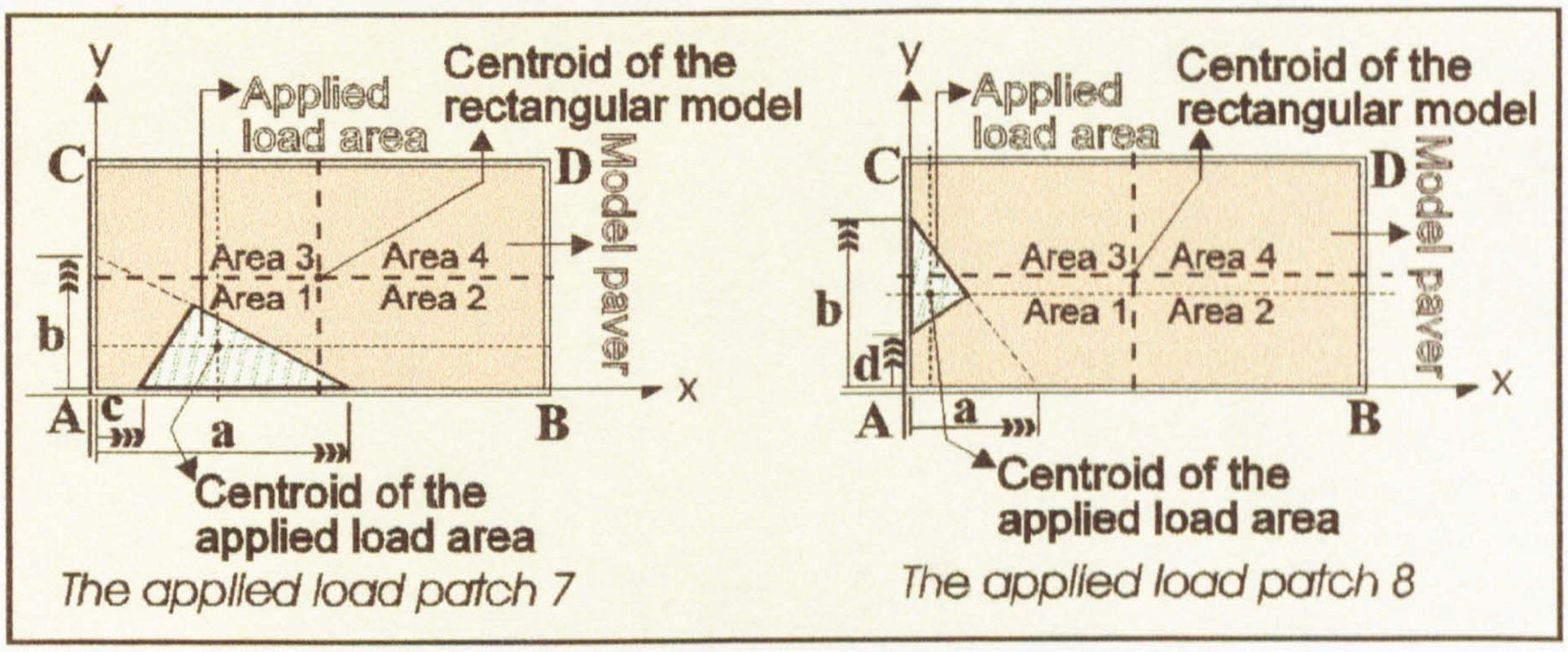

Figure 4.7: The applied load patches 7 and 8.

Load patch 7 in Figure 4.7 can be calculated similarly, the only difference is in the position of the patch. The solution to the variable surface area and its centroids is:

$$F = \frac{a\,b\,(c-a)^2}{2\left(a^2 + b^2\right)},\quad \overline{Y} = \frac{a\,b\,(a-c)}{3\left(a^2 + b^2\right)} \text{ and } \overline{X} = \frac{a^3 + 2\,a\,b^2 + 2\,a^2\,c + b^2\,c}{3\left(a^2 + b^2\right)}$$

For patch loading 8 shown in Figure 4.7 when the distance **a** moves in the x direction, the distances **b** and **d** (**d**<**b**) change in the y direction and they scan the paver in a similar way. The solution to this possible applied load patch is:

$$F = \frac{a\,b\,(d-b)^2}{2\left(a^2+b^2\right)},\quad \overline{Y} = \frac{2\,a^2\,b+b^3+a^2\,d+2\,b^2\,d}{3\left(a^2+b^2\right)} \text{ and } \overline{X} = \frac{a\,b\,(b-d)}{3\left(a^2+b^2\right)}$$

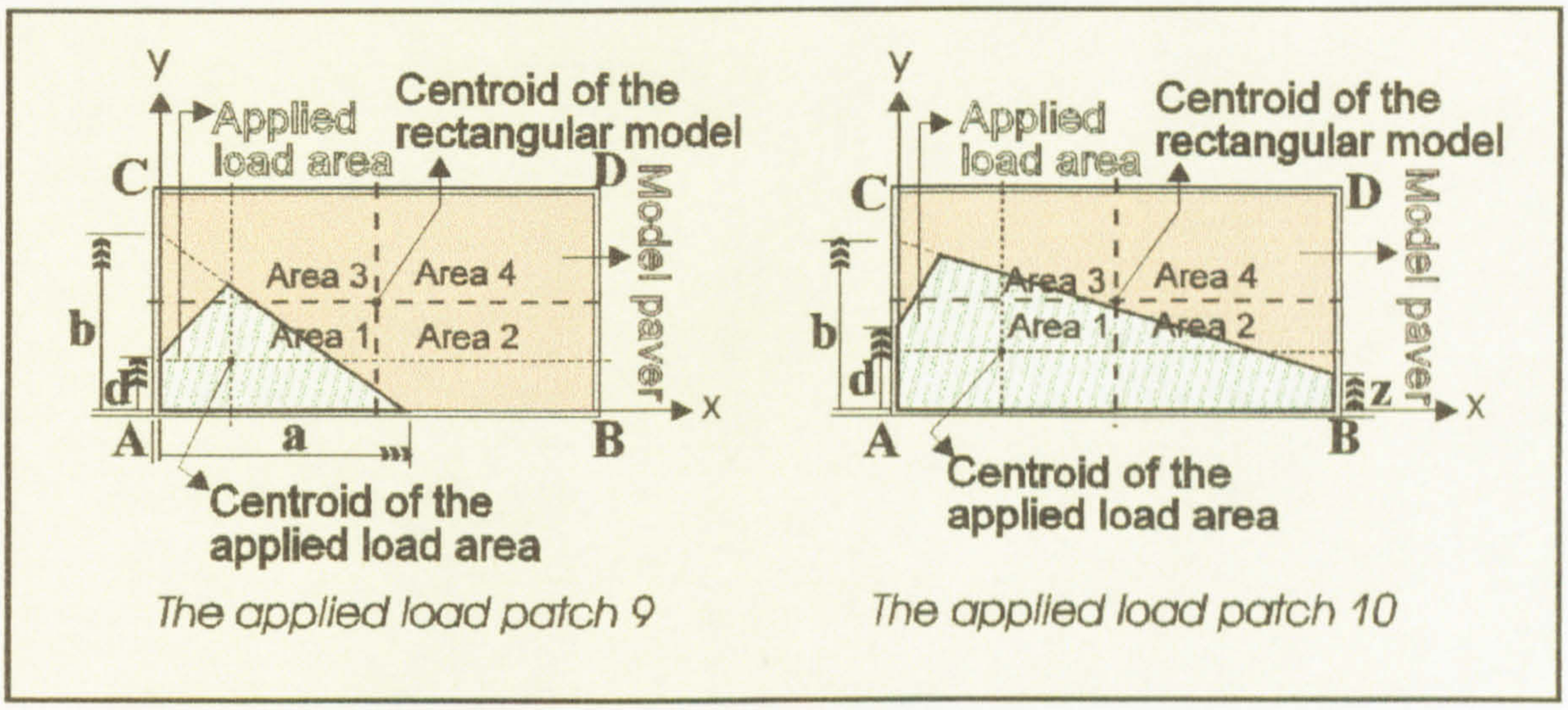

Figure 4.8: The applied load patches 9 and 10.

The varying surface area and the centroids of patch load 9 shown in Figure 4.8 can be solved in a similar manner to patch load 8. The only difference is the position of the load patch. The equations are:

$$F = \frac{a\,b\left(a^2+2\,b\,d-d^2\right)}{2\left(a^2+b^2\right)},\quad \overline{Y} = \frac{a^4\,b+3\,a^2\,b^2\,d+3\,b^3\,d^2-a^2\,d^3-2\,b^2\,d^3}{3\left(a^2+b^2\right)\left(a^2+2\,b\,d-d^2\right)},$$

$$\overline{X} = \frac{a\left(a^4+2\,a^2\,b^2+3\,b^3\,d-3\,b^2\,d^2+b\,d^3\right)}{3\left(a^2+b^2\right)\left(a^2+2\,b\,d-d^2\right)}$$

For patch load 10 illustrated in Figure 4.8, when the distance **z** (**z**<**b**) moves in the y direction, the distances **b** and **d** (**d**≤ **b**) change from corner **A** to **C**. It can be recalled that the centroids of the applied load surfaces must be in **Area 1**. Therefore, the relation between the distance **b**, **z** and **d** should be **z**<**b** and **d**≤ **b**. The equations for the surface areas and for their centroids are as follows:

$$F = \frac{95\left(36100\,b + 2\,b^2 d - b\,d^2 + 36100\,z - 2\,b\,d\,z + d^2\,z - b\,z^2 + z^3\right)}{36100 + b^2 - 2\,b\,z + z^2},$$

$$\overline{Y} = (-1303210000\,b^2 - 108300\,b^3\,d - 3\,b^4\,d^2 + 36100\,b\,d^3 + 2\,b^3\,d^3 - 1303210000\,b\,z$$
$$+108300\,b^2\,d\,z + 9\,b^3\,d^2\,z - 36100\,d^3\,z - 6\,b^2\,d^3\,z - 1303210000\,z^2 - 9\,b^2\,d^2\,z^2$$
$$+6\,b\,d^3\,z^2 + 72200\,b\,z^3 + b^3\,z^3 + 3\,b\,d^2\,z^3 - 2\,d^3\,z^3 - 72200\,z^4 - 3\,b^2\,z^4 + 3\,b\,z^5 - z^6)$$
$$\Big/ (3\,(36100 + b^2 - 2\,b\,z + z^2)\,(-36100\,b - 2\,b^2\,d + b\,d^2 - 36100\,z + 2\,b\,d\,z - d^2\,z$$
$$+b\,z^2 - z^3)),$$
$$\overline{X} = (190(-1303210000\,b - 72200\,b^3 - 3\,b^4\,d + 3\,b^3\,d^2 - b^2\,d^3 - 2606420000\,z$$
$$+216600\,b^2\,z - 216600\,b\,d\,z + 12\,b^3\,d\,z - 12\,b^2\,d^2\,z + 2\,b\,d^3\,z - 3\,b^3\,z^2$$
$$+216600\,d\,z^2 - 9\,b^2\,d\,z^2 + 15\,b\,d^2\,z^2 - d^3\,z^2 - 144400\,z^3 + 4\,b^2\,z^3 - 6\,b\,d\,z^3 - 6\,d^2\,z^3$$
$$+b\,z^4 + 6\,d\,z^4 - 2\,z^5)) \Big/ (3\,(36100 + b^2 - 2\,b\,z + z^2)\,(-36100\,b - 2\,b^2\,d + b\,d^2$$
$$-36100\,z + 2\,b\,d\,z - d^2\,z + b\,z^2 - z^3))$$

As can be seen in Figure 4.9, when the distances **z** and **b** move along the short side of the paver, the distance **c** varies in the **x** direction. In that case, the distance **z** should be smaller than the distance **b** and the position of the patch load surface area's centroids should be in **Area 1** in terms of the varying distance **c** in the **x** direction. Hence, the general solution of patch load 11 to the surface area and its centroids is:

$$F = \frac{95\left(36100\,b - 380\,b\,c + b\,c^2 + 36100\,z - c^2\,z - b\,z^2 + z^3\right)}{36100 + b^2 - 2\,b\,z + z^2},$$

$$\overline{Y} = (24760990000\,b^2 - 390963000\,b^2\,c + 2057700\,b^2\,c^2 - 3610\,b^2\,c^3 + 24760990000\,b\,z$$
$$-2057700\,b\,c^2\,z + 7220\,b\,c^3\,z + 20851360000\,z^2 - 216600\,b^2\,z^2 - 3\,b^4\,z^2 - 3610\,c^3\,z^2$$
$$-938600\,b\,z^3 - 7\,b^3\,z^3 + 1155200\,z^4 + 39\,b^2\,z^4 - 45\,b\,z^5 + 16\,z^6) \Big/ (57\,(36100 + b^2$$
$$-2\,b\,z + z^2)\,(36100\,b - 380\,b\,c + b\,c^2 + 36100\,z - c^2\,z - b\,z^2 + z^3)),$$
$$\overline{X} = (247609900000\,b + 13718000\,b^3 - 108300\,b^3\,c - 20577000\,b\,c^2 + 72200\,b\,c^3$$
$$+b^3\,c^3 + 495219800000\,z + 108300\,b^2\,c\,z - 72200\,c^3\,z - 3\,b^2\,c^3\,z - 41154000\,b\,z^2$$
$$-570\,b^3\,z^2 + 3\,b\,c^3\,z^2 + 27436000\,z^3 + 1520\,b^2\,z^3 - c^3\,z^3 - 1330\,b\,z^4 + 380\,z^5)$$
$$\Big/ (3\,(36100 + b^2 - 2\,b\,z + z^2)\,(36100\,b - 380\,b\,c + b\,c^2 + 36100\,z - c^2\,z - b\,z^2 + z^3))$$

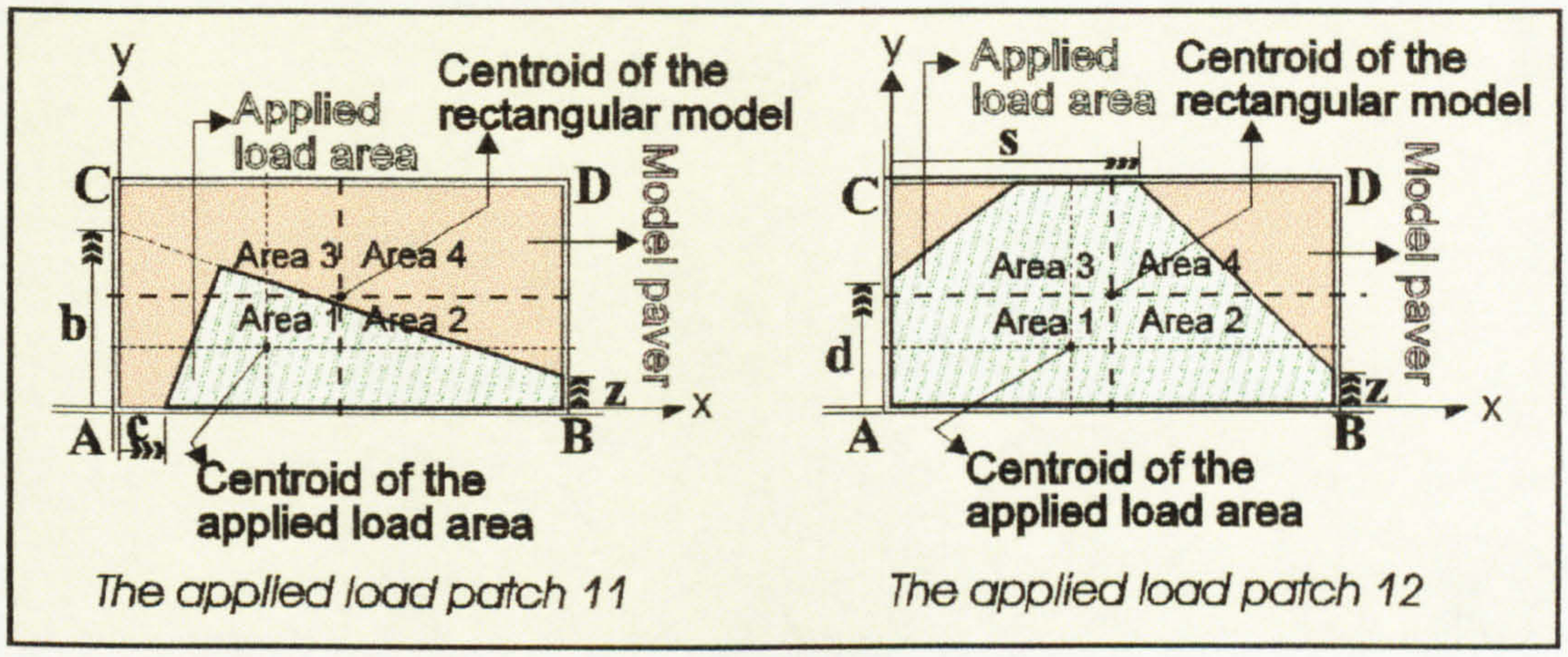

Figure 4.9: The applied load patches 11 and 12.

Another load patch shown in Figure 4.9 has a trapezium shape whereby the distances **z** and **d** change along the short side of the model while the distance **s** scans the paver in order to find the probable patch load surface areas having their centroids in **Area 1**. The solution to this contact load area and to its centroids according to the changeable distances (**d**, **s**, **z**) is:

$$F = \frac{-2520000 - 16200\,d + 90\,d^2 + 90\,s^2 - 44200\,z + 180\,d\,z - d^2\,z + 380\,s\,z - s^2\,z}{2\,(-190 + s)},$$

$$\overline{Y} = (161190000 + 2187000\,d - 90\,d^3 + 1539000\,s - 16200\,s^2 + 4707000\,z - 24300\,d\,z + d^3\,z - 34200\,s\,z + 90\,s^2\,z + 36100\,z^2 - 380\,s\,z^2 + s^2\,z^2) \Big/ (3\,(2520000 + 16200\,d - 90\,d^2 - 90\,s^2 + 44200\,z - 180\,d\,z + d^2\,z - 380\,s\,z + s^2\,z))$$

$$\overline{X} = (-111384000000 - 196830000\,d + 2187000\,d^2 - 8100\,d^3 + 617310000\,s + 17100\,s^3 - 90\,s^4 - 2737640000\,z + 4374000\,d\,z - 48600\,d^2\,z + 180\,d^3\,z + 34295000\,s\,z - 108300\,s^2\,z - 190\,s^3\,z + s^4\,z + 729000\,z^2 - 24300\,d\,z^2 + 270\,d^2\,z^2 - d^3\,z^2) \Big/ (3\,(-190 + s)\,(2520000 + 16200\,d - 90\,d^2 - 90\,s^2 + 44200\,z - 180\,d\,z + d^2\,z - 380\,s\,z + s^2\,z))$$

In the applied patch load 13 illustrated in Figure 4.10, the distances **a** and **s** change along the long side of the model while the distance **d** scans the paver in the y direction in order to find the probable patch load surface areas having their centroids in **Area 1**.

The solution to this contact area and to its centroids according to the changeable distances (**a**, **d**, **s**) is:

$$F = \frac{45\left(8100 - a^2 - 180\,d + d^2 + s^2\right)}{-a + s},$$

$$\overline{Y} = \frac{1458000 - 90\,a^2 - 24300\,d + d^3 - 90\,a\,s + 180\,s^2}{3\left(8100 - a^2 - 180\,d + d^2 + s^2\right)},$$

$$\overline{X} = \frac{-65610000 + a^4 + 2187000\,d + 90\,d^3 - a^3\,s - a\,s^3 + s^4}{3\left(-a + s\right)\left(8100 - a^2 - 180\,d + d^2 + s^2\right)}$$

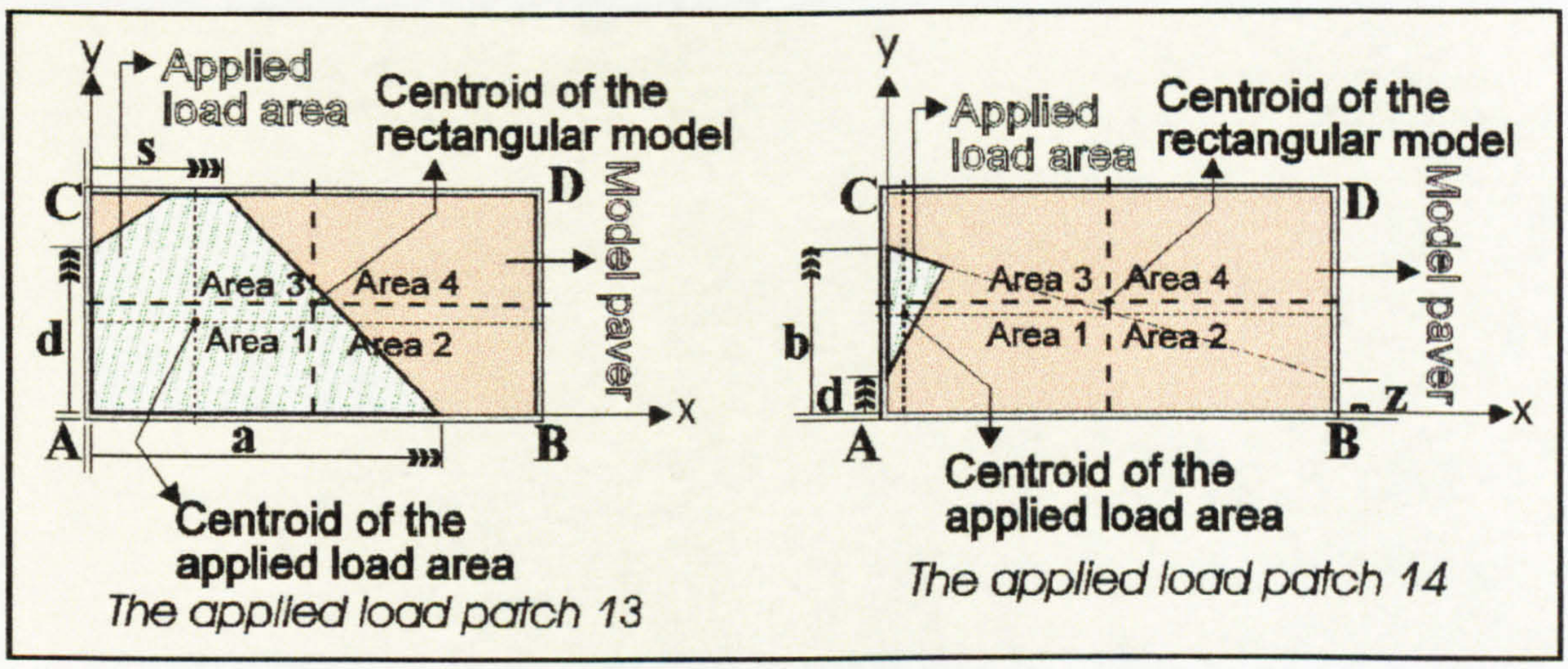

Figure 4.10: The applied load patches 13 and 14.

In load patch 14 shown in Figure 4.10, while the distances **b** and **z** scan the model paver in the y direction, the distance **d** varies along the short side to ensure that the load patch surface area has its centroids in **Area 1**. The general solutions are:

$$F = \frac{95\left(d - b\right)^2\left(b - z\right)}{36100 + b^2 - 2\,b\,z + z^2},$$

$$\overline{Y} = \frac{72200\,b + b^3 + 36100\,d + 2\,b^2\,d - 2\,b^2 z - 4\,b\,d\,z + b\,z^2 + 2\,d\,z^2}{3\left(36100 + b^2 - 2\,b\,z + z^2\right)},$$

$$\overline{X} = \frac{190\left(-b^3 + 2\,b^2\,d - b\,d^2 - 216600\,z + b^2\,z - 8\,b\,d\,z + d^2\,z + 6\,b\,z^2 + 6\,d\,z^2 - 6\,z^3\right)}{3\left(-b + d\right)\left(36100 + b^2 - 2\,b\,z + z^2\right)}$$

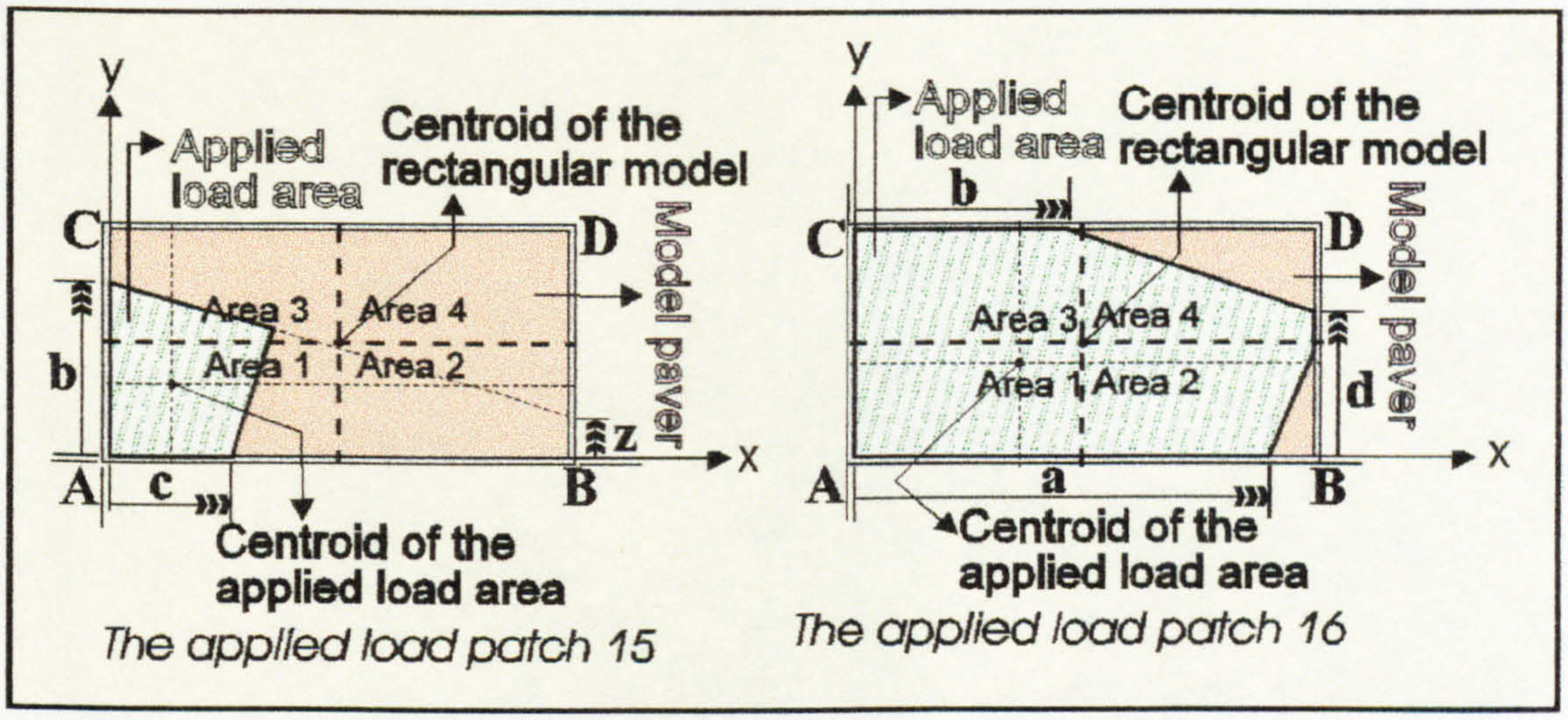

Figure 4.11: The applied load patches 15 and 16.

As can be seen in Figure 4.11, the distances **b** and **z** ($z \le b$) vary in the y direction while the distance **c** scans the paver in the x direction. The simplified general solution of patch 15 to the surface area and its centroids is:

$$F = \frac{95\left(b^3 + 380\,b\,c - b\,c^2 - b^2\,z + c^2\,z\right)}{36100 + b^2 - 2\,b\,z + z^2}$$

$$\overline{Y} = (72200\,b^4 + b^6 + 20577000\,b^2\,c - 108300\,b^2\,c^2 + 190\,b^2 c^3 - 72200\,b^3\,z - 3\,b^5\,z + 108300\,b\,c^2\,z - 380\,b\,c^3\,z + 3\,b^4\,z^2 + 190\,c^3\,z^2 - b^3\,z^3) \Big/ (3\,(b^3 + 380\,b\,c - b\,c^2 - b^2\,z + c^2\,z)\,(36100 + b^2 - 2\,b\,z + z^2)),$$

$$\overline{X} = (190\,b^5 + 108300\,b^3\,c + 20577000\,b\,c^2 - 72200\,b\,c^3 - b^3\,c^3 - 380\,b^4\,z - 108300\,b^2\,c\,z + 72200\,c^3\,z + 3\,b^2\,c^3\,z + 190\,b^3\,z^2 - 3\,b\,c^3\,z^2 + c^3\,z^3) \Big/ (3\,(b^3 + 380\,b\,c - b\,c^2 - b^2\,z + c^2\,z)\,(36100 + b^2 - 2\,b\,z + z^2))$$

The surface area of load patch 16 and its centroids illustrated in Figure 4.11 can be solved according to the varying distances **a**, **b** and **d** which change in the y and x directions respectively. The solutions are:

$$F = \frac{5320000 - 72200\,a + 190\,a^2 - 44200\,b + 380\,a\,b - a^2\,b + 180\,b\,d + 190\,d^2 - b\,d^2}{2(-90 + d)},$$

$$\overline{Y} = (235144000000 - 3909630000\,a + 20577000\,a^2 - 36100\,a^3 - 2737640000\,b$$
$$+41154000\,a\,b - 216600\,a^2\,b + 380\,a^3\,b + 6859000\,b^2 - 108300\,a\,b^2 + 570\,a^2\,b^2 - a^3\,b^2$$
$$+138510000\,d + 3645000\,b\,d - 24300\,b\,d^2 + 17100\,d^3 - 90\,b\,d^3 - 190\,d^4 + b\,d^4) \Big/$$
$$(3\,(-90 + d)\,(-5320000 + 72200\,a - 190\,a^2 + 44200\,b - 380\,a\,b + a^2\,b - 180\,b\,d - 190\,d^2$$
$$+b\,d^2)),$$

$$\overline{X} = (-2314010000 + 20577000\,a - 190\,a^3 + 15257000\,b - 108300\,a\,b + a^3\,b + 8100\,b^2$$
$$+3249000\,d - 34200\,b\,d - 180\,b^2\,d - 72200\,d^2 + 190\,b\,d^2 + b^2\,d^2) \Big/ (3\,(-5320000$$
$$+72200\,a - 190\,a^2 + 44200\,b - 380\,a\,b + a^2\,b - 180\,b\,d - 190\,d^2 + b\,d^2))$$

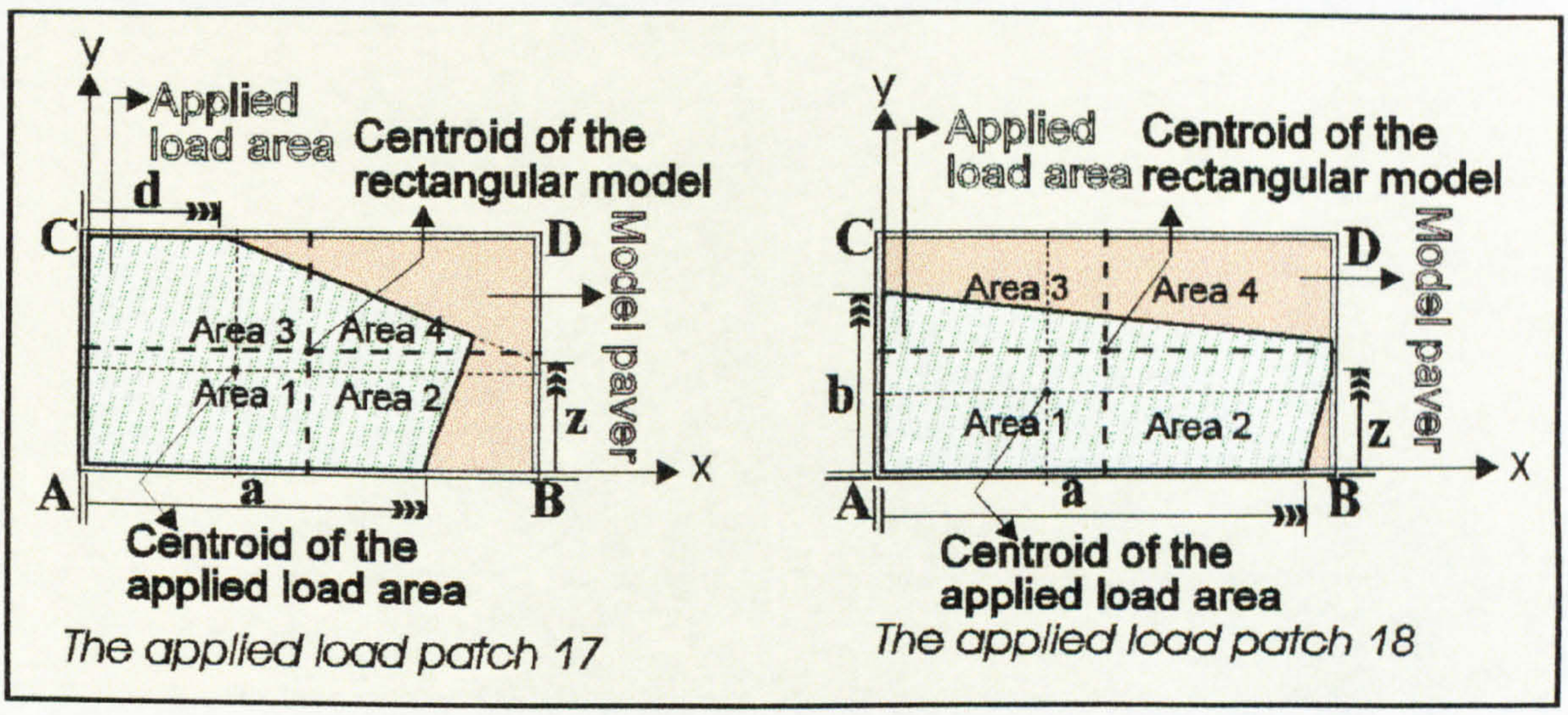

Figure 4.12: The applied load patches 17 and 18.

For load patch 17 shown in Figure 4.12, the distances **a** and **d** progress in the long side of the paver while the distance **z** scans the paver in the y direction. The general geometrical solution to the surface area and its centroides can be expressed as the following equations.

$$F = (138510000 + 6498000\,a - 17100\,a^2 + 729000\,d - 34200\,a\,d + 90\,a^2\,d - 17100\,d^2$$
$$+90\,d^3 - 1539000\,z + 190\,a^2\,z - 24300\,d\,z - 380\,a\,d\,z - a^2\,d\,z + 190\,d^2\,z + 2\,a\,d^2\,z$$
$$-d^3\,z + 180\,d\,z^2) \Big/ (2\,(44200 - 380\,d + d^2 - 180\,z + z^2)),$$

$$\overline{Y} = (2\,(44200 - 380\,d + d^2 - 180\,z + z^2)(((-190 + d)^2\,(-90 + z)\,(17100 - 90\,a + a\,z - d\,z)^3) \Big/ (6\,(44200 - 380\,d + d^2 - 180\,z + z^2)^3) + ((-190 + d)\,(-90 + z)\,(-8100 - 190\,a + 190\,d + a\,d - d^2 + 90\,z)^2\,(-11205000 + 17100\,a + 85500\,d - 90\,a\,d - 180\,d^2 + 32400\,z - 190\,a\,z + 190\,d\,z + a\,d\,z - d^2\,z - 180\,z^2)) \Big/ (6\,(44200 - 380\,d + d^2 - 180\,z + z^2)^3 + (4050\,(1539000 + 36100\,a - 380\,a\,d + a\,d^2 - 17100\,z - 90\,d\,z + d\,z^2)) \Big/ (44200 - 380\,d + d^2 - 180\,z + z^2))) \Big/ (138510000 + 6498000\,a - 17100\,a^2 + 729000\,d - 34200\,a\,d + 90\,a^2\,d - 17100\,d^2 + 90\,d^3 - 1539000\,z + 190\,a^2\,z - 24300\,d\,z - 380\,a\,d\,z - a^2\,d\,z + 190\,d^2\,z + 2\,a\,d^2\,z - d^3\,z + 180\,d\,z^2),$$

$$\overline{X} = (2\,(44200 - 380\,d + d^2 - 180\,z + z^2)\,((45\,(1539000 + 36100\,a - 380\,a\,d + a\,d^2 - 17100\,z - 90\,d\,z + d\,z^2)^2) \Big/ (44200 - 380\,d + d^2 - 180\,z + z^2)^2 + ((190 - d)\,(-90 + z)\,(17100 - 90\,a + a\,z - d\,z)^2\,(3078000 + 116400\,a - 1140\,a\,d + 3\,a\,d^2 - 34200\,z - 180\,a\,z - 180\,d\,z + az2 + 2dz2)) \Big/ (6\,(44200 - 380\,d + d^2 - 180\,z + z^2)^3) + ((190 - d)\,(-90 + z)\,(-8100 - 190\,a + 190\,d + a\,d - d^2 + 90\,z)^2\,(3078000 + 72200\,a + 44200\,d - 760\,a\,d - 380\,d^2 + 2\,a\,d^2 + d^3 - 34200\,z - 360\,d\,z + 3\,d\,z^2)) \Big/ (6\,(44200 - 380\,d + d^2 - 180\,z + z^2)^3))) \Big/ (138510000 + 6498000\,a - 17100\,a^2 + 729000\,d - 34200\,a\,d + 90\,a^2\,d - 17100\,d^2 + 90\,d^3 - 1539000\,z + 190\,a^2\,z - 24300\,d\,z - 380\,a\,d\,z - a^2\,d\,z + 190\,d^2\,z + 2\,a\,d^2\,z - d^3\,z + 180\,d\,z^2)$$

As can be seen in Figure 4.12, for load patch 18, while the distances **z** and **b** change in the x direction, the distance **a** scans the paver to determine the possible surface areas having their centroids in **Area 1**. The general geometrical solution to this load patch is:

$$F = 190\,b - \frac{3429500}{z} + \frac{18050\,a}{z} - 95\,z + \frac{a\,z}{2},$$

$$\overline{X} = (247609900000 - 2606420000\,a + 6859000\,a^2 - 20577000\,b\,z + 108300\,a\,b\,z + 570\,b^2\,z^2 - 190\,z^4 + a\,z^4) \Big/ (3\,z\,(-6859000 + 36100\,a + 380\,b\,z - 190\,z^2 + a\,z^2)),$$

$$\overline{Y} = (-2606420000 + 13718000\,a + 108300\,b\,z - 72200\,z^2 + 190\,a\,z^2 + a^2\,z^2) \Big/ (3\,z\,(-6859000 + 36100\,a + 380\,b\,z - 190\,z^2 + a\,z^2))$$

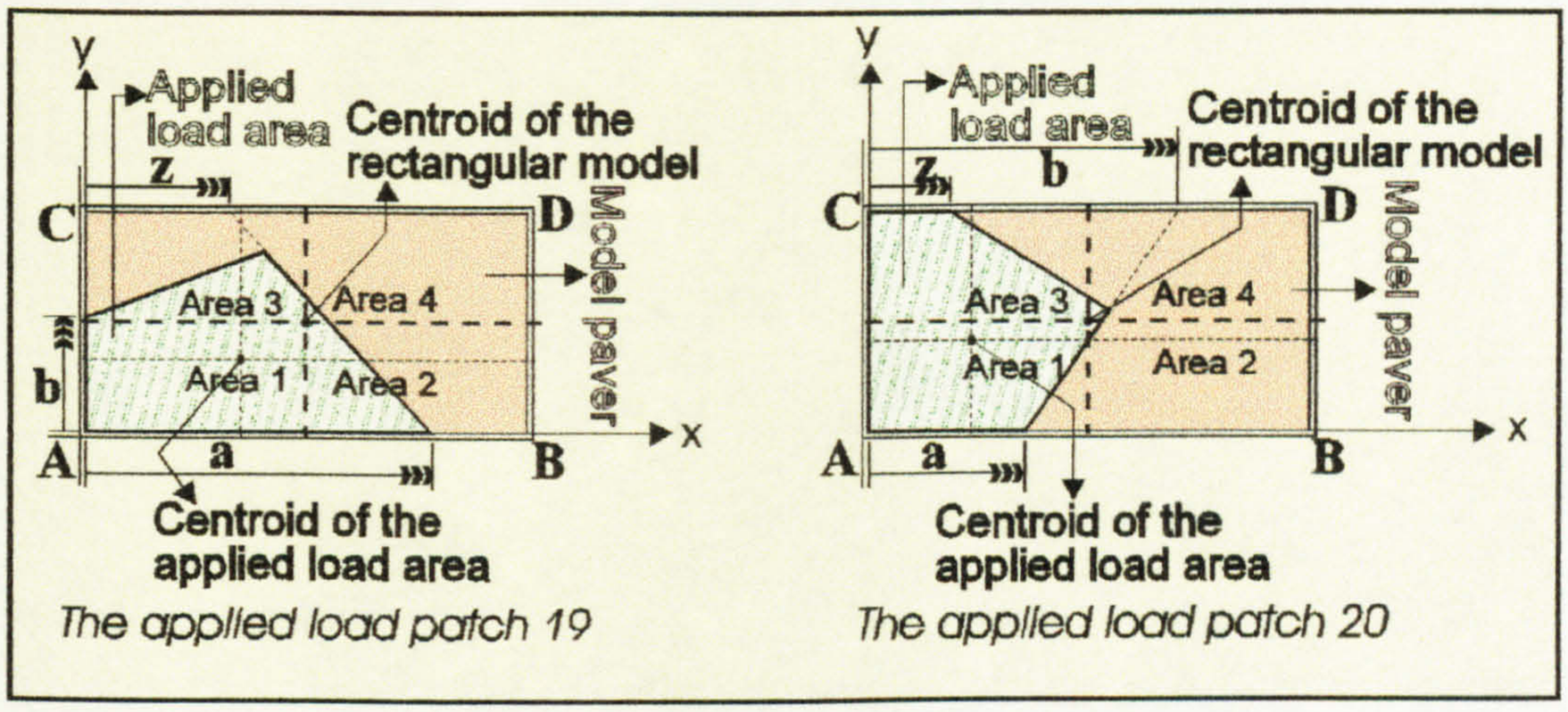

Figure 4.13: The applied load patches 19 and 20.

For load patch 19 shown in Figure 4.13, while the distance **a** and **z** (**z<a**) vary in the x direction, the distance **b** scans the model paver to determine possible load patch surface areas having their centroids in **Area 1**. The general solution to the surface area and its centroids for this load patch is:

$$F = \frac{45\left(a^3 + 180\,a\,b - a\,b^2 - a^2\,z + b^2\,z\right)}{8100 + a^2 - 2\,a\,z + z^2},$$

$$\overline{X} = (16200\,a^4 + a^6 + 2187000\,a^2\,b - 24300\,a^2\,b^2 + 90\,a^2\,b^3 - 16200\,a^3\,z - 3\,a^5\,z + 24300\,a\,b^2\,z - 180\,a\,b^3\,z + 3\,a^4\,z^2 + 90\,b^3\,z^2 - a^3\,z^3) \Big/ (3\,(a^3 + 180\,a\,b - a\,b^2 - a^2\,z + b^2\,z)\,(8100 + a^2 - 2\,a\,z + z^2)),$$

$$\overline{Y} = (90\,a^5 + 24300\,a^3\,b + 2187000\,a\,b^2 - 16200\,a\,b^3 - a^3\,b^3 - 180\,a^4\,z - 24300\,a^2\,b\,z + 16200\,b^3\,z + 3\,a^2\,b^3\,z + 90\,a^3\,z^2 - 3\,a\,b^3\,z^2 + b^3\,z^3) \Big/ (3\,(a^3 + 180\,a\,b - a\,b^2 - a^2\,z + b^2\,z)\,(8100 + a^2 - 2\,a\,z + z^2))$$

In the case of load patch 20's application illustrated in Figure 4.13, the distances **a**, **b** and **z** (**z<b**) change in the x direction of the model paver. The general geometrical solution of this changeable load patch surface area and its centroids is:

$$F = \frac{45\left(8100\,a + a^3 + 8100\,b - a^2\,b - 2\,a\,b\,z + 2\,b^2\,z + a\,z^2 - b\,z^2\right)}{8100 + a^2 - 2\,a\,b + b^2},$$

$$\overline{X} = (30\,(-65610000\,a - 16200\,a^3 - a^5 - 131220000\,b + 2\,a^4\,b + 24300\,a\,b^2 - a^3\,b^2$$
$$-8100\,b^3 + 48600\,a\,b\,z + 6\,a^3\,b\,z - 48600\,b^2\,z - 15\,a^2\,b^2\,z + 12\,a\,b^3\,z - 3\,b^4\,z$$
$$-24300\,a\,z^2 - 3\,a^3\,z^2 + 24300\,b\,z^2 + 6\,a^2\,b\,z^2 - 3\,a\,b^2\,z^2 + a^2\,z^3 - 2\,a\,b\,z^3 + b^2\,z^3))$$
$$\Big/ ((8100 + a^2 - 2\,a\,b + b^2)\,(-8100\,a - a^3 - 8100\,b + a^2\,b + 2\,a\,b\,z - 2\,b^2\,z - a\,z^2$$
$$+b\,z^2)),$$

$$\overline{Y} = (65610000\,a^2 + 16200\,a^4 + a^6 + 65610000\,a\,b - 16200\,a^3\,b - 3\,a^5\,b + 65610000\,b^2$$
$$+3\,a^4\,b^2 - a^3\,b^3 - 24300\,a\,b^2\,z + 24300\,b^3\,z - 3\,a^3\,b\,z^2 + 9\,a^2\,b^2\,z^2 - 9\,a\,b^3\,z^2 + 3\,b^4\,z^2$$
$$+8100\,a\,z^3 + 2\,a^3\,z^3 - 8100\,b\,z^3 - 6\,a^2\,b\,z^3 + 6\,a\,b^2\,z^3 - 2\,b^3\,z^3) \Big/ (3\,(8100 + a^2$$
$$-2\,a\,b + b^2)\,(8100\,a + a^3 + 8100\,b - a^2\,b - 2\,a\,b\,z + 2\,b^2\,z + a\,z^2 - b\,z^2))$$

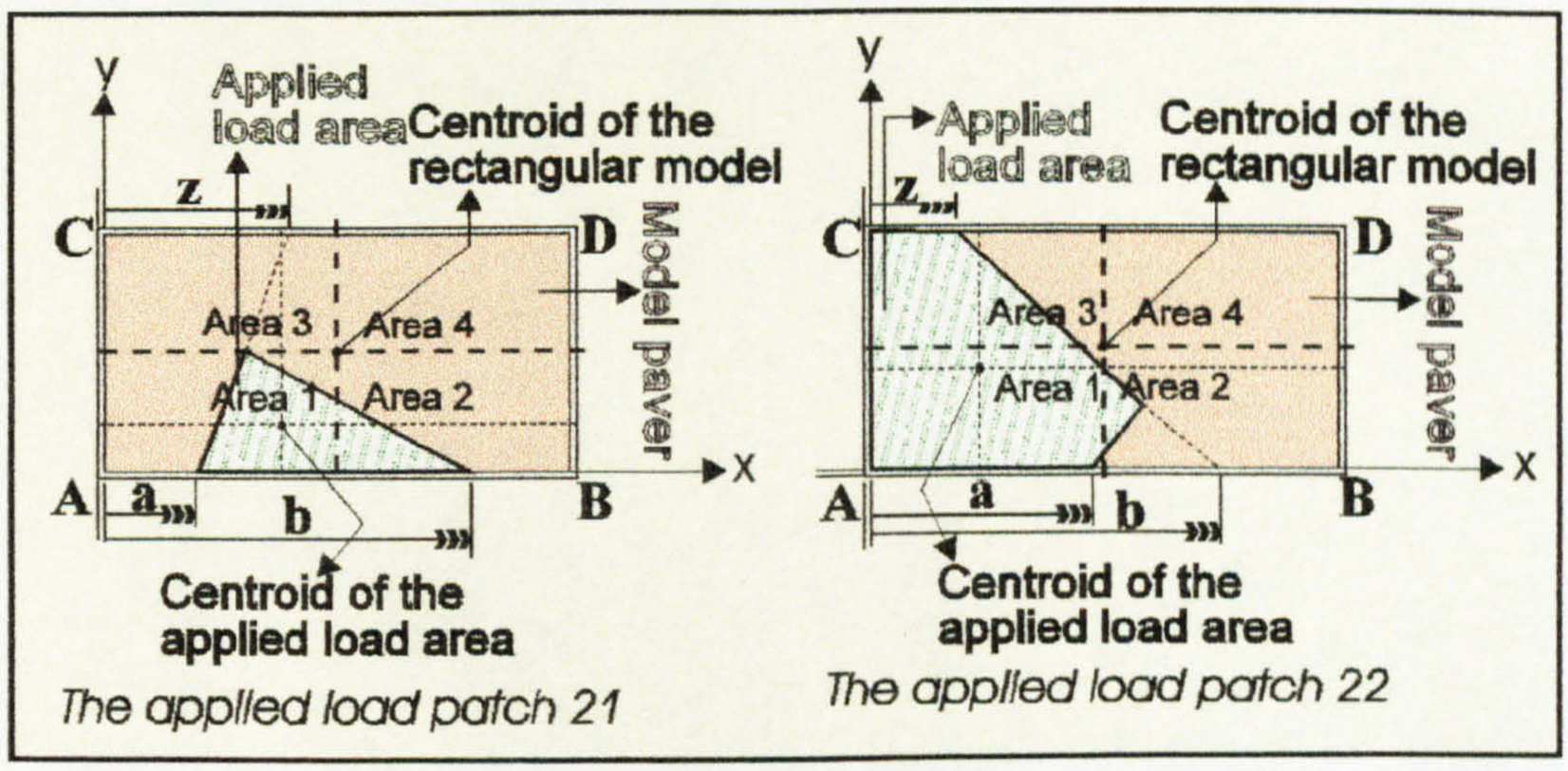

Figure 4.14: The applied load patches 21 and 22.

Figure 4.14 shows the possible applied load patches 21 and 22. In the triangular load patch 21, while the distances **a** and **b** (**a**<**b**) vary in the long side of the model paver, the distance **z** scans the paver by changing in the same direction in order to determine the possible load patch surface areas having their centroids in **Area 1**. In this case the general geometrical solutions are as follows:

$$F = \frac{45\,(-a + b)^2\,(-a + z)}{8100 + a^2 - 2\,a\,z + z^2},$$

$$\overline{X} = \frac{30\,(-a+b)\,(-a+z)}{8100+a^2-2\,a\,z+z^2},$$

$$\overline{Y} = \frac{16200\,a+a^3+8100\,b+2\,a^2\,b-2\,a^2\,z-4\,a\,b\,z+a\,z^2+2\,b\,z^2}{3\left(8100+a^2-2\,a\,z+z^2\right)}$$

For load patch 22, the distances **a**, **b** and **z** (**a<b**) vary in the long side of the model paver in order to determine the possible load patch surface areas having their centroids in **Area 1**. The difference between load patch 20 and 22 is that the line through the distance **z** in patch 20 (see Figure 4.13) can exceed the long side of the model paver. Although the results of some surface areas can be similar both in load patches 20 and 22, they basically generate different patch loadings. The general geometrical solution to load patch 22's surface area and its centroids is:

$$F = \frac{45\left(8100\,b-a^2\,b+2\,a\,b^2+8100\,z+a^2\,z-2\,a\,b\,z-b\,z^2+z^3\right)}{8100+b^2-2\,b\,z+z^2},$$

$$\begin{aligned}\overline{X} = (&30\,(65610000\,b+a^3\,b^2+16200\,b^3-3\,a^2\,b^3+3\,a\,b^4+131220000\,z-2\,a^3\,b\,z\\&+6\,a^2\,b^2z-6\,a\,b^3\,z+a^3\,z^2-48600\,b\,z^2-3\,a^2\,b\,z^2+3\,a\,b^2\,z^2-3\,b^3\,z^2+32400\,z^3\\&+8\,b^2\,z^3-7\,b\,z^4+2\,z^5))\Big/((8100+b^2-2\,b\,z+z^2)\,(8100\,b-a^2\,b+2\,a\,b^2+8100\,z\\&+a^2\,z-2\,a\,b\,z-b\,z^2+z^3)),\end{aligned}$$

$$\begin{aligned}\overline{Y} = (&-8100\,a^3\,b+65610000\,b^2+24300\,a\,b^3-2\,a^3\,b^3+3\,a^2\,b^4+8100\,a^3\,z\\&+65610000\,b\,z-24300\,a\,b^2\,z+6\,a^3\,b^2\,z-9\,a^2\,b^3\,z+65610000\,z^2-6\,a^3\,b\,z^2\\&+9\,a^2b^2\,z^2+2\,a^3\,z^3-16200\,b\,z^3-3\,a^2\,b\,z^3-b^3\,z^3+16200\,z^4+3\,b^2\,z^4\\&-3\,b\,z^5+z^6)\Big/(3\,(8100+b^2-2\,b\,z+z^2)\,(8100\,b-a^2\,b+2\,a\,b^2+8100\,z\\&+a^2\,z-2\,a\,b\,z-b\,z^2+z^3))\end{aligned}$$

As can be seen in Figure 4.15, the triangular load patch surface area and its centroids which should be in **Area 1** can be calculated using geometrical calculus. The distances **a** and **b** (**a<b**) change in the long side of the model paver, while the distance **z** scans the paver in the same direction. The difference between load patch 21 and 23 is that the line through the point **a** cuts through the long side of the model paver in load patch 23 and it

cuts through the short side of the model paver in load patch 21. Some load patch surface areas and their centroids might be similar, but they basically generate different patch loadings. The simplified general geometrical solutions of the possible varying load patch 23's surface area and its centroids can be found using the following equations:

$$F = \frac{45\,(a-b)^2\,(b-z)}{8100+b^2-2\,b\,z+z^2},$$

$$\overline{Y} = \frac{30\,(a-b)\,(-b+z)}{8100+b^2-2\,b\,z+z^2},$$

$$\overline{X} = \frac{8100\,a+16200\,b+2\,a\,b^2+b^3-4\,a\,b\,z-2\,b^2z+2\,a\,z^2+b\,z^2}{3\left(8100+b^2-2\,b\,z+z^2\right)}$$

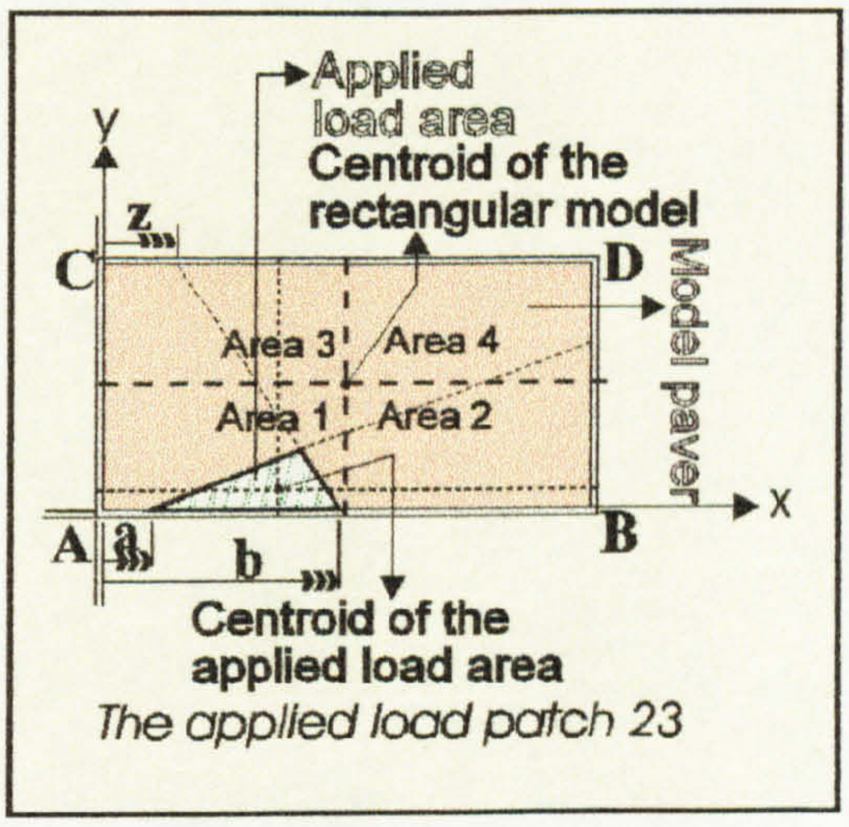

Figure 4.15: The applied load patch 23.

4.3. The selected special load patch applied to rectangular pavers

A special load patch which allows the comparison of the analysed pavers (see Figure 5.1) in terms of their vertical compressive stress distributions was selected (see Figure 4.16). This special load patch functionally generates the maximum stress value was assumed for analysing each proprietory shaped paver (see Chapter 5). The special patch load which is applied to all shaped pavers scans the circumscribing rectangular border from its lower left corner to its upper right corner with defining distances **a** and **b** **(b=a/2)** in the longitudinal and in the transverse axes respectively (see Chapter 5 for

more detail). If the special patch loads are initially considered acting on rectangular pavers, the solutions are as follows.

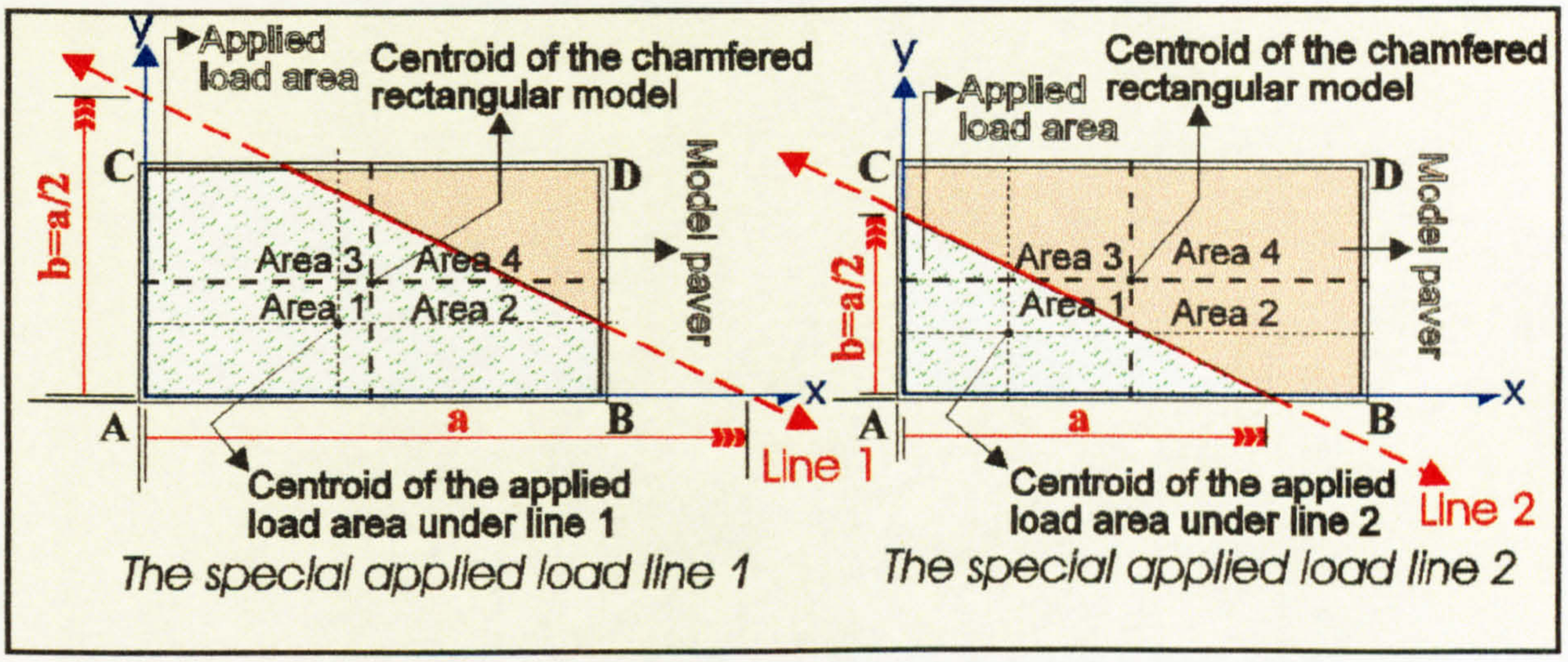

Figure 4.16: The special load patch application for chamfered rectangular paver.

As can be seen in Figure 4.16 the special patch loads are bordered by **Line 1** and **Line 2** which scan the paver from its lower left corner to its upper right corner with distances **a** and **b (b=a/2)**. For both **Line 1** and **Line 2** cases, the patch load's surface areas and centroids can be calculated by using the following equations:

For **Line 1** (see Figure 4.16):

$$F = \frac{-68500 + 740a - a^2}{4}, \qquad \overline{X} = \frac{7886000 - 11100\,a - 540\,a^2 + a^3}{3\left(68500 - 740\,a + a^2\right)},$$

$$\overline{Y} = \frac{4805000 + 11100\,a - 570\,a^2 + a^3}{6\left(68500 - 740\,a + a^2\right)}$$

For **Line 2** (see Figure 4.16):

$$F = \frac{a^2}{4}, \quad \overline{X} = \frac{a}{3} \quad \text{and} \quad \overline{Y} = \frac{a}{6}$$

Figure 4.17 illustrates the application of the selected special patch load for a non-chamfered rectangular paver formed by **Line 1** and **Line 2** which scan the paver from its upper right corner to its lower left corner with distances **a** and **b (b=a/2)**. In terms of the changeable distance **a**, the patch load's surface areas and centroids can be calculated by using the following equations:

For **Line 1** (see Figure 4.17):

$$F = -20000 + 200\,a - \frac{a^2}{4}, \qquad \overline{X} = \frac{8000000 - 600\,a^2 + a^3}{3\left(80000 - 800a + a^2\right)},$$

$$\overline{Y} = \frac{8000000 - 600\,a^2 + a^3}{6\left(80000 - 800a + a^2\right)}$$

For **Line 2** (see Figure 4.17):

$$F = \frac{a^2}{4}, \quad \overline{X} = \frac{a}{3} \quad \text{and} \quad \overline{Y} = \frac{a}{6}$$

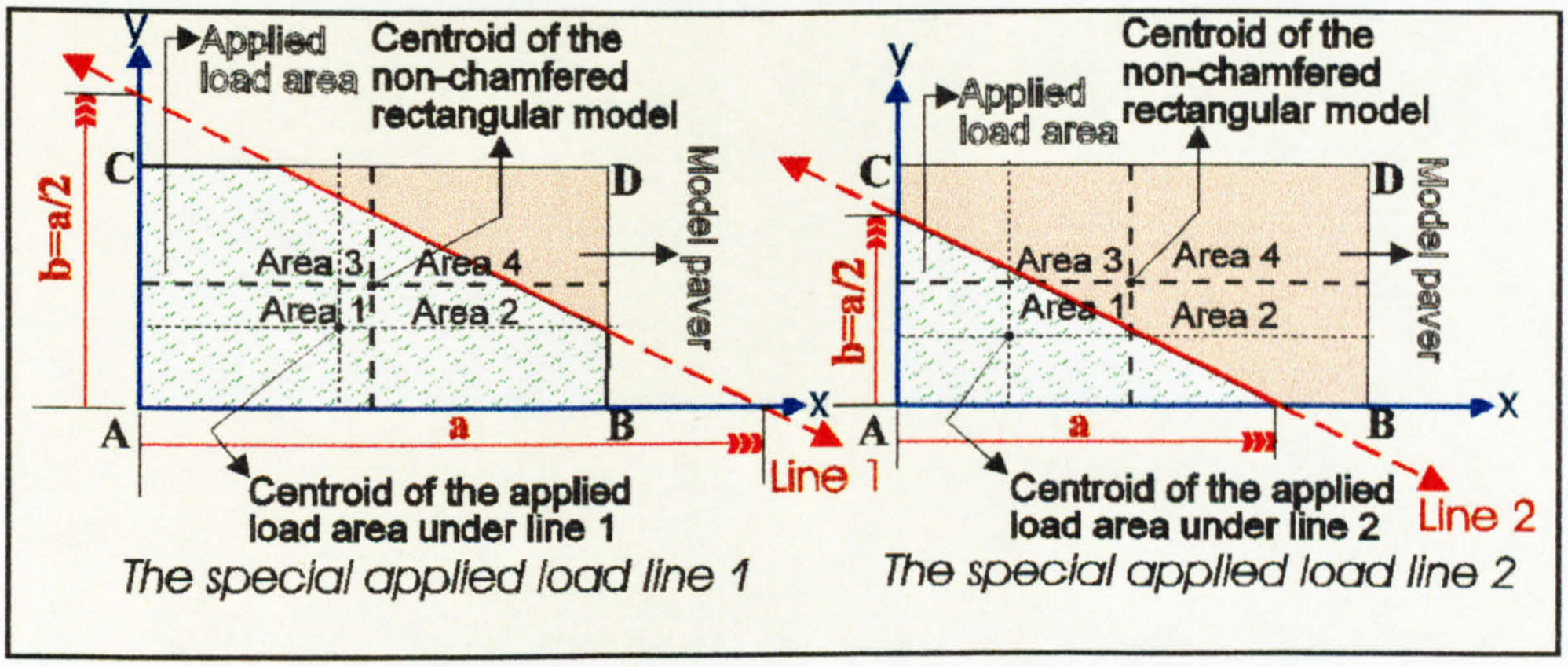

Figure 4.17: The special load patch application for non-chamfered rectangular paver.

4.4. Conclusion

This chapter defined a method to calculate the variations of the patch loads for rectangular pavers. It will be shown in Chapter 6 that there is a direct relation between the pressure applied onto a paver surface and resulting vertical compressive stress distribution; and there are five main vertical compressive stress regimes (see Figure 6.1) which can occur beneath rectangular pavers according to magnitude and position of patch loads. Because of this reason, this Chapter developed the general equations to the total applied pressures and the centroid distances of the variations of all realistically possible patch loadings for rectangular pavers. It is therefore necessary to select a particular patch loading applied onto paver before the stresses in the bedding material can be analysed. The vertical compressive stresses in the bedding material are calculated for rectangular pavers in Chapter 6 by considering vertical and rotational equilibrium of the pressures (which are defined in this Chapter) applied to the upper and lower horizontal paver surfaces (see Figures 4.3 to 4.17, 6.2 to 6.16, and 6.21). Many analytical design procedures assume that the load patch is a disk whose diameter can be determined on the basis of assessing wheel load and contact stress (see Chapter 3). It will be shown in Chapter 6 that pavement analysis must take into account the true shape of the patch loading (see Figures 4.1 and 4.2). Highway loadings must be considered as direct input criteria rather than static circular plate load assumptions because of the unique behaviour of pavers on the surface level of a paver pavement (see Chapter 6). The true behaviour of concrete block paving under highway loading can be understood only when the way in which asymmetrically loaded pavers transmit wearing surface applied patch loads into the underlying bedding sand has been studied (see Chapters 6 and 9). This Chapter also included the selected special load patch applied to rectangular pavers. This load patch which functionally generates the maximum stress value allows the comparison of the analysed pavers (see Figure 5.1) in terms of their vertical compressive stress distributions.

References

1 Knapton, J., Algin, H.M., (1995), *The Mathematical Solution to Interlock in Flexibly Bedded Clay Paving.* Proc. of the 4th. Int. Masonry Conf. No. 7, Vol. 2, p 307-313. London.

2 Algin, H.M., Knapton, J., (1996), *Research into paver interlock*, Jrnl. of the Institution of Highway & Transportation & IHIE, Vol. 43, No. 03, p 20-24.

3 Knapton, J., Algin, H.M., (1996), *The Mathematical Solution to Interlock in Concrete Block Paving.* Proc. of the 5th. Int. Conf. on Concrete Block Paving, p 261-278, Tel-Aviv.

4 Knapton, J., and Barber, S. D., (1980*), UK Research into Concrete Block Pavement Design*, Proc. of the 1st. Int. Conf. on Concrete Block Paving, University of Newcastle upon Tyne, UK, pp 33-37.

5 Lilley A. A.,(1991). *A Handbook of Segmental Paving*, Chapman & Hall, London.

CHAPTER FIVE

PATCH LOADING APPLIED TO PROPRIETORY SHAPED PAVERS

Synopsis

This Chapter concentrates on calculating the vertical pressures applied onto the selected nine proprietory shaped pavers (see Figure 5.1) by rolling loads. The calculation technique used in this Chapter for analysing the pressures applied onto proprietory shaped pavers is based on the method described in the previous chapter for rectangular pavers. The vertical compressive stress regimes in the bedding material are calculated for proprietory shaped pavers (see Chapters 7, 8 and 9) by considering vertical and rotational equilibrium of the pressures applied to the upper and lower horizontal paver surfaces. It is therefore necessary to calculate the patch loadings applied onto proprietory shaped pavers before the stresses in the bedding material can be analysed in Chapters 7, 8 and 9. This Chapter develops the general equations to the total applied pressures and the centroid distances of the variations of a realistically possible patch loading which is specially selected for proprietory shaped pavers in order to compare the pavers in terms of the stress distributions which they generate.

5.1. Introduction

Figure 5.1 illustrates the paver shapes which were studied. Apart from chamfered and non-chamfered rectangular pavers whose load patches were described in Chapter 4 , the most commonly used 9 proprietory shaped pavers' patch loadings have been analysed using an extension of the method described for the rectangular pavers (see Chapter 4). From the analysis previously set out in Chapter 4, it has been possible to identify the patch load configuration which leads to the greatest vertical compressive stress values beneath the pavers. The greatest stresses are produced when the special patch load illustrated in Figure 4.16 and 4.17 is applied. This is now used in the patch loading analyses of 9 proprietory shaped pavers shown in Figure 5.1.

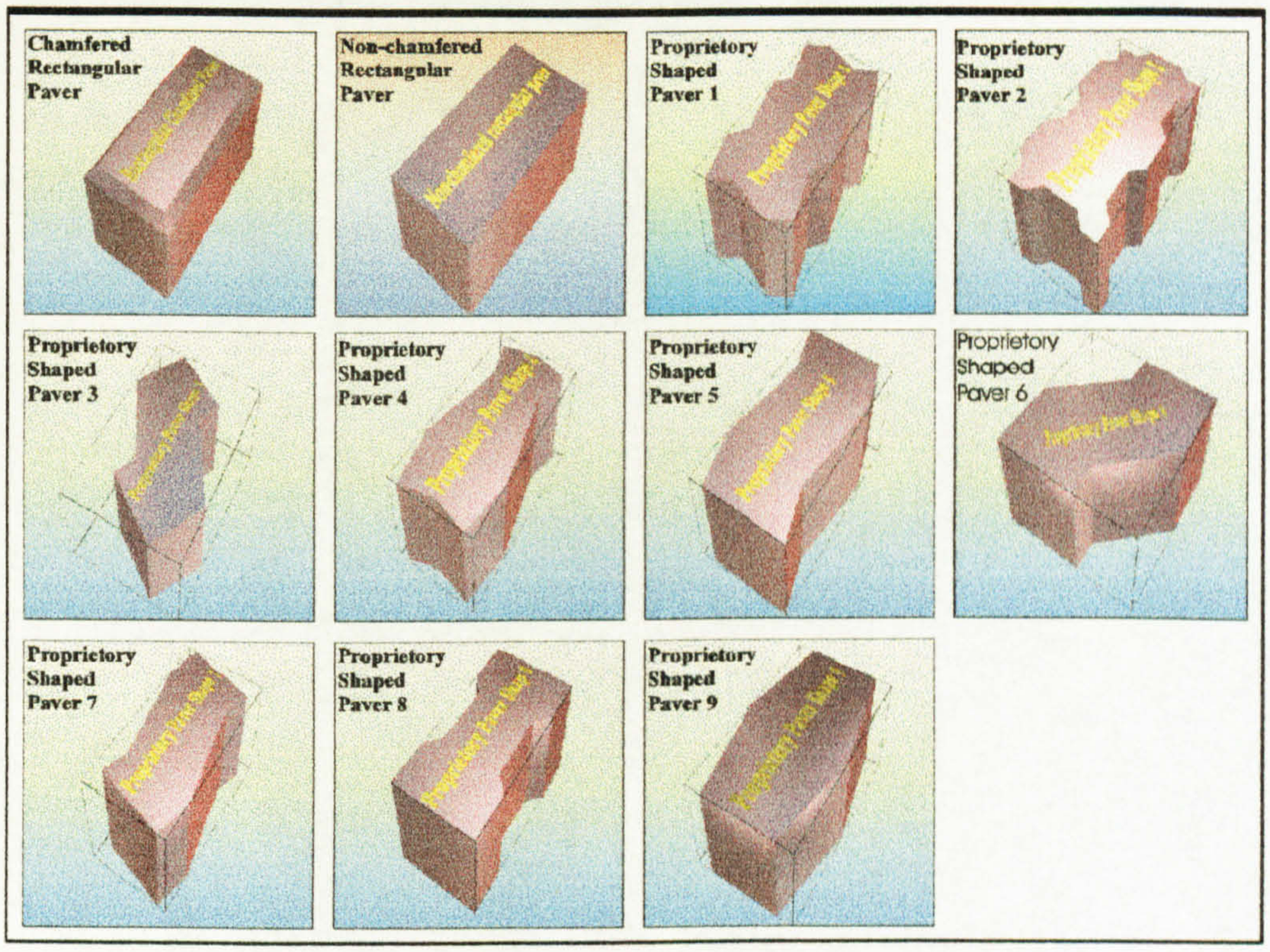

Figure 5.1: The two rectangular (chamfered and non-chamfered) and nine proprietory shaped pavers were analysed.

If each proprietory shape is considered of having a circumscribing rectangular paver, all patch loadings for shaped pavers can be analysed by placing x, y transverse and longitudinal axes on the circumscribing rectangular surface and by calculating the

function for each actual boundary line. In order to reduce the geometrical complexity of the work, a special load patch which functionally achieves the maximum vertical compressive stress values was assumed for analysing each proprietory shaped paver. This selected special patch loading which were analysed for rectangular pavers in Section 4.3 is useful for allowing a meaningful comparison of the pavers in terms of the maximum stress values which they generate. This special patch load applied to all of the shaped pavers scans the circumscribing rectangular border from its lower left corner to its upper right corner with defining distances **a** and **b (b=a/2)** in the longitudinal and in the transverse axes respectively (see Figure 5.2). Therefore, according to the distances **a** in the longitudinal direction, the real loading area of the shaped blocks is computed using the shaped blocks' real border line functions. Hence the centre of gravity of the special patch loading when applied to each of the shaped paver can be computed in order to analyse the stresses generated by each paver. The Chapter defines the application of this selected special patch load to 9 proprietory shaped pavers.

5.2 The selected special patch load applied to proprietory shaped paver 1

The special patch load which characterises the maximum idealised vertical compressive stress value was selected for proprietory shaped paver 1 as described in Section 4.3 and 5.1. Common patch loadings which functionally generate maximum corner stress values were applied to the shaped pavers so allowing a meaningful comparison of the effectiveness of each shape in load dissipation. In each case, a circumscribing rectangular paver has been analysed and the negative effects generated by the dentations have been included in the results. Figure 5.2 shows the application of the critical load patch shape to the proprietory shaped paver 1. 15 different patch load applications can be generated in which the lines which form the boundaries of the patch loadings can scan the paver from its lower left corner to its upper right corner with distances **a** and **b (b=a/2)**. The patch load application 1 can be seen in Figure 5.2 and is bordered by **Line 1**. **Line 1** scans the paver from corner **h** to **i** in terms of the changeable distance **a** in the x direction. If x, y transverse and longitudinal axes have their origin corner **A** of this circumscribing rectangular shape, it can be seen that each corner of the actual paver is connected by lines which form the real shape of the paver. The functions of these lines

can be calculated using basic geometrical rules. The boundary line functions for proprietory shaped paver 1 are shown in Table 5.1.

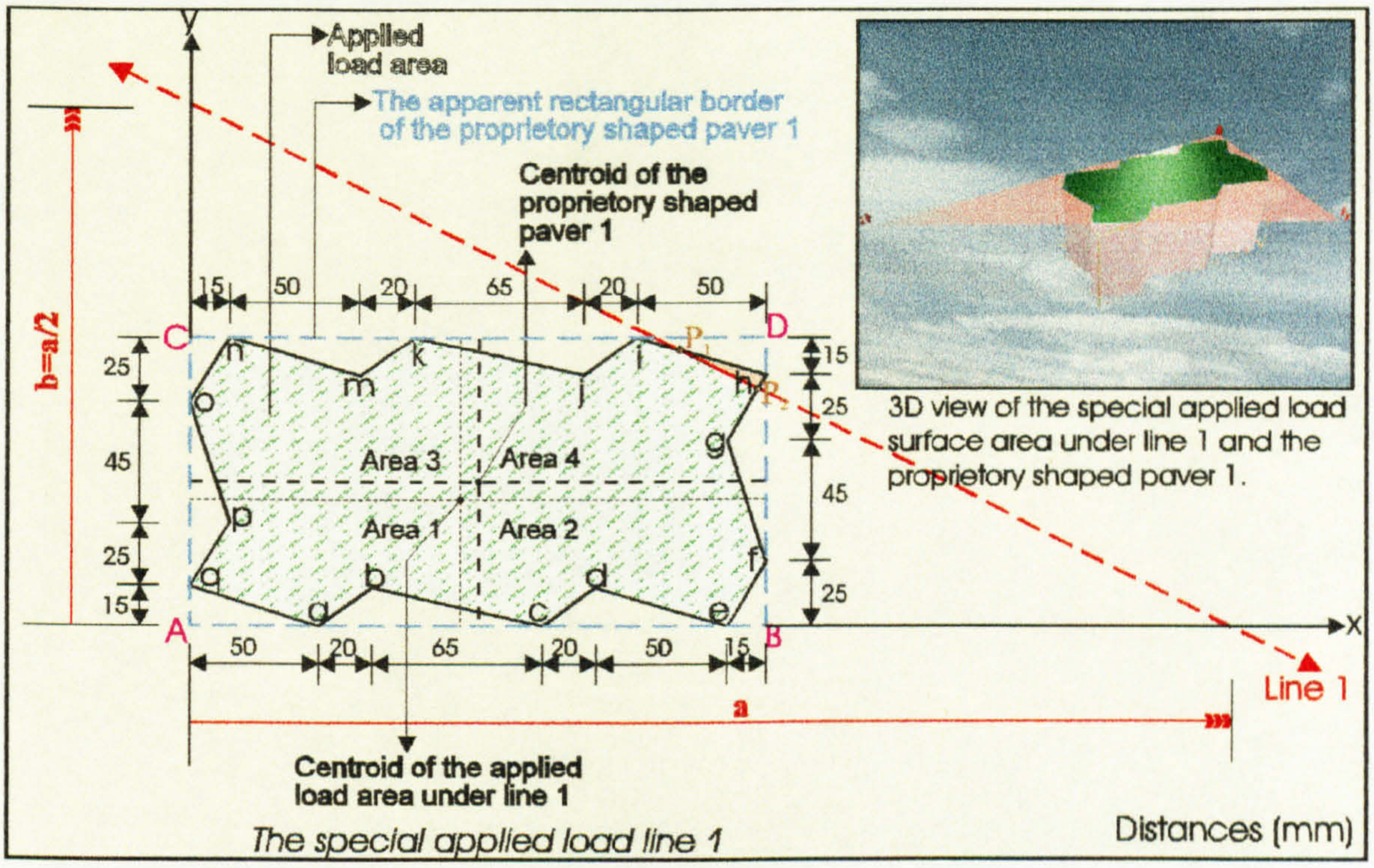

Figure 5.2: The selected special patch load application 1 for proprietory shaped paver 1.

$qax = 50 - 3.\bar{3}y$ $qay = 15 - 0.3x$	$abx = 50 + 1.\bar{3}y$ $aby = 0.75x - 37.5$	$bcx = 135 - 4.\bar{3}y$ $bcy = 31.154 - 0.230x$	$cdx = 135 + 1.\bar{3}y$ $cdy = 0.75x - 101.25$
$dex = 205 - 3.\bar{3}y$ $dey = 61.5 - 0.3x$	$efx = 205 + 0.6y$ $efy = 1.\bar{6}x - 341.\bar{6}$	$fgx = 228.\bar{3} - 0.\bar{3}y$ $fgy = 685 - 3x$	$ghx = 163 + 0.6y$ $ghy = 1.\bar{6}x - 271.\bar{6}$
$hix = 536.\bar{6} - 3.\bar{3}y$ $hiy = 161 - 0.3x$	$jix = 23.\bar{3} + 1.\bar{3}y$ $jiy = 0.75x - 17.5$	$kjx = 561.\bar{6} - 4.\bar{3}y$ $kjy = 129.615 - 0.2301x$	$mkx = 1.\bar{3}y - 61.\bar{6}$ $mky = 46.25 + 0.75x$
$nmx = 381.\bar{6} - 3.\bar{3}y$ $nmy = 114.5 - 0.3x$	$onx = 0.6y - 51$ $ony = 85 + 1.\bar{6}x$	$pox = 28.\bar{3} - 0.\bar{3}y$ $poy = 85 - 3x$	$qpx = 0.6y - 9$ $qpy = 15 + 1.\bar{6}x$

Table 5.1: Boundary line functions for proprietory shaped paver 1.

In Table 5.1 the first two letters of each line function characterise the corner names as can be seen in Figure 5.2 . By using the line functions in Table 5.1 for shaped paver 1 and the line functions which define the patch load boundaries, which are of the form

$f_y = b(1-\frac{x}{a})$, $f_x = a(1-\frac{y}{b})$ in the x and y axes, the intersection points between the paver boundary lines and the load patch boundary line can be calculated mathematically. Table 5.2 shows the intersection points which can be seen in Figures from 5.2 to 5.16.

$P_{1x} = \frac{a(b-161)}{b-0.3a}$ and $P_{1y} = \frac{b(a-536.\bar{6})}{a-3.\bar{3}b}$	$P_{2x} = \frac{a(b+271.\bar{6})}{b+1.\bar{6}a}$ and $P_{2y} = \frac{b(a-163)}{a+0.6b}$
$P_{3x} = \frac{a(b+17.5)}{b+0.75a}$ and $P_{3y} = \frac{b(a-23.\bar{3})}{a+1.\bar{3}b}$	$P_{4x} = \frac{a(b-129.615)}{b-0.2301a}$ and $P_{4y} = \frac{b(a-561.\bar{6})}{a-4.\bar{3}b}$
$P_{5x} = \frac{a(b-685)}{b-3a}$ and $P_{5y} = \frac{b(a-228.\bar{3})}{a-0.\bar{3}b}$	$P_{6x} = \frac{a(b-46.25)}{b+0.75a}$ and $P_{6y} = \frac{b(a+61.\bar{6})}{a+1.\bar{3}b}$
$P_{7x} = \frac{a(b-114.5)}{b-0.3a}$ and $P_{7y} = \frac{b(a-381.\bar{6})}{a-3.\bar{3}b}$	$P_{8x} = \frac{a(b+341.\bar{6})}{b+1.\bar{6}a}$ and $P_{8y} = \frac{b(a-205)}{a+0.6b}$
$P_{9x} = \frac{a(b-61.5)}{b-0.3a}$ and $P_{9y} = \frac{b(a-205)}{a-3.\bar{3}b}$	$P_{10x} = \frac{a(b-85)}{b+1.\bar{6}a}$ and $P_{10y} = \frac{b(a+51)}{a+0.6b}$
$P_{11x} = \frac{a(b+101.25)}{b+0.75a}$ and $P_{11y} = \frac{b(a-135)}{a+1.\bar{3}b}$	$P_{12x} = \frac{a(b-31.154)}{b-0.23a}$ and $P_{12y} = \frac{b(a-135)}{a-4.\bar{3}b}$
$P_{13x} = \frac{a(b-85)}{b-3a}$ and $P_{13y} = \frac{b(a-28.\bar{3})}{a-0.\bar{3}b}$	$P_{14x} = \frac{a(b+37.5)}{b+0.75a}$ and $P_{14y} = \frac{b(a-50)}{a+1.\bar{3}b}$
$P_{15x} = \frac{0.6a(b-15)}{a+0.6b}$ and $P_{15y} = \frac{b(a+9)}{a+0.6b}$	$P_{16x} = \frac{a(b-15)}{b-0.3a}$ and $P_{16y} = \frac{b(a-50)}{a-3.\bar{3}b}$

Table 5.2: The intersection points between the lines which form the patch load boundary with distances a and b in the x and y directions and line functions bounding the proprietory shaped paver 1.

The surface area and centroid distances for the system illustrated in Figure 5.2 can be calculated using the data in Table 5.1 and Table 5.2 and are as follows:

$$F = \int_0^{220} fy\,dx - \int_{205}^{P_{2x}} ghy\,dx + \int_{205}^{P_{2x}} fgy\,dx - \int_{P_{2x}}^{220} fy\,dx + \int_{P_{2x}}^{220} fgy\,dx - \int_{205}^{220} efy\,dx$$
$$- \int_0^{50} qay\,dx - \int_{50}^{70} aby\,dx - \int_{70}^{135} fy\,dx - \int_{135}^{155} cdy\,dx - \int_{155}^{205} fy\,dx - \int_0^{15} poy\,dx + \int_0^{15} qpy\,dx$$
$$- \int_0^{15} 110\,dx + \int_0^{15} ony\,dx - \int_0^{15} fy\,dx + \int_0^{15} 110\,dx - \int_{15}^{P_{1x}} fy\,dx + \int_{15}^{65} nmy\,dx + \int_{65}^{85} mky\,dx$$

$$+\int_{85}^{150} kjy\,dx+\int_{150}^{170} jiy\,dx+\int_{170}^{P_{1x}} ihy\,dx$$

The evaluation of the integrals yields the following equation:

$$F=-75665.2+465.194a-0.567306a^2$$

$$\begin{aligned}\overline{X}=\frac{1}{F}\Bigg[&\int_{0}^{220} x\,fy\,dx-\int_{205}^{P_{2x}} x\,ghy\,dx+\int_{205}^{P_{2x}} x\,fgy\,dx-\int_{P_{2x}}^{220} x\,fy\,dx+\int_{P_{2x}}^{220} x\,fgy\,dx-\int_{205}^{220} x\,efy\,dx\\&-\int_{0}^{50} x\,qay\,dx-\int_{50}^{70} x\,aby\,dx-\int_{70}^{135} x\,fy\,dx-\int_{135}^{155} x\,cdy\,dx-\int_{155}^{205} x\,fy\,dx-\int_{0}^{15} x\,poy\,dx\\&+\int_{0}^{15} x\,qpy\,dx-\int_{0}^{15} x\,110\,dx+\int_{0}^{15} x\,ony\,dx-\int_{0}^{15} x\,fy\,dx+\int_{0}^{15} x\,110\,dx-\int_{15}^{P_{1x}} x\,fy\,dx\\&+\int_{15}^{65} x\,nmy\,dx+\int_{65}^{85} x\,mky\,dx+\int_{85}^{150} x\,kjy\,dx+\int_{150}^{170} x\,jiy\,dx+\int_{170}^{P_{1x}} x\,ihy\,dx\Bigg]\end{aligned}$$

The evaluation of the integrals yields the following equation:

$$\overline{X}=\frac{0.910259(-519.342+a)\left(62558.4-468.969a+a^2\right)}{(-596.352+a)(-223.654+a)}$$

$$\begin{aligned}\overline{Y}=\frac{1}{F}\Bigg[&\int_{0}^{110} y\,fx\,dy-\int_{0}^{25} y\,fx\,dy+\int_{0}^{25} y\,220\,dy-\int_{25}^{P_{2y}} y\,fx\,dy+\int_{25}^{70} y\,fgx\,dy+\int_{70}^{P_{2y}} y\,ghx\,dy\\&-\int_{0}^{25} y\,220\,dy+\int_{0}^{25} y\,efx\,dy-\int_{85}^{110} y\,onx\,dy-\int_{15}^{40} y\,qpx\,dy-\int_{40}^{85} y\,pox\,dy-\int_{0}^{15} y\,dex\,dy\end{aligned}$$

$$+\int_0^{15} y\,cdx\,dy - \int_0^{15} y\,bcx\,dy + \int_0^{15} y\,abx\,dy - \int_0^{15} y\,qax\,dy - \int_{95}^{110} y\,mkx\,dy + \int_{95}^{110} y\,nmx\,dy$$

$$\left. - \int_{95}^{110} y\,jix\,dy + \int_{95}^{110} y\,kjx\,dy \int_{P_{1y}}^{110} y\,fx\,dy + \int_{P_{1y}}^{110} y\,hix\,dy \right]$$

The evaluation of the integrals yields the following equation:

$$\overline{Y} = \frac{0.121857(1161.97-a)(-568.918+a)(-278.843+a)}{(-596.361+a)(-223.68+a)}$$

Line 1 in Figure 5.2 scans the paver between corners **h** and **i**. It should therefore be noted that for the solutions above to be valid for the patch load application 1, the variable distance **a** in the x direction must lie in the range: 410>**a**>390mm.

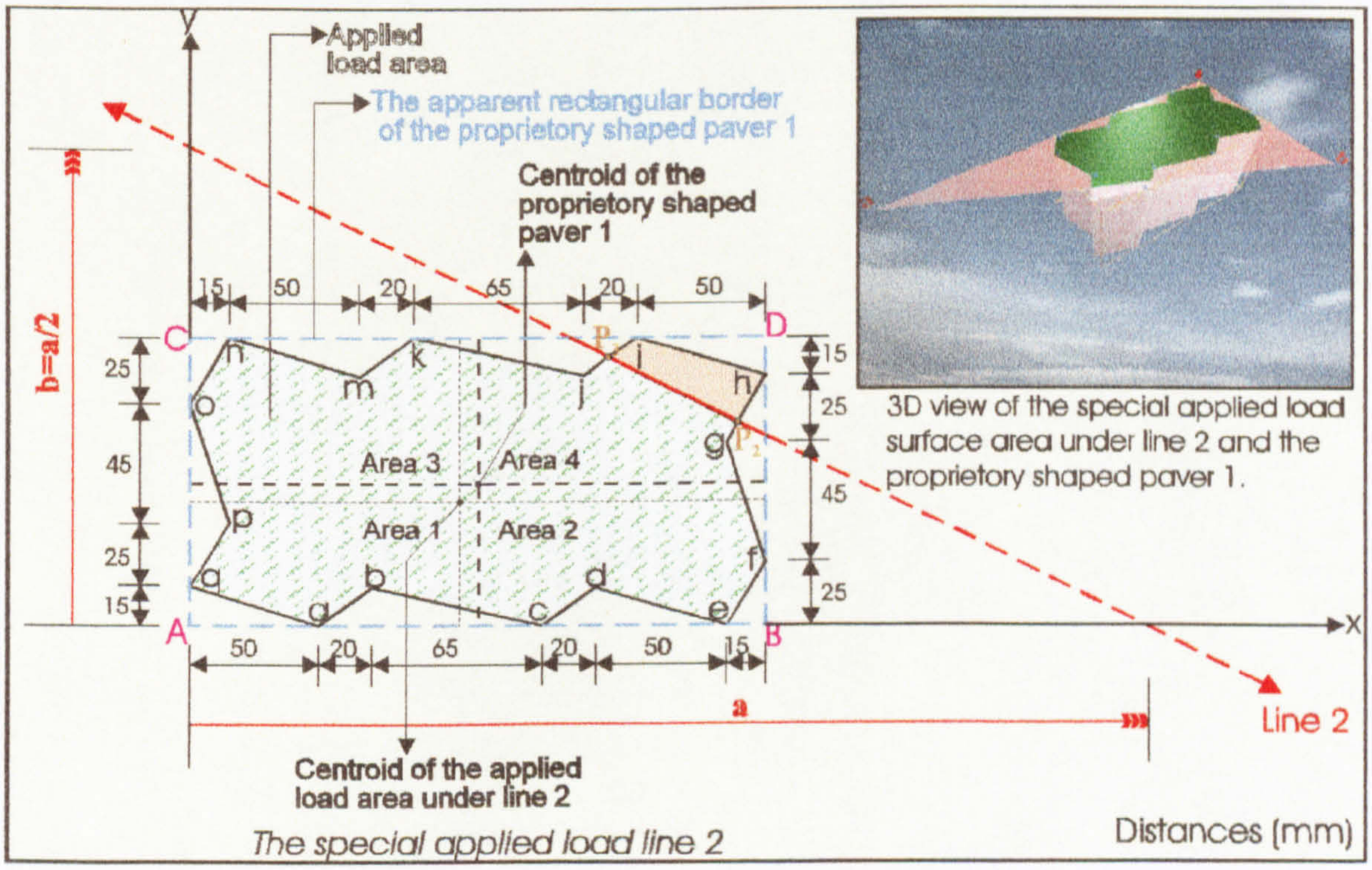

Figure 5.3: The selected special patch load application 2 for proprietory shaped paver 1.

Figure 5.3 illustrates the special patch load application 2 for the proprietory shaped paver 1. **Line 2** scans the paver between corners **i** and **g** in terms of the variable distance

a in the x direction. By using the paver line functions in Table 5.1, the equations of the intersection points in Table 5.2 and the patch load boundary line function which is $f_y = b(1-\frac{x}{a})$, $f_x = a(1-\frac{y}{b})$ in the x and y axes, the special patch load's surface area and centroid distances can be calculated as follows:

$$F = \int_0^{220} fy\,dx - \int_{205}^{P_{2x}} ghy\,dx + \int_{205}^{P_{2x}} fgy\,dx - \int_{P_{2x}}^{220} fy\,dx + \int_{P_{2x}}^{220} fgy\,dx - \int_{205}^{220} efy\,dx - \int_0^{50} qay\,dx$$
$$- \int_{50}^{70} aby\,dx - \int_{70}^{135} fy\,dx - \int_{135}^{155} cdy\,dx - \int_{155}^{205} fy\,dx - \int_0^{15} poy\,dx + \int_0^{15} qpy\,dx - \int_0^{15} 110\,dx + \int_0^{15} ony\,dx$$
$$- \int_0^{15} fy\,dx + \int_0^{15} 110\,dx - \int_{15}^{P_{3x}} fy\,dx + \int_{15}^{65} nmy\,dx + \int_{65}^{85} mky\,dx \int_{85}^{150} kjy\,dx + \int_{150}^{P_{3x}} jiy\,dx$$

The evaluation of the integrals yields the following equation:

$$F = 4187.27 + 55.6941a - 0.0423059a^2$$

$$\overline{X} = \frac{1}{F}\left[\begin{array}{l} \int_0^{220} x\,fy\,dx - \int_{205}^{P_{2x}} x\,ghy\,dx + \int_{205}^{P_{2x}} x\,fgy\,dx - \int_{P_{2x}}^{220} x\,fy\,dx + \int_{P_{2x}}^{220} x\,fgy\,dx - \int_{205}^{220} x\,efy\,dx \\ - \int_0^{50} x\,qay\,dx - \int_{50}^{70} x\,aby\,dx - \int_{70}^{135} x\,fy\,dx - \int_{135}^{155} x\,cdy\,dx - \int_{155}^{205} x\,fy\,dx - \int_0^{15} x\,poy\,dx \\ + \int_0^{15} x\,qpy\,dx - \int_0^{15} x\,110\,dx + \int_0^{15} x\,ony\,dx - \int_0^{15} x\,fy\,dx + \int_0^{15} x\,110\,dx - \int_{15}^{P_{3x}} x\,fy\,dx \\ + \int_{15}^{65} x\,nmy\,dx + \int_{65}^{85} x\,mky\,dx \int_{85}^{150} x\,kjy\,dx + \int_{150}^{P_{3x}} x\,jiy\,dx \end{array}\right]$$

The evaluation of the integrals yields the following equation:

$$\overline{X} = \frac{0.210259(-1082.68+a)(72.6617+a)(354.145+a)}{(-1387.78+a)(71.3196+a)}$$

$$\overline{Y} = \frac{1}{F}\left[\begin{array}{l}
\int_0^{110} y\,fx\,dy - \int_0^{25} y\,fx\,dy + \int_0^{25} y\,220\,dy - \int_{25}^{P_{2y}} y\,fx\,dy + \int_{25}^{70} y\,fgx\,dy + \int_{70}^{P_{2y}} y\,ghx\,dy \\
-\int_0^{25} y\,220\,dy + \int_0^{25} y\,efx\,dy - \int_{85}^{110} y\,onx\,dy - \int_{15}^{40} y\,qpx\,dy - \int_{40}^{85} y\,pox\,dy - \int_0^{15} y\,dex\,dy \\
+\int_0^{15} y\,cdx\,dy - \int_0^{15} y\,bcx\,dy + \int_0^{15} y\,abx\,dy - \int_0^{15} y\,qax\,dy - \int_{95}^{110} y\,mkx\,dy + \int_{95}^{110} y\,nmx\,dy \\
-\int_{95}^{P_{3y}} y\,jix\,dy + \int_{95}^{P_{3y}} y\,kjx\,dy - \int_{P_{3y}}^{110} y\,fx\,dy + \int_{P_{3y}}^{110} y\,kjx\,dy
\end{array}\right]$$

The evaluation of the integrals yields the following equation:

$$\overline{Y} = \frac{0.228206(-1014+a)\left(73243.9-126.002a+a^2\right)}{(-1387.76+a)(71.3502+a)}$$

Line 2 in Figure 5.3 scans the paver between corners **i** and **g**. It should therefore be noted that for the solutions above to be valid for the patch load application 2, the variable distance **a** in the x direction must lie in the range: 390>**a**>345mm.

Figure 5.4 illustrates the special patch load application 3 for the proprietory shaped paver 1. **Line 3** scans the paver between corners **g** and **j** in terms of the variable distance **a** in the x direction. By using Table 5.1, Table 5.2 and the patch load boundary line function which is $f_y = b(1-\frac{x}{a})$, $f_x = a(1-\frac{y}{b})$ in the x and y axes, the special patch load's surface area and centroid distances can be calculated according to the distance **a**.

$$F = \int_0^{220} fy\,dx - \int_{P_{5x}}^{220} fy\,dx + \int_{P_{5x}}^{220} fgy\,dx - \int_{205}^{220} efy\,dx - \int_0^{50} qay\,dx - \int_{50}^{70} aby\,dx - \int_{70}^{135} fy\,dx$$

$$-\int_{135}^{155} cdy\,dx - \int_{155}^{205} fy\,dx - \int_0^{15} poy\,dx + \int_0^{15} qpy\,dx - \int_0^{15} 110\,dx + \int_0^{15} ony\,dx - \int_0^{15} fy\,dx + \int_0^{15} 110\,dx$$

$$-\int_{15}^{P_{3x}} fy\,dx + \int_{15}^{65} nmy\,dx + \int_{65}^{85} mky\,dx + \int_{85}^{150} kjy\,dx + \int_{150}^{P_{3x}} jiy\,dx$$

The evaluation of the integrals yields the following equation:

$$F = -8626.67 + 129.972a - 0.149939a^2$$

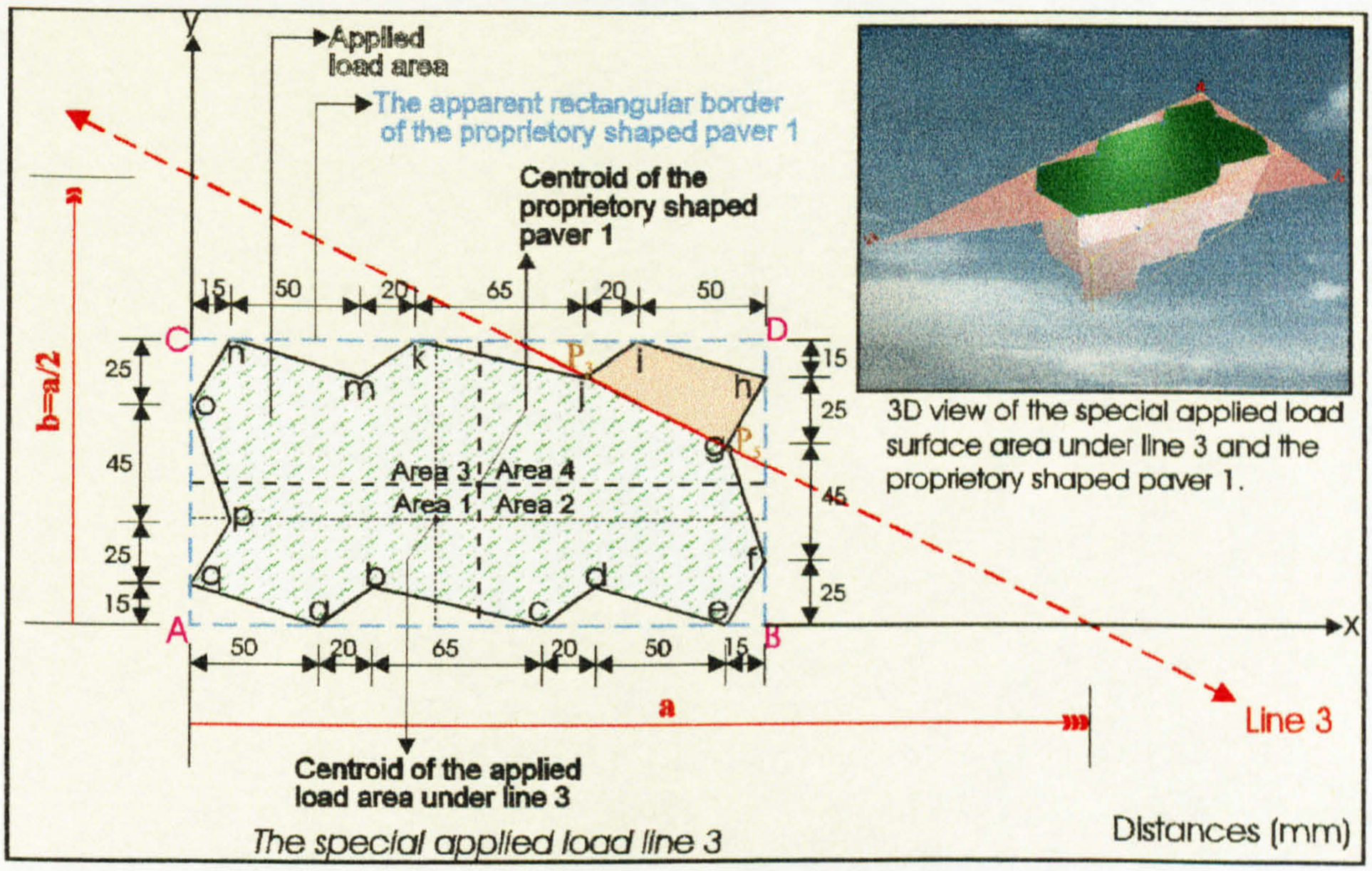

Figure 5.4: The selected special patch load application 3 for proprietory shaped paver 1.

$$\overline{X} = \frac{1}{F}\left[\int_{0}^{220} x\,fy\,dx - \int_{P_{5x}}^{220} x\,fy\,dx + \int_{P_{5x}}^{220} x\,fgy\,dx - \int_{205}^{220} x\,efy\,dx - \int_{0}^{50} x\,qay\,dx - \int_{50}^{70} x\,aby\,dx\right.$$

$$-\int_{70}^{135} x\,fy\,dx - \int_{135}^{155} x\,cdy\,dx - \int_{155}^{15} x\,fy\,dx - \int_{0}^{15} x\,poy\,dx + \int_{0}^{15} x\,qpy\,dx - \int_{0}^{15} x\,110\,dx$$

$$+\int_{0}^{15} x\,ony\,dx - \int_{0}^{P_{3x}} x\,fy\,dx + \int_{0}^{65} x\,110\,dx - \int_{15}^{65} x\,fy\,dx + \int_{15}^{85} x\,nmy\,dx + \int_{65}^{150} x\,mky\,dx$$

$$\left.+\int_{85}^{P_{3x}} x\,kjy\,dx + \int_{150}^{} x\,jiy\,dx\right]$$

The evaluation of the integrals yields the following equation:

$$\overline{X} = \frac{0.0\overline{6}(-696.505+a)(-142.67+a)(2349.18+a)}{(-794.227+a)(-72.4393+a)}$$

$$\overline{Y} = \frac{1}{F}\left[\int_0^{110} y\,fx\,dy - \int_0^{25} y\,fx\,dy + \int_0^{25} y\,220\,dy - \int_{25}^{P_{5y}} y\,fx\,dy + \int_{25}^{P_{5y}} y\,fgx\,dy - \int_0^{25} y\,220\,dy\right.$$

$$+\int_0^{25} y\,efx\,dy - \int_{85}^{110} y\,onx\,dy - \int_{15}^{40} y\,qpx\,dy - \int_{40}^{85} y\,pox\,dy - \int_0^{15} y\,dex\,dy + \int_0^{15} y\,cdx\,dy$$

$$-\int_0^{15} y\,bcx\,dy + \int_0^{15} y\,abx\,dy - \int_0^{15} y\,qax\,dy - \int_{95}^{110} y\,mkx\,dy + \int_{95}^{110} y\,nmx\,dy - \int_{95}^{P_{3y}} y\,jix\,dy$$

$$\left.+\int_{95}^{P_{3y}} y\,kjx\,dy - \int_{P_{3y}}^{110} y\,fx\,dy + \int_{P_{3y}}^{110} y\,kjx\,dy\right]$$

The evaluation of the integrals yields the following equation:

$$\overline{Y} = \frac{0.299961(-631.57+a)\left(44739.7-258.544a+a^2\right)}{(-794.414+a)(-72.424+a)}$$

Line 3 in Figure 5.4 scans the paver between corners **g** and **j**. It should therefore be noted that for the solutions above to be valid for the patch load application 3, the variable distance **a** in the x direction must lie in the range: 345>**a**>340mm.

Figure 5.5 illustrates the special patch load application 4 for the proprietory shaped paver 1. **Line 4** scans the paver between corners **j** and **k** in terms of the variable distance **a** in the x direction. By using the paver line functions in Table 5.1, the equations of the intersection points in Table 5.2 and the patch load boundary line

function which is $f_y = b(1-\frac{x}{a})$, $f_x = a(1-\frac{y}{b})$ in the x and y axes, the special patch load's surface area and centroid distances can be calculated as follows:

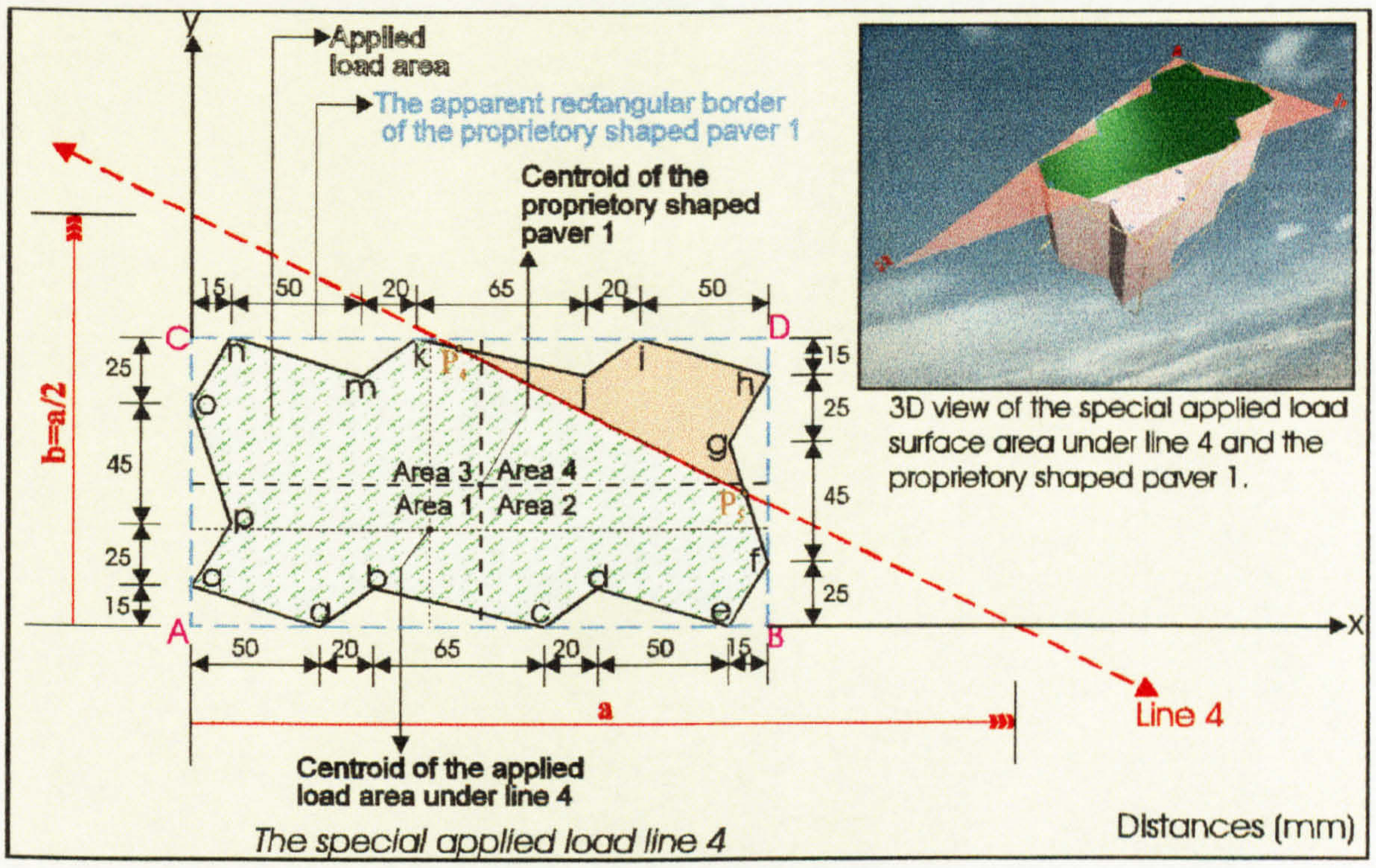

Figure 5.5: The selected special patch load application 4 for proprietory shaped paver 1.

$$F = \int_0^{220} fy\,dx - \int_{P_{5x}}^{220} fy\,dx + \int_{P_{5x}}^{220} fgy\,dx - \int_{205}^{220} efy\,dx - \int_0^{50} qay\,dx - \int_{50}^{70} aby\,dx - \int_{70}^{135} fy\,dx$$
$$- \int_{135}^{155} cdy\,dx - \int_{155}^{205} fy\,dx - \int_0^{15} poy\,dx + \int_0^{15} qpy\,dx - \int_0^{15} 110\,dx + \int_0^{15} ony\,dx - \int_0^{15} fy\,dx + \int_0^{15} 110\,dx$$
$$- \int_{15}^{P_{4x}} fy\,dx + \int_{15}^{65} nmy\,dx + \int_{65}^{85} mky\,dx + \int_{85}^{P_{4x}} kjy\,dx$$

The evaluation of the integrals yields the following equation:

$$F = -50746 + 377.721a - 0.514256a^2$$

$$\overline{X} = \frac{1}{F}\left[\begin{array}{l}
\int_0^{220} x\,fy\,dx - \int_{P_{5x}}^{220} x\,fy\,dx + \int_{P_{5x}}^{220} x\,fgy\,dx - \int_{205}^{220} x\,efy\,dx - \int_0^{50} x\,qay\,dx - \int_{50}^{70} x\,aby\,dx \\
- \int_{70}^{135} x\,fy\,dx - \int_{135}^{155} x\,cdy\,dx - \int_{155}^{205} x\,fy\,dx - \int_0^{15} x\,poy\,dx + \int_0^{15} x\,qpy\,dx - \int_0^{15} x\,110\,dx \\
+ \int_0^{15} x\,ony\,dx - \int_0^{15} x\,fy\,dx + \int_0^{15} x\,110\,dx - \int_{15}^{P_{4x}} x\,fy\,dx + \int_{15}^{65} x\,nmy\,dx + \int_{65}^{85} x\,mky\,dx \\
+ \int_{85}^{P_{4x}} x\,kjy\,dx
\end{array}\right]$$

The evaluation of the integrals yields the following equation:

$$\overline{X} = \frac{0.550846(-487.289+a)(-148.943+a)(-102.161+a)}{(-557.94+a)(-176.988+a)}$$

$$\overline{Y} = \frac{1}{F}\left[\begin{array}{l}
\int_0^{110} y\,fx\,dy - \int_0^{25} y\,fx\,dy + \int_0^{25} y\,220\,dy - \int_{25}^{P_{5y}} y\,fx\,dy + \int_{25}^{P_{5y}} y\,fgx\,dy - \int_0^{25} y\,220\,dy \\
+ \int_0^{25} y\,efx\,dy - \int_{85}^{110} y\,onx\,dy - \int_{15}^{40} y\,qpx\,dy - \int_{40}^{85} y\,pox\,dy - \int_0^{15} y\,dex\,dy + \int_0^{15} y\,cdx\,dy \\
- \int_0^{15} y\,bcx\,dy + \int_0^{15} y\,abx\,dy - \int_0^{15} y\,qax\,dy - \int_{95}^{110} y\,mkx\,dy + \int_{95}^{110} y\,nmx\,dy - \int_{P_{4y}}^{110} y\,fx\,dy \\
+ \int_{P_{4y}}^{110} y\,kjx\,dy
\end{array}\right]$$

The evaluation of the integrals yields the following equation:

$$\overline{Y} = \frac{0.0570825(-511.589+a)(-206.878+a)(1076.59+a)}{(-557.496+a)(-177.003+a)}$$

Line 4 in Figure 5.5 scans the paver between corners **j** and **k**. It should therefore be noted that for the solutions above to be valid for the patch load application 4, the variable distance **a** in the x direction must lie in the range: 340>**a**>305mm.

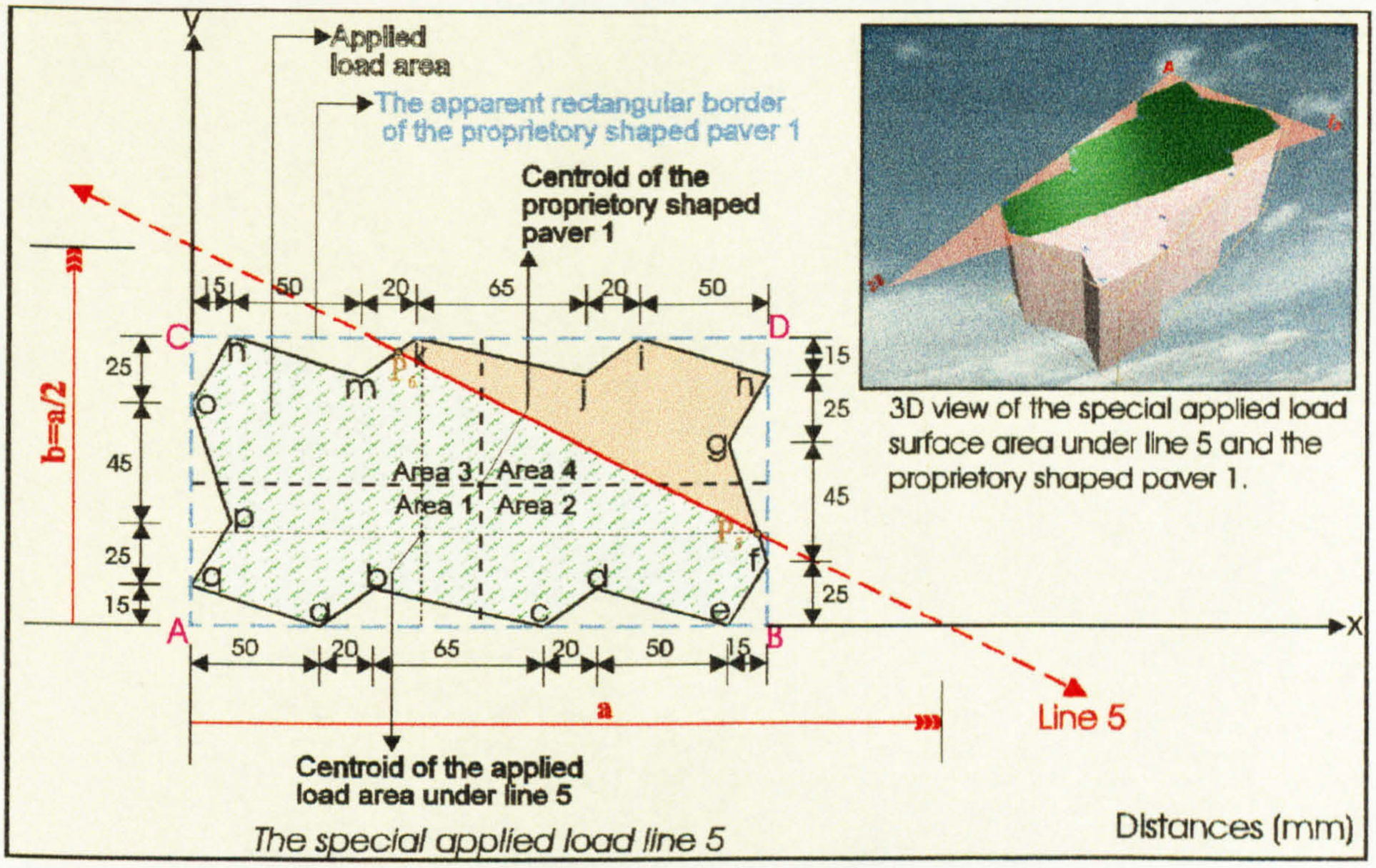

The special applied load line 5

Figure 5.6: The selected special patch load application 5 for proprietory shaped paver 1.

Figure 5.6 illustrates the special patch load application 5 for the proprietory shaped paver 1. **Line 5** scans the paver between corners **k** and **f** in terms of the variable distance **a** in the x direction. By using Table 5.1, Table 5.2 and the patch load boundary line function which is $f_y = b(1-\frac{x}{a})$, $f_x = a(1-\frac{y}{b})$ in the x and y axes, the special patch load's surface area and centroid distances can be calculated according to the distance **a**.

$$F = \int_0^{220} fy\,dx - \int_{P_{5x}}^{220} fy\,dx + \int_{P_{5x}}^{220} fgy\,dx - \int_{205}^{220} efy\,dx - \int_0^{50} qay\,dx - \int_{50}^{70} aby\,dx - \int_{70}^{135} fy\,dx - \int_{135}^{155} cdy\,dx$$
$$- \int_{155}^{205} fy\,dx - \int_0^{15} poy\,dx + \int_0^{15} qpy\,dx - \int_0^{15} 110\,dx + \int_0^{15} ony\,dx - \int_0^{15} fy\,dx + \int_0^{15} 110\,dx - \int_{15}^{P_{6x}} fy\,dx$$

$$+\int_{15}^{65} nmy\,dx + \int_{65}^{P_{6x}} mky\,dx$$

The evaluation of the integrals yields the following equation:

$$F = -16852.6 + 155.474a - 0.149925a^2$$

$$\overline{X} = \frac{1}{F}\left[\begin{array}{l}\int_{0}^{220} x\,fy\,dx - \int_{P_{5x}}^{220} x\,fy\,dx + \int_{P_{5x}}^{220} fgy\,dx - \int_{205}^{220} x\,efy\,dx - \int_{0}^{50} x\,qay\,dx - \int_{50}^{70} x\,aby\,dx \\ -\int_{70}^{135} x\,fy\,dx - \int_{135}^{155} x\,cdy\,dx - \int_{155}^{205} x\,fy\,dx - \int_{0}^{15} x\,poy\,dx + \int_{0}^{15} x\,qpy\,dx - \int_{0}^{15} x\,110\,dx \\ +\int_{0}^{15} x\,ony\,dx - \int_{0}^{15} x\,fy\,dx + \int_{0}^{15} x\,110\,dx - \int_{15}^{P_{6x}} x\,fy\,dx + \int_{15}^{65} x\,nmy\,dx + \int_{65}^{P_{6x}} x\,mky\,dx\end{array}\right]$$

The evaluation of the integrals yields the following equation:

$$\overline{X} = \frac{0.0\overline{6}(-825.297 + a)(-168.643 + a)(1993.94 + a)}{(-913.653 + a)(-123.014 + a)}$$

$$\overline{Y} = \frac{1}{F}\left[\begin{array}{l}\int_{0}^{110} y\,fx\,dy - \int_{0}^{25} y\,fx\,dy + \int_{0}^{25} y\,220\,dy - \int_{25}^{P_{5y}} y\,fx\,dy + \int_{25}^{P_{5y}} y\,fgx\,dy - \int_{0}^{25} y\,220\,dy \\ +\int_{0}^{25} y\,efx\,dy - \int_{85}^{110} y\,onx\,dy - \int_{15}^{40} y\,qpx\,dy - \int_{40}^{85} y\,pox\,dy - \int_{0}^{15} y\,dex\,dy + \int_{0}^{15} y\,cdx\,dy \\ -\int_{0}^{15} y\,bcx\,dy + \int_{0}^{15} y\,abx\,dy - \int_{0}^{15} y\,qax\,dy - \int_{95}^{110} y\,65\,dy + \int_{95}^{110} y\,nmx\,dy - \int_{95}^{P_{6y}} y\,mkx\,dy \\ +\int_{95}^{P_{6y}} y\,65\,dy - \int_{P_{6y}}^{110} y\,fx\,dy + \int_{P_{6y}}^{110} y\,65\,dy\end{array}\right]$$

The evaluation of the integrals yields the following equation:

$$\overline{Y} = \frac{0.29997(-728.9+a)\left(25229.9-246.33a+a^2\right)}{(-914.033+a)(-122.979+a)}$$

Line 5 in Figure 5.6 scans the paver between corners **k** and **f**. It should therefore be noted that for the solutions above to be valid for the patch load application 5, the variable distance **a** in the x direction must lie in the range: 305>**a**>270mm.

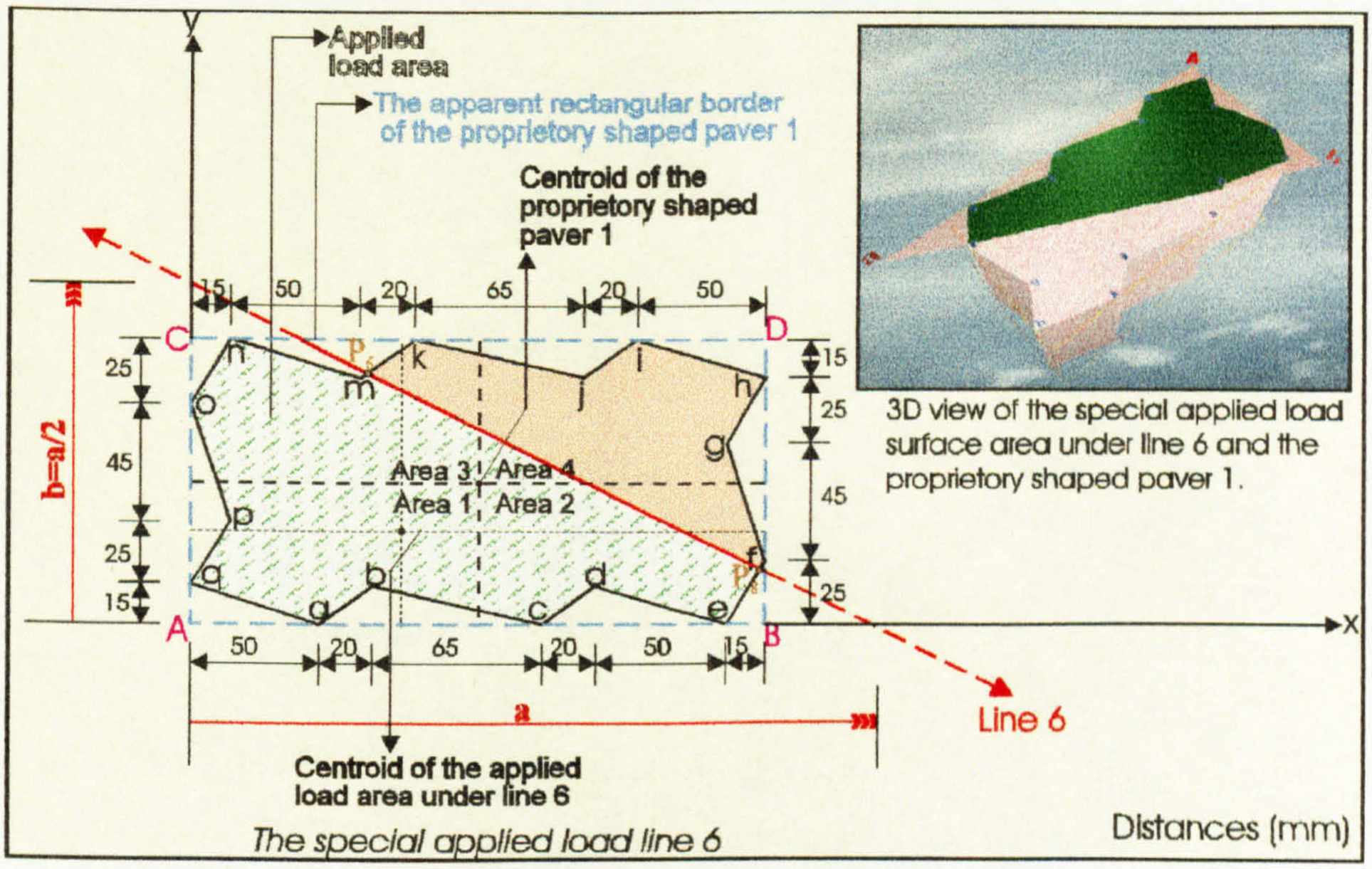

Figure 5.7: The selected special patch load application 6 for proprietory shaped paver 1.

Figure 5.7 illustrates the special patch load application 6 for the proprietory shaped paver 1. **Line 6** scans the paver between corners **f** and **m** in terms of the variable distance **a** in the x direction. By using Table 5.1, Table 5.2 and the patch load boundary line function which is $f_y = b(1-\frac{x}{a})$, $f_x = a(1-\frac{y}{b})$ in the x and y axes, the special patch load's surface area and centroid distances can be calculated according to the distance **a**.

$$F = \int_0^{220} fy\,dx - \int_{P_{8x}}^{220} fy\,dx - \int_{205}^{P_{8x}} efy\,dx - \int_{135}^{155} cdy\,dx - \int_{155}^{205} dey\,dx - \int_{50}^{70} aby\,dx - \int_{70}^{135} bcy\,dx$$

$$-\int_0^{50} qay\,dx-\int_0^{15} poy\,dx+\int_0^{15} qpy\,dx-\int_0^{15} 110\,dx+\int_0^{15} ony\,dx-\int_0^{15} fy\,dx+\int_0^{15} 110\,dx-\int_{15}^{P_{6x}} fy\,dx$$
$$+\int_{15}^{65} nmy\,dx+\int_{65}^{P_{6x}} mky\,dx$$

The evaluation of the integrals yields the following equation:

$$F = 0.0423059(2204.47-a)(-96.5971+a)$$

$$\overline{X}=\frac{1}{F}\left[\begin{array}{l}\displaystyle\int_0^{220} x\,fy\,dx-\int_{P_{8x}}^{220} x\,fy\,dx-\int_{205}^{P_{8x}} x\,efy\,dx-\int_{135}^{155} x\,cdy\,dx-\int_{155}^{205} x\,dey\,dx-\int_{50}^{70} x\,aby\,dx \\ \displaystyle-\int_{70}^{135} x\,bcy\,dx-\int_0^{50} x\,qay\,dx-\int_0^{15} x\,poy\,dx+\int_0^{15} x\,qpy\,dx-\int_0^{15} x\,110\,dx+\int_0^{15} x\,ony\,dx \\ \displaystyle-\int_0^{15} x\,fy\,dx+\int_0^{15} x\,110\,dx-\int_{15}^{P_{6x}} x\,fy\,dx+\int_{15}^{65} x\,nmy\,dx+\int_{65}^{P_{6x}} x\,mky\,dx\end{array}\right]$$

The evaluation of the integrals yields the following equation:

$$\overline{X}=\frac{0.210259(1773.02-a)(-142.342+a)(476.583+a)}{\left(-212945+2301.06a-a^2\right)}$$

$$\overline{Y}=\frac{1}{F}\left[\begin{array}{l}\displaystyle\int_0^{110} y\,fx\,dy-\int_0^{P_{8y}} y\,fx\,dy+\int_0^{P_{8y}} y\,efx\,dy-\int_0^{15} y\,qax\,dy-\int_0^{15} y\,bcx\,dy+\int_0^{15} y\,abx\,dy \\ \displaystyle-\int_0^{15} y\,dex\,dy+\int_0^{15} y\,cdx\,dy-\int_{15}^{40} y\,qpx\,dy-\int_{40}^{85} y\,pox\,dy-\int_{85}^{110} y\,onx\,dy-\int_{P_{6y}}^{110} y\,fx\,dy \\ \displaystyle+\int_{P_{6y}}^{110} y\,nmx\,dy-\int_{85}^{P_{6y}} y\,mkx\,dy+\int_{85}^{P_{6y}} y\,nmx\,dy\end{array}\right]$$

The evaluation of the integrals yields the following equation:

$$\overline{Y} = \frac{0.228215(1691.22 - a)\left(21354.8 - 167.311a + a^2\right)}{\left(-207388 + 2301.76a - a^2\right)}$$

Line 6 in Figure 5.7 scans the paver between corners **f** and **m**. It should therefore be noted that for the solutions above to be valid for the patch load application 6, the variable distance **a** in the x direction must lie in the range: 270>**a**>255mm.

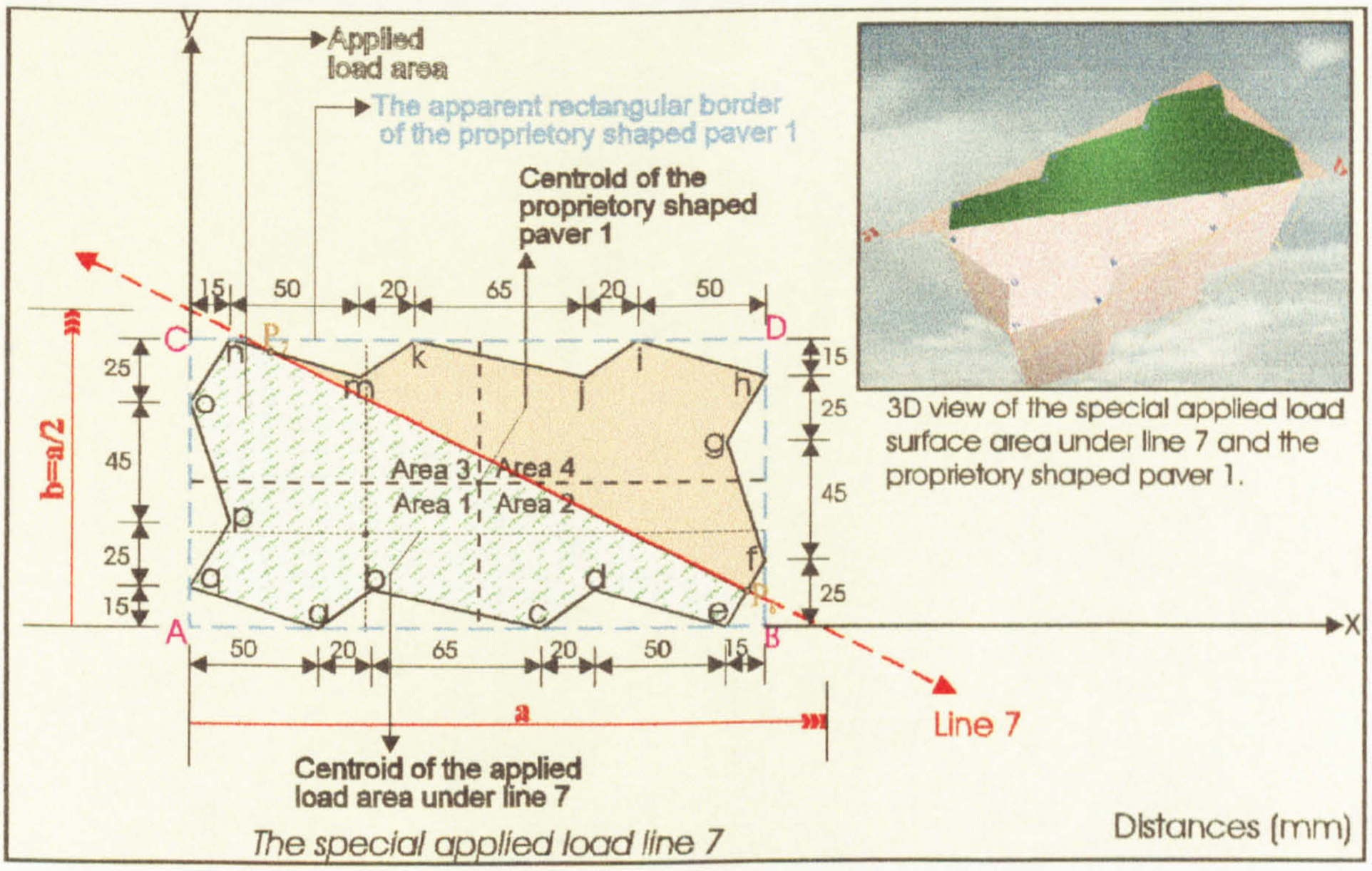

Figure 5.8: The selected special patch load application 7 for proprietory shaped paver 1.

Figure 5.8 illustrates the special patch load application 7 for the proprietory shaped paver 1. **Line 7** scans the paver between corners **m** and **n** in terms of the variable distance **a** in the x direction. By using Table 5.1, Table 5.2 and the patch load boundary line function which is $f_y = b(1-\frac{x}{a})$, $f_x = a(1-\frac{y}{b})$ in the x and y axes, the special patch load's surface area and centroid distances can be calculated according to the distance **a**.

$$F = \int_0^{220} fy\,dx - \int_{P_{8x}}^{220} fy\,dx - \int_{205}^{P_{8x}} efy\,dx - \int_{135}^{155} cdy\,dx + \int_{155}^{205} dey\,dx - \int_{50}^{70} aby\,dx - \int_{70}^{135} bcy\,dx$$
$$- \int_0^{50} qay\,dx - \int_0^{15} poy\,dx + \int_0^{15} qpy\,dx - \int_0^{15} 110\,dx + \int_0^{15} ony\,dx - \int_{15}^{P_{7x}} fy\,dx + \int_{15}^{P_{7x}} nmy\,dx$$
$$- \int_0^{15} fy\,dx + \int_0^{15} 110\,dx$$

The evaluation of the integrals yields the following equation:

$$F = -43153.8 + 365.168a - 0.567401a^2$$

$$\overline{X} = \frac{1}{F}\left[\begin{array}{l} \int_0^{220} x\,fy\,dx - \int_{P_{8x}}^{220} x\,fy\,dx - \int_{205}^{P_{8x}} x\,efy\,dx - \int_{135}^{155} x\,cdy\,dx - \int_{155}^{205} x\,dey\,dx - \int_{50}^{70} x\,aby\,dx \\ - \int_{70}^{135} x\,bcy\,dx - \int_0^{50} x\,qay\,dx - \int_0^{15} x\,poy\,dx + \int_0^{15} x\,qpy\,dx - \int_0^{15} x\,110\,dx + \int_0^{15} x\,ony\,dx \\ - \int_{15}^{P_{7x}} x\,fy\,dx + \int_{15}^{P_{7x}} x\,nmy\,dx - \int_0^{15} x\,fy\,dx + \int_0^{15} x\,110\,dx \end{array}\right]$$

The evaluation of the integrals yields the following equation:

$$\overline{X} = \frac{0.910259(-414.584 + a)\left(23944.1 - 259.939a + a^2\right)}{(-487.579 + a)(-155.987 + a)}$$

$$\overline{Y} = \frac{1}{F}\left[\begin{array}{l} \int_0^{110} y\,fx\,dy - \int_0^{P_{8y}} y\,fx\,dy + \int_0^{P_{8y}} y\,efx\,dy - \int_0^{15} y\,dex\,dy + \int_0^{15} y\,cdx\,dy - \int_0^{15} y\,bcx\,dy \\ + \int_0^{15} y\,abx\,dy - \int_0^{15} y\,qax\,dy - \int_{15}^{40} y\,qpx\,dy - \int_{40}^{85} y\,pox\,dy - \int_{85}^{110} y\,onx\,dy - \int_{P_{7y}}^{110} y\,fx\,dy + \int_{P_{7y}}^{110} y\,nmx\,dy \end{array}\right]$$

The evaluation of the integrals yields the following equation:

$$\overline{Y} = \frac{0.121857(-179.115+a)\left(-341026+1154.87a-a^2\right)}{(-487.601+a)(-155.978+a)}$$

Line 7 in Figure 5.8 scans the paver between corners **m** and **n**. It should therefore be noted that for the solutions above to be valid for the patch load application 7, the variable distance **a** in the x direction must lie in the range: 255>**a**>235mm.

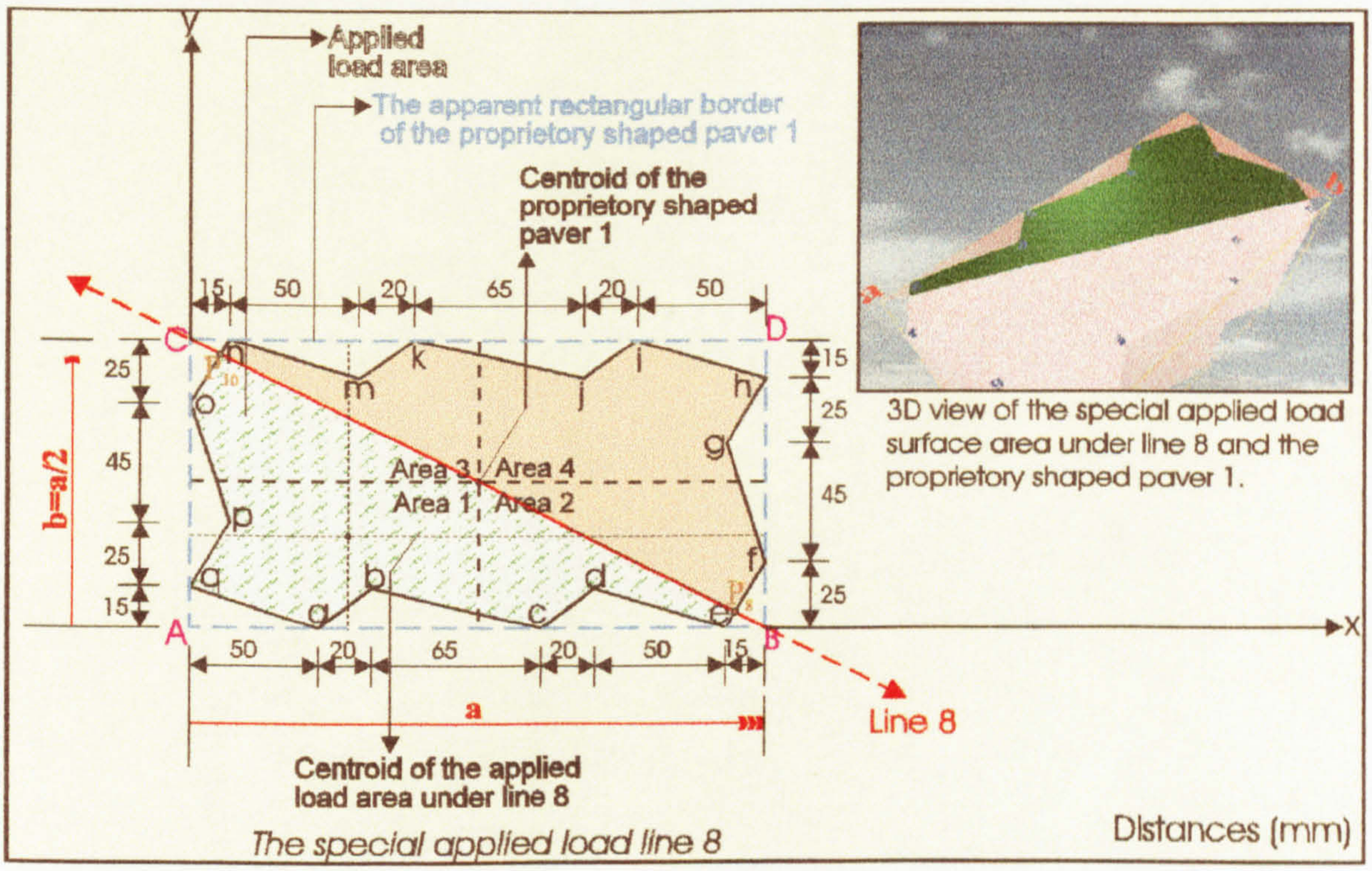

Figure 5.9: The selected special patch load application 8 for proprietory shaped paver 1.

Figure 5.9 illustrates the special patch load application 8 for the proprietory shaped paver 1. **Line 8** scans the paver between corner **n** and **e** in terms of the variable distance **a** in the x direction. By using Table 5.1, Table 5.2 and the patch load boundary line function which is $f_y = b(1-\frac{x}{a})$, $f_x = a(1-\frac{y}{b})$ in the x and y axes, the special patch load's surface area and centroid distances can be calculated as follows.

$$F = \int_0^{220} fy\,dx - \int_{205}^{P_{8x}} efy\,dx - \int_{P_{8x}}^{220} fy\,dx - \int_{155}^{205} dey\,dx - \int_{135}^{155} cdy\,dx - \int_{70}^{135} bcy\,dx - \int_{50}^{70} aby\,dx$$

$$- \int_0^{50} qay\,dx - \int_0^{15} poy\,dx + \int_0^{15} qpy\,dx - \int_0^{P_{10x}} fy\,dx + \int_0^{P_{10x}} ony\,dx$$

The evaluation of the integrals yields the following equation:

$$F = -11817.3 + 98.464a + 1.59773.10^{-6}a^2$$

$$\overline{X} = \frac{1}{F}\left[\begin{array}{l} \displaystyle\int_0^{220} x\,fy\,dx - \int_{205}^{P_{8x}} x\,efy\,dx - \int_{P_{8x}}^{220} x\,fy\,dx - \int_{155}^{205} x\,dey\,dx - \int_{135}^{155} x\,cdy\,dx - \int_{70}^{135} x\,bcy\,dx \\ \displaystyle -\int_{50}^{70} x\,aby\,dx - \int_0^{50} x\,qay\,dx - \int_0^{15} x\,poy\,dx + \int_0^{15} x\,qpy\,dx - \int_0^{P_{10x}} x\,fy\,dx + \int_0^{P_{10x}} x\,ony\,dx \end{array}\right]$$

The evaluation of the integrals yields the following equation:

$$\overline{X} = \frac{0.153851(-147.297 + a)(660.646 + a)\left(4.62198.10^7 + a\right)}{-7.39627.10^9 + 6.16274.10^7 a + a^2}$$

$$\overline{Y} = \frac{1}{F}\left[\begin{array}{l} \displaystyle\int_0^{110} y\,fx\,dy - \int_0^{P_{8y}} y\,fx\,dy + \int_0^{P_{8y}} y\,efx\,dy - \int_0^{15} y\,dex\,dy + \int_0^{15} y\,cdx\,dy - \int_0^{15} y\,bcx\,dy \\ \displaystyle +\int_0^{15} y\,abx\,dy - \int_0^{15} y\,qax\,dy - \int_{15}^{40} y\,qpx\,dy - \int_{40}^{85} y\,pox\,dy - \int_{85}^{P_{10y}} y\,onx\,dy - \int_{P_{10y}}^{110} y\,fx\,dy \end{array}\right]$$

The evaluation of the integrals yields the following equation:

$$\overline{Y} = \frac{1.18511.10^7\left(64443.81 - 154a + a^2\right)}{-7.39627.10^9 + 6.16274.10^7 a + a^2}$$

Line 8 in Figure 5.9 scans the paver between corners **n** and **e**. It should therefore be noted that for the solutions above to be valid for the patch load application 8, the variable distance **a** in the x direction must lie in the range: 235>**a**>205mm.

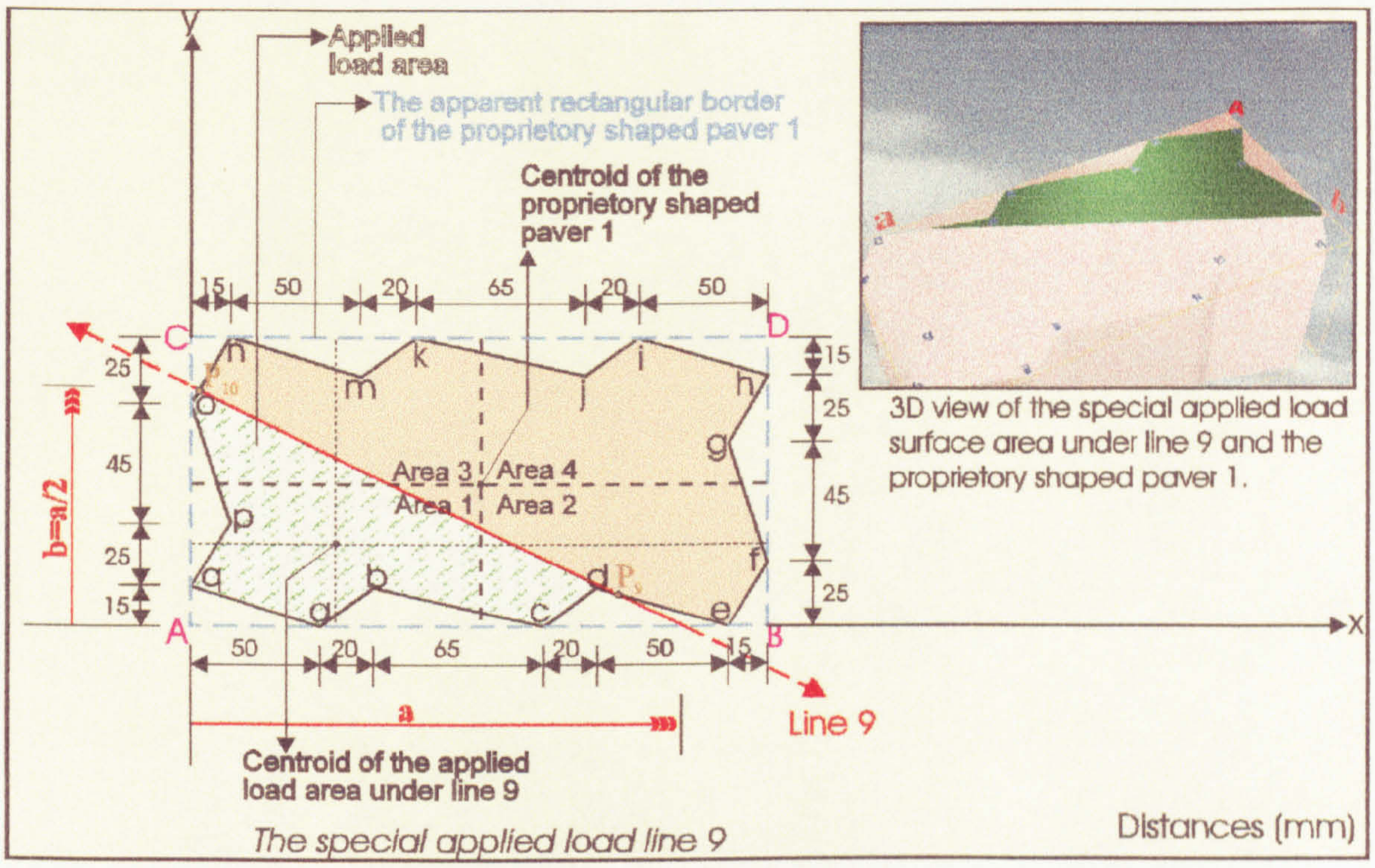

Figure 5.10: The selected special patch load application 9 for proprietory shaped paver 1.

Figure 5.10 illustrates the special patch load application 9 for the proprietory shaped paver 1. **Line 9** scans the paver between corner **e** and **d** in terms of the variable distance **a** in the x direction. By using Table 5.1, Table 5.2 and the patch load boundary line function which is $f_y = b(1-\frac{x}{a})$, $f_x = a(1-\frac{y}{b})$ in the x and y axes, the special patch load's surface area and centroid distances can be calculated as follows.

$$F = \int_0^a fy\,dx - \int_{P_{9x}}^a fy\,dx - \int_{155}^{P_{9x}} dey\,dx - \int_{135}^{155} cdy\,dx - \int_{70}^{135} bcy\,dx - \int_{50}^{70} aby\,dx - \int_0^{50} qay\,dx$$

$$- \int_0^{15} poy\,dx + \int_0^{15} qpy\,dx - \int_0^{P_{10x}} fy\,dx + \int_0^{P_{10x}} ony\,dx$$

The evaluation of the integrals yields the following equation:

$$F = 12024.4 - 134.135a + 0.567308a^2$$

$$\overline{X} = \frac{1}{F}\left[\begin{array}{l} \int_0^a x\,fy\,dx - \int_{P_{9x}}^a x\,fy\,dx - \int_{155}^{P_{9x}} x\,dey\,dx - \int_{135}^{155} x\,cdy\,dx - \int_{70}^{135} x\,bcy\,dx - \int_{50}^{70} x\,aby\,dx \\ -\int_0^{50} x\,qay\,dx - \int_0^{15} x\,poy\,dx + \int_0^{15} x\,qpy\,dx - \int_0^{P_{10x}} x\,fy\,dx + \int_0^{P_{10x}} x\,ony\,dx \end{array}\right]$$

The evaluation of the integrals yields the following equation:

$$\overline{X} = \frac{-666873 + 23254.3a - 189.924a^2 + 0.516395a^3}{12024.4 - 134.135a + 0.567308a^2}$$

$$\overline{Y} = \frac{1}{F}\left[\begin{array}{l} \int_0^b y\,fx\,dy - \int_0^{P_{9y}} y\,fx\,dy + \int_0^{P_{9y}} y\,cdx\,dy - \int_{P_{9y}}^{15} y\,dex\,dy + \int_{P_{9y}}^{15} y\,cdx\,dy - \int_0^{15} y\,bcx\,dy \\ +\int_0^{15} y\,abx\,dy - \int_0^{15} y\,qax\,dy - \int_{15}^{40} y\,qpx\,dy - \int_{40}^{85} y\,pox\,dy - \int_{85}^{P_{10y}} y\,onx\,dy - \int_{P_{10y}}^{b} y\,fx\,dy \end{array}\right]$$

The evaluation of the integrals yields the following equation:

$$\overline{Y} = \frac{717317 - 11627.7a + 61.4313a^2 - 0.069099a^3}{12024.4 - 134.135a + 0.567308a^2}$$

Line 9 in Figure 5.10 scans the paver between corners **e** and **d**. It should therefore be noted that for the solutions above to be valid for the patch load application 9, the variable distance **a** in the x direction must lie in the range: 205>**a**>185mm.

Figure 5.11 illustrates the special patch load application 10 for the proprietory shaped paver 1. **Line 10** scans the paver between corners **d** and **o** in terms of the variable

distance **a** in the x direction. By using Table 5.1, Table 5.2 and the patch load boundary line function which is $f_y = b(1-\frac{x}{a})$, $f_x = a(1-\frac{y}{b})$ in the x and y axes, the special patch load's surface area and centroid distances can be calculated as follows.

$$F = \int_0^a fy\,dx - \int_{135}^{P_{11x}} cdy\,dx - \int_{P_{11x}}^{a} fy\,dx - \int_{70}^{135} bcy\,dx - \int_{50}^{70} aby\,dx - \int_{0}^{50} qay\,dx - \int_{0}^{15} poy\,dx$$

$$+\int_0^{15} qpy\,dx - \int_0^{P_{10x}} fy\,dx + \int_0^{P_{10x}} ony\,dx$$

The evaluation of the integrals yields the following equation:

$$F = -5943.71 + 60.1154a + 0.0423075a^2$$

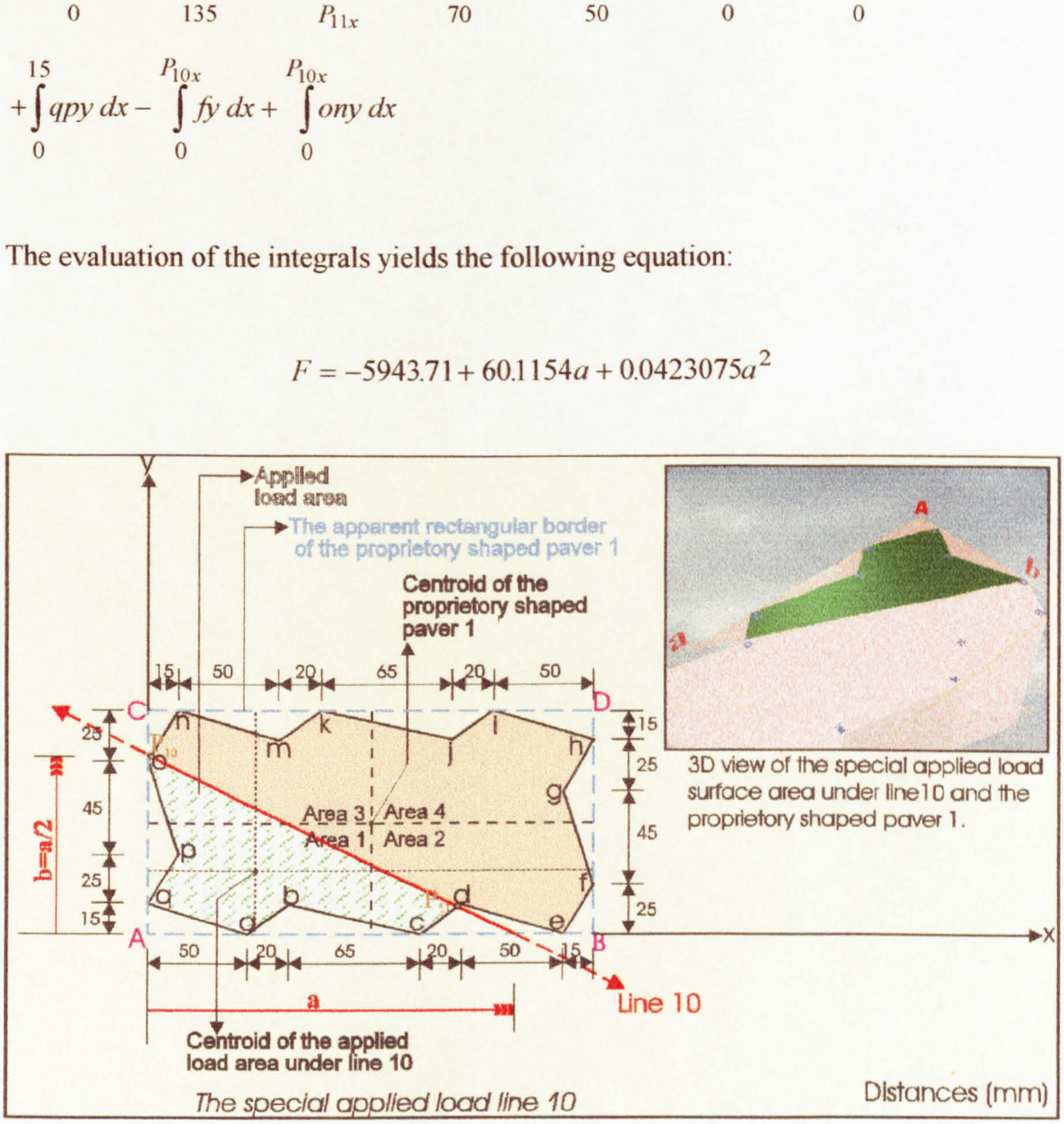

Figure 5.11: The selected special patch load application 10 for proprietory shaped paver 1.

$$\overline{X} = \frac{1}{F}\left[\int_0^a x\,fy\,dx - \int_{135}^{P_{11x}} x\,cdy\,dx - \int_{P_{11x}}^{a} x\,fy\,dx - \int_{70}^{135} x\,bcy\,dx - \int_{50}^{70} x\,aby\,dx - \int_{0}^{50} x\,qay\,dx\right.$$

$$\left. - \int_0^{15} x\,poy\,dx + \int_0^{15} x\,qpy\,dx - \int_0^{P_{10x}} x\,fy\,dx + \int_0^{P_{10x}} x\,ony\,dx\right]$$

The evaluation of the integrals yields the following equation:

$$\overline{X} = \frac{-238633 + 1255.48a + 10.3633a^2 + 0.00889544a^3}{-5943.71 + 60.1154a + 0.0423075a^2}$$

$$\overline{Y} = \frac{1}{F}\left[\int_0^b y\,fx\,dy - \int_0^{P_{11y}} y\,fx\,dy + \int_0^{P_{11y}} y\,cdx\,dy - \int_0^{15} y\,bcx\,dy + \int_0^{15} y\,abx\,dy - \int_0^{15} y\,qax\,dy\right.$$

$$\left. - \int_{15}^{40} y\,qpx\,dy - \int_{40}^{85} y\,pox\,dy - \int_{85}^{P_{10y}} y\,onx\,dy - \int_{P_{10y}}^{b} y\,fx\,dy\right]$$

The evaluation of the integrals yields the following equation:

$$\overline{Y} = \frac{-50859.6 - 627.76a + 9.84731a^2 + 0.00965453a^3}{-5943.71 + 60.1154a + 0.0423075a^2}$$

Line 10 in Figure 5.11 scans the paver between corners **d** and **o**. It should therefore be noted that for the solutions above to be valid for the patch load application 10, the variable distance **a** in the x direction must lie in the range: 185>**a**>170mm.

Figure 5.12 illustrates the special patch load application 11 for the proprietory shaped paver 1. **Line 11** scans the paver between corners **o** and **c** in terms of the variable distance **a** in the x direction. By using Table 5.1, Table 5.2 and the patch load boundary line function which is $f_y = b(1-\frac{x}{a})$, $f_x = a(1-\frac{y}{b})$ in the x and y axes, the special patch load's surface area and centroid distances can be calculated as follows.

$$F = \int_0^a fy\,dx - \int_{P_{11x}}^a fy\,dx - \int_{135}^{P_{11x}} cdy\,dx - \int_{70}^{135} bcy\,dx - \int_{50}^{70} aby\,dx - \int_0^{50} qay\,dx - \int_0^{15} 40\,dx + \int_0^{15} qpy\,dx$$

$$-\int_0^{15} fy\,dx + \int_0^{P_{13x}} fy\,dx + \int_{P_{13x}}^{15} poy\,dx$$

The evaluation of the integrals yields the following equation:

$$F = -4390.14 + 50a + 0.05a^2$$

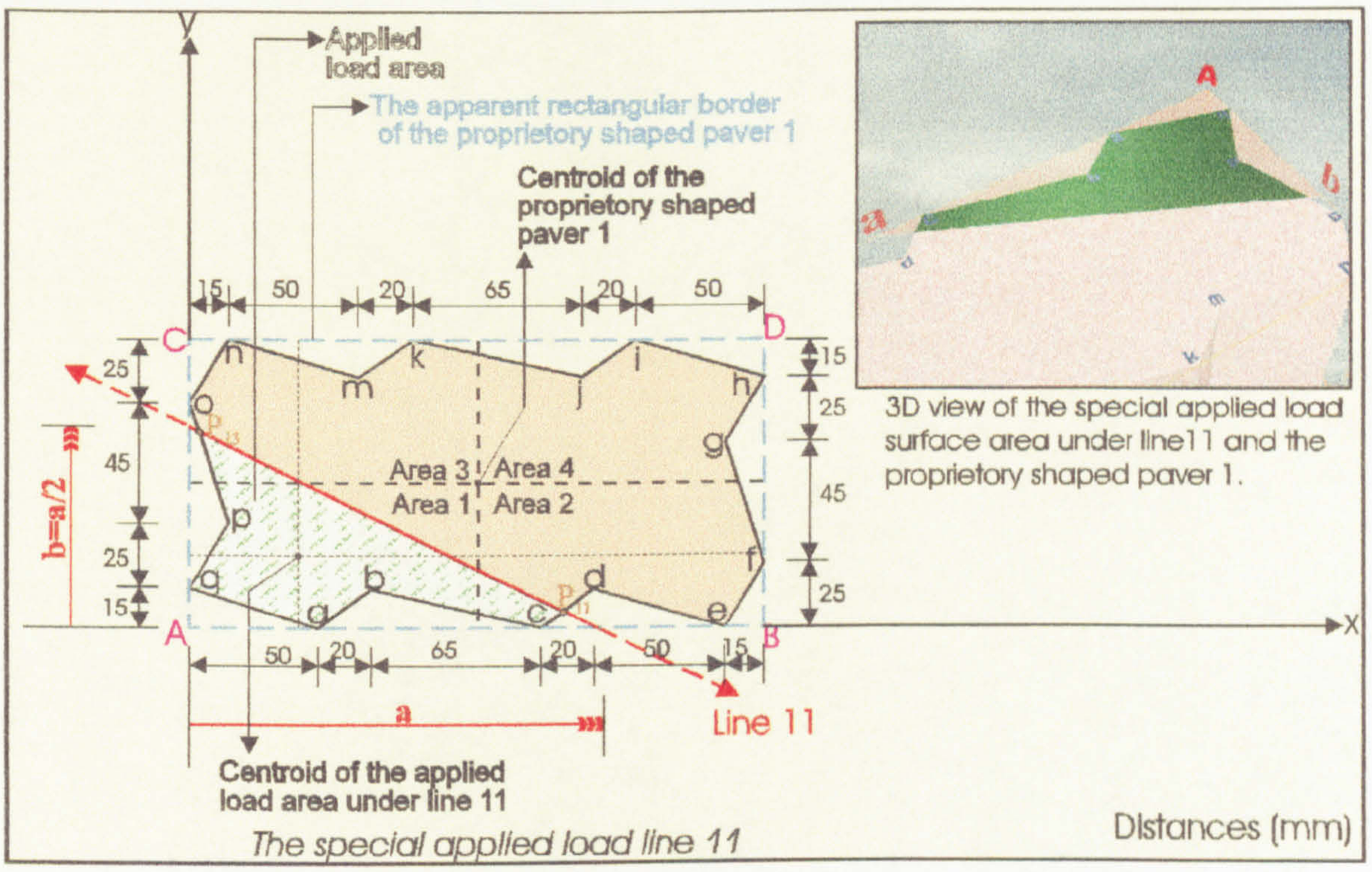

Figure 5.12: The selected special patch load application 11 for proprietory shaped paver 1.

$$\overline{X} = \frac{1}{F}\left[\int_0^a x\,fy\,dx - \int_{P_{11x}}^a x\,fy\,dx - \int_{135}^{P_{11x}} x\,cdy\,dx - \int_{70}^{135} x\,bcy\,dx - \int_{50}^{70} x\,aby\,dx - \int_0^{50} x\,qay\,dx\right.$$
$$\left. -\int_0^{15} x\,40\,dx + \int_0^{15} x\,qpy\,dx - \int_0^{15} x\,fy\,dx + \int_0^{P_{13x}} x\,fy\,dx + \int_{P_{13x}}^{15} x\,poy\,dx\right]$$

The evaluation of the integrals yields the following equation:

$$\overline{X} = \frac{-268376 + 1873a + 6.4a^2 + 0.0166667a^3}{-4390.14 + 50a + 0.05a^2}$$

$$\overline{Y} = \frac{1}{F}\left[\begin{array}{l} \int_0^b y\,fx\,dy - \int_0^{P_{11y}} y\,fx\,dy + \int_0^{P_{11y}} y\,cdx\,dy - \int_0^{15} y\,bcx\,dy + \int_0^{15} y\,abx\,dy - \int_0^{15} y\,qax\,dy \\ -\int_{15}^{40} y\,qpx\,dy - \int_{40}^{P_{13y}} y\,pox\,dy - \int_{P_{13y}}^{b} y\,fx\,dy \end{array}\right]$$

The evaluation of the integrals yields the following equation:

$$\overline{Y} = \frac{40104.4 - 675.7a + 0.977167a^2 + 0.0449757a^3}{-4390.14 + 50a + 0.05a^2}$$

Line 11 in Figure 5.12 scans the paver between corners **o** and **c**. It should therefore be noted that for the solutions above to be valid for the patch load application 11, the variable distance **a** in the x direction must lie in the range: 170>**a**>135mm.

Figure 5.13 illustrates the special patch load application 12 for the proprietory shaped paver 1. **Line 12** scans the paver between corners **c** and **b** in terms of the variable distance **a** in the x direction. By using Table 5.1, Table 5.2 and the patch load boundary line function which is $f_y = b(1-\frac{x}{a})$, $f_x = a(1-\frac{y}{b})$ in the x and y axes, the special patch load's surface area and centroid distances can be calculated as follows.

$$F = \int_0^a fy\,dx - \int_{50}^{70} aby\,dx - \int_{70}^{P_{12x}} bcy\,dx - \int_{P_{12x}}^{a} fy\,dx - \int_0^{50} qay\,dx - \int_0^{15} 40\,dx + \int_0^{15} qpy\,dx$$
$$- \int_0^{15} fy\,dx + \int_0^{P_{13x}} fy\,dx + \int_{P_{13x}}^{15} poy\,dx$$

The evaluation of the integrals yields the following equation:

$$F = 2250.88 - 48.1926a + 0.412963a^2$$

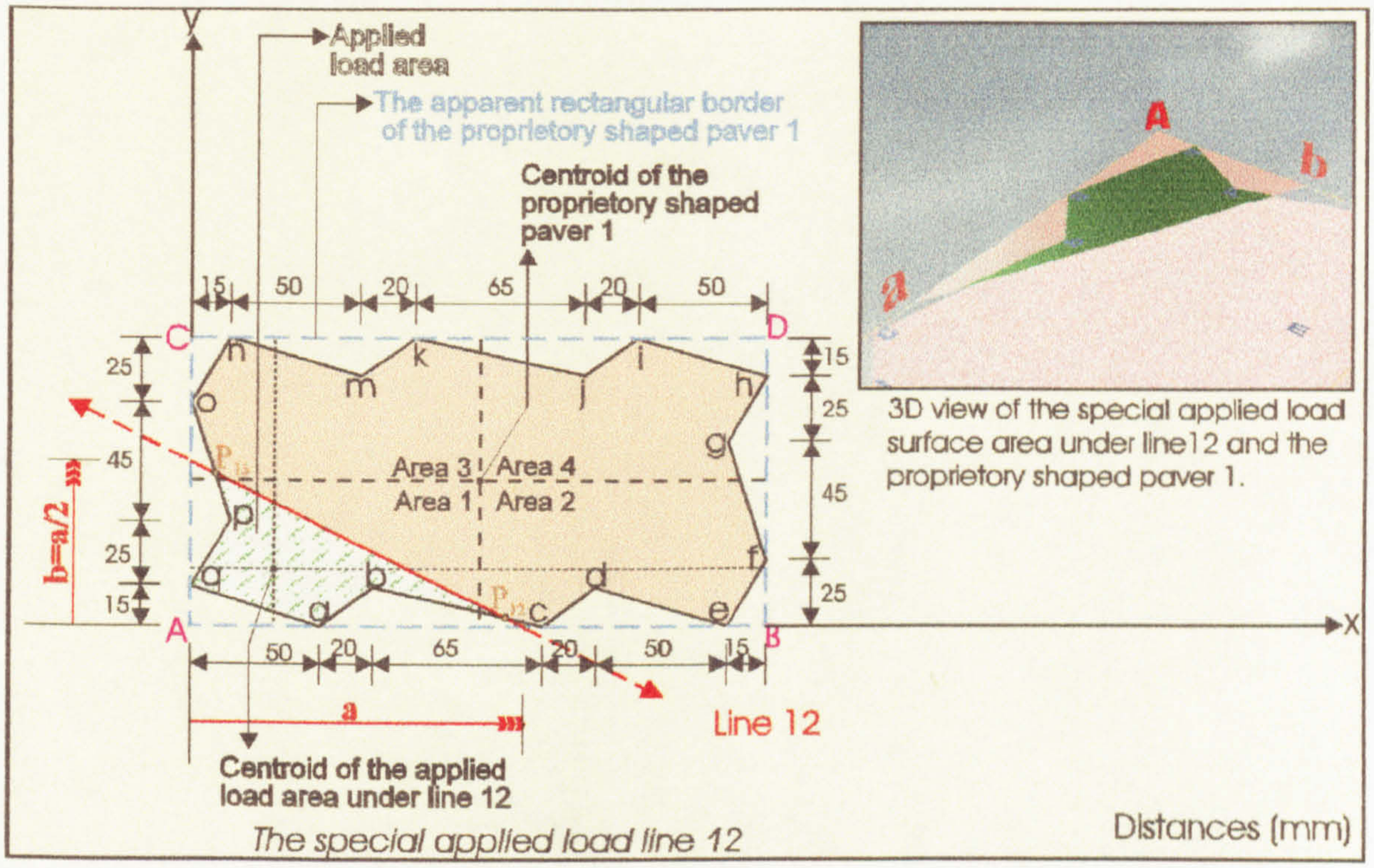

Figure 5.13: The selected special patch load application 12 for proprietory shaped paver 1.

$$\overline{X} = \frac{1}{F}\left[\begin{array}{l} \int_0^a x\,fy\,dx - \int_{50}^{70} x\,aby\,dx - \int_{70}^{P_{12x}} x\,bcy\,dx - \int_{P_{12x}}^{a} x\,fy\,dx - \int_0^{50} x\,qay\,dx - \int_0^{15} x\,40\,dx \\ + \int_0^{15} x\,qpy\,dx - \int_0^{15} x\,fy\,dx + \int_0^{P_{13x}} x\,fy\,dx + \int_{P_{13x}}^{15} x\,poy\,dx \end{array}\right]$$

The evaluation of the integrals yields the following equation:

$$\overline{X} = \frac{-45413 + 3561.19a - 55.1191a^2 + 0.289113a^3}{2250.88 - 48.1926a + 0.412963a^2}$$

$$\overline{Y} = \frac{1}{F}\left[\int_{15}^{b} y\,fx\,dy + \int_{P_{12y}}^{15} y\,fx\,dy - \int_{P_{12y}}^{15} y\,bcx\,dy + \int_0^{15} y\,abx\,dy - \int_0^{15} y\,qax\,dy - \int_{15}^{40} y\,qpx\,dy\right.$$

$$\left. - \int_{40}^{P_{13y}} y\, pox\, dy - \int_{P_{13y}}^{b} y\, fx\, dy \right]$$

The evaluation of the integrals yields the following equation:

$$\overline{Y} = \frac{78517.8 - 1529.33a + 7.30036a^2 + 0.0293629a^3}{2250.88 - 48.1926a + 0.412963a^2}$$

Line 12 in Figure 5.13 scans the paver between corners **c** and **b**. It should therefore be noted that for the solutions above to be valid for the patch load application 12, the variable distance **a** in the x direction must lie in the range: 135>**a**>100mm.

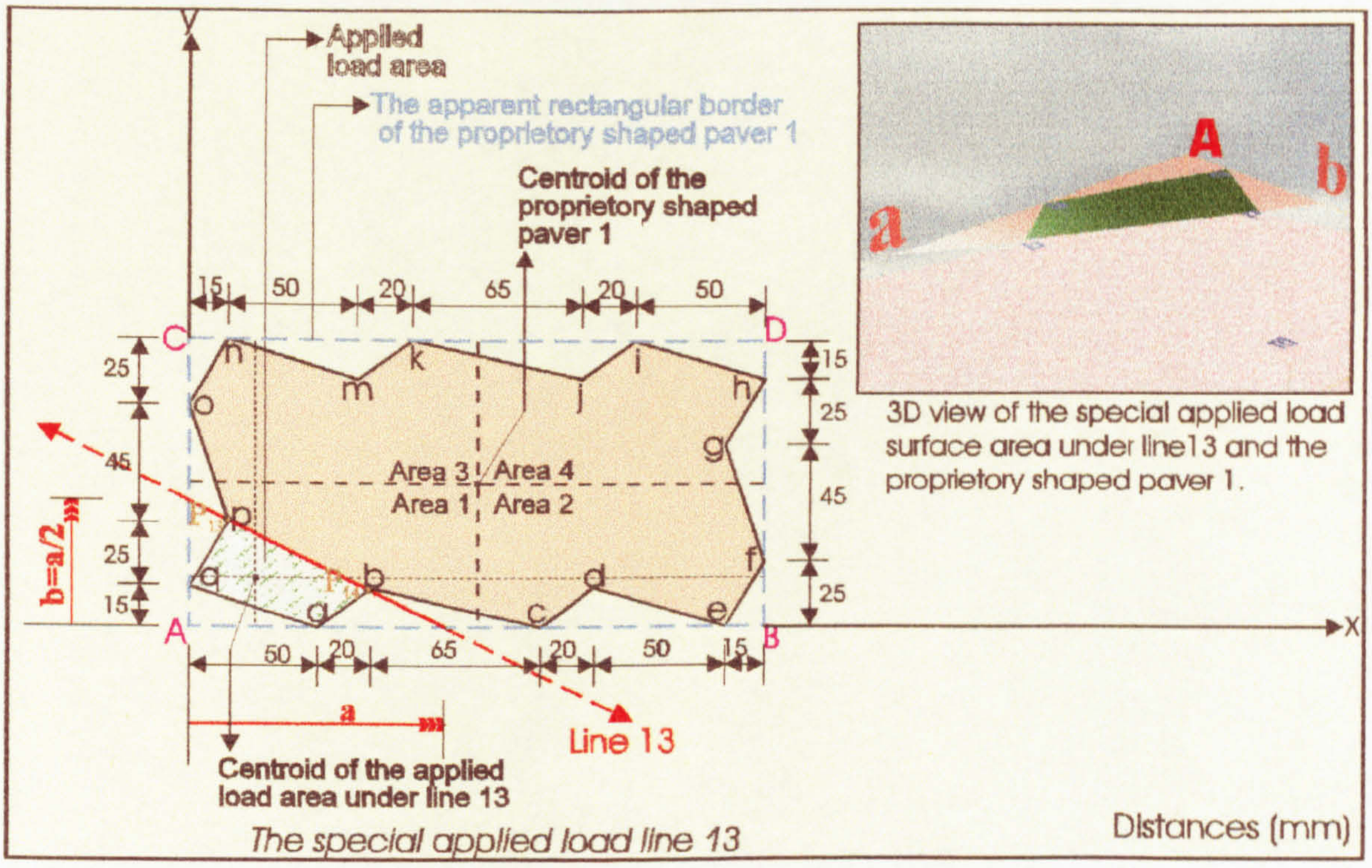

Figure 5.14: The selected special patch load application 13 for proprietory shaped paver 1.

Figure 5.14 illustrates the special patch load application 13 for the proprietory shaped paver 1. **Line 13** scans the paver between corners **b** and **p** in terms of the variable distance **a** in the x direction. By using Table 5.1, Table 5.2 and the patch load boundary

line function which is $f_y = b(1-\frac{x}{a})$, $f_x = a(1-\frac{y}{b})$ in the x and y axes, the special patch load's surface area and centroid distances can be calculated as follows.

$$F = \int_0^a fy\,dx - \int_{P_{14x}}^a fy\,dx - \int_{50}^{P_{14x}} aby\,dx - \int_0^{50} qay\,dx - \int_0^{15} 40\,dx + \int_0^{15} qpy\,dx - \int_0^{15} fy\,dx + \int_0^{P_{13x}} fy\,dx + \int_{P_{13x}}^{15} poy\,dx$$

The evaluation of the integrals yields the following equation:

$$F = -1388.76 + 24.5a + 0.05a^2$$

$$\overline{X} = \frac{1}{F}\left[\begin{array}{l} \int_0^a x\,fy\,dx - \int_{P_{14x}}^a x\,fy\,dx - \int_{50}^{P_{14x}} x\,aby\,dx - \int_0^{50} x\,qay\,dx - \int_0^{15} x\,40\,dx + \int_0^{15} x\,qpy\,dx \\ -\int_0^{15} x\,fy\,dx + \int_0^{P_{13x}} x\,fy\,dx + \int_{P_{13x}}^{15} x\,poy\,dx \end{array}\right]$$

The evaluation of the integrals yields the following equation:

$$\overline{X} = \frac{-26814.2 + 457.75a + 1.3a^2 + 0.0166667a^3}{-1388.76 + 24.5a + 0.05a^2}$$

$$\overline{Y} = \frac{1}{F}\left[\begin{array}{l} \int_0^b y\,fx\,dy - \int_0^{P_{14y}} y\,fx\,dy + \int_0^{P_{14y}} y\,abx\,dy - \int_0^{15} y\,qax\,dy - \int_{15}^{40} y\,qpx\,dy - \int_{40}^{P_{13y}} y\,pox\,dy \\ -\int_{P_{13y}}^{b} y\,fx\,dy \end{array}\right]$$

The evaluation of the integrals yields the following equation:

$$\overline{Y} = \frac{8261.34 + 31.9194a - 2.8475a^2 + 0.044973a^3}{-1388.76 + 24.5a + 0.05a^2}$$

Line 13 in Figure 5.14 scans the paver between corners **b** and **p**. It should therefore be noted that for the solutions above to be valid for the patch load application 13, the variable distance **a** in the x direction must lie in the range: 100>**a**>95mm.

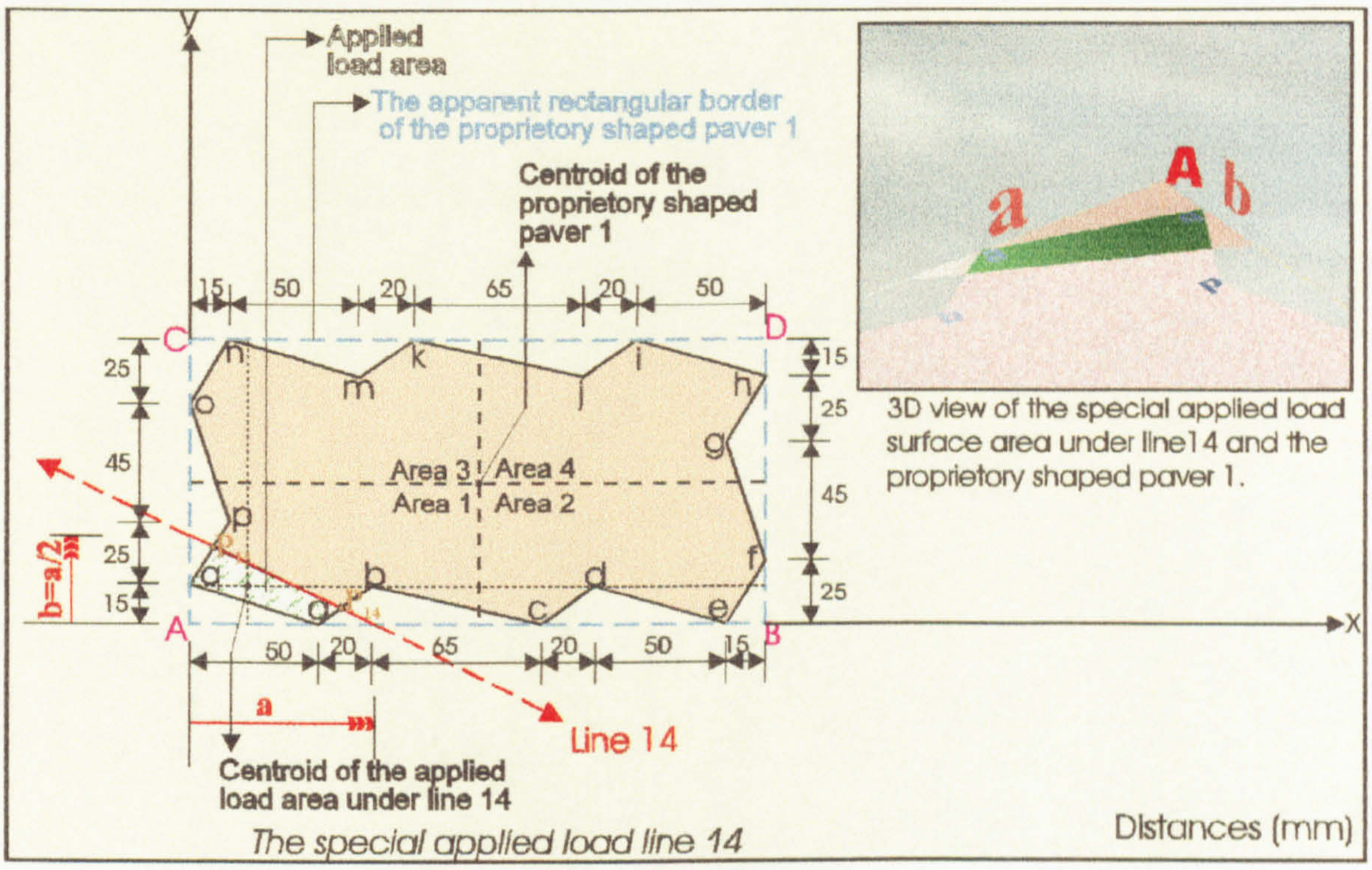

Figure 5.15: The selected special patch load application 14 for proprietory shaped paver 1.

Figure 5.15 illustrates the special patch load application 14 for the proprietory shaped paver 1. **Line 14** scans the paver between corners **p** and **a** in terms of the variable distance **a** in the x direction. By using Table 5.1, Table 5.2 and the patch load boundary line function which is $f_y = b(1-\frac{x}{a})$, $f_x = a(1-\frac{y}{b})$ in the x and y axes, the special patch load's surface area and centroid distances can be calculated as follows.

$$F = \int_0^a fy\ dx - \int_{P_{14x}}^a fy\,dx - \int_{50}^{P_{14x}} aby\,dx - \int_0^{50} qay\,dx - \int_0^{P_{15x}} fy\,dx + \int_0^{P_{15x}} qpy\,dx$$

The evaluation of the integrals yields the following equation:

$$F = -801.925 + 18.4616a + 0.0423059a^2$$

$$\overline{X} = \frac{1}{F}\left[\int_0^a x\,fy\;dx - \int_{P_{14x}}^a x\,fy\,dx - \int_{50}^{P_{14x}} x\,aby\,dx - \int_0^{50} x\,qay\,dx - \int_0^{P_{15x}} x\,fy\,dx + \int_0^{P_{15x}} x\,qpy\,dx\right]$$

The evaluation of the integrals yields the following equation:

$$\overline{X} = \frac{-161302 + 213.017a + 3.39943a^2 + 0.00889519a^3}{-801.925 + 18.4616a + 0.0423059a^2}$$

$$\overline{Y} = \frac{1}{F}\left[\int_0^b y\,fx\,dy - \int_0^{P_{14y}} y\,fx\,dy + \int_0^{P_{14y}} y\,abx\,dy - \int_0^{15} y\,qax\,dy - \int_{15}^{P_{15y}} y\,qpx\,dy - \int_{P_{15y}}^b y\,fx\,dy\right]$$

The evaluation of the integrals yields the following equation:

$$\overline{Y} = \frac{-319.155 - 106.531a + 2.91613a^2 + 0.00965183a^3}{-801.925 + 18.4616a + 0.0423059a^2}$$

Line 14 in Figure 5.15 scans the paver between corners **p** and **a**. It should therefore be noted that for the solutions above to be valid for the patch load application 14, the variable distance **a** in the x direction must lie in the range: 95>**a**>50mm.

Figure 5.16 illustrates the special patch load application 15 for the proprietory shaped paver 1. **Line 15** scans the paver between corners **a** and **q** in terms of the variable distance **a** in the x direction. By using Table 5.1, Table 5.2 and the patch load boundary line function which is $f_y = b(1-\frac{x}{a})$, $f_x = a(1-\frac{y}{b})$ in the x and y axes, the special patch load's surface area and centroid distances can be calculated as follows.

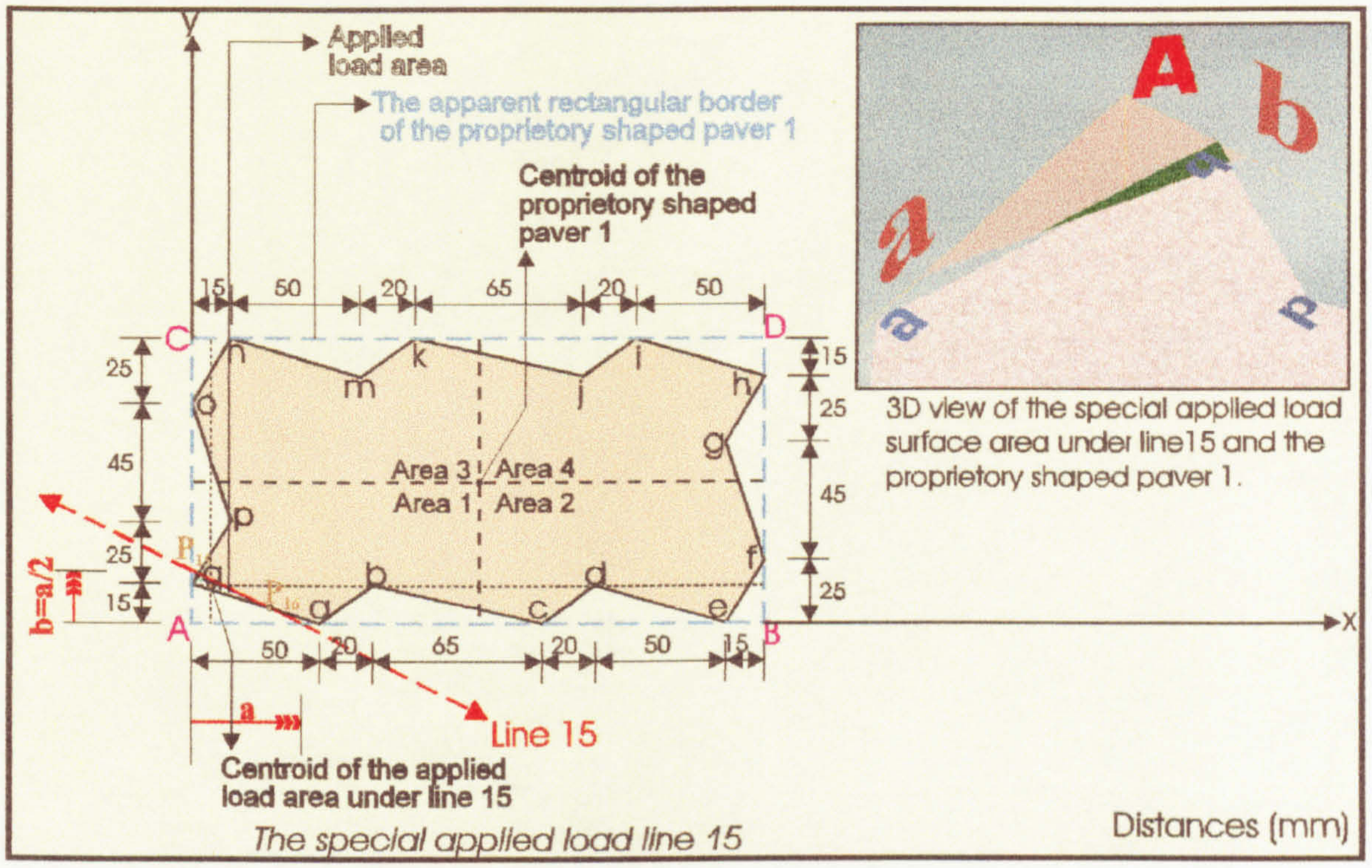

Figure 5.16: The selected special patch load application 15 for proprietory shaped paver 1.

$$F = \int_0^a fy\,dx - \int_0^{P_{16x}} qay\,dx - \int_{P_{16x}}^a fy\,dx - \int_0^{P_{15x}} fy\,dx + \int_0^{P_{15x}} qpy\,dx$$

The evaluation of the integrals yields the following equation:

$$F = 510.575 - 34.0384a + 0.567306a^2$$

$$\overline{X} = \frac{1}{F}\left[\int_0^a x\,fy\,dx - \int_0^{P_{16x}} x\,qay\,dx - \int_{P_{16x}}^a x\,fy\,dx - \int_0^{P_{15x}} x\,fy\,dx + \int_0^{P_{15x}} x\,qpy\,dx\right]$$

The evaluation of the integrals yields the following equation:

$$\overline{X} = \frac{-13942.7 + 1394.27a - 46.4756a^2 + 0.516395a^3}{510.575 - 34.0384a + 0.567306a^2}$$

$$\overline{Y} = \frac{1}{F}\left[\int_0^b y\,fx\,dy - \int_0^{P_{16y}} y\,fx\,dy - \int_{P_{16y}}^{15} y\,qax\,dy - \int_{15}^{P_{15y}} y\,qpx\,dy - \int_{P_{15y}}^{b} y\,fx\,dy\right]$$

The evaluation of the integrals yields the following equation:

$$\overline{Y} = \frac{9524.28 - 697.137a + 14.7283a^2 - 0.0690956a^3}{510.575 - 34.0384a + 0.567306a^2}$$

Line 15 in Figure 5.16 scans the paver between corners **a** and **q**. It should therefore be noted that for the solutions above to be valid for the patch load application 15, the variable distance **a** in the x direction must lie in the range: 50>**a**>30mm.

5.3. The selected special patch load applied to proprietory shaped paver 2

Figure 5.17 illustrates one of the common patch load application to proprietory shaped paver 2 (see Figure 5.1). It may be recalled that in these common load applications, the lines which define the patch loading gradually scan the paver from its lower left corner to its upper right corner with distances **a** and **b** (**b**=**a**/2). The proprietory shaped paver 2 is analysed with the similar logic described for the shaped paver 1 in Section 5.2. The patch load applications principally generate five types of idealised vertical compressive stress dissipations beneath pavers which are tetrahedral, short-pentahedral, long-pentahedral, partial-hexahedral and absolute-hexahedral as described in Chapters 6, 7 and 8. The solutions of these five vertical stress distributions were given in Chapter 6 for rectangular pavers. The solutions of the vertical compressive stress regimes for proprietory shaped pavers (see Figure 5.1) are particularly complex so iterative solutions have been used in their evaluations. The numerical solutions have been conducted by using Mathematica[1], Maple[2] and Nag[3] mathematical software. However the arithmetical solutions to the absolute-hexahedral case have been calculated for each proprietory shaped paver (see Chapters 7 and 8). For this reason the evaluations of the patch loads' integrals relating only to the absolute-hexahedral stress cases are documented in this Section for the proprietory shaped paver 2.

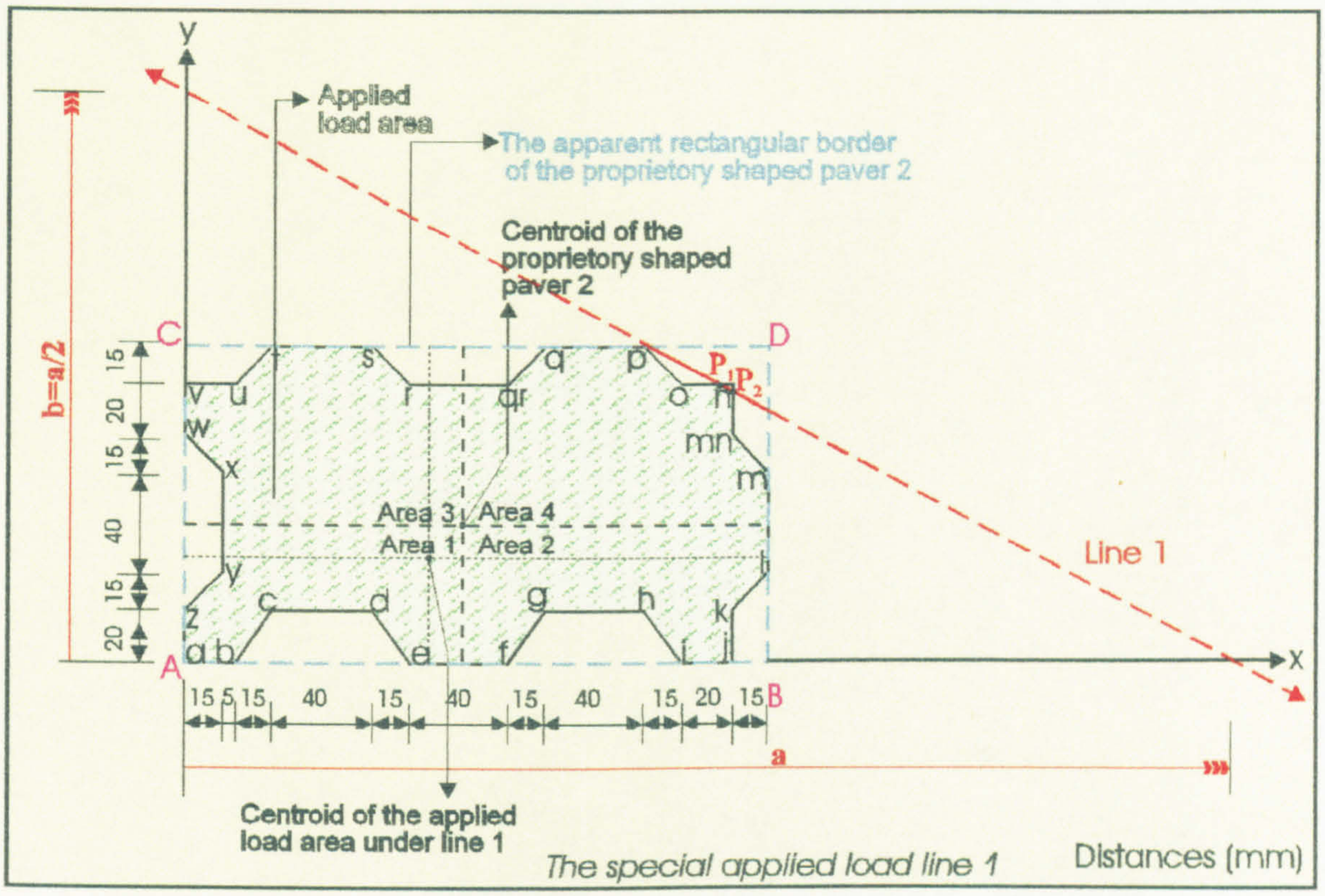

Figure 5.17: The selected special patch load application 1 for proprietory shaped paver 2.

Figure 5.17 illustrates the special patch load application 1 for the proprietory shaped paver 2. **Line 1** scans the paver between corners **n** and **p** in terms of the variable distance **a** in the x direction. It may be recalled that each shaped paver is of a circumscribing rectangular border. If x, y transverse and longitudinal axes have their original corner **A** of this circumscribing rectangular shape, it can be seen that each corner of the actual paver is connected by lines which form the real shape of the paver. The functions of these lines can be calculated using basic geometrical rules. The boundary line functions for the proprietory shaped paver 2 are shown in Table 5.3.

In Table 5.3 the first letters of each line function characterise the corner names as can be seen in Figure 5.17. By using the line functions in Table 5.3 shaped paver 2 and the line functions which define the patch load boundaries, which are of the form $f_y = b(1-\frac{x}{a})$, $f_x = a(1-\frac{y}{b})$ in the x and y axes, the intersection points between the paver boundary lines and the load patch boundary line can be calculated

mathematically. Table 5.4 shows the intersection points which can be seen in Figures 5.17 to 5.24.

$bcx = 20 + y$ $bcy = -20 + x$	$dex = 90 - y$ $dey = 90 - x$	$fgx = 130 + y$ $fgy = -130 + x$	$hix = 200 - y$ $hiy = 200 - x$
$klx = 200 + y$ $kly = -200 + x$	$mmnx = 310 - y$ $mmny = 310 - x$	$utx = -90 + y$ $uty = 90 + x$	$zyx = -26.\overline{6} + 1.\overline{3}y$ $zyy = 20 + 0.75x$
$qrqx = bcx$ $qrqy = bcy$	$wxx = dex$ $wxy = dey$	$srx = hix$ $sry = hiy$	$pox = mmnx$ $poy = mmny$

Table 5.3: Boundary line functions for proprietory shaped paver 2.

$P_{1x} = a - 220$ $P_{1y} = 110$	$P_{2y} = \frac{a}{2} - 110$ $P_{2x} = 220$	$P_{3y} = a - 310$ $P_{3x} = 620 - a$	$P_{4y} = 125$ $P_{4x} = a - 250$
$P_{5y} = a - 310$ $P_{5x} = 620 - a$	$P_{6y} = \frac{a}{2} - 117.5$ $P_{6x} = 235$	$P_{7y} = 0.\overline{3}a - 6.\overline{6}$ $P_{7x} = 13.\overline{3} + 0.\overline{3}a$	$P_{8y} = 110$ $P_{8x} = a - 220$
$P_{9y} = a - 200$ $P_{9x} = 400 - a$	$P_{10y} = 125$ $P_{10x} = a - 250$	$P_{11y} = 0.\overline{3}a - 66.\overline{6}$ $P_{11x} = 133.\overline{3} + 0.\overline{3}a$	

Table 5.4: The intersection points between the lines which form the patch load boundary with distances **a** and **b** (**b=a/2**) in the x and y directions and line functions bounding the proprietory shaped paver 2.

The surface area and centroid distances for the system illustrated in Figure 5.17 can be calculated using the data in Table 5.3 and Table 5.4 and are as follows:

$$F = \int_0^a fy\,dx - \int_{235}^a fy\,dx - \int_{220}^{235} fy\,dx + \int_{220}^{235} mmny\,dx - \int_{220}^{235} kly\,dx - \int_{185}^{200} hiy\,dx - \int_{145}^{185} 15\,dx - \int_{130}^{145} fgy\,dx$$
$$- \int_{75}^{90} dey\,dx - \int_{35}^{75} 15\,dx - \int_{20}^{35} bcy\,dx - \int_0^{15} wxy\,dx + \int_0^{15} zyy\,dx - \int_0^{P_{1x}} fy\,dx + \int_0^{20} 110\,dx + \int_{20}^{35} uty\,dx$$
$$+ \int_{35}^{75} 125\,dx + \int_{75}^{90} sry\,dx + \int_{90}^{130} 110\,dx + \int_{130}^{145} qrqy\,dx + \int_{145}^{185} 110\,dx + \int_{185}^{200} poy\,dx + \int_{200}^{P_{1x}} 110\,dx$$

The evaluation of the integrals yields the following equation:

$$F = \frac{(747.063 - a)(-132.937 + a)}{4}$$

$$\overline{X} = \frac{1}{F}\left[\begin{array}{l}
\int_{0}^{a} x\,fy\,dx - \int_{235}^{a} x\,fy\,dx - \int_{220}^{235} x\,fy\,dx + \int_{220}^{235} x\,mmny\,dx - \int_{220}^{235} x\,kly\,dx - \int_{185}^{200} x\,hiy\,dx \\
- \int_{145}^{185} x\,15\,dx - \int_{130}^{145} x\,fgy\,dx - \int_{75}^{90} x\,dey\,dx - \int_{35}^{75} x\,15\,dx - \int_{20}^{35} x\,bcy\,dx - \int_{0}^{15} x\,wxy\,dx \\
+ \int_{0}^{15} x\,zyy\,dx - \int_{0}^{P_{1x}} x\,fy\,dx + \int_{0}^{20} x\,110\,dx + \int_{20}^{35} x\,uty\,dx + \int_{35}^{75} x\,125\,dx + \int_{75}^{90} x\,sry\,dx \\
+ \int_{90}^{130} x\,110\,dx + \int_{130}^{145} x\,qrqy\,dx + \int_{145}^{185} x\,110\,dx + \int_{185}^{200} x\,poy\,dx + \int_{200}^{P_{1x}} x\,110\,dx
\end{array}\right]$$

The evaluation of the integrals yields the following equation:

$$\overline{X} = \frac{(-626.77 + a)(-161.885 + a)(128.656 + a)}{3(-747.063 + a)(-132.937 + a)}$$

$$\overline{Y} = \frac{1}{F}\left[\begin{array}{l}
\int_{0}^{b} y\,fx\,dy - \int_{125}^{b} y\,fx\,dy - \int_{110}^{125} y\,utx\,dy - \int_{110}^{125} y\,qrqx\,dy + \int_{110}^{125} y\,srx\,dy - \int_{110}^{125} y\,fx\,dy \\
+ \int_{110}^{125} y\,opx\,dy - \int_{75}^{90} y\,wxx\,dy - \int_{35}^{75} y\,15\,dy - \int_{20}^{35} y\,zyx\,dy - \int_{0}^{15} y\,dex\,dy + \int_{0}^{15} y\,bcx\,dy \\
- \int_{0}^{15} y\,hix\,dy + \int_{0}^{15} y\,fgx\,dy - \int_{0}^{P_{2y}} y\,fx\,dy + \int_{0}^{20} y\,220\,dy + \int_{20}^{35} y\,klx\,dy + \int_{35}^{75} y\,235\,dy \\
+ \int_{75}^{90} y\,mmnx\,dy + \int_{90}^{P_{2y}} y\,220\,dy
\end{array}\right]$$

The evaluation of the integrals yields the following equation:

$$\bar{Y} = \frac{(-611.173+a)(-198.878+a)(150.051+a)}{6(-750.887+a)(-129.113+a)}$$

Line 1 in Figure 5.17 scans the paver between corners **n** and **p**. It should therefore be noted that for the solutions above to be valid for the patch load application 1, the variable distance **a** in the x direction must lie in the range: 440>**a**>435mm.

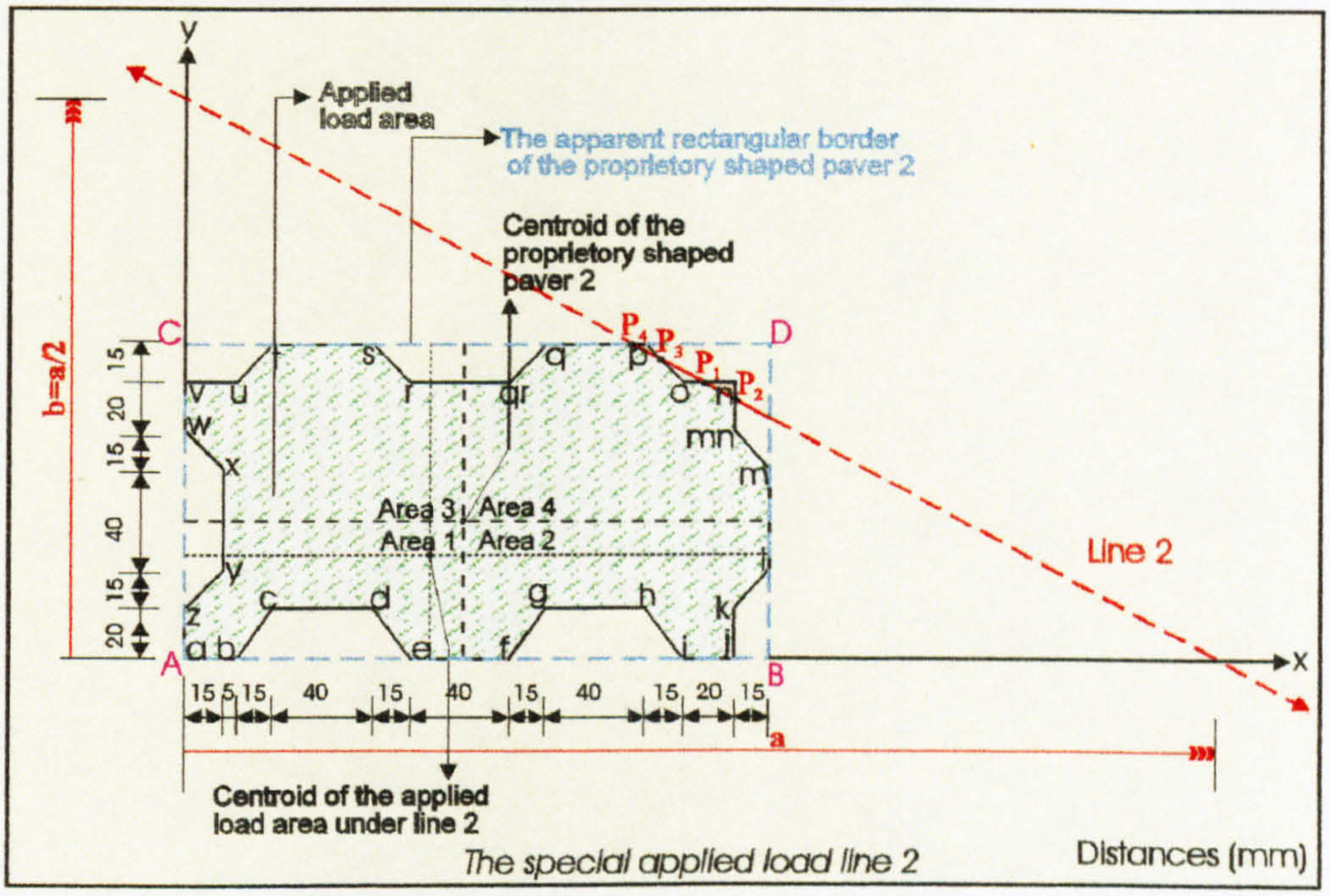

Figure 5.18: The selected special patch load application 2 for proprietory shaped paver 2.

Figure 5.18 illustrates the special patch load application 2 for the proprietory shaped paver 2. **Line 2** scans the paver between corners **p** and **o** in terms of the variable distance **a** in the x direction. By using the paver line functions in Table 5.3, the equations of the intersection points in Table 5.4 and the patch load boundary line function which is $f_y = b(1-\frac{x}{a})$, $f_x = a(1-\frac{y}{b})$ in the x and y axes, the special patch load's surface area and centroid distances can be calculated as follows:

$$F = \int_0^a fy\,dx - \int_{235}^a fy\,dx - \int_{220}^{235} fy\,dx + \int_{220}^{235} mmny\,dx - \int_{220}^{235} kly\,dx - \int_{185}^{200} hiy\,dx - \int_{145}^{185} 15\,dx - \int_{130}^{145} fgy\,dx$$

$$-\int_{75}^{90} dey\,dx-\int_{35}^{75}15\,dx-\int_{20}^{35} bcy\,dx-\int_{0}^{15} wxy\,dx+\int_{0}^{15} zyy\,dx-\int_{0}^{P_{4x}} fy\,dx+\int_{0}^{20}110\,dx+\int_{20}^{35} uty\,dx$$

$$+\int_{35}^{75}125\,dx+\int_{75}^{90} sry\,dx+\int_{90}^{130}110\,dx+\int_{130}^{145} qrqy\,dx+\int_{145}^{P_{4x}}110\,dx-\int_{P_{3x}}^{200} fy\,dx+\int_{P_{3x}}^{200} poy\,dx-\int_{200}^{P_{1x}} fy\,dx$$

$$+\int_{200}^{P_{1x}}110\,dx$$

The evaluation of the integrals yields the following equation:

$$F=\frac{3(604.122-a)(-249.212+a)}{4}$$

$$\overline{X}=\frac{1}{F}\left[\int_{0}^{a} x\,fy\,dx-\int_{235}^{a} x\,fy\,dx-\int_{220}^{235} x\,fy\,dx+\int_{220}^{235} x\,mmny\,dx-\int_{220}^{235} x\,kly\,dx-\int_{185}^{200} x\,hiy\,dx\right.$$

$$-\int_{145}^{185} x\,15\,dx-\int_{130}^{145} x\,fgy\,dx-\int_{75}^{90} x\,dey\,dx-\int_{35}^{75} x\,15\,dx-\int_{20}^{35} x\,bcy\,dx-\int_{0}^{15} x\,wxy\,dx$$

$$+\int_{0}^{15} x\,zyy\,dx-\int_{0}^{P_{4x}} x\,fy\,dx+\int_{0}^{20} x\,110\,dx+\int_{20}^{35} x\,uty\,dx+\int_{35}^{75} x\,125\,dx+\int_{75}^{90} x\,sry\,dx$$

$$+\int_{90}^{130} x\,110\,dx+\int_{130}^{145} x\,qrqy\,dx+\int_{145}^{P_{4x}} x\,110\,dx-\int_{P_{3x}}^{200} x\,fy\,dx+\int_{P_{3x}}^{200} x\,poy\,dx-\int_{200}^{P_{1x}} x\,fy\,dx$$

$$\left.+\int_{200}^{P_{1x}} x\,110\,dx\right]$$

The evaluation of the integrals yields the following equation:

$$\overline{X}=\frac{(-551.057+a)(-259.344+a)(1386.4+a)}{9(-604.122+a)(-249.212+a)}$$

$$\overline{Y} = \frac{1}{F}\left[\begin{array}{l} \int_0^b y\,fx\,dy - \int_{125}^b y\,fx\,dy - \int_{110}^{125} y\,utx\,dy - \int_{110}^{125} y\,qrqx\,dy + \int_{110}^{125} y\,srx\,dy - \int_{110}^{P_{3y}} y\,fx\,dy \\ + \int_{110}^{P_{3y}} y\,opx\,dy - \int_{75}^{90} y\,wxx\,dy - \int_{35}^{75} y\,15\,dy - \int_{20}^{35} y\,zyx\,dy - \int_{0}^{15} y\,dex\,dy + \int_{0}^{15} y\,bcx\,dy \\ - \int_0^{15} y\,hix\,dy + \int_0^{15} y\,fgx\,dy - \int_0^{P_{2y}} y\,fx\,dy + \int_0^{20} y\,220\,dy + \int_{20}^{35} y\,klx\,dy + \int_{35}^{75} y\,235\,dy \\ + \int_{75}^{90} y\,mmnx\,dy + \int_{90}^{P_{2y}} y\,220\,dy \end{array}\right]$$

The evaluation of the integrals yields the following equation:

$$\overline{Y} = \frac{5(-545.788+a)(-284.88+a)(-45.3322+a)}{18(-616.142+a)(-257.192+a)}$$

Line 2 in Figure 5.18 scans the paver between corners **p** and **o**. It should therefore be noted that for the solutions above to be valid for the patch load application 2, the variable distance **a** in the x direction must lie in the range: 435>**a**>420mm.

Figure 5.19 illustrates the special patch load application 3 for the proprietory shaped paver 2. **Line 3** scans the paver between corners **o** and **mn** in terms of the variable distance **a** in the x direction. By using the paver line functions in Table 5.3, the equations of the intersection points in Table 5.4 and the patch load boundary line function which is $f_y = b(1-\frac{x}{a})$, $f_x = a(1-\frac{y}{b})$ in the x and y axes, the special patch load's surface area and centroid distances can be calculated as follows:

$$F = \int_0^a fy\,dx - \int_{235}^a fy\,dx - \int_{220}^{235} fy\,dx + \int_{220}^{235} mmny\,dx - \int_{220}^{235} kly\,dx - \int_{185}^{200} hiy\,dx - \int_{145}^{185} 15\,dx - \int_{130}^{145} fgy\,dx$$
$$- \int_{75}^{90} dey\,dx - \int_{35}^{75} 15\,dx - \int_{20}^{35} bcy\,dx - \int_{0}^{15} wxy\,dx + \int_{0}^{15} zyy\,dx - \int_{0}^{P_{4x}} fy\,dx + \int_{0}^{20} 110\,dx + \int_{20}^{35} uty\,dx$$

$$+\int_{35}^{75} 125\,dx + \int_{75}^{90} sry\,dx + \int_{90}^{130} 110\,dx + \int_{130}^{145} qrqy\,dx + \int_{145}^{P_{4x}} 110\,dx$$

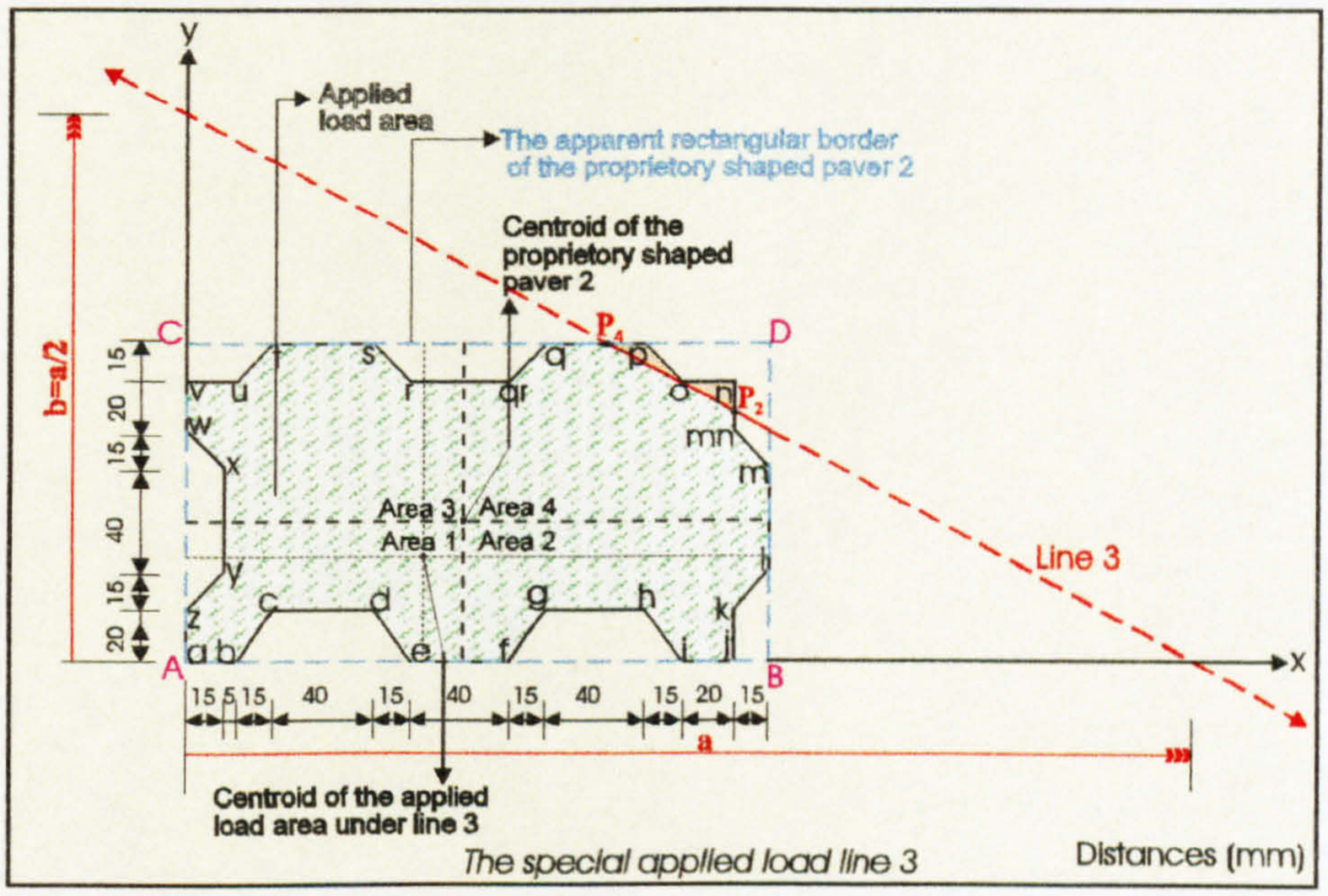

Figure 5.19: The selected special patch load application 3 for proprietory shaped paver 2.

The evaluation of the integrals yields the following equation:

$$F = \frac{(745.839 - a)(-134.161 + a)}{4}$$

$$\overline{X} = \frac{1}{F}\left[\begin{array}{l} \int_{0}^{a} x\,fy\,dx - \int_{235}^{a} x\,fy\,dx - \int_{220}^{235} x\,fy\,dx + \int_{220}^{235} x\,mmny\,dx - \int_{220}^{235} x\,kly\,dx - \int_{185}^{200} x\,hiy\,dx \\ - \int_{145}^{185} x\,15\,dx - \int_{130}^{145} x\,fgy\,dx - \int_{75}^{90} x\,dey\,dx - \int_{35}^{75} x\,15\,dx - \int_{20}^{35} x\,bcy\,dx - \int_{0}^{15} x\,wxy\,dx \\ + \int_{0}^{15} x\,zyy\,dx - \int_{0}^{P_{4x}} x\,fy\,dx + \int_{0}^{20} x\,110\,dx + \int_{20}^{35} x\,uty\,dx + \int_{35}^{75} x\,125\,dx + \int_{75}^{90} x\,sry\,dx \\ + \int_{90}^{130} x\,110\,dx + \int_{130}^{145} x\,qrqy\,dx + \int_{145}^{P_{4x}} x\,110\,dx \end{array}\right]$$

The evaluation of the integrals yields the following equation:

$$\overline{X} = \frac{(-626.525+a)(-171.504+a)(138.03+a)}{3(-745.839+a)(-134.161+a)}$$

$$\overline{Y} = \frac{1}{F}\left[\begin{array}{l} \int_0^b y\,fx\,dy - \int_{125}^b y\,fx\,dy - \int_{110}^{125} y\,utx\,dy - \int_{110}^{125} y\,qrqx\,dy + \int_{110}^{125} y\,srx\,dy - \int_{75}^{90} y\,wxx\,dy \\ -\int_{35}^{75} y\,15\,dy - \int_{20}^{35} y\,zyx\,dy - \int_{0}^{15} y\,dex\,dy + \int_{0}^{15} y\,bcx\,dy - \int_{0}^{15} y\,hix\,dy + \int_{0}^{15} y\,fgx\,dy \\ -\int_{0}^{P_{2y}} y\,fx\,dy + \int_{0}^{20} y\,220\,dy + \int_{20}^{35} y\,klx\,dy + \int_{35}^{75} y\,235\,dy + \int_{75}^{90} y\,mmnx\,dy + \int_{90}^{P_{2y}} y\,220\,dy \end{array}\right]$$

The evaluation of the integrals yields the following equation:

$$\overline{Y} = \frac{(-659.123+a)(-207.509+a)(206.632+a)}{(-783.529+a)(-156.471+a)}$$

Line 3 in Figure 5.19 scans the paver between corners **o** and **mn**. It should therefore be noted that for the solutions above to be valid for the patch load application 3, the variable distance **a** in the x direction must lie in the range: 420>**a**>400mm.

Figure 5.20 illustrates the special patch load application 4 for the proprietory shaped paver 2. **Line 4** scans the paver between corners **mn** and **q** in terms of the variable distance **a** in the x direction. By using the paver line functions in Table 5.3, the equations of the intersection points in Table 5.4 and the patch load boundary line function which is $f_y = b(1-\frac{x}{a})$, $f_x = a(1-\frac{y}{b})$ in the x and y axes, the special patch load's surface area and centroid distances can be calculated as follows:

$$F = \int_0^a fy\,dx - \int_{235}^a fy\,dx - \int_{P_{5x}}^{235} fy\,dx + \int_{P_{5x}}^{235} mmny\,dx - \int_{220}^{235} kly\,dx - \int_{185}^{200} hiy\,dx - \int_{145}^{185} 15\,dx - \int_{130}^{145} fgy\,dx$$

$$-\int_{75}^{90} dey\,dx - \int_{35}^{75} 15\,dx - \int_{20}^{35} bcy\,dx - \int_{0}^{15} wxy\,dx + \int_{0}^{15} zyy\,dx - \int_{0}^{P_{4x}} fy\,dx + \int_{0}^{20} 110\,dx + \int_{20}^{35} uty\,dx$$
$$+\int_{35}^{75} 125\,dx + \int_{75}^{90} sry\,dx + \int_{90}^{130} 110\,dx + \int_{130}^{145} qrqy\,dx + \int_{145}^{P_{4x}} 110\,dx$$

The evaluation of the integrals yields the following equation:

$$F = \frac{(636.723 - a)(-203.277 + a)}{2}$$

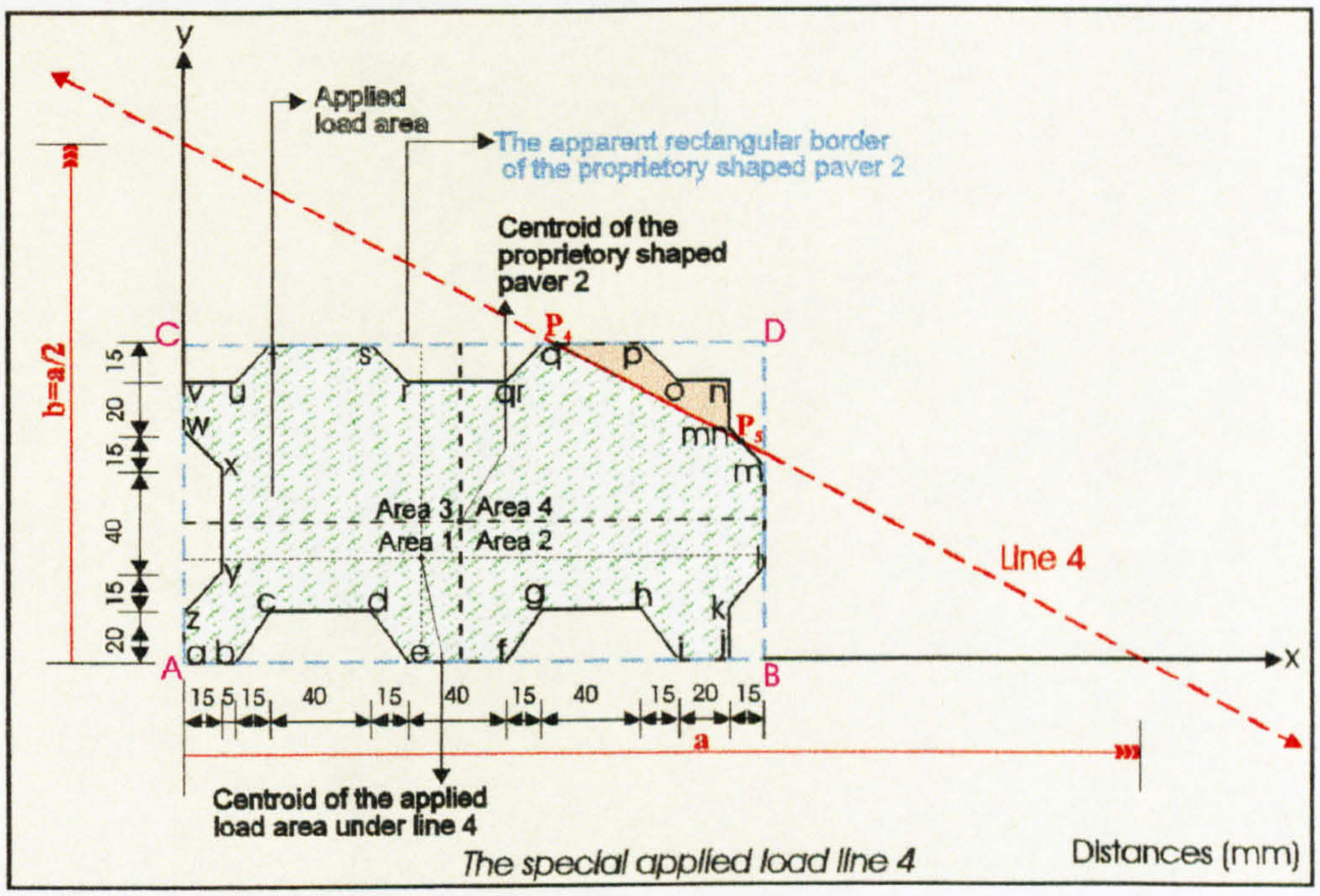

Figure 5.20: The selected special patch load application 4 for proprietory shaped paver 2.

$$\overline{X} = \frac{1}{F}\left[\begin{array}{l}
\int_{0}^{a} x\,fy\,dx - \int_{235}^{a} x\,fy\,dx - \int_{P_{5x}}^{235} x\,fy\,dx + \int_{P_{5x}}^{235} x\,mmny\,dx - \int_{220}^{235} x\,kly\,dx - \int_{185}^{200} x\,hiy\,dx - \int_{145}^{185} x\,15\,dx \\
-\int_{130}^{145} x\,fgy\,dx - \int_{75}^{90} x\,dey\,dx - \int_{35}^{75} x\,15\,dx - \int_{20}^{35} x\,bcy\,dx - \int_{0}^{15} x\,wxy\,dx + \int_{0}^{15} x\,zyy\,dx - \int_{0}^{P_{4x}} x\,fy\,dx \\
+\int_{0}^{20} x\,110\,dx + \int_{20}^{35} x\,uty\,dx + \int_{35}^{75} x\,125\,dx + \int_{75}^{90} x\,sry\,dx + \int_{90}^{130} x\,110\,dx + \int_{130}^{145} x\,qrqy\,dx + \int_{145}^{P_{4x}} x\,110\,dx
\end{array}\right]$$

The evaluation of the integrals yields the following equation:

$$\overline{X} = \frac{200(-585.991+a)(-256.259+a)}{(-636.723+a)(-203.277+a)}$$

$$\overline{Y} = \frac{1}{F}\left[\begin{array}{l} \int_0^b y\,fx\,dy - \int_{125}^b y\,fx\,dy - \int_{110}^{125} y\,utx\,dy - \int_{110}^{125} y\,qrqx\,dy + \int_{110}^{125} y\,srx\,dy - \int_{75}^{90} y\,wxx\,dy - \int_{35}^{75} y\,15\,dy \\ -\int_{20}^{35} y\,zyx\,dy - \int_0^{15} y\,dex\,dy + \int_0^{15} y\,bcx\,dy - \int_0^{15} y\,hix\,dy + \int_0^{15} y\,fgx\,dy - \int_0^{P_{5y}} y\,fx\,dy + \int_0^{20} y\,220\,dy \\ +\int_{20}^{35} y\,klx\,dy + \int_{35}^{75} y\,235\,dy + \int_{75}^{P_{5y}} y\,mmnx\,dy \end{array}\right]$$

The evaluation of the integrals yields the following equation:

$$\overline{Y} = \frac{(-561.191+a)\left(34452.7-368.809a+a^2\right)}{3(-653.918+a)(-216.082+a)}$$

Line 4 in Figure 5.20 scans the paver between corners **mn** and **q**. It should therefore be noted that for the solutions above to be valid for the patch load application 4, the variable distance **a** in the x direction must lie in the range: 400>**a**>395mm.

Figure 5.21 illustrates the special patch load application 5 for the proprietory shaped paver 2. **Line 5** scans the paver between corners **m** and **qr** in terms of the variable distance **a** in the x direction. By using the paver line functions in Table 5.3, the equations of the intersection points in Table 5.4 and the patch load boundary line function which is $f_y = b(1-\frac{x}{a})$, $f_x = a(1-\frac{y}{b})$ in the x and y axes, the special patch load's surface area and centroid distances can be calculated as follows:

$$F = \int_0^a fy\,dx - \int_{235}^a fy\,dx - \int_{220}^{235} kly\,dx - \int_{185}^{200} hiy\,dx - \int_{145}^{185} 15\,dx - \int_{130}^{145} fgy\,dx - \int_{75}^{90} dey\,dx - \int_{35}^{75} 15\,dx$$

$$-\int_{20}^{35} bcy\,dx - \int_{0}^{15} wxy\,dx + \int_{0}^{15} zyy\,dx - \int_{0}^{P_{7x}} fy\,dx + \int_{0}^{20} 110\,dx + \int_{20}^{35} uty\,dx + \int_{35}^{75} 125\,dx + \int_{75}^{90} sry\,dx$$
$$+ \int_{90}^{130} 110\,dx + \int_{130}^{P_{7x}} qrqy\,dx$$

The evaluation of the integrals yields the following equation:

$$F = \frac{(1257.67 - a)(-72.326 + a)}{12}$$

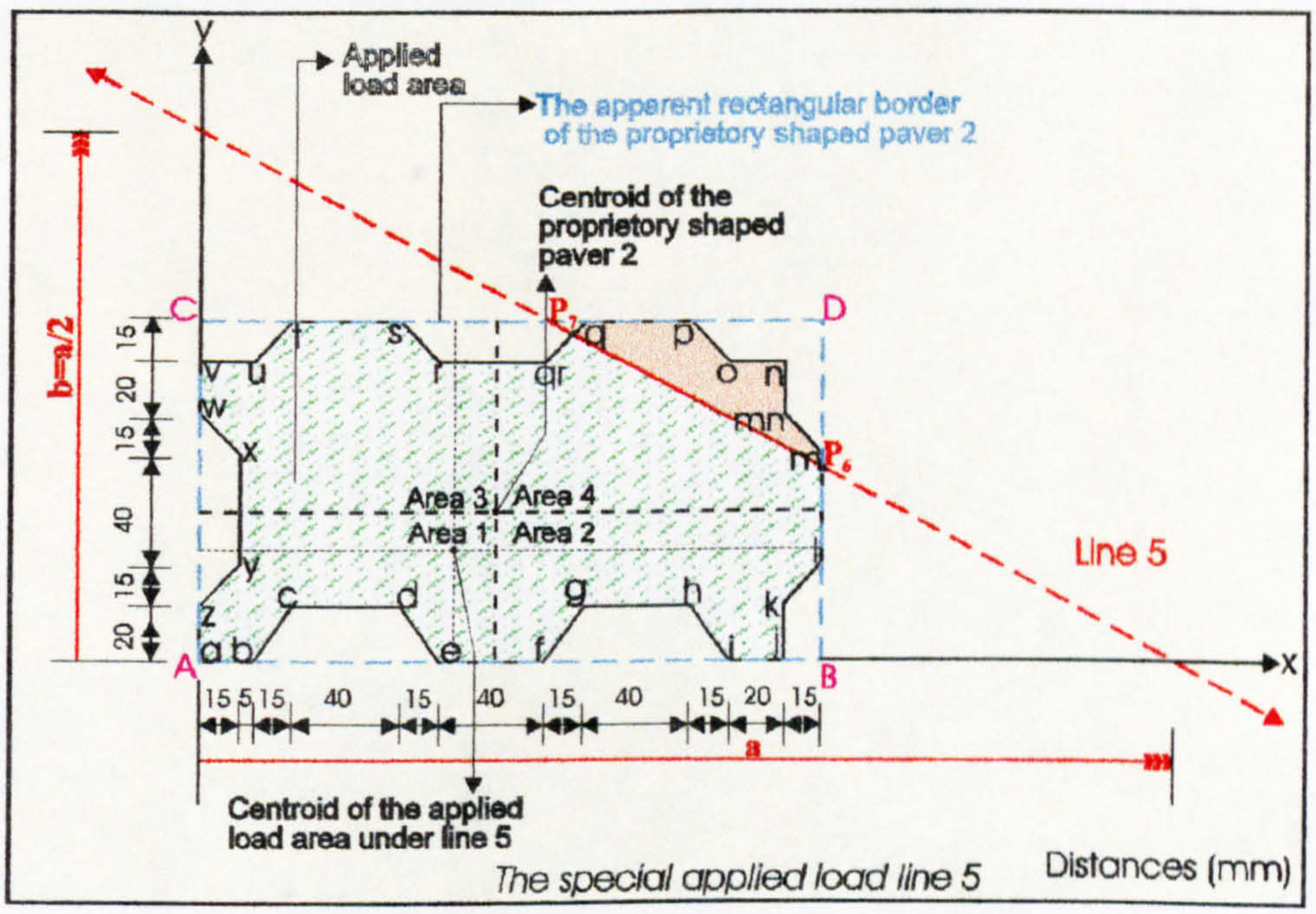

Figure 5.21: The selected special patch load application 5 for proprietory shaped paver 2.

$$\overline{X} = \frac{1}{F}\left[\begin{array}{l} \int_{0}^{a} x\,fy\,dx - \int_{235}^{a} x\,fy\,dx - \int_{220}^{235} x\,kly\,dx - \int_{185}^{200} x\,hiy\,dx - \int_{145}^{185} x\,15\,dx - \int_{130}^{145} x\,fgy\,dx - \int_{75}^{90} x\,dey\,dx \\ -\int_{35}^{75} x\,15\,dx - \int_{20}^{35} x\,bcy\,dx - \int_{0}^{15} x\,wxy\,dx + \int_{0}^{15} x\,zyy\,dx - \int_{0}^{P_{7x}} x\,fy\,dx + \int_{0}^{20} x\,110\,dx + \int_{20}^{35} x\,uty\,dx \\ +\int_{35}^{75} x\,125\,dx + \int_{75}^{90} x\,sry\,dx + \int_{90}^{130} x\,110\,dx + \int_{130}^{P_{7x}} x\,qrqy\,dx \end{array}\right]$$

The evaluation of the integrals yields the following equation:

$$\overline{X} = \frac{(-1073.59+a)(-152.208+a)(1345.8+a)}{9(-1257.67+a)(-72.326+a)}$$

$$\overline{Y} = \frac{1}{F}\left[\begin{array}{l} \int_0^b y\,fx\,dy - \int_{125}^b y\,fx\,dy - \int_{110}^{125} y\,utx\,dy - \int_{110}^{P_{7y}} y\,qrqx\,dy + \int_{110}^{P_{7y}} y\,srx\,dy - \int_{P_{7y}}^{125} y\,fx\,dy \\ + \int_{P_{7y}}^{125} y\,srx\,dy - \int_{75}^{90} y\,wxx\,dy - \int_{35}^{75} y\,15\,dy - \int_{20}^{35} y\,zyx\,dy - \int_{0}^{15} y\,dex\,dy + \int_{0}^{15} y\,bcx\,dy \\ - \int_{0}^{15} y\,hix\,dy + \int_{0}^{15} y\,fgx\,dy - \int_{0}^{P_{6y}} y\,fx\,dy + \int_{0}^{20} y\,220\,dy + \int_{20}^{35} y\,klx\,dy + \int_{35}^{P_{6y}} y\,235\,dy \end{array}\right]$$

The evaluation of the integrals yields the following equation:

$$\overline{Y} = \frac{5(-964.984+a)\left(50203.7-256.016a+a^2\right)}{18(-1257.58+a)(-72.4196+a)}$$

Line 5 in Figure 5.21 scans the paver between corners **m** and **qr**. It should therefore be noted that for the solutions above to be valid for the patch load application 5, the variable distance **a** in the x direction must lie in the range: 385>**a**>350mm.

Figure 5.22 illustrates the special patch load application 6 for the proprietory shaped paver 2. **Line 6** scans the paver between corners **qr** and **s** in terms of the variable distance **a** in the x direction. By using the paver line functions in Table 5.3, the equations of the intersection points in Table 5.4 and the patch load boundary line function which is $f_y = b(1-\frac{x}{a})$, $f_x = a(1-\frac{y}{b})$ in the x and y axes, the special patch load's surface area and centroid distances can be calculated as follows:

$$F = \int_0^a fy\,dx - \int_{235}^a fy\,dx - \int_{220}^{235} kly\,dx - \int_{185}^{200} hiy\,dx - \int_{145}^{185} 15\,dx - \int_{130}^{145} fgy\,dx - \int_{75}^{90} dey\,dx - \int_{35}^{75} 15\,dx$$

$$- \int_{20}^{35} bcy\,dx - \int_{0}^{15} wxy\,dx + \int_{0}^{15} zyy\,dx - \int_{0}^{P_{8x}} fy\,dx + \int_{0}^{20} 110\,dx + \int_{20}^{35} uty\,dx + \int_{35}^{75} 125\,dx + \int_{75}^{90} sry\,dx$$

$$+ \int_{90}^{P_{8x}} 110\,dx$$

The evaluation of the integrals yields the following equation:

$$F = \frac{(763.282 - a)(-146.718 + a)}{4}$$

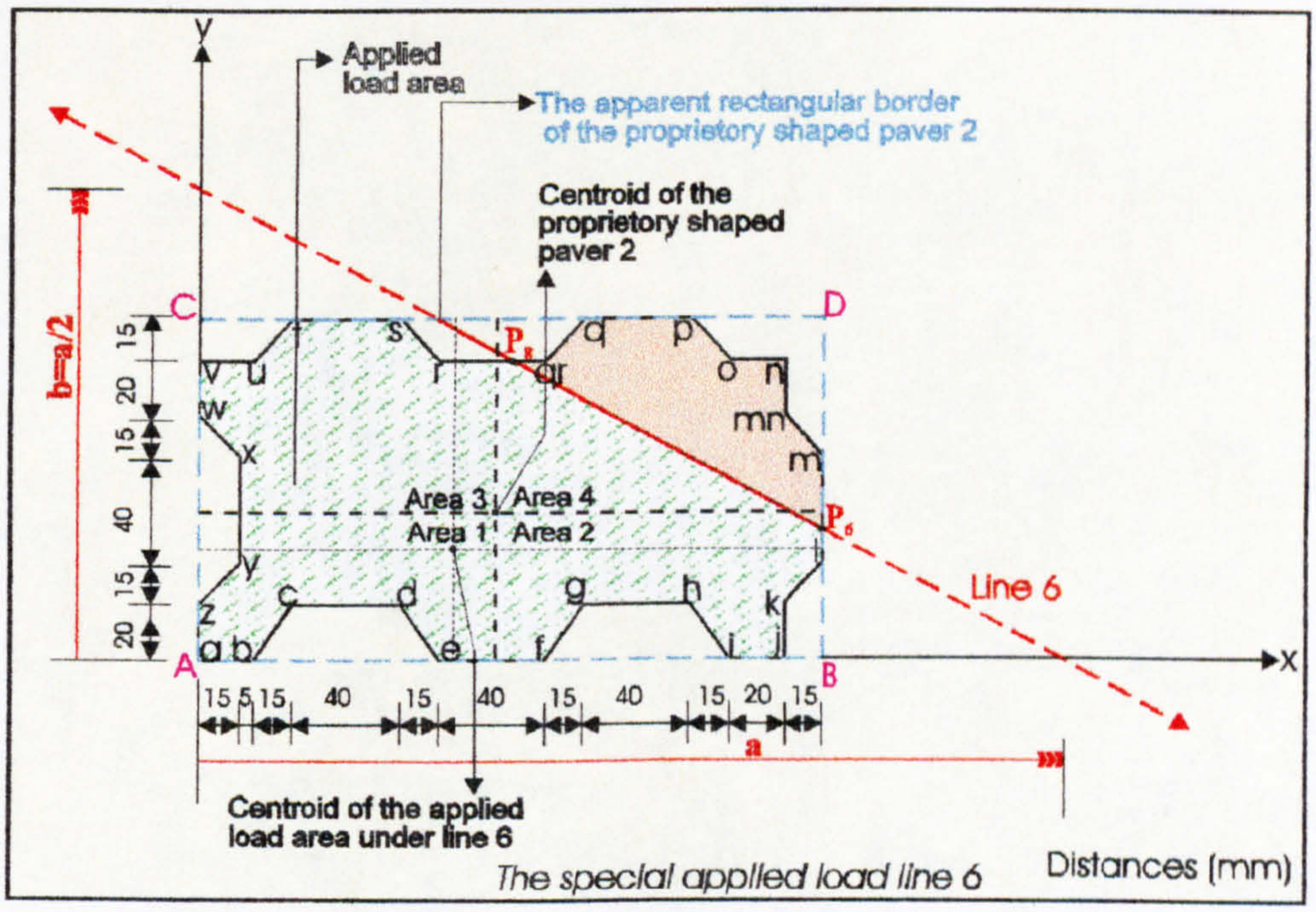

Figure 5.22: The selected special patch load application 6 for proprietory shaped paver 2.

$$\overline{X} = \frac{1}{F}\left[\int_0^a x\,fy\,dx - \int_{235}^a x\,fy\,dx - \int_{220}^{235} x\,kly\,dx - \int_{185}^{200} x\,hiy\,dx - \int_{145}^{185} x\,15\,dx - \int_{130}^{145} x\,fgy\,dx\right.$$

$$\left. - \int_{75}^{90} x\,dey\,dx - \int_{35}^{75} x\,15\,dx - \int_{20}^{35} x\,bcy\,dx - \int_{0}^{15} x\,wxy\,dx + \int_{0}^{15} x\,zyy\,dx - \int_{0}^{P_{8x}} x\,fy\,dx\right.$$

$$+\int_0^{20} x\ 110\ dx+\int_{20}^{35} x\ uty\ dx+\int_{35}^{75} x\ 125\ dx+\int_{75}^{90} x\ sry\ dx+\int_{90}^{P_{8x}} x\ 110\ dx\Bigg]$$

The evaluation of the integrals yields the following equation:

$$\overline{X}=\frac{(-648.345+a)(-173.355+a)(161.7+a)}{3(-763.282+a)(-146.718+a)}$$

$$\overline{Y}=\frac{1}{F}\Bigg[\int_0^{b} y\,fx\,dy-\int_{125}^{b} y\,fx\,dy-\int_{110}^{125} y\,utx\,dy-\int_{110}^{125} y\,fx\,dy+\int_{110}^{125} y\,srx\,dy-\int_{75}^{90} y\,wxx\,dy$$

$$-\int_{35}^{75} y\ 15\ dy-\int_{20}^{35} y\,zyx\,dy-\int_{0}^{15} y\,dex\,dy+\int_{0}^{15} y\,bcx\,dy-\int_{0}^{15} y\,hix\,dy+\int_{0}^{15} y\,fgx\,dy$$

$$-\int_{0}^{P_{6y}} y\,fx\,dy+\int_{0}^{20} y\ 220\ dy+\int_{20}^{35} y\,klx\,dy+\int_{35}^{P_{6y}} y\ 235\ dy\Bigg]$$

The evaluation of the integrals yields the following equation:

$$\overline{Y}=\frac{(-655.286+a)(-137.638+a)(87.9246+a)}{6(-763.222+a)(-146.778+a)}$$

Line 6 in Figure 5.22 scans the paver between corners **qr** and **s**. It should therefore be noted that for the solutions above to be valid for the patch load application 6, the variable distance **a** in the x direction must lie in the range: 350>**a**>325mm.

Figure 5.23 illustrates the special patch load application 7 for the proprietory shaped paver 2. **Line 7** scans the paver between corners **s** and **r** in terms of the variable distance **a** in the x direction. By using the paver line functions in Table 5.3, the equations of the intersection points in Table 5.4 and the patch load boundary line

function which is $f_y = b(1-\frac{x}{a})$, $f_x = a(1-\frac{y}{b})$ in the x and y axes, the special patch load's surface area and centroid distances can be calculated as follows:

$$F = \int_0^a fy\,dx - \int_{235}^a fy\,dx - \int_{220}^{235} kly\,dx - \int_{185}^{200} hiy\,dx - \int_{145}^{185} 15\,dx - \int_{130}^{145} fgy\,dx - \int_{75}^{90} dey\,dx - \int_{35}^{75} 15\,dx$$

$$- \int_{20}^{35} bcy\,dx - \int_0^{15} wxy\,dx + \int_0^{15} zyy\,dx - \int_0^{P_{10x}} fy\,dx + \int_0^{20} 110\,dx + \int_{20}^{35} uty\,dx + \int_{35}^{P_{10x}} 125\,dx - \int_{P_{9x}}^{90} fy\,dx$$

$$+ \int_{P_{9x}}^{90} sry\,dx - \int_{90}^{P_{8x}} fy\,dx + \int_{90}^{P_{8x}} 110\,dx$$

The evaluation of the integrals yields the following equation:

$$F = \frac{3(535.437-a)(-201.23+a)}{4}$$

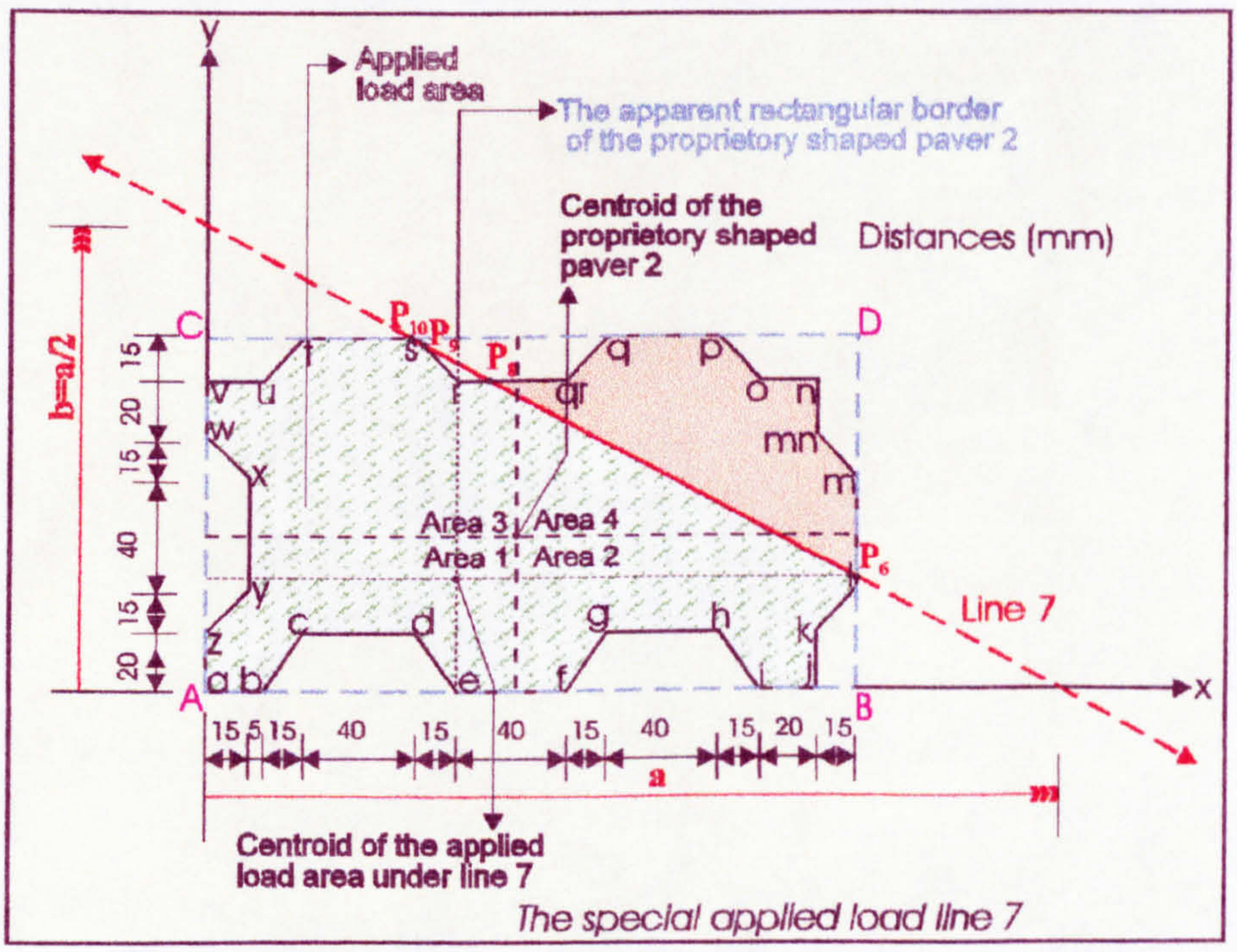

Figure 5.23: The selected special patch load application 7 for proprietory shaped paver 2.

$$\overline{X} = \frac{1}{F}\left[\int_{0}^{a} x\,fy\,dx - \int_{235}^{a} x\,fy\,dx - \int_{220}^{235} x\,kly\,dx - \int_{185}^{200} x\,hiy\,dx - \int_{145}^{185} x\,15\,dx - \int_{130}^{145} x\,fgy\,dx\right.$$

$$-\int_{75}^{90} x\,dey\,dx - \int_{35}^{75} x\,15\,dx - \int_{20}^{35} x\,bcy\,dx - \int_{0}^{15} x\,wxy\,dx + \int_{0}^{15} x\,zyy\,dx - \int_{0}^{P_{10x}} x\,fy\,dx$$

$$+\int_{0}^{20} x\,110\,dx + \int_{20}^{35} x\,uty\,dx + \int_{35}^{P_{10x}} x\,125\,dx - \int_{P_{9x}}^{90} x\,fy\,dx + \int_{P_{9x}}^{90} x\,sry\,dx - \int_{90}^{P_{8x}} x\,fy\,dx$$

$$\left.+\int_{90}^{P_{8x}} x\,110\,dx\right]$$

The evaluation of the integrals yields the following equation:

$$\overline{X} = \frac{(-559.491+a)(-209.928+a)(559.419+a)}{9(-535.437+a)(-201.23+a)}$$

$$\overline{Y} = \frac{1}{F}\left[\int_{0}^{b} y\,fx\,dy - \int_{125}^{b} y\,fx\,dy - \int_{110}^{125} y\,utx\,dy - \int_{110}^{P_{9y}} y\,fx\,dy + \int_{110}^{P_{9y}} y\,srx\,dy - \int_{75}^{90} y\,wxx\,dy\right.$$

$$-\int_{35}^{75} y\,15\,dy - \int_{20}^{35} y\,zyx\,dy - \int_{0}^{15} y\,dex\,dy + \int_{0}^{15} y\,bcx\,dy - \int_{0}^{15} y\,hix\,dy + \int_{0}^{15} y\,fgx\,dy$$

$$\left.-\int_{0}^{P_{6y}} y\,fx\,dy + \int_{0}^{20} y\,220\,dy + \int_{20}^{35} y\,klx\,dy + \int_{35}^{P_{6y}} y\,235\,dy\right]$$

The evaluation of the integrals yields the following equation:

$$\overline{Y} = \frac{5(-455.625+a)(-222.656+a)(57.281+a)}{18(-535.4+a)(-201.267+a)}$$

Line 7 in Figure 5.23 scans the paver between corners **s** and **r**. It should therefore be noted that for the solutions above to be valid for the patch load application 7, the variable distance **a** in the x direction must lie in the range: 325>**a**>310mm.

Figure 5.24 illustrates the special patch load application 8 for the proprietory shaped paver 2. **Line 8** scans the paver between corners **l** and **t** in terms of the variable distance **a** in the x direction. By using the paver line functions in Table 5.3, the equations of the intersection points in Table 5.4 and the patch load boundary line function which is $f_y = b(1-\frac{x}{a})$, $f_x = a(1-\frac{y}{b})$ in the x and y axes, the special patch load's surface area and centroid distances can be calculated as follows:

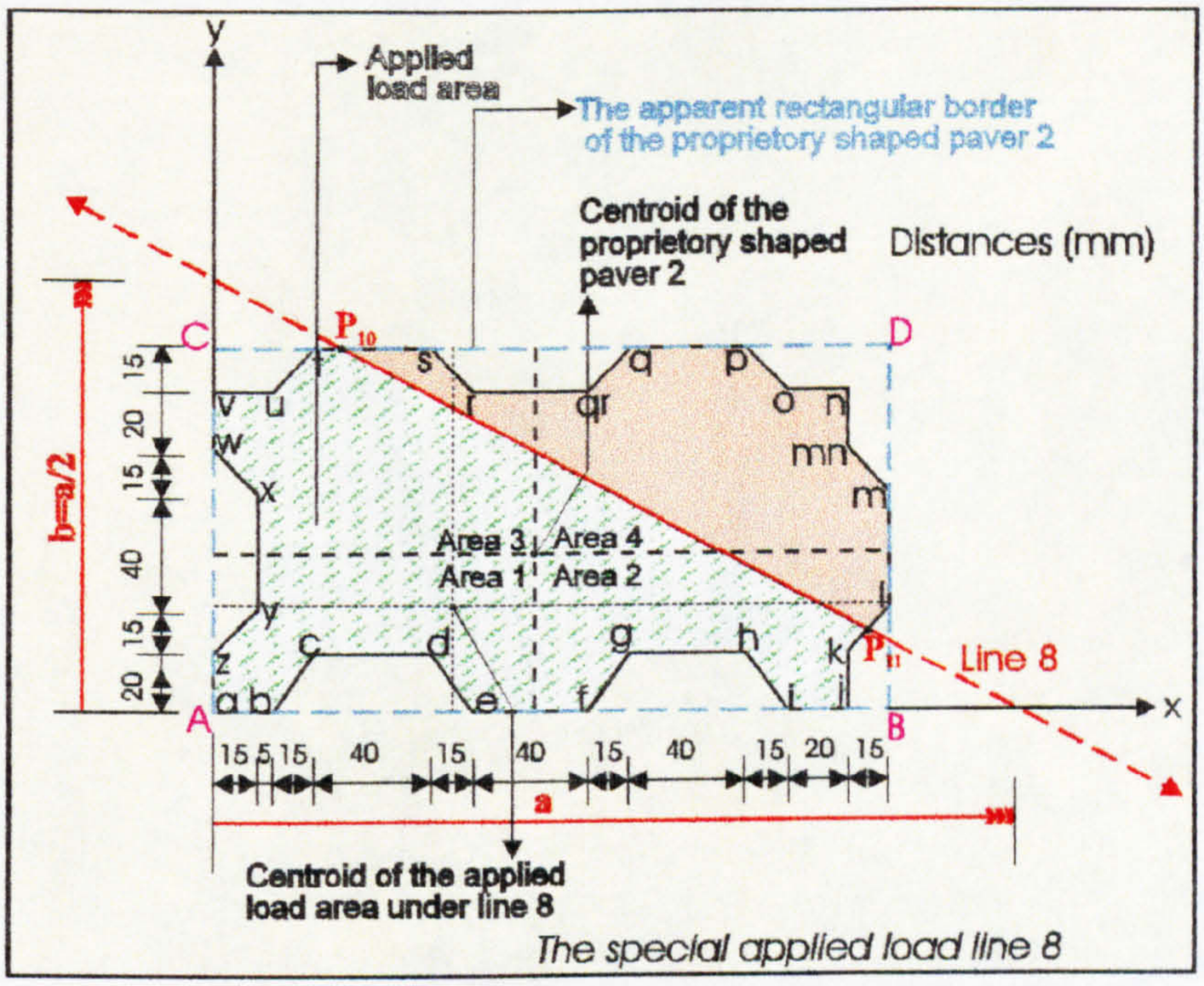

Figure 5.24: The selected special patch load application 8 for proprietory shaped paver 2.

$$F = \int_0^a fy\,dx - \int_{P_{11x}}^a fy\,dx - \int_{220}^{P_{11x}} kly\,dx - \int_{185}^{200} hiy\,dx - \int_{145}^{185} 15\,dx - \int_{130}^{145} fgy\,dx - \int_{75}^{90} dey\,dx - \int_{35}^{75} 15\,dx$$
$$- \int_{20}^{35} bcy\,dx - \int_0^{15} wxy\,dx + \int_0^{15} zyy\,dx - \int_0^{P_{10x}} fy\,dx + \int_0^{20} 110\,dx + \int_{20}^{35} uty\,dx + \int_{35}^{P_{10x}} 125\,dx$$

The evaluation of the integrals yields the following equation:

$$F = \frac{(999.949 - a)(-150.051 + a)}{6}$$

$$\overline{X} = \frac{1}{F}\left[\begin{array}{l} \int_{0}^{a} x\,fy\,dx - \int_{P_{11x}}^{a} x\,fy\,dx - \int_{220}^{P_{11x}} x\,kly\,dx - \int_{185}^{200} x\,hiy\,dx - \int_{145}^{185} x\,15\,dx - \int_{130}^{145} x\,fgy\,dx \\ -\int_{75}^{90} x\,dey\,dx - \int_{35}^{75} x\,15\,dx - \int_{20}^{35} x\,bcy\,dx - \int_{0}^{15} x\,wxy\,dx + \int_{0}^{15} x\,zyy\,dx - \int_{0}^{P_{10x}} x\,fy\,dx \\ +\int_{0}^{20} x\,110\,dx + \int_{20}^{35} x\,uty\,dx + \int_{35}^{P_{10x}} x\,125\,dx \end{array}\right]$$

The evaluation of the integrals yields the following equation:

$$\overline{X} = \frac{4(-817.324+a)(-120.479+a)(-55.9466+a)}{9(-999.949+a)(-150.051+a)}$$

$$\overline{Y} = \frac{1}{F}\left[\begin{array}{l} \int_{0}^{b} y\,fx\,dy - \int_{125}^{b} y\,fx\,dy - \int_{110}^{125} y\,utx\,dy - \int_{75}^{90} y\,wxx\,dy - \int_{35}^{75} y\,15\,dy - \int_{20}^{35} y\,zyx\,dy \\ -\int_{0}^{15} y\,dex\,dy + \int_{0}^{15} y\,bcx\,dy - \int_{0}^{15} y\,hix\,dy + \int_{0}^{15} y\,fgx\,dy - \int_{0}^{P_{11y}} y\,fx\,dy + \int_{0}^{20} y\,220\,dy \\ +\int_{20}^{P_{11y}} y\,klx\,dy \end{array}\right]$$

The evaluation of the integrals yields the following equation:

$$\overline{Y} = \frac{(-858.214+a)(-182.245+a)(440.46+a)}{9(-999.883+a)(-150.117+a)}$$

Line 8 in Figure 5.24 scans the paver between corners **l** and **t**. It should therefore be noted that for the solutions above to be valid for the patch load application 8, the variable distance **a** in the x direction must lie in the range: 305>**a**>285mm.

5.4. The selected special patch load applied to proprietory shaped paver 3

Figure 5.25 illustrates one of the common patch load application to proprietory shaped paver 3 (see Figure 5.1). It may be recalled that in these common load applications, the lines which define the patch loading gradually scan the paver from its lower left corner to its upper right corner with distances **a** and **b** (**b=a/2**). The proprietory shaped paver 3 is analysed with the similar logic described for the shaped pavers 1 and 2 (see Sections 5.2 and 5.3). The patch load applications principally generate five types of idealised vertical compressive stress dissipations beneath pavers which are tetrahedral, short-pentahedral, long-pentahedral, partial-hexahedral and absolute-hexahedral as described in Chapters 6, 7 and 8. The solutions of these five vertical stress distributions were given in Chapter 6 for rectangular pavers. The solutions of the vertical compressive stress regimes for proprietory shaped pavers (see Figure 5.1) are particularly complex so iterative solutions have been used in their evaluations. The numerical solutions have been conducted by using Mathematica[1], Maple[2] and Nag[3] mathematical software. However the arithmetical solutions to the absolute-hexahedral case have been calculated for each proprietory shaped paver (see Chapters 7 and 8). For this reason the evaluations of the patch loads' integrals relating only to the absolute-hexahedral stress cases are documented in this Section for the proprietory shaped paver 3.

Figure 5.25 illustrates the special patch load application 1 for the proprietory shaped paver 3. **Line 1** scans the paver between corners **e** and **g** in terms of the variable distance **a** in the x direction. It may be recalled that each shaped paver is of a circumscribing rectangular border. If x, y transverse and longitudinal axes have their original corner **A** of this circumscribing rectangular shape, it can be seen that each corner of the actual paver is connected by lines which form the real shape of the paver. The functions of these lines can be calculated using basic geometrical rules. The boundary line functions for the proprietory shaped paver 3 are shown in Table 5.5.

In Table 5.5 the first letters of each line function characterise the corner names as can be seen in Figure 5.25. By using the line functions in Table 5.5 shaped paver 3 and the line functions which define the patch load boundaries, which are of the form

$f_y = b(1-\frac{x}{a})$, $f_x = a(1-\frac{y}{b})$ in the x and y axes, the intersection points between the paver boundary lines and the load patch boundary line can be calculated mathematically. Table 5.6 shows the intersection points which can be seen in Figures 5.25 to 5.27.

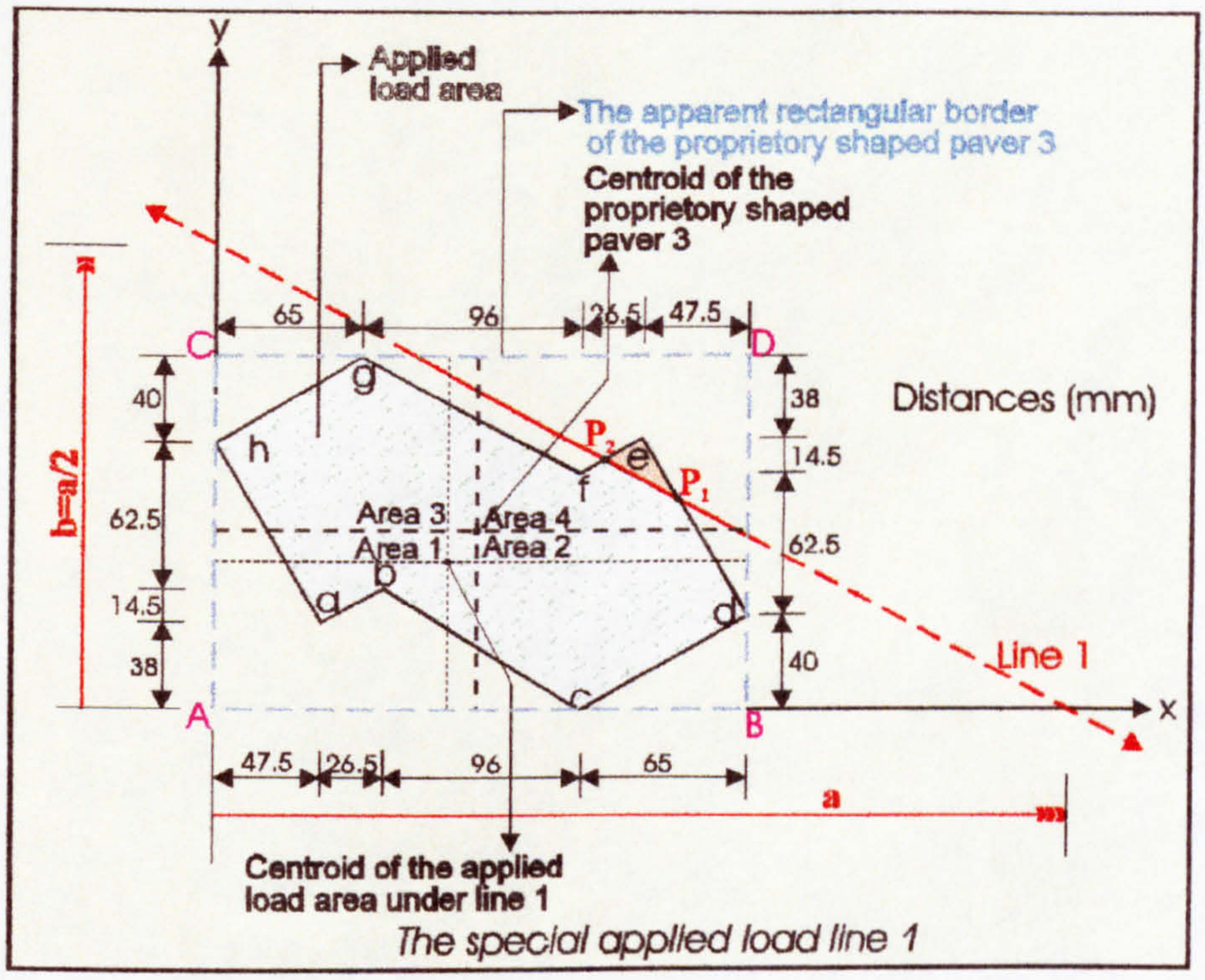

Figure 5.25: The selected special patch load application 1 for proprietory shaped paver 3.

$abx = \frac{26.5y - 318.25}{14.5}$ $aby = \frac{318.25 + 14.5x}{26.5}$	$bcx = \frac{8925 - 96y}{52.5}$ $bcy = \frac{8925 - 52.5x}{96}$	$cdx = \frac{6800 + 65y}{40}$ $cdy = \frac{40x - 6800}{65}$
$dex = \frac{19995 - 47.5y}{77}$ $dey = \frac{19995 - 77x}{47.5}$	$efx = \frac{26.5y - 381.75}{14.5}$ $efy = \frac{14.5x + 381.75}{26.5}$	$fgx = \frac{18292.5 - 96y}{52.5}$ $fgy = \frac{18292.5 - 52.5x}{96}$
$ghx = \frac{65y - 7475}{40}$ $ghy = \frac{40x + 7475}{65}$	$hax = \frac{5462.5 - 47.5y}{77}$ $hay = \frac{5462.5 - 77x}{47.5}$	

Table 5.5: Boundary line functions for proprietory shaped paver 3.

$P_{1y} = 0.725a - 188.174$	$P_{2y} = 0.261a + 6.875$
$P_{1x} = 375.848 - 0.446a$	$P_{2x} = 0.476a - 13.724$
$P_{3y} = 5.882a - 2049.588$	$P_{4y} = 0.275a + 51.482$
$P_{3x} = 3811 - 10a$	$P_{4x} = 0.446a - 102.679$

Table 5.6: The intersection points between the lines which form the patch load boundary with distances a and b (b=a/2) in the x and y directions and line functions bounding the proprietory shaped paver 3.

The surface area and centroid distances for the system illustrated in Figure 5.25 can be calculated using the data in Table 5.5 and Table 5.6 and are as follows:

$$F = \int_0^a fy\,dx - \int_{235}^a fy\,dx - \int_{170}^{235} cdy\,dx - \int_{P_{1x}}^{235} fy\,dx + \int_{P_{1x}}^{235} dey\,dx - \int_{161}^{P_{2x}} fy\,dx + \int_{161}^{P_{2x}} efy\,dx - \int_0^{161} fy\,dx$$

$$+ \int_0^{65} ghy\,dx + \int_{65}^{161} fgy\,dx - \int_0^{47.5} hay\,dx - \int_{47.5}^{74} aby\,dx - \int_{74}^{170} bcy\,dx$$

The evaluation of the integrals yields the following equation:

$$F = 0.230871(709.276 - a)(-133.727 + a)$$

$$\overline{X} = \frac{1}{F}\left[\begin{array}{l} \int_0^a x\,fy\,dx - \int_{235}^a x\,fy\,dx - \int_{170}^{235} x\,cdy\,dx - \int_{P_{1x}}^{235} x\,fy\,dx + \int_{P_{1x}}^{235} x\,dey\,dx - \int_{161}^{P_{2x}} x\,fy\,dx \\ + \int_{161}^{P_{2x}} x\,efy\,dx - \int_0^{161} x\,fy\,dx + \int_0^{65} x\,ghy\,dx + \int_{65}^{161} x\,fgy\,dx - \int_0^{47.5} x\,hay\,dx - \int_{47.5}^{74} x\,aby\,dx \\ - \int_{74}^{170} x\,bcy\,dx \end{array}\right]$$

The evaluation of the integrals yields the following equation:

$$\overline{X} = \frac{0.0104878(-647.884+a)(-192.216+a)(17453.4+a)}{(-709.274+a)(-133.727+a)}$$

$$\overline{Y} = \frac{1}{F}\left[\begin{array}{l} \int_0^b y\,fx\,dy - \int_{155}^b y\,fx\,dy - \int_{115}^{155} y\,ghx\,dy - \int_{P_{2y}}^{155} y\,fx\,dy + \int_{P_{2y}}^{155} y\,fgx\,dy - \int_{102.5}^{P_{2y}} y\,efx\,dy \\ + \int_{102.5}^{P_{2y}} y\,fgx\,dy - \int_{38}^{52.5} y\,bcx\,dy + \int_{38}^{52.5} y\,abx\,dy - \int_{0}^{38} y\,bcx\,dy - \int_{0}^{40} y\,fx\,dy + \int_{0}^{40} y\,cdx\,dy \\ - \int_{40}^{P_{1y}} y\,fx\,dy + \int_{40}^{P_{1y}} y\,dex\,dy - \int_{38}^{115} y\,hax\,dy \end{array}\right]$$

The evaluation of the integrals yields the following equation:

$$\overline{Y} = \frac{0.328085(-610.801+a)(50901.1-297.09a+a^2)}{(-709.274+a)(-133.727+a)}$$

Line 1 in Figure 5.25 scans the paver between corners **e** and **g**. It should therefore be noted that for the solutions above to be valid for the patch load application 1, the variable distance **a** in the x direction must lie in the range: 421.5>a>375mm.

Figure 5.26 illustrates the special patch load application 2 for the proprietory shaped paver 3. **Line 2** scans the paver between corners **g** and **f** in terms of the variable distance **a** in the x direction. By using the paver line functions in Table 5.5, the equations of the intersection points in Table 5.6 and the patch load boundary line function which is $f_y = b(1-\frac{x}{a})$, $f_x = a(1-\frac{y}{b})$ in the x and y axes, the special patch load's surface area and centroid distances can be calculated as follows:

$$F = \int_0^a fy\,dx - \int_{235}^a fy\,dx - \int_{170}^{235} cdy\,dx - \int_{P_{1x}}^{235} fy\,dx + \int_{P_{1x}}^{235} dey\,dx - \int_{161}^{P_{2x}} fy\,dx + \int_{161}^{P_{2x}} efy\,dx - \int_{P_{3x}}^{161} fy\,dx$$

$$+\int_{P_{3x}}^{161} fgy\,dx - \int_{0}^{P_{4x}} fy\,dx + \int_{0}^{P_{4x}} ghy\,dx - \int_{0}^{47.5} hay\,dx - \int_{47.5}^{74} aby\,dx - \int_{74}^{170} bcy\,dx$$

The evaluation of the integrals yields the following equation:

$$F = 3.0094(457.31 - a)(-299.829 + a)$$

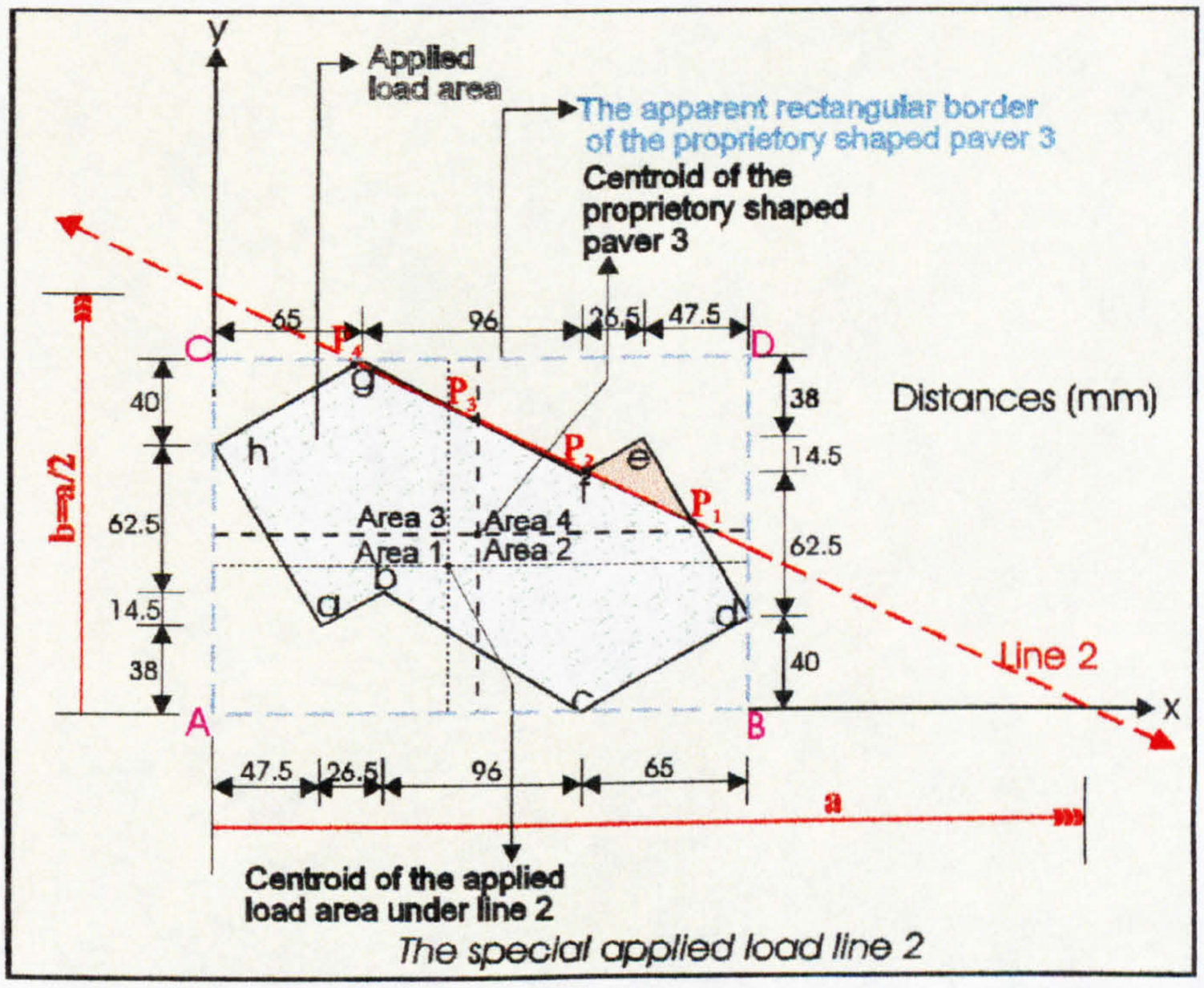

Figure 5.26: The selected special patch load application 2 for proprietory shaped paver 3.

$$\overline{X} = \frac{1}{F}\left[\begin{aligned}&\int_{0}^{a} x\,fy\,dx - \int_{235}^{a} x\,fy\,dx - \int_{170}^{235} x\,cdy\,dx - \int_{P_{1x}}^{235} x\,fy\,dx + \int_{P_{1x}}^{235} x\,dey\,dx - \int_{161}^{P_{2x}} x\,fy\,dx \\ &+ \int_{161}^{P_{2x}} x\,efy\,dx - \int_{P_{3x}}^{161} x\,fy\,dx + \int_{P_{3x}}^{161} x\,fgy\,dx - \int_{0}^{P_{4x}} x\,fy\,dx + \int_{0}^{P_{4x}} x\,ghy\,dx - \int_{0}^{47.5} x\,hay\,dx \\ &- \int_{47.5}^{74} x\,aby\,dx - \int_{74}^{170} x\,bcy\,dx\end{aligned}\right]$$

The evaluation of the integrals yields the following equation:

$$\overline{X} = \frac{3.11946(322.706-a)\left(173520-825.984a+a^2\right)}{(-457.433+a)(-299.684+a)}$$

$$\overline{Y} = \frac{1}{F}\left[\int_0^b y\,fx\,dy - \int_{P_{4y}}^{b} y\,fx\,dy - \int_{115}^{P_{4y}} y\,ghx\,dy - \int_{P_{2y}}^{P_{3y}} y\,fx\,dy + \int_{P_{2y}}^{P_{3y}} y\,fgx\,dy - \int_{102.5}^{P_{2y}} y\,efx\,dy\right.$$

$$+ \int_{102.5}^{P_{2y}} y\,fgx\,dy - \int_{38}^{52.5} y\,bcx\,dy + \int_{38}^{52.5} y\,abx\,dy - \int_{0}^{38} y\,bcx\,dy - \int_{0}^{40} y\,fx\,dy + \int_{0}^{40} y\,cdx\,dy$$

$$\left. - \int_{40}^{P_{1y}} y\,fx\,dy + \int_{40}^{P_{1y}} y\,dex\,dy - \int_{38}^{115} y\,hax\,dy\right]$$

The evaluation of the integrals yields the following equation:

$$\overline{Y} = \frac{1.90508(-421.264+a)\left(99429.6-625.759a+a^2\right)}{(-457.31+a)(-299.829+a)}$$

Line 2 in Figure 5.26 scans the paver between corners **g** and **f**. It should therefore be noted that for the solutions above to be valid for the patch load application 2, the variable distance **a** in the x direction must lie in the range: 375>**a**>366mm.

Figure 5.27 illustrates the special patch load application 3 for the proprietory shaped paver 3. **Line 3** scans the paver between corners **f** and **h** in terms of the variable distance **a** in the x direction. By using the paver line functions in Table 5.5, the equations of the intersection points in Table 5.6 and the patch load boundary line function which is $f_y = b(1-\frac{x}{a})$, $f_x = a(1-\frac{y}{b})$ in the x and y axes, the special patch load's surface area and centroid distances can be calculated as follows:

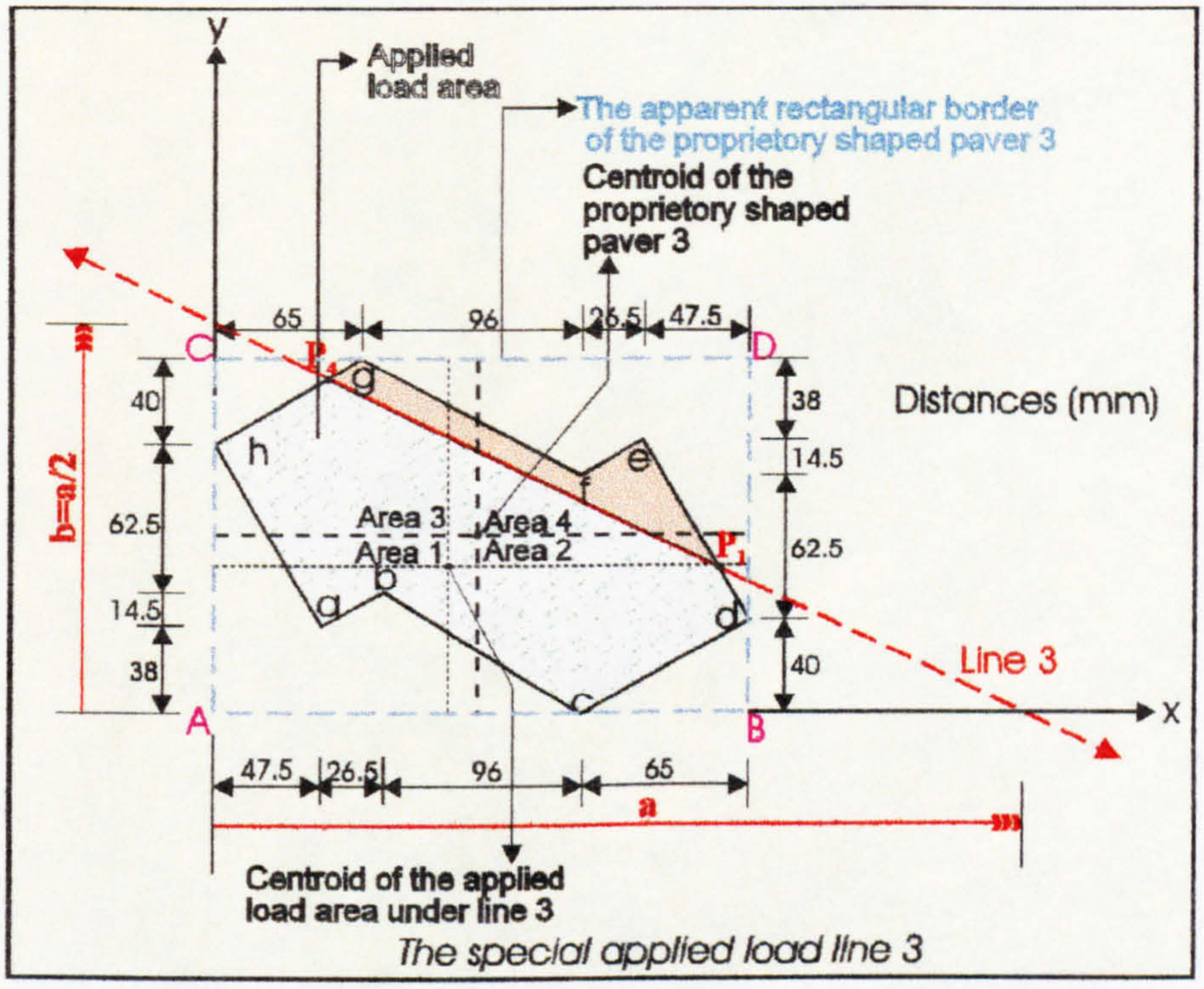

Figure 5.27: The selected special patch load application 3 for proprietory shaped paver 3.

$$F = \int_0^a fy\,dx - \int_{235}^a fy\,dx - \int_{170}^{235} cdy\,dx - \int_{P_{1x}}^{235} fy\,dx + \int_{P_{1x}}^{235} dey\,dx - \int_0^{P_{4x}} fy\,dx + \int_0^{P_{4x}} ghy\,dx - \int_0^{47.5} hay\,dx - \int_{47.5}^{74} aby\,dx - \int_{74}^{170} bcy\,dx$$

The evaluation of the integrals yields the following equation:

$$F = 0.22357(866.76 - a)(-203.587 + a)$$

$$\overline{X} = \frac{1}{F}\left[\int_0^a x\,fy\,dx - \int_{235}^a x\,fy\,dx - \int_{170}^{235} x\,cdy\,dx - \int_{P_{1x}}^{235} x\,fy\,dx + \int_{P_{1x}}^{235} x\,dey\,dx - \int_0^{P_{4x}} x\,fy\,dx + \int_0^{P_{4x}} x\,ghy\,dx - \int_0^{47.5} x\,hay\,dx - \int_{47.5}^{74} x\,aby\,dx - \int_{74}^{170} x\,bcy\,dx\right]$$

The evaluation of the integrals yields the following equation:

$$\overline{X} = \frac{0.000751889(-846.354+a)(-223.464+a)(181405-a)}{(-866.763+a)(-203.586+a)}$$

$$\overline{Y} = \frac{1}{F}\left[\int_0^b y\,fx\,dy - \int_{P_{4y}}^b y\,fx\,dy - \int_{115}^{P_{4y}} y\,ghx\,dy - \int_0^{40} y\,fx\,dy + \int_0^{40} y\,cdx\,dy - \int_{40}^{P_{1y}} y\,fx\,dy\right.$$

$$\left. + \int_{40}^{P_{1y}} y\,dex\,dy - \int_{38}^{52.5} y\,bcx\,dy + \int_{38}^{52.5} y\,abx\,dy - \int_0^{38} y\,bcx\,dy - \int_{38}^{115} y\,hax\,dy\right]$$

The evaluation of the integrals yields the following equation:

$$\overline{Y} = \frac{0.332952(-732.077+a)(-176.29+a)(-98.9176+a)}{(-866.76+a)(-203.587+a)}$$

Line 3 in Figure 5.27 scans the paver between corners **f** and **h**. It should therefore be noted that for the solutions above to be valid for the patch load application 3, the variable distance **a** in the x direction must lie in the range: 366>**a**>315mm.

5.5. The selected special patch load applied to proprietory shaped paver 4

Figure 5.28 illustrates one of the common patch load application to proprietory shaped paver 4 (see Figure 5.1). It may be recalled that in these common load applications, the lines which define the patch loading gradually scan the paver from its lower left corner to its upper right corner with distances **a** and **b** (**b**=**a**/2). The proprietory shaped paver 4 is analysed with the similar logic described previously (see Sections 5.2, 5.3 and 5.4). The patch load applications principally generate five types of idealised vertical compressive stress dissipations beneath pavers which are tetrahedral, short-pentahedral, long-pentahedral, partial-hexahedral and absolute-hexahedral as described in Chapters 6, 7 and 8. The solutions of these five vertical stress distributions were given in Chapter

6 for rectangular pavers. The solutions of the vertical compressive stress regimes for proprietory shaped pavers (see Figure 5.1) are particularly complex so iterative solutions have been used in their evaluations. The numerical solutions have been conducted by using Mathematica[1], Maple[2] and Nag[3] mathematical software. However the arithmetical solutions to the absolute-hexahedral case have been calculated for each proprietory shaped paver (see Chapters 7 and 8). For this reason the evaluations of the patch loads' integrals relating only to the absolute-hexahedral stress cases are documented in this Section for the proprietory shaped paver 4.

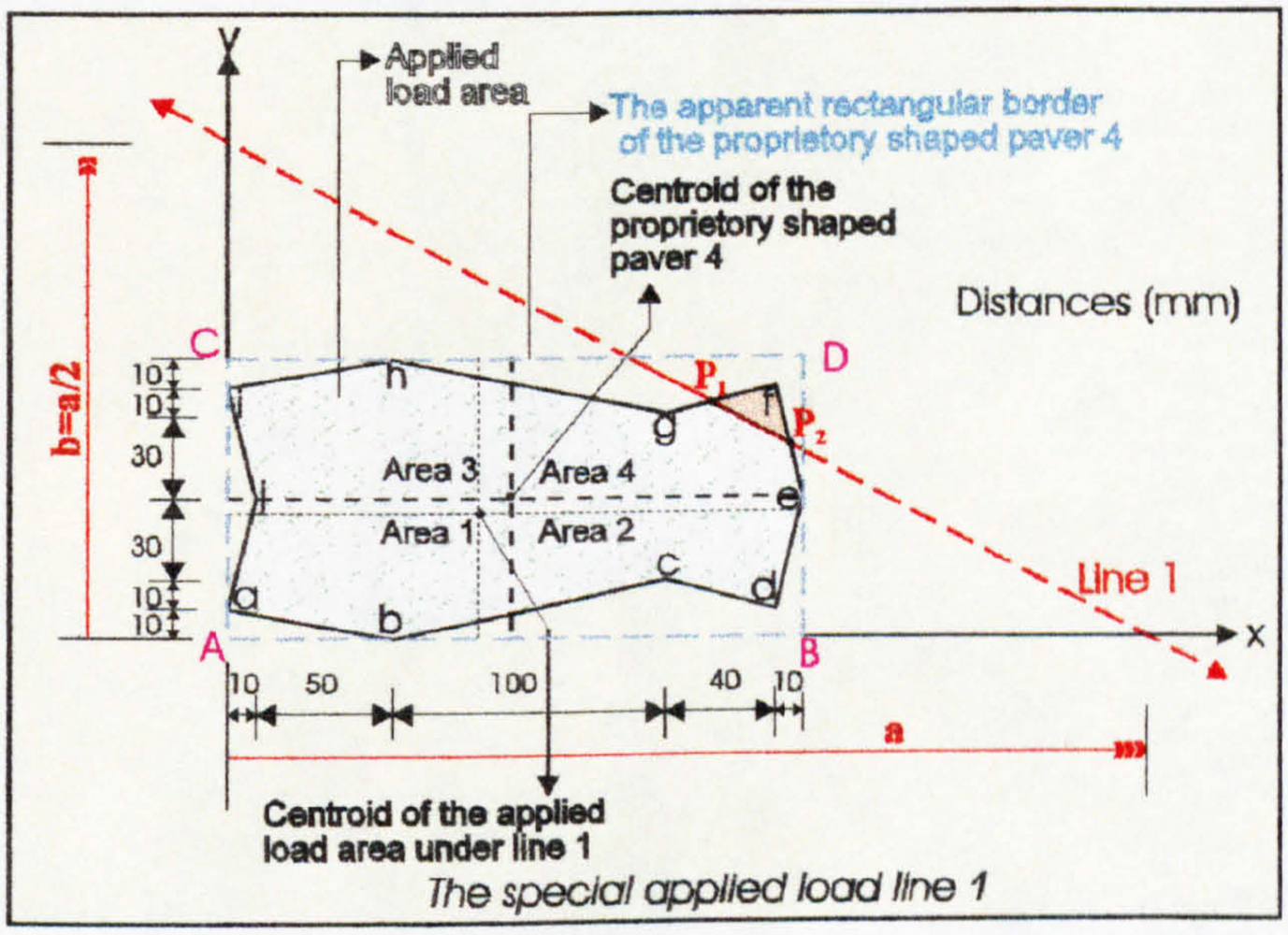

Figure 5.28: The selected special patch load application 1 for proprietory shaped paver 4.

Figure 5.28 illustrates the special patch load application 1 for the proprietory shaped paver 4. **Line 1** scans the paver between corners **f** and **e** in terms of the variable distance **a** in the x direction. It may be recalled that each shaped paver is of a circumscribing rectangular border. If x, y transverse and longitudinal axes have their original corner **A** of this circumscribing rectangular shape, it can be seen that each corner of the actual paver is connected by lines which form the real shape of the paver. The functions of these lines can be calculated using basic geometrical rules. The boundary line functions for the proprietory shaped paver 4 are shown in Table 5.7.

$abx = 60 - 6y$ $aby = 10 - 0.\overline{16}x$	$bcx = 60 + 5y$ $bcy = -12 + 0.2x$	$cdx = 240 - 4y$ $cdy = 60 - 0.25x$	$dex = 197.5 + 0.25y$ $dey = -790 + 4x$
$efx = 222.5 - 0.25y$ $efy = 890 - 4x$	$fgx = -160 + 4y$ $fgy = 40 + 0.25x$	$ghx = 560 - 5y$ $ghy = 112 - 0.2x$	$hix = -540 + 6y$ $hiy = 90 + 0.\overline{16}x$
$ijx = 22.5 - 0.25y$ $ijy = 90 - 4x$	$jax = -2.5 + 0.25y$ $jay = 10 + 4x$		

Table 5.7: Boundary line functions for proprietory shaped paver 4.

In Table 5.7 the first letters of each line function characterise the corner names as can be seen in Figure 5.28. By using the line functions in Table 5.7 shaped paver 4 and the line functions which define the patch load boundaries, which are of the form $f_y = b(1-\frac{x}{a})$, $f_x = a(1-\frac{y}{b})$ in the x and y axes, the intersection points between the paver boundary lines and the load patch boundary line can be calculated mathematically. Table 5.8 shows the intersection points which can be seen in Figures 5.28 to 5.30.

$P_{1y} = 26.\overline{6} + 0.1\overline{6}a$ $P_{1x} = 0.\overline{6}a - 53.\overline{3}$	$P_{2y} = -127.143 + 0.571a$ $P_{2x} = 254.286 - 0.143a$	$P_{3y} = 0.\overline{4}a - 87.\overline{7}$ $P_{3x} = 175.\overline{5} + 0.\overline{1}a$
$P_{4y} = 186.\overline{6} - 0.\overline{3}a$ $P_{4x} = -373.\overline{3} + 1.\overline{6}a$	$P_{5y} = 67.5 + 0.125a$ $P_{5x} = 0.75a - 135$	

Table 5.8: The intersection points between the lines which form the patch load boundary with distances **a** and **b** (**b**=**a**/2) in the x and y directions and line functions bounding the proprietory shaped paver 4.

The surface area and centroid distances for the system illustrated in Figure 5.28 can be calculated using the data in Table 5.7 and Table 5.8 and are as follows:

$$F = \int_0^a fy\,dx - \int_{210}^a fy\,dx - \int_{P_{2x}}^{210} cdy\,dx + \int_{P_{2x}}^{210} efy\,dx - \int_{200}^{210} dey\,dx - \int_{160}^{200} cdy\,dx - \int_{60}^{160} bcy\,dx - \int_0^{60} aby\,dx$$

The evaluation of the integrals yields the following equation:

$$F = 0.202381(662.926 - a)(-97.0741 + a)$$

$$\overline{X} = \frac{1}{F}\left[\begin{array}{l} \int_0^a x\,fy\,dx - \int_{210}^a x\,fy\,dx - \int_{P_{2x}}^{210} x\,cdy\,dx + \int_{P_{2x}}^{210} x\,efy\,dx - \int_{200}^{210} x\,dey\,dx - \int_{160}^{200} x\,cdy\,dx \\ -\int_{60}^{160} x\,bcy\,dx - \int_0^{60} x\,aby\,dx - \int_0^{10} x\,ijy\,dx + \int_0^{10} x\,jay\,dx - \int_0^{P_{1x}} x\,fy\,dx + \int_0^{60} x\,hiy\,dx \\ +\int_{60}^{160} x\,ghy\,dx + \int_{160}^{P_{1x}} x\,fgy\,dx \end{array}\right]$$

The evaluation of the integrals yields the following equation:

$$\overline{X} = \frac{0.174603(-564.586 + a)(-158.54 + a)(728.58 + a)}{(-662.926 + a)(-97.0741 + a)}$$

$$\overline{Y} = \frac{1}{F}\left[\begin{array}{l} \int_0^b y\,fx\,dy - \int_{100}^b y\,fx\,dy - \int_{90}^{100} y\,hix\,dy - \int_{P_{1y}}^{100} y\,fx\,dy + \int_{P_{1y}}^{100} y\,ghx\,dy - \int_{80}^{P_{1y}} y\,fgx\,dy \\ +\int_{80}^{P_{1y}} y\,ghx\,dy - \int_{50}^{90} y\,ijx\,dy - \int_{10}^{50} y\,jax\,dy - \int_0^{10} y\,abx\,dy - \int_0^{10} y\,fx\,dy + \int_0^{10} y\,bcx\,dy \\ -\int_{10}^{20} y\,cdx\,dy + \int_{10}^{20} y\,bcx\,dy - \int_{10}^{P_{2y}} y\,fx\,dy + \int_{10}^{50} y\,dex\,dy + \int_{50}^{P_{2y}} y\,efx\,dy \end{array}\right]$$

The evaluation of the integrals yields the following equation:

$$\overline{Y} = \frac{0.246032(-553.653 + a)\left(33084.2 - 220.54a + a^2\right)}{(-662.926 + a)(-97.0741 + a)}$$

Line 1 in Figure 5.28 scans the paver between corners **f** and **e**. It should therefore be noted that for the solutions above to be valid for the patch load application 1, the variable distance **a** in the x direction must lie in the range: 380>**a**>320mm.

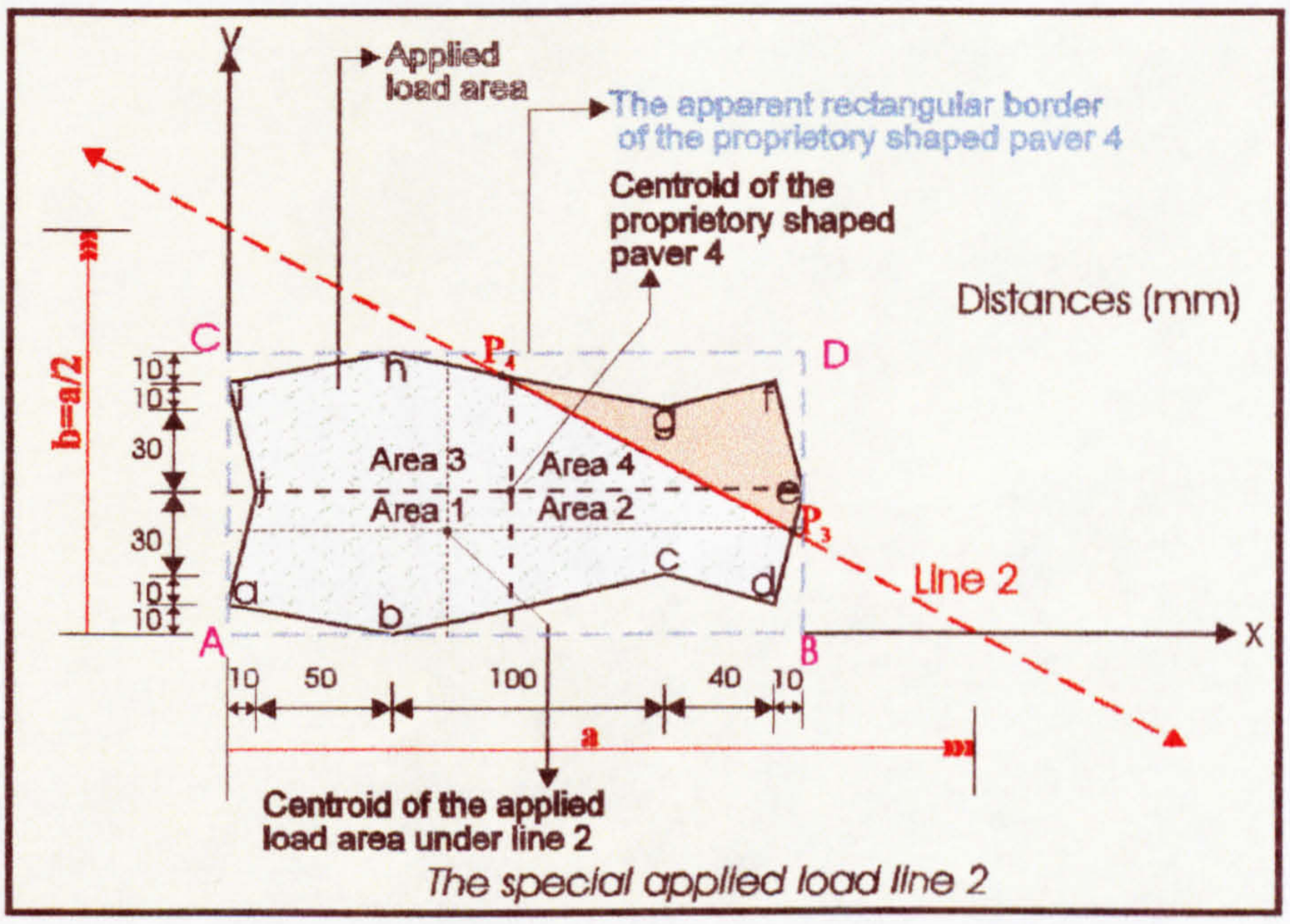

The special applied load line 2

Figure 5.29: The selected special patch load application 2 for proprietory shaped paver 4.

Figure 5.29 illustrates the special patch load application 2 for the proprietory shaped paver 4. **Line 2** scans the paver between corners **g** and **h** in terms of the variable distance **a** in the x direction. By using the paver line functions in Table 5.7, the equations of the intersection points in Table 5.8 and the patch load boundary line function which is $f_y = b(1-\frac{x}{a})$, $f_x = a(1-\frac{y}{b})$ in the x and y axes, the special patch load's surface area and centroid distances can be calculated as follows:

$$F = \int_0^a fy\,dx - \int_{200}^{P_{3x}} dey\,dx - \int_{P_{3x}}^{a} fy\,dx - \int_{160}^{200} cdy\,dx - \int_{60}^{160} bcy\,dx - \int_{0}^{60} aby\,dx - \int_{0}^{10} ijy\,dx + \int_{0}^{10} jay\,dx$$

$$- \int_{0}^{P_{4x}} ijy\,dx + \int_{0}^{60} hiy\,dx + \int_{60}^{P_{4x}} ghy\,dx$$

The evaluation of the integrals yields the following equation:

$$F = 0.388889(555.044 - a)(-150.67 + a)$$

$$\overline{X} = \frac{1}{F}\left[\begin{array}{l} \int_{0}^{a} x\,fy\,dx - \int_{200}^{P_{3x}} x\,dey\,dx - \int_{P_{3x}}^{a} x\,fy\,dx - \int_{160}^{200} x\,cdy\,dx - \int_{60}^{160} x\,bcy\,dx - \int_{0}^{60} x\,aby\,dx \\ -\int_{0}^{10} x\,ijy\,dx + \int_{0}^{10} x\,jay\,dx - \int_{0}^{P_{4x}} x\,ijy\,dx + \int_{0}^{60} x\,hiy\,dx + \int_{60}^{P_{4x}} x\,gly\,dx \end{array}\right]$$

The evaluation of the integrals yields the following equation:

$$\overline{X} = \frac{0.592593(-471.028 + a)(-143.37 + a)(-81.7627 + a)}{(-555.044 + a)(-150.67 + a)}$$

$$\overline{Y} = \frac{1}{F}\left[\begin{array}{l} \int_{0}^{b} y\,fx\,dy - \int_{100}^{b} y\,fx\,dy - \int_{90}^{100} y\,hix\,dy - \int_{P_{4y}}^{100} y\,fx\,dy + \int_{P_{4y}}^{100} y\,glx\,dy - \int_{50}^{90} y\,ijx\,dy \\ -\int_{10}^{50} y\,jax\,dy - \int_{0}^{10} y\,abx\,dy - \int_{0}^{10} y\,fx\,dy + \int_{0}^{10} y\,bcx\,dy - \int_{10}^{20} y\,cdx\,dy + \int_{10}^{20} y\,bcx\,dy \\ -\int_{10}^{P_{3y}} y\,fx\,dy + \int_{10}^{P_{3y}} y\,dex\,dy \end{array}\right]$$

The evaluation of the integrals yields the following equation:

$$\overline{Y} = \frac{0.037037(-516.683 + a)(-173.099 + a)(1495.5 + a)}{(-555.044 + a)(-150.67 + a)}$$

Line 2 in Figure 5.29 scans the paver between corners **g** and **h**. It should therefore be noted that for the solutions above to be valid for the patch load application 2, the variable distance **a** in the x direction must lie in the range: 310>**a**>260mm.

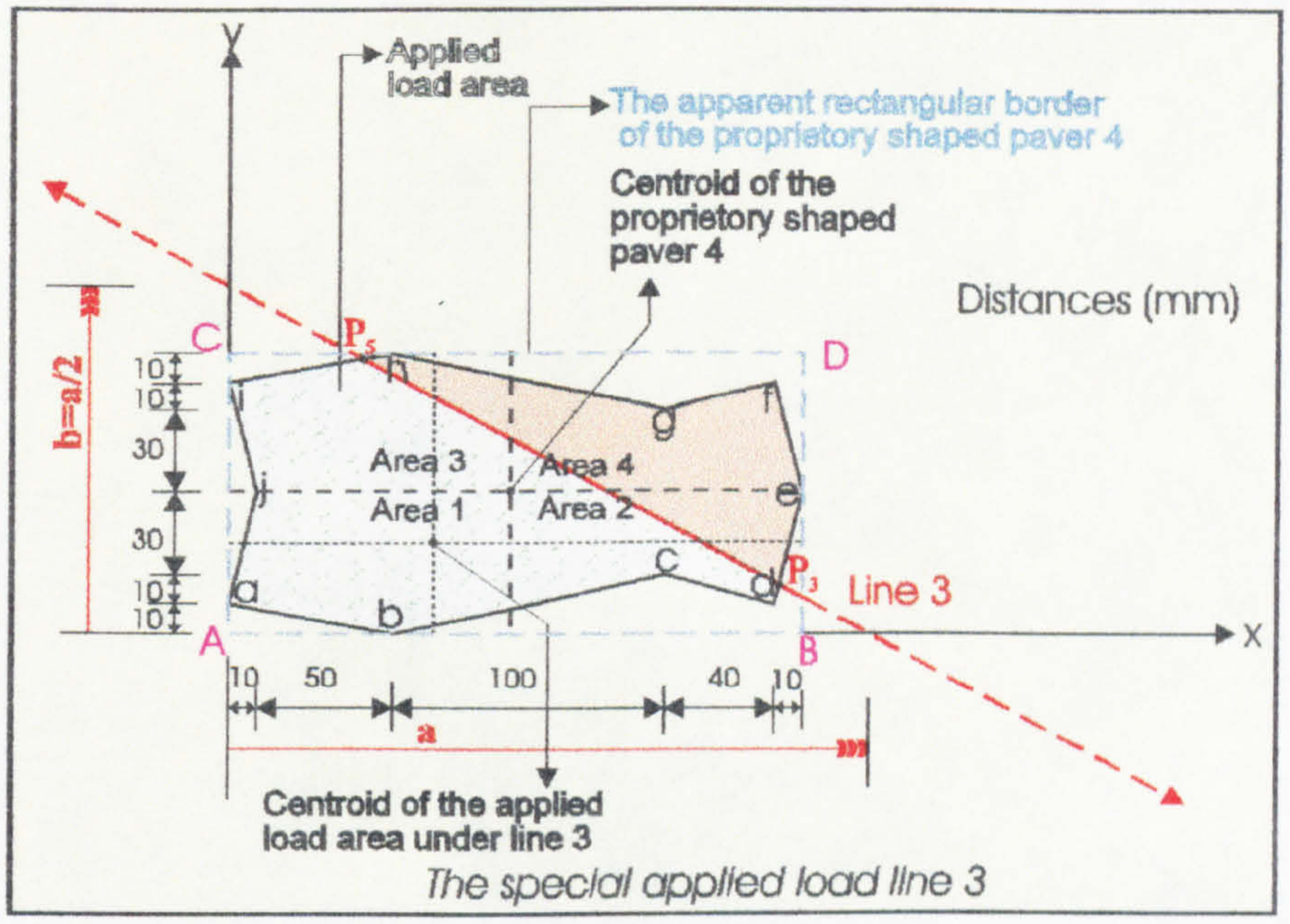

Figure 5.30: The selected special patch load application 3 for proprietory shaped paver 4.

Figure 5.30 illustrates the special patch load application 3 for the proprietory shaped paver 4. **Line 3** scans the paver between corners **h** and **d** in terms of the variable distance **a** in the x direction. By using the paver line functions in Table 5.7, the equations of the intersection points in Table 5.8 and the patch load boundary line function which is $f_y = b(1-\frac{x}{a})$, $f_x = a(1-\frac{y}{b})$ in the x and y axes, the special patch load's surface area and centroid distances can be calculated as follows:

$$F = \int_0^a fy\,dx - \int_{200}^{P_{3x}} dey\,dx - \int_{P_{3x}}^{a} fy\,dx - \int_{160}^{200} cdy\,dx - \int_{60}^{160} bcy\,dx - \int_0^{60} aby\,dx - \int_0^{10} ijy\,dx + \int_0^{10} jay\,dx$$
$$- \int_0^{P_{5x}} fy\,dx + \int_0^{P_{5x}} hiy\,dx$$

The evaluation of the integrals yields the following equation:

$$F = 0.159722(846.163 - a)(-126.011 + a)$$

$$\overline{X} = \frac{1}{F}\left[\begin{array}{l} \int_0^a x\,fy\,dx - \int_{200}^{P_{3x}} x\,dey\,dx - \int_{P_{3x}}^{a} x\,fy\,dx - \int_{160}^{200} x\,cdy\,dx - \int_{60}^{160} x\,bcy\,dx - \int_0^{60} x\,aby\,dx \\ -\int_0^{10} x\,ijy\,dx + \int_0^{10} x\,jay\,dx - \int_0^{P_{5x}} x\,fy\,dx + \int_0^{P_{5x}} x\,hiy\,dx \end{array}\right]$$

The evaluation of the integrals yields the following equation:

$$\overline{X} = \frac{0.287037(-710.099+a)(-155.008+a)(206.623+a)}{(-846.163+a)(-126.011+a)}$$

$$\overline{Y} = \frac{1}{F}\left[\begin{array}{l} \int_0^b y\,fx\,dy - \int_{P_{5y}}^{b} y\,fx\,dy - \int_{90}^{P_{5y}} y\,hix\,dy - \int_{50}^{90} y\,ijx\,dy - \int_{10}^{50} y\,jax\,dy - \int_0^{10} y\,abx\,dy \\ -\int_0^{10} y\,fx\,dy + \int_0^{10} y\,bcx\,dy - \int_{10}^{20} y\,cdx\,dy + \int_{10}^{20} y\,bcx\,dy - \int_{10}^{P_{3y}} y\,fx\,dy + \int_{10}^{P_{3y}} y\,dex\,dy \end{array}\right]$$

The evaluation of the integrals yields the following equation:

$$\overline{Y} = \frac{0.189815(-702.046+a)(-119.028+a)(38.5282+a)}{(-846.163+a)(-126.011+a)}$$

Line 3 in Figure 5.30 scans the paver between corners **h** and **d**. It should therefore be noted that for the solutions above to be valid for the patch load application 3, the variable distance **a** in the x direction must lie in the range: 260>**a**>220mm.

5.6. The selected special patch load applied to proprietory shaped paver 5

Figure 5.31 illustrates one of the common patch load application to proprietory shaped paver 5 (see Figure 5.1). It may be recalled that in these common load applications, the lines which define the patch loading gradually scan the paver from its lower left corner

to its upper right corner with distances **a** and **b** (**b=a/2**). The proprietory shaped paver 5 is analysed with the similar logic described previously (see Sections 5.2, 5.3, 5.4 and 5.5). The patch load applications principally generate five types of idealised vertical compressive stress dissipations beneath pavers which are tetrahedral, short-pentahedral, long-pentahedral, partial-hexahedral and absolute-hexahedral as described in Chapters 6, 7 and 8. The solutions of these five vertical stress distributions were given in Chapter 6 for rectangular pavers. The solutions of the vertical compressive stress regimes for proprietory shaped pavers (see Figure 5.1) are particularly complex so iterative solutions have been used in their evaluations. The numerical solutions have been conducted by using Mathematica[1], Maple[2] and Nag[3] mathematical software. However the arithmetical solutions to the absolute-hexahedral case have been calculated for each proprietory shaped paver (see Chapters 7 and 8). For this reason the evaluations of the patch loads' integrals relating only to the absolute-hexahedral stress cases are documented in this Section for the proprietory shaped paver 5.

Figure 5.31 illustrates the special patch load application 1 for the proprietory shaped paver 5. **Line 1** scans the paver between corners **e** and **f** in terms of the variable distance **a** in the x direction. It may be recalled that each shaped paver is of a circumscribing rectangular border. If x, y transverse and longitudinal axes have their original corner **A** of this circumscribing rectangular shape, it can be seen that each corner of the actual paver is connected by lines which form the real shape of the paver. The functions of these lines can be calculated using basic geometrical rules. The boundary line functions for the proprietory shaped paver 5 are shown in Table 5.9.

In Table 5.9 the first letters of each line function characterise the corner names as can be seen in Figure 5.31. By using the line functions in Table 5.9 shaped paver 5 and the line functions which define the patch load boundaries, which are of the form $f_y = b(1-\frac{x}{a})$, $f_x = a(1-\frac{y}{b})$ in the x and y axes, the intersection points between the paver boundary lines and the load patch boundary line can be calculated mathematically. Table 5.10 shows the intersection points which can be seen in Figures 5.31 and 5.32.

$abx = 3.\overline{6}y$ $aby = 0.\overline{27}x$	$bcx = 165 - 7.\overline{3}y$ $bcy = 22.5 - 0.1\overline{36}x$	$cdx = 165 + 3.\overline{6}y$ $cdy = -45 + 0.\overline{27}x$
$efx = -183.\overline{3} + 3.\overline{6}y$ $efy = 50 + 0.\overline{27}x$	$fgx = 861.\overline{6} - 7.\overline{3}y$ $fgy = 117.5 - 0.1\overline{36}x$	$ghx = -348.\overline{3} + 3.\overline{6}y$ $ghy = 95 + 0.\overline{27}x$

Table 5.9: Boundary line functions for proprietory shaped paver 5.

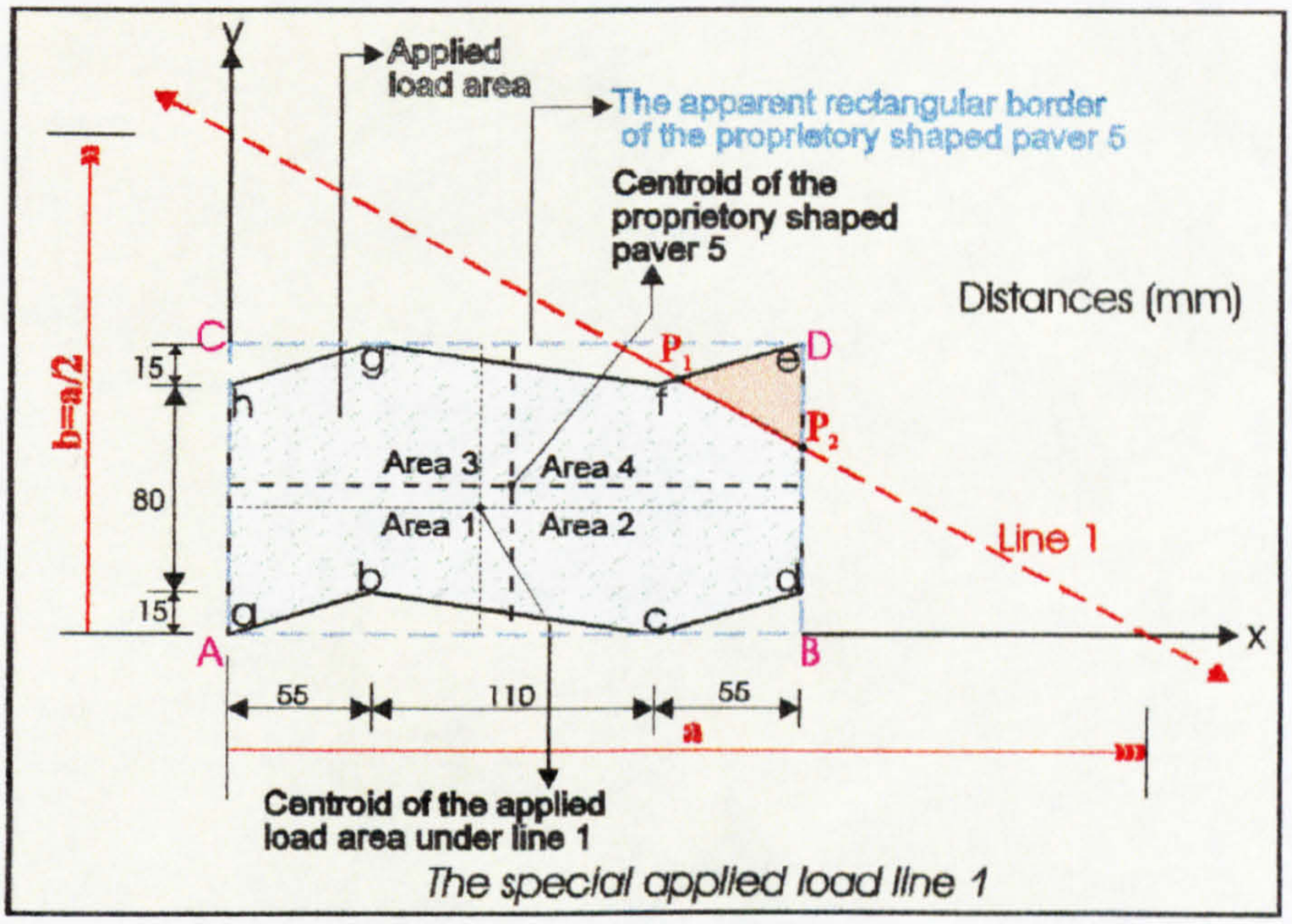

Figure 5.31: The selected special patch load application 1 for proprietory shaped paver 5.

$P_{1y} = 32.353 + 0.176a$ $P_{1x} = 0.647a - 64.706$	$P_{2y} = 0.5a - 110$ $P_{2x} = 220$	$P_{3y} = 161.55 - 0.1875a$ $P_{3x} = -323.125 + 1.375a$

Table 5.10: The intersection points between the lines which form the patch load boundary with distances **a** and **b** (**b**=**a**/2) in the x and y directions and line functions bounding the proprietory shaped paver 5.

The surface area and centroid distances for the system illustrated in Figure 5.31 can be calculated using the data in Table 5.9 and Table 5.10 and are as follows:

$$F = \int_0^a fy\,dx - \int_{220}^a fy\,dx - \int_{165}^{220} cdy\,dx - \int_{55}^{165} bcy\,dx - \int_0^{55} aby\,dx - \int_0^{P_{1x}} fy\,dx + \int_0^{55} ghy\,dx + \int_{55}^{165} fgy\,dx + \int_{165}^{P_{1x}} efy\,dx$$

The evaluation of the integrals yields the following equation:

$$F = 0.16177(799.426 - a)(-80.5503 + a)$$

$$\overline{X} = \frac{1}{F}\left[\int_0^a x\,fy\,dx - \int_{220}^a x\,fy\,dx - \int_{165}^{220} x\,cdy\,dx - \int_{55}^{165} x\,bcy\,dx - \int_0^{55} x\,aby\,dx - \int_0^{P_{1x}} x\,fy\,dx + \int_0^{55} x\,ghy\,dx + \int_{55}^{165} x\,fgy\,dx + \int_{165}^{P_{1x}} x\,efy\,dx\right]$$

The evaluation of the integrals yields the following equation:

$$\overline{X} = \frac{0.215694(669.612 - a)(-136.802 + a)(506.415 + a)}{-64394 + 879.976a - a^2}$$

$$\overline{Y} = \frac{1}{F}\left[\int_0^b y\,fx\,dy - \int_{110}^b y\,fx\,dy - \int_{95}^{110} y\,ghx\,dy - \int_{P_{1y}}^{110} y\,fx\,dy + \int_{P_{1y}}^{110} y\,fgx\,dy - \int_{95}^{P_{1y}} y\,efx\,dy + \int_{95}^{P_{1y}} y\,fgx\,dy - \int_0^{15} y\,bcx\,dy + \int_0^{15} y\,abx\,dy - \int_0^{P_{2y}} y\,fx\,dy + \int_0^{15} y\,cdx\,dy + \int_{15}^{P_{2y}} y\,220\,dy\right]$$

The evaluation of the integrals yields the following equation:

$$\overline{Y} = \frac{0.225481(652.185 - a)\left(34124.4 - 179.993a + a^2\right)}{-64394 + 879.976a - a^2}$$

Line 1 in Figure 5.31 scans the paver between corners **e** and **f**. It should therefore be noted that for the solutions above to be valid for the patch load application 1, the variable distance **a** in the x direction must lie in the range: 440>**a**>355mm.

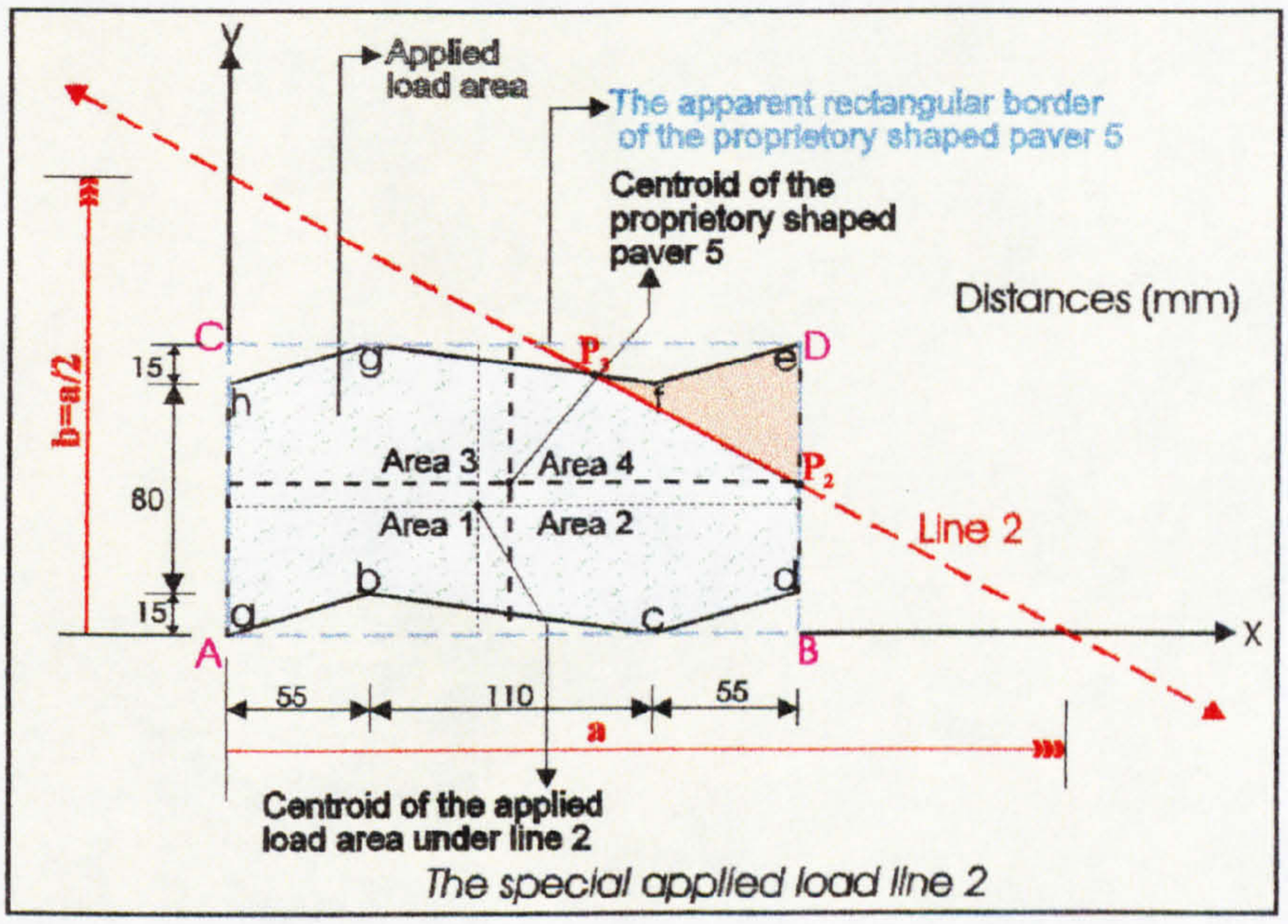

Figure 5.32: The selected special patch load application 2 for proprietory shaped paver 5.

Figure 5.32 illustrates the special patch load application 2 for the proprietory shaped paver 5. **Line 2** scans the paver between corners **f** and **d** in terms of the variable distance **a** in the x direction. By using the paver line functions in Table 5.9, the equations of the intersection points in Table 5.10 and the patch load boundary line function which is $f_y = b(1-\frac{x}{a})$, $f_x = a(1-\frac{y}{b})$ in the x and y axes, the special patch load's surface area and centroid distances can be calculated as follows:

$$F = \int_0^a fy\,dx - \int_{220}^a fy\,dx - \int_{165}^{220} cdy\,dx - \int_{55}^{165} bcy\,dx - \int_0^{55} aby\,dx - \int_0^{P_{3x}} fy\,dx + \int_0^{55} ghy\,dx + \int_{55}^{P_{3x}} fgy\,dx$$

The evaluation of the integrals yields the following equation:

$$F = 0.343747(637.904 - a)(-152.099 + a)$$

$$\overline{X} = \frac{1}{F}\left[\begin{array}{l} \int_0^a x\,fy\,dx - \int_{220}^a x\,fy\,dx - \int_{165}^{220} x\,cdy\,dx - \int_{55}^{165} x\,bcy\,dx - \int_0^{55} x\,aby\,dx - \int_0^{P_{3x}} x\,fy\,dx \\ + \int_0^{55} x\,ghy\,dx + \int_{55}^{P_{3x}} x\,fgy\,dx \end{array}\right]$$

The evaluation of the integrals yields the following equation:

$$\overline{X} = \frac{0.458329(543.217 - a)(-155.411 + a)(-6.37214 + a)}{-97024.7 + 790.003a - a^2}$$

$$\overline{Y} = \frac{1}{F}\left[\begin{array}{l} \int_0^b y\,fx\,dy - \int_{110}^b y\,fx\,dy - \int_{95}^{110} y\,ghx\,dy - \int_{P_{3y}}^{110} y\,fx\,dy + \int_{P_{3y}}^{110} y\,fgx\,dy - \int_0^{15} y\,bcx\,dy \\ + \int_0^{15} y\,abx\,dy - \int_0^{P_{2y}} y\,fx\,dy + \int_0^{15} y\,cdx\,dy + \int_{15}^{P_{2y}} y\,220\,dy \end{array}\right]$$

The evaluation of the integrals yields the following equation:

$$\overline{Y} = \frac{0.104166(568.271 - a)(-173.188 + a)(396.505 + a)}{-97024.7 + 790.003a - a^2}$$

Line 2 in Figure 5.32 scans the paver between corners **f** and **d**. It should therefore be noted that for the solutions above to be valid for the patch load application 2, the variable distance **a** in the x direction must lie in the range: 355>a>275mm.

5.7. The selected special patch load applied to proprietory shaped paver 6

Figure 5.33 illustrates one of the common patch load application to proprietory shaped paver 6 (see Figure 5.1). It may be recalled that in these common load applications, the lines which define the patch loading gradually scan the paver from its lower left corner to its upper right corner with distances **a** and **b** (**b=a/2**). The proprietory shaped paver 6 is analysed with the similar logic described previously (see Sections 5.2, 5.3, 5.4, 5.5 and 5.6). The patch load applications principally generate five types of idealised vertical compressive stress dissipations beneath pavers which are tetrahedral, short-pentahedral, long-pentahedral, partial-hexahedral and absolute-hexahedral as described in Chapters 6, 7 and 8. The solutions of these five vertical stress distributions were given in Chapter 6 for rectangular pavers. The solutions of the vertical compressive stress regimes for proprietory shaped pavers (see Figure 5.1) are particularly complex so iterative solutions have been used in their evaluations. The numerical solutions have been conducted by using Mathematica[1], Maple[2] and Nag[3] mathematical software. However the arithmetical solutions to the absolute-hexahedral case have been calculated for each proprietory shaped paver (see Chapters 7 and 8). For this reason the evaluations of the patch loads' integrals relating only to the absolute-hexahedral stress cases are documented in this Section for the proprietory shaped paver 6.

Figure 5.33 illustrates the special patch load application 1 for the proprietory shaped paver 6. **Line 1** scans the paver between corners **e** and **f** in terms of the variable distance **a** in the x direction. It may be recalled that each shaped paver is of a circumscribing rectangular border. If x, y transverse and longitudinal axes have their original corner **A** of this circumscribing rectangular shape, it can be seen that each corner of the actual paver is connected by lines which form the real shape of the paver. The functions of these lines can be calculated using basic geometrical rules. The boundary line functions for the proprietory shaped paver 6 are shown in Table 5.11.

In Table 5.11 the first letters of each line function characterise the corner names as can be seen in Figure 5.33. By using the line functions in Table 5.11 shaped paver 6 and the line functions which define the patch load boundaries, which are of the form

$f_y = b(1-\frac{x}{a})$, $f_x = a(1-\frac{y}{b})$ in the x and y axes, the intersection points between the paver boundary lines and the load patch boundary line can be calculated mathematically. Table 5.12 shows the intersection points which can be seen in Figures 5.33 to 5.35.

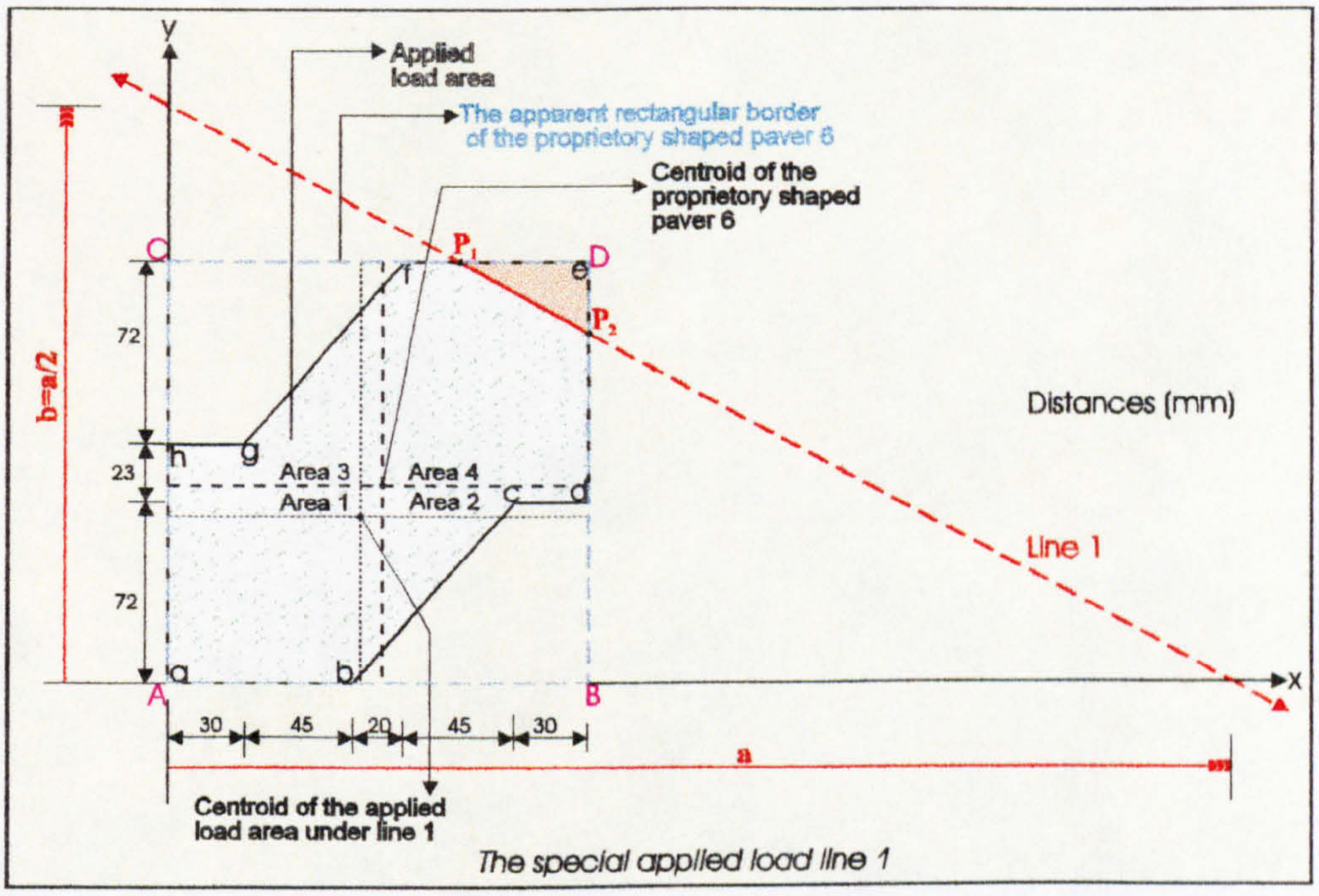

The special applied load line 1

Figure 5.33: The selected special patch load application 1 for proprietory shaped paver 6.

$bcx = 75 + 0.9027y$	$fgx = -55.7639 + 0.9027y$
$bcy = -83.077 + 1.1077x$	$fgy = 61.769 + 1.1077x$

Table 5.11: Boundary line functions for proprietory shaped paver 6.

$P_{1x} = a - 334$ $P_{1y} = 167$	$P_{2y} = 05a - 85$ $P_{2x} = 170$
$P_{3y} = 0.3445a + 19.211$ $P_{3x} = 0.311a - 38.421$	$P_{4y} = 72$ $P_{4x} = a - 144$

Table 5.12: The intersection points between the lines which form the patch load boundary with distances **a** and **b** (**b**=**a**/2) in the x and y directions and line functions bounding the proprietory shaped paver 6.

The surface area and centroid distances for the system illustrated in Figure 5.33 can be calculated using the data in Table 5.11 and Table 5.12 and are as follows:

$$F = \int_0^a fy\,dx - \int_{170}^a fy\,dx - \int_{140}^{170} 72\,dx - \int_{75}^{140} bcy\,dx - \int_0^{P_{1x}} fy\,dx + \int_0^{30} 95\,dx + \int_{30}^{95} fgy\,dx + \int_{95}^{P_{1x}} 167\,dx$$

The evaluation of the integrals yields the following equation:

$$F = -44114 + 252a - \frac{a^2}{4}$$

$$\overline{X} = \frac{1}{F}\left[\int_0^a x\,fy\,dx - \int_{170}^a x\,fy\,dx - \int_{140}^{170} x\,72\,dx - \int_{75}^{140} x\,bcy\,dx - \int_0^{P_{1x}} x\,fy\,dx + \int_0^{30} x\,95\,dx + \int_{30}^{95} x\,fgy\,dx + \int_{95}^{P_{1x}} x\,167\,dx\right]$$

The evaluation of the integrals yields the following equation:

$$\overline{X} = \frac{-18253704 + 247968a - 1002a^2 + a^3}{3\left(176456 - 1008a + a^2\right)}$$

$$\overline{Y} = \frac{1}{F}\left[\int_0^b y\,fx\,dy - \int_{167}^b y\,fx\,dy - \int_{95}^{167} y\,fgx\,dy - \int_0^{P_{2y}} y\,fx\,dy + \int_{72}^{P_{2y}} y\,170\,dy + \int_0^{72} y\,bcx\,dy\right]$$

The evaluation of the integrals yields the following equation:

$$\overline{Y} = \frac{87642408 - 247968a - 510a^2 + a^3}{6\left(176456 - 1008a + a^2\right)}$$

Line 1 in Figure 5.33 scans the paver between corners **e** and **f**. It should therefore be noted that for the solutions above to be valid for the patch load application 1, the variable distance **a** in the x direction must lie in the range: 504>**a**>429mm.

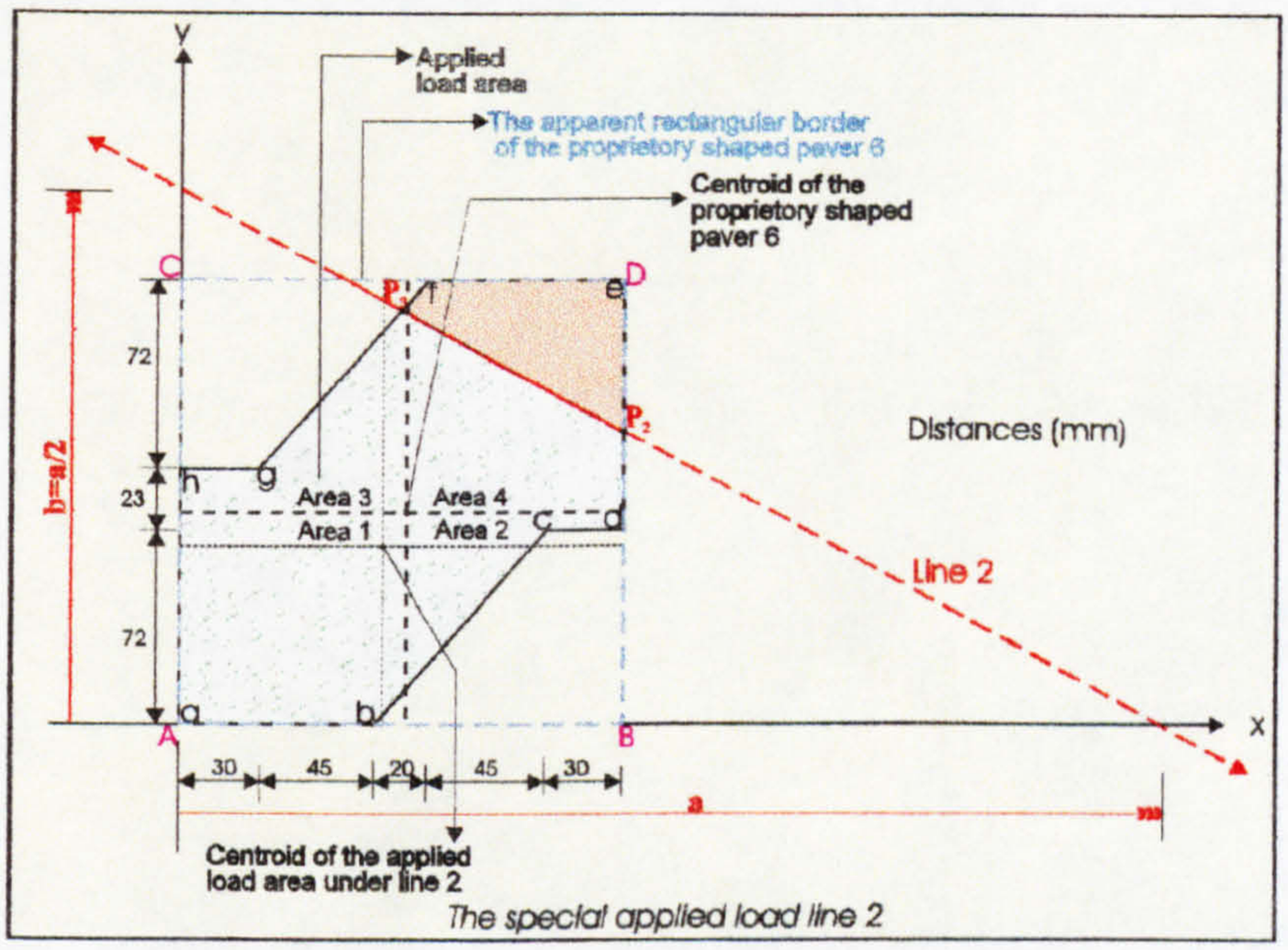

Figure 5.34: The selected special patch load application 2 for proprietory shaped paver 6.

Figure 5.34 illustrates the special patch load application 2 for the proprietory shaped paver 6. **Line 2** scans the paver between corners **f** and **d** in terms of the variable distance **a** in the x direction. By using the paver line functions in Table 5.11, the equations of the intersection points in Table 5.12 and the patch load boundary line function which is $f_y = b(1-\frac{x}{a})$, $f_x = a(1-\frac{y}{b})$ in the x and y axes, the special patch load's surface area and centroid distances can be calculated as follows:

$$F = \int_0^a fy\,dx - \int_{170}^a fy\,dx - \int_{140}^{170} 72\,dx - \int_{75}^{140} bcy\,dx - \int_0^{P_{3x}} fy\,dx + \int_0^{30} 95\,dx + \int_{30}^{P_{3x}} fgy\,dx$$

The evaluation of the integrals yields the following equation:

$$F = -12413.2 + 104.211a - 0.0777512a^2$$

$$\overline{X} = \frac{1}{F}\left[\int_0^a x\,fy\,dx - \int_{170}^{a} x\,fy\,dx - \int_{140}^{170} x\,72\,dx - \int_{75}^{140} x\,bcy\,dx - \int_0^{P_{3x}} x\,fy\,dx + \int_0^{30} x\,95\,dx + \int_{30}^{P_{3x}} x\,fgy\,dx\right]$$

The evaluation of the integrals yields the following equation:

$$\overline{X} = \frac{0.103668(-1031.01+a)(-197.764+a)(858.155+a)}{(-1208.16+a)(-132.145+a)}$$

$$\overline{Y} = \frac{1}{F}\left[\int_0^b y\,fx\,dy - \int_{P_{3y}}^{b} y\,fx\,dy - \int_{95}^{P_{3y}} y\,fgx\,dy - \int_0^{P_{2y}} y\,fx\,dy + \int_{72}^{P_{2y}} y\,170\,dy + \int_0^{72} y\,bcx\,dy\right]$$

The evaluation of the integrals yields the following equation:

$$\overline{Y} = \frac{0.281499(-963.496+a)(-128.954+a)(-29.6354+a)}{(-1208.16+a)(-132.145+a)}$$

Line 2 in Figure 5.34 scans the paver between corners **f** and **d**. It should therefore be noted that for the solutions above to be valid for the patch load application 2, the variable distance **a** in the **x** direction must lie in the range: 429>**a**>314mm.

Figure 5.35 illustrates the special patch load application 3 for the proprietory shaped paver 6. **Line 3** scans the paver between corners **d** and **c** in terms of the variable distance **a** in the **x** direction. By using the paver line functions in Table 5.11, the equations of the intersection points in Table 5.12 and the patch load boundary line

function which is $f_y = b(1-\frac{x}{a})$, $f_x = a(1-\frac{y}{b})$ in the x and y axes, the special patch load's surface area and centroid distances can be calculated as follows:

$$F = \int_0^a fy\,dx - \int_{P_{4x}}^a fy\,dx - \int_{140}^{P_{4x}} 72\,dx - \int_{75}^{140} bcy\,dx - \int_0^{P_{3x}} fy\,dx + \int_0^{30} 95\,dx + \int_{30}^{P_{3x}} fgy\,dx$$

The evaluation of the integrals yields the following equation:

$$F = 12235.8 - 52.7895a + 0.172249a^2$$

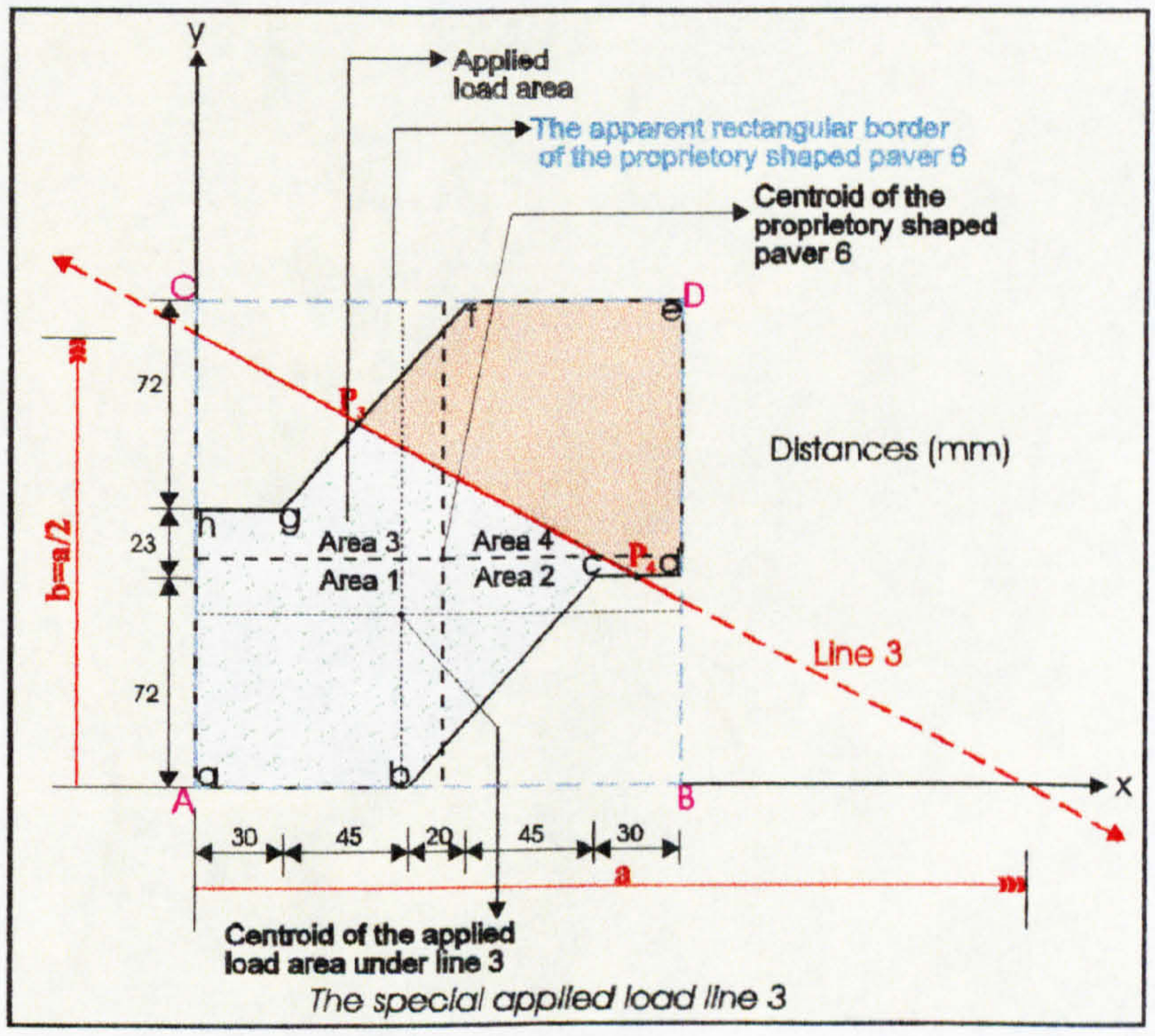

Figure 5.35: The selected special patch load application 3 for proprietory shaped paver

6.

$$\overline{X} = \frac{1}{F}\left[\int_0^a x\,fy\,dx - \int_{P_{4x}}^a x\,fy\,dx - \int_{140}^{P_{4x}} x\,72\,dx - \int_{75}^{140} x\,bcy\,dx - \int_0^{P_{3x}} x\,fy\,dx + \int_0^{30} x\,95\,dx\right.$$

$$+\int_{30}^{P_{3x}} x\,fgy\,dx\Bigg]$$

The evaluation of the integrals yields the following equation:

$$\overline{X}=\frac{0.437002(33.3447+a)\left(79702.5-471.918a+a^2\right)}{71035.9-306.472a+a^2}$$

$$\overline{Y}=\frac{1}{F}\left[\int_0^b y\,fx\,dy-\int_{P_{3y}}^b y\,fx\,dy-\int_{95}^{P_{3y}} y\,fgx\,dy-\int_0^{72} y\,fx\,dy+\int_0^{72} y\,bcx\,dy\right]$$

The evaluation of the integrals yields the following equation:

$$\overline{Y}=\frac{0.114833(513.085+a)\left(55707-345.793a+a^2\right)}{71035.9-306.472a+a^2}$$

Line 3 in Figure 5.35 scans the paver between corners **d** and **c**. It should therefore be noted that for the solutions above to be valid for the patch load application 3, the variable distance **a** in the x direction must lie in the range: **314>a>284mm.**

5.8. The selected special patch load applied to proprietory shaped paver 7

Figure 5.36 illustrates one of the common patch load application to proprietory shaped paver 7 (see Figure 5.1). It may be recalled that in these common load applications, the lines which define the patch loading gradually scan the paver from its lower left corner to its upper right corner with distances **a** and **b** (**b=a/2**). The proprietory shaped paver 7 is analysed with the similar logic described previously (see Sections 5.2, 5.3, 5.4, 5.5, 5.6 and 5.7). The patch load applications principally generate five types of idealised vertical compressive stress dissipations beneath pavers which are tetrahedral, short-pentahedral, long-pentahedral, partial-hexahedral and absolute-hexahedral as described

in Chapters 6, 7 and 8. The solutions of these five vertical stress distributions were given in Chapter 6 for rectangular pavers. The solutions of the vertical compressive stress regimes for proprietory shaped pavers (see Figure 5.1) are particularly complex so iterative solutions have been used in their evaluations. The numerical solutions have been conducted by using Mathematica[1], Maple[2] and Nag[3] mathematical software. However the arithmetical solutions to the absolute-hexahedral case have been calculated for each proprietory shaped paver (see Chapters 7 and 8). For this reason the evaluations of the patch loads' integrals relating only to the absolute-hexahedral stress cases are documented in this Section for the proprietory shaped paver 7.

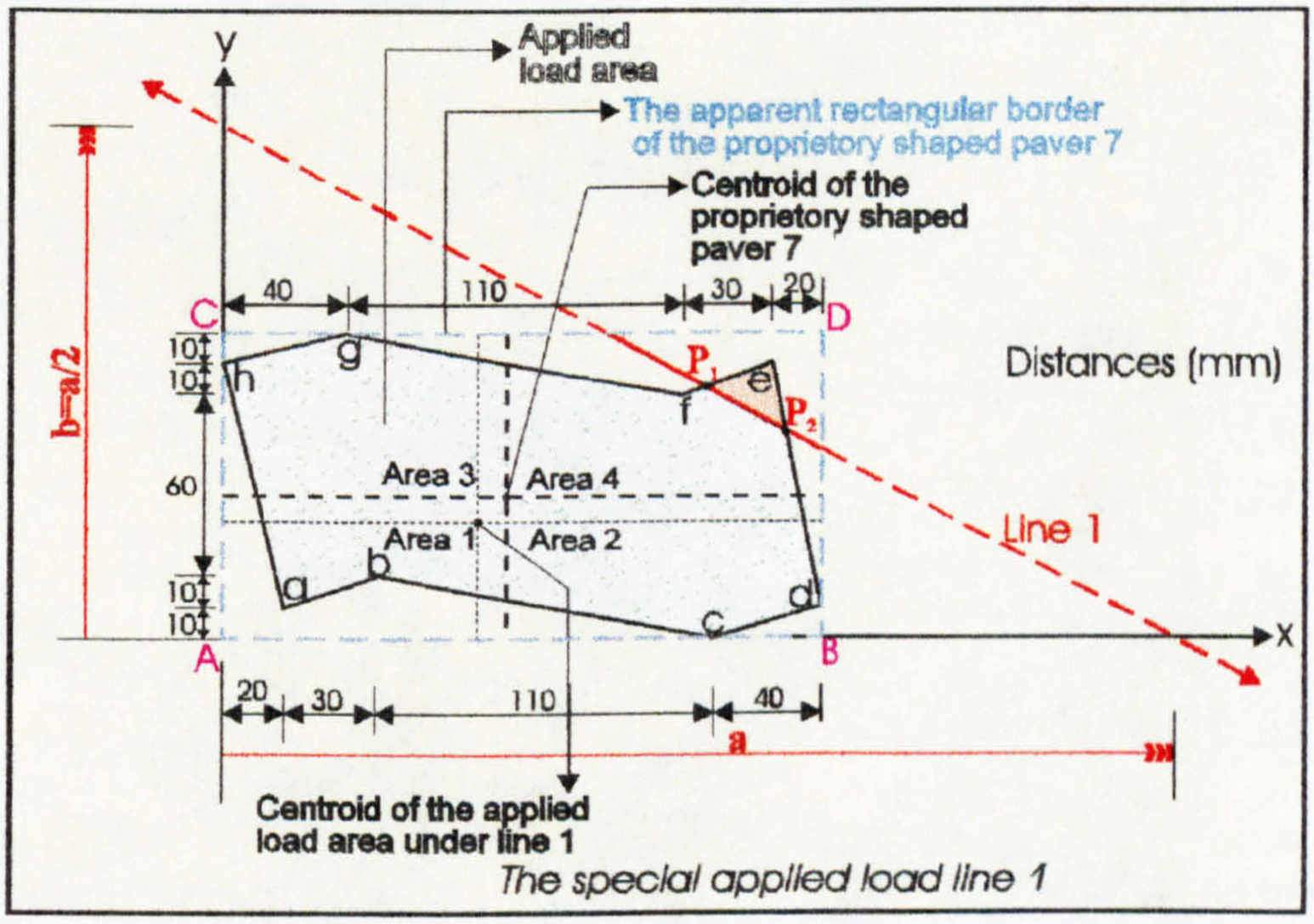

Figure 5.36: The selected special patch load application 1 for proprietory shaped paver 7.

Figure 5.36 illustrates the special patch load application 1 for the proprietory shaped paver 7. **Line 1** scans the paver between corners **e** and **f** in terms of the variable distance **a** in the x direction. It may be recalled that each shaped paver is of a circumscribing rectangular border. If x, y transverse and longitudinal axes have their original corner **A** of this circumscribing rectangular shape, it can be seen that each corner of the actual paver is connected by lines which form the real shape of the paver. The functions of

these lines can be calculated using basic geometrical rules. The boundary line functions for the proprietory shaped paver 7 are shown in Table 5.13.

In Table 5.13 the first letters of each line function characterise the corner names as can be seen in Figure 5.36. By using the line functions in Table 5.13 shaped paver 7 and the line functions which define the patch load boundaries, which are of the form $f_y = b(1-\frac{x}{a})$, $f_x = a(1-\frac{y}{b})$ in the x and y axes, the intersection points between the paver boundary lines and the load patch boundary line can be calculated mathematically. Table 5.14 shows the intersection points which can be seen in Figures 5.36 and 5.37.

$abx = -10 + 3y$ $aby = 3.\bar{3} + 0.\bar{3}x$	$bcx = 160 - 5.5y$ $bcy = 29.09 - 0.1818x$	$cdx = 160 + 4y$ $cdy = -40 + 0.25x$	$dex = 202.5 - 0.25y$ $dey = 810 - 4x$
$efx = -90 + 3y$ $efy = 30 + 0.\bar{3}x$	$fgx = 590 - 5.5y$ $fgy = 107.27 - 0.1818x$	$glx = -360 + 4y$ $gly = 90 + 0.25x$	$hax = 22.5 - 0.25y$ $hay = 90 - 4x$

Table 5.13: Boundary line functions for proprietory shaped paver 7.

$P_{1x} = 0.6a - 36$ $P_{1y} = 18 + 0.2a$	$P_{2y} = -115.714 + 0.571a$ $P_{2x} = 231.429 - 0.143a$	$P_{3y} = 168.571 - 0.286a$ $P_{3x} = -337.327 + 1.571a$

Table 5.14: The intersection points between the lines which form the patch load boundary with distances a and b (b=a/2) in the x and y directions and line functions bounding the proprietory shaped paver 7.

The surface area and centroid distances for the system illustrated in Figure 5.36 can be calculated using the data in Table 5.13 and Table 5.14 and are as follows:

$$F = \int_0^a fy\,dx - \int_{200}^a fy\,dx - \int_{160}^{200} cdy\,dx - \int_{P_{2x}}^{200} fy\,dx + \int_{P_{2x}}^{200} dey\,dx - \int_{50}^{160} bcy\,dx - \int_{20}^{50} aby\,dx - \int_0^{20} hay\,dx$$

$$- \int_0^{P_{1x}} fy\,dx + \int_0^{40} ghy\,dx + \int_{40}^{150} fgy\,dx + \int_{150}^{P_{1x}} bcy\,dx$$

The evaluation of the integrals yields the following equation:

$$F = 0.185715(639.419 - a)(-80.5792 + a)$$

$$\overline{X} = \frac{1}{F}\left[\begin{array}{l} \int_0^a x\,fy\,dx - \int_{200}^a x\,fy\,dx + \int_{160}^{200} x\,cdy\,dx - \int_{P_{2x}}^{200} x\,fy\,dx + \int_{P_{2x}}^{200} x\,dey\,dx - \int_{50}^{160} x\,bcy\,dx \\ -\int_{20}^{50} x\,aby\,dx - \int_{0}^{20} x\,hay\,dx - \int_{0}^{P_{1x}} x\,fy\,dx + \int_{0}^{40} x\,ghy\,dx + \int_{40}^{150} x\,fgy\,dx + \int_{150}^{P_{1x}} x\,bcy\,dx \end{array}\right]$$

The evaluation of the integrals yields the following equation:

$$\overline{X} = \frac{0.152382(553.083 - a)(-127.625 + a)(781.956 + a)}{-51523.9 + 719.998a - a^2}$$

$$\overline{Y} = \frac{1}{F}\left[\begin{array}{l} \int_0^b y\,fx\,dy - \int_{100}^b y\,fx\,dy - \int_{90}^{100} y\,ghx\,dy - \int_{P_{1y}}^{100} y\,fx\,dy + \int_{P_{1y}}^{100} y\,fgx\,dy - \int_{80}^{P_{1y}} y\,efx\,dy + \int_{80}^{P_{1y}} y\,efx\,dy \\ -\int_{0}^{P_{2y}} y\,efx\,dy + \int_{10}^{P_{2y}} y\,dex\,dy + \int_{0}^{10} y\,cdx\,dy - \int_{20}^{90} y\,hax\,dy - \int_{0}^{20} y\,bcx\,dy + \int_{10}^{20} y\,abx\,dy - \int_{10}^{20} y\,hax\,dy \end{array}\right]$$

The evaluation of the integrals yields the following equation:

$$\overline{Y} = \frac{0.257142(530.745 - a)\left(31046.2 - 199.255a + a^2\right)}{-51523.9 + 719.998a - a^2}$$

Line 1 in Figure 5.36 scans the paver between corners **e** and **f**. It should therefore be noted that for the solutions above to be valid for the patch load application 1, the variable distance **a** in the x direction must lie in the range: 360>**a**>310mm.

Figure 5.37 illustrates the special patch load application 2 for the proprietory shaped paver 7. **Line 2** scans the paver between corners **f** and **d** in terms of the variable

distance **a** in the x direction. By using the paver line functions in Table 5.13, the equations of the intersection points in Table 5.14 and the patch load boundary line function which is $f_y = b(1-\frac{x}{a})$, $f_x = a(1-\frac{y}{b})$ in the x and y axes, the special patch load's surface area and centroid distances can be calculated as follows:

$$F = \int_0^a fy\,dx - \int_{200}^{200} fy\,dx - \int_{160}^{200} cdy\,dx - \int_{P_{2x}}^{200} fy\,dx + \int_{P_{2x}}^{160} dey\,dx - \int_{50}^{20} bcy\,dx - \int_{20}^{0} aby\,dx - \int_{0}^{40} hay\,dx$$
$$- \int_{0}^{P_{3x}} fy\,dx + \int_{0}^{40} ghy\,dx + \int_{40}^{P_{3x}} fgy\,dx$$

The evaluation of the integrals yields the following equation:

$$F = 0.428549(513.933 - a)(-149.402 + a)$$

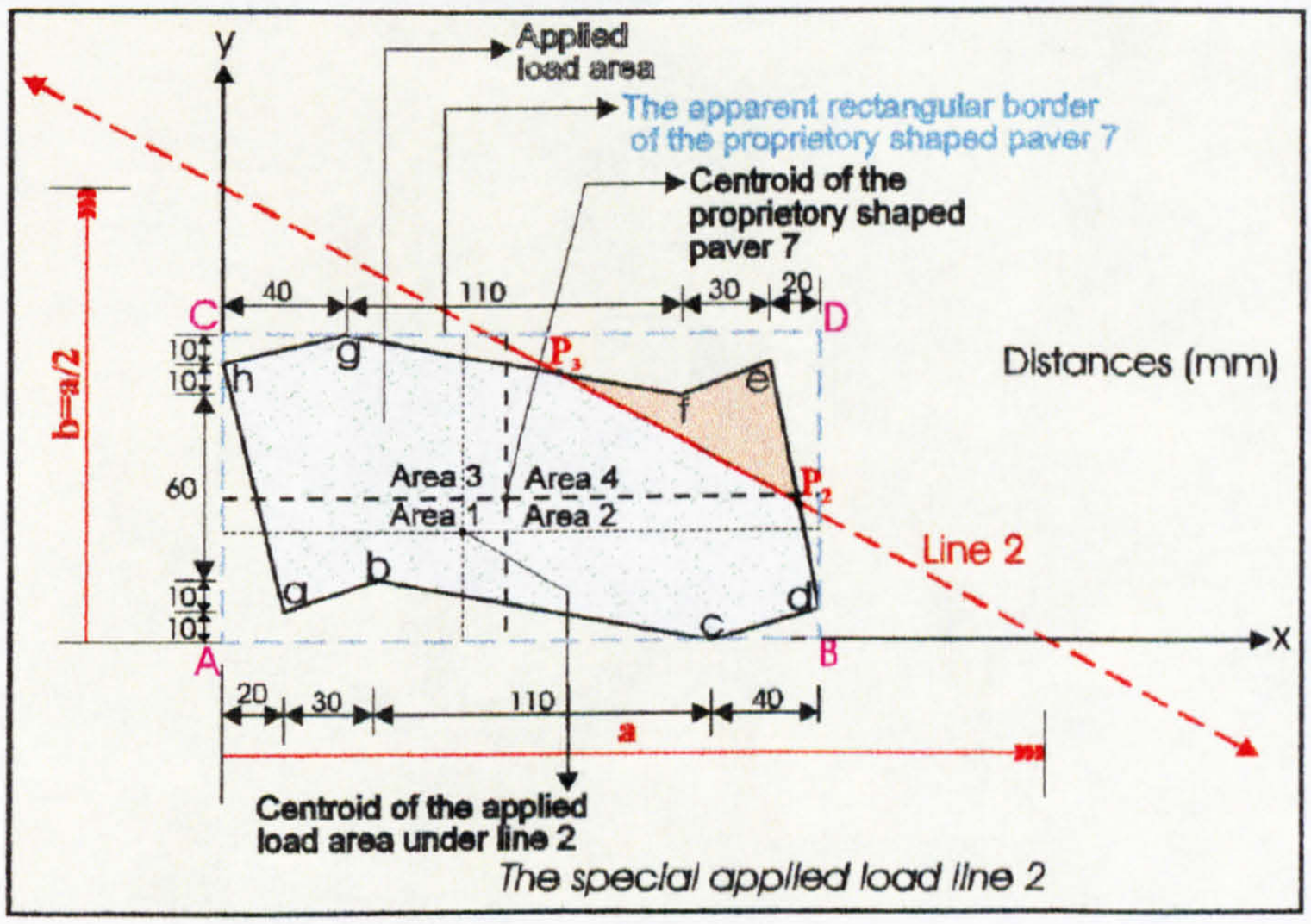

Figure 5.37: The selected special patch load application 2 for proprietory shaped paver 7.

$$\overline{X} = \frac{1}{F}\left[\int_0^a x\,fy\,dx - \int_{200}^{a} x\,fy\,dx + \int_{160}^{200} x\,cdy\,dx - \int_{P_{2x}}^{200} x\,fy\,dx + \int_{P_{2x}}^{200} x\,dey\,dx - \int_{50}^{160} x\,bcy\,dx\right.$$

$$\left.-\int_{20}^{50} x\,aby\,dx-\int_{0}^{20} x\,hay\,dx-\int_{0}^{P_{3x}} x\,fy\,dx+\int_{0}^{40} x\,ghy\,dx+\int_{40}^{P_{3x}} x\,fgy\,dx\right]$$

The evaluation of the integrals yields the following equation:

$$\overline{X}=\frac{0.476161(448.607-a)(-146.976+a)(-12.8982+a)}{-76782.8+663.336a-a^2}$$

$$\overline{Y}=\frac{1}{F}\left[\begin{array}{l}\int_{0}^{b} y\,fx\,dy-\int_{100}^{b} y\,fx\,dy-\int_{90}^{100} y\,ghx\,dy-\int_{P_{3y}}^{100} y\,fx\,dy+\int_{P_{3y}}^{100} y\,fgx\,dy-\int_{0}^{P_{2y}} y\,fx\,dy \\ +\int_{10}^{P_{2y}} y\,dex\,dy+\int_{0}^{10} y\,cdx\,dy-\int_{20}^{90} y\,hax\,dy-\int_{0}^{20} y\,bcx\,dy+\int_{10}^{20} y\,abx\,dy-\int_{10}^{20} y\,hax\,dy\end{array}\right]$$

The evaluation of the integrals yields the following equation:

$$\overline{Y}=\frac{0.0952431(469.117-a)(-163.06+a)(412.178+a)}{-76782.8+663.336a-a^2}$$

Line 2 in Figure 5.37 scans the paver between corners **f** and **d**. It should therefore be noted that for the solutions above to be valid for the patch load application 2, the variable distance **a** in the x direction must lie in the range: 310>a>240mm.

5.9. The selected special patch load applied to proprietory shaped paver 8

Figure 5.38 illustrates one of the common patch load application to proprietory shaped paver 8 (see Figure 5.1). It may be recalled that in these common load applications, the lines which define the patch loading gradually scan the paver from its lower left corner to its upper right corner with distances **a** and **b** (b=a/2). The proprietory shaped paver 8 is analysed with the similar logic described previously (see Sections 5.2, 5.3, 5.4, 5.5, 5.6, 5.7 and 5.8). The patch load applications principally generate five types of

idealised vertical compressive stress dissipations beneath pavers which are tetrahedral, short-pentahedral, long-pentahedral, partial-hexahedral and absolute-hexahedral as described in Chapters 6, 7 and 8. The solutions of these five vertical stress distributions were given in Chapter 6 for rectangular pavers. The solutions of the vertical compressive stress regimes for proprietory shaped pavers (see Figure 5.1) are particularly complex so iterative solutions have been used in their evaluations. The numerical solutions have been conducted by using Mathematica[1], Maple[2] and Nag[3] mathematical software. However the arithmetical solutions to the absolute-hexahedral case have been calculated for each proprietory shaped paver (see Chapters 7 and 8). For this reason the evaluations of the patch loads' integrals relating only to the absolute-hexahedral stress cases are documented in this Section for the proprietory shaped paver 8.

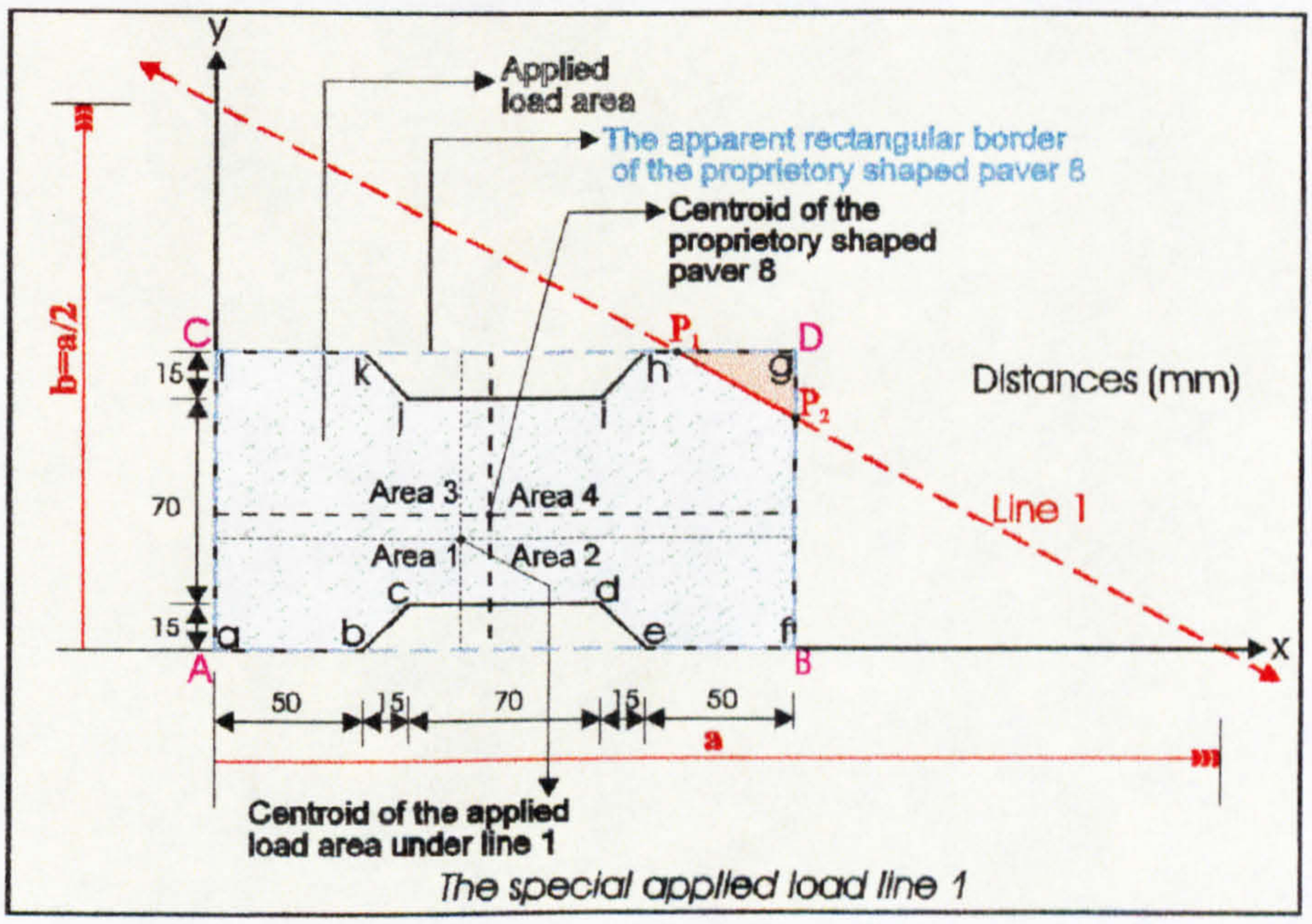

Figure 5.38: The selected special patch load application 1 for proprietory shaped paver 8.

Figure 5.38 illustrates the special patch load application 1 for the proprietory shaped paver 8. **Line 1** scans the paver between corners **g** and **h** in terms of the variable distance **a** in the x direction. It may be recalled that each shaped paver is of a circumscribing rectangular border. If x, y transverse and longitudinal axes have their

original corner **A** of this circumscribing rectangular shape, it can be seen that each corner of the actual paver is connected by lines which form the real shape of the paver. The functions of these lines can be calculated using basic geometrical rules. The boundary line functions for the proprietory shaped paver 8 are shown in Table 5.15.

In Table 5.15 the first letters of each line function characterise the corner names as can be seen in Figure 5.38. By using the line functions in Table 5.15 shaped paver 8 and the line functions which define the patch load boundaries, which are of the form $f_y = b(1-\frac{x}{a})$, $f_x = a(1-\frac{y}{b})$ in the x and y axes, the intersection points between the paver boundary lines and the load patch boundary line can be calculated mathematically. Table 5.16 shows the intersection points which can be seen in Figures 5.38 to 5.40.

$bcx = 50 + y$ $bcy = -50 + x$	$hix = 50 + y$ $hiy = -50 + x$	$dex = 150 - y$ $dey = 150 - x$	$jkx = 150 - y$ $jky = 150 - x$

Table 5.15: Boundary line functions for proprietory shaped paver 8.

$P_{1x} = a - 200$ $P_{1y} = 100$	$P_{2x} = 200$ $P_{2y} = 0.5\,a - 100$	$P_{3x} = 33.\bar{3} + 0.\bar{3}\,a$ $P_{3y} = 0.\bar{3}\,a - 16.\bar{6}\,a$	$P_{4x} = a - 170$ $P_{4y} = 85$

Table 5.16: The intersection points between the lines which form the patch load boundary with distances **a** and **b** (**b**=**a**/2) in the x and y directions and line functions bounding the proprietory shaped paver 8.

The surface area and centroid distances for the system illustrated in Figure 5.38 can be calculated using the data in Table 5.15 and Table 5.16 and are as follows:

$$F = \int_0^a fy\,dx - \int_{200}^a fy\,dx - \int_{135}^{150} dey\,dx - \int_{65}^{135} 15\,dx - \int_{50}^{65} bcy\,dx - \int_0^{P_{1x}} fy\,dx + \int_0^{50} 100\,dx + \int_{50}^{65} kjy\,dx$$

$$+ \int_{65}^{135} 85\,dx + \int_{135}^{150} hiy\,dx + \int_{150}^{P_{1x}} 100\,dx$$

The evaluation of the integrals yields the following equation:

$$F = \frac{-90200 + 800a - a^2}{4}$$

$$\overline{X} = \frac{1}{F}\left[\begin{array}{l} \int_0^a x\,fy\,dx - \int_{200}^{a} x\,fy\,dx - \int_{135}^{150} x\,dey\,dx - \int_{65}^{135} x\,15\,dx - \int_{50}^{65} x\,bcy\,dx - \int_{0}^{P_{1x}} x\,fy\,dx \\ + \int_0^{50} x\,100\,dx + \int_{50}^{65} x\,kjy\,dx + \int_{65}^{135} x\,85\,dx + \int_{135}^{150} x\,hiy\,dx + \int_{150}^{P_{1x}} x\,100\,dx \end{array}\right]$$

The evaluation of the integrals yields the following equation:

$$\overline{X} = \frac{11060000 - 600a^2 + a^3}{3\left(90200 - 800a + a^2\right)}$$

$$\overline{Y} = \frac{1}{F}\left[\begin{array}{l} \int_0^b y\,fx\,dy - \int_{100}^{b} y\,fx\,dy - \int_{85}^{100} y\,hix\,dy + \int_{85}^{100} y\,kjx\,dy - \int_{0}^{P_{2y}} y\,fx\,dy + \int_{0}^{P_{2y}} y\,200\,dy \\ - \int_0^{15} y\,dex\,dy + \int_0^{15} y\,bcx\,dy \end{array}\right]$$

The evaluation of the integrals yields the following equation:

$$\overline{Y} = \frac{11060000 - 600a^2 + a^3}{6\left(90200 - 800a + a^2\right)}$$

Line 1 in Figure 5.38 scans the paver between corners **g** and **h**. It should therefore be noted that for the solutions above to be valid for the patch load application 1, the variable distance **a** in the x direction must lie in the range: 400>**a**>350mm.

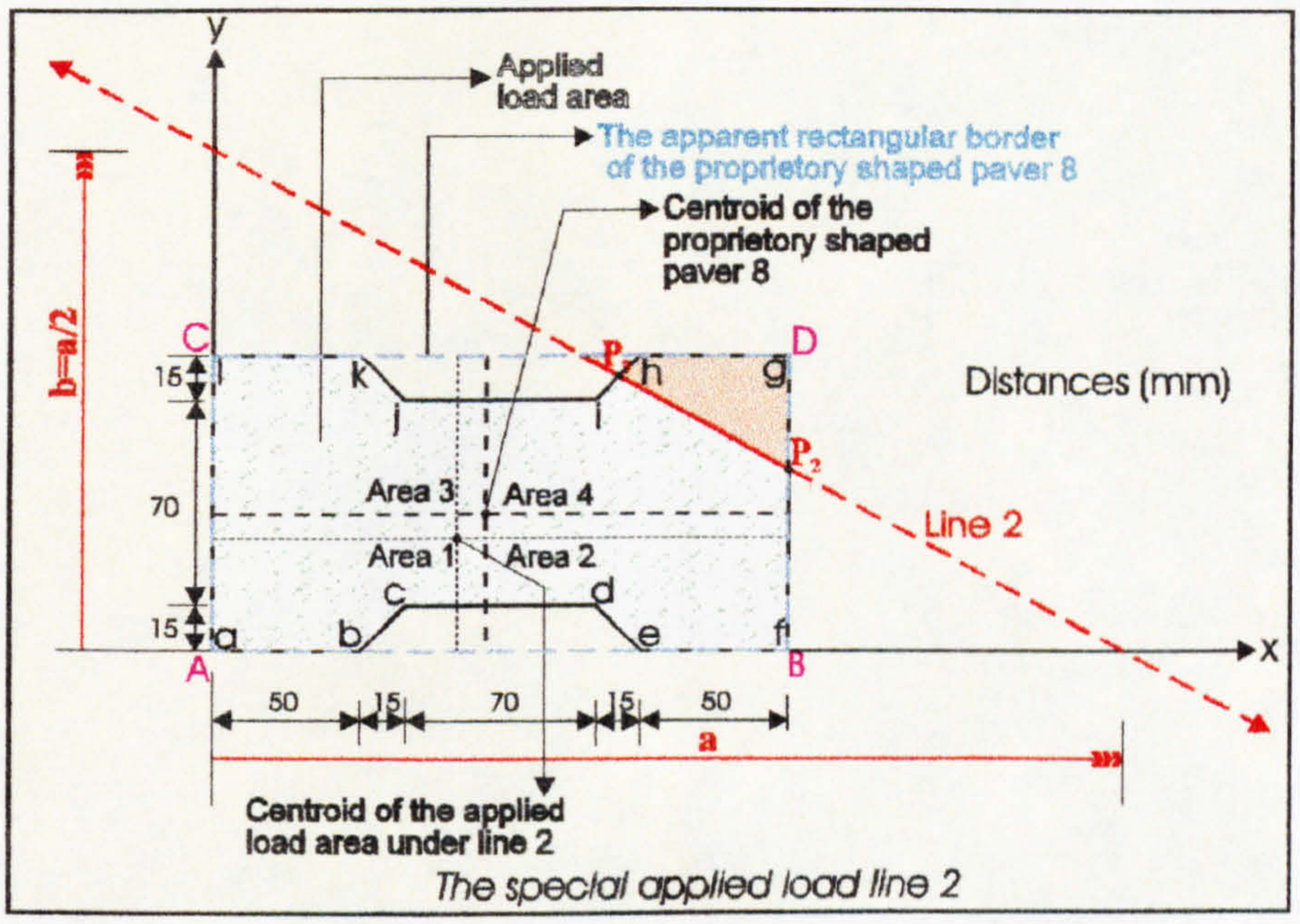

Figure 5.39: The selected special patch load application 2 for proprietory shaped paver 8.

Figure 5.39 illustrates the special patch load application 2 for the proprietory shaped paver 8. **Line 2** scans the paver between corners **h** and **i** in terms of the variable distance **a** in the x direction. By using the paver line functions in Table 5.15, the equations of the intersection points in Table 5.16 and the patch load boundary line function which is $f_y = b(1-\frac{x}{a})$, $f_x = a(1-\frac{y}{b})$ in the x and y axes, the special patch load's surface area and centroid distances can be calculated as follows:

$$F = \int_0^a fy\,dx - \int_{200}^a fy\,dx - \int_{135}^{150} dey\,dx - \int_{65}^{135} 15\,dx - \int_{50}^{65} bcy\,dx - \int_0^{P_{3x}} fy\,dx + \int_0^{50} 100\,dx + \int_{50}^{65} kjy\,dx + \int_{65}^{135} 85\,dx + \int_{135}^{P_{3x}} hiy\,dx$$

The evaluation of the integrals yields the following equation:

$$F = \frac{-25600 + 1000a - a^2}{12}$$

$$\overline{X} = \frac{1}{F}\left[\begin{array}{l} \int_0^a x\,fy\,dx - \int_{200}^{a} x\,fy\,dx - \int_{135}^{150} x\,dey\,dx - \int_{65}^{135} x\,15\,dx - \int_{50}^{65} x\,bcy\,dx - \int_{0}^{P_{3x}} x\,fy\,dx \\ + \int_0^{50} x\,100\,dx + \int_{50}^{65} x\,kjy\,dx + \int_{65}^{135} x\,85\,dx + \int_{135}^{P_{3x}} x\,hiy\,dx \end{array}\right]$$

The evaluation of the integrals yields the following equation:

$$\overline{X} = \frac{111790000 - 1050000a - 300a^2 + a^3}{9\left(25600 - 1000a + a^2\right)}$$

$$\overline{Y} = \frac{1}{F}\left[\begin{array}{l} \int_0^b y\,fx\,dy - \int_{100}^{b} y\,fx\,dy - \int_{P_{3y}}^{100} y\,fx\,dy + \int_{P_{3y}}^{100} y\,kjx\,dy - \int_{85}^{P_{3y}} y\,hix\,dy + \int_{85}^{P_{3y}} y\,kjx\,dy \\ - \int_0^{P_{2y}} y\,fx\,dy + \int_0^{P_{2y}} y\,200\,dy - \int_0^{15} y\,dex\,dy + \int_0^{15} y\,bc\,dy \end{array}\right]$$

The evaluation of the integrals yields the following equation:

$$\overline{Y} = \frac{5\left(-33992000 + 210000a - 960a^2 + a^3\right)}{18\left(25600 - 1000a + a^2\right)}$$

Line 2 in Figure 5.39 scans the paver between corners **h** and **i**. It should therefore be noted that for the solutions above to be valid for the patch load application 2, the variable distance **a** in the x direction must lie in the range: 350>**a**>305mm.

Figure 5.40 illustrates the special patch load application 3 for the proprietory shaped paver 8. **Line 3** scans the paver between corners **i** and **k** in terms of the variable distance **a** in the x direction. By using the paver line functions in Table 5.15, the equations of the intersection points in Table 5.16 and the patch load boundary line

function which is $f_y = b(1-\frac{x}{a})$, $f_x = a(1-\frac{y}{b})$ in the x and y axes, the special patch load's surface area and centroid distances can be calculated as follows:

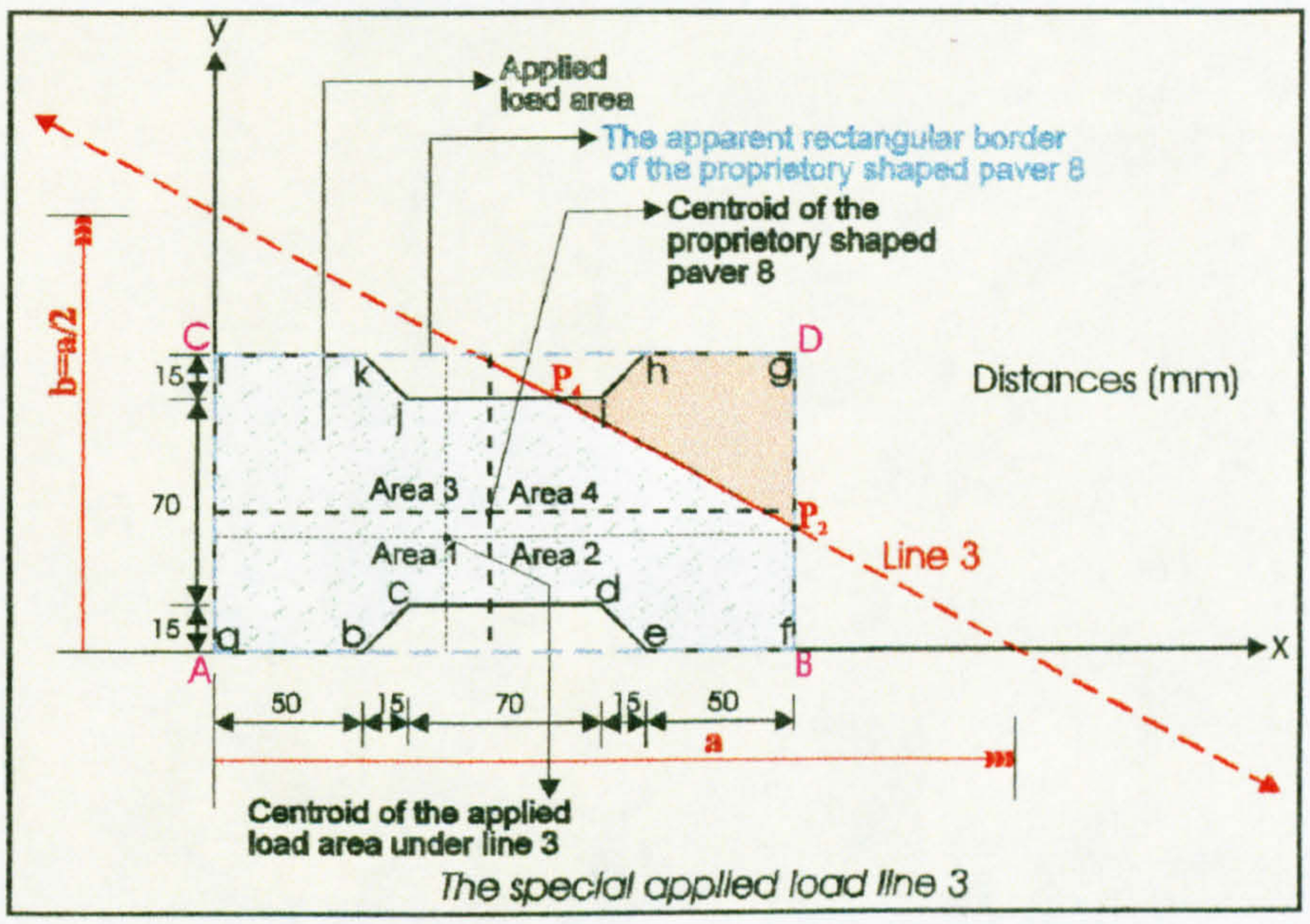

Figure 5.40: The selected special patch load application 3 for proprietory shaped paver 8.

$$F = \int_0^a fy\,dx - \int_{200}^a fy\,dx - \int_{135}^{150} dey\,dx - \int_{65}^{135} 15\,dx - \int_{50}^{65} bcy\,dx - \int_0^{P_{4x}} fy\,dx + \int_0^{50} 100\,dx + \int_{50}^{65} kjy\,dx + \int_{65}^{P_{4x}} 85\,dx$$

The evaluation of the integrals yields the following equation:

$$F = \frac{-70550 + 740a - a^2}{4}$$

$$\overline{X} = \frac{1}{F}\left[\int_0^a x\,fy\,dx - \int_{200}^a x\,fy\,dx - \int_{135}^{150} x\,dey\,dx - \int_{65}^{135} x\,15\,dx - \int_{50}^{65} x\,bcy\,dx - \int_0^{P_{4x}} x\,fy\,dx\right.$$

$$+\int_0^{50} x\,100\,dx+\int_{50}^{65} x\,kjy\,dx+\int_{65}^{P_{4x}} x\,85\,dx\Bigg]$$

The evaluation of the integrals yields the following equation:

$$\overline{X}=\frac{12317750-33300a-510a^2+a^3}{3\left(70550-740a+a^2\right)}$$

$$\overline{Y}=\frac{1}{F}\left[\begin{array}{l}\displaystyle\int_0^{b} y\,fx\,dy-\int_{100}^{b} y\,fx\,dy-\int_{85}^{100} y\,fx\,dy+\int_{85}^{100} y\,kjx\,dy-\int_0^{P_{2y}} y\,fx\,dy+\int_0^{P_{2y}} y\,200\,dy\\ \displaystyle-\int_0^{15} y\,dex\,dy+\int_0^{15} y\,bc\,dy\end{array}\right]$$

The evaluation of the integrals yields the following equation:

$$\overline{Y}=\frac{134000+33300a-600a^2+a^3}{6\left(70550-740a+a^2\right)}$$

Line 3 in Figure 5.40 scans the paver between corners **i** and **k**. It should therefore be noted that for the solutions above to be valid for the patch load application 3, the variable distance **a** in the x direction must lie in the range: 305>a>250mm.

5.10. The selected special patch load applied to proprietory shaped paver 9

Figure 5.41 illustrates one of the common patch load application to proprietory shaped paver 9 (see Figure 5.1). It may be recalled that in these common load applications, the lines which define the patch loading gradually scan the paver from its lower left corner to its upper right corner with distances **a** and **b** (**b=a/2**). The proprietory shaped paver 9 is analysed with the similar logic described previously (see Sections 5.2, 5.3, 5.4, 5.5,

5.6, 5.7, 5.8 and 5.9). The patch load applications principally generate five types of idealised vertical compressive stress dissipations beneath pavers which are tetrahedral, short-pentahedral, long-pentahedral, partial-hexahedral and absolute-hexahedral as described in Chapters 6, 7 and 8. The solutions of these five vertical stress distributions were given in Chapter 6 for rectangular pavers. The solutions of the vertical compressive stress regimes for proprietory shaped pavers (see Figure 5.1) are particularly complex so iterative solutions have been used in their evaluations. The numerical solutions have been conducted by using Mathematica[1], Maple[2] and Nag[3] mathematical software. However the arithmetical solutions to the absolute-hexahedral case have been calculated for each proprietory shaped paver (see Chapters 7 and 8). For this reason the evaluations of the patch loads' integrals relating only to the absolute-hexahedral stress cases are documented in this Section for the proprietory shaped paver 9.

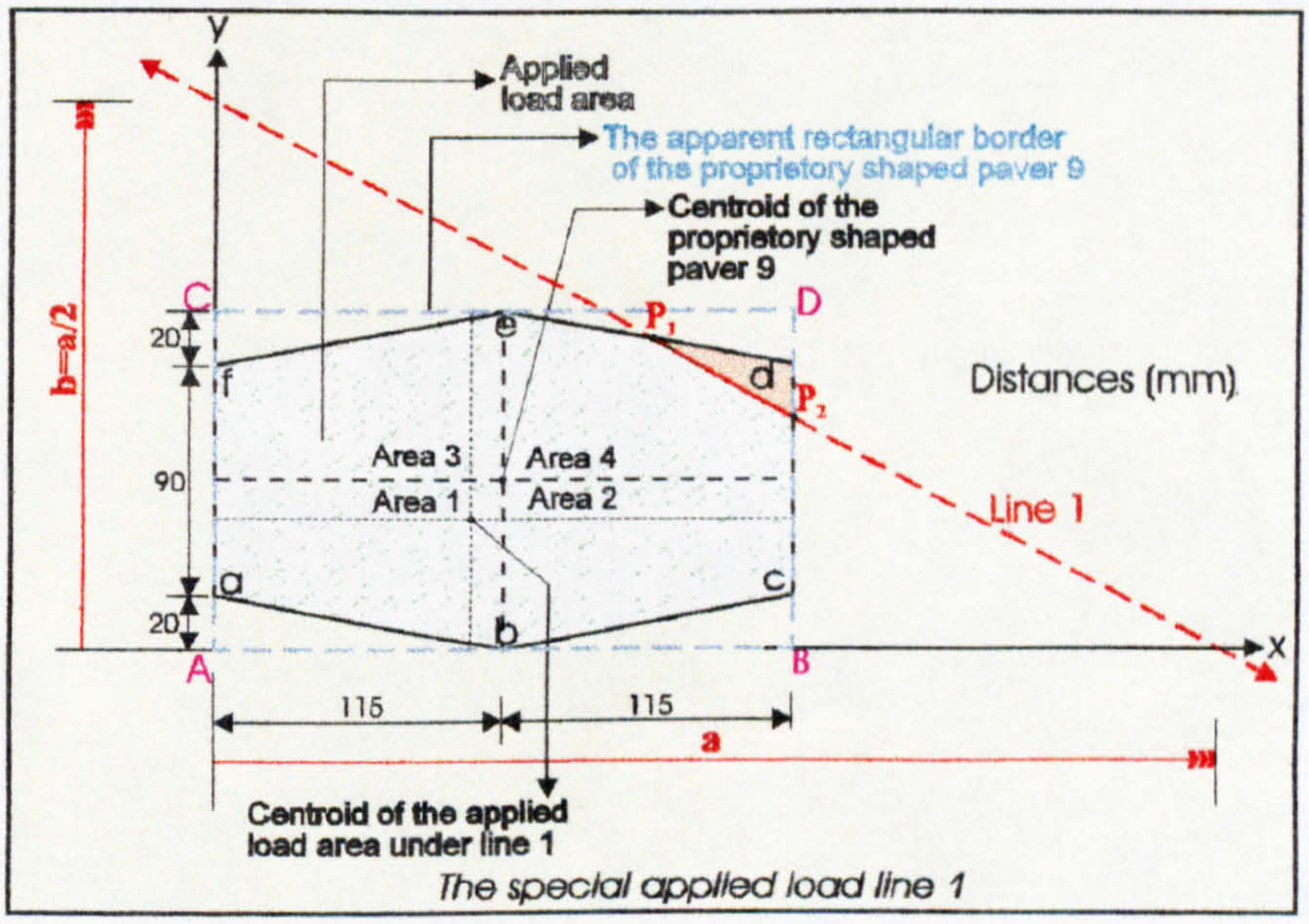

Figure 5.41: The selected special patch load application 1 for proprietory shaped paver 9.

Figure 5.41 illustrates the special patch load application 1 for the proprietory shaped paver 9. **Line 1** scans the paver between corners **d** and **e** in terms of the variable distance **a** in the x direction. It may be recalled that each shaped paver is of a circumscribing rectangular border. If x, y transverse and longitudinal axes have their

original corner **A** of this circumscribing rectangular shape, it can be seen that each corner of the actual paver is connected by lines which form the real shape of the paver. The functions of these lines can be calculated using basic geometrical rules. The boundary line functions for the proprietory shaped paver 9 are shown in Table 5.17.

In Table 5.17 the first letters of each line function characterise the corner names as can be seen in Figure 5.41. By using the line functions in Table 5.17 shaped paver 9 and the line functions which define the patch load boundaries, which are of the form $f_y = b(1-\frac{x}{a})$, $f_x = a(1-\frac{y}{b})$ in the x and y axes, the intersection points between the paver boundary lines and the load patch boundary line can be calculated mathematically. Table 5.18 shows the intersection points which can be seen in Figures 5.41 and 5.42.

$abx = 115 - 7.\bar{6}y$ $aby = 20 - 0.174x$	$dey = 150 - 0.174x$ $dex = 862.5 - 5.75y$	$bcx = 115 + 5.75y$ $bcy = 0.174x - 20$	$efx = 5.75y - 632.5$ $efy = 0.174x + 110$

Table 5.17: Boundary line functions for proprietory shaped paver 9.

$P_{1x} = 1.534a - 460.123$ $P_{1y} = 230 - 0.267a$	$P_{2x} = 230$ $P_{2y} = 0.5a - 115$	$P_{3y} = 0.129a + 81.613$ $P_{3x} = 0.742a - 163.205$

Table 5.18: The intersection points between the lines which form the patch load boundary with distances **a** and **b** (**b**=**a**/2) in the x and y directions and line functions bounding the proprietory shaped paver 9.

The surface area and centroid distances for the system illustrated in Figure 5.41 can be calculated using the data in Table 5.17 and Table 5.18 and are as follows:

$$F = \int_{P_{1x}}^{230} fy\,dx - \int_{P_{1x}}^{230} bcy\,dx + \int_{115}^{P_{1x}} dey\,dx - \int_{115}^{P_{1x}} bcy\,dx + \int_{0}^{115} efy\,dx - \int_{0}^{115} aby\,dx$$

The evaluation of the integrals yields the following equation:

$$F = 0.383318(706.918 - a)(-193.094 + a)$$

$$\overline{X} = \frac{1}{F}\left[\int_{P_{1x}}^{230} x\,fy\,dx - \int_{P_{1x}}^{230} x\,bcy\,dx + \int_{115}^{P_{1x}} x\,dey\,dx - \int_{115}^{P_{1x}} x\,bcy\,dx + \int_{0}^{115} x\,efy\,dx - \int_{0}^{115} x\,aby\,dx\right]$$

The evaluation of the integrals yields the following equation:

$$\overline{X} = \frac{0.511091(606.49 - a)\left(24483.8 - 293.51a + a^2\right)}{-136502 + 900.012a - a^2}$$

$$\overline{Y} = \frac{1}{F}\left[\int_{0}^{20} y\,bcx\,dy - \int_{0}^{20} y\,abx\,dy + \int_{20}^{P_{2y}} y\,230\,dy + \int_{P_{2y}}^{P_{1y}} y\,fx\,dy - \int_{110}^{P_{1y}} y\,efx\,dy + \int_{P_{1y}}^{130} y\,dex\,dy - \int_{P_{1y}}^{130} y\,efx\,dy\right]$$

The evaluation of the integrals yields the following equation:

$$\overline{Y} = \frac{0.0777809(635.869 - a)(-235.334 + a)(935.488 + a)}{-136502 + 900.012a - a^2}$$

Line 1 in Figure 5.41 scans the paver between corners **d** and **e**. It should therefore be noted that for the solutions above to be valid for the patch load application 1, the variable distance **a** in the x direction must lie in the range: **450>a>375mm.**

Figure 5.42 illustrates the special patch load application 2 for the proprietory shaped paver 9. **Line 2** scans the paver between corners **e** and **f** in terms of the variable distance **a** in the x direction. By using the paver line functions in Table 5.17, the equations of the intersection points in Table 5.18 and the patch load boundary line function which is

$f_y = b(1-\frac{x}{a})$, $f_x = a(1-\frac{y}{b})$ in the x and y axes, the special patch load's surface area and centroid distances can be calculated as follows:

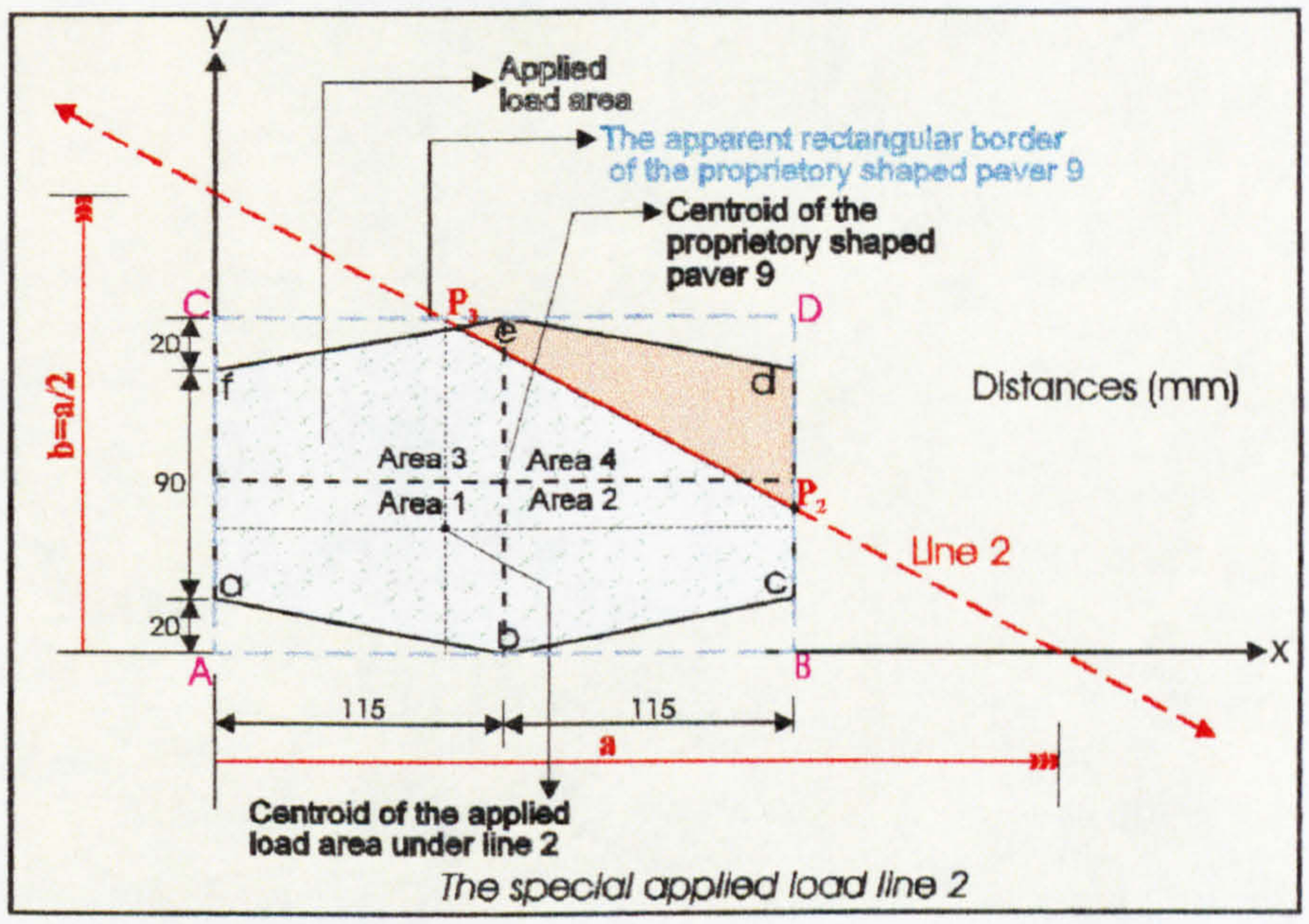

Figure 5.42: The selected special patch load application 2 for proprietory shaped paver 9.

$$F = \int_{P_{3x}}^{230} fy\,dx - \int_{P_{3x}}^{115} aby\,dx - \int_{115}^{230} bcy\,dx + \int_{0}^{P_{3x}} efy\,dx - \int_{0}^{P_{3x}} aby\,dx$$

The evaluation of the integrals yields the following equation:

$$F = 0.185487(915.735-a)(-144.253+a)$$

$$\overline{X} = \frac{1}{F}\left[\int_{P_{3x}}^{230} x\,fy\,dx - \int_{P_{3x}}^{115} x\,aby\,dx - \int_{115}^{230} x\,bcy\,dx + \int_{0}^{P_{3x}} x\,efy\,dx - \int_{0}^{P_{3x}} x\,aby\,dx\right]$$

The evaluation of the integrals yields the following equation:

$$\overline{X} = \frac{0.247317(778.894-a)(-172.969+a)(291.863+a)}{-132094+1059.99a-a^2}$$

$$\overline{Y} = \frac{1}{F}\left[\int_0^{20} y\,bcx\,dy - \int_0^{20} y\,abx\,dy + \int_{20}^{P_{2y}} y\,230\,dy + \int_{P_{2y}}^{P_{3y}} y\,fx\,dy - \int_{110}^{P_{3y}} y\,efx\,dy\right]$$

The evaluation of the integrals yields the following equation:

$$\overline{Y} = \frac{0.209693(759.797-a)(-133.642+a)(19.0785+a)}{-132097+1059.99a-a^2}$$

Line 2 in Figure 5.42 scans the paver between corners **e** and **f**. It should therefore be noted that for the solutions above to be valid for the patch load application 2, the variable distance **a** in the x direction must lie in the range: 375>a>270mm.

5.11. Conclusion

It can be recalled in Chapter 4 that a special load patch which functionally generates the maximum stress value was selected and applied to rectangular pavers in order to compare the analysed pavers (see Figure 5.1) in terms of their vertical compressive stress distributions. The nine proprietory shaped pavers analysed (see Figure 5.1) in this Thesis are commercially important on a worldwide basis. This Chapter developed the general equations to the total applied pressures and the centroid distances of the variations of a realistically possible patch loading which is specially selected for proprietory shaped pavers (see Figure 5.1) in order to compare the pavers in terms of the stress distributions which they generate. The calculation technique used in this Chapter for analysing the pressures applied onto proprietory shaped pavers is based on the method described in the previous chapter for rectangular pavers. The vertical compressive stress regimes in the bedding material are calculated for proprietory shaped pavers in Chapters 7 and 8 by considering vertical and rotational equilibrium of the pressures applied to the upper and lower horizontal paver surfaces. Chapter 9 will

show the evaluation of the algebraical solutions which are developed for the nine proprietory shaped pavers in Chapters 7 and 8 according to the variations of the common patch loading's general equations (which are defined in this Chapter) to the total applied pressures and their centroid distances in the xy-plane (see Figures 5.2 to 5.42 and 9.1 to 9.9). It is therefore necessary to calculate the patch loadings applied onto proprietory shaped pavers before the stresses in the bedding material can be analysed in Chapters 7, 8 and 9. The vertical compressive stresses in the bedding material are calculated for the shaped pavers in Chapters 7, 8 and 9 by using the application of the bedding sand stress calculation method[1, 2, 3] to proprietory shaped pavers. The bedding sand stress calculation method[1, 2, 3] which is presented in the next Chapter based on vertical and rotational equilibrium of the pressures applied to the upper and lower horizontal paver surfaces.

References

1 Algin, H.M., Knapton, J., (1996), *Research into paver interlock*, Jrnl. of the Institution of Highway & Transportation & IHIE, Vol. 43, No. 03, p 20-24.

2 Knapton, J., Algin, H.M., (1995), *The Mathematical Solution to Interlock in Flexibly Bedded Clay Paving*. Proc. of the 4th. Int. Masonry Conf. No. 7, Vol. 2, p 307-313. London.

3 Knapton, J., Algin, H.M., (1996), *The Mathematical Solution to Interlock in Concrete Block Paving*. Proc. of the 5th. Int. Conf. on Concrete Block Paving, p 261-278, Tel-Aviv.

CHAPTER SIX

BEDDING SAND STRESSES IN RECTANGULAR PAVERS

Synopsis

This Chapter presents the bedding sand stress calculation method and the mathematical solution to interlock in concrete paver pavements. The bedding sand stress calculation method which can be used for determining the vertical compressive stress distributions beneath flexibly bedded concrete pavers is based upon the relationships between the applied patch loadings (see Chapters 4 and 5) and their resulting vertical stress distributions beneath pavers. The vertical stress distributions have been found for a range of patch loadings resulting from vehicle tyres rolling across pavers. This Chapter explains the application of the method to rectangular pavers. The vertical compressive stresses resulting from load patches (see Chapter 4) have been calculated for chamfered and non-chamfered rectangular pavers. In addition, the transfer stresses have been calculated across joints for interlocking chamfered rectangular pavers laid to 45 degree herringbone pattern.

6.1. Introduction

This Chapter presents the bedding sand stress calculation method which can be used for determining the vertical compressive stress distributions beneath flexible bedded concrete pavers. This method represents the mathematical solution to interlock in paver pavements. Paver pavements are structurally complex systems consisting of individual pavers. The mathematical solution to interlock initially involves assessing the relationship between an applied load patch shape and its resulting vertical compressive stress distribution beneath individual pavers. The vertical stress distributions have been found for a range of patch loadings (described in Chapters 4 and 5) resulting from vehicle tyres rolling across pavers. In order to reduce the size of the system to one of manageable proportions, the following variables have been fixed at values which are commonly achieved in practice. Tyre pressure of $0.8N/mm^2$ has been assumed. In the case of rectangular pavers herringbone laying pattern has been assumed. Pavers of commonly installed size and shape have been analysed. The stresses resulting from load patches have been calculated for chamfered and non-chamfered rectangular pavers which are presented in this Chapter and for 9 proprietory shaped pavers (see Chapter 7, 8, 9). In addition transfer stresses presented in this Chapter have been calculated across joints for interlocking chamfered rectangular pavers laid to 45 degree herringbone pattern. The vertical stresses in the bedding sand are calculated by considering vertical and rotational equilibrium of the pressures applied to the upper and lower horizontal paver surfaces. It is assumed that the paver is structurally rigid in relation to the bedding sand so a planar stress regime can be assumed at the paver/sand interface[1, 2, 3]. This assumption is justified by the values of Young's Modulus which would normally be applied to concrete ($30,000N/mm^2$) and to sand in compression ($300N/mm^2$). If tension were to be permitted to develop between the paver and the bedding sand the solution would be relatively straightforward. Tension cannot be developed in uncemented sand so it is assumed that compressive stress is developed in some parts of the interface and zero stress is developed elsewhere.

By ensuring vertical and rotational equilibrium, three equations can be developed (one vertical equilibrium and two rotational equilibrium equations, one in each orthogonal

direction) which can be solved to obtain the values of the vertical stress in the bedding sand at each corner of the lower horizontal surface of the paver. The stress at any point along the paver boundary can then be determined by linear interpolation.

6.2. The bedding sand stress calculation method for rectangular pavers

In the case of rectangular pavers, Figure 6.1 shows the five principal bedding sand stress patterns. The five cases can be best understood by considering them sequentially. Initially, the applied upper surface patch load occupies one corner of the loaded paver. Bedding sand compressive stress occurs only at one lower paver corner and zero stress occurs at the remaining three corners. As the patch load occupies progressively more paver surface area, the situation illustrated is attained in which stresses are compressive at two paver corners. Eventually, the patch load creeps further over the paver so that three corners exhibit compressive bedding sand stress. Finally, compressive stress develops at each of the four corners. No matter how complex the patch loading might be, one of the five conditions in Figure 6.1 must represent the true state of vertical stress at the paver/bedding sand interface for rectangular pavers.

The evaluation of paver corner stresses can be understood by reference to the first of the stress blocks in Figure 6.1. For rotational equilibrium, the stress block centroid co-ordinates must be equal to the easily calculable patch load centroid co-ordinates, hence the determination of values for the two stress block lengths **l** & **t**. Once those two lengths have been so determined, vertical equilibrium can be used to determine the volume of the stress block **V** (which has a dimension of force) since its value must equal the total downward force applied to the paver. Once **V**, **l** and **t** are known, it is a simple matter to evaluate σ_A, the vertical stress beneath corner **A**.

The surface plane of the tetrahedral vertical stress distribution shown in Figure 6.1 through the three points σ_A, **l** and **t** is given by the formula:

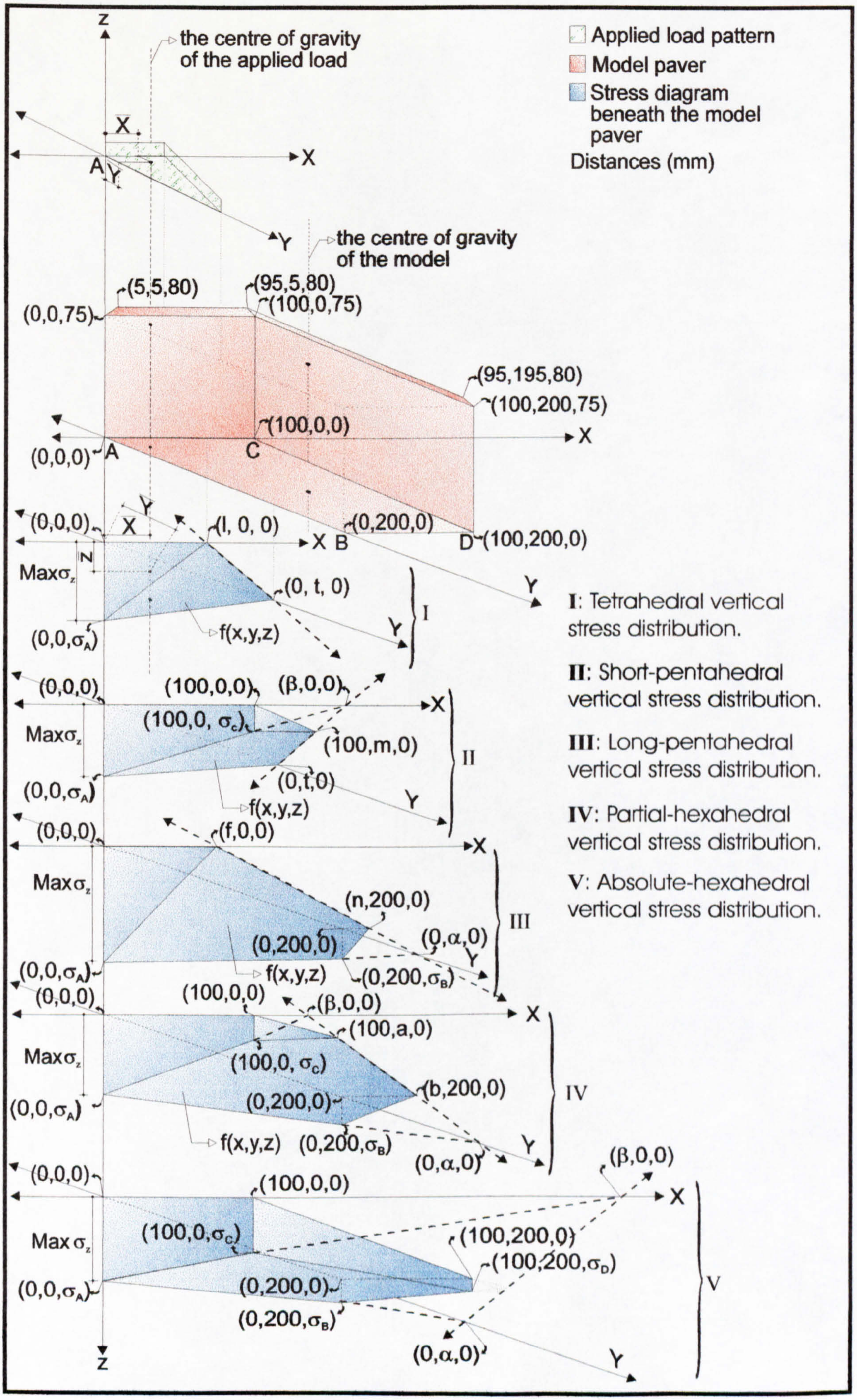

Figure 6.1: Compressive stress regimes beneath paver when patch load covers part of a paver surface. Compressive stress develops initially beneath one corner only and the stress block takes the form of a tetrahedron. Stress remains compressive for a length of **t** along one 200mm long side and for a length **l** along one 100mm short side. As the load patch progressively covers more of the paver wearing surface, stresses develop progressively from corner to corner until eventually positive stress values occur beneath each paver corner.

$$\begin{vmatrix} x & y & z & 1 \\ 0 & 0 & \sigma_A & 1 \\ l & 0 & 0 & 1 \\ 0 & t & 0 & 1 \end{vmatrix} = 0 \text{ or } z = \sigma_A\left(1-\frac{y}{t}-\frac{x}{l}\right)$$

z represents the value of the vertical stress at any in the surface

By undertaking a volume integration of this function, the volume of the tetrahedron can be determined using the boundary line function of the tetrahedron in the xy-plane ($y = t\left(1-\frac{x}{l}\right)$ or $x = l\left(1-\frac{y}{t}\right)$). This volume **V** represents the total force transmitted vertically through the paver to its underlying bedding material and is given by:

$$V = \int_0^l \int_0^{t\left(1-\frac{x}{l}\right)} \sigma_A\left(1-\frac{y}{t}-\frac{x}{l}\right) dy\, dx \Rightarrow V = \frac{\sigma_A\, t\, l}{6}$$

and the centroid distances of this volume in the xy-plane are as follows.

$$\overline{X} = \frac{1}{V}\left[\int_0^l \int_0^{t\left(1-\frac{x}{l}\right)} x\, \sigma_A\left(1-\frac{y}{t}-\frac{x}{l}\right) dy\, dx\right] \Rightarrow \overline{X} = \frac{l}{4}$$

$$\overline{Y} = \frac{1}{V}\left[\int_0^t \int_0^{l\left(1-\frac{y}{t}\right)} y\, \sigma_A\left(1-\frac{y}{t}-\frac{x}{l}\right) dx\, dy\right] \Rightarrow \overline{Y} = \frac{t}{4}$$

The following equations can be found by evaluating the tetrahedral mass and its centroid distances in terms of **l**, **t** and σ_A.

$$l = 4\overline{X},\ t = 4\overline{Y} \text{ and } \sigma_A = \frac{3\,V}{8\,\overline{X}\,\overline{Y}}$$

According to the bedding sand stress calculation method, N (total applied load) has to be equal to the total mass and the centroid of the applied load must be equal to the centroid of the vertical stress distribution occurs beneath the paver. Therefore, the equations can be formed as follows.

$$l = 4\overline{X},\ t = 4\overline{Y} \text{ and } \sigma_A = \frac{3\,\mathrm{N}}{8\,\overline{X}\,\overline{Y}}$$

Where:
$\overline{X}$ = Applied load short side centroidal distance
$\overline{Y}$ = Applied load long side centroidal distance
N = total applied load

Similar reasoning can be applied to the short-pentahedral vertical stress dissipation in Figure 6.1 in which case values are required for σ_A and σ_C. In this cases, there are three unknowns, σ_A , σ_C and t, the vertical stress run-out distance from the origin along the paver side in the y axis.

The function of the surface of the short-pentahedral vertical stress distribution shown in Figure 6.1 through the three points σ_A, β and t is given by:

$$\begin{vmatrix} x & y & z & 1 \\ 0 & 0 & \sigma_A & 1 \\ \beta & 0 & 0 & 1 \\ 0 & t & 0 & 1 \end{vmatrix} = 0 \quad \text{or} \quad z = \sigma_A\left(1 - \frac{y}{t} - \frac{x}{\beta}\right)$$

z represents the value of the vertical stress at any in the surface

From the geometry of the short-pentahedral stress distribution (see Figure 6.1),

$$\beta = \frac{100\,\sigma_A}{\sigma_A - \sigma_C} \text{ and } m = \frac{t\,\sigma_C}{\sigma_A}$$

Therefore, the stress function of the short-pentahedral mass is:

$$f(x,y) = \sigma_A\left(1 - \frac{x}{100} - \frac{y}{t}\right) + \frac{\sigma_C\,x}{100} \qquad f(x,y) = z\,(>0)$$

By undertaking a volume integration of this function, the volume of the short-pentahedral mass can be determined using the boundary line function of the short-pentahedral mass in the xy-plane. This volume V represents the total force transmitted vertically through the paver to its underlying bedding material and is given by:

$$V = \int_0^{\sigma_A}\int_0^{100}\left[\sigma_A\left(1-\frac{x}{100}-\frac{y}{t}\right)+\frac{\sigma_C x}{100}\right]dx\,dy + \int_{t\frac{\sigma_C}{\sigma_A}}^{t}\int_0^{\left[\frac{100\sigma_A}{\sigma_{A-\sigma_C}}\left(1-\frac{y}{t}\right)\right]}\left[\sigma_A\left(1-\frac{x}{100}-\frac{y}{t}\right)+\frac{\sigma_C x}{100}\right]dx\,dy \Rightarrow V=\frac{50t\left(\sigma_A^2+\sigma_A\sigma_C+\sigma_C^2\right)}{3\sigma_A}$$

and the centroid distances of this volume in the xy-plane are as follows.

$$\bar{Y}=\frac{1}{V}\left[\int_{t\frac{\sigma_C}{\sigma_A}}^{100}\int_0^{\sigma_A} y\left[\sigma_A\left(1-\frac{x}{100}-\frac{y}{t}\right)+\frac{\sigma_C x}{100}\right]dx\,dy + \int_{t\frac{\sigma_C}{\sigma_A}}^{t}\int_0^{\left[\frac{100\sigma_A}{\sigma_{A-\sigma_C}}\left(1-\frac{y}{t}\right)\right]} y\left[\sigma_A\left(1-\frac{x}{100}-\frac{y}{t}\right)+\frac{\sigma_C x}{100}\right]dx\,dy\right] \Rightarrow \bar{Y}=\frac{\left(\sigma_A+\sigma_C\right)\left(\sigma_A^2+\sigma_C^2\right)}{4\sigma_A\left(\sigma_A^2+\sigma_A\sigma_C+\sigma_C^2\right)}$$

$$\bar{X}=\frac{1}{V}\left[\int_{100}^{t\frac{\sigma_C}{\sigma_A}}\int_0^{\sigma_A} x\left[\sigma_A\left(1-\frac{x}{100}-\frac{y}{t}\right)+\frac{\sigma_C x}{100}\right]dy\,dx + \int_0^{100}\int_{t\frac{\sigma_C}{\sigma_A}}^{t\left[1-\frac{x(\sigma_A-\sigma_C)}{100\sigma_A}\right]} x\left[\sigma_A\left(1-\frac{x}{100}-\frac{y}{t}\right)+\frac{\sigma_C x}{100}\right]dy\,dx\right] \Rightarrow \bar{X}=\frac{25t\left(\sigma_A^2+2\sigma_A\sigma_C+3\sigma_C^2\right)}{\sigma_A^2+\sigma_A\sigma_C+\sigma_C^2}$$

According to the bedding sand stress calculation method, N (total applied load) has to be equal to the total mass and the centroid of the applied load must be equal to the

centroid of the vertical stress distribution beneath the paver. Therefore, the equations can be formed by evaluating the short-pentahedral mass and its centroid distances in terms of **t**, σ_A and σ_C as follows.

$$\sigma_A = \frac{N\left(50-\overline{X}+b\right)\left(-5{,}000+3\overline{X}^2+200b-3\overline{X}b\right)}{1{,}500{,}000\overline{Y}\left(\overline{X}-25\right)}$$

$$\sigma_C = \frac{N\left(-5000+3\overline{X}^2+200b-3\overline{X}b\right)}{750{,}000\overline{Y}}$$

$$t = \frac{1800\overline{Y}\left(25-\overline{X}\right)\left(50-\overline{X}+b\right)}{\left(-50+3\overline{X}+b\right)\left(5000-3\overline{X}^2-2000b+3\overline{X}b\right)}$$

Where:

$$b = \sqrt{-5{,}000+3\overline{X}-3\overline{X}^2}$$

$$N = \sum Load$$

$$\overline{X} = Applied\ load\ short\ side\ centroidal\ distance$$

$$\overline{Y} = Applied\ load\ long\ side\ centroidal\ distance$$

Note that for this solution to be valid for rectangular pavers of plan dimensions 200mm x 100mm, $\overline{X}$ must lie in the range: $21.1325 \le \overline{X} \le 78.8675 mm$

Similar reasoning can be applied to the long-pentahedral vertical stress distribution in Figure 6.1 in which case values are required for σ_A and σ_B. In this case, there are three unknowns, σ_A, σ_B and **f**, the vertical stress run-out distance from the origin along the paver side in the **x** axis.

The function of the surface of the long-pentahedral vertical stress distribution shown in Figure 6.1 through the three points σ_A, α and **t** is given by:

$$\begin{vmatrix} x & y & z & 1 \\ 0 & 0 & \sigma_A & 1 \\ f & 0 & 0 & 1 \\ 0 & \alpha & 0 & 1 \end{vmatrix} = 0 \quad \text{or } z = \sigma_A\left(1 - \frac{y}{\alpha} - \frac{x}{f}\right)$$

z represents the value of the vertical stress at any in the surface

From the geometry of the long-pentahedral stress distribution (see Figure 6.1),

$$\alpha = \frac{200\,\sigma_A}{\sigma_A - \sigma_B} \text{ and } n = \frac{f\,\sigma_B}{\sigma_A}$$

Therefore, the stress function of the long-pentahedral mass is:

$$f(x,y) = \sigma_A\left(1 - \frac{x}{f} - \frac{y}{200}\right) + \frac{\sigma_B y}{200} \qquad f(x,y) = z\ (>0)$$

By undertaking a volume integration of this function, the volume of the long-pentahedral mass can be determined using the boundary line function of long-pentahedral mass in the xy-plane. This volume V represents the total force transmitted vertically through the paver to its underlying bedding material and is given by:

$$V = \int_0^{f\frac{\sigma_B}{\sigma_A}} \int_0^{200} \left[\sigma_A\left(1 - \frac{x}{f} - \frac{y}{200}\right) + \frac{\sigma_B y}{200}\right] dy\,dx + \int_{f\frac{\sigma_B}{\sigma_A}}^{f} \int_0^{\left[\frac{200\sigma_A}{\sigma_{A-\sigma_B}}\left(1-\frac{x}{f}\right)\right]} \left[\sigma_A\left(1 - \frac{x}{f} - \frac{y}{200}\right) + \frac{\sigma_B y}{200}\right] dy\,dx$$

$$\Rightarrow V = \frac{100f\left(\sigma_A^2 + \sigma_A\sigma_B + \sigma_B^2\right)}{3\sigma_A}$$

and the centroid distances of this volume in the xy-plane are as follows.

$$\overline{X}=\frac{1}{V}\left[\begin{array}{l}\displaystyle\int_0^{f\frac{\sigma_B}{\sigma_A}}\int_0^{200} x\left[\sigma_A\left(1-\frac{x}{f}-\frac{y}{200}\right)+\frac{\sigma_B y}{200}\right]dy\,dx \\ \displaystyle+\int_{f\frac{\sigma_B}{\sigma_A}}^{f}\int_0^{\left[\frac{200\sigma_A}{\sigma_{A-}\sigma_B}\left(1-\frac{x}{f}\right)\right]} x\left[\sigma_A\left(1-\frac{x}{f}-\frac{y}{200}\right)+\frac{\sigma_B y}{200}\right]dy\,dx\end{array}\right]\Rightarrow \overline{X}=\frac{f\left(\sigma_A+\sigma_B\right)\left(\sigma_A^2+\sigma_B^2\right)}{4\sigma_A\left(\sigma_A^2+\sigma_A\sigma_B+\sigma_B^2\right)}$$

$$\overline{Y}=\frac{1}{V}\left[\begin{array}{l}\displaystyle\int_0^{200}\int_0^{f\frac{\sigma_B}{\sigma_A}} y\left[\sigma_A\left(1-\frac{x}{f}-\frac{y}{200}\right)+\frac{\sigma_B y}{200}\right]dx\,dy \\ \displaystyle+\int_0^{200}\int_{f\frac{\sigma_B}{\sigma_A}}^{f\left[1-\frac{y\left(\sigma_A-\sigma_B\right)}{200\sigma_A}\right]} y\left[\sigma_A\left(1-\frac{x}{f}-\frac{y}{200}\right)+\frac{\sigma_B y}{200}\right]dx\,dy\end{array}\right]\Rightarrow \overline{Y}=\frac{50\left(\sigma_A^2+2\sigma_A\sigma_B+3\sigma_B^2\right)}{\left(\sigma_A^2+\sigma_A\sigma_B+\sigma_B^2\right)}$$

According to the bedding sand stress calculation method, N (total applied load) has to be equal to the total mass and the centroid of the applied load must be equal to the centroid of the vertical stress distribution beneath the paver. Therefore, the equations can be formed by evaluating the long-pentahedral mass and its centroid distance in terms of f, σ_A and σ_B as follows.

$$\sigma_A=\frac{N\left(100-\overline{Y}+a\right)\left(-20{,}000+3\overline{Y}^2+400a-3\overline{Y}a\right)}{12{,}000{,}000\overline{X}\left(\overline{Y}-50\right)}$$

$$\sigma_B=\frac{N\left(-20{,}000+3\overline{Y}^2+400a-3\overline{Y}a\right)}{6{,}000{,}000\overline{X}}$$

$$f=\frac{3600\overline{X}\left(50-\overline{Y}\right)\left(100-\overline{Y}+a\right)}{\left(-100+3\overline{Y}+a\right)\left(20{,}000-3\overline{Y}^2-400a+3\overline{Y}a\right)}$$

Where:

$$a = \sqrt{-20{,}000 + 600\overline{Y} - 3\overline{Y}^2}$$

$$N = \sum Load$$

$$\overline{X} = Applied\ load\ short\ side\ centroidal\ distance$$

$$\overline{Y} = Applied\ load\ long\ side\ centroidal\ distance$$

Note that for this solution to be valid for rectangular pavers of plan dimensions 200mm x 100mm, $\overline{Y}$ must lie in the range: $42.265 \le y \le 157.735 mm$

Figure 6.1 shows the stress pattern when compressive stress occurs at three paver corners. Rotational equilibrium requires that the centroid of the stress block corresponds with the centroid of the load patch, hence values for the stress block centroid co-ordinates.

Similar reasoning can be applied to the partial-hexahedral vertical stress distribution in Figure 6.1 in which case values are required for σ_A , σ_B and σ_C. The function of the surface of the partial-hexahedral vertical stress distribution shown in Figure 6.1 through the three points σ_A, α and β is given by.

$$\begin{vmatrix} x & y & z & 1 \\ 0 & 0 & \sigma_A & 1 \\ \beta & 0 & 0 & 1 \\ 0 & \alpha & 0 & 1 \end{vmatrix} = 0 \quad \text{or} \quad z = \sigma_A\left(1 - \frac{y}{\alpha} - \frac{x}{\beta}\right)$$

z represents the value of the vertical stress at any in the surface

From the geometry of the partial-hexahedral stress distribution (see Figure 6.1),

$$\alpha = \frac{200\ \sigma_A}{\sigma_A - \sigma_B}\ ,\ \beta = \frac{100\ \sigma_A}{\sigma_A - \sigma_C},\ a = \frac{\alpha(\beta - 100)}{\beta} = \frac{200\ \sigma_C}{\sigma_A - \sigma_B} \text{ and}$$

$$b = \frac{\beta(\alpha - 200)}{\alpha} = \frac{100\ \sigma_B}{\sigma_A - \sigma_C}$$

Therefore, the stress function of the partial-hexahedral mass is:

$$f(x,y)=\sigma_A\left(1-\frac{x}{\beta}-\frac{y}{\alpha}\right) \qquad f(x,y)=z\,(>0)$$

By undertaking a volume integration of this function, the volume of the partial-hexahedral mass can be determined using the boundary line function of partial-hexahedral mass in the xy-plane. This volume **V** represents the total force transmitted vertically through the paver to its underlying bedding material and is given by:

$$V=\int_0^b\int_0^{200}\left[\sigma_A\left(1-\frac{x}{\beta}-\frac{y}{\alpha}\right)\right]dy\,dx+\int_b^{100}\int_0^{\alpha\left(1-\frac{x}{\beta}\right)}\left[\sigma_A\left(1-\frac{x}{\beta}-\frac{y}{\alpha}\right)\right]dy\,dx$$

$$\Rightarrow V=\frac{50\sigma_A\left(10000\alpha^2-300\alpha^2\beta+3\alpha^2\beta^2-1200\beta^3+6\alpha\beta^3\right)}{3\alpha\beta^2}$$

and the centroid distances of this volume in the xy-plane are as follows.

$$\overline{X}=\frac{1}{V}\left[\int_0^b\int_0^{200}x\left[\sigma_A\left(1-\frac{x}{\beta}-\frac{y}{\alpha}\right)\right]dy\,dx+\int_b^{100}\int_0^{\alpha\left(1-\frac{x}{\beta}\right)}x\left[\sigma_A\left(1-\frac{x}{\beta}-\frac{y}{\alpha}\right)\right]dy\,dx\right]$$

$$\Rightarrow \overline{X}=\frac{2\left(375000\alpha^4-10000\alpha^4\beta+75\alpha^4\beta^2+4000000\beta^4-300\alpha^2\beta^4+\alpha^3\beta^4\right)}{\alpha^2\left(10000\alpha^2-300\alpha^2\beta+3\alpha^2\beta-1200\beta^3+6\alpha\beta^3\right)}$$

$$\overline{Y}=\frac{1}{V}\left[\int_0^a\int_0^{100}y\left[\sigma_A\left(1-\frac{x}{\beta}-\frac{y}{\alpha}\right)\right]dx\,dy+\int_a^{200}\int_0^{\beta\left(1-\frac{y}{\alpha}\right)}y\left[\sigma_A\left(1-\frac{x}{\beta}-\frac{y}{\alpha}\right)\right]dx\,dy\right]\Rightarrow$$

$$\overline{Y} = \frac{-100000000\alpha^4 + 4000000\alpha^4\beta - 60000\alpha^4\beta^2 + 400\alpha^4\beta^3 + 480000000\beta^4 - 6400000\alpha\beta^4 + 240000\alpha^2\beta^4 - \alpha^4\beta^4}{400\alpha\beta\left(10000\alpha^2 - 300\alpha^2\beta + 3\alpha^2\beta^2 - 1200\beta^3 + 6\alpha\beta^3\right)}$$

According to the bedding sand stress calculation method, N (total applied load) has to be equal to the total mass and the centroid of the applied load must be equal to the centroid of the vertical stress distribution beneath the paver. Therefore, the equations can be formed by evaluating the partial-hexahedral mass and its centroid distances in terms of σ_A, α, β as follows.

$$\sigma_A = \frac{3N\alpha\beta^2}{50\left(10000\alpha^2 - 300\alpha^2\beta + 3\alpha^2\beta^2 - 1200\beta^3 + 6\alpha\beta^3\right)}$$

$$0 = 8000000\beta^4 + \alpha^4\left(-750000 + 20000\beta - 150\beta^2 + 10000\overline{X} - 300\beta\overline{X} + 3\beta^2\overline{X}\right) +$$
$$\alpha^2\left(600\beta^4 - 1200\beta^3\overline{X}\right) + \alpha^3\left(-2\beta^4 + 6\beta^3\overline{X}\right)$$

$$0 = 10.10^7\alpha^4 + \beta^4\left(-48.10^8 + 64.10^6\alpha - 24.10^4\alpha^2 + \alpha^4 - 48.10^4\alpha\overline{Y} + 2400\alpha^2\overline{Y}\right) +$$
$$\beta^2\left(60000\alpha^4 - 120000\alpha^3\overline{Y}\right) + \beta^3\left(-400\alpha^4 + 1200\alpha^3\overline{Y}\right) + \beta\left(-4.10^6\alpha^4 + 4.10^6\alpha^3\overline{Y}\right)$$

The solution to these equations is particularly complex so an iterative solution has been used in their evaluation (see Appendix).

The final part of Figure 6.1 shows compressive stress at each of the four paver corners. The function of the surface of the absolute-hexahedral vertical stress distribution shown in Figure 6.1 through the three points σ_A, α and β is given by:

$$\begin{vmatrix} x & y & z & 1 \\ 0 & 0 & \sigma_A & 1 \\ \beta & 0 & 0 & 1 \\ 0 & \alpha & 0 & 1 \end{vmatrix} = 0 \quad \text{or} \quad z = \sigma_A\left(1 - \frac{y}{\alpha} - \frac{x}{\beta}\right)$$

z represents the value of the vertical stress at any in the surface

From the geometry of the absolute-hexahedral stress distribution (see Figure 6.1),

$$\alpha = \frac{200\,\sigma_A}{\sigma_A - \sigma_B} \text{ and } \beta = \frac{100\,\sigma_A}{\sigma_A - \sigma_C}$$

Therefore, the stress function of the absolute-hexahedral mass is:

$$f(x,y) = \sigma_A - \frac{(\sigma_A - \sigma_C)x}{100} - \frac{(\sigma_A - \sigma_B)y}{200} \qquad f(x,y) = z\,(>0)$$

By undertaking a volume integration of this function, the volume of the absolute-hexahedral mass can be determined. This volume V represents the total force transmitted vertically through the paver to its underlying bedding material and is given by:

$$V = \int_0^{100}\int_0^{200}\left[\sigma_A - \frac{(\sigma_A - \sigma_C)x}{100} - \frac{(\sigma_A - \sigma_B)y}{200}\right]dy\,dx \Rightarrow V = 10000\left(\sigma_B + \sigma_C\right)$$

and the centroid distances of this volume in the xy-plane are as follows.

$$\overline{X} = \frac{1}{V}\left[\int_0^{100}\int_0^{200} x\left[\sigma_A - \frac{(\sigma_A - \sigma_C)x}{100} - \frac{(\sigma_A - \sigma_B)y}{200}\right]dy\,dx\right] \Rightarrow \overline{X} = \frac{50\left(3\sigma_B + 4\sigma_C - \sigma_A\right)}{3\left(\sigma_B + \sigma_C\right)}$$

$$\overline{Y} = \frac{1}{V}\left[\int_0^{200}\int_0^{100} y\left[\sigma_A - \frac{(\sigma_A - \sigma_C)x}{100} - \frac{(\sigma_A - \sigma_B)y}{200}\right]dx\,dy\right] \Rightarrow \overline{Y} = \frac{100\left(4\sigma_B + 3\sigma_C - \sigma_A\right)}{3\left(\sigma_B + \sigma_C\right)}$$

The solution follows the pattern of the solutions above such that three non-linear equations are established in σ_A, σ_B and σ_C. The solution of the absolute-hexahedral case is as follows:

$$\sigma_A = \frac{N(700 - 6\overline{X} - 3\overline{Y})}{2{,}000{,}000}$$

$$\sigma_B = \frac{N(100 - 6\overline{X} + 3\overline{Y})}{2{,}000{,}000}$$

$$\sigma_C = \frac{N(100 + 6\overline{X} - 3\overline{Y})}{2{,}000{,}000}$$

Where:

$$N = \sum Load$$

$$\overline{X} = Applied\ load\ short\ side\ centroidal\ distance$$

$$\overline{Y} = Applied\ load\ long\ side\ centroidal\ distance$$

Once the three corner stress values have been determined, the fourth corner stress σ_D can be determined from the following equation which is true as a result of the planarity of the stress variation:

$$\sigma_D = \sigma_C + \sigma_B - \sigma_A$$

The vertical stress analysis for non-chamfered rectangular pavers can be calculated in a similar way. The only difference is in the patch load application since the chamfer reduces surface area of the patch loading by some 20%-30%. The stress patterns shown in Figure 6.1 can also be used for non-chamfered rectangular pavers.

6.3. Evaluation of vertical stresses in bedding sand with & without interlock for rectangular paver pavement

The solutions developed in the previous section are now used to develop relationships between patch load geometry and resulting vertical stress at the paver underside for rectangular pavers. Figures 6.2 to 6.16 show the development of paver corner stresses according to the different patch load applications in the case of a chamfered rectangular paver of dimensions 100mm x 200mm. The maximum stress beneath a 0.8N/mm^2 patch

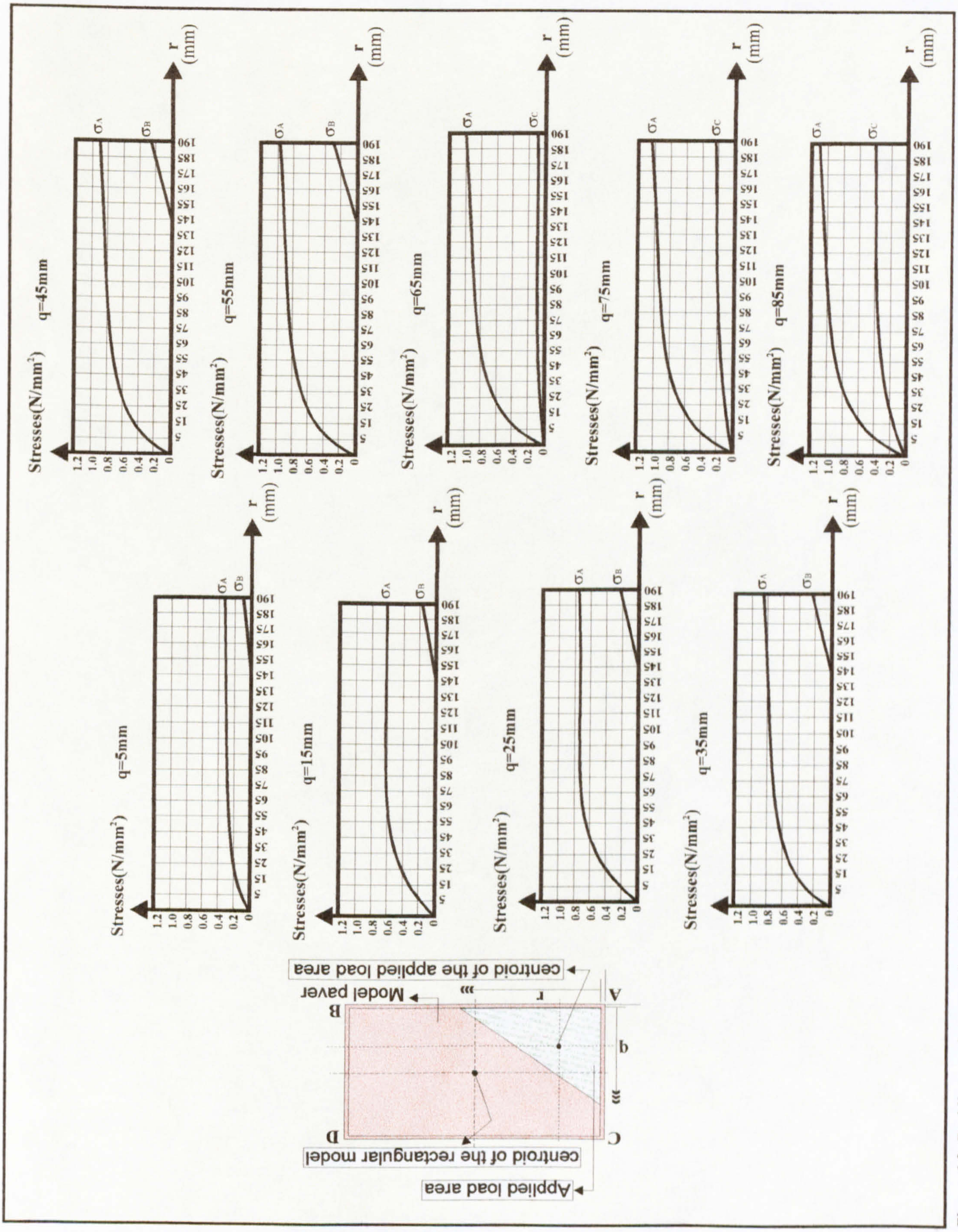

Figure 6.2: Bedding sand stress values (N/mm²) beneath the four corners of a 200mm x 100mm chamfered rectangular paver for various shapes of patch loading.

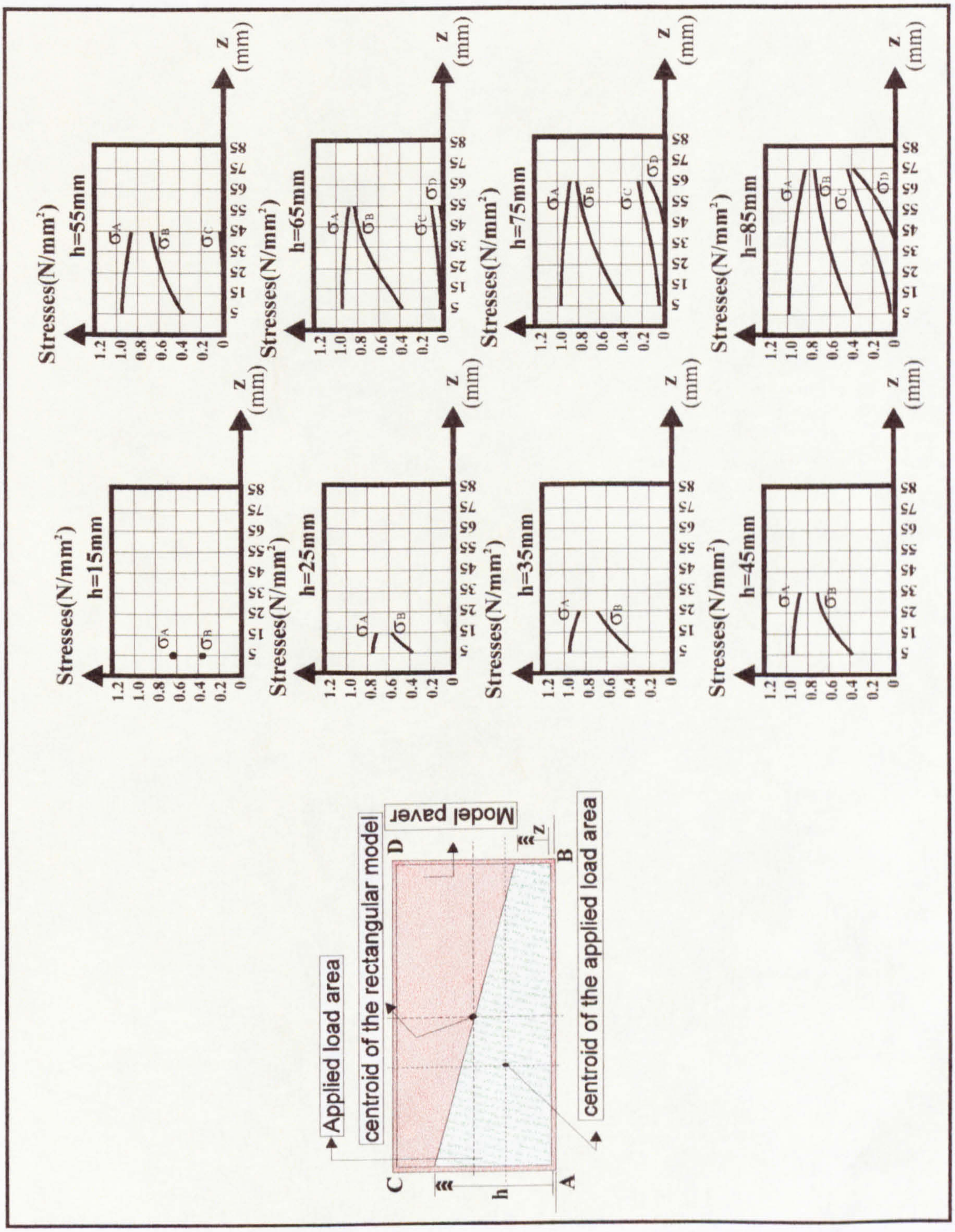

Figure 6.3: Bedding sand stress values (N/mm²) beneath the four corners of a 200mm x 100mm chamfered rectangular paver for various shapes of patch loading.

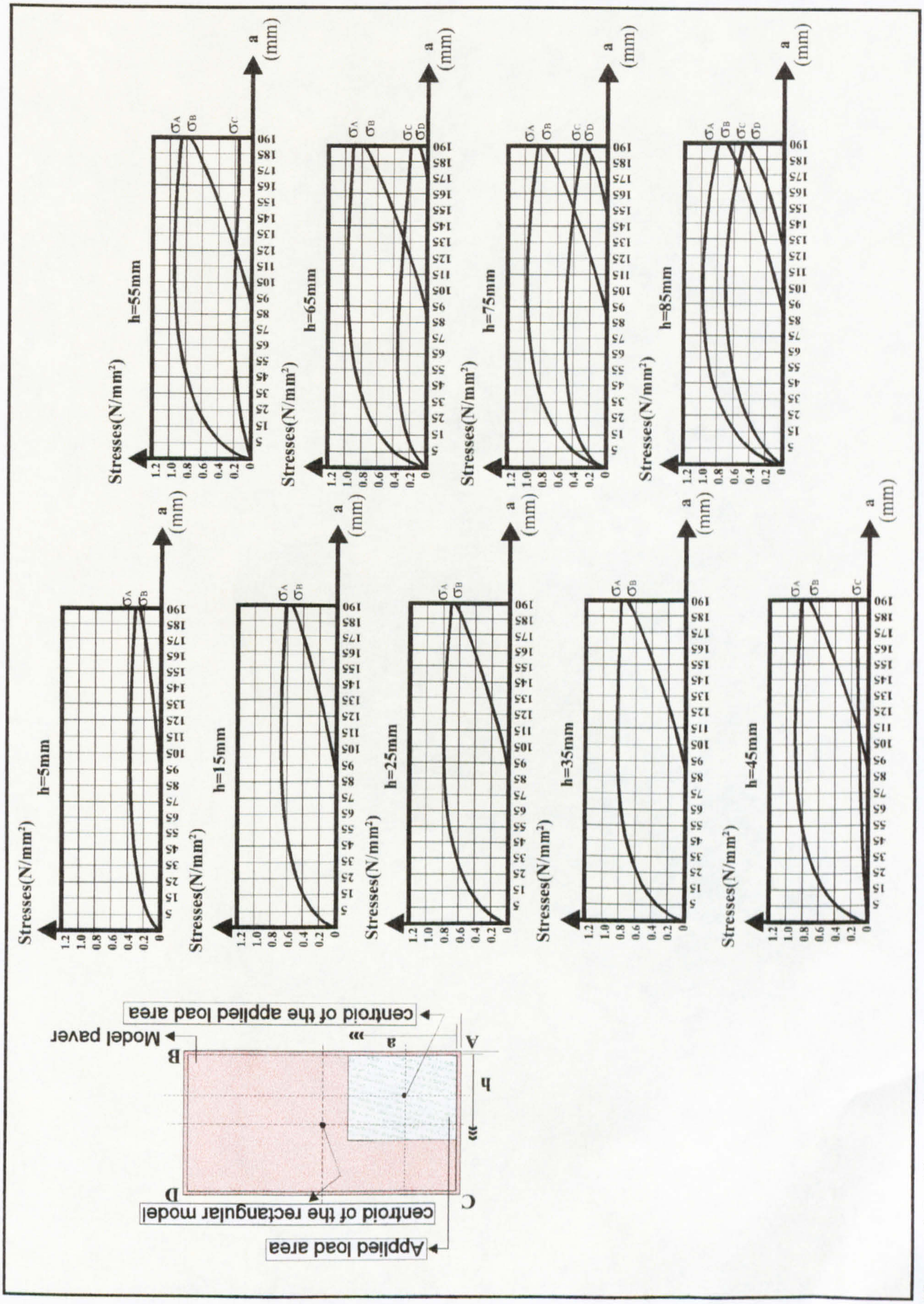

Figure 6.4: Bedding sand stress values (N/mm²) beneath the four corners of a 200mm x 100mm chamfered rectangular paver for various shapes of patch loading.

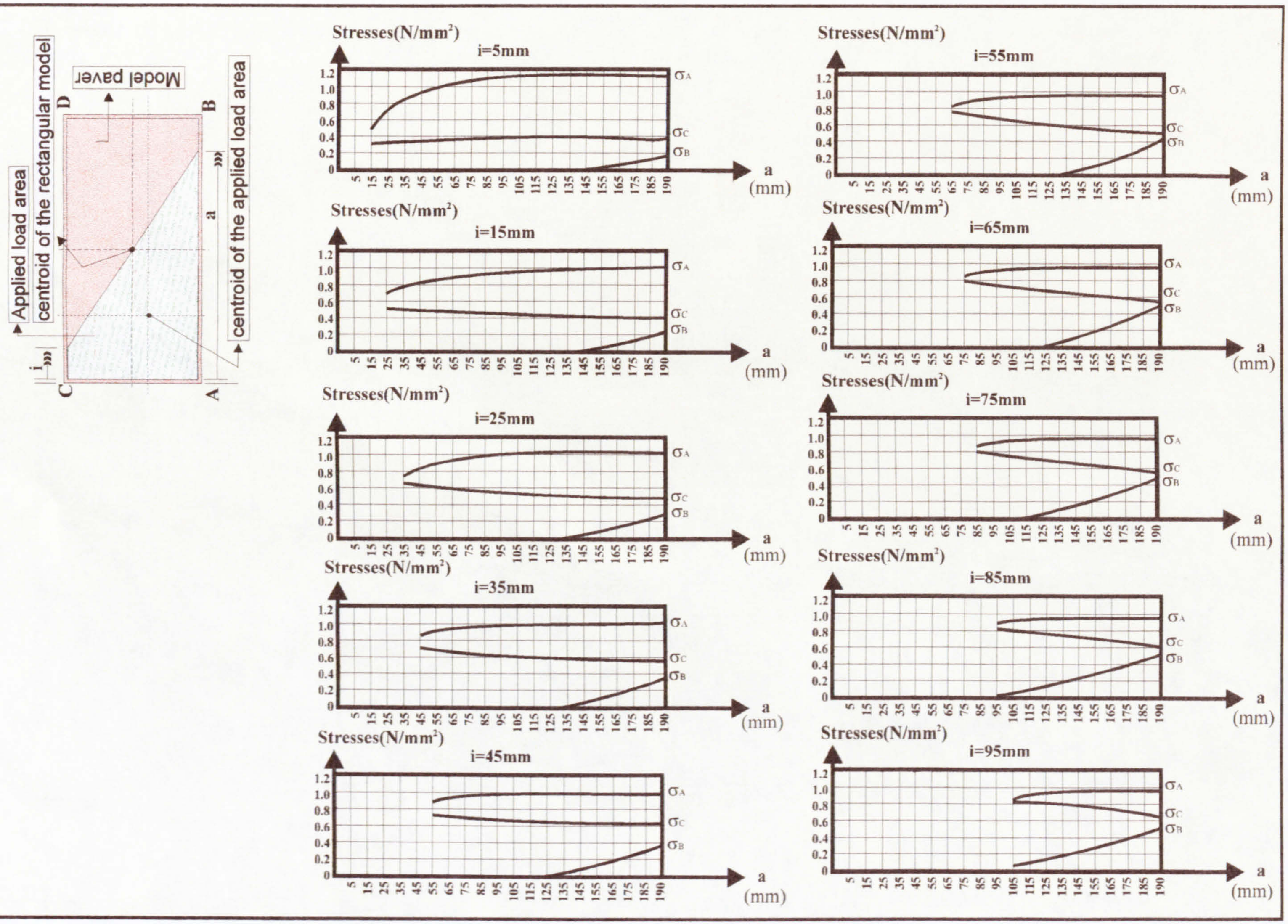

Figure 6.5(a): Bedding sand stress values (N/mm²) beneath the four corners of a 200mm x 100mm chamfered rectangular paver for various shapes of patch loading.

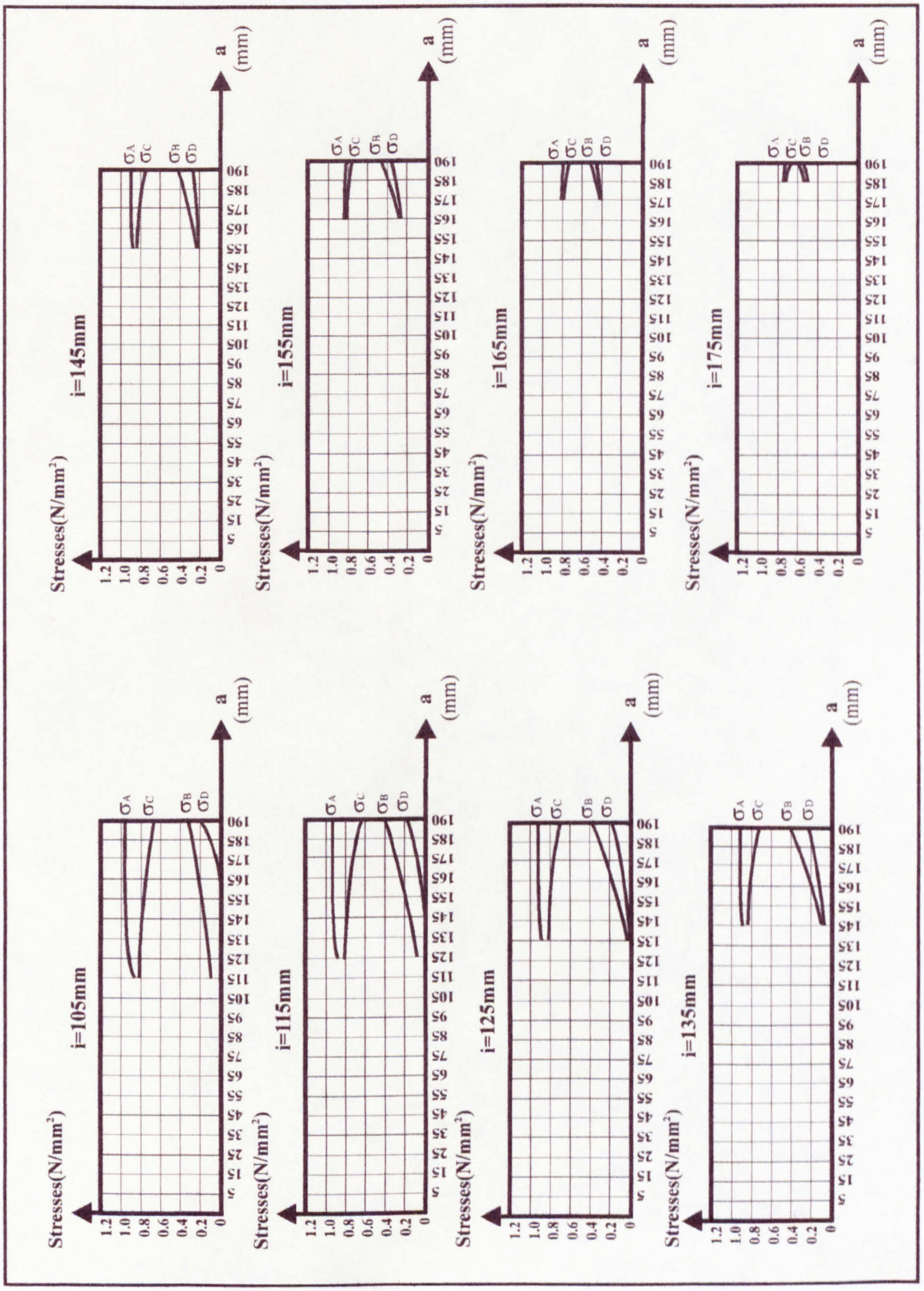

Figure 6.5(b): Bedding sand stress values (N/mm²) beneath the four corners of a 200mm x 100mm chamfered rectangular paver for various shapes of patch loading.

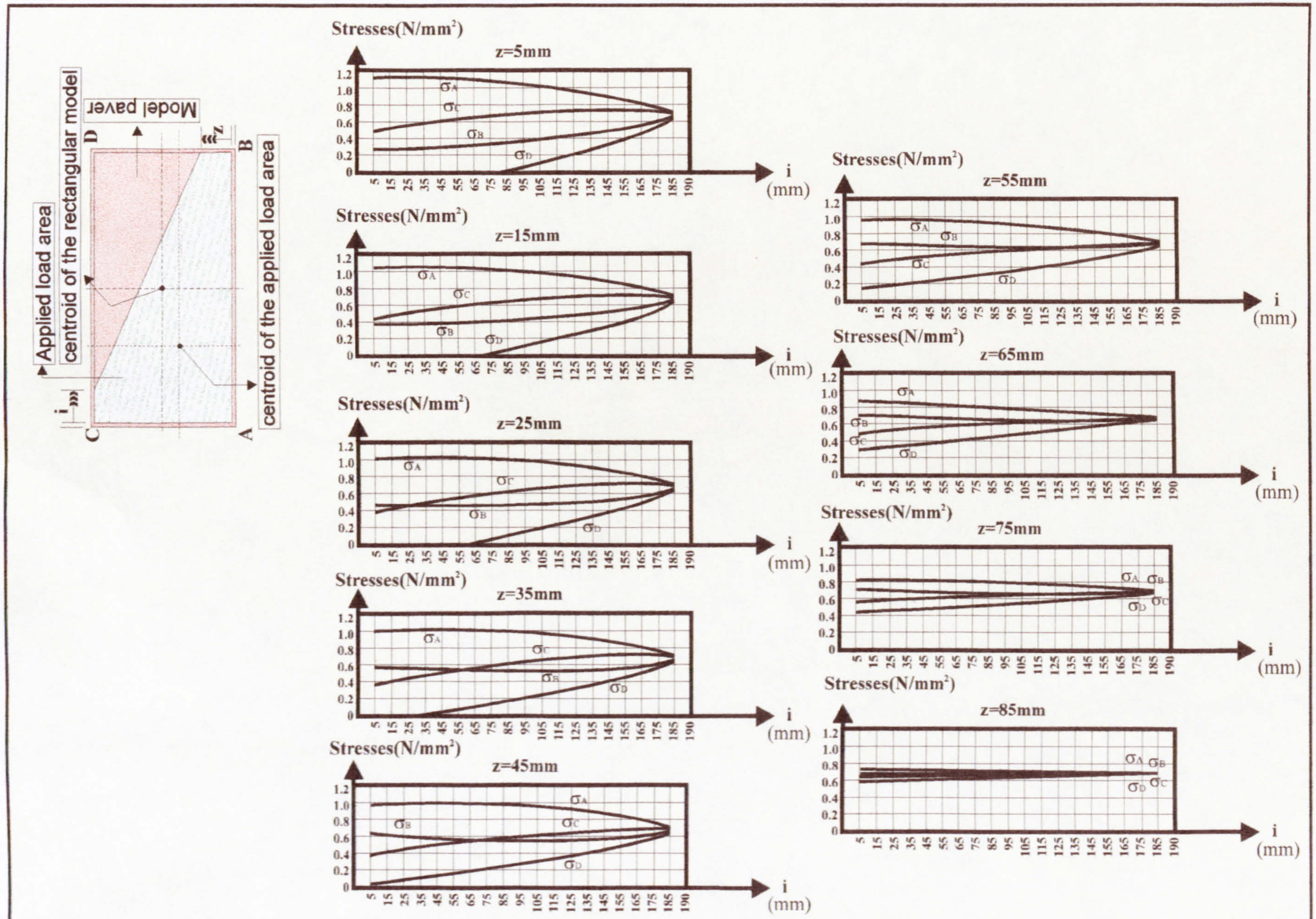

Figure 6.6: Bedding sand stress values (N/mm²) beneath the four corners of a 200mm x 100mm chamfered rectangular paver for various shapes of patch loading.

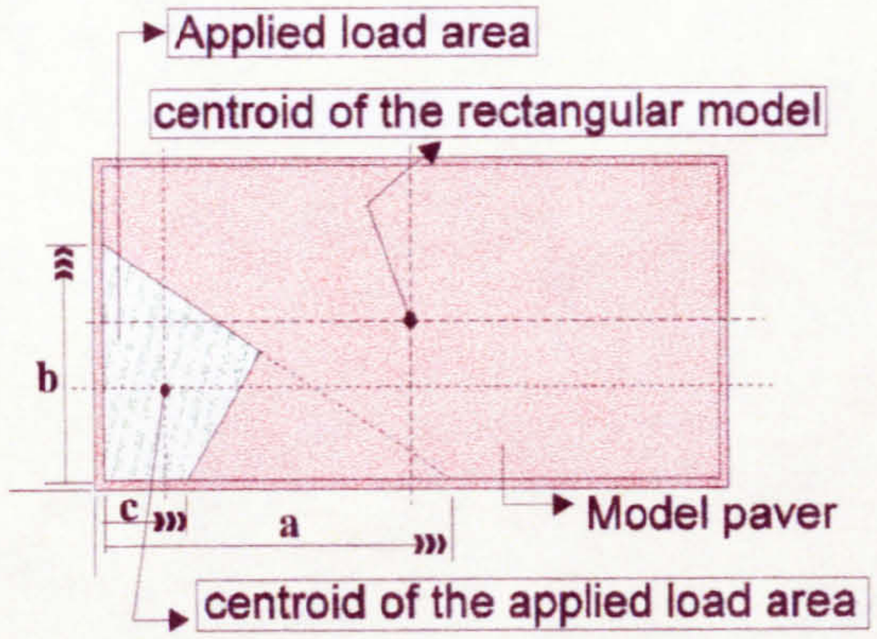

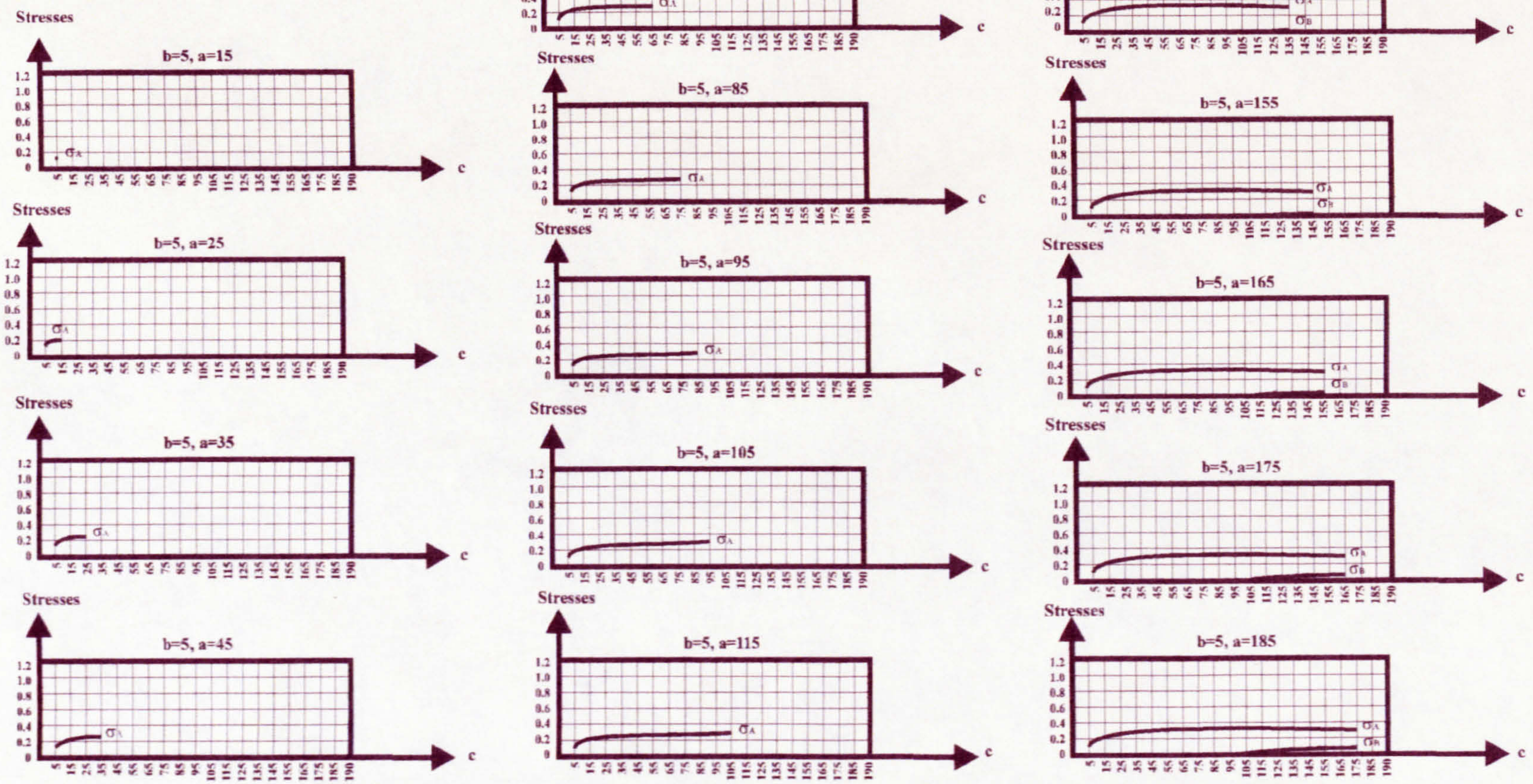

Figure 6.7(a): Bedding sand stress values (N/mm²) beneath the four corners of a 200mm x 100mm chamfered rectangular paver for various shapes of patch loading.

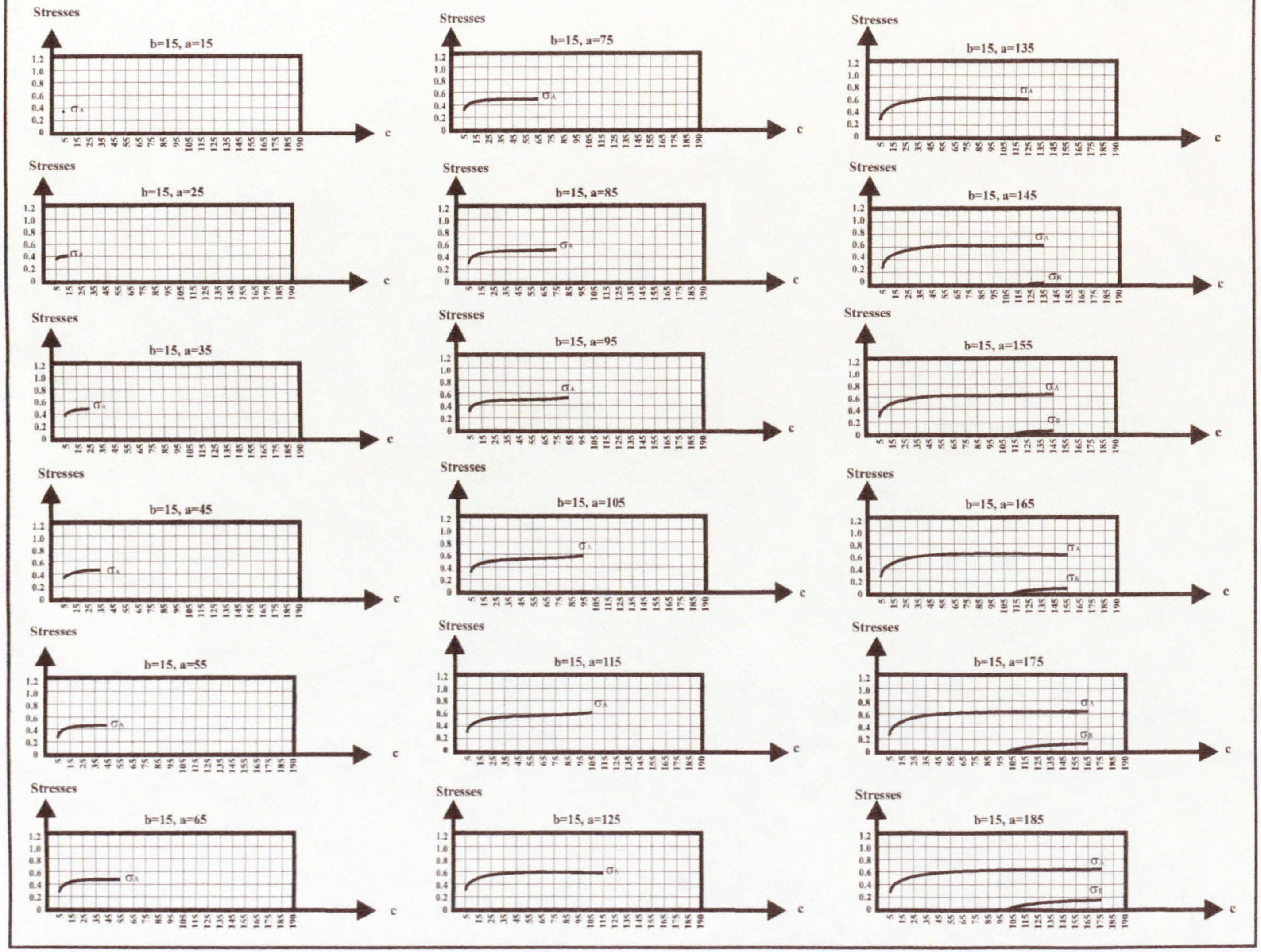

Figure 6.7(b): Bedding sand stress values (N/mm²) beneath the four corners of a 200mm x 100mm chamfered rectangular paver for various shapes of patch loading.

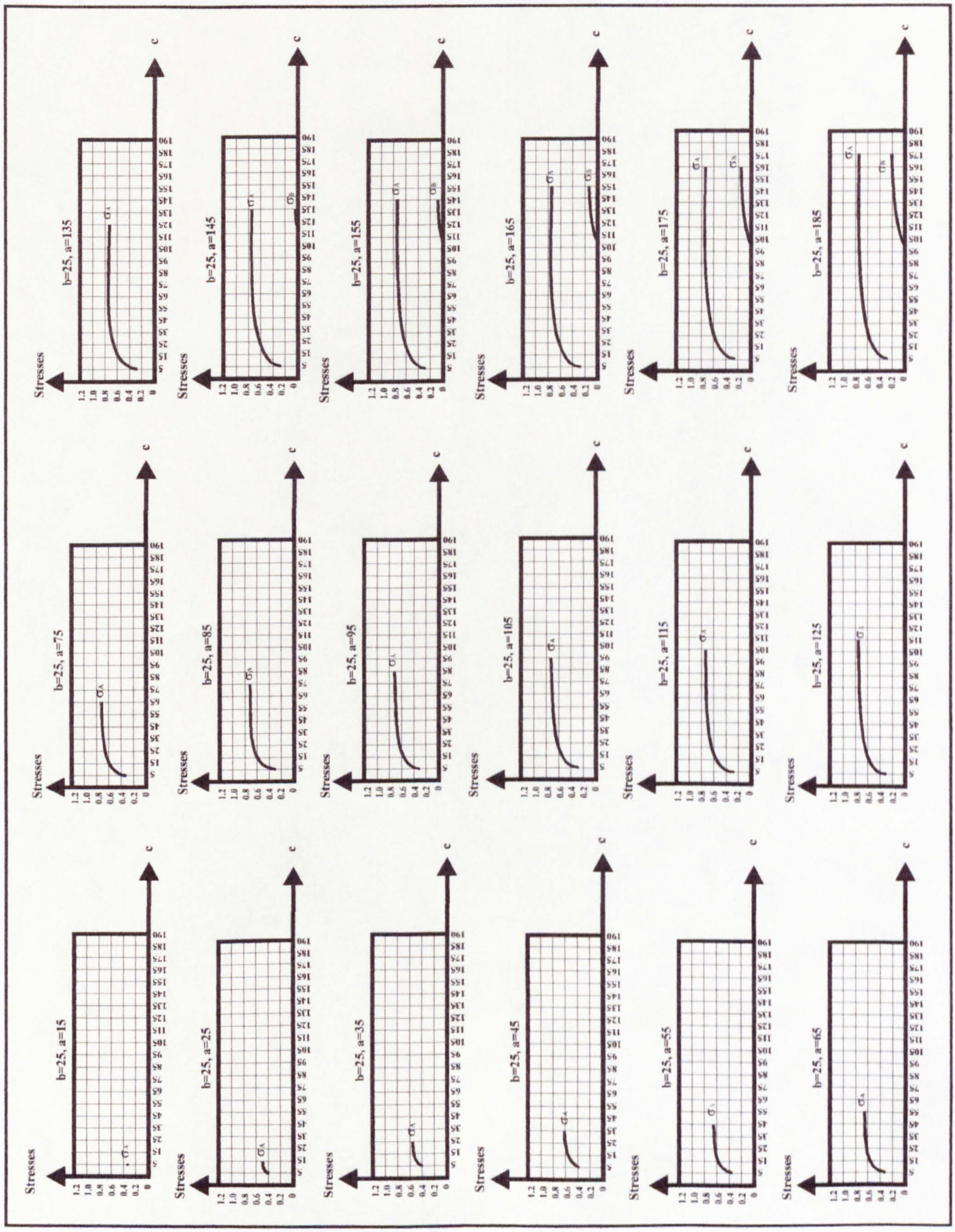

Figure 6.7(c): Bedding sand stress values (N/mm²) beneath the four corners of a 200mm x 100mm chamfered rectangular paver for various shapes of patch loading.

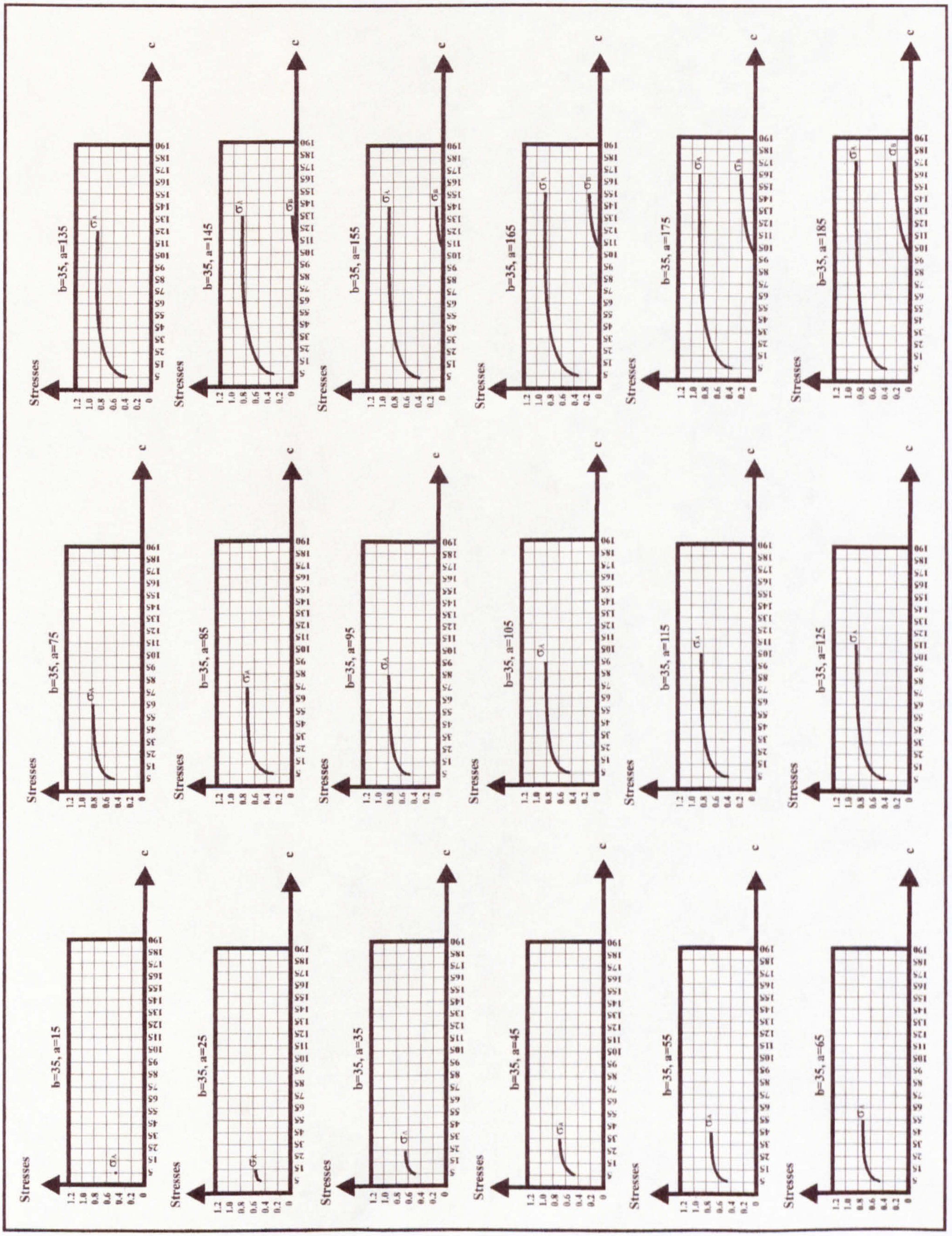

Figure 6.7(d): Bedding sand stress values (N/mm²) beneath the four corners of a 200mm x 100mm chamfered rectangular paver for various shapes of patch loading.

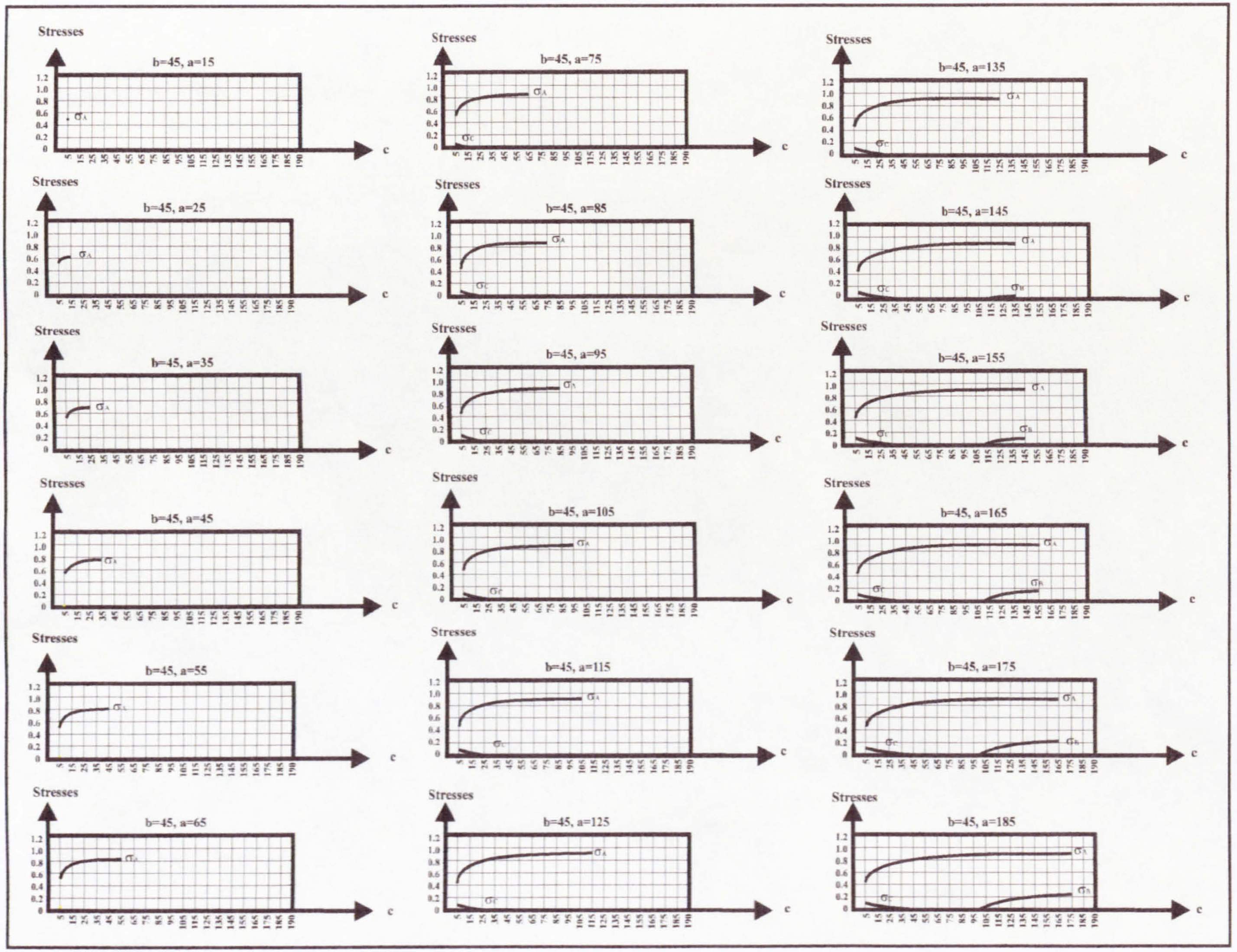

Figure 6.7(e): Bedding sand stress values (N/mm²) beneath the four corners of a 200mm x 100mm chamfered rectangular paver for various shapes of patch loading.

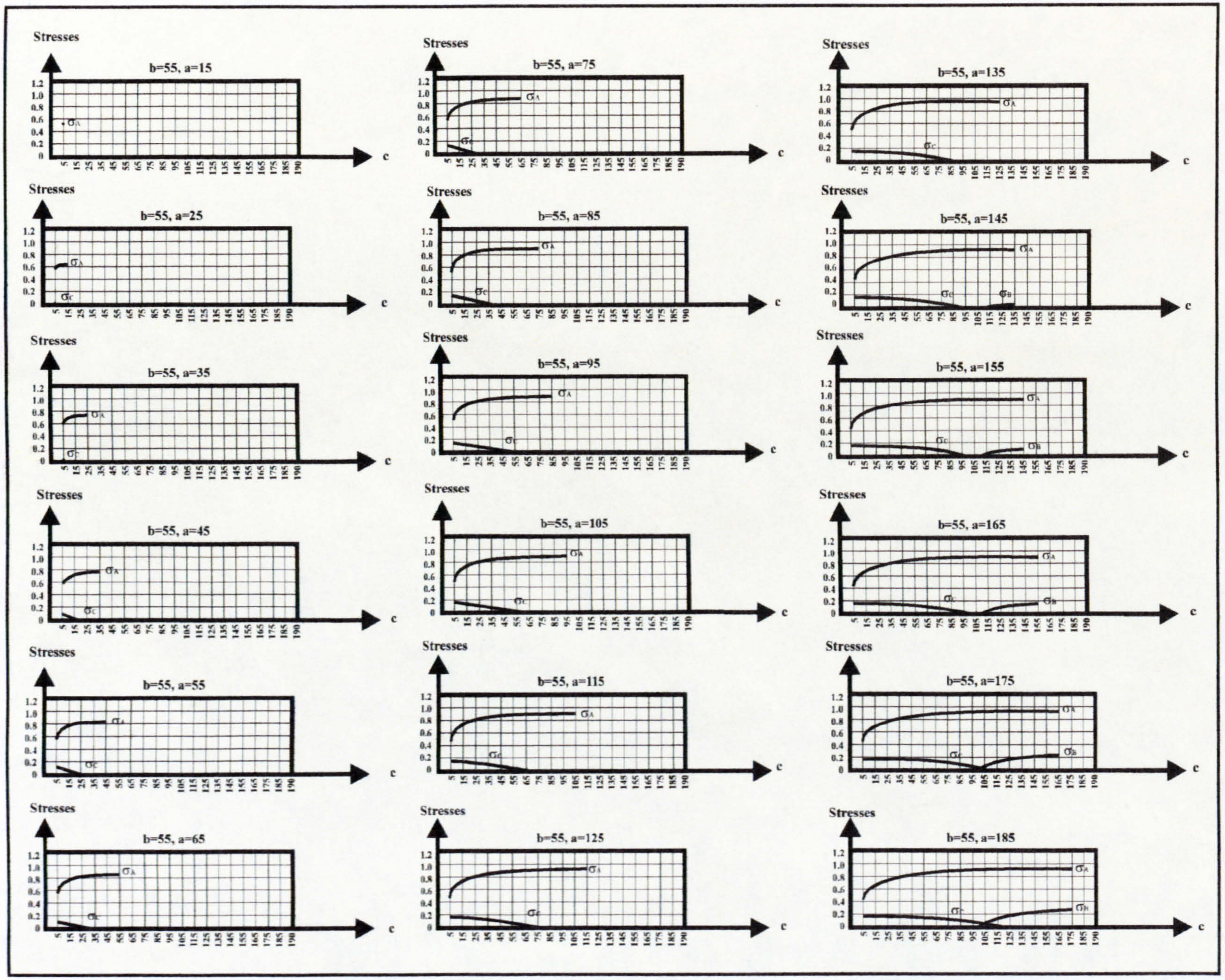

Figure 6.7(f): Bedding sand stress values (N/mm²) beneath the four corners of a 200mm x 100mm chamfered rectangular paver for various shapes of patch loading.

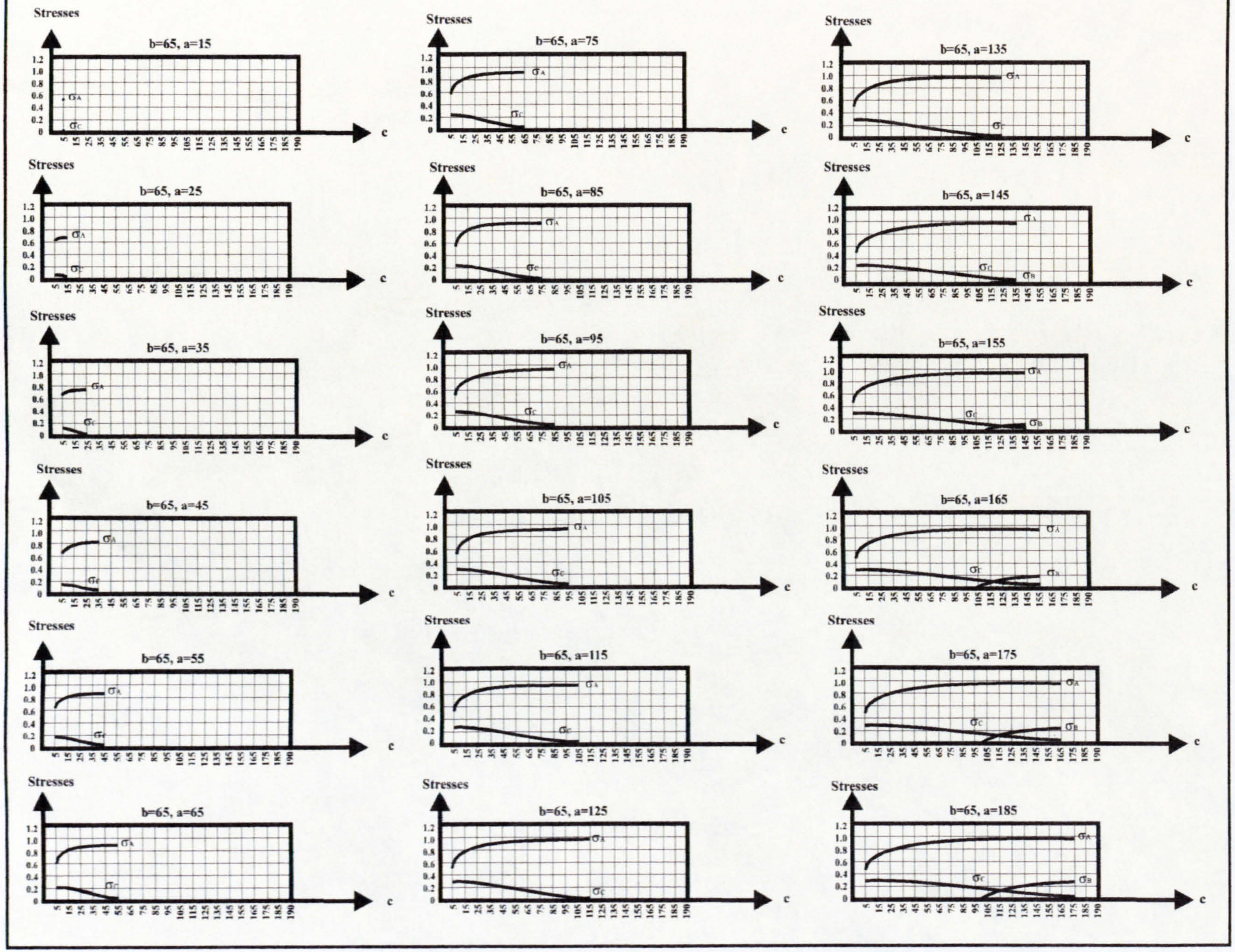

Figure 6.7(g): Bedding sand stress values (N/mm²) beneath the four corners of a 200mm x 100mm chamfered rectangular paver for various shapes of patch loading.

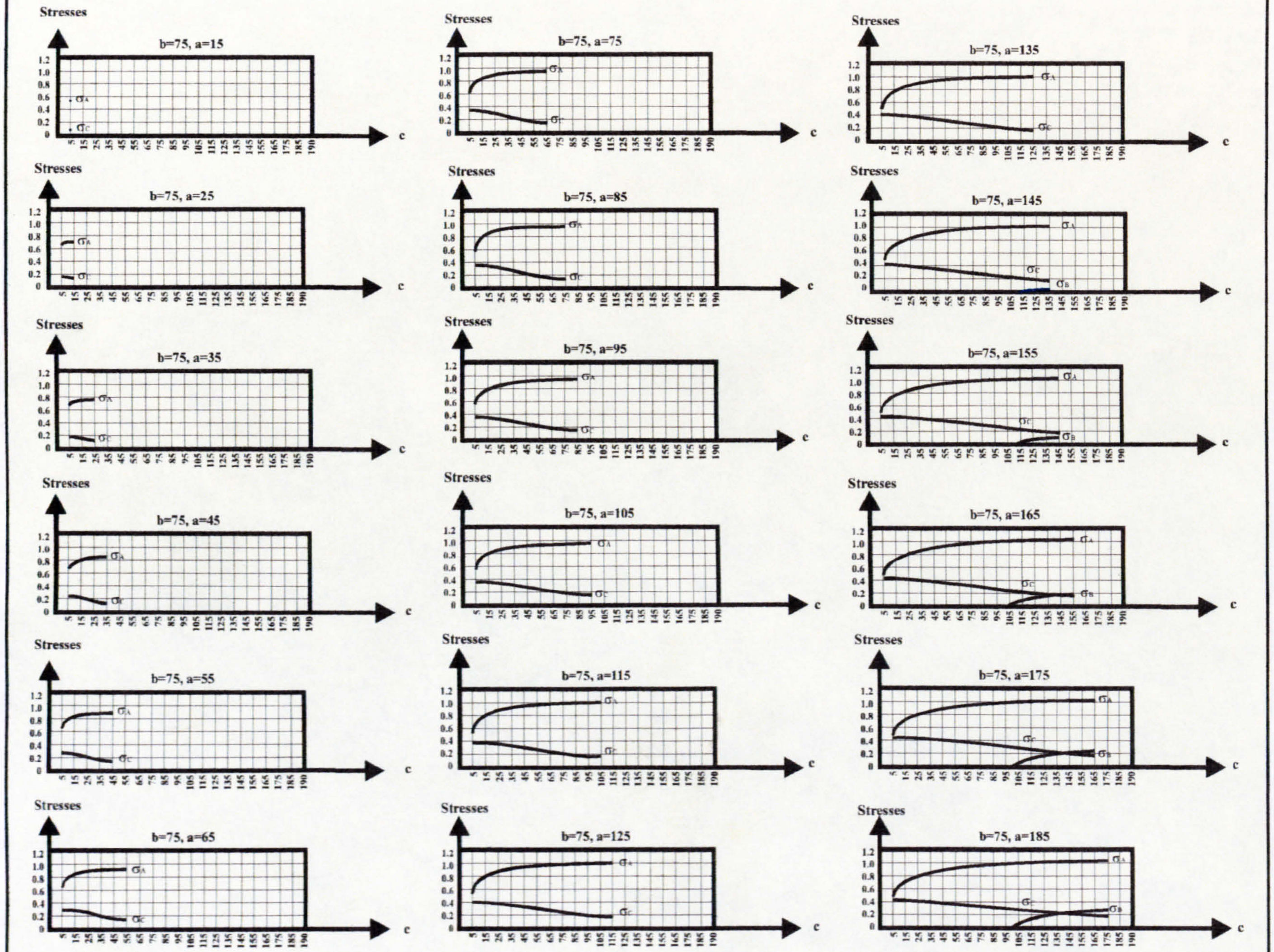

Figure 6.7(h): Bedding sand stress values (N/mm²) beneath the four corners of a 200mm x 100mm chamfered rectangular paver for various shapes of patch loading.

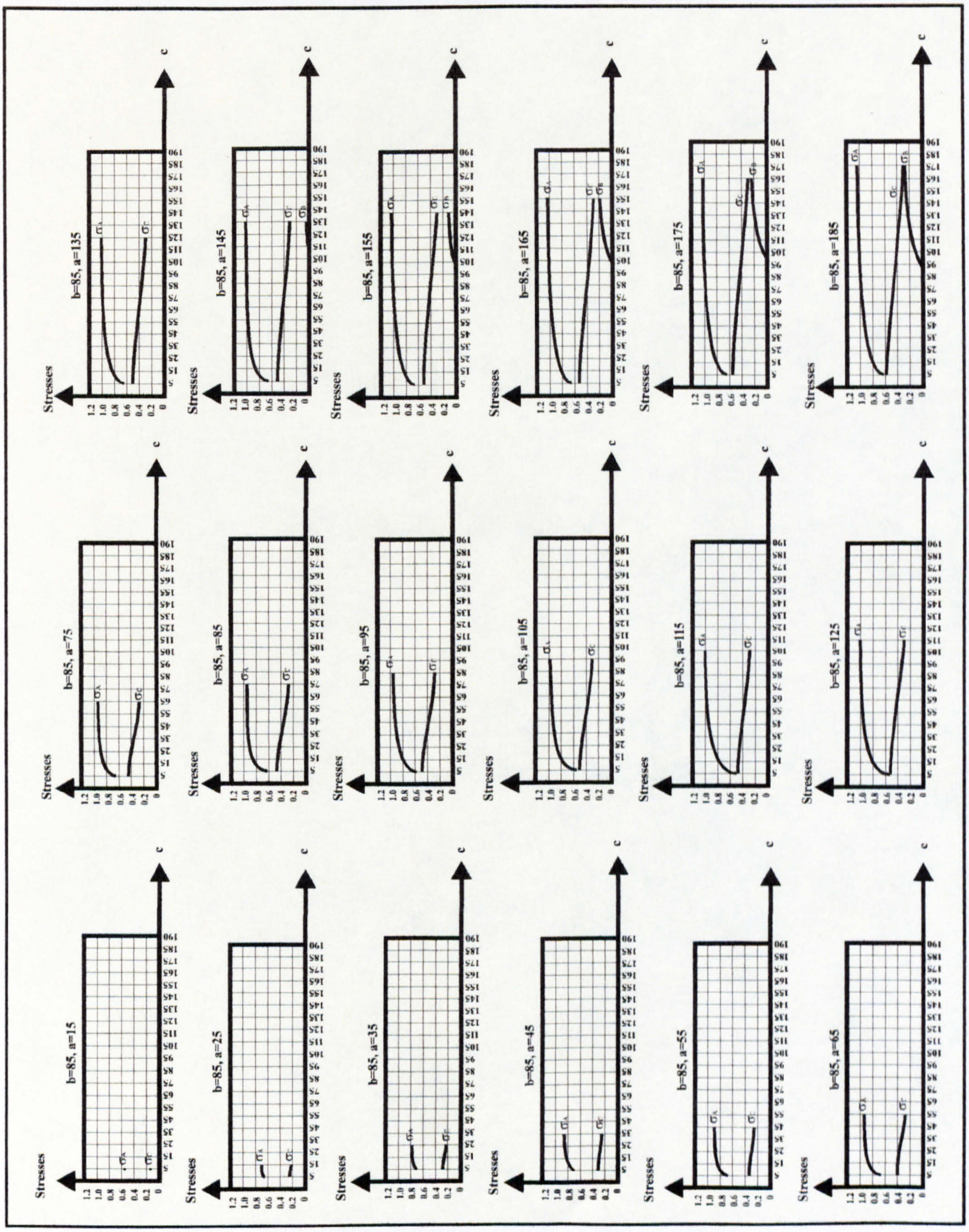

Figure 6.7(i): Bedding sand stress values (N/mm²) beneath the four corners of a 200mm x 100mm chamfered rectangular paver for various shapes of patch loading.

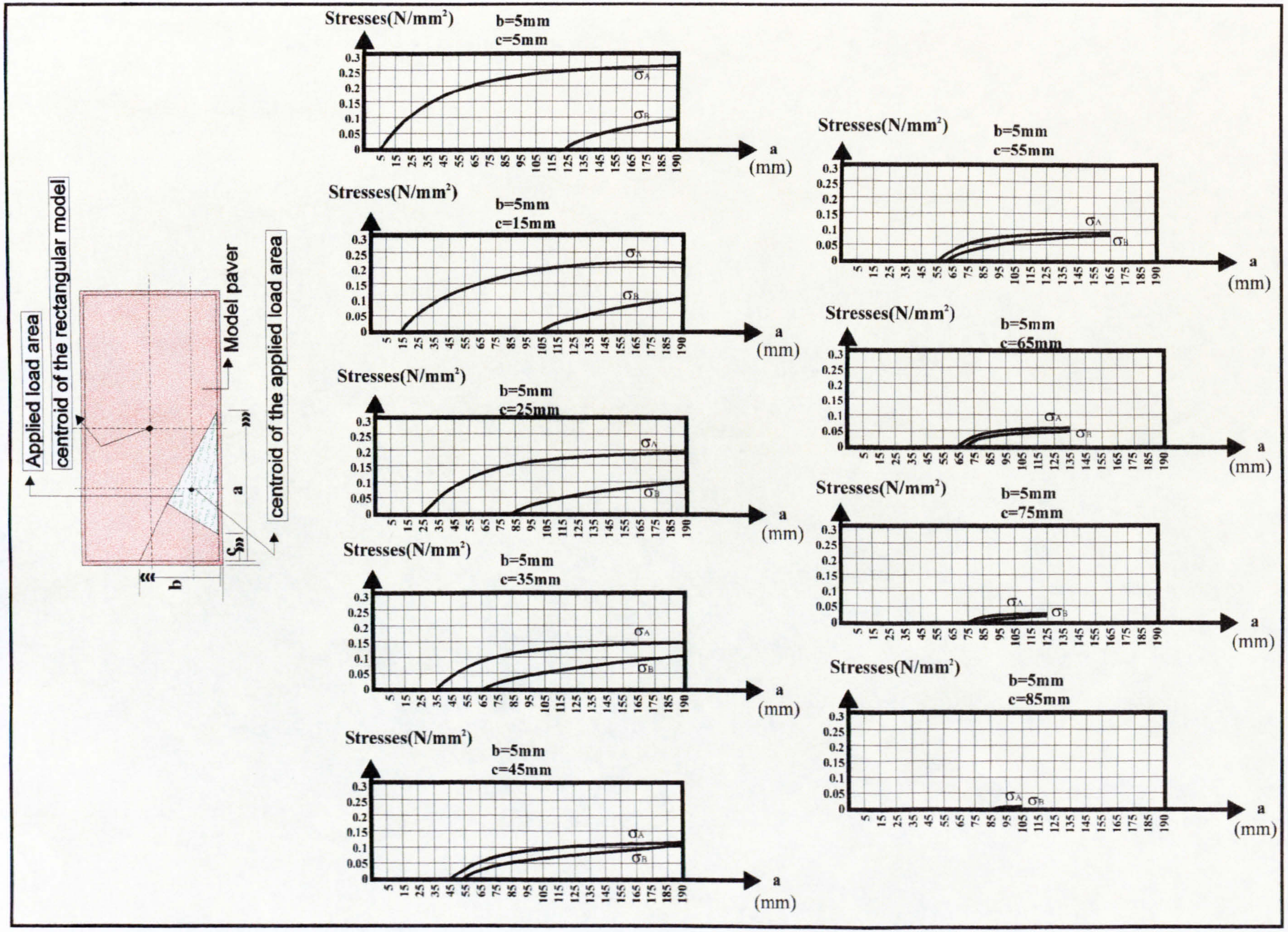

Figure 6.8(a): Bedding sand stress values (N/mm²) beneath the four corners of a 200mm x 100mm chamfered rectangular paver for various shapes of patch loading.

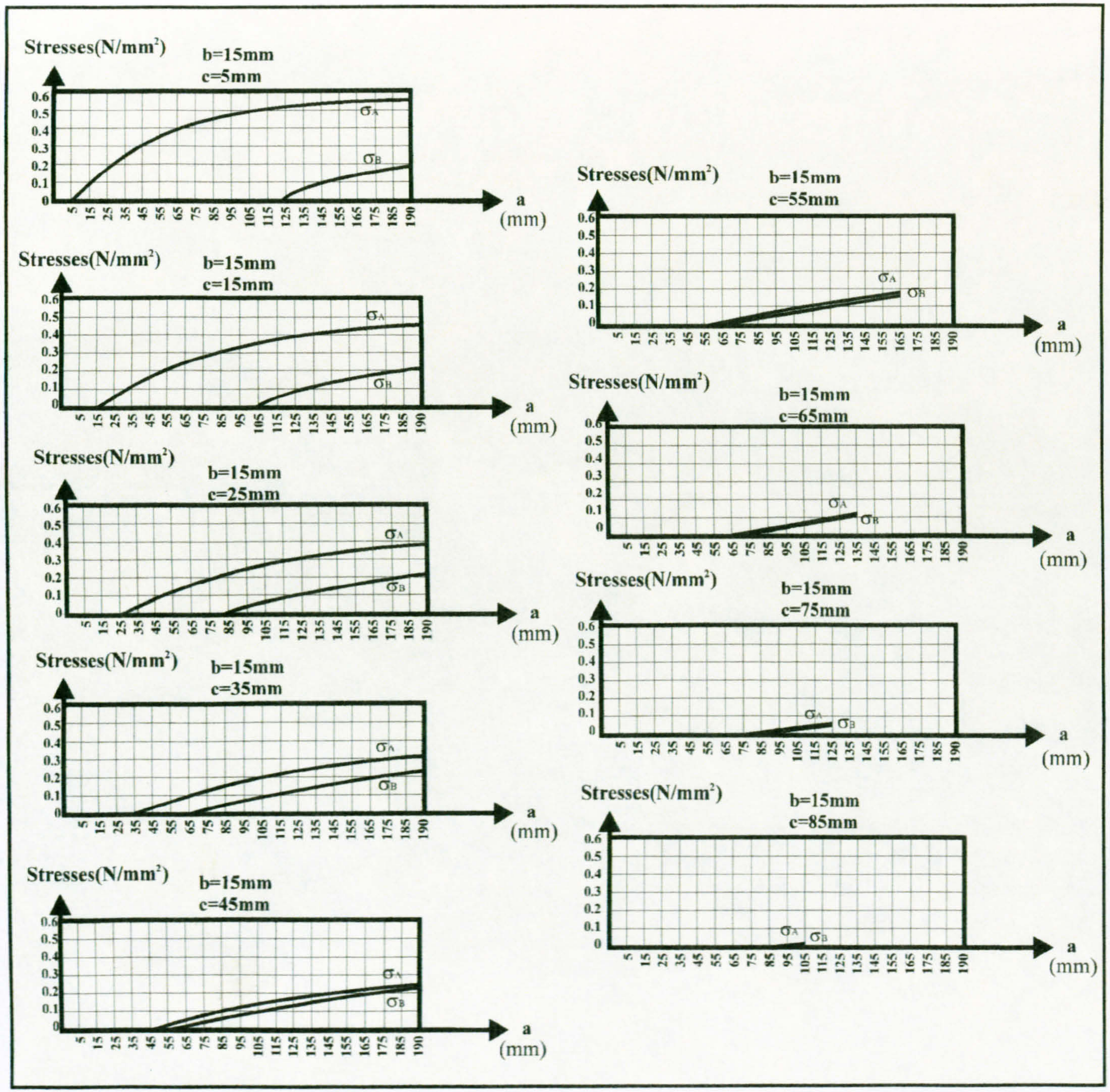

Figure 6.8(b): Bedding sand stress values (N/mm²) beneath the four corners of a 200mm x 100mm chamfered rectangular paver for various shapes of patch loading.

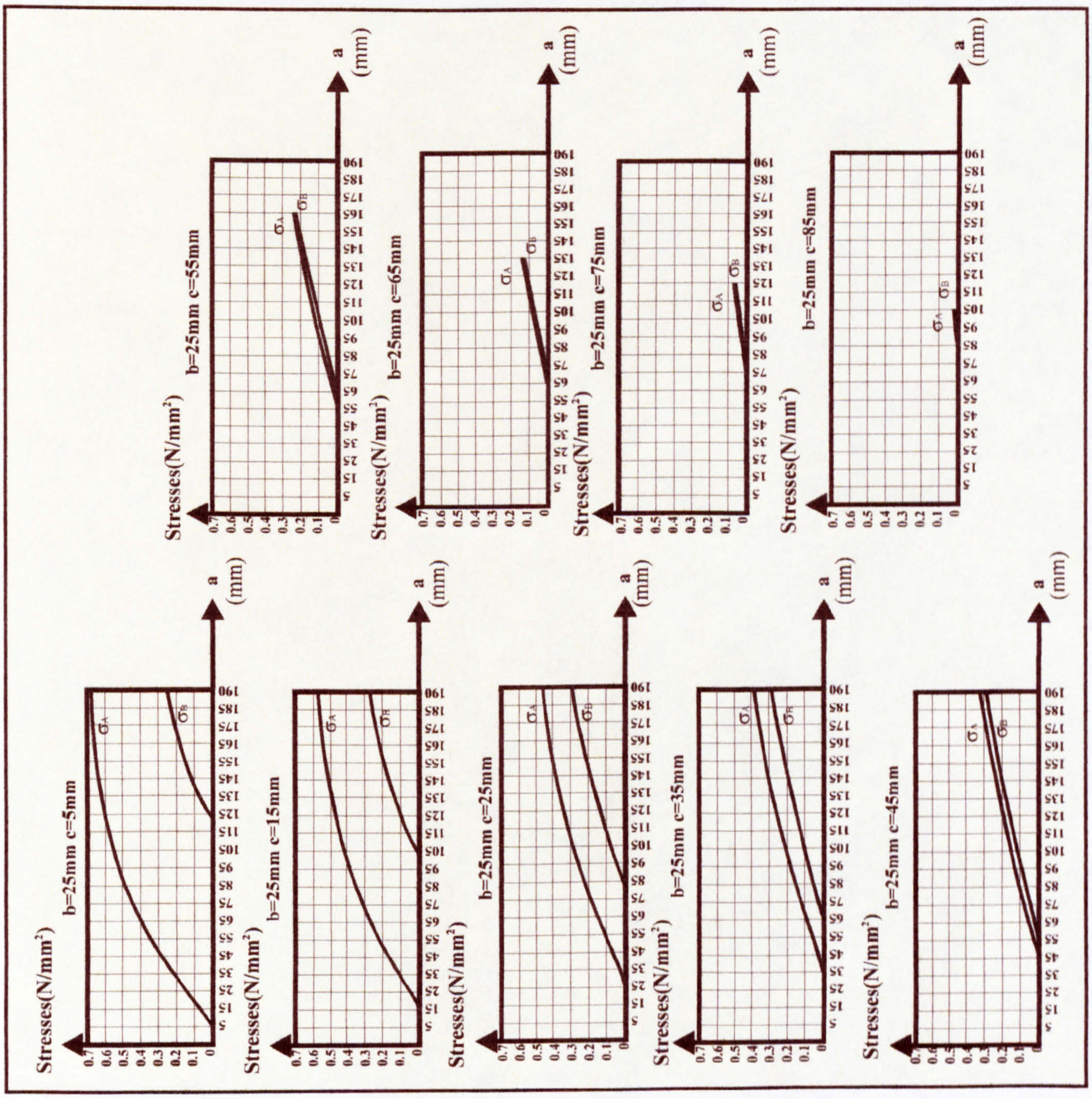

Figure 6.8(c): Bedding sand stress values (N/mm²) beneath the four corners of a 200mm x 100mm chamfered rectangular paver for various shapes of patch loading.

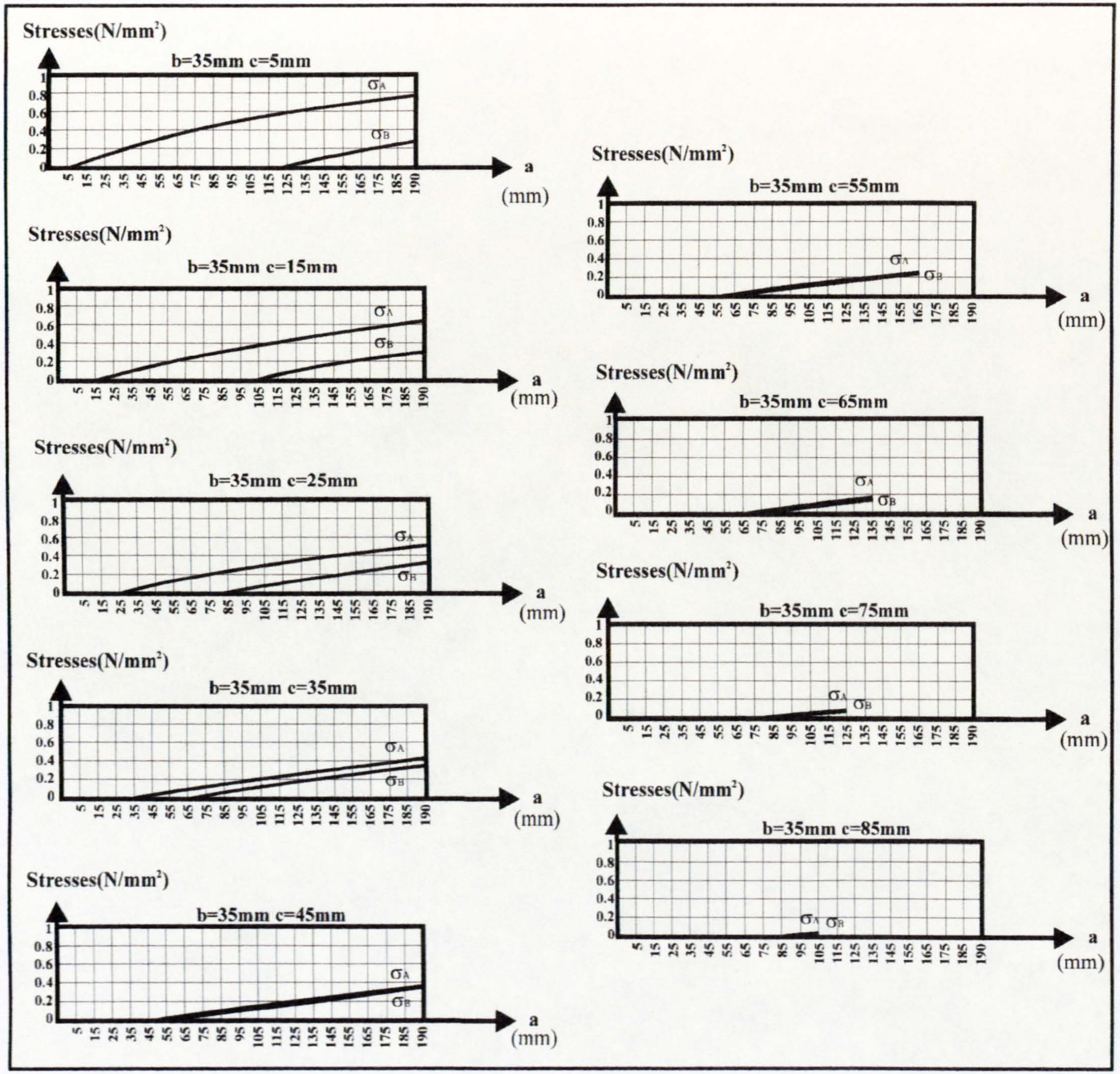

Figure 6.8(d): Bedding sand stress values (N/mm²) beneath the four corners of a 200mm x 100mm chamfered rectangular paver for various shapes of patch loading.

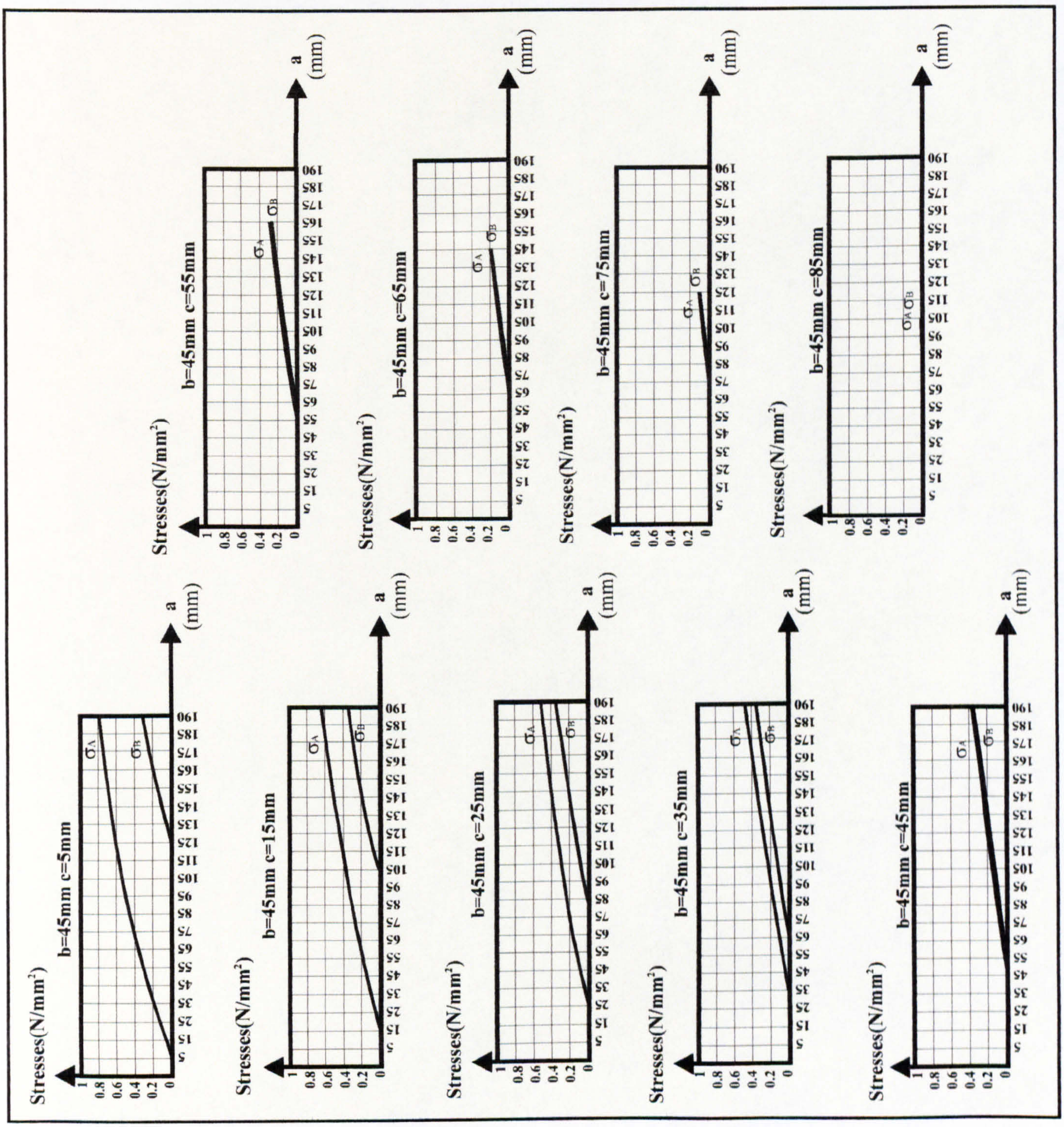

Figure 6.8(e): Bedding sand stress values (N/mm²) beneath the four corners of a 200mm x 100mm chamfered rectangular paver for various shapes of patch loading.

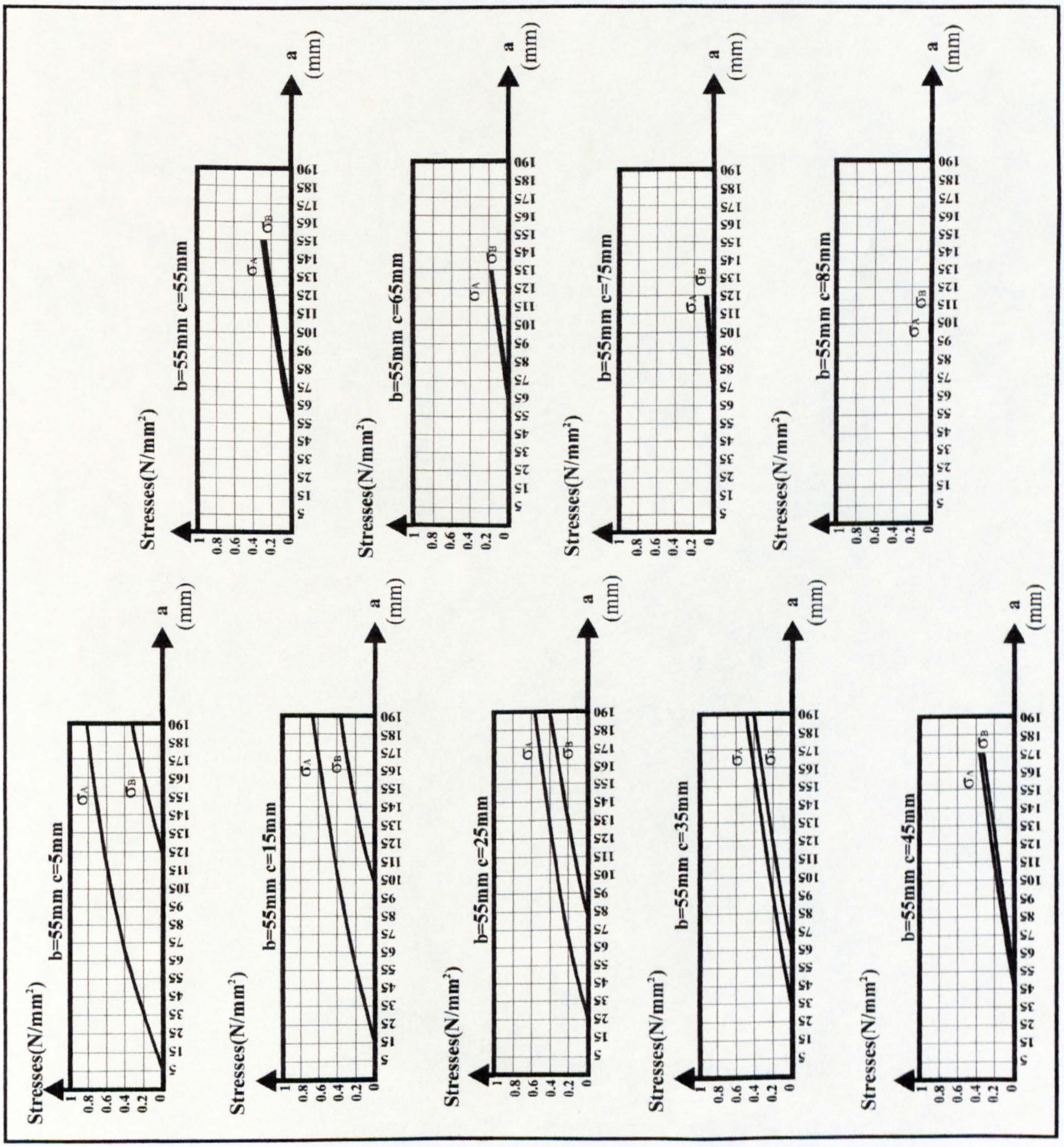

Figure 6.8(f): Bedding sand stress values (N/mm²) beneath the four corners of a 200mm x 100mm chamfered rectangular paver for various shapes of patch loading.

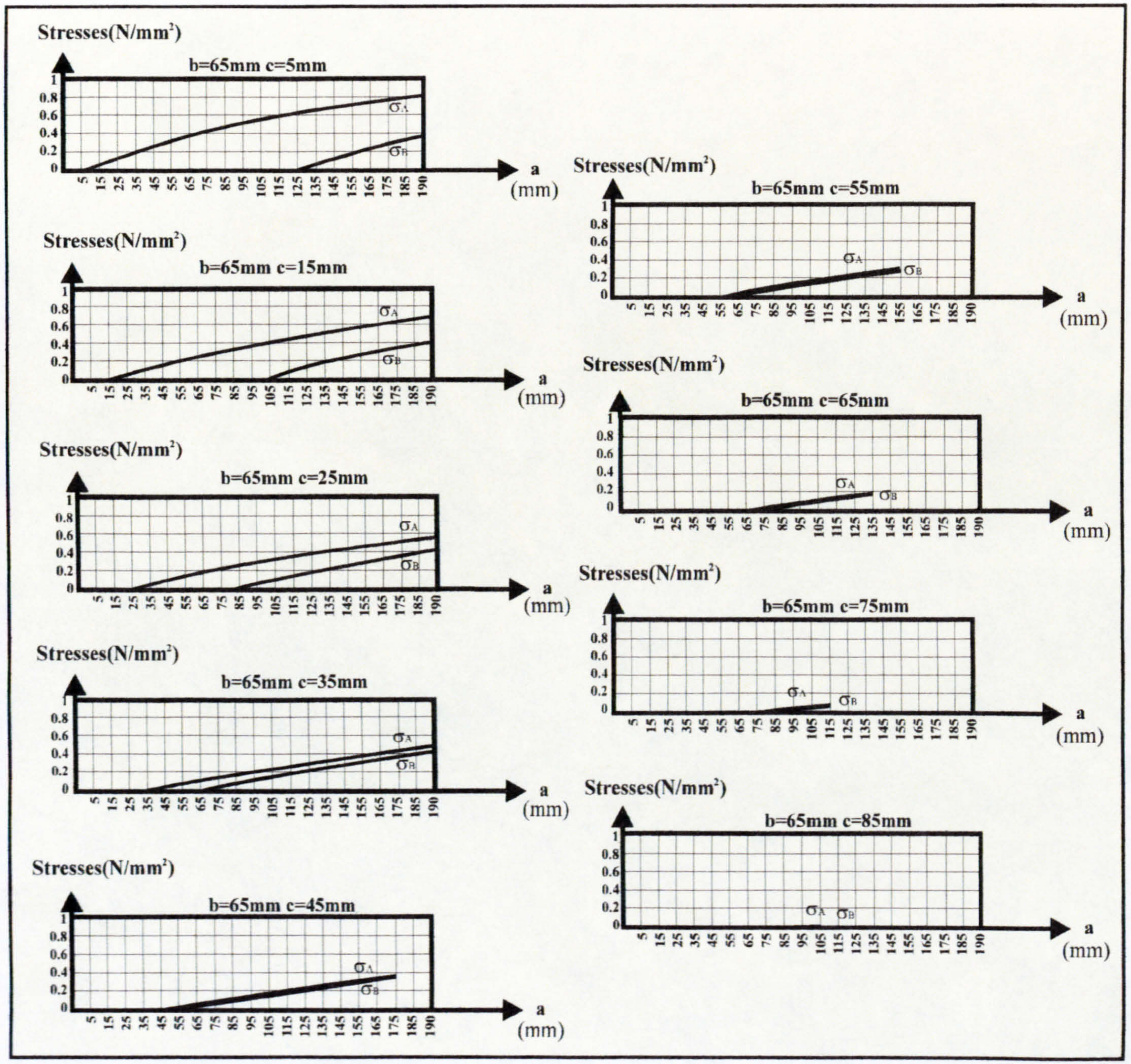

Figure 6.8(g): Bedding sand stress values (N/mm²) beneath the four corners of a 200mm x 100mm chamfered rectangular paver for various shapes of patch loading.

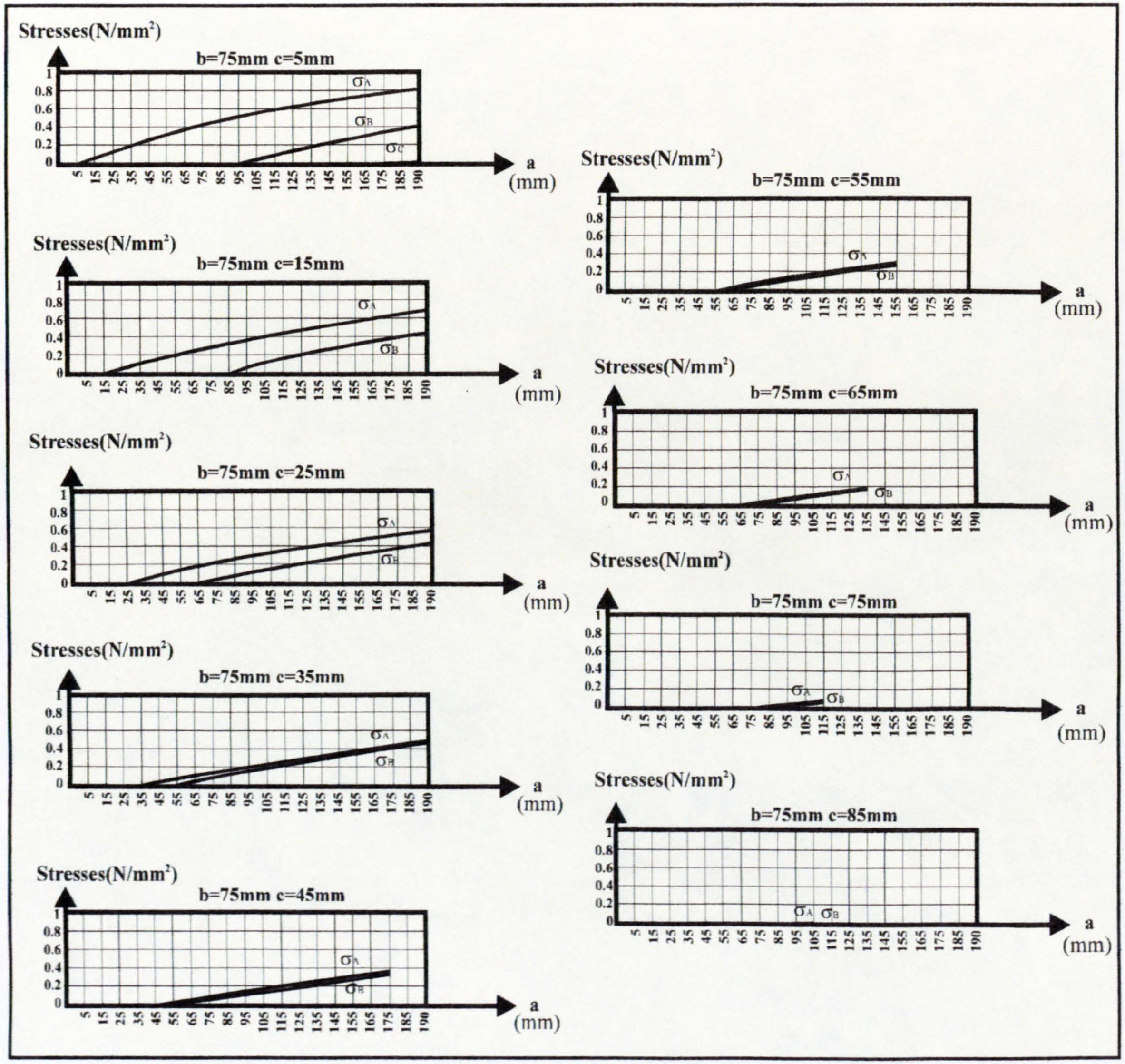

Figure 6.8(h): Bedding sand stress values (N/mm²) beneath the four corners of a 200mm x 100mm chamfered rectangular paver for various shapes of patch loading.

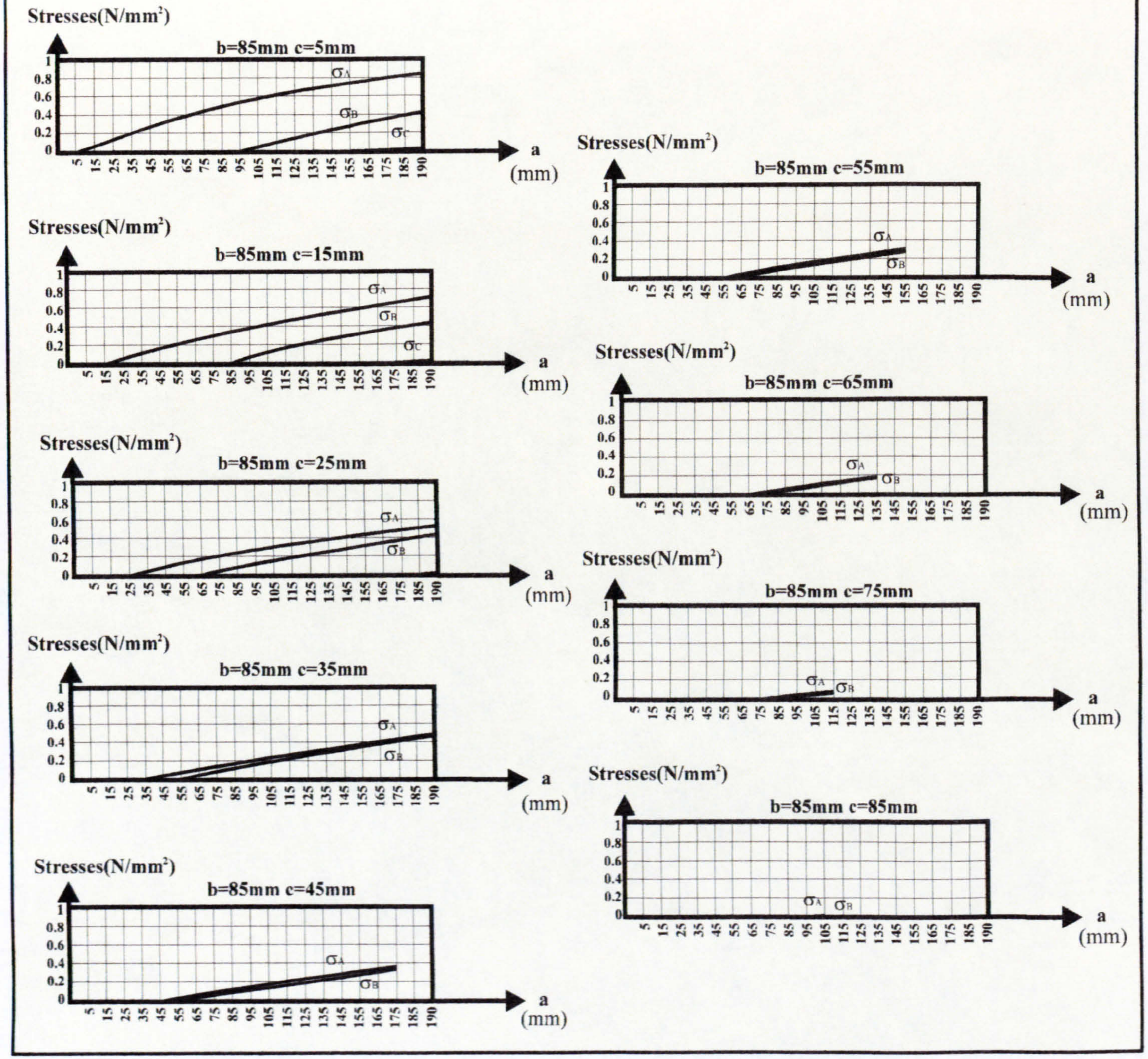

Figure 6.8(i): Bedding sand stress values (N/mm²) beneath the four corners of a 200mm x 100mm chamfered rectangular paver for various shapes of patch loading.

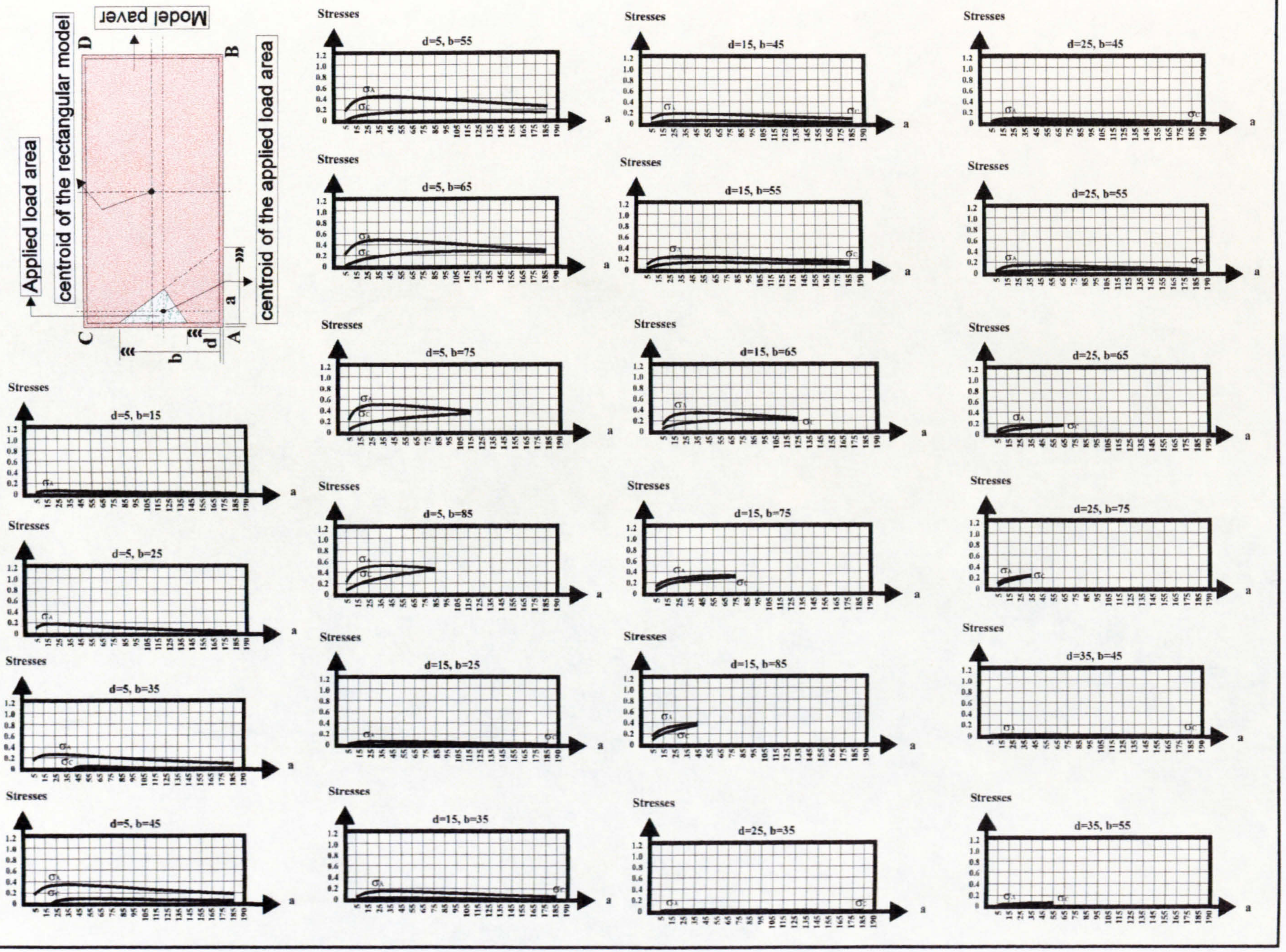

Figure 6.9: Bedding sand stress values (N/mm²) beneath the four corners of a 200mm x 100mm chamfered rectangular paver for various shapes of patch loading.

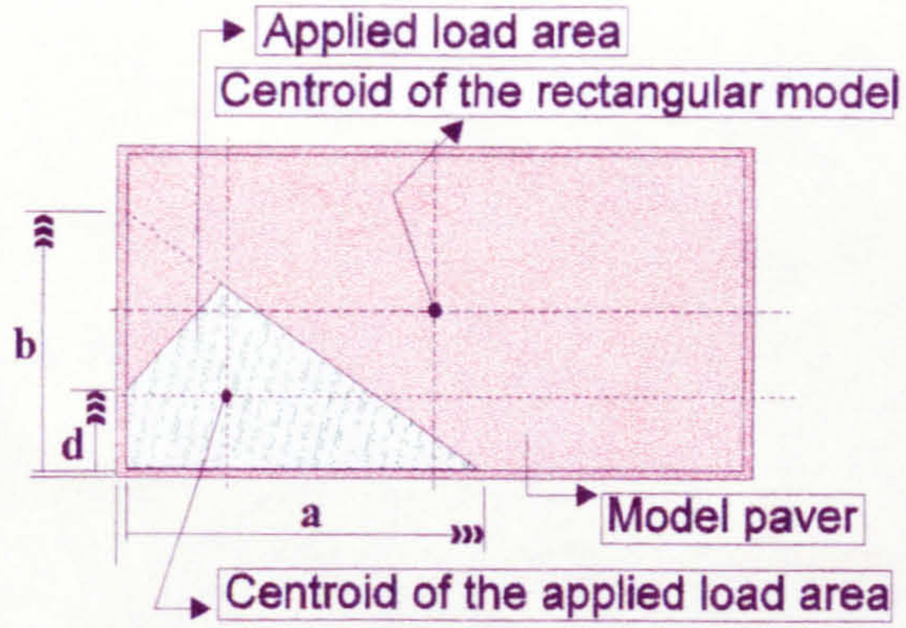

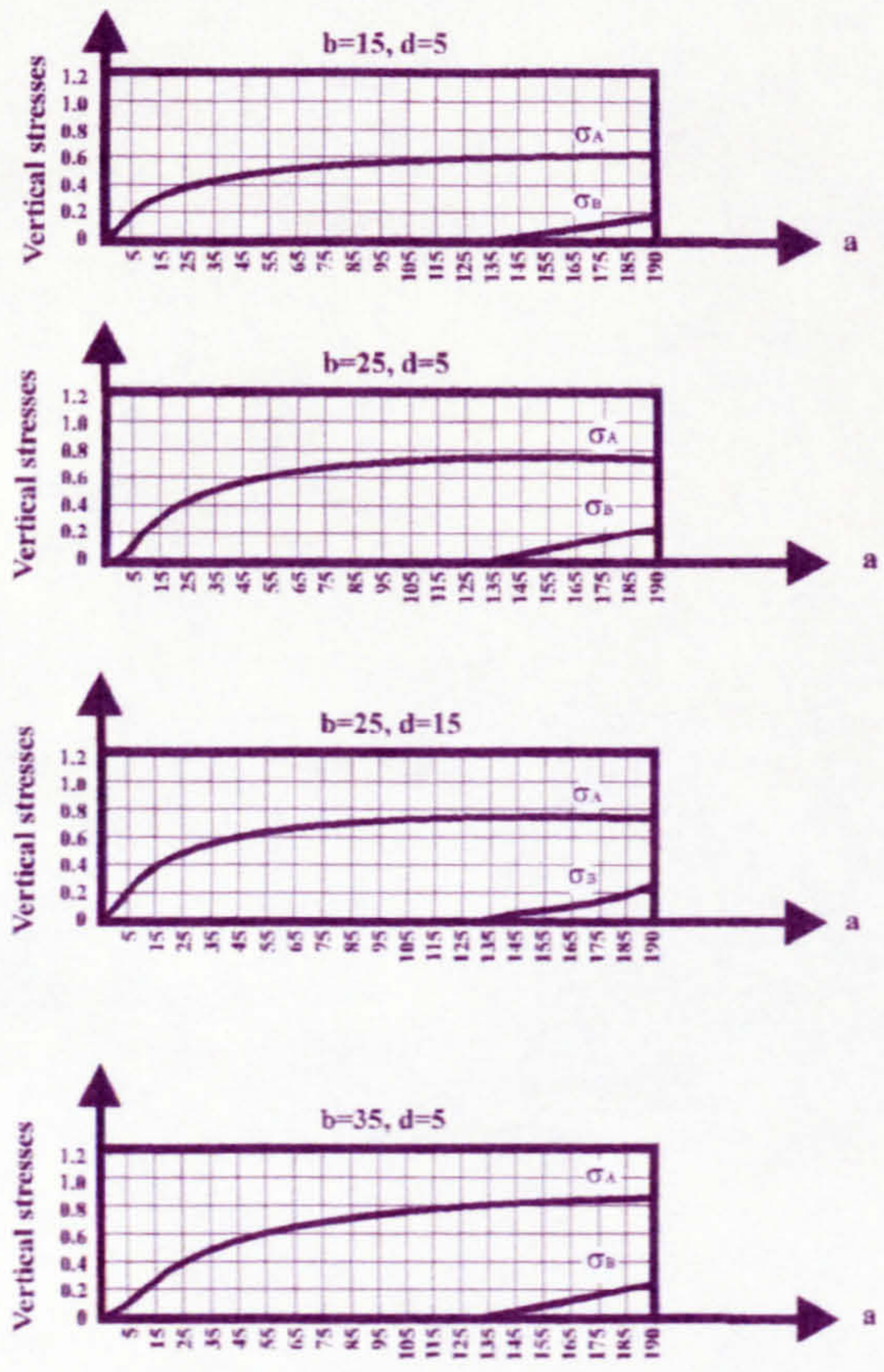

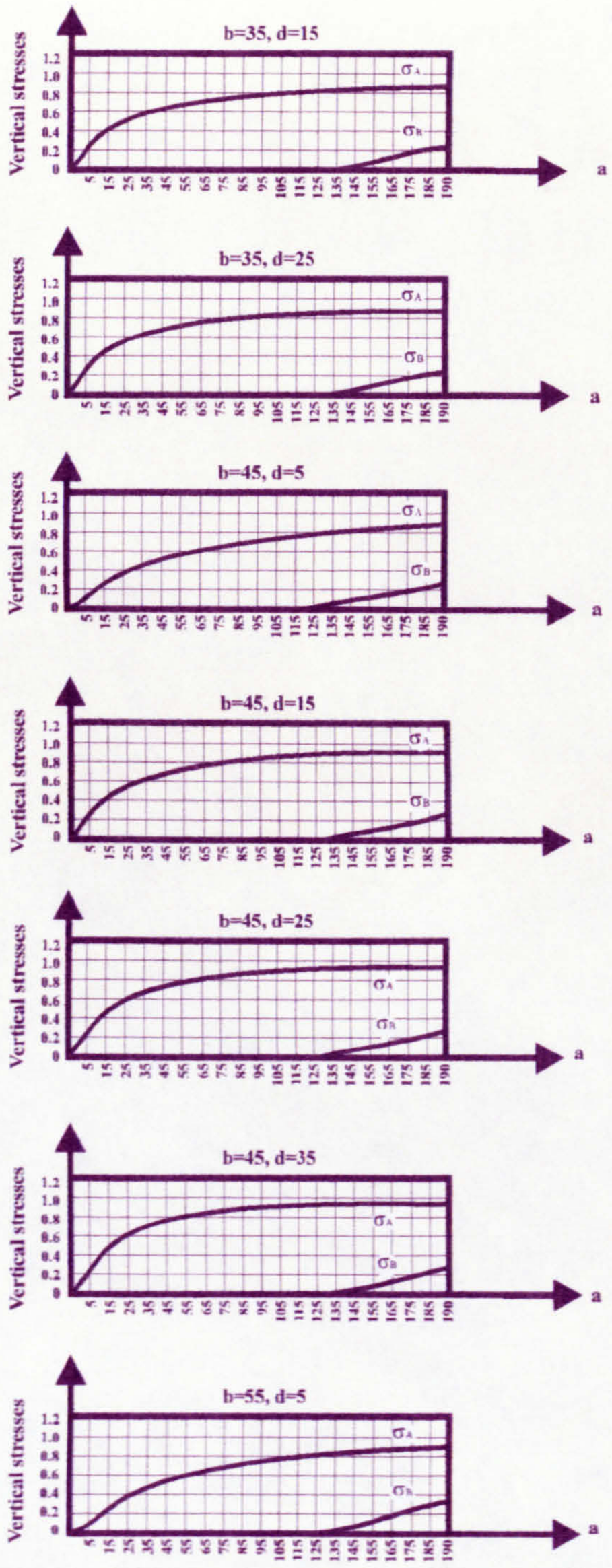

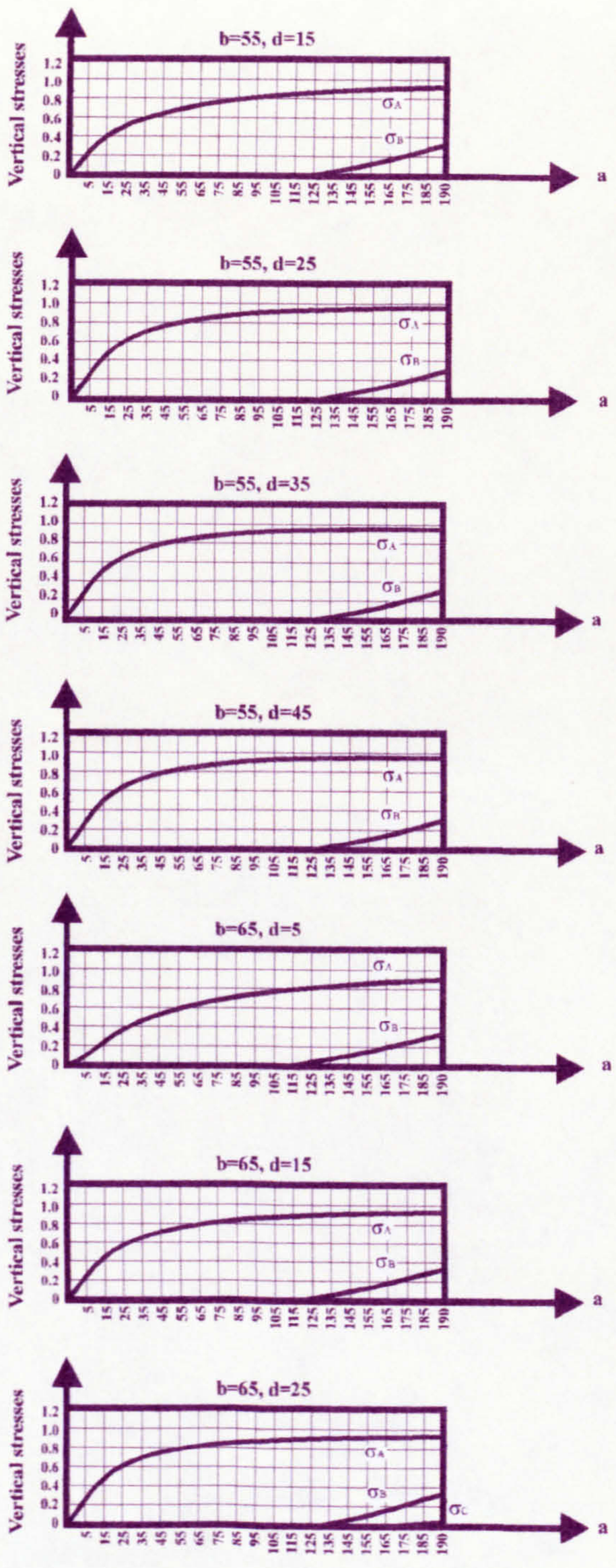

Figure 6.10(a): Bedding sand stress values (N/mm^2) beneath the four corners of a 200mm x 100mm chamfered rectangular paver for various shapes of patch loading.

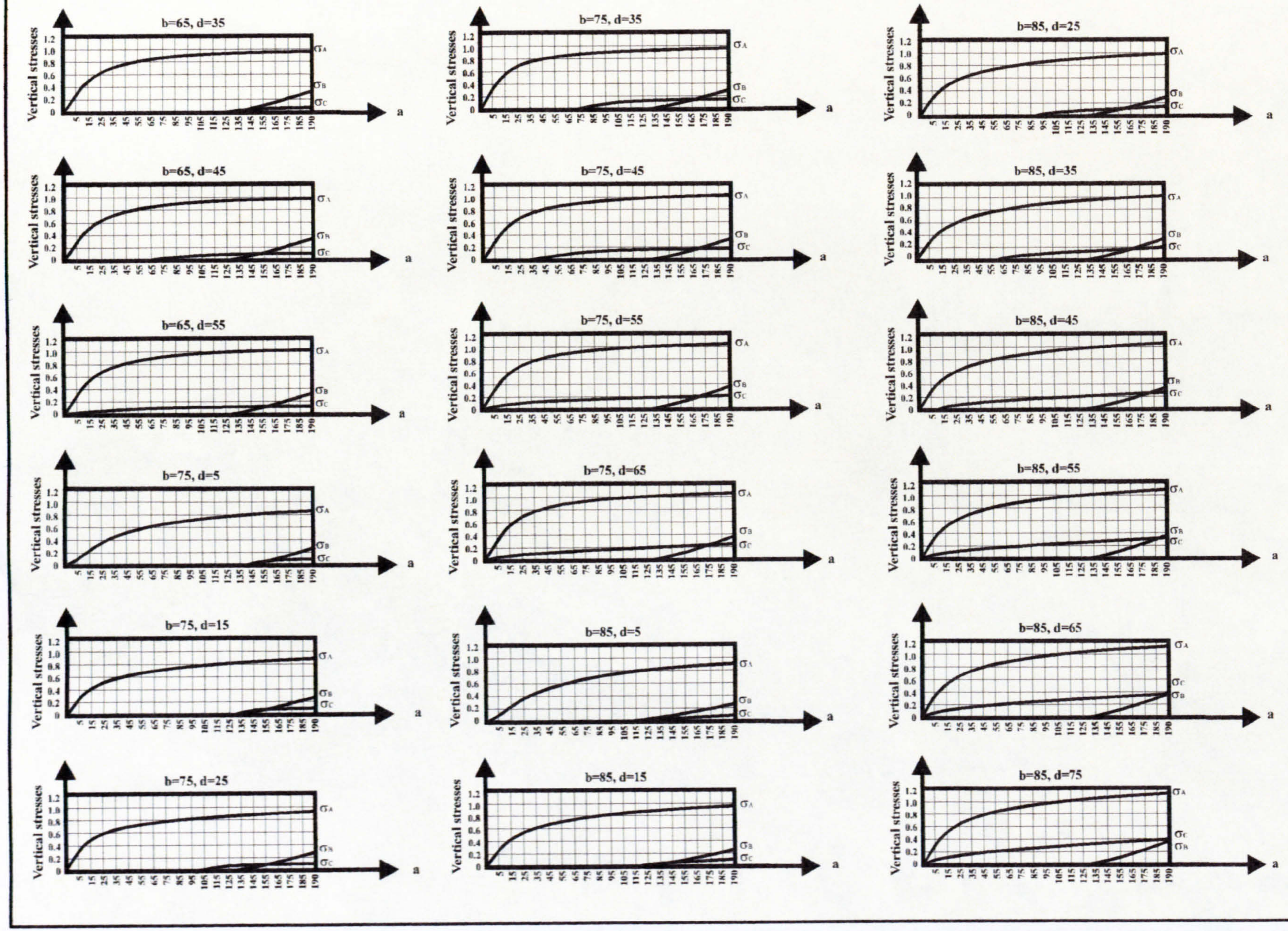

Figure 6.10(b): Bedding sand stress values (N/mm^2) beneath the four corners of a 200mm x 100mm chamfered rectangular paver for various shapes of patch loading.

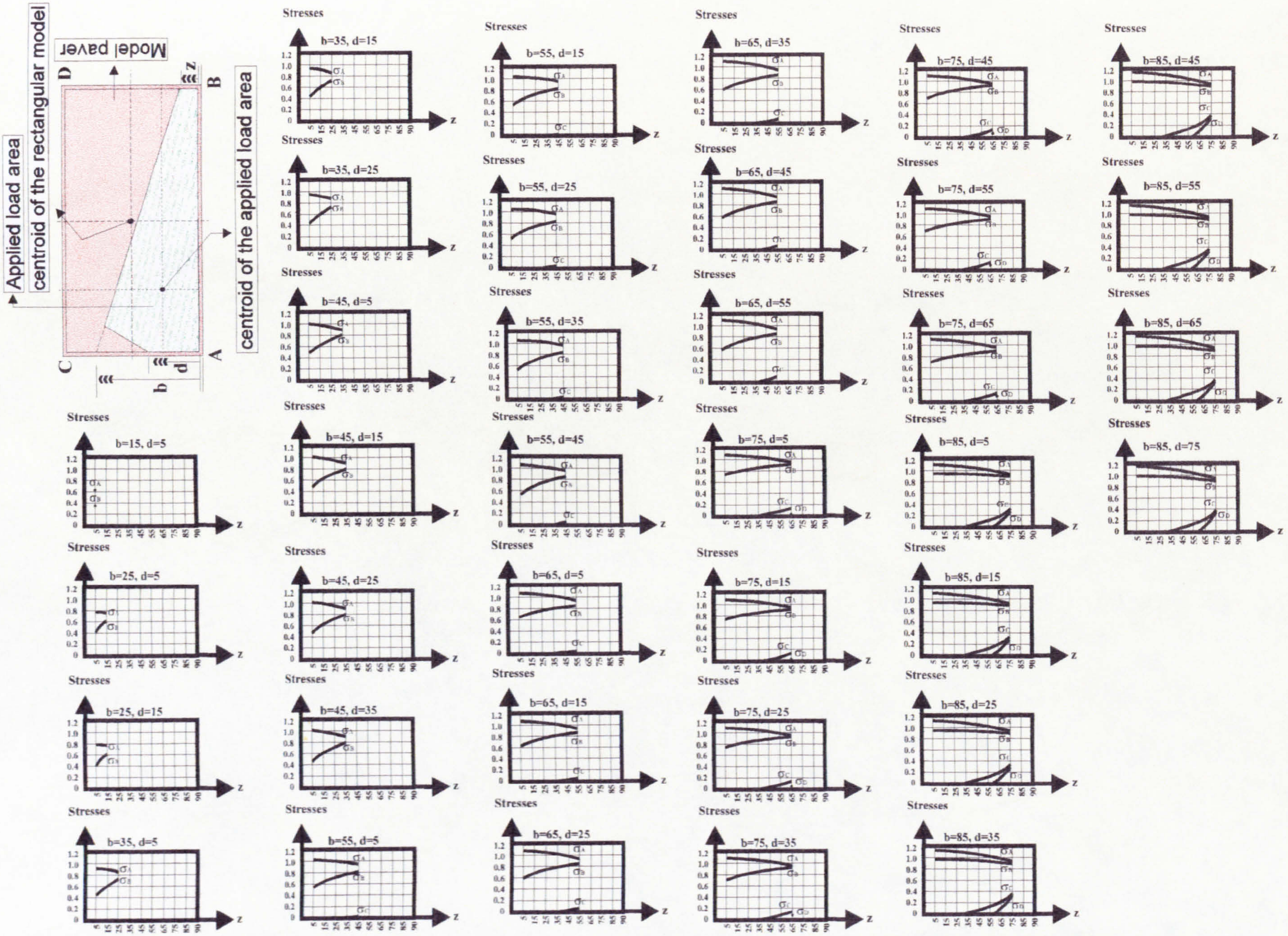

Figure 6.11: Bedding sand stress values (N/mm²) beneath the four corners of a 200mm x 100mm chamfered rectangular paver for various shapes of patch loading.

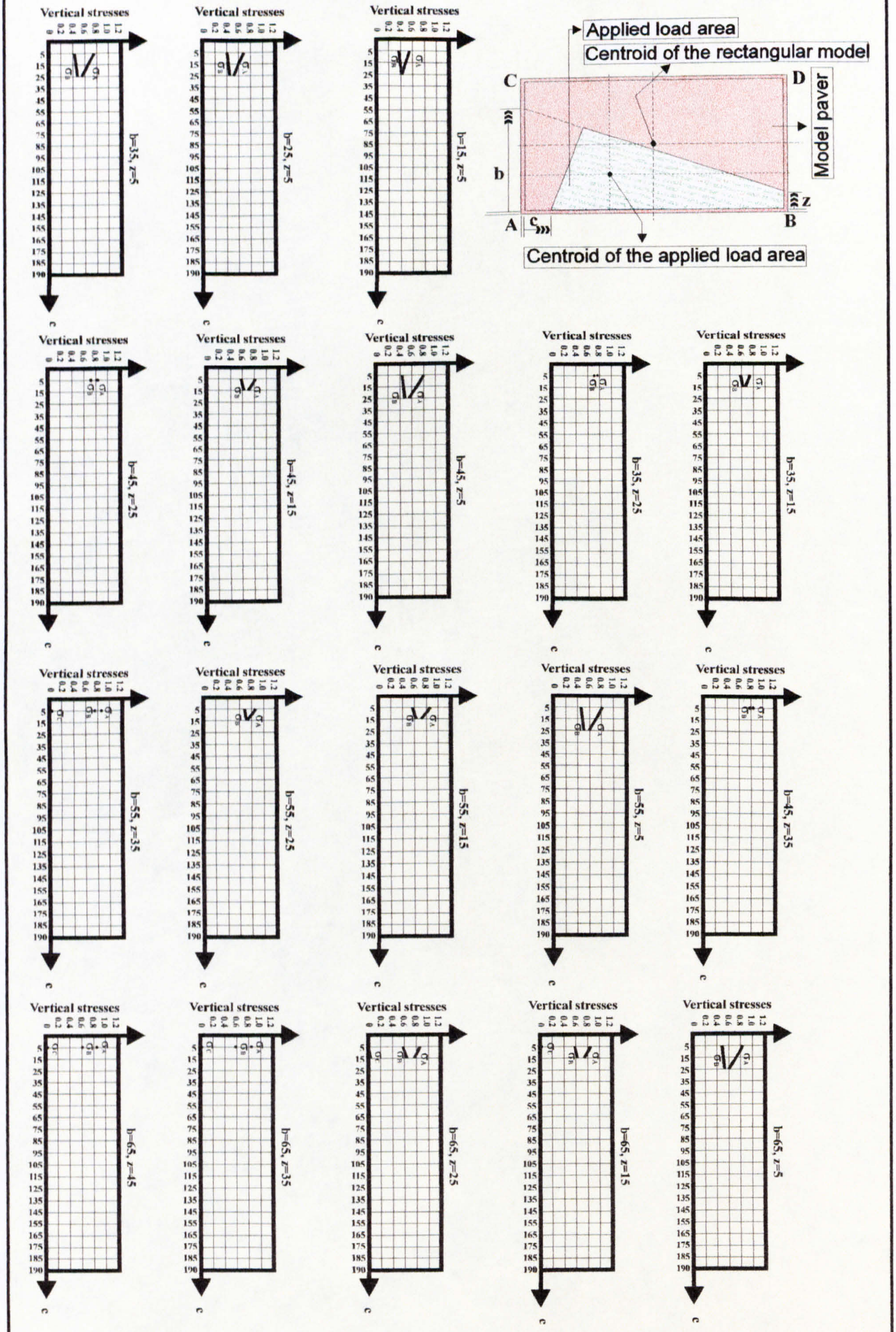

Figure 6.12(a): Bedding sand stress values (N/mm²) beneath the four corners of a 200mm x 100mm chamfered rectangular paver for various shapes of patch loading.

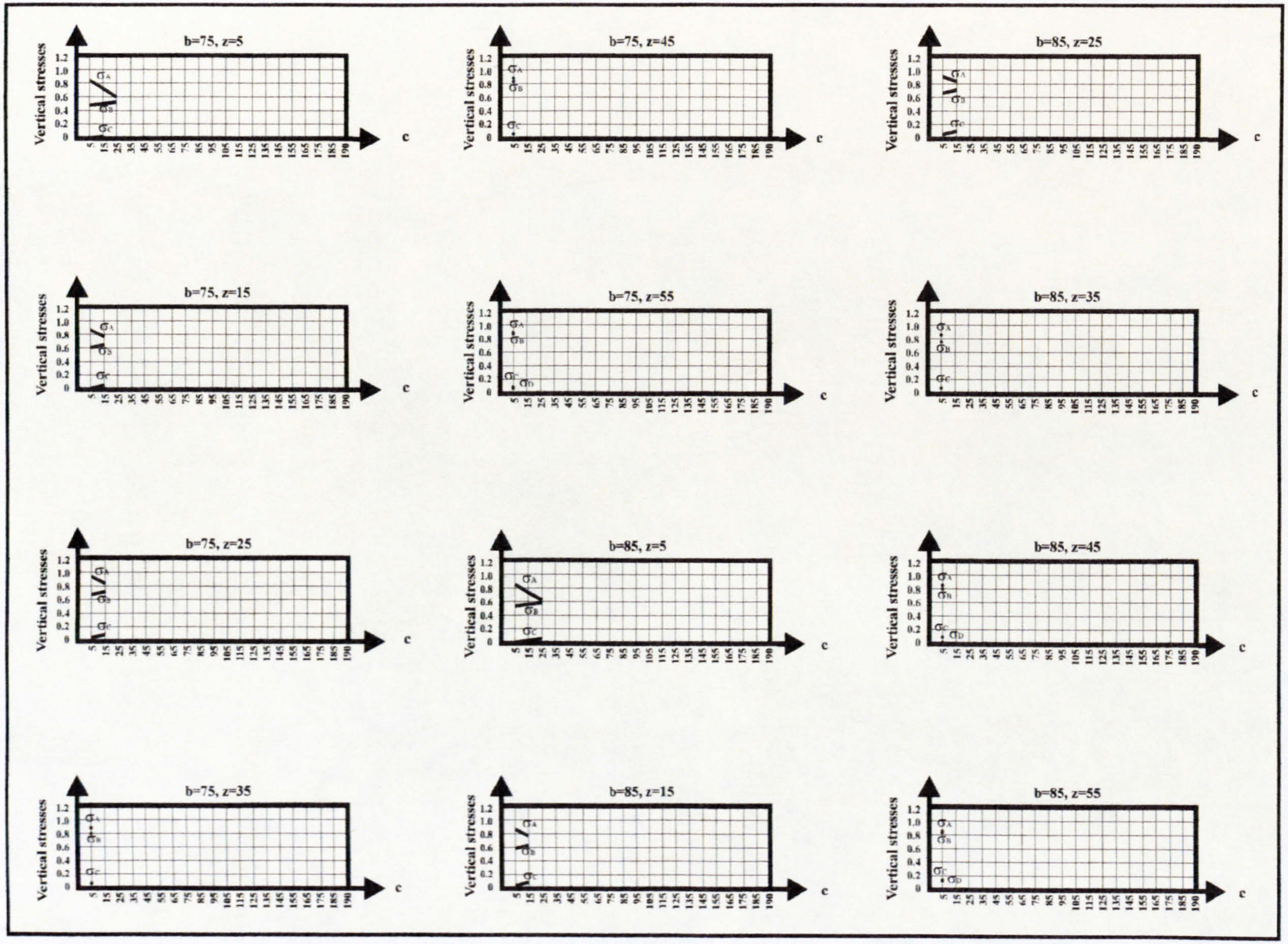

Figure 6.12(b): Bedding sand stress values (N/mm²) beneath the four corners of a 200mm x 100mm chamfered rectangular paver for various shapes of patch loading.

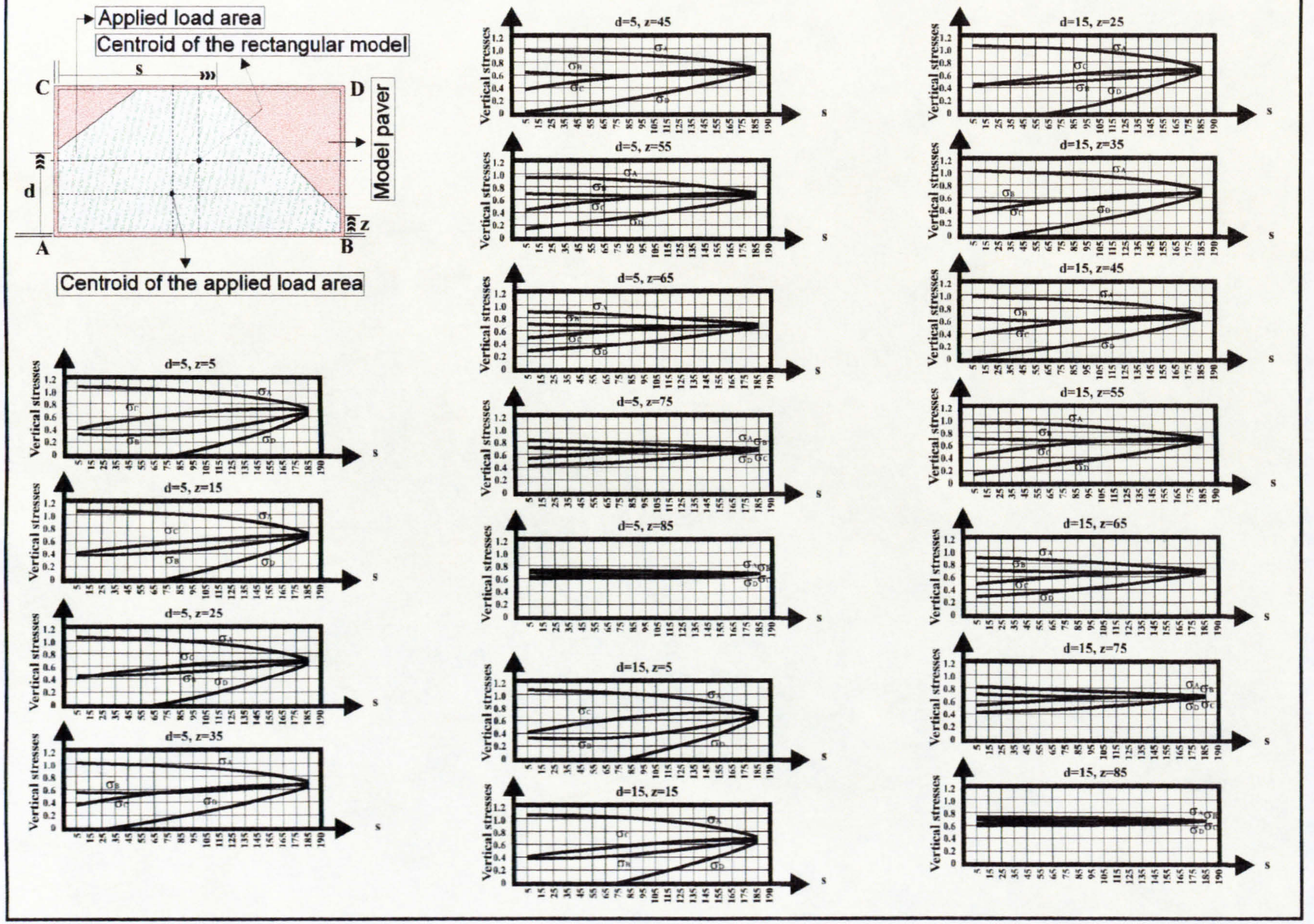

Figure 6.13(a): Bedding sand stress values (N/mm^2) beneath the four corners of a 200mm x 100mm chamfered rectangular paver for various shapes of patch loading.

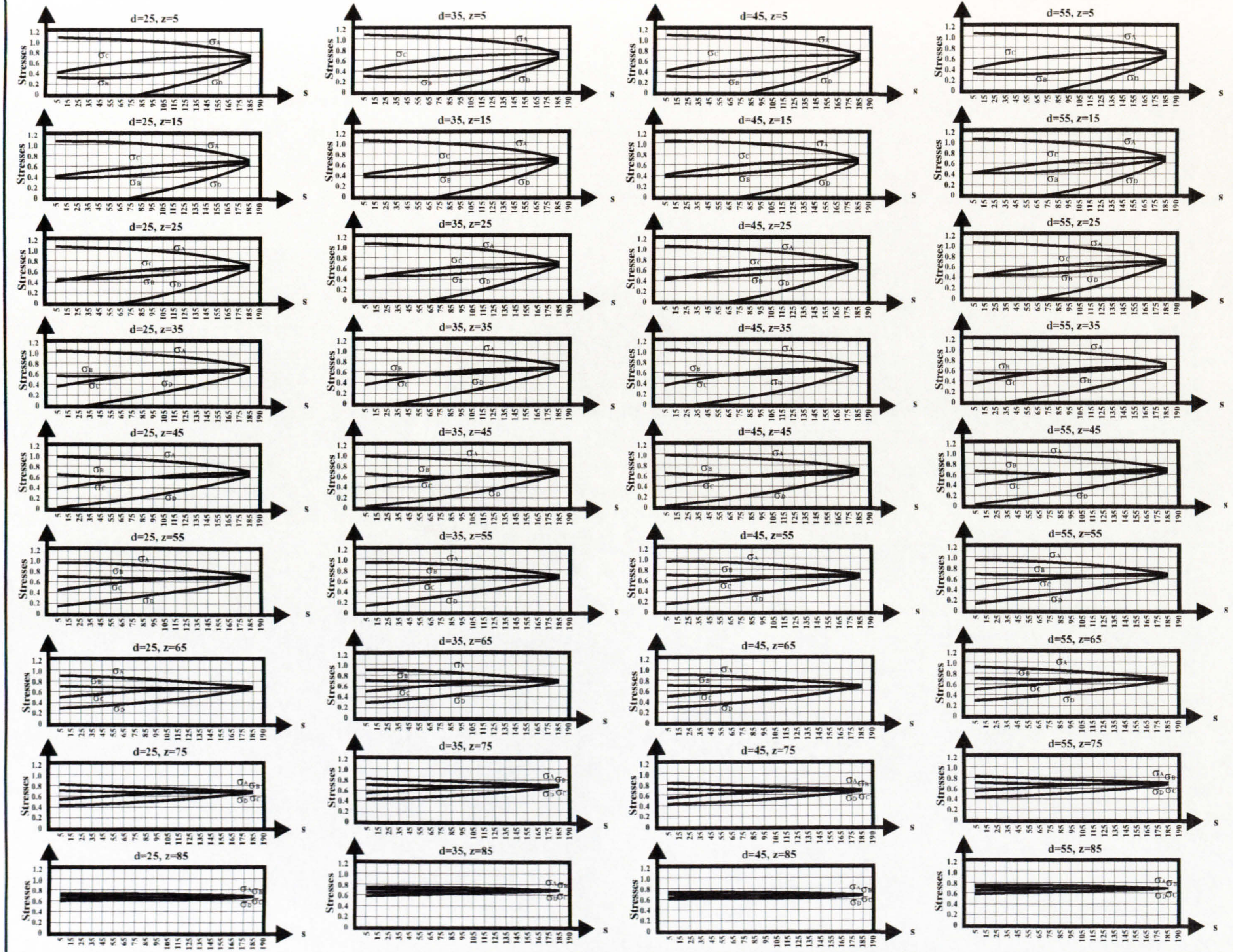

Figure 6.13(b): Bedding sand stress values (N/mm^2) beneath the four corners of a 200mm x 100mm chamfered rectangular paver for various shapes of patch loading.

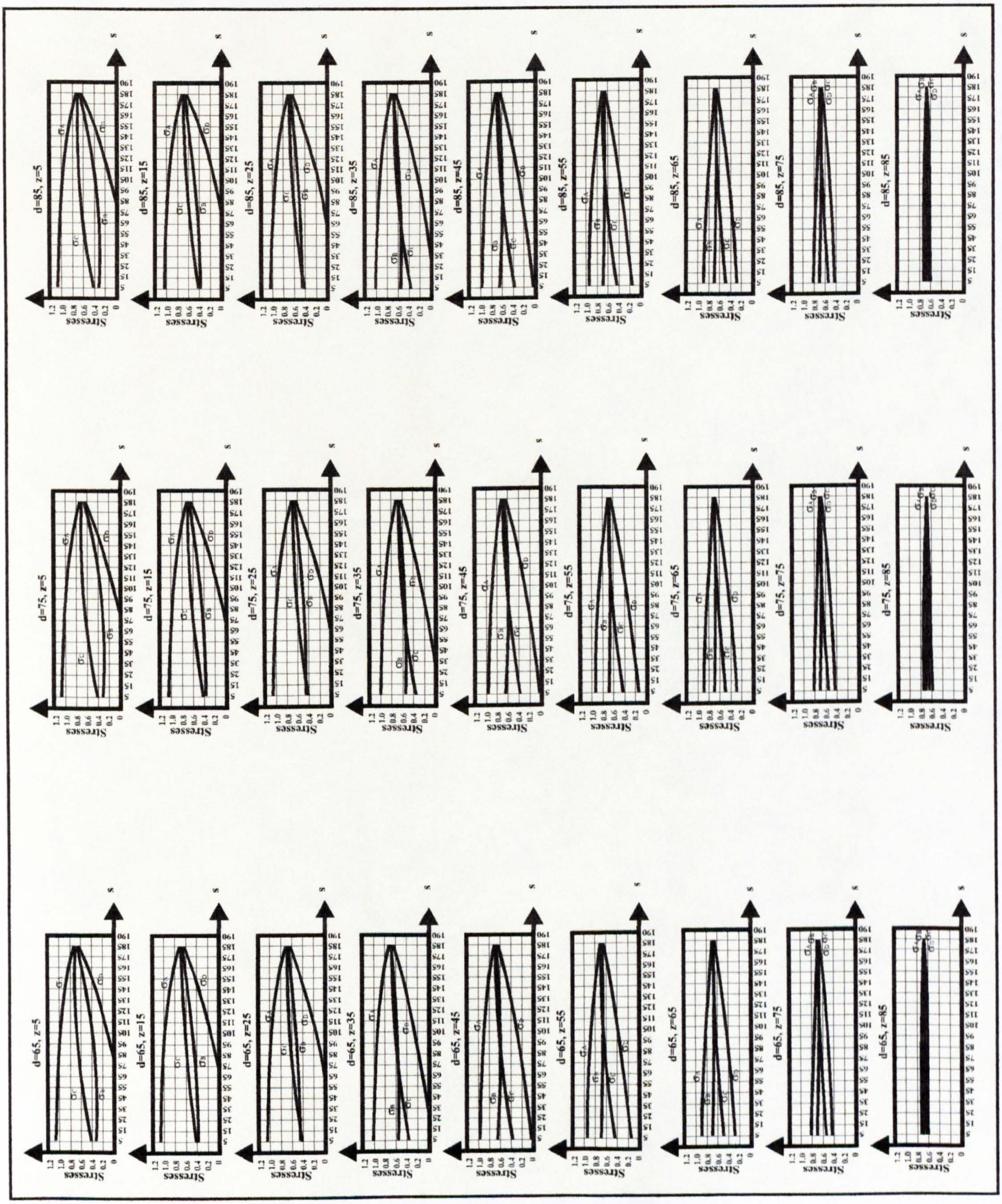

Figure 6.13(c): Bedding sand stress values (N/mm²) beneath the four corners of a 200mm x 100mm chamfered rectangular paver for various shapes of patch loading.

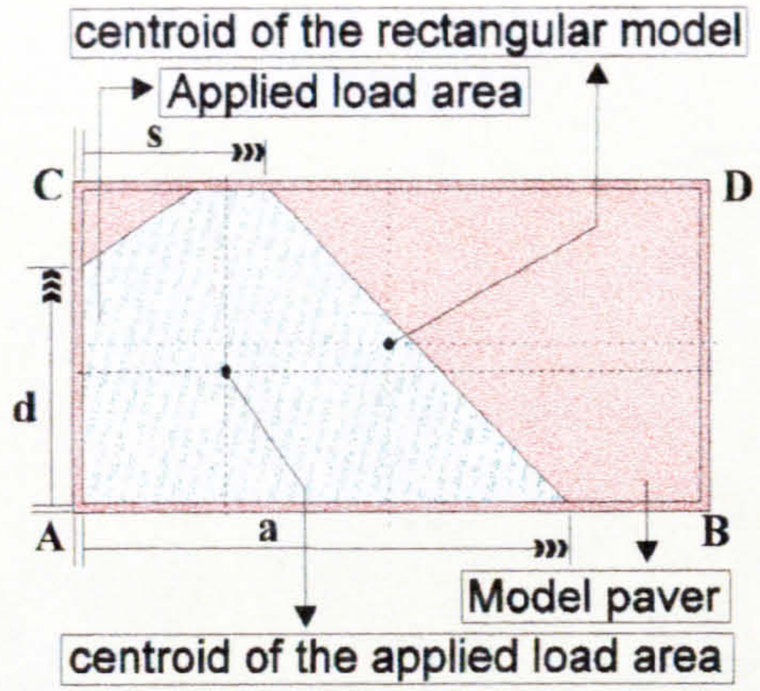

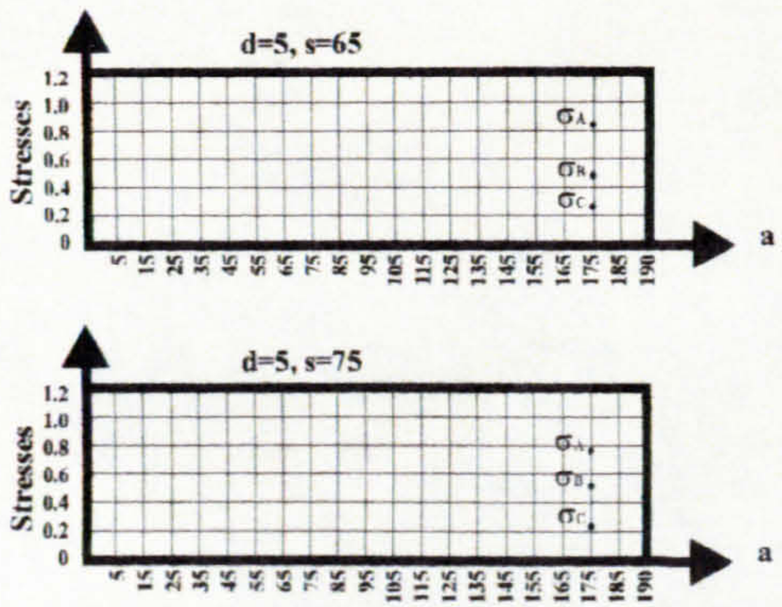

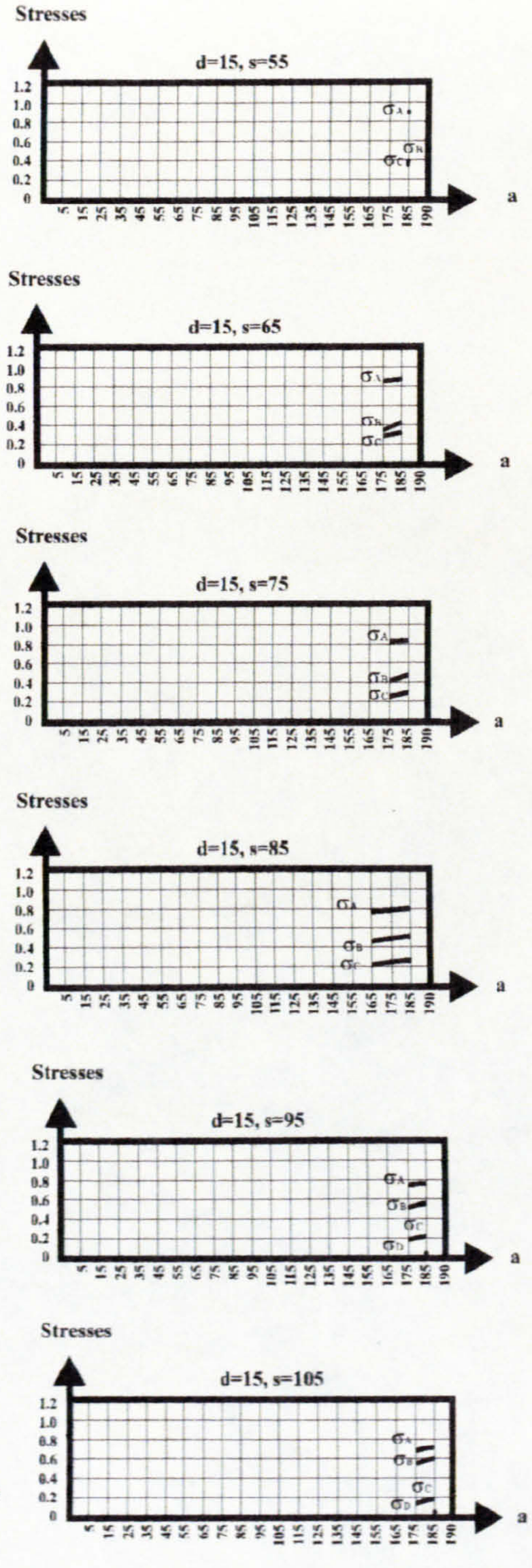

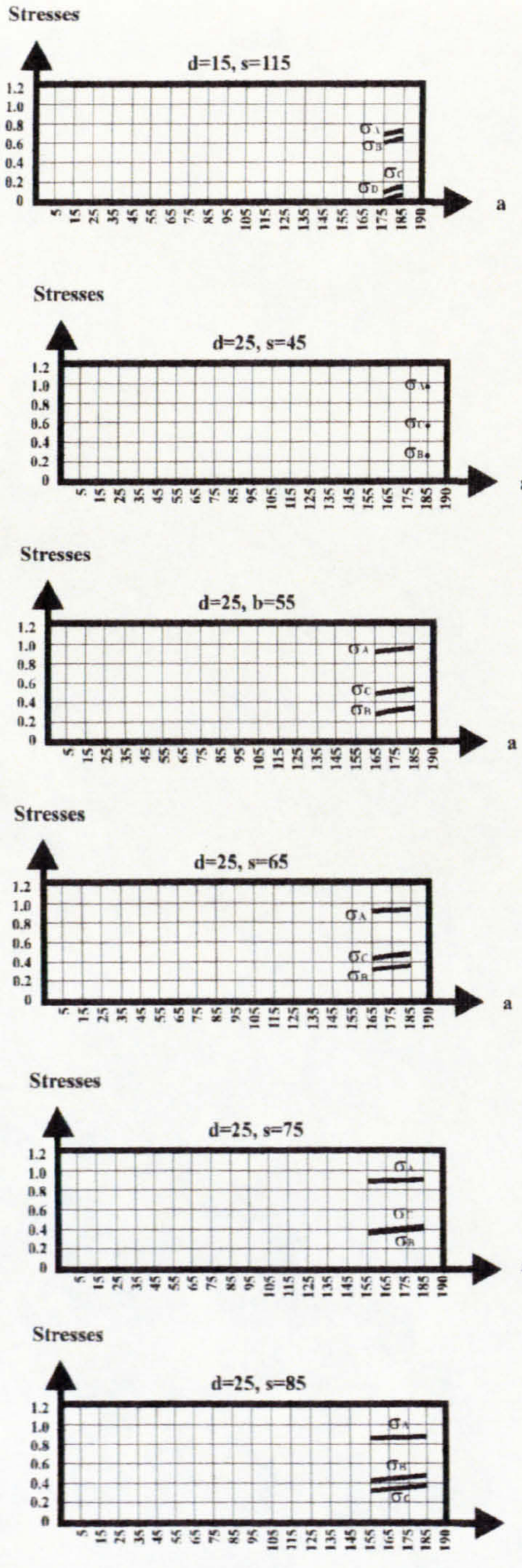

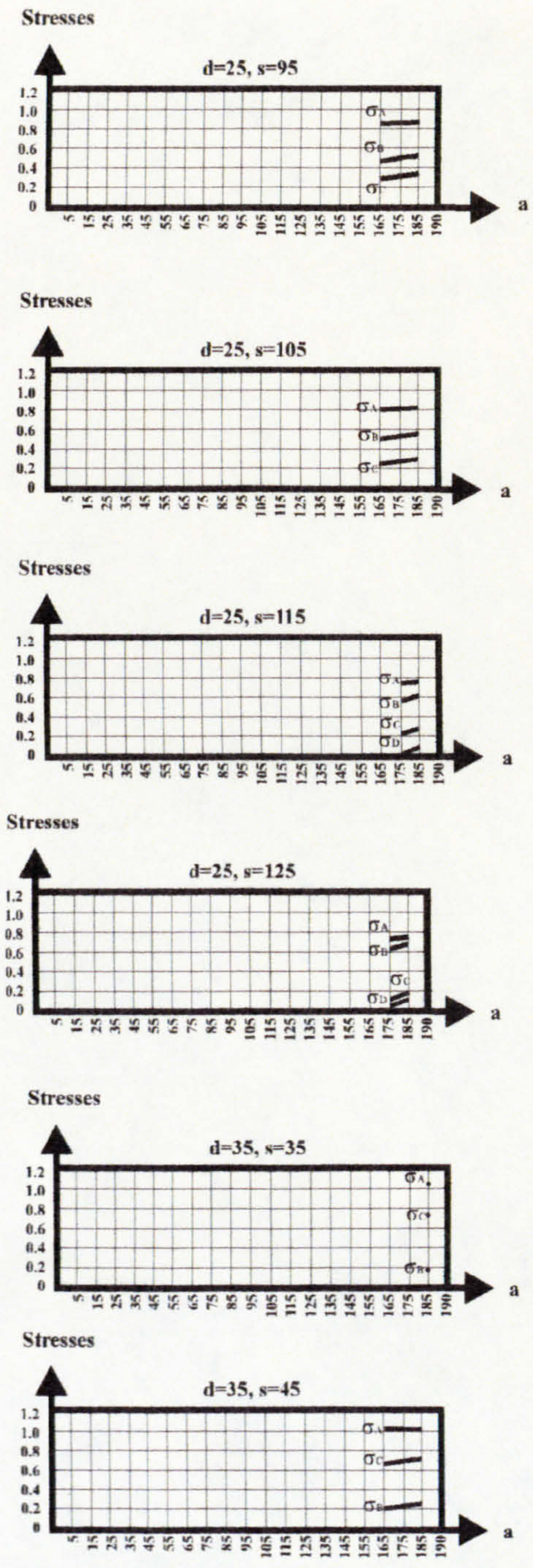

Figure 6.14(a): Bedding sand stress values (N/mm^2) beneath the four corners of a 200mm x 100mm chamfered rectangular paver for various shapes of patch loading.

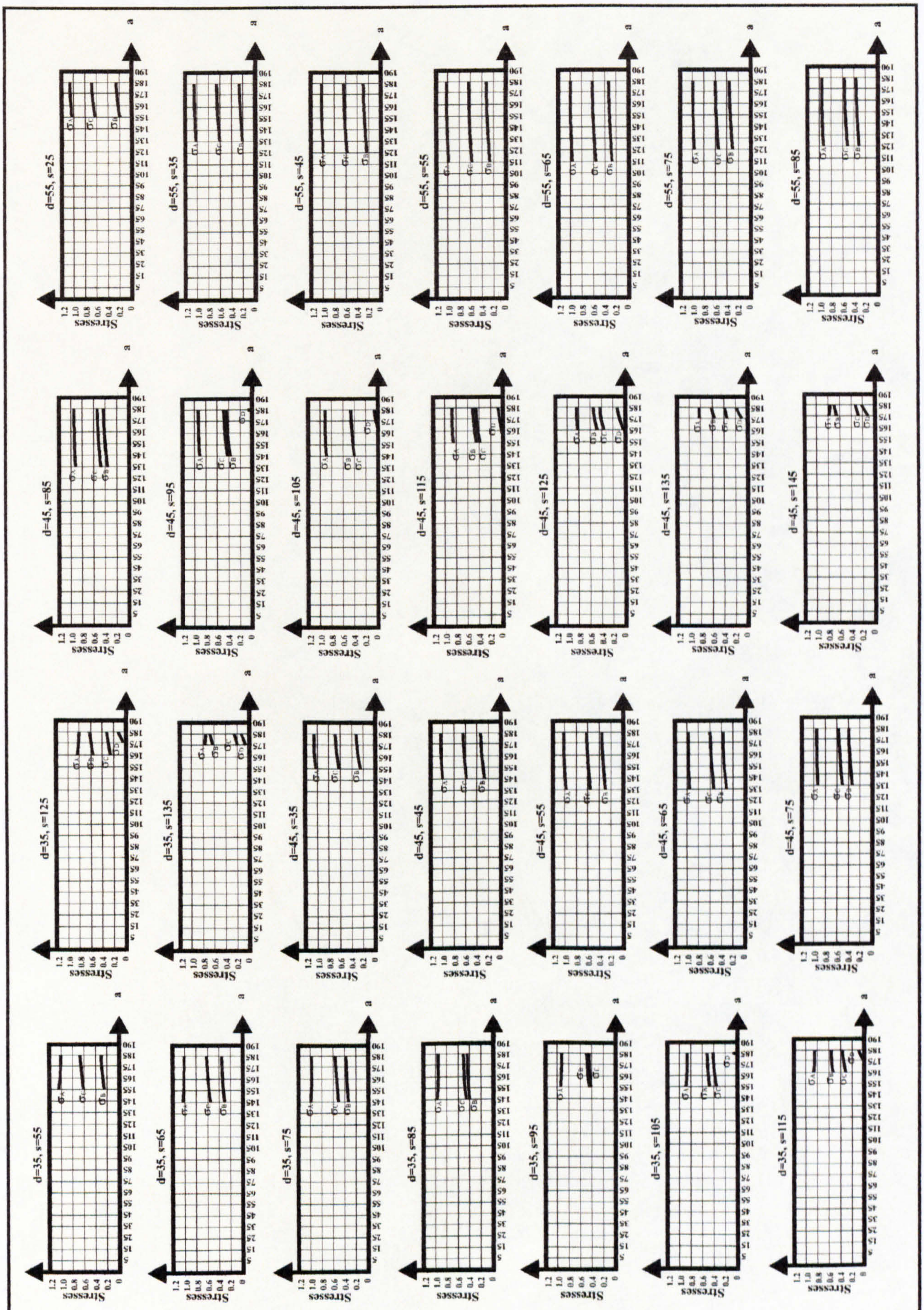

Figure 6.14(b): Bedding sand stress values (N/mm^2) beneath the four corners of a 200mm x 100mm chamfered rectangular paver for various shapes of patch loading.

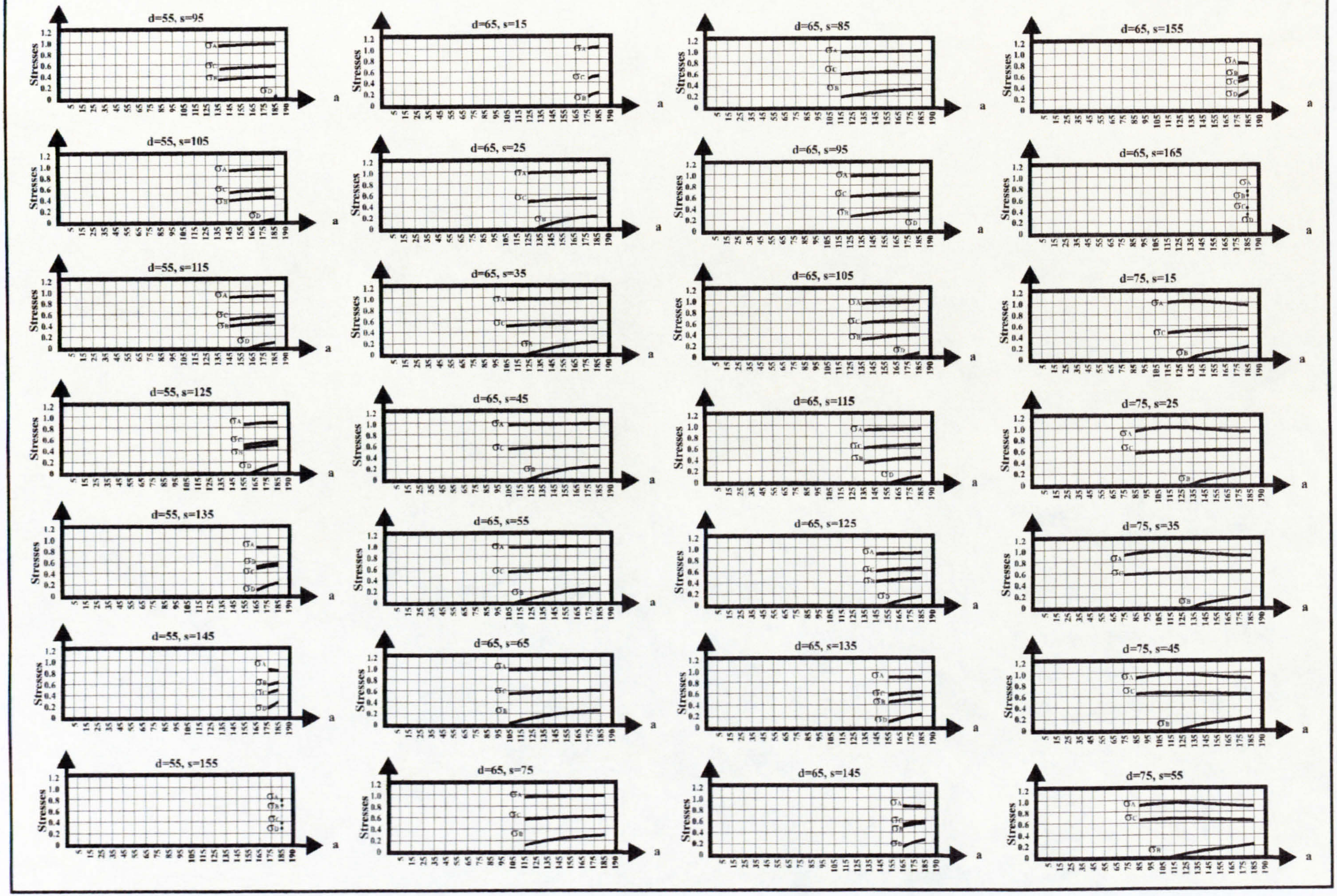

Figure 6.14(c): Bedding sand stress values (N/mm^2) beneath the four corners of a 200mm x 100mm chamfered rectangular paver for various shapes of patch loading.

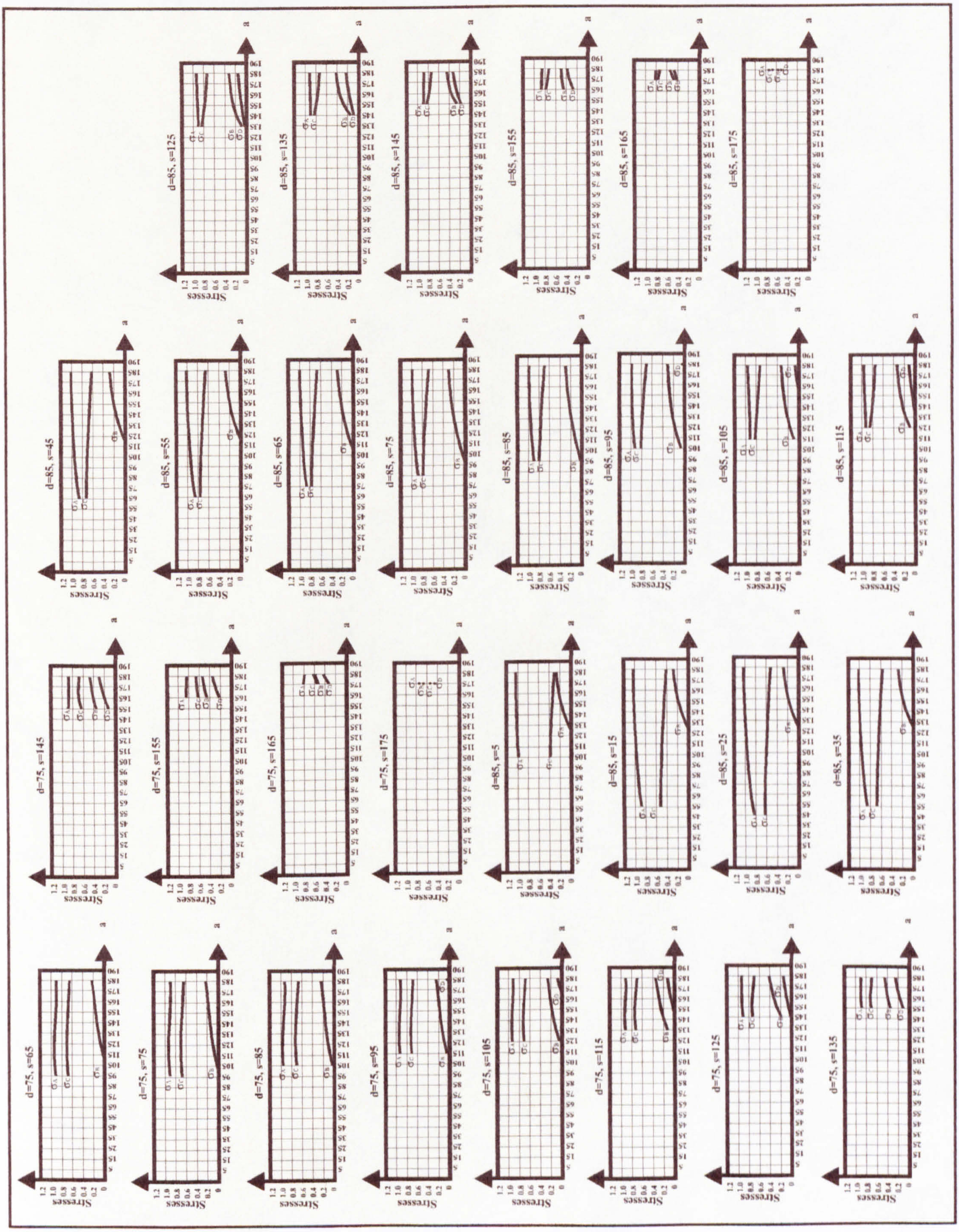

Figure 6.14(d): Bedding sand stress values (N/mm^2) beneath the four corners of a 200mm x 100mm chamfered rectangular paver for various shapes of patch loading.

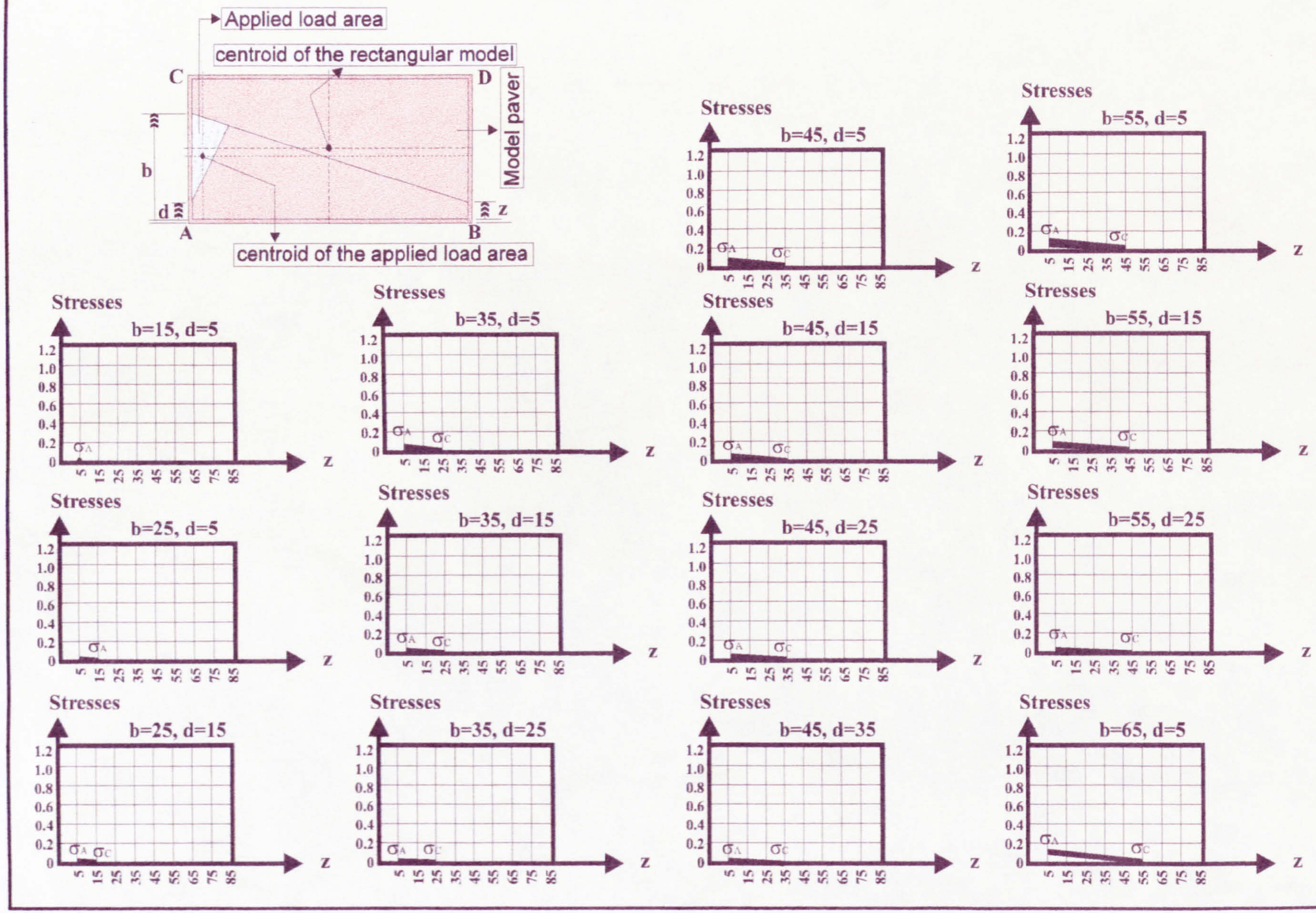

Figure 6.15: Bedding sand stress values (N/mm²) beneath the four corners of a 200mm x 100mm chamfered rectangular paver for various shapes of patch loading.

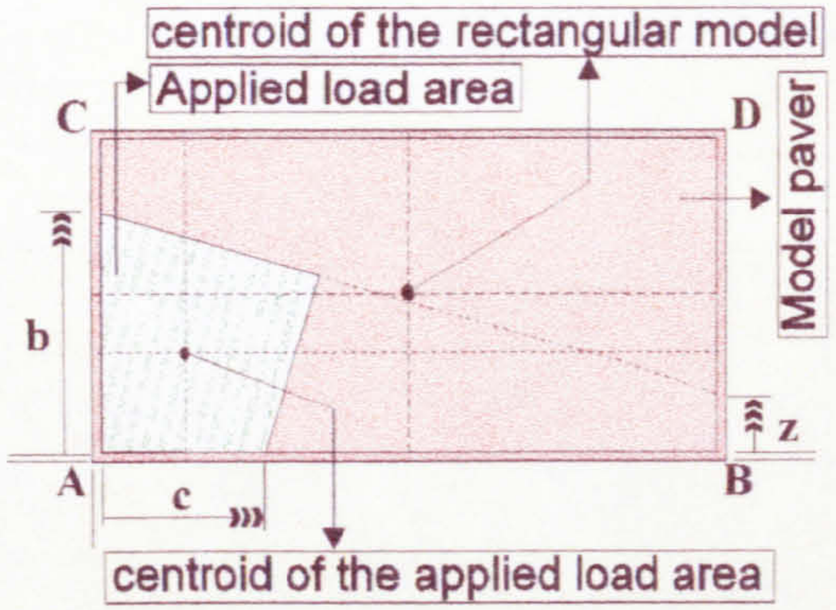

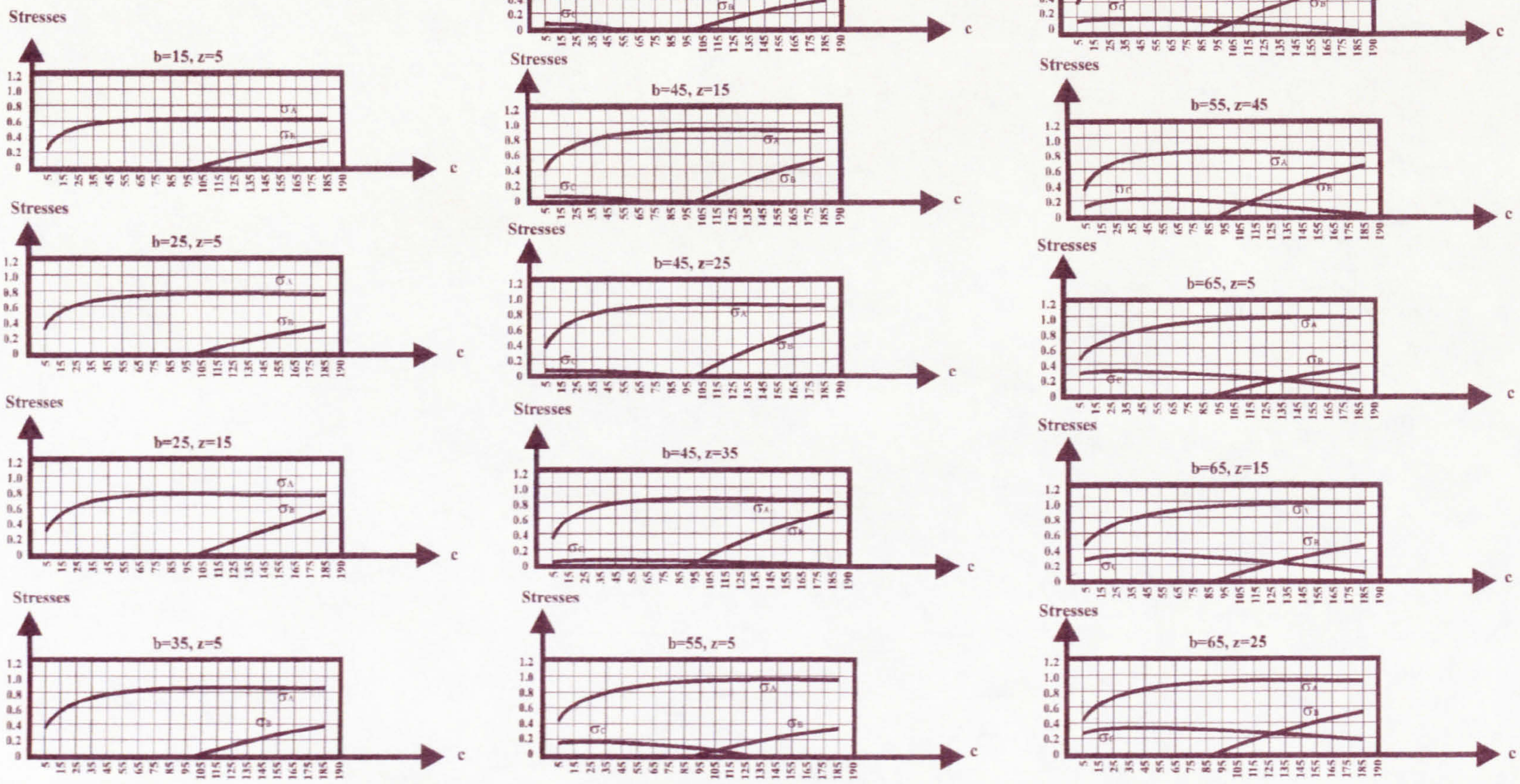

Figure 6.16(a): Bedding sand stress values (N/mm²) beneath the four corners of a 200mm x 100mm chamfered rectangular paver for various shapes of patch loading.

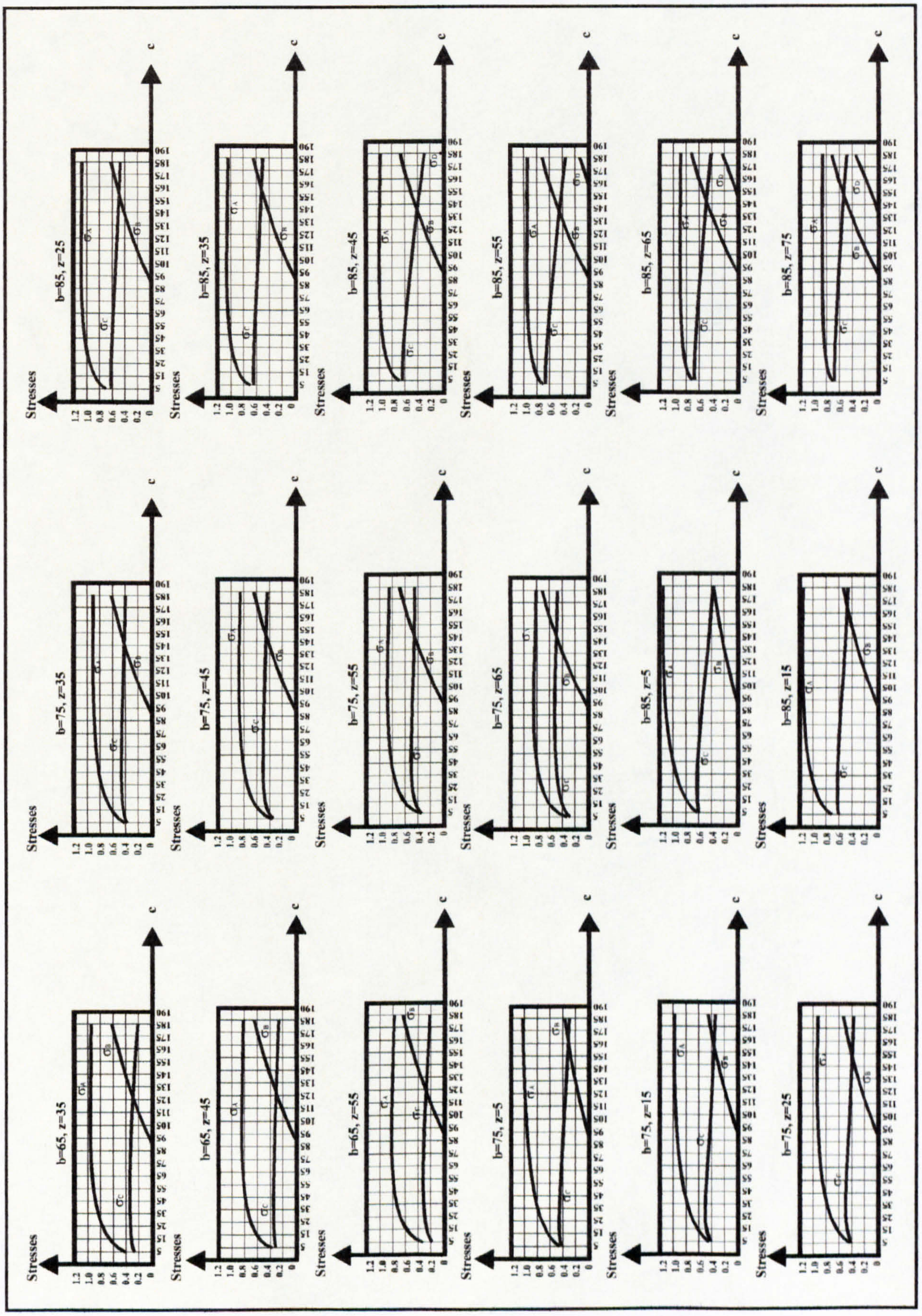

Figure 6.16(b): Bedding sand stress values (N/mm^2) beneath the four corners of a 200mm x 100mm chamfered rectangular paver for various shapes of patch loading.

load is 1.15N/mm^2 i.e. 45% overstress when only one corner of the paver develops positive stress. Figure 6.17 shows the individual and systematic behaviour of vertical stresses when the applied patch load boundaries are in line with rectangular paver boundaries (θ° =0 in Figure 4.2) . Figures 6.18, 6.19 and 6.20 show values of stress which develop within the bedding sand when a vehicle passes over rectangular pavers laid to a herringbone pattern. Figure 6.18 applies when the vehicle runs at angles of zero, 10° and 20°(as defined in Figure 4.2) to the orientation of the laying pattern, Figure 6.19 applies when the vehicle travels at 30°, 40° and 50° and Figure 6.20 applies when the vehicle travels at 60°, 70°, 80° and 90°.

Each of Figures 6.17, 6.18, 6.19 and 6.20 shows bedding sand stresses both with and in the absence of interlock. The non-interlocking stresses are taken from the solutions to the equations set out in the last Section. In the case of interlock, the definition of interlock set out in Chapter 1 (see Section 1.4.1.1) is invoked as follows. If neighbouring pavers cannot move independently of one another, the bedding sand beneath them must accept similar compressive stress values along adjoining boundaries since any difference in neighbouring stresses would lead to differential strain in the sand and loss of vertical interlock. Therefore, along all of the paver boundaries, the stresses have been modified by taking the average of the two values along the sides of adjoining pavers. This is accomplished by assessing corner stress values and stress runout distances where appropriate.

The stresses in Figures 6.17, 6.18, 6.19 and 6.20 are shown at points defined in Figure 4.2. The lines joining the points show variation of stress along paver sides. Effectively, the lines shown in Figures 6.18, 6.19 and 6.20 define the peak stresses in bedding sand and also provide an indication of the effectiveness of interlock for each vehicle/laying pattern orientation. Graphs with high peak stress values and low intermediate values indicate relatively ineffective interlock whereas uniform values with low peaks indicate more effective interlock. One interesting conclusion is that pavers are likely to perform better when their laying pattern runs in line with or at right angles to the direction of

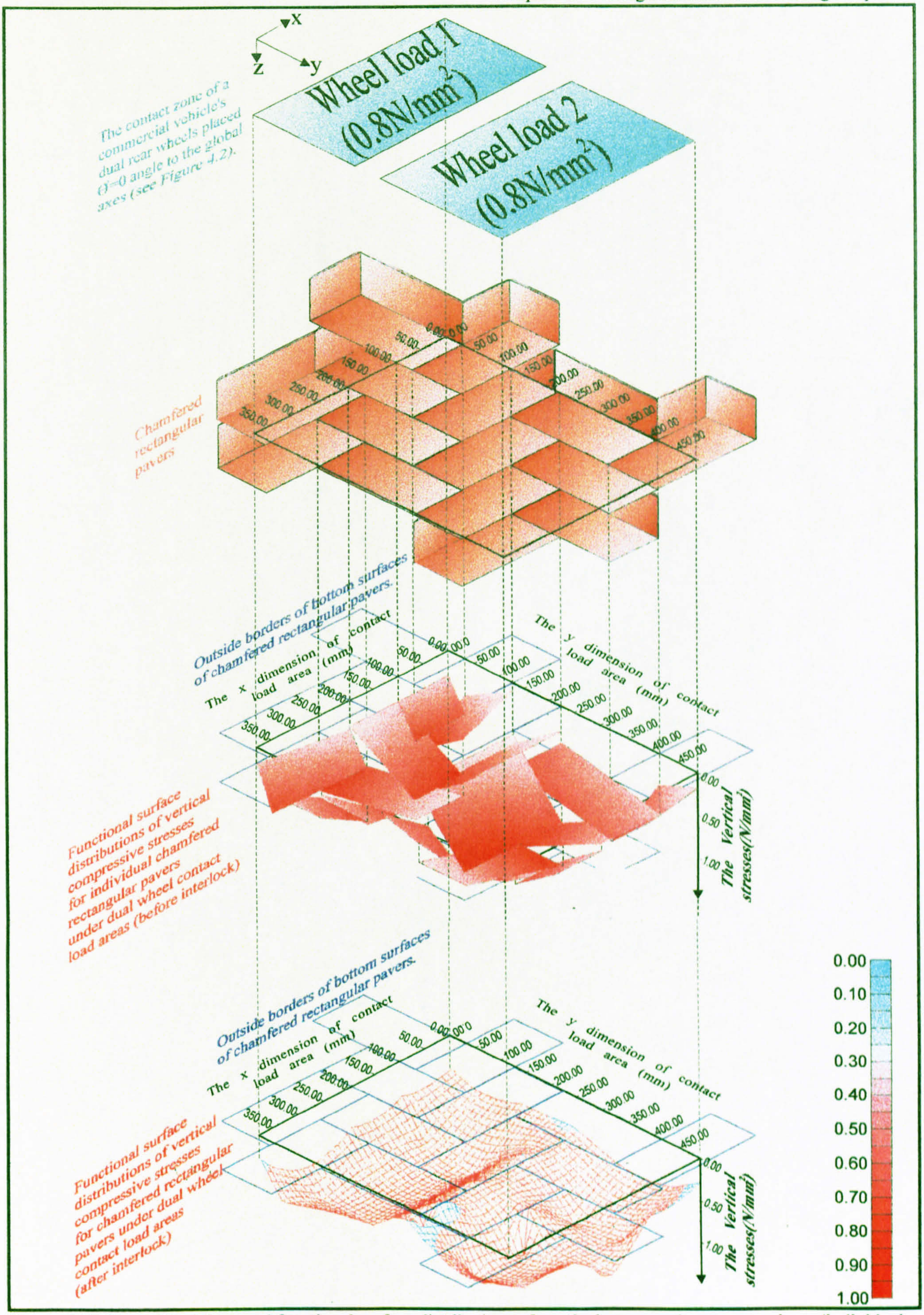

Figure 6.17: Typical bedding sand functional surface distributions of vertical compressive stress regimes (individual and systematic behaviour of paver pavement) under 0.8N/mm² applied tyre pressure for vehicle travelling at angle of zero to the orientation of the laying pattern (see Figure 4.2).

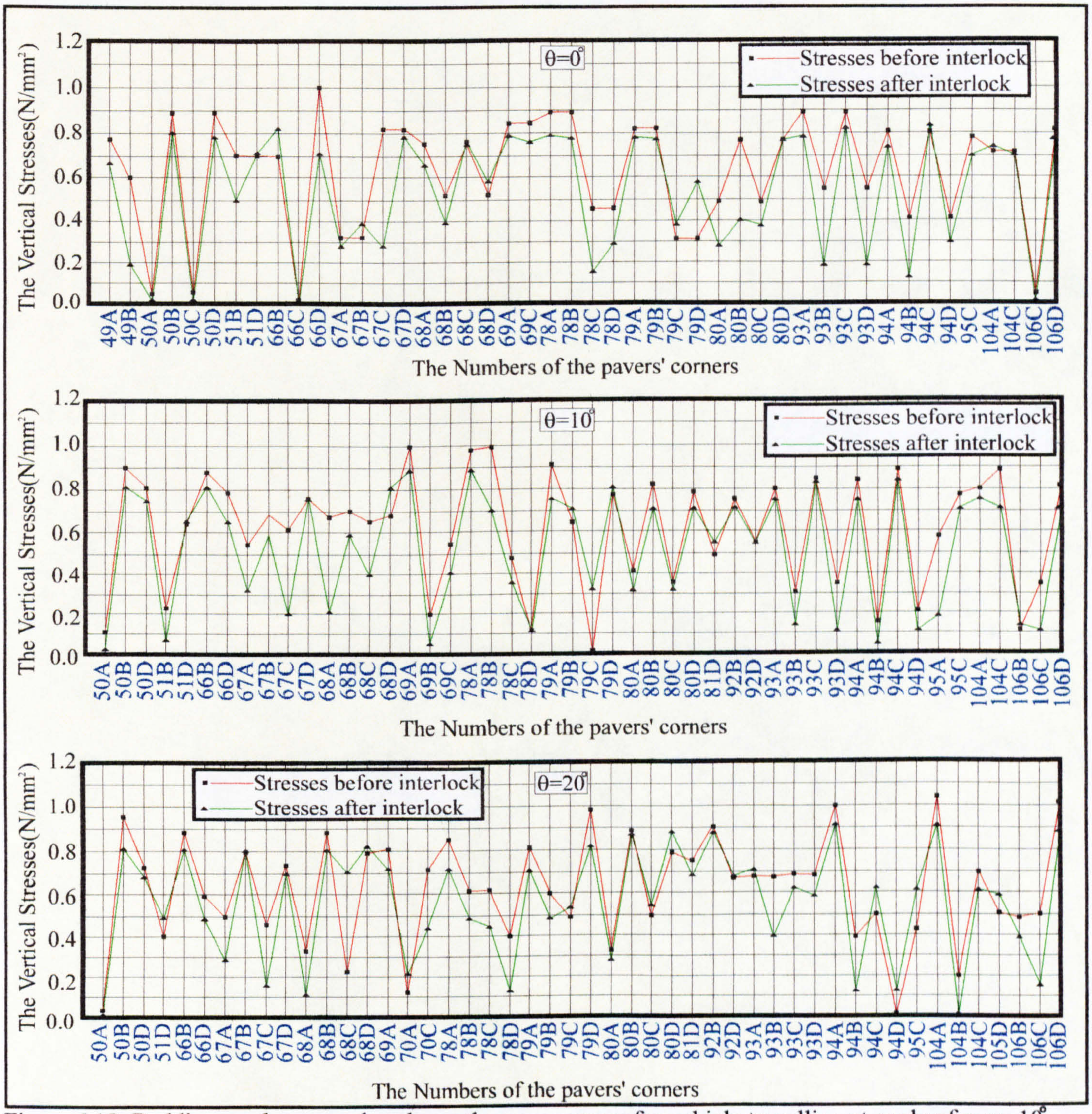

Figure 6.18: Bedding sand stress values beneath paver corners for vehicle travelling at angle of zero, 10° and 20° to the orientation of the laying pattern.

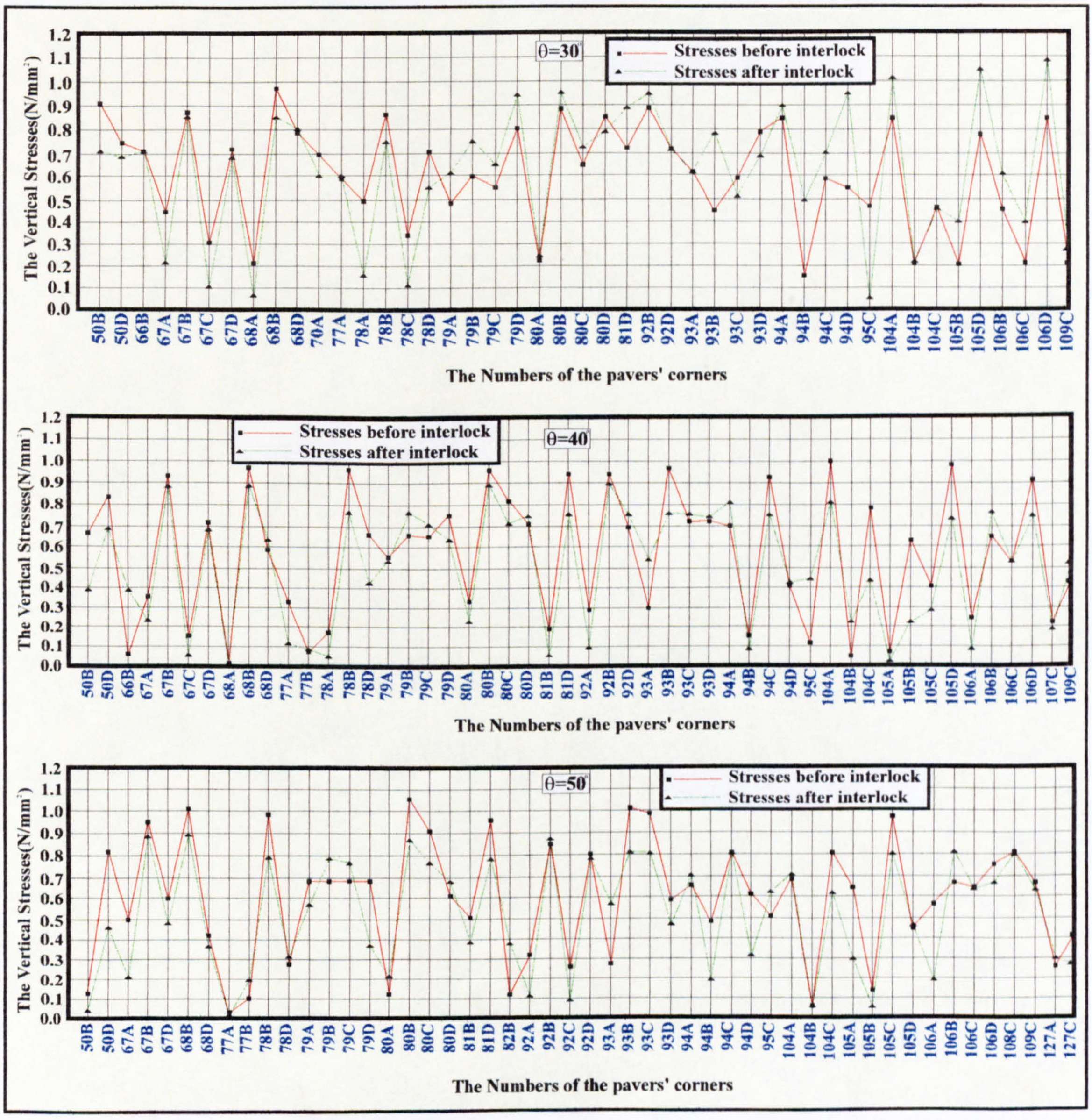

Figure 6.19: Bedding sand stress values beneath paver corners for vehicle travelling at angle of 30°, 40°, 50° to the orientation of the laying pattern.

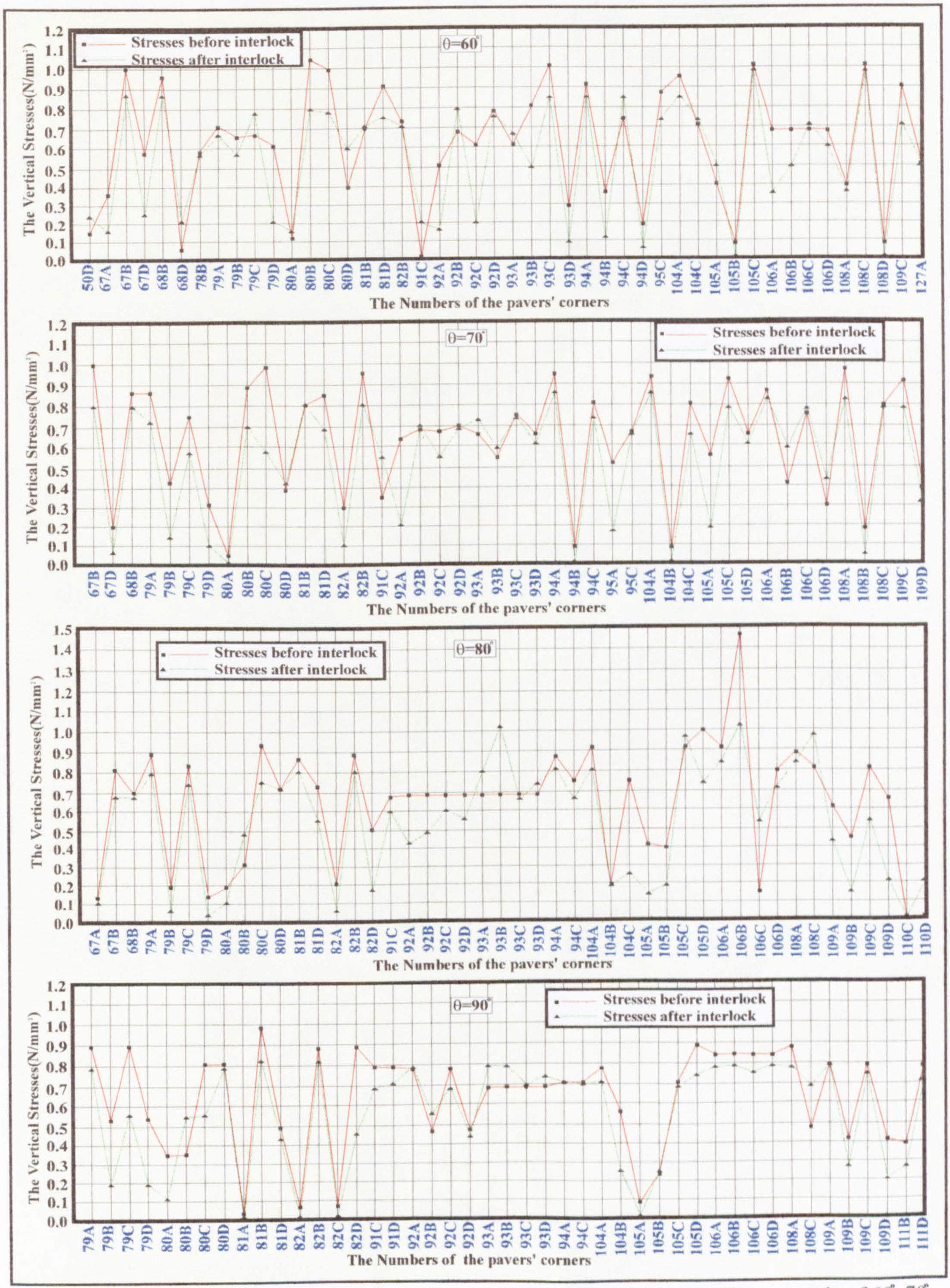

Figure 6.20: Bedding sand stress values beneath paver corners for vehicle travelling at angle of 60°, 70°, 80°, 90° to the orientation of the laying pattern.

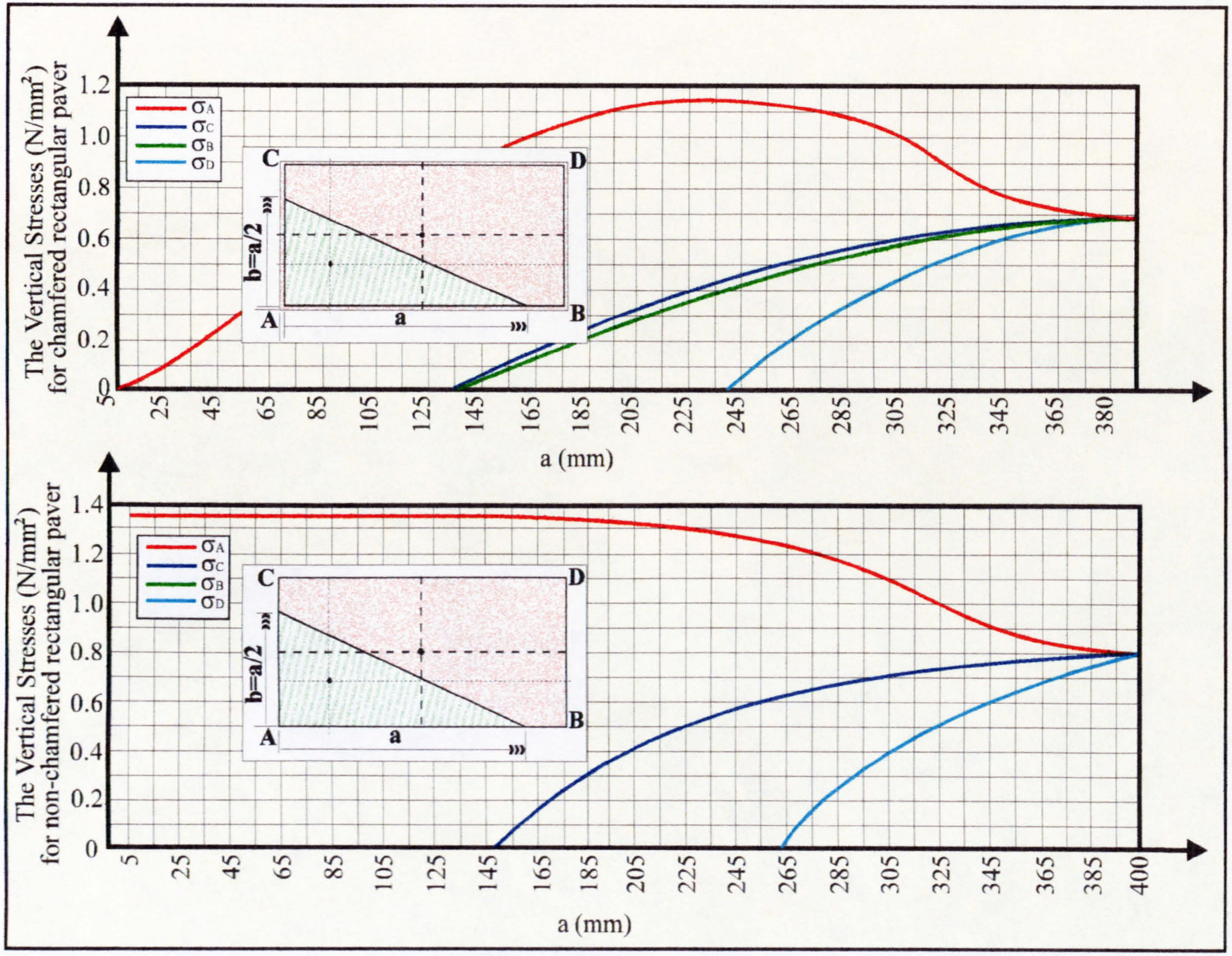

Figure 6.21: Bedding sand vertical stress distributions are developed by the variations of the common patch loading (applied pressure=0.8N/mm^2) for chamfered and non-chamfered rectangular pavers.

traffic (θ=0° or 90°). When vehicles deviate by as little as 10° from these two directions, interlock performs less effectively.

Common patch loadings which functionally generate maximum corner stress values were applied to chamfered rectangular, non- chamfered rectangular and to the nine proprietory shaped pavers (see Figure 5.1) being considered in this Thesis so allowing a meaningful comparison of the effectiveness of each paver shape in terms of load distribution. Figure 6.21 shows the vertical stress distributions beneath chamfered and non-chamfered rectangular pavers for the various common patch loadings.

6.4. Implication of results

Figures 4.2, 6.18, 6.19 and 6.20 show that the true behaviour of concrete block paving under highway loading can be understood only when the way in which asymmetrically loaded pavers transmit wearing surface applied patch loads into the underlying bedding sand has been studied. Even when full interlock is developed, any attempt to measure vertical stress in bedding sand will produce results varying from zero to nearly 70% greater than applied pressure according to the position where stresses are measured and according to the orientation of the load patch in relation to the laying pattern. The simplistic concept of spreading applied load through pavers such that stress gradually diminishes with depth does not apply to pavers. For this reason, any attempt to compare the behaviour of pavers with that of homogeneous material by comparing vertical stress in the bedding sand may lead to erroneous results. Figures 4.2, 6.18, 6.19 and 6.20 show that pavement analysis must take into account the true shape of the patch loading. Many analytical design procedures assume that the load patch is a disk whose diameter can be determined on the basis of assessing wheel load and contact stress. Such an approach must now be regarded as providing results of limited value in terms of the performance of the pavers and their bedding sand, although may still be valid in terms of overall pavement design[1, 2, 3]. Any assessment of the contribution of different laying patterns or different paver size or shape to overall pavement performance must be based upon the type of analysis presented in this Thesis.

Figures 4.2, 6.18, 6.19 and 6.20 also demonstrate why full scale testing of pavers must always be undertaken using true load patch size, pressure and shape and why rolling loads must be used if meaningful results are to be produced. At the University of Newcastle Upon Tyne, the early research into the behaviour of pavers[4] was based upon measuring stresses in bedding sand when the paver wearing surface was loaded by a static circular plate (see Chapter 1, Section 1.4.1.1). Whilst the results provided an initial understanding of the behaviour of pavers and demonstrated the existence of interlock, the inability of such methods to register stress magnification generated at paver corners led to sand specifications being inadequate in some circumstances[1, 2, 3].

The reason why some bedding sands have performed poorly under a combination of regular traffic and the presence of water can now be understood[1, 2, 3]. A combination of high levels of stress frequently develop in bedding sands and rapid changes in those stress values, in conjunction with hydrostatic pressure, have been the cause of several paver pavement failures[1, 2, 3]. Rapidly changing stress values lead to the development of normal pressures in water when the water cannot flow freely, such as is the case in sands including a significant proportion of fine material (defined as finer than 75 microns)[1,2,3]. In some cases, for example, even when full interlock is operating, bedding sand stress can change from 0.1N/mm^2 to 0.9N/mm^2 over a distance of 100mm. A vehicle travelling at 30mph(50kph) would cover 100mm in less than a hundredth of a second. This means that stress can change at a rate exceeding 100N/mm^2 /second[1, 2, 3]. Such a rapid change would lead to destabilising pressures developing in saturated bedding sands[1, 2, 3]. This Chapter indicates that specifiers should avoid those bedding materials which would be disturbed by a combination of high levels of stress and moisture. In particular, material finer that 75 microns is considered to be likely to lead to bedding sand weakness and should be kept to a minimum[1, 2, 3].

6.5. Conclusion and discussion

This Chapter has presented the bedding sand stress calculation method and the mathematical solution to interlock in rectangular paver pavements. The bedding sand stress calculation method which can be used for determining the vertical compressive

stress distributions beneath flexibly bedded concrete pavers is based upon the relationships between the applied patch loadings and their resulting vertical stress distributions beneath pavers. This Chapter has explained the application of the method to rectangular pavers. Initially, the vertical stress distributions have been found for a range of patch loadings (described in Chapters 4 and 5) resulting from vehicle tyres rolling across chamfered and non-chamfered rectangular non-interlocking pavers (see Figures 6.2 to 6.16 and Figure 6.21). It has also been demonstrated that chamfered rectangular pavers have significantly enhanced load dissipation characteristics as compared with non-chamfered pavers (see Figure 6.21). This may account for some of the observed benefits inherent in chamfered pavers[1, 2, 3]. Paver joints should be narrow and should remain narrow and well filled in service in order that full interlock is maintained[1, 2, 3]. By forcing the load patch inboard of the paver perimeter, chamfered pavers reduce bedding sand stress levels and are therefore to be preferred in trafficked pavements.

This Chapter concludes that the deformations and the stress distributions are function of the applied full contacted tyre pressures (see Figures 4.2 and 6.17) and the stresses change three dimensionally by exceeding the tyre pressures in certain points beneath pavers (see Figures 6.2 to 6.21). The vertical stresses in the bedding sand are calculated by considering vertical and rotational equilibrium of the pressures applied to the upper and lower horizontal paver surfaces. By ensuring vertical and rotational equilibrium, three equations can be developed (one vertical equilibrium and two rotational equilibrium equations, one in each orthogonal direction) which can be solved to obtain the values of the vertical stress in the bedding sand at each corner of the lower horizontal surface of the paver. It has been shown that there are five main vertical compressive stress regimes (see Figure 6.1) which can occur beneath rectangular pavers according to magnitude and position of patch loads. These are conceptually:

- tetrahedral stress regimes
- long-pentahedral stress regimes
- short-pentahedral stress regimes

- partial-hexahedral stress regimes
- absolute-hexahedral stress regimes

By determining stress values resulting from patch loading, this Chapter has illustrated discontinuities in the patterns of vertical stress beneath non-interlocking neighboring pavers. It argued that those discontinuities can occur only in the theoretical non-interlocking case (see Figure 6.17) and it used the values of the discontinuities to evaluate (for the first ever time) the true values of interlock which are established beneath neighboring pavers (see Figures 6.18, 6.19 and 6.20). The importance of this evaluation of interlock stress is in the fact that it can be used to explain many phenomena known to exist in pavers which so far have been considered to be too difficult to understand. For example, it is shown that rapid changes in levels of compressive stress in bedding sand occur even with relatively low speed traffic[1, 2, 3]. These rapid changes in the presence of water are considered to represent the reason for bedding sand instability which has been observed in some pavements[1, 2, 3]. This Chapter has also compared different laying pattern orientations and confirmed that from a stress distribution point of the view the preferred orientation of pavers is when their axis runs at 90° to and in line with the direction of traffic (see Figure 6.20). The transfer stresses have been calculated across joints for interlocking chamfered rectangular pavers laid to 45 degree herringbone pattern (see Figures 6.18, 6.19 and 6.20).

The first experimental justification[5] to the mathematical solutions presented in this Chapter has recently been conducted in Japan. The Japanese experimental study[5] concentrated on the determination of vertical compressive stress values beneath pavers and asphalt by using the pressure sensitive reactive papers which were installed to the upper surface of the sub-base of the test pavements. In this study[5] the 8tf and 5tf static circular plate loads were used for paver and asphalt pavements respectively. The rectangular and shaped paver pavements were compared between different laying pattern orientations according to the vertical compressive stress distributions beneath the wearing course. Subsequently, the results have been compared with the stress values which the flexible materials generated. Figure 6.22 shows the results of the

Japanese experimental study[5] for the vertical compressive stress distributions on the tested rectangular and shaped paver pavements' lower surface of bedding sand.

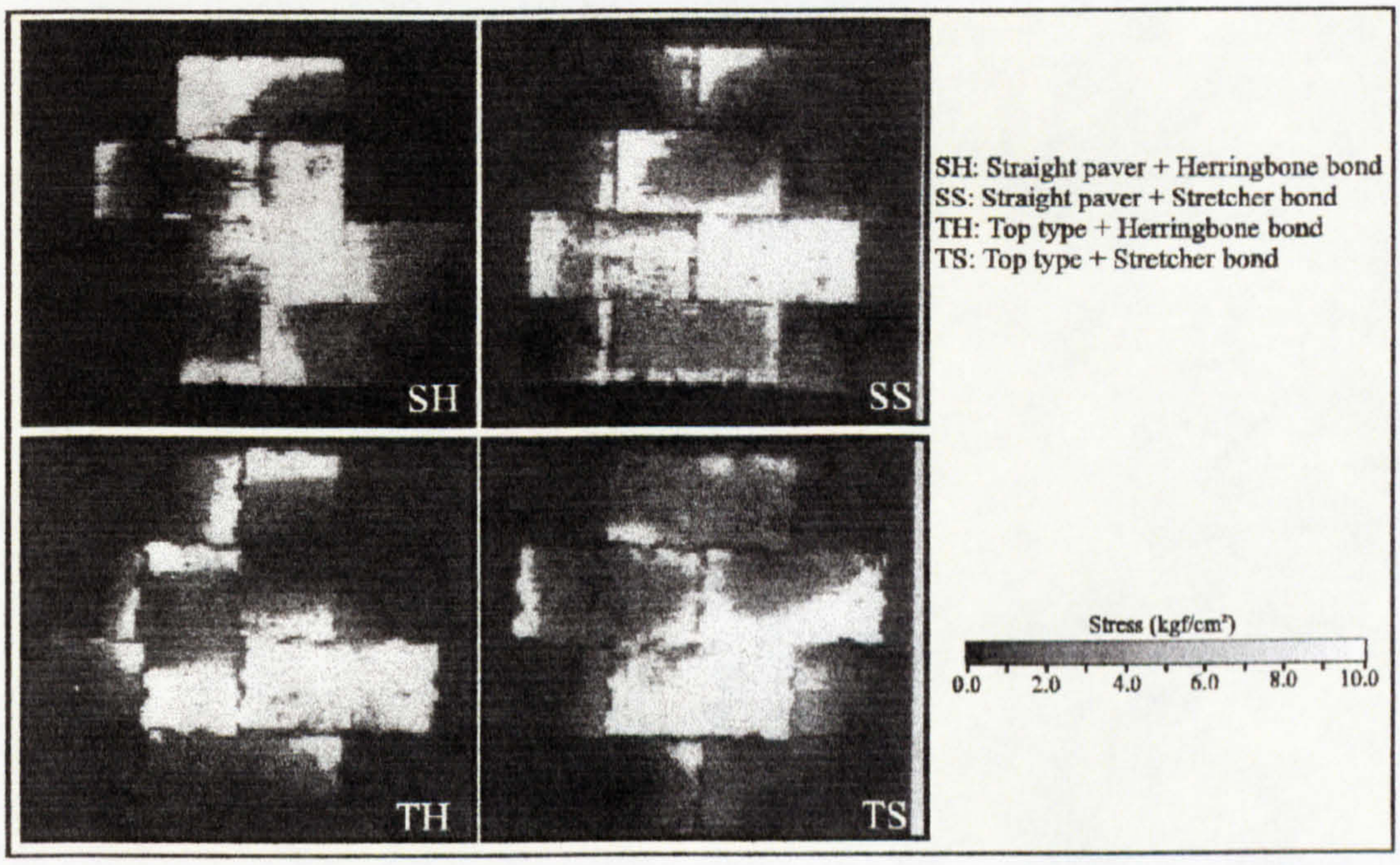

Figure 6.22: The results of the Japanese experimental study[5] for the rectangular and shaped paver pavements' vertical stress distributions at the lower surface of bedding sand.

The Japanese study[5] in Figure 6.22 illustrates the discontinuities in the patterns of the vertical stress distributions beneath the non-interlocking neighbouring pavers because of both untreated sand joints (which cause non-interlock case) and the static circular plate loads, which were used, do not address to the true wheel patch loading (see Chapter 4). It has been shown in this Chapter that those discontinuities can occur only in the theoretical non-interlocking case (see Figure 6.17). Because of this reason, the vertical compressive stress values determined in the Japanese study[5] can only be compared with the stress distributions beneath non-interlocking neighboring rectangular pavers developed in this Chapter (see Figures 6.2 to 6.21).

The most significant part of the Japanese experimental study[5] is that the vertical compressive stress regimes beneath non-interlocking rectangular pavers (see Figure 6.1) which have been developed theoretically in this Chapter can be seen in Figure 6.23.

Figure 6.23 consists of the stress distributions given in Figure 6.22 for the tested rectangular pavers (SH and SS). The red lines shown in Figure 6.23 illustrate the boundary of the stress regimes beneath non-interlocking rectangular pavers (see Figures 6.1 and 6.17).

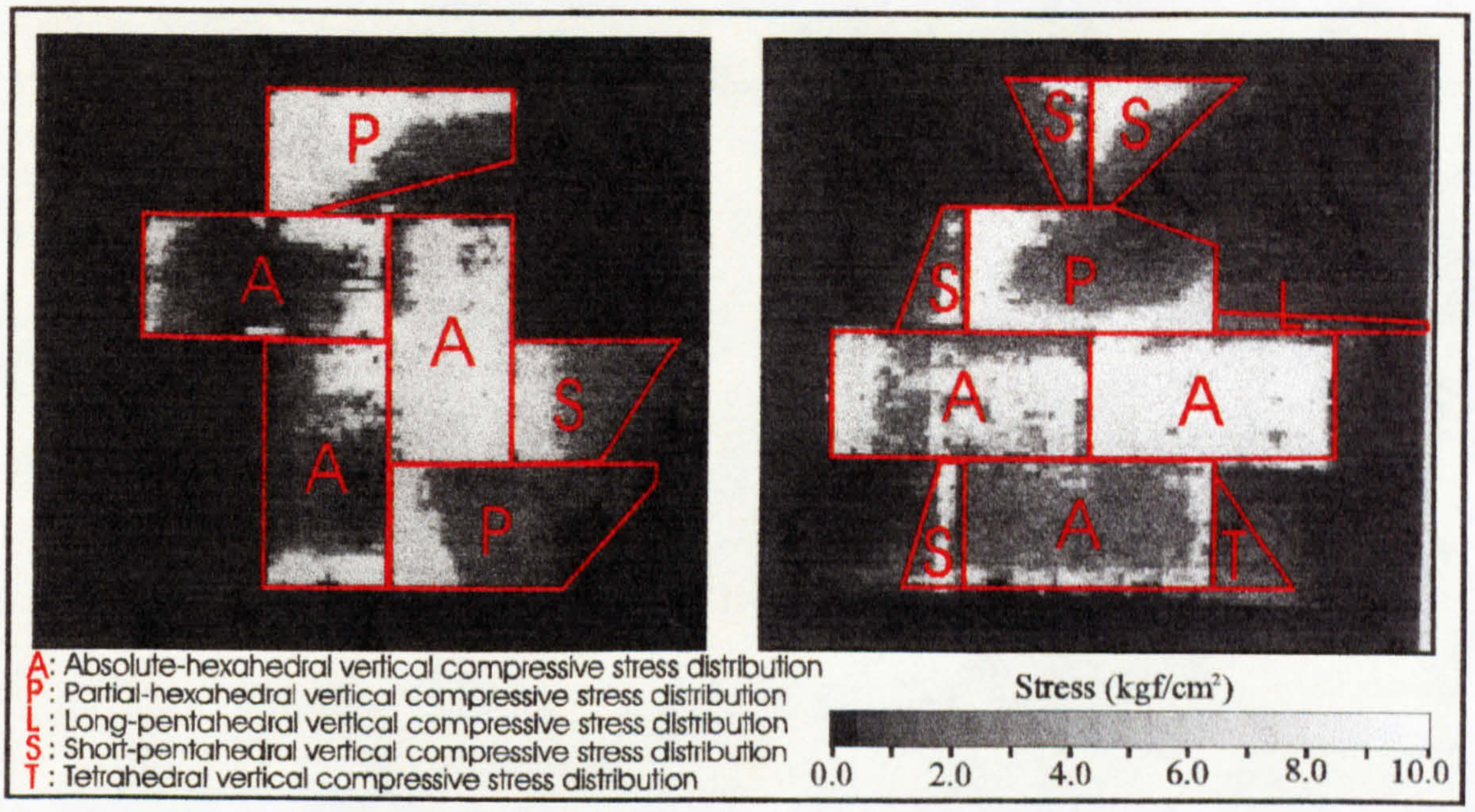

Figure 6.23: The results of the Japanese experimental study[5] for the rectangular paver pavements' vertical stress distributions at the lower surface of bedding sand and the boundary of the vertical compressive stress regimes (red lines) beneath non-interlocking rectangular pavers have been developed theoretically in this Chapter (see Figures 6.1 and 6.17).

Pavers are particularly useful paving material in that they provide a strong and flexible surface which can support concentrated loads for long periods without suffering deformation[6], and because no complex or expensive plant is involved in its construction[6]. The ability of block paving to withstand concentrated loads has led to its wide use at highway engineering applications[6]. A pavement incorporating full interlock has been proven to sustain high levels of applied load[4, 6, 7, 8]. An interlocking paver pavement can be observed to behave in a manner whereby the pavers act together as a system such that the pavement has more of the character of a flexible homogeneous material rather than that of a collection of individual units behaving independently[1, 2, 3].

Because of this, virtually all of the research into the behavior of concrete block paving has focused upon establishing relative performance factors between pavers and conventional flexible pavement construction materials[1, 2, 3].

The interlock mechanism whereby pavers act together as a coherent system which occurs as a result of load transfer and shear stress between neighbouring pavers. Pavers form the upper surface of the pavement and must therefore meet the requirements for a wearing course which are as follows. It should support traffic loads without undue deformation, present a surface with suitable characteristics for the safe and comfortable passage of traffic, and provide protection to the underlying layers of the pavement and its foundation from the harmful effects of weather and traffic[1, 2, 3]. These objectives can be achieved by ensuring that the joint and bedding course materials are successful in transferring maximum stresses without any failure. This matrix of joint materials should effectively prevent any paver from moving downwards and/or rotating which will ensure that the surface remains stable. By ensuring the sand is remained compact, the frictional forces must transfer the stresses between neigbouring pavers in the interlock mechanism. The paving is commonly agitated by a vibrating plate compactor which causes the laying course material to flow into the open joints and to be compacted, thus providing conditions in which full interlock can develop. The functions of the laying course are twofold: to fill any irregularities in the surface upon which the material is to be laid, and to bed the pavers and filling of the joints so that interlock may develop.

The principal UK paver pavement design guide, BS7533:1992[9] uses conventional flexible pavement design technology with a one to one equivalence factor between pavers and asphalt, i.e. 100mm thickness of bedding sand and pavers is equivalent structurally with 100mm asphalt. This assumption is based upon the research[10, 11] which is supported by observations of the performance of pavers on trafficked areas[12]. Because the equivalence thickness technique has been found to be adequate in day to day design, there has been no need to attempt to investigate rigorously the mechanics of the behavior of concrete block paving. Woodman[13] has reported full scale testing in which levels of vertical strain were measured beneath rolling loads at the Transport Research Laboratory(TRL). He has concluded that pavers and their bedding sand

equivalence with no more than 10mm asphalt, rather than with the value of 100mm in BS 7533[9]. Other unpublished experimental work at TRL has indicated that concrete pavers can actually magnify applied pressure such that stresses measured in the bedding sand have been found to exceed the tyre pressure of the load vehicle.

There is clearly a contradiction between the findings of some researchers and the assumptions made by designers and by those drafting codes of practice. The apparently unconservative design assumptions being made world-wide on a daily basis are not in fact leading to the premature pavement deterioration levels which some research suggests should be occurring[1, 2, 3]. This Chapter investigated to resolve this contradiction by examining in detail the way in which patch loading applied to the wearing surface of pavers is transmitted as vertical stress into the underlying bedding material. It developed the equations of vertical and rotational equilibrium which are solved to determine the values of critical stresses beneath pavers. It first of all considers the case of zero interlock i.e. each paver comprises an individual unit unconnected to its neighbours and shows that the mathematical solution to this case results in stresses which exceed applied pressure by up to 70%. This is important because it means that any attempts to measure the effect of interlock should in fact compare measured stresses not with tyre pressure but with a value up to 70% greater than tyre pressure. The Chapter concludes that those researchers who have made an assessment of the equivalence of pavers with asphalt on the basis of comparing measured stress with actual applied pressure may have drawn inaccurate conclusions. It therefore explains the contradiction between the practitioners and the researchers and explains why the design assumption of one to one equivalence may remain valid.

The complexity of the stress distribution in bedding sand may explain why some research conclusions e.g. Woodman[13] have contradicted observed performance of pavers. The high stress transients shown in Figures 6.18, 6.19 and 6.20 occur for short time periods in a rolling load situation and may be of little consequence when pavers are laid over some materials but may be more important in other situations. This might explain why some evidence[13] indicates that pavers perform better when laid over concrete bases than they do when laid over softer bitumen bound materials or granular

materials (better even when the additional stiffness inherent in concrete as compared with asphalt is taken into account)[1, 2, 3].

Many of the hitherto unexplained bedding sand failures can be understood by examining the way in which local vertical stress transients develop and travel though bedding sand. In cases where water is present in sands including a significant fraction of fine material, the mechanism whereby sand instability can develop has been explained[1, 2, 3]. Rapidly changing stress levels can result in pressure developing in water in bedding sand which can lead to instability[1, 2, 3]. Many regions permit sand specifications which can lead to instability when vehicles travelling at highway speeds use pavers bedded on saturated sand[1, 2, 3]. It is recommended that such specifications be reviewed and that sands should be specified which permit water to flow as freely as possible where traffic and water may occur concurrently[1, 2, 3].

References

1 Algin, H.M., Knapton, J., (1996), *Research into paver interlock*, Jml. of the Institution of Highway & Transportation & IHIE, Vol. 43, No. 03, Pp 20-24.

2 Knapton, J., Algin, H.M., (1995), *The Mathematical Solution to Interlock in Flexibly Bedded Clay Paving*. Proc. of the 4th. Int. Masonry Conf. No. 7, Vol. 2, Pp 307-313. London.

3 Knapton, J., Algin, H.M., (1996), *The Mathematical Solution to Interlock in Concrete Block Paving*. Proc. of the 5th. Int. Conf. on Concrete Block Paving, Tel-Aviv. Pp 261-278.

4 Knapton J. and Barber S.D., (1980), *UK Research into Concrete Block Pavement Design*. Proc. 1st Int. Conf. on Concrete Block Paving. Pp 33-37, University of Newcastle upon Tyne, UK.

5 Murai, S., Takahashi, H., Okawa, M., (1996), *Stress Distributions under Concrete Blocks*, Proc. of the 5th. Int. Conf. on Concrete Block Paving, Tel-Aviv, Pp 253-260.

6 Barber S.D., (1980). *Pavement Design For Port Areas*, Ph.D. Thesis, University of Newcastle upon Tyne, UK.

7 Lilley A. A.,(1991). *A Handbook of Segmental Paving*, Chapman & Hall, London.

8 Shackel B.,(1990). *Design and Construction of Interlocking Concrete Block Pavements*, Chapman & Hall, London.

9 BS7533:1992. *The Structural Design of Pavements Surfaced with Clay Pavers or Concrete Block Paving*. British Standards Institution, London.

10 Knapton J(1984). *Concrete Block Pavement Design in the UK*. Proc. 2nd Int. Conf. on Concrete Block Paving. Pp 129-138.

11 Knapton J(1985). *The Structural Design and Performance of Concrete Block Roads*. Proc. 3rd Int. Conf. on Concrete Pavement Design & Rehabilitation, Purdue University. Pp127-135.

12 Knapton J & Cook ID(1992). *Design Methods for Clay & Concrete Block Paving*. Proc. 4th Int. Conf. on Concrete Block Paving, Auckland, NZ. Pp 27-50.

13 Woodman GR(1992). *The Performance of Concrete Block Surfacing on a Cement-Bound Base in Airfield Pavements.* Proc. 4th Int. Conf. on Concrete Block Paving, Auckland, NZ. Pp. 253-262.

CHAPTER SEVEN

STRESS CALCULATIONS FOR A COMMON PROPRIETORY SHAPED PAVER

Synopsis

This Chapter presents the application of the bedding sand stress calculation method to a common proprietory shaped paver (see proprietory shaped paver 1 in Figure 5.1). The nine proprietory shaped pavers analysed in this Thesis are commercially important on a worldwide basis. A common proprietory shaped paver has been selected as an example in this Chapter to show how all possible vertical compressive stress regimes of proprietory shaped pavers can be calculated for all realistically possible load patches (see Chapter 5). For the remaining shapes, the developed algebraical solutions of the absolute-hexahedral compressive stress regimes which occur beneath the circumscribing rectangular borders are given in Chapter 8. In the other paver stress regimes, iterative solutions (see Appendix) have been developed and given in Figures 6.21, 9.1, 9.2, 9.3, 9.4, 9.5, 9.6, 9.7, 9.8 and 9.9.

7.1. Introduction

The Bedding sand stress calculation method for rectangular pavers described in Chapter 6 has been applied to the nine non-rectangular shapes of pavers as shown in Figure 5.1. In each case, the circumscribing rectangular paver has been analysed and the negative effects generated by the shaped paver dentations have been included in the results.

The vertical stresses for shaped pavers can be calculated by considering vertical and rotational equilibrium of the load patch pressures applied onto the upper paver surface as has already been described for rectangular pavers. For vertical equilibrium to be satisfied the total applied load must equal the total volume of the vertical compressive stress beneath the paver and for rotational equilibrium, the centroid distances of the applied load $\left(\overline{X}, \overline{Y}\right)$ must coincide with the centroid distances of the total volume of the vertical compressive stress in the bedding sand. The assumptions which were used for rectangular pavers can be applied equally to proprietory shaped pavers. These are firstly the support conditions of the paver are uniform and secondly the pavers are structurally rigid in relation to their bedding sand. As may be seen in Figure 6.1 all stress blocks geometrically have the tetrahedron surface function. However only that part of the upper surface of these volumes which contacts the lower paver surface must be considered. Therefore, a method is required which calculates that part of the volume of a tetrahedron which is truncated by the paver boundary lines. This truncated volume can then be equalised to the total applied patch load and rotational equilibrium conditions can be applied by ensuring the centroid distances of the load patch and the truncated tetrahedron coincide. The vertical compressive stress function can be calculated by using the three resulting equations. The stress function is the function satisfies the equation of the vertical equilibrium and the two equations of rotational equilibrium. The complexity of the vertical compressive stresses calculation can be reduced by using the circumscribing rectangular boundaries of the shaped blocks (see Figure 5.1), with the proviso that the volume of actual vertical stress must satisfy the vertical and rotational equilibriums in each step of evaluating the stress function. The individual proprietory shaped pavers illustrated in Figure 5.1 are now analysed to

determine the vertical stress distributions by using the common applied load patch variations which are described in Chapter 5. This Chapter presents the application of the bedding sand vertical stress calculation method for a common proprietory shaped paver (see Figure 5.1, proprietory shaped paver 1).

7.2. The Application of the bedding sand stress calculation method for proprietory shaped paver 1

The proprietory shaped paver 1 shown in Figure 5.1 is analysed by using the method described in Chapter 6. Because this shape of paver is commercially important on a worldwide basis, it has been selected as the paver for which solutions will now be developed for all possible bedding material stress block shapes. For the remaining shapes, the developed algebraical solutions of the absolute-hexahedral compressive stress regimes which occur beneath the circumscribing rectangular borders are given in Chapter 8. In the other paver stress regimes, iterative solutions (see Appendix) have been developed and given in Figures 6.21, 9.1, 9.2, 9.3, 9.4, 9.5, 9.6, 9.7, 9.8, 9.9.

Five vertical compressive stress regimes can occur beneath the circumscribing rectangular border of proprietory shaped paver 1. These are tetrahedral, short-pentahedral, long-pentahedral, partial-hexahedral and absolute-hexahedral compressive stress regimes as described in Figure 6.1. The negative effects generated by the dentations have been included in the results of these compressive stress regimes.

7.2.1. Tetrahedral compressive stress regimes beneath the circumscribing rectangular border for proprietory shaped paver 1

The intersection points which are between the line functions bounding shaped paver 1 shown in Table 5.1 and the lines (which bound the bottom surface of the tetrahedral stress in the xy-plane) have the functions $fy = l\left(1-\frac{x}{l}\right)$, $fx = l\left(1-\frac{y}{l}\right)$ in the x and y axes can be calculated mathematically. Table 7.1 shows the intersection points' formulae and the points are illustrated in Figures 7.1 to 7.24.

$T_{1x} = \frac{t(l-15)}{l-0.3t}$ and $T_{1y} = \frac{l(t-50)}{t-3.\bar{3}l}$		$T_{2x} = \frac{0.6t(l-15)}{t+0.6l}$ and $T_{2y} = \frac{l(t+9)}{t+0.6l}$	
$T_{3x} = \frac{t(l-85)}{l-3t}$ and $T_{3y} = \frac{l(t-28.\bar{3})}{t-0.\bar{3}l}$		$T_{4x} = \frac{t(l-85)}{l+1.\bar{6}t}$ and $T_{4y} = \frac{l(t+51)}{t+0.6l}$	
$T_{5x} = \frac{t(l-114.5)}{l-0.3t}$ and $T_{5y} = \frac{l(t-381.\bar{6})}{t-3.\bar{3}l}$		$T_{6x} = \frac{t(l-46.25)}{l+0.75t}$ and $T_{6y} = \frac{l(t+61.\bar{6})}{t+1.\bar{3}l}$	
$T_{7x} = \frac{t(l-129.615)}{l-0.2301t}$ and $T_{7y} = \frac{l(t-561.\bar{6})}{t-4.\bar{3}l}$		$T_{8x} = \frac{t(l+17.5)}{l+0.75t}$ and $T_{8y} = \frac{l(t-23.\bar{3})}{t+1.\bar{3}l}$	
$T_{9x} = \frac{t(l-161)}{l-0.3t}$ and $T_{9y} = \frac{l(t-536.\bar{6})}{t-3.\bar{3}l}$		$T_{10x} = \frac{t(l+271.\bar{6})}{l+1.\bar{6}t}$ and $T_{10y} = \frac{l(t-163)}{t+0.6l}$	
$T_{11x} = \frac{t(l-685)}{l-3t}$ and $T_{11y} = \frac{l(t-228.\bar{3})}{t-0.\bar{3}l}$		$T_{12x} = \frac{t(l+341.\bar{6})}{l+1.\bar{6}t}$ and $T_{12y} = \frac{l(t-205)}{t+0.6l}$	
$T_{13x} = \frac{t(l-61.5)}{l-0.3t}$ and $T_{13y} = \frac{l(t-205)}{t-3.\bar{3}l}$		$T_{14x} = \frac{t(l+101.25)}{l+0.75t}$ and $T_{14y} = \frac{l(t-135)}{t+1.\bar{3}l}$	
$T_{15x} = \frac{t(l-31.154)}{l-0.23t}$ and $T_{15y} = \frac{l(t-135)}{t-4.\bar{3}l}$		$T_{16x} = \frac{t(l+37.5)}{l+0.75t}$ and $T_{16y} = \frac{l(t-50)}{t+1.\bar{3}l}$	

Table 7.1: The intersection points between the line which forms the tetrahedral stress block in the xy-plane and the line boundary functions of proprietory shaped paver 1 (**t** and **l** are the lengths of the stress block along the x and y axes respectively as illustrated in Figure 7.1).

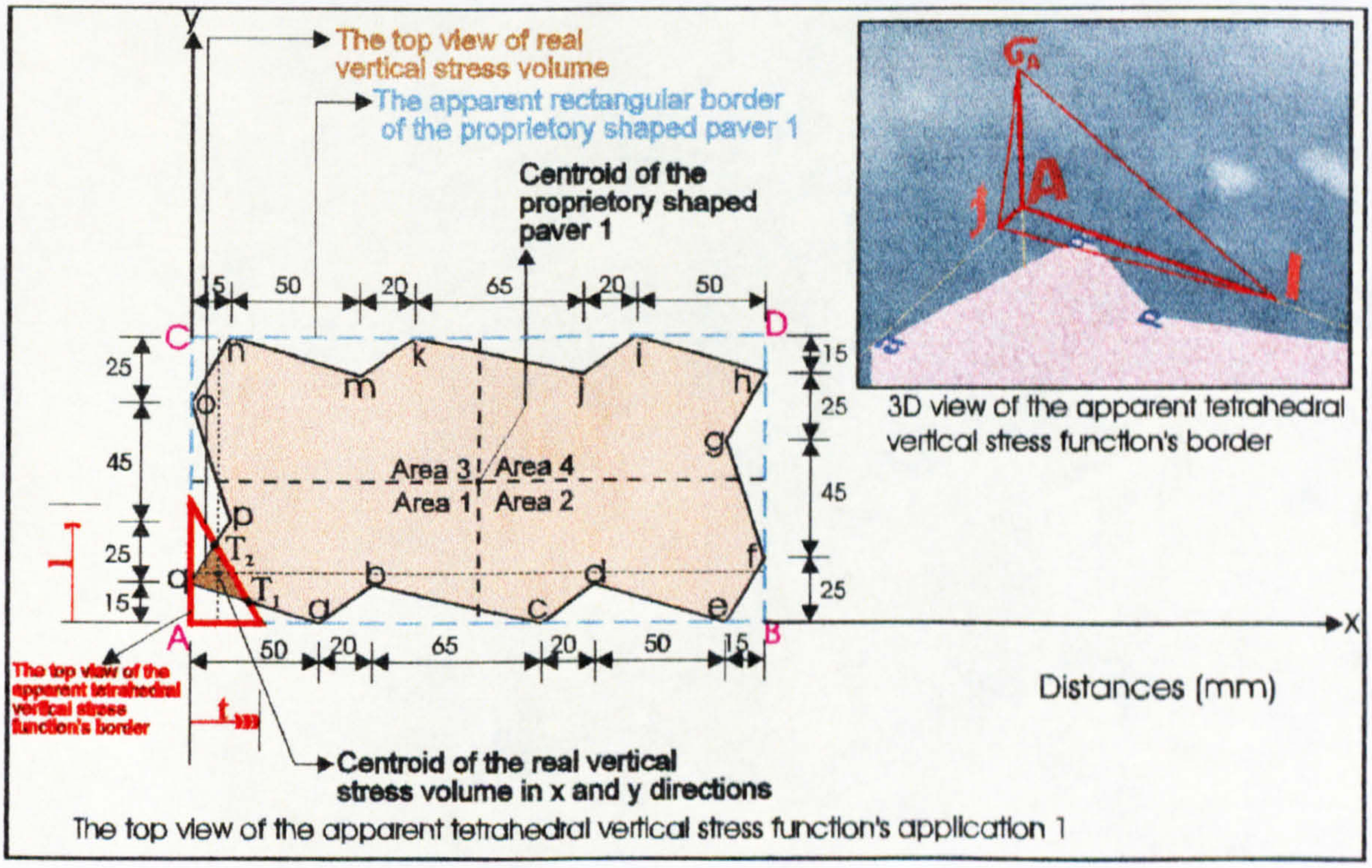

Figure 7.1: Application 1 of the tetrahedral compressive stress distribution beneath the circumscribing rectangular border of proprietory shaped paver 1.

The surface function of the tetrahedral compressive stress block beneath the circumscribing rectangular border shown in Figure 7.1 through the three point σ_A, **l** and **t** is given by:

$$\begin{vmatrix} x & y & z & 1 \\ t & 0 & 0 & 1 \\ 0 & l & 0 & 1 \\ 0 & 0 & \sigma_A & 1 \end{vmatrix} = 0 \Rightarrow f(x,y) = z = \sigma_A\left(1 - \frac{x}{t} - \frac{y}{l}\right)$$

The first application of the tetrahedral compressive stress regime beneath the circumscribing rectangular border of proprietory shaped paver 1 shown in Figure 7.1 can be calculated by using the data in Tables 5.1 and 7.1. The first two letters of each boundary line function in Table 5.1 for proprietory shaped paver 1 charecterise the corner names can be seen in Figure 7.1 (example: **qay** symbolises the boundary line function of proprietory shaped paver 1 in the **y** axis between corner **q** and **a**). The line functions which define the boundary of the tetrahedral stress block in the xy-plane (see Figure 7.1) are of the form $fy = l\left(1 - \frac{x}{t}\right)$, $fx = t\left(1 - \frac{y}{l}\right)$.

The following actual total volume **V** beneath the surface $f(x,y) = z\ (> 0)$ and above the region in the xy-plane (see Figure 7.1) is calculated by subtracting the negative volume generated by the dentations of the shaped paver from the tetrahedral volume beneath circumscribing rectangular boundary of the paver.

$$V = \int_0^t \int_0^{fy} f(x,y)\,dy\,dx - \int_{T_{1x}}^t \int_0^{fy} f(x,y)\,dy\,dx - \int_0^{T_{1x}} \int_0^{T_{1y}} f(x,y)\,dy\,dx - \int_0^{T_{1x}} \int_{T_{1y}}^{qay} f(x,y)\,dy\,dx$$

$$- \int_0^{T_{2x}} \int_{T_{2y}}^{fy} f(x,y)\,dy\,dx - \int_0^{T_{2x}} \int_{15}^{qpy} f(x,y)\,dy\,dx$$

and the centroids of this volume in the xy-plane are at distances $\overline{X}$ and $\overline{Y}$ from the axes (see Figure 7.1) which are given by the following equations.

$$\overline{X} = \frac{1}{V}\left[\begin{array}{l} \int_0^t \int_0^{fy} x f(x,y)\,dy\,dx - \int_{T_{1x}}^t \int_0^{fy} x f(x,y)\,dy\,dx - \int_0^{T_{1x}} \int_0^{T_{1y}} x f(x,y)\,dy\,dx \\ -\int_0^{T_{1x}} \int_{T_{1y}}^{qay} x f(x,y)\,dy\,dx - \int_0^{T_{2x}} \int_{T_{2y}}^{fy} x f(x,y)\,dy\,dx - \int_0^{T_{2x}} \int_{15}^{qpy} x f(x,y)\,dy\,dx \end{array}\right]$$

$$\overline{Y} = \frac{1}{V}\left[\begin{array}{l} \int_0^l \int_0^{fx} y f(x,y)\,dx\,dy - \int_0^{T_{1y}} \int_{T_{1x}}^{fx} y f(x,y)\,dx\,dy - \int_0^{T_{1y}} \int_0^{T_{1x}} y f(x,y)\,dx\,dy \\ -\int_{T_{1y}}^{15} \int_0^{qax} y f(x,y)\,dx\,dy - \int_{15}^{T_{2y}} \int_0^{qpx} y f(x,y)\,dx\,dy - \int_{T_{2y}}^{l} \int_0^{fx} y f(x,y)\,dx\,dy \end{array}\right]$$

Appendix which is included at the end of Thesis shows how to evaluate these integrates to the nonlinear system equations and how to apply the numerical analysis to those generated simultaneous equations in order to determine the roots of the equations iteratively. In the iterative solutions, the results are obtained by repeatedly performing the same sequence of steps until the specified conditions are satisfied and no longer change (see Appendix). Appendix also gives theoretical information about iterative solutions to nonlinear simultaneous equations.

Application 2 of the tetrahedral compressive stress regime beneath the circumscribing rectangular border of proprietory shaped paver 1 shown in Figure 7.2 can be calculated by using Tables 5.1 and 7.1 and the surface function of the tetrahedral compressive stress through the three points σ_A, l and t.

The total volume V beneath the surface $f(x,y) = z\ (> 0)$ and above the region in the xy-plane (see Figure 7.2) is:

$$V = \int_0^t \int_0^{fy} f(x,y)\,dy\,dx - \int_{T_{1x}}^t \int_0^{fy} f(x,y)\,dy\,dx - \int_0^{T_{1x}} \int_0^{T_{1y}} f(x,y)\,dy\,dx - \int_0^{T_{1x}} \int_{T_{1y}}^{qay} f(x,y)\,dy\,dx$$

$$- \int_0^{15} \int_{15}^{qpy} f(x,y)\,dy\,dx - \int_0^{T_{3x}} \int_{40}^{T_{3y}} f(x,y)\,dy\,dx - \int_0^{T_{3x}} \int_{T_{3y}}^{fy} f(x,y)\,dy\,dx - \int_{T_{3x}}^{15} \int_{40}^{poy} f(x,y)\,dy\,dx$$

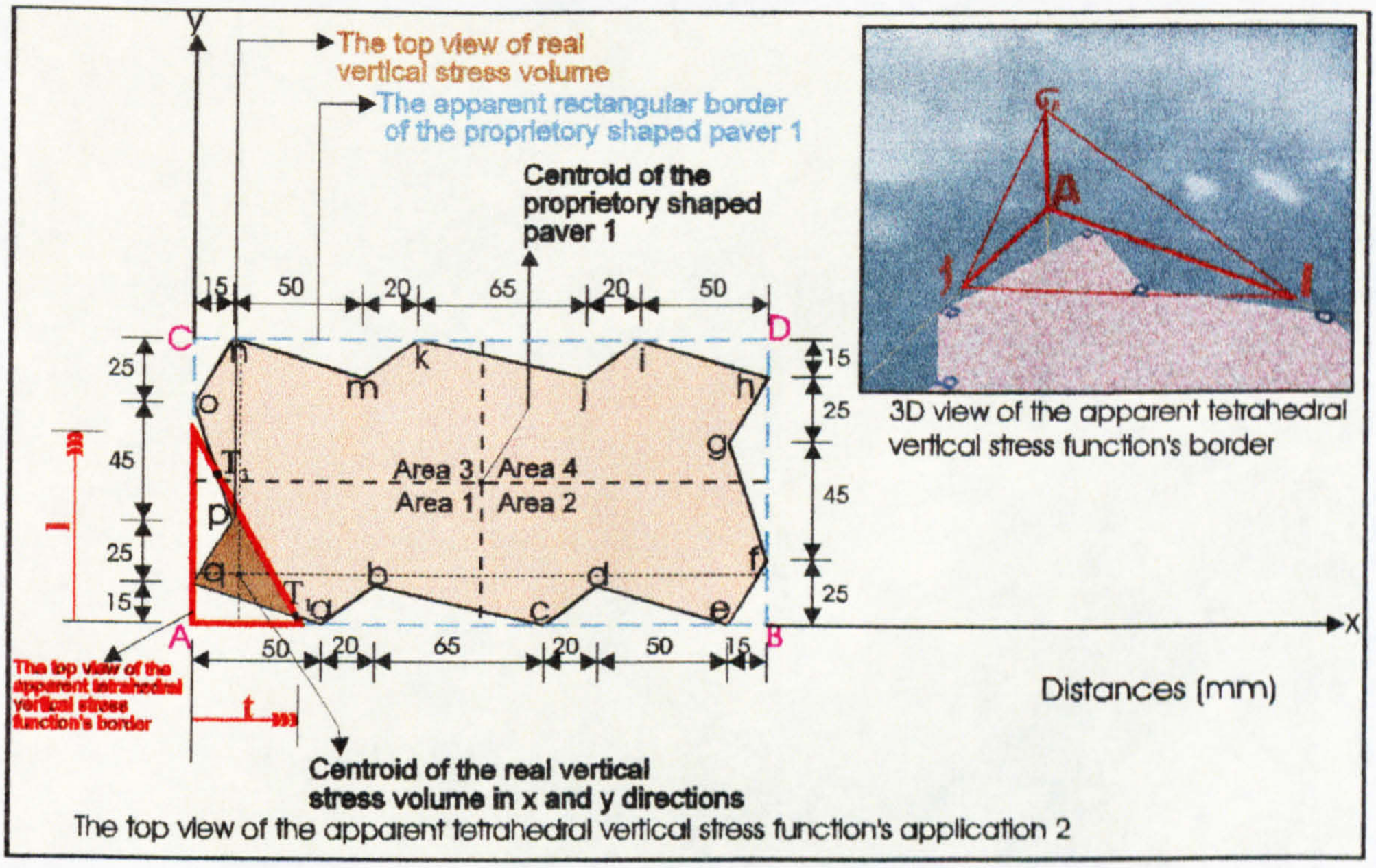

Figure 7.2: Application 2 of the tetrahedral compressive stress distribution beneath the circumscribing rectangular border of proprietory shaped paver 1.

and the centroids of this volume in the xy-plane are at distances $\overline{X}$ and $\overline{Y}$ from the axes (see Figure 7.2) which are given by the following equations.

$$\overline{X} = \frac{1}{V}\left[\int_0^t \int_0^{fy} x f(x,y)\,dy\,dx - \int_{T_{1x}}^t \int_0^{fy} x f(x,y)\,dy\,dx - \int_0^{T_{1x}} \int_0^{T_{1y}} x f(x,y)\,dy\,dx - \int_0^{T_{1x}} \int_{T_{1y}}^{qay} x f(x,y)\,dy\,dx\right.$$

$$\left. - \int_0^{15} \int_{15}^{qpy} x f(x,y)\,dy\,dx - \int_0^{T_{3x}} \int_{40}^{T_{3y}} x f(x,y)\,dy\,dx - \int_0^{T_{3x}} \int_{T_{3y}}^{fy} x f(x,y)\,dy\,dx - \int_{T_{3x}}^{15} \int_{40}^{poy} x f(x,y)\,dy\,dx\right]$$

$$\overline{Y} = \frac{1}{V}\left[\begin{array}{l} \int_{0}^{l}\int_{0}^{fx} y f(x,y)\,dx\,dy - \int_{0}^{T_{1y}}\int_{T_{1x}}^{fx} y f(x,y)\,dx\,dy - \int_{0}^{T_{1y}}\int_{0}^{T_{1x}} y f(x,y)\,dx\,dy \\ -\int_{T_{1y}}^{15}\int_{0}^{qax} y f(x,y)\,dx\,dy - \int_{15}^{40}\int_{0}^{qpx} y f(x,y)\,dx\,dy - \int_{40}^{T_{3y}}\int_{0}^{T_{3x}} y f(x,y)\,dx\,dy \\ -\int_{T_{3y}}^{l}\int_{0}^{fx} y f(x,y)\,dx\,dy - \int_{40}^{T_{3y}}\int_{T_{3x}}^{pox} y f(x,y)\,dx\,dy \end{array}\right]$$

Application 3 of the tetrahedral compressive stress regime beneath the circumscribing rectangular border of proprietory shaped paver 1 shown in Figure 7.3 can be calculated by using Tables 5.1 and 7.1 and the surface function of the tetrahedral compressive stress through the three points σ_A, **l** and **t**.

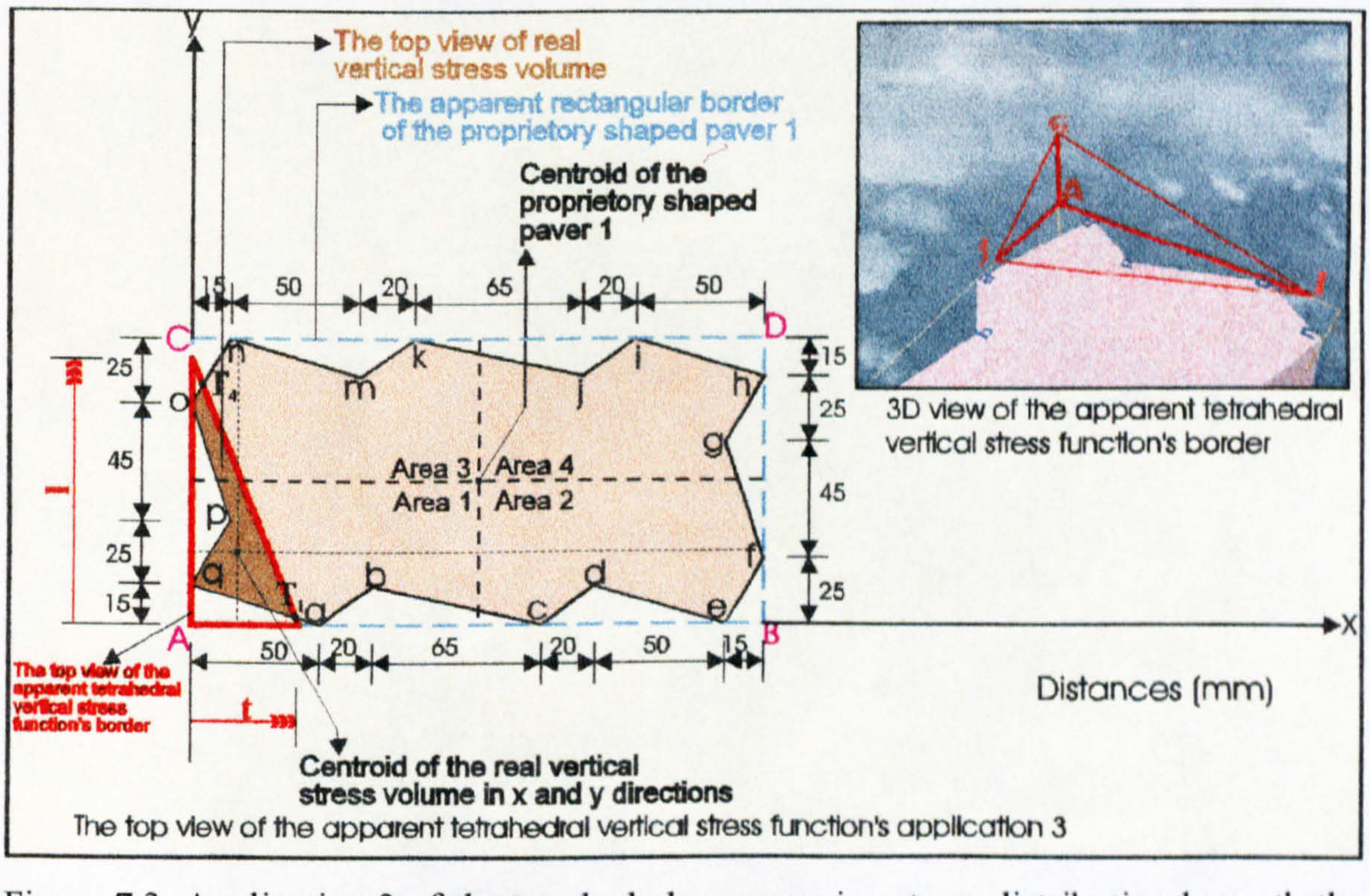

Figure 7.3: Application 3 of the tetrahedral compressive stress distribution beneath the circumscribing rectangular border of proprietory shaped paver 1.

The total volume **V** beneath the surface $f(x,y) = z\ (> 0)$ and above the region in the xy-plane (see Figure 7.3) is:

$$V = \int_0^t \int_0^{fy} f(x,y)\,dy\,dx - \int_{T_{1x}}^t \int_0^{fy} f(x,y)\,dy\,dx - \int_0^{T_{1x}} \int_0^{T_{1y}} f(x,y)\,dy\,dx - \int_0^{T_{1x}} \int_{T_{1y}}^{qay} f(x,y)\,dy\,dx$$

$$- \int_0^{15qpy} \int_{15}^{qpy} f(x,y)\,dy\,dx - \int_0^{15poy} \int_{40}^{poy} f(x,y)\,dy\,dx - \int_0^{T_{4x}} \int_{85}^{ony} f(x,y)\,dy\,dx - \int_0^{T_{4x}} \int_{T_{4y}}^{fy} f(x,y)\,dy\,dx$$

and the centroids of this volume in the xy-plane are at distances $\overline{X}$ and $\overline{Y}$ from the axes (see Figure 7.3) which are given by the following equations.

$$\overline{X} = \frac{1}{V}\left[\int_0^t \int_0^{fy} x f(x,y)\,dy\,dx - \int_{T_{1x}}^t \int_0^{fy} x f(x,y)\,dy\,dx - \int_0^{T_{1x}} \int_0^{T_{1y}} x f(x,y)\,dy\,dx\right.$$

$$- \int_0^{T_{1x}} \int_{T_{1y}}^{qay} x f(x,y)\,dy\,dx - \int_0^{15qpy} \int_{15}^{qpy} x f(x,y)\,dy\,dx - \int_0^{15poy} \int_{40}^{poy} x f(x,y)\,dy\,dx$$

$$\left. - \int_0^{T_{4x}} \int_{85}^{ony} x f(x,y)\,dy\,dx - \int_0^{T_{4x}} \int_{T_{4y}}^{fy} x f(x,y)\,dy\,dx\right]$$

$$\overline{Y} = \frac{1}{V}\left[\int_0^l \int_0^{fx} y f(x,y)\,dx\,dy - \int_0^{T_{1y}} \int_{T_{1x}}^{fx} y f(x,y)\,dx\,dy - \int_0^{T_{1y}} \int_0^{T_{1x}} y f(x,y)\,dx\,dy\right.$$

$$- \int_{T_{1y}}^{15} \int_0^{qax} y f(x,y)\,dx\,dy - \int_{15}^{40qpx} \int_0^{qpx} y f(x,y)\,dx\,dy - \int_{40}^{85pox} \int_0^{pox} y f(x,y)\,dx\,dy$$

$$\left. - \int_{85}^{T_{4y}} \int_0^{onx} y f(x,y)\,dx\,dy - \int_{T_{4y}}^l \int_0^{fx} y f(x,y)\,dx\,dy\right]$$

Application 4 of the tetrahedral compressive stress regime beneath the circumscribing rectangular border of proprietory shaped paver 1 shown in Figure 7.4 can be calculated by using Tables 5.1 and 7.1 and the surface function of the tetrahedral compressive stress through the three points σ_A, l and t.

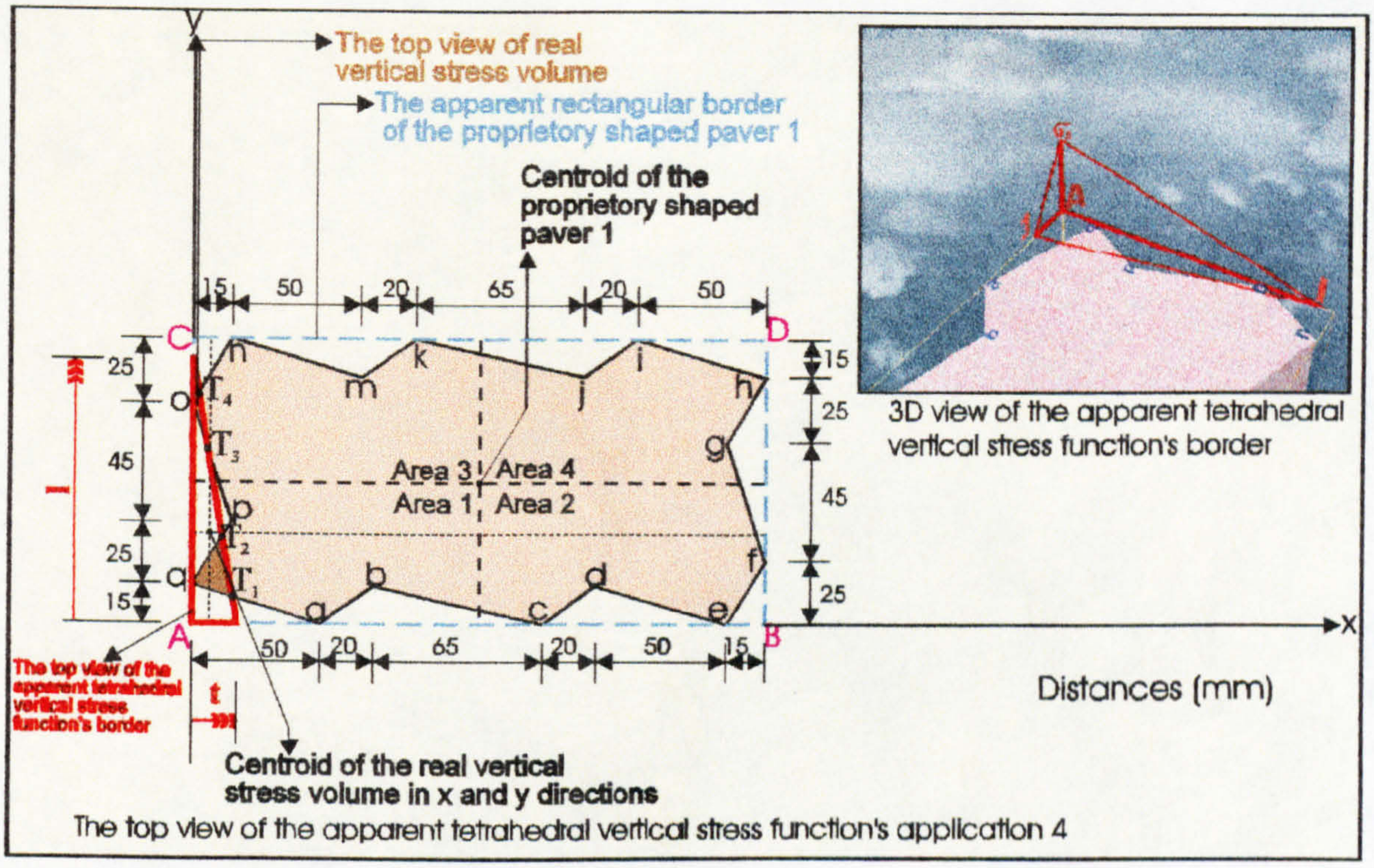

Figure 7.4: Application 4 of the tetrahedral compressive stress distribution beneath the circumscribing rectangular border of proprietory shaped paver 1.

The total volume **V** beneath the surface $f(x,y) = z\ (> 0)$ and above the region in the xy-plane (see Figure 7.4) is:

$$V = \int_0^t \int_0^{fy} f(x,y)\,dy\,dx - \int_{T_{1x}}^t \int_0^{fy} f(x,y)\,dy\,dx - \int_0^{T_{1x}} \int_0^{T_{1y}} f(x,y)\,dy\,dx - \int_0^{T_{1x}} \int_{T_{1y}}^{qay} f(x,y)\,dy\,dx$$

$$- \int_0^{T_{2x}} \int_{15}^{qpy} f(x,y)\,dy\,dx - \int_{T_{3x}}^{T_{2x}} \int_{T_{2y}}^{fy} f(x,y)\,dy\,dx - \int_{T_{4x}}^{T_{3x}} \int_{T_{3y}}^{poy} f(x,y)\,dy\,dx - \int_0^{T_{3x}} \int_{T_{2y}}^{T_{3y}} f(x,y)\,dy\,dx$$

$$- \int_0^{T_{3x}} \int_{T_{3y}}^{poy} f(x,y)\,dy\,dx - \int_0^{T_{4x}} \int_{85}^{ony} f(x,y)\,dy\,dx - \int_0^{T_{4x}} \int_{T_{4y}}^{fy} f(x,y)\,dy\,dx$$

and the centroids of this volume in the xy-plane are at distances $\overline{X}$ and $\overline{Y}$ from the axes (see Figure 7.4) which are given by the following equations.

$$\overline{X} = \frac{1}{V}\left[\begin{array}{l}
\int_0^t \int_0^{fy} x f(x,y)\,dy\,dx - \int_{T_{1x}}^t \int_0^{fy} x f(x,y)\,dy\,dx - \int_0^{T_{1x}} \int_0^{T_{1y}} x f(x,y)\,dy\,dx \\
- \int_0^{T_{1x}} \int_{T_{1y}}^{qay} x f(x,y)\,dy\,dx - \int_0^{T_{2x}} \int_{15}^{qpy} x f(x,y)\,dy\,dx - \int_{T_{3x}}^{T_{2x}} \int_{T_{2y}}^{fy} x f(x,y)\,dy\,dx \\
- \int_{T_{4x}}^{T_{3x}} \int_{T_{3y}}^{poy} x f(x,y)\,dy\,dx - \int_0^{T_{3x}} \int_{T_{2y}}^{T_{3y}} x f(x,y)\,dy\,dx - \int_0^{T_{3x}} \int_{T_{3y}}^{poy} x f(x,y)\,dy\,dx \\
- \int_{T_{4x}}^{T_{4x}} \int_{85}^{ony} x f(x,y)\,dy\,dx - \int_0^{T_{4x}} \int_{T_{4y}}^{fy} x f(x,y)\,dy\,dx
\end{array}\right]$$

$$\overline{Y} = \frac{1}{V}\left[\begin{array}{l}
\int_0^l \int_0^{fx} y f(x,y)\,dx\,dy - \int_0^{T_{1y}} \int_{T_{1x}}^{fx} y f(x,y)\,dx\,dy - \int_0^{T_{1y}} \int_0^{T_{1x}} y f(x,y)\,dx\,dy \\
- \int_{T_{1y}}^{15} \int_0^{qax} y f(x,y)\,dx\,dy - \int_{15}^{T_{2y}} \int_0^{qpx} y f(x,y)\,dx\,dy - \int_{T_{2y}}^{T_{3y}} \int_{T_{3x}}^{fx} y f(x,y)\,dx\,dy \\
- \int_{T_{2y}}^{T_{3y}} \int_0^{T_{3x}} y f(x,y)\,dx\,dy - \int_{T_{3y}}^{85} \int_0^{fx} y f(x,y)\,dx\,dy - \int_{85}^{T_{4y}} \int_0^{onx} y f(x,y)\,dx\,dy \\
- \int_{T_{3y}}^{T_{4y}} \int_{T_{4x}}^{pox} y f(x,y)\,dx\,dy - \int_{T_{4y}}^{l} \int_0^{fx} y f(x,y)\,dx\,dy
\end{array}\right]$$

Application 5 of the tetrahedral compressive stress regime beneath the circumscribing rectangular border of proprietory shaped paver 1 shown in Figure 7.5 can be calculated by using Tables 5.1 and 7.1 and the surface function of the tetrahedral compressive stress through the three points σ_A, **l** and **t**.

The total volume **V** beneath the surface $f(x,y) = z\ (> 0)$ and above the region in the xy-plane (see Figure 7.5) is:

$$V = \int_0^t \int_0^{fy} f(x,y)\,dy\,dx - \int_{T_{1x}}^{50} \int_0^{qay} f(x,y)\,dy\,dx - \int_0^{T_{1x}} \int_0^{T_{1y}} f(x,y)\,dy\,dx - \int_0^{T_{1x}} \int_{T_{1y}}^{fy} f(x,y)\,dy\,dx$$

$$- \int_{50}^{T_{16x}} \int_0^{aby} f(x,y)\,dy\,dx - \int_{T_{16x}}^{t} \int_0^{fy} f(x,y)\,dy\,dx$$

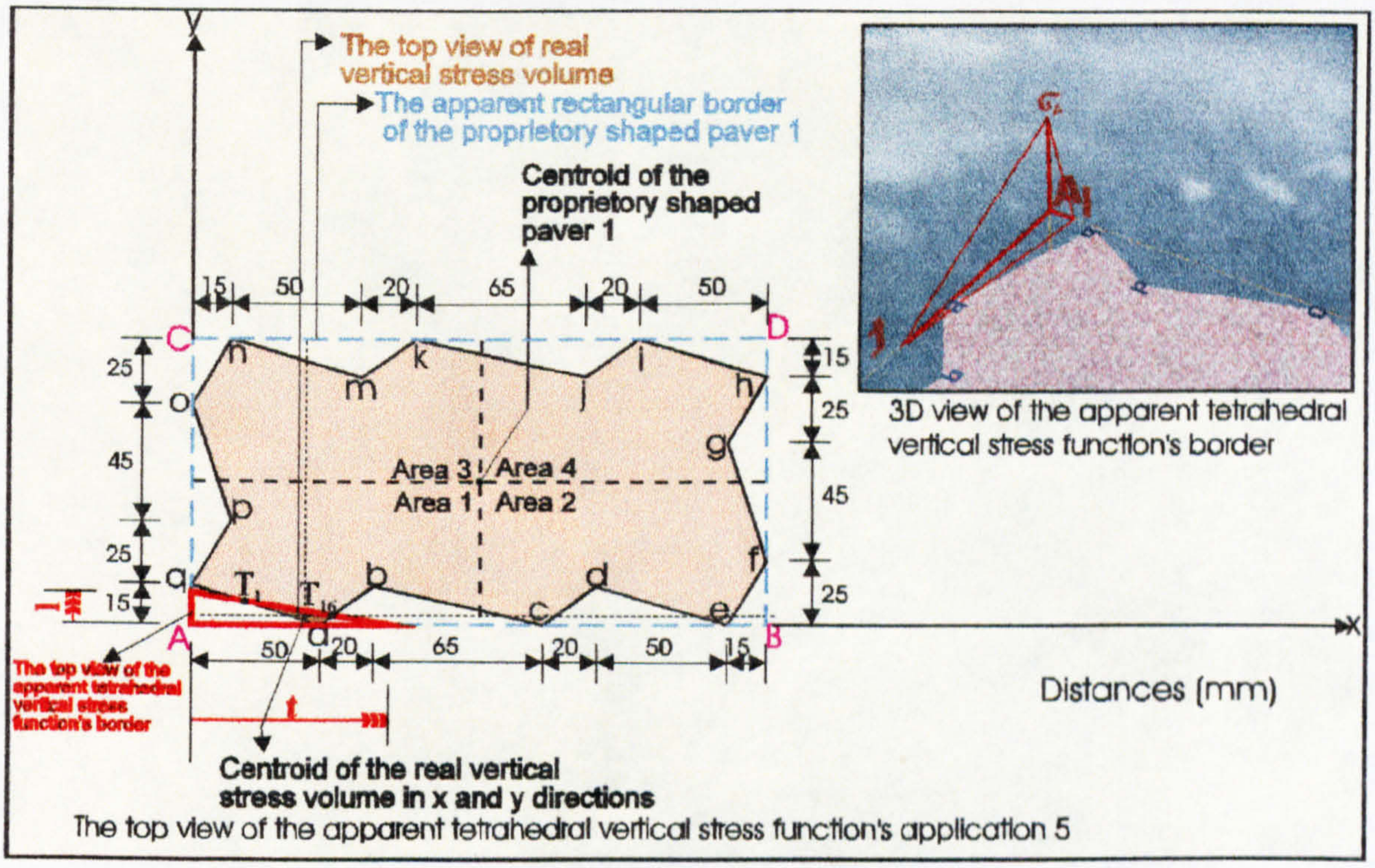

Figure 7.5: Application 5 of the tetrahedral compressive stress distribution beneath the circumscribing rectangular border of proprietory shaped paver 1.

and the centroids of this volume in the xy-plane are at distances $\overline{X}$ and $\overline{Y}$ from the axes (see Figure 7.5) which are given by the following equations.

$$\overline{X} = \frac{1}{V}\left[\int_0^t \int_0^{fy} x f(x,y)\,dy\,dx - \int_{T_{1x}}^{50} \int_0^{qay} x f(x,y)\,dy\,dx - \int_0^{T_{1x}} \int_0^{T_{1y}} x f(x,y)\,dy\,dx\right.$$
$$\left. - \int_0^{T_{1x}} \int_{T_{1y}}^{fy} x f(x,y)\,dy\,dx - \int_{50}^{T_{16x}} \int_0^{aby} x f(x,y)\,dy\,dx - \int_{T_{16x}}^{t} \int_0^{fy} x f(x,y)\,dy\,dx\right]$$

$$\overline{Y} = \frac{1}{V}\left[\begin{array}{l} \int_0^l \int_0^{fx} y f(x,y)\,dx\,dy - \int_0^{T_{1y}} \int_{T_{1x}}^{qax} y f(x,y)\,dx\,dy - \int_0^{T_{1y}} \int_0^{T_{1x}} y f(x,y)\,dx\,dy \\ -\int_{T_{1y}}^{l} \int_0^{fx} y f(x,y)\,dx\,dy - \int_0^{T_{16y}} \int_{50}^{abx} y f(x,y)\,dx\,dy - \int_0^{T_{16y}} \int_{T_{16x}}^{fx} y f(x,y)\,dx\,dy \end{array}\right]$$

Application 6 of the tetrahedral compressive stress regime beneath the circumscribing rectangular border of proprietory shaped paver 1 shown in Figure 7.6 can be calculated by using Tables 5.1 and 7.1 and the surface function of the tetrahedral compressive stress through the three points σ_A, **l** and **t**.

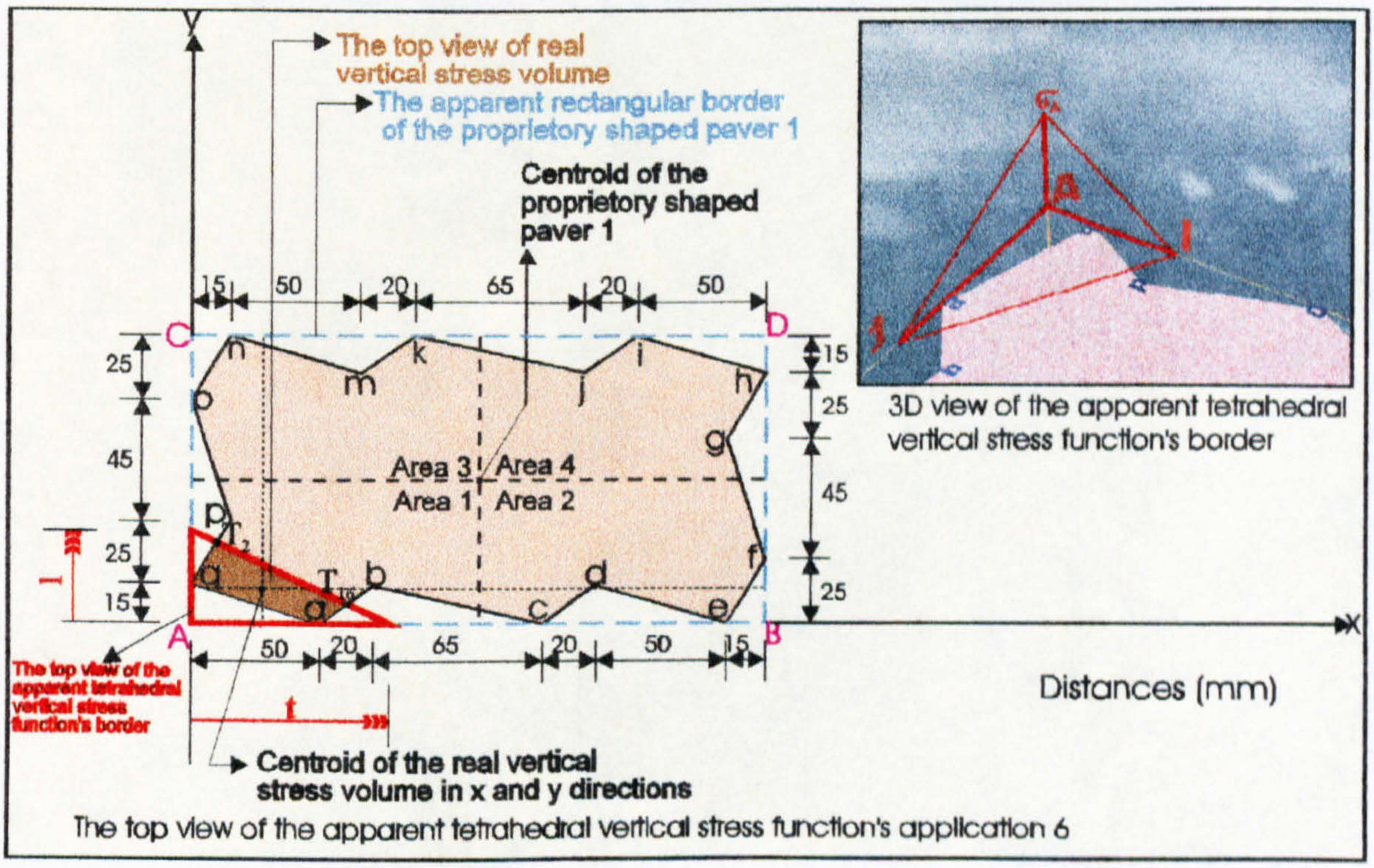

Figure 7.6: Application 6 of the tetrahedral compressive stress distribution beneath the circumscribing rectangular border of proprietory shaped paver 1.

The total volume **V** beneath the surface $f(x,y) = z\ (> 0)$ and above the region in the xy-plane (see Figure 7.6) is:

$$V = \int_0^t \int_0^{fy} f(x,y)\,dy\,dx - \int_{T_{16x}}^t \int_0^{fy} f(x,y)\,dy\,dx - \int_{50}^{T_{16x}} \int_0^{aby} f(x,y)\,dy\,dx - \int_0^{50} \int_0^{qay} f(x,y)\,dy\,dx$$

$$- \int_0^{T_{2x}} \int_{15}^{qpy} f(x,y)\,dy\,dx - \int_0^{T_{2x}} \int_{T_{2y}}^{fy} f(x,y)\,dy\,dx$$

and the centroids of this volume in the xy-plane are at distances $\overline{X}$ and $\overline{Y}$ from the axes (see Figure 7.6) which are given by the following equations.

$$\overline{X} = \frac{1}{V}\left[\int_0^t \int_0^{fy} x f(x,y)\,dy\,dx - \int_{T_{16x}}^t \int_0^{fy} x f(x,y)\,dy\,dx - \int_{50}^{T_{16x}} \int_0^{aby} x f(x,y)\,dy\,dx \right.$$
$$\left. - \int_0^{50} \int_0^{qay} x f(x,y)\,dy\,dx - \int_0^{T_{2x}} \int_{15}^{qpy} x f(x,y)\,dy\,dx - \int_0^{T_{2x}} \int_{T_{2y}}^{fy} x f(x,y)\,dy\,dx\right]$$

$$\overline{Y} = \frac{1}{V}\left[\int_0^l \int_0^{fx} y f(x,y)\,dx\,dy - \int_0^{T_{16y}} \int_{T_{16x}}^{fx} y f(x,y)\,dx\,dy - \int_0^{T_{16y}} \int_{50}^{abx} y f(x,y)\,dx\,dy \right.$$
$$\left. - \int_0^{15} \int_0^{qax} y f(x,y)\,dx\,dy - \int_0^{T_{2y}} \int_{15}^{qpx} y f(x,y)\,dx\,dy - \int_{T_{2y}}^{l} \int_0^{fx} y f(x,y)\,dx\,dy\right]$$

Application 7 of the tetrahedral compressive stress regime beneath the circumscribing rectangular border of proprietory shaped paver 1 shown in Figure 7.7 can be calculated by using Tables 5.1 and 7.1 and the surface function of the tetrahedral compressive stress through the three points σ_A, **l** and **t**.

The total volume **V** beneath the surface $f(x,y) = z\ (> 0)$ and above the region in the xy-plane (see Figure 7.7) is:

$$V = \int_0^t \int_0^{fy} f(x,y)\,dy\,dx - \int_{T_{16x}}^t \int_0^{fy} f(x,y)\,dy\,dx - \int_{50}^{T_{16x}} \int_0^{aby} f(x,y)\,dy\,dx - \int_0^{50} \int_0^{qay} f(x,y)\,dy\,dx$$

$$- \int_0^{15} \int_0^{qpy} f(x,y)\,dy\,dx - \int_0^{T_{3x}} \int_{15}^{T_{3y}} f(x,y)\,dy\,dx - \int_{T_{3x}}^{15} \int_{40}^{poy} f(x,y)\,dy\,dx - \int_0^{T_{3x}} \int_{T_{3y}}^{fy} f(x,y)\,dy\,dx$$

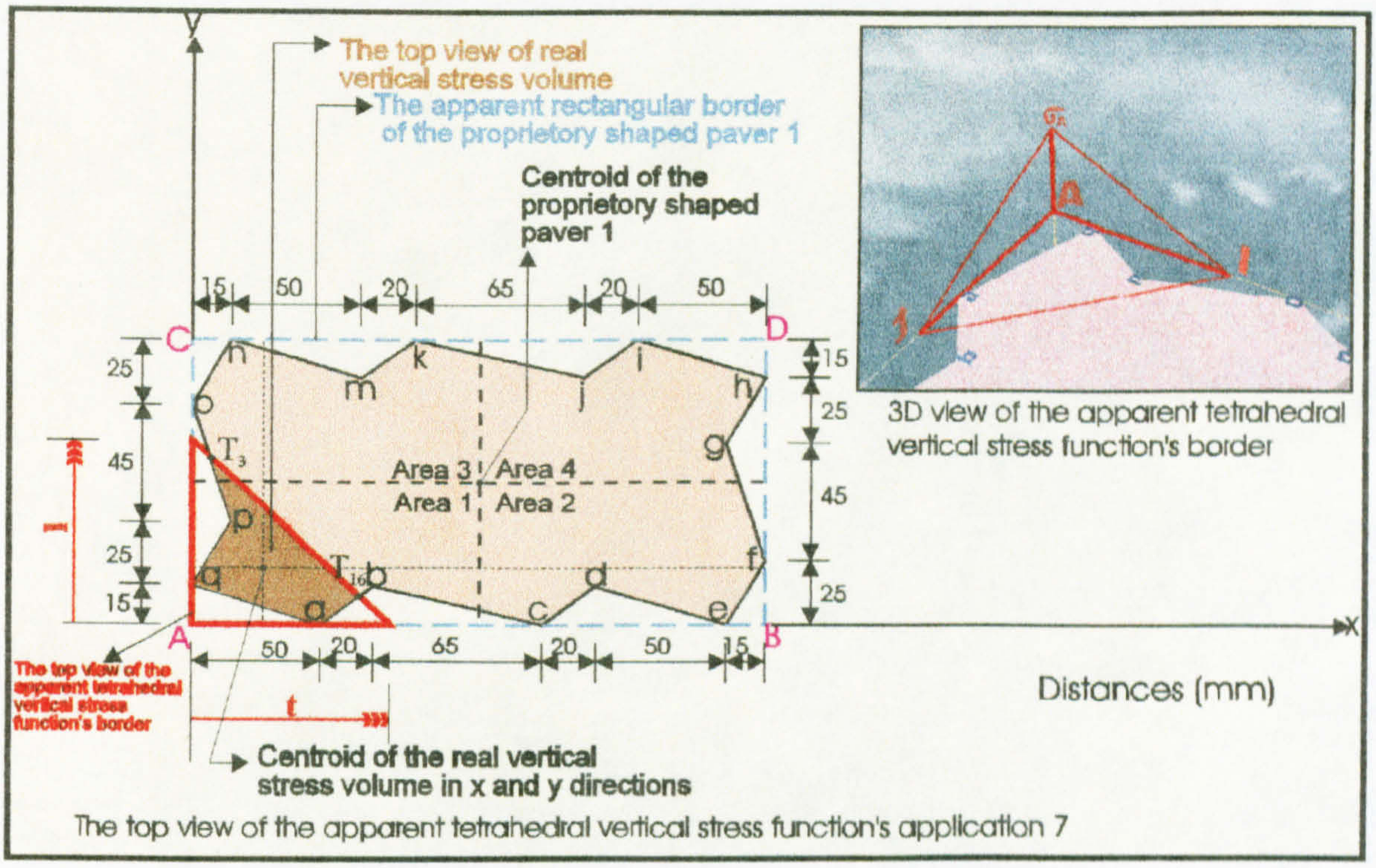

Figure 7.7: Application 7 of the tetrahedral compressive stress distribution beneath the circumscribing rectangular border of proprietory shaped paver 1.

and the centroids of this volume in the xy-plane are at distances $\overline{X}$ and $\overline{Y}$ from the axes (see Figure 7.7) which are given by the following equations.

$$\overline{X} = \frac{1}{V}\left[\int_0^t \int_0^{fy} x\,f(x,y)\,dy\,dx - \int_{T_{16x}}^t \int_0^{fy} x\,f(x,y)\,dy\,dx - \int_{50}^{T_{16x}} \int_0^{aby} x\,f(x,y)\,dy\,dx - \int_0^{50} \int_0^{qay} x\,f(x,y)\,dy\,dx\right.$$
$$\left. - \int_0^{15} \int_0^{qpy} x\,f(x,y)\,dy\,dx - \int_0^{T_{3x}} \int_{15}^{T_{3y}} x\,f(x,y)\,dy\,dx - \int_{T_{3x}}^{15} \int_{40}^{poy} x\,f(x,y)\,dy\,dx - \int_0^{T_{3x}} \int_{T_{3y}}^{fy} x\,f(x,y)\,dy\,dx\right]$$

$$\overline{Y} = \frac{1}{V}\left[\begin{array}{l} \int_0^l \int_0^{fx} y f(x,y)\,dx\,dy - \int_0^{T_{16y}} \int_{T_{16x}}^{fx} y f(x,y)\,dx\,dy - \int_0^{T_{16y}} \int_{50}^{abx} y f(x,y)\,dx\,dy \\ -\int_0^{15} \int_0^{qax} y f(x,y)\,dx\,dy - \int_{15}^{40} \int_0^{qpx} y f(x,y)\,dx\,dy - \int_{40}^{T_{3y}} \int_0^{T_{3x}} y f(x,y)\,dx\,dy \\ -\int_{40}^{T_{3y}} \int_{T_{3x}}^{pox} y f(x,y)\,dx\,dy - \int_{T_{3y}}^{l} \int_0^{fx} y f(x,y)\,dx\,dy \end{array}\right]$$

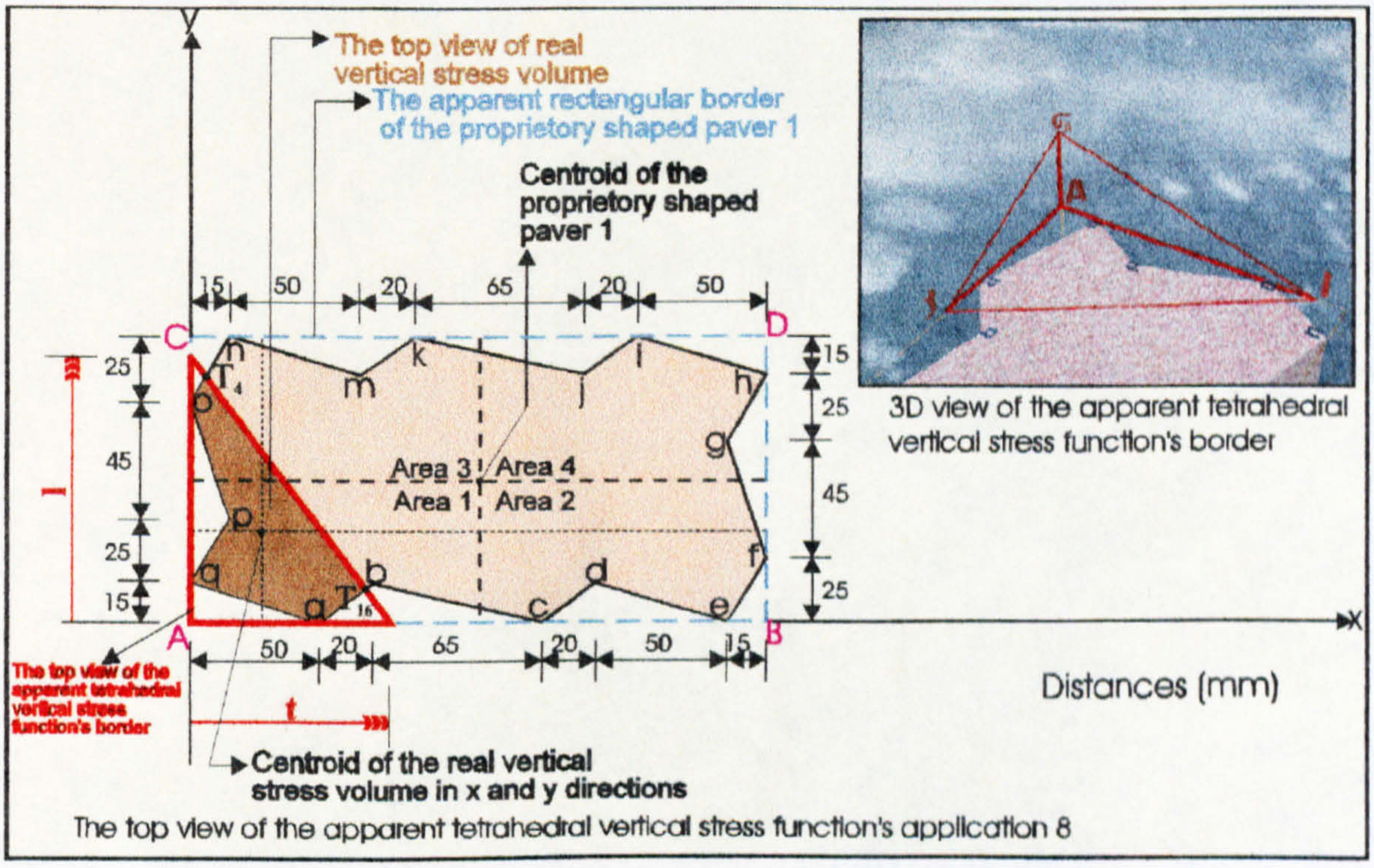

Figure 7.8: Application 8 of the tetrahedral compressive stress distribution beneath the circumscribing rectangular border of proprietory shaped paver 1.

Application 8 of the tetrahedral compressive stress regime beneath the circumscribing rectangular border of proprietory shaped paver 1 shown in Figure 7.8 can be calculated by using Tables 5.1 and 7.1 and the surface function of the tetrahedral compressive stress through the three points σ_A, **l** and **t**.

The total volume **V** beneath the surface $f(x,y) = z\ (> 0)$ and above the region in the xy-plane (see Figure 7.8) is:

$$V = \int_0^t \int_0^{fy} f(x,y)\,dy\,dx - \int_{T_{16x}}^t \int_0^{fy} f(x,y)\,dy\,dx - \int_{50}^{T_{16x}} \int_0^{aby} f(x,y)\,dy\,dx - \int_0^{50} \int_0^{qay} f(x,y)\,dy\,dx$$

$$- \int_0^{15} \int_0^{qpy} f(x,y)\,dy\,dx - \int_0^{15} \int_0^{poy} f(x,y)\,dy\,dx - \int_0^{T_{4x}} \int_{85}^{ony} f(x,y)\,dy\,dx - \int_0^{T_{4x}} \int_{T_{4y}}^{fy} f(x,y)\,dy\,dx$$

and the centroids of this volume in the xy-plane are at distances $\overline{X}$ and $\overline{Y}$ from the axes (see Figure 7.8) which are given by the following equations.

$$\overline{X} = \frac{1}{V}\left[\int_0^t \int_0^{fy} x f(x,y)\,dy\,dx - \int_{T_{16x}}^t \int_0^{fy} x f(x,y)\,dy\,dx - \int_{50}^{T_{16x}} \int_0^{aby} x f(x,y)\,dy\,dx \right.$$
$$- \int_0^{50} \int_0^{qay} x f(x,y)\,dy\,dx - \int_0^{15} \int_{15}^{qpy} x f(x,y)\,dy\,dx - \int_0^{15} \int_{40}^{poy} x f(x,y)\,dy\,dx$$
$$\left. - \int_0^{T_{4x}} \int_{85}^{ony} x f(x,y)\,dy\,dx - \int_0^{T_{4x}} \int_{T_{4y}}^{fy} x f(x,y)\,dy\,dx \right]$$

$$\overline{Y} = \frac{1}{V}\left[\int_0^l \int_0^{fx} y f(x,y)\,dx\,dy - \int_0^{T_{16y}} \int_{T_{16x}}^{fx} y f(x,y)\,dx\,dy - \int_0^{T_{16y}} \int_{50}^{abx} y f(x,y)\,dx\,dy \right.$$
$$- \int_0^{15} \int_0^{qax} y f(x,y)\,dx\,dy - \int_{15}^{40} \int_0^{qpx} y f(x,y)\,dx\,dy - \int_{40}^{85} \int_0^{pox} y f(x,y)\,dx\,dy$$
$$\left. - \int_{85}^{T_{4y}} \int_0^{onx} y f(x,y)\,dx\,dy - \int_{T_{4y}}^{l} \int_0^{fx} y f(x,y)\,dx\,dy \right]$$

Application 9 of the tetrahedral compressive stress regime beneath the circumscribing rectangular border of proprietory shaped paver 1 shown in Figure 7.9 can be calculated by using Tables 5.1 and 7.1 and the surface function of the tetrahedral compressive stress through the three points σ_A, **l** and **t**.

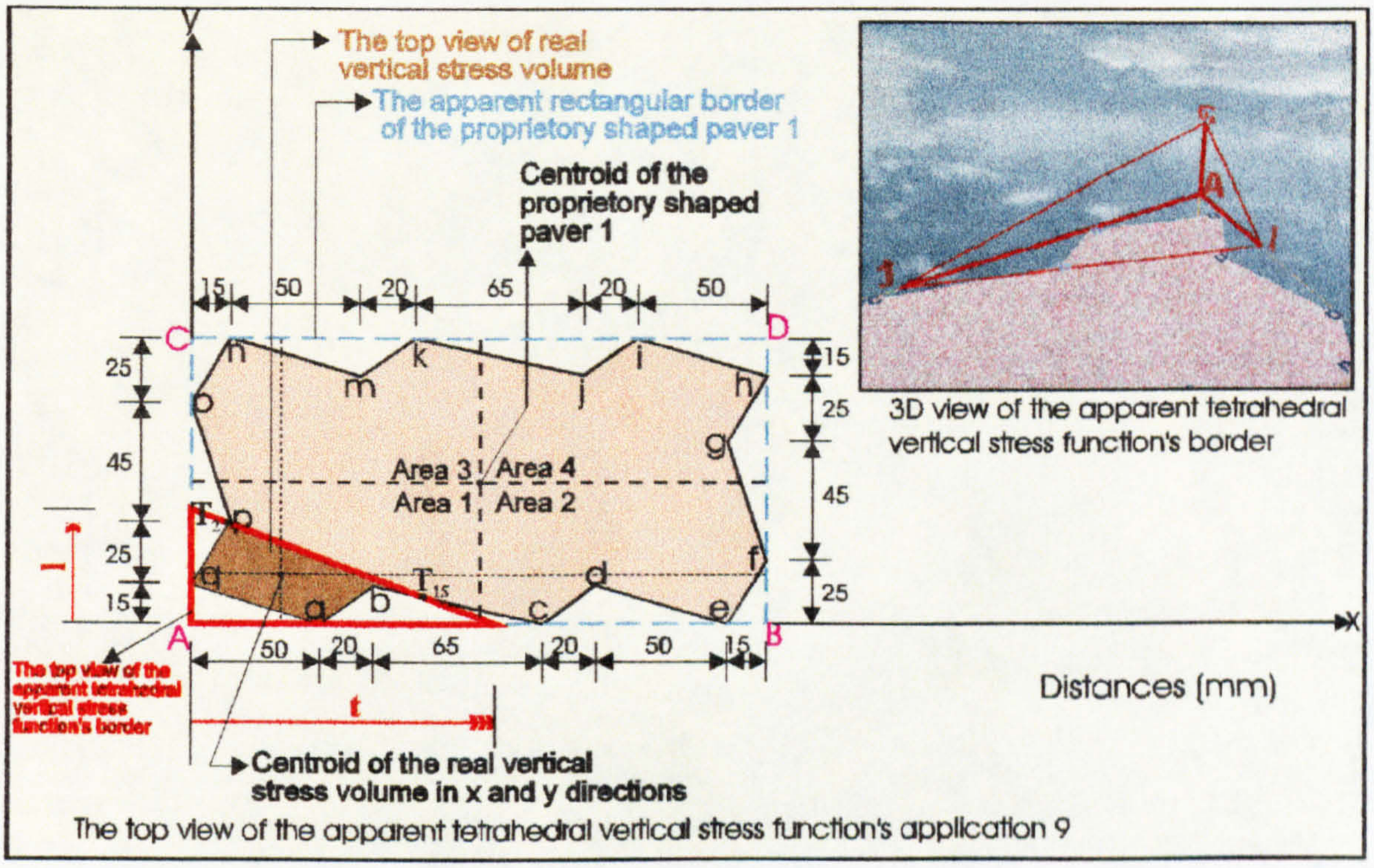

Figure 7.9: Application 9 of the tetrahedral compressive stress distribution beneath the circumscribing rectangular border of proprietory shaped paver 1.

The total volume **V** beneath the surface $f(x,y) = z\ (> 0)$ and above the region in the xy-plane (see Figure 7.9) is:

$$V = \int_0^t \int_0^{fy} f(x,y)\,dy\,dx - \int_{T_{15x}}^t \int_0^{fy} f(x,y)\,dy\,dx - \int_{70}^{T_{15x}} \int_{T_{15y}}^{bcy} f(x,y)\,dy\,dx - \int_{70}^{T_{15x}} \int_0^{T_{15y}} f(x,y)\,dy\,dx$$

$$- \int_{50}^{70} \int_{15}^{aby} f(x,y)\,dy\,dx - \int_0^{50} \int_{40}^{qay} f(x,y)\,dy\,dx - \int_0^{T_{2x}} \int_{T_{2y}}^{fy} f(x,y)\,dy\,dx - \int_0^{T_{2x}} \int_{15}^{qpy} f(x,y)\,dy\,dx$$

and the centroids of this volume in the xy-plane are at distances $\overline{X}$ and $\overline{Y}$ from the axes (see Figure 7.9) which are given by the following equations.

$$\overline{X} = \frac{1}{V}\left[\int_0^t \int_0^{fy} x f(x,y)\,dy\,dx - \int_{T_{15x}}^t \int_0^{fy} x f(x,y)\,dy\,dx - \int_{70}^{T_{15x}} \int_{T_{15y}}^{bcy} x f(x,y)\,dy\,dx\right.$$

$$-\int_{70}^{T_{15x}}\int_{0}^{T_{15y}} xf(x,y)\,dy\,dx-\int_{50}^{70}\int_{15}^{aby} xf(x,y)\,dy\,dx-\int_{0}^{50}\int_{40}^{qay} xf(x,y)\,dy\,dx$$
$$\left.-\int_{0}^{T_{2x}}\int_{T_{2y}}^{fy} xf(x,y)\,dy\,dx-\int_{0}^{T_{2x}}\int_{15}^{qpy} xf(x,y)\,dy\,dx\right]$$

$$\overline{Y}=\frac{1}{V}\left[\begin{array}{l}\displaystyle\int_{0}^{l}\int_{0}^{fx} yf(x,y)\,dx\,dy-\int_{0}^{T_{15y}}\int_{T_{15x}}^{fx} yf(x,y)\,dx\,dy-\int_{0}^{T_{15y}}\int_{70}^{T_{15x}} yf(x,y)\,dx\,dy\\ \displaystyle-\int_{T_{15y}}^{15}\int_{70}^{bcx} yf(x,y)\,dx\,dy-\int_{0}^{15}\int_{50}^{abx} yf(x,y)\,dx\,dy-\int_{0}^{15}\int_{0}^{qax} yf(x,y)\,dx\,dy\\ \displaystyle-\int_{15}^{T_{2y}}\int_{0}^{qpx} yf(x,y)\,dx\,dy-\int_{T_{2y}}^{l}\int_{0}^{fx} yf(x,y)\,dx\,dy\end{array}\right]$$

Application 10 of the tetrahedral compressive stress regime beneath the circumscribing rectangular border of proprietory shaped paver 1 shown in Figure 7.10 can be calculated by using Tables 5.1 and 7.1 and the surface function of the tetrahedral compressive stress through the three points σ_A, **l** and **t**.

The total volume **V** beneath the surface $f(x,y)=z\ (>0)$ and above the region in the xy-plane (see Figure 7.10) is:

$$V=\int_{0}^{t}\int_{0}^{fy} f(x,y)\,dy\,dx-\int_{T_{15x}}^{t}\int_{0}^{fy} f(x,y)\,dy\,dx-\int_{70}^{T_{15x}}\int_{T_{15y}}^{bcy} f(x,y)\,dy\,dx-\int_{70}^{T_{15x}}\int_{0}^{T_{15y}} f(x,y)\,dy\,dx$$
$$-\int_{50}^{70}\int_{15}^{aby} f(x,y)\,dy\,dx-\int_{0}^{50}\int_{40}^{qay} f(x,y)\,dy\,dx-\int_{0}^{15}\int_{15}^{qpy} f(x,y)\,dy\,dx-\int_{0}^{T_{3x}}\int_{40}^{T_{3y}} f(x,y)\,dy\,dx$$
$$-\int_{T_{3x}}^{15}\int_{40}^{poy} f(x,y)\,dy\,dx-\int_{0}^{T_{3x}}\int_{T_{3y}}^{fy} f(x,y)\,dy\,dx$$

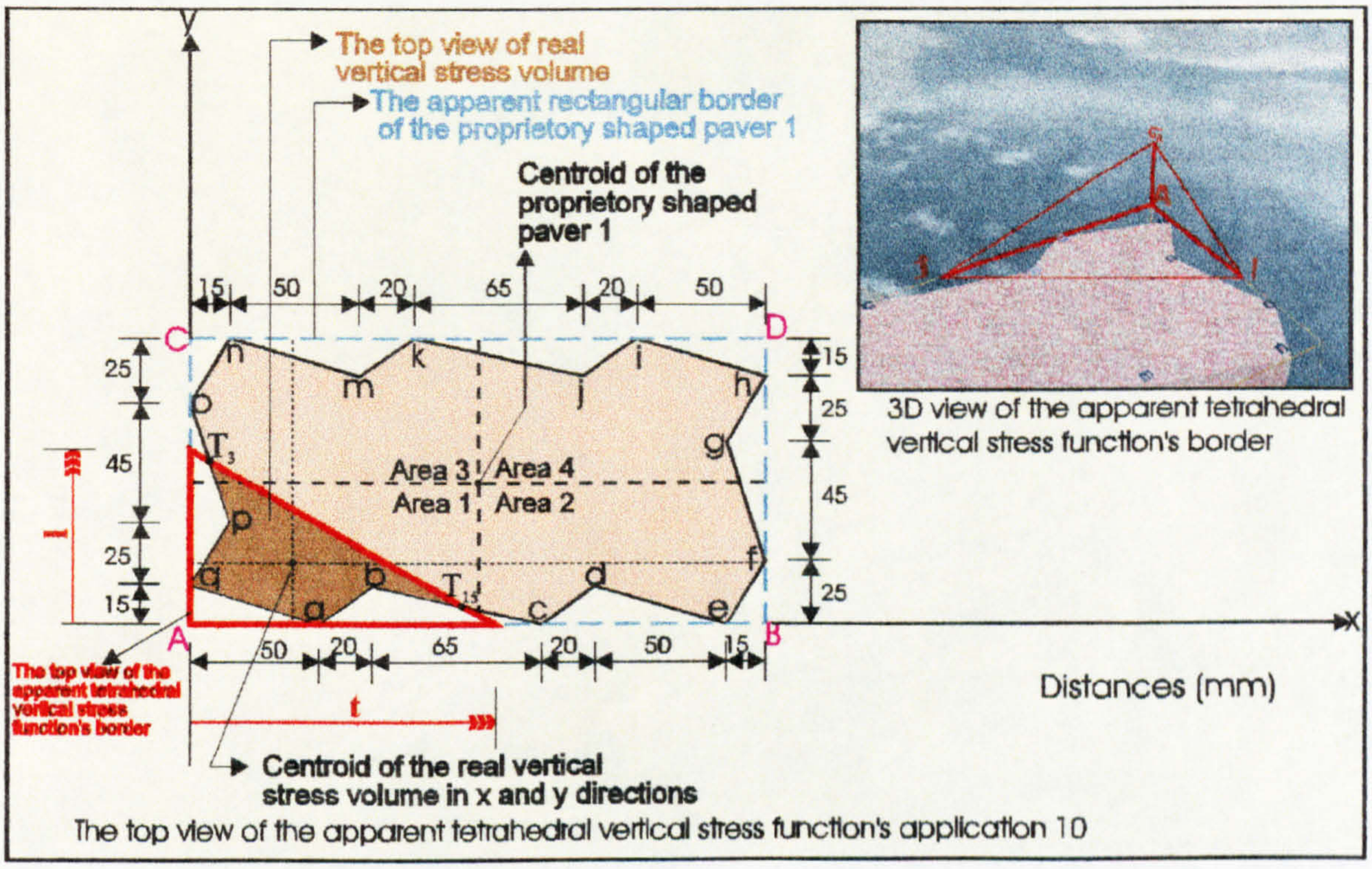

Figure 7.10: Application 10 of the tetrahedral compressive stress distribution beneath the circumscribing rectangular border of proprietory shaped paver 1.

and the centroids of this volume in the xy-plane are at distances $\overline{X}$ and $\overline{Y}$ from the axes (see Figure 7.10) which are given by the following equations.

$$\overline{X} = \frac{1}{V}\left[\begin{array}{l}
\int_0^t \int_0^{fy} x f(x,y)\,dy\,dx - \int_{T_{15x}}^t \int_0^{fy} x f(x,y)\,dy\,dx - \int_{70}^{T_{15x}} \int_{T_{15y}}^{bcy} x f(x,y)\,dy\,dx \\
- \int_{70}^{T_{15x}} \int_0^{T_{15y}} x f(x,y)\,dy\,dx - \int_{50}^{70} \int_{15}^{aby} x f(x,y)\,dy\,dx - \int_0^{50} \int_{40}^{qay} x f(x,y)\,dy\,dx \\
- \int_0^{15} \int_{15}^{qpy} x f(x,y)\,dy\,dx - \int_0^{T_{3x}} \int_{40}^{T_{3y}} x f(x,y)\,dy\,dx - \int_{T_{3x}}^{15} \int_{40}^{poy} x f(x,y)\,dy\,dx \\
- \int_0^{T_{3x}} \int_{T_{3y}}^{fy} x f(x,y)\,dy\,dx
\end{array}\right]$$

$$\overline{Y} = \frac{1}{V}\left[\begin{array}{l}
\int_0^l \int_0^{fx} y f(x,y)\,dx\,dy - \int_0^{T_{15y}} \int_{T_{15x}}^{fx} y f(x,y)\,dx\,dy - \int_0^{T_{15y}} \int_{70}^{T_{15x}} y f(x,y)\,dx\,dy \\
- \int_{T_{15y}}^{15} \int_{70}^{bcx} y f(x,y)\,dx\,dy - \int_0^{15abx} \int_{50} y f(x,y)\,dx\,dy - \int_0^{15qax} \int_0 y f(x,y)\,dx\,dy \\
- \int_{15}^{40qpx} \int_0 y f(x,y)\,dx\,dy - \int_{40}^{T_{3y}} \int_0^{T_{3x}} y f(x,y)\,dx\,dy - \int_{40}^{T_{3y}} \int_{T_{3x}}^{pox} y f(x,y)\,dx\,dy \\
- \int_{T_{3y}}^{l} \int_0^{fx} y f(x,y)\,dx\,dy
\end{array}\right]$$

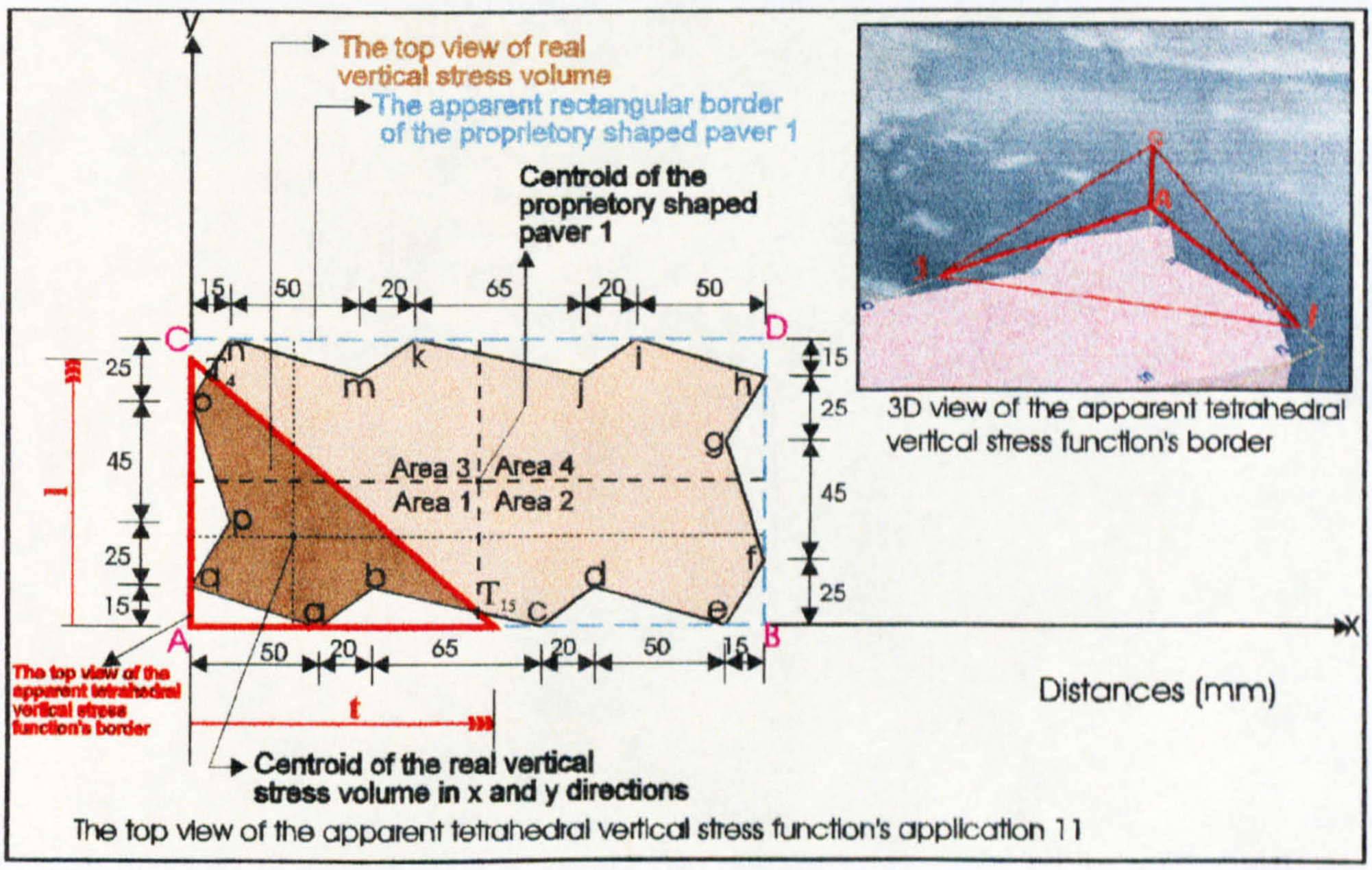

Figure 7.11: Application 11 of the tetrahedral compressive stress distribution beneath the circumscribing rectangular border of proprietory shaped paver 1.

Application 11 of the tetrahedral compressive stress regime beneath the circumscribing rectangular border of proprietory shaped paver 1 shown in Figure 7.11 can be calculated by using Tables 5.1 and 7.1 and the surface function of the tetrahedral compressive stress through the three points σ_A, **l** and **t**.

The total volume **V** beneath the surface $f(x,y) = z\ (> 0)$ and above the region in the xy-plane (see Figure 7.11) is:

$$V = \int_0^t \int_0^{fy} f(x,y)\,dy\,dx - \int_{T_{15x}}^t \int_0^{fy} f(x,y)\,dy\,dx - \int_{70}^{T_{15x}} \int_{T_{15y}}^{bcy} f(x,y)\,dy\,dx - \int_{70}^{T_{15x}} \int_0^{T_{15y}} f(x,y)\,dy\,dx$$
$$- \int_{50}^{70} \int_0^{aby} f(x,y)\,dy\,dx - \int_0^{50} \int_0^{qay} f(x,y)\,dy\,dx - \int_0^{15} \int_{15}^{qpy} f(x,y)\,dy\,dx - \int_0^{15} \int_{40}^{poy} f(x,y)\,dy\,dx$$
$$- \int_0^{T_{4x}} \int_{85}^{ony} f(x,y)\,dy\,dx - \int_0^{T_{4x}} \int_{T_{4y}}^{fy} f(x,y)\,dy\,dx$$

and the centroids of this volume in the xy-plane are at distances $\overline{X}$ and $\overline{Y}$ from the axes (see Figure 7.11) which are given by the following equations.

$$\overline{X} = \frac{1}{V}\left[\int_0^t \int_0^{fy} x f(x,y)\,dy\,dx - \int_{T_{15x}}^t \int_0^{fy} x f(x,y)\,dy\,dx - \int_{70}^{T_{15x}} \int_{T_{15y}}^{bcy} x f(x,y)\,dy\,dx\right.$$
$$- \int_{70}^{T_{15x}} \int_0^{T_{15y}} x f(x,y)\,dy\,dx - \int_{50}^{70} \int_0^{aby} x f(x,y)\,dy\,dx - \int_0^{50} \int_0^{qay} x f(x,y)\,dy\,dx$$
$$- \int_0^{15} \int_{15}^{qpy} x f(x,y)\,dy\,dx - \int_0^{15} \int_{40}^{poy} x f(x,y)\,dy\,dx - \int_0^{T_{4x}} \int_{85}^{ony} x f(x,y)\,dy\,dx$$
$$\left. - \int_0^{T_{4x}} \int_{T_{4y}}^{fy} x f(x,y)\,dy\,dx\right]$$

$$\overline{Y} = \frac{1}{V}\left[\int_0^l \int_0^{fx} y f(x,y)\,dx\,dy - \int_0^{T_{15y}} \int_{T_{15x}}^{fx} y f(x,y)\,dx\,dy - \int_0^{T_{15y}} \int_{70}^{T_{15x}} y f(x,y)\,dx\,dy\right.$$
$$- \int_{T_{15y}}^{15} \int_{70}^{bcx} y f(x,y)\,dx\,dy - \int_0^{15} \int_{50}^{abx} y f(x,y)\,dx\,dy - \int_0^{15} \int_0^{qax} y f(x,y)\,dx\,dy$$

$$-\int_{15}^{40}\int_{0}^{qpx} y f(x,y)\,dx\,dy - \int_{40}^{85}\int_{0}^{pox} y f(x,y)\,dx\,dy - \int_{85}^{T_{4y}}\int_{0}^{onx} y f(x,y)\,dx\,dy$$

$$\left. -\int_{T_{4y}}^{l}\int_{0}^{fx} y f(x,y)\,dx\,dy \right]$$

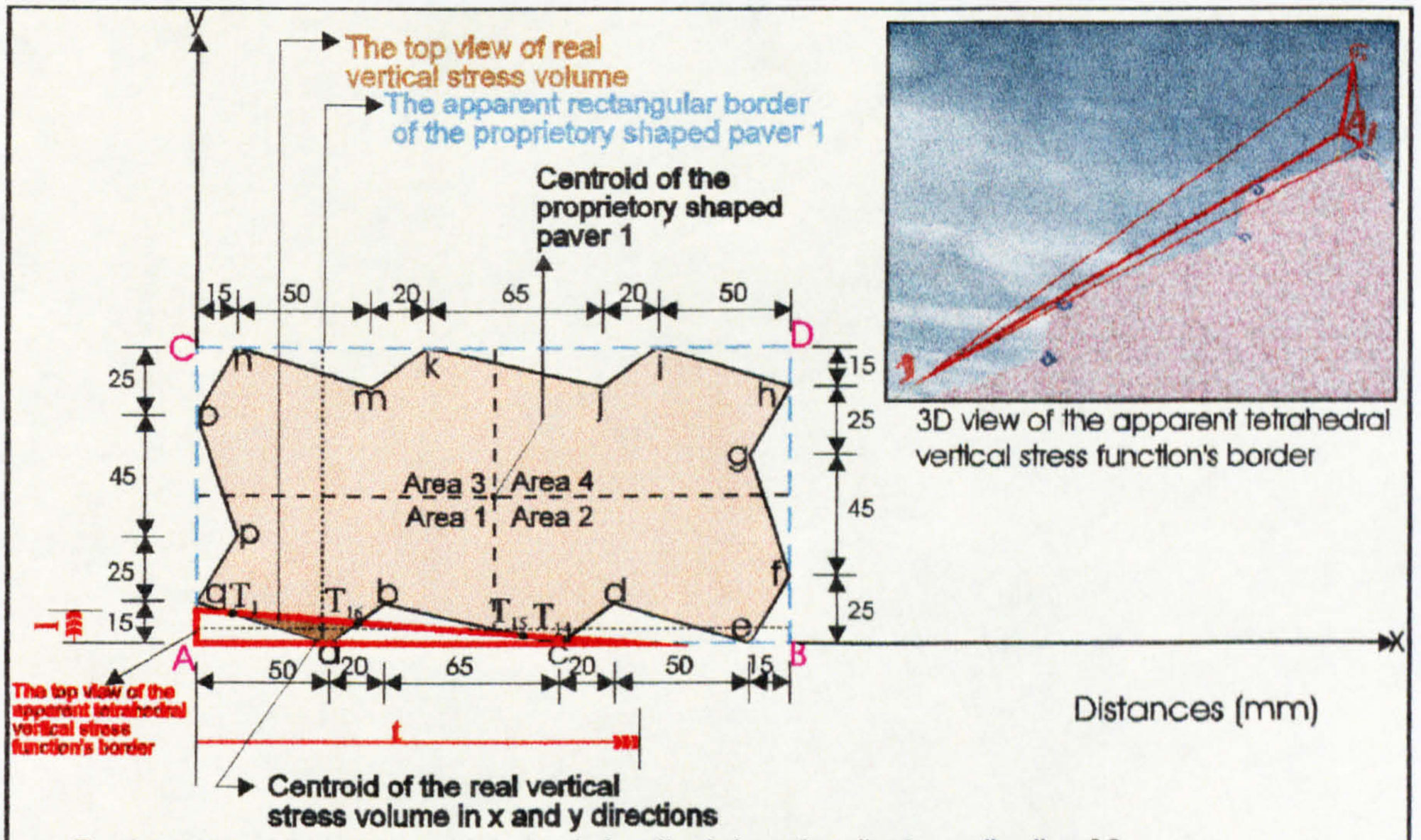

The top view of the apparent tetrahedral vertical stress function's application 12

Figure 7.12: Application 12 of the tetrahedral compressive stress distribution beneath the circumscribing rectangular border of proprietory shaped paver 1.

Application 12 of the tetrahedral compressive stress regime beneath the circumscribing rectangular border of proprietory shaped paver 1 shown in Figure 7.12 can be calculated by using Tables 5.1 and 7.1 and the surface function of the tetrahedral compressive stress through the three points σ_A, **l** and **t**.

The total volume **V** beneath the surface $f(x,y) = z\ (> 0)$ and above the region in the xy-plane (see Figure 7.12) is:

$$V = \int_0^t \int_0^{fy} f(x,y)\,dy\,dx - \int_{T_{14x}}^t \int_0^{fy} f(x,y)\,dy\,dx - \int_{135}^{T_{14x}} \int_0^{cdy} f(x,y)\,dy\,dx - \int_{T_{15x}}^{135} \int_0^{cby} f(x,y)\,dy\,dx$$
$$- \int_{T_{16x}}^{T_{15x}} \int_0^{T_{15y}} f(x,y)\,dy\,dx - \int_{T_{16x}}^{T_{15x}} \int_{T_{15y}}^{fy} f(x,y)\,dy\,dx - \int_{50}^{T_{16x}} \int_0^{aby} f(x,y)\,dy\,dx - \int_{T_{1x}}^{50} \int_0^{qay} f(x,y)\,dy\,dx$$
$$- \int_0^{T_{1x}} \int_0^{T_{1y}} f(x,y)\,dy\,dx - \int_0^{T_{1x}} \int_{T_{1y}}^{fy} f(x,y)\,dy\,dx$$

and the centroids of this volume in the xy-plane are at distances $\overline{X}$ and $\overline{Y}$ from the axes (see Figure 7.12) which are given by the following equations.

$$\overline{X} = \frac{1}{V}\left[\begin{array}{l} \int_0^t \int_0^{fy} x f(x,y)\,dy\,dx - \int_{T_{14x}}^t \int_0^{fy} x f(x,y)\,dy\,dx - \int_{135}^{T_{14x}} \int_0^{cdy} x f(x,y)\,dy\,dx \\ - \int_{T_{15x}}^{135} \int_0^{cby} x f(x,y)\,dy\,dx - \int_{T_{16x}}^{T_{15x}} \int_0^{T_{15y}} x f(x,y)\,dy\,dx - \int_{T_{16x}}^{T_{15x}} \int_{T_{15y}}^{fy} x f(x,y)\,dy\,dx \\ - \int_{50}^{T_{16x}} \int_0^{aby} x f(x,y)\,dy\,dx - \int_{T_{1x}}^{50} \int_0^{qay} x f(x,y)\,dy\,dx - \int_0^{T_{1x}} \int_0^{T_{1y}} x f(x,y)\,dy\,dx \\ - \int_0^{T_{1x}} \int_{T_{1y}}^{fy} x f(x,y)\,dy\,dx \end{array}\right]$$

$$\overline{Y} = \frac{1}{V}\left[\begin{array}{l} \int_0^l \int_0^{fx} y f(x,y)\,dx\,dy - \int_0^{T_{14y}} \int_{T_{14x}}^{fx} y f(x,y)\,dx\,dy - \int_0^{T_{14y}} \int_{135}^{cdx} y f(x,y)\,dx\,dy \\ - \int_0^{T_{15y}} \int_{T_{15x}}^{bcx} y f(x,y)\,dx\,dy - \int_0^{T_{15y}} \int_{T_{15x}}^{T_{16x}} y f(x,y)\,dx\,dy - \int_{T_{15y}}^{T_{16y}} \int_{T_{16x}}^{fx} y f(x,y)\,dx\,dy \\ - \int_0^{T_{16y}} \int_{50}^{abx} y f(x,y)\,dx\,dy - \int_0^{T_{1y}} \int_{T_{1x}}^{qax} y f(x,y)\,dx\,dy - \int_0^{T_{1y}} \int_0^{T_{1x}} y f(x,y)\,dx\,dy \end{array}\right]$$

$$\left. - \int_{T_{1y}}^{l} \int_{0}^{fx} y f(x,y)\, dx\, dy \right]$$

Application 13 of the tetrahedral compressive stress regime beneath the circumscribing rectangular border of proprietory shaped paver 1 shown in Figure 7.13 can be calculated by using Tables 5.1 and 7.1 and the surface function of the tetrahedral compressive stress through the three points σ_A, **l** and **t**.

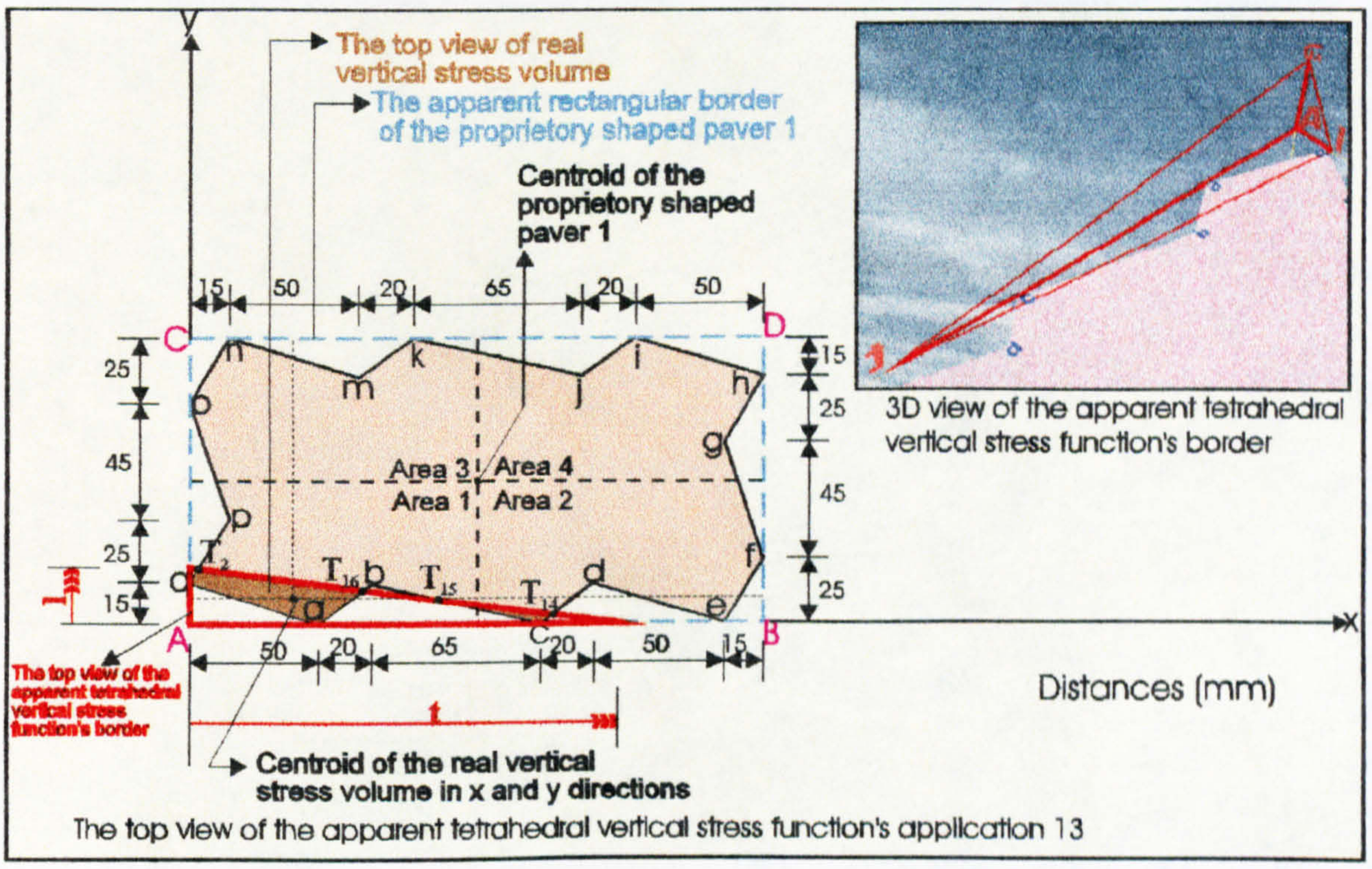

Figure 7.13: Application 13 of the tetrahedral compressive stress distribution beneath the circumscribing rectangular border of proprietory shaped paver 1.

The total volume **V** beneath the surface $f(x,y) = z\ (> 0)$ and above the region in the xy-plane (see Figure 7.13) is:

$$V = \int_{0}^{t} \int_{0}^{fy} f(x,y)\, dy\, dx - \int_{T_{14x}}^{t} \int_{0}^{fy} f(x,y)\, dy\, dx - \int_{135}^{T_{14x}cdy} \int_{0}^{} f(x,y)\, dy\, dx - \int_{T_{15x}}^{135\ cby} \int_{0}^{} f(x,y)\, dy\, dx$$

$$-\int_{T_{16x}}^{T_{15x}}\int_{0}^{T_{15y}} f(x,y)\,dy\,dx - \int_{T_{16x}}^{T_{15x}}\int_{T_{15y}}^{fy} f(x,y)\,dy\,dx - \int_{50}^{T_{16x}}\int_{0}^{aby} f(x,y)\,dy\,dx - \int_{0}^{50}\int_{0}^{qay} f(x,y)\,dy\,dx$$

$$-\int_{0}^{T_{2x}}\int_{15}^{qpy} f(x,y)\,dy\,dx - \int_{0}^{T_{2x}}\int_{T_{2y}}^{fy} f(x,y)\,dy\,dx$$

and the centroids of this volume in the xy-plane are at distances $\overline{X}$ and $\overline{Y}$ from the axes (see Figure 7.13) which are given by the following equations.

$$\overline{X} = \frac{1}{V}\left[\begin{array}{l}
\displaystyle\int_{0}^{t}\int_{0}^{fy} x f(x,y)\,dy\,dx - \int_{T_{14x}}^{t}\int_{0}^{fy} x f(x,y)\,dy\,dx - \int_{135}^{T_{14x}}\int_{0}^{cdy} x f(x,y)\,dy\,dx \\
\displaystyle -\int_{T_{15x}}^{135}\int_{0}^{cby} x f(x,y)\,dy\,dx - \int_{T_{16x}}^{T_{15x}}\int_{0}^{T_{15y}} x f(x,y)\,dy\,dx - \int_{T_{16x}}^{T_{15x}}\int_{T_{15y}}^{fy} x f(x,y)\,dy\,dx \\
\displaystyle -\int_{50}^{T_{16x}}\int_{0}^{aby} x f(x,y)\,dy\,dx - \int_{0}^{50}\int_{0}^{qay} x f(x,y)\,dy\,dx - \int_{0}^{T_{2x}}\int_{15}^{qpy} x f(x,y)\,dy\,dx \\
\displaystyle -\int_{0}^{T_{2x}}\int_{T_{2y}}^{fy} x f(x,y)\,dy\,dx
\end{array}\right]$$

$$\overline{Y} = \frac{1}{V}\left[\begin{array}{l}
\displaystyle\int_{0}^{l}\int_{0}^{fx} y f(x,y)\,dx\,dy - \int_{0}^{T_{14y}}\int_{T_{14x}}^{fx} y f(x,y)\,dx\,dy - \int_{0}^{T_{14y}}\int_{135}^{cdx} y f(x,y)\,dx\,dy \\
\displaystyle -\int_{0}^{T_{15y}}\int_{T_{15x}}^{bcx} y f(x,y)\,dx\,dy - \int_{0}^{T_{15y}}\int_{T_{16x}}^{T_{15x}} y f(x,y)\,dx\,dy - \int_{T_{15y}}^{T_{16y}}\int_{T_{16x}}^{fx} y f(x,y)\,dx\,dy \\
\displaystyle -\int_{0}^{T_{16y}}\int_{50}^{abx} y f(x,y)\,dx\,dy - \int_{0}^{15}\int_{0}^{qax} y f(x,y)\,dx\,dy - \int_{15}^{T_{2y}}\int_{0}^{qpx} y f(x,y)\,dx\,dy \\
\displaystyle -\int_{T_{2y}}^{l}\int_{0}^{fx} y f(x,y)\,dx\,dy
\end{array}\right]$$

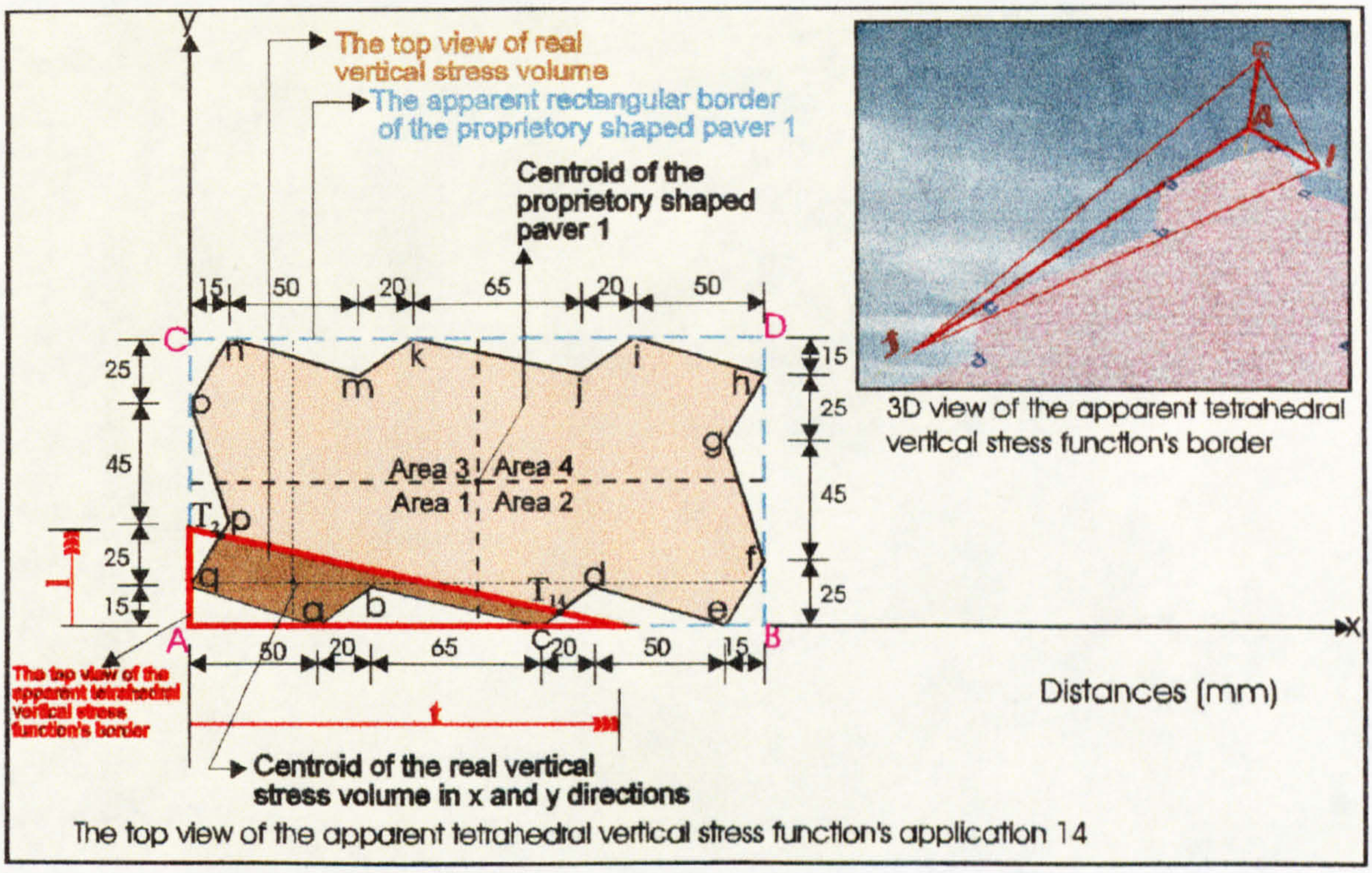

Figure 7.14: Application 14 of the tetrahedral compressive stress distribution beneath the circumscribing rectangular border of proprietory shaped paver 1.

Application 14 of the tetrahedral compressive stress regime beneath the circumscribing rectangular border of proprietory shaped paver 1 shown in Figure 7.14 can be calculated by using Tables 5.1 and 7.1 and the surface function of the tetrahedral compressive stress through the three points σ_A, **l** and **t**.

The total volume **V** beneath the surface $f(x,y) = z\ (> 0)$ and above the region in the xy-plane (see Figure 7.14) is:

$$V = \int_0^t \int_0^{fy} f(x,y)\,dy\,dx - \int_{T_{14x}}^t \int_0^{fy} f(x,y)\,dy\,dx - \int_{135}^{T_{14x}} \int_0^{cdy} f(x,y)\,dy\,dx - \int_{70}^{135} \int_0^{bcy} f(x,y)\,dy\,dx$$

$$- \int_{50}^{70} \int_0^{aby} f(x,y)\,dy\,dx - \int_0^{50} \int_0^{qay} f(x,y)\,dy\,dx - \int_0^{T_{2x}} \int_{15}^{qpy} f(x,y)\,dy\,dx - \int_0^{T_{2x}} \int_{T_{2y}}^{fy} f(x,y)\,dy\,dx$$

and the centroids of this volume in the xy-plane are at distances $\overline{X}$ and $\overline{Y}$ from the axes (see Figure 7.14) which are given by the following equations.

$$\overline{X} = \frac{1}{V}\left[\begin{array}{l} \int_0^t \int_0^{fy} x f(x,y)\,dy\,dx - \int_{T_{14x}}^{t} \int_0^{fy} x f(x,y)\,dy\,dx - \int_{135}^{T_{14x}} \int_0^{cdy} x f(x,y)\,dy\,dx \\ -\int_{70}^{135} \int_0^{bcy} x f(x,y)\,dy\,dx - \int_{50}^{70} \int_0^{aby} x f(x,y)\,dy\,dx - \int_0^{50} \int_0^{qay} x f(x,y)\,dy\,dx \\ -\int_0^{T_{2x}} \int_{15}^{qpy} x f(x,y)\,dy\,dx - \int_0^{T_{2x}} \int_{T_{2y}}^{fy} x f(x,y)\,dy\,dx \end{array}\right]$$

$$\overline{Y} = \frac{1}{V}\left[\begin{array}{l} \int_0^l \int_0^{fx} y f(x,y)\,dx\,dy - \int_0^{T_{14y}} \int_{T_{14x}}^{fx} y f(x,y)\,dx\,dy - \int_0^{T_{14y}} \int_{135}^{cdx} y f(x,y)\,dx\,dy \\ -\int_0^{15} \int_{70}^{bcx} y f(x,y)\,dx\,dy - \int_0^{15} \int_{50}^{abx} y f(x,y)\,dx\,dy - \int_0^{15} \int_0^{qax} y f(x,y)\,dx\,dy \\ -\int_{15}^{T_{2y}} \int_0^{qpx} y f(x,y)\,dx\,dy - \int_{T_{2y}}^{l} \int_0^{fx} y f(x,y)\,dx\,dy \end{array}\right]$$

Application 15 of the tetrahedral compressive stress regime beneath the circumscribing rectangular border of proprietory shaped paver 1 shown in Figure 7.15 can be calculated by using Tables 5.1 and 7.1 and the surface function of the tetrahedral compressive stress through the three points σ_A, **l** and **t**.

The total volume **V** beneath the surface $f(x,y) = z\ (> 0)$ and above the region in the xy-plane (see Figure 7.15) is:

$$V = \int_0^t \int_0^{fy} f(x,y)\,dy\,dx - \int_{T_{14x}}^{t} \int_0^{fy} f(x,y)\,dy\,dx - \int_{135}^{T_{14x}} \int_0^{cdy} f(x,y)\,dy\,dx - \int_{70}^{135} \int_0^{bcy} f(x,y)\,dy\,dx$$

$$-\int_{50}^{70}\int_{0}^{aby} f(x,y)\,dy\,dx-\int_{0}^{50}\int_{0}^{qay} f(x,y)\,dy\,dx-\int_{0}^{15}\int_{0}^{qpy} f(x,y)\,dy\,dx-\int_{0}^{T_{3x}}\int_{40}^{T_{3y}} f(x,y)\,dy\,dx$$

$$-\int_{T_{3x}}^{15}\int_{40}^{poy} f(x,y)\,dy\,dx-\int_{0}^{T_{3x}}\int_{T_{3y}}^{fy} f(x,y)\,dy\,dx$$

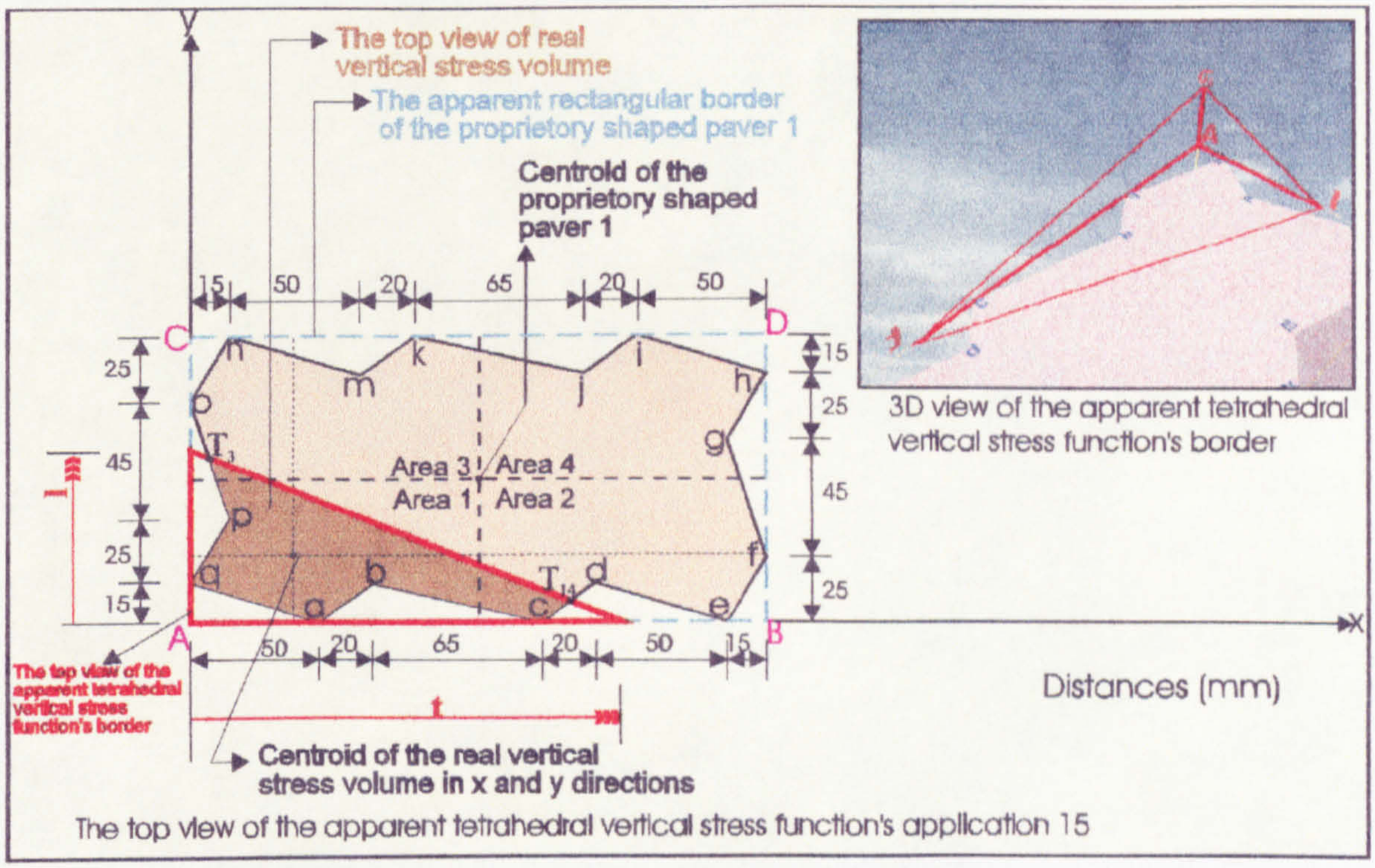

Figure 7.15: Application 15 of the tetrahedral compressive stress distribution beneath the circumscribing rectangular border of proprietory shaped paver 1.

and the centroids of this volume in the xy-plane are at distances $\overline{X}$ and $\overline{Y}$ from the axes (see Figure 7.15) which are given by the following equations.

$$\overline{X}=\frac{1}{V}\left[\int_{0}^{t}\int_{0}^{fy} x\,f(x,y)\,dy\,dx-\int_{T_{14x}}^{t}\int_{0}^{fy} x\,f(x,y)\,dy\,dx-\int_{135}^{T_{14x}}\int_{0}^{cdy} x\,f(x,y)\,dy\,dx-\int_{70}^{135}\int_{0}^{bcy} x\,f(x,y)\,dy\,dx\right.$$

$$\left.-\int_{50}^{70}\int_{0}^{aby} x\,f(x,y)\,dy\,dx-\int_{0}^{50}\int_{0}^{qay} x\,f(x,y)\,dy\,dx-\int_{0}^{15}\int_{0}^{qpy} x\,f(x,y)\,dy\,dx-\int_{0}^{T_{3x}}\int_{40}^{T_{3y}} x\,f(x,y)\,dy\,dx\right.$$

$$-\int_{T_{3x}}^{15}\int_{40}^{poy} x f(x,y)\,dy\,dx - \int_{0}^{T_{3x}}\int_{T_{3y}}^{fy} x f(x,y)\,dy\,dx\Bigg]$$

$$\left[\int_{0}^{l}\int_{0}^{fx} y f(x,y)\,dx\,dy - \int_{0}^{T_{14y}}\int_{T_{14x}}^{fx} y f(x,y)\,dx\,dy - \int_{0}^{T_{14y}}\int_{135}^{cdx} y f(x,y)\,dx\,dy\right]$$

$$\overline{Y} = \frac{1}{V}\left[\begin{array}{l} -\int_{0}^{15}\int_{70}^{bcx} y f(x,y)\,dx\,dy - \int_{0}^{15}\int_{50}^{abx} y f(x,y)\,dx\,dy - \int_{0}^{15}\int_{0}^{qax} y f(x,y)\,dx\,dy \\ -\int_{15}^{40}\int_{0}^{qpx} y f(x,y)\,dx\,dy - \int_{40}^{T_{3y}}\int_{0}^{T_{3x}} y f(x,y)\,dx\,dy - \int_{40}^{T_{3y}}\int_{T_{3x}}^{pox} y f(x,y)\,dx\,dy \\ -\int_{T_{3y}}^{l}\int_{0}^{fx} y f(x,y)\,dx\,dy \end{array}\right]$$

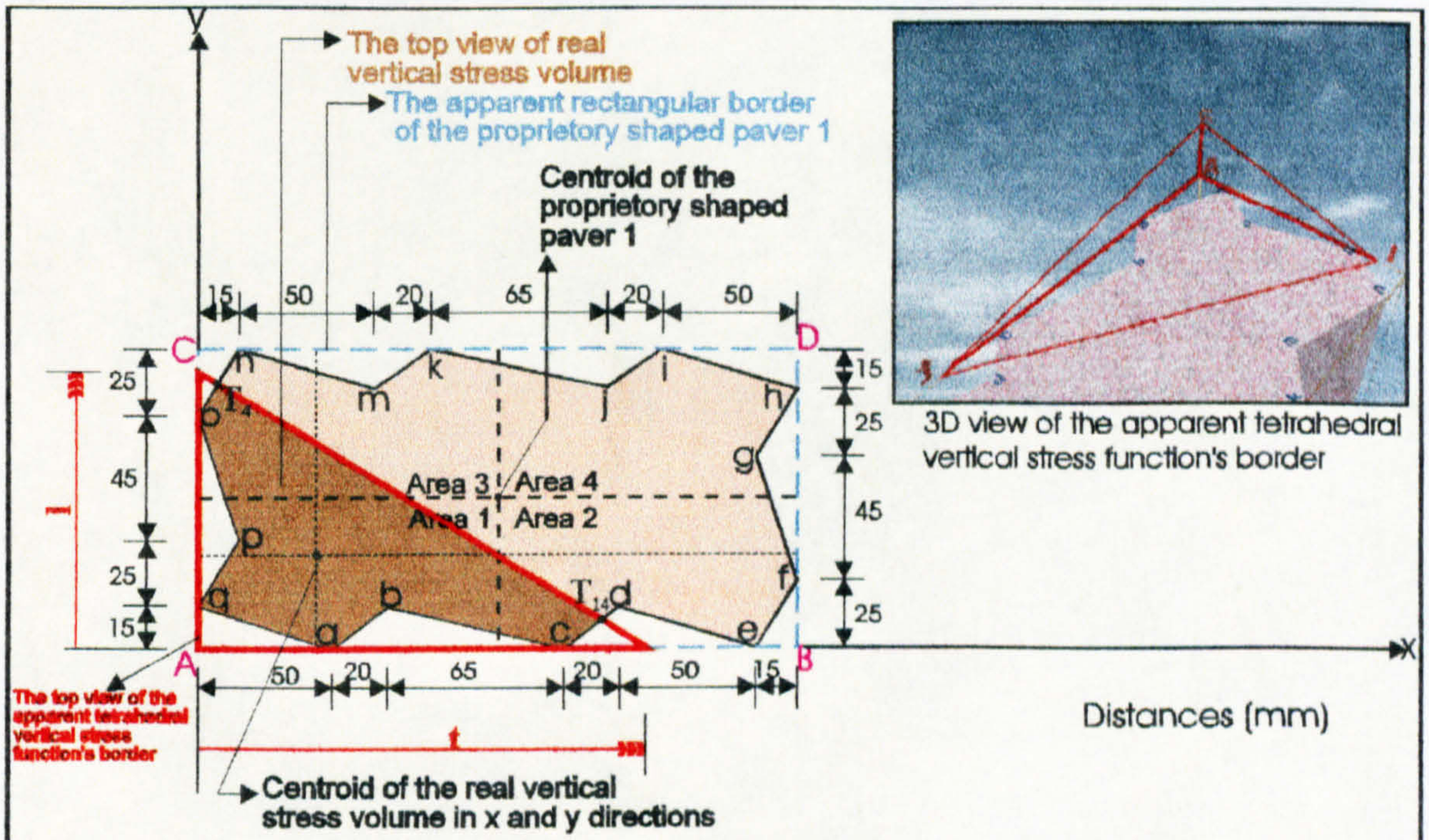

Figure 7.16: Application 16 of the tetrahedral compressive stress distribution beneath the circumscribing rectangular border of proprietory shaped paver 1.

Application 16 of the tetrahedral compressive stress regime beneath the circumscribing rectangular border of proprietory shaped paver 1 shown in Figure 7.16 can be calculated by using Tables 5.1 and 7.1 and the surface function of the tetrahedral compressive stress through the three points σ_A, **l** and **t**.

The total volume **V** beneath the surface $f(x,y) = z\ (> 0)$ and above the region in the xy-plane (see Figure 7.16) is:

$$V = \int_0^t \int_0^{fy} f(x,y)\,dy\,dx - \int_{T_{14x}}^t \int_0^{fy} f(x,y)\,dy\,dx - \int_{135}^{T_{14x}} \int_0^{cdy} f(x,y)\,dy\,dx - \int_{70}^{135} \int_0^{bcy} f(x,y)\,dy\,dx$$
$$- \int_{50}^{70} \int_0^{aby} f(x,y)\,dy\,dx - \int_0^{50} \int_0^{qay} f(x,y)\,dy\,dx - \int_0^{15} \int_{15}^{qpy} f(x,y)\,dy\,dx - \int_0^{40} \int_{15}^{poy} f(x,y)\,dy\,dx$$
$$- \int_0^{T_{4x}} \int_{85}^{ony} f(x,y)\,dy\,dx - \int_0^{T_{4x}} \int_{T_{4y}}^{fy} f(x,y)\,dy\,dx$$

and the centroids of this volume in the xy-plane are at distances $\overline{X}$ and $\overline{Y}$ from the axes (see Figure 7.16) which are given by the following equations.

$$\overline{X} = \frac{1}{V}\left[\int_0^t \int_0^{fy} x f(x,y)\,dy\,dx - \int_{T_{14x}}^t \int_0^{fy} x f(x,y)\,dy\,dx - \int_{135}^{T_{14x}} \int_0^{cdy} x f(x,y)\,dy\,dx \right.$$
$$- \int_{70}^{135} \int_0^{bcy} x f(x,y)\,dy\,dx - \int_{50}^{70} \int_0^{aby} x f(x,y)\,dy\,dx - \int_0^{50} \int_0^{qay} x f(x,y)\,dy\,dx$$
$$- \int_0^{15} \int_{15}^{qpy} x f(x,y)\,dy\,dx - \int_0^{40} \int_{15}^{poy} x f(x,y)\,dy\,dx - \int_0^{85} \int_{15}^{T_{4x}\,ony} x f(x,y)\,dy\,dx$$
$$\left. - \int_0^{T_{4x}} \int_{T_{4y}}^{fy} x f(x,y)\,dy\,dx\right]$$

$$\overline{Y} = \frac{1}{V}\left[\begin{array}{l} \int_0^l \int_0^{fx} y f(x,y)\,dx\,dy - \int_0^{T_{14y}} \int_{T_{14x}}^{fx} y f(x,y)\,dx\,dy - \int_0^{T_{14y}} \int_{135}^{cdx} y f(x,y)\,dx\,dy \\ -\int_0^{15} \int_{70}^{bcx} y f(x,y)\,dx\,dy - \int_0^{15} \int_{50}^{abx} y f(x,y)\,dx\,dy - \int_0^{15} \int_0^{qax} y f(x,y)\,dx\,dy \\ -\int_{15}^{40} \int_0^{qpx} y f(x,y)\,dx\,dy - \int_{40}^{85} \int_0^{pox} y f(x,y)\,dx\,dy - \int_{85}^{T_{4y}} \int_0^{onx} y f(x,y)\,dx\,dy \\ -\int_{T_{4y}}^{l} \int_0^{fx} y f(x,y)\,dx\,dy \end{array}\right]$$

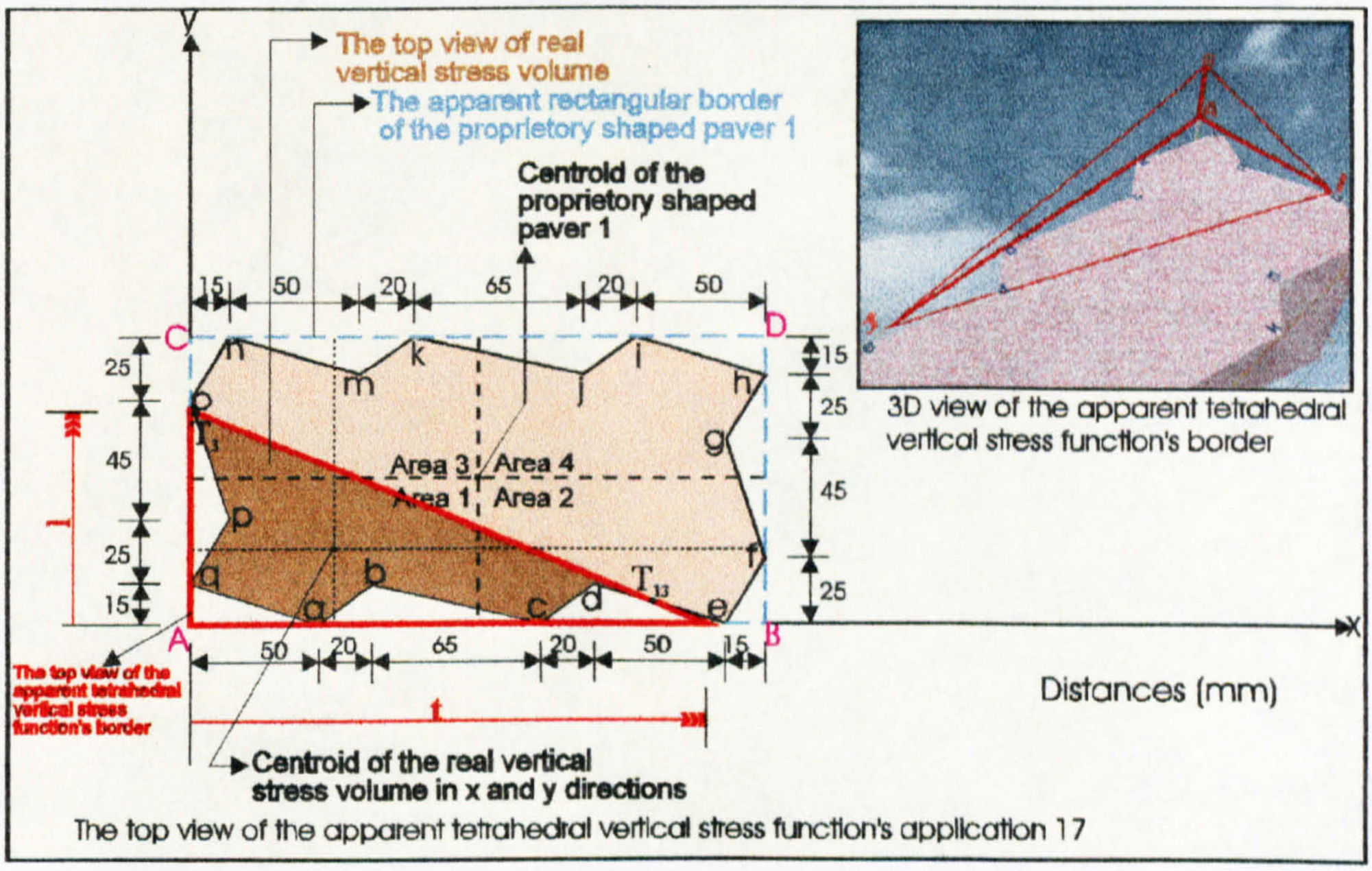

Figure 7.17: Application 17 of the tetrahedral compressive stress distribution beneath the circumscribing rectangular border of proprietory shaped paver 1.

Application 17 of the tetrahedral compressive stress regime beneath the circumscribing rectangular border of proprietory shaped paver 1 shown in Figure 7.17 can be calculated by using Tables 5.1 and 7.1 and the surface function of the tetrahedral compressive stress through the three points σ_A, **l** and **t**.

The total volume **V** beneath the surface $f(x,y) = z\ (> 0)$ and above the region in the xy-plane (see Figure 7.17) is:

$$V = \int_0^t \int_0^{fy} f(x,y)\,dy\,dx - \int_{T_{13x}}^t \int_0^{fy} f(x,y)\,dy\,dx - \int_{155}^{T_{13x}} \int_0^{T_{13y}} f(x,y)\,dy\,dx - \int_{155}^{T_{13x}} \int_{T_{13y}}^{dey} f(x,y)\,dy\,dx$$
$$- \int_{135}^{155} \int_0^{cdy} f(x,y)\,dy\,dx - \int_{70}^{135} \int_0^{bcy} f(x,y)\,dy\,dx - \int_{50}^{70} \int_0^{aby} f(x,y)\,dy\,dx - \int_0^{50} \int_0^{qay} f(x,y)\,dy\,dx$$
$$- \int_0^{T_{3x}} \int_{40}^{T_{3y}} f(x,y)\,dy\,dx - \int_{T_{3x}}^{15} \int_{40}^{poy} f(x,y)\,dy\,dx - \int_0^{T_{3x}} \int_{T_{3y}}^{fy} f(x,y)\,dy\,dx - \int_0^{15} \int_{15}^{qpy} f(x,y)\,dy\,dx$$

and the centroids of this volume in the xy-plane are at distances $\overline{X}$ and $\overline{Y}$ from the axes (see Figure 7.17) which are given by the following equations.

$$\overline{X} = \frac{1}{V}\left[\int_0^t \int_0^{fy} x f(x,y)\,dy\,dx - \int_{T_{13x}}^t \int_0^{fy} x f(x,y)\,dy\,dx - \int_{155}^{T_{13x}} \int_0^{T_{13y}} x f(x,y)\,dy\,dx - \int_{155}^{T_{13x}} \int_{T_{13y}}^{dey} x f(x,y)\,dy\,dx\right.$$
$$- \int_{135}^{155} \int_0^{cdy} x f(x,y)\,dy\,dx - \int_{70}^{135} \int_0^{bcy} x f(x,y)\,dy\,dx - \int_{50}^{70} \int_0^{aby} x f(x,y)\,dy\,dx - \int_0^{50} \int_0^{qay} x f(x,y)\,dy\,dx$$
$$\left. - \int_0^{T_{3x}} \int_{40}^{T_{3y}} x f(x,y)\,dy\,dx - \int_{T_{3x}}^{15} \int_{40}^{poy} x f(x,y)\,dy\,dx - \int_0^{T_{3x}} \int_{T_{3y}}^{fy} x f(x,y)\,dy\,dx - \int_0^{15} \int_{15}^{qpy} x f(x,y)\,dy\,dx\right]$$

$$\overline{Y} = \frac{1}{V}\left[\int_0^l \int_0^{fx} y f(x,y)\,dx\,dy - \int_0^{T_{13y}} \int_{T_{13x}}^{fx} y f(x,y)\,dx\,dy - \int_0^{T_{13y}} \int_{155}^{T_{13x}} y f(x,y)\,dx\,dy\right.$$
$$- \int_{T_{13y}}^{15} \int_{155}^{dex} y f(x,y)\,dx\,dy - \int_0^{15} \int_{135}^{cdx} y f(x,y)\,dx\,dy - \int_0^{15} \int_{70}^{bcx} y f(x,y)\,dx\,dy$$

$$-\int_{0}^{15}\int_{50}^{abx} y\,f(x,y)\,dx\,dy-\int_{0}^{15}\int_{0}^{qax} y\,f(x,y)\,dx\,dy-\int_{15}^{40}\int_{0}^{qpx} y\,f(x,y)\,dx\,dy$$

$$-\int_{40}^{T_{3y}}\int_{0}^{T_{3x}} y\,f(x,y)\,dx\,dy-\int_{40}^{T_{3y}}\int_{T_{3x}}^{pox} y\,f(x,y)\,dx\,dy-\int_{T_{3y}}^{l}\int_{0}^{fx} y\,f(x,y)\,dx\,dy\Bigg]$$

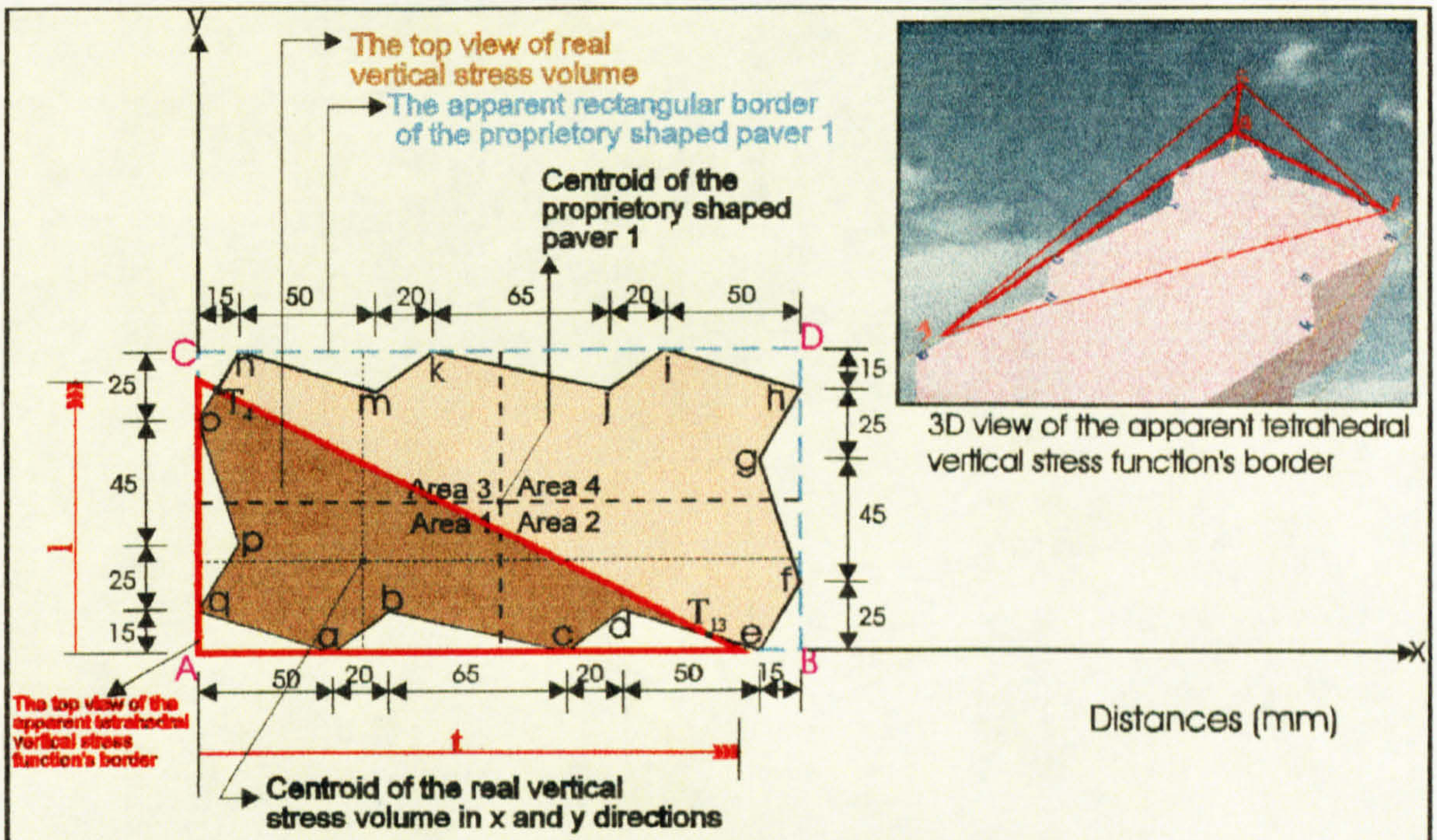

Figure 7.18: Application 18 of the tetrahedral compressive stress distribution beneath the circumscribing rectangular border of proprietory shaped paver 1.

Application 18 of the tetrahedral compressive stress regime beneath the circumscribing rectangular border of proprietory shaped paver 1 shown in Figure 7.18 can be calculated by using Tables 5.1 and 7.1 and the surface function of the tetrahedral compressive stress through the three points σ_A, **l** and **t**.

The total volume **V** beneath the surface $f(x,y)=z\ (>0)$ and above the region in the xy-plane (see Figure 7.18) is:

$$V = \int_0^t \int_0^{fy} f(x,y)\,dy\,dx - \int_{T_{13x}}^t \int_0^{fy} f(x,y)\,dy\,dx - \int_{155}^{T_{13x}} \int_0^{T_{13y}} f(x,y)\,dy\,dx - \int_{155}^{T_{13x}} \int_{T_{13y}}^{dey} f(x,y)\,dy\,dx$$
$$- \int_{135}^{155} \int_0^{cdy} f(x,y)\,dy\,dx - \int_{70}^{135} \int_0^{bcy} f(x,y)\,dy\,dx - \int_{50}^{70} \int_0^{aby} f(x,y)\,dy\,dx - \int_0^{50} \int_0^{qay} f(x,y)\,dy\,dx$$
$$- \int_0^{15} \int_{15}^{qpy} f(x,y)\,dy\,dx - \int_0^{40} \int_{15}^{poy} f(x,y)\,dy\,dx - \int_0^{85} \int_{T_{4x}}^{ony} f(x,y)\,dy\,dx - \int_0^{T_{4y}} \int_{T_{4x}}^{fy} f(x,y)\,dy\,dx$$

and the centroids of this volume in the xy-plane are at distances $\overline{X}$ and $\overline{Y}$ from the axes (see Figure 7.18) which are given by the following equations.

$$\overline{X} = \frac{1}{V}\left[\begin{array}{l} \int_0^t \int_0^{fy} x f(x,y)\,dy\,dx - \int_{T_{13x}}^t \int_0^{fy} x f(x,y)\,dy\,dx - \int_{155}^{T_{13x}} \int_0^{T_{13y}} x f(x,y)\,dy\,dx - \int_{155}^{T_{13x}} \int_{T_{13y}}^{dey} x f(x,y)\,dy\,dx \\ - \int_{135}^{155} \int_0^{cdy} x f(x,y)\,dy\,dx - \int_{70}^{135} \int_0^{bcy} x f(x,y)\,dy\,dx - \int_{50}^{70} \int_0^{aby} x f(x,y)\,dy\,dx - \int_0^{50} \int_0^{qay} x f(x,y)\,dy\,dx \\ - \int_0^{15} \int_{15}^{qpy} x f(x,y)\,dy\,dx - \int_0^{40} \int_{15}^{poy} x f(x,y)\,dy\,dx - \int_0^{85} \int_{T_{4x}}^{ony} x f(x,y)\,dy\,dx - \int_0^{T_{4y}} \int_{T_{4x}}^{fy} x f(x,y)\,dy\,dx \end{array}\right]$$

$$\overline{Y} = \frac{1}{V}\left[\begin{array}{l} \int_0^t \int_0^{fx} y f(x,y)\,dx\,dy - \int_0^{T_{13y}} \int_{T_{13x}}^{fx} y f(x,y)\,dx\,dy - \int_0^{T_{13y}} \int_{155}^{T_{13x}} y f(x,y)\,dx\,dy - \int_{T_{13y}}^{155} \int_{T_{13x}}^{dcx} y f(x,y)\,dx\,dy \\ - \int_0^{135} \int_0^{cdx} y f(x,y)\,dx\,dy - \int_0^{70} \int_0^{bcx} y f(x,y)\,dx\,dy - \int_0^{50} \int_0^{abx} y f(x,y)\,dx\,dy - \int_0^{0} \int_0^{qax} y f(x,y)\,dx\,dy \\ - \int_{15}^{0} \int_0^{qpx} y f(x,y)\,dx\,dy - \int_{40}^{0} \int_0^{pox} y f(x,y)\,dx\,dy - \int_{85}^{0} \int_0^{T_{4y}} y f(x,y)\,dx\,dy - \int_{T_{4y}}^{t} \int_0^{fx} y f(x,y)\,dx\,dy \end{array}\right]$$

Application 19 of the tetrahedral compressive stress regime beneath the circumscribing rectangular border of proprietory shaped paver 1 shown in Figure 7.19 can be calculated by using Tables 5.1 and 7.1 and the surface function of the tetrahedral compressive stress through the three points σ_A, l and t.

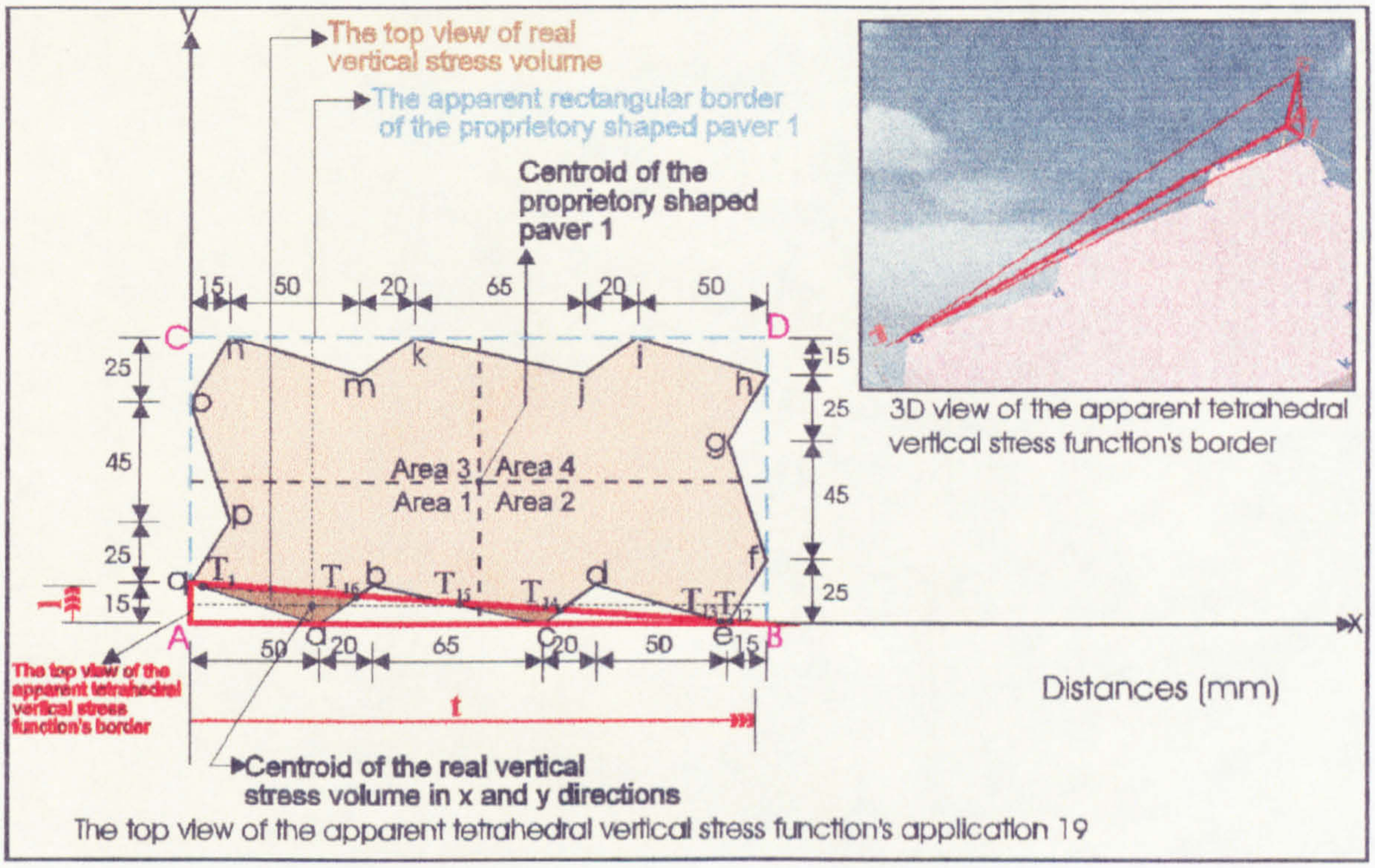

Figure 7.19: Application 19 of the tetrahedral compressive stress distribution beneath the circumscribing rectangular border of proprietory shaped paver 1.

The total volume **V** beneath the surface $f(x,y) = z\ (> 0)$ and above the region in the xy-plane (see Figure 7.19) is:

$$V = \int_0^t \int_0^{fy} f(x,y)\,dy\,dx - \int_{T_{12x}}^t \int_0^{fy} f(x,y)\,dy\,dx - \int_{205}^{T_{12x}} \int_0^{efy} f(x,y)\,dy\,dx - \int_{T_{13x}}^{205} \int_0^{dey} f(x,y)\,dy\,dx$$
$$- \int_{T_{14x}}^{T_{13x}} \int_0^{T_{13y}} f(x,y)\,dy\,dx - \int_{T_{14x}}^{T_{13x}} \int_{T_{13y}}^{fy} f(x,y)\,dy\,dx - \int_{135}^{T_{14x}} \int_0^{cdy} f(x,y)\,dy\,dx - \int_{T_{15x}}^{135} \int_0^{bcy} f(x,y)\,dy\,dx$$
$$- \int_{T_{16x}}^{T_{15x}} \int_0^{T_{15y}} f(x,y)\,dy\,dx - \int_{T_{16x}}^{T_{15x}} \int_{T_{15y}}^{fy} f(x,y)\,dy\,dx - \int_{50}^{T_{16x}} \int_0^{aby} f(x,y)\,dy\,dx - \int_{T_{1x}}^{50} \int_0^{qay} f(x,y)\,dy\,dx$$
$$- \int_0^{T_{1x}} \int_0^{T_{1y}} f(x,y)\,dy\,dx - \int_0^{T_{1x}} \int_{T_{1y}}^{fy} f(x,y)\,dy\,dx$$

and the centroids of this volume in the xy-plane are at distances $\overline{X}$ and $\overline{Y}$ from the axes (see Figure 7.19) which are given by the following equations.

$$\overline{X} = \frac{1}{V}\left[\begin{array}{l}
\int_{0}^{t}\int_{0}^{fy} x f(x,y)\,dy\,dx - \int_{T_{12x}}^{t}\int_{0}^{fy} x f(x,y)\,dy\,dx - \int_{205}^{T_{12x}}\int_{0}^{efy} x f(x,y)\,dy\,dx \\
-\int_{T_{13x}}^{205}\int_{0}^{dey} x f(x,y)\,dy\,dx - \int_{T_{14x}}^{T_{13x}}\int_{0}^{T_{13y}} x f(x,y)\,dy\,dx - \int_{T_{14x}}^{T_{13x}}\int_{T_{13y}}^{fy} x f(x,y)\,dy\,dx \\
-\int_{135}^{T_{14x}}\int_{0}^{cdy} x f(x,y)\,dy\,dx - \int_{T_{15x}}^{135}\int_{0}^{bcy} x f(x,y)\,dy\,dx - \int_{T_{16x}}^{T_{15x}}\int_{0}^{T_{15y}} x f(x,y)\,dy\,dx \\
-\int_{T_{16x}}^{T_{15x}}\int_{T_{7y}}^{fy} x f(x,y)\,dy\,dx - \int_{50}^{T_{16x}}\int_{0}^{aby} x f(x,y)\,dy\,dx - \int_{T_{1x}}^{50}\int_{0}^{qay} x f(x,y)\,dy\,dx \\
-\int_{0}^{T_{1x}}\int_{0}^{T_{1y}} x f(x,y)\,dy\,dx - \int_{0}^{T_{1x}}\int_{T_{1y}}^{fy} x f(x,y)\,dy\,dx
\end{array}\right]$$

$$\overline{Y} = \frac{1}{V}\left[\begin{array}{l}
\int_{0}^{l}\int_{0}^{fx} y f(x,y)\,dx\,dy - \int_{0}^{T_{12y}}\int_{T_{12x}}^{fx} y f(x,y)\,dx\,dy - \int_{0}^{T_{12y}}\int_{205}^{efx} y f(x,y)\,dx\,dy \\
-\int_{0}^{T_{13y}}\int_{T_{13x}}^{dcx} y f(x,y)\,dx\,dy - \int_{0}^{T_{13y}}\int_{T_{14x}}^{T_{13x}} y f(x,y)\,dx\,dy - \int_{T_{13y}}^{T_{14y}}\int_{T_{14x}}^{fx} y f(x,y)\,dx\,dy \\
-\int_{0}^{T_{14y}}\int_{135}^{cdx} y f(x,y)\,dx\,dy - \int_{0}^{T_{15y}}\int_{T_{15x}}^{bcx} y f(x,y)\,dx\,dy - \int_{0}^{T_{15y}}\int_{T_{16x}}^{T_{15x}} y f(x,y)\,dx\,dy \\
-\int_{T_{15y}}^{T_{16y}}\int_{T_{16x}}^{fx} y f(x,y)\,dx\,dy - \int_{0}^{T_{16y}}\int_{50}^{abx} y f(x,y)\,dx\,dy - \int_{0}^{T_{1y}}\int_{T_{1x}}^{qax} y f(x,y)\,dx\,dy \\
-\int_{0}^{T_{1y}}\int_{0}^{T_{1x}} y f(x,y)\,dx\,dy - \int_{T_{1y}}^{l}\int_{0}^{fx} y f(x,y)\,dx\,dy
\end{array}\right]$$

Application 20 of the tetrahedral compressive stress regime beneath the circumscribing rectangular border of proprietory shaped paver 1 shown in Figure 7.20 can be calculated by using Tables 5.1 and 7.1 and the surface function of the tetrahedral compressive stress through the three points σ_A, **l** and **t**.

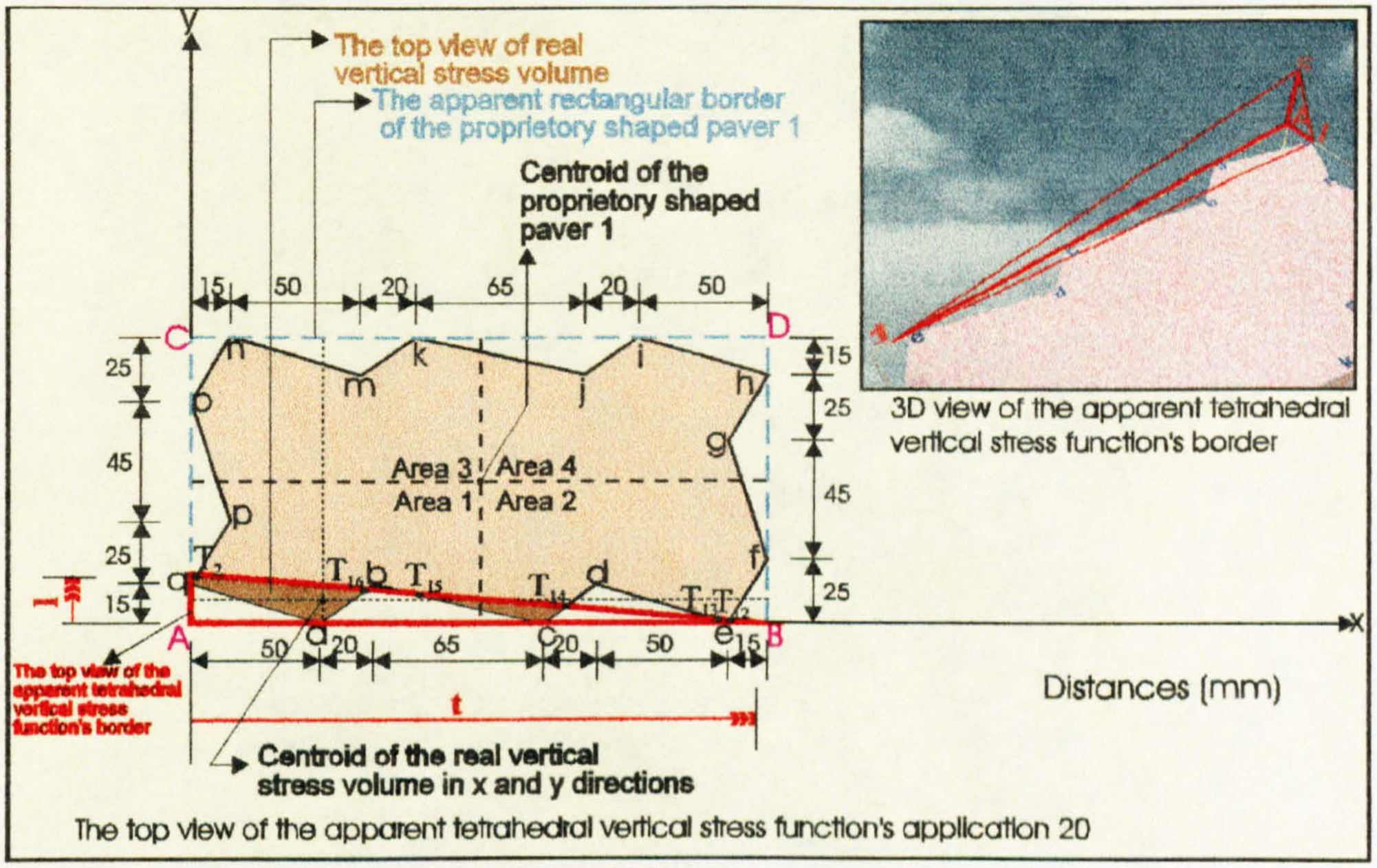

Figure 7.20: Application 20 of the tetrahedral compressive stress distribution beneath the circumscribing rectangular border of proprietory shaped paver 1.

The total volume **V** beneath the surface $f(x,y) = z\ (> 0)$ and above the region in the xy-plane (see Figure 7.20) is:

$$V = \int_0^t \int_0^{fy} f(x,y)\,dy\,dx - \int_{T_{12x}}^t \int_0^{fy} f(x,y)\,dy\,dx - \int_{205}^{T_{12x}} \int_0^{efy} f(x,y)\,dy\,dx - \int_{T_{13x}}^{205} \int_0^{dey} f(x,y)\,dy\,dx$$

$$- \int_{T_{14x}}^{T_{13x}} \int_0^{T_{13y}} f(x,y)\,dy\,dx - \int_{T_{14x}}^{T_{13x}} \int_{T_{13y}}^{fy} f(x,y)\,dy\,dx - \int_{135}^{T_{14x}} \int_0^{cdy} f(x,y)\,dy\,dx - \int_{T_{15x}}^{135} \int_0^{bcy} f(x,y)\,dy\,dx$$

$$- \int_{T_{16x}}^{T_{15x}} \int_0^{T_{15y}} f(x,y)\,dy\,dx - \int_{T_{16x}}^{T_{15x}} \int_{T_{15y}}^{fy} f(x,y)\,dy\,dx - \int_{50}^{T_{16x}} \int_0^{aby} f(x,y)\,dy\,dx - \int_{T_{1x}}^{50} \int_0^{qay} f(x,y)\,dy\,dx$$

$$- \int_0^{T_{2x}} \int_{15}^{qpy} f(x,y)\,dy\,dx - \int_0^{T_{2x}} \int_{T_{2y}}^{fy} f(x,y)\,dy\,dx$$

and the centroids of this volume in the xy-plane are at distances $\overline{X}$ and $\overline{Y}$ from the axes (see Figure 7.20) which are given by the following equations.

$$\overline{X} = \frac{1}{V}\left[\begin{array}{l}
\int_{0}^{t}\int_{0}^{fy} x f(x,y)\,dy\,dx - \int_{T_{12x}}^{t}\int_{0}^{fy} x f(x,y)\,dy\,dx - \int_{205}^{T_{12x}}\int_{0}^{efy} x f(x,y)\,dy\,dx \\
- \int_{T_{13x}}^{205}\int_{0}^{dey} x f(x,y)\,dy\,dx - \int_{T_{14x}}^{T_{13x}}\int_{0}^{T_{13y}} x f(x,y)\,dy\,dx - \int_{T_{14x}}^{T_{13x}}\int_{T_{13y}}^{fy} x f(x,y)\,dy\,dx \\
- \int_{135}^{T_{14x}}\int_{0}^{cdy} x f(x,y)\,dy\,dx - \int_{T_{15x}}^{135}\int_{0}^{bcy} x f(x,y)\,dy\,dx - \int_{T_{16x}}^{T_{15x}}\int_{0}^{T_{15y}} x f(x,y)\,dy\,dx \\
- \int_{T_{16x}}^{T_{15x}}\int_{T_{15y}}^{fy} x f(x,y)\,dy\,dx - \int_{50}^{T_{16x}}\int_{0}^{aby} x f(x,y)\,dy\,dx - \int_{T_{1x}}^{50}\int_{0}^{qay} x f(x,y)\,dy\,dx \\
- \int_{0}^{T_{2x}}\int_{15}^{qpy} x f(x,y)\,dy\,dx - \int_{0}^{T_{2x}}\int_{T_{2y}}^{fy} x f(x,y)\,dy\,dx
\end{array}\right]$$

$$\overline{Y} = \frac{1}{V}\left[\begin{array}{l}
\int_{0}^{l}\int_{0}^{fx} y f(x,y)\,dx\,dy - \int_{0}^{T_{12y}}\int_{T_{12x}}^{fx} y f(x,y)\,dx\,dy - \int_{0}^{T_{12y}}\int_{205}^{efx} y f(x,y)\,dx\,dy \\
- \int_{0}^{T_{13y}}\int_{T_{13x}}^{dcx} y f(x,y)\,dx\,dy - \int_{0}^{T_{13y}}\int_{T_{14x}}^{T_{13x}} y f(x,y)\,dx\,dy - \int_{T_{13y}}^{T_{14y}}\int_{T_{14x}}^{fx} y f(x,y)\,dx\,dy \\
- \int_{0}^{T_{14y}}\int_{135}^{cdx} y f(x,y)\,dx\,dy - \int_{0}^{T_{15y}}\int_{T_{15x}}^{bcx} y f(x,y)\,dx\,dy - \int_{0}^{T_{15y}}\int_{T_{16x}}^{T_{15x}} y f(x,y)\,dx\,dy \\
- \int_{T_{15y}}^{T_{16y}}\int_{T_{16x}}^{fx} y f(x,y)\,dx\,dy - \int_{0}^{T_{16y}}\int_{50}^{abx} y f(x,y)\,dx\,dy - \int_{0}^{15}\int_{0}^{qax} y f(x,y)\,dx\,dy \\
- \int_{15}^{T_{2y}}\int_{0}^{qpx} y f(x,y)\,dx\,dy - \int_{T_{2y}}^{l}\int_{0}^{fx} y f(x,y)\,dx\,dy
\end{array}\right]$$

Application 21 of the tetrahedral compressive stress regime beneath the circumscribing rectangular border of proprietory shaped paver 1 shown in Figure 7.21 can be calculated by using Tables 5.1 and 7.1 and the surface function of the tetrahedral compressive stress through the three points σ_A, **l** and **t**.

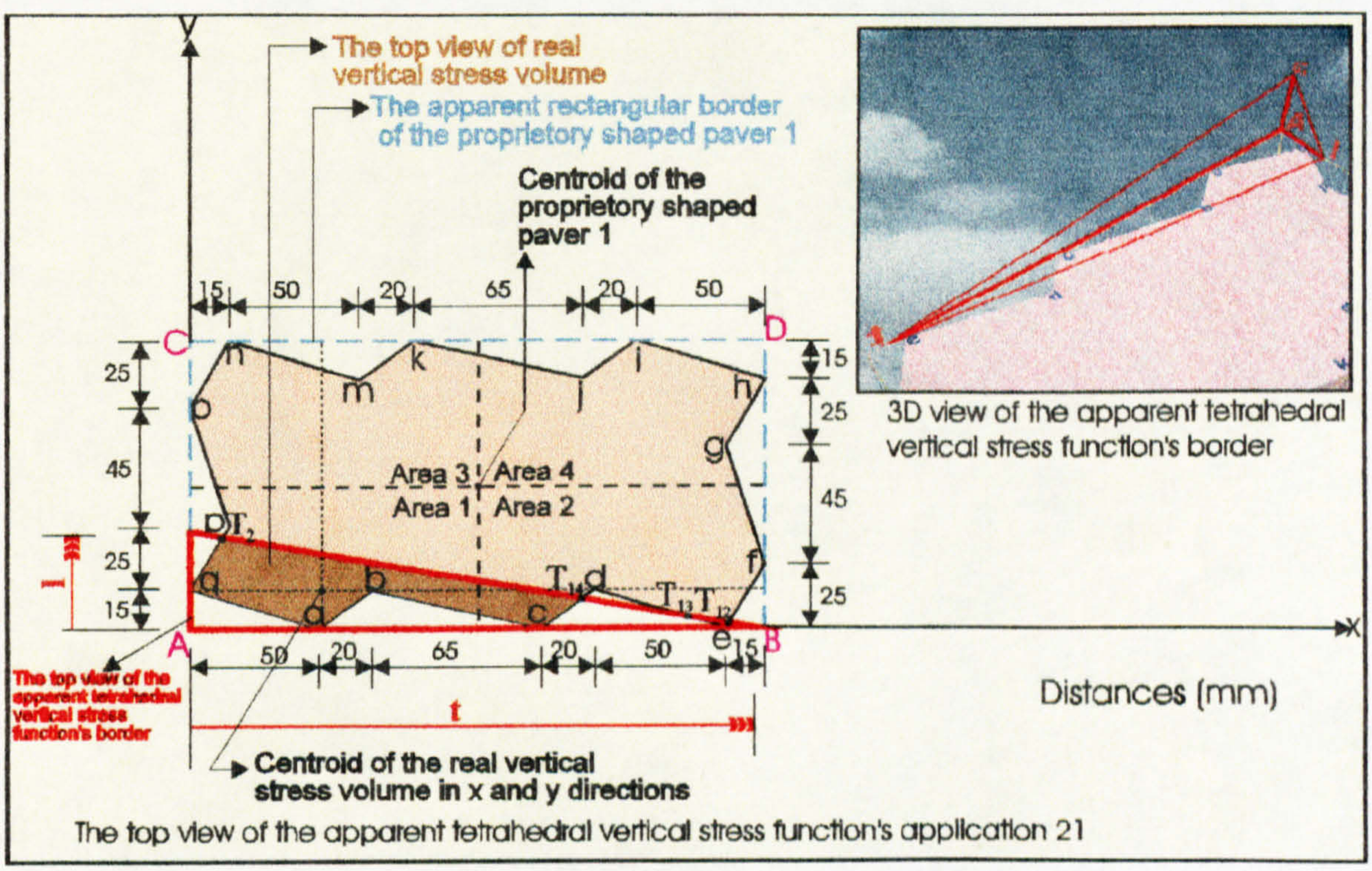

Figure 7.21: Application 21 of the tetrahedral compressive stress distribution beneath the circumscribing rectangular border of proprietory shaped paver 1.

The total volume **V** beneath the surface $f(x,y) = z\ (> 0)$ and above the region in the xy-plane (see Figure 7.21) is:

$$V = \int_0^t \int_0^{fy} f(x,y)\,dy\,dx - \int_{T_{12x}}^t \int_0^{fy} f(x,y)\,dy\,dx - \int_{205}^{T_{12x}} \int_0^{efy} f(x,y)\,dy\,dx - \int_{T_{13x}}^{205} \int_0^{dey} f(x,y)\,dy\,dx$$

$$- \int_{T_{14x}}^{T_{13x}} \int_0^{T_{13y}} f(x,y)\,dy\,dx - \int_{T_{14x}}^{T_{13x}} \int_{T_{13y}}^{fy} f(x,y)\,dy\,dx - \int_{135}^{T_{14x}} \int_0^{cdy} f(x,y)\,dy\,dx - \int_{70}^{135} \int_0^{bcy} f(x,y)\,dy\,dx$$

$$- \int_{50}^{70} \int_0^{aby} f(x,y)\,dy\,dx - \int_0^{50} \int_0^{qay} f(x,y)\,dy\,dx - \int_0^{T_{2x}} \int_{15}^{qpy} f(x,y)\,dy\,dx - \int_0^{T_{2x}} \int_{T_{2y}}^{fy} f(x,y)\,dy\,dx$$

and the centroids of this volume in the xy-plane are at distances $\overline{X}$ and $\overline{Y}$ from the axes (see Figure 7.21) which are given by the following equations.

$$\overline{X} = \frac{1}{V}\left[\begin{array}{l}
\int_{0}^{t}\int_{0}^{fy} x f(x,y)\,dy\,dx - \int_{T_{12x}}^{t}\int_{0}^{fy} x f(x,y)\,dy\,dx - \int_{205}^{T_{12x}}\int_{0}^{efy} x f(x,y)\,dy\,dx \\
-\int_{T_{13x}}^{205}\int_{0}^{dey} x f(x,y)\,dy\,dx - \int_{T_{14x}}^{T_{13x}}\int_{0}^{T_{13y}} x f(x,y)\,dy\,dx - \int_{T_{14x}}^{T_{13x}}\int_{T_{13y}}^{fy} x f(x,y)\,dy\,dx \\
-\int_{135}^{T_{14x}}\int_{0}^{cdy} x f(x,y)\,dy\,dx - \int_{70}^{135}\int_{0}^{bcy} x f(x,y)\,dy\,dx - \int_{50}^{70}\int_{0}^{aby} x f(x,y)\,dy\,dx \\
-\int_{0}^{50}\int_{0}^{qpy} x f(x,y)\,dy\,dx - \int_{0}^{T_{2x}}\int_{15}^{qpy} x f(x,y)\,dy\,dx - \int_{0}^{T_{2x}}\int_{T_{2y}}^{fy} x f(x,y)\,dy\,dx
\end{array}\right]$$

$$\overline{Y} = \frac{1}{V}\left[\begin{array}{l}
\int_{0}^{l}\int_{0}^{fx} y f(x,y)\,dx\,dy - \int_{0}^{T_{12y}}\int_{T_{12x}}^{fx} y f(x,y)\,dx\,dy - \int_{0}^{T_{12y}}\int_{205}^{efx} y f(x,y)\,dx\,dy \\
-\int_{0}^{T_{13y}}\int_{T_{13x}}^{dex} y f(x,y)\,dx\,dy - \int_{0}^{T_{13y}}\int_{T_{13x}}^{T_{14x}} y f(x,y)\,dx\,dy - \int_{T_{13y}}^{T_{14y}}\int_{T_{14x}}^{fx} y f(x,y)\,dx\,dy \\
-\int_{0}^{T_{14y}}\int_{135}^{cdx} y f(x,y)\,dx\,dy - \int_{0}^{15}\int_{70}^{bcx} y f(x,y)\,dx\,dy - \int_{0}^{15}\int_{50}^{abx} y f(x,y)\,dx\,dy \\
-\int_{0}^{15}\int_{0}^{qax} y f(x,y)\,dx\,dy - \int_{15}^{T_{2y}}\int_{0}^{qpx} y f(x,y)\,dx\,dy - \int_{T_{2y}}^{l}\int_{0}^{fx} y f(x,y)\,dx\,dy
\end{array}\right]$$

Application 22 of the tetrahedral compressive stress regime beneath the circumscribing rectangular border of proprietory shaped paver 1 shown in Figure 7.22 can be calculated by using Tables 5.1 and 7.1 and the surface function of the tetrahedral compressive stress through the three points σ_A, l and t.

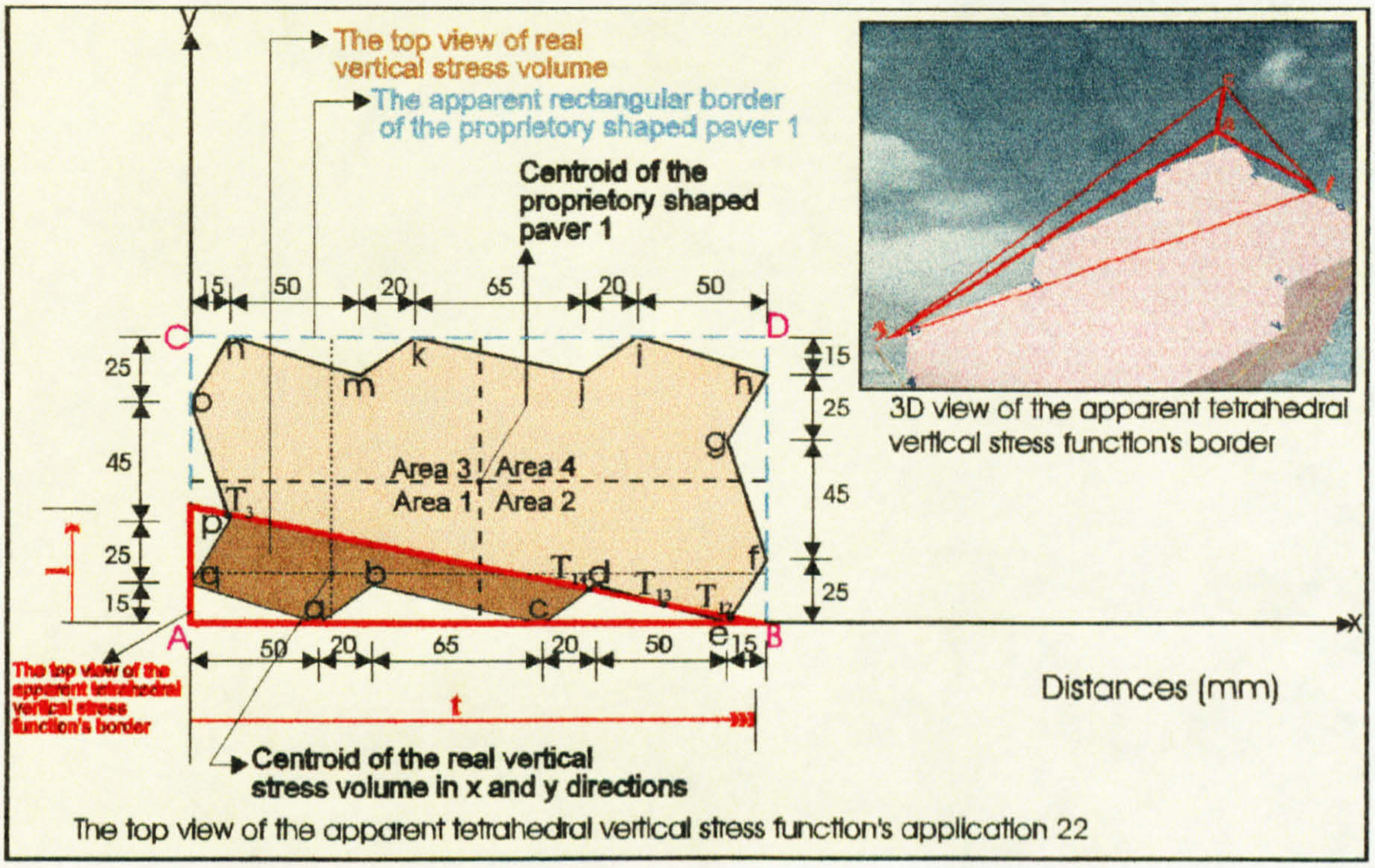

Figure 7.22: Application 22 of the tetrahedral compressive stress distribution beneath the circumscribing rectangular border of proprietory shaped paver 1.

The total volume **V** beneath the surface $f(x,y) = z\ (> 0)$ and above the region in the xy-plane (see Figure 7.22) is:

$$V = \int_0^t \int_0^{fy} f(x,y)\,dy\,dx - \int_{T_{12x}}^t \int_0^{fy} f(x,y)\,dy\,dx - \int_{205}^{T_{12x}} \int_0^{efy} f(x,y)\,dy\,dx - \int_{T_{13x}}^{205} \int_0^{dey} f(x,y)\,dy\,dx$$

$$- \int_{T_{14x}}^{T_{13x}} \int_0^{T_{13y}} f(x,y)\,dy\,dx - \int_{T_{14x}}^{T_{13x}} \int_{T_{13y}}^{fy} f(x,y)\,dy\,dx - \int_{135}^{T_{14x}} \int_0^{cdy} f(x,y)\,dy\,dx - \int_{70}^{135} \int_0^{bcy} f(x,y)\,dy\,dx$$

$$- \int_{50}^{70} \int_0^{aby} f(x,y)\,dy\,dx - \int_0^{50} \int_0^{qay} f(x,y)\,dy\,dx - \int_0^{15} \int_0^{qpy} f(x,y)\,dy\,dx - \int_{T_{3x}}^{15} \int_0^{poy} f(x,y)\,dy\,dx$$

$$- \int_0^{T_{3x}} \int_{40}^{T_{3y}} f(x,y)\,dy\,dx - \int_0^{T_{3x}} \int_{T_{3y}}^{fy} f(x,y)\,dy\,dx$$

and the centroids of this volume in the xy-plane are at distances $\overline{X}$ and $\overline{Y}$ from the axes (see Figure 7.22) which are given by the following equations.

$$\overline{X} = \frac{1}{V}\left[\begin{array}{l}
\int_0^t \int_0^{fy} x f(x,y)\,dy\,dx - \int_{T_{12x}}^{t} \int_0^{fy} x f(x,y)\,dy\,dx - \int_{205}^{T_{12x}} \int_0^{efy} x f(x,y)\,dy\,dx \\
- \int_{T_{13x}}^{205} \int_0^{dey} x f(x,y)\,dy\,dx - \int_{T_{14x}}^{T_{13x}} \int_0^{T_{13y}} x f(x,y)\,dy\,dx - \int_{T_{14x}}^{T_{13x}} \int_{T_{13y}}^{fy} x f(x,y)\,dy\,dx \\
- \int_{135}^{T_{14x}} \int_0^{cdy} x f(x,y)\,dy\,dx - \int_{70}^{135} \int_0^{bcy} x f(x,y)\,dy\,dx - \int_{50}^{70} \int_0^{axby} x f(x,y)\,dy\,dx \\
- \int_0^{50} \int_0^{qay} x f(x,y)\,dy\,dx - \int_0^{15} \int_0^{qpy} x f(x,y)\,dy\,dx - \int_{T_{3x}}^{15} \int_{40}^{pxy} x f(x,y)\,dy\,dx \\
- \int_0^{T_{3x}} \int_{40}^{T_{3y}} x f(x,y)\,dy\,dx - \int_0^{T_{3x}} \int_{T_{3y}}^{fy} x f(x,y)\,dy\,dx
\end{array}\right]$$

$$\overline{Y} = \frac{1}{V}\left[\begin{array}{l}
\int_0^l \int_0^{fx} y f(x,y)\,dx\,dy - \int_0^{T_{12y}} \int_{T_{12x}}^{fx} y f(x,y)\,dx\,dy - \int_0^{T_{12y}} \int_{205}^{efx} y f(x,y)\,dx\,dy \\
- \int_0^{T_{13y}} \int_{T_{13x}}^{dex} y f(x,y)\,dx\,dy - \int_0^{T_{13y}} \int_{T_{13x}}^{T_{13x}} y f(x,y)\,dx\,dy - \int_{T_{13y}}^{T_{14y}} \int_{T_{14x}}^{fx} y f(x,y)\,dx\,dy \\
- \int_0^{T_{14y}} \int_{135}^{cdx} y f(x,y)\,dx\,dy - \int_0^{15} \int_{70}^{bcx} y f(x,y)\,dx\,dy - \int_0^{15} \int_{50}^{abx} y f(x,y)\,dx\,dy \\
- \int_0^{15} \int_0^{qax} y f(x,y)\,dx\,dy - \int_{15}^{40} \int_0^{qpx} y f(x,y)\,dx\,dy - \int_{40}^{T_{3y}} \int_{T_{3x}}^{pax} y f(x,y)\,dx\,dy \\
- \int_{40}^{T_{3y}} \int_0^{T_{3x}} y f(x,y)\,dx\,dy - \int_{T_{3y}}^{l} \int_0^{fx} y f(x,y)\,dx\,dy
\end{array}\right]$$

Application 23 of the tetrahedral compressive stress regime beneath the circumscribing rectangular border of proprietory shaped paver 1 shown in Figure 7.23 can be calculated by using Tables 5.1 and 7.1 and the surface function of the tetrahedral compressive stress through the three points σ_A, **l** and **t**.

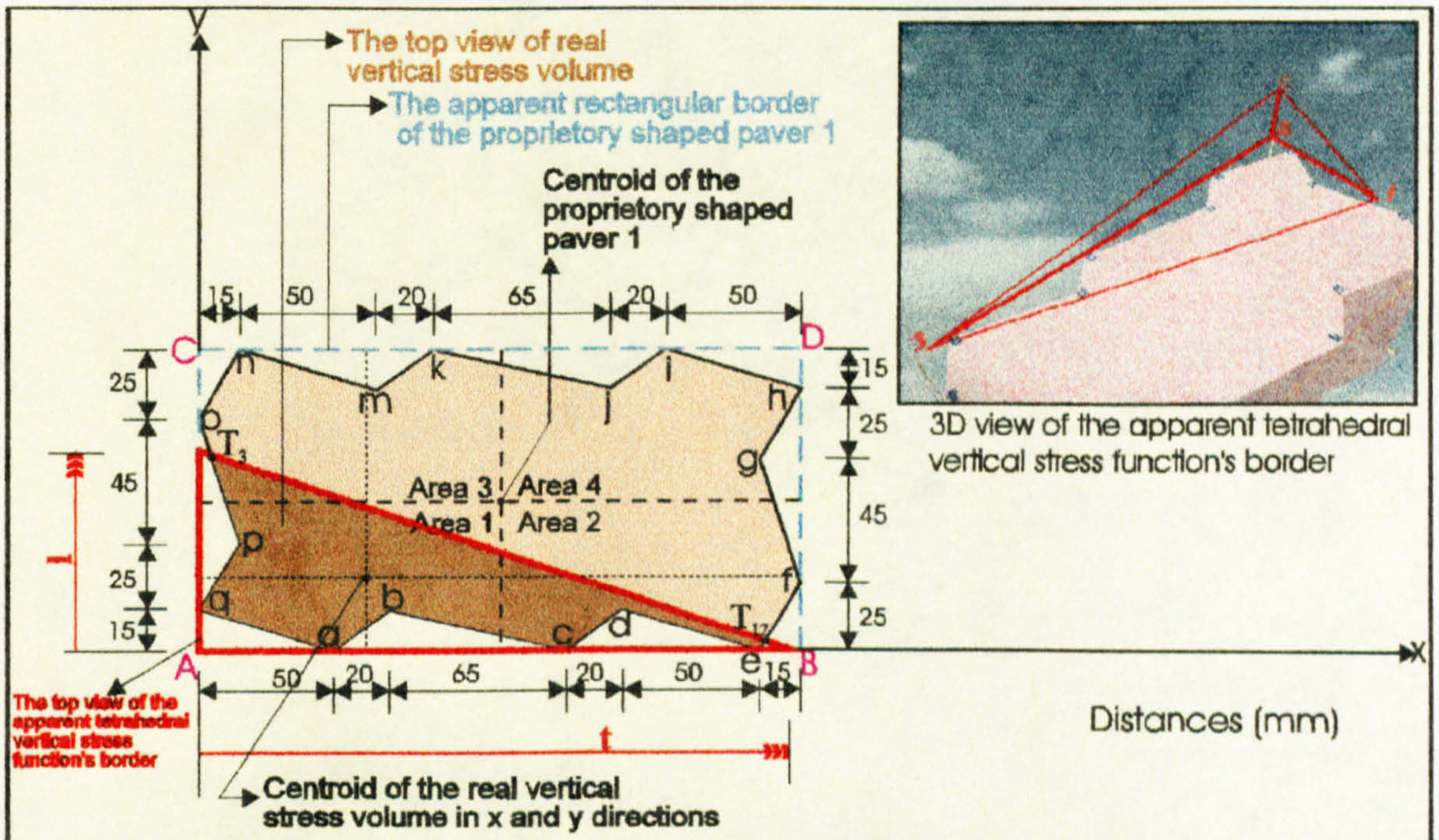

Figure 7.23: Application 23 of the tetrahedral compressive stress distribution beneath the circumscribing rectangular border of proprietory shaped paver 1.

The total volume **V** beneath the surface $f(x,y) = z\ (> 0)$ and above the region in the xy-plane (see Figure 7.23) is:

$$V = \int_0^t \int_0^{fy} f(x,y)\,dy\,dx - \int_{T_{12x}}^{t} \int_0^{fy} f(x,y)\,dy\,dx - \int_{205}^{T_{12x}} \int_0^{efy} f(x,y)\,dy\,dx - \int_{155}^{205} \int_0^{dey} f(x,y)\,dy\,dx$$

$$- \int_{135}^{155} \int_0^{cdy} f(x,y)\,dy\,dx - \int_{70}^{135} \int_0^{bcy} f(x,y)\,dy\,dx - \int_{50}^{70} \int_0^{aby} f(x,y)\,dy\,dx - \int_0^{50} \int_0^{qay} f(x,y)\,dy\,dx$$

$$- \int_0^{15} \int_{135}^{qpy} f(x,y)\,dy\,dx - \int_{T_{3x}}^{15} \int_{40}^{poy} f(x,y)\,dy\,dx - \int_0^{T_{3x}} \int_{40}^{T_{3y}} f(x,y)\,dy\,dx - \int_{T_{3y}}^{T_{3x}} \int_0^{fy} f(x,y)\,dy\,dx$$

and the centroids of this volume in the xy-plane are at distances $\overline{X}$ and $\overline{Y}$ from the axes (see Figure 7.23) which are given by the following equations.

$$\overline{X} = \frac{1}{V}\left[\begin{array}{l}
\int_{0}^{t}\int_{0}^{fy} x f(x,y)\,dy\,dx - \int_{T_{12x}}^{t}\int_{0}^{fy} x f(x,y)\,dy\,dx - \int_{205}^{T_{12x}}\int_{0}^{efy} x f(x,y)\,dy\,dx \\
-\int_{155}^{205}\int_{0}^{dey} x f(x,y)\,dy\,dx - \int_{135}^{155}\int_{0}^{cdy} x f(x,y)\,dy\,dx - \int_{70}^{135}\int_{0}^{bcy} x f(x,y)\,dy\,dx \\
-\int_{50}^{70}\int_{0}^{aby} x f(x,y)\,dy\,dx - \int_{0}^{50}\int_{0}^{qay} x f(x,y)\,dy\,dx - \int_{0}^{15}\int_{15}^{qpy} x f(x,y)\,dy\,dx \\
-\int_{T_{3x}}^{15}\int_{40}^{poy} x f(x,y)\,dy\,dx - \int_{0}^{T_{3x}}\int_{40}^{T_{3y}} x f(x,y)\,dy\,dx - \int_{0}^{T_{3x}}\int_{T_{3y}}^{fy} x f(x,y)\,dy\,dx
\end{array}\right]$$

$$\overline{Y} = \frac{1}{V}\left[\begin{array}{l}
\int_{0}^{l}\int_{0}^{fx} y f(x,y)\,dx\,dy - \int_{0}^{T_{12y}}\int_{T_{12x}}^{fx} y f(x,y)\,dx\,dy - \int_{0}^{T_{12y}}\int_{205}^{efx} y f(x,y)\,dx\,dy \\
-\int_{0}^{15}\int_{155}^{dex} y f(x,y)\,dx\,dy - \int_{0}^{15}\int_{135}^{cdx} y f(x,y)\,dx\,dy - \int_{0}^{15}\int_{70}^{bcx} y f(x,y)\,dx\,dy \\
-\int_{0}^{15}\int_{50}^{abx} y f(x,y)\,dx\,dy - \int_{0}^{15}\int_{0}^{qax} y f(x,y)\,dx\,dy - \int_{15}^{40}\int_{0}^{qpx} y f(x,y)\,dx\,dy \\
-\int_{40}^{T_{3y}}\int_{T_{3x}}^{pox} y f(x,y)\,dx\,dy - \int_{40}^{T_{3y}}\int_{0}^{T_{3x}} y f(x,y)\,dx\,dy - \int_{T_{3y}}^{l}\int_{0}^{fx} y f(x,y)\,dx\,dy
\end{array}\right]$$

Application 24 of the tetrahedral compressive stress regime beneath the circumscribing rectangular border of proprietory shaped paver 1 shown in Figure 7.24 can be calculated by using Tables 5.1 and 7.1 and the surface function of the tetrahedral compressive stress through the three points σ_A, l and t.

The total volume V beneath the surface $f(x,y) = z\ (> 0)$ and above the region in the xy-plane (see Figure 7.24) is:

$$V = \int_0^t \int_0^{fy} f(x,y)\,dy\,dx - \int_{T_{12x}}^t \int_0^{fy} f(x,y)\,dy\,dx - \int_{205}^{T_{12x}} \int_0^{efy} f(x,y)\,dy\,dx - \int_{155}^{205} \int_0^{dey} f(x,y)\,dy\,dx$$
$$- \int_{135}^{155} \int_0^{cdy} f(x,y)\,dy\,dx - \int_{70}^{135} \int_0^{bcy} f(x,y)\,dy\,dx - \int_{50}^{70} \int_0^{aby} f(x,y)\,dy\,dx - \int_0^{50} \int_0^{qay} f(x,y)\,dy\,dx$$
$$- \int_0^{15} \int_{15}^{qpy} f(x,y)\,dy\,dx - \int_0^{40} \int_{15}^{poy} f(x,y)\,dy\,dx - \int_0^{85} \int_{T_{4x}}^{ony} f(x,y)\,dy\,dx - \int_0^{T_{4y}} \int_{T_{4x}}^{fy} f(x,y)\,dy\,dx$$

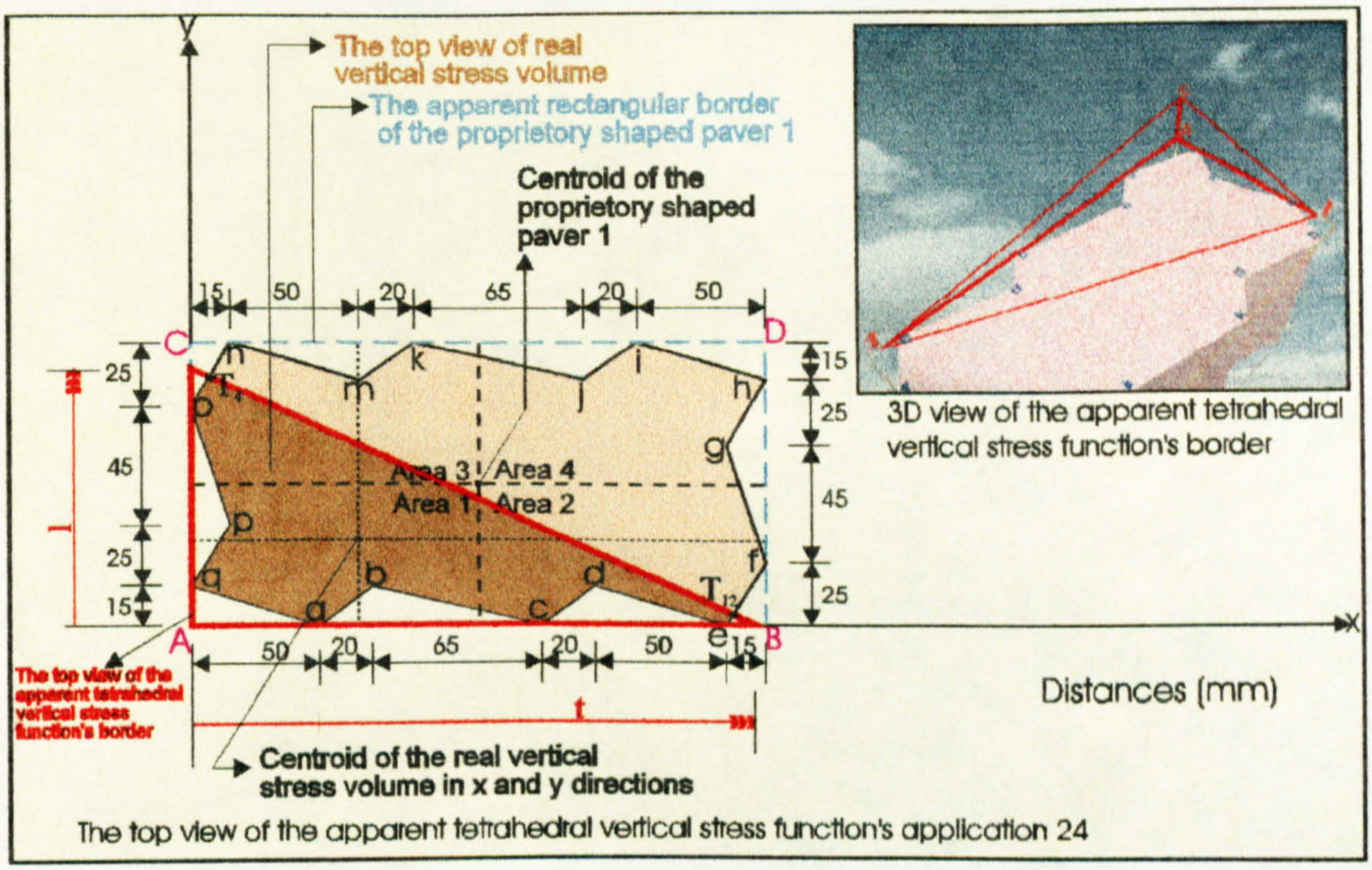

Figure 7.24: Application 24 of the tetrahedral compressive stress distribution beneath the circumscribing rectangular border of proprietory shaped paver 1.

and the centroids of this volume in the xy-plane are at distances $\overline{X}$ and $\overline{Y}$ from the axes (see Figure 7.24) which are given by the following equations.

$$\overline{X} = \frac{1}{V}\left[\int_0^t \int_0^{fy} x f(x,y)\,dy\,dx - \int_{T_{12x}}^t \int_0^{fy} x f(x,y)\,dy\,dx - \int_{205}^{T_{12x}} \int_0^{efy} x f(x,y)\,dy\,dx\right.$$
$$\left. - \int_{155}^{205} \int_0^{dey} x f(x,y)\,dy\,dx - \int_{135}^{155} \int_0^{cdy} x f(x,y)\,dy\,dx - \int_{70}^{135} \int_0^{bcy} x f(x,y)\,dy\,dx\right.$$

$$-\int_{50}^{70}\int_{0}^{aby} xf(x,y)\,dy\,dx-\int_{0}^{50}\int_{0}^{qay} xf(x,y)\,dy\,dx-\int_{0}^{15}\int_{15}^{qpy} xf(x,y)\,dy\,dx$$

$$-\int_{0}^{15}\int_{40}^{poy} xf(x,y)\,dy\,dx-\int_{0}^{T_{4x}}\int_{85}^{ony} xf(x,y)\,dy\,dx-\int_{0}^{T_{4x}}\int_{T_{4y}}^{fy} xf(x,y)\,dy\,dx\Bigg]$$

$$\overline{Y}=\frac{1}{V}\Bigg[\int_{0}^{l}\int_{0}^{fx} yf(x,y)\,dx\,dy-\int_{0}^{T_{12y}}\int_{T_{12x}}^{fx} yf(x,y)\,dx\,dy-\int_{0}^{T_{12y}}\int_{205}^{efx} yf(x,y)\,dx\,dy$$

$$-\int_{0}^{15}\int_{155}^{dex} yf(x,y)\,dx\,dy-\int_{0}^{15}\int_{135}^{cdx} yf(x,y)\,dx\,dy-\int_{0}^{15}\int_{70}^{bcx} yf(x,y)\,dx\,dy$$

$$-\int_{0}^{15}\int_{50}^{abx} yf(x,y)\,dx\,dy-\int_{0}^{15}\int_{0}^{qax} yf(x,y)\,dx\,dy-\int_{15}^{40}\int_{0}^{qpx} yf(x,y)\,dx\,dy$$

$$-\int_{40}^{85}\int_{0}^{pox} yf(x,y)\,dx\,dy-\int_{85}^{T_{4y}}\int_{0}^{onx} yf(x,y)\,dx\,dy-\int_{T_{4y}}^{l}\int_{0}^{fx} yf(x,y)\,dx\,d$$

7.2.2 Short-pentahedral compressive stress regimes beneath the circumscribing rectangular border for proprietory shaped paver 1

The intersection points which are between the line functions bounding shaped paver 1 shown in Table 5.1 and the lines (which bound the bottom surface of the short-pentahedral stress in the xy-plane) have the functions $fy = u\left(1-\frac{x}{b}\right)$, $fx = b\left(1-\frac{y}{u}\right)$ in the x and y axes can be calculated mathematically. Table 7.2 shows the intersection points' formulae and the points are illustrated in Figures 7.25 to 7.52.

The surface function of the short-pentahedral compressive stress block beneath the circumscribing rectangular border shown in Figure 7.25 through the three points σ_A, b and u is given by:

$$\begin{vmatrix} x & y & z & 1 \\ b & 0 & 0 & 1 \\ 0 & u & 0 & 1 \\ 0 & 0 & \sigma_A & 1 \end{vmatrix} = 0 \Rightarrow f(x,y) = z = \sigma_A\left(1 - \frac{x}{b} - \frac{y}{u}\right)$$

The following equalities can be obtained from the geometry of the short-pentahedral compressive stress block (see Figure 7.25).

$$a = b\left(\frac{\sigma_C}{\sigma_A}\right) \quad \text{and} \quad u = \frac{110\sigma_A}{\sigma_A - \sigma_C} \Rightarrow \sigma_C = \frac{\sigma_A(u-110)}{u}$$

therefore,

$$a = \frac{b(u-110)}{u}$$

$S_{1x} = \frac{b\,(u - 15)}{u - 0.3\,b}$ *and* $S_{1y} = \frac{u\,(b - 50)}{b - 3.\bar{3}\,u}$	$S_{2x} = \frac{0.6\,b\,(u - 15)}{b + 0.6\,u}$ *and* $S_{2y} = \frac{u\,(b + 9)}{b + 0.6\,u}$
$S_{3x} = \frac{b\,(u - 85)}{u - 3\,b}$ *and* $S_{3y} = \frac{u\,(b - 28.\bar{3})}{b - 0.\bar{3}\,u}$	$S_{4x} = \frac{b\,(u - 85)}{u + 1.\bar{6}\,b}$ *and* $S_{4y} = \frac{u\,(b + 51)}{b + 0.6\,u}$
$S_{5x} = \frac{b\,(u - 114.5)}{u - 0.3\,b}$ *and* $S_{5y} = \frac{u\,(b - 381.\bar{6})}{b - 3.\bar{3}\,u}$	$S_{6x} = \frac{b\,(u - 46.25)}{u + 0.75\,b}$ *and* $S_{6y} = \frac{u\,(b + 61.\bar{6})}{b + 1.\bar{3}\,u}$
$S_{7x} = \frac{b\,(u - 129.615)}{u - 0.2301\,b}$ *and* $S_{7y} = \frac{u\,(b - 561.\bar{6})}{b - 4.\bar{3}\,u}$	$S_{8x} = \frac{b\,(u + 17.5)}{u + 0.75\,b}$ *and* $S_{8y} = \frac{u\,(b - 23.\bar{3})}{b + 1.\bar{3}\,u}$
$S_{9x} = \frac{b\,(u - 161)}{u - 0.3\,b}$ *and* $S_{9y} = \frac{u\,(b - 536.\bar{6})}{b - 3.\bar{3}\,u}$	$S_{10x} = \frac{b\,(u + 271.\bar{6})}{u + 1.\bar{6}\,b}$ *and* $S_{10y} = \frac{u\,(b - 163)}{b + 0.6\,u}$
$S_{11x} = \frac{b\,(u - 685)}{u - 3\,b}$ *and* $S_{11y} = \frac{u\,(b - 228.\bar{3})}{b - 0.\bar{3}\,u}$	$S_{12x} = \frac{b\,(u + 341.\bar{6})}{u + 1.\bar{6}\,b}$ *and* $S_{12y} = \frac{u\,(b - 205)}{b + 0.6\,u}$
$S_{13x} = \frac{b\,(u - 61.5)}{u - 0.3\,b}$ *and* $S_{13y} = \frac{u\,(b - 205)}{b - 3.\bar{3}\,u}$	$S_{14x} = \frac{b\,(u + 101.25)}{u + 0.75\,b}$ *and* $S_{14y} = \frac{u\,(b - 135)}{b + 1.\bar{3}\,u}$
$S_{15x} = \frac{b\,(u - 31.154)}{u - 0.23\,b}$ *and* $S_{15y} = \frac{u\,(b - 135)}{b - 4.\bar{3}\,u}$	$S_{16x} = \frac{b\,(u + 37.5)}{u + 0.75\,b}$ *and* $S_{16y} = \frac{u\,(b - 50)}{b + 1.\bar{3}\,u}$

Table 7.2: The intersection points between the line which forms the short-pentahedral stress block in the xy-plane and the line boundary functions of proprietory shaped paver 1 (b and u are the lengths of the stress block along the x and y axes respectively as illustrated in Figure 7.25).

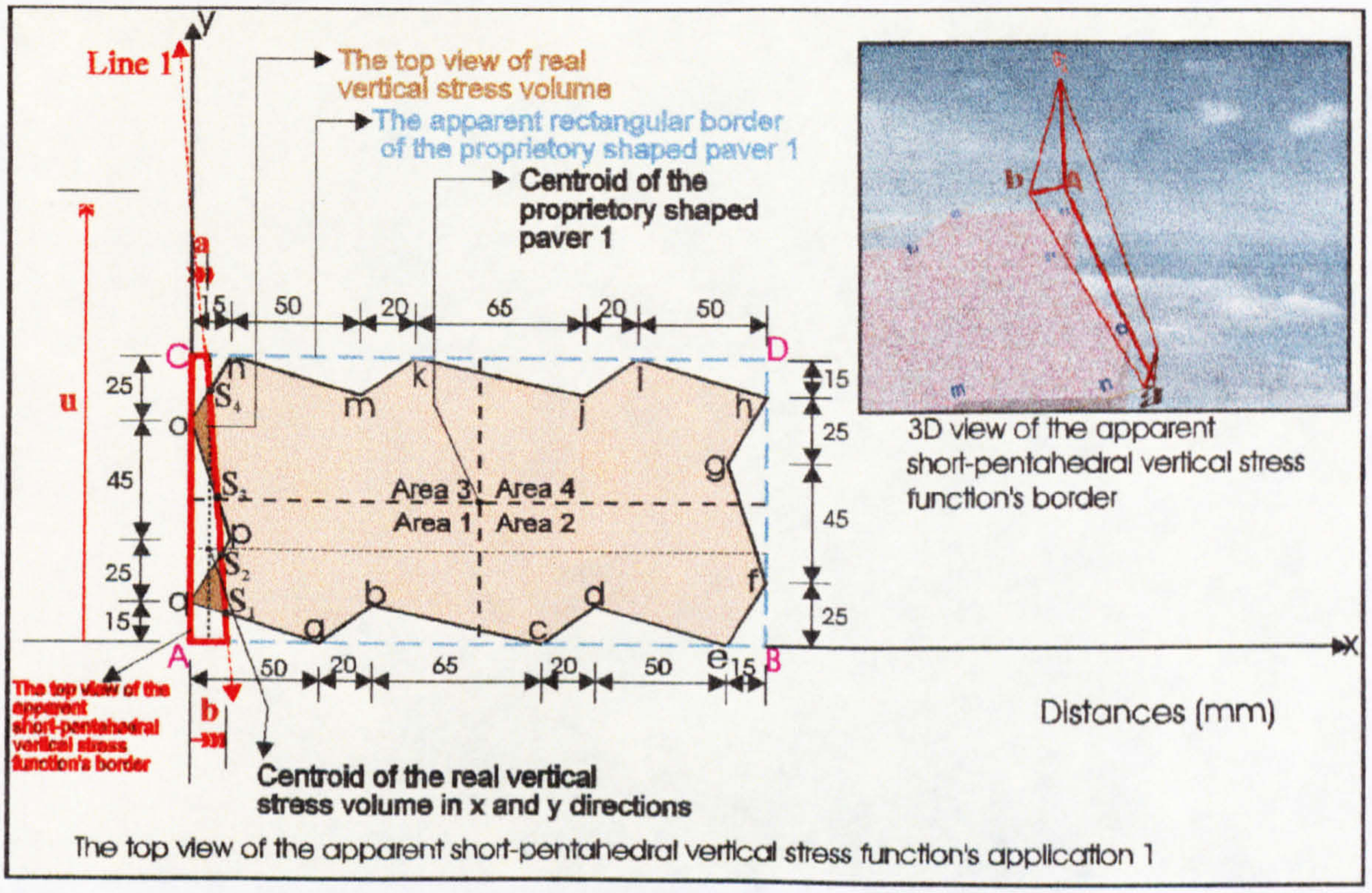

Figure 7.25: Application 1 of the short-pentahedral compressive stress distribution beneath the circumscribing rectangular border of proprietory shaped paver 1.

The first application of the short-pentahedral compressive stress regime beneath the circumscribing rectangular border of proprietory shaped paver 1 shown in Figure 7.25 can be calculated by using the data in Tables 5.1 and 7.2. The first two letters of each boundary line function in Table 5.1 for proprietory shaped paver 1 charecterise the corner names can be seen in Figure 7.25 (example: **ony** symbolises the boundary line function of proprietory shaped paver 1 in the **y** axis between corner **o** and **n**). The line functions which define the boundary of the short-pentahedral stress block in the xy-plane (see Figure 7.25) are of the form $fy = u\left(1-\frac{x}{b}\right)$, $fx = b\left(1-\frac{y}{u}\right)$.

The following actual total volume **V** beneath the surface $f(x,y) = z\ (>0)$ and above the region in the xy-plane (see Figure 7.25) is calculated by subtracting the negative volume generated by the dentations of the shaped paver from the short-pentahedral volume beneath circumscribing rectangular boundary of the paver.

$$V = \int_{0}^{a}\int_{0}^{110} f(x,y)\,dy\,dx + \int_{a}^{b}\int_{0}^{fy} f(x,y)\,dy\,dx - \int_{0}^{a}\int_{S_{4y}}^{110} f(x,y)\,dy\,dx - \int_{a}^{S_{4x}}\int_{S_{4y}}^{fy} f(x,y)\,dy\,dx$$

$$- \int_{0}^{S_{4x}}\int_{85}^{ony} f(x,y)\,dy\,dx - \int_{0}^{S_{3x}}\int_{S_{3y}}^{poy} f(x,y)\,dy\,dx - \int_{0}^{S_{3x}}\int_{S_{2y}}^{S_{3y}} f(x,y)\,dy\,dx - \int_{S_{3x}}^{S_{2x}}\int_{S_{2y}}^{fy} f(x,y)\,dy\,dx$$

$$- \int_{0}^{S_{2x}}\int_{15}^{qpy} f(x,y)\,dy\,dx - \int_{0}^{S_{1x}}\int_{0}^{S_{1y}} f(x,y)\,dy\,dx - \int_{0}^{S_{1x}}\int_{S_{1y}}^{qay} f(x,y)\,dy\,dx - \int_{S_{1x}}^{b}\int_{0}^{fy} f(x,y)\,dy\,dx$$

and the centroids of this volume in the xy-plane are at distances $\overline{X}$ and $\overline{Y}$ from the axes (see Figure 7.25) which are given by the following equations.

$$\overline{X} = \frac{1}{V}\left[\begin{array}{l} \displaystyle\int_{0}^{a}\int_{0}^{110} x f(x,y)\,dy\,dx + \int_{a}^{b}\int_{0}^{fy} x f(x,y)\,dy\,dx - \int_{0}^{a}\int_{S_{4y}}^{110} x f(x,y)\,dy\,dx - \int_{a}^{S_{4x}}\int_{S_{4y}}^{fy} x f(x,y)\,dy\,dx \\ \displaystyle - \int_{0}^{S_{4x}}\int_{85}^{ony} x f(x,y)\,dy\,dx - \int_{0}^{S_{3x}}\int_{S_{3y}}^{poy} x f(x,y)\,dy\,dx - \int_{0}^{S_{3x}}\int_{S_{2y}}^{S_{3y}} x f(x,y)\,dy\,dx - \int_{S_{3x}}^{S_{2x}}\int_{S_{2y}}^{fy} x f(x,y)\,dy\,dx \\ \displaystyle - \int_{0}^{S_{2x}}\int_{15}^{qpy} x f(x,y)\,dy\,dx - \int_{0}^{S_{1x}}\int_{0}^{S_{1y}} x f(x,y)\,dy\,dx - \int_{0}^{S_{1x}}\int_{S_{1y}}^{qay} x f(x,y)\,dy\,dx - \int_{S_{1x}}^{b}\int_{0}^{fy} x f(x,y)\,dy\,dx \end{array}\right]$$

$$\overline{Y} = \frac{1}{V}\left[\begin{array}{l} \displaystyle\int_{0}^{110}\int_{0}^{a} y f(x,y)\,dx\,dy + \int_{0}^{110}\int_{a}^{fx} y f(x,y)\,dx\,dy - \int_{S_{4y}}^{110}\int_{0}^{a} y f(x,y)\,dx\,dy - \int_{S_{4y}}^{110}\int_{a}^{fx} y f(x,y)\,dx\,dy \\ \displaystyle - \int_{85}^{S_{4y}}\int_{0}^{onx} y f(x,y)\,dx\,dy - \int_{S_{3y}}^{85}\int_{0}^{pox} y f(x,y)\,dx\,dy - \int_{S_{2y}}^{S_{3y}}\int_{0}^{S_{3x}} y f(x,y)\,dx\,dy - \int_{S_{2y}}^{S_{3y}}\int_{S_{3x}}^{fx} y f(x,y)\,dx\,dy \\ \displaystyle - \int_{15}^{S_{2y}}\int_{0}^{qpx} y f(x,y)\,dx\,dy - \int_{0}^{S_{1y}}\int_{0}^{S_{1x}} y f(x,y)\,dx\,dy - \int_{S_{1y}}^{15}\int_{0}^{qax} y f(x,y)\,dx\,dy - \int_{0}^{S_{1y}}\int_{S_{1x}}^{fx} y f(x,y)\,dx\,dy \end{array}\right]$$

Application 2 of the short-pentahedral compressive stress regime beneath the circumscribing rectangular border of proprietory shaped paver 1 shown in Figure 7.26 can be calculated by using Tables 5.1 and 7.2 and the surface function of the short-pentahedral compressive stress through the three points σ_A, **b** and **u**.

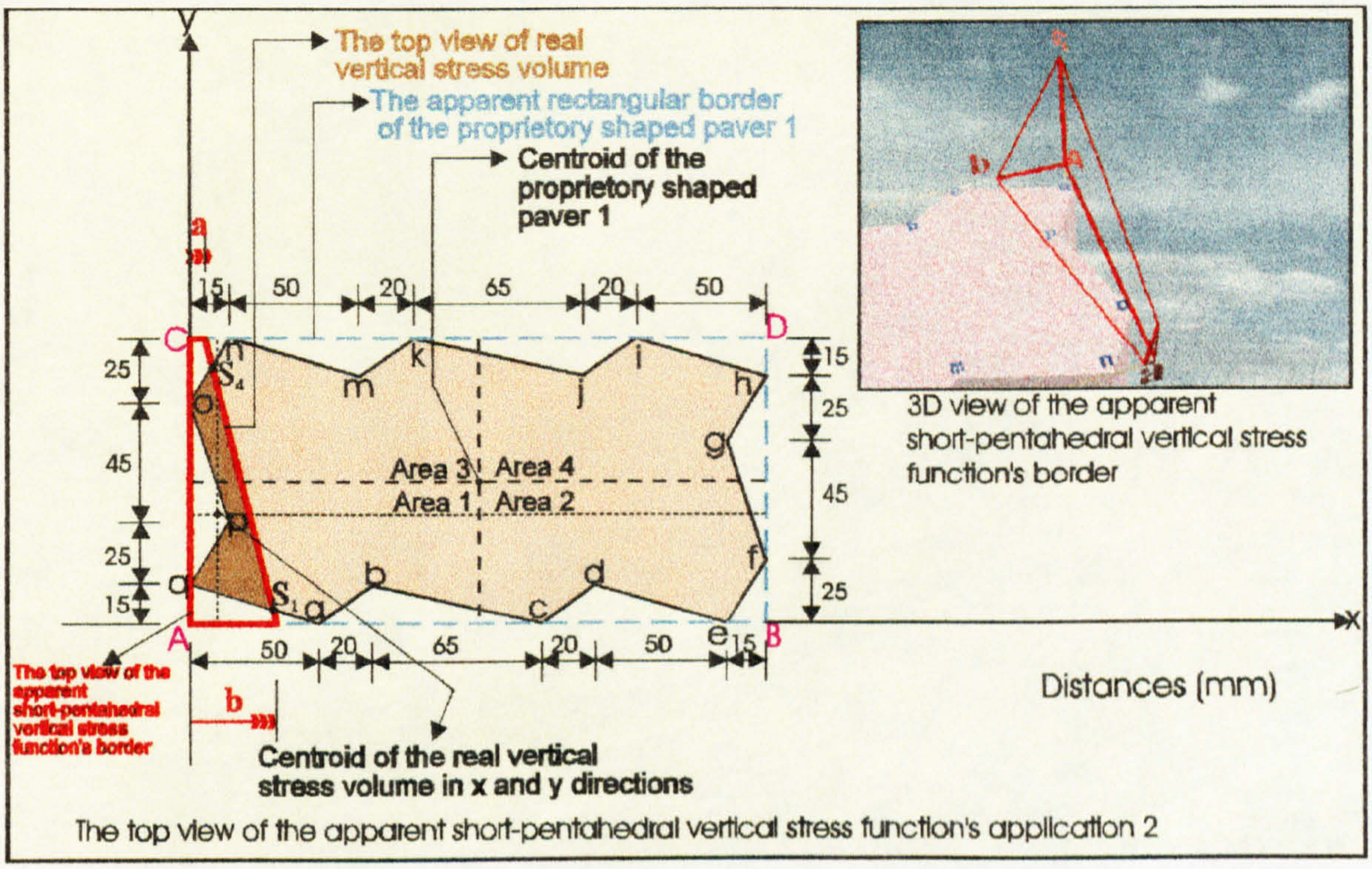

Figure 7.26: Application 2 of the short-pentahedral compressive stress distribution beneath the circumscribing rectangular border of proprietory shaped paver 1.

The total volume **V** beneath the surface $f(x,y) = z\ (> 0)$ and above the region in the xy-plane (see Figure 7.26) is:

$$V = \int_0^a \int_0^{110} f(x,y)\,dy\,dx + \int_a^{b} \int_0^{fy} f(x,y)\,dy\,dx - \int_0^{a} \int_{S_{4y}}^{110} f(x,y)\,dy\,dx - \int_a^{S_{4x}} \int_{S_{4y}}^{fy} f(x,y)\,dy\,dx$$
$$- \int_0^{S_{4x}} \int_{85}^{ony} f(x,y)\,dy\,dx - \int_0^{40} \int_{0}^{15poy} f(x,y)\,dy\,dx - \int_0^{15} \int_{0}^{15qpy} f(x,y)\,dy\,dx - \int_0^{S_{1x}} \int_{0}^{S_{1y}} f(x,y)\,dy\,dx$$
$$- \int_0^{S_{1x}} \int_{0}^{qay} f(x,y)\,dy\,dx - \int_{S_{1x}}^{b} \int_{0}^{fy} f(x,y)\,dy\,dx$$

and the centroids of this volume in the xy-plane are at distances $\overline{X}$ and $\overline{Y}$ from the axes (see Figure 7.26) which are given by the following equations.

$$\overline{X} = \frac{1}{V}\left[\begin{array}{l} \int_{0}^{a}\int_{0}^{110} x f(x,y)\,dy\,dx + \int_{a}^{b}\int_{0}^{fy} x f(x,y)\,dy\,dx - \int_{0}^{a}\int_{S_{4y}}^{110} x f(x,y)\,dy\,dx - \int_{a}^{S_{4x}}\int_{S_{4y}}^{fy} x f(x,y)\,dy\,dx \\ - \int_{0}^{S_{4x}}\int_{85}^{ony} x f(x,y)\,dy\,dx - \int_{0}^{40}\int_{0}^{15poy} x f(x,y)\,dy\,dx - \int_{0}^{15}\int_{0}^{15qpy} x f(x,y)\,dy\,dx - \int_{0}^{S_{1x}}\int_{0}^{S_{1y}} x f(x,y)\,dy\,dx \\ - \int_{0}^{S_{1x}}\int_{S_{1y}}^{qay} x f(x,y)\,dy\,dx - \int_{S_{1x}}^{b}\int_{0}^{fy} x f(x,y)\,dy\,dx \end{array}\right]$$

$$\overline{Y} = \frac{1}{V}\left[\begin{array}{l} \int_{0}^{110}\int_{0}^{a} y f(x,y)\,dx\,dy + \int_{0}^{110}\int_{a}^{fx} y f(x,y)\,dx\,dy - \int_{S_{4y}}^{110}\int_{0}^{a} y f(x,y)\,dx\,dy - \int_{S_{4y}}^{110}\int_{a}^{fx} y f(x,y)\,dx\,dy \\ - \int_{85}^{S_{4y}}\int_{0}^{onx} y f(x,y)\,dx\,dy - \int_{40}^{85}\int_{0}^{pox} y f(x,y)\,dx\,dy - \int_{15}^{40}\int_{0}^{qpx} y f(x,y)\,dx\,dy - \int_{0}^{S_{1y}}\int_{0}^{S_{1x}} y f(x,y)\,dx\,dy \\ - \int_{S_{1y}}^{15}\int_{0}^{qax} y f(x,y)\,dx\,dy - \int_{0}^{S_{1y}}\int_{S_{1x}}^{fx} y f(x,y)\,dx\,dy \end{array}\right]$$

Application 3 of the short-pentahedral compressive stress regime beneath the circumscribing rectangular border of proprietory shaped paver 1 shown in Figure 7.27 can be calculated by using Tables 5.1 and 7.2 and the surface function of the short-pentahedral compressive stress through the three points σ_A, **b** and **u**.

The total volume **V** beneath the surface $f(x,y) = z\ (> 0)$ and above the region in the xy-plane (see Figure 7.27) is:

$$V = \int_{0}^{a}\int_{0}^{110} f(x,y)\,dy\,dx + \int_{a}^{b}\int_{0}^{fy} f(x,y)\,dy\,dx - \int_{0}^{a}\int_{S_{4y}}^{110} f(x,y)\,dy\,dx - \int_{a}^{S_{4x}}\int_{S_{4y}}^{fy} f(x,y)\,dy\,dx$$
$$- \int_{0}^{S_{4x}}\int_{85}^{ony} f(x,y)\,dy\,dx - \int_{0}^{15}\int_{15}^{qpy} f(x,y)\,dy\,dx - \int_{0}^{40}\int_{0}^{15poy} f(x,y)\,dy\,dx - \int_{0}^{50}\int_{0}^{xqay} f(x,y)\,dy\,dx$$
$$- \int_{50}^{S_{16x}}\int_{0}^{aby} f(x,y)\,dy\,dx - \int_{S_{16x}}^{b}\int_{0}^{fy} f(x,y)\,dy\,dx$$

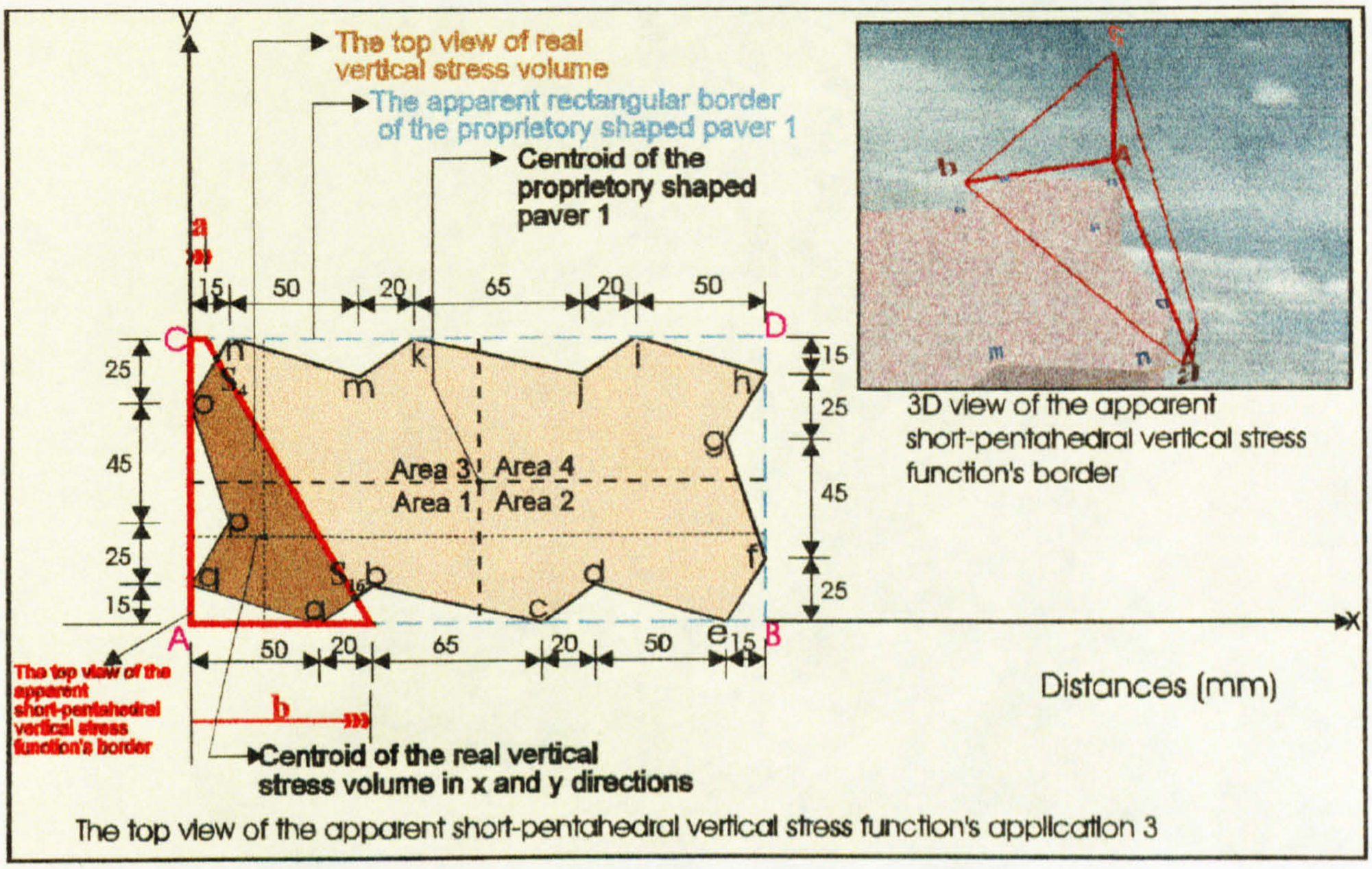

Figure 7.27: Application 3 of the short-pentahedral compressive stress distribution beneath the circumscribing rectangular border of proprietory shaped paver 1.

and the centroids of this volume in the xy-plane are at distances $\overline{X}$ and $\overline{Y}$ from the axes (see Figure 7.27) which are given by the following equations.

$$\overline{X} = \frac{1}{V}\left[\int_0^a\int_0^{110} x f(x,y)\,dy\,dx + \int_a^b\int_0^{fy} x f(x,y)\,dy\,dx - \int_0^a\int_{S_{4y}}^{110} x f(x,y)\,dy\,dx - \int_a^{S_{4x}}\int_{S_{4y}}^{fy} x f(x,y)\,dy\,dx \right.$$
$$- \int_0^{S_{4x}}\int_{85}^{ony} x f(x,y)\,dy\,dx - \int_0^{15}\int_{15}^{qpy} x f(x,y)\,dy\,dx - \int_0^{15}\int_{40}^{poy} x f(x,y)\,dy\,dx - \int_0^{50}\int_0^{qay} x f(x,y)\,dy\,dx$$
$$\left. - \int_{50}^{S_{16x}}\int_0^{aby} x f(x,y)\,dy\,dx - \int_{S_{16x}}^{b}\int_0^{fy} x f(x,y)\,dy\,dx \right]$$

$$\overline{Y} = \frac{1}{V}\left[\int_0^{110}\int_0^{a} y f(x,y)\,dx\,dy + \int_0^{110}\int_a^{fx} y f(x,y)\,dx\,dy - \int_{S_{4y}}^{110}\int_0^{a} y f(x,y)\,dx\,dy - \int_{S_{4y}}^{110}\int_a^{fx} y f(x,y)\,dx\,dy \right.$$
$$\left. - \int_{85}^{S_{4y}}\int_0^{onx} y f(x,y)\,dx\,dy - \int_{40}^{85}\int_0^{pox} y f(x,y)\,dx\,dy - \int_{15}^{40}\int_0^{qpx} y f(x,y)\,dx\,dy - \int_0^{15}\int_0^{qax} y f(x,y)\,dx\,dy \right]$$

$$\left. - \int_{0}^{S_{16y}} \int_{50}^{abx} y f(x,y)\, dx\, dy - \int_{0}^{S_{16y}} \int_{S_{16x}}^{fx} y f(x,y)\, dx\, dy \right]$$

Application 4 of the short-pentahedral compressive stress regime beneath the circumscribing rectangular border of proprietory shaped paver 1 shown in Figure 7.28 can be calculated by using Tables 5.1 and 7.2 and the surface function of the short-pentahedral compressive stress through the three points σ_A, **b** and **u**.

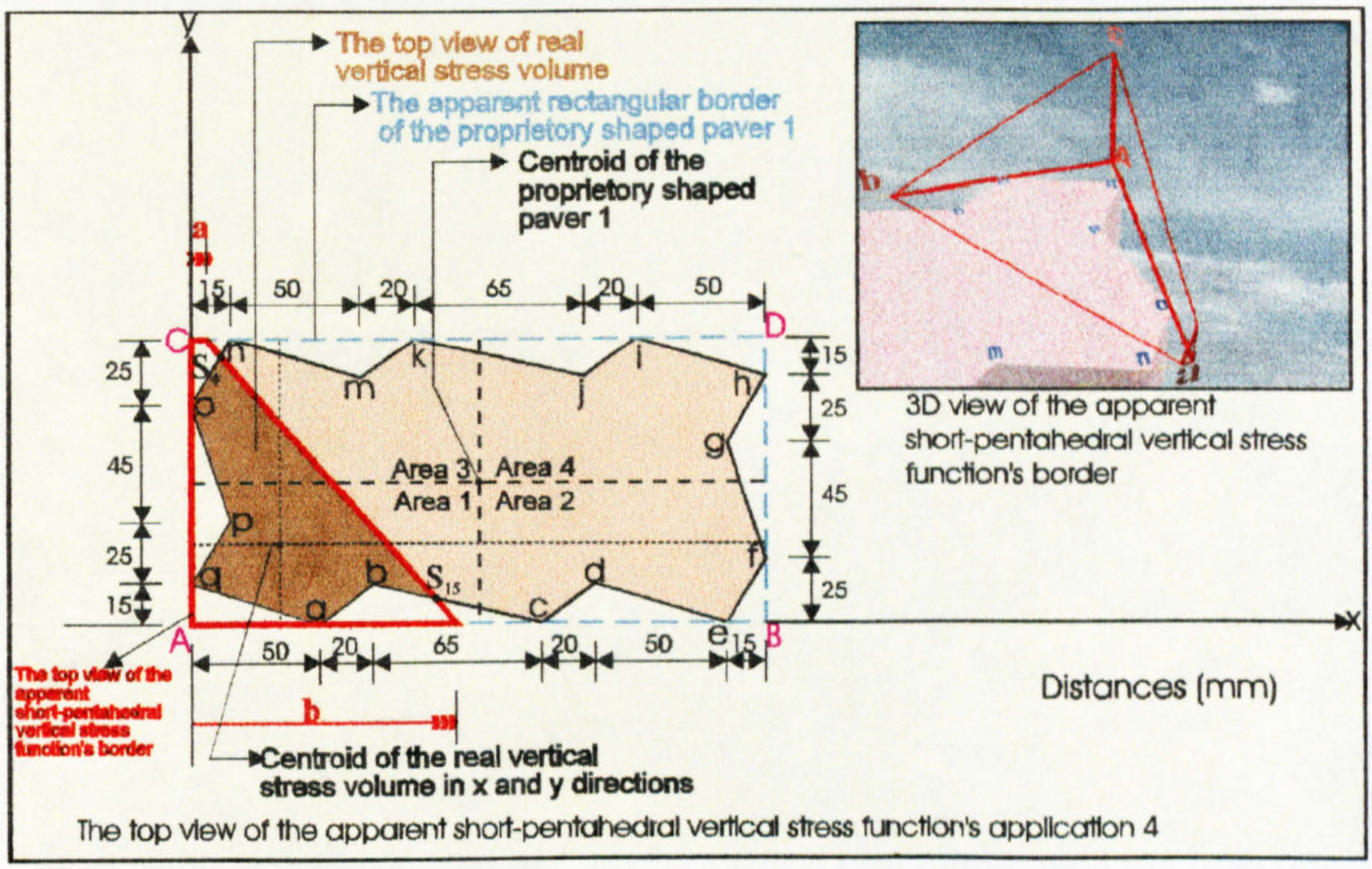

Figure 7.28: Application 4 of the short-pentahedral compressive stress distribution beneath the circumscribing rectangular border of proprietory shaped paver 1.

The total volume **V** beneath the surface $f(x,y) = z\ (> 0)$ and above the region in the xy-plane (see Figure 7.28) is:

$$V = \int_{0}^{a} \int_{0}^{110} f(x,y)\, dy\, dx + \int_{a}^{b} \int_{0}^{fy} f(x,y)\, dy\, dx - \int_{0}^{a} \int_{S_{4y}}^{110} f(x,y)\, dy\, dx - \int_{a}^{S_{4x}} \int_{S_{4y}}^{fy} f(x,y)\, dy\, dx$$

$$-\int_{0}^{S_{4x}}\int_{85}^{ony} f(x,y)\,dy\,dx-\int_{0}^{15}\int_{15}^{qpy} f(x,y)\,dy\,dx-\int_{0}^{15}\int_{40}^{poy} f(x,y)\,dy\,dx-\int_{0}^{50}\int_{0}^{qay} f(x,y)\,dy\,dx$$

$$-\int_{50}^{70}\int_{0}^{aby} f(x,y)\,dy\,dx-\int_{70}^{S_{15x}}\int_{0}^{S_{15y}} f(x,y)\,dy\,dx-\int_{70}^{S_{15x}}\int_{S_{15y}}^{bcy} f(x,y)\,dy\,dx-\int_{S_{15x}}^{b}\int_{0}^{fy} f(x,y)\,dy\,dx$$

and the centroids of this volume in the xy-plane are at distances $\overline{X}$ and $\overline{Y}$ from the axes (see Figure 7.28) which are given by the following equations.

$$\overline{X}=\frac{1}{V}\left[\begin{array}{l}\displaystyle\int_{0}^{a}\int_{0}^{110} x f(x,y)\,dy\,dx+\int_{a}^{b}\int_{0}^{fy} x f(x,y)\,dy\,dx-\int_{0}^{a}\int_{S_{4y}}^{110} x f(x,y)\,dy\,dx-\int_{a}^{S_{4x}}\int_{S_{4y}}^{fy} x f(x,y)\,dy\,dx\\ \displaystyle-\int_{0}^{S_{4x}}\int_{85}^{ony} x f(x,y)\,dy\,dx-\int_{0}^{15}\int_{15}^{qpy} x f(x,y)\,dy\,dx-\int_{0}^{15}\int_{40}^{poy} x f(x,y)\,dy\,dx-\int_{0}^{50}\int_{0}^{qay} x f(x,y)\,dy\,dx\\ \displaystyle-\int_{50}^{70}\int_{0}^{aby} x f(x,y)\,dy\,dx-\int_{70}^{S_{15x}}\int_{0}^{S_{15y}} x f(x,y)\,dy\,dx-\int_{70}^{S_{15x}}\int_{S_{15y}}^{bcy} x f(x,y)\,dy\,dx-\int_{S_{15x}}^{b}\int_{0}^{fy} x f(x,y)\,dy\,dx\end{array}\right]$$

$$\overline{Y}=\frac{1}{V}\left[\begin{array}{l}\displaystyle\int_{0}^{110}\int_{0}^{a} y f(x,y)\,dx\,dy+\int_{0}^{110}\int_{a}^{fx} y f(x,y)\,dx\,dy-\int_{S_{4y}}^{110}\int_{0}^{a} y f(x,y)\,dx\,dy-\int_{S_{4y}}^{110}\int_{a}^{fx} y f(x,y)\,dx\,dy\\ \displaystyle-\int_{85}^{S_{4y}}\int_{0}^{onx} y f(x,y)\,dx\,dy-\int_{40}^{85}\int_{0}^{pox} y f(x,y)\,dx\,dy-\int_{15}^{40}\int_{0}^{qpx} y f(x,y)\,dx\,dy-\int_{0}^{15}\int_{0}^{qax} y f(x,y)\,dx\,dy\\ \displaystyle-\int_{0}^{15}\int_{50}^{abx} y f(x,y)\,dx\,dy-\int_{0}^{S_{15y}}\int_{70}^{S_{15x}} y f(x,y)\,dx\,dy-\int_{S_{15y}}^{15}\int_{70}^{bcx} y f(x,y)\,dx\,dy-\int_{0}^{S_{15y}}\int_{S_{15x}}^{fx} y f(x,y)\,dx\,dy\end{array}\right]$$

Application 5 of the short-pentahedral compressive stress regime beneath the circumscribing rectangular border of proprietory shaped paver 1 shown in Figure 7.29 can be calculated by using Tables 5.1 and 7.2 and the surface function of the short-pentahedral compressive stress through the three points σ_A, b and u.

The total volume **V** beneath the surface $f(x,y)=z\ (>0)$ and above the region in the xy-plane (see Figure 7.29) is:

$$V = \int_0^a \int_0^{110} f(x,y)\,dy\,dx + \int_a^b \int_0^{fy} f(x,y)\,dy\,dx - \int_0^a \int_{S_{4y}}^{110} f(x,y)\,dy\,dx - \int_a^{S_{4x}} \int_{S_{4y}}^{fy} f(x,y)\,dy\,dx$$

$$- \int_0^{S_{4x}} \int_{85}^{ony} f(x,y)\,dy\,dx - \int_0^{15} \int_{15}^{qpy} f(x,y)\,dy\,dx - \int_0^{40} \int_{15}^{poy} f(x,y)\,dy\,dx - \int_0^{50} \int_0^{qay} f(x,y)\,dy\,dx$$

$$- \int_{50}^{70} \int_0^{aby} f(x,y)\,dy\,dx - \int_{70}^{135} \int_0^{bcy} f(x,y)\,dy\,dx - \int_{135}^{S_{14x}} \int_0^{cdy} f(x,y)\,dy\,dx - \int_{S_{14x}}^{b} \int_0^{fy} f(x,y)\,dy\,dx$$

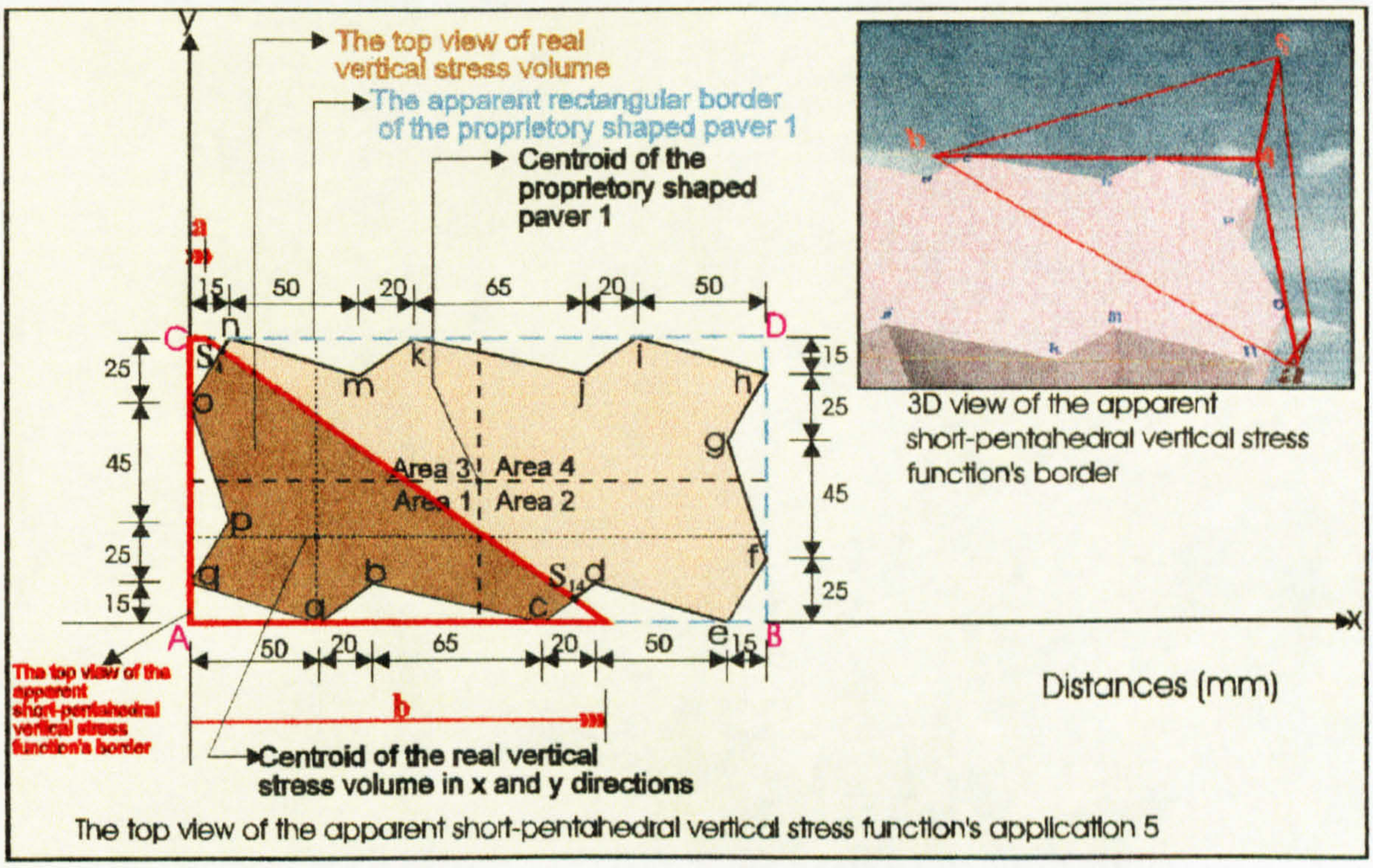

Figure 7.29: Application 5 of the short-pentahedral compressive stress distribution beneath the circumscribing rectangular border of proprietory shaped paver 1.

and the centroids of this volume in the xy-plane are at distances $\overline{X}$ and $\overline{Y}$ from the axes (see Figure 7.29) which are given by the following equations.

$$\overline{X} = \frac{1}{V}\left[\int_0^a \int_0^{110} x f(x,y)\,dy\,dx + \int_a^b \int_0^{fy} x f(x,y)\,dy\,dx - \int_0^a \int_{S_{4y}}^{110} x f(x,y)\,dy\,dx - \int_a^{S_{4x}} \int_{S_{4y}}^{fy} x f(x,y)\,dy\,dx\right.$$

$$\left. - \int_0^{S_{4x}} \int_{85}^{ony} x f(x,y)\,dy\,dx - \int_0^{15} \int_{15}^{qpy} x f(x,y)\,dy\,dx - \int_0^{40} \int_{15}^{poy} x f(x,y)\,dy\,dx - \int_0^{50} \int_0^{qay} x f(x,y)\,dy\,dx\right.$$

$$-\int_{50}^{70}\int_{0}^{aby} x f(x,y)\,dy\,dx - \int_{70}^{135}\int_{0}^{bcy} x f(x,y)\,dy\,dx - \int_{135}^{S_{14x}}\int_{0}^{cdy} x f(x,y)\,dy\,dx - \int_{S_{14x}}^{b}\int_{0}^{fy} x f(x,y)\,dy\,dx \Bigg]$$

$$\overline{Y} = \frac{1}{V}\Bigg[\int_{0}^{110}\int_{0}^{a} y f(x,y)\,dx\,dy + \int_{0}^{110}\int_{a}^{fx} y f(x,y)\,dx\,dy - \int_{S_{4y}}^{110}\int_{0}^{a} y f(x,y)\,dx\,dy - \int_{S_{4y}}^{110}\int_{a}^{fx} y f(x,y)\,dx\,dy$$
$$-\int_{85}^{S_{4y}}\int_{0}^{onx} y f(x,y)\,dx\,dy - \int_{40}^{85}\int_{0}^{pox} y f(x,y)\,dx\,dy - \int_{15}^{40}\int_{0}^{qpx} y f(x,y)\,dx\,dy - \int_{0}^{15}\int_{0}^{qax} y f(x,y)\,dx\,dy$$
$$-\int_{0}^{15}\int_{50}^{abx} y f(x,y)\,dx\,dy - \int_{0}^{15}\int_{70}^{bcx} y f(x,y)\,dx\,dy - \int_{0}^{S_{14y}}\int_{135}^{cdx} y f(x,y)\,dx\,dy - \int_{0}^{S_{14y}}\int_{S_{14x}}^{fx} y f(x,y)\,dx\,dy \Bigg]$$

Application 6 of the short-pentahedral compressive stress regime beneath the circumscribing rectangular border of proprietory shaped paver 1 shown in Figure 7.30 can be calculated by using Tables 5.1 and 7.2 and the surface function of the short-pentahedral compressive stress through the three points σ_A, **b** and **u**.

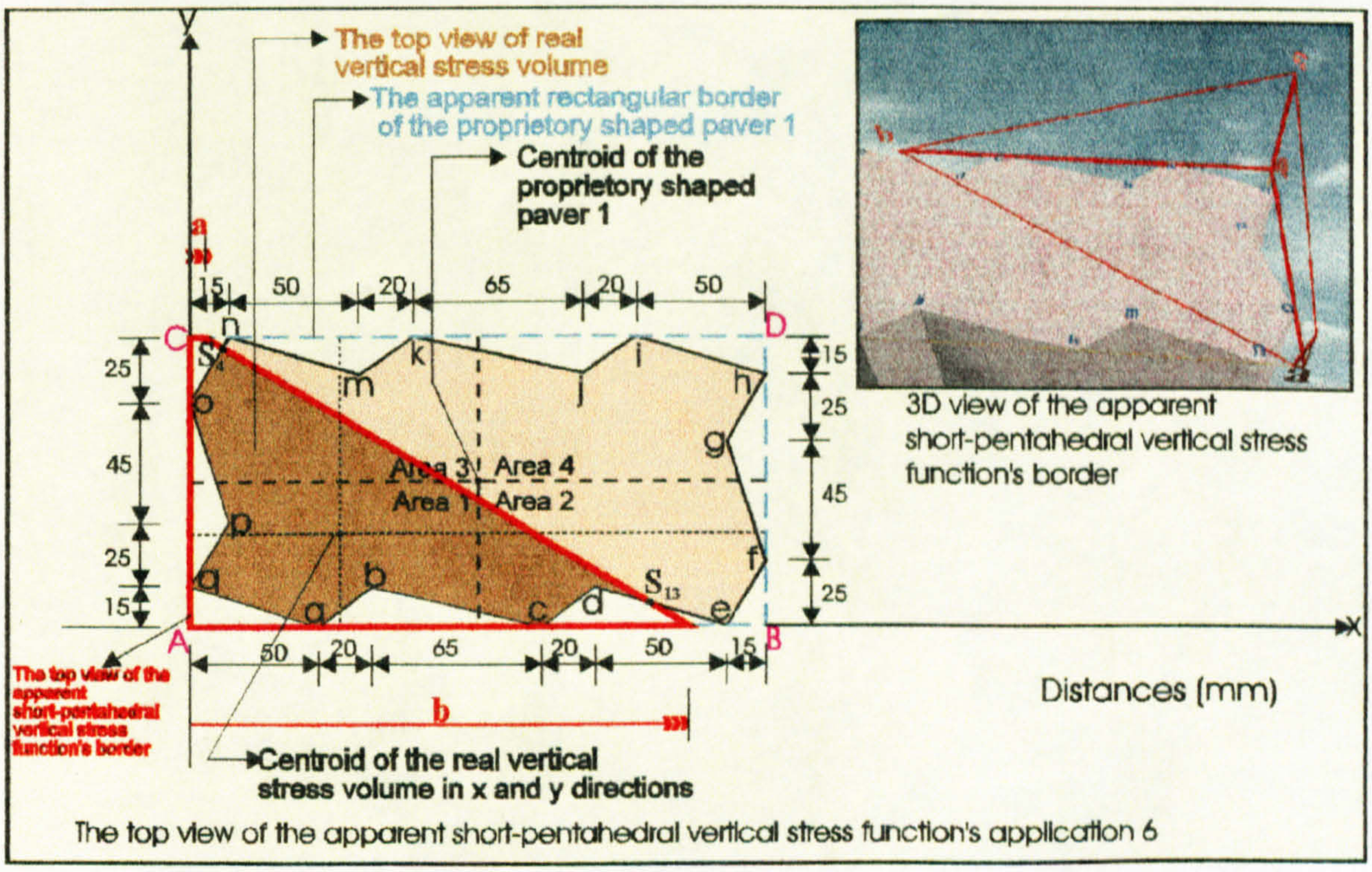

Figure 7.30: Application 6 of the short-pentahedral compressive stress distribution beneath the circumscribing rectangular border of proprietory shaped paver 1.

The total volume **V** beneath the surface $f(x,y) = z\ (> 0)$ and above the region in the xy-plane (see Figure 7.30) is:

$$V = \int_0^a \int_0^{110} f(x,y)\,dy\,dx + \int_a^b \int_0^{fy} f(x,y)\,dy\,dx - \int_0^a \int_{S_{4y}}^{110} f(x,y)\,dy\,dx - \int_a^{S_{4x}} \int_{S_{4y}}^{fy} f(x,y)\,dy\,dx$$
$$- \int_0^{S_{4x}} \int_{85}^{ony} f(x,y)\,dy\,dx - \int_0^{15} \int_{15}^{qpy} f(x,y)\,dy\,dx - \int_0^{15} \int_{40}^{poy} f(x,y)\,dy\,dx - \int_0^{50} \int_0^{qay} f(x,y)\,dy\,dx$$
$$- \int_{50}^{70} \int_0^{aby} f(x,y)\,dy\,dx - \int_{70}^{135} \int_0^{bcy} f(x,y)\,dy\,dx - \int_{135}^{155} \int_0^{cdy} f(x,y)\,dy\,dx - \int_{155}^{S_{13x}} \int_0^{S_{13y}} f(x,y)\,dy\,dx$$
$$- \int_{155}^{S_{13x}} \int_{S_{13y}}^{dey} f(x,y)\,dy\,dx - \int_{S_{13x}}^{b} \int_0^{fy} f(x,y)\,dy\,dx$$

and the centroids of this volume in the xy-plane are at distances $\overline{X}$ and $\overline{Y}$ from the axes (see Figure 7.30) which are given by the following equations.

$$\overline{X} = \frac{1}{V}\left[\int_0^a \int_0^{110} x f(x,y)\,dy\,dx + \int_a^b \int_0^{fy} x f(x,y)\,dy\,dx - \int_0^a \int_{S_{4y}}^{110} x f(x,y)\,dy\,dx - \int_a^{S_{4x}} \int_{S_{4y}}^{fy} x f(x,y)\,dy\,dx\right.$$
$$- \int_0^{S_{4x}} \int_{85}^{ony} x f(x,y)\,dy\,dx - \int_0^{15} \int_{15}^{qpy} x f(x,y)\,dy\,dx - \int_0^{15} \int_{40}^{poy} x f(x,y)\,dy\,dx - \int_0^{50} \int_0^{qay} x f(x,y)\,dy\,dx$$
$$- \int_{50}^{70} \int_0^{aby} x f(x,y)\,dy\,dx - \int_{70}^{135} \int_0^{bcy} x f(x,y)\,dy\,dx - \int_{135}^{155} \int_0^{cdy} x f(x,y)\,dy\,dx - \int_{155}^{S_{13x}} \int_0^{S_{13y}} x f(x,y)\,dy\,dx$$
$$\left. - \int_{155}^{S_{13x}} \int_{S_{13y}}^{dey} x f(x,y)\,dy\,dx - \int_{S_{13x}}^{b} \int_0^{fy} x f(x,y)\,dy\,dx\right]$$

$$\overline{Y} = \frac{1}{V}\left[\int_0^{110} \int_0^{a} y f(x,y)\,dx\,dy + \int_0^{110} \int_a^{fx} y f(x,y)\,dx\,dy - \int_{S_{4y}}^{110} \int_0^{a} y f(x,y)\,dx\,dy - \int_{S_{4y}}^{110} \int_a^{fx} y f(x,y)\,dx\,dy\right.$$
$$\left. - \int_{85}^{S_{4y}} \int_0^{onx} y f(x,y)\,dx\,dy - \int_{40}^{85} \int_0^{pox} y f(x,y)\,dx\,dy - \int_{15}^{40} \int_0^{qpx} y f(x,y)\,dx\,dy - \int_0^{15} \int_0^{qax} y f(x,y)\,dx\,dy\right]$$

$$-\int_{0}^{15}\int_{50}^{abx} y f(x,y)\,dx\,dy - \int_{0}^{15}\int_{70}^{bcx} y f(x,y)\,dx\,dy - \int_{0}^{15}\int_{135}^{cdx} y f(x,y)\,dx\,dy - \int_{0}^{S_{13y}}\int_{155}^{S_{13x}} y f(x,y)\,dx\,dy$$
$$\left. -\int_{S_{13y}}^{15}\int_{155}^{dex} y f(x,y)\,dx\,dy - \int_{0}^{S_{13y}}\int_{S_{13x}}^{fx} y f(x,y)\,dx\,dy \right]$$

Application 7 of the short-pentahedral compressive stress regime beneath the circumscribing rectangular border of proprietory shaped paver 1 shown in Figure 7.31 can be calculated by using Tables 5.1 and 7.2 and the surface function of the short-pentahedral compressive stress through the three points σ_A, **b** and **u**.

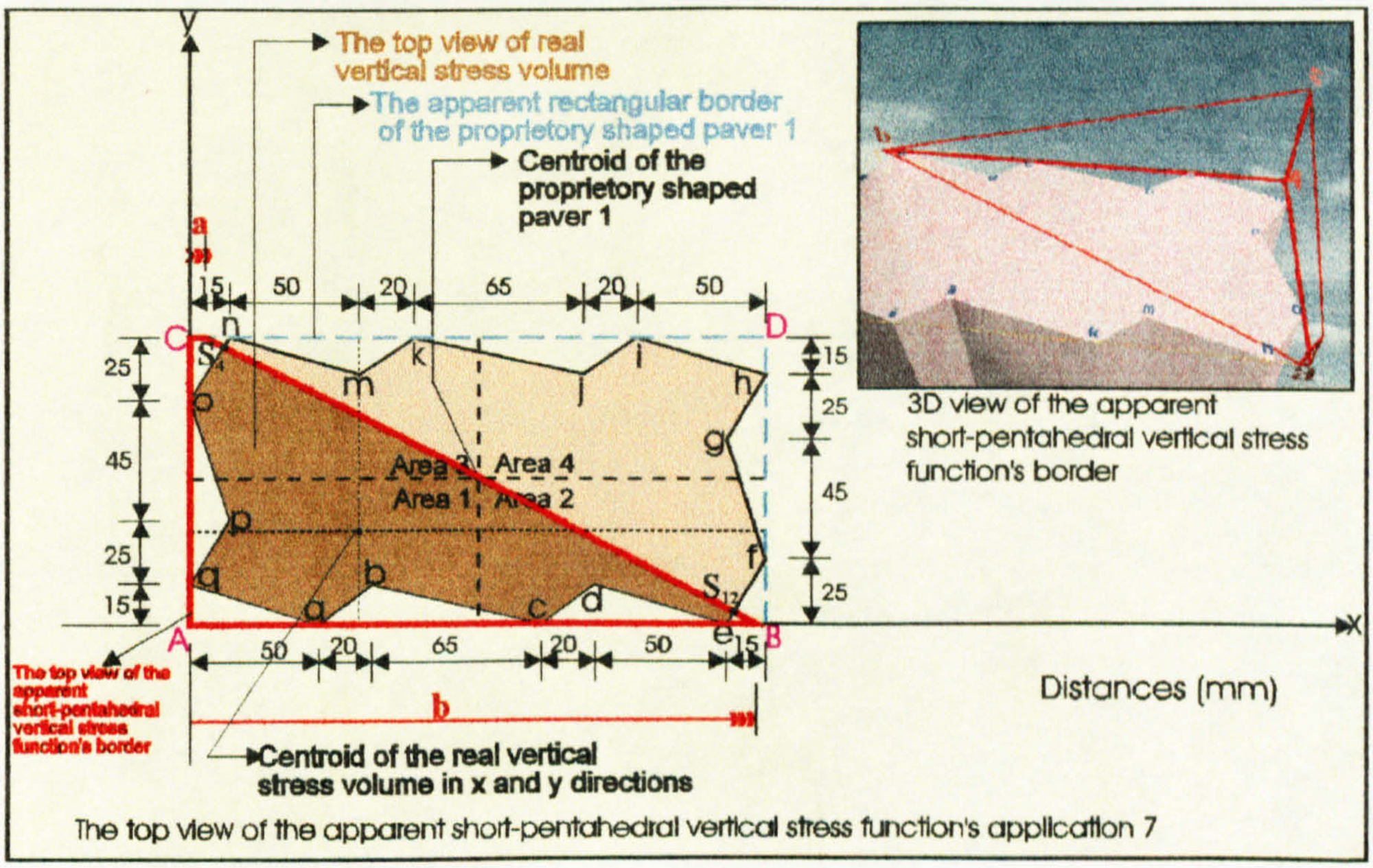

Figure 7.31: Application 7 of the short-pentahedral compressive stress distribution beneath the circumscribing rectangular border of proprietory shaped paver 1.

The total volume **V** beneath the surface $f(x,y) = z\ (> 0)$ and above the region in the xy-plane (see Figure 7.31) is:

$$V = \int_0^a \int_0^{110} f(x,y)\,dy\,dx + \int_a^b \int_0^{fy} f(x,y)\,dy\,dx - \int_0^a \int_{S_{4y}}^{110} f(x,y)\,dy\,dx - \int_a^{S_{4x}} \int_{S_{4y}}^{fy} f(x,y)\,dy\,dx$$
$$- \int_0^{S_{4x}} \int_{85}^{ony} f(x,y)\,dy\,dx - \int_0^{15} \int_{15}^{qpy} f(x,y)\,dy\,dx - \int_0^{15} \int_{40}^{poy} f(x,y)\,dy\,dx - \int_0^{50} \int_0^{qay} f(x,y)\,dy\,dx$$
$$- \int_{50}^{70} \int_0^{aby} f(x,y)\,dy\,dx - \int_{70}^{135} \int_0^{bcy} f(x,y)\,dy\,dx - \int_{135}^{155} \int_0^{cdy} f(x,y)\,dy\,dx - \int_{155}^{205} \int_0^{dey} f(x,y)\,dy\,dx$$
$$- \int_{205}^{S_{12x}} \int_0^{efy} f(x,y)\,dy\,dx - \int_{S_{12x}}^{b} \int_0^{fy} f(x,y)\,dy\,dx$$

and the centroids of this volume in the xy-plane are at distances $\overline{X}$ and $\overline{Y}$ from the axes (see Figure 7.31) which are given by the following equations.

$$\overline{X} = \frac{1}{V}\left[\begin{array}{l} \int_0^a \int_0^{110} x f(x,y)\,dy\,dx + \int_a^b \int_0^{fy} x f(x,y)\,dy\,dx - \int_0^a \int_{S_{4y}}^{110} x f(x,y)\,dy\,dx - \int_a^{S_{4x}} \int_{S_{4y}}^{fy} x f(x,y)\,dy\,dx \\ - \int_0^{S_{4x}} \int_{85}^{ony} x f(x,y)\,dy\,dx - \int_0^{15} \int_{15}^{qpy} x f(x,y)\,dy\,dx - \int_0^{15} \int_{40}^{poy} x f(x,y)\,dy\,dx - \int_0^{50} \int_0^{qay} x f(x,y)\,dy\,dx \\ - \int_{50}^{70} \int_0^{aby} x f(x,y)\,dy\,dx - \int_{70}^{135} \int_0^{bcy} x f(x,y)\,dy\,dx - \int_{135}^{155} \int_0^{cdy} x f(x,y)\,dy\,dx - \int_{155}^{205} \int_0^{dey} x f(x,y)\,dy\,dx \\ - \int_{205}^{S_{12x}} \int_0^{efy} x f(x,y)\,dy\,dx - \int_{S_{12x}}^{b} \int_0^{fy} x f(x,y)\,dy\,dx \end{array}\right]$$

$$\overline{Y} = \frac{1}{V}\left[\begin{array}{l} \int_0^{110} \int_0^{a} y f(x,y)\,dx\,dy + \int_0^{110} \int_a^{fx} y f(x,y)\,dx\,dy - \int_{S_{4y}}^{110} \int_0^{a} y f(x,y)\,dx\,dy - \int_{S_{4y}}^{110} \int_a^{fx} y f(x,y)\,dx\,dy \\ - \int_{85}^{S_{4y}} \int_0^{onx} y f(x,y)\,dx\,dy - \int_{40}^{85} \int_0^{pox} y f(x,y)\,dx\,dy - \int_{15}^{40} \int_0^{qpx} y f(x,y)\,dx\,dy - \int_0^{15} \int_0^{qax} y f(x,y)\,dx\,dy \\ - \int_0^{15} \int_{50}^{abx} y f(x,y)\,dx\,dy - \int_0^{15} \int_{70}^{bcx} y f(x,y)\,dx\,dy - \int_0^{135} \int_{135}^{cdx} y f(x,y)\,dx\,dy - \int_0^{155} \int_{155}^{dex} y f(x,y)\,dx\,dy \end{array}\right]$$

$$\left. - \int_{0}^{S_{12y}} \int_{205}^{efx} y f(x,y)\, dx\, dy - \int_{0}^{S_{12y}} \int_{S_{12x}}^{fx} y f(x,y)\, dx\, dy \right]$$

Application 8 of the short-pentahedral compressive stress regime beneath the circumscribing rectangular border of proprietory shaped paver 1 shown in Figure 7.32 can be calculated by using Tables 5.1 and 7.2 and the surface function of the short-pentahedral compressive stress through the three points σ_A, **b** and **u**.

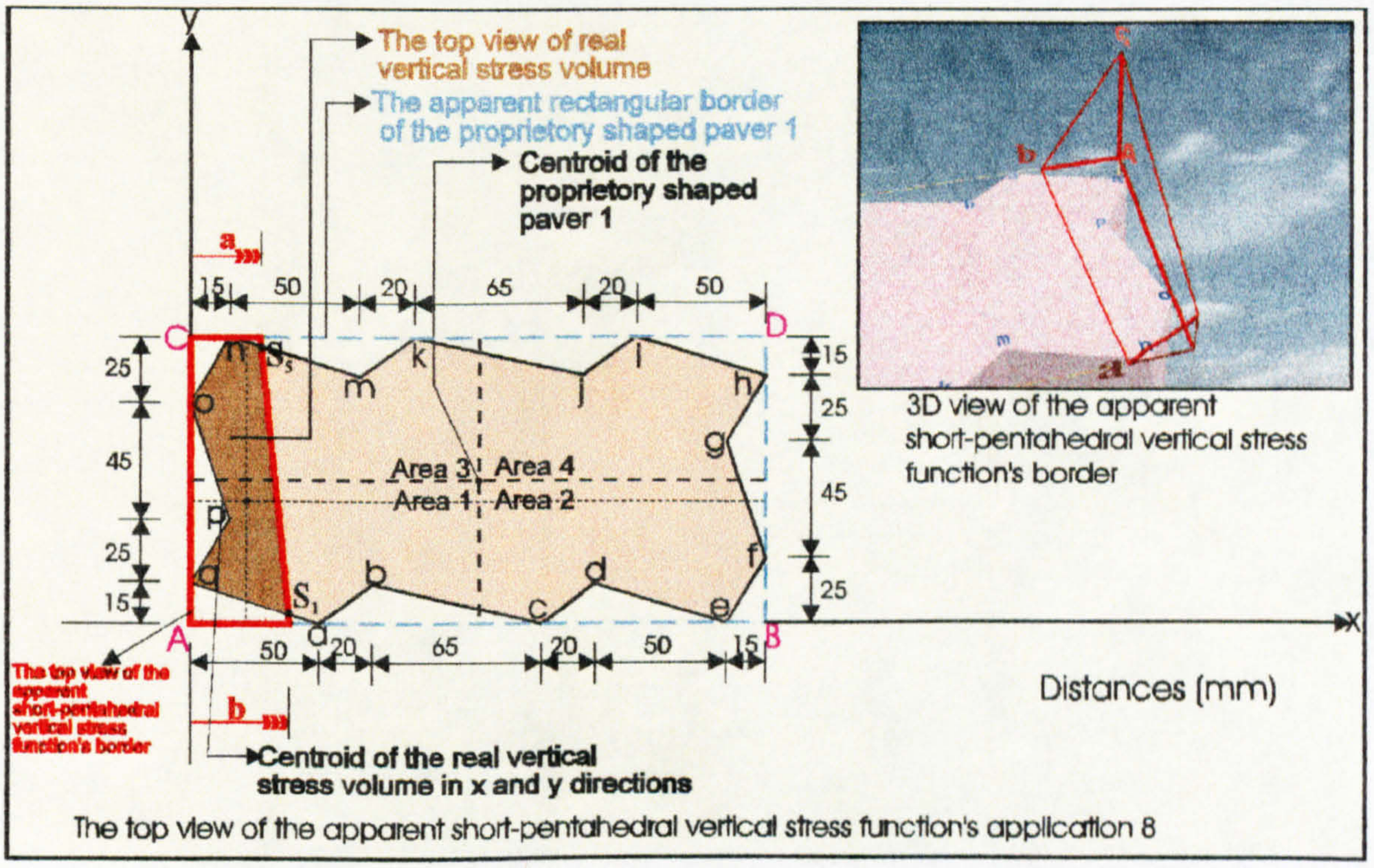

Figure 7.32: Application 8 of the short-pentahedral compressive stress distribution beneath the circumscribing rectangular border of proprietory shaped paver 1.

The total volume **V** beneath the surface $f(x,y) = z\ (> 0)$ and above the region in the xy-plane (see Figure 7.32) is:

$$V = \int_{0}^{a} \int_{0}^{110} f(x,y)\, dy\, dx + \int_{a}^{b} \int_{0}^{fy} f(x,y)\, dy\, dx - \int_{15}^{a} \int_{S_{5y}}^{110} f(x,y)\, dy\, dx - \int_{a}^{S_{5x}} \int_{S_{5y}}^{fy} f(x,y)\, dy\, dx$$

$$+\int_{15}^{S_{5x}}\int_{S_{5y}}^{nmy} f(x,y)\,dy\,dx-\int_{0}^{15}\int_{85}^{ony} f(x,y)\,dy\,dx-\int_{0}^{15}\int_{40}^{poy} f(x,y)\,dy\,dx-\int_{0}^{15}\int_{15}^{qpy} f(x,y)\,dy\,dx$$

$$-\int_{0}^{S_{1x}}\int_{0}^{S_{1y}} f(x,y)\,dy\,dx-\int_{0}^{S_{1x}}\int_{S_{1y}}^{qay} f(x,y)\,dy\,dx-\int_{S_{1x}}^{b}\int_{0}^{fy} f(x,y)\,dy\,dx$$

and the centroids of this volume in the xy-plane are at distances $\overline{X}$ and $\overline{Y}$ from the axes (see Figure 7.32) which are given by the following equations.

$$\overline{X}=\frac{1}{V}\left[\begin{array}{l}\int_{0}^{a}\int_{0}^{110} x f(x,y)\,dy\,dx+\int_{a}^{b}\int_{0}^{fy} x f(x,y)\,dy\,dx-\int_{15}^{a}\int_{S_{5y}}^{110} x f(x,y)\,dy\,dx-\int_{a}^{S_{5x}}\int_{S_{5y}}^{fy} x f(x,y)\,dy\,dx\\ +\int_{15}^{S_{5x}}\int_{S_{5y}}^{nmy} x f(x,y)\,dy\,dx-\int_{0}^{15}\int_{85}^{ony} x f(x,y)\,dy\,dx-\int_{0}^{15}\int_{40}^{poy} x f(x,y)\,dy\,dx-\int_{0}^{15}\int_{15}^{qpy} x f(x,y)\,dy\,dx\\ -\int_{0}^{S_{1x}}\int_{0}^{S_{1y}} x f(x,y)\,dy\,dx-\int_{0}^{S_{1x}}\int_{S_{1y}}^{qay} x f(x,y)\,dy\,dx-\int_{S_{1x}}^{b}\int_{0}^{fy} x f(x,y)\,dy\,dx\end{array}\right]$$

$$\overline{Y}=\frac{1}{V}\left[\begin{array}{l}\int_{0}^{110}\int_{0}^{a} y f(x,y)\,dx\,dy+\int_{0}^{110}\int_{a}^{fx} y f(x,y)\,dx\,dy-\int_{S_{5y}}^{110}\int_{15}^{a} y f(x,y)\,dx\,dy-\int_{S_{5y}}^{110}\int_{a}^{fx} y f(x,y)\,dx\,dy\\ +\int_{S_{5y}}^{110}\int_{15}^{nmx} y f(x,y)\,dx\,dy-\int_{85}^{110}\int_{0}^{onx} y f(x,y)\,dx\,dy-\int_{40}^{85}\int_{0}^{pox} y f(x,y)\,dx\,dy-\int_{15}^{40}\int_{0}^{qpx} y f(x,y)\,dx\,dy\\ -\int_{0}^{S_{1y}}\int_{0}^{S_{1x}} y f(x,y)\,dx\,dy-\int_{S_{1y}}^{15}\int_{0}^{qax} y f(x,y)\,dx\,dy-\int_{0}^{S_{1y}}\int_{S_{1x}}^{fx} y f(x,y)\,dx\,dy\end{array}\right]$$

Application 9 of the short-pentahedral compressive stress regime beneath the circumscribing rectangular border of proprietory shaped paver 1 shown in Figure 7.33 can be calculated by using Tables 5.1 and 7.2 and the surface function of the short-pentahedral compressive stress through the three points σ_A, b and u.

The total volume **V** beneath the surface $f(x,y) = z\ (> 0)$ and above the region in the xy-plane (see Figure 7.33) is:

$$V = \int_0^a \int_0^{110} f(x,y)\,dy\,dx + \int_a^b \int_0^{fy} f(x,y)\,dy\,dx - \int_{15}^{a} \int_{S_{5y}}^{110} f(x,y)\,dy\,dx - \int_a^{S_{5x}} \int_{S_{5y}}^{fy} f(x,y)\,dy\,dx$$

$$+ \int_{15}^{S_{5x}} \int_{S_{5y}}^{nmy} f(x,y)\,dy\,dx - \int_0^{85} \int_{15}^{ony} f(x,y)\,dy\,dx - \int_0^{40} \int_{15}^{poy} f(x,y)\,dy\,dx - \int_0^{15} \int_{15}^{qpy} f(x,y)\,dy\,dx$$

$$- \int_0^0 \int_0^{50qay} f(x,y)\,dy\,dx - \int_{50}^{S_{16x}} \int_0^{aby} f(x,y)\,dy\,dx - \int_{S_{16x}}^{b} \int_0^{fy} f(x,y)\,dy\,dx$$

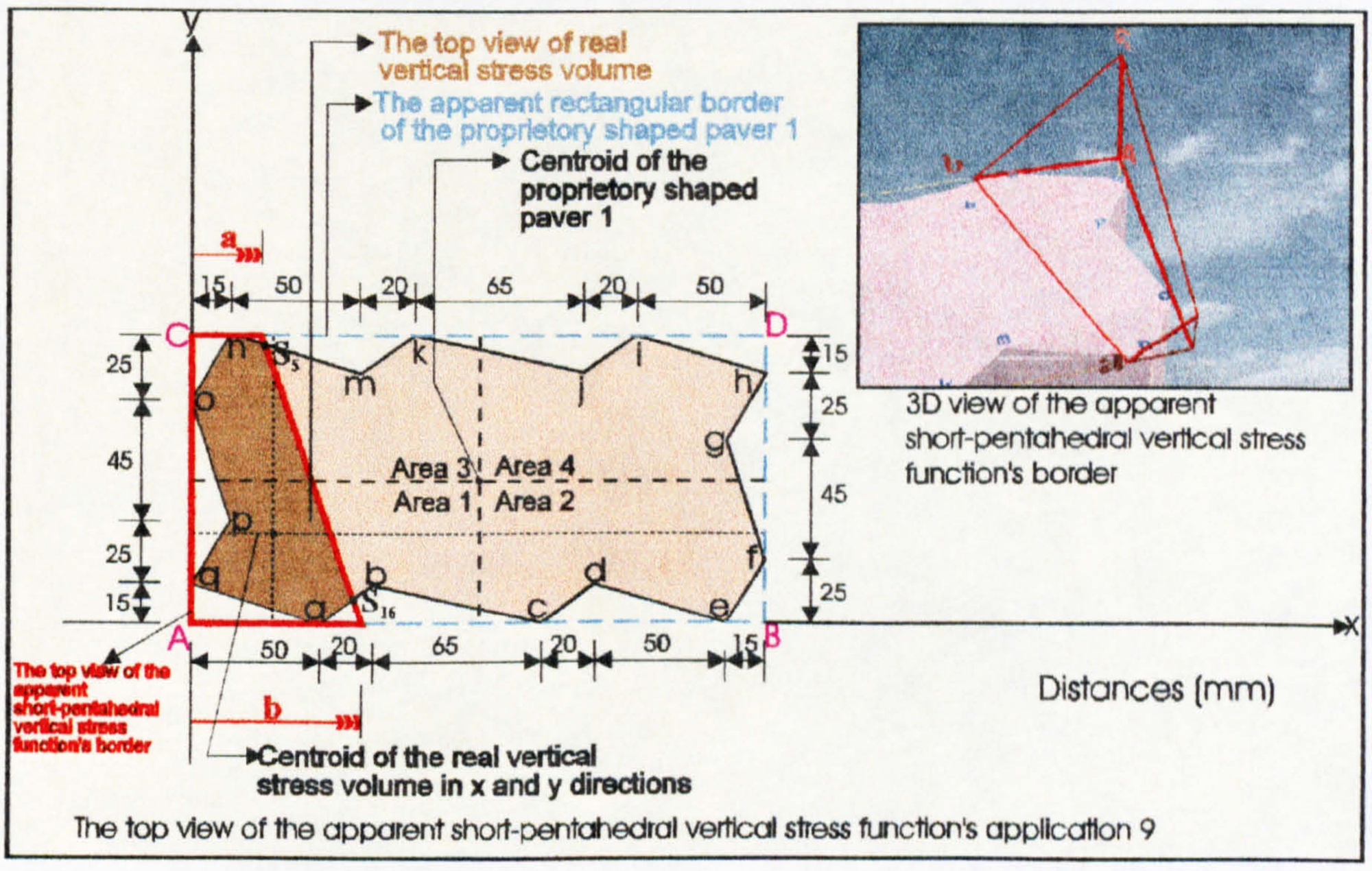

Figure 7.33: Application 9 of the short-pentahedral compressive stress distribution beneath the circumscribing rectangular border of proprietory shaped paver 1.

and the centroids of this volume in the xy-plane are at distances $\overline{X}$ and $\overline{Y}$ from the axes (see Figure 7.33) which are given by the following equations.

$$\overline{X} = \frac{1}{V}\left[\begin{array}{l}
\int_{0}^{a}\int_{0}^{110} x f(x,y)\,dy\,dx + \int_{a}^{b}\int_{0}^{fy} x f(x,y)\,dy\,dx - \int_{15}^{a}\int_{S_{5y}}^{110} x f(x,y)\,dy\,dx - \int_{a}^{S_{5x}}\int_{S_{5y}}^{fy} x f(x,y)\,dy\,dx \\
+ \int_{15}^{S_{5x}}\int_{S_{5y}}^{nmy} x f(x,y)\,dy\,dx - \int_{0}^{15}\int_{85}^{ony} x f(x,y)\,dy\,dx - \int_{0}^{15}\int_{40}^{poy} x f(x,y)\,dy\,dx - \int_{0}^{15}\int_{15}^{qpy} x f(x,y)\,dy\,dx \\
- \int_{0}^{50}\int_{0}^{qay} x f(x,y)\,dy\,dx - \int_{50}^{S_{16x}}\int_{0}^{aby} x f(x,y)\,dy\,dx - \int_{S_{16x}}^{b}\int_{0}^{fy} x f(x,y)\,dy\,dx
\end{array}\right]$$

$$\overline{Y} = \frac{1}{V}\left[\begin{array}{l}
\int_{0}^{110}\int_{0}^{a} y f(x,y)\,dx\,dy + \int_{0}^{110}\int_{a}^{fx} y f(x,y)\,dx\,dy - \int_{S_{5y}}^{110}\int_{15}^{a} y f(x,y)\,dx\,dy - \int_{S_{5y}}^{110}\int_{a}^{fx} y f(x,y)\,dx\,dy \\
+ \int_{S_{5y}}^{110}\int_{15}^{nmx} y f(x,y)\,dx\,dy - \int_{85}^{110}\int_{0}^{onx} y f(x,y)\,dx\,dy - \int_{40}^{85}\int_{0}^{pox} y f(x,y)\,dx\,dy - \int_{15}^{40}\int_{0}^{qpx} y f(x,y)\,dx\,dy \\
- \int_{0}^{15}\int_{0}^{qax} y f(x,y)\,dx\,dy - \int_{0}^{S_{16y}}\int_{50}^{abx} y f(x,y)\,dx\,dy - \int_{0}^{S_{16y}}\int_{S_{16x}}^{fx} y f(x,y)\,dx\,dy
\end{array}\right]$$

Application 10 of the short-pentahedral compressive stress regime beneath the circumscribing rectangular border of proprietory shaped paver 1 shown in Figure 7.34 can be calculated by using Tables 5.1 and 7.2 and the surface function of the short-pentahedral compressive stress through the three points σ_A, **b** and **u**.

The total volume **V** beneath the surface $f(x,y) = z\ (> 0)$ and above the region in the xy-plane (see Figure 7.34) is:

$$V = \int_{0}^{a}\int_{0}^{110} f(x,y)\,dy\,dx + \int_{a}^{b}\int_{0}^{fy} f(x,y)\,dy\,dx - \int_{15}^{a}\int_{S_{5y}}^{110} f(x,y)\,dy\,dx - \int_{a}^{S_{5x}}\int_{S_{5y}}^{fy} f(x,y)\,dy\,dx$$

$$+ \int_{15}^{S_{5x}}\int_{S_{5y}}^{nmy} f(x,y)\,dy\,dx - \int_{0}^{15}\int_{85}^{ony} f(x,y)\,dy\,dx - \int_{0}^{15}\int_{40}^{poy} f(x,y)\,dy\,dx - \int_{0}^{15}\int_{15}^{qpy} f(x,y)\,dy\,dx$$

$$- \int_{0}^{50}\int_{0}^{qay} f(x,y)\,dy\,dx - \int_{50}^{70}\int_{0}^{aby} f(x,y)\,dy\,dx - \int_{70}^{S_{15x}}\int_{0}^{S_{15y}} f(x,y)\,dy\,dx - \int_{70}^{S_{15x}}\int_{S_{15y}}^{bcy} f(x,y)\,dy\,dx$$

$$-\int_{S_{15x}}^{b}\int_{0}^{fy} f(x,y)\,dy\,dx$$

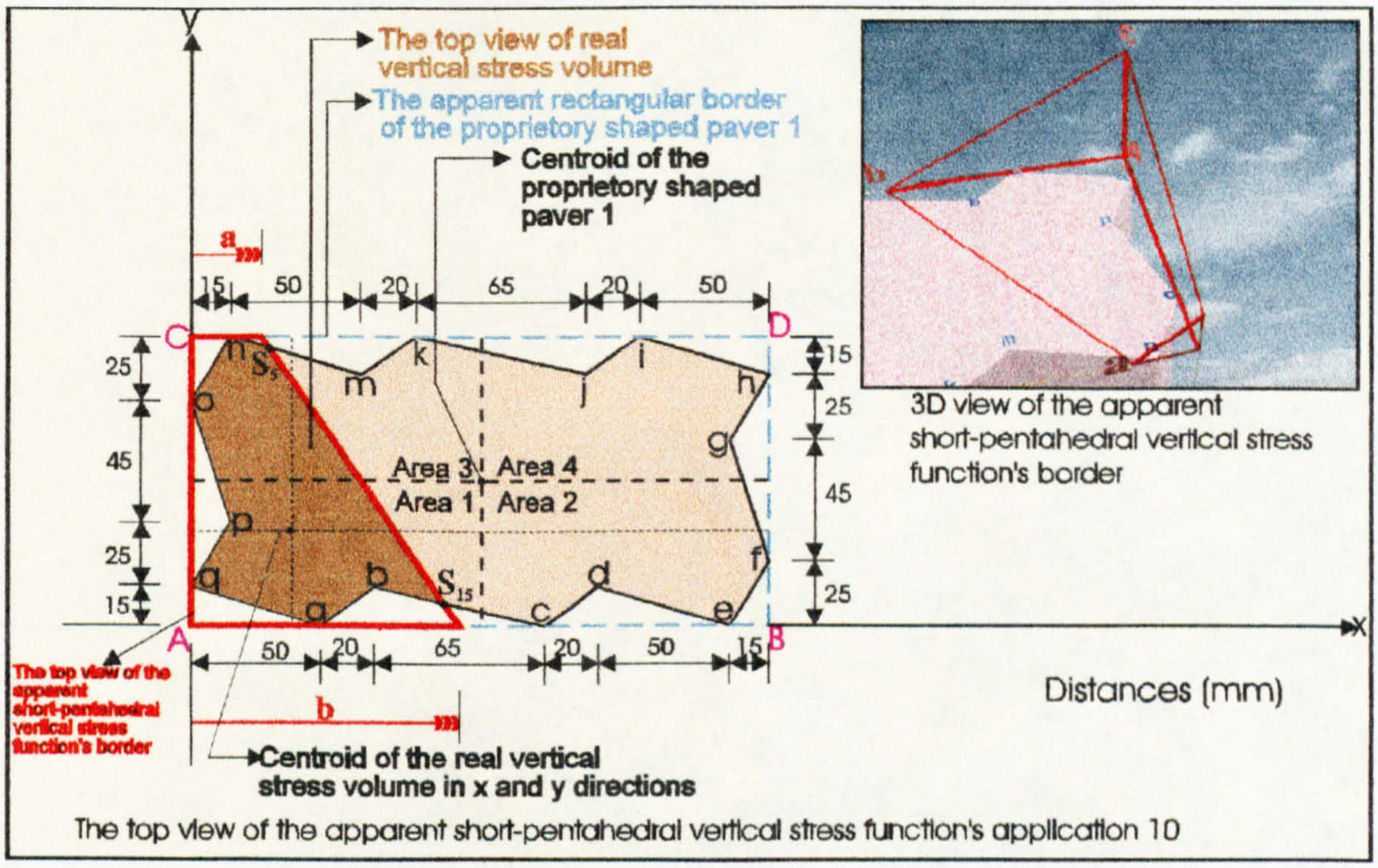

Figure 7.34: Application 10 of the short-pentahedral compressive stress distribution beneath the circumscribing rectangular border of proprietory shaped paver 1.

and the centroids of this volume in the xy-plane are at distances $\overline{\mathrm{X}}$ and $\overline{\mathrm{Y}}$ from the axes (see Figure 7.34) which are given by the following equations.

$$\overline{X} = \frac{1}{V}\left[\begin{aligned}
&\int_{0}^{a}\int_{0}^{110} x f(x,y)\,dy\,dx + \int_{a}^{b}\int_{0}^{fy} x f(x,y)\,dy\,dx - \int_{15}^{a}\int_{S_{5y}}^{110} x f(x,y)\,dy\,dx - \int_{a}^{S_{5x}}\int_{S_{5y}}^{fy} x f(x,y)\,dy\,dx \\
&+\int_{15}^{S_{5x}}\int_{S_{5y}}^{nmy} x f(x,y)\,dy\,dx - \int_{0}^{15}\int_{85}^{ony} x f(x,y)\,dy\,dx - \int_{0}^{15}\int_{40}^{poy} x f(x,y)\,dy\,dx - \int_{0}^{15}\int_{15}^{qpy} x f(x,y)\,dy\,dx \\
&-\int_{0}^{50}\int_{0}^{qay} x f(x,y)\,dy\,dx - \int_{50}^{70}\int_{0}^{aby} x f(x,y)\,dy\,dx - \int_{70}^{S_{15x}}\int_{0}^{S_{15y}} x f(x,y)\,dy\,dx - \int_{70}^{S_{15x}}\int_{S_{15y}}^{bcy} x f(x,y)\,dy\,dx \\
&-\int_{S_{15x}}^{b}\int_{0}^{fy} x f(x,y)\,dy\,dx
\end{aligned}\right]$$

$$\overline{Y} = \frac{1}{V}\left[\begin{array}{l}
\int_{0}^{110}\int_{0}^{a} y f(x,y)\,dx\,dy + \int_{0}^{110}\int_{a}^{fx} y f(x,y)\,dx\,dy - \int_{S_{5y}}^{110}\int_{15}^{a} y f(x,y)\,dx\,dy - \int_{S_{5y}}^{110}\int_{a}^{fx} y f(x,y)\,dx\,dy \\
+\int_{S_{5y}}^{110}\int_{15}^{nmx} y f(x,y)\,dx\,dy - \int_{85}^{110}\int_{0}^{onx} y f(x,y)\,dx\,dy - \int_{40}^{85}\int_{0}^{pox} y f(x,y)\,dx\,dy - \int_{15}^{40}\int_{0}^{qpx} y f(x,y)\,dx\,dy \\
-\int_{0}^{15}\int_{0}^{qax} y f(x,y)\,dx\,dy - \int_{0}^{15}\int_{50}^{abx} y f(x,y)\,dx\,dy - \int_{0}^{S_{15y}}\int_{70}^{S_{15x}} y f(x,y)\,dx\,dy - \int_{S_{15y}}^{15}\int_{70}^{bcx} y f(x,y)\,dx\,dy \\
-\int_{0}^{S_{15y}}\int_{S_{15x}}^{fx} y f(x,y)\,dx\,dy
\end{array}\right]$$

Application 11 of the short-pentahedral compressive stress regime beneath the circumscribing rectangular border of proprietory shaped paver 1 shown in Figure 7.35 can be calculated by using Tables 5.1 and 7.2 and the surface function of the short-pentahedral compressive stress through the three points σ_A, **b** and **u**.

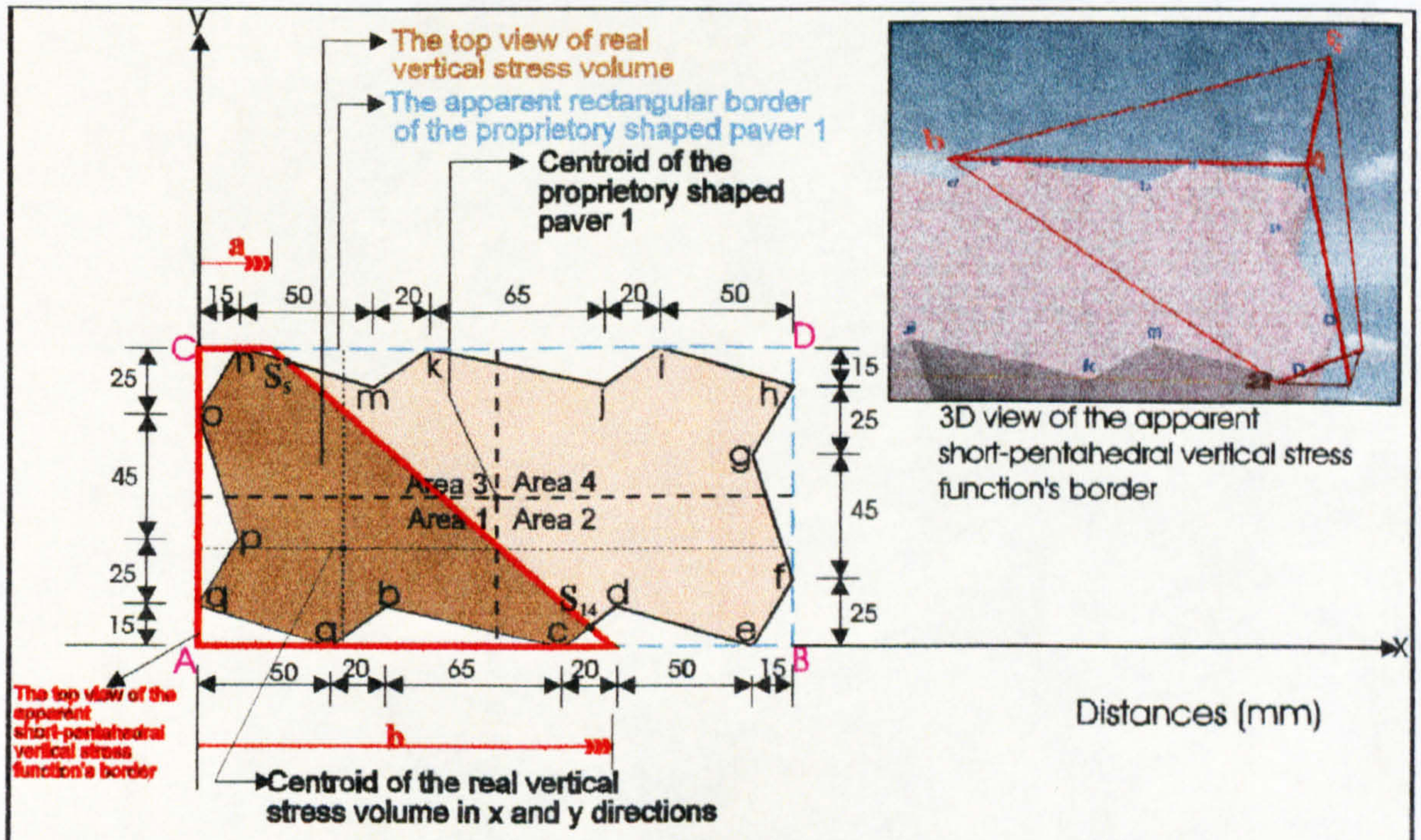

Figure 7.35: Application 11 of the short-pentahedral compressive stress distribution beneath the circumscribing rectangular border of proprietory shaped paver 1.

The total volume **V** beneath the surface $f(x,y) = z\ (> 0)$ and above the region in the xy-plane (see Figure 7.35) is:

$$V = \int_0^a \int_0^{110} f(x,y)\,dy\,dx + \int_a^b \int_0^{fy} f(x,y)\,dy\,dx - \int_{15}^a \int_{S_{5y}}^{110} f(x,y)\,dy\,dx - \int_a^{S_{5x}} \int_{S_{5y}}^{fy} f(x,y)\,dy\,dx$$
$$+ \int_{15}^{S_{5x}} \int_{S_{5y}}^{nmy} f(x,y)\,dy\,dx - \int_0^{85} \int_0^{15on y} f(x,y)\,dy\,dx - \int_0^{40} \int_0^{15po y} f(x,y)\,dy\,dx - \int_0^{15} \int_0^{15qp y} f(x,y)\,dy\,dx$$
$$- \int_0^{50} \int_0^{50qa y} f(x,y)\,dy\,dx - \int_0^{70} \int_0^{70ab y} f(x,y)\,dy\,dx - \int_0^{135} \int_0^{135bc y} f(x,y)\,dy\,dx - \int_{135}^{S_{14x}} \int_0^{cdy} f(x,y)\,dy\,dx$$
$$- \int_{S_{14x}}^b \int_0^{fy} f(x,y)\,dy\,dx$$

and the centroids of this volume in the xy-plane are at distances $\overline{X}$ and $\overline{Y}$ from the axes (see Figure 7.35) which are given by the following equations.

$$\overline{X} = \frac{1}{V}\left[\int_0^a \int_0^{110} x f(x,y)\,dy\,dx + \int_a^b \int_0^{fy} x f(x,y)\,dy\,dx - \int_{15}^a \int_{S_{5y}}^{110} x f(x,y)\,dy\,dx - \int_a^{S_{5x}} \int_{S_{5y}}^{fy} x f(x,y)\,dy\,dx\right.$$
$$+ \int_{15}^{S_{5x}} \int_{S_{5y}}^{nmy} x f(x,y)\,dy\,dx - \int_0^{85} \int_0^{15on y} x f(x,y)\,dy\,dx - \int_0^{40} \int_0^{15po y} x f(x,y)\,dy\,dx - \int_0^{15} \int_0^{15qp y} x f(x,y)\,dy\,dx$$
$$- \int_0^{50} \int_0^{50qa y} x f(x,y)\,dy\,dx - \int_0^{70} \int_0^{70ab y} x f(x,y)\,dy\,dx - \int_0^{135} \int_0^{135bc y} x f(x,y)\,dy\,dx - \int_{135}^{S_{14x}} \int_0^{cdy} x f(x,y)\,dy\,dx$$
$$\left. - \int_{S_{14x}}^b \int_0^{fy} x f(x,y)\,dy\,dx\right]$$

$$\overline{Y} = \frac{1}{V}\left[\int_0^{110} \int_0^a y f(x,y)\,dx\,dy + \int_0^{110} \int_a^{fx} y f(x,y)\,dx\,dy - \int_{S_{5y}}^{110} \int_{15}^a y f(x,y)\,dx\,dy - \int_{S_{5y}}^{110} \int_a^{fx} y f(x,y)\,dx\,dy\right.$$
$$\left. + \int_{S_{5y}}^{110} \int_{15}^{nmx} y f(x,y)\,dx\,dy - \int_{85}^{110} \int_0^{onx} y f(x,y)\,dx\,dy - \int_{40}^{85} \int_0^{pox} y f(x,y)\,dx\,dy - \int_{15}^{40} \int_0^{qpx} y f(x,y)\,dx\,dy\right]$$

$$-\int_0^{15qax}\int_0^{} y f(x,y)\,dx\,dy - \int_0^{15abx}\int_{50}^{} y f(x,y)\,dx\,dy - \int_0^{15bcx}\int_{70}^{} y f(x,y)\,dx\,dy - \int_0^{S_{14y}\,cdx}\int_{135}^{} y f(x,y)\,dx\,dy$$
$$\left.-\int_0^{S_{14y}}\int_{S_{14x}}^{fx} y f(x,y)\,dx\,dy\right]$$

Application 12 of the short-pentahedral compressive stress regime beneath the circumscribing rectangular border of proprietory shaped paver 1 shown in Figure 7.36 can be calculated by using Tables 5.1 and 7.2 and the surface function of the short-pentahedral compressive stress through the three points σ_A, **b** and **u**.

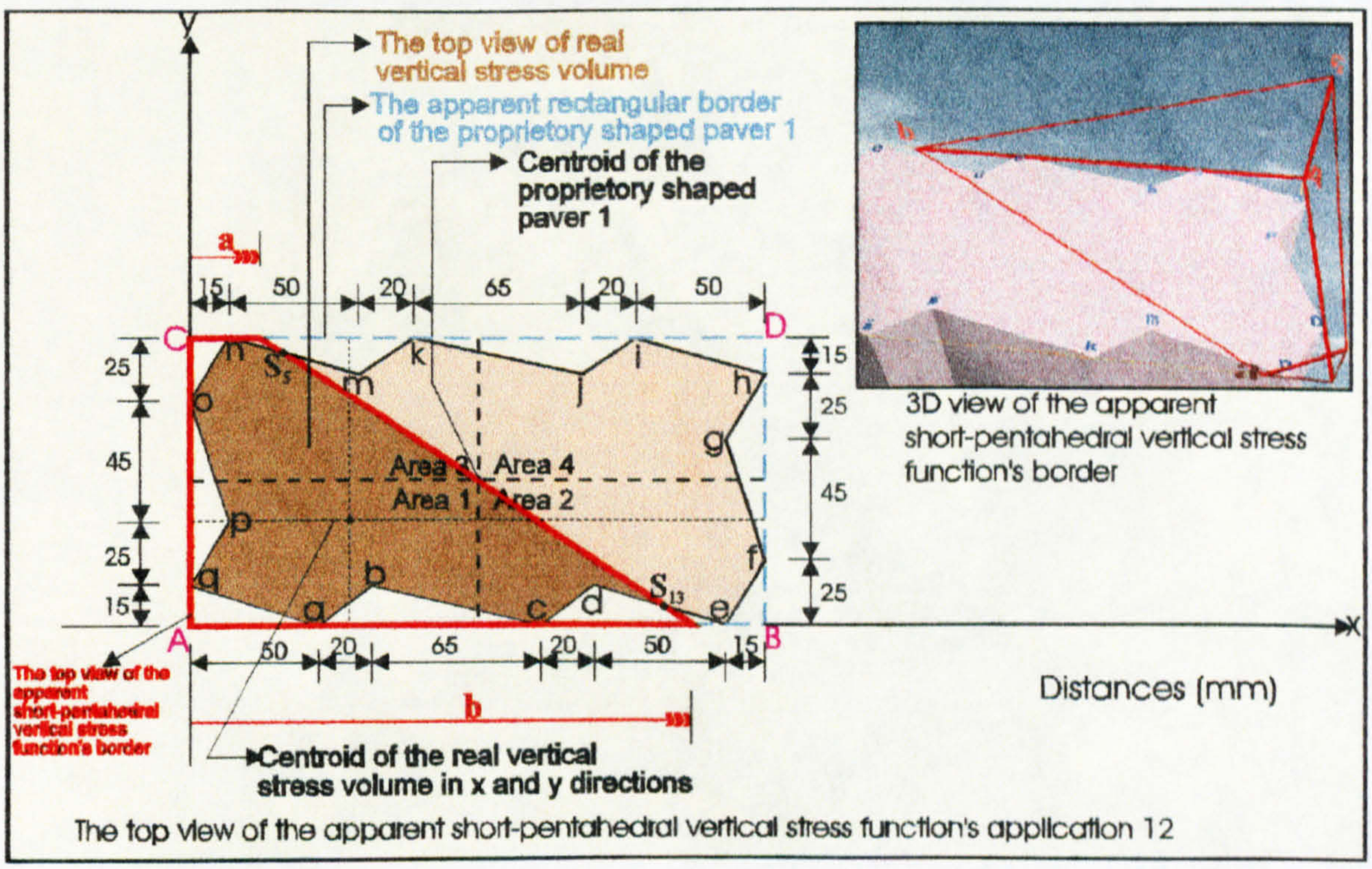

Figure 7.36: Application 12 of the short-pentahedral compressive stress distribution beneath the circumscribing rectangular border of proprietory shaped paver 1.

The total volume **V** beneath the surface $f(x,y) = z\ (> 0)$ and above the region in the xy-plane (see Figure 7.36) is:

$$V = \int_0^a \int_0^{110} f(x,y)\,dy\,dx + \int_a^b \int_0^{fy} f(x,y)\,dy\,dx - \int_{15}^{a} \int_{0}^{110} f(x,y)\,dy\,dx - \int_{a}^{S_{5x}} \int_{S_{5y}}^{fy} f(x,y)\,dy\,dx$$

$$+ \int_{15}^{S_{5x}} \int_{S_{5y}}^{nmy} f(x,y)\,dy\,dx - \int_{0}^{85} \int_{0}^{15ony} f(x,y)\,dy\,dx - \int_{0}^{40} \int_{0}^{15poy} f(x,y)\,dy\,dx - \int_{0}^{15} \int_{0}^{15qpy} f(x,y)\,dy\,dx$$

$$- \int_{0}^{50} \int_{0}^{50qay} f(x,y)\,dy\,dx - \int_{50}^{70} \int_{0}^{70aby} f(x,y)\,dy\,dx - \int_{70}^{135} \int_{0}^{135bcy} f(x,y)\,dy\,dx - \int_{135}^{155} \int_{0}^{155cdy} f(x,y)\,dy\,dx$$

$$- \int_{155}^{S_{13x}} \int_{0}^{S_{13y}} f(x,y)\,dy\,dx - \int_{155}^{S_{13x}} \int_{S_{13y}}^{dey} f(x,y)\,dy\,dx - \int_{S_{13x}}^{b} \int_{0}^{fy} f(x,y)\,dy\,dx$$

and the centroids of this volume in the xy-plane are at distances $\overline{X}$ and $\overline{Y}$ from the axes (see Figure 7.36) which are given by the following equations.

$$\overline{X} = \frac{1}{V}\left[\int_0^a \int_0^{110} x f(x,y)\,dy\,dx + \int_a^b \int_0^{fy} x f(x,y)\,dy\,dx - \int_{15}^{a} \int_{0}^{110} x f(x,y)\,dy\,dx - \int_{a}^{S_{5x}} \int_{S_{5y}}^{fy} x f(x,y)\,dy\,dx\right.$$

$$+ \int_{15}^{S_{5x}} \int_{S_{5y}}^{nmy} x f(x,y)\,dy\,dx - \int_{0}^{85} \int_{0}^{15ony} x f(x,y)\,dy\,dx - \int_{0}^{40} \int_{0}^{15poy} x f(x,y)\,dy\,dx - \int_{0}^{15} \int_{0}^{15qpy} x f(x,y)\,dy\,dx$$

$$- \int_{0}^{50} \int_{0}^{50qay} x f(x,y)\,dy\,dx - \int_{50}^{70} \int_{0}^{70aby} x f(x,y)\,dy\,dx - \int_{70}^{135} \int_{0}^{135bcy} x f(x,y)\,dy\,dx - \int_{135}^{155} \int_{0}^{155cdy} x f(x,y)\,dy\,dx$$

$$\left. - \int_{155}^{S_{13x}} \int_{0}^{S_{13y}} x f(x,y)\,dy\,dx - \int_{155}^{S_{13x}} \int_{S_{13y}}^{dey} x f(x,y)\,dy\,dx - \int_{S_{13x}}^{b} \int_{0}^{fy} x f(x,y)\,dy\,dx\right]$$

$$\overline{Y} = \frac{1}{V}\left[\int_0^{110} \int_0^{a} y f(x,y)\,dx\,dy + \int_0^{110} \int_a^{fx} y f(x,y)\,dx\,dy - \int_{S_{5y}}^{110} \int_{15}^{a} y f(x,y)\,dx\,dy - \int_{S_{5y}}^{110} \int_{a}^{fx} y f(x,y)\,dx\,dy\right.$$

$$+ \int_{S_{5y}}^{110} \int_{15}^{nmx} y f(x,y)\,dx\,dy - \int_{85}^{110} \int_{0}^{onx} y f(x,y)\,dx\,dy - \int_{40}^{85} \int_{0}^{pox} y f(x,y)\,dx\,dy - \int_{15}^{40} \int_{0}^{qpx} y f(x,y)\,dx\,dy$$

$$\left. - \int_{0}^{15} \int_{0}^{qax} y f(x,y)\,dx\,dy - \int_{0}^{15} \int_{50}^{abx} y f(x,y)\,dx\,dy - \int_{0}^{15} \int_{70}^{bcx} y f(x,y)\,dx\,dy - \int_{0}^{15} \int_{135}^{cdx} y f(x,y)\,dx\,dy\right]$$

$$- \int_{0}^{S_{13y}} \int_{155}^{S_{13x}} y f(x,y)\, dx\, dy - \int_{S_{13y}}^{15} \int_{155}^{dex} y f(x,y)\, dx\, dy - \int_{0}^{S_{13y}} \int_{S_{13x}}^{fx} y f(x,y)\, dx\, dy \Bigg]$$

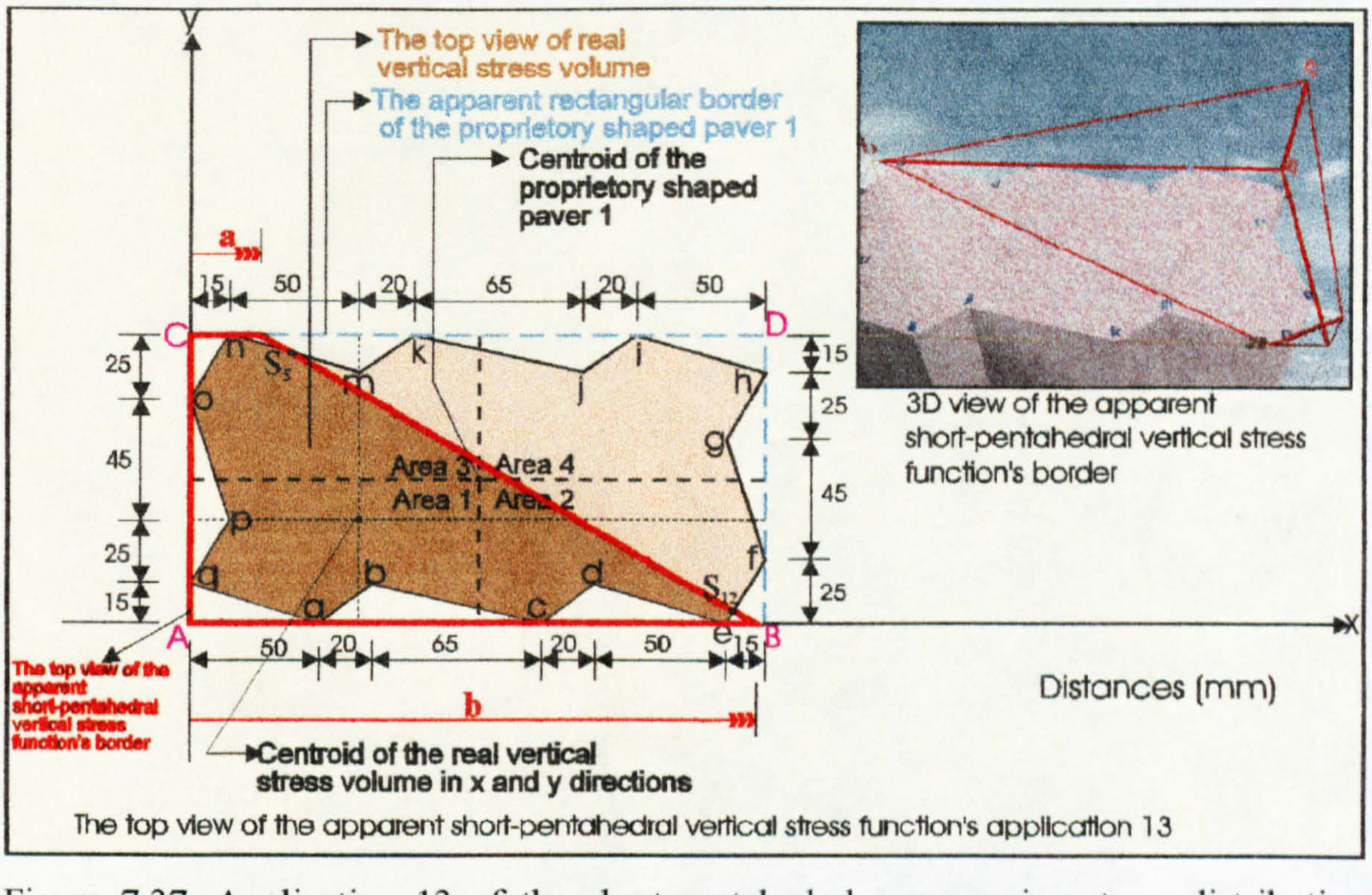

The top view of the apparent short-pentahedral vertical stress function's application 13

Figure 7.37: Application 13 of the short-pentahedral compressive stress distribution beneath the circumscribing rectangular border of proprietory shaped paver 1.

Application 13 of the short-pentahedral compressive stress regime beneath the circumscribing rectangular border of proprietory shaped paver 1 shown in Figure 7.37 can be calculated by using Tables 5.1 and 7.2 and the surface function of the short-pentahedral compressive stress through the three points σ_A, **b** and **u**.

The total volume **V** beneath the surface $f(x,y) = z\ (> 0)$ and above the region in the xy-plane (see Figure 7.37) is:

$$V = \int_{0}^{a} \int_{0}^{110} f(x,y)\, dy\, dx + \int_{a}^{b} \int_{0}^{fy} f(x,y)\, dy\, dx - \int_{15}^{a} \int_{S_{5y}}^{110} f(x,y)\, dy\, dx - \int_{a}^{S_{5x}} \int_{S_{5y}}^{fy} f(x,y)\, dy\, dx$$

$$+\int_{15}^{S_{5x}}\int_{S_{5y}}^{nmy} f(x,y)\,dy\,dx-\int_{0}^{15}\int_{85}^{ony} f(x,y)\,dy\,dx-\int_{0}^{15}\int_{40}^{poy} f(x,y)\,dy\,dx-\int_{0}^{15}\int_{15}^{qpy} f(x,y)\,dy\,dx$$

$$-\int_{0}^{50}\int_{0}^{qay} f(x,y)\,dy\,dx-\int_{50}^{70}\int_{0}^{aby} f(x,y)\,dy\,dx-\int_{70}^{135}\int_{0}^{bcy} f(x,y)\,dy\,dx-\int_{135}^{155}\int_{0}^{cdy} f(x,y)\,dy\,dx$$

$$-\int_{155}^{205}\int_{0}^{dey} f(x,y)\,dy\,dx-\int_{205}^{S_{12x}}\int_{0}^{efy} f(x,y)\,dy\,dx-\int_{S_{12x}}^{b}\int_{0}^{fy} f(x,y)\,dy\,dx$$

and the centroids of this volume in the xy-plane are at distances $\overline{X}$ and $\overline{Y}$ from the axes (see Figure 7.37) which are given by the following equations.

$$\overline{X}=\frac{1}{V}\left[\int_{0}^{a}\int_{0}^{110} x f(x,y)\,dy\,dx+\int_{a}^{b}\int_{0}^{fy} x f(x,y)\,dy\,dx-\int_{15}^{a}\int_{S_{5y}}^{110} x f(x,y)\,dy\,dx-\int_{a}^{S_{5x}}\int_{S_{5y}}^{fy} x f(x,y)\,dy\,dx\right.$$

$$+\int_{15}^{S_{5x}}\int_{S_{5y}}^{nmy} x\,xf(x,y)\,dy\,dx-\int_{0}^{15}\int_{85}^{ony} x f(x,y)\,dy\,dx-\int_{0}^{15}\int_{40}^{poy} x f(x,y)\,dy\,dx-\int_{0}^{15}\int_{15}^{qpy} x f(x,y)\,dy\,dx$$

$$-\int_{0}^{50}\int_{0}^{qay} x f(x,y)\,dy\,dx-\int_{50}^{70}\int_{0}^{aby} x f(x,y)\,dy\,dx-\int_{70}^{135}\int_{0}^{bcy} x f(x,y)\,dy\,dx-\int_{135}^{155}\int_{0}^{cdy} x f(x,y)\,dy\,dx$$

$$\left.-\int_{155}^{205}\int_{0}^{dey} x f(x,y)\,dy\,dx-\int_{205}^{S_{12x}}\int_{0}^{efy} x f(x,y)\,dy\,dx-\int_{S_{12x}}^{b}\int_{0}^{fy} x f(x,y)\,dy\,dx\right]$$

$$\overline{Y}=\frac{1}{V}\left[\int_{0}^{110}\int_{0}^{a} y f(x,y)\,dx\,dy+\int_{0}^{110}\int_{a}^{fx} y f(x,y)\,dx\,dy-\int_{S_{5y}}^{110}\int_{15}^{a} y f(x,y)\,dx\,dy-\int_{S_{5y}}^{110}\int_{a}^{fx} y f(x,y)\,dx\,dy\right.$$

$$+\int_{S_{5y}}^{110}\int_{15}^{nmx} y f(x,y)\,dx\,dy-\int_{85}^{110}\int_{0}^{onx} y f(x,y)\,dx\,dy-\int_{40}^{85}\int_{0}^{pox} y f(x,y)\,dx\,dy-\int_{15}^{40}\int_{0}^{qpx} y f(x,y)\,dx\,dy$$

$$-\int_{0}^{15}\int_{0}^{qax} y f(x,y)\,dx\,dy-\int_{0}^{15}\int_{50}^{abx} y f(x,y)\,dx\,dy-\int_{0}^{15}\int_{70}^{bcx} y f(x,y)\,dx\,dy-\int_{0}^{15}\int_{135}^{cdx} y f(x,y)\,dx\,dy$$

$$\left.-\int_{0}^{15}\int_{155}^{dex} y f(x,y)\,dx\,dy-\int_{0}^{S_{12y}}\int_{205}^{efx} y f(x,y)\,dx\,dy-\int_{0}^{S_{12y}}\int_{S_{12x}}^{fx} y f(x,y)\,dx\,dy\right]$$

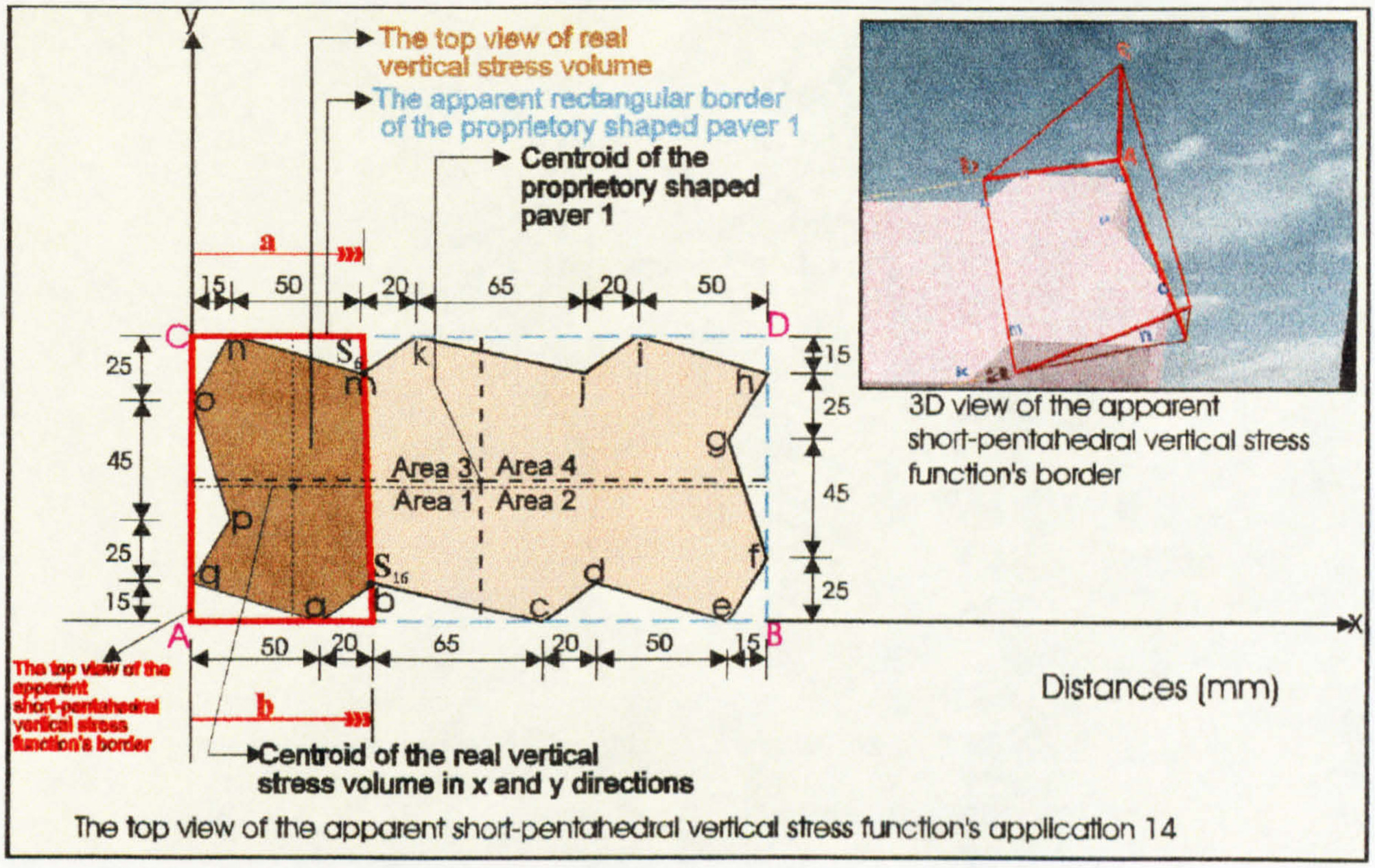

Figure 7.38: Application 14 of the short-pentahedral compressive stress distribution beneath the circumscribing rectangular border of proprietory shaped paver 1.

Application 14 of the short-pentahedral compressive stress regime beneath the circumscribing rectangular border of proprietory shaped paver 1 shown in Figure 7.38 can be calculated by using Tables 5.1 and 7.2 and the surface function of the short-pentahedral compressive stress through the three points σ_A, **b** and **u**.

The total volume **V** beneath the surface $f(x,y) = z\ (> 0)$ and above the region in the xy-plane (see Figure 7.38) is:

$$V = \int_0^a \int_0^{110} f(x,y)\,dy\,dx + \int_a^b \int_0^{fy} f(x,y)\,dy\,dx - \int_{65}^{a} \int_0^{110} f(x,y)\,dy\,dx - \int_{a}^{S_{6y}} \int_0^{fy} f(x,y)\,dy\,dx$$
$$- \int_{65}^{S_{6x}} \int_{95}^{mky} f(x,y)\,dy\,dx - \int_{15}^{65} \int_{95}^{nmy} f(x,y)\,dy\,dx - \int_0^{50} \int_0^{qay} f(x,y)\,dy\,dx - \int_0^{15} \int_{85}^{ony} f(x,y)\,dy\,dx$$
$$- \int_0^{15} \int_{40}^{poy} f(x,y)\,dy\,dx - \int_0^{15} \int_{15}^{qpy} f(x,y)\,dy\,dx - \int_{50}^{S_{16x}} \int_0^{aby} f(x,y)\,dy\,dx - \int_{S_{16x}}^{b} \int_0^{fy} f(x,y)\,dy\,dx$$

and the centroids of this volume in the xy-plane are at distances $\overline{X}$ and $\overline{Y}$ from the axes (see Figure 7.38) which are given by the following equations.

$$\overline{X} = \frac{1}{V}\left[\begin{array}{l} \int_{0}^{a}\int_{0}^{110} x f(x,y)\,dy\,dx + \int_{a}^{b}\int_{0}^{fy} x f(x,y)\,dy\,dx - \int_{65}^{a}\int_{S_{6y}}^{110} x f(x,y)\,dy\,dx - \int_{a}^{S_{6x}}\int_{S_{6y}}^{fy} x f(x,y)\,dy\,dx \\ - \int_{65}^{S_{6x}}\int_{95}^{mky} x f(x,y)\,dy\,dx - \int_{15}^{65}\int_{95}^{nmy} x f(x,y)\,dy\,dx - \int_{0}^{50}\int_{0}^{qay} x f(x,y)\,dy\,dx - \int_{0}^{15}\int_{85}^{ony} x f(x,y)\,dy\,dx \\ - \int_{0}^{15}\int_{40}^{poy} x f(x,y)\,dy\,dx - \int_{0}^{15}\int_{15}^{qpy} x f(x,y)\,dy\,dx - \int_{50}^{S_{16x}}\int_{0}^{aby} x f(x,y)\,dy\,dx - \int_{S_{16x}}^{b}\int_{0}^{fy} x f(x,y)\,dy\,dx \end{array}\right]$$

$$\overline{Y} = \frac{1}{V}\left[\begin{array}{l} \int_{0}^{110}\int_{0}^{a} y f(x,y)\,dx\,dy + \int_{0}^{110}\int_{a}^{fx} y f(x,y)\,dx\,dy - \int_{S_{6y}}^{110}\int_{65}^{a} y f(x,y)\,dx\,dy - \int_{S_{6y}}^{110}\int_{a}^{fx} y f(x,y)\,dx\,dy \\ + \int_{95}^{S_{6y}}\int_{65}^{mkx} y f(x,y)\,dx\,dy - \int_{95}^{110}\int_{15}^{nmx} y f(x,y)\,dx\,dy - \int_{0}^{15}\int_{0}^{qax} y f(x,y)\,dx\,dy - \int_{85}^{110}\int_{0}^{onx} y f(x,y)\,dx\,dy \\ - \int_{40}^{85}\int_{0}^{pox} y f(x,y)\,dx\,dy - \int_{15}^{40}\int_{0}^{qpx} y f(x,y)\,dx\,dy - \int_{0}^{S_{16y}}\int_{50}^{abx} y f(x,y)\,dx\,dy - \int_{0}^{S_{16y}}\int_{S_{16x}}^{fx} y f(x,y)\,dx\,dy \end{array}\right]$$

Application 15 of the short-pentahedral compressive stress regime beneath the circumscribing rectangular border of proprietory shaped paver 1 shown in Figure 7.39 can be calculated by using Tables 5.1 and 7.2 and the surface function of the short-pentahedral compressive stress through the three points σ_A, **b** and **u**.

The total volume **V** beneath the surface $f(x,y) = z\ (> 0)$ and above the region in the xy-plane (see Figure 7.39) is:

$$V = \int_{0}^{a}\int_{0}^{110} f(x,y)\,dy\,dx + \int_{a}^{b}\int_{0}^{fy} f(x,y)\,dy\,dx - \int_{65}^{a}\int_{S_{6y}}^{110} f(x,y)\,dy\,dx - \int_{a}^{S_{6x}}\int_{S_{6y}}^{fy} f(x,y)\,dy\,dx$$
$$- \int_{65}^{S_{6x}}\int_{95}^{mky} f(x,y)\,dy\,dx - \int_{15}^{65}\int_{95}^{nmy} f(x,y)\,dy\,dx - \int_{0}^{50}\int_{0}^{qay} f(x,y)\,dy\,dx - \int_{0}^{15}\int_{85}^{ony} f(x,y)\,dy\,dx$$

$$-\int_{0}^{15}\int_{40}^{poy} f(x,y)\,dy\,dx-\int_{0}^{15}\int_{15}^{qpy} f(x,y)\,dy\,dx-\int_{50}^{70}\int_{0}^{aby} f(x,y)\,dy\,dx-\int_{70}^{S_{15x}}\int_{0}^{S_{15y}} f(x,y)\,dy\,dx$$

$$-\int_{70}^{S_{15x}}\int_{S_{15y}}^{bcy} f(x,y)\,dy\,dx-\int_{S_{15x}}^{b}\int_{0}^{fy} f(x,y)\,dy\,dx$$

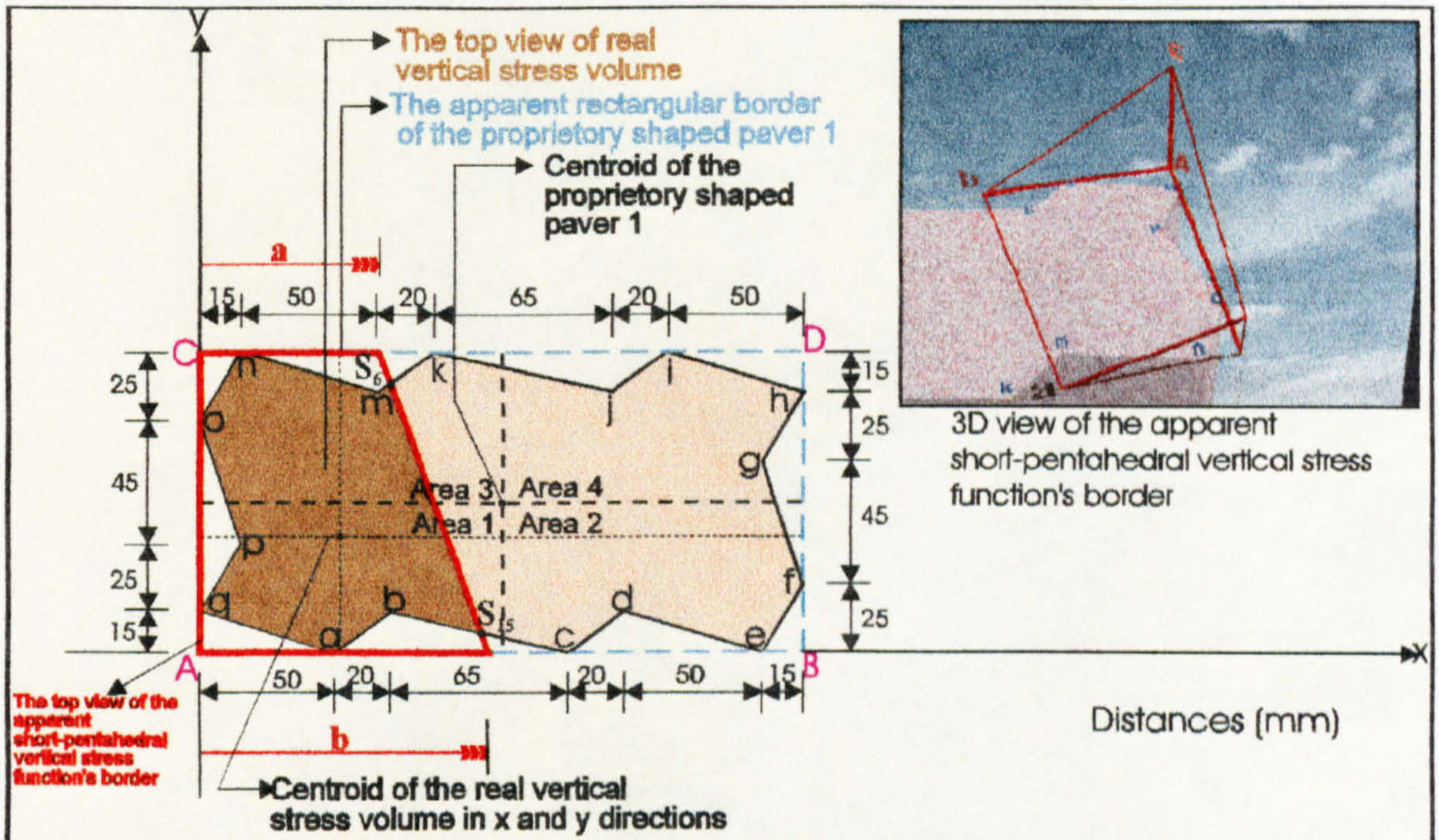

Figure 7.39: Application 15 of the short-pentahedral compressive stress distribution beneath the circumscribing rectangular border of proprietory shaped paver 1.

and the centroids of this volume in the xy-plane are at distances $\overline{X}$ and $\overline{Y}$ from the axes (see Figure 7.39) which are given by the following equations.

$$\overline{X}=\frac{1}{V}\left[\int_{0}^{a}\int_{0}^{110} x\,f(x,y)\,dy\,dx+\int_{a}^{b}\int_{0}^{fy} x\,f(x,y)\,dy\,dx-\int_{65}^{a}\int_{S_{6y}}^{110} x\,f(x,y)\,dy\,dx-\int_{a}^{S_{6x}}\int_{S_{6y}}^{fy} x\,f(x,y)\,dy\,dx\right.$$

$$-\int_{65}^{S_{6x}}\int_{95}^{mky} x\,f(x,y)\,dy\,dx-\int_{15}^{65}\int_{95}^{nmy} x\,f(x,y)\,dy\,dx-\int_{0}^{50}\int_{0}^{qay} x\,f(x,y)\,dy\,dx-\int_{0}^{15}\int_{85}^{ony} x\,f(x,y)\,dy\,dx$$

$$\left.-\int_{0}^{15}\int_{40}^{poy} x\,f(x,y)\,dy\,dx-\int_{0}^{15}\int_{15}^{qpy} x\,f(x,y)\,dy\,dx-\int_{50}^{70}\int_{0}^{aby} x\,f(x,y)\,dy\,dx-\int_{70}^{S_{15x}}\int_{0}^{S_{15y}} x\,f(x,y)\,dy\,dx\right.$$

$$-\int_{70}^{S_{15x}}\int_{S_{15y}}^{bcy} x f(x,y)\,dy\,dx - \int_{S_{15x}}^{b}\int_{0}^{fy} x f(x,y)\,dy\,dx\Bigg]$$

$$\bar{Y} = \frac{1}{V}\Bigg[\int_{0}^{110}\int_{0}^{a} y f(x,y)\,dx\,dy + \int_{0}^{110}\int_{a}^{fx} y f(x,y)\,dx\,dy - \int_{S_{6y}}^{110}\int_{65}^{a} y f(x,y)\,dx\,dy - \int_{S_{6y}}^{110}\int_{a}^{fx} y f(x,y)\,dx\,dy$$
$$+\int_{95}^{S_{6y}}\int_{65}^{mkx} y f(x,y)\,dx\,dy - \int_{95}^{110}\int_{15}^{nmx} y f(x,y)\,dx\,dy - \int_{0}^{15}\int_{0}^{qax} y f(x,y)\,dx\,dy - \int_{85}^{110}\int_{0}^{onx} y f(x,y)\,dx\,dy$$
$$-\int_{40}^{85}\int_{0}^{pox} y f(x,y)\,dx\,dy - \int_{15}^{40}\int_{0}^{qpx} y f(x,y)\,dx\,dy - \int_{0}^{15}\int_{50}^{abx} y f(x,y)\,dx\,dy - \int_{0}^{S_{15y}}\int_{70}^{S_{15x}} y f(x,y)\,dx\,dy$$
$$-\int_{S_{15y}}^{15}\int_{70}^{bcx} y f(x,y)\,dx\,dy - \int_{0}^{S_{15y}}\int_{S_{15x}}^{fx} y f(x,y)\,dx\,dy\Bigg]$$

Application 16 of the short-pentahedral compressive stress regime beneath the circumscribing rectangular border of proprietory shaped paver 1 shown in Figure 7.40 can be calculated by using Tables 5.1 and 7.2 and the surface function of the short-pentahedral compressive stress through the three points σ_A, **b** and **u**.

The total volume **V** beneath the surface $f(x,y) = z\ (> 0)$ and above the region in the xy-plane (see Figure 7.40) is:

$$V = \int_{0}^{a}\int_{0}^{110} f(x,y)\,dy\,dx + \int_{a}^{b}\int_{0}^{fy} f(x,y)\,dy\,dx - \int_{65}^{a}\int_{S_{6y}}^{110} f(x,y)\,dy\,dx - \int_{a}^{S_{6x}}\int_{S_{6y}}^{fy} f(x,y)\,dy\,dx$$
$$-\int_{65}^{S_{6x}}\int_{95}^{mky} f(x,y)\,dy\,dx - \int_{15}^{65}\int_{95}^{nmy} f(x,y)\,dy\,dx - \int_{0}^{50}\int_{0}^{qpy} f(x,y)\,dy\,dx - \int_{0}^{15}\int_{85}^{ony} f(x,y)\,dy\,dx$$
$$-\int_{0}^{15}\int_{40}^{poy} f(x,y)\,dy\,dx - \int_{0}^{15}\int_{15}^{qpy} f(x,y)\,dy\,dx - \int_{50}^{70}\int_{0}^{nby} f(x,y)\,dy\,dx - \int_{70}^{135}\int_{0}^{bcy} f(x,y)\,dy\,dx$$
$$-\int_{135}^{S_{14x}}\int_{0}^{cdy} f(x,y)\,dy\,dx - \int_{S_{14x}}^{b}\int_{0}^{fy} f(x,y)\,dy\,dx$$

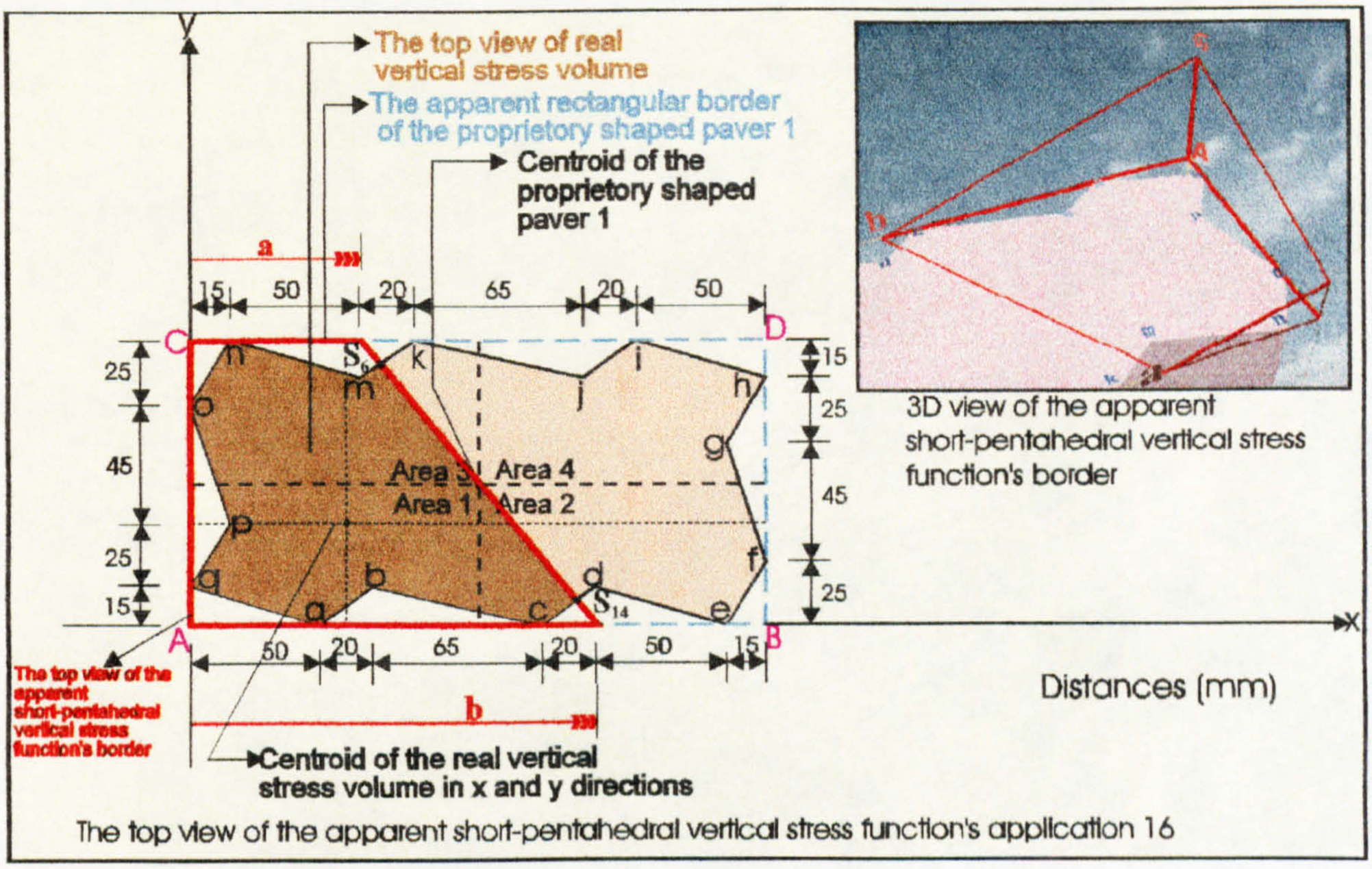

Figure 7.40: Application 16 of the short-pentahedral compressive stress distribution beneath the circumscribing rectangular border of proprietory shaped paver 1.

and the centroids of this volume in the xy-plane are at distances $\overline{X}$ and $\overline{Y}$ from the axes (see Figure 7.40) which are given by the following equations.

$$\overline{X} = \frac{1}{V}\left[\begin{array}{l} \int_0^a \int_0^{110} x f(x,y)\,dy\,dx + \int_a^b \int_0^{fy} x f(x,y)\,dy\,dx - \int_{65}^{a} \int_{S_{6y}}^{110} x f(x,y)\,dy\,dx - \int_a^{S_{6x}} \int_{S_{6y}}^{fy} x f(x,y)\,dy\,dx \\ - \int_{65}^{S_{6x}} \int_{95}^{mky} x f(x,y)\,dy\,dx - \int_{15}^{65} \int_{95}^{nmy} x f(x,y)\,dy\,dx - \int_0^{50} \int_0^{qay} x f(x,y)\,dy\,dx - \int_0^{15} \int_{85}^{ony} x f(x,y)\,dy\,dx \\ - \int_0^{15} \int_{40}^{poy} x f(x,y)\,dy\,dx - \int_0^{15} \int_{15}^{qpy} x f(x,y)\,dy\,dx - \int_{50}^{70} \int_0^{aby} x f(x,y)\,dy\,dx - \int_{70}^{135} \int_0^{bcy} x f(x,y)\,dy\,dx \\ - \int_{135}^{S_{14x}} \int_0^{cdy} x f(x,y)\,dy\,dx - \int_{S_{14x}}^{b} \int_0^{fy} x f(x,y)\,dy\,dx \end{array}\right]$$

$$\overline{Y} = \frac{1}{V}\left[\int_0^{110} \int_0^{a} y f(x,y)\,dx\,dy + \int_0^{110} \int_a^{fx} y f(x,y)\,dx\,dy - \int_{S_{6y}}^{110} \int_{65}^{a} y f(x,y)\,dx\,dy - \int_{S_{6y}}^{110} \int_a^{fx} y f(x,y)\,dx\,dy\right]$$

$$+\int_{95}^{S_{6y}}\int_{65}^{mkx} yf(x,y)\,dx\,dy-\int_{95}^{110}\int_{15}^{nmx} yf(x,y)\,dx\,dy-\int_{0}^{15}\int_{0}^{qax} yf(x,y)\,dx\,dy-\int_{85}^{110}\int_{0}^{onx} yf(x,y)\,dx\,dy$$

$$-\int_{40}^{85}\int_{0}^{pox} yf(x,y)\,dx\,dy-\int_{15}^{40}\int_{0}^{qpx} yf(x,y)\,dx\,dy-\int_{0}^{15}\int_{50}^{abx} yf(x,y)\,dx\,dy-\int_{0}^{15}\int_{70}^{bcx} yf(x,y)\,dx\,dy$$

$$-\int_{0}^{S_{14y}}\int_{135}^{cdx} yf(x,y)\,dx\,dy-\int_{0}^{S_{14y}}\int_{S_{14x}}^{fx} yf(x,y)\,dx\,dy\Bigg]$$

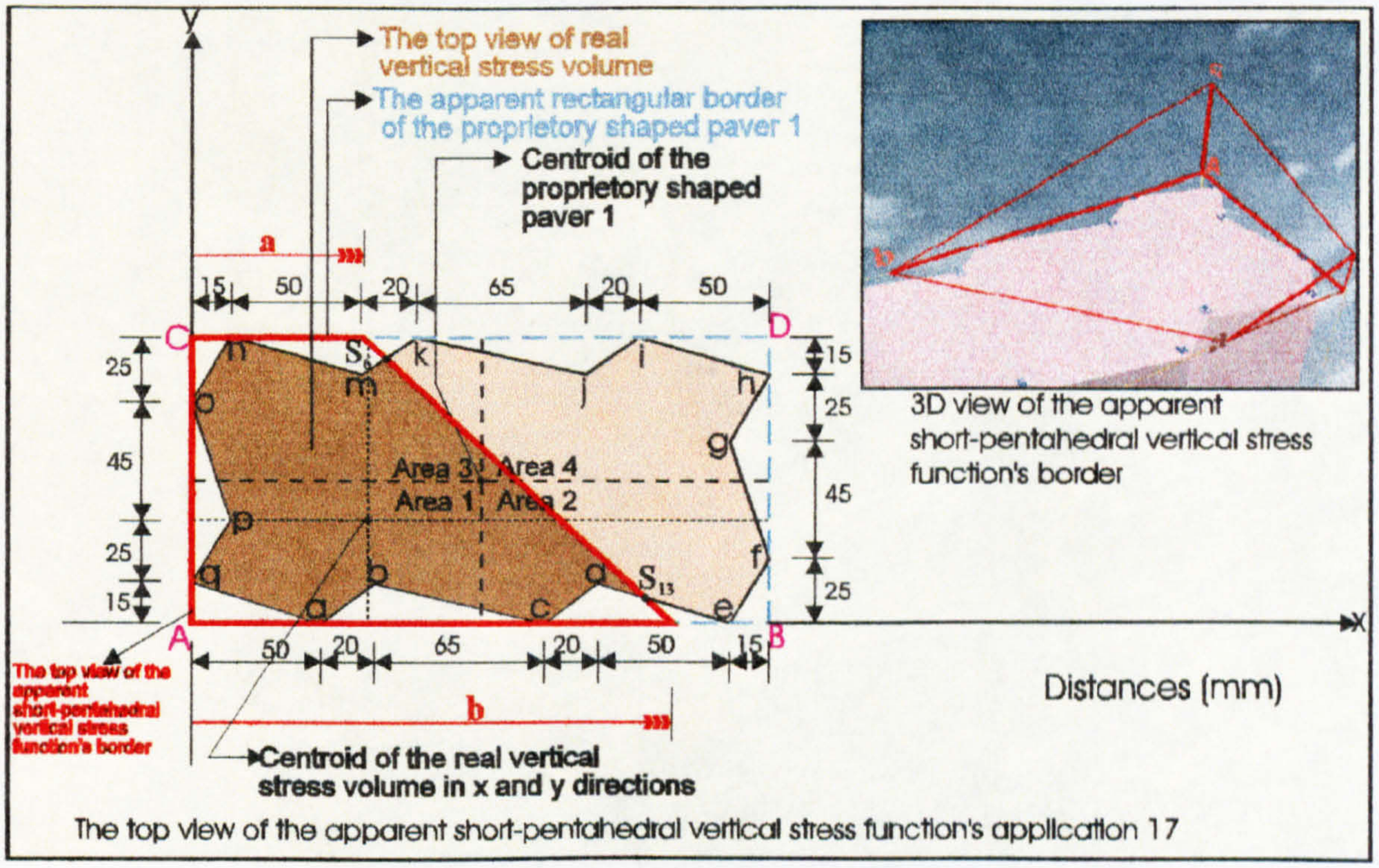

Figure 7.41: Application 17 of the short-pentahedral compressive stress distribution beneath the circumscribing rectangular border of proprietory shaped paver 1.

Application 17 of the short-pentahedral compressive stress regime beneath the circumscribing rectangular border of proprietory shaped paver 1 shown in Figure 7.41 can be calculated by using Tables 5.1 and 7.2 and the surface function of the short-pentahedral compressive stress through the three points σ_A, **b** and **u**.

The total volume **V** beneath the surface $f(x,y)=z\ (>0)$ and above the region in the xy-plane (see Figure 7.41) is:

$$V = \int_0^a \int_0^{110} f(x,y)\,dy\,dx + \int_a^b \int_0^{fy} f(x,y)\,dy\,dx - \int_{65}^{a} \int_{S_{6y}}^{110} f(x,y)\,dy\,dx - \int_a^{S_{6x}} \int_{S_{6y}}^{fy} f(x,y)\,dy\,dx$$
$$- \int_{65}^{S_{6x}} \int_{95}^{mky} f(x,y)\,dy\,dx - \int_{15}^{65} \int_{95}^{nmy} f(x,y)\,dy\,dx - \int_0^{50} \int_0^{qay} f(x,y)\,dy\,dx - \int_0^{15} \int_{85}^{ony} f(x,y)\,dy\,dx$$
$$- \int_0^{15} \int_{40}^{poy} f(x,y)\,dy\,dx - \int_0^{15} \int_{15}^{qpy} f(x,y)\,dy\,dx - \int_{50}^{70} \int_0^{ahy} f(x,y)\,dy\,dx - \int_{70}^{135} \int_0^{bcy} f(x,y)\,dy\,dx$$
$$- \int_{135}^{155} \int_0^{cdy} f(x,y)\,dy\,dx - \int_{155}^{S_{13x}} \int_0^{S_{13y}} f(x,y)\,dy\,dx - \int_{155}^{S_{13x}} \int_{S_{13y}}^{dey} f(x,y)\,dy\,dx - \int_{S_{13x}}^{b} \int_0^{fy} f(x,y)\,dy\,dx$$

and the centroids of this volume in the xy-plane are at distances $\overline{X}$ and $\overline{Y}$ from the axes (see Figure 7.41) which are given by the following equations.

$$\overline{X} = \frac{1}{V}\left[\int_0^a \int_0^{110} x f(x,y)\,dy\,dx + \int_a^b \int_0^{fy} x f(x,y)\,dy\,dx - \int_{65}^{a} \int_{S_{6y}}^{110} x f(x,y)\,dy\,dx - \int_a^{S_{6x}} \int_{S_{6y}}^{fy} x f(x,y)\,dy\,dx\right.$$
$$- \int_{65}^{S_{6x}} \int_{95}^{mky} x f(x,y)\,dy\,dx - \int_{15}^{65} \int_{95}^{nmy} x f(x,y)\,dy\,dx - \int_0^{50} \int_0^{qay} x f(x,y)\,dy\,dx - \int_0^{15} \int_{85}^{ony} x f(x,y)\,dy\,dx$$
$$- \int_0^{15} \int_{40}^{poy} x f(x,y)\,dy\,dx - \int_0^{15} \int_{15}^{qpy} x f(x,y)\,dy\,dx - \int_{50}^{70} \int_0^{axby} x f(x,y)\,dy\,dx - \int_{70}^{135} \int_0^{bcy} x f(x,y)\,dy\,dx$$
$$\left. - \int_{135}^{155} \int_0^{cdy} x f(x,y)\,dy\,dx - \int_{155}^{S_{13x}} \int_0^{S_{13y}} x f(x,y)\,dy\,dx - \int_{155}^{S_{13x}} \int_{S_{13y}}^{dey} x f(x,y)\,dy\,dx - \int_{S_{13x}}^{b} \int_0^{fy} x f(x,y)\,dy\,dx\right]$$

$$\overline{Y} = \frac{1}{V}\left[\int_0^{110} \int_0^{a} y f(x,y)\,dx\,dy + \int_0^{110} \int_a^{fx} y f(x,y)\,dx\,dy - \int_{S_{6y}}^{110} \int_{65}^{a} y f(x,y)\,dx\,dy - \int_{S_{6y}}^{110} \int_a^{fx} y f(x,y)\,dx\,dy\right.$$
$$+ \int_{95}^{S_{6y}} \int_{65}^{mkx} y f(x,y)\,dx\,dy - \int_{95}^{110} \int_{15}^{nmx} y f(x,y)\,dx\,dy - \int_0^{15} \int_0^{qax} y f(x,y)\,dx\,dy - \int_{85}^{110} \int_0^{onx} y f(x,y)\,dx\,dy$$
$$- \int_{40}^{85} \int_0^{pox} y f(x,y)\,dx\,dy - \int_{15}^{40} \int_0^{qpx} y f(x,y)\,dx\,dy - \int_0^{15} \int_{50}^{abx} y f(x,y)\,dx\,dy - \int_0^{15} \int_{70}^{bcx} y f(x,y)\,dx\,dy$$
$$\left. - \int_0^{15} \int_{135}^{cdx} y f(x,y)\,dx\,dy - \int_0^{S_{13y}} \int_{155}^{S_{13x}} y f(x,y)\,dx\,dy - \int_{S_{13y}}^{15} \int_{155}^{dex} y f(x,y)\,dx\,dy - \int_0^{S_{13y}} \int_{S_{13x}}^{fx} y f(x,y)\,dx\,dy\right]$$

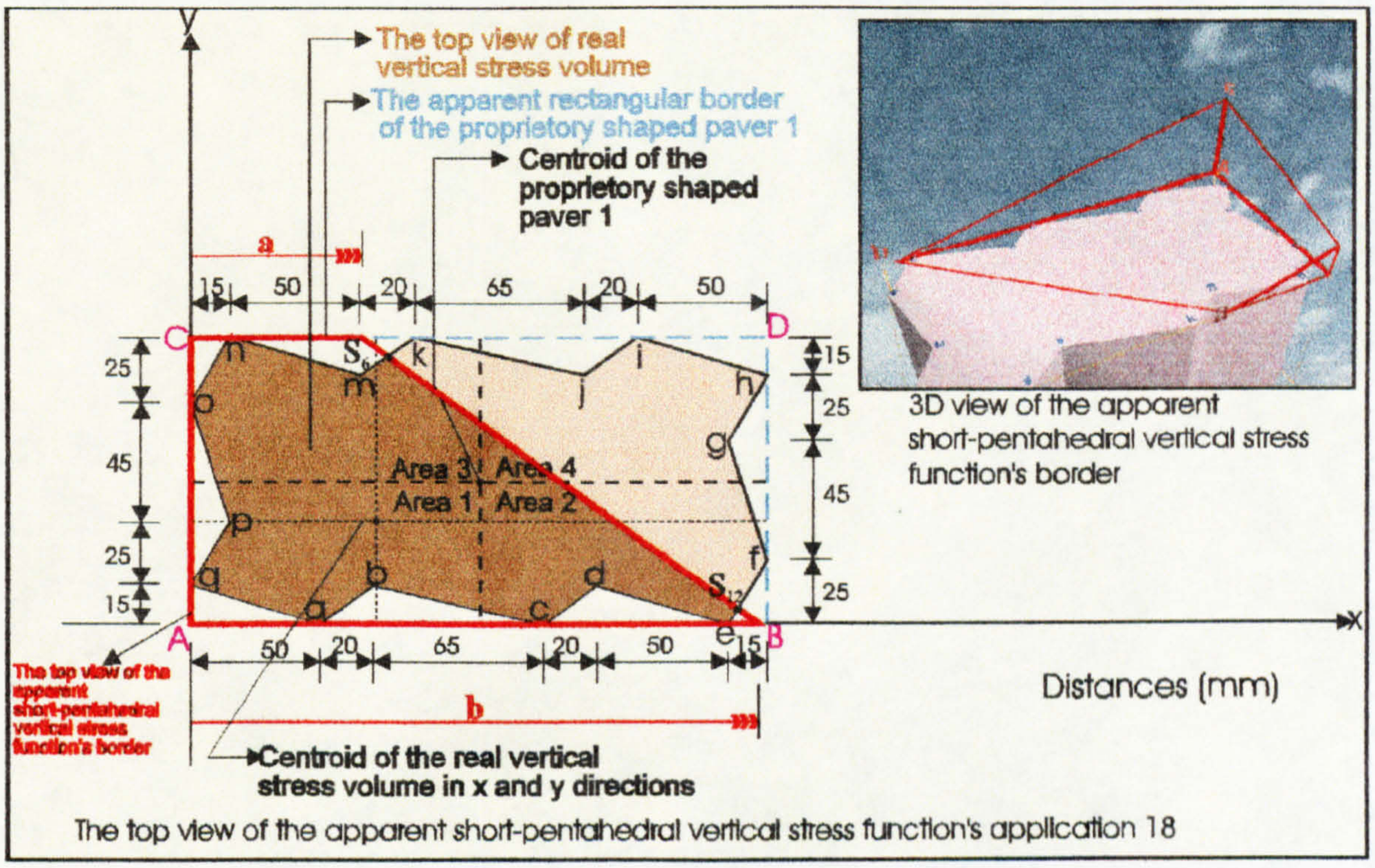

Figure 7.42: Application 18 of the short-pentahedral compressive stress distribution beneath the circumscribing rectangular border of proprietory shaped paver 1.

Application 18 of the short-pentahedral compressive stress regime beneath the circumscribing rectangular border of proprietory shaped paver 1 shown in Figure 7.42 can be calculated by using Tables 5.1 and 7.2 and the surface function of the short-pentahedral compressive stress through the three points σ_A, **b** and **u**.

The total volume **V** beneath the surface $f(x,y) = z\ (> 0)$ and above the region in the xy-plane (see Figure 7.42) is:

$$V = \int_{0}^{a}\int_{0}^{110} f(x,y)\,dy\,dx + \int_{a}^{b}\int_{0}^{fy} f(x,y)\,dy\,dx - \int_{a}^{65}\int_{0}^{110} f(x,y)\,dy\,dx - \int_{65}^{S_{6x}}\int_{S_{6y}}^{fy} f(x,y)\,dy\,dx$$

$$- \int_{65}^{S_{6x}}\int_{95}^{mky} f(x,y)\,dy\,dx - \int_{15}^{65}\int_{95}^{nmy} f(x,y)\,dy\,dx - \int_{0}^{50}\int_{0}^{qay} f(x,y)\,dy\,dx - \int_{0}^{15}\int_{85}^{ony} f(x,y)\,dy\,dx$$

$$- \int_{0}^{15}\int_{40}^{poy} f(x,y)\,dy\,dx - \int_{0}^{15}\int_{15}^{qpy} f(x,y)\,dy\,dx - \int_{50}^{70}\int_{0}^{aby} f(x,y)\,dy\,dx - \int_{70}^{135}\int_{0}^{bcy} f(x,y)\,dy\,dx$$

$$-\int_{135}^{155}\int_{0}^{cdy} f(x,y)\,dy\,dx-\int_{155}^{205}\int_{0}^{dey} f(x,y)\,dy\,dx-\int_{205}^{S_{12x}}\int_{0}^{efy} f(x,y)\,dy\,dx-\int_{S_{12x}}^{b}\int_{0}^{fy} f(x,y)\,dy\,dx$$

and the centroids of this volume in the xy-plane are at distances $\overline{X}$ and $\overline{Y}$ from the axes (see Figure 7.42) which are given by the following equations.

$$\overline{X}=\frac{1}{V}\left[\begin{array}{l}
\int_{0}^{a}\int_{0}^{110} xf(x,y)\,dy\,dx+\int_{a}^{b}\int_{0}^{fy} xf(x,y)\,dy\,dx-\int_{65}^{a}\int_{S_{6y}}^{110} xf(x,y)\,dy\,dx-\int_{a}^{S_{6x}}\int_{S_{6y}}^{fy} xf(x,y)\,dy\,dx \\
-\int_{65}^{S_{6x}}\int_{95}^{mky} xf(x,y)\,dy\,dx-\int_{15}^{65}\int_{95}^{nmy} xf(x,y)\,dy\,dx-\int_{0}^{50}\int_{0}^{qay} xf(x,y)\,dy\,dx-\int_{0}^{15}\int_{85}^{ony} xf(x,y)\,dy\,dx \\
-\int_{0}^{15}\int_{40}^{poy} xf(x,y)\,dy\,dx-\int_{0}^{15}\int_{15}^{qpy} xf(x,y)\,dy\,dx-\int_{50}^{70}\int_{0}^{xby} xf(x,y)\,dy\,dx-\int_{70}^{135}\int_{0}^{bcy} xf(x,y)\,dy\,dx \\
-\int_{135}^{155}\int_{0}^{cdy} xf(x,y)\,dy\,dx-\int_{155}^{205}\int_{0}^{dey} xf(x,y)\,dy\,dx-\int_{205}^{S_{12x}}\int_{0}^{efy} xf(x,y)\,dy\,dx-\int_{S_{12x}}^{b}\int_{0}^{fy} xf(x,y)\,dy\,dx
\end{array}\right]$$

$$\overline{Y}=\frac{1}{V}\left[\begin{array}{l}
\int_{0}^{110}\int_{0}^{a} yf(x,y)\,dx\,dy+\int_{0}^{110}\int_{a}^{fx} yf(x,y)\,dx\,dy-\int_{S_{6y}}^{110}\int_{65}^{a} yf(x,y)\,dx\,dy-\int_{S_{6y}}^{110}\int_{a}^{fx} yf(x,y)\,dx\,dy \\
+\int_{95}^{S_{6y}}\int_{65}^{mkx} yf(x,y)\,dx\,dy-\int_{95}^{110}\int_{15}^{nmx} yf(x,y)\,dx\,dy-\int_{0}^{15}\int_{0}^{qax} yf(x,y)\,dx\,dy-\int_{85}^{110}\int_{0}^{onx} yf(x,y)\,dx\,dy \\
-\int_{40}^{85}\int_{0}^{pox} yf(x,y)\,dx\,dy-\int_{15}^{40}\int_{0}^{qpx} yf(x,y)\,dx\,dy-\int_{0}^{50}\int_{0}^{abx} yf(x,y)\,dx\,dy-\int_{0}^{70}\int_{0}^{bcx} yf(x,y)\,dx\,dy \\
-\int_{0}^{135}\int_{0}^{cdx} yf(x,y)\,dx\,dy-\int_{0}^{155}\int_{0}^{dex} yf(x,y)\,dx\,dy-\int_{0}^{205}\int_{0}^{S_{12y}\,efx} yf(x,y)\,dx\,dy-\int_{0}^{S_{12x}}\int_{0}^{fx} yf(x,y)\,dx\,dy
\end{array}\right]$$

Application 19 of the short-pentahedral compressive stress regime beneath the circumscribing rectangular border of proprietory shaped paver 1 shown in Figure 7.43 can be calculated by using Tables 5.1 and 7.2 and the surface function of the short-pentahedral compressive stress through the three points σ_A, b and u.

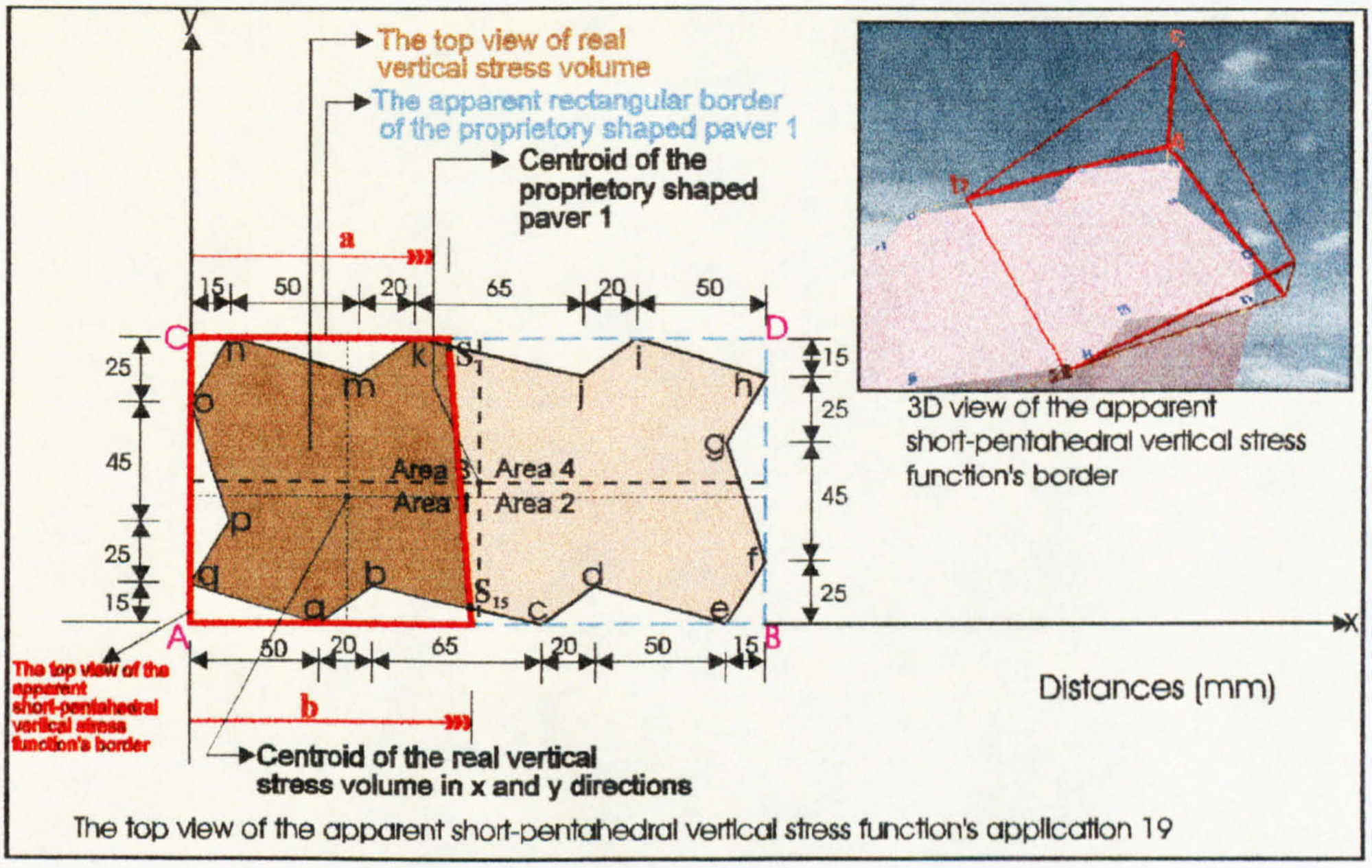

Figure 7.43: Application 19 of the short-pentahedral compressive stress distribution beneath the circumscribing rectangular border of proprietory shaped paver 1.

The total volume **V** beneath the surface $f(x,y) = z\ (> 0)$ and above the region in the xy-plane (see Figure 7.43) is:

$$V = \int_0^a \int_0^{110} f(x,y)\,dy\,dx + \int_a^b \int_0^{fy} f(x,y)\,dy\,dx - \int_{85}^{a} \int_{S_{7y}}^{110} f(x,y)\,dy\,dx - \int_a^{S_{7x}} \int_{S_{7y}}^{fy} f(x,y)\,dy\,dx$$

$$+ \int_{85}^{S_{7x}} \int_{S_{7y}}^{kjy} f(x,y)\,dy\,dx - \int_{65}^{85} \int_{95}^{mky} f(x,y)\,dy\,dx - \int_{15}^{65} \int_{95}^{nmy} f(x,y)\,dy\,dx - \int_0^{50} \int_0^{qay} f(x,y)\,dy\,dx$$

$$- \int_{50}^{70} \int_0^{aby} f(x,y)\,dy\,dx - \int_0^{85} \int_{15}^{ony} f(x,y)\,dy\,dx - \int_0^{40} \int_{15}^{poy} f(x,y)\,dy\,dx - \int_0^{15} \int_{15}^{qpy} f(x,y)\,dy\,dx$$

$$- \int_{70}^{S_{15x}} \int_0^{S_{15y}} f(x,y)\,dy\,dx - \int_{70}^{S_{15x}} \int_{S_{15y}}^{bcy} f(x,y)\,dy\,dx - \int_{S_{15x}}^{b} \int_0^{fy} f(x,y)\,dy\,dx$$

and the centroids of this volume in the xy-plane are at distances $\overline{X}$ and $\overline{Y}$ from the axes (see Figure 7.43) which are given by the following equations.

$$\overline{X} = \frac{1}{V}\left[\begin{array}{l}
\int_{0}^{a}\int_{0}^{110} x f(x,y)\,dy\,dx + \int_{a}^{b}\int_{0}^{fy} x f(x,y)\,dy\,dx - \int_{85}^{a}\int_{S_{7y}}^{110} x f(x,y)\,dy\,dx - \int_{a}^{S_{7x}}\int_{S_{7y}}^{fy} x f(x,y)\,dy\,dx \\
+ \int_{85}^{S_{7x}}\int_{S_{7y}}^{kjy} x f(x,y)\,dy\,dx - \int_{65}^{85}\int_{95}^{mky} x f(x,y)\,dy\,dx - \int_{15}^{65}\int_{95}^{nmy} x f(x,y)\,dy\,dx - \int_{0}^{50}\int_{0}^{qay} x f(x,y)\,dy\,dx \\
- \int_{50}^{70}\int_{0}^{aby} x f(x,y)\,dy\,dx - \int_{0}^{85}\int_{85}^{ony} x f(x,y)\,dy\,dx - \int_{0}^{40}\int_{0}^{poy} x f(x,y)\,dy\,dx - \int_{0}^{15}\int_{0}^{qpy} x f(x,y)\,dy\,dx \\
- \int_{70}^{S_{15x}}\int_{0}^{S_{15y}} x f(x,y)\,dy\,dx - \int_{70}^{S_{15x}}\int_{S_{15y}}^{bcy} x f(x,y)\,dy\,dx - \int_{S_{15x}}^{b}\int_{0}^{fy} x f(x,y)\,dy\,dx
\end{array}\right]$$

$$\overline{Y} = \frac{1}{V}\left[\begin{array}{l}
\int_{0}^{110}\int_{0}^{a} y f(x,y)\,dx\,dy + \int_{0}^{110}\int_{a}^{fx} y f(x,y)\,dx\,dy - \int_{S_{7y}}^{110}\int_{85}^{a} y f(x,y)\,dx\,dy - \int_{S_{7y}}^{110}\int_{a}^{fx} y f(x,y)\,dx\,dy \\
+ \int_{S_{7y}}^{110}\int_{85}^{kjx} y f(x,y)\,dx\,dy - \int_{95}^{110}\int_{65}^{mkx} y f(x,y)\,dx\,dy - \int_{95}^{110}\int_{15}^{nmx} y f(x,y)\,dx\,dy - \int_{0}^{15}\int_{0}^{qax} y f(x,y)\,dx\,dy \\
- \int_{0}^{15}\int_{50}^{abx} y f(x,y)\,dx\,dy - \int_{85}^{110}\int_{0}^{onx} y f(x,y)\,dx\,dy - \int_{40}^{85}\int_{0}^{pox} y f(x,y)\,dx\,dy - \int_{15}^{40}\int_{0}^{kjpx} y f(x,y)\,dx\,dy \\
- \int_{0}^{S_{15y}}\int_{70}^{S_{15x}} y f(x,y)\,dx\,dy - \int_{S_{15y}}^{15}\int_{70}^{bcx} y f(x,y)\,dx\,dy - \int_{0}^{S_{15y}}\int_{S_{15x}}^{fx} y f(x,y)\,dx\,dy
\end{array}\right]$$

Application 20 of the short-pentahedral compressive stress regime beneath the circumscribing rectangular border of proprietory shaped paver 1 shown in Figure 7.44 can be calculated by using Tables 5.1 and 7.2 and the surface function of the short-pentahedral compressive stress through the three points σ_A, **b** and **u**.

The total volume **V** beneath the surface $f(x,y) = z\ (> 0)$ and above the region in the xy-plane (see Figure 7.44) is:

$$V = \int_{0}^{a}\int_{0}^{110} f(x,y)\,dy\,dx + \int_{a}^{b}\int_{0}^{fy} f(x,y)\,dy\,dx - \int_{85}^{a}\int_{S_{7y}}^{110} f(x,y)\,dy\,dx - \int_{a}^{S_{7x}}\int_{S_{7y}}^{fy} f(x,y)\,dy\,dx$$

$$+\int_{85}^{S_{7x}}\int_{S_{7y}}^{kjy} f(x,y)\,dy\,dx-\int_{65}^{85}\int_{95}^{mky} f(x,y)\,dy\,dx-\int_{15}^{65}\int_{95}^{nmy} f(x,y)\,dy\,dx-\int_{0}^{50}\int_{0}^{qay} f(x,y)\,dy\,dx$$

$$-\int_{50}^{70}\int_{0}^{aby} f(x,y)\,dy\,dx-\int_{0}^{50}\int_{85}^{ony} f(x,y)\,dy\,dx-\int_{0}^{40}\int_{0}^{poy} f(x,y)\,dy\,dx-\int_{0}^{15}\int_{0}^{qpy} f(x,y)\,dy\,dx$$

$$-\int_{70}^{135}\int_{0}^{bcy} f(x,y)\,dy\,dx-\int_{135}^{S_{14x}}\int_{0}^{cdy} f(x,y)\,dy\,dx-\int_{S_{14x}}^{b}\int_{0}^{fy} f(x,y)\,dy\,dx$$

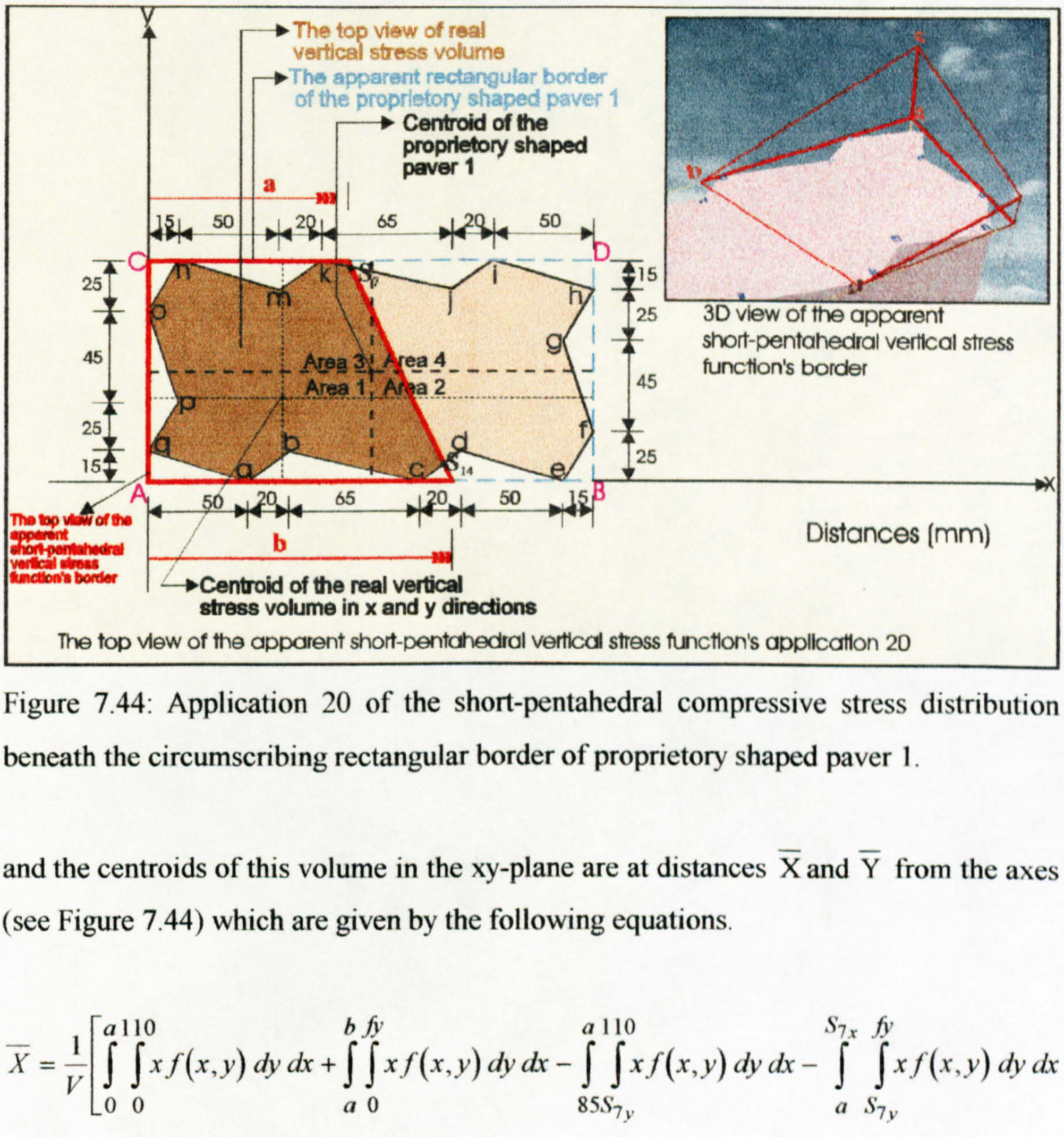

Figure 7.44: Application 20 of the short-pentahedral compressive stress distribution beneath the circumscribing rectangular border of proprietory shaped paver 1.

and the centroids of this volume in the xy-plane are at distances $\overline{X}$ and $\overline{Y}$ from the axes (see Figure 7.44) which are given by the following equations.

$$\overline{X}=\frac{1}{V}\left[\int_{0}^{a}\int_{0}^{110} x\,f(x,y)\,dy\,dx+\int_{a}^{b}\int_{0}^{fy} x\,f(x,y)\,dy\,dx-\int_{85}^{a}\int_{S_{7y}}^{110} x\,f(x,y)\,dy\,dx-\int_{a}^{S_{7x}}\int_{S_{7y}}^{fy} x\,f(x,y)\,dy\,dx\right.$$

$$+\int_{85}^{S_{7x}}\int_{S_{7y}}^{kjy} xf(x,y)\,dy\,dx-\int_{65}^{85}\int_{95}^{mky} xf(x,y)\,dy\,dx-\int_{15}^{65}\int_{95}^{nmy} xf(x,y)\,dy\,dx-\int_{0}^{50}\int_{0}^{qay} xf(x,y)\,dy\,dx$$

$$-\int_{50}^{70}\int_{0}^{aby} xf(x,y)\,dy\,dx-\int_{0}^{15}\int_{85}^{ony} xf(x,y)\,dy\,dx-\int_{0}^{15}\int_{0}^{poy} xf(x,y)\,dy\,dx-\int_{0}^{15}\int_{0}^{qpy} xf(x,y)\,dy\,dx$$

$$-\int_{70}^{135}\int_{0}^{bcy} xf(x,y)\,dy\,dx-\int_{135}^{S_{14x}}\int_{0}^{cdy} xf(x,y)\,dy\,dx-\int_{S_{14x}}^{b}\int_{0}^{fy} xf(x,y)\,dy\,dx\Bigg]$$

$$\bar{Y}=\frac{1}{V}\Bigg[\int_{0}^{110}\int_{0}^{a} yf(x,y)\,dx\,dy+\int_{0}^{110}\int_{a}^{fx} yf(x,y)\,dx\,dy-\int_{S_{7y}}^{110}\int_{85}^{a} yf(x,y)\,dx\,dy-\int_{S_{7y}}^{110}\int_{a}^{fx} yf(x,y)\,dx\,dy$$

$$+\int_{S_{7y}}^{110}\int_{85}^{kjx} yf(x,y)\,dx\,dy-\int_{95}^{110}\int_{65}^{mkx} yf(x,y)\,dx\,dy-\int_{95}^{110}\int_{15}^{nmx} yf(x,y)\,dx\,dy-\int_{0}^{15}\int_{0}^{qax} yf(x,y)\,dx\,dy$$

$$-\int_{0}^{15}\int_{50}^{abx} yf(x,y)\,dx\,dy-\int_{85}^{110}\int_{0}^{onx} yf(x,y)\,dx\,dy-\int_{40}^{85}\int_{0}^{pox} yf(x,y)\,dx\,dy-\int_{15}^{40}\int_{0}^{qpx} yf(x,y)\,dx\,dy$$

$$-\int_{0}^{15}\int_{70}^{bcx} yf(x,y)\,dx\,dy-\int_{0}^{S_{14y}}\int_{135}^{cdx} yf(x,y)\,dx\,dy-\int_{0}^{S_{14y}}\int_{S_{14x}}^{fx} yf(x,y)\,dx\,dy\Bigg]$$

Application 21 of the short-pentahedral compressive stress regime beneath the circumscribing rectangular border of proprietory shaped paver 1 shown in Figure 7.45 can be calculated by using Tables 5.1 and 7.2 and the surface function of the short-pentahedral compressive stress through the three points σ_A, **b** and **u**.

The total volume **V** beneath the surface $f(x,y)=z\ (>0)$ and above the region in the xy-plane (see Figure 7.45) is:

$$V=\int_{0}^{a}\int_{0}^{110} f(x,y)\,dy\,dx+\int_{a}^{b}\int_{0}^{fy} f(x,y)\,dy\,dx-\int_{85}^{a}\int_{S_{7y}}^{110} f(x,y)\,dy\,dx-\int_{a}^{S_{7x}}\int_{S_{7y}}^{fy} f(x,y)\,dy\,dx$$

$$+\int_{85}^{S_{7x}}\int_{S_{7y}}^{kjy} f(x,y)\,dy\,dx-\int_{65}^{85}\int_{95}^{mky} f(x,y)\,dy\,dx-\int_{15}^{65}\int_{95}^{nmy} f(x,y)\,dy\,dx-\int_{0}^{50}\int_{0}^{qpy} f(x,y)\,dy\,dx$$

$$-\int_{50}^{70}\int_{0}^{aby} f(x,y)\,dy\,dx - \int_{0}^{15}\int_{85}^{ony} f(x,y)\,dy\,dx - \int_{0}^{15}\int_{0}^{poy} f(x,y)\,dy\,dx - \int_{0}^{15}\int_{0}^{qpy} f(x,y)\,dy\,dx$$

$$-\int_{70}^{135}\int_{0}^{bcy} f(x,y)\,dy\,dx - \int_{135}^{155}\int_{0}^{cdy} f(x,y)\,dy\,dx - \int_{155}^{S_{13x}}\int_{0}^{S_{13y}} f(x,y)\,dy\,dx - \int_{155}^{S_{13x}}\int_{S_{13y}}^{dey} f(x,y)\,dy\,dx$$

$$-\int_{S_{13x}}^{b}\int_{0}^{fy} f(x,y)\,dy\,dx$$

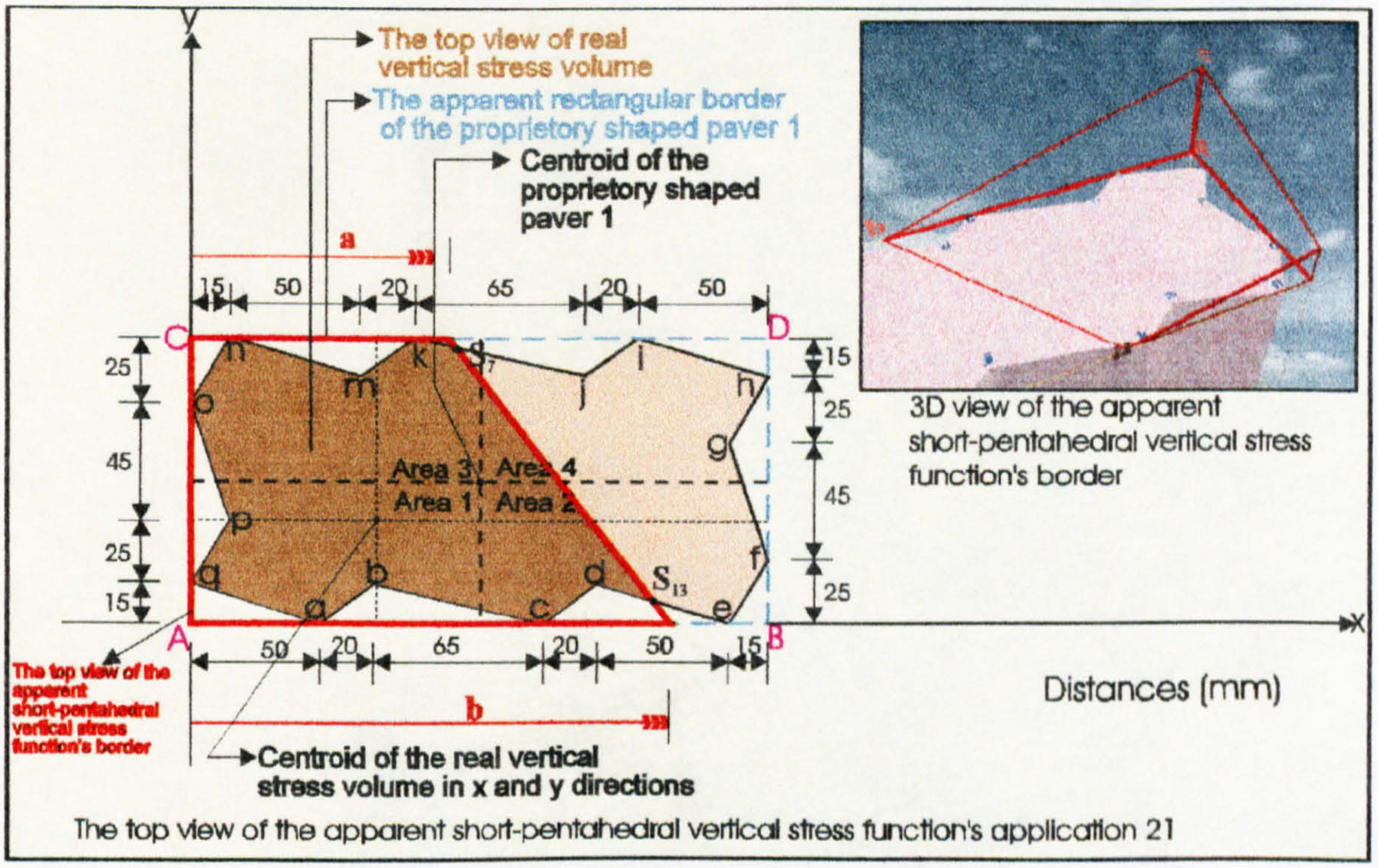

Figure 7.45: Application 21 of the short-pentahedral compressive stress distribution beneath the circumscribing rectangular border of proprietory shaped paver 1.

and the centroids of this volume in the xy-plane are at distances $\overline{X}$ and $\overline{Y}$ from the axes (see Figure 7.45) which are given by the following equations.

$$\overline{X} = \frac{1}{V}\left[\int_{0}^{a}\int_{0}^{110} x f(x,y)\,dy\,dx + \int_{a}^{b}\int_{0}^{fy} x f(x,y)\,dy\,dx - \int_{85}^{a}\int_{S_{7y}}^{110} x f(x,y)\,dy\,dx - \int_{a}^{S_{7x}}\int_{S_{7y}}^{fy} x f(x,y)\,dy\,dx\right.$$

$$\left. + \int_{85}^{S_{7x}}\int_{S_{7y}}^{kjy} x f(x,y)\,dy\,dx - \int_{65}^{85}\int_{95}^{mky} x f(x,y)\,dy\,dx - \int_{15}^{65}\int_{95}^{nmy} x f(x,y)\,dy\,dx - \int_{0}^{50}\int_{0}^{qay} x f(x,y)\,dy\,dx\right.$$

$$-\int_{50}^{70}\int_{0}^{aby} xf(x,y)\,dy\,dx-\int_{0}^{15}\int_{85}^{ony} xf(x,y)\,dy\,dx-\int_{0}^{15}\int_{40}^{poy} xf(x,y)\,dy\,dx-\int_{0}^{15}\int_{15}^{qpy} xf(x,y)\,dy\,dx$$

$$-\int_{70}^{135}\int_{0}^{bcy} xf(x,y)\,dy\,dx-\int_{135}^{155}\int_{0}^{cdy} xf(x,y)\,dy\,dx-\int_{155}^{S_{13x}}\int_{0}^{S_{13y}} xf(x,y)\,dy\,dx-\int_{155}^{S_{13x}}\int_{S_{13y}}^{dey} xf(x,y)\,dy\,dx$$

$$\left.-\int_{S_{13x}}^{b}\int_{0}^{fy} xf(x,y)\,dy\,dx\right]$$

$$\bar{Y}=\frac{1}{V}\left[\int_{0}^{110}\int_{0}^{a} yf(x,y)\,dx\,dy+\int_{0}^{110}\int_{a}^{fx} yf(x,y)\,dx\,dy-\int_{S_{7y}}^{110}\int_{85}^{a} yf(x,y)\,dx\,dy-\int_{S_{7y}}^{110}\int_{a}^{fx} yf(x,y)\,dx\,dy\right.$$

$$+\int_{S_{7y}}^{110}\int_{85}^{kjx} yf(x,y)\,dx\,dy-\int_{95}^{110}\int_{65}^{mkx} yf(x,y)\,dx\,dy-\int_{95}^{110}\int_{15}^{nmx} yf(x,y)\,dx\,dy-\int_{0}^{15}\int_{0}^{qax} yf(x,y)\,dx\,dy$$

$$-\int_{0}^{15}\int_{50}^{abx} yf(x,y)\,dx\,dy-\int_{85}^{110}\int_{0}^{onx} yf(x,y)\,dx\,dy-\int_{40}^{85}\int_{0}^{pox} yf(x,y)\,dx\,dy-\int_{15}^{40}\int_{0}^{qpx} yf(x,y)\,dx\,dy$$

$$-\int_{0}^{15}\int_{70}^{bcx} yf(x,y)\,dx\,dy-\int_{0}^{15}\int_{135}^{cdx} yf(x,y)\,dx\,dy-\int_{0}^{S_{13y}}\int_{155}^{S_{13x}} yf(x,y)\,dx\,dy-\int_{S_{13y}}^{15}\int_{155}^{dex} yf(x,y)\,dx\,dy$$

$$\left.-\int_{0}^{S_{13y}}\int_{S_{13x}}^{fx} yf(x,y)\,dx\,dy\right]$$

Application 22 of the short-pentahedral compressive stress regime beneath the circumscribing rectangular border of proprietory shaped paver 1 shown in Figure 7.46 can be calculated by using Tables 5.1 and 7.2 and the surface function of the short-pentahedral compressive stress through the three points σ_A, b and u.

The total volume V beneath the surface $f(x,y)=z\ (>0)$ and above the region in the xy-plane (see Figure 7.46) is:

$$V=\int_{0}^{a}\int_{0}^{110} f(x,y)\,dy\,dx+\int_{a}^{b}\int_{0}^{fy} f(x,y)\,dy\,dx-\int_{85}^{a}\int_{S_{7y}}^{110} f(x,y)\,dy\,dx-\int_{a}^{S_{7x}}\int_{S_{7y}}^{fy} f(x,y)\,dy\,dx$$

$$+\int_{85}^{S_{7x}}\int_{S_{7y}}^{kjy} f(x,y)\,dy\,dx-\int_{65}^{85}\int_{95}^{mky} f(x,y)\,dy\,dx-\int_{15}^{65}\int_{95}^{nmy} f(x,y)\,dy\,dx-\int_{0}^{50}\int_{0}^{qay} f(x,y)\,dy\,dx$$

$$-\int_{50}^{70}\int_{0}^{aby} f(x,y)\,dy\,dx-\int_{0}^{15}\int_{85}^{ony} f(x,y)\,dy\,dx-\int_{0}^{15}\int_{40}^{poy} f(x,y)\,dy\,dx-\int_{0}^{15}\int_{15}^{qpy} f(x,y)\,dy\,dx$$

$$-\int_{70}^{135}\int_{0}^{bcy} f(x,y)\,dy\,dx-\int_{135}^{155}\int_{0}^{cdy} f(x,y)\,dy\,dx-\int_{155}^{205}\int_{0}^{dey} f(x,y)\,dy\,dx-\int_{205}^{S_{12x}}\int_{0}^{efy} f(x,y)\,dy\,dx$$

$$-\int_{S_{12x}}^{b}\int_{0}^{fy} f(x,y)\,dy\,dx$$

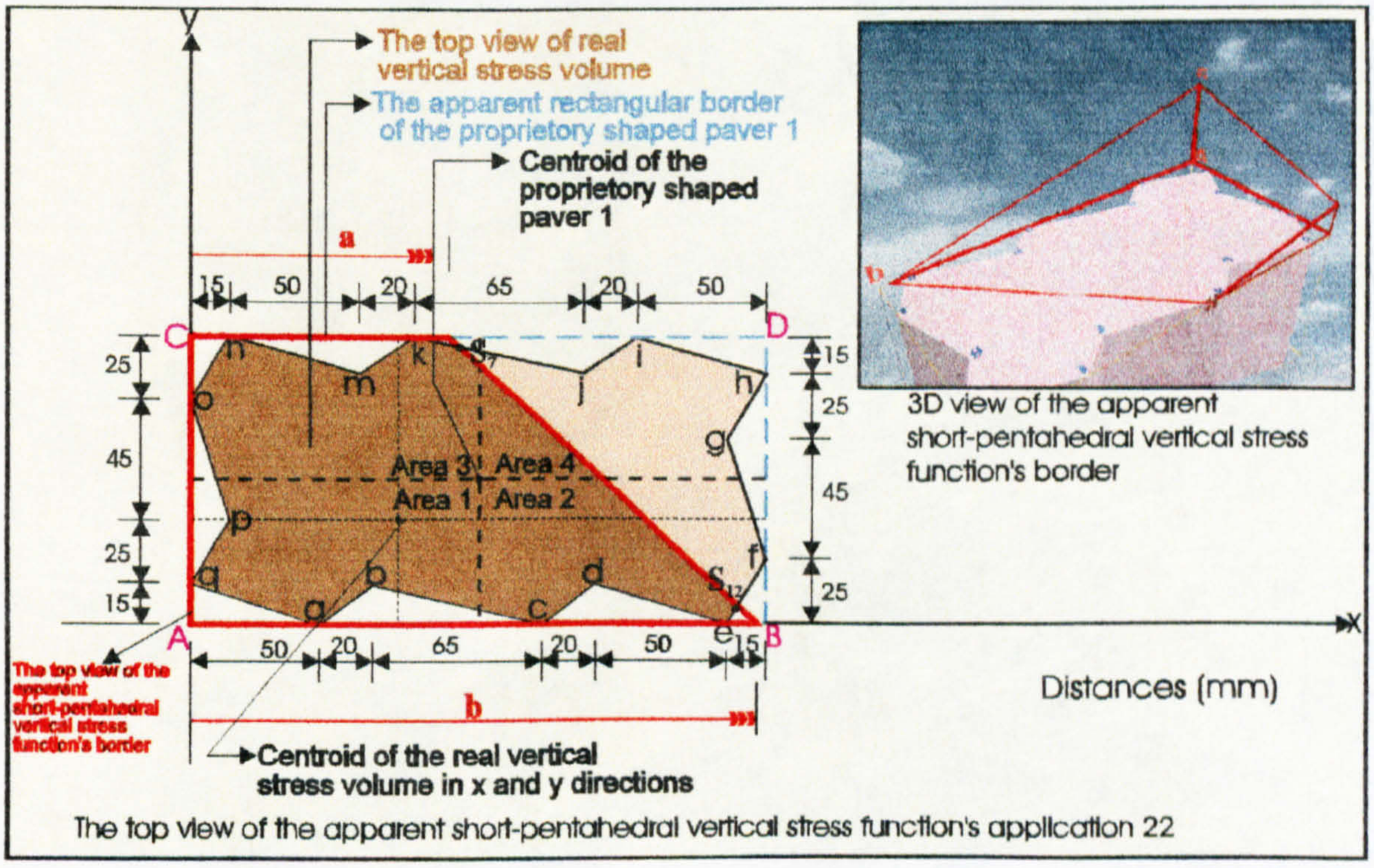

Figure 7.46: Application 22 of the short-pentahedral compressive stress distribution beneath the circumscribing rectangular border of proprietory shaped paver 1.

and the centroids of this volume in the xy-plane are at distances $\overline{X}$ and $\overline{Y}$ from the axes (see Figure 7.46) which are given by the following equations.

$$\overline{X} = \frac{1}{V}\left[\begin{array}{l}
\int_{0}^{a}\int_{0}^{110} x f(x,y)\,dy\,dx + \int_{a}^{b}\int_{0}^{fy} x f(x,y)\,dy\,dx - \int_{85}^{a}\int_{S_{7y}}^{110} x f(x,y)\,dy\,dx - \int_{a}^{S_{7x}}\int_{S_{7y}}^{fy} x f(x,y)\,dy\,dx \\
+ \int_{85}^{S_{7x}}\int_{S_{7y}}^{kjy} x f(x,y)\,dy\,dx - \int_{65}^{85}\int_{95}^{mky} x f(x,y)\,dy\,dx - \int_{15}^{65}\int_{95}^{nmy} x f(x,y)\,dy\,dx - \int_{0}^{50}\int_{0}^{qay} x f(x,y)\,dy\,dx \\
- \int_{50}^{70}\int_{0}^{aby} x f(x,y)\,dy\,dx - \int_{0}^{85}\int_{0}^{ony} x f(x,y)\,dy\,dx - \int_{0}^{40}\int_{0}^{poy} x f(x,y)\,dy\,dx - \int_{0}^{15}\int_{0}^{qpy} x f(x,y)\,dy\,dx \\
- \int_{70}^{135}\int_{0}^{bcy} x f(x,y)\,dy\,dx - \int_{135}^{155}\int_{0}^{cdy} x f(x,y)\,dy\,dx - \int_{155}^{205}\int_{0}^{dey} x f(x,y)\,dy\,dx - \int_{205}^{S_{12x}}\int_{0}^{efy} x f(x,y)\,dy\,dx \\
- \int_{S_{12x}}^{b}\int_{0}^{fy} x f(x,y)\,dy\,dx
\end{array}\right]$$

$$\overline{Y} = \frac{1}{V}\left[\begin{array}{l}
\int_{0}^{110}\int_{0}^{a} y f(x,y)\,dx\,dy + \int_{0}^{110}\int_{a}^{fx} y f(x,y)\,dx\,dy - \int_{S_{7y}}^{110}\int_{85}^{a} y f(x,y)\,dx\,dy - \int_{S_{7y}}^{110}\int_{a}^{fx} y f(x,y)\,dx\,dy \\
+ \int_{S_{7y}}^{110}\int_{85}^{kfx} y f(x,y)\,dx\,dy - \int_{95}^{110}\int_{65}^{mkx} y f(x,y)\,dx\,dy - \int_{95}^{110}\int_{15}^{nmx} y f(x,y)\,dx\,dy - \int_{0}^{15}\int_{0}^{qax} y f(x,y)\,dx\,dy \\
- \int_{0}^{15}\int_{50}^{abx} y f(x,y)\,dx\,dy - \int_{85}^{110}\int_{0}^{onx} y f(x,y)\,dx\,dy - \int_{40}^{85}\int_{0}^{pox} y f(x,y)\,dx\,dy - \int_{15}^{40}\int_{0}^{qpx} y f(x,y)\,dx\,dy \\
- \int_{0}^{15}\int_{70}^{bcx} y f(x,y)\,dx\,dy - \int_{0}^{15}\int_{135}^{cdx} y f(x,y)\,dx\,dy - \int_{0}^{15}\int_{155}^{dcx} y f(x,y)\,dx\,dy - \int_{0}^{S_{12y}}\int_{205}^{efx} y f(x,y)\,dx\,dy \\
- \int_{0}^{S_{12y}}\int_{S_{12x}}^{fx} y f(x,y)\,dx\,dy
\end{array}\right]$$

Application 23 of the short-pentahedral compressive stress regime beneath the circumscribing rectangular border of proprietory shaped paver 1 shown in Figure 7.47 can be calculated by using Tables 5.1 and 7.2 and the surface function of the short-pentahedral compressive stress through the three points σ_A, **b** and **u**.

The total volume **V** beneath the surface $f(x,y) = z\ (> 0)$ and above the region in the xy-plane (see Figure 7.47) is:

$$V = \int_{0}^{a}\int_{0}^{110} f(x,y)\,dy\,dx + \int_{a}^{b}\int_{0}^{fy} f(x,y)\,dy\,dx - \int_{150}^{S_{8x}}\int_{95}^{jiy} f(x,y)\,dy\,dx - \int_{150}^{a}\int_{S_{8y}}^{110} f(x,y)\,dy\,dx$$

$$+ \int_{85}^{150}\int_{95}^{kjy} f(x,y)\,dy\,dx - \int_{65}^{85}\int_{95}^{mky} f(x,y)\,dy\,dx - \int_{15}^{65}\int_{95}^{nmy} f(x,y)\,dy\,dx - \int_{0}^{50}\int_{0}^{qay} f(x,y)\,dy\,dx$$

$$- \int_{50}^{70}\int_{0}^{aby} f(x,y)\,dy\,dx - \int_{70}^{135}\int_{0}^{bcy} f(x,y)\,dy\,dx - \int_{a}^{S_{8x}}\int_{S_{8y}}^{fy} f(x,y)\,dy\,dx - \int_{0}^{15}\int_{85}^{ony} f(x,y)\,dy\,dx$$

$$- \int_{0}^{15}\int_{40}^{poy} f(x,y)\,dy\,dx - \int_{0}^{15}\int_{15}^{qpy} f(x,y)\,dy\,dx - \int_{135}^{S_{14x}}\int_{0}^{cdy} f(x,y)\,dy\,dx - \int_{S_{14x}}^{b}\int_{0}^{fy} f(x,y)\,dy\,dx$$

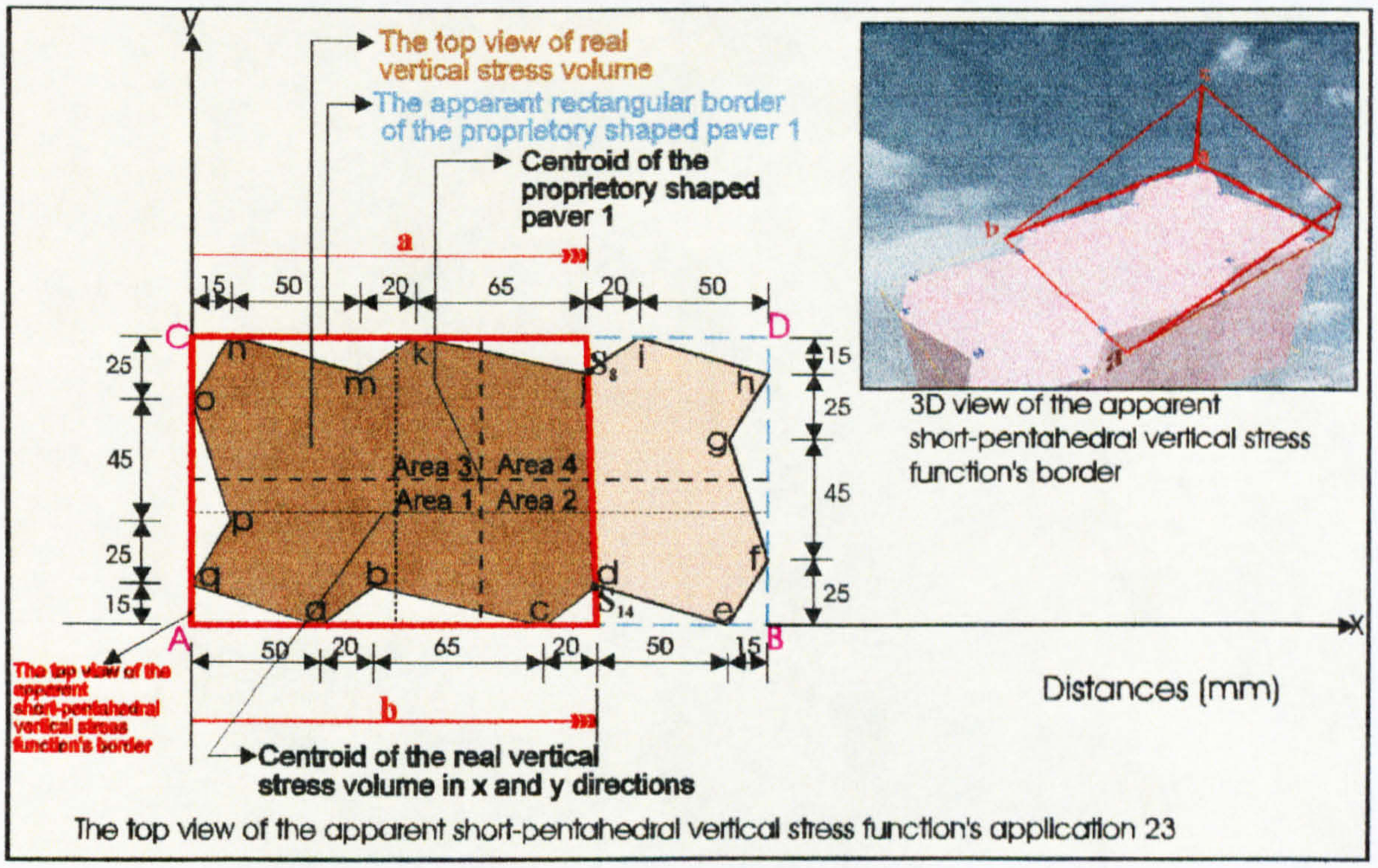

Figure 7.47: Application 23 of the short-pentahedral compressive stress distribution beneath the circumscribing rectangular border of proprietory shaped paver 1.

and the centroids of this volume in the xy-plane are at distances $\overline{X}$ and $\overline{Y}$ from the axes (see Figure 7.47) which are given by the following equations.

$$\overline{X} = \frac{1}{V}\left[\begin{array}{l}
\int_{0}^{a}\int_{0}^{110} x f(x,y)\,dy\,dx + \int_{a}^{b}\int_{0}^{fy} x f(x,y)\,dy\,dx - \int_{150}^{S_{8x}}\int_{95}^{jly} x f(x,y)\,dy\,dx - \int_{150}^{a}\int_{S_{8y}}^{110} x f(x,y)\,dy\,dx \\
+\int_{85}^{150}\int_{95}^{kjy} x f(x,y)\,dy\,dx - \int_{65}^{85}\int_{95}^{mky} x f(x,y)\,dy\,dx - \int_{15}^{65}\int_{95}^{nmy} x f(x,y)\,dy\,dx - \int_{0}^{50}\int_{0}^{qay} x f(x,y)\,dy\,dx \\
-\int_{50}^{70}\int_{0}^{aby} x f(x,y)\,dy\,dx - \int_{70}^{135}\int_{0}^{bcy} x f(x,y)\,dy\,dx - \int_{a}^{S_{8x}}\int_{S_{8y}}^{fy} x f(x,y)\,dy\,dx - \int_{0}^{15}\int_{85}^{amy} x f(x,y)\,dy\,dx \\
-\int_{0}^{15}\int_{40}^{poy} x f(x,y)\,dy\,dx - \int_{0}^{15}\int_{15}^{qpy} x f(x,y)\,dy\,dx - \int_{135}^{S_{14x}}\int_{0}^{cdy} x f(x,y)\,dy\,dx - \int_{S_{14x}}^{b}\int_{0}^{fy} x f(x,y)\,dy\,dx
\end{array}\right]$$

$$\overline{Y} = \frac{1}{V}\left[\begin{array}{l}
\int_{0}^{110}\int_{0}^{a} y f(x,y)\,dx\,dy + \int_{0}^{110}\int_{a}^{fx} y f(x,y)\,dx\,dy - \int_{95}^{S_{8y}}\int_{150}^{jix} y f(x,y)\,dx\,dy - \int_{S_{8y}}^{110}\int_{150}^{a} y f(x,y)\,dx\,dy \\
-\int_{95}^{110}\int_{85}^{kjx} y f(x,y)\,dx\,dy - \int_{95}^{110}\int_{65}^{mkx} y f(x,y)\,dx\,dy - \int_{95}^{110}\int_{15}^{nmx} y f(x,y)\,dx\,dy - \int_{0}^{15}\int_{0}^{qax} y f(x,y)\,dx\,dy \\
-\int_{0}^{15}\int_{0}^{abx} y f(x,y)\,dx\,dy - \int_{0}^{15}\int_{0}^{bcx} y f(x,y)\,dx\,dy - \int_{S_{8y}}^{110}\int_{a}^{fx} y f(x,y)\,dx\,dy - \int_{85}^{110}\int_{0}^{onx} y f(x,y)\,dx\,dy \\
-\int_{40}^{85}\int_{0}^{pox} y f(x,y)\,dx\,dy - \int_{15}^{40}\int_{0}^{qpx} y f(x,y)\,dx\,dy - \int_{0}^{S_{14y}}\int_{135}^{cdx} y f(x,y)\,dx\,dy - \int_{0}^{S_{14y}}\int_{S_{14x}}^{fx} y f(x,y)\,dx\,dy
\end{array}\right]$$

Application 24 of the short-pentahedral compressive stress regime beneath the circumscribing rectangular border of proprietory shaped paver 1 shown in Figure 7.48 can be calculated by using Tables 5.1 and 7.2 and the surface function of the short-pentahedral compressive stress through the three points σ_A, **b** and **u**.

The total volume **V** beneath the surface $f(x,y) = z\ (> 0)$ and above the region in the xy-plane (see Figure 7.48) is:

$$V = \int_{0}^{a}\int_{0}^{110} f(x,y)\,dy\,dx + \int_{a}^{b}\int_{0}^{fy} f(x,y)\,dy\,dx - \int_{150}^{S_{8x}}\int_{95}^{jiy} f(x,y)\,dy\,dx - \int_{150}^{a}\int_{S_{8y}}^{110} f(x,y)\,dy\,dx$$

$$+\int_{85}^{150}\int_{95}^{kjy} f(x,y)\,dy\,dx - \int_{65}^{85}\int_{95}^{mky} f(x,y)\,dy\,dx - \int_{15}^{65}\int_{95}^{nmy} f(x,y)\,dy\,dx - \int_{0}^{50}\int_{0}^{qay} f(x,y)\,dy\,dx$$

$$-\int_{50}^{70}\int_{0}^{aby} f(x,y)\,dy\,dx - \int_{70}^{135}\int_{0}^{bcy} f(x,y)\,dy\,dx - \int_{a}^{S_{8x}}\int_{S_{8y}}^{fy} f(x,y)\,dy\,dx - \int_{0}^{15}\int_{85}^{ony} f(x,y)\,dy\,dx$$

$$-\int_{0}^{15}\int_{40}^{poy} f(x,y)\,dy\,dx - \int_{0}^{15}\int_{15}^{qpy} f(x,y)\,dy\,dx - \int_{135}^{155}\int_{0}^{cdy} f(x,y)\,dy\,dx - \int_{155}^{S_{13x}}\int_{0}^{S_{13y}} f(x,y)\,dy\,dx$$

$$-\int_{155}^{S_{13x}}\int_{S_{13y}}^{dey} f(x,y)\,dy\,dx - \int_{S_{13x}}^{b}\int_{0}^{fy} f(x,y)\,dy\,dx$$

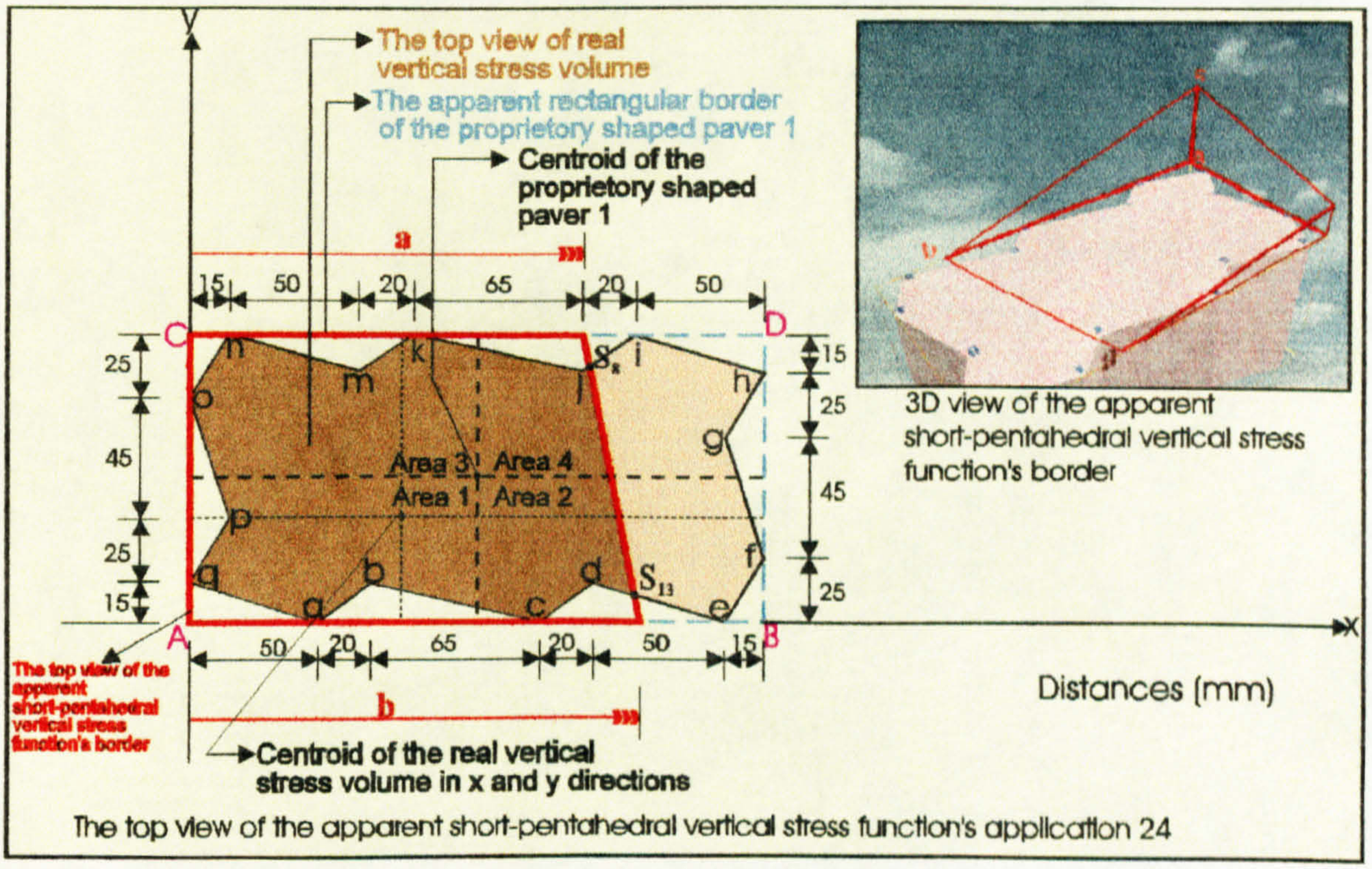

Figure 7.48: Application 24 of the short-pentahedral compressive stress distribution beneath the circumscribing rectangular border of proprietory shaped paver 1.

and the centroids of this volume in the xy-plane are at distances $\overline{X}$ and $\overline{Y}$ from the axes (see Figure 7.48) which are given by the following equations.

$$\overline{X} = \frac{1}{V}\left[\begin{array}{l}
\int_{0}^{a}\int_{0}^{110} x f(x,y)\,dy\,dx + \int_{a}^{b}\int_{0}^{fy} x f(x,y)\,dy\,dx - \int_{150}^{S_{8x}}\int_{95}^{fiy} x f(x,y)\,dy\,dx - \int_{150}^{a}\int_{S_{8y}}^{110} x f(x,y)\,dy\,dx \\
+\int_{85}^{150}\int_{95}^{kjy} x f(x,y)\,dy\,dx - \int_{65}^{85}\int_{95}^{mky} x f(x,y)\,dy\,dx - \int_{15}^{65}\int_{95}^{nmy} x f(x,y)\,dy\,dx - \int_{0}^{50}\int_{0}^{qay} x f(x,y)\,dy\,dx \\
-\int_{50}^{70}\int_{0}^{aby} x f(x,y)\,dy\,dx - \int_{70}^{135}\int_{0}^{bcy} x f(x,y)\,dy\,dx - \int_{a}^{S_{8x}}\int_{S_{8y}}^{fy} x f(x,y)\,dy\,dx - \int_{0}^{15}\int_{85}^{ony} x f(x,y)\,dy\,dx \\
-\int_{0}^{15}\int_{40}^{poy} x f(x,y)\,dy\,dx - \int_{0}^{15}\int_{15}^{qpy} x f(x,y)\,dy\,dx - \int_{135}^{155}\int_{0}^{cdy} x f(x,y)\,dy\,dx - \int_{155}^{S_{13x}}\int_{0}^{S_{13y}} x f(x,y)\,dy\,dx \\
-\int_{155}^{S_{13x}}\int_{S_{13y}}^{dey} x f(x,y)\,dy\,dx - \int_{S_{13x}}^{b}\int_{0}^{fy} x f(x,y)\,dy\,dx
\end{array}\right]$$

$$\overline{Y} = \frac{1}{V}\left[\begin{array}{l}
\int_{0}^{110}\int_{0}^{a} y f(x,y)\,dx\,dy + \int_{0}^{110}\int_{a}^{fx} y f(x,y)\,dx\,dy - \int_{95}^{S_{8y}}\int_{150}^{fix} y f(x,y)\,dx\,dy - \int_{S_{8y}}^{110}\int_{150}^{a} y f(x,y)\,dx\,dy \\
-\int_{95}^{110}\int_{85}^{kjx} y f(x,y)\,dx\,dy - \int_{95}^{110}\int_{65}^{mkx} y f(x,y)\,dx\,dy - \int_{95}^{110}\int_{15}^{nmx} y f(x,y)\,dx\,dy - \int_{0}^{15}\int_{0}^{qax} y f(x,y)\,dx\,dy \\
-\int_{0}^{15}\int_{50}^{abx} y f(x,y)\,dx\,dy - \int_{0}^{15}\int_{70}^{bcx} y f(x,y)\,dx\,dy - \int_{S_{8y}}^{110}\int_{a}^{fx} y f(x,y)\,dx\,dy - \int_{85}^{110}\int_{0}^{onx} y f(x,y)\,dx\,dy \\
-\int_{40}^{85}\int_{0}^{pox} y f(x,y)\,dx\,dy - \int_{15}^{40}\int_{0}^{qpx} y f(x,y)\,dx\,dy - \int_{0}^{135}\int_{0}^{15cdx} y f(x,y)\,dx\,dy - \int_{0}^{155}\int_{155}^{S_{13y}} y f(x,y)\,dx\,dy \\
-\int_{S_{13y}}^{155}\int_{15}^{dex} y f(x,y)\,dx\,dy - \int_{0}^{S_{13x}}\int_{S_{13x}}^{fx} y f(x,y)\,dx\,dy
\end{array}\right]$$

Application 25 of the short-pentahedral compressive stress regime beneath the circumscribing rectangular border of proprietory shaped paver 1 shown in Figure 7.49 can be calculated by using Tables 5.1 and 7.2 and the surface function of the short-pentahedral compressive stress through the three points σ_A, b and u.

The total volume V beneath the surface $f(x,y) = z\ (> 0)$ and above the region in the xy-plane (see Figure 7.49) is:

$$V = \int_{0}^{a}\int_{0}^{110} f(x,y)\,dy\,dx + \int_{a}^{b}\int_{0}^{fy} f(x,y)\,dy\,dx - \int_{150}^{S_{8x}}\int_{95}^{jiy} f(x,y)\,dy\,dx - \int_{150}^{a}\int_{S_{8y}}^{110} f(x,y)\,dy\,dx$$

$$+ \int_{85}^{150}\int_{95}^{kjy} f(x,y)\,dy\,dx - \int_{65}^{85}\int_{95}^{mky} f(x,y)\,dy\,dx - \int_{15}^{65}\int_{95}^{nmy} f(x,y)\,dy\,dx - \int_{0}^{50}\int_{0}^{qay} f(x,y)\,dy\,dx$$

$$- \int_{50}^{70}\int_{0}^{aby} f(x,y)\,dy\,dx - \int_{70}^{135}\int_{0}^{bcy} f(x,y)\,dy\,dx - \int_{a}^{S_{8x}}\int_{S_{8y}}^{fy} f(x,y)\,dy\,dx - \int_{0}^{85}\int_{0}^{15oy} f(x,y)\,dy\,dx$$

$$- \int_{0}^{40}\int_{0}^{15poy} f(x,y)\,dy\,dx - \int_{0}^{15}\int_{0}^{15qpy} f(x,y)\,dy\,dx - \int_{135}^{155}\int_{0}^{155cdy} f(x,y)\,dy\,dx - \int_{155}^{205}\int_{0}^{205dey} f(x,y)\,dy\,dx$$

$$- \int_{205}^{S_{12x}}\int_{0}^{efy} f(x,y)\,dy\,dx - \int_{S_{12x}}^{b}\int_{0}^{fy} f(x,y)\,dy\,dx$$

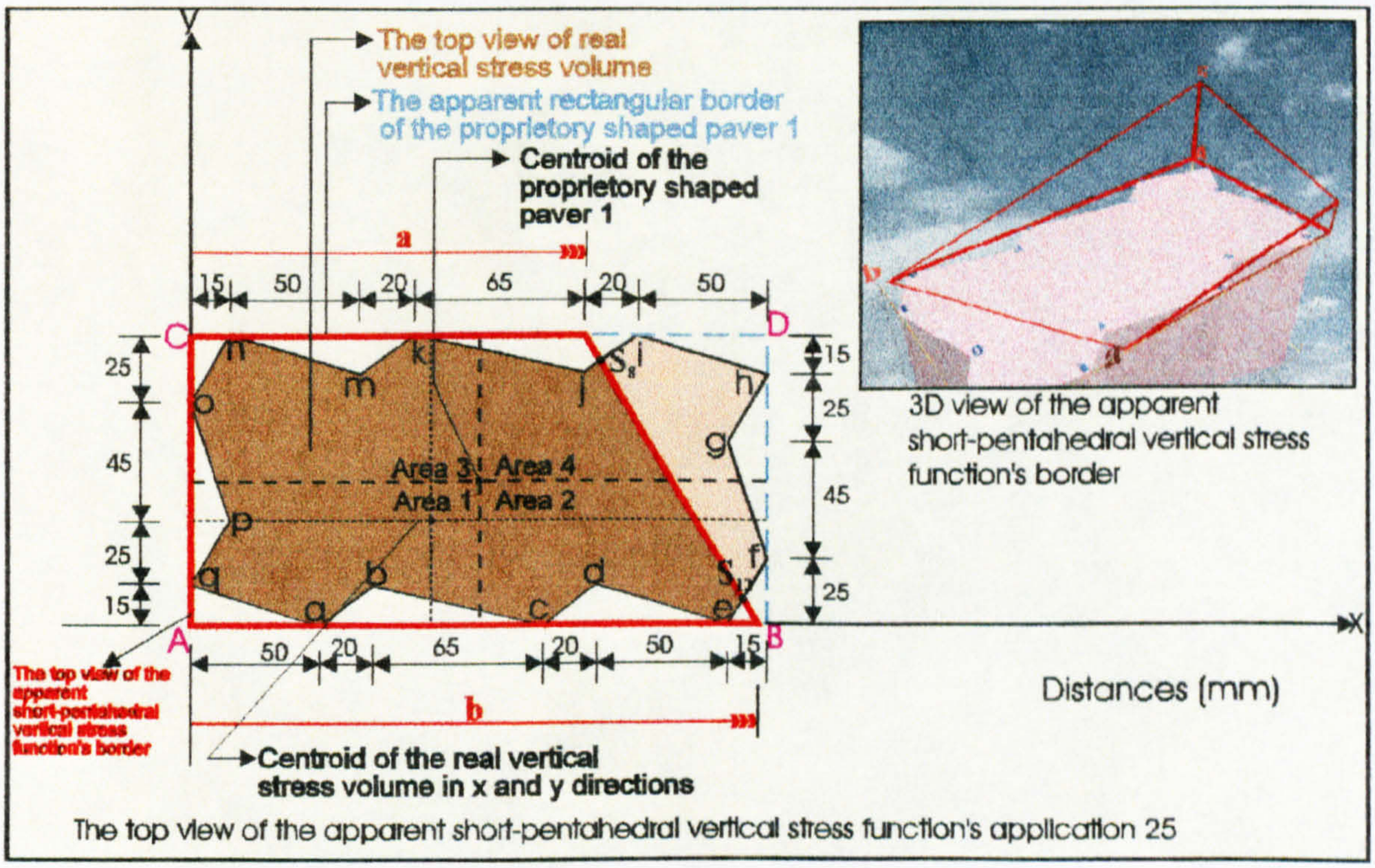

The top view of the apparent short-pentahedral vertical stress function's application 25

Figure 7.49: Application 25 of the short-pentahedral compressive stress distribution beneath the circumscribing rectangular border of proprietory shaped paver 1.

and the centroids of this volume in the xy-plane are at distances $\overline{X}$ and $\overline{Y}$ from the axes (see Figure 7.49) which are given by the following equations.

$$\overline{X} = \frac{1}{V}\left[\begin{array}{l}
\int_{0}^{a}\int_{0}^{110} x f(x,y)\,dy\,dx + \int_{a}^{b}\int_{0}^{fy} x f(x,y)\,dy\,dx - \int_{150}^{S_{8x}}\int_{95}^{jly} x f(x,y)\,dy\,dx - \int_{150}^{a}\int_{S_{8y}}^{110} x f(x,y)\,dy\,dx \\
+ \int_{85}^{150}\int_{95}^{kjy} x f(x,y)\,dy\,dx - \int_{65}^{85}\int_{95}^{mky} x f(x,y)\,dy\,dx - \int_{15}^{65}\int_{95}^{nmy} x f(x,y)\,dy\,dx - \int_{0}^{50}\int_{0}^{lay} x f(x,y)\,dy\,dx \\
- \int_{50}^{70}\int_{0}^{aby} x f(x,y)\,dy\,dx - \int_{70}^{135}\int_{0}^{bcy} x f(x,y)\,dy\,dx - \int_{a}^{S_{8x}}\int_{S_{8y}}^{fy} x f(x,y)\,dy\,dx - \int_{0}^{15}\int_{85}^{ony} x f(x,y)\,dy\,dx \\
- \int_{0}^{15}\int_{40}^{poy} x f(x,y)\,dy\,dx - \int_{0}^{15}\int_{15}^{qpy} x f(x,y)\,dy\,dx - \int_{135}^{155}\int_{0}^{cdy} x f(x,y)\,dy\,dx - \int_{155}^{205}\int_{0}^{dey} x f(x,y)\,dy\,dx \\
- \int_{205}^{S_{12x}}\int_{0}^{efy} x f(x,y)\,dy\,dx - \int_{S_{12x}}^{b}\int_{0}^{fy} x f(x,y)\,dy\,dx
\end{array}\right]$$

$$\overline{Y} = \frac{1}{V}\left[\begin{array}{l}
\int_{0}^{110}\int_{0}^{a} y f(x,y)\,dx\,dy + \int_{0}^{110}\int_{a}^{fx} y f(x,y)\,dx\,dy - \int_{95}^{S_{8y}}\int_{150}^{jlx} y f(x,y)\,dx\,dy - \int_{S_{8y}}^{110}\int_{150}^{a} y f(x,y)\,dx\,dy \\
- \int_{95}^{110}\int_{85}^{kjx} y f(x,y)\,dx\,dy - \int_{95}^{110}\int_{65}^{mkx} y f(x,y)\,dx\,dy - \int_{95}^{110}\int_{15}^{nmx} y f(x,y)\,dx\,dy - \int_{0}^{15}\int_{0}^{qax} y f(x,y)\,dx\,dy \\
- \int_{0}^{15}\int_{0}^{abx} y f(x,y)\,dx\,dy - \int_{0}^{15}\int_{50}^{bcx} y f(x,y)\,dx\,dy - \int_{S_{8y}}^{110}\int_{a}^{fx} y f(x,y)\,dx\,dy - \int_{85}^{110}\int_{0}^{cnx} y f(x,y)\,dx\,dy \\
- \int_{40}^{85}\int_{0}^{pox} y f(x,y)\,dx\,dy - \int_{15}^{40}\int_{0}^{qpx} y f(x,y)\,dx\,dy - \int_{0}^{135}\int_{0}^{cdx} y f(x,y)\,dx\,dy - \int_{0}^{155}\int_{0}^{dex} y f(x,y)\,dx\,dy \\
- \int_{0}^{S_{12y}}\int_{205}^{efx} y f(x,y)\,dx\,dy - \int_{0}^{S_{12y}}\int_{S_{12x}}^{fx} y f(x,y)\,dx\,dy
\end{array}\right]$$

Application 26 of the short-pentahedral compressive stress regime beneath the circumscribing rectangular border of proprietory shaped paver 1 shown in Figure 7.50 can be calculated by using Tables 5.1 and 7.2 and the surface function of the short-pentahedral compressive stress through the three points σ_A, b and u.

The total volume **V** beneath the surface $f(x,y) = z\ (> 0)$ and above the region in the xy-plane (see Figure 7.50) is:

$$V = \int_{0}^{a}\int_{0}^{110} f(x,y)\,dy\,dx + \int_{a}^{b}\int_{0}^{fy} f(x,y)\,dy\,dx - \int_{170}^{a}\int_{S_{9y}}^{110} f(x,y)\,dy\,dx - \int_{a}^{S_{9x}}\int_{S_{9y}}^{fy} f(x,y)\,dy\,dx$$

$$+ \int_{170}^{S_{9x}}\int_{S_{9y}}^{hiy} f(x,y)\,dy\,dx - \int_{150}^{170}\int_{95}^{jiy} f(x,y)\,dy\,dx - \int_{85}^{150}\int_{95}^{kjy} f(x,y)\,dy\,dx - \int_{65}^{85}\int_{95}^{mky} f(x,y)\,dy\,dx$$

$$- \int_{15}^{65}\int_{95}^{nmy} f(x,y)\,dy\,dx - \int_{0}^{50}\int_{0}^{qay} f(x,y)\,dy\,dx - \int_{50}^{70}\int_{0}^{aby} f(x,y)\,dy\,dx - \int_{70}^{135}\int_{0}^{bcy} f(x,y)\,dy\,dx$$

$$- \int_{135}^{155}\int_{0}^{cdy} f(x,y)\,dy\,dx - \int_{0}^{85}\int_{0}^{ony} f(x,y)\,dy\,dx - \int_{0}^{40}\int_{0}^{poy} f(x,y)\,dy\,dx - \int_{0}^{15}\int_{0}^{qpy} f(x,y)\,dy\,dx$$

$$- \int_{155}^{S_{13x}}\int_{0}^{S_{13y}} f(x,y)\,dy\,dx - \int_{155}^{S_{13x}}\int_{S_{13y}}^{dey} f(x,y)\,dy\,dx - \int_{S_{13x}}^{b}\int_{0}^{fy} f(x,y)\,dy\,dx$$

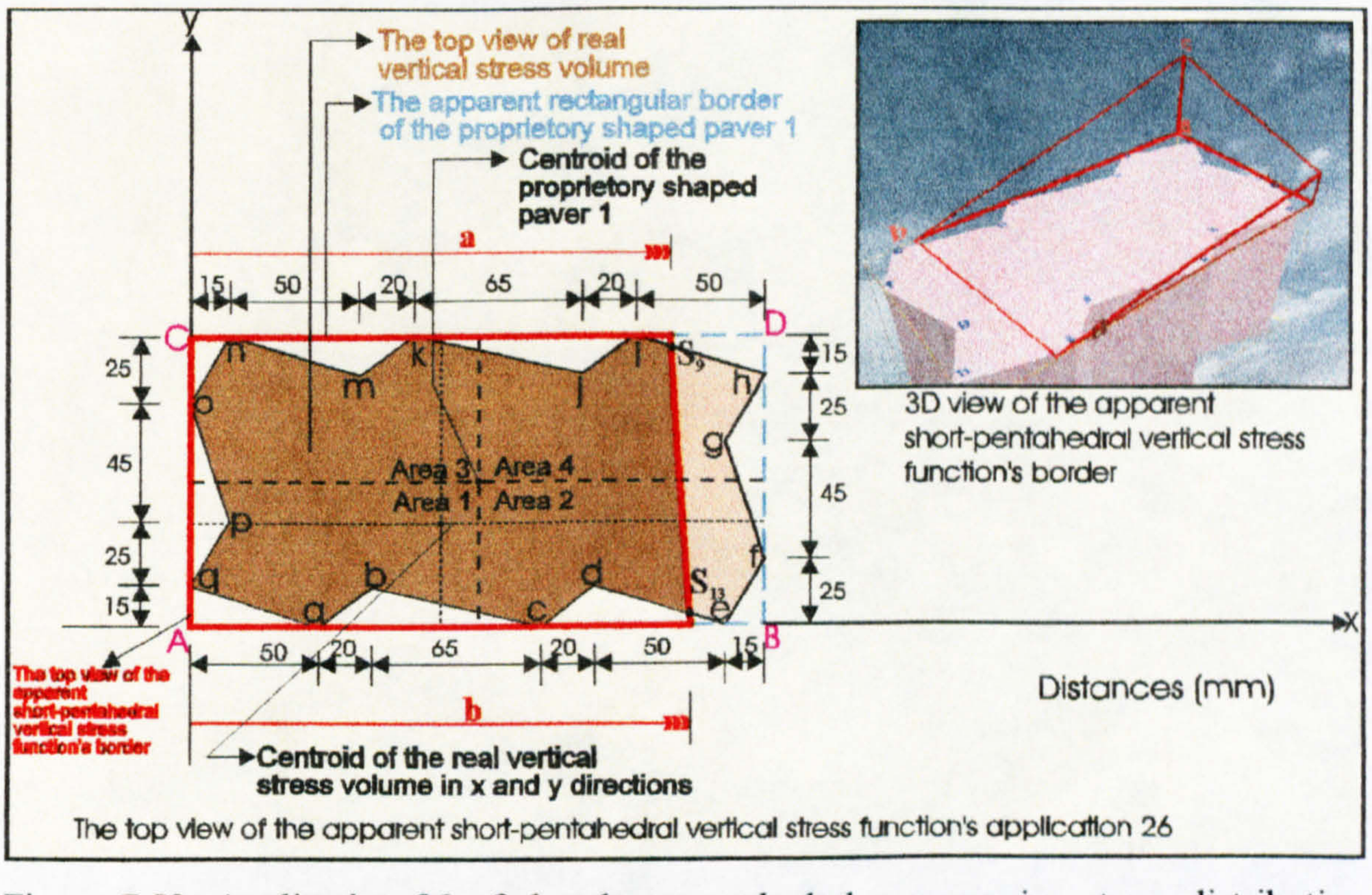

The top view of the apparent short-pentahedral vertical stress function's application 26

Figure 7.50: Application 26 of the short-pentahedral compressive stress distribution beneath the circumscribing rectangular border of proprietory shaped paver 1.

and the centroids of this volume in the xy-plane are at distances $\overline{X}$ and $\overline{Y}$ from the axes (see Figure 7.50) which are given by the following equations.

$$\overline{X} = \frac{1}{V}\left[\begin{array}{l}
\int_{0}^{a}\int_{0}^{110} x f(x,y)\,dy\,dx + \int_{a}^{b}\int_{0}^{fy} x f(x,y)\,dy\,dx - \int_{170}^{a}\int_{S_{9y}}^{110} x f(x,y)\,dy\,dx - \int_{a}^{S_{9x}}\int_{S_{9y}}^{fy} x f(x,y)\,dy\,dx \\
+\int_{170}^{S_{9x}}\int_{S_{9y}}^{hiy} x f(x,y)\,dy\,dx - \int_{150}^{170}\int_{95}^{jiy} x f(x,y)\,dy\,dx - \int_{85}^{150}\int_{95}^{kjy} x f(x,y)\,dy\,dx - \int_{65}^{85}\int_{95}^{mky} x f(x,y)\,dy\,dx \\
-\int_{15}^{65}\int_{95}^{nmy} x f(x,y)\,dy\,dx - \int_{0}^{50}\int_{0}^{qay} x f(x,y)\,dy\,dx - \int_{50}^{70}\int_{0}^{nby} x f(x,y)\,dy\,dx - \int_{70}^{135}\int_{0}^{bcy} x f(x,y)\,dy\,dx \\
-\int_{135}^{155}\int_{0}^{cdy} x f(x,y)\,dy\,dx - \int_{0}^{85}\int_{0}^{ony} x f(x,y)\,dy\,dx - \int_{0}^{40}\int_{0}^{pay} x f(x,y)\,dy\,dx - \int_{0}^{15}\int_{0}^{qpy} x f(x,y)\,dy\,dx \\
-\int_{155}^{S_{13x}}\int_{0}^{S_{13y}} x f(x,y)\,dy\,dx - \int_{155}^{S_{13x}}\int_{S_{13y}}^{dcy} x f(x,y)\,dy\,dx - \int_{S_{13x}}^{b}\int_{0}^{fy} x f(x,y)\,dy\,dx
\end{array}\right]$$

$$\overline{Y} = \frac{1}{V}\left[\begin{array}{l}
\int_{0}^{110}\int_{0}^{a} y f(x,y)\,dx\,dy + \int_{0}^{110}\int_{a}^{fx} y f(x,y)\,dx\,dy - \int_{S_{9y}}^{110}\int_{170}^{a} y f(x,y)\,dx\,dy - \int_{S_{9y}}^{110}\int_{a}^{fx} y f(x,y)\,dx\,dy \\
+\int_{S_{9y}}^{110}\int_{170}^{hix} y f(x,y)\,dx\,dy - \int_{95}^{110}\int_{150}^{jiy} y f(x,y)\,dx\,dy - \int_{95}^{110}\int_{85}^{kjx} y f(x,y)\,dx\,dy - \int_{95}^{110}\int_{65}^{mkx} y f(x,y)\,dx\,dy \\
-\int_{95}^{110}\int_{15}^{nmx} y f(x,y)\,dx\,dy - \int_{0}^{15}\int_{0}^{qax} y f(x,y)\,dx\,dy - \int_{0}^{15}\int_{50}^{abx} y f(x,y)\,dx\,dy - \int_{0}^{15}\int_{70}^{bcx} y f(x,y)\,dx\,dy \\
-\int_{0}^{15}\int_{135}^{cdx} y f(x,y)\,dx\,dy - \int_{85}^{110}\int_{0}^{onx} y f(x,y)\,dx\,dy - \int_{40}^{85}\int_{0}^{pax} y f(x,y)\,dx\,dy - \int_{15}^{40}\int_{0}^{qpx} y f(x,y)\,dx\,dy \\
-\int_{0}^{S_{13y}}\int_{155}^{S_{13x}} y f(x,y)\,dx\,dy - \int_{S_{13y}}^{15}\int_{155}^{dex} y f(x,y)\,dx\,dy - \int_{0}^{S_{13y}}\int_{S_{13x}}^{fx} y f(x,y)\,dx\,dy
\end{array}\right]$$

Application 27 of the short-pentahedral compressive stress regime beneath the circumscribing rectangular border of proprietory shaped paver 1 shown in Figure 7.51 can be calculated by using Tables 5.1 and 7.2 and the surface function of the short-pentahedral compressive stress through the three points σ_A, b and u.

The total volume V beneath the surface $f(x,y) = z\ (> 0)$ and above the region in the xy-plane (see Figure 7.51) is:

$$V = \int_{0}^{a}\int_{0}^{110} f(x,y)\,dy\,dx + \int_{a}^{b}\int_{0}^{fy} f(x,y)\,dy\,dx - \int_{170}^{a}\int_{S_{9y}}^{110} f(x,y)\,dy\,dx - \int_{a}^{S_{9x}}\int_{S_{9y}}^{fy} f(x,y)\,dy\,dx$$

$$+ \int_{170}^{S_{9x}}\int_{S_{9y}}^{hiy} f(x,y)\,dy\,dx - \int_{150}^{170}\int_{95}^{jiy} f(x,y)\,dy\,dx - \int_{85}^{150}\int_{95}^{kjy} f(x,y)\,dy\,dx - \int_{65}^{85}\int_{95}^{mky} f(x,y)\,dy\,dx$$

$$- \int_{15}^{65}\int_{95}^{mmy} f(x,y)\,dy\,dx - \int_{0}^{50}\int_{0}^{qay} f(x,y)\,dy\,dx - \int_{50}^{70}\int_{0}^{aby} f(x,y)\,dy\,dx - \int_{70}^{135}\int_{0}^{bcy} f(x,y)\,dy\,dx$$

$$- \int_{135}^{155}\int_{0}^{cdy} f(x,y)\,dy\,dx - \int_{0}^{85}\int_{0}^{ony} f(x,y)\,dy\,dx - \int_{0}^{40}\int_{0}^{poy} f(x,y)\,dy\,dx - \int_{0}^{15}\int_{0}^{qpy} f(x,y)\,dy\,dx$$

$$- \int_{155}^{205}\int_{0}^{dey} f(x,y)\,dy\,dx - \int_{205}^{S_{12x}}\int_{0}^{efy} f(x,y)\,dy\,dx - \int_{S_{12x}}^{b}\int_{0}^{fy} f(x,y)\,dy\,dx$$

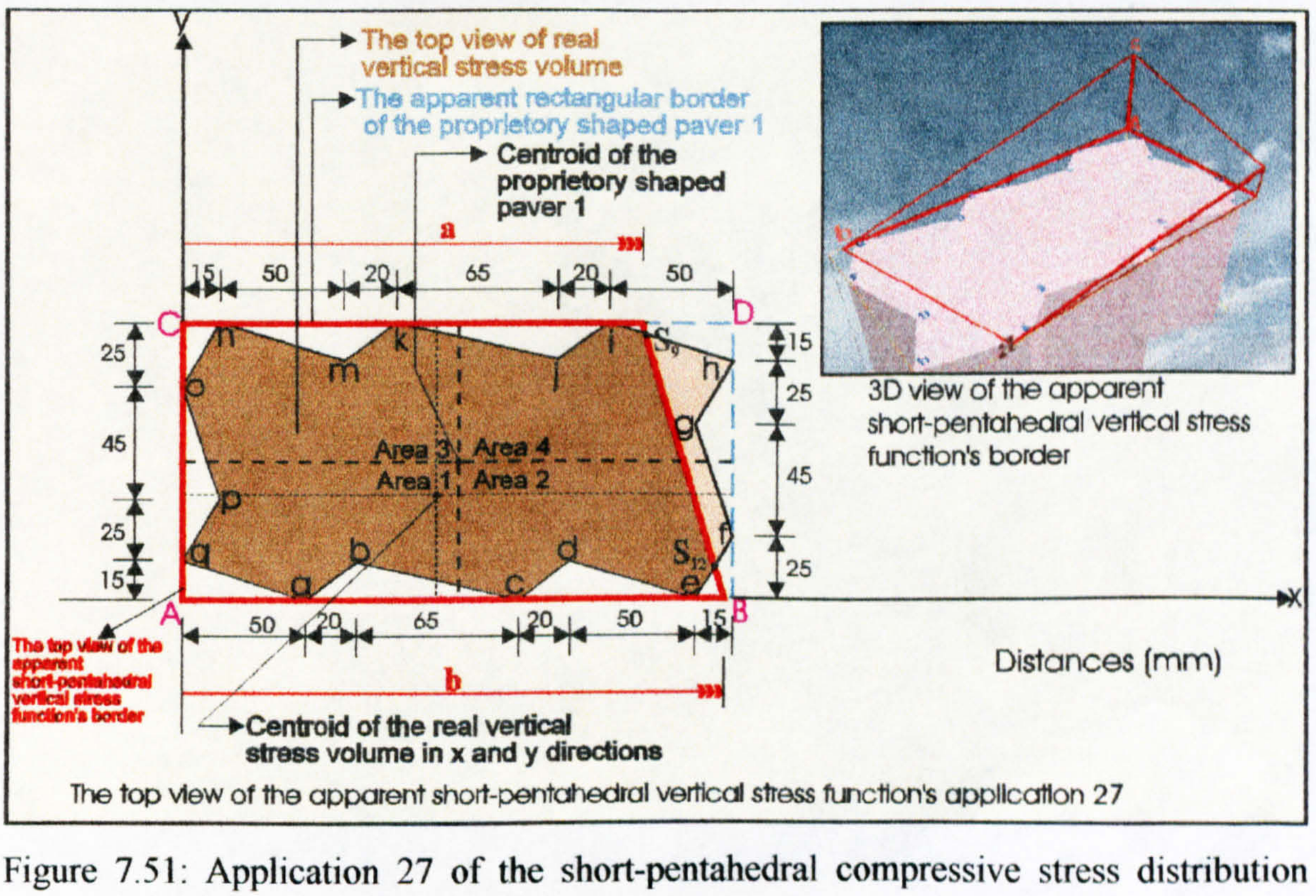

Figure 7.51: Application 27 of the short-pentahedral compressive stress distribution beneath the circumscribing rectangular border of proprietory shaped paver 1.

and the centroids of this volume in the xy-plane are at distances $\overline{X}$ and $\overline{Y}$ from the axes (see Figure 7.51) which are given by the following equations.

$$\overline{X} = \frac{1}{V}\left[\begin{array}{l}
\int_{0}^{a}\int_{0}^{110} x f(x,y)\,dy\,dx + \int_{a}^{b}\int_{0}^{fy} x f(x,y)\,dy\,dx - \int_{170}^{a}\int_{S_{9y}}^{110} x f(x,y)\,dy\,dx - \int_{a}^{S_{9x}}\int_{S_{9y}}^{fy} x f(x,y)\,dy\,dx \\
+\int_{170}^{S_{9x}}\int_{S_{9y}}^{hiy} x f(x,y)\,dy\,dx - \int_{150}^{170}\int_{95}^{jiy} x f(x,y)\,dy\,dx - \int_{85}^{150}\int_{95}^{kjy} x f(x,y)\,dy\,dx - \int_{65}^{85}\int_{95}^{mky} x f(x,y)\,dy\,dx \\
-\int_{15}^{65}\int_{95}^{nmy} x f(x,y)\,dy\,dx - \int_{0}^{50}\int_{0}^{qay} x f(x,y)\,dy\,dx - \int_{50}^{70}\int_{0}^{xhy} x f(x,y)\,dy\,dx - \int_{70}^{135}\int_{0}^{bcy} x f(x,y)\,dy\,dx \\
-\int_{135}^{155}\int_{0}^{cdy} x f(x,y)\,dy\,dx - \int_{0}^{85}\int_{0}^{ony} x f(x,y)\,dy\,dx - \int_{0}^{40}\int_{0}^{poy} x f(x,y)\,dy\,dx - \int_{0}^{15}\int_{0}^{qpy} x f(x,y)\,dy\,dx \\
-\int_{155}^{205}\int_{0}^{dey} x f(x,y)\,dy\,dx - \int_{205}^{S_{12x}}\int_{0}^{efy} x f(x,y)\,dy\,dx - \int_{S_{12x}}^{b}\int_{0}^{fy} x f(x,y)\,dy\,dx
\end{array}\right]$$

$$\overline{Y} = \frac{1}{V}\left[\begin{array}{l}
\int_{0}^{110}\int_{0}^{a} y f(x,y)\,dx\,dy + \int_{0}^{110}\int_{a}^{fx} y f(x,y)\,dx\,dy - \int_{S_{9y}}^{110}\int_{170}^{a} y f(x,y)\,dx\,dy - \int_{S_{9y}}^{110}\int_{a}^{fx} y f(x,y)\,dx\,dy \\
+\int_{S_{9y}}^{110}\int_{170}^{hix} y f(x,y)\,dx\,dy - \int_{95}^{110}\int_{150}^{jiy} y f(x,y)\,dx\,dy - \int_{95}^{110}\int_{85}^{kjx} y f(x,y)\,dx\,dy - \int_{95}^{110}\int_{65}^{mkx} y f(x,y)\,dx\,dy \\
-\int_{95}^{110}\int_{15}^{nmx} y f(x,y)\,dx\,dy - \int_{0}^{15}\int_{0}^{qax} y f(x,y)\,dx\,dy - \int_{0}^{15}\int_{50}^{xbx} y f(x,y)\,dx\,dy - \int_{0}^{15}\int_{70}^{bcx} y f(x,y)\,dx\,dy \\
-\int_{0}^{15}\int_{135}^{cdx} y f(x,y)\,dx\,dy - \int_{85}^{110}\int_{0}^{onx} y f(x,y)\,dx\,dy - \int_{40}^{85}\int_{0}^{pox} y f(x,y)\,dx\,dy - \int_{15}^{40}\int_{0}^{qpx} y f(x,y)\,dx\,dy \\
-\int_{0}^{15}\int_{155}^{dex} y f(x,y)\,dx\,dy - \int_{0}^{S_{12y}}\int_{205}^{efx} y f(x,y)\,dx\,dy - \int_{0}^{S_{12y}}\int_{S_{12x}}^{fx} y f(x,y)\,dx\,dy
\end{array}\right]$$

Application 28 of the short-pentahedral compressive stress regime beneath the circumscribing rectangular border of proprietory shaped paver 1 shown in Figure 7.52 can be calculated by using Tables 5.1 and 7.2 and the surface function of the short-pentahedral compressive stress through the three points σ_A, b and u.

The total volume V beneath the surface $f(x,y) = z\ (> 0)$ and above the region in the xy-plane (see Figure 7.52) is:

$$V=\int_{0}^{a}\int_{0}^{110} f(x,y)\,dy\,dx+\int_{a}^{b}\int_{0}^{fy} f(x,y)\,dy\,dx-\int_{170}^{a}\int_{S_{9y}}^{110} f(x,y)\,dy\,dx-\int_{a}^{S_{9x}}\int_{S_{9y}}^{fy} f(x,y)\,dy\,dx+\int_{170}^{S_{9x}}\int_{S_{9y}}^{hiy} f(x,y)\,dy\,dx$$
$$-\int_{150}^{170}\int_{95}^{jiy} f(x,y)\,dy\,dx-\int_{85}^{150}\int_{95}^{kjy} f(x,y)\,dy\,dx-\int_{65}^{85}\int_{95}^{mky} f(x,y)\,dy\,dx-\int_{15}^{65}\int_{95}^{nmy} f(x,y)\,dy\,dx-\int_{0}^{50}\int_{0}^{qay} f(x,y)\,dy\,dx$$
$$-\int_{50}^{70}\int_{0}^{aby} f(x,y)\,dy\,dx-\int_{70}^{135}\int_{0}^{bcy} f(x,y)\,dy\,dx-\int_{135}^{155}\int_{0}^{cdy} f(x,y)\,dy\,dx-\int_{0}^{15}\int_{85}^{ony} f(x,y)\,dy\,dx-\int_{0}^{15}\int_{40}^{poy} f(x,y)\,dy\,dx$$
$$-\int_{0}^{15}\int_{0}^{qpy} f(x,y)\,dy\,dx-\int_{155}^{205}\int_{0}^{dey} f(x,y)\,dy\,dx-\int_{205}^{S_{12x}}\int_{0}^{efy} f(x,y)\,dy\,dx-\int_{S_{12x}}^{b}\int_{0}^{fy} f(x,y)\,dy\,dx-\int_{205}^{220}\int_{25}^{fgy} f(x,y)\,dy\,dx$$
$$-\int_{205}^{220}\int_{70}^{ghy} f(x,y)\,dy\,dx+\int_{S_{11x}}^{220}\int_{25}^{fgy} f(x,y)\,dy\,dx+\int_{S_{11x}}^{220}\int_{S_{11y}}^{S_{10y}} f(x,y)\,dy\,dx+\int_{S_{10x}}^{S_{11x}}\int_{S_{11y}}^{fy} f(x,y)\,dy\,dx+\int_{S_{10x}}^{220}\int_{S_{10y}}^{ghy} f(x,y)\,dy\,dx$$

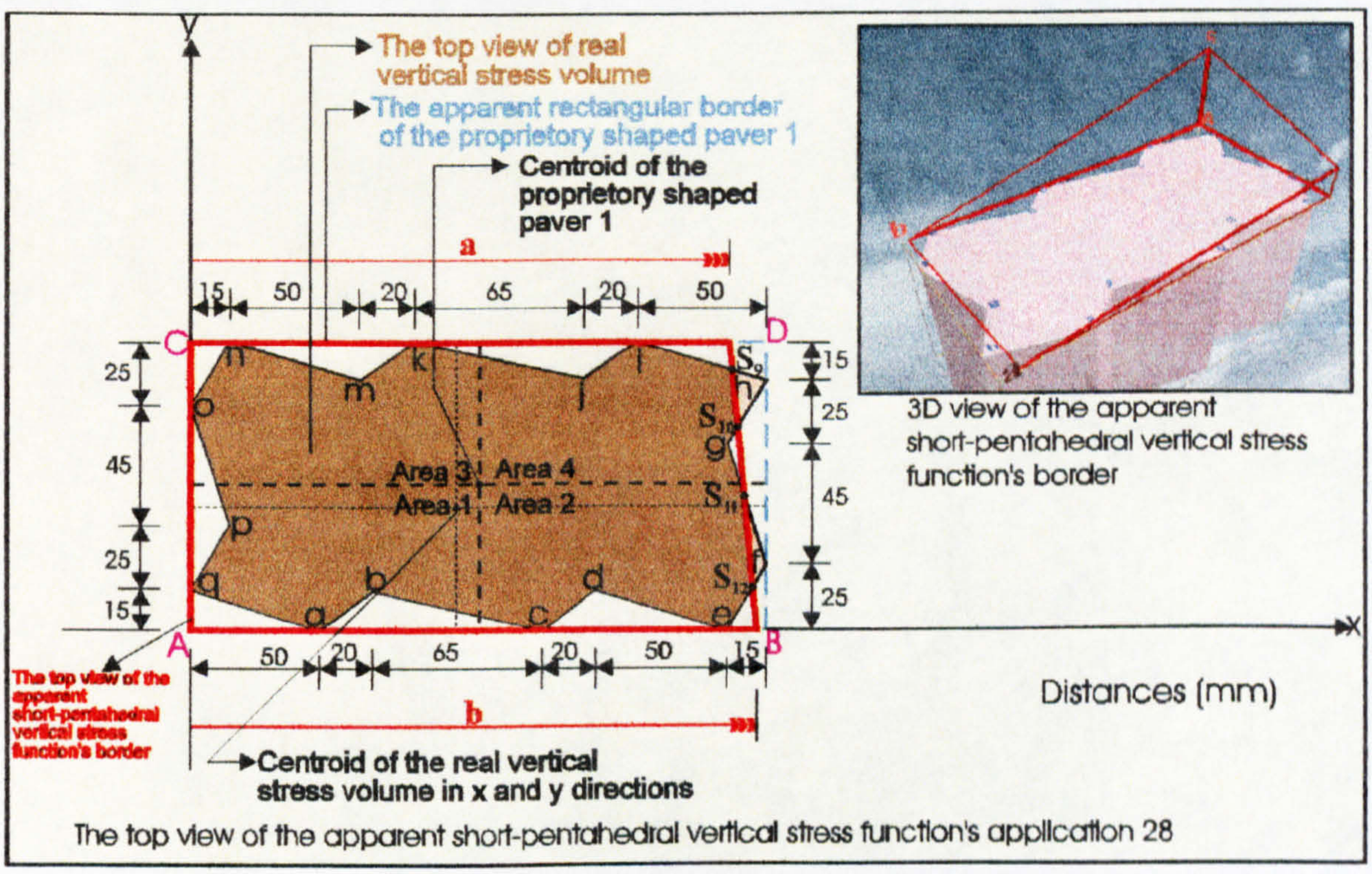

Figure 7.52: Application 28 of the short-pentahedral compressive stress distribution beneath the circumscribing rectangular border of proprietory shaped paver 1.

and the centroids of this volume in the xy-plane are at distances $\overline{X}$ and $\overline{Y}$ from the axes (see Figure 7.52) which are given by the following equations.

$$\overline{X}=\frac{1}{V}\left[\int_{0}^{a}\int_{0}^{110} x f(x,y)\,dy\,dx+\int_{a}^{b}\int_{0}^{fy} x f(x,y)\,dy\,dx-\int_{170}^{a}\int_{S_{9y}}^{110} x f(x,y)\,dy\,dx-\int_{a}^{S_{9x}}\int_{S_{9y}}^{fy} x f(x,y)\,dy\,dx\right.$$

$$+\int_{170}^{S_{9x}}\int_{S_{9y}}^{hiy} xf(x,y)\,dy\,dx-\int_{150}^{170}\int_{95}^{jiy} xf(x,y)\,dy\,dx-\int_{85}^{150}\int_{95}^{kjy} xf(x,y)\,dy\,dx-\int_{65}^{85}\int_{95}^{mky} xf(x,y)\,dy\,dx$$

$$-\int_{15}^{65}\int_{95}^{nmy} xf(x,y)\,dy\,dx-\int_{0}^{50}\int_{0}^{qay} xf(x,y)\,dy\,dx-\int_{50}^{70}\int_{0}^{aby} xf(x,y)\,dy\,dx-\int_{70}^{135}\int_{0}^{bcy} xf(x,y)\,dy\,dx$$

$$-\int_{135}^{155}\int_{0}^{cdy} xf(x,y)\,dy\,dx-\int_{0}^{85}\int_{0}^{ony} xf(x,y)\,dy\,dx-\int_{0}^{40}\int_{0}^{poy} xf(x,y)\,dy\,dx-\int_{0}^{15}\int_{0}^{qpy} xf(x,y)\,dy\,dx$$

$$-\int_{155}^{205}\int_{0}^{dey} xf(x,y)\,dy\,dx-\int_{205}^{S_{12x}}\int_{0}^{efy} xf(x,y)\,dy\,dx-\int_{S_{12x}}^{b}\int_{0}^{fy} xf(x,y)\,dy\,dx-\int_{205}^{220}\int_{25}^{fgy} xf(x,y)\,dy\,dx$$

$$-\int_{205}^{220}\int_{70}^{ghy} xf(x,y)\,dy\,dx+\int_{S_{11x}}^{220}\int_{25}^{fgy} xf(x,y)\,dy\,dx+\int_{S_{11x}}^{220}\int_{S_{11y}}^{S_{10y}} xf(x,y)\,dy\,dx+\int_{S_{10x}}^{S_{11x}}\int_{S_{11y}}^{fy} xf(x,y)\,dy\,dx$$

$$+\int_{S_{10x}}^{220}\int_{S_{10y}}^{ghy} xf(x,y)\,dy\,dx\Bigg]$$

$$\bar{Y}=\frac{1}{V}\Bigg[\int_{0}^{110}\int_{0}^{a} yf(x,y)\,dx\,dy+\int_{0}^{110}\int_{a}^{fx} yf(x,y)\,dx\,dy-\int_{S_{9y}}^{110}\int_{170}^{a} yf(x,y)\,dx\,dy-\int_{S_{9y}}^{110}\int_{a}^{fx} yf(x,y)\,dx\,dy$$

$$+\int_{S_{9y}}^{110}\int_{170}^{hix} yf(x,y)\,dx\,dy-\int_{95}^{110}\int_{150}^{jiy} yf(x,y)\,dx\,dy-\int_{95}^{110}\int_{85}^{kjx} yf(x,y)\,dx\,dy-\int_{95}^{110}\int_{65}^{mkx} yf(x,y)\,dx\,dy$$

$$-\int_{95}^{110}\int_{15}^{nmx} yf(x,y)\,dx\,dy-\int_{0}^{15}\int_{0}^{qax} yf(x,y)\,dx\,dy-\int_{0}^{15}\int_{50}^{abx} yf(x,y)\,dx\,dy-\int_{0}^{15}\int_{70}^{bcx} yf(x,y)\,dx\,dy$$

$$-\int_{0}^{15}\int_{135}^{cdx} yf(x,y)\,dx\,dy-\int_{85}^{110}\int_{0}^{onx} yf(x,y)\,dx\,dy-\int_{40}^{85}\int_{0}^{pax} yf(x,y)\,dx\,dy-\int_{15}^{40}\int_{0}^{qpx} yf(x,y)\,dx\,dy$$

$$-\int_{0}^{15}\int_{155}^{dex} yf(x,y)\,dx\,dy-\int_{0}^{S_{12y}}\int_{205}^{efx} yf(x,y)\,dx\,dy-\int_{0}^{S_{12y}}\int_{S_{12x}}^{fx} yf(x,y)\,dx\,dy-\int_{25}^{70}\int_{205}^{fgx} yf(x,y)\,dx\,dy$$

$$-\int_{70}^{95}\int_{205}^{ghx} yf(x,y)\,dx\,dy+\int_{25}^{S_{11y}}\int_{S_{11x}}^{fgx} yf(x,y)\,dx\,dy+\int_{S_{11y}}^{S_{10y}}\int_{S_{11x}}^{220} yf(x,y)\,dx\,dy+\int_{S_{10x}}^{S_{11y}}\int_{S_{10y}}^{fx} yf(x,y)\,dx\,dy$$

$$+\int_{S_{10y}}^{95}\int_{S_{10x}}^{ghx} yf(x,y)\,dx\,dy\Bigg]$$

$$\begin{vmatrix} x & y & z & 1 \\ k & 0 & 0 & 1 \\ 0 & d & 0 & 1 \\ 0 & 0 & \sigma_A & 1 \end{vmatrix} = 0 \Rightarrow f(x,y) = z = \sigma_A\left(1 - \frac{y}{d} - \frac{x}{k}\right)$$

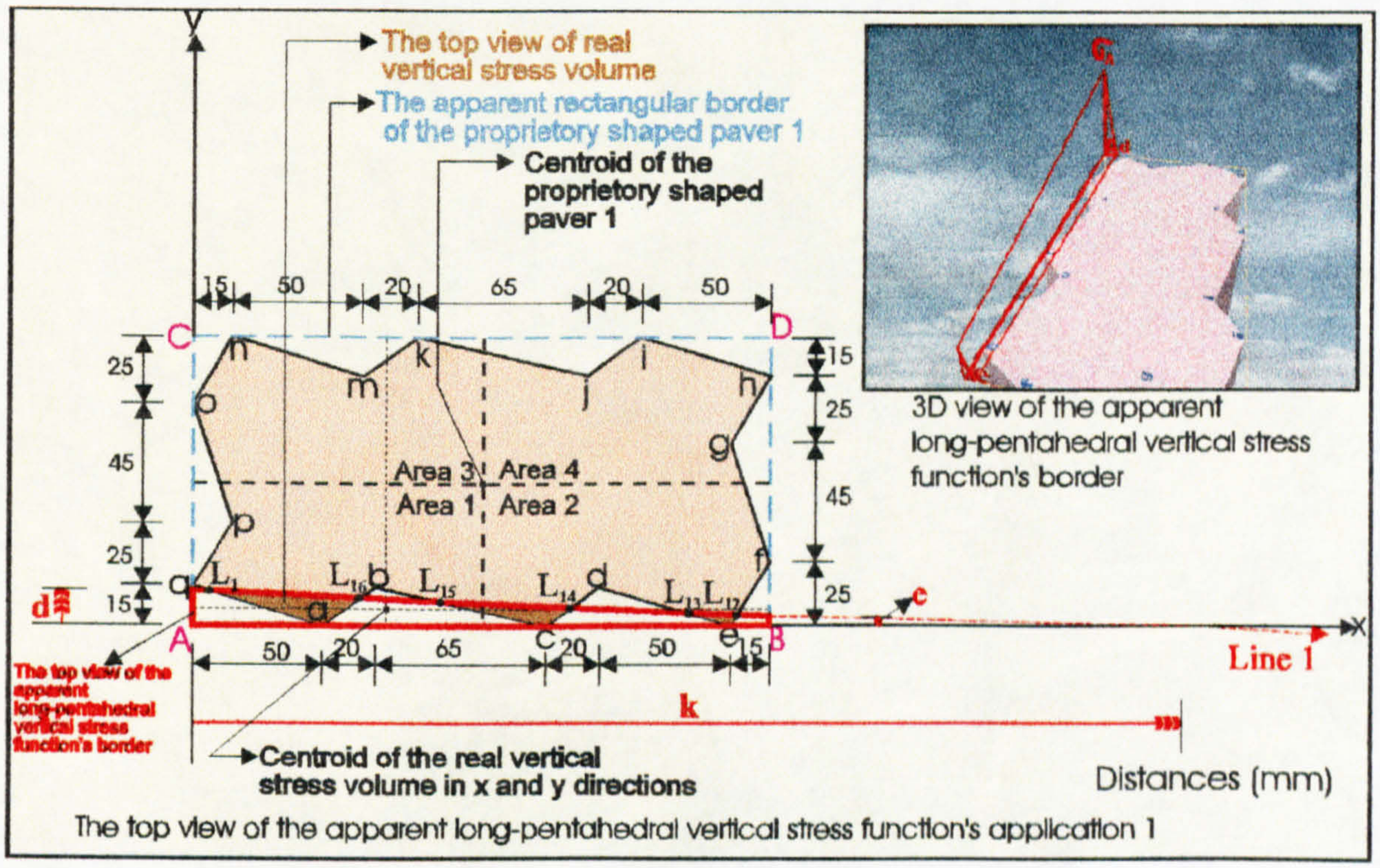

The top view of the apparent long-pentahedral vertical stress function's application 1

Figure 7.53: Application 1 of the long-pentahedral compressive stress distribution beneath the circumscribing rectangular border of proprietory shaped paver 1.

The following equalities can be obtained from the geometry of the long-pentahedral compressive stress block (see Figure 7.53).

$$e = d\left(\frac{\sigma_B}{\sigma_A}\right) \quad and \quad k = \frac{220\sigma_A}{\sigma_A - \sigma_B} \Rightarrow \sigma_C = \frac{\sigma_A(k-220)}{k}$$

therefore,

$$e = \frac{d(k-220)}{k}$$

The first application of the long-pentahedral compressive stress regime beneath the circumscribing rectangular border of proprietory shaped paver 1 shown in Figure 7.53 can be calculated by using the data in Tables 5.1 and 7.3. The first two letters of each boundary line function in Table 5.1 for proprietory shaped paver 1 charecterise the corner names can be seen in Figure 7.53 (example: qay symbolises the boundary line function of proprietory shaped paver 1 in the y axis between corner q and a). The line functions which define the boundary of the long-pentahedral stress block in the xy-plane (see Figure 7.53) are of the form $fy = d\left(1-\frac{x}{k}\right)$, $fx = k\left(1-\frac{y}{d}\right)$.

The following actual total volume V beneath the surface $f(x,y) = z\ (> 0)$ and above the region in the xy-plane (see Figure 7.53) is calculated by subtracting the negative volume generated by the dentations of the shaped paver from the long-pentahedral volume beneath circumscribing rectangular boundary of the paver.

$$V = \int_0^{220}\int_0^{e} f(x,y)\,dy\,dx + \int_0^{220}\int_e^{fy} f(x,y)\,dy\,dx - \int_{L_{12x}}^{220}\int_0^{e} f(x,y)\,dy\,dx - \int_{L_{12x}}^{220}\int_e^{fy} f(x,y)\,dy\,dx$$

$$- \int_{205}^{L_{12x}}\int_0^{efy} f(x,y)\,dy\,dx - \int_{L_{13x}}^{205}\int_0^{dey} f(x,y)\,dy\,dx - \int_{L_{14x}}^{L_{13x}}\int_0^{L_{13y}} f(x,y)\,dy\,dx - \int_{L_{14x}}^{L_{13x}}\int_{L_{13y}}^{fy} f(x,y)\,dy\,dx$$

$$- \int_{135}^{L_{14x}}\int_0^{cdy} f(x,y)\,dy\,dx - \int_{L_{15x}}^{135}\int_0^{bcy} f(x,y)\,dy\,dx - \int_{L_{16x}}^{L_{15x}}\int_0^{L_{13y}} f(x,y)\,dy\,dx - \int_{L_{16x}}^{L_{15x}}\int_{L_{15y}}^{fy} f(x,y)\,dy\,dx$$

$$- \int_{50}^{L_{16x}}\int_0^{aby} f(x,y)\,dy\,dx - \int_{L_{1x}}^{50}\int_0^{qay} f(x,y)\,dy\,dx - \int_0^{L_{1x}}\int_0^{L_{1y}} f(x,y)\,dy\,dx - \int_0^{L_{1x}}\int_{L_{1y}}^{fy} f(x,y)\,dy\,dx$$

and the centroids of this volume in the xy-plane are at distances $\overline{X}$ and $\overline{Y}$ from the axes (see Figure 7.53) which are given by the following equations.

$$\overline{X} = \frac{1}{V}\left[\int_0^{220}\int_0^{e} x f(x,y)\,dy\,dx + \int_0^{220}\int_e^{fy} x f(x,y)\,dy\,dx - \int_{L_{12x}}^{220}\int_0^{e} x f(x,y)\,dy\,dx - \int_{L_{12x}}^{220}\int_e^{fy} x f(x,y)\,dy\,dx\right.$$

$$-\int_{205}^{L_{12x}}\int_{0}^{efy} xf(x,y)\,dy\,dx-\int_{L_{13x}}^{205}\int_{0}^{dey} xf(x,y)\,dy\,dx-\int_{L_{14x}}^{L_{13x}}\int_{0}^{L_{13y}} xf(x,y)\,dy\,dx-\int_{L_{14x}}^{L_{13x}}\int_{L_{13y}}^{fy} xf(x,y)\,dy\,dx$$

$$-\int_{135}^{L_{14x}}\int_{0}^{cdy} xf(x,y)\,dy\,dx-\int_{L_{15x}}^{135}\int_{0}^{bcy} xf(x,y)\,dy\,dx-\int_{L_{16x}}^{L_{15x}}\int_{0}^{L_{13y}} xf(x,y)\,dy\,dx-\int_{L_{16x}}^{L_{15x}}\int_{L_{15y}}^{fy} xf(x,y)\,dy\,dx$$

$$-\int_{50}^{L_{16x}}\int_{0}^{aby} xf(x,y)\,dy\,dx-\int_{L_{1x}}^{50}\int_{0}^{qay} xf(x,y)\,dy\,dx-\int_{0}^{L_{1x}}\int_{0}^{L_{1y}} xf(x,y)\,dy\,dx-\int_{0}^{L_{1x}}\int_{L_{1y}}^{fy} xf(x,y)\,dy\,dx\Bigg]$$

$$\bar{Y}=\frac{1}{V}\Bigg[\int_{0}^{e}\int_{0}^{220} yf(x,y)\,dx\,dy+\int_{e}^{d}\int_{0}^{fx} yf(x,y)\,dx\,dy-\int_{0}^{e}\int_{L_{12x}}^{220} yf(x,y)\,dx\,dy-\int_{e}^{L_{12y}}\int_{L_{12x}}^{fx} yf(x,y)\,dx\,dy$$

$$-\int_{0}^{L_{12y}}\int_{205}^{efx} yf(x,y)\,dx\,dy-\int_{0}^{L_{13y}}\int_{L_{13x}}^{dex} yf(x,y)\,dx\,dy-\int_{0}^{L_{13y}}\int_{L_{14x}}^{L_{13x}} yf(x,y)\,dx\,dy-\int_{L_{13y}}^{L_{14y}}\int_{L_{14x}}^{fx} yf(x,y)\,dx\,dy$$

$$-\int_{0}^{L_{14y}}\int_{135}^{cdx} yf(x,y)\,dx\,dy-\int_{0}^{L_{15y}}\int_{L_{15x}}^{bcx} yf(x,y)\,dx\,dy-\int_{0}^{L_{15y}}\int_{L_{16x}}^{L_{15x}} yf(x,y)\,dx\,dy-\int_{L_{15y}}^{L_{16y}}\int_{L_{16x}}^{fx} yf(x,y)\,dx\,dy$$

$$-\int_{0}^{L_{16y}}\int_{50}^{abx} yf(x,y)\,dx\,dy-\int_{0}^{L_{1y}}\int_{L_{1x}}^{qax} yf(x,y)\,dx\,dy-\int_{0}^{L_{1y}}\int_{0}^{L_{1x}} yf(x,y)\,dx\,dy-\int_{L_{1y}}^{d}\int_{0}^{fx} yf(x,y)\,dx\,dy\Bigg]$$

Application 2 of the long-pentahedral compressive stress regime beneath the circumscribing rectangular border of proprietory shaped paver 1 shown in Figure 7.54 can be calculated by using Tables 5.1 and 7.3 and the surface function of the long-pentahedral compressive stress through the three points σ_A, **k** and **d**.

The total volume **V** beneath the surface $f(x,y)=z\ (>0)$ and above the region in the xy-plane (see Figure 7.54) is:

$$V=\int_{0}^{220}\int_{0}^{e} f(x,y)\,dy\,dx+\int_{0}^{220}\int_{e}^{fy} f(x,y)\,dy\,dx-\int_{L_{12x}}^{220}\int_{0}^{e} f(x,y)\,dy\,dx-\int_{L_{12x}}^{220}\int_{e}^{fy} f(x,y)\,dy\,dx$$

$$-\int_{205}^{L_{12x}}\int_{0}^{efy} f(x,y)\,dy\,dx-\int_{L_{13x}}^{205}\int_{0}^{dey} f(x,y)\,dy\,dx-\int_{L_{14x}}^{L_{13x}}\int_{0}^{L_{13y}} f(x,y)\,dy\,dx-\int_{L_{14x}}^{L_{13x}}\int_{L_{13y}}^{fy} f(x,y)\,dy\,dx$$

$$-\int_{135}^{L_{14x}}\int_{0}^{cdy} f(x,y)\,dy\,dx-\int_{L_{15x}}^{135}\int_{0}^{bcy} f(x,y)\,dy\,dx-\int_{L_{16x}}^{L_{15x}}\int_{0}^{L_{13y}} f(x,y)\,dy\,dx-\int_{L_{16x}}^{L_{15x}}\int_{L_{15y}}^{fy} f(x,y)\,dy\,dx$$

$$-\int_{50}^{L_{16x}}\int_{0}^{aby} f(x,y)\,dy\,dx-\int_{0}^{50}\int_{0}^{qay} f(x,y)\,dy\,dx-\int_{0}^{L_{2x}}\int_{15}^{qpy} f(x,y)\,dy\,dx-\int_{0}^{L_{2x}}\int_{L_{2y}}^{fy} f(x,y)\,dy\,dx$$

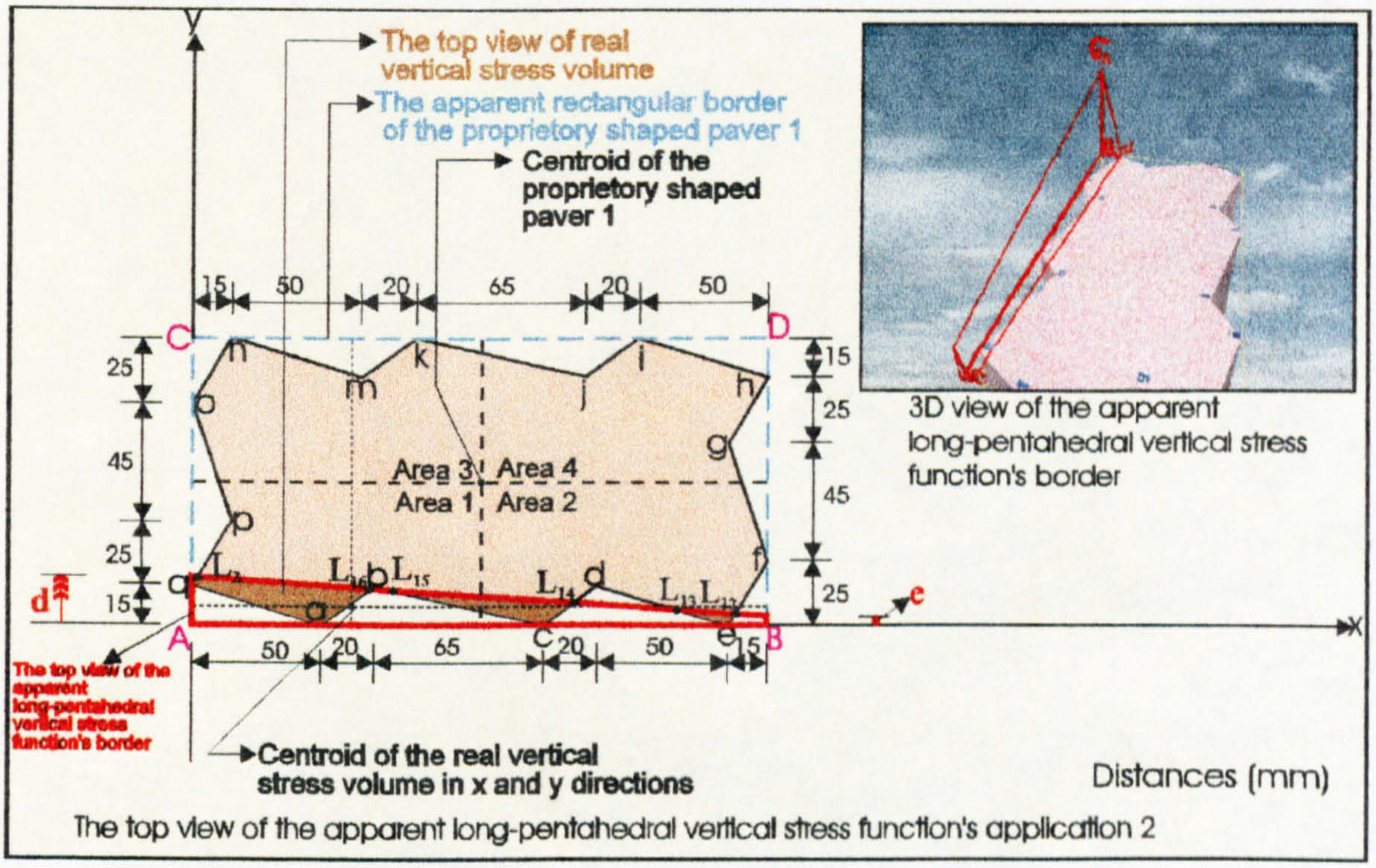

The top view of the apparent long-pentahedral vertical stress function's application 2

Figure 7.54: Application 2 of the long-pentahedral compressive stress distribution beneath the circumscribing rectangular border of proprietory shaped paver 1.

and the centroids of this volume in the xy-plane are at distances $\overline{X}$ and $\overline{Y}$ from the axes (see Figure 7.54) which are given by the following equations.

$$\overline{X}=\frac{1}{V}\left[\int_{0}^{220}\int_{0}^{e} x f(x,y)\,dy\,dx+\int_{0}^{220}\int_{e}^{fy} x f(x,y)\,dy\,dx-\int_{L_{12x}}^{220}\int_{0}^{e} x f(x,y)\,dy\,dx-\int_{L_{12x}}^{220}\int_{e}^{fy} x f(x,y)\,dy\,dx\right.$$

$$-\int_{205}^{L_{12x}}\int_{0}^{efy} x f(x,y)\,dy\,dx-\int_{L_{13x}}^{205}\int_{0}^{dey} x f(x,y)\,dy\,dx-\int_{L_{14x}}^{L_{13x}}\int_{0}^{L_{13y}} x f(x,y)\,dy\,dx-\int_{L_{14x}}^{L_{13x}}\int_{L_{13y}}^{fy} x f(x,y)\,dy\,dx$$

$$\left.-\int_{135}^{L_{14x}}\int_{0}^{cdy} x f(x,y)\,dy\,dx-\int_{L_{15x}}^{135}\int_{0}^{bcy} x f(x,y)\,dy\,dx-\int_{L_{16x}}^{L_{15x}}\int_{0}^{L_{13y}} x f(x,y)\,dy\,dx-\int_{L_{16x}}^{L_{15x}}\int_{L_{15y}}^{fy} x f(x,y)\,dy\,dx\right]$$

$$-\int_{50}^{L_{16x}}\int_{0}^{aby} x f(x,y)\,dy\,dx-\int_{0}^{50}\int_{0}^{qay} x f(x,y)\,dy\,dx-\int_{0}^{L_{2x}}\int_{15}^{qpy} x f(x,y)\,dy\,dx-\int_{0}^{L_{2x}}\int_{L_{2y}}^{fy} x f(x,y)\,dy\,dx\Bigg]$$

$$\overline{Y}=\frac{1}{V}\Bigg[\int_{0}^{e}\int_{0}^{220} y f(x,y)\,dx\,dy+\int_{e}^{d}\int_{0}^{fx} y f(x,y)\,dx\,dy-\int_{0}^{e}\int_{L_{12x}}^{220} y f(x,y)\,dx\,dy-\int_{e}^{L_{12y}}\int_{L_{12x}}^{fx} y f(x,y)\,dx\,dy$$
$$-\int_{0}^{L_{12y}}\int_{205}^{efx} y f(x,y)\,dx\,dy-\int_{0}^{L_{13y}}\int_{L_{13x}}^{dex} y f(x,y)\,dx\,dy-\int_{0}^{L_{13y}}\int_{L_{14x}}^{L_{13x}} y f(x,y)\,dx\,dy-\int_{L_{13y}}^{L_{14y}}\int_{L_{14x}}^{fx} y f(x,y)\,dx\,dy$$
$$-\int_{0}^{L_{14y}}\int_{135}^{cdx} y f(x,y)\,dx\,dy-\int_{0}^{L_{15y}}\int_{L_{15x}}^{bcx} y f(x,y)\,dx\,dy-\int_{0}^{L_{15y}}\int_{L_{16x}}^{L_{15x}} y f(x,y)\,dx\,dy-\int_{L_{15y}}^{L_{16y}}\int_{L_{16x}}^{fx} y f(x,y)\,dx\,dy$$
$$-\int_{0}^{L_{16y}}\int_{50}^{abx} y f(x,y)\,dx\,dy-\int_{0}^{15}\int_{0}^{qax} y f(x,y)\,dx\,dy-\int_{15}^{L_{2y}}\int_{0}^{qpx} y f(x,y)\,dx\,dy-\int_{L_{2y}}^{d}\int_{0}^{fx} y f(x,y)\,dx\,dy\Bigg]$$

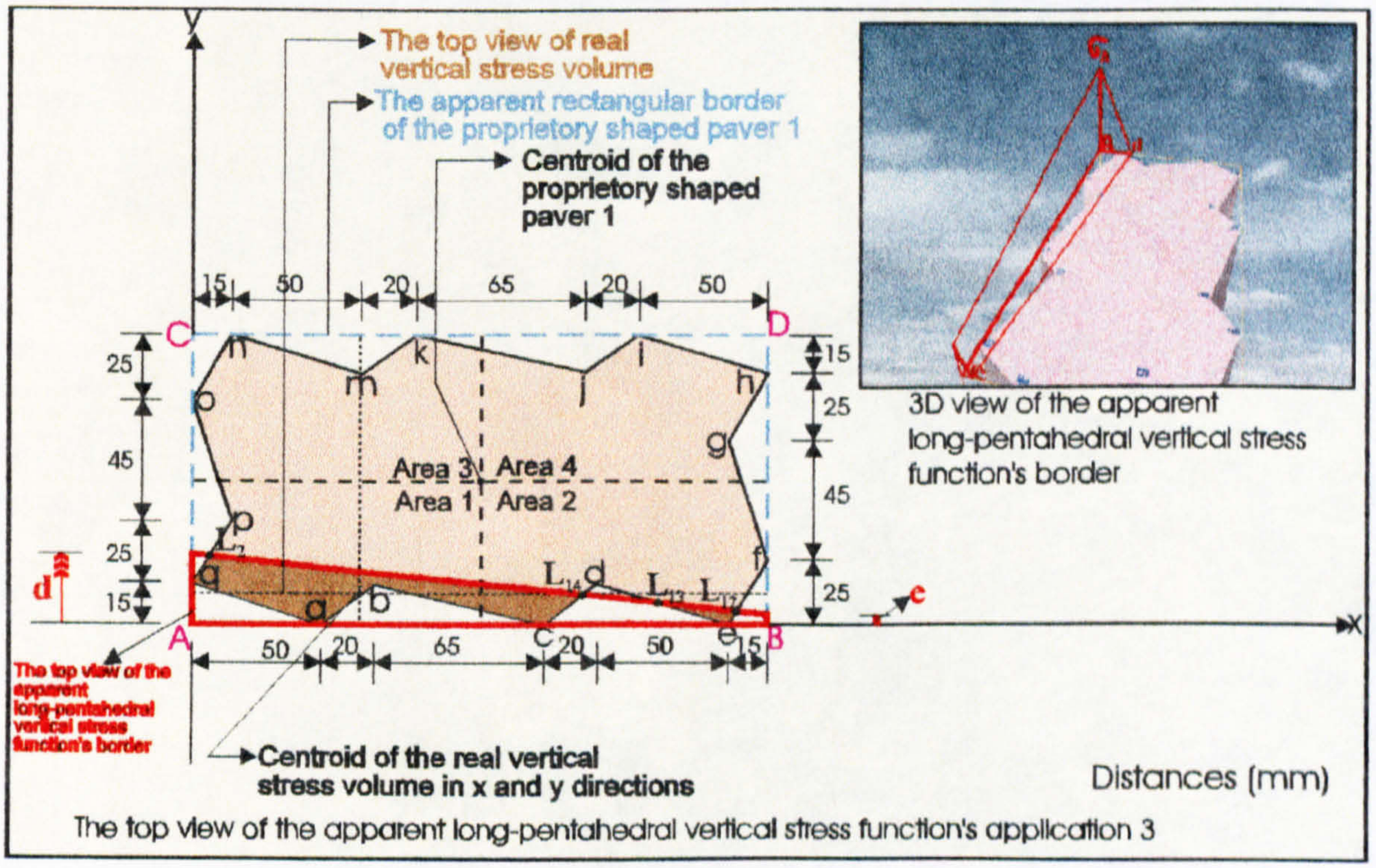

The top view of the apparent long-pentahedral vertical stress function's application 3

Figure 7.55: Application 3 of the long-pentahedral compressive stress distribution beneath the circumscribing rectangular border of proprietory shaped paver 1.

Application 3 of the long-pentahedral compressive stress regime beneath the circumscribing rectangular border of proprietory shaped paver 1 shown in Figure 7.55 can be calculated by using Tables 5.1 and 7.3 and the surface function of the long-pentahedral compressive stress through the three points σ_A, **k** and **d**.

The total volume **V** beneath the surface $f(x,y) = z\ (> 0)$ and above the region in the xy-plane (see Figure 7.55) is:

$$V = \int_0^{220}\int_0^{e} f(x,y)\,dy\,dx + \int_0^{220}\int_e^{fy} f(x,y)\,dy\,dx - \int_{L_{12x}}^{220}\int_0^{e} f(x,y)\,dy\,dx - \int_{L_{12x}}^{220}\int_e^{fy} f(x,y)\,dy\,dx$$
$$- \int_{205}^{L_{12x}}\int_0^{efy} f(x,y)\,dy\,dx - \int_{L_{13x}}^{205}\int_0^{dey} f(x,y)\,dy\,dx - \int_{L_{14x}}^{L_{13x}}\int_0^{L_{13y}} f(x,y)\,dy\,dx - \int_{L_{14x}}^{L_{13x}}\int_{L_{13y}}^{fy} f(x,y)\,dy\,dx$$
$$- \int_{135}^{L_{14x}}\int_0^{cdy} f(x,y)\,dy\,dx - \int_{70}^{135}\int_0^{bcy} f(x,y)\,dy\,dx - \int_{50}^{70}\int_0^{nby} f(x,y)\,dy\,dx - \int_0^{50}\int_0^{qay} f(x,y)\,dy\,dx$$
$$- \int_0^{L_{2x}}\int_{15}^{qpy} f(x,y)\,dy\,dx - \int_0^{L_{2x}}\int_{L_{2y}}^{fy} f(x,y)\,dy\,dx$$

and the centroids of this volume in the xy-plane are at distances $\overline{X}$ and $\overline{Y}$ from the axes (see Figure 7.55) which are given by the following equations.

$$\overline{X} = \frac{1}{V}\left[\int_0^{220}\int_0^{e} x f(x,y)\,dy\,dx + \int_0^{220}\int_e^{fy} x f(x,y)\,dy\,dx - \int_{L_{12x}}^{220}\int_0^{e} x f(x,y)\,dy\,dx - \int_{L_{12x}}^{220}\int_e^{fy} x f(x,y)\,dy\,dx\right.$$
$$- \int_{205}^{L_{12x}}\int_0^{efy} x f(x,y)\,dy\,dx - \int_{L_{13x}}^{205}\int_0^{dey} x f(x,y)\,dy\,dx - \int_{L_{14x}}^{L_{13x}}\int_0^{L_{13y}} x f(x,y)\,dy\,dx - \int_{L_{14x}}^{L_{13x}}\int_{L_{13y}}^{fy} x f(x,y)\,dy\,dx$$
$$- \int_{135}^{L_{14x}}\int_0^{cdy} x f(x,y)\,dy\,dx - \int_{70}^{135}\int_0^{bcy} x f(x,y)\,dy\,dx - \int_{50}^{70}\int_0^{nby} x f(x,y)\,dy\,dx - \int_0^{50}\int_0^{qay} x f(x,y)\,dy\,dx$$
$$\left. - \int_0^{L_{2x}}\int_{15}^{qpy} x f(x,y)\,dy\,dx - \int_0^{L_{2x}}\int_{L_{2y}}^{fy} x f(x,y)\,dy\,dx\right]$$

$$\overline{Y} = \frac{1}{V}\left[\int_0^{e}\int_0^{220} y f(x,y)\,dx\,dy + \int_e^{d}\int_0^{fx} y f(x,y)\,dx\,dy - \int_0^{e}\int_{L_{12x}}^{220} y f(x,y)\,dx\,dy - \int_e^{L_{12y}}\int_{L_{12x}}^{fx} y f(x,y)\,dx\,dy\right.$$
$$\left. - \int_0^{L_{12y}}\int_{205}^{efx} y f(x,y)\,dx\,dy - \int_0^{L_{13y}}\int_{L_{13x}}^{dex} y f(x,y)\,dx\,dy - \int_0^{L_{13y}}\int_{L_{13x}}^{L_{14x}} y f(x,y)\,dx\,dy - \int_{L_{13y}}^{L_{14y}}\int_{L_{14x}}^{fx} y f(x,y)\,dx\,dy\right]$$

$$-\int_{0}^{L_{14y}}\int_{135}^{cdx} y f(x,y)\,dx\,dy - \int_{0}^{15bcx}\int_{70} y f(x,y)\,dx\,dy - \int_{0}^{15abx}\int_{50} y f(x,y)\,dx\,dy - \int_{0}^{15qax}\int_{0} y f(x,y)\,dx\,dy$$

$$\left. -\int_{15}^{L_{2y}}\int_{0}^{qpx} y f(x,y)\,dx\,dy - \int_{L_{2y}}^{d}\int_{0}^{fx} y f(x,y)\,dx\,dy \right]$$

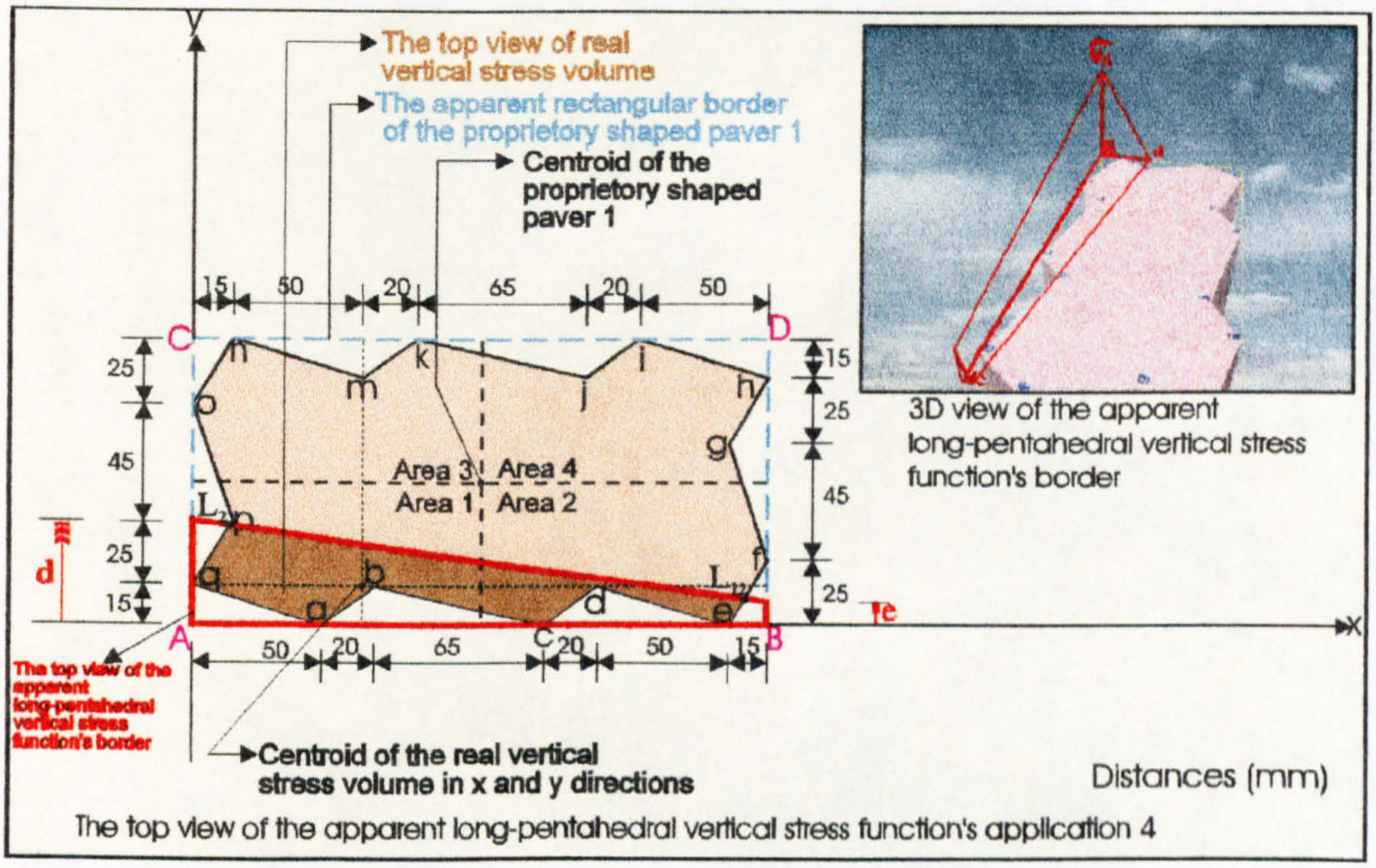

The top view of the apparent long-pentahedral vertical stress function's application 4

Figure 7.56: Application 4 of the long-pentahedral compressive stress distribution beneath the circumscribing rectangular border of proprietory shaped paver 1.

Application 4 of the long-pentahedral compressive stress regime beneath the circumscribing rectangular border of proprietory shaped paver 1 shown in Figure 7.56 can be calculated by using Tables 5.1 and 7.3 and the surface function of the long-pentahedral compressive stress through the three points σ_A, **k** and **d**.

The total volume **V** beneath the surface $f(x,y) = z\ (> 0)$ and above the region in the xy-plane (see Figure 7.56) is:

$$V = \int_0^{220}\int_0^{e} f(x,y)\,dy\,dx + \int_0^{220}\int_e^{fy} f(x,y)\,dy\,dx - \int_{L_{12x}}^{220}\int_0^{e} f(x,y)\,dy\,dx - \int_{L_{12x}}^{220}\int_e^{fy} f(x,y)\,dy\,dx$$
$$- \int_{205}^{L_{12x}}\int_0^{efy} f(x,y)\,dy\,dx - \int_{155}^{205}\int_0^{dey} f(x,y)\,dy\,dx - \int_{135}^{155}\int_0^{cdy} f(x,y)\,dy\,dx - \int_{70}^{135}\int_0^{bcy} f(x,y)\,dy\,dx$$
$$- \int_{50}^{70}\int_0^{aby} f(x,y)\,dy\,dx - \int_0^{50}\int_0^{qay} f(x,y)\,dy\,dx - \int_0^{L_{2x}}\int_{15}^{qpy} f(x,y)\,dy\,dx - \int_0^{L_{2x}}\int_{L_{2y}}^{fy} f(x,y)\,dy\,dx$$

and the centroids of this volume in the xy-plane are at distances $\overline{X}$ and $\overline{Y}$ from the axes (see Figure 7.56) which are given by the following equations.

$$\overline{X} = \frac{1}{V}\left[\int_0^{220}\int_0^{e} x f(x,y)\,dy\,dx + \int_0^{220}\int_e^{fy} x f(x,y)\,dy\,dx - \int_{L_{12x}}^{220}\int_0^{e} x f(x,y)\,dy\,dx - \int_{L_{12x}}^{220}\int_e^{fy} x f(x,y)\,dy\,dx\right.$$
$$- \int_{205}^{L_{12x}}\int_0^{efy} x f(x,y)\,dy\,dx - \int_{155}^{205}\int_0^{dey} x f(x,y)\,dy\,dx - \int_{135}^{155}\int_0^{cdy} x f(x,y)\,dy\,dx - \int_{70}^{135}\int_0^{bcy} x f(x,y)\,dy\,dx$$
$$\left.- \int_{50}^{70}\int_0^{aby} x f(x,y)\,dy\,dx - \int_0^{50}\int_0^{qay} x f(x,y)\,dy\,dx - \int_0^{L_{2x}}\int_{15}^{qpy} x f(x,y)\,dy\,dx - \int_0^{L_{2x}}\int_{L_{2y}}^{fy} x f(x,y)\,dy\,dx\right]$$

$$\overline{Y} = \frac{1}{V}\left[\int_0^{e}\int_0^{220} y f(x,y)\,dx\,dy + \int_e^{d}\int_0^{fx} y f(x,y)\,dx\,dy - \int_0^{e}\int_{L_{12x}}^{220} y f(x,y)\,dx\,dy - \int_e^{L_{12y}}\int_{L_{12x}}^{fx} y f(x,y)\,dx\,dy\right.$$
$$- \int_0^{L_{12y}}\int_{205}^{efx} y f(x,y)\,dx\,dy - \int_0^{155}\int_{205}^{dex} y f(x,y)\,dx\,dy - \int_0^{135}\int_{155}^{cdx} y f(x,y)\,dx\,dy - \int_0^{70}\int_{135}^{bcx} y f(x,y)\,dx\,dy$$
$$\left.- \int_0^{50}\int_{70}^{abx} y f(x,y)\,dx\,dy - \int_0^{0}\int_{50}^{qax} y f(x,y)\,dx\,dy - \int_{15}^{0}\int_{L_{2y}}^{qpx} y f(x,y)\,dx\,dy - \int_{L_{2y}}^{0}\int_{d}^{fx} y f(x,y)\,dx\,dy\right]$$

Application 5 of the long-pentahedral compressive stress regime beneath the circumscribing rectangular border of proprietory shaped paver 1 shown in Figure 7.57 can be calculated by using Tables 5.1 and 7.3 and the surface function of the long-pentahedral compressive stress through the three points σ_A, k and d.

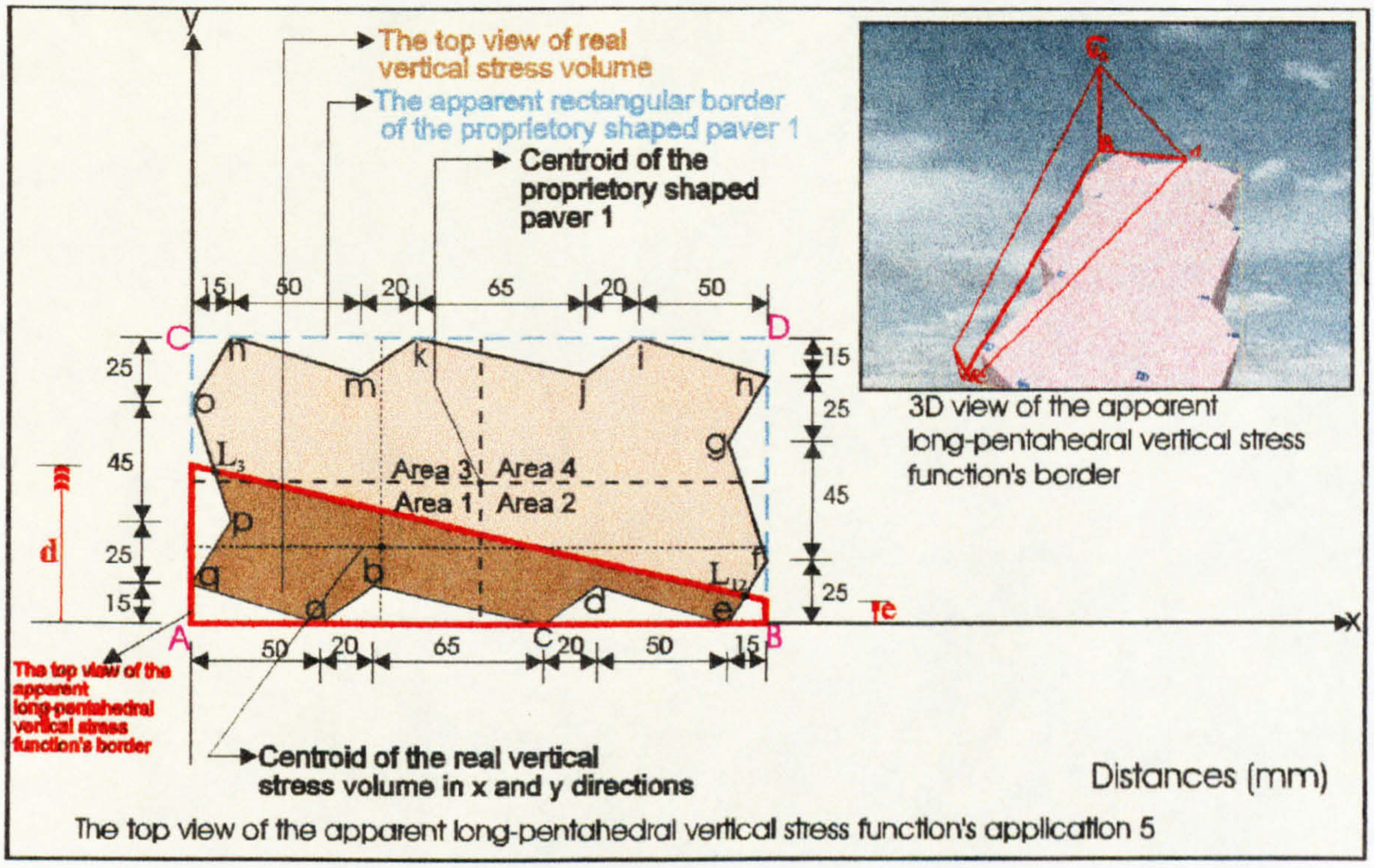

Figure 7.57: Application 5 of the long-pentahedral compressive stress distribution beneath the circumscribing rectangular border of proprietory shaped paver 1.

The total volume **V** beneath the surface $f(x,y) = z\ (> 0)$ and above the region in the xy-plane (see Figure 7.57) is:

$$V = \int_0^{220}\int_0^{e} f(x,y)\,dy\,dx + \int_0^{220}\int_e^{fy} f(x,y)\,dy\,dx - \int_{L_{12x}}^{220}\int_0^{e} f(x,y)\,dy\,dx - \int_{L_{12x}}^{220}\int_e^{fy} f(x,y)\,dy\,dx$$

$$- \int_{205}^{L_{12x}}\int_0^{efy} f(x,y)\,dy\,dx - \int_{155}^{205}\int_0^{dey} f(x,y)\,dy\,dx - \int_{135}^{155}\int_0^{cdy} f(x,y)\,dy\,dx - \int_{70}^{135}\int_0^{bcy} f(x,y)\,dy\,dx$$

$$- \int_{50}^{70}\int_0^{aby} f(x,y)\,dy\,dx - \int_{0}^{50}\int_0^{qay} f(x,y)\,dy\,dx - \int_{0}^{15}\int_0^{qpy} f(x,y)\,dy\,dx - \int_{0}^{40}\int_{L_{3x}}^{L_{3y}} f(x,y)\,dy\,dx$$

$$- \int_{L_{3x}}^{15}\int_{40}^{poy} f(x,y)\,dy\,dx - \int_{0}^{L_{3x}}\int_{L_{3y}}^{fy} f(x,y)\,dy\,dx$$

and the centroids of this volume in the xy-plane are at distances $\overline{X}$ and $\overline{Y}$ from the axes (see Figure 7.57) which are given by the following equations.

$$\overline{X} = \frac{1}{V}\left[\begin{array}{l}
\int_0^{220}\int_0^{e} x f(x,y)\,dy\,dx + \int_0^{220}\int_e^{fy} x f(x,y)\,dy\,dx - \int_{L_{12x}}^{220}\int_0^{e} x f(x,y)\,dy\,dx - \int_{L_{12x}}^{220}\int_e^{fy} x f(x,y)\,dy\,dx \\
-\int_{205}^{L_{12x}}\int_0^{efy} x f(x,y)\,dy\,dx - \int_{155}^{205}\int_0^{dey} x f(x,y)\,dy\,dx - \int_{135}^{155}\int_0^{cdy} x f(x,y)\,dy\,dx - \int_{70}^{135}\int_0^{bcy} x f(x,y)\,dy\,dx \\
-\int_{50}^{70}\int_0^{aby} x f(x,y)\,dy\,dx - \int_{0}^{50}\int_0^{qay} x f(x,y)\,dy\,dx - \int_{0}^{15}\int_0^{qpy} x f(x,y)\,dy\,dx - \int_{0}^{L_{3x}}\int_{40}^{L_{3y}} x f(x,y)\,dy\,dx \\
-\int_{L_{3x}}^{15}\int_{40}^{poy} x f(x,y)\,dy\,dx - \int_{0}^{L_{3x}}\int_{L_{3y}}^{fy} x f(x,y)\,dy\,dx
\end{array}\right]$$

$$\overline{Y} = \frac{1}{V}\left[\begin{array}{l}
\int_0^{e}\int_0^{220} y f(x,y)\,dx\,dy + \int_e^{d}\int_0^{fx} y f(x,y)\,dx\,dy - \int_0^{e}\int_{L_{12x}}^{220} y f(x,y)\,dx\,dy - \int_e^{L_{12y}}\int_{L_{12x}}^{fx} y f(x,y)\,dx\,dy \\
-\int_0^{L_{12y}}\int_{205}^{efx} y f(x,y)\,dx\,dy - \int_0^{15}\int_{155}^{dex} y f(x,y)\,dx\,dy - \int_0^{15}\int_{135}^{cdx} y f(x,y)\,dx\,dy - \int_0^{15}\int_{70}^{bcx} y f(x,y)\,dx\,dy \\
-\int_0^{15}\int_{50}^{abx} y f(x,y)\,dx\,dy - \int_0^{15}\int_{0}^{qax} y f(x,y)\,dx\,dy - \int_{15}^{40}\int_{0}^{qpx} y f(x,y)\,dx\,dy - \int_{40}^{L_{3y}}\int_{0}^{L_{3x}} y f(x,y)\,dx\,dy \\
-\int_{40}^{L_{3y}}\int_{L_{3x}}^{pox} y f(x,y)\,dx\,dy - \int_{L_{3y}}^{d}\int_{0}^{fx} y f(x,y)\,dx\,dy
\end{array}\right]$$

Application 6 of the long-pentahedral compressive stress regime beneath the circumscribing rectangular border of proprietory shaped paver 1 shown in Figure 7.58 can be calculated by using Tables 5.1 and 7.3 and the surface function of the long-pentahedral compressive stress through the three points σ_A, k and d.

The total volume V beneath the surface $f(x,y) = z\ (> 0)$ and above the region in the xy-plane (see Figure 7.58) is:

$$V = \int_0^{220}\int_0^{e} f(x,y)\,dy\,dx + \int_0^{220}\int_e^{fy} f(x,y)\,dy\,dx - \int_{L_{12x}}^{220}\int_0^{e} f(x,y)\,dy\,dx - \int_{L_{12x}}^{220}\int_e^{fy} f(x,y)\,dy\,dx$$
$$-\int_{205}^{L_{12x}}\int_0^{efy} f(x,y)\,dy\,dx - \int_{155}^{205}\int_0^{dey} f(x,y)\,dy\,dx - \int_{135}^{155}\int_0^{cdy} f(x,y)\,dy\,dx - \int_{70}^{135}\int_0^{bcy} f(x,y)\,dy\,dx$$

$$-\int_{50}^{70}\int_{0}^{aby} f(x,y)\,dy\,dx-\int_{0}^{50}\int_{0}^{qay} f(x,y)\,dy\,dx-\int_{0}^{15}\int_{15}^{qpy} f(x,y)\,dy\,dx-\int_{0}^{15}\int_{40}^{poy} f(x,y)\,dy\,dx$$

$$-\int_{0}^{L_{4x}}\int_{85}^{ony} f(x,y)\,dy\,dx-\int_{0}^{L_{4x}}\int_{L_{4y}}^{fy} f(x,y)\,dy\,dx$$

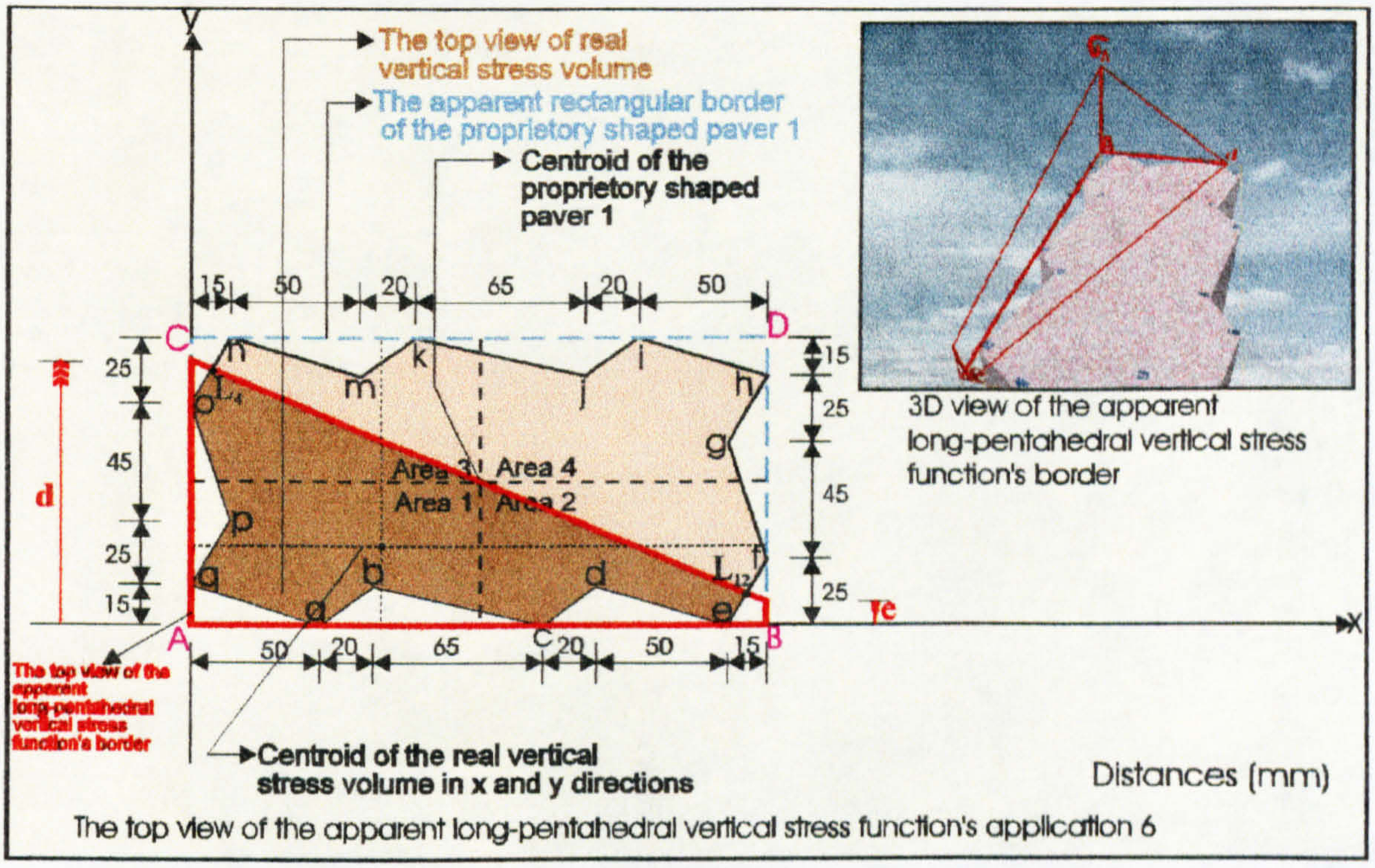

The top view of the apparent long-pentahedral vertical stress function's application 6

Figure 7.58: Application 6 of the long-pentahedral compressive stress distribution beneath the circumscribing rectangular border of proprietory shaped paver 1.

and the centroids of this volume in the xy-plane are at distances $\overline{X}$ and $\overline{Y}$ from the axes (see Figure 7.58) which are given by the following equations.

$$\overline{X}=\frac{1}{V}\left[\int_{0}^{220}\int_{0}^{e} x f(x,y)\,dy\,dx+\int_{0}^{220}\int_{e}^{fy} x f(x,y)\,dy\,dx-\int_{L_{12x}}^{220}\int_{0}^{e} x f(x,y)\,dy\,dx-\int_{L_{12x}}^{220}\int_{e}^{fy} x f(x,y)\,dy\,dx\right.$$

$$-\int_{205}^{L_{12x}}\int_{0}^{efy} x f(x,y)\,dy\,dx-\int_{155}^{205}\int_{0}^{dey} x f(x,y)\,dy\,dx-\int_{135}^{155}\int_{0}^{cdy} x f(x,y)\,dy\,dx-\int_{70}^{135}\int_{0}^{bcy} x f(x,y)\,dy\,dx$$

$$\left.-\int_{50}^{70}\int_{0}^{aby} x f(x,y)\,dy\,dx-\int_{0}^{50}\int_{0}^{qay} x f(x,y)\,dy\,dx-\int_{0}^{15}\int_{15}^{qpy} x f(x,y)\,dy\,dx-\int_{0}^{15}\int_{40}^{poy} x f(x,y)\,dy\,dx\right]$$

$$-\int_{0}^{L_{4x}}\int_{85}^{ony} x f(x,y)\,dy\,dx - \int_{0}^{L_{4x}}\int_{L_{4y}}^{fy} x f(x,y)\,dy\,dx\Bigg]$$

$$\overline{Y} = \frac{1}{V}\Bigg[\int_{0}^{e}\int_{0}^{220} y f(x,y)\,dx\,dy + \int_{e}^{d}\int_{0}^{fx} y f(x,y)\,dx\,dy - \int_{0}^{e}\int_{L_{12x}}^{220} y f(x,y)\,dx\,dy - \int_{e}^{L_{12y}}\int_{L_{12x}}^{fx} y f(x,y)\,dx\,dy$$
$$-\int_{0}^{L_{12y}}\int_{205}^{efx} y f(x,y)\,dx\,dy - \int_{0}^{155}\int_{0}^{15dex} y f(x,y)\,dx\,dy - \int_{0}^{135}\int_{0}^{15cdx} y f(x,y)\,dx\,dy - \int_{0}^{70}\int_{0}^{15bcx} y f(x,y)\,dx\,dy$$
$$-\int_{0}^{50}\int_{0}^{15abx} y f(x,y)\,dx\,dy - \int_{0}^{0}\int_{0}^{15qax} y f(x,y)\,dx\,dy - \int_{15}^{0}\int_{0}^{40qpx} y f(x,y)\,dx\,dy - \int_{40}^{0}\int_{0}^{85pox} y f(x,y)\,dx\,dy$$
$$-\int_{85}^{0}\int_{0}^{L_{4y}\,onx} y f(x,y)\,dx\,dy - \int_{L_{4y}}^{0}\int_{0}^{d\quad fx} y f(x,y)\,dx\,dy\Bigg]$$

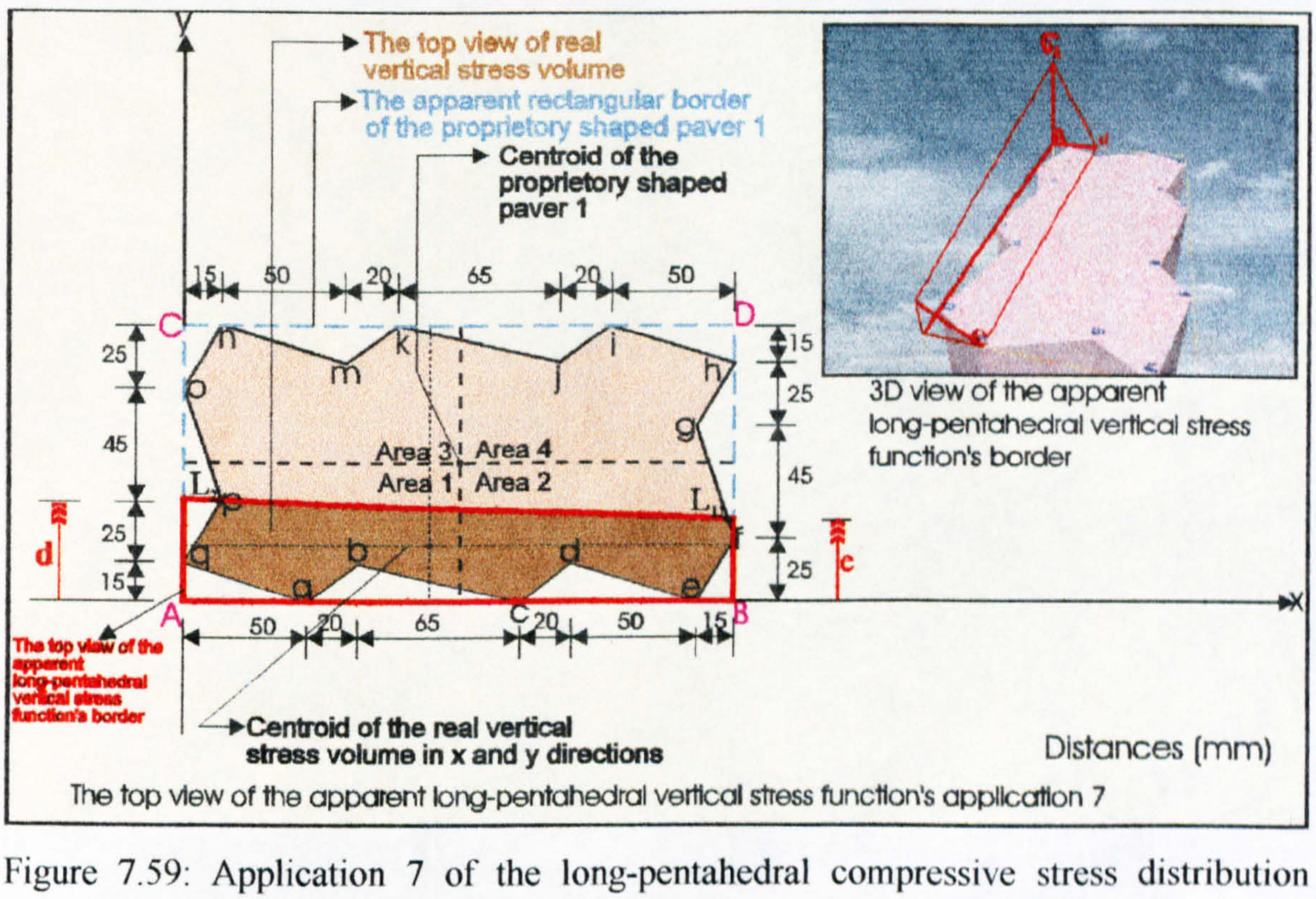

The top view of the apparent long-pentahedral vertical stress function's application 7

Figure 7.59: Application 7 of the long-pentahedral compressive stress distribution beneath the circumscribing rectangular border of proprietory shaped paver 1.

Application 7 of the long-pentahedral compressive stress regime beneath the circumscribing rectangular border of proprietory shaped paver 1 shown in Figure 7.59

can be calculated by using Tables 5.1 and 7.3 and the surface function of the long-pentahedral compressive stress through the three points σ_A, **k** and **d**.

The total volume **V** beneath the surface $f(x,y) = z\ (> 0)$ and above the region in the xy-plane (see Figure 7.59) is:

$$V = \int_0^{220}\int_0^{e} f(x,y)\,dy\,dx + \int_0^{220}\int_e^{fy} f(x,y)\,dy\,dx - \int_{L_{11x}}^{220}\int_{25}^{fgy} f(x,y)\,dy\,dx + \int_{L_{11x}}^{220}\int_e^{fy} f(x,y)\,dy\,dx - \int_{205}^{220}\int_0^{efy} f(x,y)\,dy\,dx$$
$$- \int_{155}^{205}\int_0^{dey} f(x,y)\,dy\,dx - \int_{135}^{155}\int_0^{cdy} f(x,y)\,dy\,dx - \int_{70}^{135}\int_0^{bcy} f(x,y)\,dy\,dx - \int_{50}^{70}\int_0^{kby} f(x,y)\,dy\,dx - \int_0^{50}\int_0^{qay} f(x,y)\,dy\,dx$$
$$- \int_0^{L_{2x}}\int_{15}^{qpy} f(x,y)\,dy\,dx - \int_0^{L_{2x}}\int_{L_{2y}}^{fy} f(x,y)\,dy\,dx$$

and the centroids of this volume in the xy-plane are at distances $\overline{X}$ and $\overline{Y}$ from the axes (see Figure 7.59) which are given by the following equations.

$$\overline{X} = \frac{1}{V}\left[\int_0^{220}\int_0^{e} x f(x,y)\,dy\,dx + \int_0^{220}\int_e^{fy} x f(x,y)\,dy\,dx - \int_{L_{11x}}^{220}\int_{25}^{fgy} x f(x,y)\,dy\,dx + \int_{L_{11x}}^{220}\int_e^{fy} x f(x,y)\,dy\,dx\right.$$
$$- \int_{205}^{220}\int_0^{efy} x f(x,y)\,dy\,dx - \int_{155}^{205}\int_0^{dey} x f(x,y)\,dy\,dx - \int_{135}^{155}\int_0^{cdy} x f(x,y)\,dy\,dx - \int_{70}^{135}\int_0^{bcy} x f(x,y)\,dy\,dx$$
$$\left.- \int_{50}^{70}\int_0^{aby} x f(x,y)\,dy\,dx - \int_0^{50}\int_0^{qay} x f(x,y)\,dy\,dx - \int_0^{L_{2x}}\int_{15}^{qpy} x f(x,y)\,dy\,dx - \int_0^{L_{2x}}\int_{L_{2y}}^{fy} x f(x,y)\,dy\,dx\right]$$

$$\overline{Y} = \frac{1}{V}\left[\int_0^{e}\int_0^{220} y f(x,y)\,dx\,dy + \int_e^{d}\int_0^{fx} y f(x,y)\,dx\,dy - \int_{25}^{L_{11y}}\int_{L_{11x}}^{fgx} y f(x,y)\,dx\,dy + \int_e^{L_{11y}}\int_{L_{11x}}^{fx} y f(x,y)\,dx\,dy\right.$$
$$- \int_0^{25}\int_{205}^{efx} y f(x,y)\,dx\,dy - \int_0^{15}\int_{155}^{dex} y f(x,y)\,dx\,dy - \int_0^{15}\int_{135}^{cdx} y f(x,y)\,dx\,dy - \int_0^{15}\int_{70}^{bcx} y f(x,y)\,dx\,dy$$
$$\left.- \int_0^{15}\int_{50}^{abx} y f(x,y)\,dx\,dy - \int_0^{15}\int_0^{qax} y f(x,y)\,dx\,dy - \int_{15}^{L_{2y}}\int_0^{qpx} y f(x,y)\,dx\,dy - \int_{L_{2y}}^{d}\int_0^{fx} y f(x,y)\,dx\,dy\right]$$

Application 8 of the long-pentahedral compressive stress regime beneath the circumscribing rectangular border of proprietory shaped paver 1 shown in Figure 7.60 can be calculated by using Tables 5.1 and 7.3 and the surface function of the long-pentahedral compressive stress through the three points σ_A, **k** and **d**.

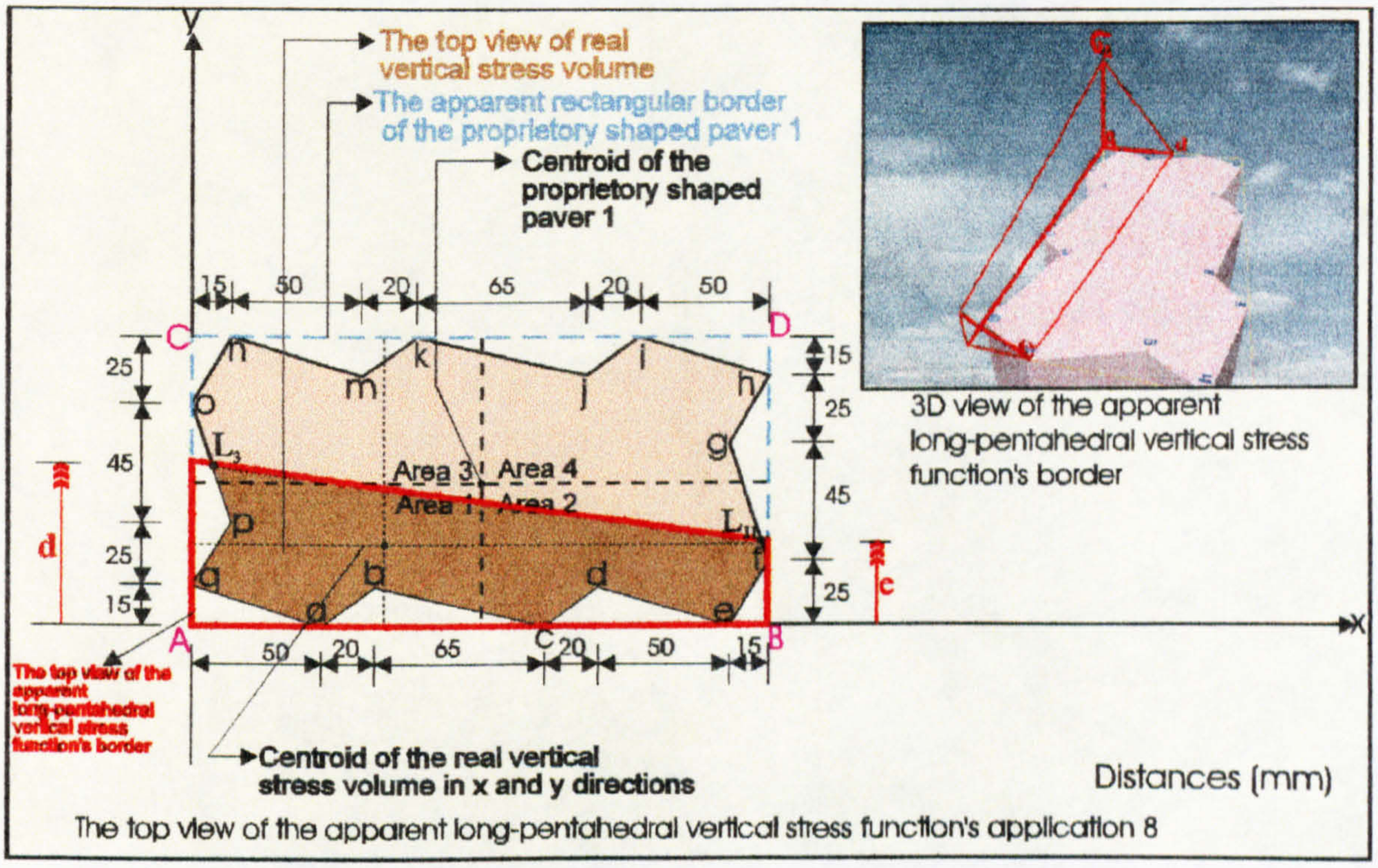

Figure 7.60: Application 8 of the long-pentahedral compressive stress distribution beneath the circumscribing rectangular border of proprietory shaped paver 1.

The total volume **V** beneath the surface $f(x,y) = z\ (> 0)$ and above the region in the xy-plane (see Figure 7.60) is:

$$V = \int_0^{220}\int_0^{e} f(x,y)\,dy\,dx + \int_0^{220}\int_e^{fy} f(x,y)\,dy\,dx - \int_{L_{11x}}^{220}\int_{25}^{fgy} f(x,y)\,dy\,dx + \int_{L_{11x}}^{220}\int_{e}^{fy} f(x,y)\,dy\,dx$$

$$- \int_{205}^{220}\int_{0}^{efy} f(x,y)\,dy\,dx - \int_{155}^{205}\int_{0}^{dey} f(x,y)\,dy\,dx - \int_{135}^{155}\int_{0}^{cdy} f(x,y)\,dy\,dx - \int_{70}^{135}\int_{0}^{bcy} f(x,y)\,dy\,dx$$

$$- \int_{50}^{70}\int_{0}^{aby} f(x,y)\,dy\,dx - \int_{0}^{50}\int_{0}^{qay} f(x,y)\,dy\,dx - \int_{0}^{15}\int_{0}^{qpy} f(x,y)\,dy\,dx - \int_{0}^{L_{3x}}\int_{40}^{L_{3y}} f(x,y)\,dy\,dx$$

$$-\int_{L_{3x}}^{15}\int_{40}^{poy} f(x,y)\,dy\,dx-\int_{0}^{L_{3x}}\int_{L_{3y}}^{fy} f(x,y)\,dy\,dx$$

and the centroids of this volume in the xy-plane are at distances $\overline{X}$ and $\overline{Y}$ from the axes (see Figure 7.60) which are given by the following equations.

$$\overline{X}=\frac{1}{V}\left[\begin{array}{l}\int_{0}^{220}\int_{0}^{e} x f(x,y)\,dy\,dx+\int_{0}^{220}\int_{e}^{fy} x f(x,y)\,dy\,dx-\int_{L_{11x}}^{220}\int_{25}^{fgy} x f(x,y)\,dy\,dx+\int_{L_{11x}}^{220}\int_{e}^{fy} x f(x,y)\,dy\,dx\\ -\int_{205}^{220}\int_{0}^{efy} x f(x,y)\,dy\,dx-\int_{155}^{205}\int_{0}^{dey} x f(x,y)\,dy\,dx-\int_{135}^{155}\int_{0}^{cdy} x f(x,y)\,dy\,dx-\int_{70}^{135}\int_{0}^{bcy} x f(x,y)\,dy\,dx\\ -\int_{50}^{70}\int_{0}^{aby} x f(x,y)\,dy\,dx-\int_{0}^{50}\int_{0}^{qay} x f(x,y)\,dy\,dx-\int_{0}^{15}\int_{0}^{qpy} x f(x,y)\,dy\,dx-\int_{0}^{L_{3x}}\int_{40}^{L_{3y}} x f(x,y)\,dy\,dx\\ -\int_{L_{3x}}^{15}\int_{40}^{poy} x f(x,y)\,dy\,dx-\int_{0}^{L_{3x}}\int_{L_{3y}}^{fy} x f(x,y)\,dy\,dx\end{array}\right]$$

$$\overline{Y}=\frac{1}{V}\left[\begin{array}{l}\int_{0}^{e}\int_{0}^{220} y f(x,y)\,dx\,dy+\int_{e}^{d}\int_{0}^{fx} y f(x,y)\,dx\,dy-\int_{25}^{L_{11y}}\int_{L_{11x}}^{fgx} y f(x,y)\,dx\,dy+\int_{e}^{L_{11y}}\int_{L_{11x}}^{fx} y f(x,y)\,dx\,dy\\ -\int_{0}^{25}\int_{205}^{efx} y f(x,y)\,dx\,dy-\int_{0}^{15}\int_{155}^{dex} y f(x,y)\,dx\,dy-\int_{0}^{15}\int_{135}^{cdx} y f(x,y)\,dx\,dy-\int_{0}^{15}\int_{70}^{bcx} y f(x,y)\,dx\,dy\\ -\int_{0}^{15}\int_{50}^{abx} y f(x,y)\,dx\,dy-\int_{0}^{15}\int_{0}^{qax} y f(x,y)\,dx\,dy-\int_{15}^{40}\int_{0}^{qpx} y f(x,y)\,dx\,dy-\int_{40}^{L_{3y}}\int_{0}^{L_{3x}} y f(x,y)\,dx\,dy\\ -\int_{40}^{L_{3y}}\int_{L_{3x}}^{pox} y f(x,y)\,dx\,dy-\int_{L_{3y}}^{d}\int_{0}^{fx} y f(x,y)\,dx\,dy\end{array}\right]$$

Application 9 of the long-pentahedral compressive stress regime beneath the circumscribing rectangular border of proprietory shaped paver 1 shown in Figure 7.61 can be calculated by using Tables 5.1 and 7.3 and the surface function of the long-pentahedral compressive stress through the three points σ_A, k and d.

The total volume **V** beneath the surface $f(x,y) = z\ (> 0)$ and above the region in the xy-plane (see Figure 7.61) is:

$$V = \int_0^{220}\int_0^{e} f(x,y)\,dy\,dx + \int_0^{220}\int_e^{fy} f(x,y)\,dy\,dx - \int_{L_{11x}}^{220}\int_{25}^{fgy} f(x,y)\,dy\,dx + \int_{L_{11x}}^{220}\int_e^{fy} f(x,y)\,dy\,dx$$
$$- \int_{205}^{220}\int_0^{efy} f(x,y)\,dy\,dx - \int_{155}^{205}\int_0^{dey} f(x,y)\,dy\,dx - \int_{135}^{155}\int_0^{cdy} f(x,y)\,dy\,dx - \int_{70}^{135}\int_0^{bcy} f(x,y)\,dy\,dx$$
$$- \int_{50}^{70}\int_0^{aby} f(x,y)\,dy\,dx - \int_0^{50}\int_0^{qay} f(x,y)\,dy\,dx - \int_0^{0}\int_{15}^{qpy} f(x,y)\,dy\,dx - \int_0^{0}\int_{40}^{poy} f(x,y)\,dy\,dx$$
$$- \int_0^{L_{4x}}\int_{85}^{ony} f(x,y)\,dy\,dx - \int_0^{L_{4x}}\int_{L_{4y}}^{fy} f(x,y)\,dy\,dx$$

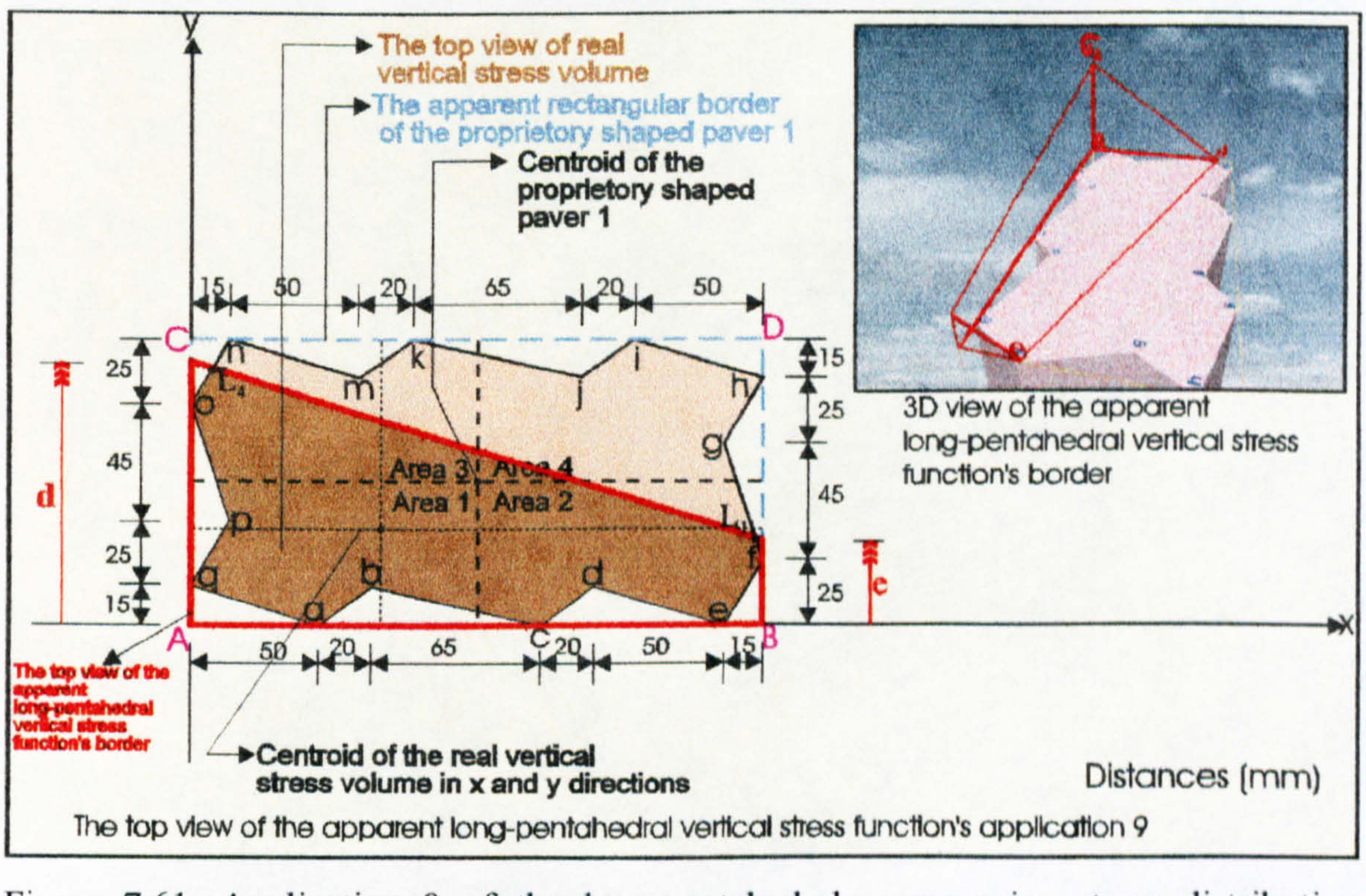

The top view of the apparent long-pentahedral vertical stress function's application 9

Figure 7.61: Application 9 of the long-pentahedral compressive stress distribution beneath the circumscribing rectangular border of proprietory shaped paver 1.

and the centroids of this volume in the xy-plane are at distances $\overline{X}$ and $\overline{Y}$ from the axes (see Figure 7.61) which are given by the following equations.

$$\overline{X} = \frac{1}{V}\left[\begin{array}{l}
\int_{0}^{220}\int_{0}^{e} x f(x,y)\,dy\,dx + \int_{0}^{220}\int_{e}^{fy} x f(x,y)\,dy\,dx - \int_{L_{11x}}^{220}\int_{25}^{fgy} x f(x,y)\,dy\,dx + \int_{L_{11x}}^{220}\int_{e}^{fy} x f(x,y)\,dy\,dx \\
-\int_{205}^{220}\int_{0}^{efy} x f(x,y)\,dy\,dx - \int_{155}^{205}\int_{0}^{dey} x f(x,y)\,dy\,dx - \int_{135}^{155}\int_{0}^{cdy} x f(x,y)\,dy\,dx - \int_{70}^{135}\int_{0}^{bcy} x f(x,y)\,dy\,dx \\
-\int_{50}^{70}\int_{0}^{aby} x f(x,y)\,dy\,dx - \int_{0}^{50}\int_{0}^{qay} x f(x,y)\,dy\,dx - \int_{0}^{15}\int_{15}^{qpy} x f(x,y)\,dy\,dx - \int_{0}^{15}\int_{40}^{poy} x f(x,y)\,dy\,dx \\
-\int_{0}^{L_{4x}}\int_{85}^{ony} x f(x,y)\,dy\,dx - \int_{0}^{L_{4x}}\int_{L_{4y}}^{fy} x f(x,y)\,dy\,dx
\end{array}\right]$$

$$\overline{Y} = \frac{1}{V}\left[\begin{array}{l}
\int_{0}^{e}\int_{0}^{220} y f(x,y)\,dx\,dy + \int_{e}^{d}\int_{0}^{fx} y f(x,y)\,dx\,dy - \int_{25}^{L_{11y}}\int_{L_{11x}}^{fgx} y f(x,y)\,dx\,dy + \int_{e}^{L_{11y}}\int_{L_{11x}}^{fx} y f(x,y)\,dx\,dy \\
-\int_{0}^{25}\int_{205}^{efx} y f(x,y)\,dx\,dy - \int_{0}^{15}\int_{155}^{dcx} y f(x,y)\,dx\,dy - \int_{0}^{15}\int_{135}^{cdx} y f(x,y)\,dx\,dy - \int_{0}^{15}\int_{70}^{bcx} y f(x,y)\,dx\,dy \\
-\int_{0}^{15}\int_{50}^{ahx} y f(x,y)\,dx\,dy - \int_{0}^{15}\int_{0}^{qax} y f(x,y)\,dx\,dy - \int_{15}^{40}\int_{0}^{qpx} y f(x,y)\,dx\,dy - \int_{40}^{85}\int_{0}^{pox} y f(x,y)\,dx\,dy \\
-\int_{85}^{L_{4y}}\int_{0}^{onx} y f(x,y)\,dx\,dy - \int_{L_{4y}}^{d}\int_{0}^{fx} y f(x,y)\,dx\,dy
\end{array}\right]$$

Application 10 of the long-pentahedral compressive stress regime beneath the circumscribing rectangular border of proprietory shaped paver 1 shown in Figure 7.62 can be calculated by using Tables 5.1 and 7.3 and the surface function of the long-pentahedral compressive stress through the three points σ_A, **k** and **d**.

The total volume **V** beneath the surface $f(x,y) = z\ (> 0)$ and above the region in the xy-plane (see Figure 7.62) is:

$$\begin{array}{l}
V = \int_{0}^{220}\int_{0}^{e} f(x,y)\,dy\,dx + \int_{0}^{220}\int_{e}^{fy} f(x,y)\,dy\,dx - \int_{205}^{l_{10x}}\int_{70}^{ghy} f(x,y)\,dy\,dx - \int_{l_{10x}}^{220}\int_{70}^{e} f(x,y)\,dy\,dx \\
-\int_{L_{10x}}^{220}\int_{e}^{fy} f(x,y)\,dy\,dx - \int_{205}^{220}\int_{25}^{fgy} f(x,y)\,dy\,dx - \int_{205}^{220}\int_{0}^{efy} f(x,y)\,dy\,dx - \int_{155}^{205}\int_{0}^{dcy} f(x,y)\,dy\,dx
\end{array}$$

$$-\int_{135}^{155}\int_{0}^{cdy} f(x,y)\,dy\,dx-\int_{70}^{135}\int_{0}^{bcy} f(x,y)\,dy\,dx-\int_{50}^{70}\int_{0}^{aby} f(x,y)\,dy\,dx-\int_{0}^{50}\int_{0}^{qay} f(x,y)\,dy\,dx$$

$$-\int_{0}^{15}\int_{15}^{qpy} f(x,y)\,dy\,dx-\int_{0}^{L_{3x}}\int_{40}^{L_{3y}} f(x,y)\,dy\,dx-\int_{L_{3x}}^{15}\int_{40}^{poy} f(x,y)\,dy\,dx-\int_{0}^{L_{3x}}\int_{L_{3y}}^{fy} f(x,y)\,dy\,dx$$

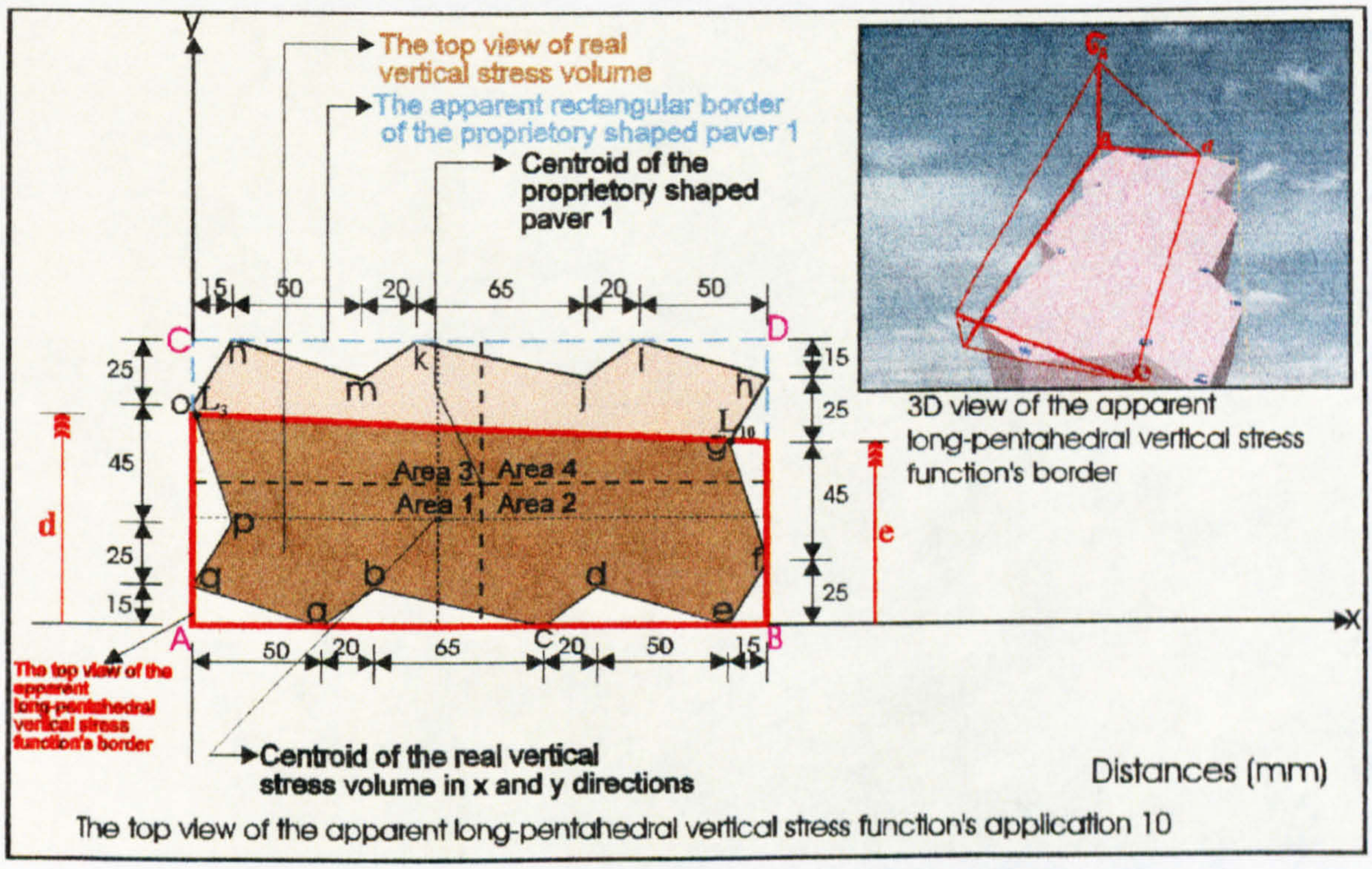

Figure 7.62: Application 10 of the long-pentahedral compressive stress distribution beneath the circumscribing rectangular border of proprietory shaped paver 1.

and the centroids of this volume in the xy-plane are at distances $\overline{X}$ and $\overline{Y}$ from the axes (see Figure 7.62) which are given by the following equations.

$$\overline{X}=\frac{1}{V}\left[\int_{0}^{220}\int_{0}^{e} x f(x,y)\,dy\,dx+\int_{0}^{220}\int_{e}^{fy} x f(x,y)\,dy\,dx-\int_{205}^{L_{10x}}\int_{70}^{ghy} x f(x,y)\,dy\,dx-\int_{L_{10x}}^{220}\int_{70}^{e} x f(x,y)\,dy\,dx\right.$$

$$-\int_{L_{10x}}^{220}\int_{e}^{fy} x f(x,y)\,dy\,dx-\int_{205}^{220}\int_{25}^{fgy} x f(x,y)\,dy\,dx-\int_{205}^{220}\int_{0}^{efy} x f(x,y)\,dy\,dx-\int_{155}^{205}\int_{0}^{dey} x f(x,y)\,dy\,dx$$

$$\left.-\int_{135}^{155}\int_{0}^{cdy} x f(x,y)\,dy\,dx-\int_{70}^{135}\int_{0}^{bcy} x f(x,y)\,dy\,dx-\int_{50}^{70}\int_{0}^{aby} x f(x,y)\,dy\,dx-\int_{0}^{50}\int_{0}^{qay} x f(x,y)\,dy\,dx\right]$$

$$-\int_{0}^{15}\int_{15}^{15qpy} x f(x,y)\,dy\,dx - \int_{0}^{L_{3x}}\int_{40}^{L_{3y}} x f(x,y)\,dy\,dx - \int_{L_{3x}}^{15}\int_{40}^{poy} x f(x,y)\,dy\,dx - \int_{0}^{L_{3x}}\int_{L_{3y}}^{fy} x f(x,y)\,dy\,dx \Bigg]$$

$$\left[\int_{0}^{e}\int_{0}^{220} y f(x,y)\,dx\,dy + \int_{e}^{d}\int_{0}^{fx} y f(x,y)\,dx\,dy - \int_{70}^{L_{10y}}\int_{205}^{ghx} y f(x,y)\,dx\,dy - \int_{70}^{e}\int_{L_{10x}}^{220} y f(x,y)\,dx\,dy\right.$$

$$\left. - \int_{e}^{L_{10y}}\int_{L_{10x}}^{fx} y f(x,y)\,dx\,dy - \int_{25}^{70}\int_{205}^{fgx} y f(x,y)\,dx\,dy - \int_{0}^{25}\int_{205}^{efx} y f(x,y)\,dx\,dy - \int_{0}^{15}\int_{155}^{dex} y f(x,y)\,dx\,dy\right.$$

$$\left. - \int_{0}^{15}\int_{135}^{cdx} y f(x,y)\,dx\,dy - \int_{0}^{15}\int_{70}^{bcx} y f(x,y)\,dx\,dy - \int_{0}^{15}\int_{50}^{abx} y f(x,y)\,dx\,dy - \int_{0}^{15}\int_{0}^{qax} y f(x,y)\,dx\,dy\right.$$

$$\left. - \int_{15}^{40}\int_{0}^{qpx} y f(x,y)\,dx\,dy - \int_{40}^{L_{3y}}\int_{0}^{L_{3x}} y f(x,y)\,dx\,dy - \int_{40}^{L_{3y}}\int_{L_{3x}}^{pox} y f(x,y)\,dx\,dy - \int_{L_{3y}}^{d}\int_{0}^{fx} y f(x,y)\,dx\,dy\right]$$

$$\overline{Y} = \frac{1}{V}$$

Application 11 of the long-pentahedral compressive stress regime beneath the circumscribing rectangular border of proprietory shaped paver 1 shown in Figure 7.63 can be calculated by using Tables 5.1 and 7.3 and the surface function of the long-pentahedral compressive stress through the three points σ_A, **k** and **d**.

The total volume **V** beneath the surface $f(x,y) = z\ (> 0)$ and above the region in the xy-plane (see Figure 7.63) is:

$$V = \int_{0}^{220}\int_{0}^{e} f(x,y)\,dy\,dx + \int_{0}^{220}\int_{e}^{fy} f(x,y)\,dy\,dx - \int_{205}^{L_{10x}}\int_{70}^{ghy} f(x,y)\,dy\,dx - \int_{L_{10x}}^{220}\int_{70}^{e} f(x,y)\,dy\,dx$$

$$- \int_{L_{10x}}^{220}\int_{e}^{fy} f(x,y)\,dy\,dx - \int_{205}^{220}\int_{25}^{fgy} f(x,y)\,dy\,dx - \int_{205}^{220}\int_{0}^{efy} f(x,y)\,dy\,dx - \int_{155}^{205}\int_{0}^{dcy} f(x,y)\,dy\,dx$$

$$- \int_{135}^{155}\int_{0}^{cdy} f(x,y)\,dy\,dx - \int_{70}^{135}\int_{0}^{bcy} f(x,y)\,dy\,dx - \int_{50}^{70}\int_{0}^{aby} f(x,y)\,dy\,dx - \int_{0}^{50}\int_{0}^{qpy} f(x,y)\,dy\,dx$$

$$- \int_{0}^{15}\int_{15}^{qpy} f(x,y)\,dy\,dx - \int_{0}^{15}\int_{40}^{poy} f(x,y)\,dy\,dx - \int_{0}^{L_{4x}}\int_{85}^{ony} f(x,y)\,dy\,dx - \int_{0}^{L_{4x}}\int_{L_{4y}}^{fy} f(x,y)\,dy\,dx$$

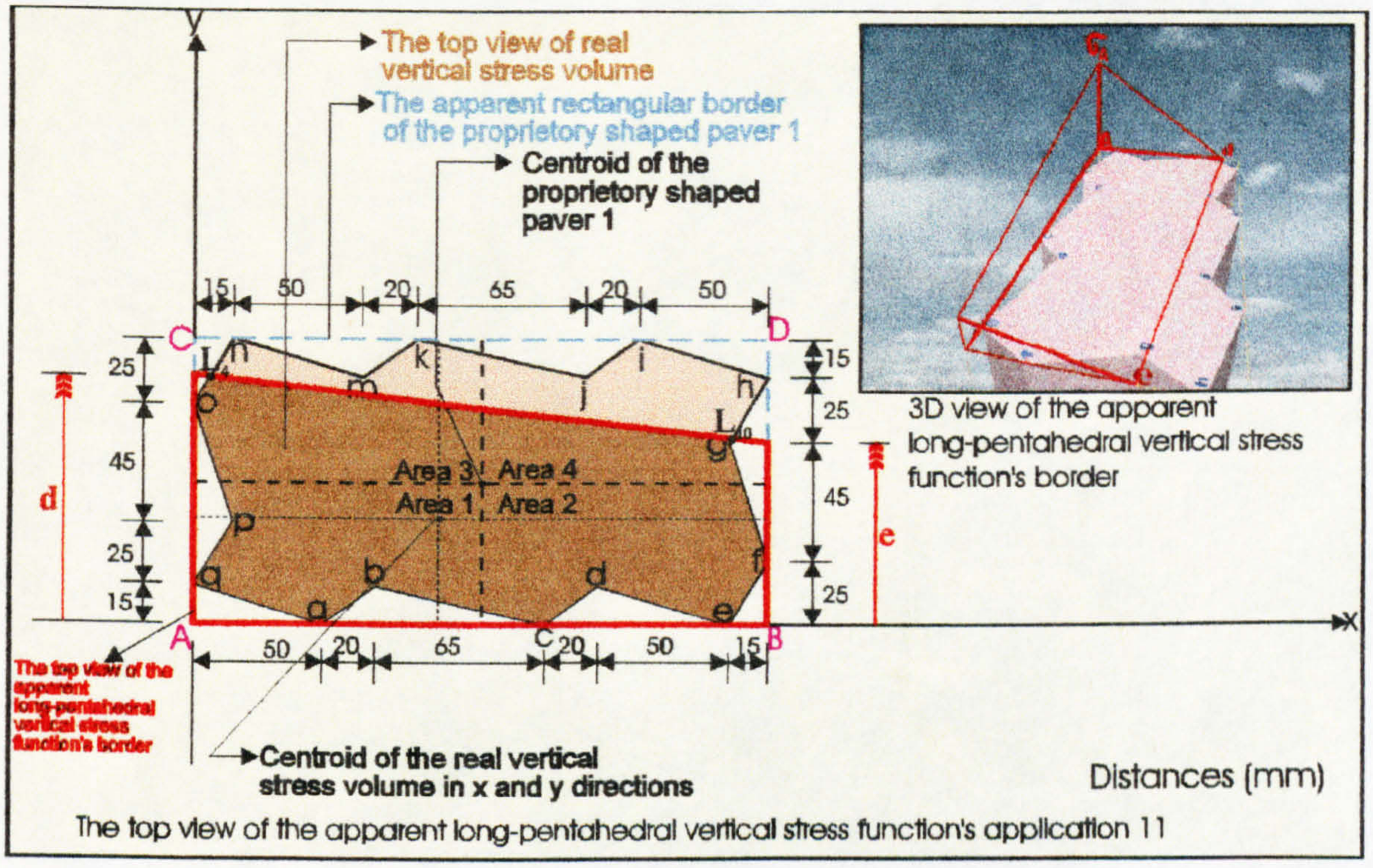

Figure 7.63: Application 11 of the long-pentahedral compressive stress distribution beneath the circumscribing rectangular border of proprietory shaped paver 1.

and the centroids of this volume in the xy-plane are at distances $\overline{X}$ and $\overline{Y}$ from the axes (see Figure 7.63) which are given by the following equations.

$$\overline{X} = \frac{1}{V}\left[\begin{array}{l}
\int_0^{220}\int_0^{e} x f(x,y)\,dy\,dx + \int_0^{220}\int_e^{fy} x f(x,y)\,dy\,dx - \int_{205}^{L_{10x}}\int_{70}^{ghy} x f(x,y)\,dy\,dx - \int_{L_{10x}}^{220}\int_{70}^{e} x f(x,y)\,dy\,dx \\
-\int_{L_{10x}}^{220}\int_{e}^{fy} x f(x,y)\,dy\,dx - \int_{205}^{220}\int_{25}^{fgy} x f(x,y)\,dy\,dx - \int_{205}^{220}\int_{0}^{efy} x f(x,y)\,dy\,dx - \int_{155}^{205}\int_{0}^{dey} x f(x,y)\,dy\,dx \\
-\int_{135}^{155}\int_{0}^{cdy} x f(x,y)\,dy\,dx - \int_{70}^{135}\int_{0}^{bcy} x f(x,y)\,dy\,dx - \int_{50}^{70}\int_{0}^{aby} x f(x,y)\,dy\,dx - \int_{0}^{50}\int_{0}^{qay} x f(x,y)\,dy\,dx \\
-\int_{0}^{15}\int_{15}^{qpy} x f(x,y)\,dy\,dx - \int_{0}^{15}\int_{40}^{poy} x f(x,y)\,dy\,dx - \int_{0}^{L_{4x}}\int_{85}^{ony} x f(x,y)\,dy\,dx - \int_{0}^{L_{4x}}\int_{L_{4y}}^{fy} x f(x,y)\,dy\,dx
\end{array}\right]$$

$$\overline{Y} = \frac{1}{V}\left[\int_0^{e}\int_0^{220} y f(x,y)\,dx\,dy + \int_e^{d}\int_0^{fx} y f(x,y)\,dx\,dy - \int_{70}^{L_{10y}}\int_{205}^{ghx} y f(x,y)\,dx\,dy - \int_{70}^{e}\int_{L_{10x}}^{220} y f(x,y)\,dx\,dy\right]$$

$$-\int_{e}^{L_{10y}}\int_{L_{10x}}^{fx} y f(x,y)\,dx\,dy - \int_{25}^{70}\int_{205}^{fgx} y f(x,y)\,dx\,dy - \int_{0}^{25}\int_{205}^{efx} y f(x,y)\,dx\,dy - \int_{0}^{15}\int_{155}^{dex} y f(x,y)\,dx\,dy$$

$$-\int_{0}^{15}\int_{135}^{cdx} y f(x,y)\,dx\,dy - \int_{0}^{15}\int_{70}^{bcx} y f(x,y)\,dx\,dy - \int_{0}^{15}\int_{50}^{abx} y f(x,y)\,dx\,dy - \int_{0}^{15}\int_{0}^{qax} y f(x,y)\,dx\,dy$$

$$\left.-\int_{15}^{40}\int_{0}^{qpx} y f(x,y)\,dx\,dy - \int_{40}^{85}\int_{0}^{pox} y f(x,y)\,dx\,dy - \int_{85}^{L_{4y}}\int_{0}^{onx} y f(x,y)\,dx\,dy - \int_{L_{4y}}^{d}\int_{0}^{fx} y f(x,y)\,dx\,dy\right]$$

Application 12 of the long-pentahedral compressive stress regime beneath the circumscribing rectangular border of proprietory shaped paver 1 shown in Figure 7.64 can be calculated by using Tables 5.1 and 7.3 and the surface function of the long-pentahedral compressive stress through the three points σ_A, **k** and **d**.

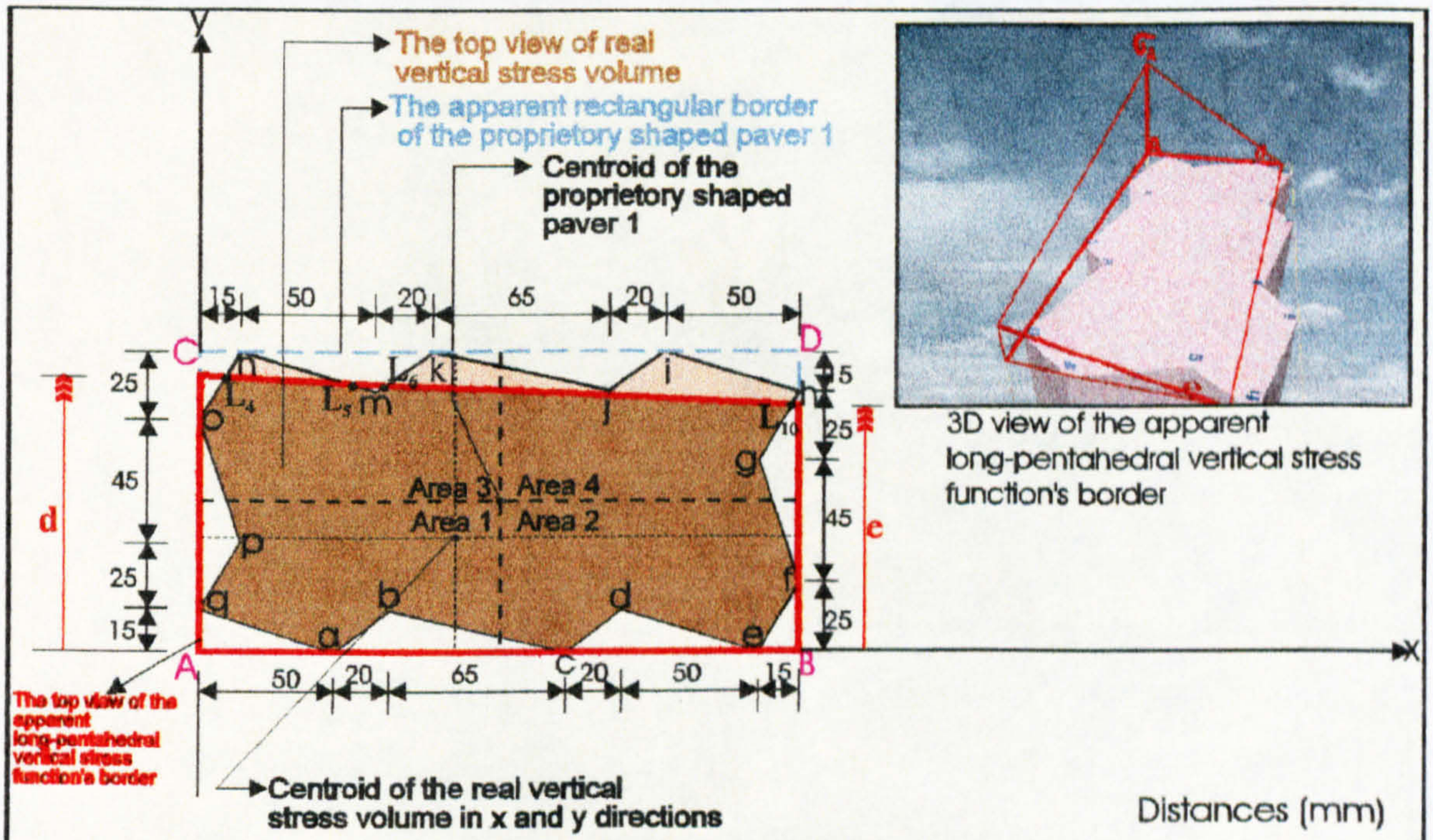

Figure 7.64: Application 12 of the long-pentahedral compressive stress distribution beneath the circumscribing rectangular border of proprietory shaped paver 1.

The total volume **V** beneath the surface $f(x,y) = z\ (> 0)$ and above the region in the xy-plane (see Figure 7.64) is:

$$V = \int_0^{220}\int_0^{e} f(x,y)\,dy\,dx + \int_0^{220}\int_e^{fy} f(x,y)\,dy\,dx - \int_{205}^{L_{10x}}\int_{70}^{ghy} f(x,y)\,dy\,dx - \int_{L_{10x}}^{220}\int_{70}^{e} f(x,y)\,dy\,dx - \int_{L_{10x}}^{220}\int_{e}^{fy} f(x,y)\,dy\,dx$$
$$- \int_{205}^{220}\int_{25}^{fgy} f(x,y)\,dy\,dx - \int_{205}^{220}\int_{0}^{efy} f(x,y)\,dy\,dx - \int_{155}^{205}\int_{0}^{dey} f(x,y)\,dy\,dx - \int_{135}^{155}\int_{0}^{cdy} f(x,y)\,dy\,dx - \int_{70}^{135}\int_{0}^{bcy} f(x,y)\,dy\,dx$$
$$- \int_{50}^{70}\int_{0}^{aby} f(x,y)\,dy\,dx - \int_{0}^{50}\int_{0}^{qay} f(x,y)\,dy\,dx - \int_{0}^{15}\int_{15}^{qpy} f(x,y)\,dy\,dx - \int_{0}^{15}\int_{40}^{poy} f(x,y)\,dy\,dx - \int_{0}^{L_{4x}}\int_{85}^{ony} f(x,y)\,dy\,dx$$
$$- \int_{0}^{L_{4x}}\int_{L_{4y}}^{fy} f(x,y)\,dy\,dx - \int_{15}^{65}\int_{95}^{nmy} f(x,y)\,dy\,dx - \int_{65}^{85}\int_{95}^{mky} f(x,y)\,dy\,dx + \int_{15}^{L_{5x}}\int_{L_{5y}}^{nmy} f(x,y)\,dy\,dx + \int_{L_{5x}}^{L_{6x}}\int_{L_{5y}}^{110} f(x,y)\,dy\,dx$$
$$+ \int_{L_{5x}}^{L_{6x}}\int_{L_{6y}}^{fy} f(x,y)\,dy\,dx + \int_{L_{6x}}^{85}\int_{L_{6y}}^{mky} f(x,y)\,dy\,dx$$

and the centroids of this volume in the xy-plane are at distances $\overline{X}$ and $\overline{Y}$ from the axes (see Figure 7.64) which are given by the following equations.

$$\overline{X} = \frac{1}{V}\left[\int_0^{220}\int_0^{e} x f(x,y)\,dy\,dx + \int_0^{220}\int_e^{fy} x f(x,y)\,dy\,dx - \int_{205}^{L_{10x}}\int_{70}^{ghy} x f(x,y)\,dy\,dx - \int_{L_{10x}}^{220}\int_{70}^{e} x f(x,y)\,dy\,dx - \int_{L_{10x}}^{220}\int_{e}^{fy} x f(x,y)\,dy\,dx\right.$$
$$- \int_{205}^{220}\int_{25}^{fgy} x f(x,y)\,dy\,dx - \int_{205}^{220}\int_{0}^{efy} x f(x,y)\,dy\,dx - \int_{155}^{205}\int_{0}^{dey} x f(x,y)\,dy\,dx - \int_{135}^{155}\int_{0}^{cdy} x f(x,y)\,dy\,dx - \int_{70}^{135}\int_{0}^{bcy} x f(x,y)\,dy\,dx$$
$$- \int_{50}^{70}\int_{0}^{aby} x f(x,y)\,dy\,dx - \int_{0}^{50}\int_{0}^{qay} x f(x,y)\,dy\,dx - \int_{0}^{15}\int_{15}^{qpy} x f(x,y)\,dy\,dx - \int_{0}^{15}\int_{40}^{poy} x f(x,y)\,dy\,dx - \int_{0}^{L_{4x}}\int_{85}^{ony} x f(x,y)\,dy\,dx$$
$$- \int_{0}^{L_{4x}}\int_{L_{4y}}^{fy} x f(x,y)\,dy\,dx - \int_{15}^{65}\int_{95}^{nmy} x f(x,y)\,dy\,dx - \int_{65}^{85}\int_{95}^{mky} x f(x,y)\,dy\,dx + \int_{15}^{L_{5x}}\int_{L_{5y}}^{nmy} x f(x,y)\,dy\,dx + \int_{L_{5x}}^{L_{6x}}\int_{L_{5y}}^{110} x f(x,y)\,dy\,dx$$
$$\left. + \int_{L_{5x}}^{L_{6x}}\int_{L_{6y}}^{fy} x f(x,y)\,dy\,dx + \int_{L_{6x}}^{85}\int_{L_{6y}}^{mky} x f(x,y)\,dy\,dx\right]$$

$$\overline{Y} = \frac{1}{V}\left[\int_0^{e}\int_0^{220} y f(x,y)\,dx\,dy + \int_e^{d}\int_0^{fx} y f(x,y)\,dx\,dy - \int_{70}^{L_{10y}}\int_{205}^{ghx} y f(x,y)\,dx\,dy - \int_{70}^{e}\int_{L_{10x}}^{220} y f(x,y)\,dx\,dy\right.$$
$$\left. - \int_{e}^{L_{10y}}\int_{L_{10x}}^{fx} y f(x,y)\,dx\,dy - \int_{25}^{205}\int_{205}^{70fgx} y f(x,y)\,dx\,dy - \int_{0}^{25}\int_{205}^{efx} y f(x,y)\,dx\,dy - \int_{0}^{15}\int_{155}^{dex} y f(x,y)\,dx\,dy\right]$$

$$-\int_{0}^{15}\int_{135}^{15c}\int^{dx} y f(x,y)\,dx\,dy-\int_{0}^{15}\int_{70}^{15b}\int^{cx} y f(x,y)\,dx\,dy-\int_{0}^{15}\int_{50}^{15a}\int^{bx} y f(x,y)\,dx\,dy-\int_{0}^{15}\int_{0}^{15q}\int^{ax} y f(x,y)\,dx\,dy$$

$$-\int_{15}^{40}\int_{0}^{40q}\int^{px} y f(x,y)\,dx\,dy-\int_{40}^{85}\int_{0}^{85p}\int^{ox} y f(x,y)\,dx\,dy-\int_{85}^{L_{4y}}\int_{0}^{L_{4y}o}\int^{nx} y f(x,y)\,dx\,dy-\int_{L_{4y}}^{d}\int_{0}^{f}\int^{x} y f(x,y)\,dx\,dy$$

$$-\int_{95}^{110}\int_{15}^{110n}\int^{mx} y f(x,y)\,dx\,dy-\int_{95}^{110}\int_{65}^{110m}\int^{kx} y f(x,y)\,dx\,dy+\int_{L_{5y}}^{110}\int_{15}^{110n}\int^{mx} y f(x,y)\,dx\,dy+\int_{L_{5y}}^{110}\int_{L_{5x}}^{110L_{6x}}\int^{x} y f(x,y)\,dx\,dy$$

$$+\left[\int_{L_{6y}}^{L_{5y}}\int_{L_{5x}}^{fx}\int^{x} y f(x,y)\,dx\,dy+\int_{L_{6y}}^{110}\int_{L_{6x}}^{110mk}\int^{x} y f(x,y)\,dx\,dy\right]$$

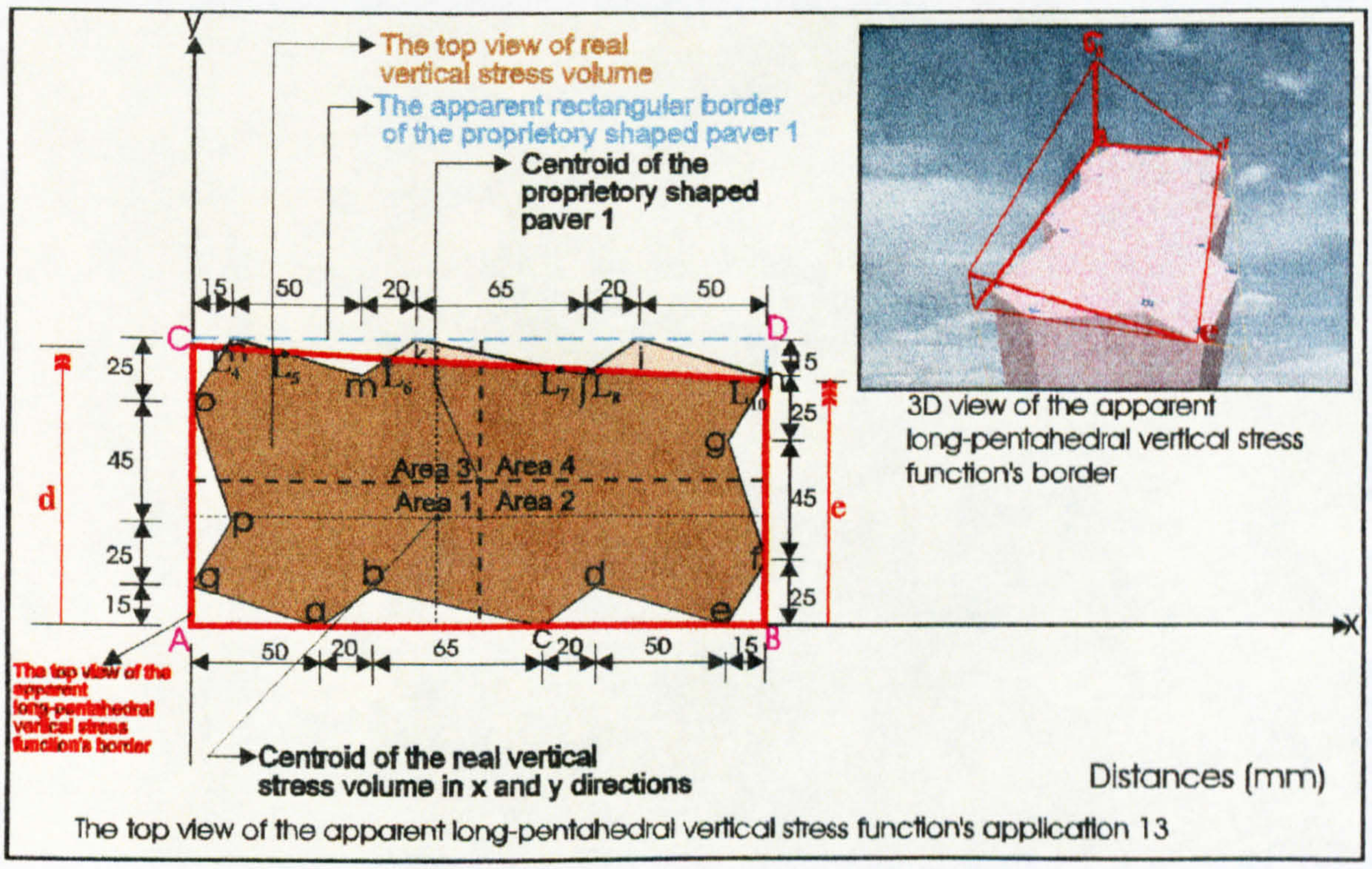

Figure 7.65: Application 13 of the long-pentahedral compressive stress distribution beneath the circumscribing rectangular border of proprietory shaped paver 1.

Application 13 of the long-pentahedral compressive stress regime beneath the circumscribing rectangular border of proprietory shaped paver 1 shown in Figure 7.65 can be calculated by using Tables 5.1 and 7.3 and the surface function of the long-pentahedral compressive stress through the three points σ_A, **k** and **d**.

The total volume **V** beneath the surface $f(x,y) = z\ (> 0)$ and above the region in the xy-plane (see Figure 7.65) is:

$$V = \int_{0}^{220}\int_{0}^{e} f(x,y)\,dy\,dx + \int_{0}^{220}\int_{e}^{fy} f(x,y)\,dy\,dx - \int_{205}^{L_{10x}}\int_{70}^{ghy} f(x,y)\,dy\,dx - \int_{L_{10x}}^{220}\int_{70}^{e} f(x,y)\,dy\,dx - \int_{L_{10x}}^{220}\int_{e}^{fy} f(x,y)\,dy\,dx$$
$$- \int_{205}^{220}\int_{25}^{fgy} f(x,y)\,dy\,dx - \int_{205}^{220}\int_{0}^{efy} f(x,y)\,dy\,dx - \int_{155}^{205}\int_{0}^{dey} f(x,y)\,dy\,dx - \int_{135}^{155}\int_{0}^{cdy} f(x,y)\,dy\,dx - \int_{70}^{135}\int_{0}^{bcy} f(x,y)\,dy\,dx$$
$$- \int_{50}^{70}\int_{0}^{aby} f(x,y)\,dy\,dx - \int_{0}^{50}\int_{0}^{qay} f(x,y)\,dy\,dx - \int_{0}^{15}\int_{15}^{qpy} f(x,y)\,dy\,dx - \int_{0}^{15}\int_{40}^{poy} f(x,y)\,dy\,dx - \int_{0}^{L_{4x}}\int_{85}^{ony} f(x,y)\,dy\,dx$$
$$- \int_{0}^{L_{4x}}\int_{L_{4y}}^{fy} f(x,y)\,dy\,dx - \int_{15}^{65}\int_{95}^{nmy} f(x,y)\,dy\,dx - \int_{65}^{85}\int_{95}^{mky} f(x,y)\,dy\,dx + \int_{15}^{L_{5x}}\int_{L_{5y}}^{nmy} f(x,y)\,dy\,dx + \int_{L_{5x}}^{L_{6x}}\int_{L_{5y}}^{110} f(x,y)\,dy\,dx$$
$$+ \int_{L_{5x}}^{L_{6x}}\int_{L_{6y}}^{fy} f(x,y)\,dy\,dx + \int_{L_{6x}}^{85}\int_{L_{6y}}^{mky} f(x,y)\,dy\,dx - \int_{85}^{150}\int_{95}^{kjy} f(x,y)\,dy\,dx - \int_{150}^{170}\int_{95}^{jiy} f(x,y)\,dy\,dx + \int_{85}^{L_{7x}}\int_{L_{7y}}^{kjy} f(x,y)\,dy\,dx$$
$$+ \int_{L_{7x}}^{L_{8x}}\int_{L_{7y}}^{110} f(x,y)\,dy\,dx + \int_{L_{7x}}^{L_{8x}}\int_{L_{8y}}^{fy} f(x,y)\,dy\,dx + \int_{L_{8x}}^{170}\int_{L_{8y}}^{jiy} f(x,y)\,dy\,dx$$

and the centroids of this volume in the xy-plane are at distances $\overline{X}$ and $\overline{Y}$ from the axes (see Figure 7.65) which are given by the following equations.

$$\overline{X} = \frac{1}{V}\left[\int_{0}^{220}\int_{0}^{e} x f(x,y)\,dy\,dx + \int_{0}^{220}\int_{e}^{fy} x f(x,y)\,dy\,dx - \int_{205}^{L_{10x}}\int_{70}^{ghy} x f(x,y)\,dy\,dx - \int_{L_{10x}}^{220}\int_{70}^{e} x f(x,y)\,dy\,dx\right.$$
$$- \int_{L_{10x}}^{220}\int_{e}^{fy} x f(x,y)\,dy\,dx - \int_{205}^{220}\int_{25}^{fgy} x f(x,y)\,dy\,dx - \int_{205}^{220}\int_{0}^{efy} x f(x,y)\,dy\,dx - \int_{155}^{205}\int_{0}^{dey} x f(x,y)\,dy\,dx$$
$$- \int_{135}^{155}\int_{0}^{cdy} x f(x,y)\,dy\,dx - \int_{70}^{135}\int_{0}^{bcy} x f(x,y)\,dy\,dx - \int_{50}^{70}\int_{0}^{aby} x f(x,y)\,dy\,dx - \int_{0}^{50}\int_{0}^{qay} x f(x,y)\,dy\,dx$$
$$- \int_{0}^{15}\int_{15}^{qpy} x f(x,y)\,dy\,dx - \int_{0}^{15}\int_{40}^{poy} x f(x,y)\,dy\,dx - \int_{0}^{L_{4x}}\int_{85}^{ony} x f(x,y)\,dy\,dx - \int_{0}^{L_{4x}}\int_{L_{4y}}^{fy} x f(x,y)\,dy\,dx$$
$$- \int_{0}^{65}\int_{95}^{nmy} x f(x,y)\,dy\,dx - \int_{65}^{85}\int_{95}^{mky} x f(x,y)\,dy\,dx + \int_{15}^{L_{5x}}\int_{L_{5y}}^{nmy} x f(x,y)\,dy\,dx + \int_{L_{5x}}^{L_{6x}}\int_{L_{5y}}^{110} x f(x,y)\,dy\,dx$$
$$\left. + \int_{L_{5x}}^{L_{6x}}\int_{L_{6y}}^{fy} x f(x,y)\,dy\,dx + \int_{L_{6x}}^{85}\int_{L_{6y}}^{mky} x f(x,y)\,dy\,dx - \int_{85}^{150}\int_{95}^{kjy} x f(x,y)\,dy\,dx - \int_{150}^{170}\int_{95}^{jiy} x f(x,y)\,dy\,dx\right]$$

$$+\int_{85}^{L_{7x}}\int_{L_{7y}}^{kjy} x f(x,y)\,dy\,dx+\int_{L_{7x}}^{L_{8x}}\int_{L_{7y}}^{110} x f(x,y)\,dy\,dx+\int_{L_{7x}}^{L_{8x}}\int_{L_{8y}}^{fy} x f(x,y)\,dy\,dx+\int_{l_{8x}}^{170}\int_{l_{8y}}^{jly} x f(x,y)\,dy\,dx\Bigg]$$

$$\overline{Y}=\frac{1}{V}\Bigg[\int_{0}^{e}\int_{0}^{220} y f(x,y)\,dx\,dy+\int_{e}^{d}\int_{0}^{fx} y f(x,y)\,dx\,dy-\int_{70}^{L_{10y}}\int_{205}^{ghx} y f(x,y)\,dx\,dy-\int_{70}^{e}\int_{L_{10x}}^{220} y f(x,y)\,dx\,dy$$

$$-\int_{e}^{L_{10y}}\int_{L_{10x}}^{fx} y f(x,y)\,dx\,dy-\int_{25}^{70}\int_{205}^{fgx} y f(x,y)\,dx\,dy-\int_{0}^{25}\int_{205}^{efx} y f(x,y)\,dx\,dy-\int_{0}^{15}\int_{155}^{dex} y f(x,y)\,dx\,dy$$

$$-\int_{0}^{15}\int_{135}^{cdx} y f(x,y)\,dx\,dy-\int_{0}^{15}\int_{70}^{bcx} y f(x,y)\,dx\,dy-\int_{0}^{15}\int_{50}^{abx} y f(x,y)\,dx\,dy-\int_{0}^{15}\int_{0}^{qax} y f(x,y)\,dx\,dy$$

$$-\int_{15}^{40}\int_{0}^{qpx} y f(x,y)\,dx\,dy-\int_{40}^{85}\int_{0}^{pox} y f(x,y)\,dx\,dy-\int_{85}^{L_{4y}}\int_{0}^{onx} y f(x,y)\,dx\,dy-\int_{L_{4y}}^{d}\int_{0}^{fx} y f(x,y)\,dx\,dy$$

$$-\int_{95}^{110}\int_{15}^{nmx} y f(x,y)\,dx\,dy-\int_{95}^{110}\int_{65}^{mkx} y f(x,y)\,dx\,dy+\int_{L_{5y}}^{110}\int_{15}^{nmx} y f(x,y)\,dx\,dy+\int_{L_{5y}}^{110}\int_{L_{5x}}^{L_{6x}} y f(x,y)\,dx\,dy$$

$$+\int_{L_{6y}}^{L_{5y}}\int_{L_{5x}}^{fx} y f(x,y)\,dx\,dy+\int_{L_{6y}}^{110}\int_{L_{6x}}^{mkx} y f(x,y)\,dx\,dy-\int_{95}^{110}\int_{85}^{kjx} y f(x,y)\,dx\,dy-\int_{95}^{110}\int_{150}^{jix} y f(x,y)\,dx\,dy$$

$$+\int_{L_{7y}}^{110}\int_{85}^{kjx} y f(x,y)\,dx\,dy+\int_{L_{7y}}^{110}\int_{L_{7x}}^{L_{8x}} y f(x,y)\,dx\,dy+\int_{L_{8y}}^{L_{7y}}\int_{L_{7x}}^{fx} y f(x,y)\,dx\,dy+\int_{l_{8y}}^{110}\int_{l_{8x}}^{jix} y f(x,y)\,dx\,dy\Bigg]$$

Application 14 of the long-pentahedral compressive stress regime beneath the circumscribing rectangular border of proprietory shaped paver 1 shown in Figure 7.66 can be calculated by using Tables 5.1 and 7.3 and the surface function of the long-pentahedral compressive stress through the three points σ_A, **k** and **d**.

The total volume **V** beneath the surface $f(x,y)=z\ (>0)$ and above the region in the xy-plane (see Figure 7.66) is:

$$V=\int_{0}^{220}\int_{0}^{e} f(x,y)\,dy\,dx+\int_{0}^{220}\int_{e}^{fy} f(x,y)\,dy\,dx-\int_{170}^{L_{9x}}\int_{l_{9y}}^{hly} f(x,y)\,dy\,dx-\int_{L_{9x}}^{220}\int_{L_{9y}}^{110} f(x,y)\,dy\,dx-\int_{L_{9x}}^{220}\int_{e}^{fy} f(x,y)\,dy\,dx$$

$$-\int_{205}^{220}\int_{25}^{fgy} f(x,y)\,dy\,dx-\int_{205}^{220}\int_{0}^{efy} f(x,y)\,dy\,dx-\int_{155}^{205}\int_{0}^{dey} f(x,y)\,dy\,dx-\int_{135}^{155}\int_{0}^{cdy} f(x,y)\,dy\,dx-\int_{70}^{135}\int_{0}^{bcy} f(x,y)\,dy\,dx$$

$$-\int_{50}^{70}\int_{0}^{aby} f(x,y)\,dy\,dx - \int_{0}^{50}\int_{0}^{qay} f(x,y)\,dy\,dx - \int_{0}^{15}\int_{15}^{qpy} f(x,y)\,dy\,dx - \int_{0}^{40}\int_{15}^{poy} f(x,y)\,dy\,dx - \int_{0}^{85}\int_{40}^{L_{4x}\,ony} f(x,y)\,dy\,dx$$

$$-\int_{0}^{L_{4x}}\int_{L_{4y}}^{fy} f(x,y)\,dy\,dx - \int_{15}^{65}\int_{95}^{nmy} f(x,y)\,dy\,dx - \int_{65}^{85}\int_{95}^{mky} f(x,y)\,dy\,dx + \int_{15}^{L_{5x}}\int_{L_{5y}}^{nmy} f(x,y)\,dy\,dx + \int_{L_{5x}}^{L_{6x}}\int_{L_{5y}}^{110} f(x,y)\,dy\,dx$$

$$+\int_{L_{5x}}^{L_{6x}}\int_{L_{6y}}^{fy} f(x,y)\,dy\,dx + \int_{L_{6x}}^{85}\int_{L_{6y}}^{mky} f(x,y)\,dy\,dx - \int_{85}^{150}\int_{95}^{kjy} f(x,y)\,dy\,dx - \int_{150}^{170}\int_{95}^{jiy} f(x,y)\,dy\,dx + \int_{85}^{L_{7x}}\int_{L_{7y}}^{kjy} f(x,y)\,dy\,dx$$

$$+\int_{L_{7x}}^{L_{8x}}\int_{L_{7y}}^{110} f(x,y)\,dy\,dx + \int_{L_{7x}}^{L_{8x}}\int_{L_{8y}}^{fy} f(x,y)\,dy\,dx + \int_{L_{8x}}^{170}\int_{L_{8y}}^{jiy} f(x,y)\,dy\,dx - \int_{205}^{220}\int_{70}^{ghy} f(x,y)\,dy\,dx$$

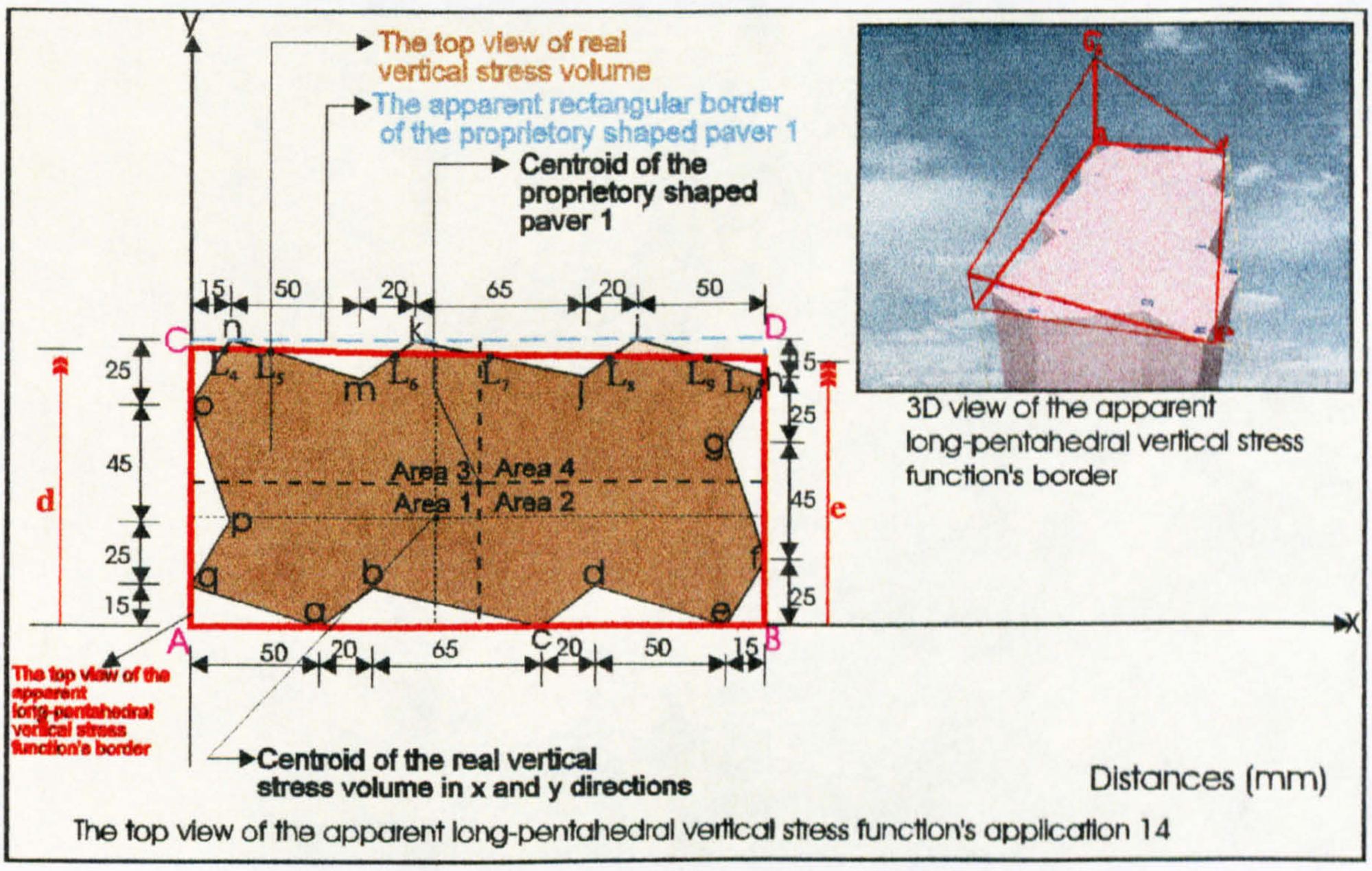

Figure 7.66: Application 14 of the long-pentahedral compressive stress distribution beneath the circumscribing rectangular border of proprietory shaped paver 1.

and the centroids of this volume in the xy-plane are at distances $\overline{X}$ and $\overline{Y}$ from the axes (see Figure 7.66) which are given by the following equations.

$$\overline{X} = \frac{1}{V}\left[\int_{0}^{220}\int_{0}^{e} x\,f(x,y)\,dy\,dx + \int_{0}^{220}\int_{e}^{fy} x\,f(x,y)\,dy\,dx - \int_{170}^{L_{9x}}\int_{L_{9y}}^{hiy} x\,f(x,y)\,dy\,dx - \int_{L_{9x}}^{220}\int_{L_{9y}}^{110} x\,f(x,y)\,dy\,dx\right.$$

$$-\int_{L_{9x}}^{220}\int_{e}^{fy} xf(x,y)\,dy\,dx-\int_{205}^{220}\int_{25}^{fgy} xf(x,y)\,dy\,dx-\int_{205}^{220}\int_{0}^{efy} xf(x,y)\,dy\,dx-\int_{155}^{205}\int_{0}^{dcy} xf(x,y)\,dy\,dx$$

$$-\int_{135}^{155}\int_{0}^{cdy} xf(x,y)\,dy\,dx-\int_{70}^{135}\int_{0}^{bcy} xf(x,y)\,dy\,dx-\int_{50}^{70}\int_{0}^{xaby} xf(x,y)\,dy\,dx-\int_{0}^{50}\int_{0}^{qay} xf(x,y)\,dy\,dx$$

$$-\int_{0}^{15}\int_{15}^{qpy} xf(x,y)\,dy\,dx-\int_{0}^{40}\int_{15}^{poy} xf(x,y)\,dy\,dx-\int_{0}^{85}\int_{L_{4x}}^{ony} xf(x,y)\,dy\,dx-\int_{0}^{L_{4y}}\int_{L_{4x}}^{fy} xf(x,y)\,dy\,dx$$

$$-\int_{15}^{95}\int_{65}^{nmy} xf(x,y)\,dy\,dx-\int_{65}^{95}\int_{85}^{mky} xf(x,y)\,dy\,dx+\int_{15}^{L_{5y}}\int_{L_{5x}}^{nmy} xf(x,y)\,dy\,dx+\int_{L_{5x}}^{L_{5y}}\int_{L_{6x}}^{110} xf(x,y)\,dy\,dx$$

$$+\int_{L_{5x}}^{L_{6y}}\int_{L_{6x}}^{fy} xf(x,y)\,dy\,dx+\int_{L_{6x}}^{L_{6y}}\int_{85}^{mky} xf(x,y)\,dy\,dx-\int_{85}^{95}\int_{150}^{kjy} xf(x,y)\,dy\,dx-\int_{150}^{95}\int_{170}^{jly} xf(x,y)\,dy\,dx$$

$$+\int_{85}^{L_{7y}}\int_{L_{7x}}^{kjy} xf(x,y)\,dy\,dx+\int_{L_{7x}}^{L_{7y}}\int_{L_{8x}}^{110} xf(x,y)\,dy\,dx+\int_{L_{7x}}^{L_{8y}}\int_{L_{8x}}^{fy} xf(x,y)\,dy\,dx+\int_{I_{8x}}^{I_{8y}}\int_{170}^{jly} xf(x,y)\,dy\,dx$$

$$-\int_{205}^{220}\int_{70}^{ghy} xf(x,y)\,dy\,dx\Bigg]$$

$$\bar{Y}=\frac{1}{V}\Bigg[\int_{0}^{e}\int_{0}^{220} yf(x,y)\,dx\,dy+\int_{e}^{d}\int_{0}^{fx} yf(x,y)\,dx\,dy-\int_{L_{9y}}^{110}\int_{170}^{hlx} yf(x,y)\,dx\,dy-\int_{L_{9y}}^{110}\int_{L_{9x}}^{220} yf(x,y)\,dx\,dy$$

$$-\int_{e}^{L_{9y}}\int_{L_{9x}}^{fx} yf(x,y)\,dx\,dy-\int_{25}^{70}\int_{205}^{fgx} yf(x,y)\,dx\,dy-\int_{0}^{25}\int_{205}^{efx} yf(x,y)\,dx\,dy-\int_{0}^{15}\int_{155}^{dcx} yf(x,y)\,dx\,dy$$

$$-\int_{0}^{15}\int_{135}^{cdx} yf(x,y)\,dx\,dy-\int_{0}^{15}\int_{70}^{bcx} yf(x,y)\,dx\,dy-\int_{0}^{15}\int_{50}^{abx} yf(x,y)\,dx\,dy-\int_{0}^{15}\int_{0}^{qax} yf(x,y)\,dx\,dy$$

$$-\int_{15}^{40}\int_{0}^{qpx} yf(x,y)\,dx\,dy-\int_{40}^{85}\int_{0}^{pox} yf(x,y)\,dx\,dy-\int_{85}^{L_{4y}}\int_{0}^{onx} yf(x,y)\,dx\,dy-\int_{L_{4y}}^{d}\int_{0}^{fx} yf(x,y)\,dx\,dy$$

$$-\int_{95}^{110}\int_{15}^{nmx} yf(x,y)\,dx\,dy-\int_{95}^{110}\int_{65}^{mkx} yf(x,y)\,dx\,dy+\int_{L_{5y}}^{110}\int_{15}^{nmx} yf(x,y)\,dx\,dy+\int_{L_{5y}}^{110}\int_{L_{5x}}^{L_{6y}} yf(x,y)\,dx\,dy$$

$$+\int_{L_{6y}}^{L_{5y}}\int_{L_{5x}}^{fx} yf(x,y)\,dx\,dy+\int_{L_{6y}}^{110}\int_{L_{6x}}^{mkx} yf(x,y)\,dx\,dy-\int_{95}^{110}\int_{85}^{kjx} yf(x,y)\,dx\,dy-\int_{95}^{110}\int_{150}^{jlx} yf(x,y)\,dx\,dy$$

$$+\int_{L_{7y}}^{110}\int_{85}^{kjx} y f(x,y)\,dx\,dy+\int_{L_{7y}}^{110}\int_{L_{7x}}^{L_{8x}} y f(x,y)\,dx\,dy+\int_{L_{8y}}^{L_{7y}}\int_{L_{7x}}^{fx} y f(x,y)\,dx\,dy+\int_{L_{8y}}^{110}\int_{L_{8x}}^{jlx} y f(x,y)\,dx\,dy$$

$$-\int_{70205}^{95ghx} y f(x,y)\,dx\,dy\Bigg]$$

7.2.4 Partial-hexahedral compressive stress regimes beneath the circumscribing rectangular border for proprietory shaped paver 1

The intersection points which are between the line functions bounding shaped paver 1 shown in Table 5.1 and the lines (which bound the bottom surface of the partial-hexahedral stress in the xy-plane) have the functions $fy = l\left(1-\frac{x}{l}\right)$, $fx = l\left(1-\frac{y}{l}\right)$ in the x and y axes can be calculated mathematically. Table 7.4 shows the intersection points' formulae and the points are illustrated in Figures 7.67 to 7.92.

The surface function of the partial-pentahedral compressive stress block beneath the circumscribing rectangular border shown in Figure 7.67 through the three points σ_A, l and t is given by:

$$\begin{vmatrix} x & y & z & 1 \\ l & 0 & 0 & 1 \\ 0 & t & 0 & 1 \\ 0 & 0 & \sigma_A & 1 \end{vmatrix} = 0 \Rightarrow f(x,y) = z = \sigma_A\left(1-\frac{y}{t}-\frac{x}{l}\right)$$

The following equalities can be obtained from the geometry of the partial-hexahedral compressive stress block (see Figure 7.67).

$$a = \frac{110\sigma_B}{\sigma_A-\sigma_C} \quad and \quad b = \frac{220\sigma_C}{\sigma_{A-}\sigma_B} \quad \text{and} \quad t = \frac{110\sigma_A}{\sigma_A-\sigma_C} \Rightarrow \sigma_C = \frac{\sigma_A(t-110)}{t}$$

$$\text{and} \quad l = \frac{220\sigma_A}{\sigma_A-\sigma_B} \Rightarrow \sigma_B = \frac{\sigma_A(l-220)}{l}$$

therefore, $a = \frac{t(l-220)}{l}$ and $b = \frac{l(t-110)}{t}$

$M_{1x} = \frac{l(t-15)}{t-0.3l}$ and $M_{1y} = \frac{t(l-50)}{l-3.\bar{3}t}$	$M_{2x} = \frac{0.6l(t-15)}{l+0.6t}$ and $M_{2y} = \frac{t(l+9)}{l+0.6t}$
$M_{3x} = \frac{l(t-85)}{t-3l}$ and $M_{3y} = \frac{t(l-28.\bar{3})}{l-0.\bar{3}t}$	$M_{4x} = \frac{l(t-85)}{t+1.6l}$ and $M_{4y} = \frac{t(l+51)}{l+0.6t}$
$M_{5x} = \frac{l(t-114.5)}{t-0.3l}$ and $M_{5y} = \frac{t(l-381.\bar{6})}{l-3.\bar{3}t}$	$M_{6x} = \frac{l(t-46.25)}{t+0.75l}$ and $M_{6y} = \frac{t(l+61.\bar{6})}{l+1.\bar{3}t}$
$M_{7x} = \frac{l(t-129.615)}{t-0.2301l}$ and $M_{7y} = \frac{t(l-561.\bar{6})}{l-4.\bar{3}t}$	$M_{8x} = \frac{l(t+17.5)}{t+0.75l}$ and $M_{8y} = \frac{t(l-23.\bar{3})}{l+1.\bar{3}t}$
$M_{9x} = \frac{l(t-161)}{t-0.3l}$ and $M_{9y} = \frac{t(l-536.\bar{6})}{l-3.\bar{3}t}$	$M_{10x} = \frac{l(t+271.\bar{6})}{t+1.6l}$ and $M_{10y} = \frac{t(l-163)}{l+0.6t}$
$M_{11x} = \frac{l(t-685)}{t-3l}$ and $M_{11y} = \frac{t(l-228.\bar{3})}{l-0.\bar{3}t}$	$M_{12x} = \frac{l(t+341.\bar{6})}{t+1.6l}$ and $M_{12y} = \frac{t(l-205)}{l+0.6t}$
$M_{13x} = \frac{l(t-61.5)}{t-0.3l}$ and $M_{13y} = \frac{t(l-205)}{l-3.\bar{3}t}$	$M_{14x} = \frac{l(t+101.25)}{t+0.75l}$ and $M_{14y} = \frac{t(l-135)}{l+1.\bar{3}t}$
$M_{15x} = \frac{l(t-31.154)}{t-0.23l}$ and $M_{15y} = \frac{t(l-135)}{l-4.\bar{3}t}$	$M_{16x} = \frac{l(t+37.5)}{t+0.75l}$ and $M_{16y} = \frac{t(l-50)}{l+1.\bar{3}t}$

Table 7.4: The intersection points between the line which forms the partial-hexahedral stress block in the xy-plane and the line boundary functions of proprietory shaped paver 1 (l and t are the lengths of the stress block along the x and y axes respectively as illustrated in Figure 7.67).

The first application of the partial-hexahedral compressive stress regime beneath the circumscribing rectangular border of proprietory shaped paver 1 shown in Figure 7.67 can be calculated by using the data in Tables 5.1 and 7.4. The first two letters of each boundary line function in Table 5.1 for proprietory shaped paver 1 charecterise the corner names can be seen in Figure 7.67 (example: **qay** symbolises the boundary line function of proprietory shaped paver 1 in the y axis between corner **q** and **a**). The line functions which define the boundary of the partial-hexahedral stress block in the xy-plane (see Figure 7.67) are of the form $fy = l\left(1-\frac{x}{l}\right)$, $fx = l\left(1-\frac{y}{l}\right)$.

The following actual total volume **V** beneath the surface $f(x,y) = z$ (> 0) and above the region in the xy-plane (see Figure 7.67) is calculated by subtracting the negative

volume generated by the dentations of the shaped paver from the partial-hexahedral volume beneath circumscribing rectangular boundary of the paver.

$$V = \int_0^b \int_0^{110} f(x,y)\,dy\,dx + \int_b^{220} \int_0^a f(x,y)\,dy\,dx + \int_b^{220} \int_a^{fy} f(x,y)\,dy\,dx - \int_0^{M_{4x}} \int_{85}^{ony} f(x,y)\,dy\,dx - \int_0^b \int_{M_{4y}}^{110} f(x,y)\,dy\,dx$$
$$- \int_b^{M_{4x}} \int_{M_{4y}}^{fy} f(x,y)\,dy\,dx - \int_0^{15poy} \int_{40}^{poy} f(x,y)\,dy\,dx - \int_0^{15qpy} \int_{15}^{qpy} f(x,y)\,dy\,dx - \int_0^{50qay} \int_0^{qay} f(x,y)\,dy\,dx - \int_{50}^{70aby} \int_0^{aby} f(x,y)\,dy\,dx$$
$$- \int_{70}^{135bcy} \int_0^{bcy} f(x,y)\,dy\,dx - \int_{135}^{155cdy} \int_0^{cdy} f(x,y)\,dy\,dx - \int_{155}^{205dey} \int_0^{dey} f(x,y)\,dy\,dx - \int_{205}^{M_{12x}} \int_0^{efy} f(x,y)\,dy\,dx - \int_{M_{12x}}^{220} \int_a^{fy} f(x,y)\,dy\,dx$$
$$- \int_{M_{12x}}^{220} \int_0^a f(x,y)\,dy\,dx$$

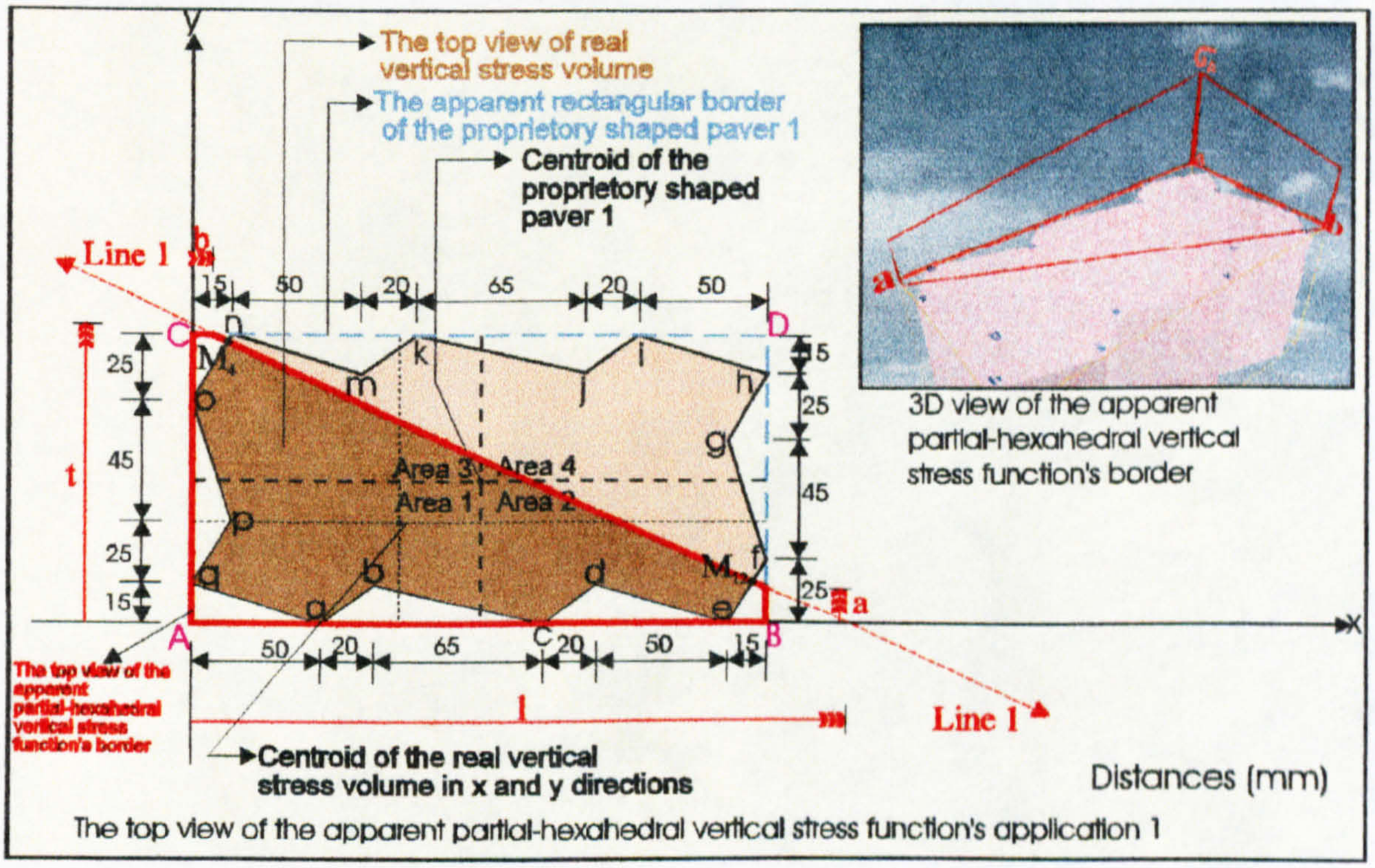

Figure 7.67: Application 1 of the partial-hexahedral compressive stress distribution beneath the circumscribing rectangular border of proprietory shaped paver 1.

and the centroids of this volume in the xy-plane are at distances $\overline{X}$ and $\overline{Y}$ from the axes (see Figure 7.67) which are given by the following equations.

$$\overline{X} = \frac{1}{V}\left[\begin{array}{l}
\int_{0}^{b}\int_{0}^{110} x f(x,y)\,dy\,dx + \int_{b}^{220}\int_{0}^{a} x f(x,y)\,dy\,dx + \int_{b}^{220}\int_{a}^{fy} x f(x,y)\,dy\,dx - \int_{0}^{M_{4x}}\int_{85}^{ony} x f(x,y)\,dy\,dx \\
-\int_{0}^{b}\int_{M_{4y}}^{110} x f(x,y)\,dy\,dx - \int_{b}^{M_{4x}}\int_{M_{4y}}^{fy} x f(x,y)\,dy\,dx - \int_{0}^{15poy}\int_{40}^{} x f(x,y)\,dy\,dx - \int_{0}^{15qpy}\int_{15}^{} x f(x,y)\,dy\,dx \\
-\int_{0}^{50qay}\int_{0}^{} x f(x,y)\,dy\,dx - \int_{50}^{70xby}\int_{0}^{} x f(x,y)\,dy\,dx - \int_{70}^{135bcy}\int_{0}^{} x f(x,y)\,dy\,dx - \int_{135}^{155cdy}\int_{0}^{} x f(x,y)\,dy\,dx \\
-\int_{155}^{205dey}\int_{0}^{} x f(x,y)\,dy\,dx - \int_{205}^{M_{12x}}\int_{0}^{efy} x f(x,y)\,dy\,dx - \int_{M_{12x}}^{220}\int_{a}^{fy} x f(x,y)\,dy\,dx - \int_{M_{12x}}^{220}\int_{0}^{a} x f(x,y)\,dy\,dx
\end{array}\right]$$

$$\overline{Y} = \frac{1}{V}\left[\begin{array}{l}
\int_{0}^{110}\int_{0}^{b} y f(x,y)\,dx\,dy + \int_{0}^{a}\int_{b}^{220} y f(x,y)\,dx\,dy + \int_{a}^{110}\int_{b}^{fx} y f(x,y)\,dx\,dy - \int_{85}^{M_{4y}}\int_{0}^{onx} y f(x,y)\,dx\,dy \\
-\int_{M_{4y}}^{110}\int_{0}^{b} y f(x,y)\,dx\,dy - \int_{M_{4y}}^{110}\int_{b}^{fx} y f(x,y)\,dx\,dy - \int_{40}^{85pox}\int_{0}^{} y f(x,y)\,dx\,dy - \int_{15}^{40qpx}\int_{0}^{} y f(x,y)\,dx\,dy \\
-\int_{0}^{15qax}\int_{0}^{} y f(x,y)\,dx\,dy - \int_{0}^{15abx}\int_{50}^{} y f(x,y)\,dx\,dy - \int_{0}^{15bcx}\int_{70}^{} y f(x,y)\,dx\,dy - \int_{0}^{15cdx}\int_{135}^{} y f(x,y)\,dx\,dy \\
-\int_{0}^{15dex}\int_{155}^{} y f(x,y)\,dx\,dy - \int_{0}^{M_{12y}}\int_{205}^{efx} y f(x,y)\,dx\,dy - \int_{a}^{M_{12y}}\int_{M_{12x}}^{fx} y f(x,y)\,dx\,dy - \int_{0}^{a}\int_{M_{12x}}^{220} y f(x,y)\,dx\,dy
\end{array}\right]$$

Application 2 of the partial-hexahedral compressive stress regime beneath the circumscribing rectangular border of proprietory shaped paver 1 shown in Figure 7.68 can be calculated by using Tables 5.1 and 7.4 and the surface function of the partial-hexahedral compressive stress through the three points σ_A, **l** and **t**.

The total volume **V** beneath the surface $f(x,y) = z\ (> 0)$ and above the region in the xy-plane (see Figure 7.68) is:

$$V = \int_{0}^{b}\int_{0}^{110} f(x,y)\,dy\,dx + \int_{b}^{220}\int_{0}^{a} f(x,y)\,dy\,dx + \int_{b}^{220}\int_{a}^{fy} f(x,y)\,dy\,dx - \int_{15}^{M_{5x}}\int_{M_{5y}}^{nmy} f(x,y)\,dy\,dx + \int_{b}^{M_{5x}}\int_{M_{5y}}^{fy} f(x,y)\,dy\,dx$$
$$-\int_{0}^{15omy}\int_{85}^{} f(x,y)\,dy\,dx - \int_{0}^{15poy}\int_{40}^{} f(x,y)\,dy\,dx - \int_{0}^{15qry}\int_{15}^{} f(x,y)\,dy\,dx - \int_{0}^{50qcy}\int_{0}^{} f(x,y)\,dy\,dx - \int_{50}^{70aby}\int_{0}^{} f(x,y)\,dy\,dx$$

$$-\int_{70}^{135}\int_{0}^{bcy} f(x,y)\,dy\,dx-\int_{135}^{155}\int_{0}^{cdy} f(x,y)\,dy\,dx-\int_{155}^{205}\int_{0}^{dey} f(x,y)\,dy\,dx-\int_{205}^{M_{12x}}\int_{0}^{efy} f(x,y)\,dy\,dx-\int_{M_{12x}}^{220}\int_{a}^{fy} f(x,y)\,dy\,dx$$
$$-\int_{M_{12x}}^{220}\int_{0}^{a} f(x,y)\,dy\,dx$$

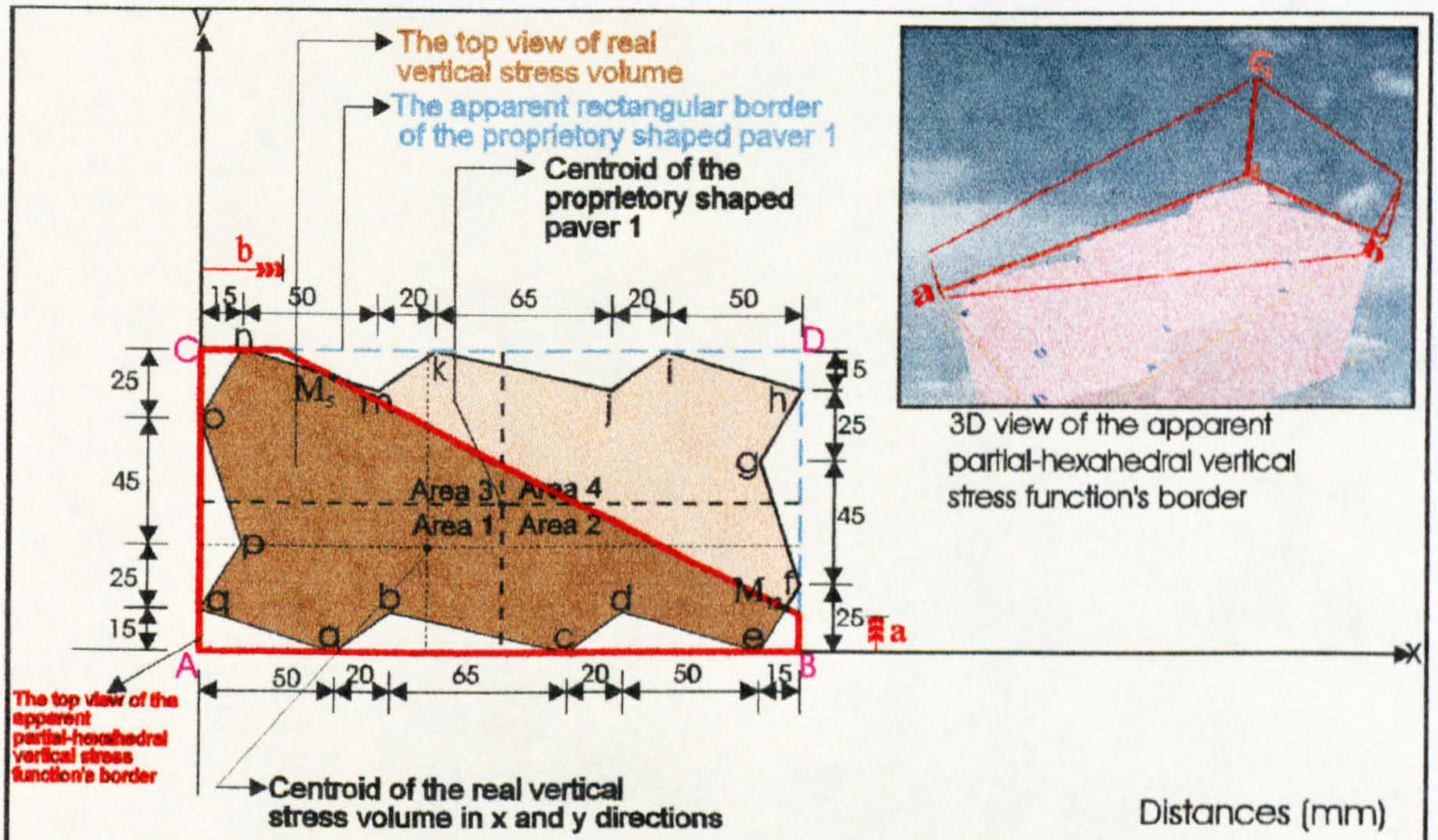

The top view of the apparent partial-hexahedral vertical stress function's application 2

Figure 7.68: Application 2 of the partial-hexahedral compressive stress distribution beneath the circumscribing rectangular border of proprietory shaped paver 1.

and the centroids of this volume in the xy-plane are at distances $\overline{X}$ and $\overline{Y}$ from the axes (see Figure 7.68) which are given by the following equations.

$$\overline{X}=\frac{1}{V}\left[\int_{0}^{b}\int_{0}^{110} x f(x,y)\,dy\,dx+\int_{b}^{220}\int_{0}^{a} x f(x,y)\,dy\,dx+\int_{b}^{220}\int_{a}^{fy} x f(x,y)\,dy\,dx-\int_{15}^{M_{5x}}\int_{M_{5y}}^{nmy} x f(x,y)\,dy\,dx\right.$$
$$+\int_{b}^{M_{5x}}\int_{M_{5y}}^{fy} x f(x,y)\,dy\,dx-\int_{0}^{15}\int_{85}^{ony} x f(x,y)\,dy\,dx-\int_{0}^{15}\int_{40}^{poy} x f(x,y)\,dy\,dx-\int_{0}^{15}\int_{15}^{qpy} x f(x,y)\,dy\,dx$$
$$\left.-\int_{0}^{50}\int_{0}^{qay} x f(x,y)\,dy\,dx-\int_{50}^{70}\int_{0}^{aby} x f(x,y)\,dy\,dx-\int_{70}^{135}\int_{0}^{bcy} x f(x,y)\,dy\,dx-\int_{135}^{155}\int_{0}^{cdy} x f(x,y)\,dy\,dx\right]$$

$$-\int_{155}^{205}\int_{0}^{dey} x f(x,y)\,dy\,dx - \int_{205}^{M_{12x}}\int_{0}^{efy} x f(x,y)\,dy\,dx - \int_{M_{12x}}^{220}\int_{a}^{fy} x f(x,y)\,dy\,dx - \int_{M_{12x}}^{220}\int_{0}^{a} x f(x,y)\,dy\,dx\Bigg]$$

$$\bar{Y} = \frac{1}{V}\Bigg[\int_{0}^{110}\int_{0}^{b} y f(x,y)\,dx\,dy + \int_{0}^{a}\int_{b}^{220} y f(x,y)\,dx\,dy + \int_{a}^{110}\int_{b}^{fx} y f(x,y)\,dx\,dy - \int_{M_{5y}}^{110}\int_{15}^{nmx} y f(x,y)\,dx\,dy$$
$$+\int_{M_{5y}}^{110}\int_{b}^{fx} y f(x,y)\,dx\,dy - \int_{85}^{110}\int_{0}^{onx} y f(x,y)\,dx\,dy - \int_{40}^{85}\int_{0}^{pox} y f(x,y)\,dx\,dy - \int_{15}^{40}\int_{0}^{qpx} y f(x,y)\,dx\,dy$$
$$-\int_{0}^{15}\int_{0}^{qax} y f(x,y)\,dx\,dy - \int_{0}^{50}\int_{50}^{abx} y f(x,y)\,dx\,dy - \int_{0}^{70}\int_{70}^{bcx} y f(x,y)\,dx\,dy - \int_{0}^{135}\int_{135}^{cdx} y f(x,y)\,dx\,dy$$
$$-\int_{0}^{155}\int_{155}^{dex} y f(x,y)\,dx\,dy - \int_{0}^{205}\int_{205}^{M_{12y}} y f(x,y)\,dx\,dy - \int_{a}^{M_{12x}}\int_{M_{12x}}^{fx} y f(x,y)\,dx\,dy - \int_{0}^{M_{12x}}\int_{M_{12x}}^{a} y f(x,y)\,dx\,dy\Bigg]$$

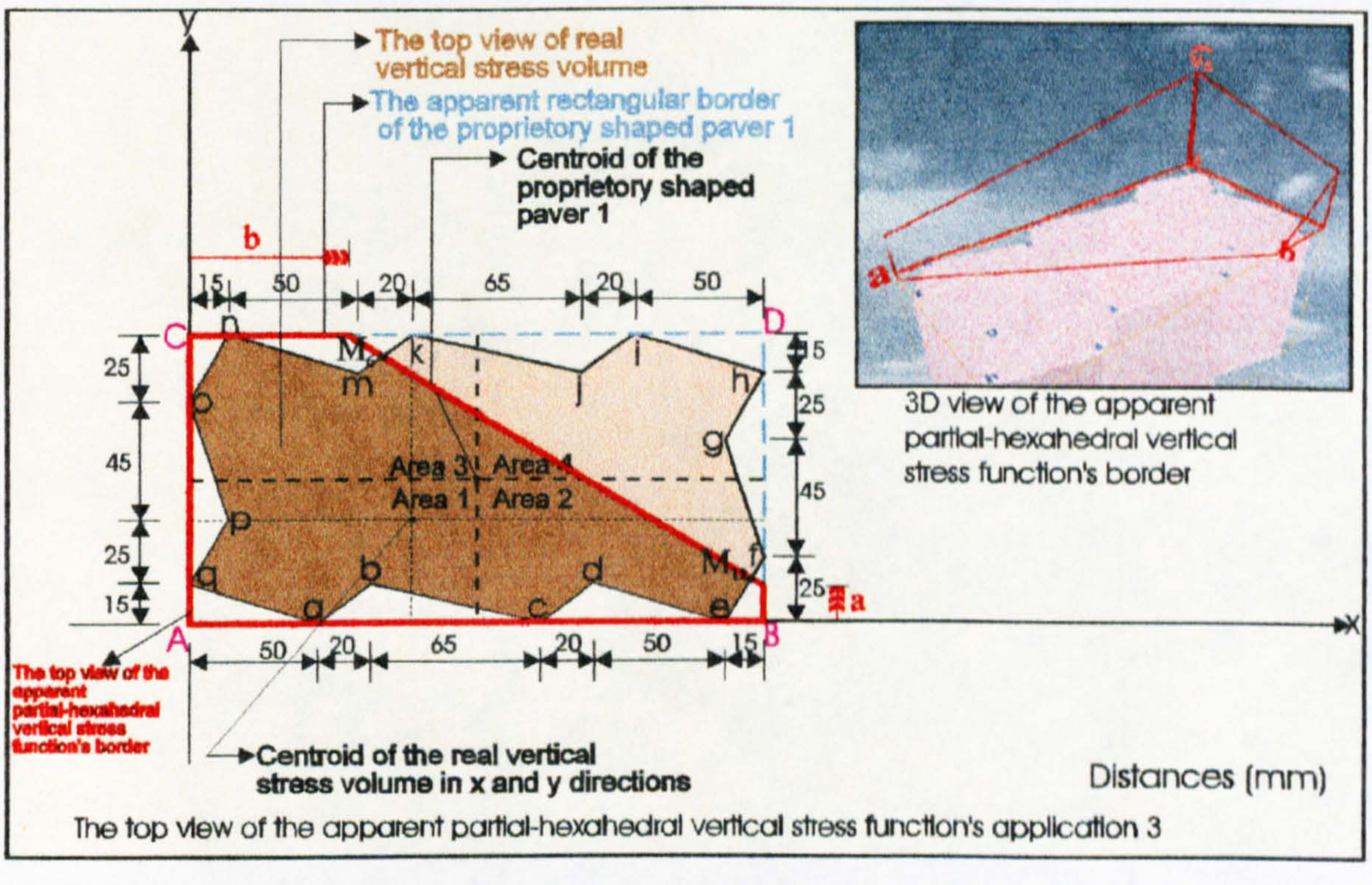

Figure 7.69: Application 3 of the partial-hexahedral compressive stress distribution beneath the circumscribing rectangular border of proprietory shaped paver 1.

Application 3 of the partial-hexahedral compressive stress regime beneath the circumscribing rectangular border of proprietory shaped paver 1 shown in Figure 7.69

can be calculated by using Tables 5.1 and 7.4 and the surface function of the partial-hexahedral compressive stress through the three points σ_A, **l** and **t**.

The total volume **V** beneath the surface $f(x,y) = z\ (> 0)$ and above the region in the xy-plane (see Figure 7.69) is:

$$V = \int_0^b \int_0^{110} f(x,y)\,dy\,dx + \int_b^{220} \int_0^a f(x,y)\,dy\,dx + \int_b^{220} \int_a^{fy} f(x,y)\,dy\,dx - \int_{15}^{65} \int_{95}^{nmy} f(x,y)\,dy\,dx - \int_{65}^{85} \int_{95}^{nky} f(x,y)\,dy\,dx$$
$$+ \int_b^{M_{6x}} \int_{M_{6y}}^{fy} f(x,y)\,dy\,dx + \int_{M_{6x}}^{85} \int_{M_{6y}}^{mky} f(x,y)\,dy\,dx - \int_0^{15} \int_{85}^{ony} f(x,y)\,dy\,dx - \int_0^{15} \int_{40}^{poy} f(x,y)\,dy\,dx - \int_0^{15} \int_{15}^{qpy} f(x,y)\,dy\,dx$$
$$- \int_0^{50} \int_0^{qay} f(x,y)\,dy\,dx - \int_{50}^{70} \int_0^{aby} f(x,y)\,dy\,dx - \int_{70}^{135} \int_0^{bcy} f(x,y)\,dy\,dx - \int_{135}^{155} \int_0^{cdy} f(x,y)\,dy\,dx - \int_{155}^{205} \int_0^{dey} f(x,y)\,dy\,dx$$
$$- \int_{205}^{M_{12x}} \int_0^{efy} f(x,y)\,dy\,dx - \int_{M_{12x}}^{220} \int_a^{fy} f(x,y)\,dy\,dx - \int_{M_{12x}}^{220} \int_0^{a} f(x,y)\,dy\,dx$$

and the centroids of this volume in the xy-plane are at distances $\overline{X}$ and $\overline{Y}$ from the axes (see Figure 7.69) which are given by the following equations.

$$\overline{X} = \frac{1}{V}\left[\int_0^b \int_0^{110} x f(x,y)\,dy\,dx + \int_b^{220} \int_0^a x f(x,y)\,dy\,dx + \int_b^{220} \int_a^{fy} x f(x,y)\,dy\,dx - \int_{15}^{65} \int_{95}^{nmy} x f(x,y)\,dy\,dx\right.$$
$$- \int_{65}^{85} \int_{95}^{nky} x f(x,y)\,dy\,dx + \int_b^{M_{6x}} \int_{M_{6y}}^{fy} x f(x,y)\,dy\,dx + \int_{M_{6x}}^{85} \int_{M_{6y}}^{mky} x f(x,y)\,dy\,dx - \int_0^{15} \int_{85}^{ony} x f(x,y)\,dy\,dx$$
$$- \int_0^{15} \int_{40}^{poy} x f(x,y)\,dy\,dx - \int_0^{15} \int_{15}^{qpy} x f(x,y)\,dy\,dx - \int_0^{50} \int_0^{qay} x f(x,y)\,dy\,dx - \int_{50}^{70} \int_0^{aby} x f(x,y)\,dy\,dx$$
$$\left. - \int_{70}^{135} \int_0^{bcy} x f(x,y)\,dy\,dx - \int_{135}^{155} \int_0^{cdy} x f(x,y)\,dy\,dx - \int_{155}^{205} \int_0^{dey} x f(x,y)\,dy\,dx - \int_{205}^{M_{12x}} \int_0^{efy} x f(x,y)\,dy\,dx\right.$$
$$\left. - \int_{M_{12x}}^{220} \int_a^{fy} x f(x,y)\,dy\,dx - \int_{M_{12x}}^{220} \int_0^{a} x f(x,y)\,dy\,dx\right]$$

$$\overline{Y} = \frac{1}{V}\left[\begin{array}{l}
\int_{0}^{110}\int_{0}^{b} y f(x,y)\,dx\,dy + \int_{0}^{a}\int_{b}^{220} y f(x,y)\,dx\,dy + \int_{a}^{110}\int_{b}^{fx} y f(x,y)\,dx\,dy - \int_{95}^{110}\int_{15}^{nmx} y f(x,y)\,dx\,dy \\
-\int_{95}^{110}\int_{65}^{mkx} y f(x,y)\,dx\,dy + \int_{M_{6y}}^{110}\int_{b}^{fx} y f(x,y)\,dx\,dy + \int_{M_{6y}}^{110}\int_{M_{6x}}^{mkx} y f(x,y)\,dx\,dy - \int_{85}^{110}\int_{0}^{onx} y f(x,y)\,dx\,dy \\
-\int_{40}^{85}\int_{0}^{pox} y f(x,y)\,dx\,dy - \int_{15}^{40}\int_{0}^{qpx} y f(x,y)\,dx\,dy - \int_{0}^{15}\int_{0}^{qax} y f(x,y)\,dx\,dy - \int_{0}^{15}\int_{50}^{abx} y f(x,y)\,dx\,dy \\
-\int_{0}^{15}\int_{70}^{bcx} y f(x,y)\,dx\,dy - \int_{0}^{15}\int_{135}^{cdx} y f(x,y)\,dx\,dy - \int_{0}^{15}\int_{155}^{dex} y f(x,y)\,dx\,dy - \int_{0}^{M_{12y}}\int_{205}^{efx} y f(x,y)\,dx\,dy \\
-\int_{a}^{M_{12y}}\int_{M_{12x}}^{fx} y f(x,y)\,dx\,dy - \int_{0}^{a}\int_{M_{12x}}^{220} y f(x,y)\,dx\,dy
\end{array}\right]$$

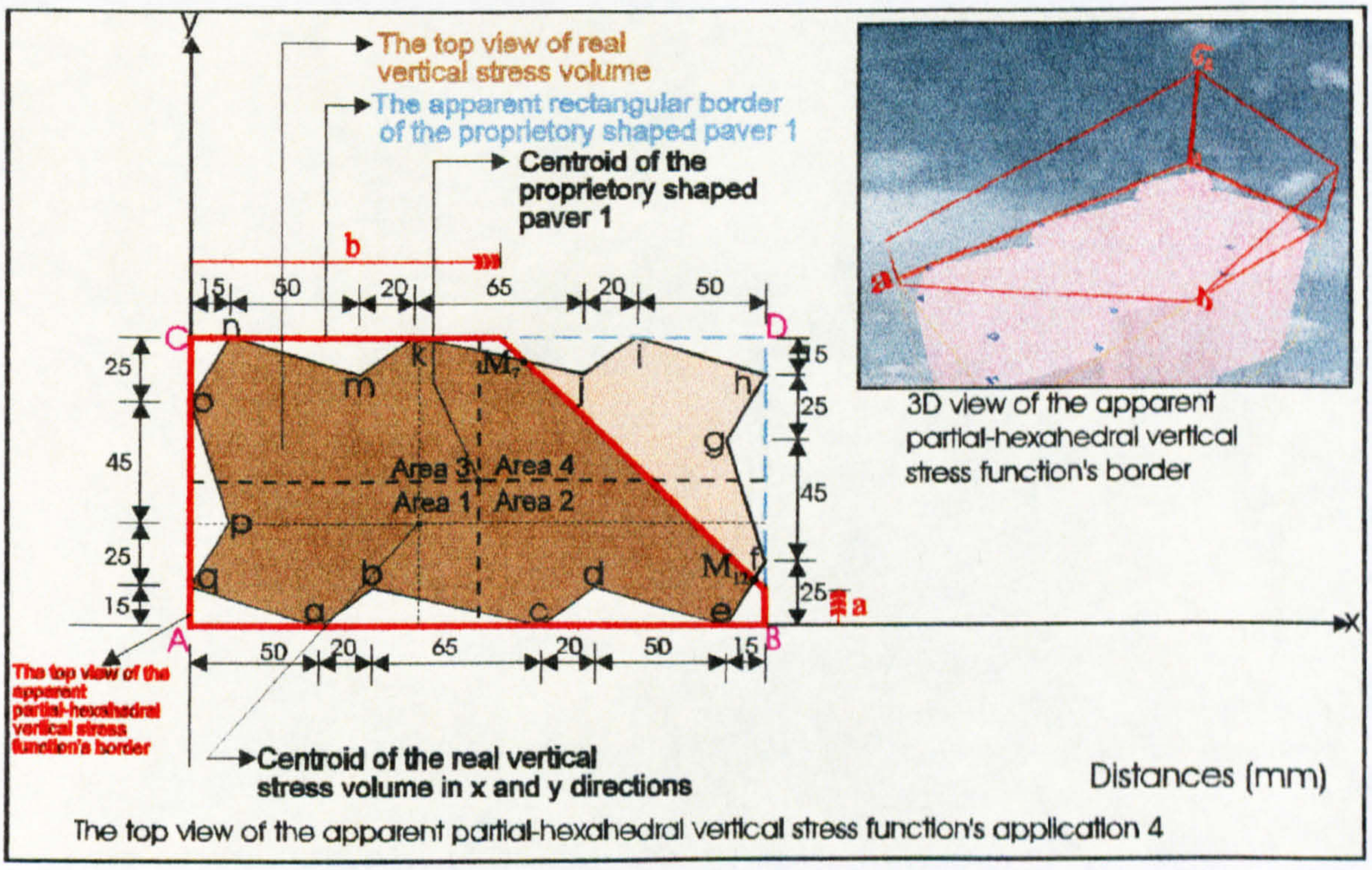

Figure 7.70: Application 4 of the partial-hexahedral compressive stress distribution beneath the circumscribing rectangular border of proprietory shaped paver 1.

Application 4 of the partial-hexahedral compressive stress regime beneath the circumscribing rectangular border of proprietory shaped paver 1 shown in Figure 7.70 can be calculated by using Tables 5.1 and 7.4 and the surface function of the partial-hexahedral compressive stress through the three points σ_A, **I** and **t**.

The total volume **V** beneath the surface $f(x,y) = z\ (> 0)$ and above the region in the xy-plane (see Figure 7.70) is:

$$V = \int_0^b \int_0^{110} f(x,y)\,dy\,dx + \int_b^{220} \int_0^a f(x,y)\,dy\,dx + \int_b^{220} \int_a^{fy} f(x,y)\,dy\,dx - \int_{15}^{65} \int_{95}^{nmy} f(x,y)\,dy\,dx - \int_{65}^{85} \int_{95}^{nky} f(x,y)\,dy\,dx$$
$$- \int_{85}^{M_{7x}} \int_{kjy}^{} f(x,y)\,dy\,dx + \int_{b}^{M_{7x}} \int_{fy}^{} f(x,y)\,dy\,dx - \int_{0}^{85} \int_{ony}^{} f(x,y)\,dy\,dx - \int_{0}^{40} \int_{poy}^{} f(x,y)\,dy\,dx - \int_{0}^{15} \int_{qpy}^{} f(x,y)\,dy\,dx$$
$$- \int_{0}^{50} \int_{0}^{qay} f(x,y)\,dy\,dx - \int_{50}^{70} \int_{0}^{aby} f(x,y)\,dy\,dx - \int_{70}^{135} \int_{0}^{bcy} f(x,y)\,dy\,dx - \int_{135}^{155} \int_{0}^{cdy} f(x,y)\,dy\,dx - \int_{155}^{205} \int_{0}^{dey} f(x,y)\,dy\,dx$$
$$- \int_{205}^{M_{12x}} \int_{0}^{efy} f(x,y)\,dy\,dx - \int_{M_{12x}}^{220} \int_{a}^{fy} f(x,y)\,dy\,dx - \int_{M_{12x}}^{220} \int_{0}^{a} f(x,y)\,dy\,dx$$

and the centroids of this volume in the xy-plane are at distances $\overline{X}$ and $\overline{Y}$ from the axes (see Figure 7.70) which are given by the following equations.

$$\overline{X} = \frac{1}{V}\left[\int_0^b \int_0^{110} x f(x,y)\,dy\,dx + \int_b^{220} \int_0^a x f(x,y)\,dy\,dx + \int_b^{220} \int_a^{fy} x f(x,y)\,dy\,dx - \int_{15}^{65} \int_{95}^{nmy} x f(x,y)\,dy\,dx\right.$$
$$- \int_{65}^{85} \int_{95}^{mky} x f(x,y)\,dy\,dx - \int_{85}^{M_{7x}} \int_{kjy}^{} x f(x,y)\,dy\,dx + \int_{b}^{M_{7x}} \int_{fy}^{} x f(x,y)\,dy\,dx - \int_{0}^{85} \int_{ony}^{} x f(x,y)\,dy\,dx$$
$$- \int_{0}^{40} \int_{poy}^{} x f(x,y)\,dy\,dx - \int_{0}^{15} \int_{qpy}^{} x f(x,y)\,dy\,dx - \int_{0}^{50} \int_{0}^{qay} x f(x,y)\,dy\,dx - \int_{50}^{70} \int_{0}^{xiby} x f(x,y)\,dy\,dx$$
$$- \int_{70}^{135} \int_{0}^{bcy} x f(x,y)\,dy\,dx - \int_{135}^{155} \int_{0}^{cdy} x f(x,y)\,dy\,dx - \int_{155}^{205} \int_{0}^{dey} x f(x,y)\,dy\,dx - \int_{205}^{M_{12x}} \int_{0}^{efy} x f(x,y)\,dy\,dx$$
$$\left. - \int_{M_{12x}}^{220} \int_{a}^{fy} x f(x,y)\,dy\,dx - \int_{M_{12x}}^{220} \int_{0}^{a} x f(x,y)\,dy\,dx\right]$$

$$\overline{Y} = \frac{1}{V}\left[\int_0^{110} \int_0^b y f(x,y)\,dx\,dy + \int_0^a \int_b^{220} y f(x,y)\,dx\,dy + \int_a^{110} \int_b^{fx} y f(x,y)\,dx\,dy - \int_{95}^{110} \int_{15}^{nmx} y f(x,y)\,dx\,dy\right.$$
$$\left. - \int_{95}^{110} \int_{65}^{mkx} y f(x,y)\,dx\,dy - \int_{M_{7y}}^{110} \int_{85}^{kjx} y f(x,y)\,dx\,dy + \int_{M_{7y}}^{110} \int_{85}^{fx} y f(x,y)\,dx\,dy - \int_{85}^{110} \int_{0}^{onx} y f(x,y)\,dx\,dy\right]$$

$$-\int_{40}^{85}\int_{0}^{pox} y f(x,y)\,dx\,dy - \int_{15}^{40}\int_{0}^{qpx} y f(x,y)\,dx\,dy - \int_{0}^{15}\int_{0}^{qax} y f(x,y)\,dx\,dy - \int_{0}^{15}\int_{50}^{abx} y f(x,y)\,dx\,dy$$

$$-\int_{0}^{15}\int_{70}^{bcx} y f(x,y)\,dx\,dy - \int_{0}^{15}\int_{135}^{cdx} y f(x,y)\,dx\,dy - \int_{0}^{15}\int_{155}^{dex} y f(x,y)\,dx\,dy - \int_{0}^{M_{12y}}\int_{205}^{efx} y f(x,y)\,dx\,dy$$

$$-\left[\int_{a}^{M_{12y}}\int_{M_{12x}}^{fx} y f(x,y)\,dx\,dy - \int_{0}^{a}\int_{M_{12x}}^{220} y f(x,y)\,dx\,dy\right]$$

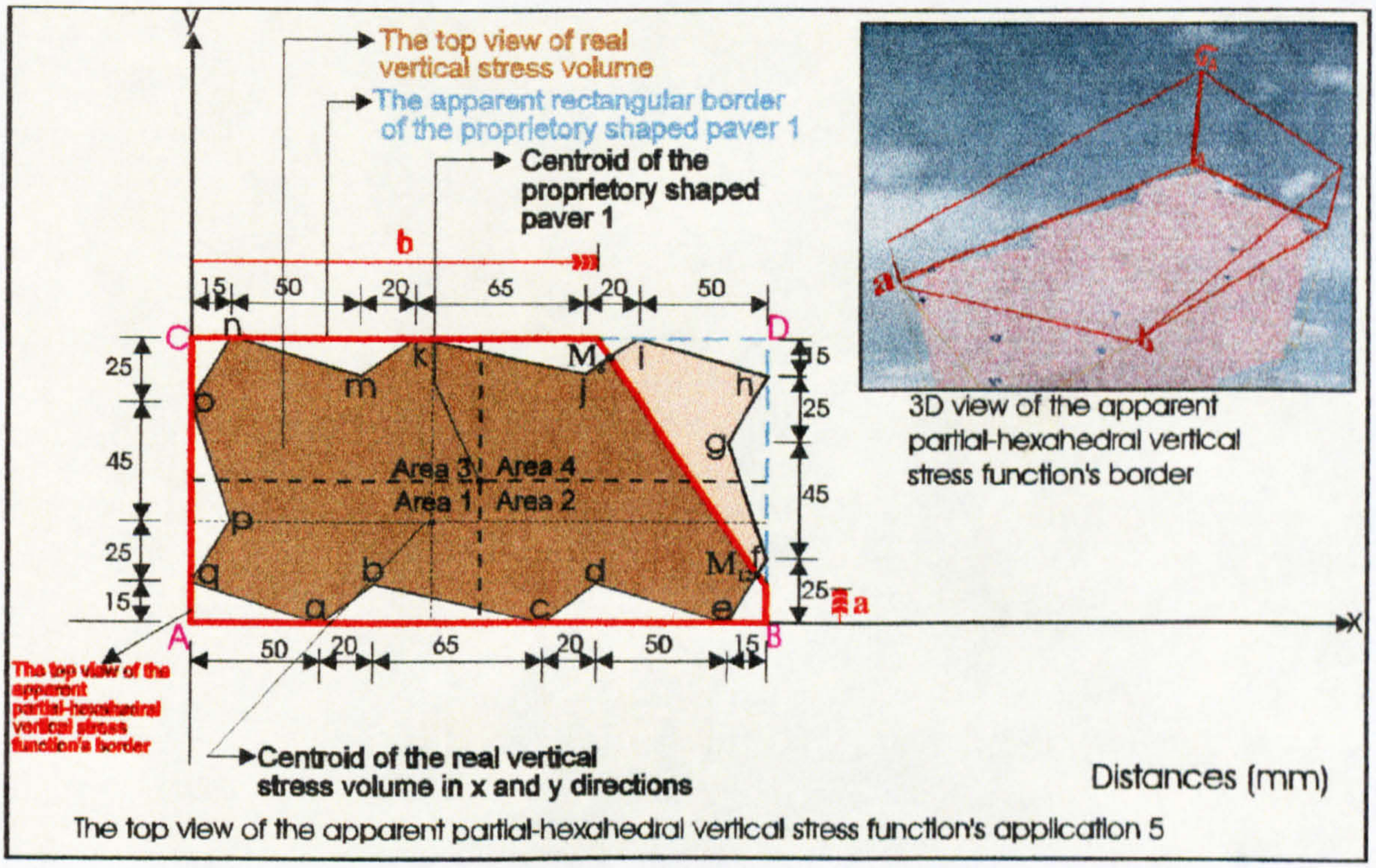

Figure 7.71: Application 5 of the partial-hexahedral compressive stress distribution beneath the circumscribing rectangular border of proprietory shaped paver 1.

Application 5 of the partial-hexahedral compressive stress regime beneath the circumscribing rectangular border of proprietory shaped paver 1 shown in Figure 7.71 can be calculated by using Tables 5.1 and 7.4 and the surface function of the partial-hexahedral compressive stress through the three points σ_A, **l** and **t**.

The total volume **V** beneath the surface $f(x,y) = z\ (> 0)$ and above the region in the xy-plane (see Figure 7.71) is:

$$V = \int_{0}^{b}\int_{0}^{110} f(x,y)\,dy\,dx + \int_{b}^{220}\int_{0}^{a} f(x,y)\,dy\,dx + \int_{b}^{220}\int_{a}^{fy} f(x,y)\,dy\,dx - \int_{15}^{65}\int_{95}^{nmy} f(x,y)\,dy\,dx - \int_{65}^{85}\int_{95}^{mky} f(x,y)\,dy\,dx$$
$$- \int_{85}^{150}\int_{95}^{kjy} f(x,y)\,dy\,dx - \int_{150}^{170}\int_{95}^{jiy} f(x,y)\,dy\,dx + \int_{b}^{M_{8x}}\int_{M_{8y}}^{fy} f(x,y)\,dy\,dx + \int_{M_{8x}}^{170}\int_{M_{8y}}^{jiy} f(x,y)\,dy\,dx - \int_{0}^{15}\int_{85}^{ony} f(x,y)\,dy\,dx$$
$$- \int_{0}^{15}\int_{40}^{poy} f(x,y)\,dy\,dx - \int_{0}^{15}\int_{15}^{qpy} f(x,y)\,dy\,dx - \int_{0}^{50}\int_{0}^{qay} f(x,y)\,dy\,dx - \int_{50}^{70}\int_{0}^{xhy} f(x,y)\,dy\,dx - \int_{70}^{135}\int_{0}^{bcy} f(x,y)\,dy\,dx$$
$$- \int_{135}^{155}\int_{0}^{cdy} f(x,y)\,dy\,dx - \int_{155}^{205}\int_{0}^{dey} f(x,y)\,dy\,dx - \int_{205}^{M_{12x}}\int_{0}^{efy} f(x,y)\,dy\,dx - \int_{M_{12x}}^{220}\int_{a}^{fy} f(x,y)\,dy\,dx - \int_{M_{12x}}^{220}\int_{0}^{a} f(x,y)\,dy\,dx$$

and the centroids of this volume in the xy-plane are at distances $\overline{X}$ and $\overline{Y}$ from the axes (see Figure 7.71) which are given by the following equations.

$$\overline{X} = \frac{1}{V}\left[\begin{array}{l}
\int_{0}^{b}\int_{0}^{110} x f(x,y)\,dy\,dx + \int_{b}^{220}\int_{0}^{a} x f(x,y)\,dy\,dx + \int_{b}^{220}\int_{a}^{fy} x f(x,y)\,dy\,dx - \int_{15}^{65}\int_{95}^{nmy} x f(x,y)\,dy\,dx \\
- \int_{65}^{85}\int_{95}^{mky} x f(x,y)\,dy\,dx - \int_{85}^{150}\int_{95}^{kjy} x f(x,y)\,dy\,dx - \int_{150}^{170}\int_{95}^{jiy} x f(x,y)\,dy\,dx + \int_{b}^{M_{8x}}\int_{M_{8y}}^{fy} x f(x,y)\,dy\,dx \\
+ \int_{M_{8x}}^{170}\int_{M_{8y}}^{jiy} x f(x,y)\,dy\,dx - \int_{0}^{15}\int_{85}^{ony} x f(x,y)\,dy\,dx - \int_{0}^{15}\int_{40}^{poy} x f(x,y)\,dy\,dx - \int_{0}^{15}\int_{15}^{qpy} x f(x,y)\,dy\,dx \\
- \int_{0}^{50}\int_{0}^{qay} x f(x,y)\,dy\,dx - \int_{50}^{70}\int_{0}^{aby} x f(x,y)\,dy\,dx - \int_{70}^{135}\int_{0}^{bcy} x f(x,y)\,dy\,dx - \int_{135}^{155}\int_{0}^{cdy} x f(x,y)\,dy\,dx \\
- \int_{155}^{205}\int_{0}^{dey} x f(x,y)\,dy\,dx - \int_{205}^{M_{12x}}\int_{0}^{efy} x f(x,y)\,dy\,dx - \int_{M_{12x}}^{220}\int_{a}^{fy} x f(x,y)\,dy\,dx - \int_{M_{12x}}^{220}\int_{0}^{a} x f(x,y)\,dy\,dx
\end{array}\right]$$

$$\overline{Y} = \frac{1}{V}\left[\begin{array}{l}
\int_{0}^{110}\int_{0}^{b} y f(x,y)\,dx\,dy + \int_{0}^{a}\int_{0}^{220} y f(x,y)\,dx\,dy + \int_{a}^{110}\int_{b}^{fx} y f(x,y)\,dx\,dy - \int_{95}^{110}\int_{15}^{nmx} y f(x,y)\,dx\,dy \\
- \int_{95}^{110}\int_{65}^{mkx} y f(x,y)\,dx\,dy - \int_{95}^{110}\int_{85}^{kjx} y f(x,y)\,dx\,dy - \int_{95}^{110}\int_{150}^{jix} y f(x,y)\,dx\,dy + \int_{M_{8y}}^{110}\int_{b}^{fx} y f(x,y)\,dx\,dy \\
+ \int_{M_{8y}}^{110}\int_{M_{8x}}^{jix} y f(x,y)\,dx\,dy - \int_{85}^{110}\int_{0}^{onx} y f(x,y)\,dx\,dy - \int_{40}^{85}\int_{0}^{pax} y f(x,y)\,dx\,dy - \int_{15}^{40}\int_{0}^{qpx} y f(x,y)\,dx\,dy \\
- \int_{0}^{15}\int_{0}^{qax} y f(x,y)\,dx\,dy - \int_{0}^{15}\int_{50}^{abx} y f(x,y)\,dx\,dy - \int_{0}^{15}\int_{70}^{bcx} y f(x,y)\,dx\,dy - \int_{0}^{15}\int_{135}^{cdx} y f(x,y)\,dx\,dy
\end{array}\right]$$

$$-\int_{0}^{15}\int_{155}^{dex} y f(x,y)\,dx\,dy - \int_{0}^{M_{12y}}\int_{205}^{efx} y f(x,y)\,dx\,dy - \int_{a}^{M_{12y}}\int_{M_{12x}}^{fx} y f(x,y)\,dx\,dy - \int_{0}^{a}\int_{M_{12x}}^{220} y f(x,y)\,dx\,dy\Bigg]$$

Application 6 of the partial-hexahedral compressive stress regime beneath the circumscribing rectangular border of proprietory shaped paver 1 shown in Figure 7.72 can be calculated by using Tables 5.1 and 7.4 and the surface function of the partial-hexahedral compressive stress through the three points σ_A, **I** and **t**.

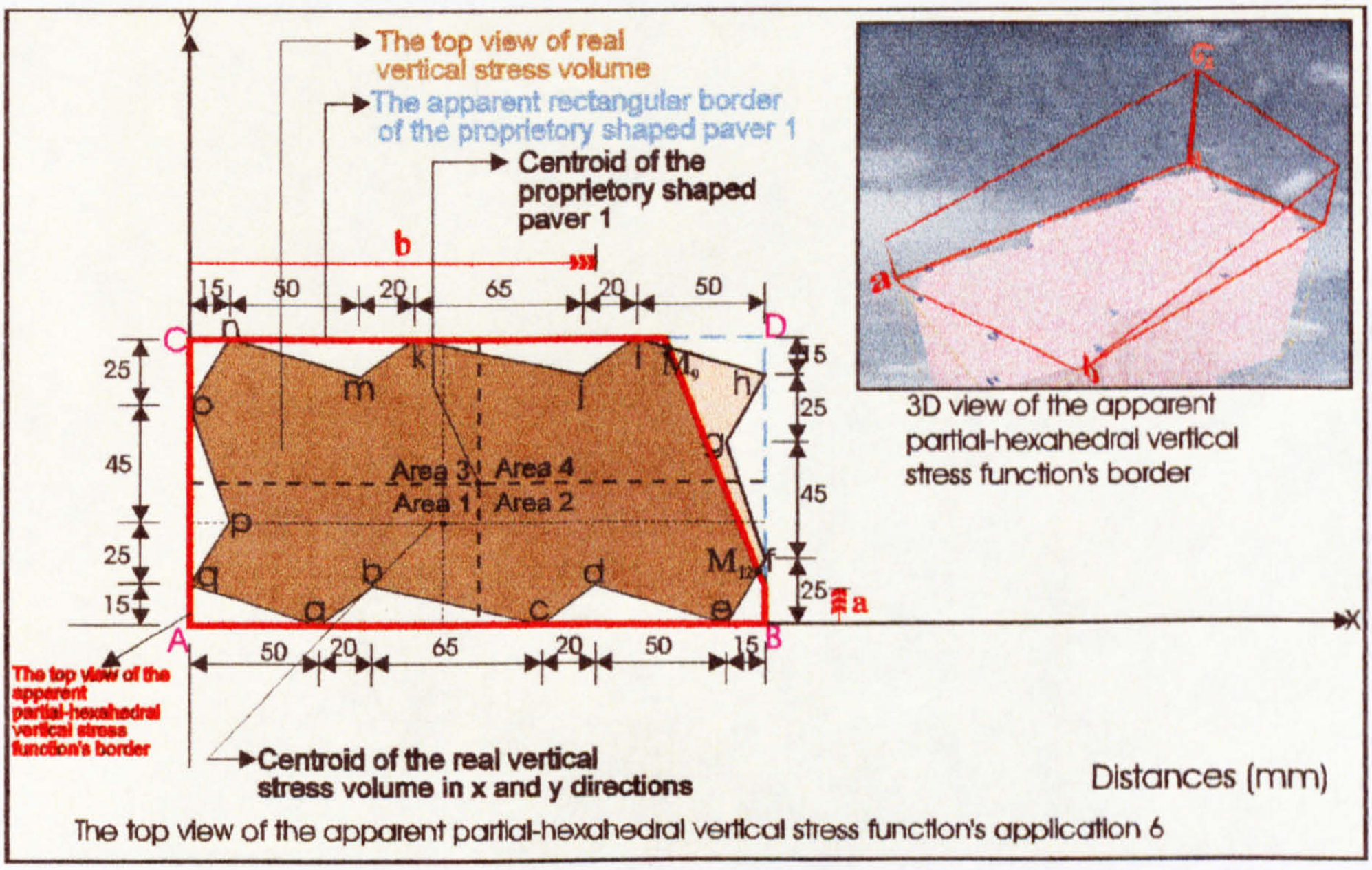

Figure 7.72: Application 6 of the partial-hexahedral compressive stress distribution beneath the circumscribing rectangular border of proprietory shaped paver 1.

The total volume **V** beneath the surface $f(x,y) = z\ (> 0)$ and above the region in the xy-plane (see Figure 7.72) is:

$$V = \int_{0}^{b}\int_{0}^{110} f(x,y)\,dy\,dx + \int_{b}^{220}\int_{0}^{a} f(x,y)\,dy\,dx + \int_{b}^{220}\int_{a}^{fy} f(x,y)\,dy\,dx - \int_{15}^{65}\int_{95}^{nmy} f(x,y)\,dy\,dx - \int_{65}^{85}\int_{95}^{mky} f(x,y)\,dy\,dx$$
$$- \int_{85}^{150}\int_{95}^{kjy} f(x,y)\,dy\,dx - \int_{150}^{170}\int_{95}^{jiy} f(x,y)\,dy\,dx - \int_{170}^{M_{9x}}\int_{M_{9y}}^{hiy} f(x,y)\,dy\,dx + \int_{b}^{M_{9x}}\int_{M_{9y}}^{fy} f(x,y)\,dy\,dx - \int_{0}^{15}\int_{85}^{ony} f(x,y)\,dy\,dx$$

$$-\int_{0}^{15}\int_{40}^{poy} f(x,y)\,dy\,dx - \int_{0}^{15}\int_{15}^{qpy} f(x,y)\,dy\,dx - \int_{0}^{50}\int_{0}^{qay} f(x,y)\,dy\,dx - \int_{50}^{70}\int_{0}^{aby} f(x,y)\,dy\,dx - \int_{70}^{135}\int_{0}^{bcy} f(x,y)\,dy\,dx$$

$$-\int_{135}^{155}\int_{0}^{cdy} f(x,y)\,dy\,dx - \int_{155}^{205}\int_{0}^{dey} f(x,y)\,dy\,dx - \int_{205}^{M_{12x}}\int_{0}^{efy} f(x,y)\,dy\,dx - \int_{M_{12x}}^{220}\int_{a}^{fy} f(x,y)\,dy\,dx - \int_{M_{12x}}^{220}\int_{0}^{a} f(x,y)\,dy\,dx$$

and the centroids of this volume in the xy-plane are at distances $\overline{X}$ and $\overline{Y}$ from the axes (see Figure 7.72) which are given by the following equations.

$$\overline{X} = \frac{1}{V}\left[\begin{array}{l}
\int_{0}^{b}\int_{0}^{110} xf(x,y)\,dy\,dx + \int_{b}^{220}\int_{0}^{a} xf(x,y)\,dy\,dx + \int_{b}^{220}\int_{a}^{fy} xf(x,y)\,dy\,dx - \int_{15}^{65}\int_{95}^{nmy} xf(x,y)\,dy\,dx \\
-\int_{65}^{85}\int_{95}^{mky} xf(x,y)\,dy\,dx - \int_{85}^{150}\int_{95}^{kjy} xf(x,y)\,dy\,dx - \int_{150}^{170}\int_{95}^{jiy} xf(x,y)\,dy\,dx - \int_{170}^{M_{9x}}\int_{M_{9y}}^{hiy} xf(x,y)\,dy\,dx \\
+\int_{b}^{M_{9x}}\int_{M_{9y}}^{fy} xf(x,y)\,dy\,dx - \int_{0}^{15}\int_{85}^{ony} xf(x,y)\,dy\,dx - \int_{0}^{15}\int_{40}^{poy} xf(x,y)\,dy\,dx - \int_{0}^{15}\int_{15}^{qpy} xf(x,y)\,dy\,dx \\
-\int_{0}^{50}\int_{0}^{qay} xf(x,y)\,dy\,dx - \int_{50}^{70}\int_{0}^{aby} xf(x,y)\,dy\,dx - \int_{70}^{135}\int_{0}^{bcy} xf(x,y)\,dy\,dx - \int_{135}^{155}\int_{0}^{cdy} xf(x,y)\,dy\,dx \\
-\int_{155}^{205}\int_{0}^{dey} xf(x,y)\,dy\,dx - \int_{205}^{M_{12x}}\int_{0}^{efy} xf(x,y)\,dy\,dx - \int_{M_{12x}}^{220}\int_{a}^{fy} xf(x,y)\,dy\,dx - \int_{M_{12x}}^{220}\int_{0}^{a} xf(x,y)\,dy\,dx
\end{array}\right]$$

$$\overline{Y} = \frac{1}{V}\left[\begin{array}{l}
\int_{0}^{110}\int_{0}^{b} yf(x,y)\,dx\,dy + \int_{0}^{a}\int_{b}^{220} yf(x,y)\,dx\,dy + \int_{a}^{110}\int_{b}^{fx} yf(x,y)\,dx\,dy - \int_{95}^{110}\int_{15}^{nmx} yf(x,y)\,dx\,dy \\
-\int_{95}^{110}\int_{65}^{mkx} yf(x,y)\,dx\,dy - \int_{95}^{110}\int_{85}^{kjx} yf(x,y)\,dx\,dy - \int_{95}^{110}\int_{150}^{jix} yf(x,y)\,dx\,dy - \int_{M_{9y}}^{110}\int_{170}^{hix} yf(x,y)\,dx\,dy \\
+\int_{M_{9y}}^{110}\int_{b}^{fx} yf(x,y)\,dx\,dy - \int_{85}^{110}\int_{0}^{onx} yf(x,y)\,dx\,dy - \int_{40}^{85}\int_{0}^{pox} yf(x,y)\,dx\,dy - \int_{15}^{40}\int_{0}^{qpx} yf(x,y)\,dx\,dy \\
-\int_{0}^{15}\int_{0}^{qax} yf(x,y)\,dx\,dy - \int_{0}^{15}\int_{50}^{abx} yf(x,y)\,dx\,dy - \int_{0}^{15}\int_{70}^{bcx} yf(x,y)\,dx\,dy - \int_{0}^{15}\int_{135}^{cdx} yf(x,y)\,dx\,dy \\
-\int_{0}^{15}\int_{155}^{dex} yf(x,y)\,dx\,dy - \int_{0}^{M_{12y}}\int_{205}^{efx} yf(x,y)\,dx\,dy - \int_{a}^{M_{12y}}\int_{M_{12x}}^{fx} yf(x,y)\,dx\,dy - \int_{0}^{a}\int_{M_{12x}}^{220} yf(x,y)\,dx\,dy
\end{array}\right]$$

Application 7 of the partial-hexahedral compressive stress regime beneath the circumscribing rectangular border of proprietory shaped paver 1 shown in Figure 7.73 can be calculated by using Tables 5.1 and 7.4 and the surface function of the partial-hexahedral compressive stress through the three points σ_A, **l** and **t**.

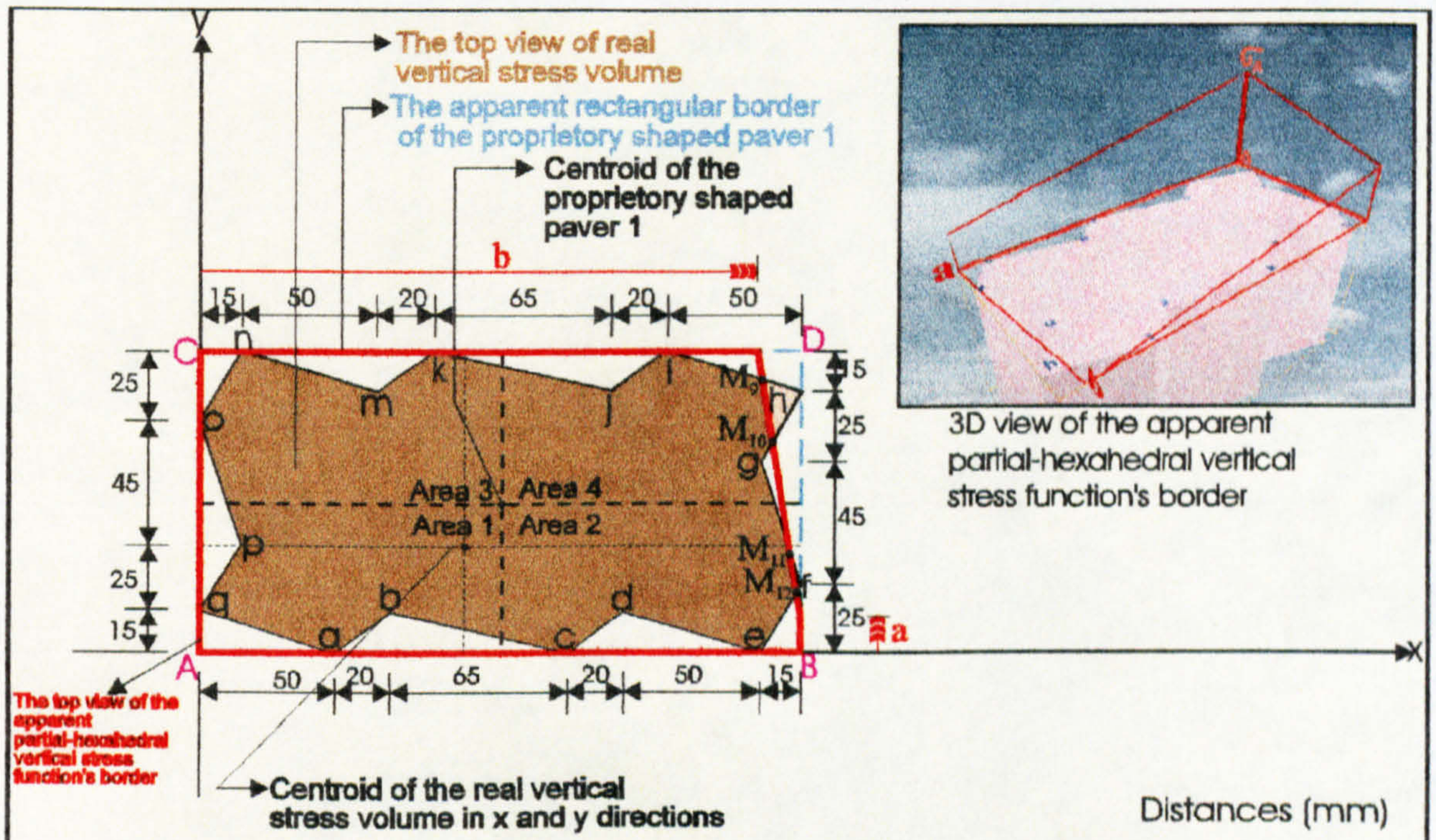

The top view of the apparent partial-hexahedral vertical stress function's application 7

Figure 7.73: Application 7 of the partial-hexahedral compressive stress distribution beneath the circumscribing rectangular border of proprietory shaped paver 1.

The total volume **V** beneath the surface $f(x,y) = z\ (> 0)$ and above the region in the xy-plane (see Figure 7.73) is:

$$V = \int_0^{b}\int_0^{110} f(x,y)\,dy\,dx + \int_b^{220}\int_0^{a} f(x,y)\,dy\,dx + \int_b^{220}\int_a^{fy} f(x,y)\,dy\,dx - \int_{15}^{65}\int_{95}^{nmy} f(x,y)\,dy\,dx - \int_{65}^{85}\int_{95}^{mky} f(x,y)\,dy\,dx$$

$$- \int_{85}^{150}\int_{95}^{kjy} f(x,y)\,dy\,dx - \int_{150}^{170}\int_{95}^{jiy} f(x,y)\,dy\,dx - \int_{170}^{M_{9x}}\int_{M_{9y}}^{hiy} f(x,y)\,dy\,dx + \int_{b}^{M_{9x}}\int_{M_{9y}}^{fy} f(x,y)\,dy\,dx - \int_{0}^{15}\int_{85}^{ony} f(x,y)\,dy\,dx$$

$$- \int_{0}^{15}\int_{40}^{poy} f(x,y)\,dy\,dx - \int_{0}^{15}\int_{15}^{qpy} f(x,y)\,dy\,dx - \int_{0}^{50}\int_{0}^{qay} f(x,y)\,dy\,dx - \int_{50}^{70}\int_{0}^{aby} f(x,y)\,dy\,dx - \int_{70}^{135}\int_{0}^{bcy} f(x,y)\,dy\,dx$$

$$- \int_{135}^{155}\int_{0}^{cdy} f(x,y)\,dy\,dx - \int_{155}^{205}\int_{0}^{dey} f(x,y)\,dy\,dx - \int_{205}^{M_{12x}}\int_{0}^{efy} f(x,y)\,dy\,dx - \int_{M_{12x}}^{220}\int_{a}^{fy} f(x,y)\,dy\,dx - \int_{M_{12x}}^{220}\int_{0}^{a} f(x,y)\,dy\,dx$$

$$-\int_{205}^{220}\int_{70}^{ghy} f(x,y)\,dy\,dx-\int_{205}^{220}\int_{25}^{fgy} f(x,y)\,dy\,dx+\int_{M_{10x}}^{220}\int_{M_{10y}}^{ghy} f(x,y)\,dy\,dx+\int_{M_{11x}}^{220}\int_{M_{11y}}^{M_{10y}} f(x,y)\,dy\,dx+\int_{M_{10x}}^{M_{11x}}\int_{M_{11y}}^{fy} f(x,y)\,dy\,dx$$
$$+\int_{M_{11x}}^{220}\int_{25}^{fgy} f(x,y)\,dy\,dx$$

and the centroids of this volume in the xy-plane are at distances $\overline{X}$ and $\overline{Y}$ from the axes (see Figure 7.73) which are given by the following equations.

$$\overline{X}=\frac{1}{V}\left[\int_{0}^{b}\int_{0}^{110} xf(x,y)\,dy\,dx+\int_{b}^{220}\int_{0}^{a} xf(x,y)\,dy\,dx+\int_{b}^{220}\int_{a}^{fy} xf(x,y)\,dy\,dx-\int_{15}^{65}\int_{95}^{nmy} xf(x,y)\,dy\,dx\right.$$
$$-\int_{65}^{85}\int_{95}^{nky} xf(x,y)\,dy\,dx-\int_{85}^{150}\int_{95}^{kjy} xf(x,y)\,dy\,dx-\int_{150}^{170}\int_{95}^{jiy} xf(x,y)\,dy\,dx-\int_{170}^{M_{9x}}\int_{M_{9y}}^{hiy} xf(x,y)\,dy\,dx$$
$$+\int_{b}^{M_{9x}}\int_{M_{9y}}^{fy} xf(x,y)\,dy\,dx-\int_{0}^{15}\int_{85}^{ony} xf(x,y)\,dy\,dx-\int_{0}^{15}\int_{40}^{poy} xf(x,y)\,dy\,dx-\int_{0}^{15}\int_{15}^{qpy} xf(x,y)\,dy\,dx$$
$$-\int_{0}^{50}\int_{0}^{qay} xf(x,y)\,dy\,dx-\int_{50}^{70}\int_{0}^{aby} xf(x,y)\,dy\,dx-\int_{70}^{135}\int_{0}^{bcy} xf(x,y)\,dy\,dx-\int_{135}^{155}\int_{0}^{cdy} xf(x,y)\,dy\,dx$$
$$-\int_{155}^{205}\int_{0}^{dey} xf(x,y)\,dy\,dx-\int_{205}^{M_{12x}}\int_{0}^{efy} xf(x,y)\,dy\,dx-\int_{M_{12x}}^{220}\int_{a}^{fy} xf(x,y)\,dy\,dx-\int_{M_{12x}}^{220}\int_{0}^{a} xf(x,y)\,dy\,dx$$
$$-\int_{205}^{220}\int_{70}^{ghy} xf(x,y)\,dy\,dx-\int_{205}^{220}\int_{25}^{fgy} xf(x,y)\,dy\,dx+\int_{M_{10x}}^{220}\int_{M_{10y}}^{ghy} xf(x,y)\,dy\,dx+\int_{M_{11x}}^{220}\int_{M_{11y}}^{M_{10y}} xf(x,y)\,dy\,dx$$
$$\left.+\int_{M_{10x}}^{M_{11x}}\int_{M_{11y}}^{fy} xf(x,y)\,dy\,dx+\int_{M_{11x}}^{220}\int_{25}^{fgy} xf(x,y)\,dy\,dx\right]$$

$$\overline{Y}=\frac{1}{V}\left[\int_{0}^{110}\int_{0}^{b} yf(x,y)\,dx\,dy+\int_{0}^{a}\int_{b}^{220} yf(x,y)\,dx\,dy+\int_{a}^{110}\int_{b}^{fx} yf(x,y)\,dx\,dy-\int_{95}^{110}\int_{15}^{nmx} yf(x,y)\,dx\,dy\right.$$
$$-\int_{95}^{110}\int_{65}^{mkx} yf(x,y)\,dx\,dy-\int_{95}^{110}\int_{85}^{kjx} yf(x,y)\,dx\,dy-\int_{95}^{110}\int_{150}^{jix} yf(x,y)\,dx\,dy-\int_{M_{9y}}^{110}\int_{170}^{hix} yf(x,y)\,dx\,dy$$
$$+\int_{M_{9y}}^{110}\int_{b}^{fx} yf(x,y)\,dx\,dy-\int_{85}^{110}\int_{0}^{onx} yf(x,y)\,dx\,dy-\int_{40}^{85}\int_{0}^{pax} yf(x,y)\,dx\,dy-\int_{15}^{40}\int_{0}^{qpx} yf(x,y)\,dx\,dy$$
$$\left.-\int_{0}^{15}\int_{0}^{qax} yf(x,y)\,dx\,dy-\int_{0}^{15}\int_{50}^{abx} yf(x,y)\,dx\,dy-\int_{0}^{15}\int_{70}^{bcx} yf(x,y)\,dx\,dy-\int_{0}^{15}\int_{135}^{cdx} yf(x,y)\,dx\,dy\right]$$

$$-\int_{0}^{15}\int_{155}^{dex} y f(x,y)\,dx\,dy - \int_{0}^{M_{12y}}\int_{205}^{efx} y f(x,y)\,dx\,dy - \int_{a}^{M_{12y}}\int_{M_{12x}}^{fx} y f(x,y)\,dx\,dy - \int_{0}^{a}\int_{M_{12x}}^{220} y f(x,y)\,dx\,dy$$

$$-\int_{70}^{95}\int_{205}^{ghx} y f(x,y)\,dx\,dy - \int_{25}^{70}\int_{205}^{fgx} y f(x,y)\,dx\,dy + \int_{M_{10y}}^{95}\int_{M_{10x}}^{ghx} y f(x,y)\,dx\,dy + \int_{M_{11y}}^{M_{10y}}\int_{M_{11x}}^{220} y f(x,y)\,dx\,dy$$

$$+\int_{M_{11y}}^{M_{10y}}\int_{M_{10x}}^{fx} y f(x,y)\,dx\,dy + \int_{25}^{M_{11y}}\int_{M_{11x}}^{fgx} y f(x,y)\,dx\,dy\Bigg]$$

Application 8 of the partial-hexahedral compressive stress regime beneath the circumscribing rectangular border of proprietory shaped paver 1 shown in Figure 7.74 can be calculated by using Tables 5.1 and 7.4 and the surface function of the partial-hexahedral compressive stress through the three points σ_A, **I** and **t**.

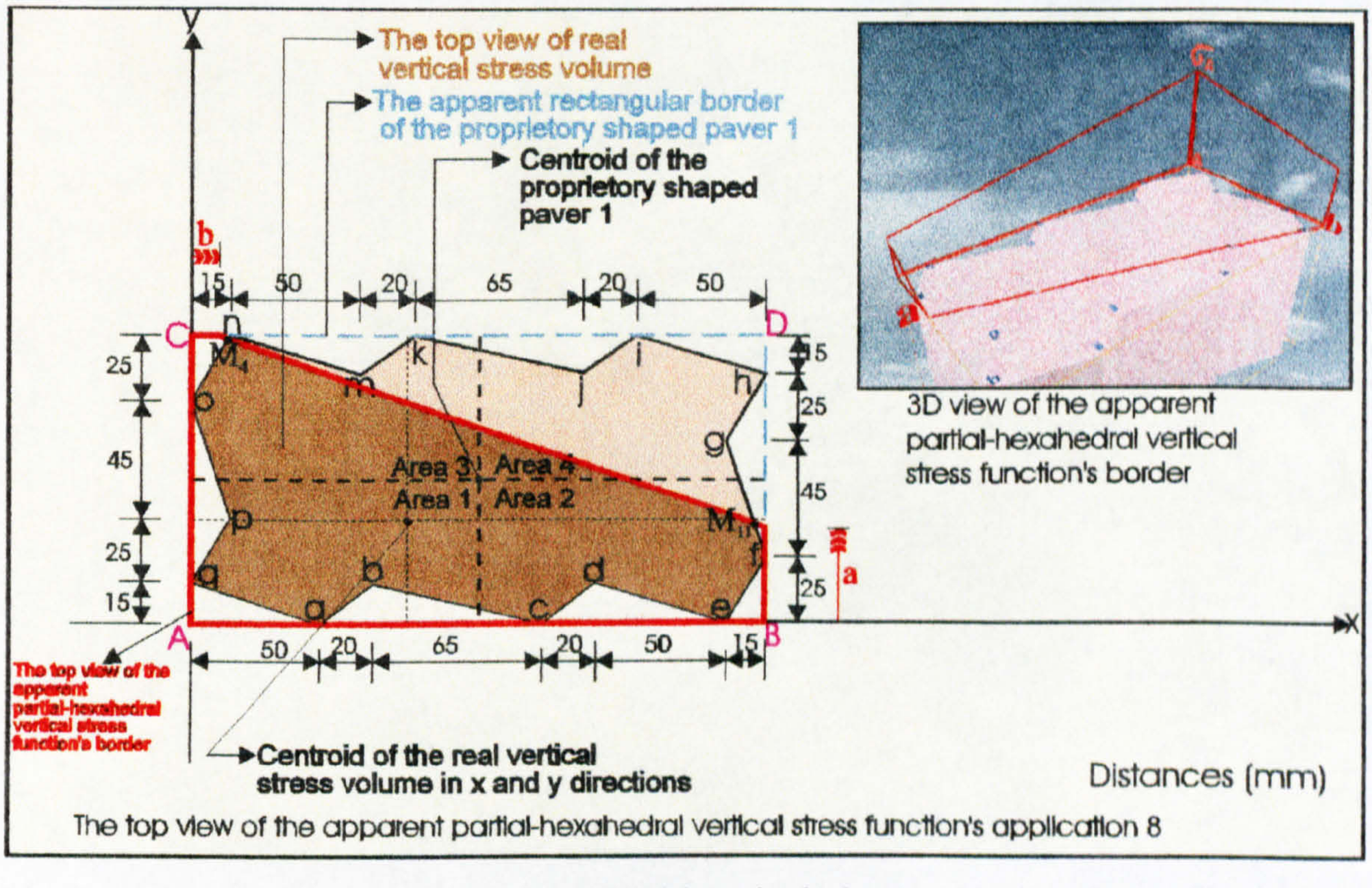

The top view of the apparent partial-hexahedral vertical stress function's application 8

Figure 7.74: Application 8 of the partial-hexahedral compressive stress distribution beneath the circumscribing rectangular border of proprietory shaped paver 1.

The total volume **V** beneath the surface $f(x,y) = z\ (> 0)$ and above the region in the xy-plane (see Figure 7.74) is:

$$V = \int_0^b \int_0^{110} f(x,y)\,dy\,dx + \int_b^{220} \int_0^a f(x,y)\,dy\,dx + \int_b^{220} \int_a^{fy} f(x,y)\,dy\,dx - \int_0^{M_{4x}} \int_{85}^{ony} f(x,y)\,dy\,dx - \int_0^b \int_{M_{4y}}^{110} f(x,y)\,dy\,dx$$
$$- \int_b^{M_{4x}} \int_{M_{4y}}^{fy} f(x,y)\,dy\,dx - \int_0^{15} \int_{40}^{poy} f(x,y)\,dy\,dx - \int_0^{15} \int_{15}^{qpy} f(x,y)\,dy\,dx - \int_0^{50} \int_0^{qay} f(x,y)\,dy\,dx - \int_{50}^{70} \int_0^{xiby} f(x,y)\,dy\,dx$$
$$- \int_{70}^{135} \int_0^{bcy} f(x,y)\,dy\,dx - \int_{135}^{155} \int_0^{cdy} f(x,y)\,dy\,dx - \int_{155}^{205} \int_0^{dey} f(x,y)\,dy\,dx - \int_{205}^{220} \int_0^{efy} f(x,y)\,dy\,dx - \int_{M_{11x}}^{220} \int_{25}^{fgy} f(x,y)\,dy\,dx$$
$$+ \int_{M_{11x}}^{220} \int_a^{fy} f(x,y)\,dy\,dx$$

and the centroids of this volume in the xy-plane are at distances $\overline{X}$ and $\overline{Y}$ from the axes (see Figure 7.74) which are given by the following equations.

$$\overline{X} = \frac{1}{V}\left[\int_0^b \int_0^{110} x f(x,y)\,dy\,dx + \int_b^{220} \int_0^a x f(x,y)\,dy\,dx + \int_b^{220} \int_a^{fy} x f(x,y)\,dy\,dx - \int_0^{M_{4x}} \int_{85}^{ony} x f(x,y)\,dy\,dx \right.$$
$$- \int_0^b \int_{M_{4y}}^{110} x f(x,y)\,dy\,dx - \int_b^{M_{4x}} \int_{M_{4y}}^{fy} x f(x,y)\,dy\,dx - \int_0^{15} \int_{40}^{poy} x f(x,y)\,dy\,dx - \int_0^{15} \int_{15}^{qpy} x f(x,y)\,dy\,dx$$
$$- \int_0^{50} \int_0^{qay} x f(x,y)\,dy\,dx - \int_{50}^{70} \int_0^{xiby} x f(x,y)\,dy\,dx - \int_{70}^{135} \int_0^{bcy} x f(x,y)\,dy\,dx - \int_{135}^{155} \int_0^{cdy} x f(x,y)\,dy\,dx$$
$$\left. - \int_{155}^{205} \int_0^{dey} x f(x,y)\,dy\,dx - \int_{205}^{220} \int_0^{efy} x f(x,y)\,dy\,dx - \int_{M_{11x}}^{220} \int_{25}^{fgy} x f(x,y)\,dy\,dx + \int_{M_{11x}}^{220} \int_a^{fy} x f(x,y)\,dy\,dx \right]$$

$$\overline{Y} = \frac{1}{V}\left[\int_0^{110} \int_0^b y f(x,y)\,dx\,dy + \int_0^{a} \int_b^{220} y f(x,y)\,dx\,dy + \int_a^{110} \int_b^{fx} y f(x,y)\,dx\,dy - \int_{85}^{M_{4y}} \int_0^{onx} y f(x,y)\,dx\,dy \right.$$
$$- \int_{M_{4y}}^{110} \int_0^b y f(x,y)\,dx\,dy - \int_{M_{4y}}^{110} \int_b^{fx} y f(x,y)\,dx\,dy - \int_{40}^{85} \int_0^{pox} y f(x,y)\,dx\,dy - \int_{15}^{40} \int_0^{qpx} y f(x,y)\,dx\,dy$$
$$- \int_0^{15} \int_0^{qax} y f(x,y)\,dx\,dy - \int_0^{15} \int_{50}^{abx} y f(x,y)\,dx\,dy - \int_0^{15} \int_{70}^{bcx} y f(x,y)\,dx\,dy - \int_0^{135} \int_{15}^{cdx} y f(x,y)\,dx\,dy$$
$$\left. - \int_0^{155} \int_{15}^{dex} y f(x,y)\,dx\,dy - \int_0^{205} \int_{25}^{efx} y f(x,y)\,dx\,dy - \int_{25}^{M_{11y}} \int_{M_{11x}}^{fgx} y f(x,y)\,dx\,dy + \int_a^{M_{11y}} \int_{M_{11x}}^{fx} y f(x,y)\,dx\,dy \right]$$

Application 9 of the partial-hexahedral compressive stress regime beneath the circumscribing rectangular border of proprietory shaped paver 1 shown in Figure 7.75 can be calculated by using Tables 5.1 and 7.4 and the surface function of the partial-hexahedral compressive stress through the three points σ_A, **l** and **t**.

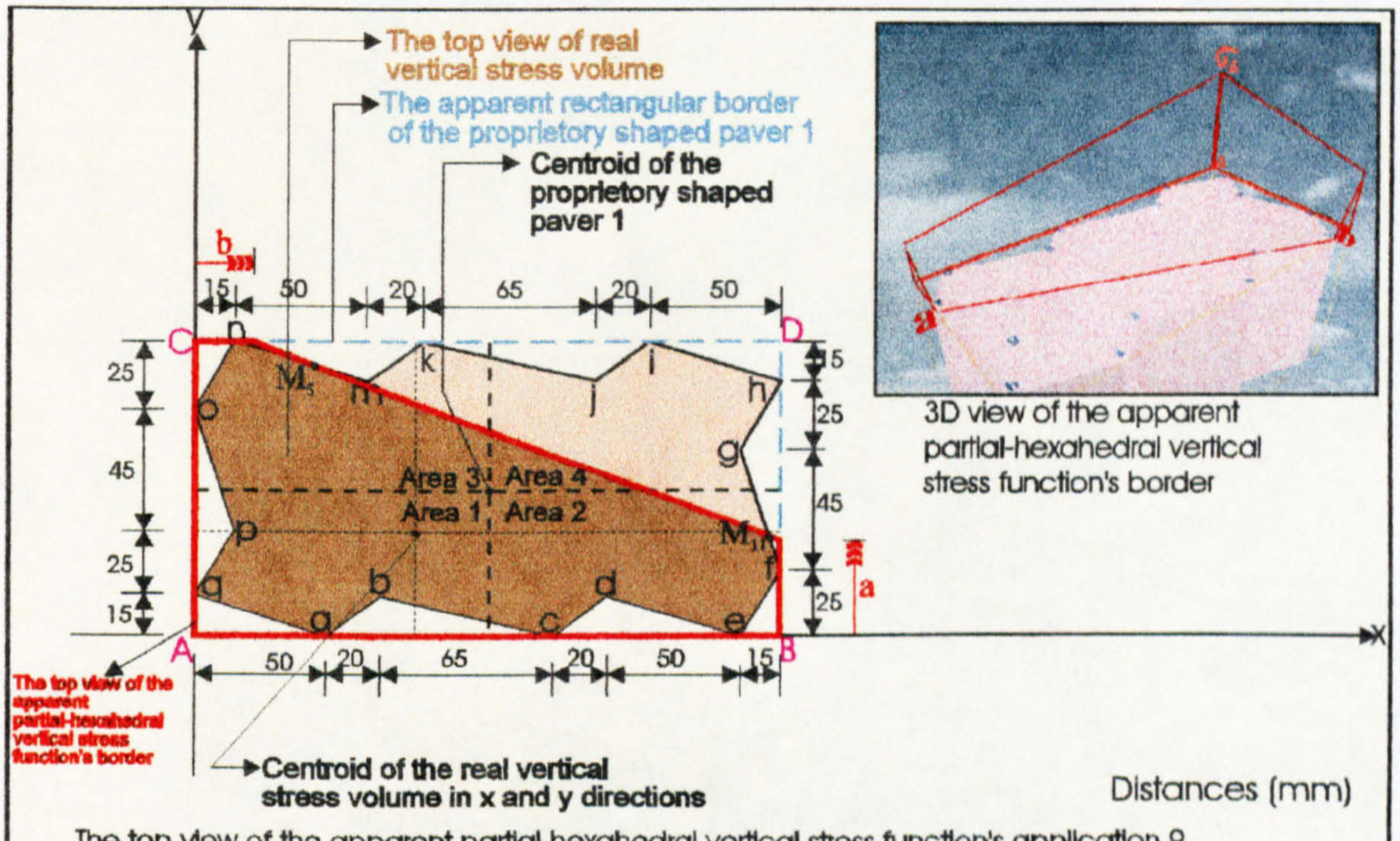

Figure 7.75: Application 9 of the partial-hexahedral compressive stress distribution beneath the circumscribing rectangular border of proprietory shaped paver 1.

The total volume **V** beneath the surface $f(x,y) = z\ (> 0)$ and above the region in the xy-plane (see Figure 7.75) is:

$$V = \int_0^b \int_0^{110} f(x,y)\,dy\,dx + \int_b^{220} \int_0^a f(x,y)\,dy\,dx + \int_b^{220} \int_a^{fy} f(x,y)\,dy\,dx - \int_{15}^{M_{5x}} \int_{M_{5y}}^{nmy} f(x,y)\,dy\,dx + \int_b^{M_{5x}} \int_{M_{5y}}^{fy} f(x,y)\,dy\,dx$$

$$- \int_0^{15} \int_{85}^{ony} f(x,y)\,dy\,dx - \int_0^{15} \int_{40}^{poy} f(x,y)\,dy\,dx - \int_0^{15} \int_{15}^{qpy} f(x,y)\,dy\,dx - \int_0^{50} \int_0^{qay} f(x,y)\,dy\,dx - \int_{50}^{70} \int_0^{aby} f(x,y)\,dy\,dx$$

$$- \int_{70}^{135} \int_0^{bcy} f(x,y)\,dy\,dx - \int_{135}^{155} \int_0^{cdy} f(x,y)\,dy\,dx - \int_{155}^{205} \int_0^{dey} f(x,y)\,dy\,dx - \int_{205}^{220} \int_0^{efy} f(x,y)\,dy\,dx - \int_{M_{11x}}^{220} \int_{25}^{fgy} f(x,y)\,dy\,dx$$

$$+ \int_{M_{11x}}^{220} \int_a^{fy} f(x,y)\,dy\,dx$$

and the centroids of this volume in the xy-plane are at distances $\overline{X}$ and $\overline{Y}$ from the axes (see Figure 7.75) which are given by the following equations.

$$\overline{X} = \frac{1}{V}\left[\begin{array}{l}
\int_{0}^{b}\int_{0}^{110} x f(x,y)\,dy\,dx + \int_{b}^{220}\int_{0}^{a} x f(x,y)\,dy\,dx + \int_{b}^{220}\int_{a}^{fy} x f(x,y)\,dy\,dx - \int_{15}^{M_{5x}}\int_{M_{5y}}^{nmy} x f(x,y)\,dy\,dx \\
+ \int_{b}^{M_{5x}}\int_{M_{5y}}^{fy} x f(x,y)\,dy\,dx - \int_{0}^{15}\int_{85}^{onv} x f(x,y)\,dy\,dx - \int_{0}^{15}\int_{40}^{poy} x f(x,y)\,dy\,dx - \int_{0}^{15}\int_{15}^{qpy} x f(x,y)\,dy\,dx \\
- \int_{0}^{50}\int_{0}^{qay} x f(x,y)\,dy\,dx - \int_{50}^{70}\int_{0}^{aby} x f(x,y)\,dy\,dx - \int_{70}^{135}\int_{0}^{bcy} x f(x,y)\,dy\,dx - \int_{135}^{155}\int_{0}^{cdy} x f(x,y)\,dy\,dx \\
- \int_{155}^{205}\int_{0}^{dey} x f(x,y)\,dy\,dx - \int_{205}^{220}\int_{0}^{efy} x f(x,y)\,dy\,dx - \int_{M_{11x}}^{220}\int_{25}^{fgy} x f(x,y)\,dy\,dx + \int_{M_{11x}}^{220}\int_{a}^{fy} x f(x,y)\,dy\,dx
\end{array}\right]$$

$$\overline{Y} = \frac{1}{V}\left[\begin{array}{l}
\int_{0}^{110}\int_{0}^{b} y f(x,y)\,dx\,dy + \int_{0}^{a}\int_{b}^{220} y f(x,y)\,dx\,dy + \int_{a}^{110}\int_{b}^{fx} y f(x,y)\,dx\,dy - \int_{M_{5y}}^{110}\int_{15}^{nmx} y f(x,y)\,dx\,dy \\
+ \int_{M_{5y}}^{110}\int_{b}^{fx} y f(x,y)\,dx\,dy - \int_{85}^{110}\int_{0}^{onx} y f(x,y)\,dx\,dy - \int_{40}^{85}\int_{0}^{pox} y f(x,y)\,dx\,dy - \int_{15}^{40}\int_{0}^{qpx} y f(x,y)\,dx\,dy \\
- \int_{0}^{15}\int_{0}^{qax} y f(x,y)\,dx\,dy - \int_{0}^{15}\int_{50}^{abx} y f(x,y)\,dx\,dy - \int_{0}^{15}\int_{70}^{bcx} y f(x,y)\,dx\,dy - \int_{0}^{15}\int_{135}^{cdx} y f(x,y)\,dx\,dy \\
- \int_{0}^{15}\int_{155}^{dex} y f(x,y)\,dx\,dy - \int_{0}^{25}\int_{205}^{efx} y f(x,y)\,dx\,dy - \int_{25}^{M_{11y}}\int_{M_{11x}}^{fgx} y f(x,y)\,dx\,dy + \int_{a}^{M_{11y}}\int_{M_{11x}}^{fx} y f(x,y)\,dx\,dy
\end{array}\right]$$

Application 10 of the partial-hexahedral compressive stress regime beneath the circumscribing rectangular border of proprietory shaped paver 1 shown in Figure 7.76 can be calculated by using Tables 5.1 and 7.4 and the surface function of the partial-hexahedral compressive stress through the three points σ_A, l and t.

The total volume V beneath the surface $f(x,y) = z\ (> 0)$ and above the region in the xy-plane (see Figure 7.76) is:

$$V = \int_{0}^{b}\int_{0}^{110} f(x,y)\,dy\,dx + \int_{b}^{220}\int_{0}^{a} f(x,y)\,dy\,dx + \int_{b}^{220}\int_{a}^{fy} f(x,y)\,dy\,dx - \int_{15}^{65}\int_{95}^{nmy} f(x,y)\,dy\,dx - \int_{65}^{85}\int_{95}^{mky} f(x,y)\,dy\,dx$$

$$+\int_{b}^{M_{6x}}\int_{M_{6y}}^{fy} f(x,y)\,dy\,dx+\int_{M_{6x}}^{85}\int_{M_{6y}}^{mky} f(x,y)\,dy\,dx-\int_{0}^{15}\int_{85}^{ony} f(x,y)\,dy\,dx-\int_{0}^{15}\int_{40}^{poy} f(x,y)\,dy\,dx-\int_{0}^{15}\int_{15}^{qpy} f(x,y)\,dy\,dx$$

$$-\int_{0}^{50}\int_{0}^{qay} f(x,y)\,dy\,dx-\int_{50}^{70}\int_{0}^{aby} f(x,y)\,dy\,dx-\int_{70}^{135}\int_{0}^{bcy} f(x,y)\,dy\,dx-\int_{135}^{155}\int_{0}^{cdy} f(x,y)\,dy\,dx-\int_{155}^{205}\int_{0}^{dey} f(x,y)\,dy\,dx$$

$$-\int_{205}^{220}\int_{0}^{efy} f(x,y)\,dy\,dx-\int_{M_{11x}}^{220}\int_{25}^{fgy} f(x,y)\,dy\,dx+\int_{M_{11x}}^{220}\int_{a}^{fy} f(x,y)\,dy\,dx$$

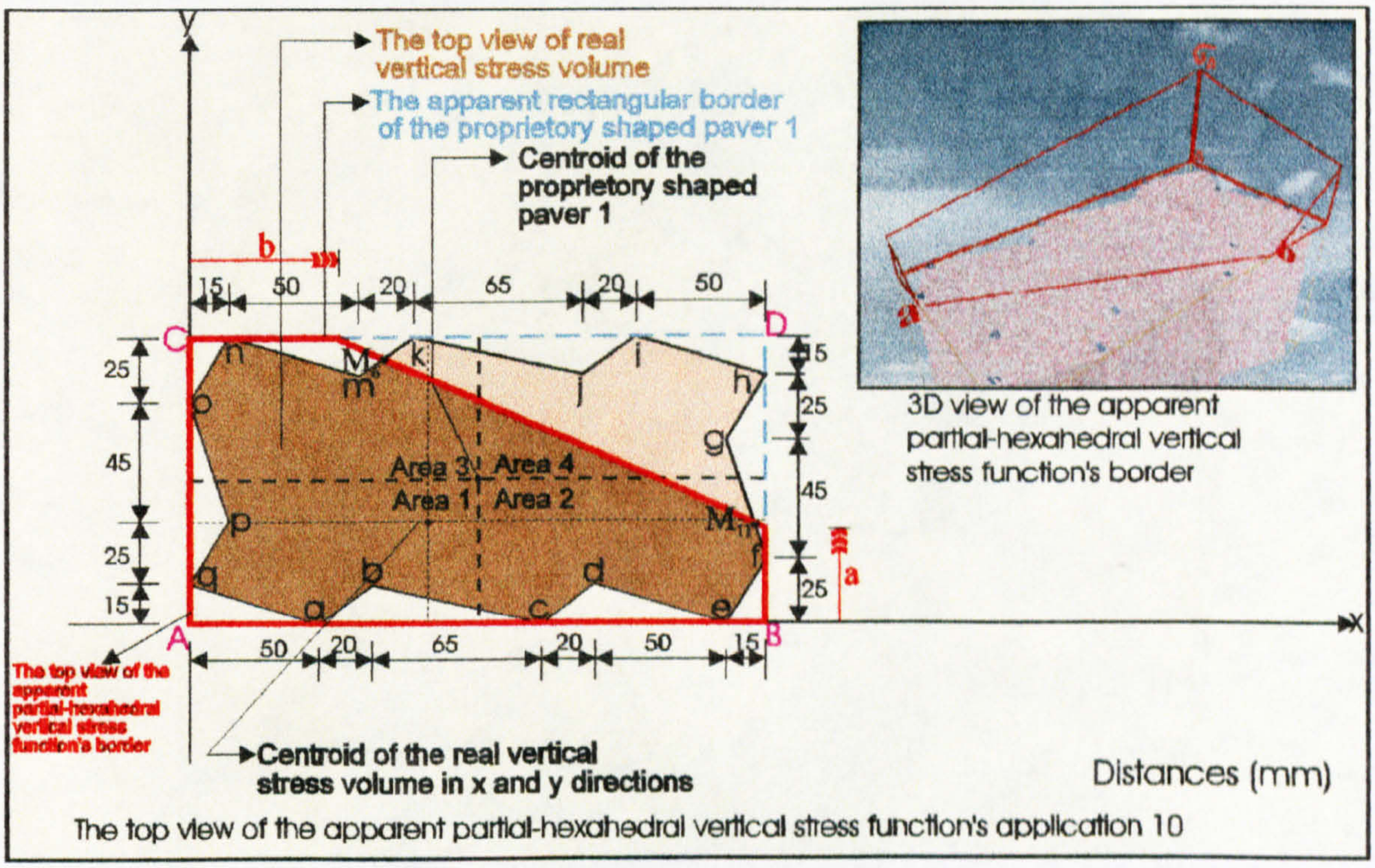

Figure 7.76: Application 10 of the partial-hexahedral compressive stress distribution beneath the circumscribing rectangular border of proprietory shaped paver 1.

and the centroids of this volume in the xy-plane are at distances $\overline{X}$ and $\overline{Y}$ from the axes (see Figure 7.76) which are given by the following equations.

$$\overline{X}=\frac{1}{V}\left[\int_{0}^{b}\int_{0}^{110} x\,f(x,y)\,dy\,dx+\int_{b}^{220}\int_{0}^{a} x\,f(x,y)\,dy\,dx+\int_{b}^{220}\int_{a}^{fy} x\,f(x,y)\,dy\,dx-\int_{15}^{65}\int_{95}^{nmy} x\,f(x,y)\,dy\,dx\right.$$

$$-\int_{65}^{85}\int_{95}^{mky} x\,f(x,y)\,dy\,dx+\int_{b}^{M_{6x}}\int_{M_{6y}}^{fy} x\,f(x,y)\,dy\,dx+\int_{M_{6x}}^{85}\int_{M_{6y}}^{mky} x\,f(x,y)\,dy\,dx-\int_{0}^{15}\int_{85}^{ony} x\,f(x,y)\,dy\,dx$$

$$\left.-\int_{0}^{15}\int_{40}^{poy} x\,f(x,y)\,dy\,dx-\int_{0}^{15}\int_{15}^{qpy} x\,f(x,y)\,dy\,dx-\int_{0}^{50}\int_{0}^{qay} x\,f(x,y)\,dy\,dx-\int_{50}^{70}\int_{0}^{aby} x\,f(x,y)\,dy\,dx\right.$$

$$-\int_{70}^{135}\int_{0}^{bcy} xf(x,y)\,dy\,dx-\int_{135}^{155}\int_{0}^{cdy} xf(x,y)\,dy\,dx-\int_{155}^{205}\int_{0}^{dey} xf(x,y)\,dy\,dx-\int_{205}^{220}\int_{0}^{efy} xf(x,y)\,dy\,dx$$

$$\left.-\int_{M_{11x}}^{220}\int_{25}^{fgy} xf(x,y)\,dy\,dx+\int_{M_{11x}}^{220}\int_{a}^{fy} xf(x,y)\,dy\,dx\right]$$

$$\overline{Y}=\frac{1}{V}\left[\begin{array}{l}
\int_{0}^{110}\int_{0}^{b} yf(x,y)\,dx\,dy+\int_{0}^{a}\int_{b}^{220} yf(x,y)\,dx\,dy+\int_{a}^{110}\int_{b}^{fx} yf(x,y)\,dx\,dy-\int_{95}^{110}\int_{15}^{nmx} yf(x,y)\,dx\,dy \\
-\int_{95}^{110}\int_{65}^{mkx} yf(x,y)\,dx\,dy+\int_{M_{6y}}^{110}\int_{b}^{fx} yf(x,y)\,dx\,dy+\int_{M_{6y}}^{110}\int_{M_{6x}}^{mkx} yf(x,y)\,dx\,dy-\int_{85}^{110}\int_{0}^{onx} yf(x,y)\,dx\,dy \\
-\int_{40}^{85}\int_{0}^{pox} yf(x,y)\,dx\,dy-\int_{15}^{40}\int_{0}^{qpx} yf(x,y)\,dx\,dy-\int_{0}^{15}\int_{0}^{qax} yf(x,y)\,dx\,dy-\int_{0}^{15}\int_{50}^{abx} yf(x,y)\,dx\,dy \\
-\int_{0}^{15}\int_{70}^{bcx} yf(x,y)\,dx\,dy-\int_{0}^{15}\int_{135}^{cdx} yf(x,y)\,dx\,dy-\int_{0}^{15}\int_{155}^{dex} yf(x,y)\,dx\,dy-\int_{0}^{25}\int_{205}^{efx} yf(x,y)\,dx\,dy \\
-\int_{25}^{M_{11y}}\int_{M_{11x}}^{fgx} yf(x,y)\,dx\,dy+\int_{a}^{M_{11y}}\int_{M_{11x}}^{fx} yf(x,y)\,dx\,dy
\end{array}\right]$$

Application 11 of the partial-hexahedral compressive stress regime beneath the circumscribing rectangular border of proprietory shaped paver 1 shown in Figure 7.77 can be calculated by using Tables 5.1 and 7.4 and the surface function of the partial-hexahedral compressive stress through the three points σ_A, **l** and **t**.

The total volume **V** beneath the surface $f(x,y) = z\ (> 0)$ and above the region in the xy-plane (see Figure 7.77) is:

$$V=\int_{0}^{b}\int_{0}^{110} f(x,y)\,dy\,dx+\int_{b}^{220}\int_{0}^{a} f(x,y)\,dy\,dx+\int_{b}^{220}\int_{a}^{fy} f(x,y)\,dy\,dx-\int_{15}^{65}\int_{95}^{nmy} f(x,y)\,dy\,dx-\int_{65}^{85}\int_{95}^{mky} f(x,y)\,dy\,dx$$

$$-\int_{85}^{M_{7x}}\int_{M_{7y}}^{kjy} f(x,y)\,dy\,dx+\int_{b}^{M_{7x}}\int_{M_{7y}}^{fy} f(x,y)\,dy\,dx-\int_{0}^{15}\int_{85}^{ony} f(x,y)\,dy\,dx-\int_{0}^{15}\int_{40}^{poy} f(x,y)\,dy\,dx-\int_{0}^{15}\int_{15}^{qpy} f(x,y)\,dy\,dx$$

$$-\int_{0}^{50}\int_{0}^{qay} f(x,y)\,dy\,dx-\int_{50}^{70}\int_{0}^{aby} f(x,y)\,dy\,dx-\int_{70}^{135}\int_{0}^{bcy} f(x,y)\,dy\,dx-\int_{135}^{155}\int_{0}^{cdy} f(x,y)\,dy\,dx-\int_{155}^{205}\int_{0}^{dky} f(x,y)\,dy\,dx$$

$$-\int_{205}^{220}\int_{0}^{efy} f(x,y)\,dy\,dx - \int_{M_{11x}}^{220}\int_{25}^{fgy} f(x,y)\,dy\,dx + \int_{M_{11x}}^{220}\int_{a}^{fy} f(x,y)\,dy\,dx$$

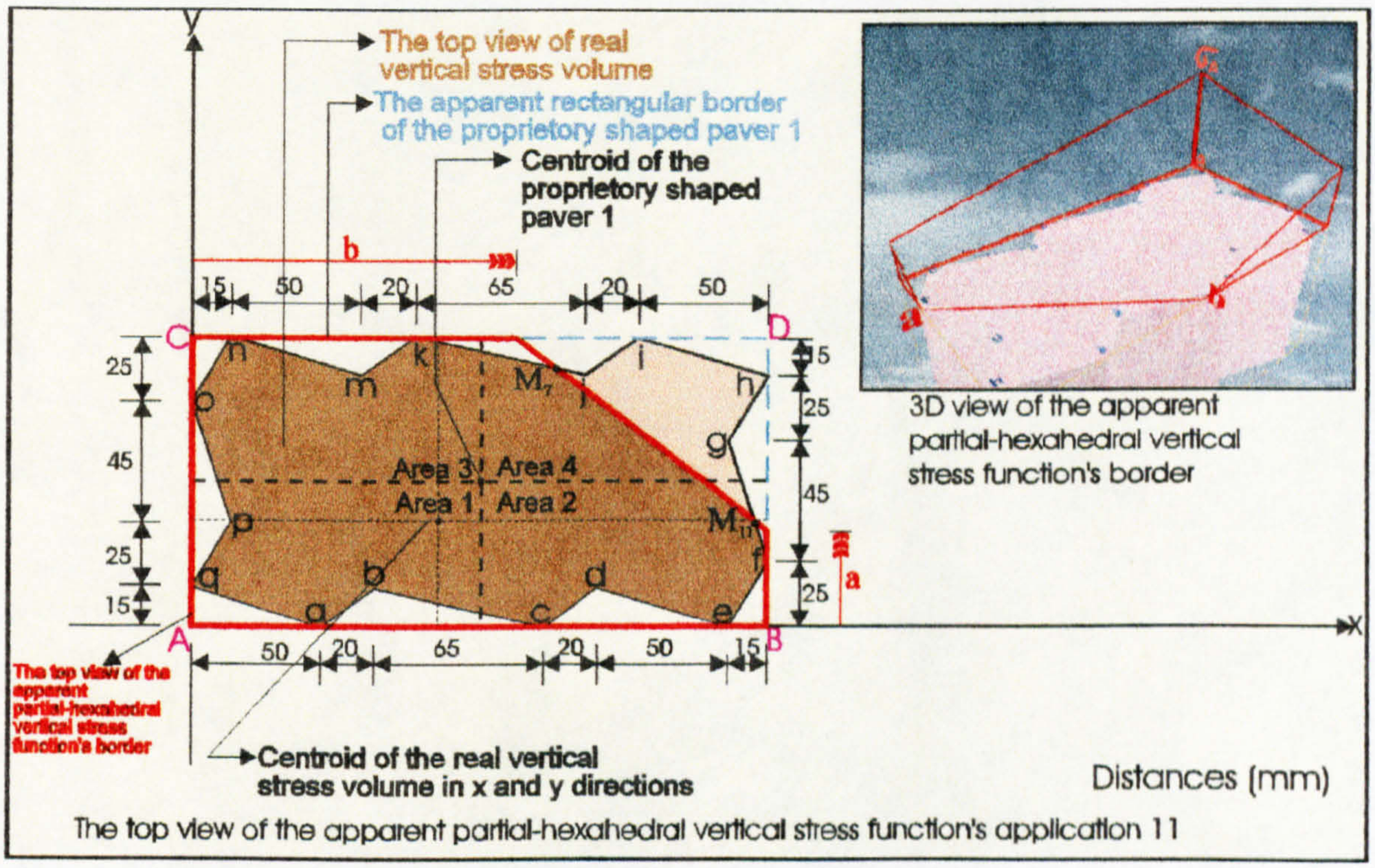

Figure 7.77: Application 11 of the partial-hexahedral compressive stress distribution beneath the circumscribing rectangular border of proprietory shaped paver 1.

and the centroids of this volume in the xy-plane are at distances $\overline{X}$ and $\overline{Y}$ from the axes (see Figure 7.77) which are given by the following equations.

$$\overline{X} = \frac{1}{V}\left[\int_{0}^{b}\int_{0}^{110} x f(x,y)\,dy\,dx + \int_{b}^{220}\int_{0}^{a} x f(x,y)\,dy\,dx + \int_{b}^{220}\int_{a}^{fy} x f(x,y)\,dy\,dx - \int_{15}^{65}\int_{95}^{nmy} x f(x,y)\,dy\,dx\right.$$

$$-\int_{65}^{85}\int_{95}^{mky} x f(x,y)\,dy\,dx - \int_{85}^{M_{7x}}\int_{M_{7y}}^{kjy} x f(x,y)\,dy\,dx + \int_{b}^{M_{7x}}\int_{M_{7y}}^{fy} x f(x,y)\,dy\,dx - \int_{0}^{15}\int_{85}^{ony} x f(x,y)\,dy\,dx$$

$$-\int_{0}^{15}\int_{40}^{poy} x f(x,y)\,dy\,dx - \int_{0}^{15}\int_{15}^{qpy} x f(x,y)\,dy\,dx - \int_{0}^{50}\int_{0}^{qay} x f(x,y)\,dy\,dx - \int_{50}^{70}\int_{0}^{aby} x f(x,y)\,dy\,dx$$

$$\left.-\int_{70}^{135}\int_{0}^{bcy} x f(x,y)\,dy\,dx - \int_{135}^{155}\int_{0}^{cdy} x f(x,y)\,dy\,dx - \int_{155}^{205}\int_{0}^{dey} x f(x,y)\,dy\,dx - \int_{205}^{220}\int_{0}^{efy} x f(x,y)\,dy\,dx\right]$$

$$-\int_{M_{11x}}^{220}\int_{25}^{fgy} x f(x,y)\,dy\,dx + \int_{M_{11x}}^{220}\int_{a}^{fy} x f(x,y)\,dy\,dx\Bigg]$$

$$\bar{Y} = \frac{1}{V}\left[\begin{array}{l}
\int_{0}^{110}\int_{0}^{b} y f(x,y)\,dx\,dy + \int_{0}^{a}\int_{b}^{220} y f(x,y)\,dx\,dy + \int_{a}^{110}\int_{b}^{fx} y f(x,y)\,dx\,dy - \int_{95}^{110}\int_{15}^{nmx} y f(x,y)\,dx\,dy \\
-\int_{95}^{110}\int_{65}^{mkx} y f(x,y)\,dx\,dy - \int_{M_{7y}}^{110}\int_{85}^{kjx} y f(x,y)\,dx\,dy + \int_{M_{7y}}^{110}\int_{85}^{fx} y f(x,y)\,dx\,dy - \int_{85}^{110}\int_{0}^{onx} y f(x,y)\,dx\,dy \\
-\int_{40}^{85}\int_{0}^{pox} y f(x,y)\,dx\,dy - \int_{15}^{40}\int_{0}^{qpx} y f(x,y)\,dx\,dy - \int_{0}^{15}\int_{0}^{qax} y f(x,y)\,dx\,dy - \int_{0}^{15}\int_{50}^{abx} y f(x,y)\,dx\,dy \\
-\int_{0}^{15}\int_{70}^{bcx} y f(x,y)\,dx\,dy - \int_{0}^{15}\int_{135}^{cdx} y f(x,y)\,dx\,dy - \int_{0}^{15}\int_{155}^{dex} y f(x,y)\,dx\,dy - \int_{0}^{25}\int_{205}^{efx} y f(x,y)\,dx\,dy \\
-\int_{25}^{M_{11y}}\int_{M_{11x}}^{fgx} y f(x,y)\,dx\,dy + \int_{a}^{M_{11y}}\int_{M_{11x}}^{fx} y f(x,y)\,dx\,dy
\end{array}\right]$$

Application 12 of the partial-hexahedral compressive stress regime beneath the circumscribing rectangular border of proprietory shaped paver 1 shown in Figure 7.78 can be calculated by using Tables 5.1 and 7.4 and the surface function of the partial-hexahedral compressive stress through the three points σ_A, **l** and **t**.

The total volume **V** beneath the surface $f(x,y) = z\ (> 0)$ and above the region in the xy-plane (see Figure 7.78) is:

$$V = \int_{0}^{b}\int_{0}^{110} f(x,y)\,dy\,dx + \int_{b}^{220}\int_{0}^{a} f(x,y)\,dy\,dx + \int_{b}^{220}\int_{a}^{fy} f(x,y)\,dy\,dx - \int_{15}^{65}\int_{95}^{nmy} f(x,y)\,dy\,dx - \int_{65}^{85}\int_{95}^{mky} f(x,y)\,dy\,dx$$

$$-\int_{85}^{150}\int_{95}^{kjy} f(x,y)\,dy\,dx - \int_{150}^{170}\int_{95}^{jiy} f(x,y)\,dy\,dx + \int_{b}^{M_{8x}}\int_{M_{8y}}^{fy} f(x,y)\,dy\,dx + \int_{M_{8x}}^{170}\int_{M_{8y}}^{jiy} f(x,y)\,dy\,dx - \int_{0}^{15}\int_{85}^{omy} f(x,y)\,dy\,dx$$

$$-\int_{0}^{15}\int_{40}^{poy} f(x,y)\,dy\,dx - \int_{0}^{15}\int_{15}^{qpy} f(x,y)\,dy\,dx - \int_{0}^{50}\int_{0}^{qay} f(x,y)\,dy\,dx - \int_{50}^{70}\int_{0}^{aby} f(x,y)\,dy\,dx - \int_{70}^{135}\int_{0}^{bcy} f(x,y)\,dy\,dx$$

$$-\int_{135}^{155}\int_{0}^{cdy} f(x,y)\,dy\,dx - \int_{155}^{205}\int_{0}^{dey} f(x,y)\,dy\,dx - \int_{205}^{220}\int_{0}^{efy} f(x,y)\,dy\,dx - \int_{M_{11x}}^{220}\int_{25}^{fgy} f(x,y)\,dy\,dx + \int_{M_{11x}}^{220}\int_{a}^{fy} f(x,y)\,dy\,dx$$

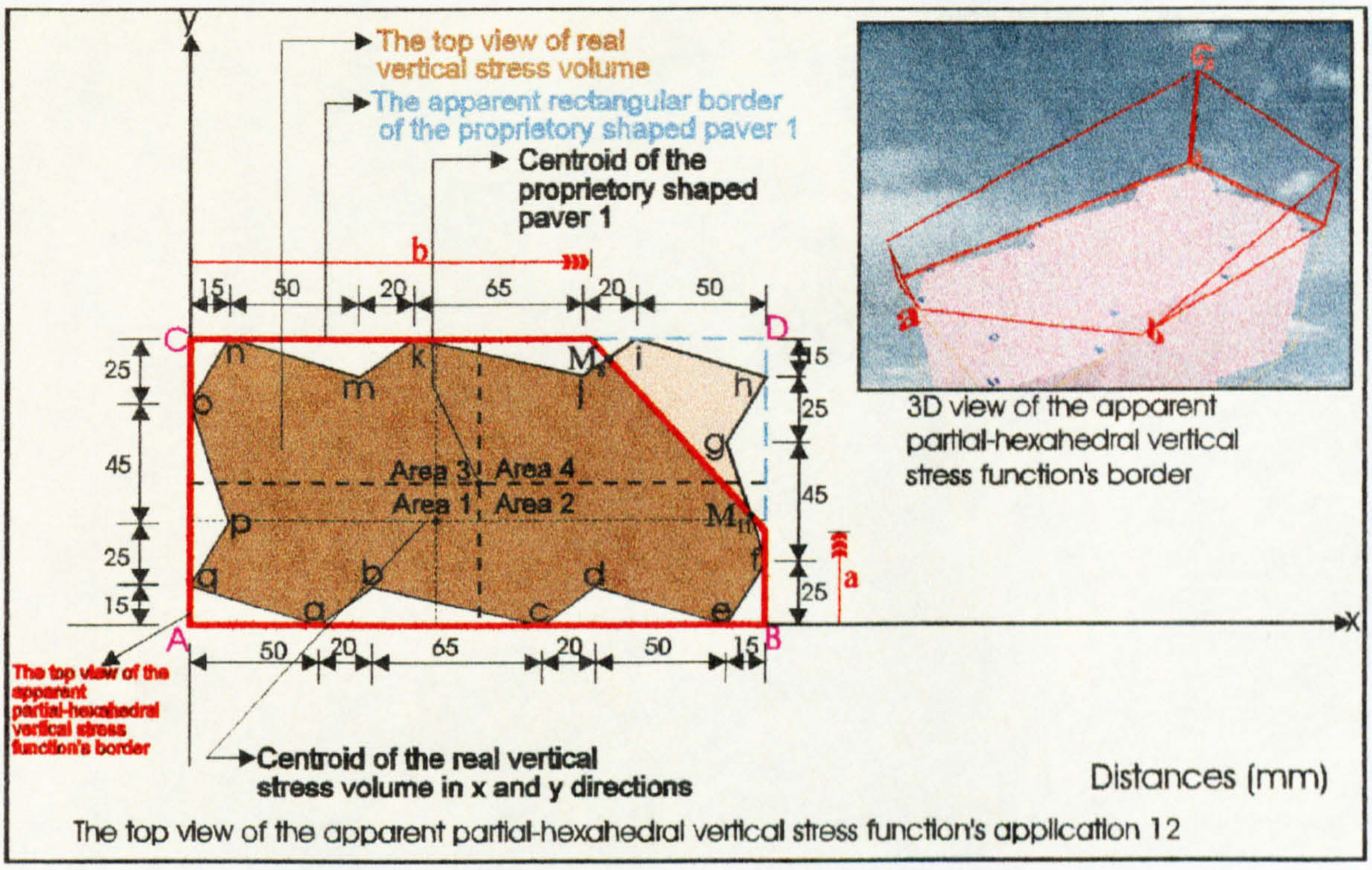

The top view of the apparent partial-hexahedral vertical stress function's application 12

Figure 7.78: Application 12 of the partial-hexahedral compressive stress distribution beneath the circumscribing rectangular border of proprietory shaped paver 1.

and the centroids of this volume in the xy-plane are at distances $\overline{X}$ and $\overline{Y}$ from the axes (see Figure 7.78) which are given by the following equations.

$$\overline{X} = \frac{1}{V}\left[\int_0^b\int_0^{110} x f(x,y)\,dy\,dx + \int_b^{220}\int_0^{a} x f(x,y)\,dy\,dx + \int_b^{220}\int_a^{fy} x f(x,y)\,dy\,dx - \int_{15}^{65}\int_{95}^{nmy} x f(x,y)\,dy\,dx\right.$$
$$- \int_{65}^{85}\int_{95}^{mky} x f(x,y)\,dy\,dx - \int_{85}^{150}\int_{95}^{kjy} x f(x,y)\,dy\,dx - \int_{150}^{170}\int_{95}^{jiy} x f(x,y)\,dy\,dx + \int_b^{M_{8x}}\int_{M_{8y}}^{fy} x f(x,y)\,dy\,dx$$
$$+ \int_{M_{8x}}^{170}\int_{M_{8y}}^{jiy} x f(x,y)\,dy\,dx - \int_0^{85}\int_{15}^{ony} x f(x,y)\,dy\,dx - \int_0^{40}\int_{15}^{poy} x f(x,y)\,dy\,dx - \int_0^{15}\int_{15}^{qpy} x f(x,y)\,dy\,dx$$
$$- \int_0^{50}\int_0^{qay} x f(x,y)\,dy\,dx - \int_{50}^{70}\int_0^{aby} x f(x,y)\,dy\,dx - \int_{70}^{135}\int_0^{bcy} x f(x,y)\,dy\,dx - \int_{135}^{155}\int_0^{cdy} x f(x,y)\,dy\,dx$$
$$\left. - \int_{155}^{205}\int_0^{dey} x f(x,y)\,dy\,dx - \int_{205}^{220}\int_0^{efy} x f(x,y)\,dy\,dx - \int_{M_{11x}}^{220}\int_{25}^{fgy} x f(x,y)\,dy\,dx + \int_{M_{11x}}^{220}\int_{a}^{fy} x f(x,y)\,dy\,dx\right]$$

$$\overline{Y} = \frac{1}{V}\left[\begin{array}{l}
\int_{0}^{110}\int_{0}^{b} yf(x,y)\,dx\,dy + \int_{0}^{a}\int_{b}^{220} yf(x,y)\,dx\,dy + \int_{a}^{110}\int_{b}^{fx} yf(x,y)\,dx\,dy - \int_{95}^{110}\int_{15}^{nmx} yf(x,y)\,dx\,dy \\
-\int_{95}^{110}\int_{65}^{mkx} yf(x,y)\,dx\,dy - \int_{95}^{110}\int_{85}^{kjx} yf(x,y)\,dx\,dy - \int_{95}^{110}\int_{150}^{jix} yf(x,y)\,dx\,dy + \int_{M_{8y}}^{110}\int_{b}^{fx} yf(x,y)\,dx\,dy \\
+\int_{M_{8y}}^{110}\int_{M_{8x}}^{jix} yf(x,y)\,dx\,dy - \int_{85}^{110}\int_{0}^{onx} yf(x,y)\,dx\,dy - \int_{40}^{85}\int_{0}^{pox} yf(x,y)\,dx\,dy - \int_{15}^{40}\int_{0}^{kjpx} yf(x,y)\,dx\,dy \\
-\int_{0}^{15}\int_{0}^{qax} yf(x,y)\,dx\,dy - \int_{0}^{15}\int_{50}^{abx} yf(x,y)\,dx\,dy - \int_{0}^{15}\int_{70}^{bcx} yf(x,y)\,dx\,dy - \int_{0}^{15}\int_{135}^{cdx} yf(x,y)\,dx\,dy \\
-\int_{0}^{15}\int_{155}^{dex} yf(x,y)\,dx\,dy - \int_{0}^{25}\int_{205}^{efx} yf(x,y)\,dx\,dy - \int_{25}^{M_{11y}}\int_{M_{11x}}^{fgx} yf(x,y)\,dx\,dy + \int_{a}^{M_{11y}}\int_{M_{11x}}^{fx} yf(x,y)\,dx\,dy
\end{array}\right]$$

Application 13 of the partial-hexahedral compressive stress regime beneath the circumscribing rectangular border of proprietory shaped paver 1 shown in Figure 7.79 can be calculated by using Tables 5.1 and 7.4 and the surface function of the partial-hexahedral compressive stress through the three points σ_A, **l** and **t**.

The total volume **V** beneath the surface $f(x,y) = z\ (> 0)$ and above the region in the xy-plane (see Figure 7.79) is:

$$\begin{array}{l}
V = \int_{0}^{b}\int_{0}^{110} f(x,y)\,dy\,dx + \int_{b}^{220}\int_{0}^{a} f(x,y)\,dy\,dx + \int_{b}^{220}\int_{a}^{fy} f(x,y)\,dy\,dx - \int_{15}^{65}\int_{95}^{nmy} f(x,y)\,dy\,dx - \int_{65}^{85}\int_{95}^{mky} f(x,y)\,dy\,dx \\
-\int_{85}^{150}\int_{95}^{kjy} f(x,y)\,dy\,dx - \int_{150}^{170}\int_{95}^{jiy} f(x,y)\,dy\,dx - \int_{170}^{M_{9x}}\int_{M_{9y}}^{hiy} f(x,y)\,dy\,dx + \int_{b}^{M_{9x}}\int_{M_{9y}}^{fy} f(x,y)\,dy\,dx - \int_{0}^{15}\int_{85}^{omy} f(x,y)\,dy\,dx \\
-\int_{0}^{15}\int_{40}^{poy} f(x,y)\,dy\,dx - \int_{0}^{15}\int_{0}^{qpy} f(x,y)\,dy\,dx - \int_{50}^{70}\int_{0}^{qay} f(x,y)\,dy\,dx - \int_{70}^{135}\int_{0}^{uby} f(x,y)\,dy\,dx - \int_{135}^{155}\int_{0}^{bcy} f(x,y)\,dy\,dx \\
-\int_{155}^{205}\int_{0}^{cdy} f(x,y)\,dy\,dx - \int_{205}^{220}\int_{0}^{dey} f(x,y)\,dy\,dx - \int_{M_{11x}}^{220}\int_{25}^{efy} f(x,y)\,dy\,dx + \int_{M_{11x}}^{220}\int_{a}^{fxy} f(x,y)\,dy\,dx
\end{array}$$

and the centroids of this volume in the xy-plane are at distances $\overline{X}$ and $\overline{Y}$ from the axes (see Figure 7.79) which are given by the following equations.

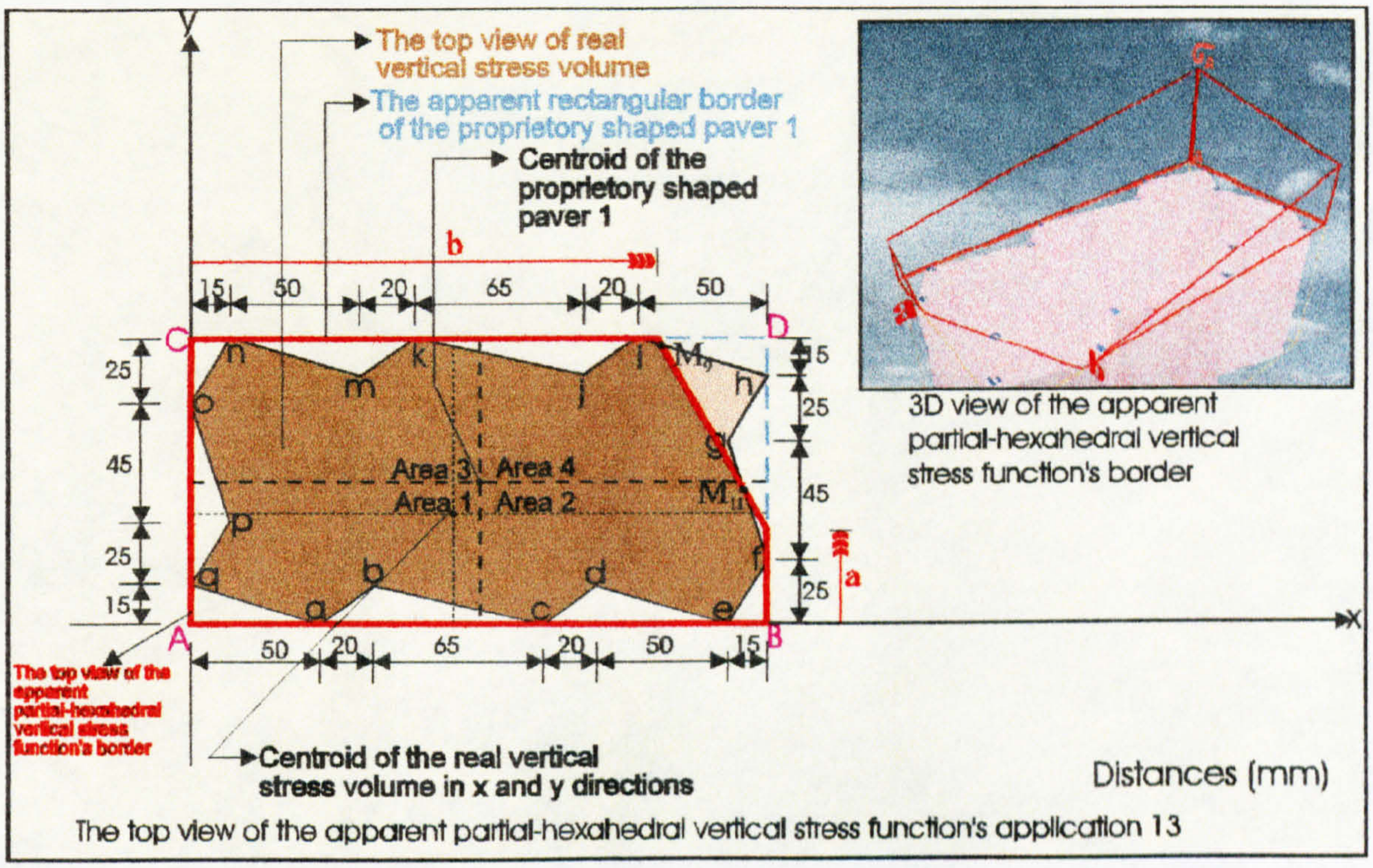

Figure 7.79: Application 13 of the partial-hexahedral compressive stress distribution beneath the circumscribing rectangular border of proprietory shaped paver 1.

$$\overline{X} = \frac{1}{V}\left[\int_0^b\int_0^{110} x f(x,y)\,dy\,dx + \int_b^{220}\int_0^a x f(x,y)\,dy\,dx + \int_b^{220}\int_a^{fy} x f(x,y)\,dy\,dx - \int_{15}^{65}\int_{95}^{nmy} x f(x,y)\,dy\,dx - \int_{65}^{85}\int_{95}^{mky} x f(x,y)\,dy\,dx - \int_{85}^{150}\int_{95}^{kjy} x f(x,y)\,dy\,dx - \int_{150}^{170}\int_{95}^{jiy} x f(x,y)\,dy\,dx - \int_{170}^{M_{9x}}\int_{M_{9y}}^{hiy} x f(x,y)\,dy\,dx + \int_b^{M_{9x}}\int_{M_{9y}}^{fy} x f(x,y)\,dy\,dx - \int_0^{85}\int_{15}^{ony} x f(x,y)\,dy\,dx - \int_0^{40}\int_{15}^{poy} x f(x,y)\,dy\,dx - \int_0^{15}\int_{15}^{qpy} x f(x,y)\,dy\,dx - \int_0^{0}\int_{50}^{qay} x f(x,y)\,dy\,dx - \int_{50}^{0}\int_{70}^{aby} x f(x,y)\,dy\,dx - \int_{70}^{0}\int_{135}^{bcy} x f(x,y)\,dy\,dx - \int_{135}^{0}\int_{155}^{cdy} x f(x,y)\,dy\,dx - \int_{155}^{0}\int_{205}^{dey} x f(x,y)\,dy\,dx - \int_{205}^{0}\int_{M_{11x}}^{efy} x f(x,y)\,dy\,dx - \int_{M_{11x}}^{25}\int_{a}^{fgy} x f(x,y)\,dy\,dx + \int_{M_{11x}}^{a}\int_{a}^{fy} x f(x,y)\,dy\,dx\right]$$

$$\overline{Y} = \frac{1}{V}\left[\int_0^{110}\int_0^{b} y f(x,y)\,dx\,dy + \int_0^{a}\int_b^{220} y f(x,y)\,dx\,dy + \int_a^{110}\int_b^{fx} y f(x,y)\,dx\,dy - \int_{95}^{110}\int_{15}^{nmx} y f(x,y)\,dx\,dy - \int_{95}^{110}\int_{65}^{mkx} y f(x,y)\,dx\,dy - \int_{95}^{110}\int_{85}^{kjx} y f(x,y)\,dx\,dy - \int_{95}^{110}\int_{150}^{jix} y f(x,y)\,dx\,dy - \int_{M_{9y}}^{110}\int_{170}^{hix} y f(x,y)\,dx\,dy\right]$$

$$+\int_{M_{9y}}^{110}\int_{b}^{fx} y f(x,y)\,dx\,dy-\int_{85}^{110}\int_{0}^{onx} y f(x,y)\,dx\,dy-\int_{40}^{85}\int_{0}^{pox} y f(x,y)\,dx\,dy-\int_{15}^{40}\int_{0}^{qpx} y f(x,y)\,dx\,dy$$

$$-\int_{0}^{15}\int_{0}^{qax} y f(x,y)\,dx\,dy-\int_{0}^{15}\int_{50}^{abx} y f(x,y)\,dx\,dy-\int_{0}^{15}\int_{70}^{bcx} y f(x,y)\,dx\,dy-\int_{0}^{15}\int_{135}^{cdx} y f(x,y)\,dx\,dy$$

$$-\int_{0}^{15}\int_{155}^{dex} y f(x,y)\,dx\,dy-\int_{0}^{25}\int_{205}^{efx} y f(x,y)\,dx\,dy-\int_{25}^{M_{11y}}\int_{M_{11x}}^{fgx} y f(x,y)\,dx\,dy+\int_{a}^{M_{11y}}\int_{M_{11x}}^{fx} y f(x,y)\,dx\,dy\Bigg]$$

Application 14 of the partial-hexahedral compressive stress regime beneath the circumscribing rectangular border of proprietory shaped paver 1 shown in Figure 7.80 can be calculated by using Tables 5.1 and 7.4 and the surface function of the partial-hexahedral compressive stress through the three points σ_A, **l** and **t**.

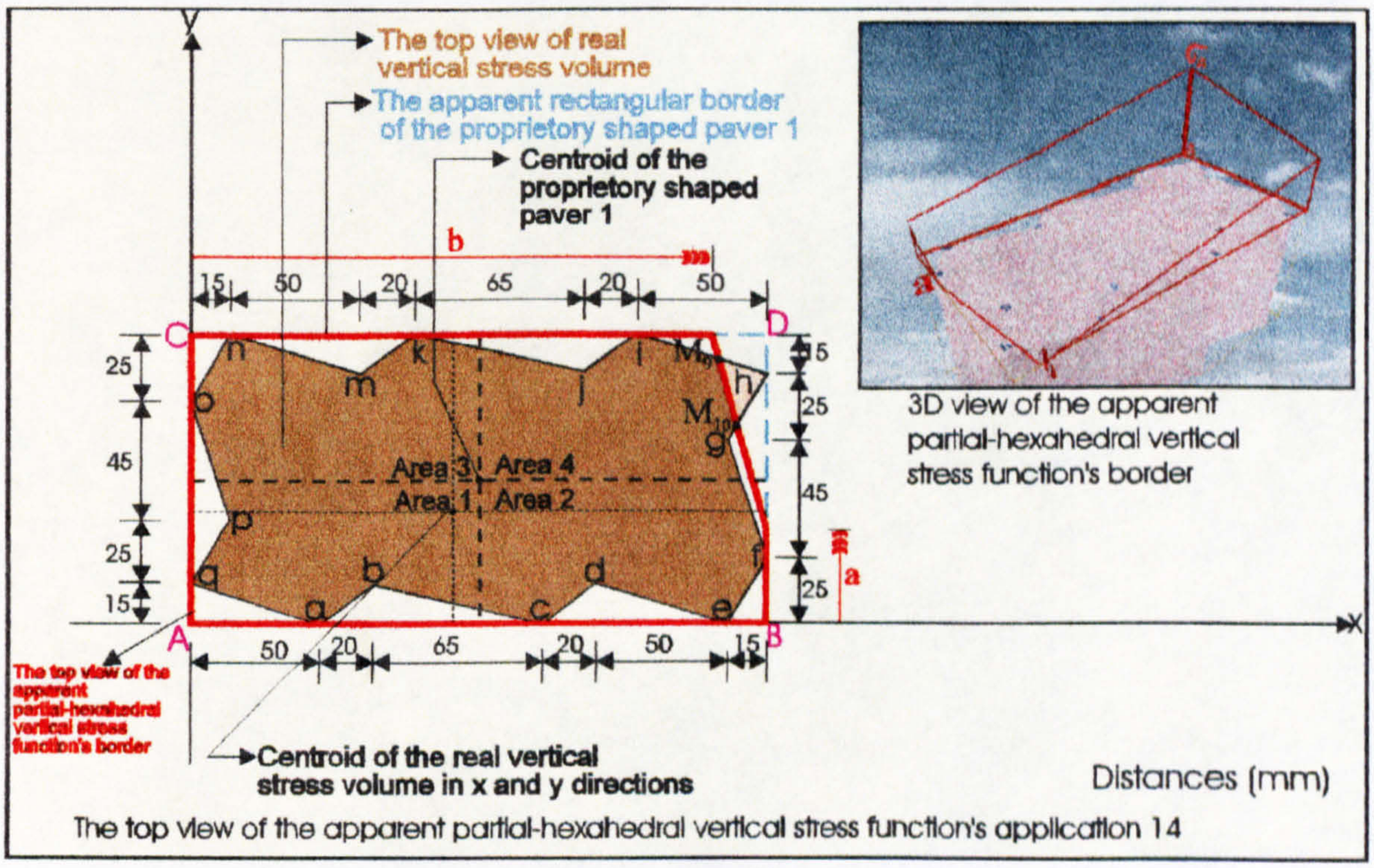

Figure 7.80: Application 14 of the partial-hexahedral compressive stress distribution beneath the circumscribing rectangular border of proprietory shaped paver 1.

The total volume **V** beneath the surface $f(x,y) = z\ (> 0)$ and above the region in the xy-plane (see Figure 7.80) is:

$$V = \int_0^b \int_0^{110} f(x,y)\,dy\,dx + \int_b^{220} \int_0^a f(x,y)\,dy\,dx + \int_b^{220} \int_a^{fy} f(x,y)\,dy\,dx - \int_{15}^{65} \int_{95}^{smy} f(x,y)\,dy\,dx - \int_{65}^{85} \int_{95}^{nky} f(x,y)\,dy\,dx$$
$$- \int_{85}^{150} \int_{95}^{kjy} f(x,y)\,dy\,dx - \int_{150}^{170} \int_{95}^{jiy} f(x,y)\,dy\,dx - \int_{170}^{M_{9x}} \int_{M_{9y}}^{hiy} f(x,y)\,dy\,dx + \int_b^{M_{9x}} \int_{M_{9y}}^{fy} f(x,y)\,dy\,dx - \int_0^{15} \int_{85}^{smy} f(x,y)\,dy\,dx$$
$$- \int_0^{15} \int_{40}^{poy} f(x,y)\,dy\,dx - \int_0^{15} \int_{15}^{qpy} f(x,y)\,dy\,dx - \int_0^{50} \int_0^{qay} f(x,y)\,dy\,dx - \int_{50}^{70} \int_0^{nby} f(x,y)\,dy\,dx - \int_{70}^{135} \int_0^{bcy} f(x,y)\,dy\,dx$$
$$- \int_{135}^{155} \int_0^{cdy} f(x,y)\,dy\,dx - \int_{155}^{205} \int_0^{dey} f(x,y)\,dy\,dx - \int_{205}^{220} \int_0^{efy} f(x,y)\,dy\,dx - \int_{M_{11x}}^{220} \int_{25}^{fgy} f(x,y)\,dy\,dx + \int_{M_{11x}}^{220} \int_a^{fy} f(x,y)\,dy\,dx$$
$$- \int_{205}^{220} \int_{70}^{ghy} f(x,y)\,dy\,dx - \int_{205}^{220} \int_{25}^{fgy} f(x,y)\,dy\,dx + \int_{M_{10x}}^{220} \int_{M_{10y}}^{ghy} f(x,y)\,dy\,dx + \int_{M_{10x}}^{220} \int_a^{fy} f(x,y)\,dy\,dx$$

and the centroids of this volume in the xy-plane are at distances $\overline{X}$ and $\overline{Y}$ from the axes (see Figure 7.80) which are given by the following equations.

$$\overline{X} = \frac{1}{V}\left[\int_0^b \int_0^{110} x f(x,y)\,dy\,dx + \int_b^{220} \int_0^a x f(x,y)\,dy\,dx + \int_b^{220} \int_a^{fy} x f(x,y)\,dy\,dx - \int_{15}^{65} \int_{95}^{smy} x f(x,y)\,dy\,dx - \int_{65}^{85} \int_{95}^{mky} x f(x,y)\,dy\,dx - \int_{85}^{150} \int_{95}^{kjy} x f(x,y)\,dy\,dx - \int_{150}^{170} \int_{95}^{jiy} x f(x,y)\,dy\,dx - \int_{170}^{M_{9x}} \int_{M_{9y}}^{hiy} x f(x,y)\,dy\,dx \right.$$
$$+ \int_b^{M_{9x}} \int_{M_{9y}}^{fy} x f(x,y)\,dy\,dx - \int_0^{15} \int_{85}^{smy} x f(x,y)\,dy\,dx - \int_0^{15} \int_{40}^{poy} x f(x,y)\,dy\,dx - \int_0^{15} \int_{15}^{qpy} x f(x,y)\,dy\,dx$$
$$- \int_0^{50} \int_0^{qay} x f(x,y)\,dy\,dx - \int_{50}^{70} \int_0^{nby} x f(x,y)\,dy\,dx - \int_{70}^{135} \int_0^{bcy} x f(x,y)\,dy\,dx - \int_{135}^{155} \int_0^{cdy} x f(x,y)\,dy\,dx$$
$$- \int_{155}^{205} \int_0^{dey} x f(x,y)\,dy\,dx - \int_{205}^{220} \int_0^{efy} x f(x,y)\,dy\,dx - \int_{M_{11x}}^{220} \int_{25}^{fgy} x f(x,y)\,dy\,dx + \int_{M_{11x}}^{220} \int_a^{fy} x f(x,y)\,dy\,dx$$
$$\left. - \int_{205}^{220} \int_{70}^{ghy} x f(x,y)\,dy\,dx - \int_{205}^{220} \int_{25}^{fgy} x f(x,y)\,dy\,dx + \int_{M_{10x}}^{220} \int_{M_{10y}}^{ghy} x f(x,y)\,dy\,dx + \int_{M_{10x}}^{220} \int_a^{fy} x f(x,y)\,dy\,dx \right]$$

$$\overline{Y} = \frac{1}{V}\left[\int_0^{110} \int_0^b y f(x,y)\,dx\,dy + \int_0^a \int_b^{220} y f(x,y)\,dx\,dy + \int_a^{110} \int_b^{fx} y f(x,y)\,dx\,dy - \int_{95}^{110} \int_{15}^{nmx} y f(x,y)\,dx\,dy \right.$$
$$- \int_{95}^{110} \int_{65}^{mkx} y f(x,y)\,dx\,dy - \int_{95}^{110} \int_{85}^{kjx} y f(x,y)\,dx\,dy - \int_{95}^{110} \int_{150}^{jix} y f(x,y)\,dx\,dy - \int_{M_{9y}}^{110} \int_{170}^{hix} y f(x,y)\,dx\,dy$$

$$+\int_{M_{9y}}^{110}\int_{b}^{fx} y f(x,y)\,dx\,dy-\int_{85}^{110}\int_{0}^{onx} y f(x,y)\,dx\,dy-\int_{40}^{85}\int_{0}^{pox} y f(x,y)\,dx\,dy-\int_{15}^{40}\int_{0}^{qpx} y f(x,y)\,dx\,dy$$

$$-\int_{0}^{15}\int_{0}^{qax} y f(x,y)\,dx\,dy-\int_{0}^{15}\int_{50}^{abx} y f(x,y)\,dx\,dy-\int_{0}^{15}\int_{70}^{bcx} y f(x,y)\,dx\,dy-\int_{0}^{15}\int_{135}^{cdx} y f(x,y)\,dx\,dy$$

$$-\int_{0}^{15}\int_{155}^{dex} y f(x,y)\,dx\,dy-\int_{0}^{25}\int_{205}^{efx} y f(x,y)\,dx\,dy-\int_{25}^{M_{11y}}\int_{M_{11x}}^{fgx} y f(x,y)\,dx\,dy+\int_{a}^{M_{11y}}\int_{M_{11x}}^{fx} y f(x,y)\,dx\,dy$$

$$-\int_{70}^{95}\int_{205}^{ghx} y f(x,y)\,dx\,dy-\int_{25}^{70}\int_{205}^{fgx} y f(x,y)\,dx\,dy+\int_{M_{10y}}^{95}\int_{M_{10x}}^{ghx} y f(x,y)\,dx\,dy+\int_{a}^{70}\int_{M_{10x}}^{fx} y f(x,y)\,dx\,dy\Bigg]$$

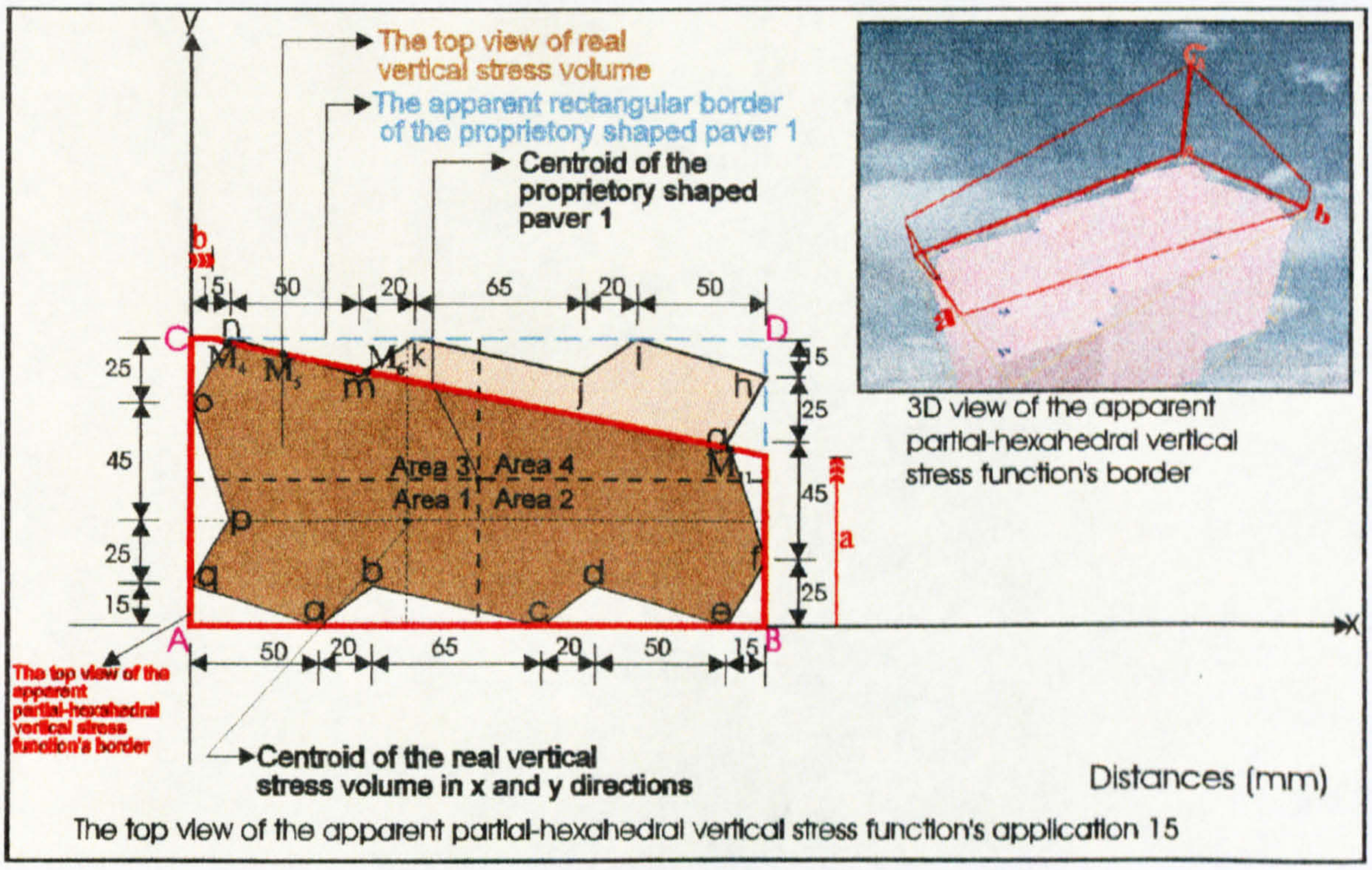

Figure 7.81: Application 15 of the partial-hexahedral compressive stress distribution beneath the circumscribing rectangular border of proprietory shaped paver 1.

Application 15 of the partial-hexahedral compressive stress regime beneath the circumscribing rectangular border of proprietory shaped paver 1 shown in Figure 7.81 can be calculated by using Tables 5.1 and 7.4 and the surface function of the partial-hexahedral compressive stress through the three points σ_A, **l** and **t**.

The total volume **V** beneath the surface $f(x,y) = z\ (> 0)$ and above the region in the xy-plane (see Figure 7.81) is:

$$V = \int_0^b \int_0^{110} f(x,y)\,dy\,dx + \int_b^{220} \int_0^a f(x,y)\,dy\,dx + \int_b^{220} \int_a^{fy} f(x,y)\,dy\,dx - \int_0^{M_{4x}} \int_{85}^{ony} f(x,y)\,dy\,dx - \int_0^b \int_{M_{4y}}^{110} f(x,y)\,dy\,dx$$
$$- \int_b^{M_{4x}} \int_{M_{4y}}^{fy} f(x,y)\,dy\,dx - \int_{15}^{65} \int_{95}^{nmy} f(x,y)\,dy\,dx - \int_{65}^{85} \int_{95}^{mky} f(x,y)\,dy\,dx + \int_{15}^{M_{3x}} \int_{M_{5y}}^{nmy} f(x,y)\,dy\,dx + \int_{M_{5x}}^{M_{6x}} \int_{M_{5y}}^{110} f(x,y)\,dy\,dx$$
$$+ \int_{M_{5x}}^{M_{6x}} \int_{M_{6y}}^{fy} f(x,y)\,dy\,dx + \int_{M_{6x}}^{85} \int_{M_{6y}}^{mky} f(x,y)\,dy\,dx - \int_0^{15} \int_{40}^{poy} f(x,y)\,dy\,dx - \int_0^{15} \int_{15}^{qpy} f(x,y)\,dy\,dx - \int_0^{50} \int_0^{qay} f(x,y)\,dy\,dx$$
$$- \int_{50}^{70} \int_0^{aby} f(x,y)\,dy\,dx - \int_{70}^{135} \int_0^{bcy} f(x,y)\,dy\,dx - \int_{135}^{155} \int_0^{cdy} f(x,y)\,dy\,dx - \int_{155}^{205} \int_0^{dey} f(x,y)\,dy\,dx - \int_{205}^{220} \int_0^{efy} f(x,y)\,dy\,dx$$
$$- \int_{M_{11x}}^{220} \int_{25}^{fgy} f(x,y)\,dy\,dx + \int_{M_{11x}}^{220} \int_a^{fy} f(x,y)\,dy\,dx$$

and the centroids of this volume in the xy-plane are at distances $\overline{X}$ and $\overline{Y}$ from the axes (see Figure 7.81) which are given by the following equations.

$$\overline{X} = \frac{1}{V}\left[\int_0^b \int_0^{110} x f(x,y)\,dy\,dx + \int_b^{220} \int_0^a x f(x,y)\,dy\,dx + \int_b^{220} \int_a^{fy} x f(x,y)\,dy\,dx - \int_0^{M_{4x}} \int_{85}^{ony} x f(x,y)\,dy\,dx \right.$$
$$- \int_0^b \int_{M_{4y}}^{110} x f(x,y)\,dy\,dx - \int_b^{M_{4x}} \int_{M_{4y}}^{fy} x f(x,y)\,dy\,dx - \int_{15}^{65} \int_{95}^{nmy} x f(x,y)\,dy\,dx - \int_{65}^{85} \int_{95}^{mky} x f(x,y)\,dy\,dx$$
$$+ \int_{15}^{M_{5x}} \int_{M_{5y}}^{nmy} x f(x,y)\,dy\,dx + \int_{M_{5x}}^{M_{6x}} \int_{M_{5y}}^{110} x f(x,y)\,dy\,dx + \int_{M_{5x}}^{M_{6x}} \int_{M_{6y}}^{fy} x f(x,y)\,dy\,dx + \int_{M_{6x}}^{85} \int_{M_{6y}}^{mky} x f(x,y)\,dy\,dx$$
$$- \int_0^{15} \int_{40}^{poy} x f(x,y)\,dy\,dx - \int_0^{15} \int_{15}^{qpy} x f(x,y)\,dy\,dx - \int_0^{50} \int_0^{qay} x f(x,y)\,dy\,dx - \int_{50}^{70} \int_0^{aby} x f(x,y)\,dy\,dx$$
$$- \int_{70}^{135} \int_0^{bcy} x f(x,y)\,dy\,dx - \int_{135}^{155} \int_0^{cdy} x f(x,y)\,dy\,dx - \int_{155}^{205} \int_0^{dey} x f(x,y)\,dy\,dx - \int_{205}^{220} \int_0^{efy} x f(x,y)\,dy\,dx$$
$$\left. - \int_{M_{11x}}^{220} \int_{25}^{fgy} x f(x,y)\,dy\,dx + \int_{M_{11x}}^{220} \int_a^{fy} x f(x,y)\,dy\,dx \right]$$

$$\overline{Y} = \frac{1}{V}\left[\int_0^{110} \int_0^b y f(x,y)\,dx\,dy + \int_0^a \int_b^{220} y f(x,y)\,dx\,dy + \int_a^{110} \int_b^{fx} y f(x,y)\,dx\,dy - \int_{85}^{M_{4y}} \int_0^{onx} y f(x,y)\,dx\,dy \right.$$

$$-\int_{M_{4y}}^{110}\int_{0}^{b} yf(x,y)\,dx\,dy-\int_{M_{4y}}^{110}\int_{b}^{fx} yf(x,y)\,dx\,dy-\int_{95}^{110}\int_{15}^{nmx} yf(x,y)\,dx\,dy-\int_{95}^{110}\int_{65}^{mkx} yf(x,y)\,dx\,dy$$

$$+\int_{M_{5y}}^{110}\int_{15}^{nmx} yf(x,y)\,dx\,dy+\int_{M_{5y}}^{110}\int_{M_{5x}}^{M_{6x}} yf(x,y)\,dx\,dy+\int_{M_{6y}}^{M_{5y}}\int_{M_{5x}}^{fx} yf(x,y)\,dx\,dy+\int_{M_{6y}}^{110}\int_{M_{6x}}^{mkx} yf(x,y)\,dx\,dy$$

$$-\int_{40}^{85}\int_{0}^{pox} yf(x,y)\,dx\,dy-\int_{15}^{40}\int_{0}^{qpx} yf(x,y)\,dx\,dy-\int_{0}^{15}\int_{0}^{qax} yf(x,y)\,dx\,dy-\int_{0}^{15}\int_{50}^{abx} yf(x,y)\,dx\,dy$$

$$-\int_{0}^{15}\int_{70}^{bcx} yf(x,y)\,dx\,dy-\int_{0}^{15}\int_{135}^{cdx} yf(x,y)\,dx\,dy-\int_{0}^{15}\int_{155}^{dex} yf(x,y)\,dx\,dy-\int_{0}^{25}\int_{205}^{efx} yf(x,y)\,dx\,dy$$

$$\left.-\int_{25}^{M_{11y}}\int_{M_{11x}}^{fgx} yf(x,y)\,dx\,dy+\int_{a}^{M_{11y}}\int_{M_{11x}}^{fx} yf(x,y)\,dx\,dy\right]$$

Application 16 of the partial-hexahedral compressive stress regime beneath the circumscribing rectangular border of proprietory shaped paver 1 shown in Figure 7.82 can be calculated by using Tables 5.1 and 7.4 and the surface function of the partial-hexahedral compressive stress through the three points σ_A, **I** and **t**.

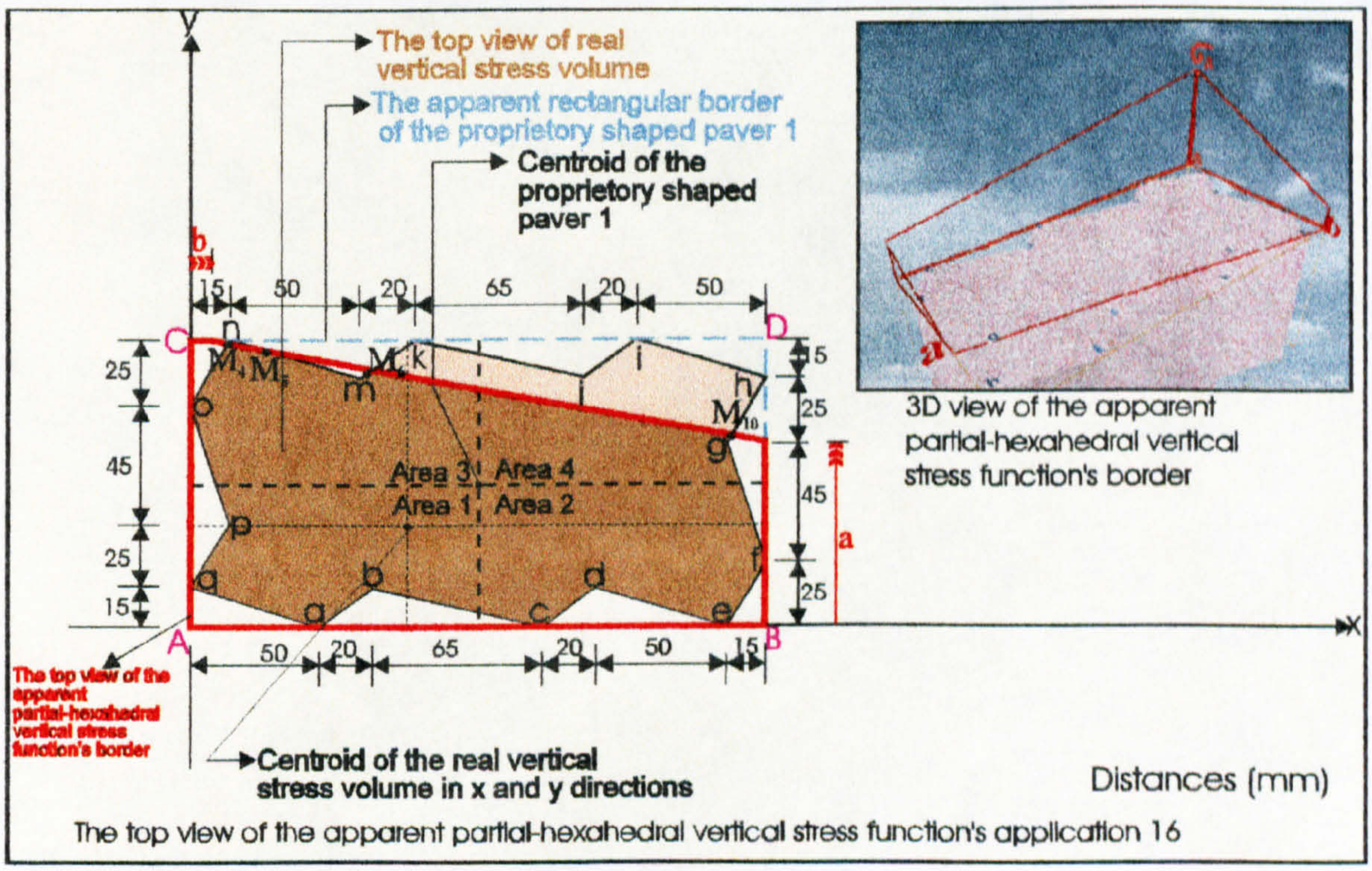

Figure 7.82: Application 16 of the partial-hexahedral compressive stress distribution beneath the circumscribing rectangular border of proprietory shaped paver 1.

The total volume **V** beneath the surface $f(x,y) = z\ (> 0)$ and above the region in the xy-plane (see Figure 7.82) is:

$$V = \int_0^b \int_0^{110} f(x,y)\,dy\,dx + \int_b^{220} \int_0^a f(x,y)\,dy\,dx + \int_b^{220} \int_a^{fy} f(x,y)\,dy\,dx - \int_0^{M_{4x}} \int_{85}^{ony} f(x,y)\,dy\,dx - \int_b^{M_{4x}} \int_{M_{4y}}^{fy} f(x,y)\,dy\,dx - \int_{15}^{65nmy} \int_{95}^{nmy} f(x,y)\,dy\,dx - \int_{65}^{85mky} \int_{95}^{mky} f(x,y)\,dy\,dx + \int_{15}^{M_{5x}} \int_{M_{5y}}^{nmy} f(x,y)\,dy\,dx + \int_{M_{5x}}^{M_{6x}} \int_{M_{5y}}^{110} f(x,y)\,dy\,dx + \int_{M_{5x}}^{M_{6x}} \int_{M_{6y}}^{fy} f(x,y)\,dy\,dx + \int_{M_{6x}}^{85} \int_{M_{6y}}^{mky} f(x,y)\,dy\,dx - \int_0^{15poy} \int_{40}^{poy} f(x,y)\,dy\,dx - \int_0^{15qpy} \int_{15}^{qpy} f(x,y)\,dy\,dx - \int_0^{50qay} \int_0^{qay} f(x,y)\,dy\,dx - \int_{50}^{70aby} \int_0^{aby} f(x,y)\,dy\,dx - \int_{70}^{135bcy} \int_0^{bcy} f(x,y)\,dy\,dx - \int_{135}^{155cdy} \int_0^{cdy} f(x,y)\,dy\,dx - \int_{155}^{205dey} \int_0^{dey} f(x,y)\,dy\,dx - \int_{205}^{220efy} \int_0^{efy} f(x,y)\,dy\,dx - \int_{205}^{220ghy} \int_{70}^{ghy} f(x,y)\,dy\,dx - \int_{205}^{220fgy} \int_{25}^{fgy} f(x,y)\,dy\,dx + \int_{M_{10x}}^{220} \int_{M_{10y}}^{ghy} f(x,y)\,dy\,dx + \int_{M_{10x}}^{220} \int_a^{fy} f(x,y)\,dy\,dx$$

and the centroids of this volume in the xy-plane are at distances $\overline{X}$ and $\overline{Y}$ from the axes (see Figure 7.82) which are given by the following equations.

$$\overline{X} = \frac{1}{V}\left[\int_0^b \int_0^{110} x f(x,y)\,dy\,dx + \int_b^{220} \int_0^a x f(x,y)\,dy\,dx + \int_b^{220} \int_a^{fy} x f(x,y)\,dy\,dx - \int_0^{M_{4x}} \int_{85}^{ony} x f(x,y)\,dy\,dx - \int_0^b \int_{M_{4y}}^{110} x f(x,y)\,dy\,dx - \int_b^{M_{4x}} \int_{M_{4y}}^{fy} x f(x,y)\,dy\,dx - \int_{15}^{65nmy} \int_{95}^{nmy} x f(x,y)\,dy\,dx - \int_{65}^{85mky} \int_{95}^{mky} x f(x,y)\,dy\,dx + \int_{15}^{M_{5x}} \int_{M_{5y}}^{nmy} x f(x,y)\,dy\,dx + \int_{M_{5x}}^{M_{6x}} \int_{M_{5y}}^{110} x f(x,y)\,dy\,dx + \int_{M_{5x}}^{M_{6x}} \int_{M_{6y}}^{fy} x f(x,y)\,dy\,dx + \int_{M_{6x}}^{85} \int_{M_{6y}}^{mky} x f(x,y)\,dy\,dx - \int_0^{15poy} \int_{40}^{poy} x f(x,y)\,dy\,dx - \int_0^{15qpy} \int_{15}^{qpy} x f(x,y)\,dy\,dx - \int_0^{50qay} \int_0^{qay} x f(x,y)\,dy\,dx - \int_{50}^{70aby} \int_0^{aby} x f(x,y)\,dy\,dx - \int_{70}^{135bcy} \int_0^{bcy} x f(x,y)\,dy\,dx - \int_{135}^{155cdy} \int_0^{cdy} x f(x,y)\,dy\,dx - \int_{155}^{205dey} \int_0^{dey} x f(x,y)\,dy\,dx - \int_{205}^{220efy} \int_0^{efy} x f(x,y)\,dy\,dx - \int_{205}^{220ghy} \int_{70}^{ghy} x f(x,y)\,dy\,dx - \int_{205}^{220fgy} \int_{25}^{fgy} x f(x,y)\,dy\,dx + \int_{M_{10x}}^{220} \int_{M_{10y}}^{ghy} x f(x,y)\,dy\,dx + \int_{M_{10x}}^{220} \int_a^{fy} x f(x,y)\,dy\,dx\right]$$

$$\overline{Y} = \frac{1}{V}\left[\begin{array}{l}
\int_{0}^{110}\int_{0}^{b} y\,f(x,y)\,dx\,dy + \int_{0}^{a}\int_{b}^{220} y\,f(x,y)\,dx\,dy + \int_{a}^{110}\int_{b}^{fx} y\,f(x,y)\,dx\,dy - \int_{85}^{M_{4y}}\int_{0}^{onx} y\,f(x,y)\,dx\,dy \\
- \int_{M_{4y}}^{110}\int_{0}^{b} y\,f(x,y)\,dx\,dy - \int_{M_{4y}}^{110}\int_{b}^{fx} y\,f(x,y)\,dx\,dy - \int_{95}^{110}\int_{15}^{nmx} y\,f(x,y)\,dx\,dy - \int_{95}^{110}\int_{65}^{mkx} y\,f(x,y)\,dx\,dy \\
+ \int_{M_{5y}}^{110}\int_{15}^{nmx} y\,f(x,y)\,dx\,dy + \int_{M_{5y}}^{110}\int_{M_{5x}}^{M_{6x}} y\,f(x,y)\,dx\,dy + \int_{M_{6y}}^{M_{5y}}\int_{M_{5x}}^{fx} y\,f(x,y)\,dx\,dy + \int_{M_{6y}}^{110}\int_{M_{6x}}^{mkx} y\,f(x,y)\,dx\,dy \\
- \int_{40}^{85}\int_{0}^{pox} y\,f(x,y)\,dx\,dy - \int_{15}^{40}\int_{0}^{qpx} y\,f(x,y)\,dx\,dy - \int_{0}^{15}\int_{0}^{qax} y\,f(x,y)\,dx\,dy - \int_{0}^{15}\int_{50}^{abx} y\,f(x,y)\,dx\,dy \\
- \int_{0}^{15}\int_{70}^{bcx} y\,f(x,y)\,dx\,dy - \int_{0}^{135}\int_{70}^{cdx} y\,f(x,y)\,dx\,dy - \int_{0}^{155}\int_{70}^{dex} y\,f(x,y)\,dx\,dy - \int_{0}^{205}\int_{70}^{efx} y\,f(x,y)\,dx\,dy \\
- \int_{70}^{95}\int_{205}^{ghx} y\,f(x,y)\,dx\,dy - \int_{25}^{70}\int_{205}^{fgx} y\,f(x,y)\,dx\,dy + \int_{M_{10y}}^{95}\int_{M_{10x}}^{ghx} y\,f(x,y)\,dx\,dy + \int_{a}^{70}\int_{M_{10x}}^{fx} y\,f(x,y)\,dx\,dy
\end{array}\right]$$

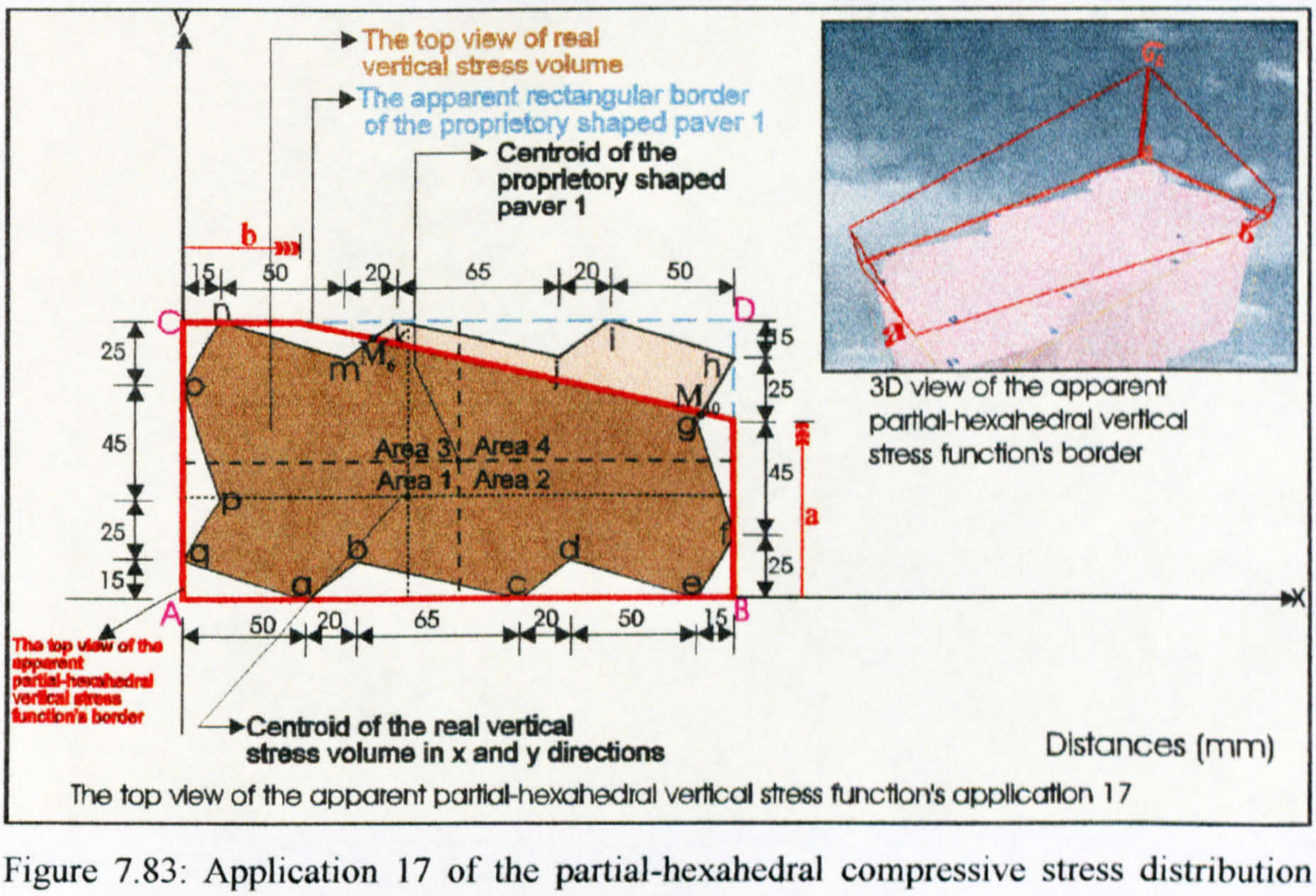

The top view of the apparent partial-hexahedral vertical stress function's application 17

Figure 7.83: Application 17 of the partial-hexahedral compressive stress distribution beneath the circumscribing rectangular border of proprietory shaped paver 1.

Application 17 of the partial-hexahedral compressive stress regime beneath the circumscribing rectangular border of proprietory shaped paver 1 shown in Figure 7.83

can be calculated by using Tables 5.1 and 7.4 and the surface function of the partial-hexahedral compressive stress through the three points σ_A, **l** and **t**.

The total volume **V** beneath the surface $f(x,y) = z\ (> 0)$ and above the region in the xy-plane (see Figure 7.83) is:

$$V = \int_0^b \int_0^{110} f(x,y)\,dy\,dx + \int_b^{220} \int_0^a f(x,y)\,dy\,dx + \int_b^{220} \int_a^{fy} f(x,y)\,dy\,dx - \int_{15}^{65} \int_{95}^{nmy} f(x,y)\,dy\,dx - \int_{65}^{85} \int_{95}^{mky} f(x,y)\,dy\,dx$$
$$+ \int_b^{M_{6x}} \int_{M_{6y}}^{fy} f(x,y)\,dy\,dx + \int_{M_{6x}}^{85} \int_{M_{6y}}^{mky} f(x,y)\,dy\,dx - \int_0^{15} \int_{85}^{ony} f(x,y)\,dy\,dx - \int_0^{15} \int_{40}^{poy} f(x,y)\,dy\,dx - \int_0^{15} \int_{15}^{qpy} f(x,y)\,dy\,dx$$
$$- \int_0^{50} \int_0^{qay} f(x,y)\,dy\,dx - \int_{50}^{70} \int_0^{aby} f(x,y)\,dy\,dx - \int_{70}^{135} \int_0^{bcy} f(x,y)\,dy\,dx - \int_{135}^{155} \int_0^{cdy} f(x,y)\,dy\,dx - \int_{155}^{205} \int_0^{dey} f(x,y)\,dy\,dx$$
$$- \int_{205}^{220} \int_0^{efy} f(x,y)\,dy\,dx - \int_{205}^{220} \int_{70}^{ghy} f(x,y)\,dy\,dx - \int_{205}^{220} \int_{25}^{fgy} f(x,y)\,dy\,dx + \int_{M_{10x}}^{220} \int_{M_{10y}}^{ghy} f(x,y)\,dy\,dx + \int_{M_{10x}}^{220} \int_a^{fy} f(x,y)\,dy\,dx$$

and the centroids of this volume in the xy-plane are at distances $\overline{X}$ and $\overline{Y}$ from the axes (see Figure 7.83) which are given by the following equations.

$$\overline{X} = \frac{1}{V}\left[\int_0^b \int_0^{110} x f(x,y)\,dy\,dx + \int_b^{220} \int_0^a x f(x,y)\,dy\,dx + \int_b^{220} \int_a^{fy} x f(x,y)\,dy\,dx - \int_{15}^{65} \int_{95}^{nmy} x f(x,y)\,dy\,dx - \int_{65}^{85} \int_{95}^{mky} x f(x,y)\,dy\,dx + \int_b^{M_{6x}} \int_{M_{6y}}^{fy} x f(x,y)\,dy\,dx + \int_{M_{6x}}^{85} \int_{M_{6y}}^{mky} x f(x,y)\,dy\,dx - \int_0^{15} \int_{85}^{ony} x f(x,y)\,dy\,dx - \int_0^{15} \int_{40}^{poy} x f(x,y)\,dy\,dx - \int_0^{15} \int_{15}^{qpy} x f(x,y)\,dy\,dx - \int_0^{50} \int_0^{qay} x f(x,y)\,dy\,dx - \int_{50}^{70} \int_0^{aby} x f(x,y)\,dy\,dx - \int_{70}^{135} \int_0^{bcy} x f(x,y)\,dy\,dx - \int_{135}^{155} \int_0^{cdy} x f(x,y)\,dy\,dx - \int_{155}^{205} \int_0^{dey} x f(x,y)\,dy\,dx - \int_{205}^{220} \int_0^{efy} x f(x,y)\,dy\,dx - \int_{205}^{220} \int_{70}^{ghy} x f(x,y)\,dy\,dx - \int_{205}^{220} \int_{25}^{fgy} x f(x,y)\,dy\,dx + \int_{M_{10x}}^{220} \int_{M_{10y}}^{ghy} x f(x,y)\,dy\,dx + \int_{M_{10x}}^{220} \int_a^{fy} x f(x,y)\,dy\,dx\right]$$

$$\overline{Y} = \frac{1}{V}\left[\int_0^{110} \int_0^b y f(x,y)\,dx\,dy + \int_0^a \int_b^{220} y f(x,y)\,dx\,dy + \int_a^{110} \int_b^{fx} y f(x,y)\,dx\,dy - \int_{95}^{110} \int_{15}^{nmx} y f(x,y)\,dx\,dy\right.$$

$$-\int_{95}^{110}\int_{65}^{mkx} y f(x,y)\,dx\,dy+\int_{M_{6y}}^{110}\int_{b}^{fx} y f(x,y)\,dx\,dy+\int_{M_{6y}}^{110}\int_{M_{6x}}^{mkx} y f(x,y)\,dx\,dy-\int_{85}^{110}\int_{0}^{onx} y f(x,y)\,dx\,dy$$

$$-\int_{40}^{85}\int_{0}^{pox} y f(x,y)\,dx\,dy-\int_{15}^{40}\int_{0}^{qpx} y f(x,y)\,dx\,dy-\int_{0}^{15}\int_{0}^{qax} y f(x,y)\,dx\,dy-\int_{0}^{15}\int_{50}^{abx} y f(x,y)\,dx\,dy$$

$$-\int_{0}^{15}\int_{70}^{bcx} y f(x,y)\,dx\,dy-\int_{0}^{15}\int_{135}^{cdx} y f(x,y)\,dx\,dy-\int_{0}^{15}\int_{155}^{dex} y f(x,y)\,dx\,dy-\int_{0}^{25}\int_{205}^{efx} y f(x,y)\,dx\,dy$$

$$\left.-\int_{70}^{95}\int_{205}^{ghx} y f(x,y)\,dx\,dy-\int_{25}^{70}\int_{205}^{fgx} y f(x,y)\,dx\,dy+\int_{M_{10y}}^{95}\int_{M_{10x}}^{ghx} y f(x,y)\,dx\,dy+\int_{a}^{70}\int_{M_{10x}}^{fx} y f(x,y)\,dx\,dy\right]$$

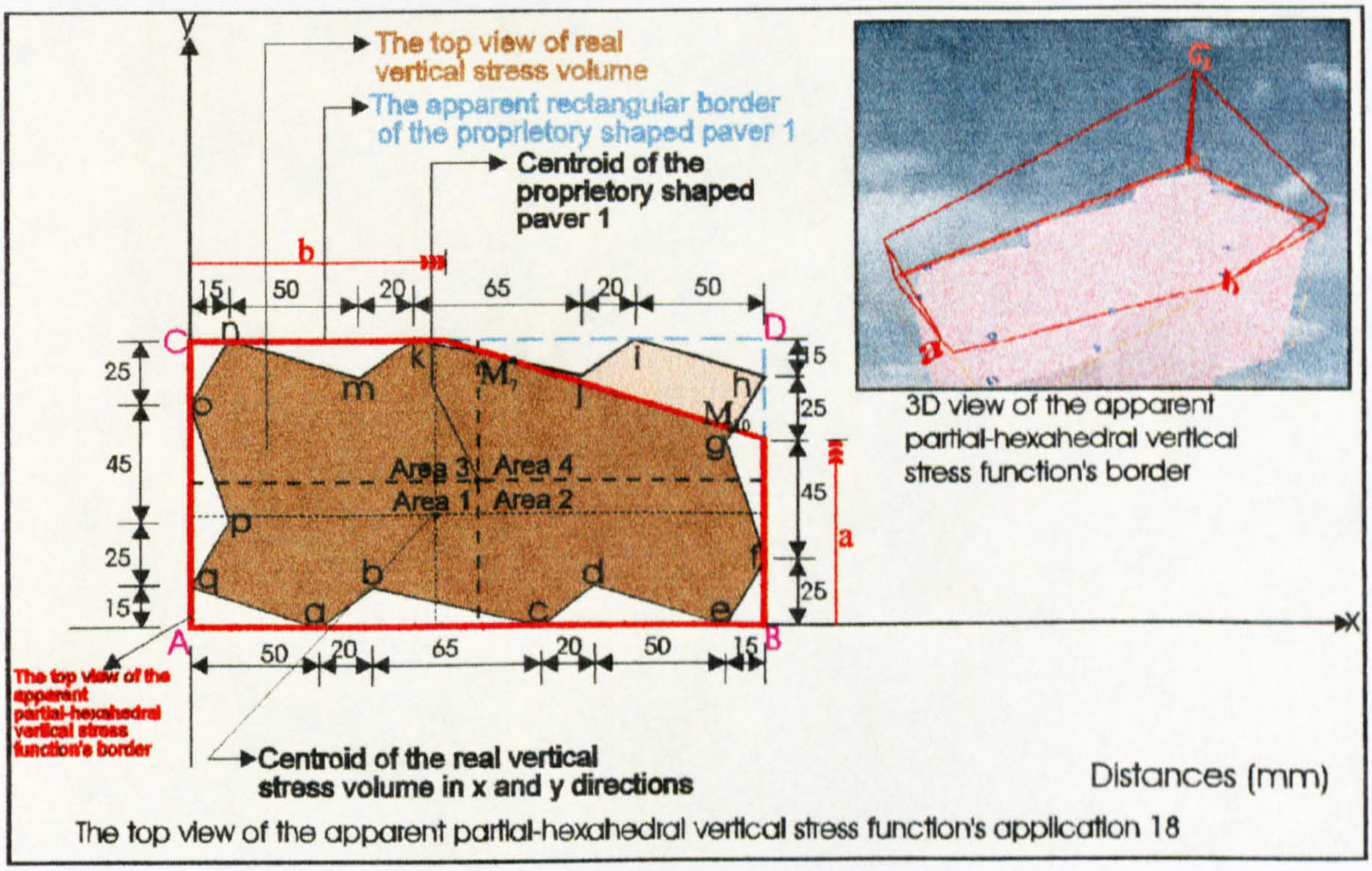

The top view of the apparent partial-hexahedral vertical stress function's application 18

Figure 7.84: Application 18 of the partial-hexahedral compressive stress distribution beneath the circumscribing rectangular border of proprietory shaped paver 1.

Application 18 of the partial-hexahedral compressive stress regime beneath the circumscribing rectangular border of proprietory shaped paver 1 shown in Figure 7.84 can be calculated by using Tables 5.1 and 7.4 and the surface function of the partial-hexahedral compressive stress through the three points σ_A, **l** and **t**.

The total volume **V** beneath the surface $f(x,y) = z\ (> 0)$ and above the region in the xy-plane (see Figure 7.84) is:

$$V = \int_0^{b}\int_0^{110} f(x,y)\,dy\,dx + \int_b^{220}\int_0^{a} f(x,y)\,dy\,dx + \int_b^{220}\int_a^{fy} f(x,y)\,dy\,dx - \int_{85}^{Mf_{7x}}\int_{Mf_{7y}}^{kjy} f(x,y)\,dy\,dx + \int_b^{Mf_{7x}}\int_{Mf_{7y}}^{fy} f(x,y)\,dy\,dx$$
$$- \int_{15}^{65}\int_{95}^{nmy} f(x,y)\,dy\,dx - \int_{65}^{85}\int_{95}^{mky} f(x,y)\,dy\,dx - \int_{0}^{15}\int_{85}^{ony} f(x,y)\,dy\,dx - \int_{0}^{15}\int_{40}^{poy} f(x,y)\,dy\,dx - \int_{0}^{15}\int_{15}^{qpy} f(x,y)\,dy\,dx$$
$$- \int_{0}^{50}\int_{0}^{qay} f(x,y)\,dy\,dx - \int_{50}^{70}\int_{0}^{ahy} f(x,y)\,dy\,dx - \int_{70}^{135}\int_{0}^{bcy} f(x,y)\,dy\,dx - \int_{135}^{155}\int_{0}^{cdy} f(x,y)\,dy\,dx - \int_{155}^{205}\int_{0}^{dey} f(x,y)\,dy\,dx$$
$$- \int_{205}^{220}\int_{0}^{efy} f(x,y)\,dy\,dx - \int_{205}^{220}\int_{70}^{ghy} f(x,y)\,dy\,dx - \int_{205}^{220}\int_{25}^{fxy} f(x,y)\,dy\,dx + \int_{Mf_{10x}}^{220}\int_{Mf_{10y}}^{ghy} f(x,y)\,dy\,dx + \int_{Mf_{10x}}^{220}\int_{a}^{fy} f(x,y)\,dy\,dx$$

and the centroids of this volume in the xy-plane are at distances $\overline{X}$ and $\overline{Y}$ from the axes (see Figure 7.84) which are given by the following equations.

$$\overline{X} = \frac{1}{V}\left[\int_0^{b}\int_0^{110} x f(x,y)\,dy\,dx + \int_b^{220}\int_0^{a} x f(x,y)\,dy\,dx + \int_b^{220}\int_a^{fy} x f(x,y)\,dy\,dx - \int_{85}^{Mf_{7x}}\int_{Mf_{7y}}^{kjv} x f(x,y)\,dy\,dx\right.$$
$$+ \int_b^{Mf_{7x}}\int_{Mf_{7y}}^{fy} x f(x,y)\,dy\,dx - \int_{15}^{65}\int_{95}^{nmy} x f(x,y)\,dy\,dx - \int_{65}^{85}\int_{95}^{mky} x f(x,y)\,dy\,dx - \int_{0}^{15}\int_{85}^{ony} x f(x,y)\,dy\,dx$$
$$- \int_{0}^{15}\int_{40}^{poy} x f(x,y)\,dy\,dx - \int_{0}^{15}\int_{15}^{qpy} x f(x,y)\,dy\,dx - \int_{0}^{50}\int_{0}^{qay} x f(x,y)\,dy\,dx - \int_{50}^{70}\int_{0}^{ahy} x f(x,y)\,dy\,dx$$
$$- \int_{70}^{135}\int_{0}^{bcy} x f(x,y)\,dy\,dx - \int_{135}^{155}\int_{0}^{cdy} x f(x,y)\,dy\,dx - \int_{155}^{205}\int_{0}^{dey} x f(x,y)\,dy\,dx - \int_{205}^{220}\int_{0}^{efy} x f(x,y)\,dy\,dx$$
$$\left. - \int_{205}^{220}\int_{70}^{ghy} x f(x,y)\,dy\,dx - \int_{205}^{220}\int_{25}^{fgy} x f(x,y)\,dy\,dx + \int_{Mf_{10x}}^{220}\int_{Mf_{10y}}^{ghy} x f(x,y)\,dy\,dx + \int_{Mf_{10x}}^{220}\int_{a}^{fy} x f(x,y)\,dy\,dx\right]$$

$$\overline{Y} = \frac{1}{V}\left[\int_0^{110}\int_0^{b} y f(x,y)\,dx\,dy + \int_0^{a}\int_b^{220} y f(x,y)\,dx\,dy + \int_a^{110}\int_b^{fx} y f(x,y)\,dx\,dy - \int_{Mf_{7y}}^{110}\int_{85}^{kjx} y f(x,y)\,dx\,dy\right.$$
$$\left. + \int_{M_{7y}}^{110}\int_{85}^{fx} y f(x,y)\,dx\,dy - \int_{95}^{110}\int_{15}^{nmx} y f(x,y)\,dx\,dy - \int_{95}^{110}\int_{65}^{mkx} y f(x,y)\,dx\,dy - \int_{85}^{110}\int_{0}^{onx} y f(x,y)\,dx\,dy\right]$$

$$-\int_{40}^{85}\int_{0}^{pox} y f(x,y)\,dx\,dy - \int_{15}^{40}\int_{0}^{qpx} y f(x,y)\,dx\,dy - \int_{0}^{15}\int_{0}^{qax} y f(x,y)\,dx\,dy - \int_{0}^{15}\int_{50}^{abx} y f(x,y)\,dx\,dy$$

$$-\int_{0}^{15}\int_{70}^{bcx} y f(x,y)\,dx\,dy - \int_{0}^{15}\int_{135}^{cdx} y f(x,y)\,dx\,dy - \int_{0}^{15}\int_{155}^{dex} y f(x,y)\,dx\,dy - \int_{0}^{25}\int_{205}^{efx} y f(x,y)\,dx\,dy$$

$$-\int_{70}^{95}\int_{205}^{ghx} y f(x,y)\,dx\,dy - \int_{25}^{70}\int_{205}^{fgx} y f(x,y)\,dx\,dy + \int_{M_{10y}}^{95}\int_{M_{10x}}^{ghx} y f(x,y)\,dx\,dy + \int_{a}^{70}\int_{M_{10x}}^{fx} y f(x,y)\,dx\,dy$$

Application 19 of the partial-hexahedral compressive stress regime beneath the circumscribing rectangular border of proprietory shaped paver 1 shown in Figure 7.85 can be calculated by using Tables 5.1 and 7.4 and the surface function of the partial-hexahedral compressive stress through the three points σ_A, **l** and **t**.

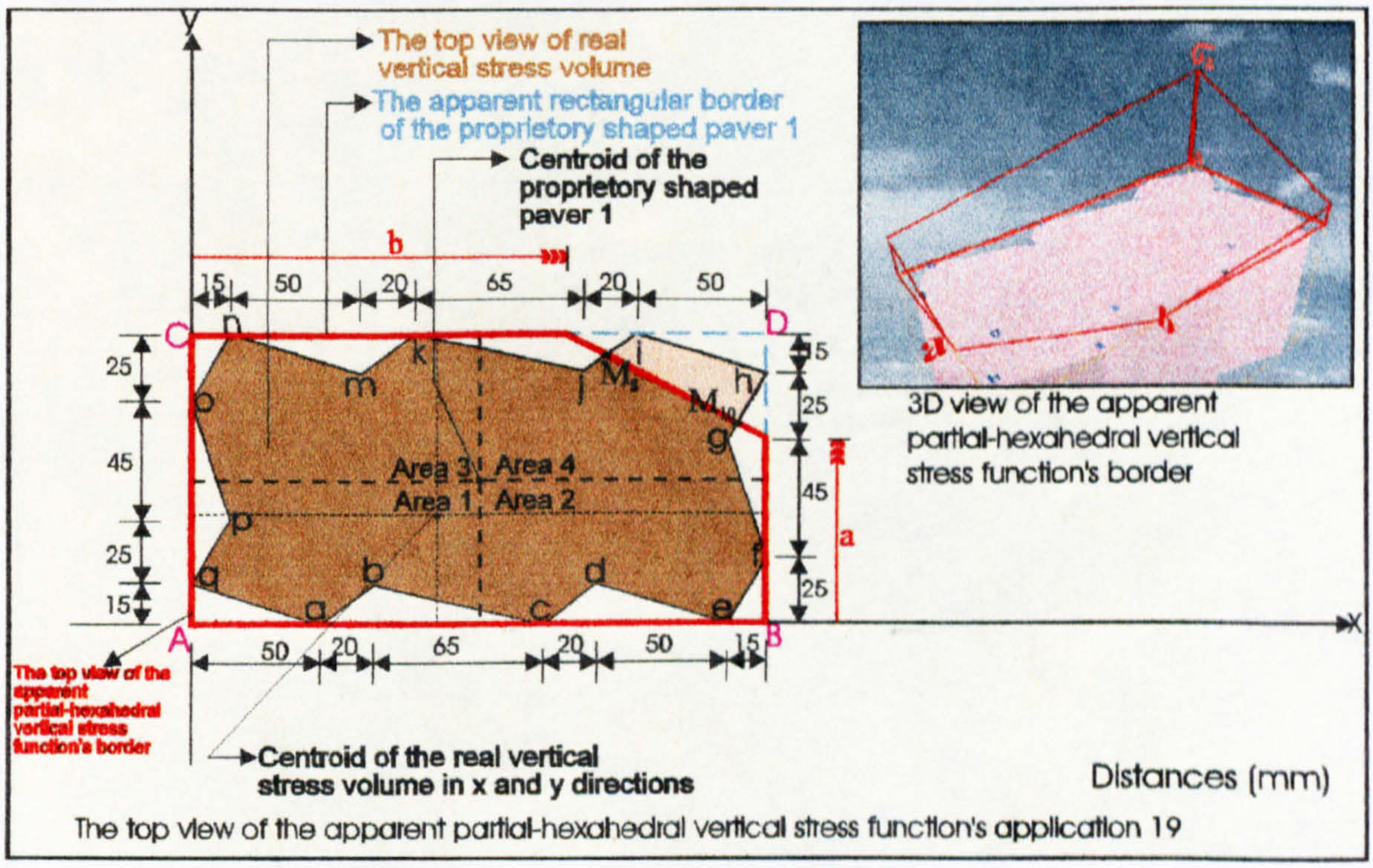

The top view of the apparent partial-hexahedral vertical stress function's application 19

Figure 7.85: Application 19 of the partial-hexahedral compressive stress distribution beneath the circumscribing rectangular border of proprietory shaped paver 1.

The total volume **V** beneath the surface $f(x,y) = z\ (> 0)$ and above the region in the xy-plane (see Figure 7.85) is:

$$V = \int_{0}^{b}\int_{0}^{110} f(x,y)\,dy\,dx + \int_{b}^{220}\int_{0}^{a} f(x,y)\,dy\,dx + \int_{b}^{220}\int_{a}^{fy} f(x,y)\,dy\,dx + \int_{b}^{M_{8x}}\int_{M_{8y}}^{fy} f(x,y)\,dy\,dx + \int_{M_{8x}}^{170}\int_{M_{8y}}^{jiy} f(x,y)\,dy\,dx$$
$$- \int_{85}^{150}\int_{95}^{kjy} f(x,y)\,dy\,dx - \int_{150}^{170}\int_{95}^{jiy} f(x,y)\,dy\,dx - \int_{15}^{65}\int_{95}^{nmy} f(x,y)\,dy\,dx - \int_{65}^{85}\int_{95}^{mky} f(x,y)\,dy\,dx - \int_{0}^{15}\int_{85}^{ony} f(x,y)\,dy\,dx$$
$$- \int_{0}^{15}\int_{0}^{poy} f(x,y)\,dy\,dx - \int_{0}^{15}\int_{40}^{qpy} f(x,y)\,dy\,dx - \int_{0}^{50}\int_{0}^{qay} f(x,y)\,dy\,dx - \int_{50}^{70}\int_{0}^{aby} f(x,y)\,dy\,dx - \int_{70}^{135}\int_{0}^{bcy} f(x,y)\,dy\,dx$$
$$- \int_{135}^{155}\int_{0}^{cdy} f(x,y)\,dy\,dx - \int_{155}^{205}\int_{0}^{dey} f(x,y)\,dy\,dx - \int_{205}^{220}\int_{0}^{efy} f(x,y)\,dy\,dx - \int_{205}^{220}\int_{70}^{ghy} f(x,y)\,dy\,dx - \int_{205}^{220}\int_{25}^{fxy} f(x,y)\,dy\,dx$$
$$+ \int_{M_{10x}}^{220}\int_{M_{10y}}^{ghy} f(x,y)\,dy\,dx + \int_{M_{10x}}^{220}\int_{a}^{fy} f(x,y)\,dy\,dx$$

and the centroids of this volume in the xy-plane are at distances $\overline{X}$ and $\overline{Y}$ from the axes (see Figure 7.85) which are given by the following equations.

$$\overline{X} = \frac{1}{V}\left[\int_{0}^{b}\int_{0}^{110} x f(x,y)\,dy\,dx + \int_{b}^{220}\int_{0}^{a} x f(x,y)\,dy\,dx + \int_{b}^{220}\int_{a}^{fy} x f(x,y)\,dy\,dx + \int_{b}^{M_{8x}}\int_{M_{8y}}^{fy} x f(x,y)\,dy\,dx + \int_{M_{8x}}^{170}\int_{M_{8y}}^{jiy} x f(x,y)\,dy\,dx\right.$$
$$- \int_{85}^{150}\int_{95}^{kjy} x f(x,y)\,dy\,dx - \int_{150}^{170}\int_{95}^{jiy} x f(x,y)\,dy\,dx - \int_{15}^{65}\int_{95}^{nmy} x f(x,y)\,dy\,dx - \int_{65}^{85}\int_{95}^{mky} x f(x,y)\,dy\,dx - \int_{0}^{15}\int_{85}^{ony} x f(x,y)\,dy\,dx$$
$$- \int_{0}^{15}\int_{0}^{poy} x f(x,y)\,dy\,dx - \int_{0}^{15}\int_{40}^{qpy} x f(x,y)\,dy\,dx - \int_{0}^{50}\int_{0}^{qay} x f(x,y)\,dy\,dx - \int_{50}^{70}\int_{0}^{aby} x f(x,y)\,dy\,dx - \int_{70}^{135}\int_{0}^{bcy} x f(x,y)\,dy\,dx$$
$$- \int_{135}^{155}\int_{0}^{cdy} x f(x,y)\,dy\,dx - \int_{155}^{205}\int_{0}^{dey} x f(x,y)\,dy\,dx - \int_{205}^{220}\int_{0}^{efy} x f(x,y)\,dy\,dx - \int_{205}^{220}\int_{70}^{ghy} x f(x,y)\,dy\,dx - \int_{205}^{220}\int_{25}^{fxy} x f(x,y)\,dy\,dx$$
$$\left. + \int_{M_{10x}}^{220}\int_{M_{10y}}^{ghy} x f(x,y)\,dy\,dx + \int_{M_{10x}}^{220}\int_{a}^{fy} x f(x,y)\,dy\,dx\right]$$

$$\overline{Y} = \frac{1}{V}\left[\int_{0}^{110}\int_{0}^{b} y f(x,y)\,dx\,dy + \int_{0}^{a}\int_{b}^{220} y f(x,y)\,dx\,dy + \int_{a}^{110}\int_{b}^{fx} y f(x,y)\,dx\,dy + \int_{M_{8y}}^{110}\int_{b}^{fx} y f(x,y)\,dx\,dy\right.$$
$$\left. + \int_{M_{8y}}^{110}\int_{M_{8x}}^{jix} y f(x,y)\,dx\,dy - \int_{95}^{110}\int_{85}^{kjx} y f(x,y)\,dx\,dy - \int_{95}^{110}\int_{150}^{jix} y f(x,y)\,dx\,dy - \int_{95}^{110}\int_{15}^{nmx} y f(x,y)\,dx\,dy\right]$$

$$-\int_{95}^{110}\int_{65}^{mkx} y f(x,y)\,dx\,dy - \int_{85}^{110}\int_{0}^{onx} y f(x,y)\,dx\,dy - \int_{40}^{85}\int_{0}^{pox} y f(x,y)\,dx\,dy - \int_{15}^{40}\int_{0}^{qpx} y f(x,y)\,dx\,dy$$

$$-\int_{0}^{15}\int_{0}^{qax} y f(x,y)\,dx\,dy - \int_{0}^{15}\int_{50}^{abx} y f(x,y)\,dx\,dy - \int_{0}^{15}\int_{70}^{bcx} y f(x,y)\,dx\,dy - \int_{0}^{15}\int_{135}^{cdx} y f(x,y)\,dx\,dy$$

$$-\int_{0}^{15}\int_{155}^{dex} y f(x,y)\,dx\,dy - \int_{0}^{25}\int_{205}^{efx} y f(x,y)\,dx\,dy - \int_{70}^{95}\int_{205}^{ghx} y f(x,y)\,dx\,dy - \int_{25}^{70}\int_{205}^{fgx} y f(x,y)\,dx\,dy$$

$$+\int_{M_{10y}}^{95}\int_{M_{10x}}^{ghx} y f(x,y)\,dx\,dy + \int_{a}^{70}\int_{M_{10x}}^{fx} y f(x,y)\,dx\,dy\Bigg]$$

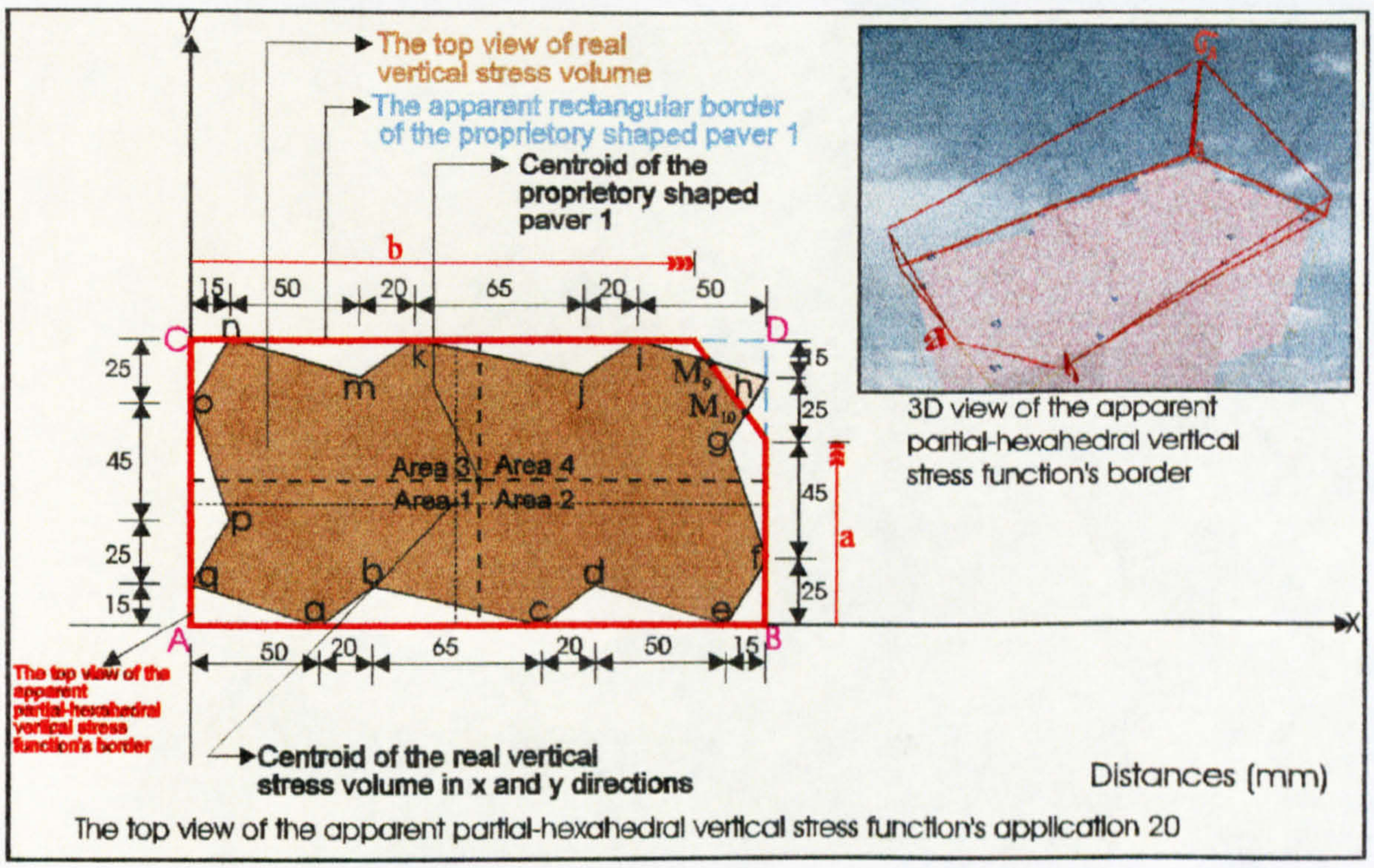

Figure 7.86: Application 20 of the partial-hexahedral compressive stress distribution beneath the circumscribing rectangular border of proprietory shaped paver 1.

Application 20 of the partial-hexahedral compressive stress regime beneath the circumscribing rectangular border of proprietory shaped paver 1 shown in Figure 7.86 can be calculated by using Tables 5.1 and 7.4 and the surface function of the partial-hexahedral compressive stress through the three points σ_A, **l** and **t**.

The total volume **V** beneath the surface $f(x,y) = z\ (> 0)$ and above the region in the xy-plane (see Figure 7.86) is:

$$V = \int_0^b \int_0^{110} f(x,y)\,dy\,dx + \int_b^{220} \int_0^a f(x,y)\,dy\,dx + \int_b^{220} \int_a^{fy} f(x,y)\,dy\,dx - \int_{170}^{Mlo_x} \int_{Mlo_y}^{hly} f(x,y)\,dy\,dx + \int_b^{Mlo_x} \int_{Mlo_y}^{fy} f(x,y)\,dy\,dx$$
$$- \int_{85}^{150} \int_{95}^{kjy} f(x,y)\,dy\,dx - \int_{150}^{170} \int_{95}^{jiy} f(x,y)\,dy\,dx - \int_{15}^{65} \int_{95}^{umy} f(x,y)\,dy\,dx - \int_{0}^{85} \int_{95}^{mky} f(x,y)\,dy\,dx - \int_{0}^{15} \int_{85}^{ony} f(x,y)\,dy\,dx$$
$$- \int_{0}^{15} \int_{40}^{poy} f(x,y)\,dy\,dx - \int_{0}^{15} \int_{15}^{qpy} f(x,y)\,dy\,dx - \int_{0}^{50} \int_{0}^{qay} f(x,y)\,dy\,dx - \int_{50}^{70} \int_{0}^{xby} f(x,y)\,dy\,dx - \int_{70}^{135} \int_{0}^{bcy} f(x,y)\,dy\,dx$$
$$- \int_{135}^{155} \int_{0}^{cdy} f(x,y)\,dy\,dx - \int_{155}^{205} \int_{0}^{dey} f(x,y)\,dy\,dx - \int_{205}^{220} \int_{0}^{efy} f(x,y)\,dy\,dx - \int_{205}^{220} \int_{70}^{ghy} f(x,y)\,dy\,dx - \int_{205}^{220} \int_{25}^{fgy} f(x,y)\,dy\,dx$$
$$+ \int_{M_{10x}}^{220} \int_{M_{10y}}^{ghy} f(x,y)\,dy\,dx + \int_{M_{10x}}^{220} \int_{a}^{fy} f(x,y)\,dy\,dx$$

and the centroids of this volume in the xy-plane are at distances $\overline{X}$ and $\overline{Y}$ from the axes (see Figure 7.86) which are given by the following equations.

$$\overline{X} = \frac{1}{V}\left[\int_0^b \int_0^{110} x f(x,y)\,dy\,dx + \int_b^{220} \int_0^a x f(x,y)\,dy\,dx + \int_b^{220} \int_a^{fy} x f(x,y)\,dy\,dx - \int_{170}^{M_{9x}} \int_{M_{9y}}^{hly} x f(x,y)\,dy\,dx\right.$$
$$+ \int_b^{M_{9x}} \int_{M_{9y}}^{fy} x f(x,y)\,dy\,dx - \int_{85}^{150} \int_{95}^{kjy} x f(x,y)\,dy\,dx - \int_{150}^{170} \int_{95}^{jiy} x f(x,y)\,dy\,dx - \int_{15}^{65} \int_{95}^{nmy} x f(x,y)\,dy\,dx$$
$$- \int_{65}^{85} \int_{95}^{mky} x f(x,y)\,dy\,dx - \int_{0}^{85} \int_{85}^{ony} x f(x,y)\,dy\,dx - \int_{0}^{40} \int_{0}^{poy} x f(x,y)\,dy\,dx - \int_{0}^{15} \int_{15}^{qpy} x f(x,y)\,dy\,dx$$
$$- \int_{0}^{50} \int_{0}^{qay} x f(x,y)\,dy\,dx - \int_{50}^{70} \int_{0}^{aby} x f(x,y)\,dy\,dx - \int_{70}^{135} \int_{0}^{bcy} x f(x,y)\,dy\,dx - \int_{135}^{155} \int_{0}^{cdy} x f(x,y)\,dy\,dx$$
$$- \int_{155}^{205} \int_{0}^{dey} x f(x,y)\,dy\,dx - \int_{205}^{220} \int_{0}^{efy} x f(x,y)\,dy\,dx - \int_{205}^{220} \int_{70}^{ghy} x f(x,y)\,dy\,dx - \int_{205}^{220} \int_{25}^{fgy} x f(x,y)\,dy\,dx$$
$$\left. + \int_{M_{10x}}^{220} \int_{M_{10y}}^{ghy} x f(x,y)\,dy\,dx + \int_{M_{10x}}^{220} \int_{a}^{fy} x f(x,y)\,dy\,dx\right]$$

$$\overline{Y} = \frac{1}{V}\left[\begin{array}{l}
\int_{0}^{110}\int_{0}^{b} y f(x,y)\,dx\,dy + \int_{0}^{a}\int_{b}^{220} y f(x,y)\,dx\,dy + \int_{a}^{110}\int_{b}^{fx} y f(x,y)\,dx\,dy - \int_{M_{9y}}^{110}\int_{170}^{hix} y f(x,y)\,dx\,dy \\
+ \int_{M_{9y}}^{110}\int_{b}^{fx} y f(x,y)\,dx\,dy - \int_{95}^{110}\int_{85}^{kjx} y f(x,y)\,dx\,dy - \int_{95}^{110}\int_{150}^{jix} y f(x,y)\,dx\,dy - \int_{95}^{110}\int_{15}^{nmx} y f(x,y)\,dx\,dy \\
- \int_{95}^{110}\int_{65}^{mkx} y f(x,y)\,dx\,dy - \int_{85}^{110}\int_{0}^{onx} y f(x,y)\,dx\,dy - \int_{40}^{85}\int_{0}^{pox} y f(x,y)\,dx\,dy - \int_{15}^{40}\int_{0}^{qpx} y f(x,y)\,dx\,dy \\
- \int_{0}^{15}\int_{0}^{qax} y f(x,y)\,dx\,dy - \int_{0}^{15}\int_{50}^{abx} y f(x,y)\,dx\,dy - \int_{0}^{15}\int_{70}^{bcx} y f(x,y)\,dx\,dy - \int_{0}^{15}\int_{135}^{cdx} y f(x,y)\,dx\,dy \\
- \int_{0}^{15}\int_{155}^{dex} y f(x,y)\,dx\,dy - \int_{0}^{25}\int_{205}^{efx} y f(x,y)\,dx\,dy - \int_{70}^{95}\int_{205}^{ghx} y f(x,y)\,dx\,dy - \int_{25}^{70}\int_{205}^{fgx} y f(x,y)\,dx\,dy \\
+ \int_{M_{10y}}^{95}\int_{M_{10x}}^{ghx} y f(x,y)\,dx\,dy + \int_{a}^{70}\int_{M_{10x}}^{fx} y f(x,y)\,dx\,dy
\end{array}\right]$$

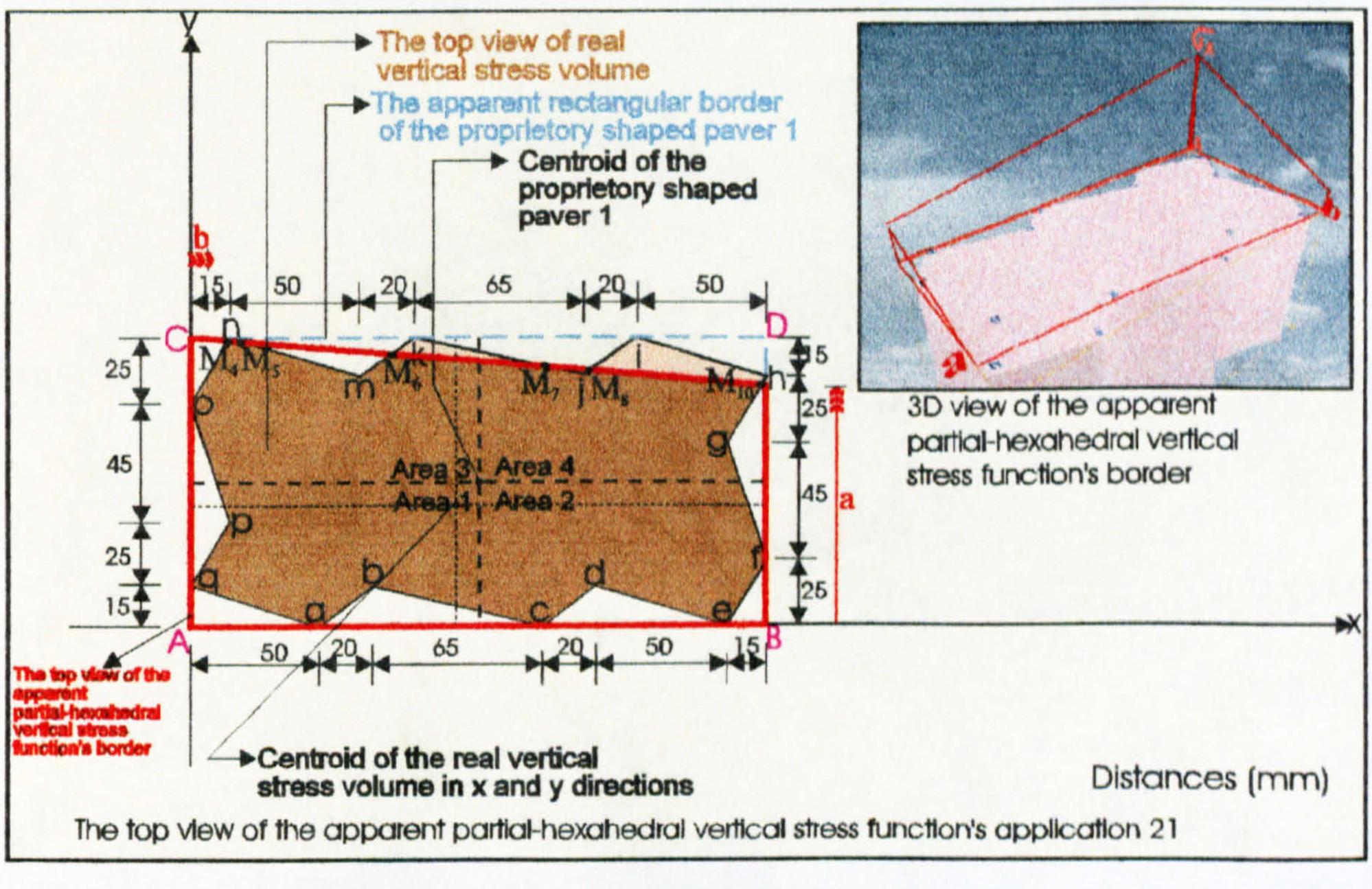

The top view of the apparent partial-hexahedral vertical stress function's application 21

Figure 7.87: Application 21 of the partial-hexahedral compressive stress distribution beneath the circumscribing rectangular border of proprietory shaped paver 1.

Application 21 of the partial-hexahedral compressive stress regime beneath the circumscribing rectangular border of proprietory shaped paver 1 shown in Figure 7.87

can be calculated by using Tables 5.1 and 7.4 and the surface function of the partial-hexahedral compressive stress through the three points σ_A, **l** and **t**.

The total volume **V** beneath the surface $f(x,y) = z\ (> 0)$ and above the region in the xy-plane (see Figure 7.87) is:

$$V = \int_0^b \int_0^{110} f(x,y)\,dy\,dx + \int_b^{220a} \int_0^{220} f(x,y)\,dy\,dx + \int_b^{220fy} \int_a^{M_{4x}onv} f(x,y)\,dy\,dx - \int_0^b \int_{85}^{110} f(x,y)\,dy\,dx - \int_0^{M_{4x}} \int_{0}^{M_{4y}} f(x,y)\,dy\,dx$$

$$- \int_b^{M_{4x}} \int_{M_{4y}}^{fy} f(x,y)\,dy\,dx - \int_{15}^{65nmy} \int_{95}^{65} f(x,y)\,dy\,dx - \int_{65}^{85mky} \int_{95}^{85} f(x,y)\,dy\,dx + \int_{15}^{M_{5x}} \int_{M_{5y}}^{nmy} f(x,y)\,dy\,dx + \int_{M_{5x}}^{M_{6x}} \int_{M_{5y}}^{110} f(x,y)\,dy\,dx$$

$$+ \int_{M_{5x}}^{M_{6x}} \int_{M_{6y}}^{fy} f(x,y)\,dy\,dx + \int_{M_{6x}}^{85} \int_{M_{6y}}^{mky} f(x,y)\,dy\,dx - \int_{205}^{220ghy} \int_{70}^{220} f(x,y)\,dy\,dx - \int_{205}^{220fgv} \int_{25}^{220} f(x,y)\,dy\,dx + \int_{M_{10x}}^{220} \int_{M_{10y}}^{ghy} f(x,y)\,dy\,dx$$

$$+ \int_{M_{10x}}^{220} \int_{a}^{fy} f(x,y)\,dy\,dx - \int_{85}^{150kjv} \int_{95}^{150} f(x,y)\,dy\,dx - \int_{150}^{170jiv} \int_{95}^{170} f(x,y)\,dy\,dx + \int_{85}^{M_{7x}} \int_{M_{7y}}^{kjv} f(x,y)\,dy\,dx + \int_{M_{7x}}^{M_{8x}} \int_{M_{7y}}^{110} f(x,y)\,dy\,dx$$

$$+ \int_{M_{7x}}^{M_{8x}} \int_{M_{8y}}^{fy} f(x,y)\,dy\,dx + \int_{M_{8x}}^{170} \int_{M_{8y}}^{jiy} f(x,y)\,dy\,dx - \int_{0}^{15pqy} \int_{40}^{15} f(x,y)\,dy\,dx - \int_{0}^{15qry} \int_{15}^{50} f(x,y)\,dy\,dx - \int_{0}^{50rqv} \int_{0}^{0} f(x,y)\,dy\,dx$$

$$- \int_{50}^{70aby} \int_{0}^{0} f(x,y)\,dy\,dx - \int_{70}^{135bcy} \int_{0}^{0} f(x,y)\,dy\,dx - \int_{135}^{155cdy} \int_{0}^{0} f(x,y)\,dy\,dx - \int_{155}^{205dey} \int_{0}^{0} f(x,y)\,dy\,dx - \int_{205}^{220efv} \int_{0}^{0} f(x,y)\,dy\,dx$$

and the centroids of this volume in the xy-plane are at distances $\overline{X}$ and $\overline{Y}$ from the axes (see Figure 7.87) which are given by the following equations.

$$\overline{X} = \frac{1}{V}\left[\int_0^b \int_0^{110} x f(x,y)\,dy\,dx + \int_b^{220a} \int_0^{220} x f(x,y)\,dy\,dx + \int_b^{220fy} \int_a^{M_{4x}onv} x f(x,y)\,dy\,dx - \int_0^{M_{4x}} \int_{85}^{onv} x f(x,y)\,dy\,dx\right.$$

$$- \int_0^b \int_{85}^{110} x f(x,y)\,dy\,dx - \int_b^{M_{4x}} \int_{M_{4y}}^{fy} x f(x,y)\,dy\,dx - \int_{15}^{65nmv} \int_{95}^{65} x f(x,y)\,dy\,dx - \int_{65}^{85mkv} \int_{95}^{85} x f(x,y)\,dy\,dx$$

$$+ \int_{15}^{M_{5x}} \int_{M_{5y}}^{nmy} x f(x,y)\,dy\,dx + \int_{M_{5x}}^{M_{6x}} \int_{M_{5y}}^{110} x f(x,y)\,dy\,dx + \int_{M_{5x}}^{M_{6x}} \int_{M_{6y}}^{fy} x f(x,y)\,dy\,dx + \int_{M_{6x}}^{85} \int_{M_{6y}}^{mky} x f(x,y)\,dy\,dx$$

$$\left. - \int_{205}^{220ghy} \int_{70}^{220} x f(x,y)\,dy\,dx - \int_{205}^{220fgv} \int_{25}^{220} x f(x,y)\,dy\,dx + \int_{M_{10x}}^{220} \int_{M_{10y}}^{ghy} x f(x,y)\,dy\,dx + \int_{M_{10x}}^{220} \int_{a}^{fy} x f(x,y)\,dy\,dx\right.$$

$$-\int_{85}^{150}\int_{95}^{kjy} x f(x,y)\,dy\,dx - \int_{150}^{170}\int_{95}^{jiy} x f(x,y)\,dy\,dx + \int_{85}^{Mf_{7x}}\int_{Mf_{7y}}^{kjy} x f(x,y)\,dy\,dx + \int_{Mf_{7x}}^{Mf_{8x}}\int_{Mf_{7y}}^{110} x f(x,y)\,dy\,dx$$

$$+\int_{Mf_{7x}}^{Mf_{8x}}\int_{Mf_{8y}}^{fy} x f(x,y)\,dy\,dx + \int_{Mf_{8x}}^{170}\int_{Mf_{8y}}^{jiy} x f(x,y)\,dy\,dx - \int_{0}^{15}\int_{0}^{40poy} x f(x,y)\,dy\,dx - \int_{0}^{15}\int_{0}^{15qpy} x f(x,y)\,dy\,dx$$

$$-\int_{0}^{50}\int_{0}^{50qay} x f(x,y)\,dy\,dx - \int_{50}^{70}\int_{0}^{70aby} x f(x,y)\,dy\,dx - \int_{70}^{135}\int_{0}^{135bcy} x f(x,y)\,dy\,dx - \int_{135}^{155}\int_{0}^{155cdy} x f(x,y)\,dy\,dx$$

$$-\int_{155}^{205}\int_{0}^{205dey} x f(x,y)\,dy\,dx - \int_{205}^{220}\int_{0}^{220efy} x f(x,y)\,dy\,dx\Bigg]$$

$$\left[\int_{0}^{110}\int_{0}^{b} y f(x,y)\,dx\,dy + \int_{0}^{a}\int_{b}^{220} y f(x,y)\,dx\,dy + \int_{a}^{110}\int_{b}^{fx} y f(x,y)\,dx\,dy - \int_{85}^{Mf_{4y}}\int_{0}^{onx} y f(x,y)\,dx\,dy\right.$$

$$-\int_{Mf_{4y}}^{110}\int_{0}^{b} y f(x,y)\,dx\,dy - \int_{Mf_{4y}}^{110}\int_{b}^{fx} y f(x,y)\,dx\,dy - \int_{95}^{110}\int_{15}^{nmx} y f(x,y)\,dx\,dy - \int_{95}^{110}\int_{65}^{mkx} y f(x,y)\,dx\,dy$$

$$+\int_{Mf_{5y}}^{110}\int_{15}^{nmx} y f(x,y)\,dx\,dy + \int_{Mf_{5y}}^{110}\int_{Mf_{5x}}^{Mf_{6x}} y f(x,y)\,dx\,dy + \int_{Mf_{6y}}^{Mf_{5y}}\int_{Mf_{5x}}^{fx} y f(x,y)\,dx\,dy + \int_{Mf_{6y}}^{110}\int_{Mf_{6x}}^{mkx} y f(x,y)\,dx\,dy$$

$$-\int_{70}^{205}\int_{95}^{ghx} y f(x,y)\,dx\,dy - \int_{25}^{205}\int_{70}^{fgx} y f(x,y)\,dx\,dy + \int_{Mf_{10y}}^{Mf_{10x}}\int_{95}^{ghx} y f(x,y)\,dx\,dy + \int_{a}^{Mf_{10x}}\int_{70}^{fx} y f(x,y)\,dx\,dy$$

$$-\int_{95}^{110}\int_{85}^{kjx} y f(x,y)\,dx\,dy - \int_{95}^{110}\int_{150}^{jix} y f(x,y)\,dx\,dy + \int_{Mf_{7y}}^{110}\int_{85}^{kjx} y f(x,y)\,dx\,dy + \int_{Mf_{7y}}^{110}\int_{Mf_{7x}}^{Mf_{8x}} y f(x,y)\,dx\,dy$$

$$+\int_{Mf_{8y}}^{Mf_{7y}}\int_{Mf_{7x}}^{fx} y f(x,y)\,dx\,dy + \int_{Mf_{8y}}^{110}\int_{Mf_{8x}}^{jix} y f(x,y)\,dx\,dy - \int_{40}^{85}\int_{0}^{pox} y f(x,y)\,dx\,dy - \int_{15}^{40}\int_{0}^{qpx} y f(x,y)\,dx\,dy$$

$$-\int_{0}^{15}\int_{0}^{15qax} y f(x,y)\,dx\,dy - \int_{0}^{15}\int_{50}^{15abx} y f(x,y)\,dx\,dy - \int_{0}^{15}\int_{70}^{15bcx} y f(x,y)\,dx\,dy - \int_{0}^{15}\int_{135}^{15cdx} y f(x,y)\,dx\,dy$$

$$\left.-\int_{0}^{15}\int_{155}^{15dex} y f(x,y)\,dx\,dy - \int_{0}^{25}\int_{205}^{efx} y f(x,y)\,dx\,dy\right]$$

$$\overline{Y} = \frac{1}{V}$$

Application 22 of the partial-hexahedral compressive stress regime beneath the circumscribing rectangular border of proprietory shaped paver 1 shown in Figure 7.88 can be calculated by using Tables 5.1 and 7.4 and the surface function of the partial-hexahedral compressive stress through the three points σ_A, **l** and **t**.

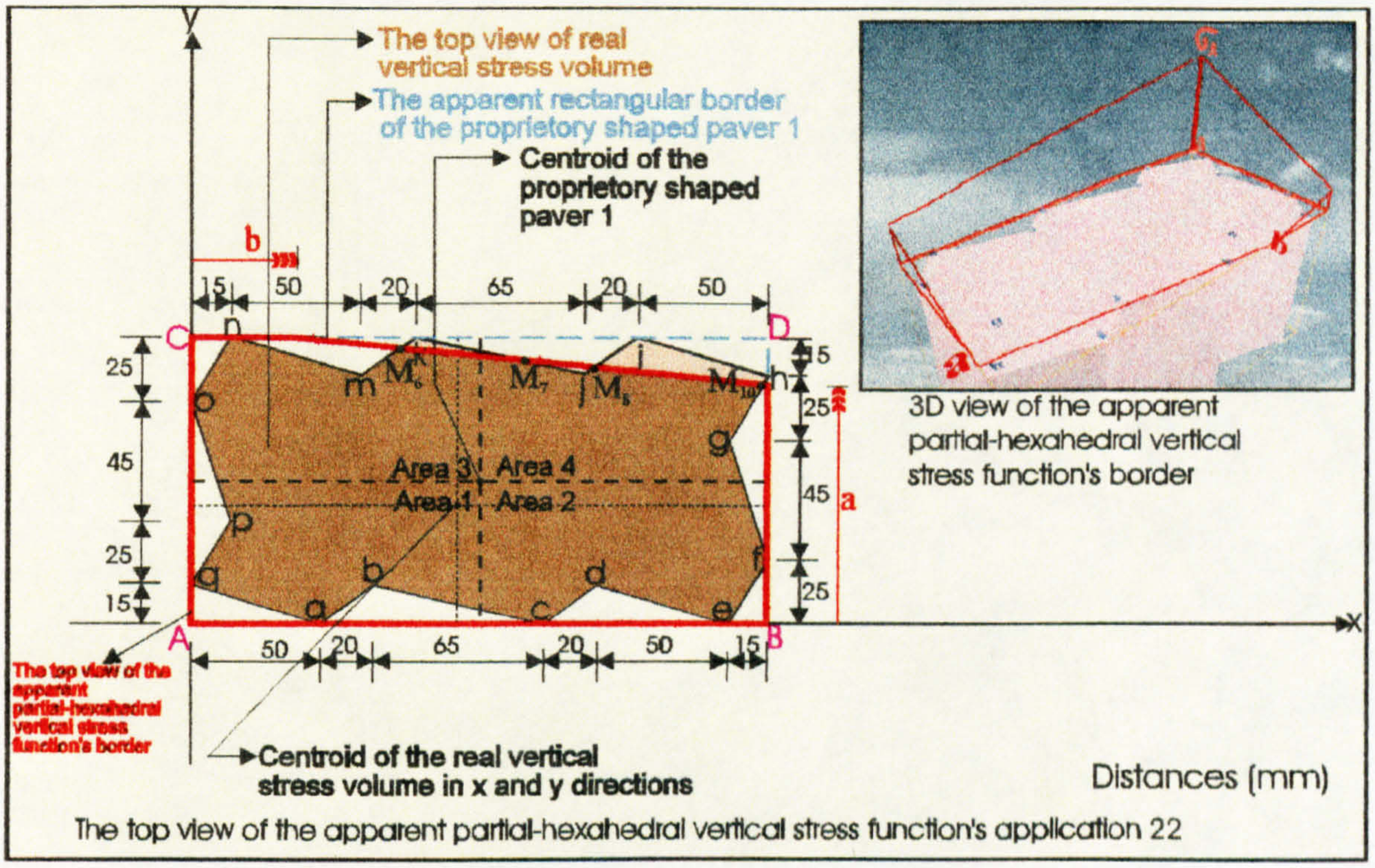

Figure 7.88: Application 22 of the partial-hexahedral compressive stress distribution beneath the circumscribing rectangular border of proprietory shaped paver 1.

The total volume **V** beneath the surface $f(x,y) = z\ (> 0)$ and above the region in the xy-plane (see Figure 7.88) is:

$$V = \int_0^b \int_0^{110} f(x,y)\,dy\,dx + \int_b^{220} \int_0^{a} f(x,y)\,dy\,dx + \int_b^{220} \int_a^{fy} f(x,y)\,dy\,dx - \int_{15}^{65} \int_{95}^{nmy} f(x,y)\,dy\,dx - \int_{65}^{85} \int_{95}^{mky} f(x,y)\,dy\,dx$$

$$+ \int_b^{M_{6x}} \int_{M_{6y}}^{fy} f(x,y)\,dy\,dx + \int_{M_{6x}}^{85} \int_{M_{6y}}^{mky} f(x,y)\,dy\,dx - \int_{205}^{220} \int_{70}^{ghy} f(x,y)\,dy\,dx - \int_{205}^{220} \int_{25}^{fgy} f(x,y)\,dy\,dx + \int_{M_{10x}}^{220} \int_{M_{10y}}^{ghy} f(x,y)\,dy\,dx$$

$$+ \int_{M_{10x}}^{220} \int_{a}^{fy} f(x,y)\,dy\,dx - \int_{85}^{150} \int_{95}^{kjy} f(x,y)\,dy\,dx - \int_{150}^{170} \int_{95}^{jiy} f(x,y)\,dy\,dx + \int_{85}^{M_{7x}} \int_{M_{7y}}^{kjy} f(x,y)\,dy\,dx + \int_{M_{7x}}^{M_{8x}} \int_{M_{7y}}^{110} f(x,y)\,dy\,dx$$

$$+ \int_{M_{7x}}^{M_{8x}} \int_{M_{8y}}^{fy} f(x,y)\,dy\,dx + \int_{M_{8x}}^{170} \int_{M_{8y}}^{jiy} f(x,y)\,dy\,dx - \int_{0}^{15} \int_{85}^{ony} f(x,y)\,dy\,dx - \int_{0}^{40} \int_{85}^{poy} f(x,y)\,dy\,dx - \int_{0}^{15} \int_{85}^{qpy} f(x,y)\,dy\,dx$$

$$- \int_0^{50} \int_0^{qay} f(x,y)\,dy\,dx - \int_{50}^{70} \int_0^{aby} f(x,y)\,dy\,dx - \int_{70}^{135} \int_0^{bcy} f(x,y)\,dy\,dx - \int_{135}^{155} \int_0^{cdy} f(x,y)\,dy\,dx - \int_{155}^{205} \int_0^{dey} f(x,y)\,dy\,dx$$

$$- \int_{205}^{220} \int_0^{efy} f(x,y)\,dy\,dx$$

and the centroids of this volume in the xy-plane are at distances $\overline{X}$ and $\overline{Y}$ from the axes (see Figure 7.88) which are given by the following equations.

$$\overline{X} = \frac{1}{V}\left[\begin{array}{l}
\int_{0}^{b}\int_{0}^{110} xf(x,y)\,dy\,dx + \int_{b}^{220}\int_{0}^{a} xf(x,y)\,dy\,dx + \int_{b}^{220}\int_{a}^{fy} xf(x,y)\,dy\,dx - \int_{15}^{65}\int_{95}^{mny} xf(x,y)\,dy\,dx \\
-\int_{65}^{85}\int_{95}^{mky} xf(x,y)\,dy\,dx + \int_{b}^{M_{6x}}\int_{M_{6y}}^{fy} xf(x,y)\,dy\,dx + \int_{M_{6x}}^{85}\int_{M_{6y}}^{mky} xf(x,y)\,dy\,dx - \int_{205}^{220}\int_{70}^{gly} xf(x,y)\,dy\,dx \\
-\int_{205}^{220}\int_{25}^{fgy} xf(x,y)\,dy\,dx + \int_{M_{10x}}^{220}\int_{M_{10y}}^{gly} xf(x,y)\,dy\,dx + \int_{M_{10x}}^{220}\int_{a}^{fy} xf(x,y)\,dy\,dx - \int_{85}^{150}\int_{95}^{kjy} xf(x,y)\,dy\,dx \\
-\int_{150}^{170}\int_{95}^{jiy} xf(x,y)\,dy\,dx + \int_{85}^{M_{7x}}\int_{M_{7y}}^{kjy} xf(x,y)\,dy\,dx + \int_{M_{7x}}^{M_{8x}}\int_{M_{7y}}^{110} xf(x,y)\,dy\,dx + \int_{M_{7x}}^{M_{8x}}\int_{M_{8y}}^{fy} xf(x,y)\,dy\,dx \\
+\int_{M_{8x}}^{170}\int_{M_{8y}}^{jiy} xf(x,y)\,dy\,dx - \int_{0}^{15}\int_{85}^{ony} xf(x,y)\,dy\,dx - \int_{0}^{15}\int_{40}^{poy} xf(x,y)\,dy\,dx - \int_{0}^{15}\int_{15}^{qjy} xf(x,y)\,dy\,dx \\
-\int_{0}^{50}\int_{0}^{qay} xf(x,y)\,dy\,dx - \int_{50}^{70}\int_{0}^{aby} xf(x,y)\,dy\,dx - \int_{70}^{135}\int_{0}^{bcy} xf(x,y)\,dy\,dx - \int_{135}^{155}\int_{0}^{cdy} xf(x,y)\,dy\,dx \\
-\int_{155}^{205}\int_{0}^{dey} xf(x,y)\,dy\,dx - \int_{205}^{220}\int_{0}^{efy} xf(x,y)\,dy\,dx
\end{array}\right]$$

$$\overline{Y} = \frac{1}{V}\left[\begin{array}{l}
\int_{0}^{110}\int_{0}^{b} yf(x,y)\,dx\,dy + \int_{0}^{a}\int_{b}^{220} yf(x,y)\,dx\,dy + \int_{a}^{110}\int_{b}^{fx} yf(x,y)\,dx\,dy - \int_{95}^{110}\int_{15}^{mnx} yf(x,y)\,dx\,dy \\
-\int_{95}^{110}\int_{65}^{mkx} yf(x,y)\,dx\,dy + \int_{M_{6y}}^{110}\int_{b}^{fx} yf(x,y)\,dx\,dy + \int_{M_{6y}}^{110}\int_{M_{6x}}^{mkx} yf(x,y)\,dx\,dy - \int_{70}^{205}\int_{95}^{ghx} yf(x,y)\,dx\,dy \\
-\int_{25}^{70}\int_{205}^{fgx} yf(x,y)\,dx\,dy + \int_{M_{10y}}^{95}\int_{M_{10x}}^{ghx} yf(x,y)\,dx\,dy + \int_{a}^{70}\int_{M_{10x}}^{fx} yf(x,y)\,dx\,dy - \int_{95}^{110}\int_{85}^{kjx} yf(x,y)\,dx\,dy \\
-\int_{95}^{110}\int_{150}^{jix} yf(x,y)\,dx\,dy + \int_{M_{7y}}^{110}\int_{85}^{kjx} yf(x,y)\,dx\,dy + \int_{M_{7y}}^{110}\int_{M_{7x}}^{M_{8x}} yf(x,y)\,dx\,dy + \int_{M_{8y}}^{M_{7y}}\int_{M_{7x}}^{fx} yf(x,y)\,dx\,dy \\
+\int_{M_{8y}}^{110}\int_{M_{8x}}^{jix} yf(x,y)\,dx\,dy - \int_{85}^{110}\int_{0}^{onx} yf(x,y)\,dx\,dy - \int_{40}^{85}\int_{0}^{pnx} yf(x,y)\,dx\,dy - \int_{15}^{40}\int_{0}^{qjnx} yf(x,y)\,dx\,dy \\
-\int_{0}^{15}\int_{0}^{qax} yf(x,y)\,dx\,dy - \int_{0}^{15}\int_{50}^{abx} yf(x,y)\,dx\,dy - \int_{0}^{15}\int_{70}^{bcx} yf(x,y)\,dx\,dy - \int_{0}^{15}\int_{135}^{cdx} yf(x,y)\,dx\,dy \\
-\int_{0}^{15}\int_{155}^{dex} yf(x,y)\,dx\,dy - \int_{0}^{25}\int_{205}^{efx} yf(x,y)\,dx\,dy
\end{array}\right]$$

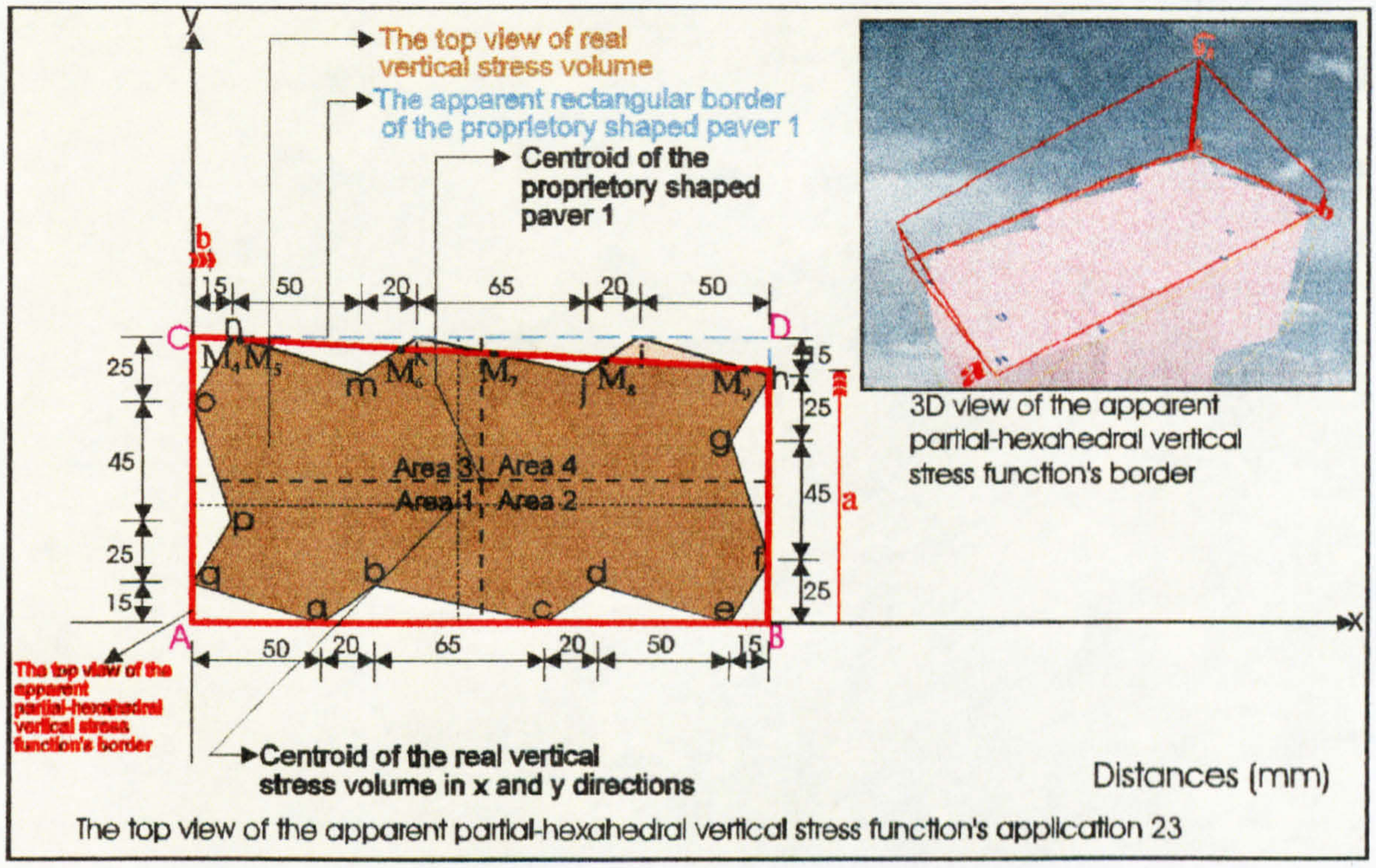

Figure 7.89: Application 23 of the partial-hexahedral compressive stress distribution beneath the circumscribing rectangular border of proprietory shaped paver 1.

Application 23 of the partial-hexahedral compressive stress regime beneath the circumscribing rectangular border of proprietory shaped paver 1 shown in Figure 7.89 can be calculated by using Tables 5.1 and 7.4 and the surface function of the partial-hexahedral compressive stress through the three points σ_A, **l** and **t**.

The total volume **V** beneath the surface $f(x,y) = z\ (> 0)$ and above the region in the xy-plane (see Figure 7.89) is:

$$V = \int_0^b \int_0^{110} f(x,y)\,dy\,dx + \int_b^{220} \int_0^a f(x,y)\,dy\,dx + \int_{220}^{fy} \int_b^a f(x,y)\,dy\,dx - \int_{M_{4x}}^{ony} \int_0^{85} f(x,y)\,dy\,dx - \int_b^{110} \int_0^{M_{4y}} f(x,y)\,dy\,dx$$

$$- \int_{M_{4x}}^{b} \int_{M_{4y}}^{fy} f(x,y)\,dy\,dx - \int_{15}^{65} \int_{95}^{nmy} f(x,y)\,dy\,dx - \int_{65}^{85} \int_{95}^{mky} f(x,y)\,dy\,dx + \int_{15}^{M_{5x}} \int_{M_{5y}}^{nmy} f(x,y)\,dy\,dx + \int_{M_{5x}}^{M_{6x}} \int_{M_{5y}}^{110} f(x,y)\,dy\,dx$$

$$+ \int_{M_{5x}}^{M_{6x}} \int_{M_{6y}}^{fy} f(x,y)\,dy\,dx + \int_{M_{6x}}^{85} \int_{M_{6y}}^{mky} f(x,y)\,dy\,dx - \int_{M_{9x}}^{220} \int_{95}^{hiy} f(x,y)\,dy\,dx + \int_{M_{9x}}^{220} \int_{a}^{fy} f(x,y)\,dy\,dx - \int_{85}^{150} \int_{95}^{kjy} f(x,y)\,dy\,dx$$

$$-\int_{150}^{170}\int_{95}^{jiy} f(x,y)\,dy\,dx+\int_{85}^{M_{7x}}\int_{M_{7y}}^{kjy} f(x,y)\,dy\,dx+\int_{M_{7x}}^{M_{8x}}\int_{M_{7y}}^{110} f(x,y)\,dy\,dx+\int_{M_{7x}}^{M_{8x}}\int_{M_{8y}}^{fy} f(x,y)\,dy\,dx+\int_{M_{8x}}^{170}\int_{M_{8y}}^{jiv} f(x,y)\,dy\,dx$$

$$-\int_{205}^{220}\int_{70}^{ghy} f(x,y)\,dy\,dx-\int_{205}^{220}\int_{25}^{fgv} f(x,y)\,dy\,dx-\int_{0}^{15}\int_{40}^{poy} f(x,y)\,dy\,dx-\int_{0}^{15}\int_{15}^{qjpy} f(x,y)\,dy\,dx-\int_{0}^{50}\int_{0}^{qkny} f(x,y)\,dy\,dx$$

$$-\int_{50}^{70}\int_{0}^{aby} f(x,y)\,dy\,dx-\int_{70}^{135}\int_{0}^{bcy} f(x,y)\,dy\,dx-\int_{135}^{155}\int_{0}^{cdy} f(x,y)\,dy\,dx-\int_{155}^{205}\int_{0}^{dey} f(x,y)\,dy\,dx-\int_{205}^{220}\int_{0}^{efy} f(x,y)\,dy\,dx$$

and the centroids of this volume in the xy-plane are at distances $\overline{X}$ and $\overline{Y}$ from the axes (see Figure 7.89) which are given by the following equations.

$$\overline{X}=\frac{1}{Vx}\left[\begin{array}{l}
\int_{0}^{b}\int_{0}^{110} xf(x,y)\,dy\,dx+\int_{b}^{220}\int_{0}^{a} xf(x,y)\,dy\,dx+\int_{b}^{220}\int_{a}^{fy} xf(x,y)\,dy\,dx-\int_{0}^{M_{4x}}\int_{85}^{omy} xf(x,y)\,dy\,dx \\
-\int_{0}^{b}\int_{M_{4y}}^{110} xf(x,y)\,dy\,dx-\int_{b}^{M_{4x}}\int_{M_{4y}}^{fy} xf(x,y)\,dy\,dx-\int_{15}^{65}\int_{95}^{nmy} xf(x,y)\,dy\,dx-\int_{65}^{85}\int_{95}^{mky} xf(x,y)\,dy\,dx \\
+\int_{15}^{M_{5x}}\int_{M_{5y}}^{nny} xf(x,y)\,dy\,dx+\int_{M_{5x}}^{M_{6x}}\int_{M_{5y}}^{110} xf(x,y)\,dy\,dx+\int_{M_{5x}}^{M_{6x}}\int_{M_{6y}}^{fy} xf(x,y)\,dy\,dx+\int_{M_{6x}}^{85}\int_{M_{6y}}^{mky} xf(x,y)\,dy\,dx \\
-\int_{M_{9x}}^{220}\int_{95}^{hiy} xf(x,y)\,dy\,dx+\int_{M_{9x}}^{220}\int_{a}^{fy} xf(x,y)\,dy\,dx-\int_{85}^{150}\int_{95}^{kjv} xf(x,y)\,dy\,dx-\int_{150}^{170}\int_{95}^{jlv} xf(x,y)\,dy\,dx \\
+\int_{85}^{M_{7x}}\int_{M_{7y}}^{kjy} xf(x,y)\,dy\,dx+\int_{M_{7x}}^{M_{8x}}\int_{M_{7y}}^{110} xf(x,y)\,dy\,dx+\int_{M_{7x}}^{M_{8x}}\int_{M_{8y}}^{fy} xf(x,y)\,dy\,dx+\int_{M_{8x}}^{170}\int_{M_{8y}}^{jlv} xf(x,y)\,dy\,dx \\
-\int_{205}^{220}\int_{70}^{ghy} xf(x,y)\,dy\,dx-\int_{205}^{220}\int_{25}^{fgv} xf(x,y)\,dy\,dx-\int_{0}^{15}\int_{40}^{poy} xf(x,y)\,dy\,dx-\int_{0}^{15}\int_{15}^{qjpy} xf(x,y)\,dy\,dx \\
-\int_{0}^{50}\int_{0}^{qay} xf(x,y)\,dy\,dx-\int_{50}^{70}\int_{0}^{uhy} xf(x,y)\,dy\,dx-\int_{70}^{135}\int_{0}^{bcy} xf(x,y)\,dy\,dx-\int_{135}^{155}\int_{0}^{cdy} xf(x,y)\,dy\,dx \\
-\int_{155}^{205}\int_{0}^{dey} xf(x,y)\,dy\,dx-\int_{205}^{220}\int_{0}^{efy} xf(x,y)\,dy\,dx
\end{array}\right]$$

$$\overline{Y}=\frac{1}{V}\left[\begin{array}{l}
\int_{0}^{110}\int_{0}^{b} y\,f(x,y)\,dx\,dy+\int_{0}^{a}\int_{b}^{220} yf(x,y)\,dx\,dy+\int_{a}^{110}\int_{b}^{fx} yf(x,y)\,dx\,dy-\int_{85}^{M_{4y}}\int_{0}^{onx} yf(x,y)\,dx\,dy \\
-\int_{M_{4y}}^{110}\int_{0}^{b} yf(x,y)\,dx\,dy-\int_{M_{4y}}^{110}\int_{b}^{fx} yf(x,y)\,dx\,dy-\int_{95}^{110}\int_{15}^{nmx} yf(x,y)\,dx\,dy-\int_{95}^{110}\int_{65}^{mkx} yf(x,y)\,dx\,dy
\end{array}\right]$$

$$+\int_{M_{5y}}^{110}\int_{15}^{nmx} y f(x,y)\,dx\,dy+\int_{M_{5y}}^{110}\int_{M_{5x}}^{M_{6x}} y f(x,y)\,dx\,dy+\int_{M_{6y}}^{M_{5y}}\int_{M_{5x}}^{fx} y f(x,y)\,dx\,dy+\int_{M_{6y}}^{110}\int_{M_{6x}}^{mkx} y f(x,y)\,dx\,dy$$

$$-\int_{95}^{M_{9y}}\int_{M_{9x}}^{hix} y f(x,y)\,dx\,dy+\int_{a}^{M_{9y}}\int_{M_{9x}}^{fx} y f(x,y)\,dx\,dy-\int_{95}^{110}\int_{85}^{kjx} y f(x,y)\,dx\,dy-\int_{95}^{110}\int_{150}^{jix} y f(x,y)\,dx\,dy$$

$$+\int_{M_{7y}}^{110}\int_{85}^{kjx} y f(x,y)\,dx\,dy+\int_{M_{7y}}^{110}\int_{M_{7x}}^{M_{8x}} y f(x,y)\,dx\,dy+\int_{M_{8y}}^{M_{7y}}\int_{M_{7x}}^{fx} y f(x,y)\,dx\,dy+\int_{M_{8y}}^{110}\int_{M_{8x}}^{jix} y f(x,y)\,dx\,dy$$

$$-\int_{70}^{95}\int_{205}^{ghx} y f(x,y)\,dx\,dy-\int_{25}^{70}\int_{205}^{fgx} y f(x,y)\,dx\,dy-\int_{40}^{85}\int_{0}^{pox} y f(x,y)\,dx\,dy-\int_{15}^{40}\int_{0}^{qpx} y f(x,y)\,dx\,dy$$

$$-\int_{0}^{15}\int_{0}^{qax} y f(x,y)\,dx\,dy-\int_{0}^{15}\int_{50}^{abx} y f(x,y)\,dx\,dy-\int_{0}^{15}\int_{70}^{bcx} y f(x,y)\,dx\,dy-\int_{0}^{15}\int_{135}^{cdx} y f(x,y)\,dx\,dy$$

$$-\int_{0}^{15}\int_{155}^{dex} y f(x,y)\,dx\,dy-\int_{0}^{25}\int_{205}^{efx} y f(x,y)\,dx\,dy\Bigg]$$

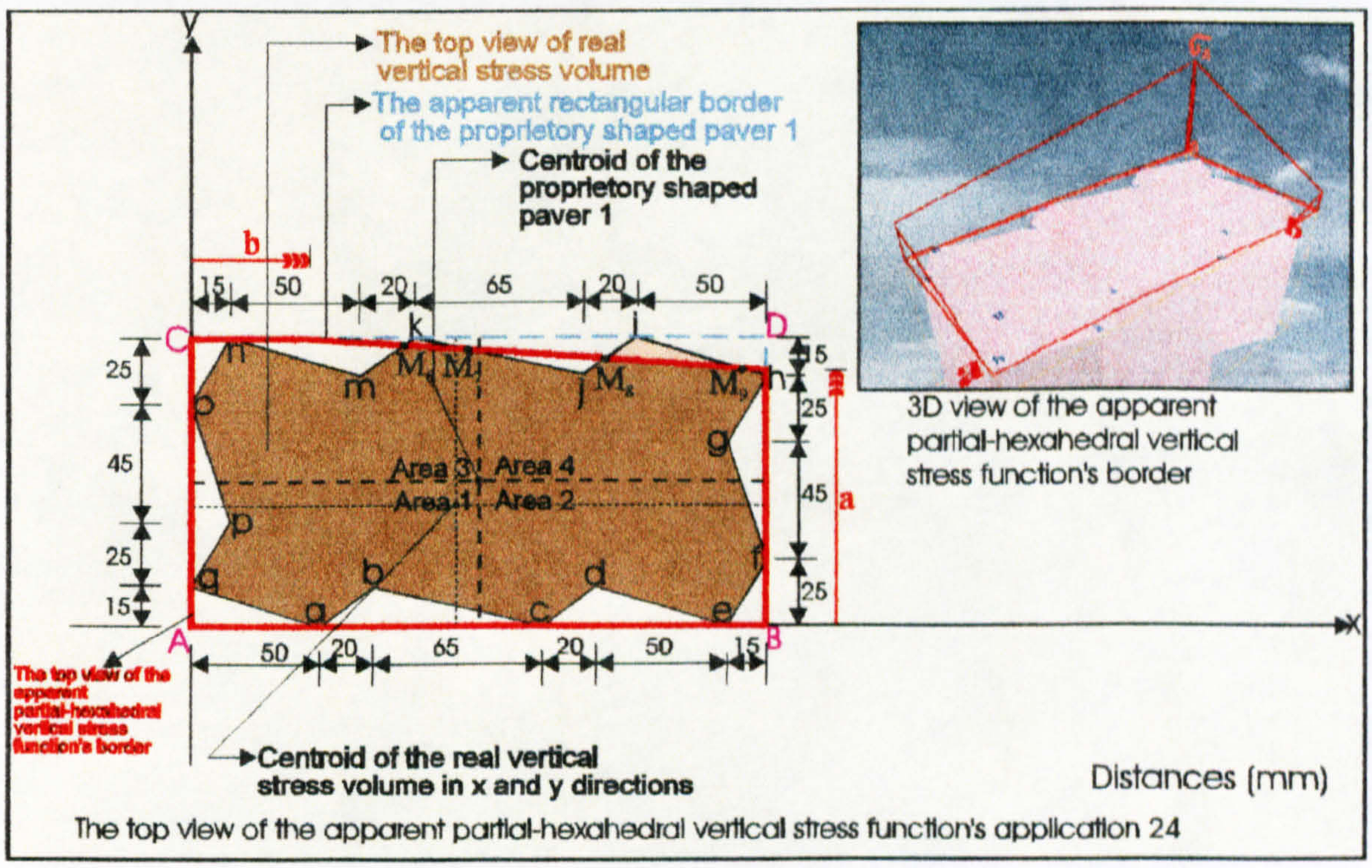

The top view of the apparent partial-hexahedral vertical stress function's application 24

Figure 7.90: Application 24 of the partial-hexahedral compressive stress distribution beneath the circumscribing rectangular border of proprietory shaped paver 1.

Application 24 of the partial-hexahedral compressive stress regime beneath the circumscribing rectangular border of proprietory shaped paver 1 shown in Figure 7.90

can be calculated by using Tables 5.1 and 7.4 and the surface function of the partial-hexahedral compressive stress through the three points σ_A, **I** and **t**.

The total volume **V** beneath the surface $f(x,y) = z\ (> 0)$ and above the region in the xy-plane (see Figure 7.90) is:

$$V = \int_0^b \int_0^{110} f(x,y)\,dy\,dx + \int_b^{220} \int_0^a f(x,y)\,dy\,dx + \int_b^{220} \int_a^{fy} f(x,y)\,dy\,dx - \int_{15}^{65} \int_{95}^{nmy} f(x,y)\,dy\,dx - \int_{65}^{85} \int_{95}^{mky} f(x,y)\,dy\,dx$$
$$+ \int_b^{M_{6x}} \int_{M_{6y}}^{fy} f(x,y)\,dy\,dx + \int_{M_{6x}}^{85} \int_{M_{6y}}^{mky} f(x,y)\,dy\,dx - \int_{M_{9x}}^{220} \int_{95}^{hiy} f(x,y)\,dy\,dx + \int_{M_{9x}}^{220} \int_a^{fv} f(x,y)\,dy\,dx - \int_{85}^{150} \int_{95}^{kjv} f(x,y)\,dy\,dx$$
$$- \int_{150}^{170} \int_{95}^{jiy} f(x,y)\,dy\,dx + \int_{85}^{M_{7x}} \int_{M_{7y}}^{kjy} f(x,y)\,dy\,dx + \int_{M_{7x}}^{M_{8x}} \int_{M_{7y}}^{110} f(x,y)\,dy\,dx + \int_{M_{7x}}^{M_{8x}} \int_{M_{8y}}^{fv} f(x,y)\,dy\,dx + \int_{M_{8x}}^{170} \int_{M_{8y}}^{jiv} f(x,y)\,dy\,dx$$
$$- \int_0^{15} \int_{85}^{ony} f(x,y)\,dy\,dx - \int_{205}^{220} \int_{70}^{ghy} f(x,y)\,dy\,dx - \int_{205}^{220} \int_{25}^{fgy} f(x,y)\,dy\,dx - \int_0^{15} \int_{40}^{pcy} f(x,y)\,dy\,dx - \int_0^{15} \int_{15}^{qpy} f(x,y)\,dy\,dx$$
$$- \int_0^{50} \int_0^{qay} f(x,y)\,dy\,dx - \int_{50}^{70} \int_0^{aby} f(x,y)\,dy\,dx - \int_{70}^{135} \int_0^{bcy} f(x,y)\,dy\,dx - \int_{135}^{155} \int_0^{cdy} f(x,y)\,dy\,dx - \int_{155}^{205} \int_0^{dey} f(x,y)\,dy\,dx$$
$$- \int_{205}^{220} \int_0^{efy} f(x,y)\,dy\,dx$$

and the centroids of this volume in the xy-plane are at distances $\overline{X}$ and $\overline{Y}$ from the axes (see Figure 7.90) which are given by the following equations.

$$\overline{X} = \frac{1}{V}\left[\int_0^b \int_0^{110} x f(x,y)\,dy\,dx + \int_b^{220} \int_0^a x f(x,y)\,dy\,dx + \int_b^{220} \int_a^{fy} x f(x,y)\,dy\,dx - \int_{15}^{65} \int_{95}^{nmy} x f(x,y)\,dy\,dx\right.$$
$$- \int_{65}^{85} \int_{95}^{mky} x f(x,y)\,dy\,dx + \int_b^{M_{6x}} \int_{M_{6y}}^{fy} x f(x,y)\,dy\,dx + \int_{M_{6x}}^{85} \int_{M_{6y}}^{mky} x f(x,y)\,dy\,dx - \int_{M_{9x}}^{220} \int_{95}^{hiy} x f(x,y)\,dy\,dx$$
$$+ \int_{M_{9x}}^{220} \int_a^{fy} x f(x,y)\,dy\,dx - \int_{85}^{150} \int_{95}^{kjy} x f(x,y)\,dy\,dx - \int_{150}^{170} \int_{95}^{jiy} x f(x,y)\,dy\,dx + \int_{85}^{M_{7x}} \int_{M_{7y}}^{kjy} x f(x,y)\,dy\,dx$$
$$+ \int_{M_{7x}}^{M_{8x}} \int_{M_{7y}}^{110} x f(x,y)\,dy\,dx + \int_{M_{7x}}^{M_{8x}} \int_{M_{8y}}^{fy} x f(x,y)\,dy\,dx + \int_{M_{8x}}^{170} \int_{M_{8y}}^{jiy} x f(x,y)\,dy\,dx - \int_0^{15} \int_{85}^{ony} x f(x,y)\,dy\,dx$$
$$\left. - \int_{205}^{220} \int_{70}^{ghy} x f(x,y)\,dy\,dx - \int_{205}^{220} \int_{25}^{fgy} x f(x,y)\,dy\,dx - \int_0^{15} \int_{40}^{pcy} x f(x,y)\,dy\,dx - \int_0^{15} \int_{15}^{qpy} x f(x,y)\,dy\,dx\right.$$

$$-\int_{0}^{50}\int_{0}^{qay} xf(x,y)\,dy\,dx-\int_{50}^{70}\int_{0}^{aby} xf(x,y)\,dy\,dx-\int_{70}^{135}\int_{0}^{bcy} xf(x,y)\,dy\,dx-\int_{135}^{155}\int_{0}^{cdy} xf(x,y)\,dy\,dx$$
$$-\int_{155}^{205}\int_{0}^{dey} xf(x,y)\,dy\,dx-\int_{205}^{220}\int_{0}^{efy} xf(x,y)\,dy\,dx\Bigg]$$

$$\overline{Y}=\frac{1}{V}\Bigg[\int_{0}^{110}\int_{0}^{b} yf(x,y)\,dx\,dy+\int_{0}^{a}\int_{b}^{220} yf(x,y)\,dx\,dy+\int_{a}^{110}\int_{b}^{fx} yf(x,y)\,dx\,dy-\int_{95}^{110}\int_{15}^{nmx} yf(x,y)\,dx\,dy$$
$$-\int_{95}^{110}\int_{65}^{mkx} yf(x,y)\,dx\,dy+\int_{Mf_{6y}}^{110}\int_{b}^{fx} yf(x,y)\,dx\,dy+\int_{Mf_{6y}}^{110}\int_{Mf_{6x}}^{mkx} yf(x,y)\,dx\,dy-\int_{95}^{Mf_{9y}}\int_{Mf_{9x}}^{hlx} yf(x,y)\,dx\,dy$$
$$+\int_{a}^{Mf_{9y}}\int_{Mf_{9x}}^{fx} yf(x,y)\,dx\,dy-\int_{95}^{110}\int_{85}^{kjx} yf(x,y)\,dx\,dy-\int_{95}^{110}\int_{150}^{jlx} yf(x,y)\,dx\,dy+\int_{Mf_{7y}}^{110}\int_{85}^{kjx} yf(x,y)\,dx\,dy$$
$$+\int_{Mf_{7y}}^{110}\int_{Mf_{7x}}^{Mf_{8x}} yf(x,y)\,dx\,dy+\int_{Mf_{8y}}^{Mf_{7y}}\int_{Mf_{7x}}^{fx} yf(x,y)\,dx\,dy+\int_{Mf_{8y}}^{110}\int_{Mf_{8x}}^{jlx} yf(x,y)\,dx\,dy-\int_{85}^{110}\int_{0}^{onx} yf(x,y)\,dx\,dy$$
$$-\int_{70}^{95}\int_{205}^{ghx} yf(x,y)\,dx\,dy-\int_{25}^{70}\int_{205}^{fgx} yf(x,y)\,dx\,dy-\int_{40}^{85}\int_{0}^{pox} yf(x,y)\,dx\,dy-\int_{15}^{40}\int_{0}^{lnpx} yf(x,y)\,dx\,dy$$
$$-\int_{0}^{15}\int_{0}^{qax} yf(x,y)\,dx\,dy-\int_{0}^{15}\int_{50}^{abx} yf(x,y)\,dx\,dy-\int_{0}^{15}\int_{70}^{bcx} yf(x,y)\,dx\,dy-\int_{0}^{15}\int_{135}^{cdx} yf(x,y)\,dx\,dy$$
$$-\int_{0}^{15}\int_{155}^{dex} yf(x,y)\,dx\,dy-\int_{0}^{25}\int_{205}^{efx} yf(x,y)\,dx\,dy\Bigg]$$

Application 25 of the partial-hexahedral compressive stress regime beneath the circumscribing rectangular border of proprietory shaped paver 1 shown in Figure 7.91 can be calculated by using Tables 5.1 and 7.4 and the surface function of the partial-hexahedral compressive stress through the three points σ_A, l and t.

The total volume **V** beneath the surface $f(x,y)=z\ (>0)$ and above the region in the xy-plane (see Figure 7.91) is:

$$V=\int_{0}^{b}\int_{0}^{110} f(x,y)\,dy\,dx+\int_{b}^{220}\int_{0}^{a} f(x,y)\,dy\,dx+\int_{b}^{220}\int_{a}^{fy} f(x,y)\,dy\,dx-\int_{85}^{150}\int_{95}^{kjy} f(x,y)\,dy\,dx-\int_{150}^{170}\int_{95}^{jly} f(x,y)\,dy\,dx$$

$$+\int_{b}^{M_{8x}}\int_{M_{8y}}^{fy} f(x,y)\,dy\,dx+\int_{M_{8x}}^{170}\int_{M_{8y}}^{jiy} f(x,y)\,dy\,dx-\int_{M_{9x}}^{220}\int_{95}^{hiy} f(x,y)\,dy\,dx+\int_{M_{9x}}^{220}\int_{a}^{fy} f(x,y)\,dy\,dx-\int_{0}^{15}\int_{85}^{ony} f(x,y)\,dy\,dx$$

$$-\int_{205}^{220}\int_{70}^{ghy} f(x,y)\,dy\,dx-\int_{205}^{220}\int_{25}^{fgy} f(x,y)\,dy\,dx-\int_{0}^{15}\int_{40}^{poy} f(x,y)\,dy\,dx-\int_{0}^{15}\int_{15}^{qpy} f(x,y)\,dy\,dx-\int_{0}^{50}\int_{0}^{qay} f(x,y)\,dy\,dx$$

$$-\int_{50}^{70}\int_{0}^{aby} f(x,y)\,dy\,dx-\int_{70}^{135}\int_{0}^{bcy} f(x,y)\,dy\,dx-\int_{135}^{155}\int_{0}^{cdy} f(x,y)\,dy\,dx-\int_{155}^{205}\int_{0}^{dey} f(x,y)\,dy\,dx-\int_{205}^{220}\int_{0}^{efy} f(x,y)\,dy\,dx$$

$$-\int_{15}^{65}\int_{95}^{nmy} f(x,y)\,dy\,dx-\int_{65}^{85}\int_{95}^{mky} f(x,y)\,dy\,dx$$

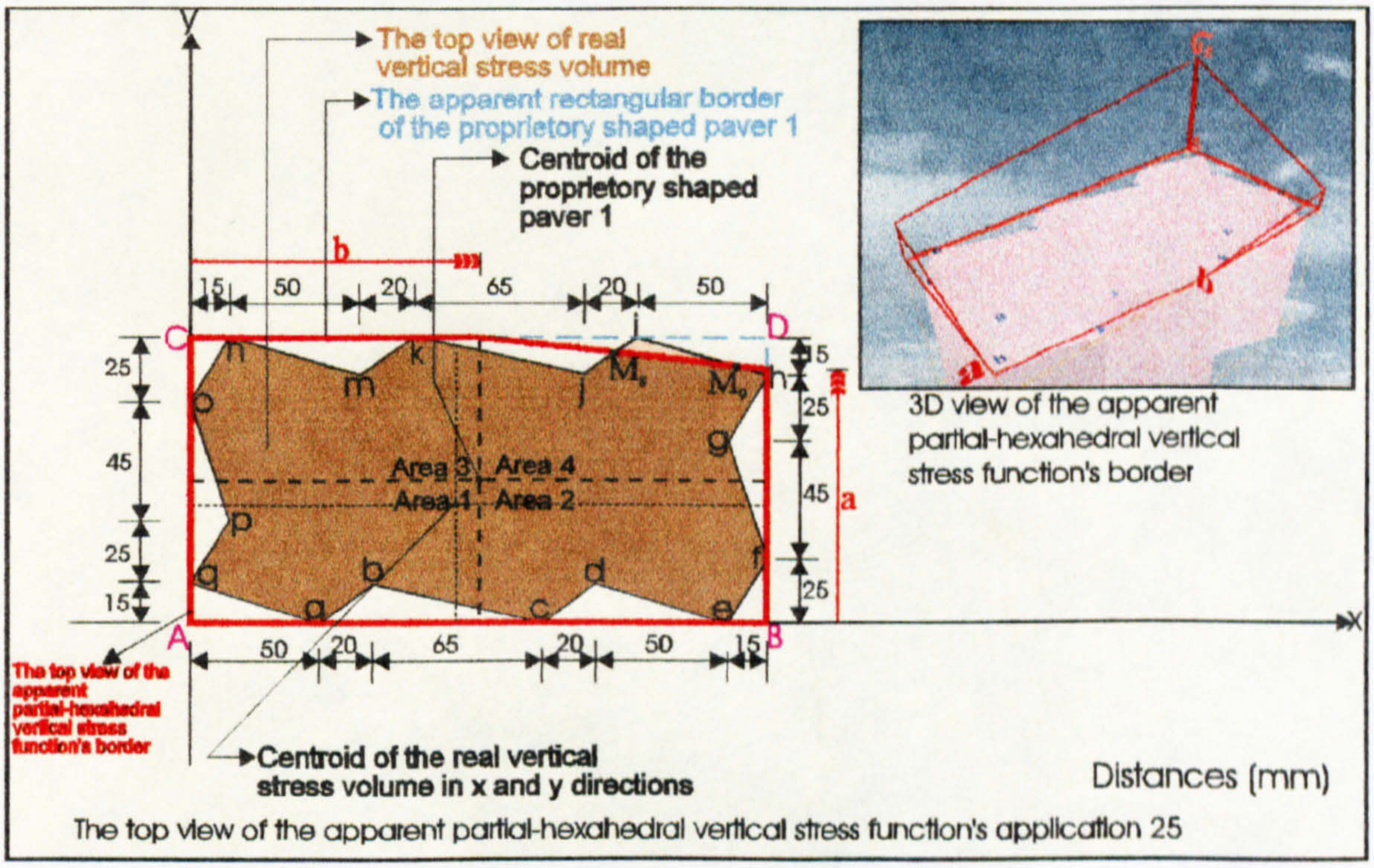

Figure 7.91: Application 25 of the partial-hexahedral compressive stress distribution beneath the circumscribing rectangular border of proprietory shaped paver 1.

and the centroids of this volume in the xy-plane are at distances $\overline{X}$ and $\overline{Y}$ from the axes (see Figure 7.91) which are given by the following equations.

$$\overline{X}=\frac{1}{V}\left[\int_{0}^{b}\int_{0}^{110} x\,f(x,y)\,dy\,dx+\int_{b}^{220}\int_{0}^{a} x\,f(x,y)\,dy\,dx+\int_{b}^{220}\int_{a}^{fy} x\,f(x,y)\,dy\,dx-\int_{85}^{150}\int_{95}^{kjy} x\,f(x,y)\,dy\,dx\right.$$

$$\left.-\int_{150}^{170}\int_{95}^{jiy} x\,f(x,y)\,dy\,dx+\int_{b}^{M_{8x}}\int_{M_{8y}}^{fy} x\,f(x,y)\,dy\,dx+\int_{M_{8x}}^{170}\int_{M_{8y}}^{jiy} x\,f(x,y)\,dy\,dx-\int_{M_{9x}}^{220}\int_{95}^{hiy} x\,f(x,y)\,dy\,dx\right.$$

$$+\int_{M_{9x}}^{220}\int_{a}^{fy} xf(x,y)\,dy\,dx-\int_{0}^{15}\int_{85}^{ony} xf(x,y)\,dy\,dx-\int_{205}^{220}\int_{70}^{ghy} xf(x,y)\,dy\,dx-\int_{205}^{220}\int_{25}^{fgy} xf(x,y)\,dy\,dx$$

$$-\int_{0}^{15}\int_{40}^{poy} xf(x,y)\,dy\,dx-\int_{0}^{15}\int_{15}^{qpy} xf(x,y)\,dy\,dx-\int_{0}^{50}\int_{0}^{qay} xf(x,y)\,dy\,dx-\int_{50}^{70}\int_{0}^{iby} xf(x,y)\,dy\,dx$$

$$-\int_{70}^{135}\int_{0}^{bcy} xf(x,y)\,dy\,dx-\int_{135}^{155}\int_{0}^{cdy} xf(x,y)\,dy\,dx-\int_{155}^{205}\int_{0}^{dey} xf(x,y)\,dy\,dx-\int_{205}^{220}\int_{0}^{efy} xf(x,y)\,dy\,dx$$

$$-\int_{15}^{65}\int_{95}^{nmy} xf(x,y)\,dy\,dx-\int_{65}^{85}\int_{95}^{mky} xf(x,y)\,dy\,dx\Bigg]$$

$$\overline{Y}=\frac{1}{V}\Bigg[\int_{0}^{110}\int_{0}^{b} yf(x,y)\,dx\,dy+\int_{0}^{a}\int_{b}^{220} yf(x,y)\,dx\,dy+\int_{a}^{110}\int_{b}^{fx} yf(x,y)\,dx\,dy-\int_{95}^{110}\int_{85}^{kjx} yf(x,y)\,dx\,dy$$

$$-\int_{95}^{110}\int_{150}^{jix} yf(x,y)\,dx\,dy+\int_{M_{8y}}^{110}\int_{b}^{fx} yf(x,y)\,dx\,dy+\int_{M_{8y}}^{110}\int_{M_{8x}}^{jix} yf(x,y)\,dx\,dy-\int_{95}^{M_{9y}}\int_{M_{9x}}^{hlx} yf(x,y)\,dx\,dy$$

$$+\int_{a}^{M_{9y}}\int_{M_{9x}}^{fx} yf(x,y)\,dx\,dy-\int_{85}^{110}\int_{0}^{onx} yf(x,y)\,dx\,dy-\int_{70}^{95}\int_{205}^{ghx} yf(x,y)\,dx\,dy-\int_{25}^{70}\int_{205}^{fgx} yf(x,y)\,dx\,dy$$

$$-\int_{40}^{85}\int_{0}^{pox} yf(x,y)\,dx\,dy-\int_{15}^{40}\int_{0}^{qpx} yf(x,y)\,dx\,dy-\int_{0}^{15}\int_{0}^{qax} yf(x,y)\,dx\,dy-\int_{0}^{15}\int_{50}^{abx} yf(x,y)\,dx\,dy$$

$$-\int_{0}^{15}\int_{70}^{bcx} yf(x,y)\,dx\,dy-\int_{0}^{15}\int_{135}^{cdx} yf(x,y)\,dx\,dy-\int_{0}^{15}\int_{155}^{dex} yf(x,y)\,dx\,dy-\int_{0}^{25}\int_{205}^{efx} yf(x,y)\,dx\,dy$$

$$-\int_{95}^{110}\int_{15}^{nmx} yf(x,y)\,dx\,dy-\int_{95}^{110}\int_{65}^{mkx} yf(x,y)\,dx\,dy\Bigg]$$

Application 26 of the partial-hexahedral compressive stress regime beneath the circumscribing rectangular border of proprietory shaped paver 1 shown in Figure 7.92 can be calculated by using Tables 5.1 and 7.4 and the surface function of the partial-hexahedral compressive stress through the three points σ_A, **l** and **t**.

The total volume **V** beneath the surface $f(x,y)=z\ (>0)$ and above the region in the xy-plane (see Figure 7.92) is:

$$V = \int_{0}^{b}\int_{0}^{110} f(x,y)\,dy\,dx + \int_{b}^{220}\int_{0}^{a} f(x,y)\,dy\,dx + \int_{b}^{220}\int_{a}^{fy} f(x,y)\,dy\,dx - \int_{170}^{220}\int_{95}^{hiy} f(x,y)\,dy\,dx + \int_{b}^{220}\int_{a}^{fy} f(x,y)\,dy\,dx$$

$$- \int_{0}^{15}\int_{85}^{ony} f(x,y)\,dy\,dx - \int_{205}^{220}\int_{70}^{ghy} f(x,y)\,dy\,dx - \int_{205}^{220}\int_{25}^{fgy} f(x,y)\,dy\,dx - \int_{0}^{15}\int_{40}^{poy} f(x,y)\,dy\,dx - \int_{0}^{15}\int_{15}^{qpy} f(x,y)\,dy\,dx$$

$$- \int_{0}^{50}\int_{0}^{qay} f(x,y)\,dy\,dx - \int_{50}^{70}\int_{0}^{aby} f(x,y)\,dy\,dx - \int_{70}^{135}\int_{0}^{bcy} f(x,y)\,dy\,dx - \int_{135}^{155}\int_{0}^{cdy} f(x,y)\,dy\,dx - \int_{155}^{205}\int_{0}^{dey} f(x,y)\,dy\,dx$$

$$- \int_{205}^{220}\int_{0}^{efy} f(x,y)\,dy\,dx - \int_{15}^{65}\int_{95}^{nmy} f(x,y)\,dy\,dx - \int_{65}^{85}\int_{95}^{mky} f(x,y)\,dy\,dx - \int_{85}^{150}\int_{95}^{kjy} f(x,y)\,dy\,dx - \int_{150}^{170}\int_{95}^{jiy} f(x,y)\,dy\,dx$$

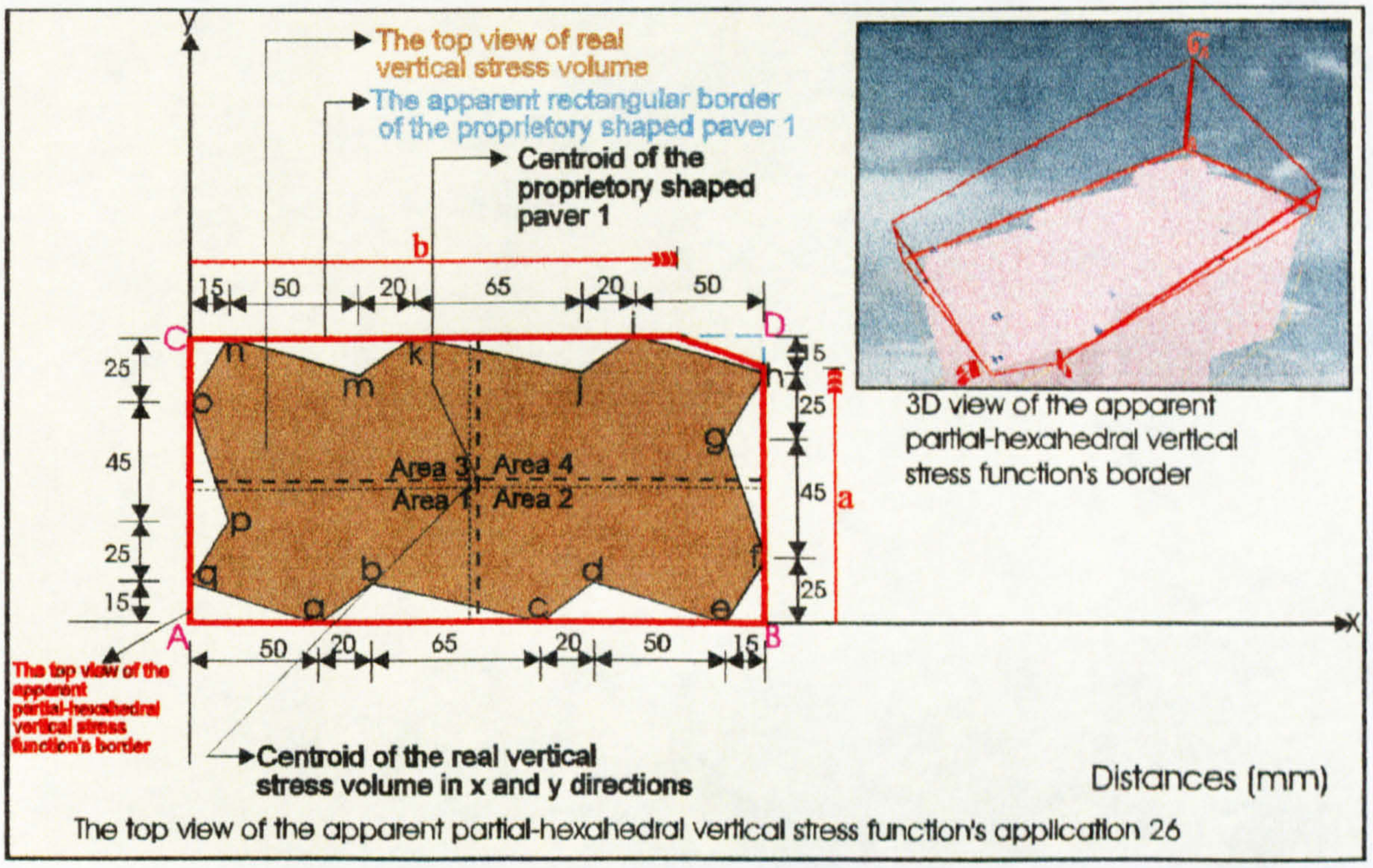

Figure 7.92: Application 26 of the partial-hexahedral compressive stress distribution beneath the circumscribing rectangular border of proprietory shaped paver 1.

and the centroids of this volume in the xy-plane are at distances $\overline{X}$ and $\overline{Y}$ from the axes (see Figure 7.92) which are given by the following equations.

$$\overline{X} = \frac{1}{V}\left[\int_{0}^{b}\int_{0}^{110} x f(x,y)\,dy\,dx + \int_{b}^{220}\int_{0}^{a} x f(x,y)\,dy\,dx + \int_{b}^{220}\int_{a}^{fy} x f(x,y)\,dy\,dx - \int_{170}^{220}\int_{95}^{hiy} x f(x,y)\,dy\,dx\right.$$

$$\left. + \int_{b}^{220}\int_{a}^{fy} x f(x,y)\,dy\,dx - \int_{0}^{15}\int_{85}^{ony} x f(x,y)\,dy\,dx - \int_{205}^{220}\int_{70}^{ghy} x f(x,y)\,dy\,dx - \int_{205}^{220}\int_{25}^{fgy} x f(x,y)\,dy\,dx\right.$$

$$-\int_{0}^{15}\int_{40}^{poy} xf(x,y)\,dy\,dx-\int_{0}^{15}\int_{15}^{qpy} xf(x,y)\,dy\,dx-\int_{0}^{50}\int_{0}^{qay} xf(x,y)\,dy\,dx-\int_{50}^{70}\int_{0}^{aby} xf(x,y)\,dy\,dx$$

$$-\int_{70}^{135}\int_{0}^{bcy} xf(x,y)\,dy\,dx-\int_{135}^{155}\int_{0}^{cdy} xf(x,y)\,dy\,dx-\int_{155}^{205}\int_{0}^{dey} xf(x,y)\,dy\,dx-\int_{205}^{220}\int_{0}^{efy} xf(x,y)\,dy\,dx$$

$$\left.-\int_{15}^{65}\int_{95}^{nmy} xf(x,y)\,dy\,dx-\int_{65}^{85}\int_{95}^{mky} xf(x,y)\,dy\,dx-\int_{85}^{150}\int_{95}^{kjy} xf(x,y)\,dy\,dx-\int_{150}^{170}\int_{95}^{jiy} xf(x,y)\,dy\,dx\right]$$

$$\overline{Y}=\frac{1}{V}\left[\begin{array}{l}\displaystyle\int_{0}^{110}\int_{0}^{b} yf(x,y)\,dx\,dy+\int_{0}^{a}\int_{b}^{220} yf(x,y)\,dx\,dy+\int_{a}^{110}\int_{b}^{fx} yf(x,y)\,dx\,dy-\int_{170}^{220}\int_{95}^{hiy} yf(x,y)\,dx\,dy\\ \displaystyle+\int_{a}^{110}\int_{b}^{fx} yf(x,y)\,dx\,dy-\int_{85}^{110}\int_{0}^{onx} yf(x,y)\,dx\,dy-\int_{70}^{95}\int_{205}^{ghx} yf(x,y)\,dx\,dy-\int_{25}^{70}\int_{205}^{fgx} yf(x,y)\,dx\,dy\\ \displaystyle-\int_{40}^{85}\int_{0}^{pox} yf(x,y)\,dx\,dy-\int_{15}^{40}\int_{0}^{qpx} yf(x,y)\,dx\,dy-\int_{0}^{15}\int_{0}^{qax} yf(x,y)\,dx\,dy-\int_{0}^{15}\int_{50}^{abx} yf(x,y)\,dx\,dy\\ \displaystyle-\int_{0}^{15}\int_{70}^{bcx} yf(x,y)\,dx\,dy-\int_{0}^{15}\int_{135}^{cdx} yf(x,y)\,dx\,dy-\int_{0}^{15}\int_{155}^{dex} yf(x,y)\,dx\,dy-\int_{0}^{25}\int_{205}^{efx} yf(x,y)\,dx\,dy\\ \displaystyle-\int_{95}^{110}\int_{15}^{nmx} yf(x,y)\,dx\,dy-\int_{95}^{110}\int_{65}^{mkx} yf(x,y)\,dx\,dy-\int_{95}^{110}\int_{85}^{kjx} yf(x,y)\,dx\,dy-\int_{95}^{110}\int_{150}^{jix} yf(x,y)\,dx\,dy\end{array}\right]$$

7.2.5. Absolute-hexahedral compressive stress regimes beneath the circumscribing rectangular border for proprietory shaped paver 1

The application of the absolute-hexahedral compressive stress regime beneath the circumscribing rectangular border of proprietory shaped paver 1 shown in Figure 7.93 can be calculated by using the data in Tables 5.1. The first two letters of each boundary line function in Table 5.1 for proprietory shaped paver 1 charecterise the corner names can be seen in Figure 7.93 (example: **qay** symbolises the boundary line function of proprietory shaped paver 1 in the **y** axis between corner **q** and **a**). The line functions which define the boundary of the absolute-hexahedral stress block in the xy-plane (see Figure 7.93) are of the form $fy = l\left(1-\frac{x}{l}\right)$, $fx = l\left(1-\frac{y}{l}\right)$.

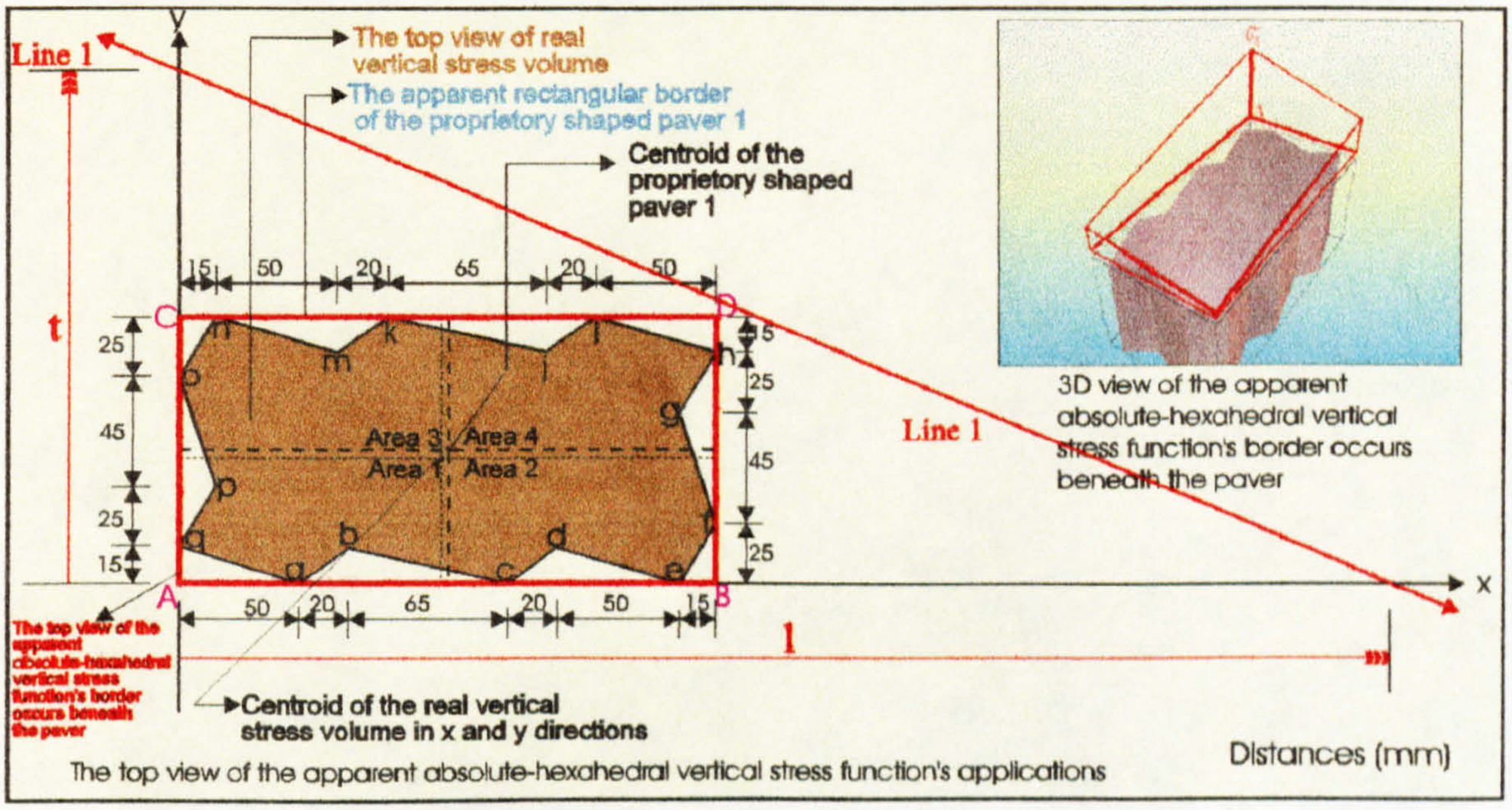

Figure 7.93: The application of the absolute-hexahedral compressive stress distribution beneath the circumscribing rectangular border of proprietory shaped paver 1.

The surface function of the absolute-hexahedral compressive stress block beneath the circumscribing rectangular border shown in Figure 7.93 through the three points σ_A, **l** and **t** is given by:

$$\begin{vmatrix} x & y & z & 1 \\ t & 0 & 0 & 1 \\ 0 & l & 0 & 1 \\ 0 & 0 & \sigma_A & 1 \end{vmatrix} = 0 \Rightarrow f(x,y) = z = \sigma_A\left(1 - \frac{x}{t} - \frac{y}{l}\right)$$

The following actual total volume **V** beneath the surface $f(x,y) = z\ (> 0)$ and above the region in the xy-plane (see Figure 7.93) is calculated by subtracting the negative volume generated by the dentations of the shaped paver from the absolute-hexahedral volume beneath circumscribing rectangular boundary of the paver.

$$V = \int_0^{220}\int_0^{110} f(x,y)\,dy\,dx - \int_{170}^{220}\int_{95}^{hiy} f(x,y)\,dy\,dx - \int_0^{15}\int_{85}^{ony} f(x,y)\,dy\,dx - \int_{205}^{220}\int_{70}^{ghy} f(x,y)\,dy\,dx - \int_{205}^{220}\int_{25}^{fgy} f(x,y)\,dy\,dx$$
$$- \int_0^{15}\int_{40}^{poy} f(x,y)\,dy\,dx - \int_0^{15}\int_{15}^{qpy} f(x,y)\,dy\,dx - \int_0^{50}\int_0^{qay} f(x,y)\,dy\,dx - \int_{50}^{70}\int_0^{aby} f(x,y)\,dy\,dx - \int_{70}^{135}\int_0^{bcy} f(x,y)\,dy\,dx$$

$$-\int_{135}^{155}\int_{0}^{cdy} f(x,y)\,dy\,dx-\int_{155}^{205}\int_{0}^{dey} f(x,y)\,dy\,dx-\int_{205}^{220}\int_{0}^{efy} f(x,y)\,dy\,dx-\int_{15}^{65}\int_{95}^{nmy} f(x,y)\,dy\,dx-\int_{65}^{85}\int_{95}^{nky} f(x,y)\,dy\,dx$$
$$-\int_{85}^{150}\int_{95}^{kjy} f(x,y)\,dy\,dx-\int_{150}^{170}\int_{95}^{jiy} f(x,y)\,dy\,dx$$

and the centroids of this volume in the xy-plane are at distances $\overline{X}$ and $\overline{Y}$ from the axes (see Figure 7.93) which are given by the following equations.

$$\overline{X}=\frac{1}{V}\left[\begin{array}{l}\int_{0}^{220}\int_{0}^{110} x f(x,y)\,dy\,dx-\int_{170}^{220}\int_{95}^{hiy} x f(x,y)\,dy\,dx-\int_{0}^{15}\int_{85}^{ony} x f(x,y)\,dy\,dx-\int_{205}^{220}\int_{70}^{ghy} x f(x,y)\,dy\,dx\\ -\int_{205}^{220}\int_{25}^{fgy} x f(x,y)\,dy\,dx-\int_{0}^{15}\int_{40}^{poy} x f(x,y)\,dy\,dx-\int_{0}^{15}\int_{15}^{qpy} x f(x,y)\,dy\,dx-\int_{0}^{50}\int_{0}^{qay} x f(x,y)\,dy\,dx\\ -\int_{50}^{70}\int_{0}^{aby} x f(x,y)\,dy\,dx-\int_{70}^{135}\int_{0}^{bcy} x f(x,y)\,dy\,dx-\int_{135}^{155}\int_{0}^{cdy} x f(x,y)\,dy\,dx-\int_{155}^{205}\int_{0}^{dey} x f(x,y)\,dy\,dx\\ -\int_{205}^{220}\int_{0}^{efy} x f(x,y)\,dy\,dx-\int_{15}^{65}\int_{95}^{nmy} x f(x,y)\,dy\,dx-\int_{65}^{85}\int_{95}^{mky} x f(x,y)\,dy\,dx-\int_{85}^{150}\int_{95}^{kfy} x f(x,y)\,dy\,dx\\ -\int_{150}^{170}\int_{95}^{jiy} x f(x,y)\,dy\,dx\end{array}\right]$$

$$\overline{Y}=\frac{1}{V}\left[\begin{array}{l}\int_{0}^{110}\int_{0}^{220} y f(x,y)\,dx\,dy-\int_{170}^{220}\int_{95}^{hiy} y f(x,y)\,dx\,dy-\int_{85}^{110}\int_{0}^{onx} y f(x,y)\,dx\,dy-\int_{70}^{95}\int_{205}^{ghx} y f(x,y)\,dx\,dy\\ -\int_{25}^{70}\int_{205}^{fgx} y f(x,y)\,dx\,dy-\int_{40}^{85}\int_{0}^{pox} y f(x,y)\,dx\,dy-\int_{15}^{40}\int_{0}^{qpx} y f(x,y)\,dx\,dy-\int_{0}^{15}\int_{0}^{qax} y f(x,y)\,dx\,dy\\ -\int_{0}^{15}\int_{50}^{abx} y f(x,y)\,dx\,dy-\int_{0}^{15}\int_{70}^{bcx} y f(x,y)\,dx\,dy-\int_{0}^{15}\int_{135}^{cdx} y f(x,y)\,dx\,dy-\int_{0}^{15}\int_{155}^{dex} y f(x,y)\,dx\,dy\\ -\int_{0}^{25}\int_{205}^{efx} y f(x,y)\,dx\,dy-\int_{95}^{110}\int_{15}^{nmx} y f(x,y)\,dx\,dy-\int_{95}^{110}\int_{65}^{mkx} y f(x,y)\,dx\,dy-\int_{95}^{110}\int_{85}^{kfx} y f(x,y)\,dx\,dy\\ -\int_{95}^{110}\int_{150}^{jix} y f(x,y)\,dx\,dy\end{array}\right]$$

The $V,\overline{X}$ and $\overline{Y}$ values can analytically be evaluated in terms of l,t and σ_A. The following results which indicate the proportions of the absolute-hexahedral vertical

compressive stress block (see Figure 7.93) can be determined by applying vertical and rotational equilibrium between load patch and vertical compressive stress distribution (see Chapter 6). For vertical equilibrium condition the equality between the truncated volume (V) and the total applied patch load (N) must be satisfied and for rotational equilibrium conditions the centroid distances of the load patch ($\overline{X}$, $\overline{Y}$) must be coincided with the centroid distances of the truncated vertical stress block ($\overline{X}$, $\overline{Y}$).

$$l = 3.75(-0.1800509936.10^{19}\overline{X} + 0.3104471197.10^{17}\overline{XY} + 0.4906910692.10^{21}$$
$$-0.1284362480.10^{20}\overline{Y} + 0.2724068857.10^{14}\overline{XY}^2 + 0.7181726473.10^{17}\overline{Y}^2)$$
$$\Big/ (0.6684767863.10^{12}\overline{XY}^2 + 0.1074937353.10^{16}\overline{XY} - 0.7237517192.10^{14}\overline{Y}^2$$
$$-0.1196081166.10^{18}\overline{Y} - 0.6150290347.10^{17}\overline{X} + 0.6837281081.10^{19})$$

$$t = -(-0.8763823140.10^{12}\overline{X} - 0.7334003330.10^{9}\overline{XY} + 0.2388395454.10^{15}$$
$$-0.1933534306.10^{13}\overline{Y}) \Big/ (0.359.10^{7}\overline{XY} - 0.1842560800.10^{9}\overline{X} + 0.3599480970.10^{11}\overline{Y}$$
$$-0.1993029722.10^{13})$$

$$\sigma_A = -75N(0.8763823140.10^{12}\overline{X} + 0.733400333.10^{9}\overline{XY} - 0.2388395454.10^{15}$$
$$+0.1933534306.10^{13}\overline{Y})(-0.1800509936.10^{15}\overline{X} + 0.3104471197.10^{13}\overline{XY}$$
$$+0.4906910692.10^{17} - 0.1284362480.10^{16}\overline{Y} + 0.2724068857.10^{10}\overline{XY}^2$$
$$+0.7181726473.10^{13}\overline{Y}^2) \Big/ (-0.6321413654.10^{33}\overline{XY} + 0.2536425027.10^{35}\overline{X}$$
$$+0.1300519976.10^{35}\overline{Y} + 0.3024622010.10^{31}\overline{XY}^2 - 0.6710577439.10^{32}\overline{Y}^2$$
$$-0.8623981487.10^{32}\overline{X}^2 + 0.1435118023.10^{31}\overline{X}^2\overline{Y} + 0.2198660499.10^{28}\overline{X}^2\overline{Y}^2$$
$$+0.7843684608.10^{24}\overline{X}^2\overline{Y}^3 + 0.2052762250.10^{28}\overline{XY}^3 - 0.3992629612.10^{29}\overline{Y}^3$$
$$-0.5072866600.10^{36})$$

Therefore, the function of the absolute-hexahedral vertical compressive stress regimes can be determined as follows by inserting the **l**, **t** and σ_A values into $f(x,y) = z = \sigma_A\left(1 - \frac{x}{l} - \frac{y}{t}\right)$.

$$f(x,y) = z = N0.46875.10^{-25}(0.2179210525.10^{40}\overline{XY} - 0.8600659493.10^{41}\overline{X}$$
$$-0.4016333524.10^{42}\overline{Y} - 0.1070397239.10^{38}\overline{XY}^2 + 0.4198639202.10^{40}\overline{Y}^2$$
$$+0.1238347382.10^{33}y\overline{XY}^3 + 0.9779407197.10^{28}y\overline{X}^2\overline{Y}^3 + 0.1577935064.10^{39}\overline{X}^2$$
$$-0.2588654193.10^{37}\overline{X}^2\overline{Y} - 0.4664145978.10^{34}\overline{X}^2\overline{Y}^2 - 0.1997833007.10^{31}\overline{X}^2\overline{Y}^3$$
$$-0.1053416117.10^{35}\overline{XY}^3 - 0.1388611451.10^{38}\overline{Y}^3 - 0.4354701614.10^{41}x$$
$$-0.9779618852.10^{41}y - 0.1437334850.10^{37}x\overline{X}^2 + 0.5515039393.10^{39}x\overline{X}$$
$$-0.5706142496.10^{37}x\overline{Y}^2 + 0.1114327086.10^{40}x\overline{Y} - 0.3731730075.10^{34}x\overline{Y}^3$$
$$+0.3317549028.10^{35}y\overline{Y}^2 + 0.3664535055.10^{32}x\overline{X}^2\overline{Y}^2 + 0.2391866227.10^{35}x\overline{X}^2\overline{Y}$$
$$+0.4713654944.10^{35}x\overline{XY}^2 - 0.1267902657.10^{38}x\overline{XY} + 0.1307362927.10^{29}x\overline{X}^2\overline{Y}^3$$
$$+0.3305180864.10^{32}x\overline{XY}^3 - 0.121840076.10^{34}y\overline{X}^2\overline{Y} - 0.1225539493.10^{38}y\overline{XY}$$
$$+0.1064312535.10^{32}y\overline{X}^2\overline{Y}^2 + 0.1003815617.10^{36}y\overline{XY}^2 + 0.3498057004.10^{39}y\overline{X}$$
$$+0.4326005762.10^{40}y\overline{Y} - 0.6054377737.10^{38}y\overline{Y}^2 + 0.2585048777.10^{36}y\overline{Y}^3$$
$$+0.1171964319.10^{44}) \Big/ (-0.3950883409.10^{18}\overline{XY} + 0.1585265642.10^{20}\overline{X}$$
$$+0.8128249850.10^{19}\overline{Y} + 0.1890388756.10^{16}\overline{XY}^2 - 0.4194110899.10^{17}\overline{Y}^2$$
$$-0.5389988429.10^{17}\overline{X}^2 + 0.8969487644.10^{15}\overline{X}^2\overline{Y} + 0.1374162812.10^{13}\overline{X}^2\overline{Y}^2$$
$$+0.490230288.10^{9}\overline{X}^2\overline{Y}^3 + 0.1282976406.10^{13}\overline{XY}^3 - 0.2495393508.10^{14}\overline{Y}^3$$
$$-0.3170541625.10^{21})$$

The stress values beneath the corners of proprietory shaped paver 1 for the absolute-hexahedral vertical compressive stress regimes can now be determined by inserting the corner co-ordinates in the xy-plane into the stress function defined above (see Figure 7.93).

The vertical compressive stress beneath the corner a is

$$\sigma_a = -0.0000234375N(-0.1931573996.10^{18}\overline{XY} + 0.7303924745.10^{19}\overline{X}$$
$$+0.4323962476.10^{20}\overline{Y} + 0.1043393115.10^{16}\overline{XY}^2 - 0.4891665096.10^{18}\overline{Y}^2$$
$$-0.1074084549.10^{17}\overline{X}^2 + 0.1740901349.10^{15}\overline{X}^2\overline{Y} + 0.3539848063.10^{12}\overline{X}^2\overline{Y}^2$$
$$+0.168018943.10^{9}\overline{X}^2\overline{Y}^3 + 0.1110196342.10^{13}\overline{XY}^3 + 0.1759087626.10^{16}\overline{Y}^3$$

$$-0.1192786548.10^{22}) \Big/ (-0.2469302131.10^{17}\overline{XY} + 0.9907910263.10^{18}\overline{X}$$
$$+0.5080156156.10^{18}\overline{Y} + 0.1181492973.10^{15}\overline{XY}^2 - 0.2621319312.10^{16}\overline{Y}^2$$
$$-0.3368742768.10^{16}\overline{X}^2 + 0.5605929778.10^{14}\overline{X}^2\overline{Y} + 0.8588517575.10^{11}\overline{X}^2\overline{Y}^2$$
$$+0.30639393.10^{8}\overline{X}^2\overline{Y}^3 + 0.8018602538.10^{11}\overline{XY}^3 - 0.1559620943.10^{13}\overline{Y}^3$$
$$-0.1981588516.10^{20})$$

The vertical compressive stress beneath the corner **b** is

$$\sigma_b = -0.000146484375N(-0.2215695482.10^{17}\overline{XY} + 0.8430846734.10^{18}\overline{X}$$
$$+0.5174807400.10^{19}\overline{Y} + 0.1179738101.10^{15}\overline{XY}^2 - 0.5782105132.10^{17}\overline{Y}^2$$
$$-0.1153553985.10^{16}\overline{X}^2 + 0.1865247690.10^{14}\overline{X}^2\overline{Y} + 0.3878649118.10^{11}\overline{X}^2\overline{Y}^2$$
$$+0.18719757.10^{8}\overline{X}^2\overline{Y}^3 + 0.1272602698.10^{12}\overline{XY}^3 + 0.2053952490.10^{15}\overline{Y}^3$$
$$-0.1440881846.10^{21}) \Big/ (-0.2469302131.10^{17}\overline{XY} + 0.9907910263.10^{18}\overline{X}$$
$$+0.5080156156.10^{18}\overline{Y} + 0.1181492973.10^{15}\overline{XY}^2 - 0.2621319312.10^{16}\overline{Y}^2$$
$$-0.3368742768.10^{16}\overline{X}^2 + 0.5605929778.10^{14}\overline{X}^2\overline{Y} + 0.8588517575.10^{11}\overline{X}^2\overline{Y}^2$$
$$+0.30639393.10^{8}\overline{X}^2\overline{Y}^3 + 0.8018602538.10^{11}\overline{XY}^3 - 0.1559620943.10^{13}\overline{Y}^3$$
$$-0.1981588516.10^{20})$$

The vertical compressive stress beneath the corner **c** is

$$\sigma_c = -0.00004687 5N(-0.2922137113.10^{17}\overline{XY} + 0.7220976950.10^{18}\overline{X}$$
$$+0.1569994974.10^{20}\overline{Y} + 0.2712836385.10^{15}\overline{XY}^2 - 0.2142693728.10^{18}\overline{Y}^2$$
$$+0.2265418650.10^{16}\overline{X}^2 - 0.4002282581.10^{14}\overline{X}^2\overline{Y} - 0.1768602163.10^{11}\overline{X}^2\overline{Y}^2$$
$$+0.14555816.10^{8}\overline{X}^2\overline{Y}^3 + 0.3795104378.10^{12}\overline{XY}^3 + 0.8993686294.10^{15}\overline{Y}^3$$
$$-0.3650497507.10^{21}) \Big/ (-0.2469302131.10^{17}\overline{XY} + 0.9907910263.10^{18}\overline{X}$$
$$+0.5080156156.10^{18}\overline{Y} + 0.1181492973.10^{15}\overline{XY}^2 - 0.2621319312.10^{16}\overline{Y}^2$$
$$-0.3368742768.10^{16}\overline{X}^2 + 0.5605929778.10^{14}\overline{X}^2\overline{Y} + 0.8588517575.10^{11}\overline{X}^2\overline{Y}^2$$
$$+0.30639393.10^{8}\overline{X}^2\overline{Y}^3 + 0.8018602538.10^{11}\overline{XY}^3 - 0.1559620943.10^{13}\overline{Y}^3$$

$-0.1981588516.10^{20}$)

The vertical compressive stress beneath the corner **d** is

$$\sigma_d = 0.5859375000.10^{-5} N(0.1506524150.10^{17}\overline{XY} + 0.2361800583.10^{19}\overline{X}$$
$$-0.8201128385.10^{20}\overline{Y} - 0.9460419005.10^{15}\overline{XY}^2 + 0.1203015227.10^{19}\overline{Y}^2$$
$$-0.3224788153.10^{17}\overline{X}^2 + 0.5502312240.10^{15}\overline{X}^2\overline{Y} + 0.5877651185.10^{12}\overline{X}^2\overline{Y}^2$$
$$+0.87635319.10^{8}\overline{X}^2\overline{Y}^3 - 0.1776804879.10^{13}\overline{XY}^3 - 0.5293479755.10^{16}\overline{Y}^3$$
$$+0.1751456430.10^{22}) \Big/ (-0.2469302131.10^{17}\overline{XY} + 0.9907910263.10^{18}\overline{X}$$
$$+0.5080156156.10^{18}\overline{Y} + 0.1181492973.10^{15}\overline{XY}^2 - 0.2621319312.10^{16}\overline{Y}^2$$
$$-0.3368742768.10^{16}\overline{X}^2 + 0.5605929778.10^{14}\overline{X}^2\overline{Y} + 0.8588517575.10^{11}\overline{X}^2\overline{Y}^2$$
$$+0.30639393.10^{8}\overline{X}^2\overline{Y}^3 + 0.8018602538.10^{11}\overline{XY}^3 - 0.1559620943.10^{13}\overline{Y}^3$$
$$-0.1981588516.10^{20})$$

The vertical compressive stress beneath the corner **e** is

$$\sigma_e = 0.2929687500.10^{-5} N(-0.4199899220.10^{18}\overline{XY} + 0.2705171267.10^{20}\overline{X}$$
$$-0.1731962998.10^{21}\overline{Y} - 0.1040979755.10^{16}\overline{XY}^2 + 0.3028879990.10^{19}\overline{Y}^2$$
$$-0.1368601379.10^{18}\overline{X}^2 + 0.2314671572.10^{16}\overline{X}^2\overline{Y} + 0.2848150885.10^{13}\overline{X}^2\overline{Y}^2$$
$$+0.682260993.10^{9}\overline{X}^2\overline{Y}^3 - 0.3758540399.10^{13}\overline{XY}^3 - 0.1465111918.10^{17}\overline{Y}^3$$
$$+0.2792504881.10^{22}) \Big/ (-0.2469302131.10^{17}\overline{XY} + 0.9907910263.10^{18}\overline{X}$$
$$+0.5080156156.10^{18}\overline{Y} + 0.1181492973.10^{15}\overline{XY}^2 - 0.2621319312.10^{16}\overline{Y}^2$$
$$-0.3368742768.10^{16}\overline{X}^2 + 0.5605929778.10^{14}\overline{X}^2\overline{Y} + 0.8588517575.10^{11}\overline{X}^2\overline{Y}^2$$
$$+0.30639393.10^{8}\overline{X}^2\overline{Y}^3 + 0.8018602538.10^{11}\overline{XY}^3 - 0.1559620943.10^{13}\overline{Y}^3$$
$$-0.1981588516.10^{20})$$

The vertical compressive stress beneath the corner **f** is

$$\sigma_f = 0.00001171875 N(-0.2291400483.10^{18}\overline{XY} + 0.1101735355.10^{20}\overline{X}$$

$$-0.1208281235.10^{20}\overline{Y}+0.5439018833.10^{15}\overline{XY}^2+0.3574233548.10^{18}\overline{Y}^2$$
$$-0.3939769333.10^{17}\overline{X}^2+0.6607478718.10^{15}\overline{X}^2\overline{Y}+0.9159773193.10^{12}\overline{X}^2\overline{Y}^2$$
$$+0.280712653.10^{9}\overline{X}^2\overline{Y}^3-0.4172370350.10^{11}\overline{XY}^3-0.2061118296.10^{16}\overline{Y}^3$$
$$-0.7640126750.10^{20})\Big/(-0.2469302131.10^{17}\overline{XY}+0.9907910263.10^{18}\overline{X}$$
$$+0.5080156156.10^{18}\overline{Y}+0.1181492973.10^{15}\overline{XY}^2-0.2621319312.10^{16}\overline{Y}^2$$
$$-0.3368742768.10^{16}\overline{X}^2+0.5605929778.10^{14}\overline{X}^2\overline{Y}+0.8588517575.10^{11}\overline{X}^2\overline{Y}^2$$
$$+0.30639393.10^{8}\overline{X}^2\overline{Y}^3+0.8018602538.10^{11}\overline{XY}^3-0.1559620943.10^{13}\overline{Y}^3$$
$$-0.1981588516.10^{20})$$

The vertical compressive stress beneath the corner g is

$$\sigma_g=0.29296875.10^{-5}N(-0.1277867567.10^{19}\overline{XY}+0.5153811170.10^{20}\overline{X}$$
$$+0.1296241035.10^{21}\overline{Y}+0.5985729564.10^{16}\overline{XY}^2-0.1209184426.10^{19}\overline{Y}^2$$
$$-0.1345378536.10^{18}\overline{X}^2+0.2229383519.10^{16}\overline{X}^2\overline{Y}+0.3593169660.10^{13}\overline{X}^2\overline{Y}^2$$
$$+0.1366819497.10^{10}\overline{X}^2\overline{Y}^3+0.4909891275.10^{13}\overline{XY}^3+0.3444222270.10^{16}\overline{Y}^3$$
$$-0.4053228320.10^{22})\Big/(-0.2469302131.10^{17}\overline{XY}+0.9907910263.10^{18}\overline{X}$$
$$+0.5080156156.10^{18}\overline{Y}+0.1181492973.10^{15}\overline{XY}^2-0.2621319312.10^{16}\overline{Y}^2$$
$$-0.3368742768.10^{16}\overline{X}^2+0.5605929778.10^{14}\overline{X}^2\overline{Y}+0.8588517575.10^{11}\overline{X}^2\overline{Y}^2$$
$$+0.30639393.10^{8}\overline{X}^2\overline{Y}^3+0.8018602538.10^{11}\overline{XY}^3-0.1559620943.10^{13}\overline{Y}^3$$
$$-0.1981588516.10^{20})$$

The vertical compressive stress beneath the corner h is

$$\sigma_h=0.00001171875N(-0.4436094595.10^{18}\overline{XY}+0.1713895330.10^{20}\overline{X}$$
$$+0.6362228848.10^{20}\overline{Y}+0.2300579213.10^{16}\overline{XY}^2-0.7020927493.10^{18}\overline{Y}^2$$
$$-0.3881712225.10^{17}\overline{X}^2+0.6394258585.10^{15}\overline{X}^2\overline{Y}+0.1102232013.10^{13}\overline{X}^2\overline{Y}^2$$
$$+0.451852279.10^{9}\overline{X}^2\overline{Y}^3+0.2125384215.10^{13}\overline{XY}^3+0.2462717063.10^{16}\overline{Y}^3$$
$$-0.1787834568.10^{22})\Big/(-0.2469302131.10^{17}\overline{XY}+0.9907910263.10^{18}\overline{X}$$

$$+0.5080156156.10^{18}\overline{Y}+0.1181492973.10^{15}\overline{XY}^2-0.2621319312.10^{16}\overline{Y}^2$$
$$-0.3368742768.10^{16}\overline{X}^2+0.5605929778.10^{14}\overline{X}^2\overline{Y}+0.8588517575.10^{11}\overline{X}^2\overline{Y}^2$$
$$+0.30639393.10^{8}\overline{X}^2\overline{Y}^3+0.8018602538.10^{11}\overline{XY}^3-0.1559620943.10^{13}\overline{Y}^3$$
$$-0.1981588516.10^{20})$$

The vertical compressive stress beneath the corner **i** is

$$\sigma_i = 0.29296875.10^{-5}N(-0.1324317434.10^{19}\overline{XY}+0.4622770179.10^{20}\overline{X}$$
$$+0.2636628860.10^{21}\overline{Y}+0.8351212805.10^{16}\overline{XY}^2-0.3431220533.10^{19}\overline{Y}^2$$
$$-0.8290411417.10^{17}\overline{X}^2+0.1343494309.10^{16}\overline{X}^2\overline{Y}+0.2736307405.10^{13}\overline{X}^2\overline{Y}^2$$
$$+0.1300418761.10^{10}\overline{X}^2\overline{Y}^3+0.8706467499.10^{13}\overline{XY}^3+0.1391502793.10^{17}\overline{Y}^3$$
$$-0.6440930290.10^{22})\Big/(-0.2469302131.10^{17}\overline{XY}+0.9907910263.10^{18}\overline{X}$$
$$+0.5080156156.10^{18}\overline{Y}+0.1181492973.10^{15}\overline{XY}^2-0.2621319312.10^{16}\overline{Y}^2$$
$$-0.3368742768.10^{16}\overline{X}^2+0.5605929778.10^{14}\overline{X}^2\overline{Y}+0.8588517575.10^{11}\overline{X}^2\overline{Y}^2$$
$$+0.30639393.10^{8}\overline{X}^2\overline{Y}^3+0.8018602538.10^{11}\overline{XY}^3-0.1559620943.10^{13}\overline{Y}^3$$
$$-0.1981588516.10^{20})$$

The vertical compressive stress beneath the corner **j** is

$$\sigma_j = 0.00001171875N(-0.2217264948.10^{18}\overline{XY}+0.7487634378.10^{19}\overline{X}$$
$$+0.4412156448.10^{20}\overline{Y}+0.1475689597.10^{16}\overline{XY}^2-0.6022352555.10^{18}\overline{Y}^2$$
$$-0.1366376238.10^{17}\overline{X}^2+0.2208492690.10^{15}\overline{X}^2\overline{Y}+0.4609383783.10^{12}\overline{X}^2\overline{Y}^2$$
$$+0.223063767.10^{9}\overline{X}^2\overline{Y}^3+0.1546977564.10^{13}\overline{XY}^3+0.2528022340.10^{16}\overline{Y}^3$$
$$-0.1025761785.10^{22})\Big/(-0.2469302131.10^{17}\overline{XY}+0.9907910263.10^{18}\overline{X}$$
$$+0.5080156156.10^{18}\overline{Y}+0.1181492973.10^{15}\overline{XY}^2-0.2621319312.10^{16}\overline{Y}^2$$
$$-0.3368742768.10^{16}\overline{X}^2+0.5605929778.10^{14}\overline{X}^2\overline{Y}+0.8588517575.10^{11}\overline{X}^2\overline{Y}^2$$
$$+0.30639393.10^{8}\overline{X}^2\overline{Y}^3+0.8018602538.10^{11}\overline{XY}^3-0.1559620943.10^{13}\overline{Y}^3$$
$$-0.1981588516.10^{20})$$

The vertical compressive stress beneath the corner **k** is

$$\sigma_k = 0.29296875.10^{-5}N(-0.246600175.10^{18}\overline{XY} - 0.6501330500.10^{18}\overline{X}$$
$$+0.1689450837.10^{21}\overline{Y} + 0.4344606102.10^{16}\overline{XY}^2 - 0.294619842 1.10^{19}\overline{Y}^2$$
$$+0.3926934803.10^{17}\overline{X}^2 - 0.6895919840.10^{15}\overline{X}^2\overline{Y} - 0.3785473920.10^{12}\overline{X}^2\overline{Y}^2$$
$$+0.189160273.10^{9}\overline{X}^2\overline{Y}^3 + 0.5897063764.10^{13}\overline{XY}^3 + 0.1423222498.10^{17}\overline{Y}^3$$
$$-0.2739433920.10^{22}) \Big/ (-0.246930213 1.10^{17}\overline{XY} + 0.9907910263.10^{18}\overline{X}$$
$$+0.5080156156.10^{18}\overline{Y} + 0.1181492973.10^{15}\overline{XY}^2 - 0.2621319312.10^{16}\overline{Y}^2$$
$$-0.3368742768.10^{16}\overline{X}^2 + 0.5605929778.10^{14}\overline{X}^2\overline{Y} + 0.8588517575.10^{11}\overline{X}^2\overline{Y}^2$$
$$+0.30639393.10^{8}\overline{X}^2\overline{Y}^3 + 0.8018602538.10^{11}\overline{XY}^3 - 0.1559620943.10^{13}\overline{Y}^3$$
$$-0.1981588516.10^{20})$$

The vertical compressive stress beneath the corner **m** is

$$\sigma_m = -0.29296875.10^{-5}N(-0.1908112799.10^{18}\overline{XY} + 0.1692729734.10^{20}\overline{X}$$
$$-0.8176845559.10^{20}\overline{Y} - 0.1896151686.10^{16}\overline{XY}^2 + 0.1923918910.10^{19}\overline{Y}^2$$
$$-0.6751841273.10^{17}\overline{X}^2 + 0.1149689217.10^{16}\overline{X}^2\overline{Y} + 0.1271101284.10^{13}\overline{X}^2\overline{Y}^2$$
$$+0.219003421.10^{9}\overline{X}^2\overline{Y}^3 - 0.3378506522.10^{13}\overline{XY}^3 - 0.1042928642.10^{17}\overline{Y}^3$$
$$+0.4015507700.10^{21}) \Big/ (-0.246930213 1.10^{17}\overline{XY} + 0.9907910263.10^{18}\overline{X}$$
$$+0.5080156156.10^{18}\overline{Y} + 0.1181492973.10^{15}\overline{XY}^2 - 0.2621319312.10^{16}\overline{Y}^2$$
$$-0.3368742768.10^{16}\overline{X}^2 + 0.5605929778.10^{14}\overline{X}^2\overline{Y} + 0.8588517575.10^{11}\overline{X}^2\overline{Y}^2$$
$$+0.30639393.10^{8}\overline{X}^2\overline{Y}^3 + 0.8018602538.10^{11}\overline{XY}^3 - 0.1559620943.10^{13}\overline{Y}^3$$
$$-0.1981588516.10^{20})$$

The vertical compressive stress beneath the corner **n** is

$$\sigma_n = -0.0000234375N(-0.8011646055.10^{17}\overline{XY} + 0.49069261.10^{19}\overline{X}$$
$$-0.1136777346.10^{20}\overline{Y} - 0.1306309553.10^{15}\overline{XY}^2 + 0.3183460558.10^{18}\overline{Y}^2$$
$$-0.1748534845.10^{17}\overline{X}^2 + 0.2954872929.10^{15}\overline{X}^2\overline{Y} + 0.3679652414.10^{12}\overline{X}^2\overline{Y}^2$$

$$+0.90749222.10^{8}\overline{X}^{2}\overline{Y}^{3}-0.4479296450.10^{12}\overline{XY}^{3}-0.1811680761.10^{16}\overline{Y}^{3}$$
$$-0.3860715125.10^{20})\Big/(-0.2469302131.10^{17}\overline{XY}+0.9907910263.10^{18}\overline{X}$$
$$+0.5080156156.10^{18}\overline{Y}+0.1181492973.10^{15}\overline{XY}^{2}-0.2621319312.10^{16}\overline{Y}^{2}$$
$$-0.3368742768.10^{16}\overline{X}^{2}+0.5605929778.10^{14}\overline{X}^{2}\overline{Y}+0.8588517575.10^{11}\overline{X}^{2}\overline{Y}^{2}$$
$$+0.30639393.10^{8}\overline{X}^{2}\overline{Y}^{3}+0.8018602538.10^{11}\overline{XY}^{3}-0.1559620943.10^{13}\overline{Y}^{3}$$
$$-0.1981588516.10^{20})$$

The vertical compressive stress beneath the corner **o** is

$$\sigma_o = -0.000014648437 5N(-0.2275003912.10^{18}\overline{XY}+0.1125462208.10^{20}\overline{X}$$
$$+0.6784572520.10^{19}\overline{Y}+0.4343079290.10^{15}\overline{XY}^{2}+0.1895163748.10^{18}\overline{Y}^{2}$$
$$+0.1641684.10^{10}\overline{XY}^{3}+0.233316679.10^{9}\overline{X}^{2}\overline{Y}^{3}-0.3212268462.10^{17}\overline{X}^{2}$$
$$+0.5384436516.10^{15}\overline{X}^{2}\overline{Y}+0.7518960646.10^{12}\overline{X}^{2}\overline{Y}^{2}-0.1617360018.10^{16}\overline{Y}^{3}$$
$$-0.6813934332.10^{21})\Big/(-0.2469302131.10^{17}\overline{XY}+0.9907910263.10^{18}\overline{X}$$
$$+0.5080156156.10^{18}\overline{Y}+0.1181492973.10^{15}\overline{XY}^{2}-0.2621319312.10^{16}\overline{Y}^{2}$$
$$-0.3368742768.10^{16}\overline{X}^{2}+0.5605929778.10^{14}\overline{X}^{2}\overline{Y}+0.8588517575.10^{11}\overline{X}^{2}\overline{Y}^{2}$$
$$+0.30639393.10^{8}\overline{X}^{2}\overline{Y}^{3}+0.8018602538.10^{11}\overline{XY}^{3}-0.1559620943.10^{13}\overline{Y}^{3}$$
$$-0.1981588516.10^{20})$$

The vertical compressive stress beneath the corner **p** is

$$\sigma_p = -0.000117187 5N(-0.3747023323.10^{17}\overline{XY}+0.1593545196.10^{19}\overline{X}$$
$$+0.5296955390.10^{19}\overline{Y}+0.1495415420.10^{15}\overline{XY}^{2}-0.4228239925.10^{17}\overline{Y}^{2}$$
$$-0.3439012583.10^{16}\overline{X}^{2}+0.5696525723.10^{14}\overline{X}^{2}\overline{Y}+0.9221851765.10^{11}\overline{X}^{2}\overline{Y}^{2}$$
$$+0.35263807.10^{8}\overline{X}^{2}\overline{Y}^{3}+0.1271248628.10^{12}\overline{XY}^{3}+0.9004738375.10^{14}\overline{Y}^{3}$$
$$-0.1788647602.10^{21})\Big/(-0.2469302131.10^{17}\overline{XY}+0.9907910263.10^{18}\overline{X}$$
$$+0.5080156156.10^{18}\overline{Y}+0.1181492973.10^{15}\overline{XY}^{2}-0.2621319312.10^{16}\overline{Y}^{2}$$
$$-0.3368742768.10^{16}\overline{X}^{2}+0.5605929778.10^{14}\overline{X}^{2}\overline{Y}+0.8588517575.10^{11}\overline{X}^{2}\overline{Y}^{2}$$

$$+0.30639393.10^{8}\overline{X}^{2}\overline{Y}^{3}+0.8018602538.10^{11}\overline{XY}^{3}-0.15596209 43.10^{13}\overline{Y}^{3}$$
$$-0.1981588516.10^{20})$$

The vertical compressive stress beneath the corner **q** is

$$\sigma_q = -0.29296875.10^{-5}N(-0.1995379601.10^{19}\overline{XY}+0.8075950942.10^{20}\overline{X}$$
$$+0.3367432660.10^{21}\overline{Y}+0.9198248964.10^{16}\overline{XY}^{2}-0.3290482541.10^{19}\overline{Y}^{2}$$
$$+0.8676640097.10^{13}\overline{XY}^{3}+0.1851141899.10^{10}\overline{X}^{2}\overline{Y}^{3}-0.1582911388.10^{18}\overline{X}^{2}$$
$$+0.2606930204.10^{16}\overline{X}^{2}\overline{Y}+0.4504499098.10^{13}\overline{X}^{2}\overline{Y}^{2}+0.1000854134.10^{17}\overline{Y}^{3}$$
$$-0.1025270036.10^{23})\Big/(-0.2469302131.10^{17}\overline{XY}+0.9907910263.10^{18}\overline{X}$$
$$+0.5080156156.10^{18}\overline{Y}+0.1181492973.10^{15}\overline{XY}^{2}-0.2621319312.10^{16}\overline{Y}^{2}$$
$$-0.3368742768.10^{16}\overline{X}^{2}+0.5605929778.10^{14}\overline{X}^{2}\overline{Y}+0.8588517575.10^{11}\overline{X}^{2}\overline{Y}^{2}$$
$$+0.30639393.10^{8}\overline{X}^{2}\overline{Y}^{3}+0.8018602538.10^{11}\overline{XY}^{3}-0.1559620943.10^{13}\overline{Y}^{3}$$
$$-0.1981588516.10^{20})$$

7.3. Conclusion

This Chapter explained the application of the bedding sand stress calculation method[1,2,3] (see Chapter 6, Section 6.2) to a common proprietory shaped paver (see proprietory shaped paver 1 in Figure 5.1). The nine proprietory shaped pavers (see Figure 5.1) analysed in this Thesis are commercially important on a worldwide basis. A common proprietory shaped paver has been selected as an example in this Chapter to show how all possible vertical compressive stress blocks of proprietory shaped pavers can be calculated for all realistically possible load patches. This Chapter also algebraically developed the general equations to the variations of the absolute-hexahedral stress blocks' total volumes and the centroid distances for proprietory shaped paver 1 (see Section 7.2.5). The calculation technique used in this Chapter for analysing the stress distributions beneath individual proprietory shaped pavers 1 is based on the method described in the previous chapter for rectangular pavers. For the remaining shapes, the algebraical solutions which are given in Chapter 8 have been

developed for the absolute-hexahedral compressive stress blocks that occur beneath the circumscribing rectangular borders. In the other paver stress blocks, iterative solutions (see Appendix) have been developed and given in Figures 6.21, 9.1, 9.2, 9.3, 9.4, 9.5, 9.6, 9.7, 9.8 and 9.9. The vertical compressive stress blocks in the bedding material are calculated for proprietory shaped pavers in this Chapter and in Chapter 8 by considering vertical and rotational equilibrium of the pressures applied to the upper and lower horizontal paver surfaces. Chapter 9 will show the evaluation of the algebraical solutions which are developed for the nine proprietory shaped pavers (see Sections 7.2.5 and 8.2 to 8.9) according to the variations of the common patch loading's general equations (which are determined in Chapter 5) to the total applied pressures and their centroid distances in the xy-plane (see Figures 5.2 to 5.42 and 9.1 to 9.9). The vertical compressive stresses in the bedding material are calculated for the shaped pavers by using the application of the bedding sand stress calculation method[1, 2, 3] to proprietory shaped pavers (see Sections 6.2, 6.3 and 6.4 for the detail of the bedding sand stress calculation mathod[1, 2, 3]).

References

1 Algin, H.M., Knapton, J., (1996), *Research into paver interlock*, Jrnl. of the Institution of Highway & Transportation & IHIE, Vol. 43, No. 03, p 20-24.

2 Knapton, J., Algin, H.M., (1995), *The Mathematical Solution to Interlock in Flexibly Bedded Clay Paving.* Proc. of the 4th. Int. Masonry Conf. No. 7, Vol. 2, p 307-313. London.

3 Knapton, J., Algin, H.M., (1996), *The Mathematical Solution to Interlock in Concrete Block Paving.* Proc. of the 5th. Int. Conf. on Concrete Block Paving, p 261-278, Tel-Aviv.

CHAPTER EIGHT

CALCULATION OF STRESSES BENEATH EIGHT COMMON SHAPED PAVERS TAKING INTO ACCOUNT LOADS GENERATING ABSOLUTE-HEXAHEDRAL STRESS PATTERN

Synopsis

The absolute-hexahedral vertical compressive stress regimes which occur beneath the circumscribing rectangular border of eight proprietory shaped pavers (see proprietory shaped pavers 2, 3, 4, 5, 6, 7, 8 and 9 in Figure 5.1) can be analysed by using the similar method described in the previous chapter for proprietory shaped paver 1. This Chapter presents the application of the bedding sand stress calculation method (see Chapters 6 and 7) to eight common proprietory shaped pavers in order to determine the algebraical solutions to the absolute-hexahedral vertical compressive stress regimes for all realistically possible load patches. In the other paver stress regimes, iterative solutions (see Appendix) have been developed and given in Figures 6.21, 9.1, 9.2, 9.3, 9.4, 9.5, 9.6, 9.7, 9.8 and 9.9.

8.1. Introduction

The proprietory shaped pavers 2, 3, 4, 5, 6, 7, 8 and 9 shown in Figure 5.1 are analysed by using the similar method presented in Chapter 7 for proprietory shaped paver 1. Five vertical compressive stress regimes can occur beneath the circumscribing rectangular border of the shaped pavers. These are conceptually tetrahedral, short-pentahedral, long-pentahedral, partial-hexahedral and absolute-hexahedral compressive stress regimes defined in Chapter 6. The chosen proprietory shaped pavers are commercially important on a worldwide basis. The all possible bedding material vertical stress regimes of proprietory shaped paver 1 have been described in Chapter 7. For the remaining shapes, only the arithmetical solutions of the absolute-hexahedral compressive stress regimes are documented in this Chapter. In the other paver stress regimes, iterative solutions (see Appendix) have been developed. The Bedding sand stress calculation method for rectangular pavers described in Chapter 6 has been applied to the nine non-rectangular shapes of pavers as shown in Figure 5.1. In each case, the circumscribing rectangular paver has been analysed and the negative effects generated by the shaped paver dentations have been included in the results. The vertical stresses for shaped pavers can be calculated by considering vertical and rotational equilibrium of the load patch pressures applied onto the upper paver surface as has already been described for rectangular pavers. For vertical equilibrium to be satisfied the total applied load must equal the total volume of the vertical compressive stress beneath the paver and for rotational equilibrium, the centroid distances of the applied load $\left(\overline{X}, \overline{Y}\right)$ must coincide with the centroid distances of the total volume of the vertical compressive stress in the bedding sand. The assumptions which were used for rectangular pavers can be applied equally to proprietory shaped pavers. These are firstly the support conditions of the paver are uniform and secondly the pavers are structurally rigid in relation to their bedding sand. As may be seen in Figure 6.1 all stress blocks geometrically have the tetrahedron surface function. However only that part of the upper surface of these volumes which contacts the lower paver surface must be considered. Therefore, a method is required which calculates that part of the volume of a tetrahedron which is truncated by the paver boundary lines. This truncated volume can

then be equalised to the total applied patch load and rotational equilibrium conditions can be applied by ensuring the centroid distances of the load patch and the truncated tetrahedron coincide. The vertical compressive stress function can be calculated by using the three resulting equations. The stress function is the function satisfies the equation of the vertical equilibrium and the two equations of rotational equilibrium. The complexity of the vertical compressive stresses calculation can be reduced by using the circumscribing rectangular boundaries of the shaped blocks (see Figure 5.1), with the proviso that the volume of actual vertical stress must satisfy the vertical and rotational equilibriums in each step of evaluating the stress function. The eight individual proprietory shaped pavers (the absolute-hexahedral vertical stress distribution of proprietory shaped paver 1 is analysed in Chapter 7, Section 7.2.5) illustrated in Figure 5.1 are now analysed to determine the absolute-hexahedral vertical stress distributions beneath the circumscribing rectangular borders by using the common applied load patch variations which are described in Chapter 5.

8.2. Absolute-hexahedral compressive stress regimes beneath the circumscribing rectangular border for proprietory shaped paver 2

The application of the absolute-hexahedral compressive stress regime beneath the circumscribing rectangular border of proprietory shaped paver 2 shown in Figure 8.1 can be calculated by using the data in Tables 5.3. The first two letters of each boundary line function in Table 5.3 for proprietory shaped paver 2 charecterise the corner names can be seen in Figure 8.1 (example: **bcy** symbolises the boundary line function of proprietory shaped paver 2 in the **y** axis between corner **b** and **c**). The line functions which define the boundary of the absolute-hexahedral stress block in the xy-plane (see Figure 8.1) are of the form $fy = l\left(1-\frac{x}{l}\right)$, $fx = l\left(1-\frac{y}{l}\right)$.

The surface function of the absolute-hexahedral compressive stress block beneath the circumscribing rectangular border shown in Figure 8.1 through the three points σ_A, **l** and **t** is given by:

$$\begin{vmatrix} x & y & z & 1 \\ t & 0 & 0 & 1 \\ 0 & l & 0 & 1 \\ 0 & 0 & \sigma_A & 1 \end{vmatrix} = 0 \Rightarrow f(x,y) = z = \sigma_A\left(1 - \frac{x}{t} - \frac{y}{l}\right)$$

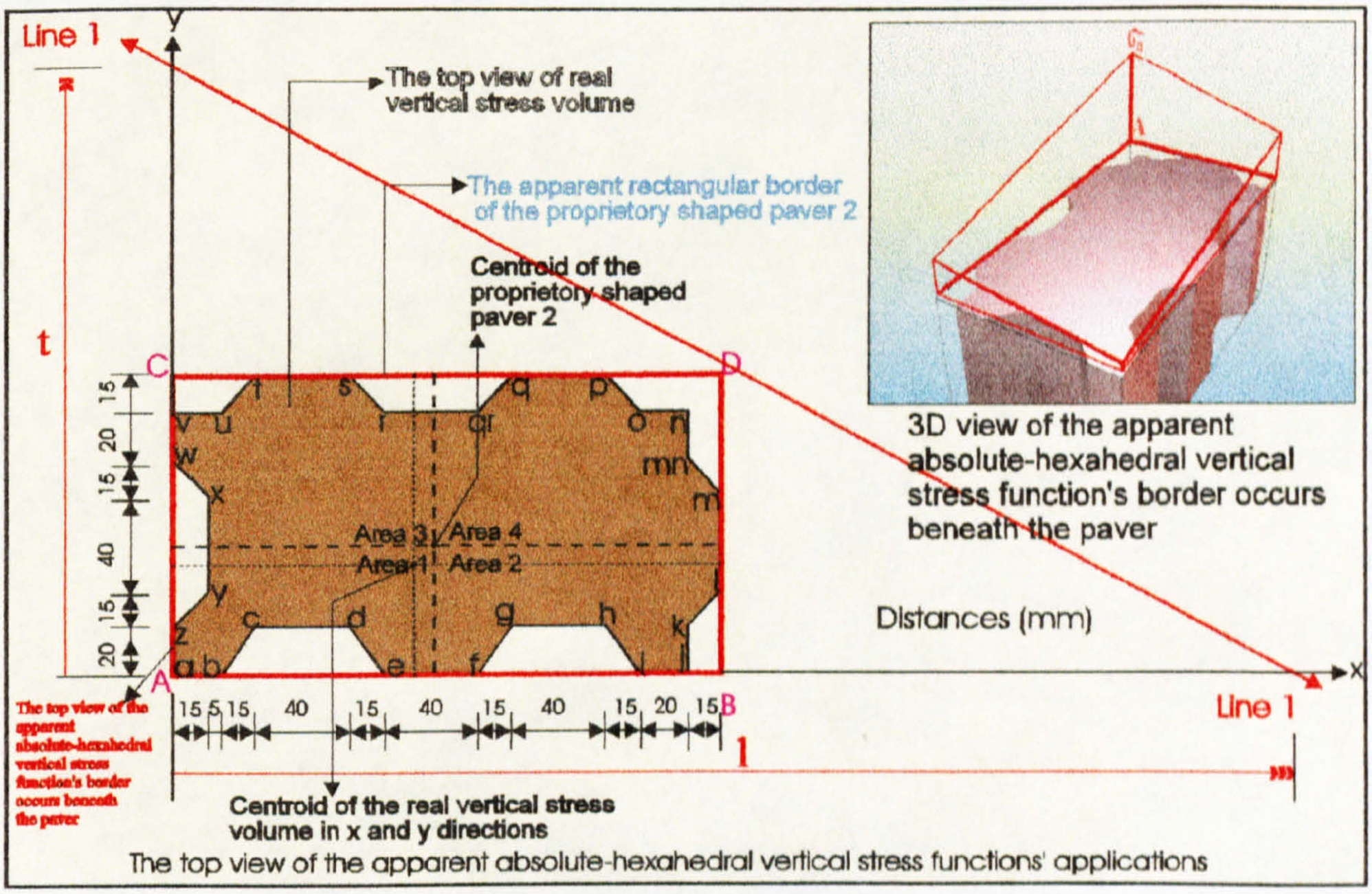

Figure 8.1: The application of the absolute-hexahedral compressive stress distribution beneath the circumscribing rectangular border of proprietory shaped paver 2.

The following actual total volume **V** beneath the surface $f(x,y) = z\ (> 0)$ and above the region in the xy-plane (see Figure 8.1) is calculated by subtracting the negative volume generated by the dentations of the shaped paver from the absolute-hexahedral volume beneath circumscribing rectangular boundary of the paver.

$$V = \int_0^{235}\int_0^{125} f(x,y)\,dy\,dx - \int_{20}^{35}\int_0^{bcy} f(x,y)\,dy\,dx - \int_{35}^{75}\int_0^{15} f(x,y)\,dy\,dx - \int_{75}^{90}\int_0^{dey} f(x,y)\,dy\,dx - \int_{130}^{145}\int_0^{fgy} f(x,y)\,dy\,dx$$
$$- \int_{145}^{185}\int_0^{15} f(x,y)\,dy\,dx - \int_{185}^{200}\int_0^{hiy} f(x,y)\,dy\,dx - \int_{220}^{235}\int_0^{20} f(x,y)\,dy\,dx - \int_{220}^{235}\int_{20}^{klv} f(x,y)\,dy\,dx - \int_{220}^{235}\int_{75}^{mmny} f(x,y)\,dy\,dx$$
$$- \int_{220}^{235}\int_{90}^{110} f(x,y)\,dy\,dx - \int_{200}^{235}\int_{110}^{125} f(x,y)\,dy\,dx - \int_{185}^{200}\int_{110}^{poy} f(x,y)\,dy\,dx - \int_{130}^{145}\int_{110}^{qrqy} f(x,y)\,dy\,dx - \int_{90}^{130}\int_{110}^{125} f(x,y)\,dy\,dx$$

$$-\int_{75}^{90}\int_{110}^{sry} f(x,y)\,dy\,dx - \int_{20}^{35}\int_{110}^{uty} f(x,y)\,dy\,dx - \int_{0}^{20}\int_{110}^{125} f(x,y)\,dy\,dx - \int_{0}^{20}\int_{75}^{wxy} f(x,y)\,dy\,dx - \int_{0}^{20}\int_{35}^{75} f(x,y)\,dy\,dx$$
$$-\int_{0}^{20}\int_{20}^{zyy} f(x,y)\,dy\,dx$$

and the centroids of this volume in the xy-plane are at distances $\overline{X}$ and $\overline{Y}$ from the axes (see Figure 8.1) which are given by the following equations.

$$\overline{X} = \frac{1}{V}\left[\int_{0}^{235}\int_{0}^{125} x f(x,y)\,dy\,dx - \int_{20}^{35}\int_{0}^{bcy} x f(x,y)\,dy\,dx - \int_{35}^{75}\int_{0}^{15} x f(x,y)\,dy\,dx - \int_{75}^{90}\int_{0}^{kcy} x f(x,y)\,dy\,dx\right.$$
$$-\int_{130}^{145}\int_{0}^{fgy} x f(x,y)\,dy\,dx - \int_{145}^{185}\int_{0}^{15} x f(x,y)\,dy\,dx - \int_{185}^{200}\int_{0}^{hiy} x f(x,y)\,dy\,dx - \int_{220}^{235}\int_{0}^{20} x f(x,y)\,dy\,dx$$
$$-\int_{220}^{235}\int_{20}^{kly} x f(x,y)\,dy\,dx - \int_{220}^{235}\int_{75}^{mmny} x f(x,y)\,dy\,dx - \int_{220}^{235}\int_{90}^{110} x f(x,y)\,dy\,dx - \int_{200}^{235}\int_{110}^{125} x f(x,y)\,dy\,dx$$
$$-\int_{185}^{200}\int_{110}^{poy} x f(x,y)\,dy\,dx - \int_{130}^{145}\int_{110}^{qrqy} x f(x,y)\,dy\,dx - \int_{90}^{130}\int_{110}^{125} x f(x,y)\,dy\,dx - \int_{75}^{90}\int_{110}^{sry} x f(x,y)\,dy\,dx$$
$$-\int_{20}^{35}\int_{110}^{uty} x f(x,y)\,dy\,dx - \int_{0}^{20}\int_{110}^{125} x f(x,y)\,dy\,dx - \int_{0}^{20}\int_{75}^{wxy} x f(x,y)\,dy\,dx - \int_{0}^{20}\int_{35}^{75} x f(x,y)\,dy\,dx$$
$$\left.-\int_{0}^{20}\int_{20}^{zyy} x f(x,y)\,dy\,dx\right]$$

$$\overline{Y} = \frac{1}{V}\left[\int_{0}^{125}\int_{0}^{235} y f(x,y)\,dx\,dy - \int_{0}^{20}\int_{0}^{bcx} y f(x,y)\,dx\,dy - \int_{0}^{35}\int_{0}^{15} y f(x,y)\,dx\,dy - \int_{0}^{75}\int_{0}^{dex} y f(x,y)\,dx\,dy\right.$$
$$-\int_{0}^{130}\int_{0}^{fgx} y f(x,y)\,dx\,dy - \int_{0}^{145}\int_{0}^{15} y f(x,y)\,dx\,dy - \int_{0}^{185}\int_{0}^{hix} y f(x,y)\,dx\,dy - \int_{0}^{220}\int_{0}^{235} y f(x,y)\,dx\,dy$$
$$-\int_{20}^{220}\int_{0}^{klx} y f(x,y)\,dx\,dy - \int_{75}^{220}\int_{0}^{mmnx} y f(x,y)\,dx\,dy - \int_{90}^{220}\int_{0}^{235} y f(x,y)\,dx\,dy - \int_{110}^{200}\int_{0}^{235} y f(x,y)\,dx\,dy$$
$$-\int_{110}^{185}\int_{0}^{pox} y f(x,y)\,dx\,dy - \int_{110}^{130}\int_{0}^{qrqx} y f(x,y)\,dx\,dy - \int_{110}^{90}\int_{0}^{125} y f(x,y)\,dx\,dy - \int_{110}^{75}\int_{0}^{srx} y f(x,y)\,dx\,dy$$
$$-\int_{110}^{20}\int_{0}^{utx} y f(x,y)\,dx\,dy - \int_{110}^{0}\int_{0}^{125} y f(x,y)\,dx\,dy - \int_{75}^{0}\int_{0}^{wxx} y f(x,y)\,dx\,dy - \int_{35}^{0}\int_{0}^{75} y f(x,y)\,dx\,dy$$

$$\left.-\int_{20}^{35}\int_{0}^{zyx} y f(x,y)\,dx\,dy\right]$$

The $V, \overline{X}$ and $\overline{Y}$ values can analytically be evaluated in terms of l, t and σ_A. The following results which indicate the proportions of the absolute-hexahedral vertical compressive stress block (see Figure 8.1) can be determined by applying vertical and rotational equilibrium between load patch and vertical compressive stress distribution (see Chapter 6). For vertical equilibrium condition the equality between the truncated volume (V) and the total applied patch load (N) must be satisfied and for rotational equilibrium conditions the centroid distances of the load patch ($\overline{X}$, $\overline{Y}$) must be coincided with the centroid distances of the truncated vertical stress block ($\overline{X}$, $\overline{Y}$).

$$l = 0.8(0.1186410.10^{7}\overline{Y} - 0.73621579.10^{8})(0.306082571.10^{9}\overline{YX} + 0.2501661605.10^{13}\overline{Y} + 0.1258002658.10^{13}\overline{X} - 0.3500377064.10^{15}) \Big/ (0.9733856445.10^{16}\overline{YX} + 0.1421470447.10^{13}\overline{Y}^{2}\overline{X} - 0.1231894319.10^{19}\overline{Y} + 0.4662524862.10^{15}\overline{Y}^{2} - 0.6094991582.10^{18}\overline{X} + 0.7464866404.10^{20})$$

$$t = \frac{4\begin{pmatrix}0.306082571.10^{9}\overline{YX} + 0.2501661605.10^{13}\overline{Y} + 0.1258002658.10^{13}\overline{X} \\ -0.3500377064.10^{15}\end{pmatrix}}{\begin{pmatrix}0.2066552432.10^{10}\overline{X} + 0.8202625.10^{7}\overline{YX} - 0.1007908704.10^{14} \\ +0.1560928582.10^{12}\overline{Y}\end{pmatrix}}$$

$$\sigma_A = -10N(0.1186410.10^{7}\overline{Y} - 0.73621579.10^{8})(0.306082571.10^{9}\overline{YX} + 0.2501661605.10^{13}\overline{Y} + 0.1258002658.10^{13}\overline{X} - 0.3500377064.10^{15}) \Big/ (0.6053741109.10^{16}\overline{YX} + 0.6407001075.10^{12}\overline{Y}^{2}\overline{X} + 0.1177822264.10^{26}\overline{Y} + 0.1680996933.10^{22}\overline{Y}^{2} - 0.3773511452.10^{18}\overline{X} - 0.7373597779.10^{27})$$

Therefore, the function of the absolute-hexahedral vertical compressive stress regimes can be determined as follows by inserting the **l**, **t** and σ_A values into $f(x,y) = z = \sigma_A\left(1 - \frac{x}{l} - \frac{y}{t}\right)$.

$$f(x,y) = z = 0.001N(-0.1452557692.10^{16}\overline{Y}^2\overline{X} - 0.1187198538.10^{20}\overline{Y}^2$$
$$-0.5879890605.10^{19}\overline{YX} + 0.2397858051.10^{22}\overline{Y} + 0.3704645683.10^{21}\overline{X}$$
$$-0.1030813146.10^{24} + 0.4866928223.10^{17}x\overline{YX} + 0.7107352235.10^{13}x\overline{Y}^2\overline{X}$$
$$-0.6159471595.10^{19}x\overline{Y} + 0.2331262431.10^{16}x\overline{Y}^2 - 0.3047495791.10^{19}x\overline{X}$$
$$+0.3732433202.10^{21}x + 0.1847888266.10^{16}y\overline{YX} + 0.9731676326.10^{13}y\overline{Y}^2\overline{X}$$
$$-0.2344973235.10^{20}y\overline{Y} + 0.1851901279.10^{18}y\overline{Y}^2 - 0.1521428531.10^{18}y\overline{X}$$
$$+0.7420383028.10^{21}y) \Big/ (0.2421496444.10^{13}\overline{YX} + 0.256280043.10^{9}\overline{Y}^2\overline{X}$$
$$+0.4711289056.10^{22}\overline{Y} + 0.6723987732.10^{18}\overline{Y}^2 - 0.1509404581.10^{15}\overline{X}$$
$$-0.2949439112.10^{24})$$

The stress values beneath the corners of proprietory shaped paver 2 for the absolute-hexahedral vertical compressive stress regimes can now be determined by inserting the corner co-ordinates in the xy-plane into the stress function defined above (see Figure 8.1).

The vertical compressive stress beneath the corner **a** is

$$\sigma_a = -4000N(0.363139423.10^{9}\overline{Y}^2\overline{X} + 0.2967996345.10^{13}\overline{Y}^2 + 0.1469972651.10^{13}\overline{YX}$$
$$-0.5994645128.10^{15}\overline{Y} - 0.9261614208.10^{14}\overline{X} + 0.2577032865.10^{17})$$
$$\Big/ (0.2421496444.10^{13}\overline{YX} + 0.256280043.10^{9}\overline{Y}^2\overline{X} + 0.4711289056.10^{22}\overline{Y}$$
$$+0.6723987732.10^{18}\overline{Y}^2 - 0.1509404581.10^{15}\overline{X} - 0.2949439112.10^{24})$$

The vertical compressive stress beneath the corner **b** is

$$\sigma_b = -1000N(0.1310410647.10^{10}\overline{Y}^2\overline{X} + 0.1182536013.10^{14}\overline{Y}^2 + 0.4906504960.10^{13}\overline{YX}$$
$$-0.2274668619.10^{16}\overline{Y} - 0.3095146525.10^{15}\overline{X} + 0.9561644820.10^{17})$$
$$\Big/ (0.2421496444.10^{13}\overline{YX} + 0.256280043.10^{9}\overline{Y}^2\overline{X} + 0.4711289056.10^{22}\overline{Y}$$
$$+0.6723987732.10^{18}\overline{Y}^2 - 0.1509404581.10^{15}\overline{X} - 0.2949439112.10^{24})$$

The vertical compressive stress beneath the corner **c** is

$$\sigma_c = -1000N(0.1057825219.10^{10}\overline{Y}^2\overline{X} + 0.9012539276.10^{13}\overline{Y}^2 + 0.4148747403.10^{13}\overline{YX}$$
$$-0.1830530560.10^{16}\overline{Y} - 0.2615200728.10^{15}\overline{X} + 0.7888722385.10^{17})$$
$$\Big/ (0.2421496444.10^{13}\overline{YX} + 0.256280043.10^{9}\overline{Y}^2\overline{X} + 0.4711289056.10^{22}\overline{Y}$$
$$+0.6723987732.10^{18}\overline{Y}^2 - 0.1509404581.10^{15}\overline{X} - 0.2949439112.10^{24})$$

The vertical compressive stress beneath the corner **d** is

$$\sigma_d = -200N(0.38676556647.10^{10}\overline{Y}^2\overline{X} + 0.4459644390.10^{14}\overline{Y}^2 + 0.1100988057.10^{14}\overline{YX}$$
$$-0.7920758480.10^{16}\overline{Y} - 0.6981012060.10^{15}\overline{X} + 0.3197874552.10^{18})$$
$$\Big/ (0.2421496444.10^{13}\overline{YX} + 0.256280043.10^{9}\overline{Y}^2\overline{X} + 0.4711289056.10^{22}\overline{Y}$$
$$+0.6723987732.10^{18}\overline{Y}^2 - 0.1509404581.10^{15}\overline{X} - 0.2949439112.10^{24})$$

The vertical compressive stress beneath the corner **e** is

$$\sigma_e = -400N(0.2032239977.10^{10}\overline{Y}^2\overline{X} + 0.2915542940.10^{14}\overline{Y}^2 + 0.3749138010.10^{13}\overline{YX}$$
$$-0.4608764018.10^{16}\overline{Y} - 0.2404748678.10^{15}\overline{X} + 0.1737235395.10^{18})$$
$$\Big/ (0.2421496444.10^{13}\overline{YX} + 0.256280043.10^{9}\overline{Y}^2\overline{X} + 0.4711289056.10^{22}\overline{Y}$$
$$+0.6723987732.10^{18}\overline{Y}^2 - 0.1509404581.10^{15}\overline{X} - 0.2949439112.10^{24})$$

The vertical compressive stress beneath the corner **f** is

$$\sigma_f = -200N(0.2643009507.10^{10}\overline{Y}^2\overline{X} + 0.5784460630.10^{14}\overline{Y}^2 - 0.2235580425.10^{13}\overline{YX}$$
$$-0.7985633720.10^{16}\overline{Y} + 0.1285494225.10^{15}\overline{X} + 0.2727984149.10^{18})$$
$$/\,(0.2421496444.10^{13}\overline{YX} + 0.256280043.10^{9}\overline{Y}^2\overline{X} + 0.4711289056.10^{22}\overline{Y}$$
$$+0.6723987732.10^{18}\overline{Y}^2 - 0.1509404581.10^{15}\overline{X} - 0.2949439112.10^{24})$$

The vertical compressive stress beneath the corner g is

$$\sigma_g = -1000N(0.276016473.10^{9}\overline{Y}^2\overline{X} + 0.8756100409.10^{13}\overline{Y}^2 - 0.1204873642.10^{13}\overline{YX}$$
$$-0.1152988685.10^{16}\overline{Y} + 0.7370446420.10^{14}\overline{X} + 0.3783045863.10^{17})$$
$$/\,(0.2421496444.10^{13}\overline{YX} + 0.256280043.10^{9}\overline{Y}^2\overline{X} + 0.4711289056.10^{22}\overline{Y}$$
$$+0.6723987732.10^{18}\overline{Y}^2 - 0.1509404581.10^{15}\overline{X} - 0.2949439112.10^{24})$$

The vertical compressive stress beneath the corner h is

$$\sigma_h = 8000N(0.1034702.10^{7}\overline{Y}^2\overline{X} - 0.1082856239.10^{13}\overline{Y}^2 + 0.3939556165.10^{12}\overline{YX}$$
$$+0.1133262276.10^{15}\overline{Y} - 0.2445053698.10^{14}\overline{X} - 0.2862590728.10^{16})$$
$$/\,(0.2421496444.10^{13}\overline{YX} + 0.256280043.10^{9}\overline{Y}^2\overline{X} + 0.4711289056.10^{22}\overline{Y}$$
$$+0.6723987732.10^{18}\overline{Y}^2 - 0.1509404581.10^{15}\overline{X} - 0.2949439112.10^{24})$$

The vertical compressive stress beneath the corner i is

$$\sigma_i = -5000N(0.6217449.10^{7}\overline{Y}^2\overline{X} + 0.2281146578.10^{13}\overline{Y}^2 - 0.7707931682.10^{12}\overline{YX}$$
$$-0.2331927464.10^{15}\overline{Y} + 0.4780691798.10^{14}\overline{X} + 0.5686530112.10^{16})$$
$$/\,(0.2421496444.10^{13}\overline{YX} + 0.256280043.10^{9}\overline{Y}^2\overline{X} + 0.4711289056.10^{22}\overline{Y}$$
$$+0.6723987732.10^{18}\overline{Y}^2 - 0.1509404581.10^{15}\overline{X} - 0.2949439112.10^{24})$$

The vertical compressive stress beneath the corner j is

$$\sigma_j = 200000N(555299\overline{Y}^2\overline{X} - 0.5679553825.10^{11}\overline{Y}^2 + 0.2413675743.10^{11}\overline{YX}$$
$$+0.5213871500.10^{13}\overline{Y} - 0.1499922529.10^{13}\overline{X} - 0.1048389208.10^{15})$$
$$/(0.2421496444.10^{13}\overline{YX} + 0.256280043.10^{9}\overline{Y}^2\overline{X} + 0.4711289056.10^{22}\overline{Y}$$
$$+0.6723987732.10^{18}\overline{Y}^2 - 0.1509404581.10^{15}\overline{X} - 0.2949439112.10^{24})$$

The vertical compressive stress beneath the corner k is

$$\sigma_k = 2000N(0.152846663.10^{9}\overline{Y}^2\overline{X} - 0.3827652544.10^{13}\overline{Y}^2 + 0.2432154625.10^{13}\overline{YX}$$
$$+0.2868898265.10^{15}\overline{Y} - 0.1515136814.10^{15}\overline{X} - 0.3063509050.10^{16})$$
$$/(0.2421496444.10^{13}\overline{YX} + 0.256280043.10^{9}\overline{Y}^2\overline{X} + 0.4711289056.10^{22}\overline{Y}$$
$$+0.6723987732.10^{18}\overline{Y}^2 - 0.1509404581.10^{15}\overline{X} - 0.2949439112.10^{24})$$

The vertical compressive stress beneath the corner l is

$$\sigma_l = 2000N(0.279139377.10^{9}\overline{Y}^2\overline{X} - 0.2421242116.10^{13}\overline{Y}^2 + 0.2811033402.10^{13}\overline{YX}$$
$$+0.6482079700.10^{14}\overline{Y} - 0.1755109713.10^{15}\overline{X} + 0.5301103125.10^{16})$$
$$/(0.2421496444.10^{13}\overline{YX} + 0.256280043.10^{9}\overline{Y}^2\overline{X} + 0.4711289056.10^{22}\overline{Y}$$
$$+0.6723987732.10^{18}\overline{Y}^2 - 0.1509404581.10^{15}\overline{X} - 0.2949439112.10^{24})$$

The vertical compressive stress beneath the corner m is

$$\sigma_m = 2500N(0.379018323.10^{9}\overline{Y}^2\overline{X} + 0.1026048352.10^{13}\overline{Y}^2 + 0.2278392934.10^{13}\overline{YX}$$
$$-0.3233390800.10^{15}\overline{Y} - 0.1428430626.10^{15}\overline{X} + 0.1611349534.10^{17})$$
$$/(0.2421496444.10^{13}\overline{YX} + 0.256280043.10^{9}\overline{Y}^2\overline{X} + 0.4711289056.10^{22}\overline{Y}$$
$$+0.6723987732.10^{18}\overline{Y}^2 - 0.1509404581.10^{15}\overline{X} - 0.2949439112.10^{24})$$

The vertical compressive stress beneath the corner mn is

$$\sigma_{mn} = 100N(0.9869106693.10^{10}\overline{Y}^2\overline{X} + 0.5308003865.10^{14}\overline{Y}^2 + 0.4993661429.10^{14}\overline{YX}$$
$$-0.1067701612.10^{17}\overline{Y} - 0.3136773625.10^{16}\overline{X} + 0.4581566309.10^{18})$$
$$\Big/ (0.2421496444.10^{13}\overline{YX} + 0.256280043.10^{9}\overline{Y}^2\overline{X} + 0.4711289056.10^{22}\overline{Y}$$
$$+0.6723987732.10^{18}\overline{Y}^2 - 0.1509404581.10^{15}\overline{X} - 0.2949439112.10^{24})$$

The vertical compressive stress beneath the corner **n** is

$$\sigma_{n} = 4000N(0.295386049.10^{9}\overline{Y}^2\overline{X} + 0.2252951606.10^{13}\overline{Y}^2 + 0.1257654799.10^{13}\overline{YX}$$
$$-0.3841740648.10^{15}\overline{Y} - 0.7918005488.10^{14}\overline{X} + 0.1516410729.10^{17})$$
$$\Big/ (0.2421496444.10^{13}\overline{YX} + 0.256280043.10^{9}\overline{Y}^2\overline{X} + 0.4711289056.10^{22}\overline{Y}$$
$$+0.6723987732.10^{18}\overline{Y}^2 - 0.1509404581.10^{15}\overline{X} - 0.2949439112.10^{24})$$

The vertical compressive stress beneath the corner **o** is

$$\sigma_{o} = 1000N(0.1039397151.10^{10}\overline{Y}^2\overline{X} + 0.8965181176.10^{13}\overline{Y}^2 + 0.4057233550.10^{13}\overline{YX}$$
$$-0.1413506827.10^{16}\overline{Y} - 0.2557703037.10^{15}\overline{X} + 0.5319156275.10^{17})$$
$$\Big/ (0.2421496444.10^{13}\overline{YX} + 0.256280043.10^{9}\overline{Y}^2\overline{X} + 0.4711289056.10^{22}\overline{Y}$$
$$+0.6723987732.10^{18}\overline{Y}^2 - 0.1509404581.10^{15}\overline{X} - 0.2949439112.10^{24})$$

The vertical compressive stress beneath the corner **p** is

$$\sigma_{p} = 4000N(0.269690503.10^{9}\overline{Y}^2\overline{X} + 0.2927016040.10^{13}\overline{Y}^2 + 0.8387281603.10^{12}\overline{YX}$$
$$-0.4182151845.10^{15}\overline{Y} - 0.5308500240.10^{14}\overline{X} + 0.1468087187.10^{17})$$
$$\Big/ (0.2421496444.10^{13}\overline{YX} + 0.256280043.10^{9}\overline{Y}^2\overline{X} + 0.4711289056.10^{22}\overline{Y}$$
$$+0.6723987732.10^{18}\overline{Y}^2 - 0.1509404581.10^{15}\overline{X} - 0.2949439112.10^{24})$$

The vertical compressive stress beneath the corner **q** is

$$\sigma_q = 1000N(0.794467923.10^9\overline{Y}^2\overline{X} + 0.11614813 66.10^{14}\overline{Y}^2 + 0.140814135 1.10^{13}\overline{YX}$$
$$-0.1426481874.10^{16}\overline{Y} - 0.9044017800.10^{14}\overline{X} + 0.4379375468.10^{17})$$
$$\Big/(0.2421496444.10^{13}\overline{YX} + 0.256280043.10^9\overline{Y}^2\overline{X} + 0.4711289056.10^{22}\overline{Y}$$
$$+0.6723987732.10^{18}\overline{Y}^2 - 0.1509404581.10^{15}\overline{X} - 0.2949439112.10^{24})$$

The vertical compressive stress beneath the corner **qr** is

$$\sigma_{qr} = 200N(0.2709412473.10^{10}\overline{Y}^2\overline{X} + 0.4400996403.10^{14}\overline{Y}^2 + 0.3251918970.10^{13}\overline{YX}$$
$$-0.4911719077.10^{16}\overline{Y} - 0.2122279915.10^{15}\overline{X} + 0.1353226517.10^{18})$$
$$\Big/(0.2421496444.10^{13}\overline{YX} + 0.256280043.10^9\overline{Y}^2\overline{X} + 0.4711289056.10^{22}\overline{Y}$$
$$+0.6723987732.10^{18}\overline{Y}^2 - 0.1509404581.10^{15}\overline{X} - 0.2949439112.10^{24})$$

The vertical compressive stress beneath the corner **r** is

$$\sigma_r = 400N(0.643971013.10^9\overline{Y}^2\overline{X} + 0.2177185577.10^{14}\overline{Y}^2 - 0.3240968738.10^{13}\overline{YX}$$
$$-0.1839912379.10^{16}\overline{Y} + 0.1986355833.10^{15}\overline{X} + 0.3033699383.10^{17})$$
$$\Big/(0.2421496444.10^{13}\overline{YX} + 0.256280043.10^9\overline{Y}^2\overline{X} + 0.4711289056.10^{22}\overline{Y}$$
$$+0.6723987732.10^{18}\overline{Y}^2 - 0.1509404581.10^{15}\overline{X} - 0.2949439112.10^{24})$$

The vertical compressive stress beneath the corner **s** is

$$\sigma_s = 200N(0.1484766333.10^{10}\overline{Y}^2\overline{X} + 0.5725812645.10^{14}\overline{Y}^2 - 0.9993542025.10^{13}\overline{YX}$$
$$-0.4976594313.10^{16}\overline{Y} + 0.6144226370.10^{15}\overline{X} + 0.8833361135.10^{17})$$
$$\Big/(0.2421496444.10^{13}\overline{YX} + 0.256280043.10^9\overline{Y}^2\overline{X} + 0.4711289056.10^{22}\overline{Y}$$
$$+0.6723987732.10^{18}\overline{Y}^2 - 0.1509404581.10^{15}\overline{X} - 0.2949439112.10^{24})$$

The vertical compressive stress beneath the corner **t** is

$$\sigma_t = 400N(0.31647943.10^8\overline{Y}^2\overline{X} + 0.2839593700.10^{14}\overline{Y}^2 - 0.9863699235.10^{13}\overline{YX}$$
$$-0.1872349997.10^{16}\overline{Y} - 0.6119608975.10^{15}\overline{X} + 0.6842473650.10^{16})$$
$$/\,(0.2421496444.10^{13}\overline{YX} + 0.256280043.10^9\overline{Y}^2\overline{X} + 0.4711289056.10^{22}\overline{Y}$$
$$+0.6723987732.10^{18}\overline{Y}^2 - 0.1509404581.10^{15}\overline{X} - 0.2949439112.10^{24})$$

The vertical compressive stress beneath the corner **u** is

$$\sigma_u = -100N(0.23992625 13.10^{10}\overline{Y}^2\overline{X} - 0.8545553939.10^{14}\overline{Y}^2 + 0.4703237251.10^{14}\overline{YX}$$
$$+0.3048019399.10^{16}\overline{Y} - 0.2927789387.10^{16}\overline{X} + 0.1399223489.10^{18})$$
$$/\,(0.2421496444.10^{13}\overline{YX} + 0.256280043.10^9\overline{Y}^2\overline{X} + 0.4711289056.10^{22}\overline{Y}$$
$$+0.6723987732.10^{18}\overline{Y}^2 - 0.1509404581.10^{15}\overline{X} - 0.2949439112.10^{24})$$

The vertical compressive stress beneath the corner **v** is

$$\sigma_v = -16000N(0.23879581.10^8\overline{Y}^2\overline{X} - 0.5311830431.10^{12}\overline{Y}^2 + 0.3547889310.10^{12}\overline{YX}$$
$$+0.1135078175.10^{14}\overline{Y} - 0.2210805341.10^{14}\overline{X} + 0.1341068831.10^{16})$$
$$/\,(0.2421496444.10^{13}\overline{YX} + 0.256280043.10^9\overline{Y}^2\overline{X} + 0.4711289056.10^{22}\overline{Y}$$
$$+0.6723987732.10^{18}\overline{Y}^2 - 0.1509404581.10^{15}\overline{X} - 0.2949439112.10^{24})$$

The vertical compressive stress beneath the corner **w** is

$$\sigma_w = -100N(0.5767068227.10^{10}\overline{Y}^2\overline{X} - 0.4795126130.10^{14}\overline{Y}^2 + 0.5713580661.10^{14}\overline{YX}$$
$$-0.2873821390.10^{16}\overline{Y} - 0.3567717115.10^{16}\overline{X} + 0.3629786735.10^{18})$$
$$/\,(0.2421496444.10^{13}\overline{YX} + 0.256280043.10^9\overline{Y}^2\overline{X} + 0.4711289056.10^{22}\overline{Y}$$
$$+0.6723987732.10^{18}\overline{Y}^2 - 0.1509404581.10^{15}\overline{X} - 0.2949439112.10^{24})$$

The vertical compressive stress beneath the corner **x** is

$$\sigma_x = -400N(0.1451337307.10^{10}\overline{Y}^2\overline{X} - 0.5159748648.10^{13}\overline{Y}^2 + 0.1191978335.10^{14}\overline{YX}$$
$$-0.1289846733.10^{16}\overline{Y} - 0.7452598463.10^{15}\overline{X} + 0.9990893873.10^{17})$$
$$/\,(0.2421496444.10^{13}\overline{YX} + 0.256280043.10^{9}\overline{Y}^2\overline{X} + 0.4711289056.10^{22}\overline{Y}$$
$$+0.6723987732.10^{18}\overline{Y}^2 - 0.1509404581.10^{15}\overline{X} - 0.2949439112.10^{24})$$

The vertical compressive stress beneath the corner **y** is

$$\sigma_y = -100N(0.9698019763.10^{10}\overline{Y}^2\overline{X} + 0.5343705654.10^{14}\overline{Y}^2 + 0.484182887 1.10^{14}\overline{YX}$$
$$-0.1453927987.10^{17}\overline{Y} - 0.3041896526.10^{16}\overline{X} + 0.6964510760.10^{18})$$
$$/\,(0.2421496444.10^{13}\overline{YX} + 0.256280043.10^{9}\overline{Y}^2\overline{X} + 0.4711289056.10^{22}\overline{Y}$$
$$+0.6723987732.10^{18}\overline{Y}^2 - 0.1509404581.10^{15}\overline{X} - 0.2949439112.10^{24})$$

The vertical compressive stress beneath the corner **z** is

$$\sigma_z = -2000N(0.628962083.10^{9}\overline{Y}^2\overline{X} + 0.4084091411.10^{13}\overline{Y}^2 + 0.2921466420.10^{13}\overline{YX}$$
$$-0.9644317020.10^{15}\overline{Y} - 0.1837108556.10^{15}\overline{X} + 0.4412027427.10^{17})$$
$$/\,(0.2421496444.10^{13}\overline{YX} + 0.256280043.10^{9}\overline{Y}^2\overline{X} + 0.4711289056.10^{22}\overline{Y}$$
$$+0.6723987732.10^{18}\overline{Y}^2 - 0.1509404581.10^{15}\overline{X} - 0.2949439112.10^{24})$$

8.3. Absolute-hexahedral compressive stress regimes beneath the circumscribing rectangular border for proprietory shaped paver 3

The application of the absolute-hexahedral compressive stress regime beneath the circumscribing rectangular border of proprietory shaped paver 3 shown in Figure 8.2 can be calculated by using the data in Tables 5.5. The first two letters of each boundary line function in Table 5.5 for proprietory shaped paver 3 charecterise the corner names can be seen in Figure 8.2 (example: **bcy** symbolises the boundary line function of proprietory shaped paver 3 in the **y** axis between corner **b** and **c**). The line functions

which define the boundary of the absolute-hexahedral stress block in the xy-plane (see Figure 8.2) are of the form $fy = t\left(1-\frac{x}{l}\right)$, $fx = l\left(1-\frac{y}{t}\right)$.

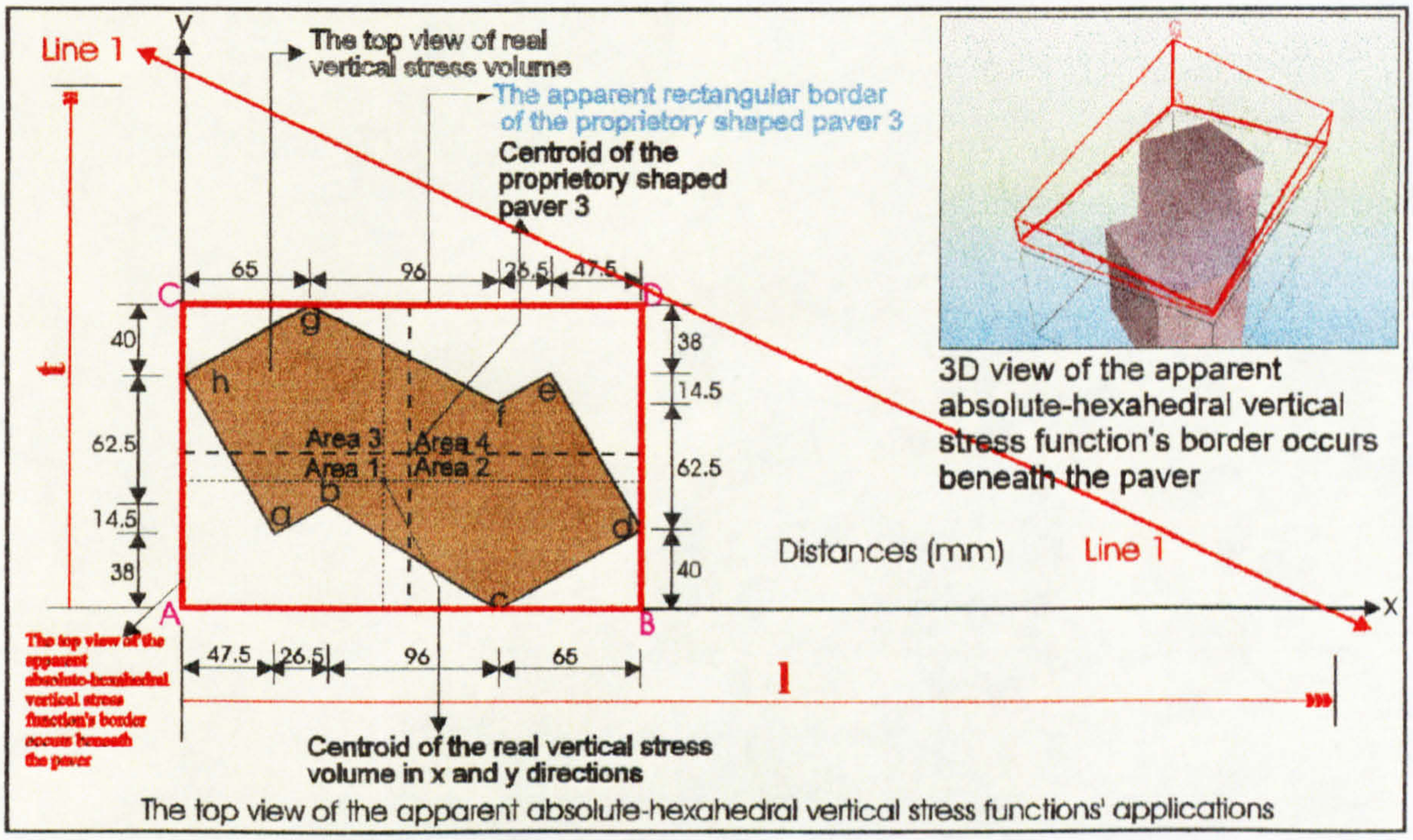

Figure 8.2: The application of the absolute-hexahedral compressive stress distribution beneath the circumscribing rectangular border of proprietory shaped paver 3.

The surface function of the absolute-hexahedral compressive stress block beneath the circumscribing rectangular border shown in Figure 8.2 through the three points σ_A, **l** and **t** is given by:

$$\begin{vmatrix} x & y & z & 1 \\ t & 0 & 0 & 1 \\ 0 & l & 0 & 1 \\ 0 & 0 & \sigma_A & 1 \end{vmatrix} = 0 \Rightarrow f(x,y) = z = \sigma_A\left(1-\frac{x}{t}-\frac{y}{l}\right)$$

The following actual total volume **V** beneath the surface $f(x,y) = z\ (> 0)$ and above the region in the xy-plane (see Figure 8.2) is calculated by subtracting the negative volume generated by the dentations of the shaped paver from the absolute-hexahedral volume beneath circumscribing rectangular boundary of the paver.

$$V = \int_0^{235}\int_0^{155} f(x,y)\,dy\,dx - \int_0^{47.5}\int_{38}^{hay} f(x,y)\,dy\,dx - \int_0^{74}\int_0^{38} f(x,y)\,dy\,dx - \int_{74}^{161}\int_0^{bcy} f(x,y)\,dy\,dx - \int_{170}^{235}\int_0^{cdy} f(x,y)\,dy\,dx$$
$$- \int_{187.5}^{235}\int_{40}^{dey} f(x,y)\,dy\,dx - \int_{161}^{235}\int_{117}^{155} f(x,y)\,dy\,dx - \int_{161}^{187.5}\int_{102.5}^{efy} f(x,y)\,dy\,dx - \int_{65}^{161}\int_{102.5}^{fgy} f(x,y)\,dy\,dx - \int_0^{65}\int_{115}^{ghy} f(x,y)\,dy\,dx$$

and the centroids of this volume in the xy-plane are at distances $\overline{X}$ and $\overline{Y}$ from the axes (see Figure 8.2) which are given by the following equations.

$$\overline{X} = \frac{1}{V}\left[\int_0^{235}\int_0^{155} x f(x,y)\,dy\,dx - \int_0^{47.5}\int_{38}^{hay} x f(x,y)\,dy\,dx - \int_0^{74}\int_0^{38} x f(x,y)\,dy\,dx - \int_{74}^{161}\int_0^{bcy} x f(x,y)\,dy\,dx - \int_{170}^{235}\int_0^{cdy} x f(x,y)\,dy\,dx - \int_{187.5}^{235}\int_{40}^{dey} x f(x,y)\,dy\,dx - \int_{161}^{235}\int_{117}^{155} x f(x,y)\,dy\,dx - \int_{161}^{187.5}\int_{102.5}^{efy} x f(x,y)\,dy\,dx - \int_{65}^{161}\int_{102.5}^{fgy} x f(x,y)\,dy\,dx - \int_0^{65}\int_{115}^{ghy} x f(x,y)\,dy\,dx\right]$$

$$\overline{Y} = \frac{1}{V}\left[\int_0^{155}\int_0^{235} y f(x,y)\,dx\,dy - \int_0^{115}\int_{38}^{hax} y f(x,y)\,dx\,dy - \int_0^{38}\int_0^{74} y f(x,y)\,dx\,dy - \int_0^{52.5}\int_{74}^{bcx} y f(x,y)\,dx\,dy - \int_0^{40}\int_{170}^{cdx} y f(x,y)\,dx\,dy - \int_{40}^{117}\int_{187.5}^{dex} y f(x,y)\,dx\,dy - \int_{117}^{155}\int_{161}^{235} y f(x,y)\,dx\,dy - \int_{102.5}^{155}\int_{161}^{efx} y f(x,y)\,dx\,dy - \int_{102.5}^{155}\int_{65}^{fgx} y f(x,y)\,dx\,dy - \int_{115}^{155}\int_0^{ghx} y f(x,y)\,dx\,dy\right]$$

The $V, \overline{X}$ and $\overline{Y}$ values can analytically be evaluated in terms of l, t and σ_A. The following results which indicate the proportions of the absolute-hexahedral vertical compressive stress block (see Figure 8.2) can be determined by applying vertical and rotational equilibrium between load patch and vertical compressive stress distribution (see Chapter 6). For vertical equilibrium condition the equality between the truncated volume (V) and the total applied patch load (N) must be satisfied and for rotational equilibrium conditions the centroid distances of the load patch ($\overline{X}$, $\overline{Y}$) must be coincided with the centroid distances of the truncated vertical stress block ($\overline{X}$, $\overline{Y}$).

$$l = 1250(-0.1855540422.10^{15} + 0.6044669461.10^{12}\overline{X} + 0.1032919928.10^{13}\overline{Y} + 0.1424415491.10^{10}\overline{XY})(-0.7344198 1.10^{8} + 0.484628\overline{X}) \Big/ ((-0.5543205905.10^{13} + 0.7373610375.10^{10}\overline{X} + 0.5183906455.10^{11}\overline{Y} + 0.46109166.10^{8}\overline{YX})(0.9310745833.10^{10} - 0.605785.10^{9}(-0.1855540422.10^{15} + 0.6044669461.10^{12}\overline{X} + 0.1032919928.10^{13}\overline{Y} + 0.1424415491.10^{10}\overline{YX}) \Big/ (-0.5543205905.10^{13} + 0.7373610375.10^{10}\overline{X} + 0.5183906455.10^{11}\overline{Y} + 0.46109166.10^{8}\overline{YX}) - 0.82722.10^{8}\overline{X} + 0.5.10^{7}(-0.1855540422.10^{15} + 0.6044669461.10^{12}\overline{X} + 0.1032919928.10^{13}\overline{Y} + 0.1424415491.10^{10}\overline{YX})\overline{X} \Big/ (-0.5543205905.10^{13} + 0.7373610375.10^{10}\overline{X} + 0.5183906455.10^{11}\overline{Y} + 0.46109166.10^{8}\overline{YX}))$$

$$t = \frac{5\begin{pmatrix} -0.1855540422.10^{15} + 0.6044669461.10^{12}\overline{X} + 0.1032919928.10^{13}\overline{Y} \\ +0.1424415491.10^{10}\overline{YX} \end{pmatrix}}{\begin{pmatrix} -0.5543205905.10^{13} + 0.7373610375.10^{10}\overline{X} + 0.5183906455.10^{11}\overline{Y} \\ +0.46109166.10^{8}\overline{YX} \end{pmatrix}}$$

$$\sigma_A = \frac{-62500N(-0.7344198 1.10^{8} + 484628\overline{X})\begin{pmatrix} -0.1855540422.10^{15} + 0.6044669461.10^{12}\overline{X} \\ +0.1032919928.10^{13}\overline{Y} + 0.1424415491.10^{10}\overline{YX} \end{pmatrix}}{\begin{pmatrix} -0.1207889122.10^{31} + 0.7970603203.10^{28}\overline{X} - 0.1201590023.10^{28}\overline{Y} \\ +0.7929036736.10^{25}\overline{YX} + 0.6924301845.10^{17}\overline{X}^2 + 0.1385603579.10^{15}\overline{YX}^2 \end{pmatrix}}$$

Therefore, the function of the absolute-hexahedral vertical compressive stress regimes can be determined as follows by inserting the **l**, **t** and σ_A values into $f(x,y) = z = \sigma_A\left(1 - \frac{x}{l} - \frac{y}{t}\right)$.

$$f(x,y) = z = 0.0005N(-0.533007989.10^{25} + 0.7509456425.10^{23}\overline{X} - 0.2634400900.10^{21}\overline{X}^2 - 0.1463134614.10^{23}\overline{Y} + 0.1299564890.10^{21}\overline{YX} - 0.2204479923.10^{18}\overline{YX}^2) \Big/ (-0.1207889122.10^{26} + 0.7970603203.10^{23}\overline{X} - 0.1201590023.10^{23}\overline{Y} + 0.7929036736.10^{20}\overline{YX} + 0.6924301845.10^{12}\overline{X}^2 + 0.1385603579.10^{10}\overline{YX}^2)$$

The stress values beneath the corners of proprietory shaped paver 3 for the absolute-hexahedral vertical compressive stress regimes can now be determined by inserting the corner co-ordinates in the xy-plane into the stress function defined above (see Figure 8.2).

The vertical compressive stress beneath the corner **a** is

$$\sigma_a = -50000N(0.1027909481.10^{18} - 0.1008115815.10^{16}\overline{X} + 0.2176413481.10^{13}\overline{X}^2 - 0.5186086842.10^{15}\overline{Y} + 0.2674350372.10^{13}\overline{YX} + 0.4934823419.10^{10}\overline{YX}^2) \Big/ (-0.1207889122.10^{26} + 0.7970603203.10^{23}\overline{X} - 0.1201590023.10^{23}\overline{Y} + 0.7929036736.10^{20}\overline{YX} + 0.6924301845.10^{12}\overline{X}^2 + 0.1385603579.10^{10}\overline{YX}^2)$$

The vertical compressive stress beneath the corner **b** is

$$\sigma_b = -250000N(0.1438457832.10^{17} - 0.1375830429.10^{15}\overline{X} + 0.2815192540.10^{12}\overline{X}^2 - 0.6853724742.10^{14}\overline{Y} + 0.3538139444.10^{12}\overline{YX} + 0.6596429.10^{9}\overline{YX}^2) \Big/ (-0.1207889122.10^{26} + 0.7970603203.10^{23}\overline{X} - 0.1201590023.10^{23}\overline{Y} + 0.7929036736.10^{20}\overline{YX} + 0.6924301845.10^{12}\overline{X}^2 + 0.1385603579.10^{10}\overline{YX}^2)$$

The vertical compressive stress beneath the corner **c** is

$$\sigma_c = -50000N(0.6699259940.10^{17} - 0.3755020200.10^{15}\overline{X} - 0.4392672970.10^{12}\overline{X}^2 - 0.7050320963.10^{15}\overline{Y} + 0.4196882753.10^{13}\overline{YX} + 0.3005575839.10^{10}\overline{YX}^2) \Big/ (-0.1207889122.10^{26} + 0.7970603203.10^{23}\overline{X} - 0.1201590023.10^{23}\overline{Y} + 0.7929036736.10^{20}\overline{YX} + 0.6924301845.10^{12}\overline{X}^2 + 0.1385603579.10^{10}\overline{YX}^2)$$

The vertical compressive stress beneath the corner **d** is

$$\sigma_d = 50000N(0.1323421108.10^{17} - 0.4456769280.10^{15}\overline{X} + 0.2364656809.10^{13}\overline{X}^2$$
$$+0.2313221581.10^{15}\overline{Y} - 0.1735438061.10^{13}\overline{YX} + 0.1379096217.10^{10}\overline{YX}^2)$$
$$/(-0.1207889122.10^{26} + 0.7970603203.10^{23}\overline{X} - 0.1201590023.10^{23}\overline{Y}$$
$$+0.7929036736.10^{20}\overline{YX} + 0.6924301845.10^{12}\overline{X}^2 + 0.1385603579.10^{10}\overline{YX}^2)$$

The vertical compressive stress beneath the corner **e** is

$$\sigma_e = 50000N(0.6272436030.10^{17} - 0.7028471012.10^{15}\overline{X} + 0.1906669389.10^{13}\overline{X}^2$$
$$-0.4335999875.10^{15}\overline{Y} + 0.2238477200.10^{13}\overline{YX} + 0.4109439713.10^{10}\overline{YX}^2)$$
$$/(-0.1207889122.10^{26} + 0.7970603203.10^{23}\overline{X} - 0.1201590023.10^{23}\overline{Y}$$
$$+0.7929036736.10^{20}\overline{YX} + 0.6924301845.10^{12}\overline{X}^2 + 0.1385603579.10^{10}\overline{YX}^2)$$

The vertical compressive stress beneath the corner **f** is

$$\sigma_f = 50000N(0.3185630371.10^{17} - 0.3826465005.10^{15}\overline{X} + 0.1137852178.10^{13}\overline{X}^2$$
$$-0.2576775406.10^{15}\overline{Y} + 0.1333196552.10^{13}\overline{YX} + 0.2422828439.10^{10}\overline{YX}^2)$$
$$/(-0.1207889122.10^{26} + 0.7970603203.10^{23}\overline{X} - 0.1201590023.10^{23}\overline{Y}$$
$$+0.7929036736.10^{20}\overline{YX} + 0.6924301845.10^{12}\overline{X}^2 + 0.1385603579.10^{10}\overline{YX}^2)$$

The vertical compressive stress beneath the corner **g** is

$$\sigma_g = 50000N(0.2692601150.10^{17} - 0.7023330590.10^{14}\overline{X} - 0.7090113890.10^{12}\overline{X}^2$$
$$-0.6200234002.10^{15}\overline{Y} + 0.3761009582.10^{13}\overline{YX} + 0.2180192133.10^{10}\overline{YX}^2)$$
$$/(-0.1207889122.10^{26} + 0.7970603203.10^{23}\overline{X} - 0.1201590023.10^{23}\overline{Y}$$
$$+0.7929036736.10^{20}\overline{YX} + 0.6924301845.10^{12}\overline{X}^2 + 0.1385603579.10^{10}\overline{YX}^2)$$

The vertical compressive stress beneath the corner **h** is

$$\sigma_h = -50000N(0.5330079890.10^{17} - 0.7509456425.10^{15}\overline{X} + 0.2634400900.10^{13}\overline{X}^2$$
$$+0.1463134614.10^{15}\overline{Y} - 0.1299564890.10^{13}\overline{YX} + 0.2204479923.10^{10}\overline{YX}^2)$$
$$/(-0.1207889122.10^{26} + 0.7970603203.10^{23}\overline{X} - 0.1201590023.10^{23}\overline{Y}$$
$$+0.7929036736.10^{20}\overline{YX} + 0.6924301845.10^{12}\overline{X}^2 + 0.1385603579.10^{10}\overline{YX}^2)$$

8.4. Absolute-hexahedral compressive stress regimes beneath the circumscribing rectangular border for proprietory shaped paver 4

The application of the absolute-hexahedral compressive stress regime beneath the circumscribing rectangular border of proprietory shaped paver 4 shown in Figure 8.3 can be calculated by using the data in Tables 5.7. The first two letters of each boundary line function in Table 5.7 for proprietory shaped paver 4 charecterise the corner names can be seen in Figure 8.3 (example: **bcy** symbolises the boundary line function of proprietory shaped paver 4 in the **y** axis between corner **b** and **c**). The line functions which define the boundary of the absolute-hexahedral stress block in the xy-plane (see Figure 8.3) are of the form $fy = t\left(1-\frac{x}{l}\right)$, $fx = l\left(1-\frac{y}{t}\right)$.

The surface function of the absolute-hexahedral compressive stress block beneath the circumscribing rectangular border shown in Figure 8.3 through the three points σ_A, **l** and **t** is given by:

$$\begin{vmatrix} x & y & z & 1 \\ t & 0 & 0 & 1 \\ 0 & l & 0 & 1 \\ 0 & 0 & \sigma_A & 1 \end{vmatrix} = 0 \Rightarrow f(x,y) = z = \sigma_A\left(1-\frac{x}{t}-\frac{y}{l}\right)$$

The following actual total volume **V** beneath the surface $f(x,y) = z\ (>0)$ and above the region in the xy-plane (see Figure 8.3) is calculated by subtracting the negative volume generated by the dentations of the shaped paver from the absolute-hexahedral volume beneath circumscribing rectangular boundary of the paver.

$$V = \int_{0}^{210}\int_{0}^{100} f(x,y)\,dy\,dx - \int_{0}^{60}\int_{0}^{aby} f(x,y)\,dy\,dx - \int_{60}^{160}\int_{0}^{bcy} f(x,y)\,dy\,dx - \int_{160}^{200}\int_{10}^{cdy} f(x,y)\,dy\,dx - \int_{160}^{200}\int_{0}^{10} f(x,y)\,dy\,dx$$
$$- \int_{200}^{210}\int_{0}^{10} f(x,y)\,dy\,dx - \int_{200}^{210}\int_{10}^{dey} f(x,y)\,dy\,dx - \int_{200}^{210}\int_{50}^{efy} f(x,y)\,dy\,dx - \int_{160}^{210}\int_{90}^{100} f(x,y)\,dy\,dx - \int_{160}^{200}\int_{80}^{fgy} f(x,y)\,dy\,dx$$
$$- \int_{60}^{160}\int_{80}^{ghy} f(x,y)\,dy\,dx - \int_{0}^{60}\int_{90}^{hiy} f(x,y)\,dy\,dx - \int_{0}^{10}\int_{50}^{ijy} f(x,y)\,dy\,dx - \int_{0}^{10}\int_{10}^{jay} f(x,y)\,dy\,dx$$

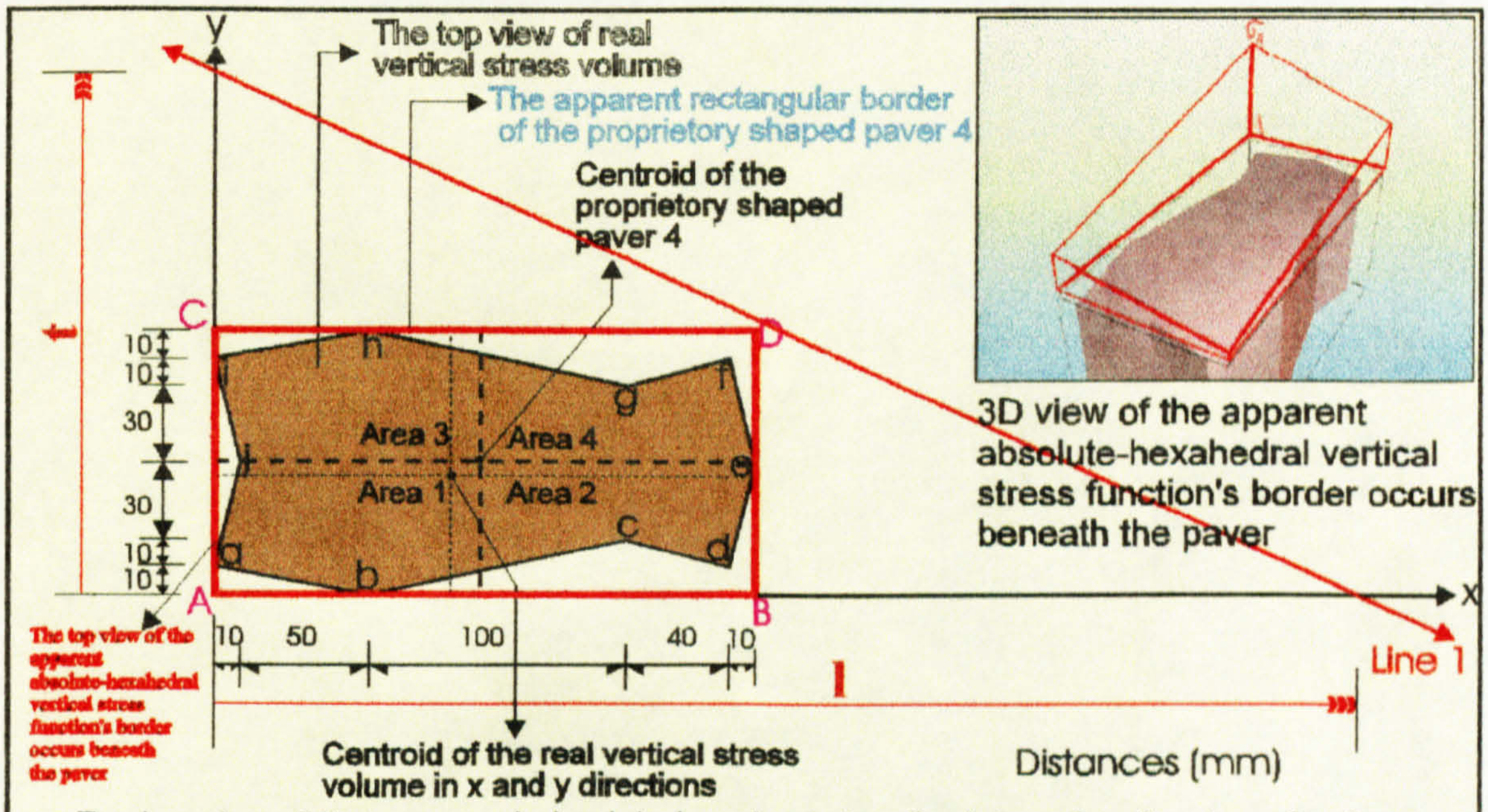

Figure 8.3: The application of the absolute-hexahedral compressive stress distribution beneath the circumscribing rectangular border of proprietory shaped paver 4.

and the centroids of this volume in the xy-plane are at distances $\overline{X}$ and $\overline{Y}$ from the axes (see Figure 8.3) which are given by the following equations.

$$\overline{X} = \frac{1}{V}\left[\int_{0}^{210}\int_{0}^{100} x f(x,y)\,dy\,dx - \int_{0}^{60}\int_{0}^{aby} x f(x,y)\,dy\,dx - \int_{60}^{160}\int_{0}^{bcy} x f(x,y)\,dy\,dx - \int_{160}^{200}\int_{10}^{cdy} x f(x,y)\,dy\,dx\right.$$
$$- \int_{160}^{200}\int_{0}^{10} x f(x,y)\,dy\,dx - \int_{200}^{210}\int_{0}^{10} x f(x,y)\,dy\,dx - \int_{200}^{210}\int_{10}^{dey} x f(x,y)\,dy\,dx - \int_{200}^{210}\int_{50}^{efy} x f(x,y)\,dy\,dx$$
$$\left. - \int_{160}^{210}\int_{90}^{100} x f(x,y)\,dy\,dx - \int_{160}^{200}\int_{80}^{fgy} x f(x,y)\,dy\,dx - \int_{60}^{160}\int_{80}^{ghy} x f(x,y)\,dy\,dx - \int_{0}^{60}\int_{90}^{hiy} x f(x,y)\,dy\,dx\right]$$

$$-\int_{0}^{10}\int_{50}^{ijy} x f(x,y)\,dy\,dx - \int_{0}^{10}\int_{10}^{jay} x f(x,y)\,dy\,dx\Bigg]$$

$$\bar{Y} = \frac{1}{V}\left[\begin{array}{l}
\int_{0}^{100}\int_{0}^{210} y f(x,y)\,dx\,dy - \int_{0}^{10}\int_{0}^{abx} y f(x,y)\,dx\,dy - \int_{0}^{20}\int_{60}^{bcx} y f(x,y)\,dx\,dy - \int_{10}^{20}\int_{60}^{cdx} y f(x,y)\,dx\,dy \\
-\int_{0}^{10}\int_{160}^{200} y f(x,y)\,dx\,dy - \int_{0}^{10}\int_{200}^{210} y f(x,y)\,dx\,dy - \int_{10}^{50}\int_{200}^{dex} y f(x,y)\,dx\,dy - \int_{50}^{90}\int_{200}^{efx} y f(x,y)\,dx\,dy \\
-\int_{90}^{100}\int_{160}^{210} y f(x,y)\,dx\,dy - \int_{80}^{90}\int_{160}^{fgx} y f(x,y)\,dx\,dy - \int_{80}^{100}\int_{60}^{ghx} y f(x,y)\,dx\,dy - \int_{90}^{100}\int_{0}^{hix} y f(x,y)\,dx\,dy \\
-\int_{50}^{90}\int_{0}^{ijx} y f(x,y)\,dx\,dy - \int_{10}^{50}\int_{0}^{jax} y f(x,y)\,dx\,dy
\end{array}\right]$$

The $V, \overline{X}$ and $\overline{Y}$ values can analytically be evaluated in terms of l, t and σ_A. The following results which indicate the proportions of the absolute-hexahedral vertical compressive stress block (see Figure 8.3) can be determined by applying vertical and rotational equilibrium between load patch and vertical compressive stress distribution (see Chapter 6). For vertical equilibrium condition the equality between the truncated volume (V) and the total applied patch load (N) must be satisfied and for rotational equilibrium conditions the centroid distances of the load patch ($\overline{X}$, $\overline{Y}$) must be coincided with the centroid distances of the truncated vertical stress block ($\overline{X}$, $\overline{Y}$).

$$l = \frac{50185t\left(-133973 + 1000\overline{X}\right)}{0.25845576 13.10^{10} - 0.50185000.10^{8} t - 0.25421800.10^{8}\overline{X} + 500000\overline{X}t}$$

$$t = \frac{0.05\left(\begin{array}{l} -0.7920623795.10^{13} + 0.2753687945.10^{11}\overline{X} + 0.6984601100.10^{11}\overline{Y} \\ +0.110339381.10^{9}\overline{YX} \end{array}\right)}{\left(-0.3880304200.10^{10} - 0.3343750.10^{7}\overline{X} + 0.77606084.10^{8}\overline{Y} + 66875\overline{YX}\right)}$$

$$\sigma_A = \frac{-0.1.10^8 N(-133973+1000\overline{X})\begin{pmatrix}-0.7920623795.10^{13}+0.2753687945.10^{11}\overline{X}\\+0.6984601100.10^{11}\overline{Y}+0.110339381.10^{9}\overline{YX}\end{pmatrix}}{\begin{pmatrix}-0.2218734814.10^{29}+0.1464907843.10^{27}\overline{X}+0.1427139043.10^{24}\overline{X}^2\\+0.1007861518.10^{21}\overline{Y}-0.1318078007.10^{19}\overline{YX}+0.4217437635.10^{16}\overline{YX}^2\end{pmatrix}}$$

Therefore, the function of the absolute-hexahedral vertical compressive stress regimes can be determined as follows by inserting the **l**, **t** and σ_A values into $f(x,y) = z = \sigma_A\left(1-\frac{x}{l}-\frac{y}{t}\right)$.

$$f(x,y) = z = 0.4.10^{-12} N(-0.5305748658.10^{31}+0.5804911073.10^{29}\overline{X}$$
$$-0.1376843973.10^{27}\overline{X}^2+0.4678739816.10^{29}\overline{Y}-0.2753175655.10^{27}\overline{YX}$$
$$-0.5516969050.10^{24}\overline{YX}^2+0.196193195 1.10^{29}x-0.3529148288.10^{27}x\overline{X}$$
$$+0.5044593427.10^{26}x\overline{Y}-0.6590871229.10^{24}x\overline{YX}+0.1541150005.10^{25}x\overline{X}^2$$
$$+0.2109.10^{22}x\overline{YX}^2+0.5198559946.10^{29}y-0.3432331981.10^{27}y\overline{X}$$
$$-0.334375.10^{24}y\overline{X}^2-0.1039711989.10^{28}y\overline{Y}+0.6864663963.10^{25}y\overline{YX}$$
$$+0.66875.10^{22}y\overline{YX}^2)\Big/(-0.4437469628.10^{22}+0.2929815686.10^{20}\overline{X}$$
$$+0.2854278086.10^{17}\overline{X}^2+0.2015723036.10^{14}\overline{Y}-0.2636156014.10^{12}\overline{YX}$$
$$+0.843487527.10^{9}\overline{YX}^2)$$

The stress values beneath the corners of proprietory shaped paver 4 for the absolute-hexahedral vertical compressive stress regimes can now be determined by inserting the corner co-ordinates in the xy-plane into the stress function defined above (see Figure 8.3).

The vertical compressive stress beneath the corner **a** is

$$\sigma_a = -2000N(0.9571785326.10^{15}-0.1092335575.10^{14}\overline{X}+0.2820562946.10^{11}\overline{X}^2$$
$$-0.7278055654.10^{13}\overline{Y}-0.4133418518.10^{11}\overline{YX}+0.96964381.10^{8}\overline{YX}^2)$$

$$/\,(-0.4437469628.10^{22}+0.2929815686.10^{20}\overline{X}+0.2854278086.10^{17}\overline{X}^2$$

$$+0.2015723036.10^{14}\overline{Y}-0.2636156014.10^{12}\overline{YX}+0.843487527.10^{9}\overline{YX}^2)$$

The vertical compressive stress beneath the corner **b** is

$$\sigma_b=-2000N(0.8257178974.10^{15}-0.7374844200.10^{13}\overline{X}+0.9043079400.10^{10}\overline{X}^2$$
$$-0.9962830844.10^{13}\overline{Y}+0.6297255858.10^{11}\overline{YX}+0.8503138 1.10^{8}\overline{YX}^2)$$
$$/\,(-0.4437469628.10^{22}+0.2929815686.10^{20}\overline{X}+0.2854278086.10^{17}\overline{X}^2$$
$$+0.2015723036.10^{14}\overline{Y}-0.2636156014.10^{12}\overline{YX}+0.843487527.10^{9}\overline{YX}^2)$$

The vertical compressive stress beneath the corner **c** is

$$\sigma_c=-2000N(0.2253891094.10^{15}+0.1056385168.10^{13}\overline{X}-0.2044242070.10^{11}\overline{X}^2$$
$$-0.6812901572.10^{13}\overline{Y}+0.4869564518.10^{11}\overline{YX}+0.16101381.10^{8}\overline{YX}^2)$$
$$/\,(-0.4437469628.10^{22}+0.2929815686.10^{20}\overline{X}+0.2854278086.10^{17}\overline{X}^2$$
$$+0.2015723036.10^{14}\overline{Y}-0.2636156014.10^{12}\overline{YX}+0.843487527.10^{9}\overline{YX}^2)$$

The vertical compressive stress beneath the corner **d** is

$$\sigma_d=-2000N(0.1724057523.10^{15}+0.3193237402.10^{13}\overline{X}-0.3344037074.10^{11}\overline{X}^2$$
$$-0.9295893024.10^{13}\overline{Y}+0.6769767010.10^{11}\overline{YX}+0.12604381.10^{8}\overline{YX}^2)$$
$$/\,(-0.4437469628.10^{22}+0.2929815686.10^{20}\overline{X}+0.2854278086.10^{17}\overline{X}^2$$
$$+0.2015723036.10^{14}\overline{Y}-0.2636156014.10^{12}\overline{YX}+0.843487527.10^{9}\overline{YX}^2)$$

The vertical compressive stress beneath the corner **e** is

$$\sigma_e=2000N(0.2827176824.10^{15}-0.6644932646.10^{13}\overline{X}+0.3384767076.10^{11}\overline{X}^2$$

$$+0.1079088982.10^{13}\overline{Y}-0.1409853262.10^{11}\overline{YX}+0.45113619.10^{8}\overline{YX}^{2})$$

$$/\,(-0.4437469628.10^{22}+0.2929815686.10^{20}\overline{X}+0.2854278086.10^{17}\overline{X}^{2}$$

$$+0.2015723036.10^{14}\overline{Y}-0.2636156014.10^{12}\overline{YX}+0.843487527.10^{9}\overline{YX}^{2})$$

The vertical compressive stress beneath the corner **f** is

$$\sigma_f = 2000N(0.6593638390.10^{15}-0.8684968572.10^{13}\overline{X}+0.2809037074.10^{11}\overline{X}^{2}$$

$$-0.7339498800.10^{13}\overline{Y}+0.4213695332.10^{11}\overline{YX}+0.943956191.10^{8}\overline{YX}^{2})$$

$$/\,(-0.4437469628.10^{22}+0.2929815686.10^{20}\overline{X}+0.2854278086.10^{17}\overline{X}^{2}$$

$$+0.2015723036.10^{14}\overline{Y}-0.2636156014.10^{12}\overline{YX}+0.843487527.10^{9}\overline{YX}^{2})$$

The vertical compressive stress beneath the corner **g** is

$$\sigma_g = 2000N(0.3984380842.10^{15}-0.5175183546.10^{13}\overline{X}+0.1642992070.10^{11}\overline{X}^{2}$$

$$-0.5663642296.10^{13}\overline{Y}+0.3368032236.10^{11}\overline{YX}+0.64148619.10^{8}\overline{YX}^{2})$$

$$/\,(-0.4437469628.10^{22}+0.2929815686.10^{20}\overline{X}+0.2854278086.10^{17}\overline{X}^{2}$$

$$+0.2015723036.10^{14}\overline{Y}-0.2636156014.10^{12}\overline{YX}+0.843487527.10^{9}\overline{YX}^{2})$$

The vertical compressive stress beneath the corner **h** is

$$\sigma_h = 2000N(0.2139940918.10^{15}+0.5101802380.10^{12}\overline{X}-0.1573057940.10^{11}\overline{X}^{2}$$

$$-0.1083140894.10^{14}\overline{Y}+0.7432072068.10^{11}\overline{YX}+0.48718619.10^{8}\overline{YX}^{2})$$

$$/\,(-0.4437469628.10^{22}+0.2929815686.10^{20}\overline{X}+0.2854278086.10^{17}\overline{X}^{2}$$

$$+0.2015723036.10^{14}\overline{Y}-0.2636156014.10^{12}\overline{YX}+0.843487527.10^{9}\overline{YX}^{2})$$

The vertical compressive stress beneath the corner **i** is

$$\sigma_i = 2000N(0.1254089414.10^{15} + 0.5431624580.10^{13}\overline{X} - 0.3355562946.10^{11}\overline{X}^2$$
$$-0.9357336170.10^{13}\overline{Y} + 0.6850043824.10^{11}\overline{YX} + 0.10035619.10^{8}\overline{YX}^2)$$
$$/\,(-0.4437469628.10^{22} + 0.2929815686.10^{20}\overline{X} + 0.2854278086.10^{17}\overline{X}^2$$
$$+0.2015723036.10^{14}\overline{Y} - 0.2636156014.10^{12}\overline{YX} + 0.843487527.10^{9}\overline{YX}^2)$$

The vertical compressive stress beneath the corner **j** is

$$\sigma_j = -2000N(0.5020550980.10^{15} - 0.7471660506.10^{13}\overline{X} + 0.2779832946.10^{11}\overline{X}^2$$
$$+0.9387483894.10^{12}\overline{Y} - 0.1226495229.10^{11}\overline{YX} + 0.3924638 1.10^{8}\overline{YX}^2)$$
$$/\,(-0.4437469628.10^{22} + 0.2929815686.10^{20}\overline{X} + 0.2854278086.10^{17}\overline{X}^2$$
$$+0.2015723036.10^{14}\overline{Y} - 0.2636156014.10^{12}\overline{YX} + 0.843487527.10^{9}\overline{YX}^2)$$

8.5. Absolute-hexahedral compressive stress regimes beneath the circumscribing rectangular border for proprietory shaped paver 5

The application of the absolute-hexahedral compressive stress regime beneath the circumscribing rectangular border of proprietory shaped paver 5 shown in Figure 8.4 can be calculated by using the data in Tables 5.9. The first two letters of each boundary line function in Table 5.9 for proprietory shaped paver 5 charecterise the corner names can be seen in Figure 8.4 (example: **bcy** symbolises the boundary line function of proprietory shaped paver 5 in the **y** axis between corner **b** and **c**). The line functions which define the boundary of the absolute-hexahedral stress block in the xy-plane (see Figure 8.4) are of the form $fy = t\left(1-\frac{x}{l}\right)$, $fx = l\left(1-\frac{y}{t}\right)$.

The surface function of the absolute-hexahedral compressive stress block beneath the circumscribing rectangular border shown in Figure 8.4 through the three points σ_A, **l** and **t** is given by:

$$\begin{vmatrix} x & y & z & 1 \\ t & 0 & 0 & 1 \\ 0 & l & 0 & 1 \\ 0 & 0 & \sigma_A & 1 \end{vmatrix} = 0 \Rightarrow f(x,y) = z = \sigma_A\left(1 - \frac{x}{t} - \frac{y}{l}\right)$$

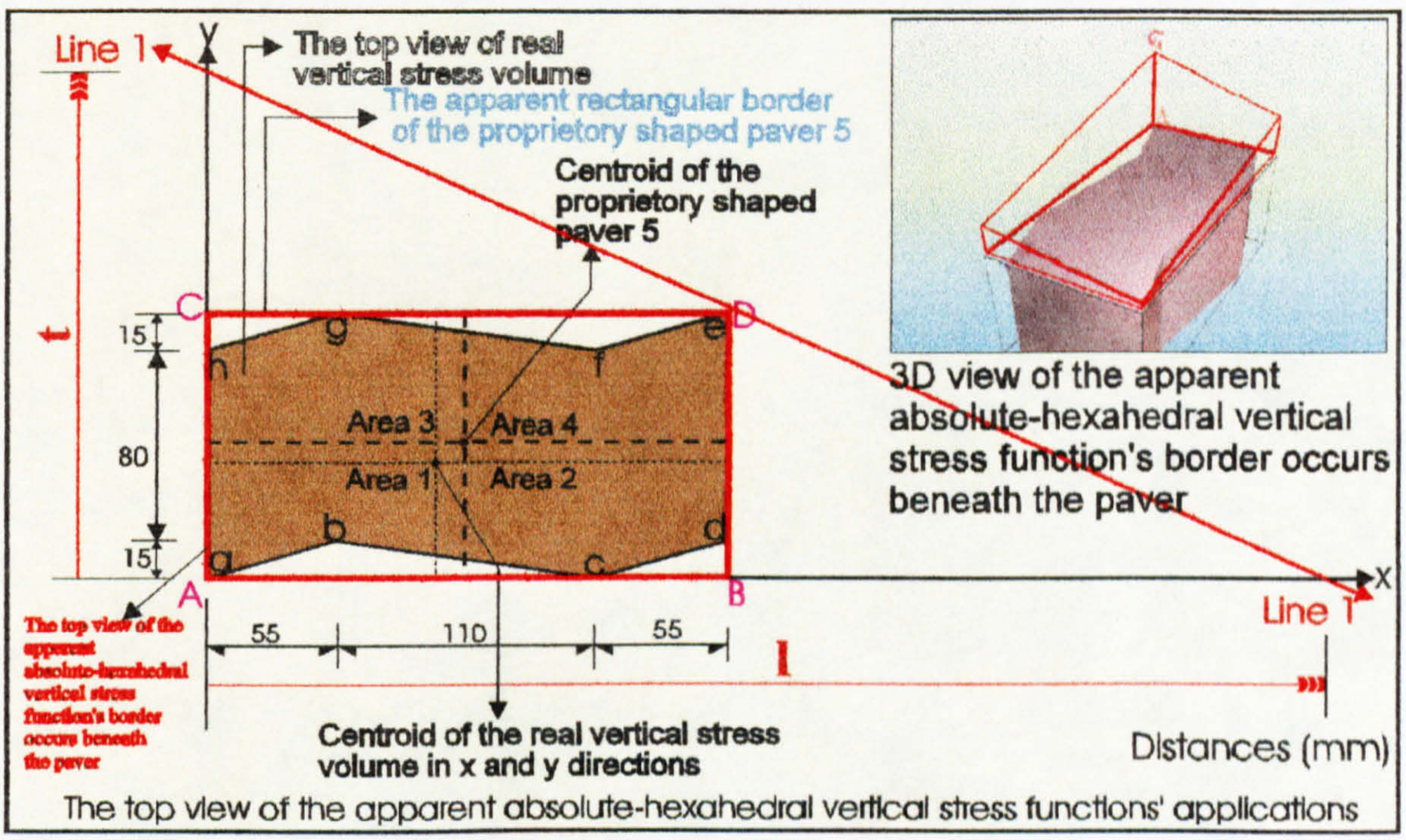

Figure 8.4: The application of the absolute-hexahedral compressive stress distribution beneath the circumscribing rectangular border of proprietory shaped paver 5.

The following actual total volume **V** beneath the surface $f(x,y) = z\ (> 0)$ and above the region in the xy-plane (see Figure 8.4) is calculated by subtracting the negative volume generated by the dentations of the shaped paver from the absolute-hexahedral volume beneath circumscribing rectangular boundary of the paver.

$$V = \int_0^{220}\int_0^{110} f(x,y)\,dy\,dx - \int_0^{55}\int_0^{aby} f(x,y)\,dy\,dx - \int_{55}^{165}\int_0^{bcy} f(x,y)\,dy\,dx - \int_{165}^{220}\int_0^{cdy} f(x,y)\,dy\,dx - \int_{165}^{220}\int_{95}^{efy} f(x,y)\,dy\,dx - \int_{55}^{165}\int_{95}^{fgy} f(x,y)\,dy\,dx$$

and the centroids of this volume in the xy-plane are at distances $\overline{X}$ and $\overline{Y}$ from the axes (see Figure 8.4) which are given by the following equations.

$$\overline{X} = \frac{1}{V}\left[\int_0^{220}\int_0^{110} x f(x,y)\,dy\,dx - \int_0^{55}\int_0^{aby} x f(x,y)\,dy\,dx - \int_{55}^{165}\int_0^{bcy} x f(x,y)\,dy\,dx - \int_{165}^{220}\int_0^{cdy} x f(x,y)\,dy\,dx - \int_{165}^{220}\int_{95}^{efy} x f(x,y)\,dy\,dx - \int_{55}^{165}\int_{95}^{fgy} x f(x,y)\,dy\,dx\right]$$

$$\overline{Y} = \frac{1}{V}\left[\int_0^{110}\int_0^{220} y\, f(x,y)\,dx\,dy - \int_0^{15}\int_0^{abx} y\, f(x,y)\,dx\,dy - \int_0^{15}\int_{55}^{bcx} y\, f(x,y)\,dx\,dy - \int_0^{15}\int_{165}^{cdx} y\, f(x,y)\,dx\,dy - \int_{95}^{110}\int_{165}^{efx} y\, f(x,y)\,dx\,dy - \int_{95}^{110}\int_{55}^{fgx} y\, f(x,y)\,dx\,dy\right]$$

The $V, \overline{X}$ and $\overline{Y}$ values can analytically be evaluated in terms of l, t and σ_A. The following results which indicate the proportions of the absolute-hexahedral vertical compressive stress block (see Figure 8.4) can be determined by applying vertical and rotational equilibrium between load patch and vertical compressive stress distribution (see Chapter 6). For vertical equilibrium condition the equality between the truncated volume (V) and the total applied patch load (N) must be satisfied and for rotational equilibrium conditions the centroid distances of the load patch ($\overline{X}$, $\overline{Y}$) must be coincided with the centroid distances of the truncated vertical stress block ($\overline{X}$, $\overline{Y}$).

$$l = 52.5(15818\overline{X} - 0.2327587.10^{7})(0.941915451.10^{9}\overline{XY} + 0.6286380310.10^{12}\overline{X} + 0.1582393543.10^{13}\overline{Y} - 0.1871575247.10^{15}) \Big/ (-0.6428037852.10^{15}\overline{XY} + 0.2499772043.10^{13}\overline{X}^{2}\overline{Y} - 0.1280759908.10^{19}\overline{X} + 0.4966222642.10^{16}\overline{X}^{2} + 0.4046089285.10^{17}\overline{Y} + 0.8092995561.10^{20})$$

$$t = 1.5(0.941915451.10^{9}\overline{XY} + 0.6286380310.10^{12}\overline{X} + 0.1582393543.10^{13}\overline{Y} - 0.1871575247.10^{15}) \Big/ (0.4417000085.10^{11}\overline{Y} + 0.1648022 5.10^{8}\overline{XY} - 0.2429145642.10^{13} - 0.907801488.10^{9}\overline{X})$$

$$\sigma_A = -105N(15818\overline{X} - 0.2327587.10^{7})(0.941915451.10^{9}\overline{XY} + 0.6286380310.10^{12}\overline{X}$$

$$+0.1582393543.10^{13}\overline{Y} - 0.1871575247.10^{15}) \Big/ (0.4212997008.10^{21}\overline{XY}$$
$$+0.6072454491.10^{12}\overline{X}^2\overline{Y} + 0.8372042509.10^{24}\overline{X} - 0.3961850825.10^{15}\overline{X}^2$$
$$-0.6199341981.10^{23}\overline{Y} - 0.1231929188.10^{27})$$

Therefore, the function of the absolute-hexahedral vertical compressive stress regimes can be determined as follows by inserting the **l**, **t** and σ_A values into $f(x,y) = z = \sigma_A\left(1 - \frac{x}{l} - \frac{y}{t}\right)$.

$$f(x,y) = z = 0.105.10^{-9}N(-0.1489921860.10^{24}\overline{X}^2\overline{Y} - 0.9943796374.10^{26}\overline{X}^2$$
$$-0.2283791090.10^{27}\overline{XY} + 0.4423667434.10^{29}\overline{X} + 0.3683158640.10^{29}\overline{Y}$$
$$-0.4356254214.10^{31} - 0.1224388162.10^{24}x\overline{XY} + 0.4761470559.10^{21}\overline{X}^2\overline{Y}$$
$$-0.2439542682.10^{27}x\overline{X} + 0.9459471700.10^{24}x\overline{X}^2 + 0.7706836734.10^{25}x\overline{Y}$$
$$+0.1541522964.10^{29}x + 0.4402146107.10^{25}y\overline{XY} + 0.1737894660.10^{22}y\overline{X}^2\overline{Y}$$
$$-0.2420749255.10^{27}y\overline{X} - 0.9573069292.10^{23}y\overline{X}^2 - 0.6853967985.10^{27}y\overline{Y}$$
$$+0.3769365212.10^{29}y) \Big/ (0.4212997008.10^{19}\overline{XY} + 0.6072454491.10^{10}\overline{X}^2\overline{Y}$$
$$+0.8372042509.10^{22}\overline{X} - 0.3961850825.10^{13}\overline{X}^2 - 0.6199341981.10^{21}\overline{Y}$$
$$-0.1231929188.10^{25})$$

The stress values beneath the corners of proprietory shaped paver 5 for the absolute-hexahedral vertical compressive stress regimes can now be determined by inserting the corner co-ordinates in the xy-plane into the stress function defined above (see Figure 8.4).

The vertical compressive stress beneath the corner a is

$$\sigma_a = -210000N(0.74496093.10^{8}\overline{X}^2\overline{Y} + 0.4971898187.10^{11}\overline{X}^2$$
$$+0.1141895545.10^{12}\overline{XY} - 0.2211833717.10^{14}\overline{X} - 0.1841579320.10^{14}\overline{Y}$$
$$+0.2178127107.10^{16}) \Big/ (0.4212997008.10^{19}\overline{XY} + 0.6072454491.10^{10}\overline{X}^2\overline{Y}$$

$$+0.8372042509.10^{22}\overline{X}-0.3961850825.10^{13}\overline{X}^2-0.6199341981.10^{21}\overline{Y}$$
$$-0.1231929188.10^{25})$$

The vertical compressive stress beneath the corner **b** is

$$\sigma_b=-1050N(0.9673567803.10^{10}\overline{X}^2\overline{Y}+0.4884682975.10^{13}\overline{X}^2$$
$$+0.1690810523.10^{14}\overline{XY}-0.2718806571.10^{16}\overline{X}-0.2697451044.10^{16}\overline{Y}$$
$$+0.2943011802.10^{18})\Big/(0.4212997008.10^{19}\overline{XY}+0.6072454491.10^{10}\overline{X}^2\overline{Y}$$
$$+0.8372042509.10^{22}\overline{X}-0.3961850825.10^{13}\overline{X}^2-0.6199341981.10^{21}\overline{Y}$$
$$-0.1231929188.10^{25})$$

The vertical compressive stress beneath the corner **c** is

$$\sigma_c=-2100N(0.3521396089.10^{10}\overline{X}^2\overline{Y}-0.2832165968.10^{13}\overline{X}^2$$
$$+0.1242907569.10^{14}\overline{XY}-0.1992110045.10^{15}\overline{X}-0.1905160723.10^{16}\overline{Y}$$
$$+0.9063706615.10^{17})\Big/(0.4212997008.10^{19}\overline{XY}+0.6072454491.10^{10}\overline{X}^2\overline{Y}$$
$$+0.8372042509.10^{22}\overline{X}-0.3961850825.10^{13}\overline{X}^2-0.6199341981.10^{21}\overline{Y}$$
$$-0.1231929188.10^{25})$$

The vertical compressive stress beneath the corner **d** is

$$\sigma_d=-10500N(0.442398337.10^{9}\overline{X}^2\overline{Y}-0.1086704137.10^{13}\overline{X}^2$$
$$+0.2553156486.10^{13}\overline{XY}+0.9433264660.10^{14}\overline{X}-0.3852709048.10^{15}\overline{Y}$$
$$+0.9649036930.10^{16})\Big/(0.4212997008.10^{19}\overline{XY}+0.6072454491.10^{10}\overline{X}^2\overline{Y}$$
$$+0.8372042509.10^{22}\overline{X}-0.3961850825.10^{13}\overline{X}^2-0.6199341981.10^{21}\overline{Y}$$
$$-0.1231929188.10^{25})$$

The vertical compressive stress beneath the corner **e** is

$$\sigma_e = 10500N(0.1469285789.10^{10}\overline{X}^2\overline{Y} + 0.9814003740.10^{12}\overline{X}^2 + 0.2289204232.10^{13}\overline{XY} - 0.3606150647.10^{15}\overline{X} - 0.3686655736.10^{15}\overline{Y} + 0.3181398040.10^{17}) \Big/ (0.4212997008.10^{19}\overline{XY} + 0.6072454491.10^{10}\overline{X}^2\overline{Y} + 0.8372042509.10^{22}\overline{X} - 0.3961850825.10^{13}\overline{X}^2 - 0.6199341981.10^{21}\overline{Y} - 0.1231929188.10^{25})$$

The vertical compressive stress beneath the corner f is

$$\sigma_f = 4200N(0.2366801773.10^{10}\overline{X}^2\overline{Y} + 0.1188722588.10^{13}\overline{X}^2 + 0.4240559163.10^{13}\overline{XY} - 0.4753224458.10^{15}\overline{X} - 0.6752370350.10^{15}\overline{Y} + 0.4420389070.10^{17}) \Big/ (0.4212997008.10^{19}\overline{XY} + 0.6072454491.10^{10}\overline{X}^2\overline{Y} + 0.8372042509.10^{22}\overline{X} - 0.3961850825.10^{13}\overline{X}^2 - 0.6199341981.10^{21}\overline{Y} - 0.1231929188.10^{25})$$

The vertical compressive stress beneath the corner g is

$$\sigma_g = 1050N(0.6836431467.10^{10}\overline{X}^2\overline{Y} - 0.5794124565.10^{13}\overline{X}^2 + 0.2491228279.10^{14}\overline{XY} + 0.4190947780.10^{15}\overline{X} - 0.3813818542.10^{16}\overline{Y} + 0.6378851490.10^{17}) \Big/ (0.4212997008.10^{19}\overline{XY} + 0.6072454491.10^{10}\overline{X}^2\overline{Y} + 0.8372042509.10^{22}\overline{X} - 0.3961850825.10^{13}\overline{X}^2 - 0.6199341981.10^{21}\overline{Y} - 0.1231929188.10^{25})$$

The vertical compressive stress beneath the corner h is

$$\sigma_h = 10500N(0.161078067.10^{9}\overline{X}^2\overline{Y} - 0.1085323796.10^{13}\overline{X}^2 + 0.1898247712.10^{13}\overline{XY} + 0.2123955642.10^{15}\overline{X} - 0.2828110946.10^{15}\overline{Y} - 0.7753572630.10^{16}) \Big/ (0.4212997008.10^{19}\overline{XY} + 0.6072454491.10^{10}\overline{X}^2\overline{Y} + 0.8372042509.10^{22}\overline{X} - 0.3961850825.10^{13}\overline{X}^2 - 0.6199341981.10^{21}\overline{Y} - 0.1231929188.10^{25})$$

8.6. Absolute-hexahedral compressive stress regimes beneath the circumscribing rectangular border for proprietory shaped paver 6

The application of the absolute-hexahedral compressive stress regime beneath the circumscribing rectangular border of proprietory shaped paver 6 shown in Figure 8.5 can be calculated by using the data in Tables 5.11. The first two letters of each boundary line function in Table 5.11 for proprietory shaped paver 6 charecterise the corner names can be seen in Figure 8.5 (example: **bcy** symbolises the boundary line function of proprietory shaped paver 6 in the **y** axis between corner **b** and **c**). The line functions which define the boundary of the absolute-hexahedral stress block in the xy-plane (see Figure 8.5) are of the form $fy = t\left(1-\frac{x}{l}\right)$, $fx = t\left(1-\frac{y}{t}\right)$.

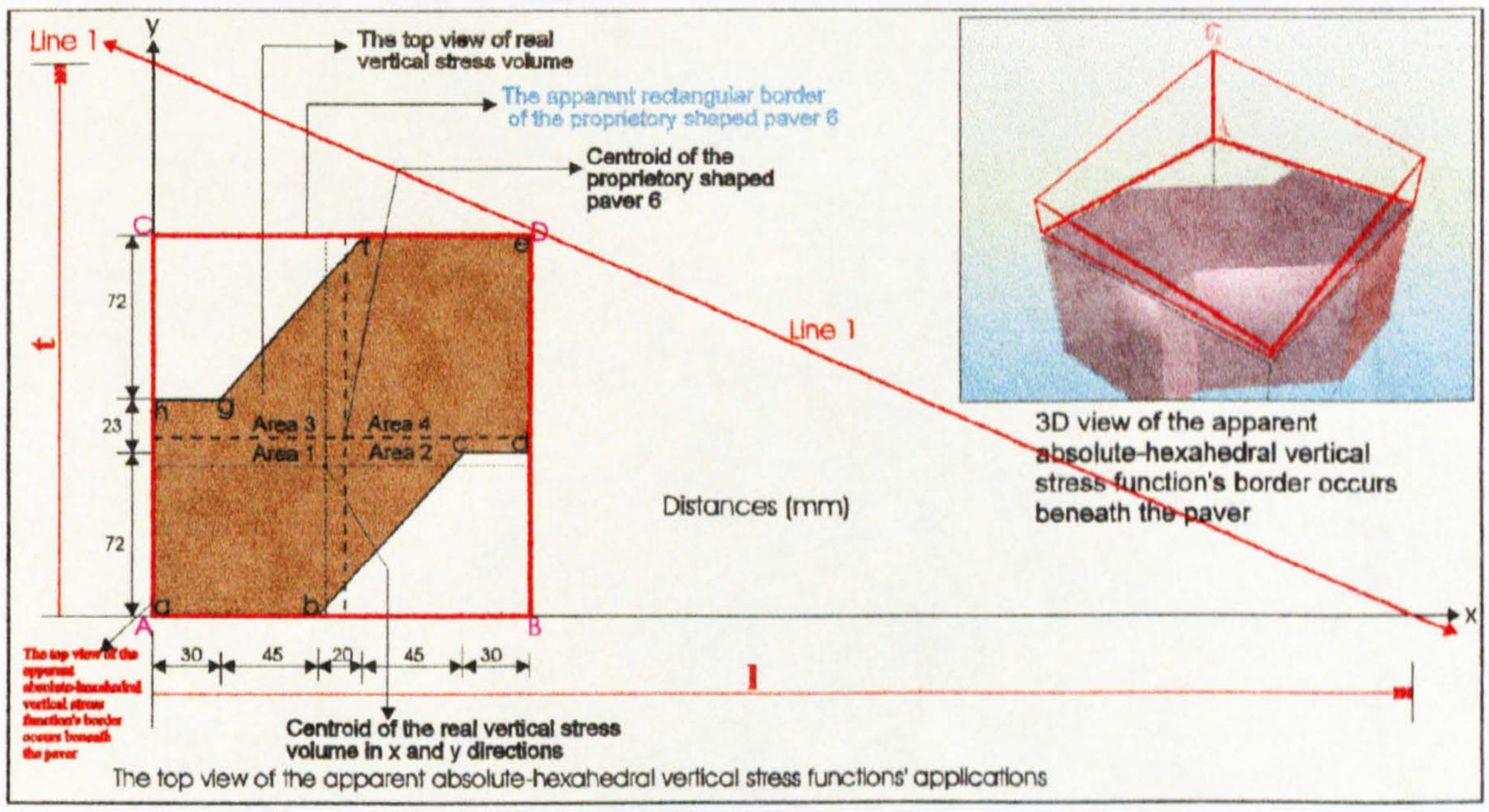

Figure 8.5: The application of the absolute-hexahedral compressive stress distribution beneath the circumscribing rectangular border of proprietory shaped paver 6.

The surface function of the absolute-hexahedral compressive stress block beneath the circumscribing rectangular border shown in Figure 8.5 through the three points σ_A, **l** and **t** is given by:

$$\begin{vmatrix} x & y & z & 1 \\ t & 0 & 0 & 1 \\ 0 & l & 0 & 1 \\ 0 & 0 & \sigma_A & 1 \end{vmatrix} = 0 \Rightarrow f(x,y) = z = \sigma_A\left(1 - \frac{x}{t} - \frac{y}{l}\right)$$

The following actual total volume **V** beneath the surface $f(x,y) = z\ (> 0)$ and above the region in the xy-plane (see Figure 8.5) is calculated by subtracting the negative volume generated by the dentations of the shaped paver from the absolute-hexahedral volume beneath circumscribing rectangular boundary of the paver.

$$V = \int_0^{170}\int_0^{167} f(x,y)\,dy\,dx - \int_{75}^{140}\int_0^{bcy} f(x,y)\,dy\,dx - \int_{140}^{170}\int_0^{72} f(x,y)\,dy\,dx - \int_{30}^{95}\int_0^{fgv} f(x,y)\,dy\,dx - \int_0^{30}\int_{95}^{167} f(x,y)\,dy\,dx$$

and the centroids of this volume in the xy-plane are at distances $\overline{X}$ and $\overline{Y}$ from the axes (see Figure 8.5) which are given by the following equations.

$$\overline{X} = \frac{1}{V}\left[\int_0^{170}\int_0^{167} x f(x,y)\,dy\,dx - \int_{75}^{140}\int_0^{bcy} x f(x,y)\,dy\,dx - \int_{140}^{170}\int_0^{72} x f(x,y)\,dy\,dx - \int_{30}^{95}\int_{95}^{fgy} x f(x,y)\,dy\,dx - \int_0^{30}\int_{95}^{167} x f(x,y)\,dy\,dx\right]$$

$$\overline{Y} = \frac{1}{V}\left[\int_0^{167}\int_0^{170} y f(x,y)\,dx\,dy - \int_0^{72}\int_{75}^{bcx} y f(x,y)\,dx\,dy - \int_0^{72}\int_{140}^{170} y f(x,y)\,dx\,dy - \int_{95}^{167}\int_{30}^{fgx} y f(x,y)\,dx\,dy - \int_{95}^{167}\int_0^{30} y f(x,y)\,dx\,dy\right]$$

The $V, \overline{X}$ and $\overline{Y}$ values can analytically be evaluated in terms of l, t and σ_A. The following results which indicate the proportions of the absolute-hexahedral vertical compressive stress block (see Figure 8.5) can be determined by applying vertical and rotational equilibrium between load patch and vertical compressive stress distribution (see Chapter 6). For vertical equilibrium condition the equality between the truncated

volume (V) and the total applied patch load (N) must be satisfied and for rotational equilibrium conditions the centroid distances of the load patch ($\overline{X}$, $\overline{Y}$) must be coincided with the centroid distances of the truncated vertical stress block ($\overline{\overline{X}}$, $\overline{\overline{Y}}$).

$$l=\left(\frac{5215}{3}\right)\left(\frac{-315784067125+390004905\overline{X}+335419410\overline{Y}+24112296\overline{XY}}{75784839745\overline{X}+2613461760\overline{XY}-2583993225145-66932974620\overline{Y}}\right)$$

$$t=\left(\frac{1043}{6}\right)\left(\frac{-315784067125+390004905\overline{X}+335419410\overline{Y}+24112296\overline{XY}}{-270693930865-6441933258\overline{X}+7998875530\overline{Y}+23593752\overline{Y}\,\overline{X}}\right)$$

$$\sigma_A=(-0.02)N\left(\frac{-315784067125+390004905\overline{X}+335419410\overline{Y}+24112296\overline{XY}}{22796259150449+181453583376\overline{Y}}\right)$$

Therefore, the function of the absolute-hexahedral vertical compressive stress regimes can be determined as follows by inserting the l, t and σ_A values into

$$f(x,y)=z=\sigma_A\left(1-\frac{x}{l}-\frac{y}{t}\right).$$

$$f(x,y)=z=(1\,/\,260750)N(1646813910056875-2033875579575\overline{X}-1749212223150\overline{Y}$$
$$-1257456236\overline{40}\,\overline{YX}+227354519235x\overline{X}+784038528x\overline{Y}\,\overline{X}-7751979675435x$$
$$-2007989238\overline{60}x\overline{Y}-8120817925950y-193257997740y\overline{X}+239966265900y\overline{Y}$$
$$+707812560y\overline{Y}\,\overline{X})\,/\,(22796259150449+181453583376\overline{Y})$$

The stress values beneath the corners of proprietory shaped paver 6 for the absolute-hexahedral vertical compressive stress regimes can now be determined by inserting the corner co-ordinates in the xy-plane into the stress function defined above (see Figure 8.5).

The vertical compressive stress beneath the corner a is

$$\sigma_a = (-0.02)N\left(\frac{-315784067125+390004905\overline{X}+335419410\overline{Y}+24112296\overline{YX}}{227962591504 49+181453583376\overline{Y}}\right)$$

The vertical compressive stress beneath the corner b is

$$\sigma_b = \left(-\frac{1}{26075}\right)\frac{\begin{pmatrix}-106541543439925-150177133630 5\overline{X}+168091315126 5\overline{Y}\\+6694273404\overline{YX}\end{pmatrix}}{227962591504 49+181453583376\overline{Y}}$$

The vertical compressive stress beneath the corner c is

$$\sigma_c = \left(\frac{1}{52150}\right)\frac{\begin{pmatrix}-4632427034485+317623625520 9\overline{X}-251669808375 0\overline{Y}\\+6996454920\overline{YX}\end{pmatrix}}{227962591504 49+181453583376\overline{Y}}$$

The vertical compressive stress beneath the corner d is

$$\sigma_d = \left(\frac{1}{52150}\right)\frac{\begin{pmatrix}-511443050870 95+454036337061 9\overline{X}-372149162691 0\overline{Y}\\+11700686088\overline{YX}\end{pmatrix}}{227962591504 49+181453583376\overline{Y}}$$

The vertical compressive stress beneath the corner e is

$$\sigma_e = \left(\frac{1}{350}\right)\frac{\left(-137879091060 5+582860009 1\overline{X}+562327131 0\overline{Y}+16878607 2\overline{YX}\right)}{227962591504 49+181453583376\overline{Y}}$$

The vertical compressive stress beneath the corner f is

$$\sigma_f = \left(\frac{1}{26075}\right)\frac{\begin{pmatrix}-445800752743 10-127092818748 3\overline{X}+192492564154 5\overline{Y}\\+6694273404\overline{YX}\end{pmatrix}}{227962591504 49+181453583376\overline{Y}}$$

The vertical compressive stress beneath the corner g is

$$\sigma_g = \left(-\frac{1}{10430}\right)\frac{\begin{pmatrix}-25711072673143+542909991513\overline{X}-600944612862\overline{Y}\\+1399290984\overline{YX}\end{pmatrix}}{227962591504 49+181453583376\overline{Y}}$$

The vertical compressive stress beneath the corner g is

$$\sigma_h = \left(-\frac{1}{52150}\right)\frac{\begin{pmatrix}-175067241418325+4078677072975\overline{X}-4209516607470\overline{Y}\\+11700686088\overline{YX}\end{pmatrix}}{227962591504 49+181453583376\overline{Y}}$$

8.7 Absolute-hexahedral compressive stress regimes beneath the circumscribing rectangular border for proprietory shaped paver 7

The application of the absolute-hexahedral compressive stress regime beneath the circumscribing rectangular border of proprietory shaped paver 7 shown in Figure 8.6 can be calculated by using the data in Tables 5.13. The first two letters of each boundary line function in Table 5.13 for proprietory shaped paver 7 charecterise the corner names can be seen in Figure 8.6 (example: bcy symbolises the boundary line function of proprietory shaped paver 7 in the y axis between corner b and c). The line functions which define the boundary of the absolute-hexahedral stress block in the xy-plane (see Figure 8.6) are of the form $fy = l\left(1-\frac{x}{l}\right)$, $fx = l\left(1-\frac{y}{l}\right)$.

The surface function of the absolute-hexahedral compressive stress block beneath the circumscribing rectangular border shown in Figure 8.6 through the three points σ_A, l and t is given by:

$$\begin{vmatrix} x & y & z & 1 \\ t & 0 & 0 & 1 \\ 0 & l & 0 & 1 \\ 0 & 0 & \sigma_A & 1 \end{vmatrix} = 0 \Rightarrow f(x,y) = z = \sigma_A\left(1 - \frac{x}{t} - \frac{y}{l}\right)$$

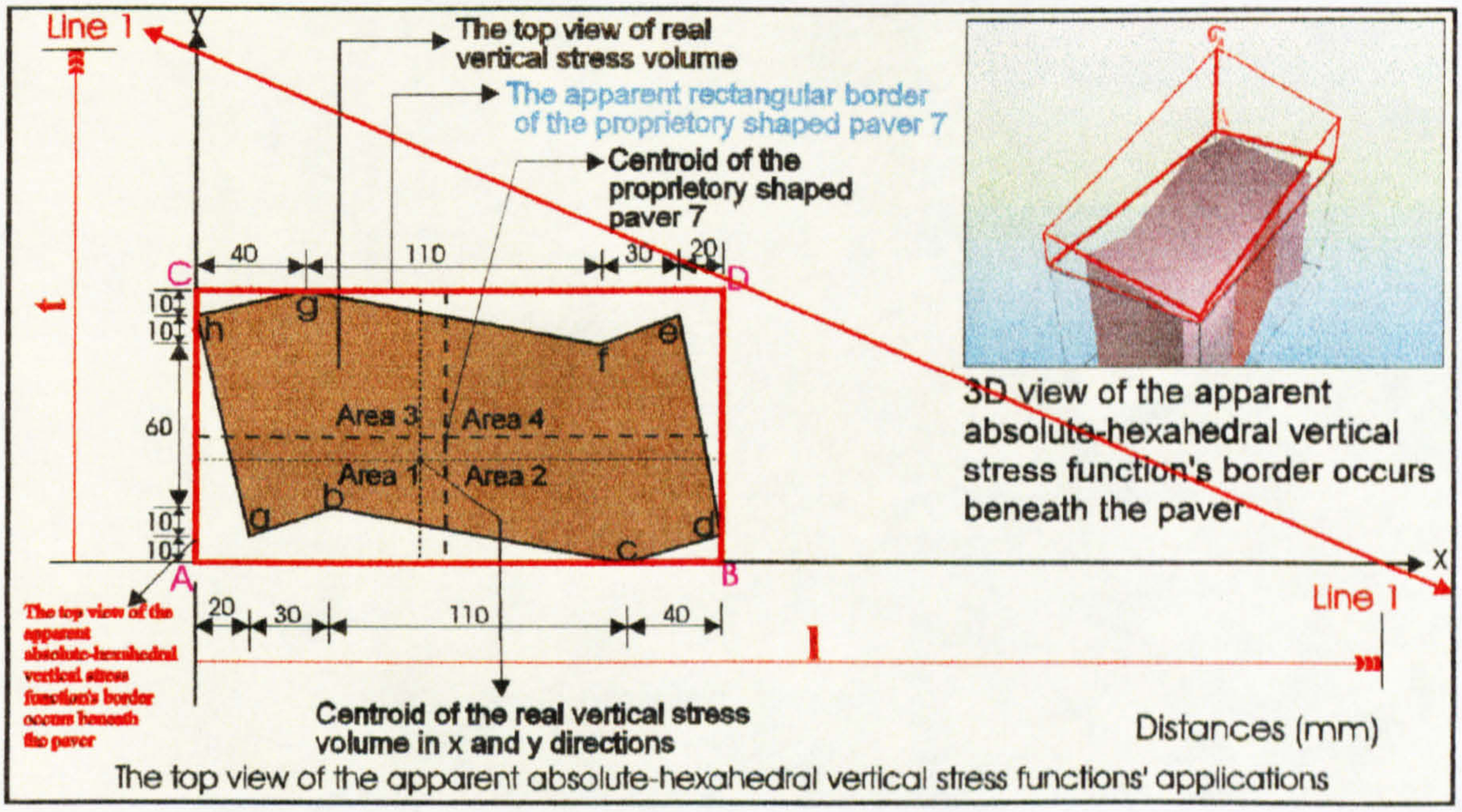

The top view of the apparent absolute-hexahedral vertical stress functions' applications

Figure 8.6: The application of the absolute-hexahedral compressive stress distribution beneath the circumscribing rectangular border of proprietory shaped paver 7.

The following actual total volume **V** beneath the surface $f(x,y) = z\ (> 0)$ and above the region in the xy-plane (see Figure 8.6) is calculated by subtracting the negative volume generated by the dentations of the shaped paver from the absolute-hexahedral volume beneath circumscribing rectangular boundary of the paver.

$$V = \int_0^{200}\int_0^{100} f(x,y)\,dy\,dx - \int_0^{20}\int_0^{10} f(x,y)\,dy\,dx - \int_0^{50}\int_0^{10} f(x,y)\,dy\,dx - \int_{20}^{160}\int_{10}^{aby} f(x,y)\,dy\,dx - \int_{50}^{160}\int_{0}^{bcy} f(x,y)\,dy\,dx$$
$$- \int_{160}^{200}\int_{0}^{cdy} f(x,y)\,dy\,dx - \int_{180}^{200}\int_{10}^{dey} f(x,y)\,dy\,dx - \int_{180}^{200}\int_{90}^{100} f(x,y)\,dy\,dx - \int_{150}^{180}\int_{90}^{100} f(x,y)\,dy\,dx - \int_{150}^{180}\int_{80}^{efy} f(x,y)\,dy\,dx$$
$$- \int_{40}^{150}\int_{80}^{fgy} f(x,y)\,dy\,dx - \int_{0}^{40}\int_{90}^{ghy} f(x,y)\,dy\,dx - \int_{0}^{20}\int_{10}^{hay} f(x,y)\,dy\,dx$$

and the centroids of this volume in the xy-plane are at distances $\overline{X}$ and $\overline{Y}$ from the axes (see Figure 8.6) which are given by the following equations.

$$\overline{X} = \frac{1}{V}\left[\begin{array}{l}
\int_{0}^{200}\int_{0}^{100} x f(x,y)\,dy\,dx - \int_{0}^{2010}\int_{0}^{0} x f(x,y)\,dy\,dx - \int_{200}^{5010}\int_{0}^{0} x f(x,y)\,dy\,dx - \int_{20}^{50}\int_{10}^{by} x f(x,y)\,dy\,dx \\
-\int_{50}^{160}\int_{0}^{bcy} x f(x,y)\,dy\,dx - \int_{160}^{200}\int_{0}^{cdy} x f(x,y)\,dy\,dx - \int_{180}^{200}\int_{10}^{dey} x f(x,y)\,dy\,dx - \int_{180}^{200}\int_{90}^{100} x f(x,y)\,dy\,dx \\
-\int_{150}^{180}\int_{90}^{100} x f(x,y)\,dy\,dx - \int_{150}^{180}\int_{80}^{efy} x f(x,y)\,dy\,dx - \int_{40}^{150}\int_{80}^{fgy} x f(x,y)\,dy\,dx - \int_{0}^{40}\int_{90}^{ghy} x f(x,y)\,dy\,dx \\
-\int_{0}^{20}\int_{10}^{hay} x f(x,y)\,dy\,dx
\end{array}\right]$$

$$\overline{Y} = \frac{1}{V}\left[\begin{array}{l}
\int_{0}^{100}\int_{0}^{200} y f(x,y)\,dx\,dy - \int_{0}^{1020}\int_{0}^{0} y f(x,y)\,dx\,dy - \int_{0}^{1050}\int_{20}^{0} y f(x,y)\,dx\,dy - \int_{10}^{20}\int_{20}^{bx} y f(x,y)\,dx\,dy \\
-\int_{0}^{20}\int_{50}^{bcx} y f(x,y)\,dx\,dy - \int_{0}^{10}\int_{160}^{cdx} y f(x,y)\,dx\,dy - \int_{10}^{90}\int_{180}^{dex} y f(x,y)\,dx\,dy - \int_{90}^{100}\int_{180}^{200} y f(x,y)\,dx\,dy \\
-\int_{90}^{100}\int_{150}^{180} y f(x,y)\,dx\,dy - \int_{80}^{90}\int_{150}^{efx} y f(x,y)\,dx\,dy - \int_{80}^{100}\int_{40}^{fgx} y f(x,y)\,dx\,dy - \int_{90}^{100}\int_{0}^{ghx} y f(x,y)\,dx\,dy \\
-\int_{10}^{90}\int_{0}^{hax} y f(x,y)\,dx\,dy
\end{array}\right]$$

The $V, \overline{X}$ and $\overline{Y}$ values can analytically be evaluated in terms of l, t and σ_A. The following results which indicate the proportions of the absolute-hexahedral vertical compressive stress block (see Figure 8.6) can be determined by applying vertical and rotational equilibrium between load patch and vertical compressive stress distribution (see Chapter 6). For vertical equilibrium condition the equality between the truncated volume (V) and the total applied patch load (N) must be satisfied and for rotational equilibrium conditions the centroid distances of the load patch ($\overline{X}$, $\overline{Y}$) must be coincided with the centroid distances of the truncated vertical stress block ($\overline{X}$, $\overline{Y}$).

$$l = \frac{15\left(34479\overline{Y} - 0.1737100.10^{7}\right)\begin{pmatrix}0.374969963.10^{9}\overline{YX} + 0.8115167190.10^{12}\overline{Y} \\ +0.3440348828.10^{12}\overline{X} - 0.8856006375.10^{14}\end{pmatrix}}{\begin{pmatrix}0.1290601680.10^{16}\overline{YX} + 0.2989329300.10^{13}\overline{Y}^{2}\overline{X} - 0.1949576103.10^{18}\overline{Y} \\ +0.2783753631.10^{15}\overline{Y}^{2} - 0.7261007719.10^{17}\overline{X} + 0.9115639805.10^{19}\end{pmatrix}}$$

$$t = \frac{-0.25\begin{pmatrix}0.374969963.10^{9}\overline{YX} + 0.8115167190.10^{12}\overline{Y} + 0.3440348828.10^{12}\overline{X} \\ -0.8856006375.10^{14}\end{pmatrix}}{\left(-0.251634742.10^{9}\overline{X} + 0.1073750.10^{7}\overline{YX} + 0.2093923374.10^{12} - 0.3641094245.10^{10}\overline{Y}\right)}$$

$$\sigma_A = \frac{-25N\left(34479\overline{Y} - 0.17371.10^{7}\right)\begin{pmatrix}0.374969963.10^{9}\overline{YX} + 0.811516719.10^{12}\overline{Y} \\ +0.3440348828.10^{12}\overline{X} - 0.8856006375.10^{14}\end{pmatrix}}{\begin{pmatrix}0.8660844086.10^{14}\overline{YX} + 0.2051995274.10^{12}\overline{Y}^{2}\overline{X} + 0.8282032771.10^{23}\overline{Y} \\ +0.2117408088.10^{21}\overline{Y}^{2} - 0.4910010330.10^{16}\overline{X} - 0.4710061792.10^{25}\end{pmatrix}}$$

Therefore, the function of the absolute-hexahedral vertical compressive stress regimes can be determined as follows by inserting the **l**, **t** and σ_A values into $f(x,y) = z = \sigma_A\left(1 - \frac{x}{l} - \frac{y}{t}\right)$.

$$f(x,y) = z = 0.125.10^{-6}N(-0.1292858935.10^{20}\overline{Y}^{2}\overline{X} - 0.2798028495.10^{23}\overline{Y}^{2}$$
$$-0.1121061840.10^{23}\overline{YX} + 0.4463148131.10^{25}\overline{Y} + 0.5976229949.10^{24}\overline{X}$$
$$-0.1538376867.10^{27} + 0.8604011200.10^{20}x\overline{YX} + 0.1992886200.10^{18}x\overline{Y}^{2}\overline{X}$$
$$-0.1299717402.10^{23}x\overline{Y} + 0.1855835754.10^{20}x\overline{Y}^{2} - 0.4840671813.10^{22}x\overline{X}$$
$$+0.6077093204.10^{24}x + 0.4216530158.10^{20}y\overline{YX} - 0.1480873050.10^{18}y\overline{Y}^{2}\overline{X}$$
$$-0.5417833286.10^{23}y\overline{Y} + 0.5021651539.10^{21}y\overline{Y}^{2} - 0.1748458841.10^{22}y\overline{X}$$
$$+0.1454941717.10^{25}y) \Big/ (0.4330422043.10^{12}\overline{YX} + 0.1025997637.10^{10}\overline{Y}^{2}\overline{X}$$
$$+0.4141016386.10^{21}\overline{Y} + 0.1058704044.10^{19}\overline{Y}^{2} - 0.2455005165.10^{14}\overline{X}$$
$$-0.2355030896.10^{23})$$

The stress values beneath the corners of proprietory shaped paver 7 for the absolute-hexahedral vertical compressive stress regimes can now be determined by inserting the corner co-ordinates in the xy-plane into the stress function defined above (see Figure 8.6).

The vertical compressive stress beneath the corner a is

$$\sigma_a = -0.125.10^7 N(0.1042369.10^7\overline{Y}^2\overline{X} + 0.2258746626.10^{10}\overline{Y}^2 + 0.906816314.10^9\overline{YX}$$
$$-0.3661421322.10^{12}\overline{Y} - 0.4833249702.10^{11}\overline{X} + 0.127134083 1.10^{14})$$
$$/\,(0.4330422043.10^{12}\overline{YX} + 0.1025997637.10^{10}\overline{Y}^2\overline{X} + 0.4141016386.10^{21}\overline{Y}$$
$$+0.1058704044.10^{19}\overline{Y}^2 - 0.2455005165.10^{14}\overline{X} - 0.2355030896.10^{23})$$

The vertical compressive stress beneath the corner b is

$$\sigma_b = -6250N(0.118518089.10^9\overline{Y}^2\overline{X} + 0.3401812798.10^{12}\overline{Y}^2 + 0.1213061345.10^{12}\overline{YX}$$
$$-0.5459445546.10^{14}\overline{Y} - 0.6412404548.10^{13}\overline{X} + 0.1887067727.10^{16})$$
$$/\,(0.4330422043.10^{12}\overline{YX} + 0.1025997637.10^{10}\overline{Y}^2\overline{X} + 0.4141016386.10^{21}\overline{Y}$$
$$+0.1058704044.10^{19}\overline{Y}^2 - 0.2455005165.10^{14}\overline{X} - 0.2355030896.10^{23})$$

The vertical compressive stress beneath the corner c is

$$\sigma_c = 6250N(0.379151797.10^9\overline{Y}^2\overline{X} - 0.5002189548.10^{12}\overline{Y}^2 + 0.5111599040.10^{11}\overline{YX}$$
$$+0.4767200576.10^{14}\overline{Y} - 0.3537689904.10^{13}\overline{X} - 0.1132083909.10^{16})$$
$$/\,(0.4330422043.10^{12}\overline{YX} + 0.1025997637.10^{10}\overline{Y}^2\overline{X} + 0.4141016386.10^{21}\overline{Y}$$
$$+0.1058704044.10^{19}\overline{Y}^2 - 0.2455005165.10^{14}\overline{X} - 0.2355030896.10^{23})$$

The vertical compressive stress beneath the corner d is

$$\sigma_d = 100000N(0.31810327.10^8\overline{Y}^2\overline{X} - 0.2405870238.10^{11}\overline{Y}^2 + 0.8023821275.10^{10}\overline{YX}$$
$$+0.1652412498.10^{13}\overline{Y} - 0.4849949451.10^{12}\overline{X} - 0.2218300679.10^{14})$$
$$/(0.4330422043.10^{12}\overline{YX} + 0.1025997637.10^{10}\overline{Y}^2\overline{X} + 0.4141016386.10^{21}\overline{Y}$$
$$+0.1058704044.10^{19}\overline{Y}^2 - 0.2455005165.10^{14}\overline{X} - 0.2355030896.10^{23})$$

The vertical compressive stress beneath the corner e is

$$\sigma_e = 50000N(0.24038762.10^8\overline{Y}^2\overline{X} + 0.5138770815.10^{11}\overline{Y}^2 + 0.2017869726.10^{11}\overline{YX}$$
$$+0.6880982875.10^{13}\overline{Y} - 0.1077648068.10^{13}\overline{X} + 0.2162368638.10^{15})$$
$$/(0.4330422043.10^{12}\overline{YX} + 0.1025997637.10^{10}\overline{Y}^2\overline{X} + 0.4141016386.10^{21}\overline{Y}$$
$$+0.1058704044.10^{19}\overline{Y}^2 - 0.2455005165.10^{14}\overline{X} - 0.2355030896.10^{23})$$

The vertical compressive stress beneath the corner f is

$$\sigma_f = 31250N(0.20470877.10^8\overline{Y}^2\overline{X} + 0.5990672396.10^{11}\overline{Y}^2 + 0.2027449010.10^{11}\overline{YX}$$
$$-0.7282778404.10^{13}\overline{Y} - 0.1073417938.10^{13}\overline{X} + 0.2148561950.10^{15})$$
$$/(0.4330422043.10^{12}\overline{YX} + 0.1025997637.10^{10}\overline{Y}^2\overline{X} + 0.4141016386.10^{21}\overline{Y}$$
$$+0.1058704044.10^{19}\overline{Y}^2 - 0.2455005165.10^{14}\overline{X} - 0.2355030896.10^{23})$$

The vertical compressive stress beneath the corner g is

$$\sigma_g = -6250N(0.395315501.10^9\overline{Y}^2\overline{X} - 0.4595712948.10^{12}\overline{Y}^2 + 0.7104967524.10^{11}\overline{YX}$$
$$+0.2949144232.10^{14}\overline{Y} - 0.4583004766.10^{13}\overline{X} - 0.3192971560.10^{15})$$
$$/(0.4330422043.10^{12}\overline{YX} + 0.1025997637.10^{10}\overline{Y}^2\overline{X} + 0.4141016386.10^{21}\overline{Y}$$
$$+0.1058704044.10^{19}\overline{Y}^2 - 0.2455005165.10^{14}\overline{X} - 0.2355030896.10^{23})$$

The vertical compressive stress beneath the corner h is

$$\sigma_h = -50000N(0.65641117.10^8\overline{Y}^2\overline{X} - 0.4303644725.10^{11}\overline{Y}^2 + 0.1853935315.10^{11}\overline{YX}$$
$$+0.1032254565.10^{13}\overline{Y} - 0.1100654248.10^{13}\overline{X} + 0.5723233050.10^{14})$$
$$/\,(0.4330422043.10^{12}\overline{YX} + 0.1025997637.10^{10}\overline{Y}^2\overline{X} + 0.4141016386.10^{21}\overline{Y}$$
$$+0.1058704044.10^{19}\overline{Y}^2 - 0.2455005165.10^{14}\overline{X} - 0.2355030896.10^{23})$$

8.8. Absolute-hexahedral compressive stress regimes beneath the circumscribing rectangular border for proprietory shaped paver 8

The application of the absolute-hexahedral compressive stress regime beneath the circumscribing rectangular border of proprietory shaped paver 8 shown in Figure 8.7 can be calculated by using the data in Tables 5.15. The first two letters of each boundary line function in Table 5.15 for proprietory shaped paver 8 charecterise the corner names can be seen in Figure 8.7 (example: bcy symbolises the boundary line function of proprietory shaped paver 8 in the y axis between corner b and c). The line functions which define the boundary of the absolute-hexahedral stress block in the xy-plane (see Figure 8.7) are of the form $fy = t\left(1-\frac{x}{t}\right)$, $fx = t\left(1-\frac{y}{t}\right)$.

The surface function of the absolute-hexahedral compressive stress block beneath the circumscribing rectangular border shown in Figure 8.7 through the three points σ_A, l and t is given by:

$$\begin{vmatrix} x & y & z & 1 \\ t & 0 & 0 & 1 \\ 0 & t & 0 & 1 \\ 0 & 0 & \sigma_A & 1 \end{vmatrix} = 0 \Rightarrow f(x,y) = z = \sigma_A\left(1-\frac{x}{t}-\frac{y}{t}\right)$$

The following actual total volume V beneath the surface $f(x,y) = z\ (> 0)$ and above the region in the xy-plane (see Figure 8.7) is calculated by subtracting the negative volume generated by the dentations of the shaped paver from the absolute-hexahedral volume beneath circumscribing rectangular boundary of the paver.

$$V = \int_0^{200}\int_0^{100} f(x,y)\,dy\,dx - \int_{50}^{65}\int_0^{bcy} f(x,y)\,dy\,dx - \int_{65}^{135}\int_0^{15} f(x,y)\,dy\,dx - \int_{135}^{150}\int_0^{dey} f(x,y)\,dy\,dx - \int_{135}^{150}\int_{85}^{hiy} f(x,y)\,dy\,dx$$
$$- \int_{65}^{135}\int_{85}^{100} f(x,y)\,dy\,dx - \int_{50}^{65}\int_{85}^{jky} f(x,y)\,dy\,dx$$

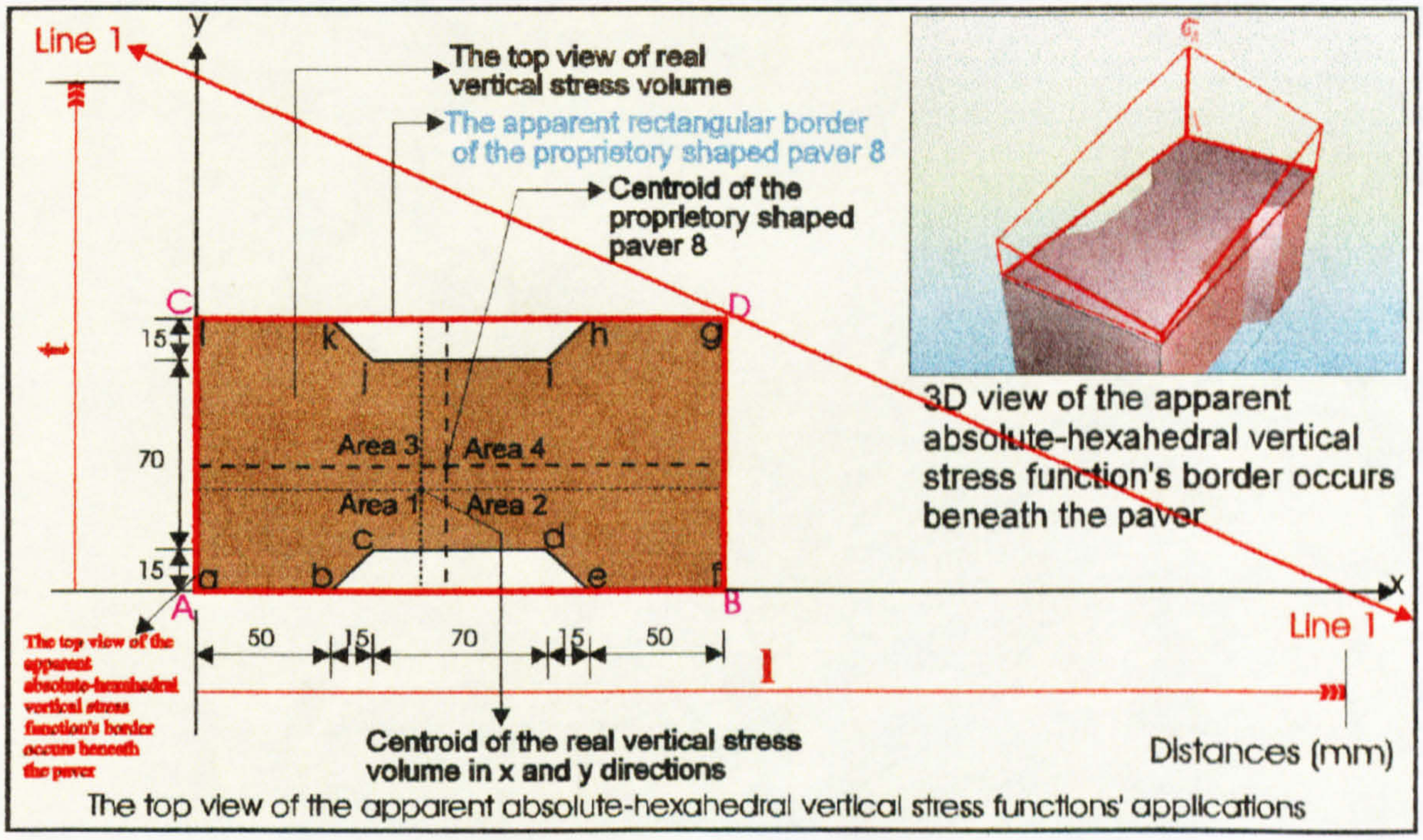

The top view of the apparent absolute-hexahedral vertical stress functions' applications

Figure 8.7: The application of the absolute-hexahedral compressive stress distribution beneath the circumscribing rectangular border of proprietory shaped paver 8.

and the centroids of this volume in the xy-plane are at distances $\overline{X}$ and $\overline{Y}$ from the axes (see Figure 8.7) which are given by the following equations.

$$\overline{X} = \frac{1}{V}\left[\int_0^{200}\int_0^{100} x f(x,y)\,dy\,dx - \int_{50}^{65}\int_0^{bcy} x f(x,y)\,dy\,dx - \int_{65}^{135}\int_0^{15} x f(x,y)\,dy\,dx - \int_{135}^{150}\int_0^{dey} x f(x,y)\,dy\,dx\right.$$
$$\left. - \int_{135}^{150}\int_{85}^{hiy} x f(x,y)\,dy\,dx - \int_{65}^{135}\int_{85}^{100} x f(x,y)\,dy\,dx - \int_{50}^{65}\int_{85}^{jky} x f(x,y)\,dy\,dx\right]$$

$$\overline{Y} = \frac{1}{V}\left[\int_0^{100}\int_0^{200} y f(x,y)\,dx\,dy - \int_0^{15}\int_{50}^{bcx} y f(x,y)\,dx\,dy - \int_0^{15}\int_{65}^{135} y f(x,y)\,dx\,dy - \int_0^{15}\int_{135}^{dex} y f(x,y)\,dx\,dy\right.$$

$$\left. -\int_{85}^{100}\int_{135}^{hix} yf(x,y)\,dx\,dy - \int_{85}^{100}\int_{65}^{135} yf(x,y)\,dx\,dy - \int_{85}^{100}\int_{50}^{jkx} yf(x,y)\,dx\,dy \right]$$

The $V, \overline{X}$ and $\overline{Y}$ values can analytically be evaluated in terms of l, t and σ_A. The following results which indicate the proportions of the absolute-hexahedral vertical compressive stress block (see Figure 8.7) can be determined by applying vertical and rotational equilibrium between load patch and vertical compressive stress distribution (see Chapter 6). For vertical equilibrium condition the equality between the truncated volume (V) and the total applied patch load (N) must be satisfied and for rotational equilibrium conditions the centroid distances of the load patch ($\overline{X}$, $\overline{Y}$) must be coincided with the centroid distances of the truncated vertical stress block ($\overline{X}$, $\overline{Y}$).

$$l = \left(\frac{5}{2094}\right)\left(\frac{1696869\overline{Y}\,\overline{X} + 11989579350\overline{X} + 32490640500\overline{Y} - 3281654295100}{27\overline{Y}\,\overline{X} + 286960\overline{X} - 28696000 - 2700\overline{Y}}\right)$$

$$t = \left(\frac{5}{2094}\right)\left(\frac{1696869\overline{Y}\,\overline{X} + 11989579350\overline{X} + 32490640500\overline{Y} - 3281654295100}{1557010\overline{Y} + 27\overline{Y}\,\overline{X} - 77850500 - 1350\overline{X}}\right)$$

$$\sigma_A = \left(-\frac{N}{27216939500}\right)\left(\frac{\begin{array}{l}1696869\overline{Y}\,\overline{X} + 11989579350\overline{X} + 32490640500\overline{Y} \\ -3281654295100\end{array}}{27\overline{Y} + 286960}\right)$$

Therefore, the function of the absolute-hexahedral vertical compressive stress regimes can be determined as follows by inserting the l, t and σ_A values into $f(x,y) = z = \sigma_A\left(1 - \frac{x}{l} - \frac{y}{t}\right)$.

$$f(x,y) = z = \left(\frac{N}{136084697500}\right)(56538x\overline{Y}\,\overline{X} + 600894240x\overline{X} - 59947896750\overline{X}$$

$$-2826900y\overline{X} - 8484345\overline{Y}\,\overline{X} + 56538y\overline{Y}\,\overline{X} - 60089424000x - 5653800x\overline{Y} + 3260378940y\overline{Y}$$
$$-162453202500\overline{Y} - 163018947000y + 1640827147500) \Big/ (27\overline{Y} + 286960)$$

The stress values beneath the corners of proprietory shaped paver 8 for the absolute-hexahedral vertical compressive stress regimes can now be determined by inserting the corner co-ordinates in the xy-plane into the stress function defined above (see Figure 8.7).

The vertical compressive stress beneath the corner **a** is

$$\sigma_a = \left(\frac{-N}{27216939500}\right)\left(\frac{1696869\overline{Y}\,\overline{X} + 11989579350\overline{X} + 32490640500\overline{Y} - 3281654295100}{27\overline{Y} + 286960}\right)$$

The vertical compressive stress beneath the corner **b** is

$$\sigma_b = \left(\frac{-N}{27216939500}\right)\left(\frac{1131489\overline{Y}\,\overline{X} + 5980636950\overline{X} - 2680760055100 + 32547178500\overline{Y}}{27\overline{Y} + 286960}\right)$$

The vertical compressive stress beneath the corner **c** is

$$\sigma_c = \left(\frac{-N}{27216939500}\right)\left(\frac{792261\overline{Y}\,\overline{X} + 4186434930\overline{X} - 2011434942100 + 22783003080\overline{Y}}{27\overline{Y} + 286960}\right)$$

The vertical compressive stress beneath the corner **d** is

$$\sigma_d = \left(\frac{-N}{27216939500}\right)\left(\frac{729\overline{Y}\,\overline{X} - 4226084430\overline{X} - 1170183006100 + 22862156280\overline{Y}}{27\overline{Y} + 286960}\right)$$

The vertical compressive stress beneath the corner **e** is

$$\sigma_e = \left(\frac{-N}{27216939500}\right)\left(\frac{729\overline{Y}\,\overline{X} - 6037247850\overline{X} - 1478971575100 + 32660254500\overline{Y}}{27\overline{Y} + 286960}\right)$$

The vertical compressive stress beneath the corner **f** is

$$\sigma_f = \left(\frac{N}{27216939500}\right)\left(\frac{564651\overline{Y}\overline{X} + 12046190250\overline{X} + 878077335100 - 32716792500\overline{Y}}{27\overline{Y} + 286960}\right)$$

The vertical compressive stress beneath the corner **g** is

$$\sigma_g = \left(\frac{N}{27216939500}\right)\left(\frac{1695411\overline{Y}\overline{X} + 11989652250\overline{X} - 2382301604900 + 32490786300\overline{Y}}{27\overline{Y} + 286960}\right)$$

The vertical compressive stress beneath the corner **h** is

$$\sigma_h = \left(\frac{N}{27216939500}\right)\left(\frac{1130031\overline{Y}\overline{X} + 5980709850\overline{X} - 1781407364900 + 32547324300\overline{Y}}{27\overline{Y} + 286960}\right)$$

The vertical compressive stress beneath the corner **i** is

$$\sigma_i = \left(\frac{N}{27216939500}\right)\left(\frac{790803\overline{Y}\overline{X} + 4186507830\overline{X} - 1112082251900 + 22783148880\overline{Y}}{27\overline{Y} + 286960}\right)$$

The vertical compressive stress beneath the corner **j** is

$$\sigma_j = \left(\frac{-N}{27216939500}\right)\left(\frac{729\overline{Y}\overline{X} + 4226011530\overline{X} + 270830315900 - 22862302080\overline{Y}}{27\overline{Y} + 286960}\right)$$

The vertical compressive stress beneath the corner **k** is

$$\sigma_k = \left(\frac{-N}{27216939500}\right)\left(\frac{729\overline{Y}\overline{X} + 6037174950\overline{X} + 579618884900 - 32660400300\overline{Y}}{27\overline{Y} + 286960}\right)$$

The vertical compressive stress beneath the corner **l** is

$$\sigma_l = \left(\frac{-N}{27216939500}\right)\left(\frac{12046117350\overline{X} + 566109\overline{Y}\overline{X} - 32716938300\overline{Y} - 21275355100}{27\overline{Y} + 286960}\right)$$

8.9. Absolute-hexahedral compressive stress regimes beneath the circumscribing rectangular border for proprietory shaped paver 9

The application of the absolute-hexahedral compressive stress regime beneath the circumscribing rectangular border of proprietory shaped paver 9 shown in Figure 8.8 can be calculated by using the data in Tables 5.17. The first two letters of each boundary line function in Table 5.17 for proprietory shaped paver 9 charecterise the corner names can be seen in Figure 8.8 (example: **bcy** symbolises the boundary line function of proprietory shaped paver 9 in the **y** axis between corner **b** and **c**). The line functions which define the boundary of the absolute-hexahedral stress block in the xy-plane (see Figure 8.8) are of the form $fy = t\left(1-\frac{x}{l}\right)$, $fx = l\left(1-\frac{y}{t}\right)$.

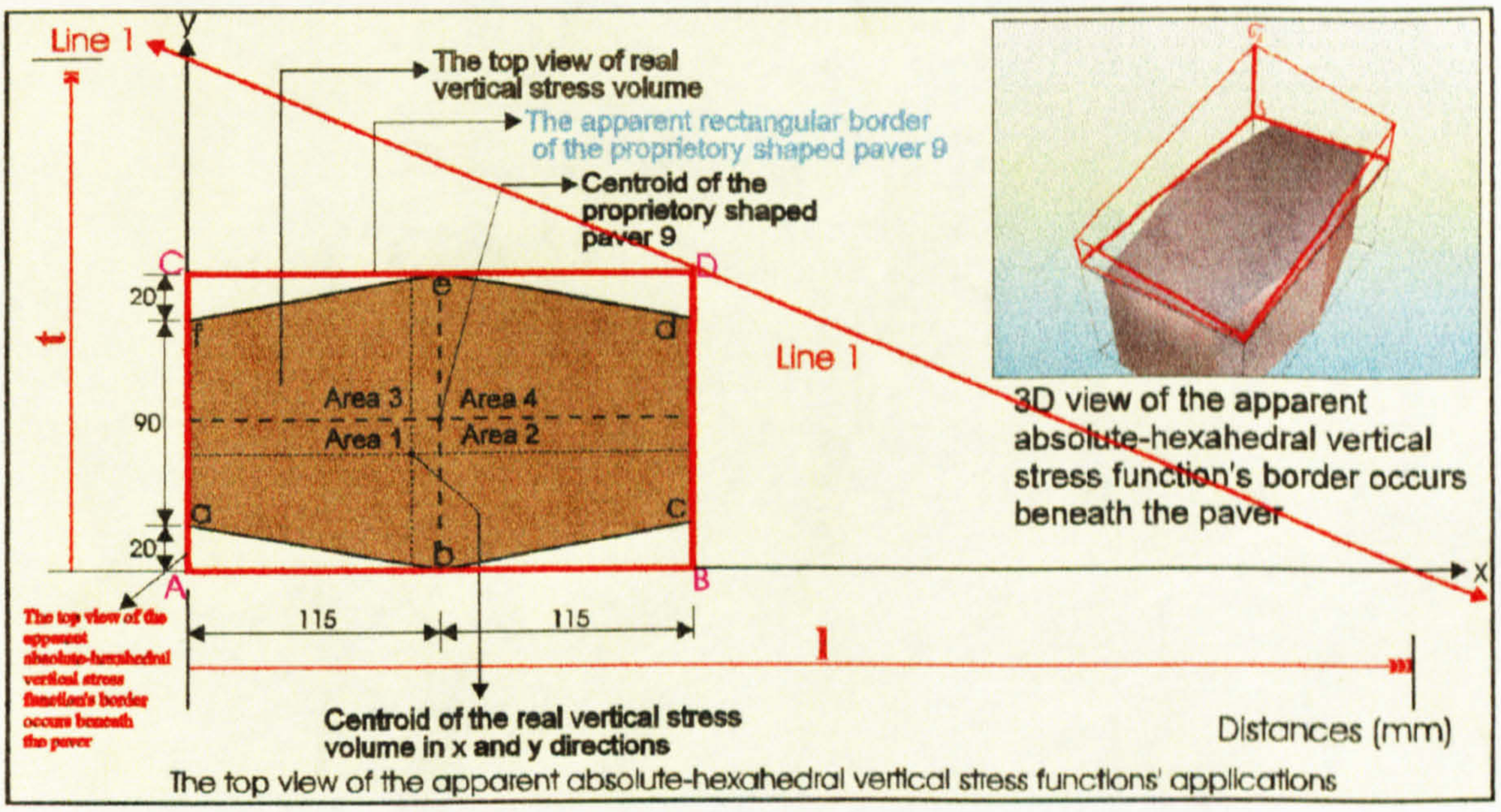

Figure 8.8: The application of the absolute-hexahedral compressive stress distribution beneath the circumscribing rectangular border of proprietory shaped paver 9.

The surface function of the absolute-hexahedral compressive stress block beneath the circumscribing rectangular border shown in Figure 8.8 through the three points σ_A, **l** and **t** is given by:

$$\begin{vmatrix} x & y & z & 1 \\ t & 0 & 0 & 1 \\ 0 & l & 0 & 1 \\ 0 & 0 & \sigma_A & 1 \end{vmatrix} = 0 \Rightarrow f(x,y) = z = \sigma_A\left(1 - \frac{x}{t} - \frac{y}{l}\right)$$

The following actual total volume **V** beneath the surface $f(x,y) = z\ (> 0)$ and above the region in the xy-plane (see Figure 8.8) is calculated by subtracting the negative volume generated by the dentations of the shaped paver from the absolute-hexahedral volume beneath circumscribing rectangular boundary of the paver.

$$V = \int_0^{230}\int_0^{130} f(x,y)\,dy\,dx - \int_0^{115}\int_0^{aby} f(x,y)\,dy\,dx - \int_{115}^{230}\int_0^{bcy} f(x,y)\,dy\,dx - \int_{115}^{230}\int_{110}^{dey} f(x,y)\,dy\,dx - \int_0^{115}\int_{110}^{efy} f(x,y)\,dy\,dx$$

and the centroids of this volume in the xy-plane are at distances $\overline{X}$ and $\overline{Y}$ from the axes (see Figure 8.8) which are given by the following equations.

$$\overline{X} = \frac{1}{V}\left[\int_0^{230}\int_0^{130} x f(x,y)\,dy\,dx - \int_0^{115}\int_0^{aby} x f(x,y)\,dy\,dx - \int_{115}^{230}\int_0^{bcy} x f(x,y)\,dy\,dx - \int_{115}^{230}\int_{110}^{dey} x f(x,y)\,dy\,dx - \int_0^{115}\int_{110}^{efy} x f(x,y)\,dy\,dx\right]$$

$$\overline{Y} = \frac{1}{V}\left[\int_0^{130}\int_0^{230} y f(x,y)\,dx\,dy - \int_0^{20}\int_0^{abx} y f(x,y)\,dx\,dy - \int_0^{20}\int_{115}^{bcx} y f(x,y)\,dx\,dy - \int_{110}^{130}\int_{115}^{dex} y f(x,y)\,dx\,dy - \int_{110}^{130}\int_0^{efx} y f(x,y)\,dx\,dy\right]$$

The $V, \overline{X}$ and $\overline{Y}$ values can analytically be evaluated in terms of l, t and σ_A. The following results which indicate the proportions of the absolute-hexahedral vertical compressive stress block (see Figure 8.8) can be determined by applying vertical and rotational equilibrium between load patch and vertical compressive stress distribution (see Chapter 6). For vertical equilibrium condition the equality between the truncated

volume (V) and the total applied patch load (N) must be satisfied and for rotational equilibrium conditions the centroid distances of the load patch ($\overline{X}$, $\overline{Y}$) must be coincided with the centroid distances of the truncated vertical stress block ($\overline{X}$, $\overline{Y}$).

$$l = \frac{126500\left(3\overline{X}-460\right)\begin{pmatrix}0.749018859.10^{9}\overline{XY}+0.269720068.10^{12}\overline{X}+0.6303096566.10^{12}\overline{Y}\\-0.8965914682.10^{14}\end{pmatrix}}{\begin{pmatrix}-0.3548542872.10^{15}\overline{XY}+0.1322438337.10^{13}\overline{X}^{2}\overline{Y}-0.2687283564.10^{18}\overline{X}\\+0.1001472136.10^{16}\overline{X}^{2}+0.2331899602.10^{17}\overline{Y}+0.1765929200.10^{20}\end{pmatrix}}$$

$$t = \frac{500\begin{pmatrix}0.749018859.10^{9}\overline{XY}+0.2697620068.10^{12}\overline{X}+0.6303096566.10^{12}\overline{Y}\\-0.8965914682.10^{14}\end{pmatrix}}{\begin{pmatrix}0.5272045601.10^{13}\overline{Y}+0.2654327709.10^{10}\overline{XY}-0.3286746505.10^{15}\\-0.25694575580.10^{12}\overline{X}\end{pmatrix}}$$

$$\sigma_A = \frac{-0.1304347826N\left(3\overline{X}-460\right)\begin{pmatrix}0.749018859.10^{9}\overline{XY}+0.2697620068.10^{12}\overline{X}\\+0.6303096566.10^{12}\overline{Y}-0.8965914682.10^{14}\end{pmatrix}}{\begin{pmatrix}0.1520804086.10^{15}\overline{XY}+891\overline{X}^{2}\overline{Y}+0.1151692957.10^{18}\overline{X}+0.1038000.10^{7}\overline{X}^{2}\\-0.2331899603.10^{17}\overline{Y}-0.1765929199.10^{20}\end{pmatrix}}$$

Therefore, the function of the absolute-hexahedral vertical compressive stress regimes can be determined as follows by inserting the **l**, **t** and σ_A values into $f(x,y)=z=\sigma_A\left(1-\frac{x}{l}-\frac{y}{t}\right)$.

$$\begin{aligned}f(x,y)=z=\;&0.2608695652.10^{-11}N(-0.1123528289.10^{21}\overline{X}^{2}\overline{Y}-0.4046430102.10^{23}\overline{X}^{2}\\&-0.7731901473.10^{23}\overline{XY}+0.1965339818.10^{26}\overline{X}+0.1449712210.10^{26}\overline{Y}\\&-0.2062160377.10^{28}-0.1402586115.10^{21}x\overline{XY}+0.5227029000.10^{18}x\overline{X}^{2}\overline{Y}\\&-0.1062167417.10^{24}x\overline{X}+0.3958387889.10^{21}x\overline{X}^{2}+0.9216994474.10^{22}x\overline{Y}\\&+0.6979957312.10^{25}x+0.1459514606.10^{22}y\overline{XY}+0.7962983127.10^{18}y\overline{X}^{2}\overline{Y}\end{aligned}$$

$$-0.8678289028.10^{23}y\overline{X}-0.7708372740.10^{20}y\overline{X}^2-0.2425140976.10^{24}y\overline{Y}$$
$$+0.1511903392.10^{26}y)\Big/(0.1520804086.10^{15}\overline{XY}+891\overline{X}^2\overline{Y}+0.1151692957.10^{18}\overline{X}$$
$$+0.1038000.10^{7}\overline{X}^2-0.2331899603.10^{17}\overline{Y}-0.1765929199.10^{20})$$

The stress values beneath the corners of proprietory shaped paver 9 for the absolute-hexahedral vertical compressive stress regimes can now be determined by inserting the corner co-ordinates in the xy-plane into the stress function defined above (see Figure 8.8).

The vertical compressive stress beneath the corner **a** is

$$\sigma_a=-0.1304347826N(0.1928537253.10^{10}\overline{X}^2\overline{Y}+0.8401195114.10^{12}\overline{X}^2$$
$$+0.9625744522.10^{12}\overline{XY}-0.3583548074.10^{15}\overline{X}-0.1929368030.10^{15}\overline{Y}$$
$$+0.3519559398.10^{17})\Big/(0.1520804086.10^{15}\overline{XY}+891\overline{X}^2\overline{Y}+0.1151692957.10^{18}\overline{X}$$
$$+0.1038000.10^{7}\overline{X}^2-0.2331899603.10^{17}\overline{Y}-0.1765929199.10^{20})$$

The vertical compressive stress beneath the corner **b** is

$$\sigma_b=-.0.5217391304N(0.261209977.10^{9}\overline{X}^2\overline{Y}-0.2528579850.10^{11}\overline{X}^2$$
$$+0.4672437753.10^{12}\overline{XY}-0.3719236440.10^{14}\overline{X}-0.7778538235.10^{14}\overline{Y}$$
$$+0.6297326430.10^{16})\Big/(0.1520804086.10^{15}\overline{XY}+891\overline{X}^2\overline{Y}+0.1151692957.10^{18}\overline{X}$$
$$+0.1038000.10^{7}\overline{X}^2-0.2331899603.10^{17}\overline{Y}-0.1765929199.10^{20})$$

The vertical compressive stress beneath the corner **c** is

$$\sigma_c=0.1304347826N(0.475896087.10^{9}\overline{X}^2\overline{Y}+0.9807389176.10^{12}\overline{X}^2$$
$$-0.1607764065.10^{13}\overline{XY}-0.1302422044.10^{15}\overline{X}+0.2353349776.10^{15}\overline{Y}$$
$$-0.3087790332.10^{16})\Big/(0.1520804086.10^{15}\overline{XY}+891\overline{X}^2\overline{Y}+0.1151692957.10^{18}\overline{X}$$

$$+0.1038000.10^{7}\overline{X}^{2}-0.2331899603.10^{17}\overline{Y}-0.1765929199.10^{20})$$

The vertical compressive stress beneath the corner **d** is

$$\sigma_d = 6.521739130N(0.38184661.10^{8}\overline{X}^{2}\overline{Y}+0.1683976417.10^{11}\overline{X}^{2}$$
$$+0.2038724453.10^{11}\overline{XY}-0.5729028136.10^{13}\overline{X}-0.4023807964.10^{13}\overline{Y}$$
$$+0.4825294144.10^{15})\Big/(0.1520804086.10^{15}\overline{XY}+891\overline{X}^{2}\overline{Y}+0.115169295 7.10^{18}\overline{X}$$
$$+0.1038000.10^{7}\overline{X}^{2}-0.2331899603.10^{17}\overline{Y}-0.1765929199.10^{20})$$

The vertical compressive stress beneath the corner **e** is

$$\sigma_e = 0.2608695652N(0.512767853.10^{9}\overline{X}^{2}\overline{Y}-0.4963724860.10^{11}\overline{X}^{2}$$
$$+0.9628814378.10^{12}\overline{XY}-0.3843302860.10^{14}\overline{X}-0.1596975623.10^{15}\overline{Y}$$
$$+0.7060091240.10^{16})\Big/(0.1520804086.10^{15}\overline{XY}+891\overline{X}^{2}\overline{Y}+0.115169295 7.10^{18}\overline{X}$$
$$+0.1038000.10^{7}\overline{X}^{2}-0.2331899603.10^{17}\overline{Y}-0.1765929199.10^{20})$$

The vertical compressive stress beneath the corner **f** is

$$\sigma_f = -1.304347826N(0.49520029.10^{8}\overline{X}^{2}\overline{Y}+0.9788702206.10^{11}\overline{X}^{2}$$
$$-0.1664551839.10^{12}\overline{XY}-0.2021456050.10^{14}\overline{X}+0.2435885728.10^{14}\overline{Y}$$
$$+0.7981332920.10^{15})\Big/(0.1520804086.10^{15}\overline{XY}+891\overline{X}^{2}\overline{Y}+0.115169295 7.10^{18}\overline{X}$$
$$+0.1038000.10^{7}\overline{X}^{2}-0.2331899603.10^{17}\overline{Y}-0.1765929199.10^{20})$$

8.10. Conclusion

It has been demonstrated in this Chapter that how the bedding sand stress calculation method[1, 2, 3] (see Sections 6.2, 6.3 and 6.4 for the detail of the bedding sand stress calculation mathod[1, 2, 3]) can be applied to proprietory shaped pavers. The absolute-hexahedral vertical compressive stress regimes which occur beneath the circumscribing rectangular border of eight proprietory shaped pavers (see proprietory shaped pavers 2, 3, 4, 5, 6, 7, 8 and 9 in Figure 5.1) has been analysed in this Chapter by using the similar method described in the previous chapter for proprietory shaped paver 1. This Chapter presented the application of the bedding sand stress calculation method[1, 2, 3] (see Chapters 6 and 7) to eight common proprietory shaped pavers in order to determine the algebraical solutions to the absolute-hexahedral vertical compressive stress blocks' total volumes and centroid distances in the xy-plane for all realistically possible load patches. These developed equations for the absolute-hexahedral stress blocks will be used in Chapter 9 to evaluate the vertical compressive stresses beneath the proprietory shaped pavers resulting from the variations of the common patch loading described in Chapter 5 (see Figures 5.2 to 5.42 and 9.1 to 9.9). In the other paver stress regimes, iterative solutions (see Appendix) have been developed and given in Figures 6.21, 9.1, 9.2, 9.3, 9.4, 9.5, 9.6, 9.7, 9.8 and 9.9. The vertical compressive stresses in the bedding material are calculated for the shaped pavers (see Sections 7.2.5 and 8.2 to 8.9) by using the application of the bedding sand stress calculation method[1, 2, 3] to proprietory shaped pavers.

References

1 Algin, H.M., Knapton, J., (1996), *Research into paver interlock*, Jrnl. of the Institution of Highway & Transportation & IHIE, Vol. 43, No. 03, p 20-24.

2 Knapton, J., Algin, H.M., (1995), *The Mathematical Solution to Interlock in Flexibly Bedded Clay Paving.* Proc. of the 4th. Int. Masonry Conf. No. 7, Vol. 2, p 307-313. London.

3 Knapton, J., Algin, H.M., (1996), *The Mathematical Solution to Interlock in Concrete Block Paving.* Proc. of the 5th. Int. Conf. on Concrete Block Paving, p 261-278, Tel-Aviv.

CHAPTER NINE

EVALUATION OF STRESSES IN BEDDING SAND WITHOUT INTERLOCK FOR PROPRIETORY SHAPED PAVERS

Synopsis

This Chapter explains how the solutions developed in Chapters 5, 7 and 8 can be used in the evaluation of vertical stresses in the bedding sand for the nine proprietory shaped pavers. The common patch loading (see Chapter 5) which functionally achieves the maximum stress values is used to compare the pavers in terms of the stress distributions which they generate. The vertical compressive stresses beneath the most commonly used nine shaped pavers (see Figure 5.1) can be analysed by applying the bedding sand stress calculation method (see Chapter 6) between the variations of the common patch loading and the stress regimes developed in Chapters 7 and 8. The developed algebrical solutions to the absolute-hexahedral stress blocks for the shaped pavers can directly be applied to the evaluation of the vertical stresses by using the variations of the common patch loading. In the other paver stress regimes, iterative solutions (see Appendix) have been developed and given in Figures 6.21, 9.1, 9.2, 9.3, 9.4, 9.5, 9.6, 9.7, 9.8 and 9.9.

9.1. Introduction

The solutions developed for the nine proprietory shaped pavers (see Figure 5.1) in Chapters 5, 7 and 8 are now used to determine relationship between patch load geometry (see Chapter 5) and resulting vertical compressive stress patterns (see Chapters 7 and 8). It may be recalled that apart from chamfered and non-chamfered rectangular pavers whose load patches and stress distributions have been described in Chapters 4 and 6 respectively, the most commonly used nine proprietory shaped pavers' patch loadings were analysed in Chapter 5 by using an extension of the method described for the rectangular pavers (see Chapter 4). It was shown in Chapter 6 that it has been possible to identify the patch load configuration which leads to the greatest vertical compressive stress values beneath the rectangular pavers. Therefore, in order to reduce the geometrical complexity of the work, a special load patch which functionally achieves the maximum vertical compressive stress values was assumed for analysing each proprietory shaped paver (see Chapter 5). This selected special patch loading which has also been applied to rectangular pavers in Chapter 6 (see Figure 6.21) is useful for allowing a meaningful comparison of the pavers in terms of the maximum stress values which they generate. The Chapter compares the proprietory shaped pavers according to the common patch loadings resulting vertical compressive stress patterns in bedding sand defined in Chapters 7 and 8.

9.2. Evaluation of vertical compressive stresses in bedding sand without interlock for proprietory shaped pavers

Common patch loadings which functionally generate maximum corner stress values have been applied to the shaped pavers so allowing a meaningful comparison of the effectiveness of each shape in load dissipation. Figures 9.1 to 9.9 show the bedding sand vertical compressive stress distributions are developed by the variations of the common patch loading for the analysed non-chamfered proprietory shaped pavers (see Figure 5.1). The stress values are taken from the solutions to the equations set out in Chapters 5, 7 and 8. The developed algebraical solutions of the absolute-hexahedral compressive stress regimes which occur beneath the circumscribing rectangular borders are given in

Chapters 7 and 8. In the other paver stress regimes, iterative solutions (see Appendix) have been developed. The following simple program for the proprietory shaped pavers is given as an example to explain how the solutions of the common patch loadings defined in Chapter 5 can be used in the evaluation of the algebraical solutions to the absolute-hexahedral compressive stress regimes are developed in Chapters 7 and 8.

```
1001 LPRINT "Calculation of vertical compressive stress distribution beneath proprietory shaped paver1 taking into account the selected special common patch load application 1's variations generating absolute-hexahedral stress pattern beneath the circumscribing rectangular border (see Figures 5.2 and 7 93 )"
1002 FOR o = 410 TO 390 STEP -5
1003 f = -75665 2 + 465 194 * o - .567306 * (o ^ 2)
1004 n = f * 8
1005 a = (.910259 * (-519 342 + o) * (62558 4 - 468 969 * o + o ^ 2)) / ((-596 352 + o) * (-223 654 + o))
1006 b = (.121857 * (1161 97 - o) * (-568 918 + o) * (-278 843 + o)) / ((-596 361 + o) * (-223 68 + o))
1007 s1 = - 0000234375# * n * (- 19315739961# * (10 ^ 18) * a * b + 7303924745# * (10 ^ 19) * a + .4323962476# * (10 ^ 20) * b + 1043393115# * (10 ^ 16) * a * (b ^ 2) - 4891665096# * (10 ^ 18) * (b ^ 2) - 107408454491# * (10 ^ 17) * (a ^ 2) + 17409013491# * (10 ^ 15) * (a ^ 2) * b + 353984880631# * (10 ^ 12) * (a ^ 2) * (b ^ 2) + 16801894381# * (10 ^ 9) * (a ^ 2) * (b ^ 3) + .1110196342# * (10 ^ 13) * a * (b ^ 3) + 175908762681# * (10 ^ 16) * (b ^ 3) - 119278654881# * (10 ^ 22))
1008 s2 = (-.2469302131# * (10 ^ 17) * a * b + .9907910263# * (10 ^ 18) * a + .5080156156# * (10 ^ 18) * b + 1181492973# * (10 ^ 15) * a * (b ^ 2) - .2621319312# * (10 ^ 16) * (b ^ 2) - 3368742768# * (10 ^ 16) * (a ^ 2) + 560592977799999991# * (10 ^ 14) * (a ^ 2) * b + 858851757581# * (10 ^ 11) * (a ^ 2) * (b ^ 2) + 30639393# * (10 ^ 8) * (a ^ 2) * (b ^ 3) + 801860253#1# * (10 ^ 11) * a * (b ^ 3) - .1559620943# * (10 ^ 13) * (b ^ 3) - .1981588516# * (10 ^ 20))
1009 sa = s1 / s2
1010 s3 = (-.00014648437#) * n * (-.2215695482# * (10 ^ 17) * a * b + 84308467341# * (10 ^ 18) * a + 51748074# * (10 ^ 19) * b + 1179738101# * (10 ^ 15) * a * (b ^ 2) - 5782105132000001# * (10 ^ 17) * (b ^ 2) - .1153553985# * (10 ^ 16) * (a ^ 2) + .1865247691# * (10 ^ 14) * (a ^ 2) * b + .3878649118# * (10 ^ 11) * (a ^ 2) * (b ^ 2) + 18719757# * (10 ^ 8) * (a ^ 2) * (b ^ 3) + .1272602698# * (10 ^ 12) * a * (b ^ 3) + .2053952491# * (10 ^ 15) * (b ^ 3) - .1440881846# * (10 ^ 21))
1011 sb = s3 / s2
1012 s4 = - 000046875# * n * (-.2922137113# * (10 ^ 17) * a * b + .7220976951# * (10 ^ 18) * a + 15699949741# * (10 ^ 20) * b + 271283631851# * (10 ^ 15) * a * (b ^ 2) - 214269372881# * (10 ^ 18) * (b ^ 2) + .2265418651# * (10 ^ 16) * (a ^ 2) - .4002282581# * (10 ^ 14) * (a ^ 2) * b - 1768602168# * (10 ^ 11) * (a ^ 2) * (b ^ 2) + 14555816# * (10 ^ 8) * (a ^ 2) * (b ^ 3) + 3795104378# * (10 ^ 12) * a * (b ^ 3) + .8993686294# * (10 ^ 15) * (b ^ 3) - 3650497507# * (10 ^ 21))
1013 sc = s4 / s2
1014 s5 = (.5859375# * (10 ^ -5)) * n * ( 150652415# * (10 ^ 17) * a * b + 2361800583# * (10 ^ 19) * a - 8201128385000001# * (10 ^ 20) * b - 94604190051# * (10 ^ 15) * a * (b ^ 2) + 1203015227# * (10 ^ 19) * (b ^ 2) - .3224788153# * (10 ^ 17) * (a ^ 2) + 550231224# * (10 ^ 15) * (a ^ 2) * b + .5877651185# * (10 ^ 12) * (a ^ 2) * (b ^ 2) + 87635319# * (10 ^ 8) * (a ^ 2) * (b ^ 3) - .1776804879# * (10 ^ 13) * a * (b ^ 3) - 52934797551# * (10 ^ 16) * (b ^ 3) + .1751456431# * (10 ^ 22))
1015 sd = s5 / s2
1016 s6 = (.29296875# * (10 ^ -5)) * n * (-.4199899221# * (10 ^ 18) * a * b + .2705171267# * (10 ^ 20) * a - 1731962998# * (10 ^ 21) * b - 104097975551# * (10 ^ 16) * a * (b ^ 2) + .3028879991# * (10 ^ 19) * (b ^ 2) - .1368601379# * (10 ^ 18) * (a ^ 2) + .2314671572# * (10 ^ 16) * (a ^ 2) * b + .2848150885# * (10 ^ 13) * (a ^ 2) * (b ^ 2) + .6822609931# * (10 ^ 9) * (a ^ 2) * (b ^ 3) - 3758540399# * (10 ^ 13) * a * (b ^ 3) - 14651119181# * (10 ^ 17) * (b ^ 3) + 2792504881# * (10 ^ 22))
1017 se = s6 / s2
1018 s7 = 00001171875# * n * (-.2291400483# * (10 ^ 18) * a * b + .1101735355# * (10 ^ 20) * a - .1208281235# * (10 ^ 20) * b + 54390188331# * (10 ^ 15) * a * (b ^ 2) + .3574233548# * (10 ^ 18) * (b ^ 2) - .3939769333# * (10 ^ 17) * (a ^ 2) + 6607478718000001# * (10 ^ 15) * (a ^ 2) * b + 91997731931# * (10 ^ 12) * (a ^ 2) * (b ^ 2) + 2807126531# * (10 ^ 9) * (a ^ 2) * (b ^ 3) - 417237035# * (10 ^ 11) * a * (b ^ 3) - 2061118296# * (10 ^ 16) * (b ^ 3) - 764012675# * (10 ^ 20))
1019 sf = s7 / s2
1020 s8 = ( 29296875# * (10 ^ -5)) * n * (- 12778675671# * (10 ^ 19) * a * b + 515381171# * (10 ^ 20) * a + 12962410351# * (10 ^ 21) * b + 5985729564# * (10 ^ 16) * a * (b ^ 2) - 12091844261# * (10 ^ 19) * (b ^ 2) - 13453785361# * (10 ^ 18) * (a ^ 2) + .2229383519# * (10 ^ 16) * (a ^ 2) * b + 35931696661# * (10 ^ 13) * (a ^ 2) * (b ^ 2) + 1366819497# * (10 ^ 10) * (a ^ 2) * (b ^ 3) + .4909891275# * (10 ^ 13) * a * (b ^ 3) + 344422227# * (10 ^ 16) * (b ^ 3) - 405322832# * (10 ^ 22))
1021 sg = s8 / s2
1022 s9 = 00001171875# * n * (-.4436094595# * (10 ^ 18) * a * b + 171389533# * (10 ^ 20) * a + .6362228848# * (10 ^ 20) * b + 23005792131# * (10 ^ 16) * a * (b ^ 2) - 7020927493# * (10 ^ 18) * (b ^ 2) - 38817122251# * (10 ^ 17) * (a ^ 2) + .6394258585# * (10 ^ 15) * (a ^ 2) * b + 11022320131# * (10 ^ 13) * (a ^ 2) * (b ^ 2) + 451852279# * (10 ^ 9) * (a ^ 2) * (b ^ 3) + .2125384215# * (10 ^ 13) * a * (b ^ 3) + 24627170631# * (10 ^ 16) * (b ^ 3) - 178783456#8 * (10 ^ 22))
1023 sh = s9 / s2
1024 h1 = (.29296875# * (10 ^ -5)) * n * (-.1324317434# * (10 ^ 19) * a * b + 46227701791# * (10 ^ 20) * a + 2636628861# * (10 ^ 21) * b + 835121280#5 * (10 ^ 16) * a * (b ^ 2) - 3431220533# * (10 ^ 19) * (b ^ 2) - 8290411417# * (10 ^ 17) * (a ^ 2) + 1343494309# * (10 ^ 16) * (a ^ 2) * b + 2736307405# * (10 ^ 13) * (a ^ 2) * (b ^ 2) + 1300418761# * (10 ^ 10) * (a ^ 2) * (b ^ 3) + .8706467499# * (10 ^ 13) * a * (b ^ 3) + .1391502793# * (10 ^ 17) * (b ^ 3) - .6440930291# * (10 ^ 22))
1025 si = h1 / s2
1026 h2 = .00001171875# * n * (-.2217264948# * (10 ^ 18) * a * b + 7487634378# * (10 ^ 19) * a + 4412156448# * (10 ^ 20) * b + 1475689597# * (10 ^ 16) * a * (b ^ 2) - 6022352555# * (10 ^ 18) * (b ^ 2) - .1366376238# * (10 ^ 17) * (a ^ 2) + 2208492691# * (10 ^ 15) * (a ^ 2) * b + 4609383783# * (10 ^ 12) * (a ^ 2) * (b ^ 2) + 223063767# * (10 ^ 9) * (a ^ 2) * (b ^ 3) + 1546977564# * (10 ^ 13) * a * (b ^ 3) + .2528022341# * (10 ^ 16) * (b ^ 3) - 1025761785# * (10 ^ 22))
1027 sj = h2 / s2
1028 h3 = (.29296875# * (10 ^ -5)) * n * (-.2466001751# * (10 ^ 18) * a * b - .6501330511# * (10 ^ 18) * a + 16894508371# * (10 ^ 21) * b + 4344606102# * (10 ^ 16) * a * (b ^ 2) - 2946198421# * (10 ^ 19) * (b ^ 2) + 3926934803# * (10 ^ 17) * (a ^ 2) - .6895919841# * (10 ^ 15) * (a ^ 2) * b - 3785473921# * (10 ^ 12) * (a ^ 2) * (b ^ 2) + 189160271# * (10 ^ 9) * (a ^ 2) * (b ^ 3) + .5897063764# * (10 ^ 13) * a * (b ^ 3) + .1423222498# * (10 ^ 17) * (b ^ 3) - 273943392# * (10 ^ 22))
1029 sk = h3 / s2
1030 h4 = (-.29296875# * (10 ^ -5)) * n * (-.1908112799# * (10 ^ 18) * a * b + .1692729734# * (10 ^ 20) * a - 8176845559# * (10 ^ 20) * b - 1896151686# * (10 ^ 16) * a * (b ^ 2) + 1923918911# * (10 ^ 19) * (b ^ 2) - .6751841273#9 * (10 ^ 17) * (a ^ 2) + 1149689217# * (10 ^ 16) * (a ^ 2) * b + 1271101284# * (10 ^ 13) * (a ^ 2) * (b ^ 2) + 219034211# * (10 ^ 9) * (a ^ 2) * (b ^ 3) - 3378506522# * (10 ^ 13) * a * (b ^ 3) - 10429286421# * (10 ^ 17) * (b ^ 3) + 401550771# * (10 ^ 21))
1031 sm = h4 / s2
1032 h5 = - 0000234375# * n * (-.8011646055# * (10 ^ 17) * a * b + 490692611# * (10 ^ 19) * a - 1136777346# * (10 ^ 20) * b - 1306309553# * (10 ^ 15) * a * (b ^ 2) + 3183460558# * (10 ^ 18) * (b ^ 2) - 1748534845# * (10 ^ 17) * (a ^ 2) + 2954872929# * (10 ^ 15) * (a ^ 2) * b + 367965241#4 * (10 ^ 12) * (a ^ 2) * (b ^ 2) + 90749222# * (10 ^ 8) * (a ^ 2) * (b ^ 3) - 447929645# * (10 ^ 12) * a * (b ^ 3) - .1811680761# * (10 ^ 16) * (b ^ 3) - .3860715125# * (10 ^ 20))
1033 sn = h5 / s2
1034 h6 = (- 00001464843751#) * n * (-.2275003912# * (10 ^ 18) * a * b + 1125462208# * (10 ^ 20) * a + .6784572521# * (10 ^ 19) * b + 434307929# * (10 ^ 15) * a * (b ^ 2) + 1895163748# * (10 ^ 18) * (b ^ 2) + 1641684# * (10 ^ 10) * a * (b ^ 3) + .2333166791# * (10 ^ 9) * (a ^ 2) * (b ^ 3) - 3212268462# * (10 ^ 17) * (a ^ 2) + 538443651#6 * (10 ^ 15) * (a ^ 2) * b + 7518960646# * (10 ^ 12) * (a ^ 2) * (b ^ 2) - 1617360018# * (10 ^ 16) * (b ^ 3) - 6813934332# * (10 ^ 21))
1035 so = h6 / s2
1036 h7 = (- 0001171875#) * n * (-.3747023323# * (10 ^ 17) * a * b + .1593545196# * (10 ^ 19) * a + .5296955391# * (10 ^ 19) * b + 149541542# * (10 ^ 15) * a * (b ^ 2) - .4228239925# * (10 ^ 17) * (b ^ 2) - 3439012583# * (10 ^ 16) * (a ^ 2) + 5696525723# * (10 ^ 14) * (a ^ 2) * b + 9221851765# * (10 ^ 11) * (a ^ 2) * (b ^ 2) + 35263807# * (10 ^ 8) * (a ^ 2) * (b ^ 3) + 1271248628# * (10 ^ 12) * a * (b ^ 3) + 9004738375# * (10 ^ 14) * (b ^ 3) - .1788647602# * (10 ^ 21))
1037 sp = h7 / s2
1038 h8 = (-.29296875# * (10 ^ -5)) * n * (-.1995379601# * (10 ^ 19) * a * b + 8075950942# * (10 ^ 20) * a + 336743266# * (10 ^ 21) * b + 9198248964# * (10 ^ 16) * a * (b ^ 2) - 3290482541# * (10 ^ 19) * (b ^ 2) + 867664009791# * (10 ^ 13) * a * (b ^ 3) + 185114189#9 * (10 ^ 10) * (a ^ 2) * (b ^ 3) - 158291138#8 * (10 ^ 18) * (a ^ 2) + .2606930204# * (10 ^ 16) * (a ^ 2) * b + .4504499098# * (10 ^ 13) * (b ^ 2) * (a ^ 2) + .1000854134# * (10 ^ 17) * (b ^ 3) - 102527003#6 * (10 ^ 23))
1039 sq = h8 / s2
1040 LPRINT "a=", a, "F=", f, "N=", n, "X=", a, "Y=", b
1041 LPRINT "Stress at Point A=", sa, "Stress at Point B=", sb
1042 LPRINT "Stress at Point C=", sc, "Stress at Point D=", sd
1043 LPRINT "Stress at Point E=", se, "Stress at Point F=", sf
1044 LPRINT "Stress at Point G=", sg, "Stress at Point H=", sh
1045 LPRINT "Stress at Point I=", si, "Stress at Point J=", sj
1046 LPRINT "Stress at Point K=", sk, "Stress at Point M=", sm
1047 LPRINT "Stress at Point N=", sn, "Stress at Point O=", so
```

```
1048 LPRINT "Stress at Point P=", sp, "Stress at Point Q=", sq
1049 NEXT o
1050 o=0 f=0 n=0 a=0 b=0 s1=0: s2=0: s3=0: s4=0: s5=0: s6=0: s7=0 s8=0: s9=0 h1=0 h2=0 h3=0: h4=0 h5=0. h6=0 h7=0 h8=0 sa=0 sb=0 sc=0 sd=0 se=0 sf=0 sg=0 sh=0 si=0 sj=0 sk=0 sm=0: sn=0: so=0: sp=0: sq=0
1051 LPRINT "Calculation of vertical compressive stress distribution beneath proprietory shaped paver 2 taking into account the selected special common patch load application 1's variations generating absolute-hexahedral stress pattern beneath the circumscribing rectangular border (see Figures 5 17 and 8 1)"
1052 FOR o = 440 TO 435 STEP -5
1053 f = (747.063 - o) * (-132.937 + o) / 4
1054 n = f * .8
1055 a = (-626.77 + o) * (-161 885 + o) * (128 656 + o) / (3 * (-747 063 + o) * (-132 937 + o))
1056 b = (-611 173 + o) * (-198 878 + o) * (150 051 + o) / (6 * (-750 887 + o) * (-129 113 + o))
1057 s1 = -4000 * n * (.363139423# * (10 ^ 9) * (b ^ 2) * a + .2967996345# * (10 ^ 13) * (b ^ 2) + 1469972651# * (10 ^ 13) * b * a - 5994645128# * (10 ^ 15) * b - 9261614208# * (10 ^ 14) * a + .2577032865# * (10 ^ 17))
1058 s2 = (.2421496444# * (10 ^ 13) * b * a + 256280043# * (10 ^ 9) * (b ^ 2) * a + 471128905 6# * (10 ^ 22) * b + .6723987732# * (10 ^ 18) * (b ^ 2) - 1509404581# * (10 ^ 15) * a - .2949439112# * (10 ^ 24))
1059 sa = s1 / s2
1060 s3 = -1000 * n * (.1310410647# * (10 ^ 10) * (b ^ 2) * a + .1182536013# * (10 ^ 14) * (b ^ 2) + 490650496# * (10 ^ 13) * b * a - .2274668619# * (10 ^ 16) * b - .3095146525# * (10 ^ 15) * a + .956164482# * (10 ^ 17))
1061 sb = s3 / s2
1062 s4 = -1000 * n * ( 1057825219# * (10 ^ 10) * (b ^ 2) * a + .9012539276# * (10 ^ 13) * (b ^ 2) + .4148747403# * (10 ^ 13) * b * a - 1830536 56# * (10 ^ 16) * b - 2615207028# * (10 ^ 15) * a + 7888722385# * (10 ^ 17))
1063 sc = s4 / s2
1064 s5 = -200 * n * (.3867655647# * (10 ^ 10) * (b ^ 2) * a + 445964439# * (10 ^ 14) * (b ^ 2) + .1100989057# * (10 ^ 14) * b * a - 7920758 48# * (10 ^ 16) * b - 698101206# * (10 ^ 15) * a + 3197874552# * (10 ^ 18))
1065 sd = s5 / s2
1066 s6 = -400 * n * (.2032239977# * (10 ^ 10) * (b ^ 2) * a + 291554294# * (10 ^ 14) * (b ^ 2) + .374913801# * (10 ^ 13) * b * a - 4608764018# * (10 ^ 16) * b - 240474 8678# * (10 ^ 15) * a + 1737235395# * (10 ^ 18))
1067 se = s6 / s2
1068 s7 = -200 * n * (.2643009507# * (10 ^ 10) * (b ^ 2) * a + .578446063# * (10 ^ 14) * (b ^ 2) - 2235580425# * (10 ^ 13) * b * a - 798563372# * (10 ^ 16) * b + 1285494225# * (10 ^ 15) * a + .2727984149# * (10 ^ 18))
1069 sf = s7 / s2
1070 s8 = -1000 * n * (.276016473# * (10 ^ 9) * (b ^ 2) * a + 875610040900000 1# * (10 ^ 13) * (b ^ 2) - 1204873642# * (10 ^ 13) * b * a - .115298 8685# * (10 ^ 16) * b + 7370446 42# * (10 ^ 14) * a + .3783045863# * (10 ^ 17))
1071 sg = s8 / s2
1072 s9 = 8000 * n * ( 1034702# * (10 ^ 7) * (b ^ 2) * a - .1082856239# * (10 ^ 13) * (b ^ 2) + .3939556165# * (10 ^ 12) * b * a + .1133262276# * (10 ^ 15) * b - 24450 3698# * (10 ^ 14) * a - 2862590728# * (10 ^ 16))
1073 sh = s9 / s2
1074 p1 = -5000 * n * ( 6217449# * (10 ^ 7) * (b ^ 2) * a + .2281146578# * (10 ^ 13) * (b ^ 2) - .7707931682# * (10 ^ 12) * b * a - .2331927464# * (10 ^ 15) * b + 4780691798# * (10 ^ 14) * a + 5686530112# * (10 ^ 16))
1075 si = p1 / s2
1076 p2 = 200000 * n * (555299 * (b ^ 2) * a - .5679553825# * (10 ^ 11) * (b ^ 2) + .2413675743# * (10 ^ 11) * b * a + 52138715# * (10 ^ 13) * b - 1499922529# * (10 ^ 13) * a - 1048389208# * (10 ^ 15))
1077 sj = p2 / s2
1078 p3 = 2000 * n * (.152846663# * (10 ^ 9) * (b ^ 2) * a - .3827652544# * (10 ^ 13) * (b ^ 2) + .2432154625# * (10 ^ 13) * b * a + 2868898265# * (10 ^ 15) * b - .1515136814# * (10 ^ 15) * a - 306350905# * (10 ^ 16))
1079 sk = p3 / s2
1080 p4 = 2000 * n * ( 279139377# * (10 ^ 9) * (b ^ 2) * a - .2421242116# * (10 ^ 13) * (b ^ 2) + .2811033402# * (10 ^ 13) * b * a + .64820797# * (10 ^ 14) * b - .1755109713# * (10 ^ 15) * a + 5301103125# * (10 ^ 16))
1081 sl = p4 / s2
1082 p5 = 2500 * n * ( 379018323# * (10 ^ 9) * (b ^ 2) * a + .1026048352# * (10 ^ 13) * (b ^ 2) + .2278192934# * (10 ^ 13) * b * a - 32333908# * (10 ^ 15) * b - 1428430626# * (10 ^ 15) * a + .1611349534# * (10 ^ 17))
1083 sm = p5 / s2
1084 p6 = 100 * n * ( 9869106693# * (10 ^ 10) * (b ^ 2) * a + 5308003865000001# * (10 ^ 14) * (b ^ 2) + .4993661429# * (10 ^ 14) * b * a - 10677016 12# * (10 ^ 17) * b - 3136773625# * (10 ^ 16) * a + .4581566309# * (10 ^ 18))
1085 smn = p6 / s2
1086 p7 = 4000 * n * (.295386049# * (10 ^ 9) * (b ^ 2) * a + .2252951606# * (10 ^ 13) * (b ^ 2) + 125765479 9# * (10 ^ 13) * b * a - 3841740648# * (10 ^ 15) * b - 7918005487999999# * (10 ^ 14) * a + 1516410729# * (10 ^ 17))
1087 sn = p7 / s2
1088 p8 = 1000 * n * ( 1039397151# * (10 ^ 10) * (b ^ 2) * a + 896518117 6# * (10 ^ 13) * (b ^ 2) + 405723355# * (10 ^ 13) * b * a - 1413506827# * (10 ^ 16) * b - 25577030 37# * (10 ^ 15) * a + .5319156275# * (10 ^ 17))
1089 so = p8 / s2
1090 p9 = 4000 * n * ( 269690503# * (10 ^ 9) * (b ^ 2) * a + 292701604# * (10 ^ 13) * (b ^ 2) + .8387281603# * (10 ^ 12) * b * a - 4182151845# * (10 ^ 15) * b - 530850024# * (10 ^ 14) * a + .1468087187# * (10 ^ 17))
1091 sp = p9 / s2
1092 h1 = 1000 * n * ( 794467923# * (10 ^ 9) * (b ^ 2) * a + .1161481366# * (10 ^ 14) * (b ^ 2) + 140814135 1# * (10 ^ 13) * b * a - 1426481874# * (10 ^ 16) * b - 90440178# * (10 ^ 14) * a + 4379375468# * (10 ^ 17))
1093 sq = h1 / s2
1094 h2 = 200 * n * ( 2709412473# * (10 ^ 10) * (b ^ 2) * a + 4400996403# * (10 ^ 14) * (b ^ 2) + 325191897# * (10 ^ 13) * b * a - .4911719077# * (10 ^ 16) * b - 21222799 15# * (10 ^ 15) * a + 1353226517# * (10 ^ 18))
1095 qr = h2 / s2
1096 h3 = 400 * n * ( 643971013# * (10 ^ 9) * (b ^ 2) * a + .2177185577# * (10 ^ 14) * (b ^ 2) - 324096873 8# * (10 ^ 13) * b * a - 1839912379# * (10 ^ 16) * b + 1986355833# * (10 ^ 15) * a + 3033699383# * (10 ^ 17))
1097 sr = h3 / s2
1098 h4 = 200 * n * ( 1484766333# * (10 ^ 10) * (b ^ 2) * a + 57258126 45# * (10 ^ 14) * (b ^ 2) - 9993542025# * (10 ^ 13) * b * a - 4976594313# * (10 ^ 16) * b + 614422637# * (10 ^ 15) * a + 8833361135# * (10 ^ 17))
1099 ss = h4 / s2
1100 h5 = 400 * n * ( 31647943# * (10 ^ 8) * (b ^ 2) * a + .28395937# * (10 ^ 14) * (b ^ 2) - 9863699235# * (10 ^ 13) * b * a - 1872349997# * (10 ^ 16) * b + 6119608975# * (10 ^ 15) * a + 684247365000000 1# * (10 ^ 16))
1101 st = h5 / s2
1102 h6 = -100 * n * ( 2399262513# * (10 ^ 10) * (b ^ 2) * a - 8545553939# * (10 ^ 14) * (b ^ 2) + 4703237251# * (10 ^ 14) * b * a + 3048019399# * (10 ^ 16) * b - 2927789387# * (10 ^ 16) * a + 13992234 89# * (10 ^ 18))
1103 su = h6 / s2
1104 h7 = -16000 * n * ( 23879581# * (10 ^ 8) * (b ^ 2) * a - 5311830431# * (10 ^ 12) * (b ^ 2) + 3547889 31# * (10 ^ 12) * b * a + 1135078175# * (10 ^ 14) * b - 2210805341# * (10 ^ 14) * a + .1341068831# * (10 ^ 16))
1105 sv = h7 / s2
1106 h8 = -100 * n * ( 5767068227# * (10 ^ 10) * (b ^ 2) * a - .4795126 13# * (10 ^ 14) * (b ^ 2) + 5713580661# * (10 ^ 14) * b * a - 2873821 39# * (10 ^ 16) * b - 3567717115# * (10 ^ 16) * a + 3629786735# * (10 ^ 18))
1107 sw = h8 / s2
1108 h9 = -400 * n * ( 1451337307# * (10 ^ 10) * (b ^ 2) * a - 5159748648# * (10 ^ 13) * (b ^ 2) + 1191978335# * (10 ^ 14) * b * a - 1289846733# * (10 ^ 16) * b - 7452598463# * (10 ^ 15) * a + 9990893873# * (10 ^ 17))
1109 sx = h9 / s2
1110 g1 = -100 * n * ( 9698019763# * (10 ^ 10) * (b ^ 2) * a + .5343705654000001# * (10 ^ 14) * (b ^ 2) + 484182887 1# * (10 ^ 14) * b * a - 1453927987# * (10 ^ 17) * b - 3041896526# * (10 ^ 16) * a + .696451076# * (10 ^ 18))
1111 sy = g1 / s2
1112 g2 = -2000 * n * ( 628962083# * (10 ^ 9) * (b ^ 2) * a + 40840914 11# * (10 ^ 13) * (b ^ 2) + 292146642# * (10 ^ 13) * b * a - 9644317019999999# * (10 ^ 15) * b - 1837108556# * (10 ^ 15) * a + .4412027427# * (10 ^ 17))
1113 sz = g2 / s2
1114 LPRINT "a=", o, "F=", f, "N=", n, "X=", a, "Y=", b
1115 LPRINT "Stress at Point A=", sa, "Stress at Point B=", sb
1116 LPRINT "Stress at Point C=", sc, "Stress at Point D=", sd
```

```
1117 LPRINT "Stress at Point E=", se, "Stress at Point F=", sf
1118 LPRINT "Stress at Point G=", sg, "Stress at Point H=", sh
1119 LPRINT "Stress at Point I=", si, "Stress at Point J=", sj
1120 LPRINT "Stress at Point K=", sk, "Stress at Point L=", sl
1121 LPRINT "Stress at Point M=", sm, "Stress at Point MN=", smn
1122 LPRINT "Stress at Point N=", sn, "Stress at Point O=", so
1123 LPRINT "Stress at Point P=", sp, "Stress at Point Q=", sq
1124 LPRINT "Stress at Point QR=", qr, "Stress at Point R=", sr
1125 LPRINT "Stress at Point S=", ss, "Stress at Point T=", st
1126 LPRINT "Stress at Point U=", su, "Stress at Point V=", sv
1127 LPRINT "Stress at Point W=", sw, "Stress at Point X=", sx
1128 LPRINT "Stress at Point Y=", sy, "Stress at Point Z=", sz
1129 NEXT o
1130 o=0 f=0 n=0 a=0 b=0 s1=0 s2=0. s3=0 s4=0 s5=0 s6=0 s7=0 s8=0 s9=0 h1=0 h2=0 h3=0 h4=0: h5=0 h6=0 h7=0 h8=0 h9=0 p1=0. p2=0 p3=0 p4=0 p5=0 p6=0 p7=0
p8=0: p9=0 g1=0 g2=0 sa=0 sb=0 sc=0 sd=0 se=0 sf=0: sg=0. sh=0 si=0 sj=0: sk=0 sl=0 sm=0: smn=0 sn=0 so=0 sp=0 sq=0 qr=0 sr=0 ss=0 st=0 su=0 sv=0 sw=0 sx=0
sy=0 sz=0
1131 LPRINT "Calculation of vertical compressive stress distribution beneath proprietory shaped paver 3 taking into account the selected special common patch load application 1's variations
generating absolute-hexahedral stress pattern beneath the circumscribing rectangular border (see Figures 5 25 and 8 2)"
1132 FOR o = 421.5 TO 375 STEP -5
1133 f = 230871 * (709 276 - o) * (-133 727 + o)
1134 n = f * 8
1135 a = 0104878 * (-647.884 + o) * (-192.216 + o) * (17453.4 + o) / ((-709 276 + o) * (-133 727 + o))
1136 b = 328085 * (-610 801 + o) * (50901 1 - 297 09 * o + o ^ 2) / ((-709 276 + o) * (-133 727 + o))
1137 s1 = -50000 * n * ( 10279094814# * (10 ^ 18) - 1008115815# * (10 ^ 16) * a + 2176413481# * (10 ^ 13) * (a ^ 2) - .5186086841999999# * (10 ^ 15) * b + .2674350372# * (10 ^ 13) *
a * b + 4934823419# * (10 ^ 10) * b * (a ^ 2))
1138 s2 = -.1207889122# * (10 ^ 26) + .7970603203# * (10 ^ 23) * a - 1201590023# * (10 ^ 23) * b + 7929036736# * (10 ^ 20) * b * a + 6924301845# * (10 ^ 12) * (a ^ 2) +
.1385603579# * (10 ^ 10) * b * (a ^ 2)
1139 sa = s1 / s2
1140 s3 = -250000 * n * (.1438457832# * (10 ^ 17) - 1375830429# * (10 ^ 15) * a + 2815192543# * (10 ^ 12) * (a ^ 2) - 6853724742999999# * (10 ^ 14) * b + 3538139444# * (10 ^ 12) *
a * b + 6496424299# * (10 ^ 9) * b * (a ^ 2))
1141 sb = s3 / s2
1142 s4 = -50000 * n * (.669925994# * (10 ^ 17) - 37550202# * (10 ^ 15) * a - 439267297# * (10 ^ 12) * (a ^ 2) - 7050320963999999# * (10 ^ 15) * b + 4196882753# * (10 ^ 13) * a * b
+ 3005575839# * (10 ^ 10) * b * (a ^ 2))
1143 sc = s4 / s2
1144 s5 = 50000 * n * ( 1323421108# * (10 ^ 17) - .4456769283# * (10 ^ 15) * a + 2364656809# * (10 ^ 13) * (a ^ 2) + 2313221581999999# * (10 ^ 15) * b - 1735438061# * (10 ^ 13) * a
* b + 1379096217# * (10 ^ 10) * b * (a ^ 2))
1145 sd = s5 / s2
1146 s6 = 50000 * n * ( 627243603# * (10 ^ 17) - .7028471012# * (10 ^ 15) * a + 1906669389# * (10 ^ 13) * (a ^ 2) - 4335999875999999# * (10 ^ 15) * b + 2238477 2# * (10 ^ 13) * a *
b + 4109439713# * (10 ^ 10) * b * (a ^ 2))
1147 se = s6 / s2
1148 s7 = 50000 * n * ( 3185630371# * (10 ^ 17) - .3826465005# * (10 ^ 15) * a + 1137852178# * (10 ^ 13) * (a ^ 2) - 2576775406999999# * (10 ^ 15) * b + 1331965524# * (10 ^ 13) *
a * b + .2422828439# * (10 ^ 10) * b * (a ^ 2))
1149 sf = s7 / s2
1150 s8 = 50000 * n * (.269260115# * (10 ^ 17) - .7023330594# * (10 ^ 14) * a - .7090113894# * (10 ^ 12) * (a ^ 2) - .6200234002999999# * (10 ^ 15) * b + 3761009582# * (10 ^ 13) * a * b
+ .2180192133# * (10 ^ 10) * b * (a ^ 2))
1151 sg = s8 / s2
1152 s9 = -50000 * n * ( 5330079894# * (10 ^ 17) - 7509456425# * (10 ^ 15) * a + .2634400994# * (10 ^ 13) * (a ^ 2) + .1463134614999999# * (10 ^ 15) * b - 1299564894# * (10 ^ 13) * a * b
+ 2204479923# * (10 ^ 10) * b * (a ^ 2))
1153 sh = s9 / s2
1154 LPRINT "a=", o, "F=", f, "N=", n, "X=", a, "Y=", b
1155 LPRINT "Stress at Point A=", sa, "Stress at Point B=", sb
1156 LPRINT "Stress at Point C=", sc, "Stress at Point D=", sd
1157 LPRINT "Stress at Point E=", se, "Stress at Point F=", sf
1158 LPRINT "Stress at Point G=", sg, "Stress at Point H=", sh
1159 NEXT o
1160 o=0 f=0 n=0 a=0 b=0 s1=0 s2=0 s3=0: s4=0 s5=0: s6=0 s7=0 s8=0 s9=0 sa=0 sb=0 sc=0 sd=0: se=0 sf=0 sg=0 sh=0
1161 LPRINT "Calculation of vertical compressive stress distribution beneath proprietory shaped paver 4 taking into account the selected special common patch load application 1's variations
generating absolute-hexahedral stress pattern beneath the circumscribing rectangular border (see Figures 5 28 and 8 3)"
1162 FOR o = 380 TO 320 STEP -5
1163 f = 202381 * (662.926 - o) * (-97.0741 + o)
1164 n = f * 8
1165 a = 174603 * (-564 586 + o) * (-158 54 + o) * (728 58 + o) / ((-662.926 + o) * (-97 0741 + o))
1166 b = 246032 * (-553 653 + o) * (33084.2 - 220 54 * o + o ^ 2) / ((-662 926 + o) * (-97 0741 + o))
1167 s1 = -2000 * n * ( 9571785326# * (10 ^ 15) - 1092335575# * (10 ^ 14) * a + 2820562946# * (10 ^ 11) * (a ^ 2) - 727805565# * (10 ^ 13) * b + 4133418518# * (10 ^ 11) * a * b +
96964381# * (10 ^ 8) * b * (a ^ 2))
1168 s2 = - 4437469628# * (10 ^ 22) + .2929815686# * (10 ^ 20) * a + .2854278086# * (10 ^ 17) * (a ^ 2) + 2015723036# * (10 ^ 14) * b - 2636156014# * (10 ^ 12) * a * b +
843487527# * (10 ^ 9) * b * (a ^ 2)
1169 sa = s1 / s2
1170 s3 = -2000 * n * ( 8257178974# * (10 ^ 15) - 73748442# * (10 ^ 13) * a + .9043079 4# * (10 ^ 10) * (a ^ 2) - 9962830844# * (10 ^ 13) * b + 6297255858# * (10 ^ 11) * a * b +
85031380999999999# * (10 ^ 8) * b * (a ^ 2))
1171 sb = s3 / s2
1172 s4 = -2000 * n * ( 2253891094# * (10 ^ 15) + .1056385168# * (10 ^ 13) * a - 204424207# * (10 ^ 11) * (a ^ 2) - 6812901572# * (10 ^ 13) * b + 4869564518# * (10 ^ 11) * a * b +
16101381# * (10 ^ 8) * b * (a ^ 2))
1173 sc = s4 / s2
1174 s5 = -2000 * n * (.1724057523# * (10 ^ 15) + 3193237402# * (10 ^ 13) * a - .3344037074# * (10 ^ 11) * (a ^ 2) - .9295891024# * (10 ^ 13) * b + 676976701# * (10 ^ 11) * a * b +
12604381# * (10 ^ 8) * b * (a ^ 2))
1175 sd = s5 / s2
1176 s6 = 2000 * n * (.2827176824# * (10 ^ 15) - .6644932646# * (10 ^ 13) * a + 3384767076# * (10 ^ 11) * (a ^ 2) + .1079088982# * (10 ^ 13) * b - .1409853262# * (10 ^ 11) * a * b +
45113619# * (10 ^ 8) * b * (a ^ 2))
1177 se = s6 / s2
1178 s7 = 2000 * n * ( 659363839# * (10 ^ 15) - 8684968572# * (10 ^ 13) * a + 2809037074# * (10 ^ 11) * (a ^ 2) - 7339498800000001# * (10 ^ 13) * b + 4213695332# * (10 ^ 11) * a *
b + 94395619# * (10 ^ 8) * b * (a ^ 2))
1179 sf = s7 / s2
1180 s8 = 2000 * n * (.3984380842# * (10 ^ 15) - .5175183546# * (10 ^ 13) * a + .1642992 7# * (10 ^ 11) * (a ^ 2) - 5663642296# * (10 ^ 13) * b + 3368032236# * (10 ^ 11) * a * b +
.64148619# * (10 ^ 8) * b * (a ^ 2))
1181 sg = s8 / s2
1182 s9 = 2000 * n * ( 2139940918# * (10 ^ 15) + 5101802 8# * (10 ^ 12) * a - 157305794# * (10 ^ 11) * (a ^ 2) - 1083140894# * (10 ^ 14) * b + 7432072068# * (10 ^ 11) * a * b +
48718619# * (10 ^ 8) * b * (a ^ 2))
1183 sh = s9 / s2
1184 p1 = 2000 * n * (-.1254089414# * (10 ^ 15) + .5431624 8# * (10 ^ 13) * a - 3355562946# * (10 ^ 11) * (a ^ 2) - 935731617# * (10 ^ 13) * b + 6850043823999999# * (10 ^ 11) * a *
b + 10035619# * (10 ^ 8) * b * (a ^ 2))
1185 si = p1 / s2
1186 p2 = -2000 * n * ( 502055098# * (10 ^ 15) - 7471660506# * (10 ^ 13) * a + 2779832946# * (10 ^ 11) * (a ^ 2) + 9387483894# * (10 ^ 12) * b - .1226495229# * (10 ^ 11) * a * b +
39246381# * (10 ^ 8) * b * (a ^ 2))
1187 sj = p2 / s2
1188 LPRINT "a=", o, "F=", f, "N=", n, "X=", a, "Y=", b
1189 LPRINT "Stress at Point A=", sa, "Stress at Point B=", sb
1190 LPRINT "Stress at Point C=", sc, "Stress at Point D=", sd
1191 LPRINT "Stress at Point E=", se, "Stress at Point F=", sf
1192 LPRINT "Stress at Point G=", sg, "Stress at Point H=", sh
```

```
1193 LPRINT "Stress at Point I="; si, "Stress at Point J="; sj
1194 NEXT o
1195 o=0 f=0 n=0 a=0 b=0 s1=0: s2=0: s3=0: s4=0: s5=0: s6=0: s7=0: s8=0: s9=0: p1=0: p2=0 sa=0: sb=0: sc=0: sd=0: se=0: sf=0: sg=0: sh=0: si=0: sj=0
1196 LPRINT "Calculation of vertical compressive stress distribution beneath proprietory shaped paver 5 taking into account the selected special common patch load application 1's variations generating absolute-hexahedral stress pattern beneath the circumscribing rectangular border (see Figures 5 31 and 8 4)"
1197 FOR o = 440 TO 355 STEP -5
1198 f = .16177 * (799 426 - o) * (-80.5503 + o)
1199 n = f * .8
1200 a = (.215694 * (669.612 - o) * (-136 802 + o) * (506 415 + o)) / (-64394 + 879 976 * o - (o ^ 2))
1201 b = (.225481 * (652.185 - o) * (34124 4 - 179 993 * o + (o ^ 2))) / (-64394 + 879 976 * o - (o ^ 2))
1202 s1 = -210000 * n * ( 74496093# * (10 ^ 8) * (a ^ 2) * b + 4971898187# * (10 ^ 11) * (a ^ 2) + .1141895545# * (10 ^ 12) * a * b - .2211833717# * (10 ^ 14) * a - 184157932# * (10 ^ 14) * b + 2178127107# * (10 ^ 16))
1203 s2 = (.4212997008# * (10 ^ 19) * a * b + .6072454491# * (10 ^ 10) * (a ^ 2) * b + .8372042508999999# * (10 ^ 22) * a - .3961850825# * (10 ^ 13) * (a ^ 2) - .6199341980999999# * (10 ^ 21) * b - .12319291 88# * (10 ^ 25))
1204 sa = s1 / s2
1205 s3 = -1050 * n * (.9673567803000001# * (10 ^ 10) * (a ^ 2) * b + .4884682975# * (10 ^ 13) * (a ^ 2) + .1690810523# * (10 ^ 14) * a * b - 2718806571# * (10 ^ 16) * a - 2697451044# * (10 ^ 16) * b + .2943011802# * (10 ^ 18))
1206 sb = s3 / s2
1207 s4 = -2100 * n * (.3521396089# * (10 ^ 10) * (a ^ 2) * b - .2832165968# * (10 ^ 13) * (a ^ 2) + 1242907569# * (10 ^ 14) * a * b - 1992110045# * (10 ^ 15) * a - 1905160723# * (10 ^ 16) * b + 9063706615# * (10 ^ 17))
1208 sc = s4 / s2
1209 s5 = -10500 * n * ( 442398337# * (10 ^ 9) * (a ^ 2) * b - .1086704137# * (10 ^ 13) * (a ^ 2) + .2553156486# * (10 ^ 13) * a * b + 9433264 66# * (10 ^ 14) * a - 385270948# * (10 ^ 15) * b + .964903693# * (10 ^ 16))
1210 sd = s5 / s2
1211 s6 = 10500 * n * ( 1469285789# * (10 ^ 10) * (a ^ 2) * b + .981400374# * (10 ^ 12) * (a ^ 2) + 2289204232# * (10 ^ 13) * a * b - 3606150647# * (10 ^ 15) * a - 3686655736# * (10 ^ 15) * b + 318139804# * (10 ^ 17))
1212 se = s6 / s2
1213 s7 = 4200 * n * ( 2366801773# * (10 ^ 10) * (a ^ 2) * b + .1188722588# * (10 ^ 13) * (a ^ 2) + 4240559163# * (10 ^ 13) * a * b - 4753224458# * (10 ^ 15) * a - 675237035# * (10 ^ 15) * b + .4420389 07# * (10 ^ 17))
1214 sf = s7 / s2
1215 s8 = 1050 * n * ( 6836431467# * (10 ^ 10) * (a ^ 2) * b - .5794124565# * (10 ^ 13) * (a ^ 2) + .2491228279# * (10 ^ 14) * a * b + 419094778# * (10 ^ 15) * a - .3813818542# * (10 ^ 16) * b + 637885149# * (10 ^ 17))
1216 sg = s8 / s2
1217 s9 = 10500 * n * (.161078067# * (10 ^ 9) * (a ^ 2) * b - .1085323796# * (10 ^ 13) * (a ^ 2) + .1898247712# * (10 ^ 13) * a * b + 2123955642# * (10 ^ 15) * a - 282811094 6# * (10 ^ 15) * b - 775357263# * (10 ^ 16))
1218 sh = s9 / s2
1219 LPRINT "a="; o, "F="; f, "N="; n, "X="; a, "Y="; b
1220 LPRINT "Stress at Point A="; sa, "Stress at Point B="; sb
1221 LPRINT "Stress at Point C="; sc, "Stress at Point D="; sd
1222 LPRINT "Stress at Point E="; se, "Stress at Point F="; sf
1223 LPRINT "Stress at Point G="; sg, "Stress at Point H="; sh
1224 NEXT o
1225 o=0 f=0.n=0.a=0.b=0.s1=0: s2=0: s3=0: s4=0 s5=0: s6=0: s7=0: s8=0: s9=0 sa=0: sb=0: sc=0: sd=0 se=0 sf=0: sg=0: sh=0
1226 LPRINT "Calculation of vertical compressive stress distribution beneath proprietory shaped paver 6 taking into account the selected special common patch load application 1's variations generating absolute-hexahedral stress pattern beneath the circumscribing rectangular border (see Figures 5 33 and 8 5)"
1227 FOR o = 504 TO 429 STEP -5
1228 f = -44114 + 252 * o - (o ^ 2) / 4
1229 n = f * .8
1230 a = (-18253704 + 247968 * o - 1002 * (o ^ 2) + (o ^ 3)) / (3 * (176456 - 1008 * o + o ^ 2))
1231 b = (87642408 - 247968 * o - 510 * (o ^ 2) + (o ^ 3)) / (6 * (176456 - 1008 * o + o ^ 2))
1232 s1 = (-1 / 50) * (n * (-315784067125# + 390004905 * a + 335419410 * b + 24112296 * a * b))
1233 s2 = (22796259150449# + 181453583376# * b)
1234 sa = s1 / s2
1235 s3 = (-1 / 26075) * (n * (-1065415434399925# - 1501771336305# * a + 1680913151265# * b + 66942734 04# * a * b))
1236 sb = s3 / s2
1237 s4 = (1 / 52150) * (n * (-4632427034485# + 3176236255209# * a - 25166980 83750# * b + 69964549 20# * a * b))
1238 sc = s4 / s2
1239 s5 = (1 / 52150) * (n * (-51144305087095# + 4540363370619# * a - 3721491626910# * b + 1170068 6088# * a * b))
1240 sd = s5 / s2
1241 s6 = (1 / 350) * (n * (-1378790910605# + 582860009 1# * a + 562327 1310# * b + 168786072 * a * b))
1242 se = s6 / s2
1243 s7 = (1 / 26075) * (n * (-445800752743 10# - 1270928187483# * a + 1924925641545# * b + 66942734 04# * a * b))
1244 sf = s7 / s2
1245 s8 = (-1 / 10430) * (n * (-25711072673143# + 542909991513# * a - 600944612862# * b + 1399290984 * a * b))
1246 sg = s8 / s2
1247 s9 = (-1 / 52150) * (n * (-175067241418325# + 40786770729 75# * a - 4209516607470# * b + 1170068 6088# * a * b))
1248 sh = s9 / s2
1249 LPRINT "a="; o, "F="; f, "N="; n, "X="; a, "Y="; b
1250 LPRINT "Stress at Point A="; sa, "Stress at Point B="; sb
1251 LPRINT "Stress at Point C="; sc, "Stress at Point D="; sd
1252 LPRINT "Stress at Point E="; se, "Stress at Point F="; sf
1253 LPRINT "Stress at Point G="; sg, "Stress at Point H="; sh
1254 NEXT o
1255 o=0 f=0:n=0 a=0 b=0:s1=0: s2=0: s3=0. s4=0: s5=0: s6=0: s7=0: s8=0 s9=0 sa=0 sb=0 sc=0 sd=0 se=0 sf=0 sg=0. sh=0
1256 LPRINT "Calculation of vertical compressive stress distribution beneath proprietory shaped paver 7 taking into account the selected special common patch load application 1's variations generating absolute-hexahedral stress pattern beneath the circumscribing rectangular border (see Figures 5 36 and 8 6)"
1257 FOR o = 360 TO 310 STEP -5
1258 f = 185715 * (639 419 - o) * (-80 5792 + o)
1259 n = f * .8
1260 a = ( 152382 * (553 083 - o) * (-127 625 + o) * (781 956 + o)) / (-51523 9 + 719 998 * o - o ^ 2)
1261 b = ( 257142 * (530 745 - o) * (31046.2 - 199 255 * o + o ^ 2)) / (-51523 9 + 719 998 * o - o ^ 2)
1262 s1 = - 125 * (10 ^ 7) * n * ( 1042369 * (10 ^ 7) * (b ^ 2) * a + 2258746626# * (10 ^ 10) * (b ^ 2) + 906816314# * (10 ^ 9) * a * b - 3661421322# * (10 ^ 12) * b - 4833249702# * (10 ^ 11) * a + 1271340831# * (10 ^ 14))
1263 s2 = (.4330422043# * (10 ^ 12) * a * b + .1025997637# * (10 ^ 10) * (b ^ 2) * a + .41410163 86# * (10 ^ 21) * b + 1058704044# * (10 ^ 19) * (b ^ 2) - 2455005165# * (10 ^ 14) * a - 2355030896# * (10 ^ 23))
1264 sa = s1 / s2
1265 s3 = -6250 * n * ( 118518089# * (10 ^ 9) * (b ^ 2) * a + 3401812798# * (10 ^ 12) * (b ^ 2) + .1213061354# * (10 ^ 12) * a * b - 5459445546# * (10 ^ 14) * b - .6412404548# * (10 ^ 13) * a + 1887067727# * (10 ^ 16))
1266 sb = s3 / s2
1267 s4 = 6250 * n * ( 379151797# * (10 ^ 9) * (b ^ 2) * a - 5002189548# * (10 ^ 12) * (b ^ 2) + 5111599 04# * (10 ^ 11) * a * b + .4767200576# * (10 ^ 14) * b - 3537689904# * (10 ^ 13) * a - .1132083909# * (10 ^ 16))
1268 sc = s4 / s2
1269 s5 = 100000 * n * ( 31810327# * (10 ^ 8) * (b ^ 2) * a - .2405870238# * (10 ^ 11) * (b ^ 2) + .8023821275# * (10 ^ 10) * a * b + 1652412498# * (10 ^ 13) * b - 4849949451# * (10 ^ 12) * a - 2218300679# * (10 ^ 14))
1270 sd = s5 / s2
1271 s6 = 50000 * n * (.24038762# * (10 ^ 8) * (b ^ 2) * a + .5138770815# * (10 ^ 11) * (b ^ 2) + 2017869726# * (10 ^ 11) * a * b - 6880982875# * (10 ^ 13) * b - .1077648068# * (10 ^ 13) * a + 2162368638# * (10 ^ 15))
1272 se = s6 / s2
1273 s7 = 31250 * n * (.20470877# * (10 ^ 8) * (b ^ 2) * a + 5990672396# * (10 ^ 11) * (b ^ 2) + .2027449 01# * (10 ^ 11) * a * b - .7282778404# * (10 ^ 13) * b - 1073417938# * (10 ^ 13) * a + 214856195# * (10 ^ 15))
```

```
1274 sf = s7 / s2
1275 s8 = -6250 * n * (.395315501# * (10 ^ 9) * (b ^ 2) * a - .4595712948# * (10 ^ 12) * (b ^ 2) + 7104967524# * (10 ^ 11) * a * b + 2949144232# * (10 ^ 14) * b - .4583004766# * (10 ^
13) * a - 319297156# * (10 ^ 15))
1276 sg = s8 / s2
1277 s9 = -50000 * n * ( 65641117# * (10 ^ 8) * (b ^ 2) * a - .4303644725# * (10 ^ 11) * (b ^ 2) + 1853935315# * (10 ^ 11) * a * b + 1032254565# * (10 ^ 13) * b - 110065424## * (10 ^
13) * a + .57232330499999999# * (10 ^ 14))
1278 sh = s9 / s2
1279 LPRINT "a="; o, "F="; f, "N="; n, "X="; a, "Y="; b
1280 LPRINT "Stress at Point A="; sa, "Stress at Point B="; sb
1281 LPRINT "Stress at Point C="; sc, "Stress at Point D="; sd
1282 LPRINT "Stress at Point E="; se, "Stress at Point F="; sf
1283 LPRINT "Stress at Point G="; sg, "Stress at Point H="; sh
1284 NEXT o
1285 o=0.f=0 n=0 a=0 b=0 s1=0: s2=0 s3=0: s4=0: s5=0. s6=0: s7=0: s8=0: s9=0.sa=0: sb=0: sc=0: sd=0. se=0: sf=0: sg=0: sh=0
1286 LPRINT "Calculation of vertical compressive stress distribution beneath proprietory shaped paver 8 taking into account the selected special common patch load application 1's variations
generating absolute-hexahedral stress pattern beneath the circumscribing rectangular border (see Figures 5 38 and 8 7)"
1287 FOR o = 400 TO 350 STEP -5
1288 f = (-90200 + 800 * o - (o ^ 2)) / 4
1289 n = f * 8
1290 a = (11060000 - 600 * (o ^ 2) + (o ^ 3)) / (3 * (90200 - 800 * o + (o ^ 2)))
1291 b = (11060000 - 600 * (o ^ 2) + (o ^ 3)) / (6 * (90200 - 800 * o + (o ^ 2)))
1292 s1 = -n * (1696869 * a * b + 11989579350# * a + 32490640500# * b - 32816542951004)
1293 s2 = 27216939500# * (27 * b + 286960)
1294 sa = s1 / s2
1295 s3 = -n * (1131489 * a * b + 5980636950# * a - 2680760055100# + 32547178500# * b)
1296 sb = s3 / s2
1297 s4 = -n * (792261 * a * b + 4186434930# * a - 2011434942100# + 22783003080# * b)
1298 sc = s4 / s2
1299 s5 = -n * (729 * a * b - 4226084430# * a - 1170183006100# + 22862156280# * b)
1300 sd = s5 / s2
1301 s6 = -n * (729 * a * b - 6037247850# * a - 1478971575100# + 32660254500# * b)
1302 se = s6 / s2
1303 s7 = n * (564651 * a * b + 12046190250# * a + 878077335100# - 32716792500# * b)
1304 sf = s7 / s2
1305 s8 = n * (1695411 * a * b + 11989652250# * a - 2382301604900# + 32490786300# * b)
1306 sg = s8 / s2
1307 s9 = n * (1130031 * a * b + 5980709850# * a - 1781407364900# + 32547324300# * b)
1308 sh = s9 / s2
1309 p1 = n * (790803 * a * b + 4186507830# * a - 1112082251900# + 22783148880# * b)
1310 si = p1 / s2
1311 p2 = -n * (729 * a * b + 4226011530# * a + 270830315900# - 22862302080# * b)
1312 sj = p2 / s2
1313 p3 = -n * (729 * a * b + 6037174950# * a + 579618884900# - 32660400300# * b)
1314 sk = p3 / s2
1315 p4 = -n * (12046117350# * a + 566109 * a * b - 32716938300# * b - 21275355100#)
1316 sl = p4 / s2
1317 LPRINT "a="; o, "F="; f, "N="; n, "X="; a, "Y="; b
1318 LPRINT "Stress at Point A="; sa, "Stress at Point B="; sb
1319 LPRINT "Stress at Point C="; sc, "Stress at Point D="; sd
1320 LPRINT "Stress at Point E="; se, "Stress at Point F="; sf
1321 LPRINT "Stress at Point G="; sg, "Stress at Point H="; sh
1322 LPRINT "Stress at Point I="; si, "Stress at Point J="; sj
1323 LPRINT "Stress at Point K="; sk, "Stress at Point L="; sl
1324 NEXT o
1325 o=0 f=0 n=0 a=0 b=0.s1=0: s2=0: s3=0. s4=0: s5=0: s6=0: s7=0: s8=0. s9=0: p1=0. p2=0: p3=0. p4=0 sa=0 sb=0 sc=0 sd=0 se=0 sf=0: sg=0. sh=0: si=0: sj=0 sk=0 sl=0
1326 LPRINT "Calculation of vertical compressive stress distribution beneath proprietory shaped paver 9 taking into account the selected special common patch load application 1's variations
generating absolute-hexahedral stress pattern beneath the circumscribing rectangular border (see Figures 5 41 and 8 8)"
1327 FOR o = 450 TO 375 STEP -5
1328 f = .383318 * (706 918 - o) * (-193 094 + o)
1329 n = f * .8
1330 a = ( 511091 * (606 49 - o) * (24483 8 - 293 51 * o + o ^ 2)) / (-136502 + 900 012 * o - o ^ 2)
1331 b = ( 077809 * (635 868 - o) * (-235.334 + o) * (935 488 + o)) / (-136502 + 900 012 * o - o ^ 2)
1332 s1 = - 1304347826# * n * ( 19285372534 * (10 ^ 10) * (a ^ 2) * b + .8401195114# * (10 ^ 12) * (a ^ 2) + 9625744522# * (10 ^ 12) * a * b - .358354#074# * (10 ^ 15) * a -
192936803# * (10 ^ 15) * b + 35195593984 * (10 ^ 17))
1333 s2 = ( 1520804086# * (10 ^ 15) * a * b + 891 * (a ^ 2) * b + 1151692957# * (10 ^ 18) * a + 1038# * (10 ^ 7) * (a ^ 2) - 2331899603# * (10 ^ 17) * b - 17659291994 * (10 ^ 20))
1334 sa = s1 / s2
1335 s3 = - 5217391304# * n * (.261209774 * (10 ^ 9) * (a ^ 2) * b - 252857985# * (10 ^ 11) * (a ^ 2) + 4672437753# * (10 ^ 12) * a * b - .3719236444 * (10 ^ 14) * a - 7778538235# *
(10 ^ 14) * b + 629732643# * (10 ^ 16))
1336 sb = s3 / s2
1337 s4 = .1304347826# * n * ( 475896087# * (10 ^ 9) * (a ^ 2) * b + .9807389176# * (10 ^ 12) * (a ^ 2) - 1607764065# * (10 ^ 13) * a * b - 1302422044# * (10 ^ 15) * a + 2353349776#
* (10 ^ 15) * b - 3087790332# * (10 ^ 16))
1338 sc = s4 / s2
1339 s5 = 6 52173913# * n * ( 38184661# * (10 ^ 8) * (a ^ 2) * b + 1683976417# * (10 ^ 11) * (a ^ 2) + .2038724453# * (10 ^ 11) * a * b - 5729028135999999# * (10 ^ 13) * a -
40238079644 * (10 ^ 13) * b + .4825294144# * (10 ^ 15))
1340 sd = s5 / s2
1341 s6 = 2608695652# * n * ( 51276785300000014 * (10 ^ 9) * (a ^ 2) * b - 496372486# * (10 ^ 11) * (a ^ 2) + .9628814378# * (10 ^ 12) * a * b - 3843302864 * (10 ^ 14) * a -
1596975623# * (10 ^ 15) * b + .7060912444 * (10 ^ 16))
1342 se = s6 / s2
1343 s7 = -1.304347826# * n * (.49520029# * (10 ^ 8) * (a ^ 2) * b + 97887022064 * (10 ^ 11) * (a ^ 2) - 16645518394 * (10 ^ 12) * a * b - 2021456054 * (10 ^ 14) * a + 2435885728# *
(10 ^ 14) * b + 798133292# * (10 ^ 15))
1344 sf = s7 / s2
1345 LPRINT "a="; o, "F="; f, "N="; n, "X="; a, "Y="; b
1346 LPRINT "Stress at Point A="; sa, "Stress at Point B="; sb
1347 LPRINT "Stress at Point C="; sc, "Stress at Point D="; sd
1348 LPRINT "Stress at Point E="; se, "Stress at Point F="; sf
1349 NEXT o
1350 END
```

The results of this program can be seen in the last sections of the a distances which define the position of the common patch load applications in Figures 9.1 to 9.9. Figures 6.21, 9.1, 9.2, 9.3, 9.4, 9.5, 9.6, 9.7, 9.8 and 9.9 show the vertical compressive stress

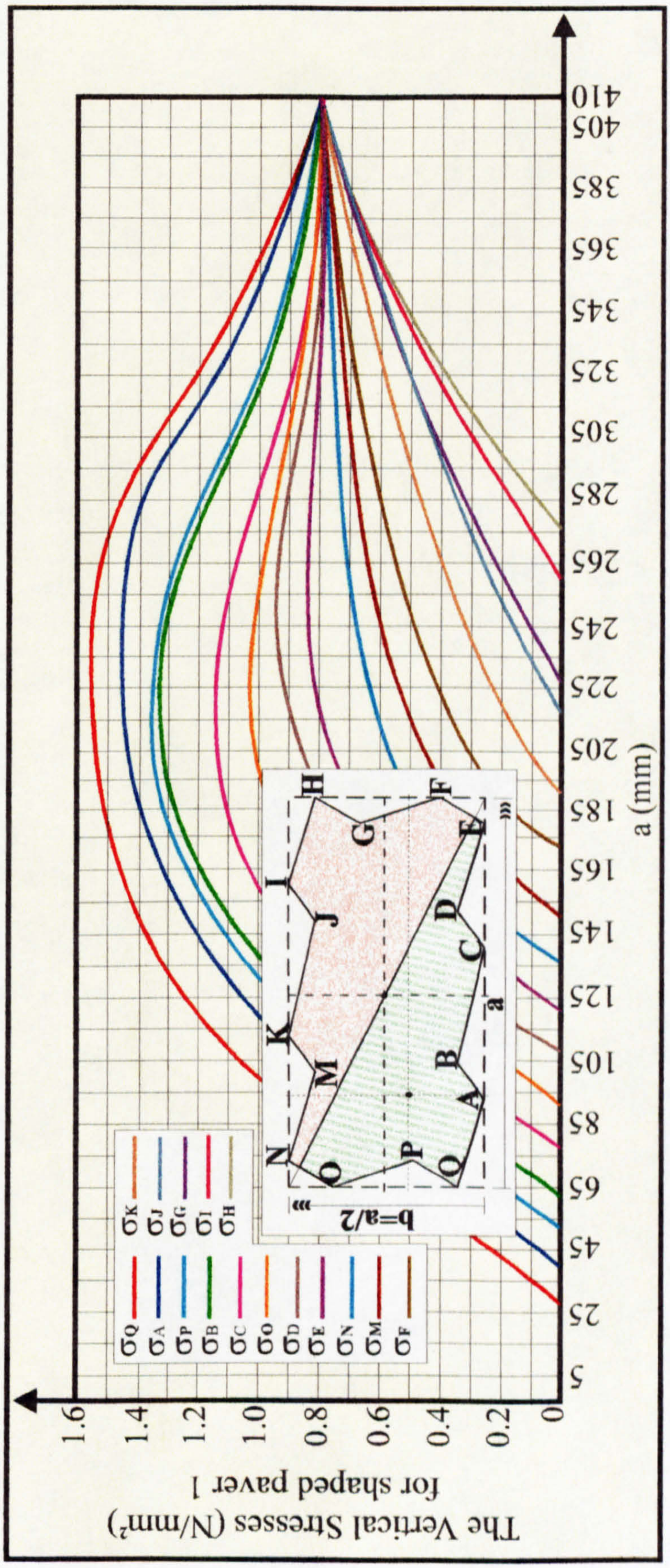

Figure 9.1: Bedding sand vertical stress distributions are developed by the variations of common patch loading (applied pressure= 0.8N/mm²) for non-chamfered common proprietory shaped paver 1.

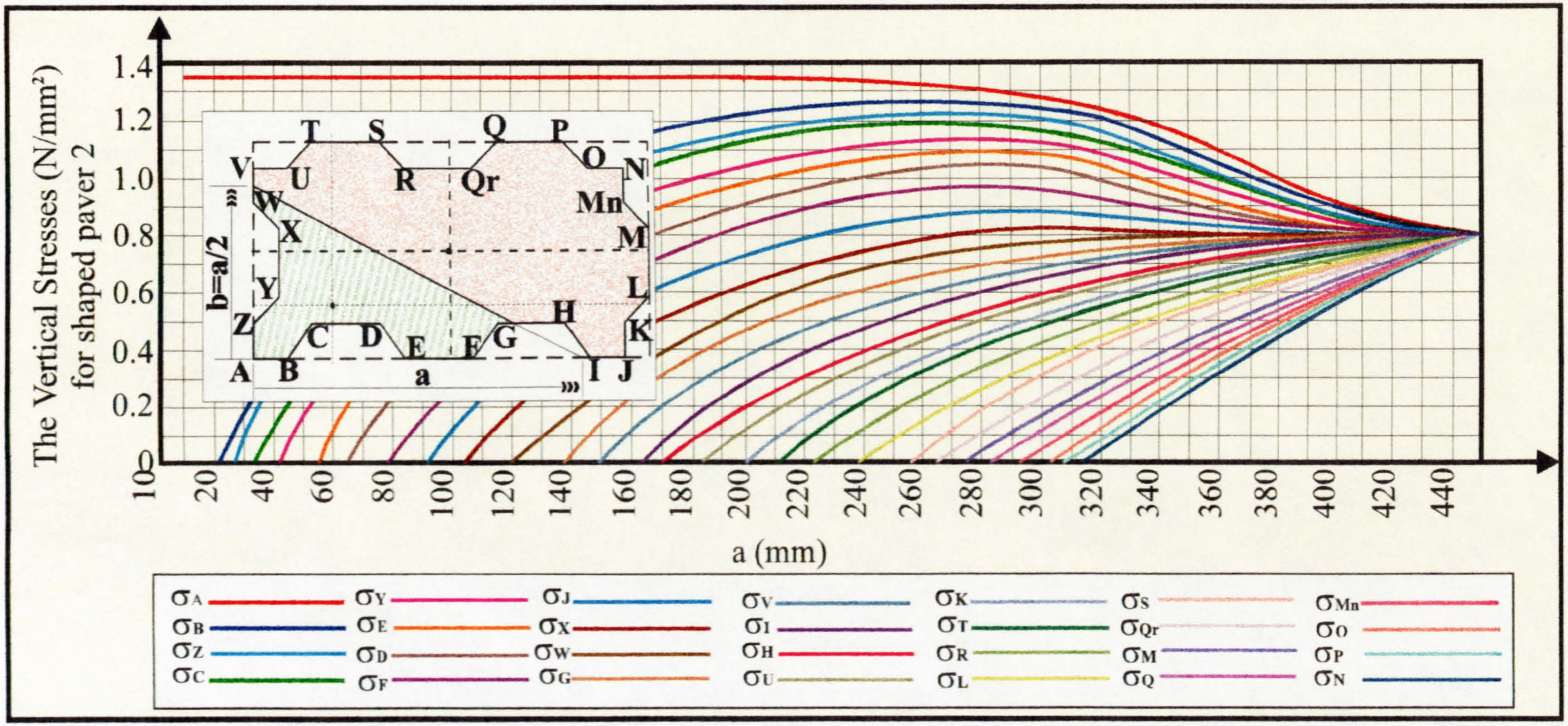

Figure 9.2: Bedding sand vertical stress distributions are developed by the variations of common patch loading (applied pressure= 0.8N/mm²) for non-chamfered common proprietory shaped paver 2.

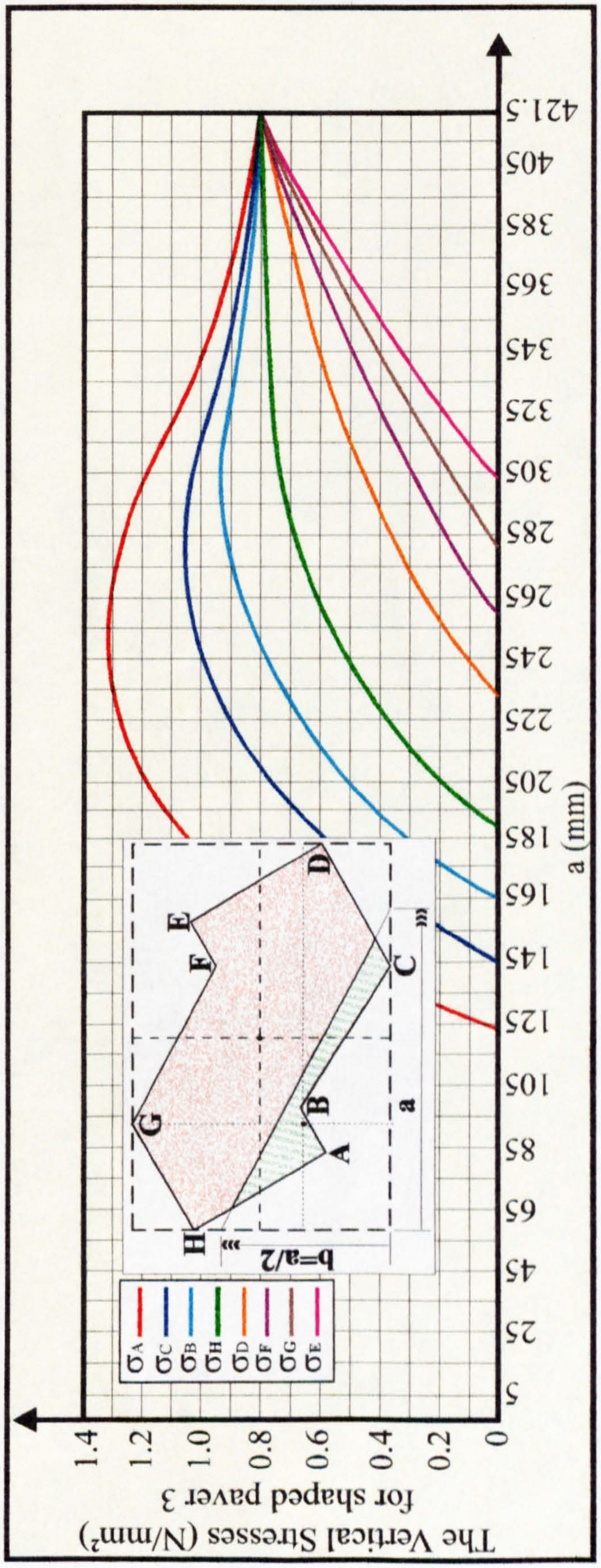

Figure 9.3: Bedding sand vertical stress distributions are developed by the variations of common patch loading (applied pressure= 0.8N/mm^2) for non-chamfered common proprietory shaped paver 3.

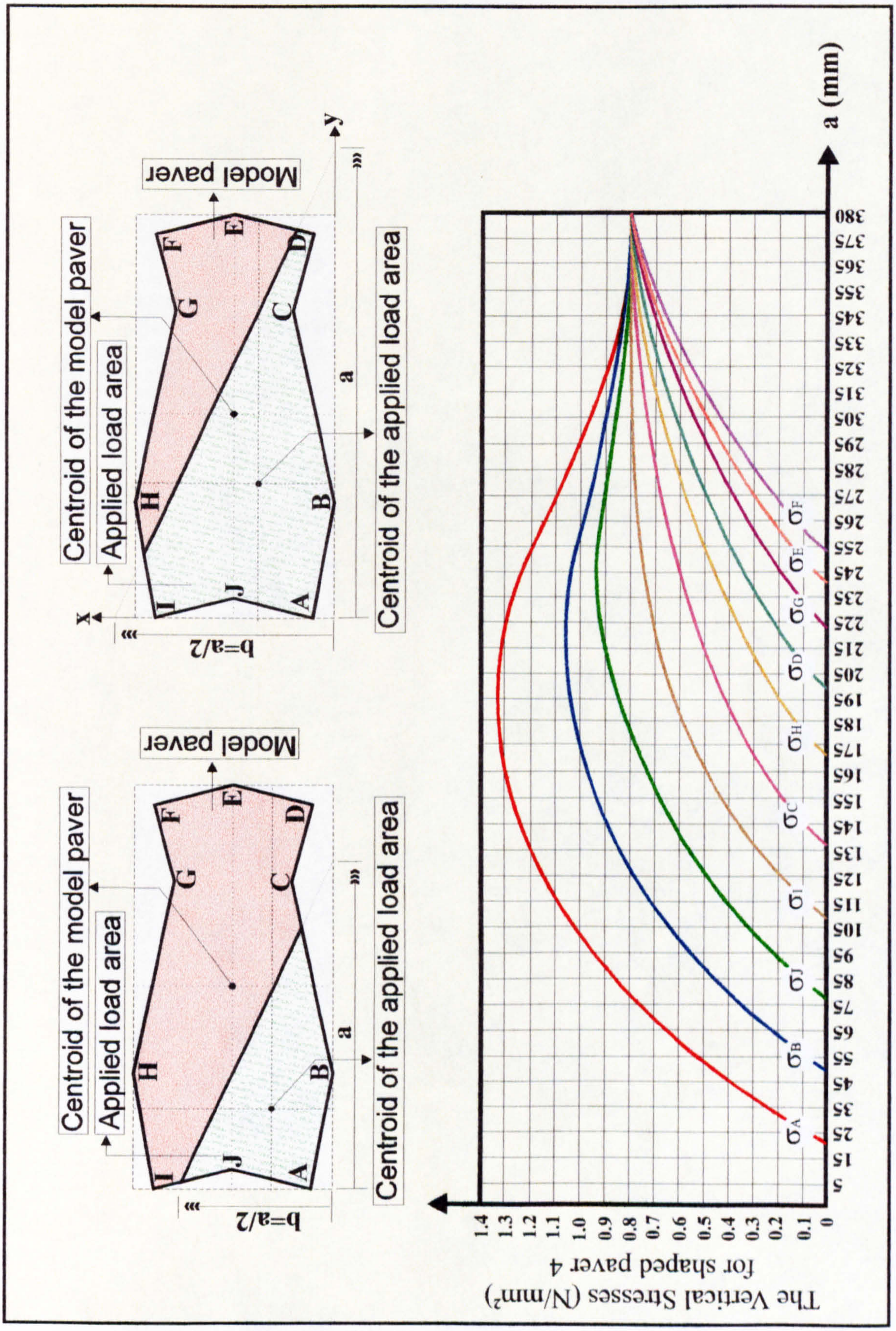

Figure 9.4: Bedding sand vertical stress distributions are developed by the variations of common patch loading (applied pressure= 0.8N/mm²) for non-chamfered common proprietory shaped pavers 4.

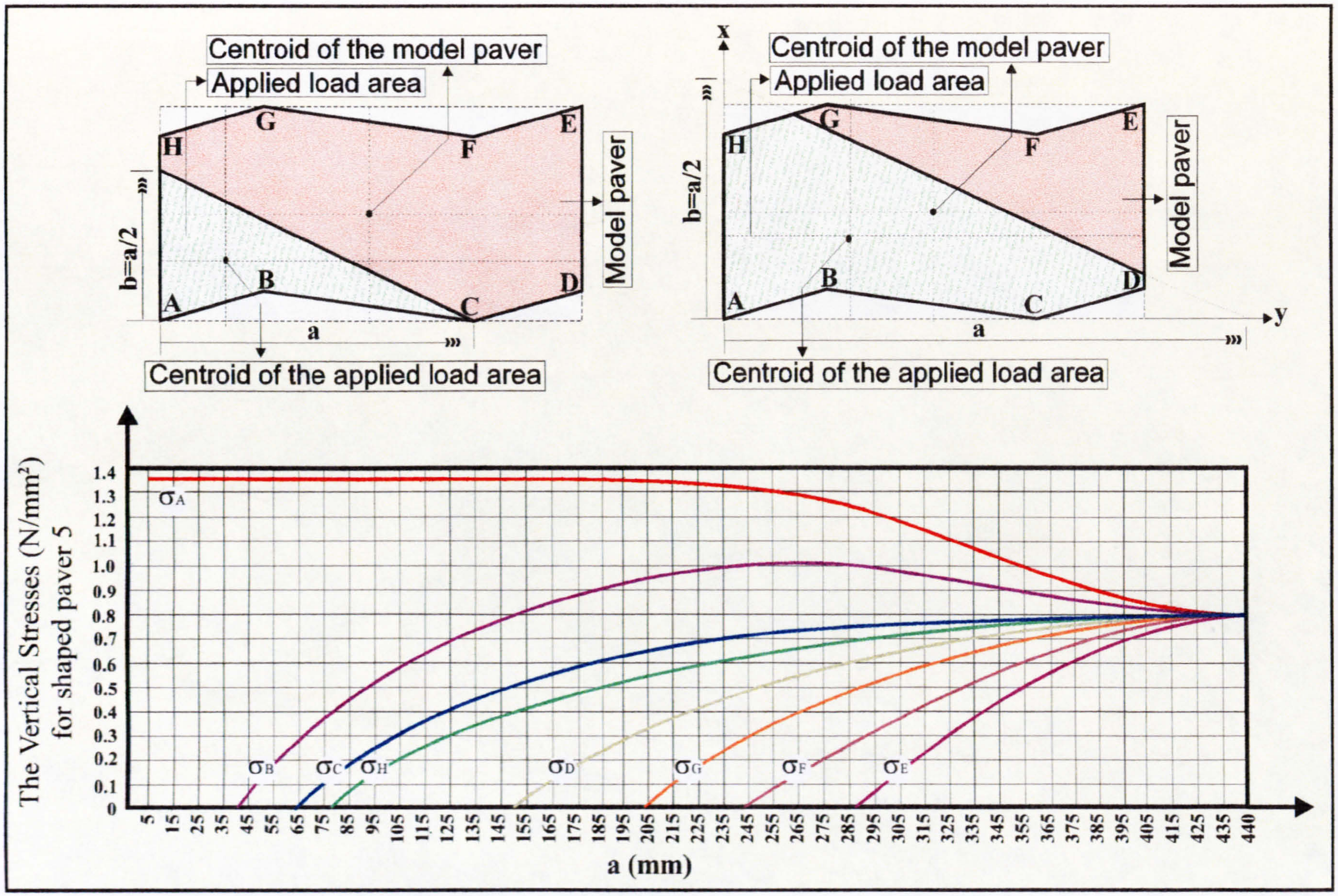

Figure 9.5: Bedding sand vertical stress distributions are developed by the variations of common patch loading (applied pressure= 0.8N/mm^2) for non-chamfered common proprietory shaped paver 5.

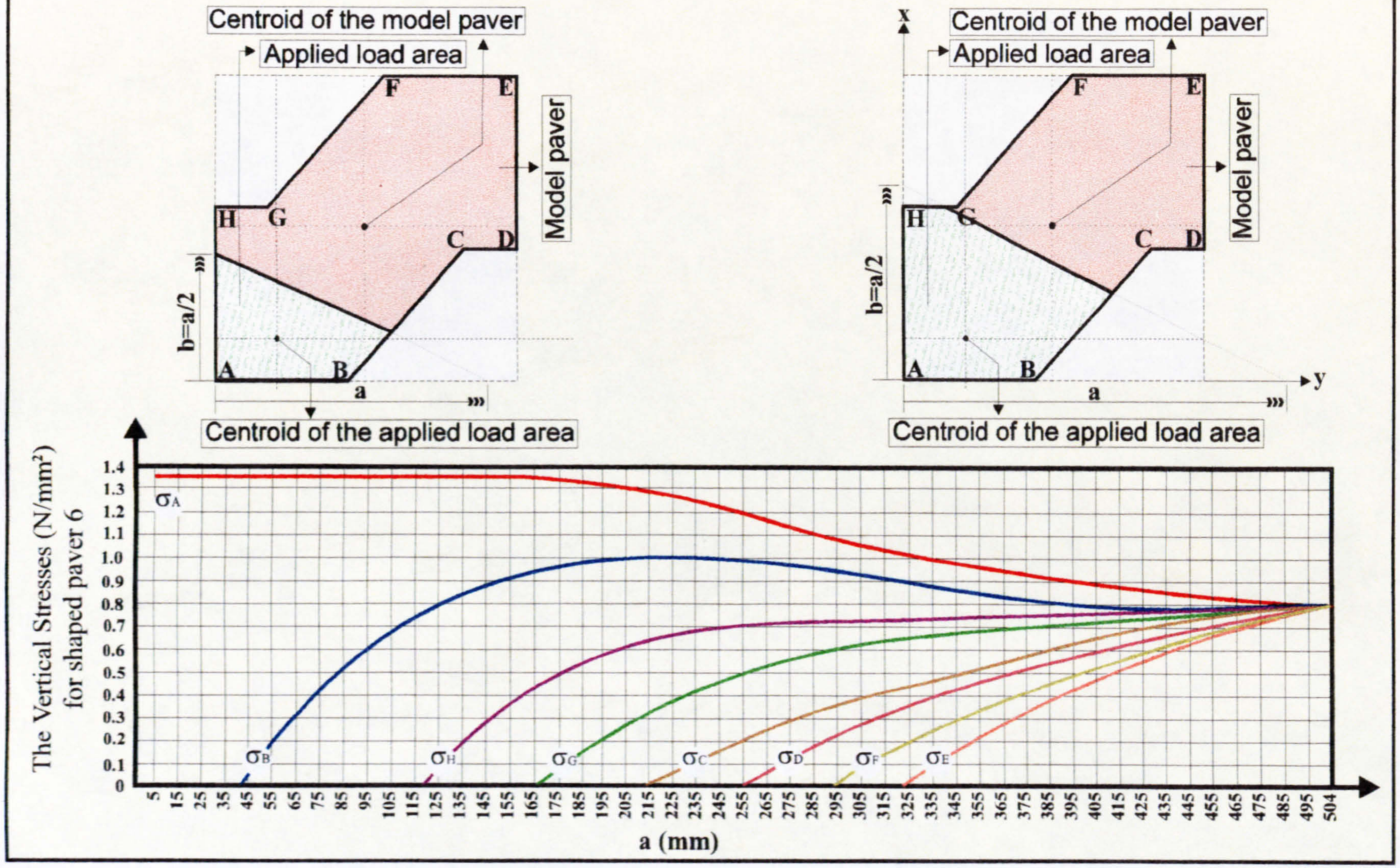

Figure 9.6: Bedding sand vertical stress distributions are developed by the variations of common patch loading (applied pressure= 0.8N/mm²) for non-chamfered common proprietory shaped paver 6.

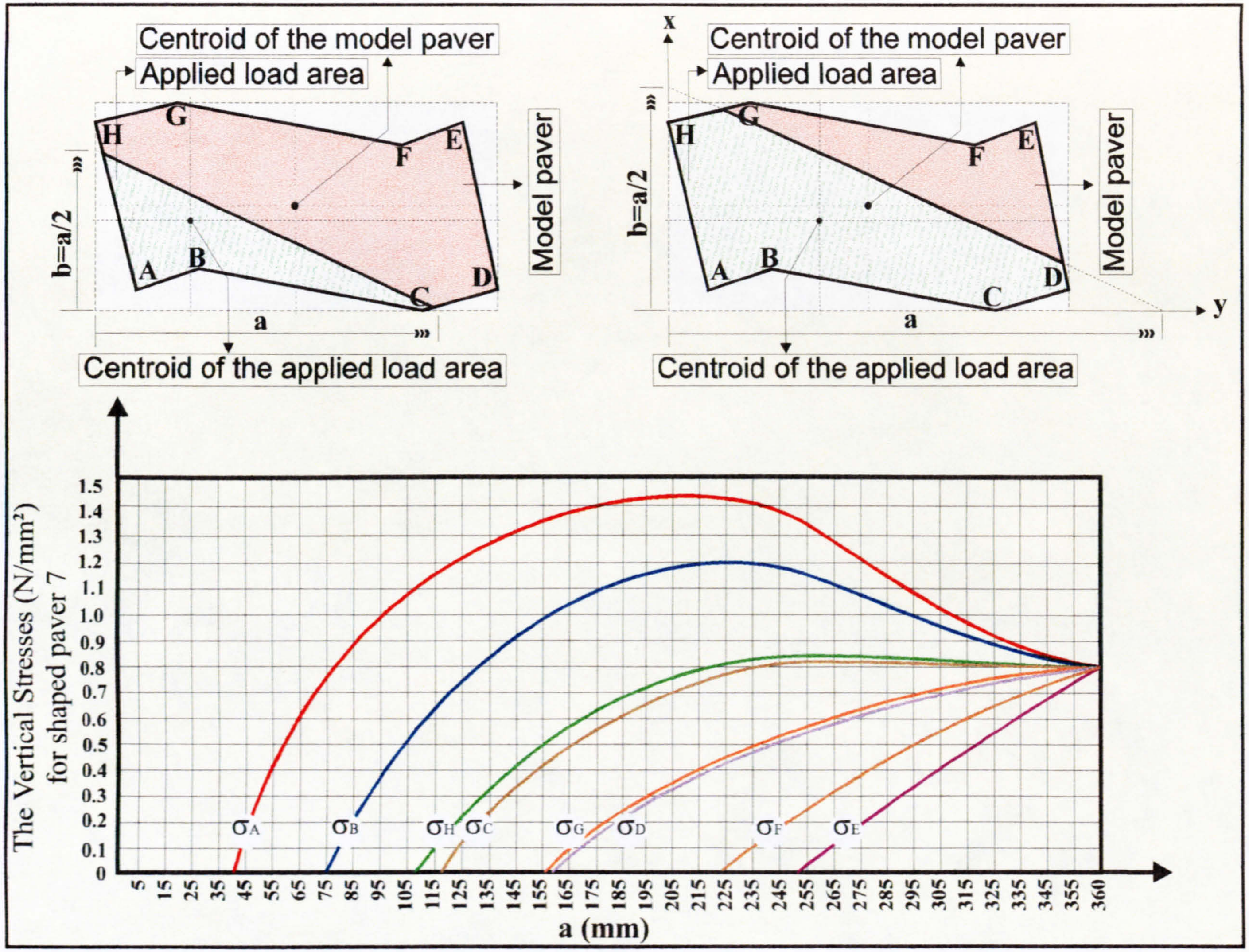

Figure 9.7: Bedding sand vertical stress distributions are developed by the variations of common patch loading (applied pressure= 0.8N/mm^2) for non-chamfered common proprietory shaped paver 7.

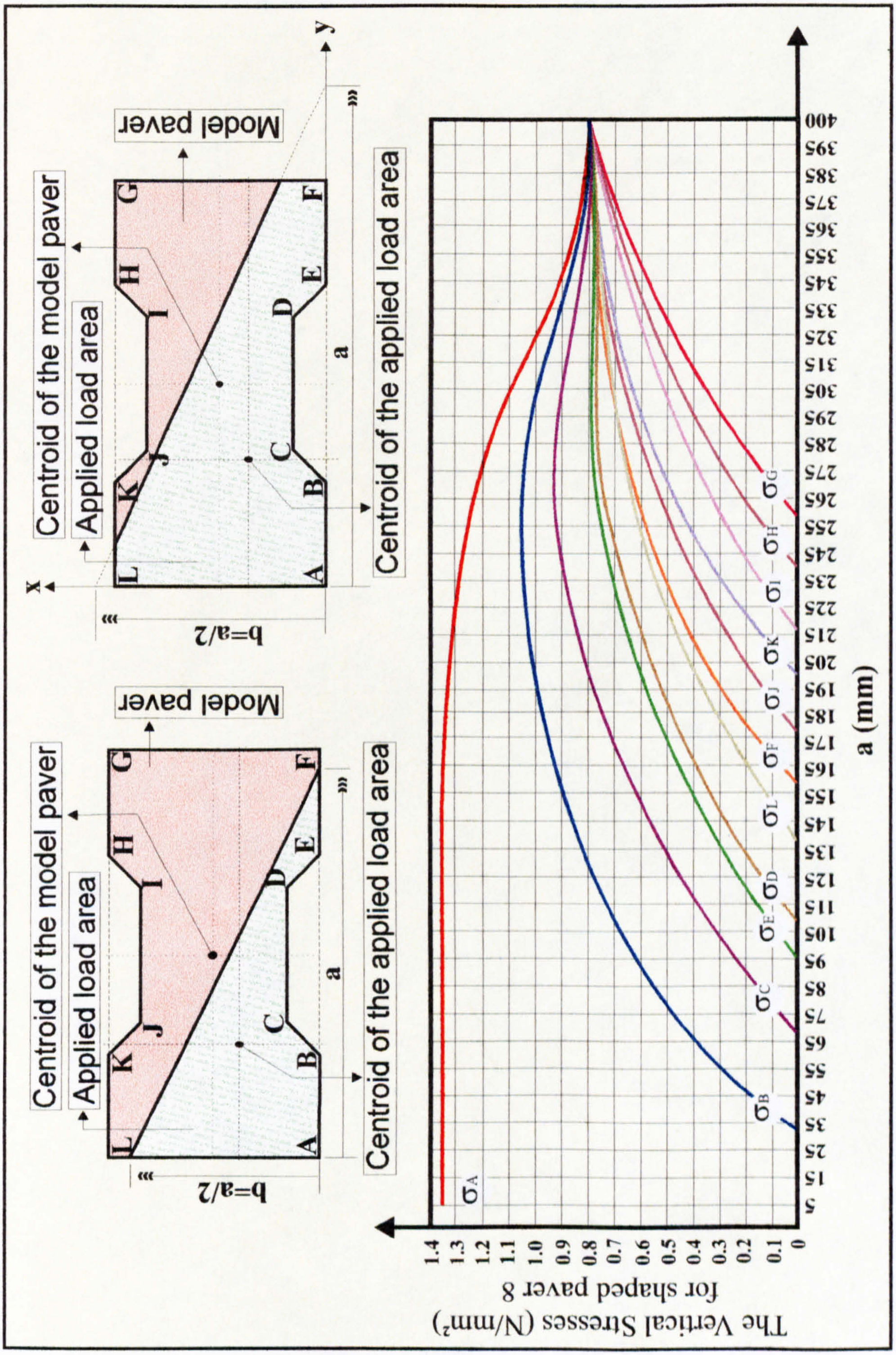

Figure 9.8: Bedding sand vertical stress distributions are developed by the variations of common patch loading (applied pressure= 0.8N/mm²) for non-chamfered common proprietory shaped paver 8.

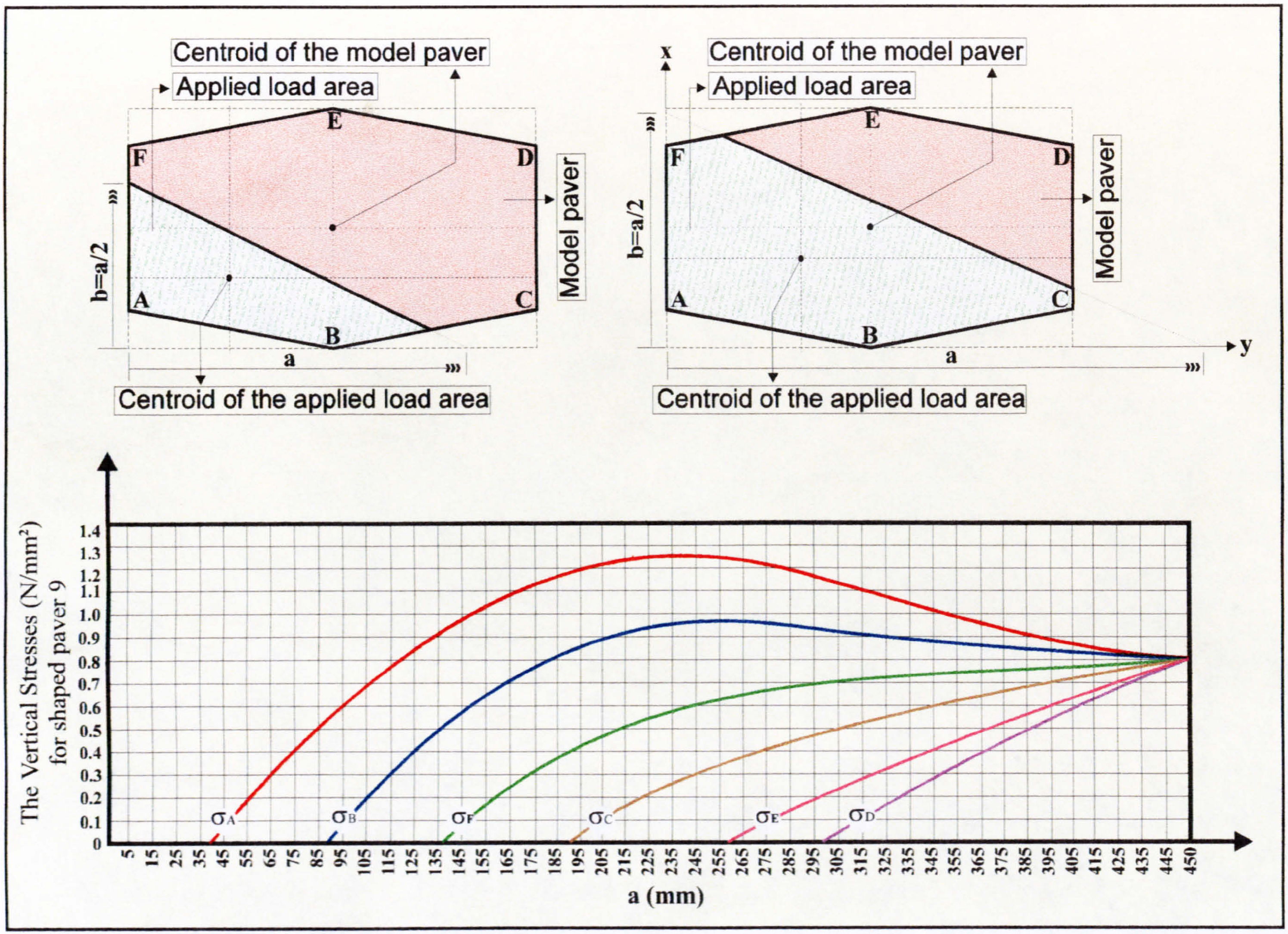

Figure 9.9: Bedding sand vertical stress distributions are developed by the variations of common patch loading (applied pressure= 0.8N/mm^2) for non-chamfered common proprietory shaped paver 9.

PAGE NUMBERING AS ORIGINAL

distributions beneath the shaped pavers while the common patch loading varies with distance a which scans the paver from its lower left corner to its upper right corner. Figures 9.1 to 9.9 show that the true behaviour of concrete block paving for non-interlocking case of the shaped pavers under highway loading can be understood only when the way in which asymmetrically loaded pavers transmit wearing surface applied patch loads into the underlying bedding sand has been studied. If the rectangular pavers (with or without chamfer) are compared with the nine common proprietory paver shapes in terms of maximum stress values (see Figures 6.21 and 9.1 to 9.9), it can be seen that there is no major difference in structural performance. The load spreading capability of both shaped and rectangular block is similar. Figures 9.1 and 9.7 indicate proprietory shaped pavers 1 and 7 which generate stresses which are greater than those which rectangular pavers develop (see Figure 6.21). The shaped pavers 2, 3, 4, 5, 6, 8, and 9 in Figures 9.2, 9.3, 9.4, 9.5, 9.6, 9.8 and 9.9 show the dentated pavers which develop stresses similar to rectangular paver stress distributions (see Figure 6.21).

9.3. Conclusion

This Chapter has demonstrated that how the algebraical solutions developed in Chapters 7 and 8 can be evaluated in order to determine vertical compressive stress values beneath the dentated pavers. The algebraical solutions to absolute-hexahedral stress blocks has been developed for all realistically possible load patches by using the application of the bedding sand stress calculation method[1, 2, 3] (see Chapters 6 and 7). These developed equations for the variations of the absolute-hexahedral stress blocks have been evaluated by using the variations of the common patch loading described in Chapter 5 (see Figures 5.2 to 5.42). The results of these evaluations have been given in Figures 9.1 to 9.9. In the other paver stress regimes, iterative solutions (see Appendix) have been developed and included in the results.

Figures 9.1 to 9.9 show that the true behaviour of concrete block paving under highway loading can be understood only when the way in which asymmetrically loaded pavers transmit wearing surface applied patch loads into the underlying bedding sand has been studied. The simplistic concept of spreading applied load through pavers such that

stress gradually diminishes with depth does not apply to pavers. For this reason, any attempt to compare the behaviour of pavers with that of homogeneous material by comparing vertical stress in the bedding sand may lead to erroneous results. Figures 9.1 to 9.9 demonstrate that pavement analysis must take into account the true shape of the patch loading.

9.4. General conclusion of the Thesis

Many analytical design procedures assume that the load patch is a disk whose diameter can be determined on the basis of assessing wheel load and contact stress[1, 2, 3]. Such an approach must now be regarded as providing results of limited value in terms of the performance of the pavers and their bedding sand, although may still be valid in terms of overall pavement design[1, 2, 3]. Any assessment of the contribution of different laying patterns or different paver size or shape to overall pavement performance must be based upon the type of analysis presented in this Thesis. Figures 9.1 to 9.9 also show why full scale testing of pavers must always be undertaken using true load patch size, pressure and shape and why rolling loads must be used if meaningful results are to be produced. At the University of Newcastle Upon Tyne, the early research into the behaviour of pavers[4] was based upon measuring stresses in bedding sand when the paver wearing surface was loaded by a static circular plate. Whilst the results provided an initial understanding of the behaviour of pavers and demonstrated the existence of interlock, the inability of such methods to register stress magnification generated at paver corners led to sand specifications being inadequate in some circumstances.

The reason why some bedding sands have performed poorly under a combination of regular traffic and the presence of water can now be understood. A combination of high levels of stress (see Figures 6.2 to 6.21 and 9.1 to 9.9) shows to frequently develop in bedding sands and rapid changes in those stress values, in conjunction with hydrostatic pressure, have been the cause of several paver pavement failures[1, 2, 3]. Rapidly changing stress values lead to the development of normal pressures in water when the water cannot flow freely, such as is the case in sands including a significant proportion of fine material (defined as finer than 75 microns) [1, 2, 3]. In some cases, for example, even

when full interlock is operating, bedding sand stress can change from 0.1N/mm^2 to 0.9N/mm^2 over a distance of 100mm. A vehicle travelling at 30mph(50kph) would cover 100mm in less than a hundredth of a second. This means that stress can change at a rate exceeding 100N/mm^2 /second. Such a rapid change would lead to destabilising pressures developing in saturated bedding sands[1, 2, 3]. This Thesis indicates that specifiers should avoid those bedding materials which would be disturbed by a combination of high levels of stress and moisture. In particular, material finer that 75 microns is considered to be likely to lead to bedding sand weakness and should be kept to a minimum[1, 2, 3]. The complexity of the stress distribution in bedding sand may explain why some research conclusions e.g. Woodman[5] (see Section 6.5) have contradicted observed performance of pavers. The high stress transients shown in Figures 6.17, 6.18 and 6.19 occur for short time periods in a rolling load situation and may be of little consequence when pavers are laid over some materials but may be more important in other situations. This might explain why some evidence[5] indicates that pavers perform better when laid over concrete bases than they do when laid over softer bitumen bound materials or granular materials (better even when the additional stiffness inherent in concrete as compared with asphalt is taken into account).

If the rectangular pavers (with or without chamfer) are compared with the nine common proprietory paver shapes (see Figures 6.21 and 9.1 to 9.9) in terms of maximum stress values, it can be seen that there is no major difference in structural performance: the load spreading capability of both shaped and rectangular block is similar. Figures 9.1 and 9.7 indicate proprietory shaped pavers 1 and 7 which generate stresses which are greater than those which rectangular pavers develop (see Figure 6.21). The shaped pavers 2, 3, 4, 5, 6, 8, and 9 in Figures 9.2, 9.3, 9.4, 9.5, 9.6, 9.8 and 9.9 respectively show the dentated pavers which develop stresses similar to rectangular paver stress distributions (see Figure 6.21). Because experience indicates that rectangular pavers can be lain to more uniform and close joint spacing than some dentated pavers, the above conclusion suggests that rectangular pavers may exhibit enhanced performance in practice. Interestingly chamfered rectangular pavers have significantly enhanced load dissipation characteristics as compared with non-chamfered pavers (see Figure 6.21). This may account for some of the observed benefits inherent in chamfered pavers.

Paver joints should be narrow and should remain narrow and well filled in service in order that full interlock is maintained.

It has been demonstrated that in typical highway loading situations, the pattern of stress development in paver bedding sand is complex and depends upon the size, shape, orientation and speed of the load as well as paver geometry and laying pattern. Many of the hitherto unexplained bedding sand failures can be understood by examining the way in which local vertical stress transients develop and travel though bedding sand. In cases where water is present in sands including a significant fraction of fine material, the mechanism whereby sand instability can develop has been explained[1, 2, 3]. Rapidly changing stress levels can result in pressure developing in water in bedding sand which can lead to instability[1, 2, 3]. Many regions permit sand specifications which can lead to instability when vehicles travelling at highway speeds use pavers bedded on saturated sand. It is recommended that such specifications be reviewed and that sands should be specified which permit water to flow as freely as possible where traffic and water may occur concurrently[1, 2, 3]. The data relating to pavers of different geometries indicate that there are differences in the performance of different pavers although the effect is likely to be of minor structural consequence. The only exception to this is the difference between chamfered and non-chamfered pavers. By forcing the load patch inboard of the paver perimeter, chamfered pavers reduce bedding sand stress levels and are therefore to be preferred in trafficked pavements.

9.5. Recommendations to further researches

In this Thesis, a way in which pavers distribute stresses resulting from rolling loads has been investigated and an understanding of the interlocking process thereby developed. This Thesis explains the theoretical analysis and demonstrates how it can be used to establish the nature and value of interlock. The benefit of this type of analysis is that it provides a very clear understanding of the complex pattern of time dependent stresses in bedding sands when the pavement is subjected to rolling loads. The achievement of full interlock in the surface level of a paver pavement is an essential part of any successful paver pavement. The behavior of paver pavement at the surface shows unique

characteristics (see Figure 6.17), the solution by directly applying the flexible pavements' mathematical modeling techniques cannot be compatible. The patch load applications on the surface varies in terms of contact load area's position (see Chapters 4 and 5). There are five main vertical compressive stress regimes (tetrahedral, long-pentahedral, short-pentahedral, partial-hexahedral and absolute-hexahedral stress regimes) which can occur beneath individual pavers according to magnitude and position of patch loads (see Chapter 6). The compression area beneath pavers bounded by force equilibrium line can only behave elastically and the other bottom surface area (apart from compression section) has zero stress value, so elastic behavior in this area cannot occur because tension cannot be developed in uncemented sand so that compressive stress is developed in some parts of interface and zero stress is developed elsewhere. Deflections and stress distributions are function of applied tyre pressure and they change three dimensionally by exceeding tyre pressure in certain points beneath pavers. Behaviour of paver pavement systems should not be attempted to solve by referring first to conceptually simple structural assemblies involving linearly elastic springs, because force-deformation relationships of construction materials are also function of time, moisture contents, temperature etc. The problem relates with dynamic and non-linear mechanistic behaviour of paver pavements and equilibrium of force, force-deformation relationships should be satisfied. In addition, material categorisations are closely related with accuracy of mathematical modeling. Especially bedding sand has direct influence to stress distribution. It has to be categorised properly in terms of maximum stress values. Stress distribution can change for stabilised and non-stabilised joints. This should also be considered in mathematical modeling. The mathematical analyses have been presented in this Thesis address accurately the nature of interlocking paver pavements at the surface level and provide more accurate inputs for analysing the behaviour of paver pavement's courses beneath the surface. Although paver pavements appear to be very simple structures they are in reality very complicated. In order to predict the future performance of paver pavements, a vast number off simplifications must therefore be made. One of the most promising approaches to this is to apply accurate modelled Finite Element Analysis obtaining the data related with systematic behaviour of paver pavements on the surface level from the results of this Thesis. The finite element method although shown to be capable of closely modeling the observed

load/deflection behavior of paver pavements, is more suited as a research tool than for routine design. All materials used in pavement construction are non-isotropic and exhibit varying degrees of elastic, plastic and viscous characteristics. A mathematical model can be no more accurate than the accuracy of the input variables, hence research into material characterisation has followed closely behind the development of the analysis methods. The only analytical technique available that encompassed this degree of complexity is the finite element method. Accurate computation of stresses and strains in pavement structures consisting of different layers and materials whose behaviour is usually influenced greatly by time, temperature, moisture, etc., is an extremely complex task. As a result the finite element method needs correct and appropriate inputs modelling the true behavior of interlocking paver pavements. Therefore, the result of the mathematical analysis can be used in finite element analysis in order to achieve more accurate design procedures for the whole paver pavement structure.

References

1 Algin, H.M., Knapton, J., (1996), *Research into paver interlock*, Jrnl. of the Institution of Highway & Transportation & IHIE, Vol. 43, No. 03, p 20-24.

2 Knapton, J., Algin, H.M., (1995), *The Mathematical Solution to Interlock in Flexibly Bedded Clay Paving*. Proc. of the 4th. Int. Masonry Conf. No. 7, Vol. 2, p 307-313. London.

3 Knapton, J., Algin, H.M., (1996), *The Mathematical Solution to Interlock in Concrete Block Paving*. Proc. of the 5th. Int. Conf. on Concrete Block Paving, p 261-278, Tel-Aviv.

4 Knapton J. and Barber S.D., (1980), *UK Research into Concrete Block Pavement Design*. Proc. 1st Int. Conf. on Concrete Block Paving. Pp 33-37, University of Newcastle upon Tyne, UK.

5 Woodman GR(1992). *The Performance of Concrete Block Surfacing on a Cement-Bound Base in Airfield Pavements*. Proc. 4th Int. Conf. on Concrete Block Paving, Auckland, NZ. Pp. 253-262.

Appendix

Iterative Solutions to the Nonlinear Simultaneous Equations

A.1. Introduction

This Section concentrated on explaining the solutions of the two-dimensional nonlinear simultaneous equations which have been encountered in the calculations of vertical compressive stress distributions beneath pavers (see partial-hexahedral case in Chapter 6, Section 6.1 and respectively tetrahedral, short-pentahedral, long-pentahedral, partial-hexahedral cases in Chapter 7, Sections 7.1, 7.2, 7.3,7.4).

A.2. Iterative solutions to the nonlinear simultaneous equations

An equation that contains expressions such as

$$x^3,\ y^{-2},\ xy,\ \frac{\sqrt{y}}{x},\ (2y-z)^2,\ \sin x,\ e^{yz},\ z\sqrt{x+y}$$

is called nonlinear in x, y, z, ... because it cannot be written as

$$ax+by+cz+....= \text{constant} \qquad \text{(a linear equation in } x, y, z, ...)$$

There are no direct methods available for solving the nonlinear system of equations presented in Chapters 6 and 7 such as are available for linear sets. In general, iterative approaches must be used, which require initial guesses or approximations of the solution values to get started. In the solutions of the two formed nonlinear equations are considered as $f(x,y) = 0$ and $g(x,y) = 0$ the two approaches have been used are:

1) to reduce the equations to $f(x) = 0$ form, then, to use numerical approximations to determine the positive roots.
2) numerical determination the positive roots using the system equations.

The first approach is used for the evaluation of the partial-hexahedral stress regimes presented in Chapter 6. The second approach is used for the evaluation of the tetrahedral, short-pentahedral, long-pentahedral, partial-hexahedral stress regimes presented in Chapter 7. The Newton-Raphson Method (Newton's Method of Tangents)[1] has been used in the numerical calculations of both the first and the second approaches.

A.2.1. The Newton-Raphson method for $f(x) = 0$ forms

Assume that an initial estimate x_0 is known for the desired root α of $f(x) = 0$ (see Figure A.1). Newton- Raphson method[1] will produce a sequence of iterates $\{x_n : n \geq 1\}$, which is anticipated to converge to α. Since x_0 is assumed close to α, approximate the graph of $y = f(x)$ in the vicinity of its root α by constructing its tangent line at $(x_0, f(x_0))$. Then use the root of this tangent line to approximate α; call this new approximation x_1. Repeat this process, to obtain a sequence of iterates x_n. This leads to the following iteration formula.

$$x_{n+1} = x_n - \frac{f(x_n)}{f'(x_n)} \qquad n \geq 0 \qquad \text{(Eq. A.1.)}$$

The process is illustrated in Figure A.1, for the iterates x_1 and x_2.

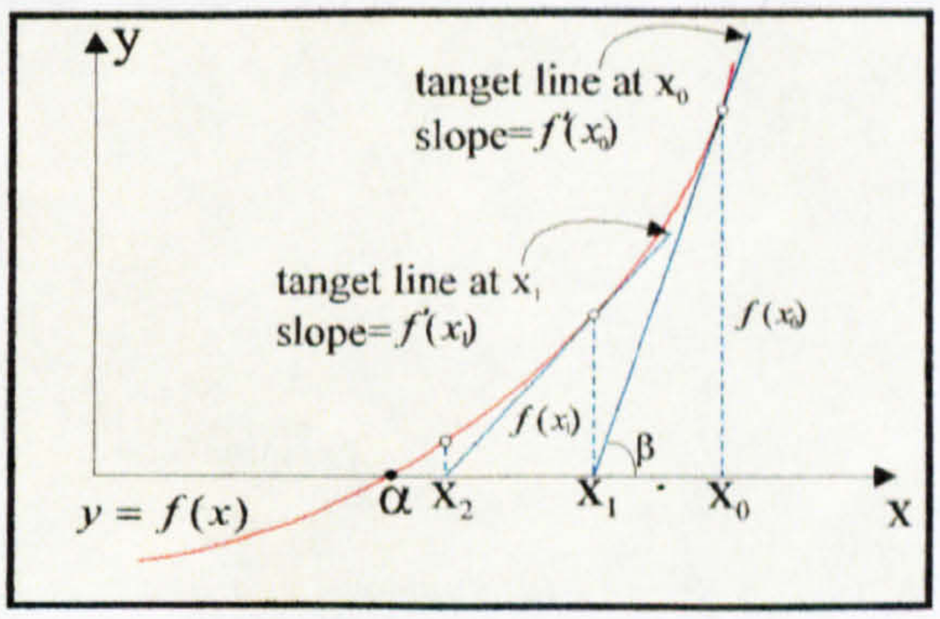

Figure A.1: The Newton-Raphson method[1].

Newton- Raphson method[1] is the best known procedure for finding the roots of an equation. It has been generalised in many ways for the solution of the other more difficult nonlinear problems, for example, systems of nonlinear equations and nonlinear integral and differential equations. It is not always the best method for a given problem, but its formal simplicity and its great speed often lead it to be the first method that people use in attempting to solve a nonlinear problem. An approach to Eq. A.1 is to use a Taylor* series development. Expanding $f(x)$ about x_n,

$$f(x) = f(x_n) + (x - x_n)f'(x_n) + \frac{(x - x_n)^2}{2} f''(\xi)$$

with ξ between x and x_n. Letting $x=\alpha$ and using $f(\alpha) = 0$, The following formula is obtained form the solution of the formula above for α.

$$\alpha = x_n - \frac{f(x_n)}{f'(x_n)} - \frac{(\alpha - x_n)^2}{2} \frac{f''(\xi_n)}{f'(x_n)}$$

with ξ_n between x_n and α. The error term (the last term) can be dropped to obtain a better approximation to α than x_n, and it can be recognised that this approximation as x_{n+1} from Eq. A.1. Then

$$\alpha - x_{n+1} = -(\alpha - x_n)^2 \frac{f''(\xi_n)}{2f'(x_n)} \qquad n \geq 0$$

This formula is used to show that Newton- Raphson method[1] has a quadratic order of convergence. The Newton- Raphson method[1] is widely used in practice because of its generally rapid convergence. However, there are cases in which convergence does not

---

* For a discussion of Taylor's series see any advanced calculus book.

occur. One such example is shown in Figure A.2 (a) where $f''(x)$ changes sign near the root. A second case in which convergence may not occur is illustrated in Figure A.2 (b). In this example, the initial approximation to the root was not sufficiently close to the true value, and the tangent to the curve for x_n has a very small slope, resulting in x_{n+1} being far to the right where a local maximum in the curve causes the difficulty. Other functions could be illustrated in which there is a jump to a root other than the one nearest to the first approximation. These difficulties can be avoided by having the initial approximation sufficiently close to the root value, but sometimes this is not possible. In that case other approximation methods can be used such as Broyden's method[1], the Secant method[1], Steepest Descend techniques[1] etc.

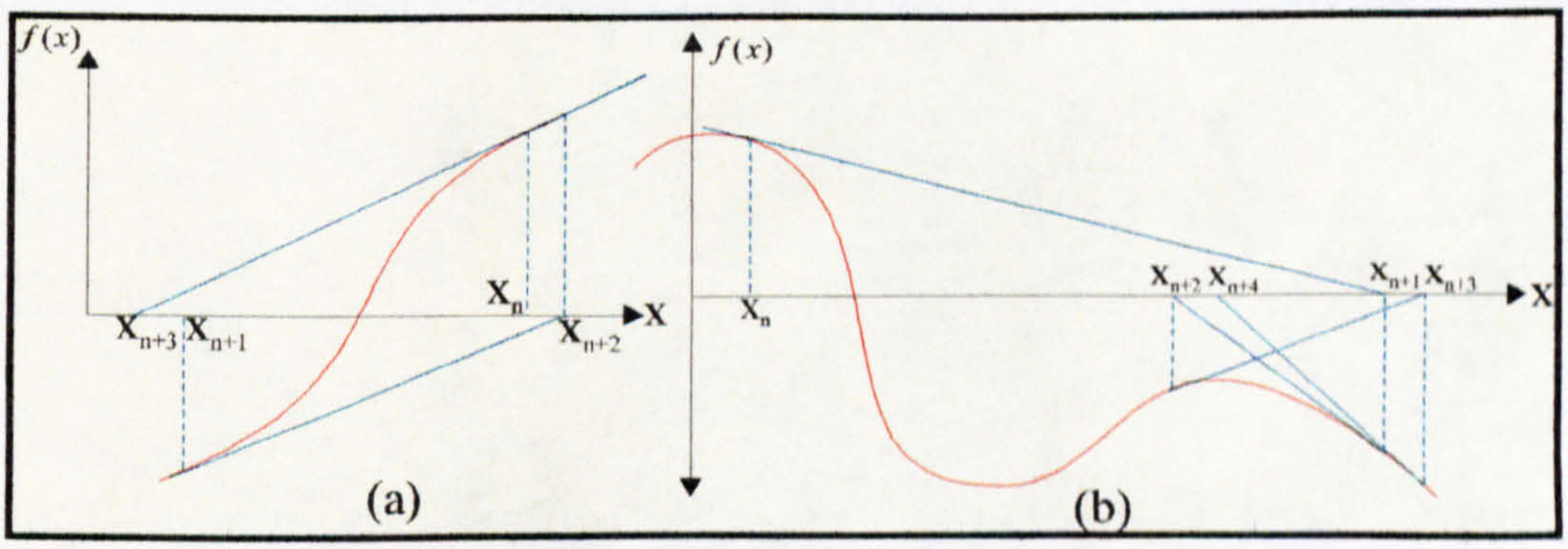

Figure A.2: (a) A case of no convergence. (b) A second case of no convergence.

Error estimation is calculated as follows using the mean value theorem:

$$f(x_n) = f(x_n) - f(\alpha) = f'(\xi_n)(x_n - \alpha) \qquad \Rightarrow \qquad \alpha - x_n = \frac{f(x_n)}{f'(\xi_n)}$$

with ξ_n between x_n and α. If $f'(x)$ is not changing rapidly between x_n and α, then we have $f'(\xi_n) \doteq f'(x_n)$, and

$$\alpha - x_n \doteq \frac{-f(x_n)}{f'(x_n)} = x_{n+1} - x_n$$

with the last equality following from the definition of Newton- Raphson method[1]. For Newton- Raphson method[1], the standard error estimate is

$$\alpha - x_n \triangleq x_{n+1} - x_n$$

For relative error, the following equality is used:

$$\frac{\alpha - x_n}{\alpha} \triangleq \frac{x_{n+1} - x_n}{x_{n+1}}$$

A.2.1.1. The Example of the Newton-Raphson method's application

The variations of the partial-hexahedral vertical stress regime presented in Chapter 6 (Section 6.1) has iterativelly been calculated as follows.

As can be recognised that the following three equations has already been developed in Chapter 6 (Section 6.1).

$$\sigma_A = \frac{3N\alpha\beta^2}{50\left(10000\alpha^2 - 300\alpha^2\beta + 3\alpha^2\beta^2 - 1200\beta^3 + 6\alpha\beta^3\right)} \qquad \text{(Eq. A.2)}$$

$$0 = 8000000\beta^4 + \alpha^4\left(-750000 + 20000\beta - 150\beta^2 + 10000\overline{X} - 300\beta\overline{X} + 3\beta^2\overline{X}\right) +$$
$$\alpha^2\left(600\beta^4 - 1200\beta^3\overline{X}\right) + \alpha^3\left(-2\beta^4 + 6\beta^3\overline{X}\right)$$

$$0 = 10.10^7\alpha^4 + \beta^4\left(-48.10^8 + 64.10^6\alpha - 24.10^4\alpha^2 + \alpha^4 - 48.10^4\alpha\overline{Y} + 2400\alpha^2\overline{Y}\right) +$$
$$\beta^2\left(60000\alpha^4 - 120000\alpha^3\overline{Y}\right) + \beta^3\left(-400\alpha^4 + 1200\alpha^3\overline{Y}\right) + \beta\left(-4.10^6\alpha^4 + 4.10^6\alpha^3\overline{Y}\right)$$

σ_A can be evaluated from the solutions of the last two equations which are reformed to the following form owing to the notational simplification by replacing α with x and β with y.

$$0 = 8000000y^4 + x^4\left(-750000 + 20000y - 150y^2 + 10000\overline{X} - 300y\overline{X} + 3y^2\overline{X}\right) + x^2\left(600y^4 - 1200y^3\overline{X}\right) + x^3\left(-2y^4 + 6y^3\overline{X}\right) \quad \text{(Eq. A.3)}$$

$$0 = 10.10^7x^4 + y^4\left(-48.10^8 + 64.10^6x - 24.10^4x^2 + x^4 - 48.10^4x\overline{Y} + 2400x^2\overline{Y}\right) + y^2\left(60000x^4 - 120000x^3\overline{Y}\right) + y^3\left(-400x^4 + 1200x^3\overline{Y}\right) + y\left(-4.10^6x^4 + 4.10^6x^3\overline{Y}\right) \quad \text{(Eq. A.4)}$$

The arithmetical solution of Eq. A.3 according to x values yields the following positive root of the equation depends upon y.

x=-((3X-y)(y^3))/(2(-750000+10000X+20000y-300Xy-150(y^2)+3X(y^2)))-((((3X-y)^2)(y^6))/(-750000+10000X+20000y- 300Xy-150(y^2)+3X(y^2))^2-(400(y^3)(-2X+y))/(-750000+ 10000X+20000y-300Xy-150(y^2)+3X)y^2))+(2^(1/3)(360000(y^6)((-2X+y)^2)-96000000(y^4)(-750000+10000X+20000y-300Xy-150(y^2)+3X(y^2))))/(3(-750000+10000X+20000y-300Xy-150(y^2)+3X(y^2))(-864000000((3X-y)^2)(y^10)+432000000(y^9)((-2X+y)^3)+345600000000(y^7)(-2X+y)(-750000+10000X +20000y-300Xy-150(y^2)+3X(y^2))+(-4(360000(y^6)((-2X+ y)^2)-96000000(y^4)(-750000+10000X+20000y-300Xy-150(y^2)+3X(y^2)))^3+ (-864000000((3X-y)^2)(y^10)+432000000(y^9)((-2X+y)^3)+345600000000(y^7)(-2X+y)(-750000+10000X+20000y -300Xy-150(y^2)+3X (y^2)))^2)^(1/2))^(1/3))+(-864000000((3X-y)^2)(y^10)+432000000(y^9)((-2X+y)^3)+345600000000(y^7)(-2X+y)(-750000+10000X+ 20000y-300Xy-150(y^2)+3X(y^2))+(-4(360000(y^6)((-2X+y)^2)-96000000(y^4)(-750000+10000X+ 20000y-300Xy-150(y^2)+3X(y^2)))^3+(-864000000((3X-y)^2)(y^10)+432000000(y^9)((-2X+y)^3)+345600000000(y^7)(-2X+y)(-750000+10000X+20000y-300Xy-150(y^2)+3X(y^2)))^2)^(1/2))^(1/3)/ (3(2^(1/3))(-750000+10000X+20000y-300Xy-150(y^2)+3X(y^2))))^(1/2)/2 +((2 ((3X-y)^2)(y^6))/(-750000+ 10000X+20000y-300Xy-150(y^2)+3X(y^2))^2-(800(y^3)(-2X+y))/(-750000+10000X+20000y-300Xy-150(y^2) +3X(y^2))-(2^(1/3)(360000(y^6)((-2*X+y))^2-96000000(y^4)(-750000+ 10000X+20000y-300Xy-150(y^2)+3X(y^2))))/(3(-750000+10000X+20000y-300Xy-150(y^2)+3X(y^2))(-864000000((3 X-y)^2)(y^10)+432000000(y^9)((-2X+y)^3)+345600000000(y^7)(-2X+y)(-750000+10000X+20000y-300Xy-150(y^2)+3X(y^2))+ (-4(360000(y^6)((-2X+y)^2)-96000000(y^4)(-750000+10000X+ 20000y-300Xy-150(y^2) +3X(y^2))) ^3+(-864000000((3X- y)^ 2)(y ^10)+432000000(y^9)((-2X+y)^3)+345600000000(y^7)(-2X+y)(-750000+10000 X+20000 y -300Xy-150(y^2)+3X(y^2))^2)^(1/2))^(1/3)-(-864000000((3X-y)^2)(y^10)+ 432000000 (y^9)((2X+y)^3)+345600000000(y^7)(-2X+y)(-750000+10000X+20000y - 300Xy-150(y^2)+3X(y^2))+(-4(360000(y^6)((-2X+y)^2)- 96000000(y^4)(-750000+ 10000X+20000y-300Xy-150(y^2) +3X(y^2)))^3+(-864000000((3X-y)^2)(y^10)+ 432000000(y^9)((-2X+y)^3)+345600000000(y^7)(-2X+y)(-750000+10000X+20000y- 300Xy-150(y^2) +3X (y^2)))^2)^(1/2))^(1/3)/(3(2^(1/3))(-750000+ 10000X+20000y-

```
300X̄y-150(y^2) +3X̄(y^2)))-((-8((3X̄-y)^3)(y^9))/(-750000+10000X̄+20000y-300X̄y-
150(y^2) +3X̄(y^2))^3 +(4800(3X̄-y)(y^6)(-2X̄+y))/(-750000+10000X̄+20000y-300X̄y-
150(y^2)+3X̄(y^2))^2)/(4((((3X̄-y)^2)(y^6))/(-750000+ 10000X̄+20000y-300X̄y-150
(y^2)+3X̄(y^2))^2-(400(y^3)(-2X̄+y))/(-750000+10000X̄+20000y-300X̄y-150(y^2)+
3X̄(y^2))+(2^(1/3)(360000(y^6)((-2X̄+y)^2)-96000000(y^4)(-750000 + 10000X̄+20000y-
300X̄y-150(y^2)+3X̄(y^2))))/(3(-750000+10000X̄+20000y-300X̄y-150(y^2)+3X̄(y^2))(-
864000000((3X̄-y)^2) (y^10)+432000000(y^9)((-2X̄+y)^3)+345600000000(y^7)(-2X̄+y)(-
750000+10000X̄+20000y-300X̄y-150(y^2)+3X̄(y^2))+(-4( 360000(y^6)((-2X̄+y)^2)-
96000000(y^4)(-750000+10000X̄+20000y-300X̄y-150(y^2)+3X̄(y^2)))^3+(-864000000
((3X̄-y)^2)(y^10)+ 432000000(y^9)((-2X̄+y)^3)+345600000000(y^7)(-2X̄+y)(750000
+10000X̄+20000y-300X̄y-150(y^2)+3X̄(y^2)))^2)^(1/2))^(1/3))+(-864000000((3X̄-y)^2)
(y^10)+432000000(y^9)((-2X̄+y)^3)+ 345600000000(y^7)(-2X̄+y)(-50000+10000 X̄+
20000y-300X̄y-150(y^2)+3X̄(y^2))+(-4(360000(y^6)((-2X̄+y)^2)-96000000(y^4)(-750000
+10000 X̄+20000y-300X̄y-150(y^2)+3X̄(y^2)))^3+(-864000000((3X̄-y)^2)(y^10)+
432000000(y^9)((-2X̄+y)^3)+ 345600000000(y^7)(-2X̄+y)(-750000+10000X̄+ 20000y-
300X̄y -150(y^2)+3X̄(y^2)))^2)^(1/2))^(1/3)/(3(2^(1/3))(-750000+10000X̄+20000y-300
X̄y-150(y^2)+3X̄(y^2))))^(1/2)))^(1/2)/2
```

According to this x value which is the algebraical solution of Eq. A.3, Eq. A.4 can be reformed and solved numerically by using the following program written for Mathematica computer softwear[2]. This program is based on the Newton-Raphson method[1] which is one of the most powerful and well-known numerical methods for solving a root-finding problem $f(x)=0$. The Newton iteration proceeds by finding better and better approximations to a zero of function with the formula $x_{i+1} = x_i - f(x_i)/f'(x_i)$. The package of this program which is written by using Mathematica software's language[2] defines two functions, F(x)zero[ ] to find roots of functions, and F(x)FixedPoint[ ] to find fixed points of functions. The F(x)zero[ ] implements Newton-Raphson method[1]'s iteration formula (Eq. A.1). It is called as F(x)zero[expression, variation, starting point]. It can also be called as F(x)zero[function, starting point]. The command F(x)FixedPoint[function, starting point] finds a fixed point of the function f starting the iteration at starting point. Both functions perform up to $RecursionLimit many iterations to find a root or fixed point of the given function. If they cannot find one within the precision of the starting point given, they print a message and return the value found so far. F(x)zero[f_, x0_] first finds the precision of x0 and then artificially raises the precision of the starting point by some amount so that the fixed-point calculations are performed at a higher precision. It then commutes the derivative f' of the given function f. The result is assigned to a local variable so that it does

not need to be recomputed at each iteration step. The fixed point of the pure function (#-f[#]/fp[#])& which corresponds to Newton's formula $x_{i+1} = x_i - f(x_i)/f'(x_i)$ can then be found. After returning from the fixed point calculation, f[res] is calculated. If the fixed point could not be found f[res] would be close to zero. The expression Accuracy[x0a]-Precision[x0a] finds the number of zeros to the right of the decimal point in x0a. If this number is less than the precision was started with, a message is printed. To find a fixed point of the function f(x), a numerical root of the function f(x)-x is found in the program. F(x)FixedPoint[function, starting point] therefore simply calls F(x)zero[ ] with the pure function (f[#]-#)&. The program goes through many levels of contracting new pure function from old ones by calling F(x)FixedPoint[function, starting point]. Nevertheless, it is capable of differentiating them correctly.

```
BeginPackage["F(x)NewtonIteration"]
F(x)zero::usage="F(x)zero[expr, x, x0] finds a zero of expr as a function of x using the
        initial guess x0  to start the iteration. F(x)zero[f, x0] finds a numerical root of the
        function f. The recursion limit determines the maximum number of iteration steps
        that are performed."
F(x)FixedPoint::usage=" F(x)FixedPoint[f, x0] finds a fixed point of the function f using
        the initial guess x0 to start the iteration."
F(x)NewtonIteration::noconv="Iteration did not converge in '1' steps."
Begin["`Private`"]
F(x)zero[expr_, x_, x0_] :=F(x)zero[Function[x, expr], x0 ]
F(x)zero[f_, x0_] :=
        Block[{res, x0a, prec=Precision[x0], fp=f'},
            x0a=SetPrecision[x0, prec + 10];
            res=FixedPoint[(# - f[#]/fp[#])&, x0a, $RecursionLimit];
            x0a=f[res];
            If [Accuracy[x0a]-Precision[x0a]<prec,
            Message[F(x)NewtonIteration::noconv, $RecursionLimit]];
            N[res,prec]
        ]
F(x)FixedPoint[f_, x0_] :=F(x)zero[(f[#]-#)&, x0]
End[ ]
Protect[F(x)zero, F(x)FixedPoint]
EndPackage[ ]
```

Here is a example by considering non-chamfered rectangular paver and the special patch load applications (see Figure 4.17):

Consider a=155mm and b=77.5mm (see Figure 4.17). Therefore N=4805N, $\overline{X}$=51.66667mm and $\overline{Y}$=25.83333mm can be found. By using the evaluated equation (Eq. A.4) and the program given above for Mathematica computer software (F(x)zero[Eq. A.4, y, 100]) y=103.06912mm can be found. By using the given positive root of Eq. A.3 x=206.13824mm can be calculated. By inserting these values into Eq. A.2, the vertical compressive stress(σ_A) beneath the corner A of the non-chamfered rectangular paver can be found as 1.34999N/mm^2. If these values are inserted into the surface function of the vertical compressive stress, any point beneath the surface can then be evaluated with considering the co-ordinate points wished to be calculated such as σ_B=0.04019941N/ mm^2 can be found for x=0 and y=100, σ_C=0.04019941 N/mm^2 can be determined for x=200 and y=0.

By applying same procedure for a=160mm (see Figure 4.17), the following results can be determined N=5120N, $\overline{X}$=53.33333mm, $\overline{Y}$=26.66667mm, y=107.85707mm, x=215.71414 mm, σ_A=1.321379 N/ mm^2, σ_B=0.09625863 N/ mm^2 and σ_C=0.09625867 N/ mm^2.

Likewise for a=165mm, the following results can be determined N=5445N, $\overline{X}$=55mm, $\overline{Y}$=27.5mm, y=112.26826mm, x=223.87883mm, σ_A=1.303089N/ mm^2, σ_B=0.138987 N/ mm^2 and σ_C=0.1423968 N/ mm^2.

The results can be seen in Figure 6.21.

A.2.2. The Newton-Raphson method for 2 x 2 systems

Rather than use subscripts, a general 2 x 2 nonlinear system is denoted by the simplified notation.

(E1) $f(x,y) = 0$, *or simply* $f(\mathbf{x})=0$

(E2) $g(x,y) = 0$, *or simply* $g(\mathbf{x})=0$

where $\mathbf{x}=\begin{bmatrix} x \\ y \end{bmatrix}$ (Eq. A.5.)

The vector **x** is identified with the point (x, y) on the xy-plane. As a result, roots $\mathbf{x}=\begin{bmatrix} \bar{x} & \bar{y} \end{bmatrix}^T$ of Eq. A.5 can be interpreted geometrically. The graphs of the equations $z = f(x, y)$ and $z = g(x, y)$ are surfaces Σ_f and Σ_g whose intersection is a curve **C** in xyz-space, as illustrated in Figure A.3 (a). Setting $f(x, y)$ and $g(x, y)$ to zero corresponds to intersecting Σ_f and Σ_g with the xy-plane (z=0). So a root **x** of E1 and E2 corresponds to a point at which the curve **C** meets the xy-plane. Let $\mathbf{x}_k=(x_k, y_k)$ be a current approximation of $\mathbf{x}=(\bar{x}, \bar{y})$. If Π_f denotes the tangents plane to Σ_f at the point $l'_f(\mathbf{x}_k, f(\mathbf{x}_k))$ and Π_g denotes the tangents plane to Σ_g at the point $l'_g(\mathbf{x}_k, g(\mathbf{x}_k))$, then Π_f and Π_g will intersect in a line **L**, as shown in Figure A.3 (b). For $\mathbf{x}_k$ sufficiently close to **x**, **L** will lie near the curve **C**, and so the point $\mathbf{x}_{k+1}$ where **L** meets the xy-plane should be closer to the desired root **x** than $\mathbf{x}_k$. If points $\mathbf{x}=(x, y)$ near $\mathbf{x}_k$ are written as

$$\mathbf{x}=(x, y), \qquad \text{where } x = x_k + dx \quad \text{and} \quad y = y_k + dy$$

then the z-coordinate of points (x, y, z) on the planes Π_f and Π_g can be found using the tangent plane equation obtained in calculus:

On Π_f: $$z = f(x_k,y_k) + \frac{\partial}{\partial x} f(x_k,y_k)dx + \frac{\partial}{\partial y} f(x_k,y_k)dy \qquad \text{(Eq. A.6a)}$$

On Π_g: $$z = g(x_k,y_k) + \frac{\partial}{\partial x} g(x_k,y_k)dx + \frac{\partial}{\partial y} g(x_k,y_k)dy \qquad \text{(Eq. A.6b)}$$

Setting z=0 in Eq. A.6 yields a linear system in the variable dx and dy. Its matrix from is J_k **dx**=-**f**($\mathbf{x_k}$), that is,

$$\underbrace{\begin{bmatrix} \frac{\partial}{\partial x} f(\mathbf{x_k}) & \frac{\partial}{\partial y} f(\mathbf{x_k}) \\ \frac{\partial}{\partial x} g(\mathbf{x_k}) & \frac{\partial}{\partial y} g(\mathbf{x_k}) \end{bmatrix}}_{\boldsymbol{J_k}} \underbrace{\begin{bmatrix} dx \\ dy \end{bmatrix}}_{\mathbf{dx}} = \underbrace{-\begin{bmatrix} f(\mathbf{x_k}) \\ g(\mathbf{x_k}) \end{bmatrix}}_{-\mathbf{f}(\mathbf{x_k})} \qquad \text{(Eq. A.7.)}$$

The solution of Eq. A.7, which is denoted as $\mathbf{dx_k}$, is what must be added to $\mathbf{x_k}$ to get $\mathbf{x_{k+1}}$ where the line **L** meets the xy-plane in Figure A.3(b). Thus, the iteration depicted in Figure A.3(b) is

$\mathbf{x_{k+1}}=\mathbf{x_k}+\mathbf{dx_k}$, where $\mathbf{dx_k}$ is obtained by solving $\mathbf{J_k}\ \mathbf{dx}=-\mathbf{f}(\mathbf{x_k})$ (Eq. A.8.)

The 2 x 2 matrix that is evaluates at $\mathbf{x_k}$ to get $\mathbf{J_k}$ in Eq. A.7 is

$$\mathbf{f'(x)}=\begin{bmatrix} \frac{\partial}{\partial x} f(x,y) & \frac{\partial}{\partial y} f(x,y) \\ \frac{\partial}{\partial x} g(x,y) & \frac{\partial}{yx} g(x,y) \end{bmatrix}, \text{ the } \textbf{Jacobian Matrix} \text{ at } \mathbf{x}=\begin{bmatrix} x \\ y \end{bmatrix} \text{ for } \mathbf{f(x)}=\begin{bmatrix} f(x,y) \\ g(x,y) \end{bmatrix} \text{ (Eq.A.9)}$$

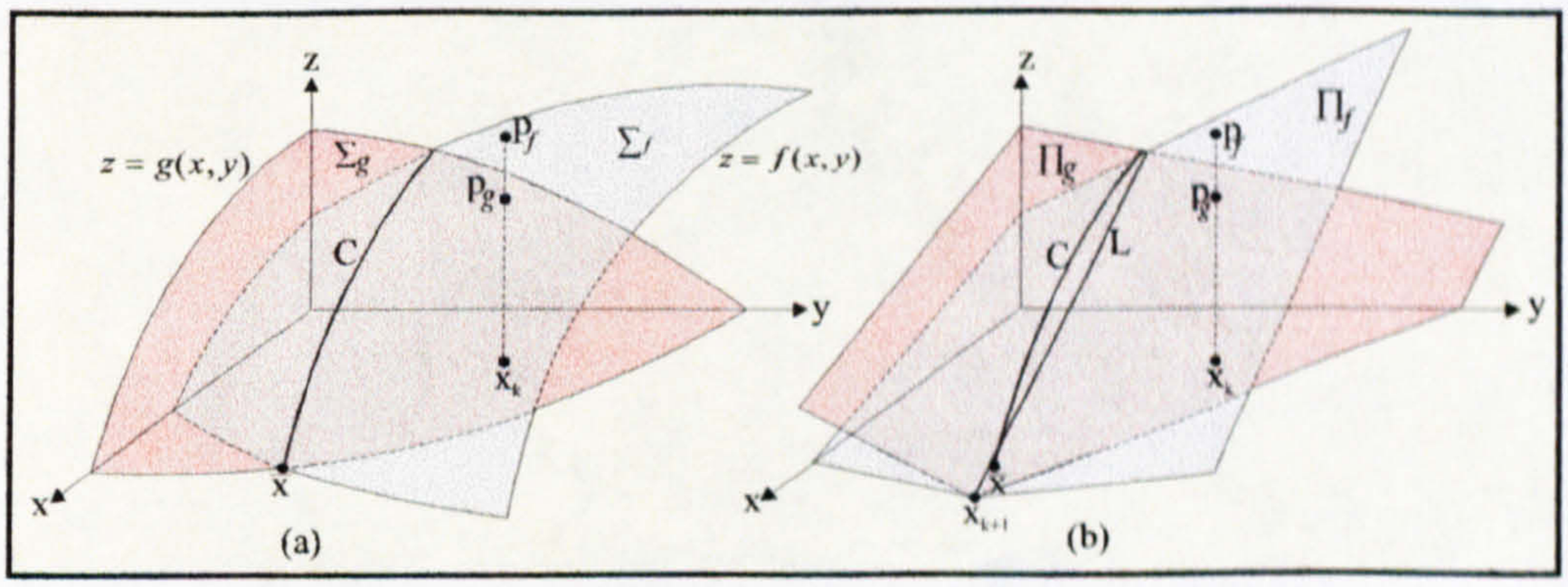

Figure A.3: (a) Surface Σ_f and Σ_g; (b) Their Tangent Planes, Π_f and Π_g, at $\mathbf{x_k}$.

Since $\mathbf{J_k}=\mathbf{f'(x_k)}$, the increment in Eq. A.8 can be expressed as $\mathbf{dx_k} = -[\mathbf{f'(x_k)}]^{-1}\ \mathbf{f(x_k)}$. Accordingly, the iteration (Eq. A.8) is referred as the Newton-Raphson method[1] for solving the 2 x 2 system $\mathbf{f(x)}=0$.

A.2.2.1. The Example of the Newton-Raphson method's application

The most of the two dimensional nonlinear simultaneous equations which have been encountered in the calculations of vertical compressive stress regimes (see tetrahedral, short-pentahedral, long-pentahedral, partial-hexahedral cases in Chapter 7, Sections 7.1, 7.2, 7.3, 7.4 respectively) have been calculated using the Newton-Raphson method described above. The following example gives the details of the application of this method to the equations.

Application 1 of the tetrahedral vertical compressive stress regime for proprietory shaped paver 1 can be calculated using the following program which is based on Newton's method for solving two nonlinear system equations written for Mathematica computer software (see Section 7.2.1 in Chapter 7).

---

qpx=0.6 y-9; qpy=15+1.6666666 x; poy=85-3 x; pox=28.3333-0.3333 y;ony=85+1.6666 x; onx=0.6 y-51; nmy=114.5-0.3 x; nmx=381.6666-3.3333 y;mky=46.25+0.75 x; mkx=1.3333 y-61.6666;kjy=129.615-0.2301 x; kjx=561.6666-4.3333 y; jiy=0.75 x-17.5;jix=23.3333+ 1.3333 y;hiy=161-0.3 x; hix=536.6666-3.3333 y; ghy=1.6666 x-271.6666; ghx=163+0.6 y; fgy=685-3 x; fgx=228.3333-0.3333 y; efy=1.6666 x-341.6666; efx=205+0.6 y; dcy=61.5-0.3 x; dex=205-3.3333 y; qax=50-3.3333 y; qay=15-0.3 x; abx=50+1.3333 y; aby=0.75 x-37.5; bcx=135-4.3333 y; bcy=31.154-0.23 x; cdx=135+1.3333 y; cdy=0.75 x-101.25; t10x =t(l+271.6666)/(l+1.6666 t);t10y=l(t-163)/(t+0.6 l);t11x=t(l-685)/(l-3 t); t11y=l(t-228.3333)/(t-0.3333 l);t12x=t(l+341.6666)/(l+1.6666 t);t12y=l(t-205)/(t+0.6 l); t13x=t(l-61.5)/(l-0.3 t);t13y=l(t-205)/(t-3.3333 l);t14x=t(l+101.25)/(l+0.75 t); t14y=l(t-135)/(t+1.3333 l); t15x=t(l-31.154)/(l-0.23 t); t15y=l(t-135)/(t-4.3333 l); t16x=t(l+37.5)/(l+0.75 t); t16y=l(t-50)/(t+1.3333 l); t1x=t(l-15)/(l-0.3 t);t1y=l(t-50)/(t-3.3333 l);t2x=0.6 t(l-15)/(t+0.6 l); t2y=l(t+9)/(t+0.6 l); t3x=t(l-85)/(l-3 t); t3y=l(t-28.3333)/(t-0.3333 l);t4x=t(l-85)/(l+1.6666 t); t4y=l (t+51)/(t+0.6 l);t5x=t(l-114.5)/(l-0.3 t); t5y=l(t-381.6666)/(t-3.3333 l);t6x=t(l-46.25)/(l+0.75 t); t6y=l(t+61.6666)/(t+1.3333 l);t7x=t(l-129.615)/(l-0.2301 t); t7y=l(t-561.6666)/(t-4.3333 l);t8x=t(l+17.5)/(l+0.75 t); t8y=l(t-23.3333)/(t+1.3333 l); t9x=t(l-161)/(l-0.3 t); t9y=l(t-536.6666)/(t-3.3333 l);fy=l(1-x/t);fx=t(1-y/l);f=σ_A(1-x/t-y/l);v=Factor[Collect[Simplify[

```
Integrate [f,{x,0,t},{y,0,fy}]- Integrate[f,{x,t1x,t},{y,0,fy}]-Integrate[f,{x,0,t1x},{y,0,t1y}]-
Integrate[f,{x,0,t1x},{y,t1y,qay}]- Integrate[f,{x,0,t2x},{y,t2y,fy}]-Integrate[f,{x,0,t2x},{y,
15,qpy}]],σA ]]; X̄ =Factor[Collect[Simplify[ 1/v (Integrate [f x,{x,0,t},{y,0,fy}]-Integrate
[f x,{x,t1x,t},{y,0,fy}]-Integrate[f x,{x,0,t1x},{y,0,t1y}]- Integrate[fx,{x,0,t1x},{y,t1y, qay
}]-Integrate[f x,{x,0,t2x},{y,t2y,fy}]-Integrate[f x,{x,0,t2x},{y, 15,qpy}])],l ]]; Ȳ =Factor[
Collect[Simplify[1/v (Integrate[f y,{y,0,l},{x,0,fx}]- Integrate[f y,{y,0,t1y},{x,t1x,fx}]-
Integrate[f y,{y,0,t1y},{x,0,t1x}]- Integrate[f y,{y,t1y,15},{x,0,qax}]- Integrate[f y,{y, 15,
t2y},{x,0,qpx}]- Integrate[f y,{y,t2y,l},{x,0,fx}])],t]]; Solve[v= =N, σA ];σA=σA ./%;
eq1=Collect [Expand[xx Denominator[ X̄ ])-Numerator[ X̄ ]],l]= =0; X̄ =.;eq1=%% ./xx-
> X̄ ; eq2= Collect[Expand[yy Denominator[ Ȳ ])-Numerator[ Ȳ ]],t]= =0; Ȳ =.;eq2=%%
./xx-> Ȳ ;Do[{ {eq1=f(l,t)= =0; eq2=f(l,t)= =0}; j21=D[eq2,l]; j22=D[eq2, t]; j12=D[eq1,t];
j11=D[eq1,l]; j={{j11,j12},{j21,j22}}; f={{eq1,0},{eq2,0}}; y=f Inverse[j]; itersolition= {
{l,0},{ t,0}}+y; l=Part[itersolition[[1]],1]; t=Part[itersolition [[2]],1]; Print[l,t]},{20}]; σA
```

Therefore, the following tetrahedral stress regime's volume can be found from the program.

$$
\begin{aligned}
V = (&2.77556.10^{-17}\sigma_A(-174l^7t + 792.5l^8t - 40.5469l^9t + l^{10}t - 7.36352.10^{19}l^6t^2 + \\
&1.4727.10^{19}l^7t^2 - 9.81803.10^{17}l^8t^2 + 2.18178.10^{16}l^9t^2 + 2.19367.10^{19}l^5t^3 - 4.38734.10^{18}l^6t^3 \\
&+2.9249.10^{17}l^7t^3 - 6.49977.10^{15}l^8t^3 - 8.76484.10^{19}l^4t^4 + 1.75297.10^{19}l^5t^4 - 1.16865.10^{18}l^6t^4 \\
&+2.59699.10^{16}l^7t^4 + 1.25207.10^{20}l^3t^5 - 2.50415.10^{19}l^4t^5 + 1.66943.10^{18}l^5t^5 - 3.70985.10^{16}l^6t^5 \\
&-6.23327.10^{19}l^2t^6 + 1.24665.10^{19}l^3t^6 - 8.31102.10^{17}l^4t^6 + 1.84689.10^{16}l^5t^6 + 1.32448.10^{19}l.t^7 \\
&-2.64896.10^{18}l^2t^7 + 1.76598.10^{17}l^3t^7 - 3.92439.10^{15}l^4t^7 - 1.03378.10^{18}t^8 + 2.06755.10^{17}l.t^8 \\
&-1.03378.10^{18}t^8 + 2.06755.10^{17}l.t^8 - 1.37837.10^{16}l^2t^8 + 3.06304.10^{14}l^3t^8)) \Big/ (l(l - 0.30003t)^2 \\
&(l - 0.3t)^3(l + 1.66667t)^3)
\end{aligned}
\qquad \text{(Eq. A.10)}
$$

The following centroid distances $\overline{X}$ and $\overline{Y}$ can be determined from the program.

$$
\begin{aligned}
\overline{X} = (&5.90492.10^{15}(-2.77464.10^{-12}l^9t^2 - 3.46829.10^{-13}l^{10}t^2 - 1.08384.10^{-14}l^{11}t^2 + \\
&50625.l^7t^3 - 13500.l^8t^3 + 1350.l^9t^3 - 60.l^{10}t^3 + l^{11}t^3 - 417.977.l^6t^4 + 111.461.l^7t^4 - \\
&11.1461.l^8t^4 + 0.49538.l^9t^4 - 0.00825633.l^{10}t^4 + 296664.l^5t^5 - 79110.4.l^6t^5 + 7911.04.l^7t^5 \\
&-351.602.l^8t^5 + 5.86003.l^9t^5 - 299760.l^4t^6 + 79935.9.l^5t^6 - 7993.59.l^6t^6 + 355.271.l^7t^6 - \\
&5.92118.l^8t^6 + 785758.l^3t^7 - 20953.6.l^4t^7 + 2095.36.l^5t^7 - 93.1269.l^6t^7 + 1.55212.l^7t^7 +
\end{aligned}
\qquad \text{(Eq. A.11)}
$$

$$8520.02.l^2t^8 - 2272.01.l^3t^8 + 227.201.l^4t^8 - 10.0978.l^5t^8 + 0.168297.l^6t^8 - 6220.59.l.t^9 +$$
$$1658.82.l^2t^9 - 165.882.l^3t^9 + 7.37255.l^4t^9 - 0.122876.l^5t^9 + 674.22.t^{10} - 179.792.l.t^{10} +$$
$$17.9792.l^2t^{10} - 0.799076.l^3t^{10} + 0.0133179.l^4t^{10})) \Big/ ((l - 0.3t)(l + 1.66667.t)(-174l^7t +$$
$$792.5l^8t - 40.5469l^9t + l^{10}t - 7.36352.10^{19}l^6t^2 + 1.4727.10^{19}l^7t^2 - 9.81803.10^{17}l^8t^2 +$$
$$2.18178.10^{16}l^9t^2 + 2.19367.10^{19}l^5t^3 - 4.38734.10^{18}l^6t^3 + 2.9249.10^{17}l^7t^3 - 6.49977.10^{15}l^8t^3$$
$$-8.76484.10^{19}l^4t^4 + 1.75297.10^{19}l^5t^4 - 1.16865.10^{18}l^6t^4 + 2.59699.10^{16}l^7t^4 + 1.25207.10^{20}l^3t^5$$
$$-2.50415.10^{19}l^4t^5 + 1.66943.10^{18}l^5t^5 - 3.70985.10^{16}l^6t^5 - 6.23327.10^{19}l^2t^6 + 1.24665.10^{19}l^3t^6$$
$$-8.31102.10^{17}l^4t^6 + 1.84689.10^{16}l^5t^6 + 1.32448.10^{19}l.t^7 - 2.64896.10^{18}l^2t^7 + 1.76598.10^{17}l^3t^7$$
$$-3.92439.10^{15}l^4t^7 - 1.03378.10^{18}t^8 + 2.06755.10^{17}l.t^8 - 1.03378.10^{18}t^8 + 2.06755.10^{17}l.t^8$$
$$-1.37837.10^{16}l^2t^8 + 3.06304.10^{14}l^3t^8))$$

$$\bar{Y} = (4.03489.10^{15}(-8.13156.10^{-7}l^{15} - 4.94871.10^{-6}l^{14}t + 1.15256.10^{-7}l^{15}t - 0.226033.l^{13}t^2 +$$
$$0.030137.l^{14}t^2 - 0.00100455.l^{15}t^2 - 148172.l^{12}t^3 + 29634.3.l^{13}t^3 - 1975.61.l^{14}t^3 + 43.9025.l^{15}t^3$$
$$-290146.l^{11}t^4 + 54654.2.l^{12}t^4 - 3193.61.l^{13}t^4 + 40.9691.l^{14}t^4 + l^{15}t^4 + 295735.l^{10}t^5 - 59826.8.l^{11}t^5$$
$$+4079.11.l^{12}t^5 - 96.691.l^{13}t^5 + 0.201476.l^{14}t^5 + 412150.l^9t^6 - 71004.7.l^{10}t^6 + 3210.3.l^{11}t^6 +$$
$$30.2169.l^{12}t^6 - 3.38522.l^{13}t^6 - 508212.l^8t^7 + 94220.5.l^9t^7 - 5291.79.l^{10}t^7 + 51.6234.l^{11}t^7 +$$
$$2.19905.l^{12}t^7 - 13096.7.l^7t^8 - 5362.06.l^8t^8 + 1421.66.l^9t^8 - 102.538.l^{10}t^8 + 2.36487.l^{11}t^8 +$$
$$295941.l^6t^9 - 44690.9.l^7t^9 + 1046.41.l^8t^9 + 105.612.l^9t^9 - 4.29552.l^{10}t^9 - 217875.l^5t^{10} +$$
$$33679.l^6t^{10} - 925.797.l^7t^{10} - 67.3912.l^8t^{10} + 2.93215.l^9t^{10} + 82111.1.l^4t^{11} - 12549.5.l^5t^{11} +$$
$$320.272.l^6t^{11} + 27.3068.l^7t^{11} - 1.14747.l^8t^{11} - 18600.5.l^3t^{12} + 2778.12.l^4t^{12} - 59.6123.l^5t^{12} -$$
$$7.04831.l^6t^{12} + 0.279101.l^7t^{12} + 2565.61.l^2t^{13} - 371.622.l^3t^{13} + 5.90825.l^4t^{13} + 1.12647.l^5t^{13} -$$
$$0.0419255.l^6t^{13} - 199.695.l.t^{14} + 27.8567.l^2t^{14} - 0.246161.l^3t^{14} - 0.101927.l^7t^{14} + 0.00357989.l^5t^{14}$$
$$+6.75442.t^{15} - 0.900589.l.t^{15} + 0.00400261.l^3t^{15} - 0.00013342.l^4t^{15} + 3.02537.10^{-20}l^3t^{16})) \Big/$$
$$((l - 0.30003.t)^3(l - 0.3.t)^2t.(l + 1.66667.t)(-174l^7t + 792.5l^8t - 40.5469l^9t + l^{10}t - 7.36352.10^{19}l^6t^2$$
$$+1.4727.10^{19}l^7t^2 - 9.81803.10^{17}l^8t^2 + 2.18178.10^{16}l^9t^2 + 2.19367.10^{19}l^5t^3 - 4.38734.10^{18}l^6t^3$$
$$+2.9249.10^{17}l^7t^3 - 6.49977.10^{15}l^8t^3 - 8.76484.10^{19}l^4t^4 + 1.75297.10^{19}l^5t^4 - 1.16865.10^{18}l^6t^4$$
$$+2.59699.10^{16}l^7t^4 + 1.25207.10^{20}l^3t^5 - 2.50415.10^{19}l^4t^5 + 1.66943.10^{18}l^5t^5 - 3.70985.10^{16}l^6t^5$$
$$-6.23327.10^{19}l^2t^6 + 1.24665.10^{19}l^3t^6 - 8.31102.10^{17}l^4t^6 + 1.84689.10^{16}l^5t^6 + 1.32448.10^{19}l.t^7$$
$$-2.64896.10^{18}l^2t^7 + 1.76598.10^{17}l^3t^7 - 3.92439.10^{15}l^4t^7 - 1.03378.10^{18}t^8 + 2.06755.10^{17}l.t^8$$
$$-1.03378.10^{18}t^8 + 2.06755.10^{17}l.t^8 - 1.37837.10^{16}l^2t^8 + 3.06304.10^{14}l^3t^8)) \qquad \text{(Eq. A.12)}$$

The program evaluates the following σ_A value from Eq. A.10 by applying the rotational and vertical equilibrium (see Chapter 6).

$$\sigma_A = (-l.N.(l-0.30003.t)^2(-l+0.3)^3(l+1.66667.t)^3) \Big/ (-4.82974.10^{-15}l^7t + 2.19963.10^{-14}l^8t$$
$$-1.1254.10^{-15}l^9t + 2.77556.10^{-17}l^{10}t - 2043.79.l^6t^2 + 408.757.l^7t^2 - 27.2505.l^8t^2 + 0.605567.l^9t^2 \quad \text{(Eq. A.13)}$$
$$+608.866.l^5t^3 - 121.773.l^6t^3 + 8.11822.l^7t^3 - 0.180405.l^8t^3 - 2432.73.l^4t^4 + 486.546.l^5t^4 -$$
$$32.4364.l^6t^4 + 0.720809.l^7t^4 + 3475.2.l^3t^5 - 695.04.l^4t^5 + 46.336.l^5t^5 - 1.02969.l^6t^5 - 1730.08.l^2t^6$$
$$+346.016.l^3t^6 - 23.0677.l^4t^6 + 0.512616.l^5t^6 + 367.618.l.t^7 - 73.5235.l^2t^7 + 4.90157.l^3t^7 -$$
$$0.108924.l^4t^7 - 28.6931.t^8 + 5.73862.l.t^8 - 0.382574.l^2t^8 + 0.00850166.l^3t^8)$$

The program evaluates the following equations from Eq. A.11 and Eq. A.12 by applying the rotational and vertical equilibrium (see Chapter 6).

$$0 = -3.98122.10^{18}t^{10} + l^{12}t.\overline{X} + 5.16889.10^{17}t^{10}\overline{X} + l^{11}(64.t^2 - 5.90492.10^{15}t^3 - 40.5469.t.\overline{X}$$
$$+2.18178.10^{16}t^2\overline{X}) + l^{10}(2048.t^2 + 3.54295.10^{17}t^3 + 4.8753.10^{13}t^4 + 792.5.t.\overline{X} -$$
$$9.81803.10^{17}t^2\overline{X} + 2.33179.10^{16}t^3\overline{X}) + l^9(16384.t^2 - 7.97164.10^{18}t^3 - 2.92518.10^{15}t^4 -$$
$$3.4603.10^{16}t^5 - 174.t.\overline{X} + 1.4727.10^{19}t^2\overline{X} - 1.04931.10^{18}t^3\overline{X} + 6.17795.10^{15}t^4\overline{X}) +$$
$$l^8(7.97164.10^{19}t^3 + 6.58165.10^{16}t^4 + 2.07618.10^{18}t^5 + 3.49641.10^{16}t^6 - 7.36352.10^{19}t^2\overline{X}$$
$$+1.57396.10^{19}t^3\overline{X} - 2.78008.10^{17}t^4\overline{X} + 1.64362.10^{15}t^5\overline{X}) + l^7(-2.98937.10^{20}t^3 -$$
$$6.58165.10^{17}t^4 - 4.67141.10^{19}t^5 - 2.09784.10^{18}t^6 - 9.16512.10^{15}t^7 - 7.86981.10^{19}t^3\overline{X} +$$
$$4.17012.10^{18}t^4\overline{X} - 7.39629.10^{16}t^5\overline{X} - 4.52172.10^{16}t^6\overline{X}) + l^6(2.46812.10^{18}t^4 + 4.67141.10^{20}t^5$$
$$+4.72015.10^{19}t^6 + 5.49907.10^{17}t^7 - 9.93778.10^{14}t^8 - 2.08506.10^{19}t^4\overline{X} + 1.10944.10^{18}t^5\overline{X}$$
$$+2.03478.10^{18}t^6\overline{X} + 3.98657.10^{16}t^7\overline{X}) + l^5(-1.75178.10^{21}t^5 - 4.72015.10^{20}t^6 - 1.23729.10^{19}t^7$$
$$+5.96267.10^{16}t^8 + 7.25572.10^{14}t^9 - 5.54722.10^{18}t^5\overline{X} - 3.05216.10^{19}t^6\overline{X} - 1.79396.10^{18}t^7\overline{X}$$
$$-1.42915.10^{16}t^8\overline{X}) + l^4(1.77006.10^{21}t^6 + 1.23729.10^{20}t^7 - 1.3416.10^{18}t^8 - 4.35343.10^{16}t^9 -$$
$$7.86413.10^{13}t^{10} + 1.52608.10^{20}t^6\overline{X} + 2.69094.10^{19}t^7\overline{X} + 6.43117.10^{17}t^8\overline{X} + 2.38081.10^{15}t^9\overline{X})$$
$$+l.(3.67321.10^{19}t^9 + 1.06166.10^{18}t^{10} - 8.03524.10^{18}t^9\overline{X} - 1.03378.10^{17}t^{10}\overline{X}) + l^3(-4.63984.10^{20}t^7 \quad \text{(Eq. A.14)}$$
$$+1.3416.10^{19}t^8 + 9.79523.10^{17}t^9 + 4.71848.10^{15}t^{10} - 1.34547.10^{20}t^7\overline{X} - 9.64676.10^{18}t^8\overline{X} -$$
$$1.07137.10^{17}t^9\overline{X} - 1.53152.10^{14}t^{10}\overline{X}) + l^2(-5.031.10^{19}t^8 - 9.79523.10^{18}t^9 - 1.06166.10^{17}t^{10} +$$
$$4.82338.10^{19}t^8\overline{X} + 1.60705.10^{18}t^9\overline{X} + 6.89185.10^{15}t^{10}\overline{X})$$

$$0 = 3.28099.10^9l^{15} + (1.99675.10^{10}l^{14} - 4.65043.10^{18}l^{15}).t - 0.00012207.l^3t^{16} + t^{15}(-2.72534.10^{16} +$$
$$3.63378.10^{15}l - 1.61501.10^{13}l^3 + 5.38336.10^{11}l^4 + 4.18805.10^{15}\overline{Y} - 8.37611.10^{14}l.\overline{Y} + 5.58407.10^{13}l^2\overline{Y} \quad \text{(Eq. A.15)}$$
$$-1.24091.10^{12}l^3\overline{Y}) + t^{14}(8.05746.10^{17}l - 1.12399.10^{17}l^2 + 9.93231.10^{14}l^3 + 4.11262.10^{14}l^4 -$$
$$1.44445.10^{13}l^5 - 1.20942.10^{17}l.\overline{Y} + 2.41883.10^{16}l^2\overline{Y} - 1.61255.10^{15}l^3\overline{Y} + 3.58345.10^{13}l^4\overline{Y})$$
$$+t^{13}(-1.03519.10^{19}l^2 + 1.49945.10^{18}l^3 - 2.38391.10^{16}l^4 - 4.54519.10^{15}l^5 + 1.69165.10^{14}l^6$$

$$+1.53797.10^{18}l^2\bar{Y} - 3.07595.10^{17}l^3\bar{Y} + 2.05063.10^{16}l^4\bar{Y} - 4.55696.10^{14}l^5\bar{Y}) + t^{12}(7.50508.10^{19}l^3$$
$$-1.12094.10^{19}l^4 + 2.40529.10^{17}l^5 + 2.84392.10^{16}l^6 - 1.12614.10^{15}l^7 - 1.12606.10^{19}l^3\bar{Y}$$
$$+2.25211.10^{18}l^4\bar{Y} - 1.50141.10^{17}l^5\bar{Y} + 3.33647.10^{15}l^6\bar{Y}) + t^{11}(-3.31309.10^{20}l^4 + 5.06359.10^{19}l^5$$
$$-1.29226.10^{18}l^6 - 1.1018.10^{17}l^7 + 4.6299.10^{15}l^8 + 5.19809.10^{19}l^4\bar{Y} - 1.03962.10^{19}l^5\bar{Y} +$$
$$6.93078.10^{17}l^6\bar{Y} - 1.54017.10^{16}l^7\bar{Y}) + t^{10}(8.79103.10^{20}l^5 - 1.35891.10^{20}l^6 + 3.73549.10^{18}l^7 +$$
$$2.71916.10^{17}l^8 - 1.18309.10^{16}l^9 - 1.55117.10^{20}l^5\bar{Y} + 3.10233.10^{19}l^6\bar{Y} - 2.06822.10^{18}l^7\bar{Y} +$$
$$4.59605.10^{16}l^8\bar{Y}) + t^9(-1.19409.10^{21}l^6 + 1.80323.10^{20}l^7 - 4.22213.10^{18}l^8 - 4.26133.10^{17}l^9 +$$
$$1.73319.10^{16}l^{10} + 2.92553.10^{20}l^6\bar{Y} - 5.85106.10^{19}l^7\bar{Y} + 3.90071.10^{18}l^8\bar{Y} - 8.66824.10^{16}l^9\bar{Y}) + t^8$$
$$(5.28436.10^{19}l^7 + 2.16353.10^{19}l^8 - 5.73623.10^{18}l^9 + 4.13731.10^{17}l^{10} - 9.54197.10^{15}l^{11} -$$
$$3.19072.10^{20}l^7\bar{Y} + 6.38143.10^{19}l^8\bar{Y} - 4.25429.10^{18}l^9\bar{Y} + 9.45397.10^{16}l^{10}\bar{Y}) + t^7(2.05058.10^{21}l^8 -$$
$$3.8017.10^{20}l^9 + 2.13518.10^{19}l^{10} - 2.08295.10^{17}l^{11} - 8.87295.10^{15}l^{12} + 1.55909.10^{20}l^8\bar{Y} -$$
$$3.11818.10^{19}l^9\bar{Y} + 2.07879.10^{18}l^{10}\bar{Y} - 4.61953.10^{16}l^{11}\bar{Y}) + t^6(-1.66298.10^{21}l^9 + 2.86496.10^{20}l^{10} -$$
$$1.29532.10^{19}l^{11} - 1.21922.10^{17}l^{12} + 1.3659.10^{16}l^{13} - 1.50736.10^{19}l^9\bar{Y} + 3.01471.10^{18}l^{10}\bar{Y} -$$
$$2.00981.10^{17}l^{11}\bar{Y} + 4.46624.10^{15}l^{12}\bar{Y}) + t^5(-1.19326.10^{21}l^{10} + 2.41395.10^{20}l^{11} - 1.64588.10^{19}l^{12} +$$
$$3.90138.10^{17}l^{13} - 8.12933.10^{14}l^{14} + 3.38252.10^{19}l^{10}\bar{Y} - 6.76504.10^{18}l^{11}\bar{Y} + 4.51002.10^{17}l^{12}\bar{Y} -$$
$$1.00223.10^{16}l^{13}\bar{Y}) + t^4(1.17071.10^{21}l^{11} - 2.20524.10^{20}l^{12} + 1.28859.10^{19}l^{13} - 1.65306.10^{17}l^{14} -$$
$$4.03489.10^{15}l^{15} + 9.67082.10^{18}l^{11}\bar{Y} - 1.93416.10^{18}l^{12}\bar{Y} + 1.28944.10^{17}l^{13}\bar{Y} - 2.86543.10^{15}l^{14}\bar{Y}) + t^3$$
$$(5.97857.10^{20}l^{12} - 1.1957.10^{20}l^{13} + 7.97139.10^{18}l^{14} - 1.77142.10^{17}l^{15} - 7.36352.10^{19}l^{12}\bar{Y} +$$
$$1.4727.10^{19}l^{13}\bar{Y} - 9.81803.10^{17}l^{14}\bar{Y} + 2.18178.10^{16}l^{15}\bar{Y}) + t^2(9.12017.10^{14}l^{13} - 1.216.10^{14}l^{14} +$$
$$4.05325.10^{12}l^{15} - 174.l^{13}\bar{Y} + 792.5.l^{14}\bar{Y} - 40.5469.l^{15}\bar{Y} + l^{16}\bar{Y})$$

The program calculates the roots of Eq. A.14 and Eq. A.15. Then, the results allow to determine σ_A from Eq. A.13. By using the procedure described in Section A.2.1.1 the stress function and the stress beneath the corners can be determined. The results are shown in Figure 9.1.

References

1 Ostrowski, A. M., (1966), Solutions of Equations and Systems of Equations, 2nd. Ed. (New York: Academic Press).

2 Mathematica Computer Software: Wolfram Research, Inc., 100 Trade Centre Drive, Champaign, Illinois, 61820-7237, USA. Telephone: 217-398-0700.